FOUNDED IN 1906 AS THE AMERICAN QUARTERLY OF ROENTGENOLOGY

# THE AMERICAN JOURNAL OF ROENTGENOLOGY RADIUM THERAPY AND NUCLEAR MEDICINE

CALCUTTA UNIVERSITY CENTRAL LIBRARY

OFFICIAL ORGAN OF

THE AMERICAN ROENTGEN RAY SOCIETY
THE AMERICAN RADIUM SOCIETY

20

TRAIAN LEUCUTIA, Editor

KENNETH L. KRABBENHOFT, Assistant to the Editor

ASSOCIATE EDITORS

HARRY HAUSER    RUSSELL H. MORGAN    EDWARD B. D. NEUHAUSER
WENDELL G. SCOTT

CONSULTING EDITORIAL BOARD

PAUL C. AEBERSOLD
OSCAR V. BATSON
JOHN CAFFEY
ROSS GOLDEN
PAUL C. HODGES
HOWARD B. HUNT
JOHN H. LAWRENCE
REED M. NESBIT
EUGENE P. PENDERGRASS
U. V. PORTMANN
LAURISTON S. TAYLOR
OWEN H. WANGENSTEEN
SHIELDS WARREN

*Issued Monthly for the American Roentgen Ray Society by*

CHARLES C THOMAS · PUBLISHER · SPRINGFIELD · ILLINOIS

VOLUME 94    JULY, 1965    NUMBER 3

Sixty-sixth Annual Meeting, American Roentgen Ray Society
Washington-Hilton Hotel, Washington, D.C.
September 28-October 1, 1965
PROGRAM NUMBER

II

# BARNES-HIND BAROTRAST®

□ Barotrast suspends easily—and **stays** in suspension. Coverage is complete... coating is thin, elastic, tenacious... flow is steady, consistent, and columnar. Barotrast is ideal for routinely precise examinations. □ BAROTRAST® (Specially compounded and micronized form of barium sulfate) □

**BARNES-HIND BARIUM PRODUCTS**
DIVISION OF BARNES-HIND PHARMACEUTICALS, INC.
Sunnyvale, California

615.842305
AM35

the original
high-density barium product
for unsurpassed delineation

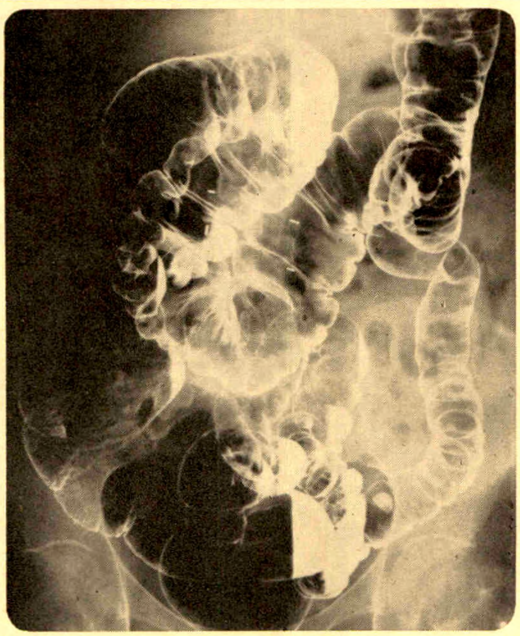

Barotrast used in an air contrast study of the mid transverse colon.

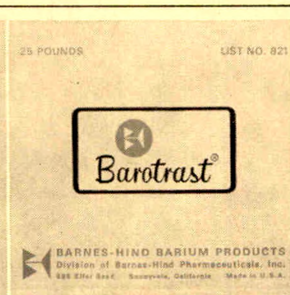


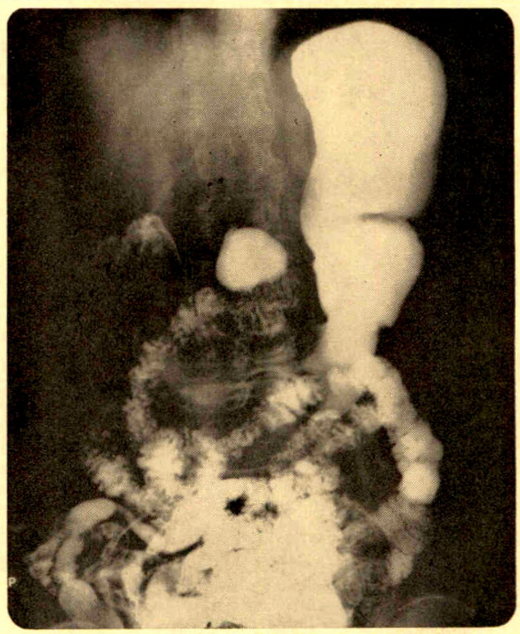

Barotrast used in an upper GI study of the stomach.

©1964 BPA 101

CULC HC3408-20-627/678

27 YEARS of integrity have helped us to become America's largest buyers of

# USED X-RAY FILM

- We purchase all makes and sizes from any point in the nation, and pay the freight cost.
- We remit in advance if desired, or promptly after receipt and tally of the value.
- Write for prices today. We will send shipping labels, and direct your film to our nearest plant.

**DONALD McELROY, INC.**

53 W. Jackson Blvd., Chicago 4, Ill.

***Who squeezed enough x-ray solution for 10,000 films into a 7-inch square box?***

***Urell did.***

The question is "why?" Why a box?

Well, you just don't stop upgrading the quality of Urell Hyper-Concentrated X-ray Solutions. They always develop up to 10,000 films of highest contrast and detail from the same tank—before changing. But for years Urell has searched for comparable efficiency in packaging. Here it is. Simply and logically. A box.

Fitted inside each 7-inch square box is an extraordinary cube-square of strong, airtight, leakproof plastic. All you do is pull-out the retractable spout, uncap and pour. Then on with the cap, in with the spout. Easier to handle and easier to store. And you'll find at least 83 uses for the empty plastic cubes.

If you're looking for economy with superior performance in your x-ray concentrates, try Urell. Developer, replenisher, fixer & replenisher in 5-gallon sizes. Unconditionally guaranteed to meet all your developing requirements by America's oldest exclusive manufacturer.

***Urell***

*2630 Humboldt Street*
*Los Angeles, California 90031*
*"It's Urell first to last"*

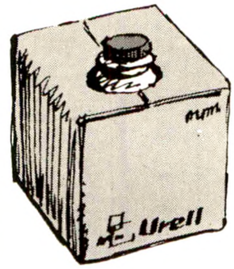

# 8 OUTSTANDING NEW BOOKS FOR ROENTGENOLOGISTS

**History · Techniques · Procedures**

- ☐ CLASSIC DESCRIPTIONS IN DIAGNOSTIC ROENTGENOLOGY *edited by* **André J. Bruwer**, *Tucson Medical Center, Tucson, Ariz. (With 35 Contributors) (In Two Volumes)* '64, 2094 pp. (7 × 10), 1727 il., $49.50
- ☐ RADIOTHERAPY OF BENIGN DISEASE *by* **Stephen B. Dewing**, *Hunterdon Medical Center, Flemington, N.J. With a chapter contributed by* **Ralph Wier Grover**, *Nassau County Tuberculosis Sanatorium, Farmingdale, N.Y.* '65, 320 pp., $9.75
- ☐ PRACTICAL GAMMA SPECTROMETRY *by* **A. J. Duivenstijn**, *Eindhoven, and* **L. A. J. Venverloo**, *Veldhoven. Both of The Netherlands. Translated by* **G. du Cloux**, *Wallington, England.* '63, 154 pp., 87 il., $7.50
- ☐ THE SCIENCE OF IONIZING RADIATION: Modes of Application *compiled and edited by* **Lewis E. Etter**, *Univ. of Pittsburgh, Pittsburgh, Pa. (With 35 Contributors) Foreword by* **Otto Glasser.** '65, 804 pp. (6¾ × 9¾), 483 il., 29 tables, $26.50
- ☐ THE TRAIL OF THE INVISIBLE LIGHT *by* **E. R. N. Grigg**, *Cook County Hosp., Chicago, Ill.* About 600 pp. (8½ × 11), 1,404 figs., (Amer. Lec. Roentgen Diagnosis edited by **Lewis E. Etter**). In Press
- ☐ DOSEMETERS FOR X-RAY DIAGNOSIS *by* **K. Reinsma**, *Philips' Industrial Division for X-Ray and other Medical Equipment, Eindhoven, The Netherlands. Translated by* **A. F. Jolmers**, *Beckenham, England.* '62, 100 pp., 40 il., 16 tables, $4.50
- ☐ UTEROSALPINGOGRAPHY IN GYNECOLOGY: Its Application in Physiological and Pathological Conditions *by* **Samuel Rozin**, *Hebrew University-Hadassah Medical School, Jerusalem, Israel.* '65, 376 pp. (8½ × 11), 369 il., $20.50
- ☐ MYELOGRAPHY *by* **Vincenzo Valentino**, *Univ. of Naples, Naples, Italy.* '65, 292 pp. (8½ × 11), 276 il., (3 color plates), $19.50

**CHARLES C THOMAS · PUBLISHER**

301-327 East Lawrence Avenue

Springfield, Illinois



HANLEY ECONOMY 14 x 17 X-RAY CABINET
SPECIAL DESIGN SLIDING DOORS
*QUALITY AT LOW PRICES*
Vertical Filing
We Build Special Size X-Ray Cabinets
SPECIAL SIZE, 83 H x 19½ D x 40 W, W/DOORS
5 COMPARTMENT SIZE—DIVIDERS 14 x 17 ............$114.70
3 COMPARTMENT SIZE—DIVIDERS 14 x 17 ............ 90.00
APPROVAL GUARANTEED—F.O.B. FACTORY—CATALOGUE

**HANLEY MEDICAL EQUIPMENT CO.**
5614 South Grand X-ray Division St. Louis 11, Mo.



In reply to advertisers please mention that you saw their advertisement in

THE AMERICAN JOURNAL OF ROENTGENOLOGY, RADIUM THERAPY AND NUCLEAR MEDICINE

• • •

CHARLES C THOMAS
PUBLISHER
Springfield · Illinois



***An Authorized Binding for***

**THE AMERICAN JOURNAL OF ROENTGENOLOGY RADIUM THERAPY AND NUCLEAR MEDICINE**

Arrangements have been made for subscribers to have their journals bound into distinctively designed books.

Six issues, January through June or July through December, bound in best grade garnet washable buckram imprinted with your name on cover, cost but $5.95 per volume.

Bound journals serve as an immediate reference for information and research. They conserve space and permanently preserve the important communications from becoming mislaid or lost. Most important of all, they save time!

Ship journals parcel post. Within forty-five days after receipt, bound volumes will be shipped prepaid anywhere in the U.S.A. Full remittance must accompany order.

**PUBLISHERS' AUTHORIZED BINDERY SERVICE**
***(Binders of all Journals)***
**430 W. Erie St., Chicago, Illinois 60610**

[FOUNDED IN 1906 AS THE AMERICAN QUARTERLY OF ROENTGENOLOGY]

# The AMERICAN JOURNAL OF ROENTGENOLOGY RADIUM THERAPY AND NUCLEAR MEDICINE

*Editor*: TRAIAN LEUCUTIA, M.D.

*Assistant to the Editor*: KENNETH L. KRABBENHOFT, M.D.

VOLUME 94

MAY–AUGUST, 1965

LIBRARY UNIVERSITY

CHARLES C THOMAS : SPRINGFIELD, ILLINOIS
1965

25678

Copyright, 1965
By AMERICAN ROENTGEN RAY SOCIETY, Inc.

# CONTENTS OF VOLUME 94

MAY, 1965. NUMBER 1

*When*

*the clinical situation demands*
*conclusive, differential diagnosis*
*consider these contrast media*

**Hytrast**® (iopydone, iopydol)
**Ethiodol**® (ethiodized oil)
**Lipiodol**® **28%** (iodized oil)
**Lipiodol**® **40%** (iodized oil)
**Ascendant Lipiodol**® (floating iodized oil)
**Visciodol**® (Lipiodol-sulfanilamide)

*...and procedural aids*

**Colo-Bar**® (ready-to-eat cholagogue)
**Polysorb**® **Hydrate** (for radiation dry skin)

CONTRAST MEDIA — DEVELOPMENTS OF GUERBET LABORATORIES

FOUGERA **E. FOUGERA & COMPANY, INC.** HICKSVILLE, L. I., NEW YORK

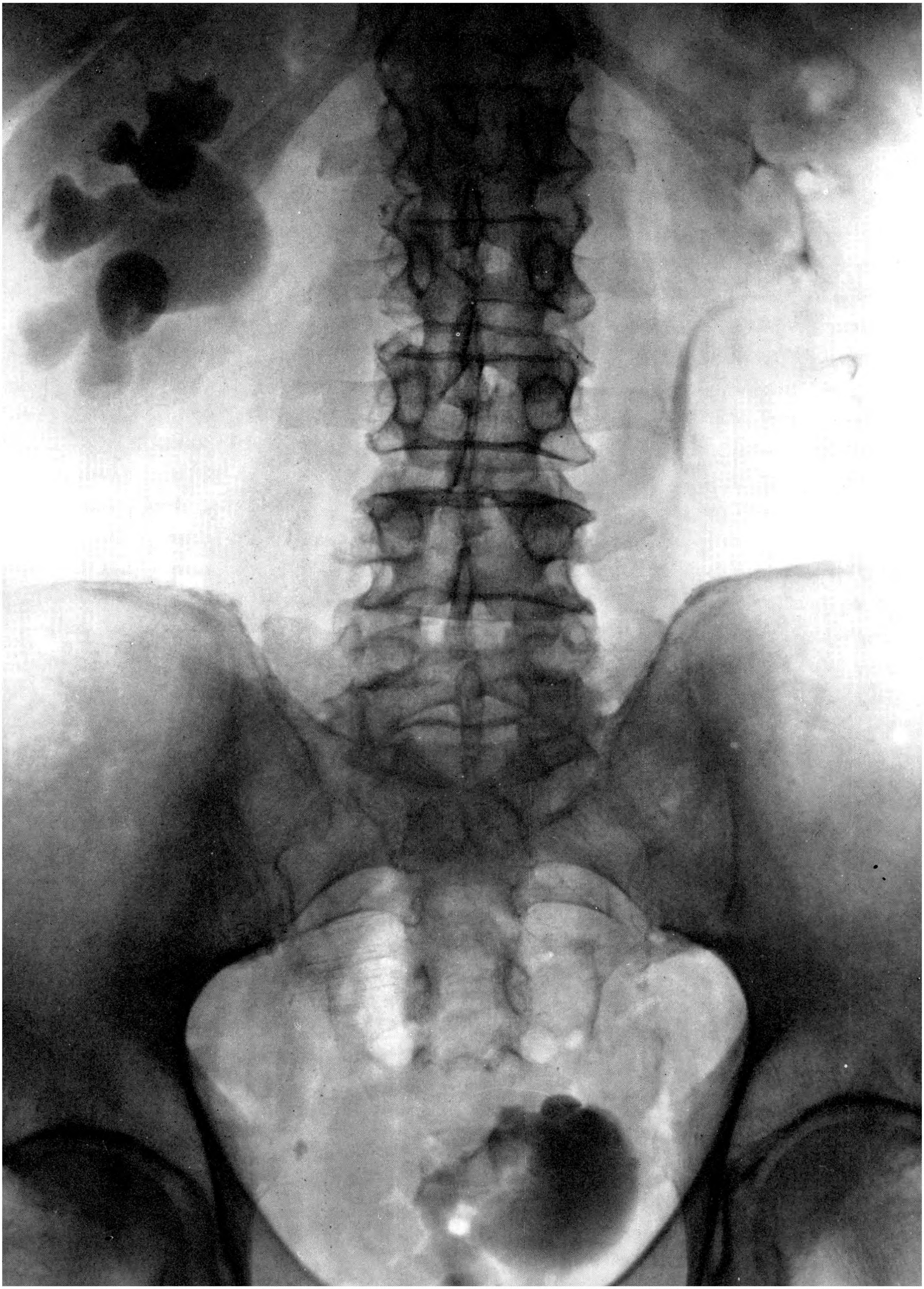

Excretory urogram with Hypaque 50 per cent (30 cc.) Hydronephrosis, right, secondary to cancer of the bladder, blocking the orifice of the right ureter; 25 minute film.

## when instrumentation is undesirable
### precise excretory urography

There are many patients where cystoscopy or catheterization is either undesirable or impossible in determining urinary tract pathology. This may be due to mechanical difficulties (e.g., deformity, anomaly, etc.), debilitated states, infancy, advanced age, infection, pregnancy or after extensive pelvic operations.

In such cases, Hypaque Sodium 50% often provides precisely defined urograms of the kidneys, ureters and bladder, with valuable information about their functional activities, undisturbed by instrumentation. Further advantages are: (1) no age limit to the procedure, and (2) no need to administer an anesthetic.

*Contraindications:* Advanced renal destruction associated with severe uremia, and severe liver disorders.

*Precautions:* Caution is advised in patients with hyperthyroidism, hypertension, severe cardiovascular disease, active tuberculosis, and a history of asthma or other allergy, especially to iodine. Because of the possibility of temporary suppression of urine, it is wise to allow an interval of at least 48 hours before repeating retrograde or excretory urography in patients with unilateral or bilateral reduction of normal renal function.

*Side effects:* Excretory urographic agents may produce symptoms of an anaphylactic* nature in sensitive persons. Patients should be watched carefully during injection as serious reactions, including fatalities, have occurred with all commonly used mediums. Minor reactions, such as nausea, vomiting, excessive salivation, flushing, dizziness, urticaria, and muscular twitching may occur.

*Supplied:* In sterile aqueous solution. Ampuls of 30 cc. (with 1 cc. test ampuls), boxes of 1, 10 and 25. Also, rubber stoppered vials of 20 cc. and 30 cc., boxes of 1, 10 and 25.

*Physicians should study the package insert for information on preventive measures and management of untoward reactions *before* administering Hypaque (diatrizoate sodium).

## Urograms with excellent anatomical detail
# Hypaque® Sodium 50%
## brand of diatrizoate sodium

*an illustrated booklet with complete information is available by writing to Winthrop Laboratories*

Winthrop PIONEERS IN PRODUCTS FOR RADIOLOGIC DIAGNOSIS

WINTHROP LABORATORIES,
NEW YORK, N.Y. 10016

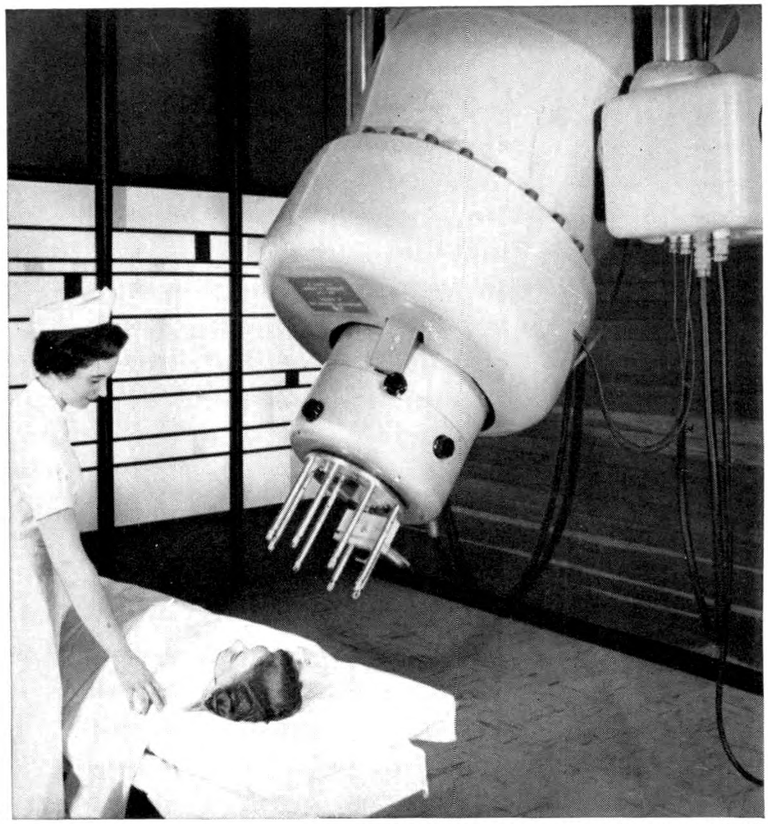

Improved Model AM Van de Graaff is the result of experience gained in 40 previous installations.

# IMPROVED *Van de Graaff*® ACCELERATOR MEETS THE MODERN NEED FOR LOW-COST PRECISION THERAPY

Today's Model AM 2 MeV Van de Graaff Therapy Unit continues to keep pace with the trend to low-cost precision therapy in leading hospitals and cancer clinics throughout the Free World. And for five good reasons:

- Its less than 3 mm "point source" of x-rays allows optimum technics for both large and small treatment fields.
- Its treatment beam is accompanied by negligible penumbra.
- Its Roentgen output exceeds that of a 5000 curie cobalt source.
- Its x-ray output will not fall off. You can hold treatment techniques and parameters constant.
- It can be operated easily by a technician without a staff physicist in attendance.

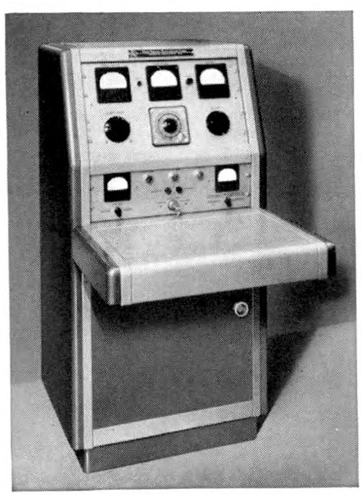

Today's Model AM is routinely operated by an easily-trained technician.

The Model AM Van de Graaff is a reliable, proven source of high-energy radiation. It offers more roentgens-per-dollar and has demonstrated less overall cost-per-treatment than any other comparable supervoltage source available today — including radioisotopes.

Full time use of the reliable Model AM 2 MeV Van de Graaff Therapy Unit will amplify your technic range and expand your patient handling capacity. It is backed by the international reputation of the leading manufacturer of particle accelerators — High Voltage Engineering Corporation. Write Medical Sales.

HIGH VOLTAGE ENGINEERING CORPORATION
BURLINGTON, MASSACHUSETTS

RICHARD SCHATZKI

CALDWELL LECTURER

CENTRAL LIBRARY UNIVERSITY

THE AMERICAN JOURNAL OF ROENTGENOLOGY RADIUM THERAPY AND NUCLEAR MEDICINE

VOL. 94 JULY, 1965 NO. 3

# ESOPHAGUS: PROGRESS AND PROBLEMS*

## THE CALDWELL LECTURE, 1964

*By* RICHARD SCHATZKI, M.D.
CAMBRIDGE, MASSACHUSETTS

*Eugene Wilson Caldwell, who started as an electrical engineer, became a radiologist by "buying out" a photographer.[12] His reputation as a radiologist grew so rapidly that 4 years later he was appointed Director of the Gibbs Laboratory, the new x-ray department of the Bellevue Hospital Medical College in New York City. Only then did he matriculate in medical school. Before he graduated, he had become the co-author of a highly praised textbook on the therapeutic and diagnostic applications of the roentgen rays. Two years after his graduation from Medical School, he was elected to the presidency of the American Roentgen Ray Society. When, in 1918, Caldwell died from radiation cancer at the age of 48, a life full of drive, accomplishment and suffering had ended. Two years later Dr. Walter Alvarez delivered the first Caldwell lecture at the meeting of the American Roentgen Ray Society in Minneapolis.*

FOR someone who has had a special interest in the esophagus through the greater part of his professional life, the request to deliver this lecture offers a tempting occasion to review radiology of the esophagus from a retrospective and prospective viewpoint.

Only 3 months after Professor Röntgen had sent his first observations to the Physicomedical Society of Würzburg, Becher[6] described the use of lead acetate for the roentgen demonstration of the intestines of killed guinea pigs. In his short publication, Becher postulated the two requisites which are still paramount for the demonstration of the gastrointestinal tract in humans: The medium must be dense and it must be nontoxic.

In the same year, the Harvard medical student Walter Bradford Cannon[13] started his little notebook in which he recorded in simple straightforward sentences his roentgenologic observations on the swallowing act in geese and dogs. Cannon used bismuth subnitrate in capsules as well as in the form of "a soft mass of bismuth subnitrate with mush." Roentgenology of the esophagus had started.

In the next year, bismuth subnitrate was employed in humans. Rumpel[31] of Ham-

* Presented at the Sixty-fifth Annual Meeting of the American Roentgen Ray Society, Minneapolis, Minnesota, September 29–October 2, 1964.

burg in a paper on fusiform dilatation of the esophagus showed what was praised by others as "extremely beautiful actinograms."

One year later, Boas and Levy-Dorn[9] used capsules with bismuth to demonstrate obstruction and delay in the gastrointestinal tract of humans.

The clinical significance of the new method was brilliantly demonstrated in 1900 when a young assistant of the Medical Clinic of Professor Nothnagel in Vienna, Dr. Guido Holzknecht,[21] published a paper on the roentgen diagnosis of esophageal stenosis. He used bismuth subnitrate in various forms, as a watery mixture, as a paste, and wrapped in wafers. The paper described the results in 22 cases of esophageal stenosis, 14 of them due to cancer of the esophagus. The importance of the right anterior oblique diameter for the examination of the esophagus was emphasized. Holzknecht was the originator of the art of fluoroscopy for which the Viennese School became so famous.

Bismuth salts were not without danger and quite expensive. It was therefore of practical importance that in 1910, Bachem and Günther,[4] a pharmacologist and an internist, replaced them by the much safer and less expensive barium sulfate which since has remained the standard contrast medium for the gastrointestinal tract.

A great technical step forward was the introduction of "spot" films by my teacher, Hans Heinrich Berg[7,8] in 1923. His technique made it possible to interpose a cassette rapidly between patient and screen while shifting almost instantaneously from fluoroscopy to roentgenography. These spot films represented a much truer facsimile of the optimal fluoroscopic image than the haphazard roentgenograms that had been obtained before.

In the early 1950's, a new era was opened by the introduction of the screen intensifier. With it came the first practical cineroentgenographic studies of the esophagus. Some cine-studies had been done as far back as 1912,[26] but not before the era of the screen intensifier were good moving pictures of the esophagus obtained, with ease and with minimal exposure to the patient. Cinefluororoentgenography finally permitted to study at leisure of what, since Cannon's and Holzknecht's time, generations of older radiologists had laboriously observed during fluoroscopy.

In the last decade, great strides have been made in manometric measurements of the act of deglutition. The development of the cinefluororoentgenography has made it possible to combine such pressure observations with simultaneous roentgenologic barium studies of the esophagus.

What clinical significance did the various phases of these technical developments have? Was the improvement in technique paralleled by increasing knowledge?

The earlier examiners of the esophagus had studied metallic foreign bodies and obstruction due to cancer and corrosive strictures. They had filled Zenker's diverticula. They demonstrated displacement of the esophagus and narrowing by mediastinal tumors and by aneurysms. They studied the dilatation of the esophagus caused by cardiospasm.

By the time I started my training in radiology in the mid twenties, isolated cases of benign tumors of the esophagus and a few isolated cases of congenital strictures had been seen roentgenologically. There seemed to be little new to be expected from further roentgenologic investigation of this simple cylindric, anatomically and physiologically rather uninteresting structure.

How erroneous this turned out to be! The progress made in roentgenology of the esophagus in the intervening four decades is remarkable. The interest in this organ instead of decreasing appears to have grown constantly, as is indicated by the large number of papers and textbooks which continue to appear about it. There are several reasons for this. The roentgenologic methods have improved. New physiologic modalities in the study of the esophagus have been developed. Finally, and most importantly, the advances in surgery have

tremendously added to our knowledge of the chest and its organs and have, at the same time, increased the demand for more roentgenologic information.

One of the instances in which roentgenologic information preceded surgical applicability is the roentgen demonstration of esophageal varices. In 1928, Günther Wolf,[45] a young assistant in internal medicine in one of the municipal hospitals of Berlin, published 2 cases in which he had demonstrated esophageal varices fluoroscopically and roentgenographically. Three years later, I showed the roentgenologic appearance of varices in the stomach.[32] In 1933, based on a material of 45 cases, the roentgen morphology of varices and the clinical significance of their demonstration were discussed in detail.[33] It is astonishing that it took more than a decade before many clinicians recognized the help derived from the demonstration of varices in the diagnosis of portal hypertension, in the study of a bleeding patient and in the differential diagnosis of splenomegaly. Due to technical progress, the recognition of early varices has slightly improved in the intervening decades. More recently cinefluororadiography offers advantages in doubtful cases.[1,14]

Even now, the diagnosis is frequently not easy. This is due to several factors, one of which is inadequate coating of the esophageal wall, another is changing degree of filling of varices under certain conditions. Varices may disappear completely in upright position. They may do so even in horizontal position, during contraction of the esophagus (Fig. 1, *A* and *B*) and during certain phases of respiration. The influence of projection is another factor. The esophagus may appear normal in one direction and show varices in another due to the fact that varices may be "polarized," that is, they may be serpentine in one plane only (Fig. 2, *A* and *B*). The roentgen demonstration of varices is a classic example of the fact that roentgenology, especially roentgenology of the gastrointestinal tract, is not just "taking pictures." Even with the most modern equipment, one may not see the lesion unless the optimal conditions have been created by the knowledgeable, determined and indefatigable examiner.

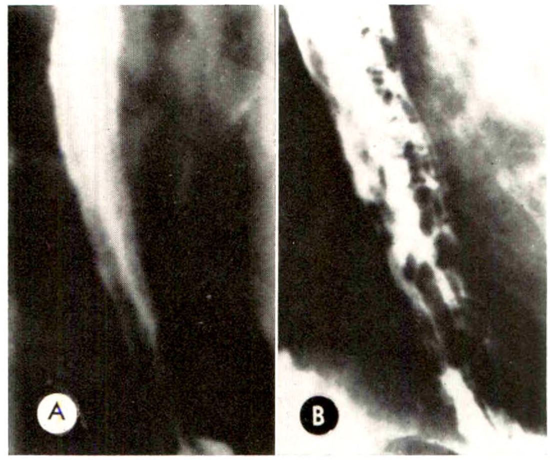


Fig. 1. Varices of the esophagus disappearing during contraction of the esophagus. (*A*) Contracting phase. (*B*) Resting phase. (Courtesy of *Archives of Surgery*, 1940, *41*, 1084–1100.[32])

Our understanding of esophageal diverticula has greatly increased during the period which we are discussing, mainly due to concepts introduced by Fleischner. In repeated publications, especially one in 1932,[20] Fleischner attacked the old division of pulsion and traction diverticula of the esophagus, as well as the more recently added category of functional diverticula.

Fleischner proved convincingly that, if one omits the Zenker's diverticula at the junction of hypopharynx and esophagus and perhaps a few rare congenital diverticula of the esophagus proper, all diverticula are produced by localized adherence of the esophagus to its surroundings. The shape and size of the diverticula depend on the length and shape of the adherence, but at least as much also on the secondary wall changes and on the pressure within the esophagus during the contraction. In other words, all these diverticula are really adhesion diverticula. They may be visible only during the contraction of the esophagus (Fig. 3, *A*, *B* and *C*), as are the so-called functional diverticula of Bársony, or may be visible at all times if there is extensive

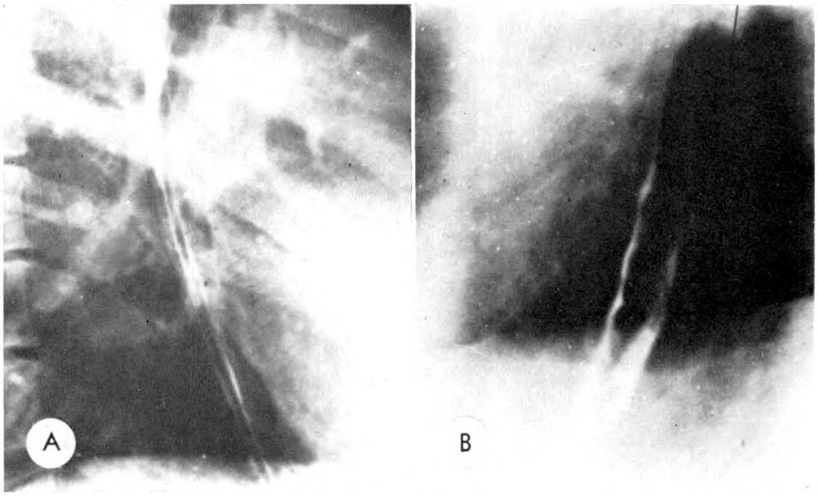


FIG. 2. Influence of projection on demonstrability of varicose vein which undulates in one plane only. The dilated vein is not visible in the right anterior oblique (*A*), but is clearly visible in the left anterior oblique view (*B*). (Courtesy of *Archives of Surgery*, 1940, *41*, 1084–1100.[32])

scarring with loss of tissue in the immediate neighborhood of the esophagus. The significance which this mechanism has on our concept of spasm and other so-called functional abnormalities of the esophagus will be discussed later.

When I started in radiology, inflammatory processes of the esophagus, except for those caused by acid and lye burns, appeared to be of negligible practical significance. In 1935, Winkelstein[42] reported inflammatory changes in the lower esophagus produced by reflux of gastric juice. Some of his patients also had peptic ulcers of the duodenum or the stomach. Winkelstein coined the name of "peptic esophagitis" for this lesion. Allison, Johnstone and Royce[2] in the 1940s recognized the importance of hiatus hernia in the etiology of esophagitis (Fig. 4, *A* and *B*). In 1950, Barrett[5] showed that a sheet of atypical gastric mucosa in some of these cases may extend high up into the esophagus (columnar-lined esophagus) (Fig. 5, *A* and *B*). The importance of hiatus hernia in this whole complex became more and more obvious. Jutras *et al.*[25] and Wolf *et al.*[43] demonstrated the significance of subtle

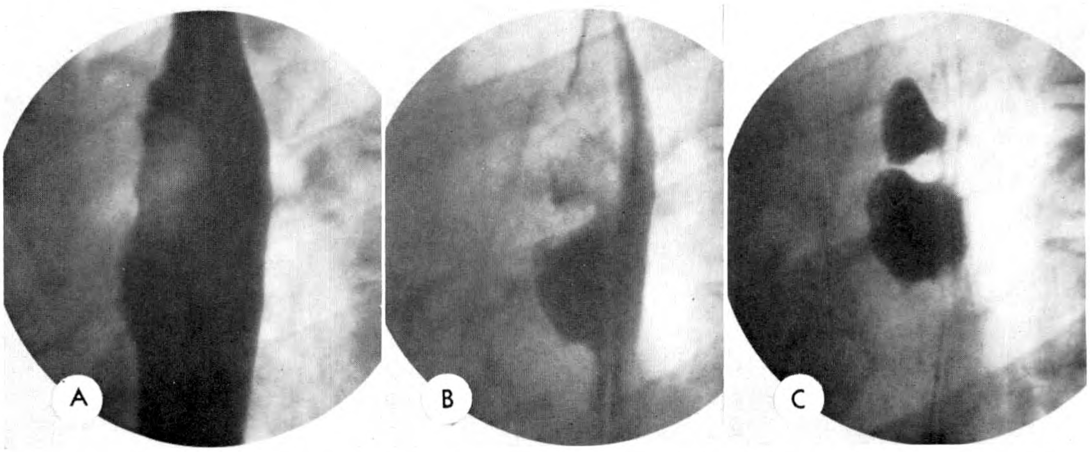


FIG. 3. (*A*, *B* and *C*) Two small adhesion diverticula visible only during the contraction phase of the esophagus. (Courtesy of *Acta radiologica*, Supplement 18, 1933, p. 58.[33])

changes in distensibility close to the herniated cardia as evidence of esophagitis (Fig. 6, *A* and *B*). They may be easily missed but can be the cause of repeated episodes of dysphagia. Whenever the bolus is too big for this particular area, dysphagia will result. The older literature described many patients who suddenly became unable to swallow. Either esophagoscopy or just simple retching relieved the patient, who then was able to swallow normally. Roentgenologic follow-up examinations showed no abnormality. The diagnosis of a functional anomaly, spasm of the esophagus, appeared to be the only explanation. One probably can say safely that the majority of these patients did not have spasm but had organic narrowing which had escaped the examiners. It is quite likely that these patients had either an area of scarring from esophagitis or had a lower esophageal ring. Both these lesions may be easily missed unless they are specifically looked for.

In 1947, I saw a dentist who complained of episodes of dysphagia which occurred only when he ate solid food in a great hurry. The only abnormality noticeable was a thin in-folding in the lower esophagus. I was not certain that this was the actual cause of the symptoms until about 3 months later when

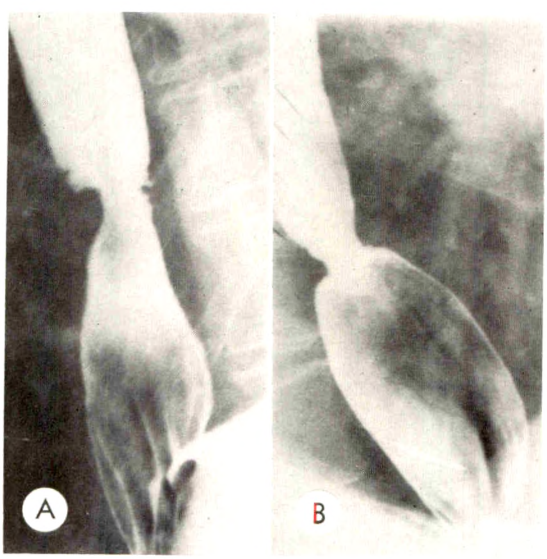


Fig. 4. (*A* and *B*) Two cases of esophagitis above small hiatus hernia.

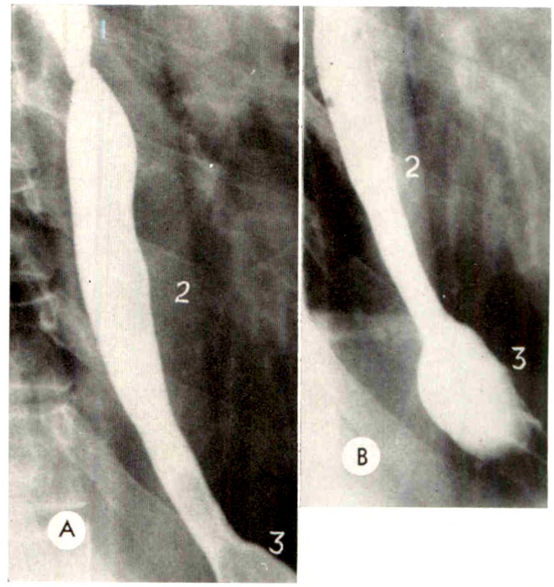


Fig. 5. (*A* and *B*) Columnar-lined esophagus with stricture at the junction of columnar and squamous epithelium close to the arch of the aorta. As usual, the upper stricture caused the patient's dysphagia. 1—Squamous lined esophagus; 2—columnar lined esophagus; 3—herniated portion of the stomach.

I saw a similar diaphragm-like narrowing in another patient with episodical dysphagia (Fig. 7, *A* and *B*). The impression that this was a heretofore unrecognized cause of dysphagia was confirmed in the following years. The first descriptions of this clinical entity appeared in 2 papers from Boston in 1953.[22,34] The lesion was called the lower esophageal ring. In 1944, Templeton[38] had shown a similar but asymptomatic narrowing in the lower esophagus. Were the two diaphragm-like structures the same entity with symptoms occurring when the opening became narrower? This assumption appeared likely and was confirmed in follow-up studies (Fig. 8, *A* and *B*).[35] The symptomatic lower esophageal ring is not rare. When properly looked for (Fig. 9, *A* and *B*), it has proved to be the most common cause of episodic dysphagia.

At least as important as the clinical significance of the ring, however, was the fact that the ring was found by most authors to be located at the junction of esophageal and gastric mucosa (Fig. 10, *A* and *B*; and 11, *A* and *B*). When present, this roent-

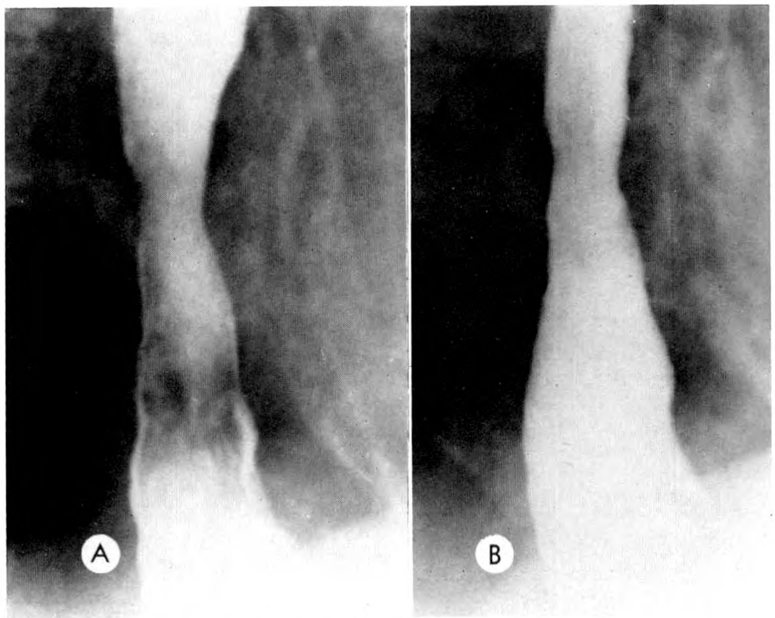


Fig. 6. (*A* and *B*) Esophagitis above small hiatus hernia. The esophagus appeared normal until the area of rigidity was demonstrated when the esophagus was filled and distended as much as possible.

genologically very distinct entity represents a landmark, actually the first definite one in this long and still disputed region of the gastrointestinal tract. More about this a little later.

Progress solves problems, and progress creates problems. Anyone who has tried to satisfy an inquiring child knows this only too well. I shall select a few of the many unsolved problems of the esophagus, some of which have been frequently discussed in the recent past.

Two of these are very basic and they are somewhat connected with each other: (1) where does the esophagus end and where does the stomach start, and (2) what forms the closing mechanism at the upper end of the stomach?

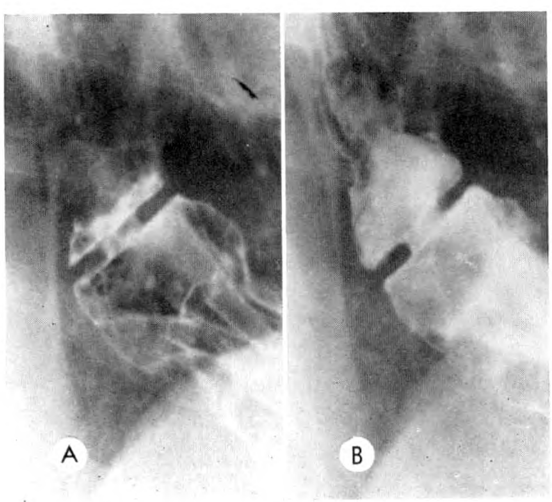


Fig. 7. (*A* and *B*) Lower esophageal ring with many years of episodical dysphagia (see also Figure 10 and 11). (Courtesy of *New England J. Med.*, 1958, *259*, 1–8.[27])

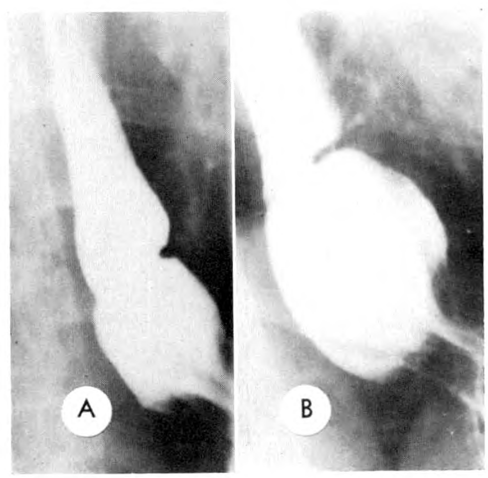


Fig. 8. Lower esophageal ring, measuring 19 mm., asymptomatic in 1954, (*A*). The patient developed frequent episodes of dysphagia in 1960. These persisted in 1962 when the ring measured 15 mm. (*B*).

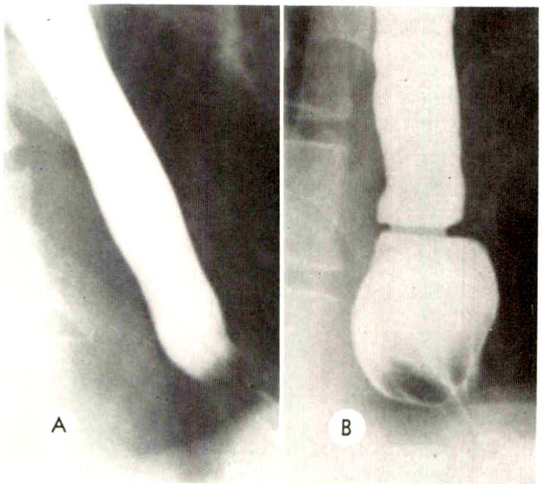

Fig. 9. (*A*) Symptomatic 15 mm. lower esophageal ring visible only after maximal distention produced by compression of the epigastrium with a pressure pad. (*B*) Without this distention the patient's dysphagia would have remained unexplained.

If a person takes a deep breath after having swallowed barium, the barium is held up, or an already existing barium column is cut off, near the diaphragm (Fig. 12, *A* and *B*).

Actually, the cutoff is not at the level of the visible diaphragm but slightly higher.

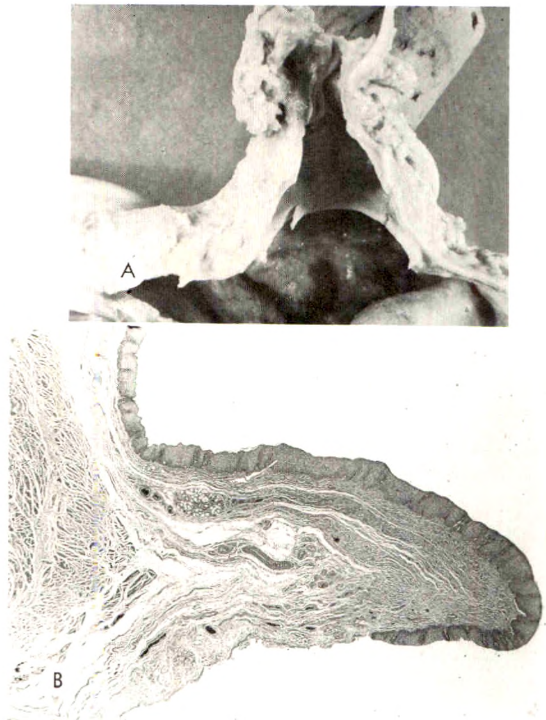

Fig. 11. (*A* and *B*) Autopsy specimen of the same ring as in Figure 7 and 10. The esophageal mucosa extends just beyond the free edge of the ring. (Courtesy of *New England J. Med.*, 1958, *259*, 1–8.[27])

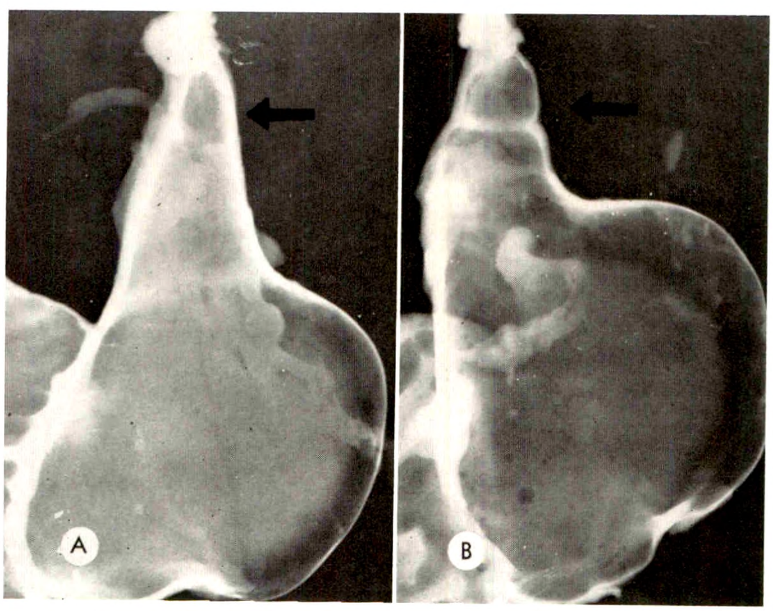

Fig. 10. (*A*) Autopsy specimen with lower esophageal ring, visible only after the stomach and esophagus are sufficiently blown up with air (*B*). The specimen also shows status following subtotal gastric resection for cancer. (See also Figure 7 and 11 of the same patient. Courtesy of *New England J. Med.*, 1958, *259*, 1–8.[27])

This is not, as was thought in the past, caused by any purely roentgenologic projection phenomenon. The right crus, that is, the muscular sling which almost completely surrounds the esophagus at the hiatus, actually lies slightly higher than the surrounding portion of the diaphragm. Monges[29] and Botha[10] proved this by attaching clips to the edges of the hiatus (Fig. 13, *A* and *B*). During surgery, I have actually felt the crus protruding above the level of the adjacent diaphragm. This protruding portion of the diaphragm is not visible roentgenographically, since it is apparently not in immediate contact with the air containing lung.

During the inspiratory arrest of the flow of barium, an empty space lies between the obvious esophagus and the obvious stomach. In expiration, there is a funnel-shaped tube connecting the two (Fig. 12 *B*). Pressure studies have confirmed that this segment lies in the abdomen, partially in the oblique hiatal canal.[17,19]

Much—and rather useless—discussion has taken place regarding the proper name for this segment. Is it part of the esophagus, namely, the abdominal esophagus, or part of the stomach, or should it be given a special name like abdominal gullet, junctional zone, submerged segment, empty segment, cardia etc.? I personally feel that, anatomically and physiologically, it best be considered part of the stomach. For discussion's sake, I shall accept the descriptive term of "empty segment." What relationship does this segment have to the mucosal junction of esophagus and stomach?

During the last 15 years, we have been told that the position of this mucosal junc-

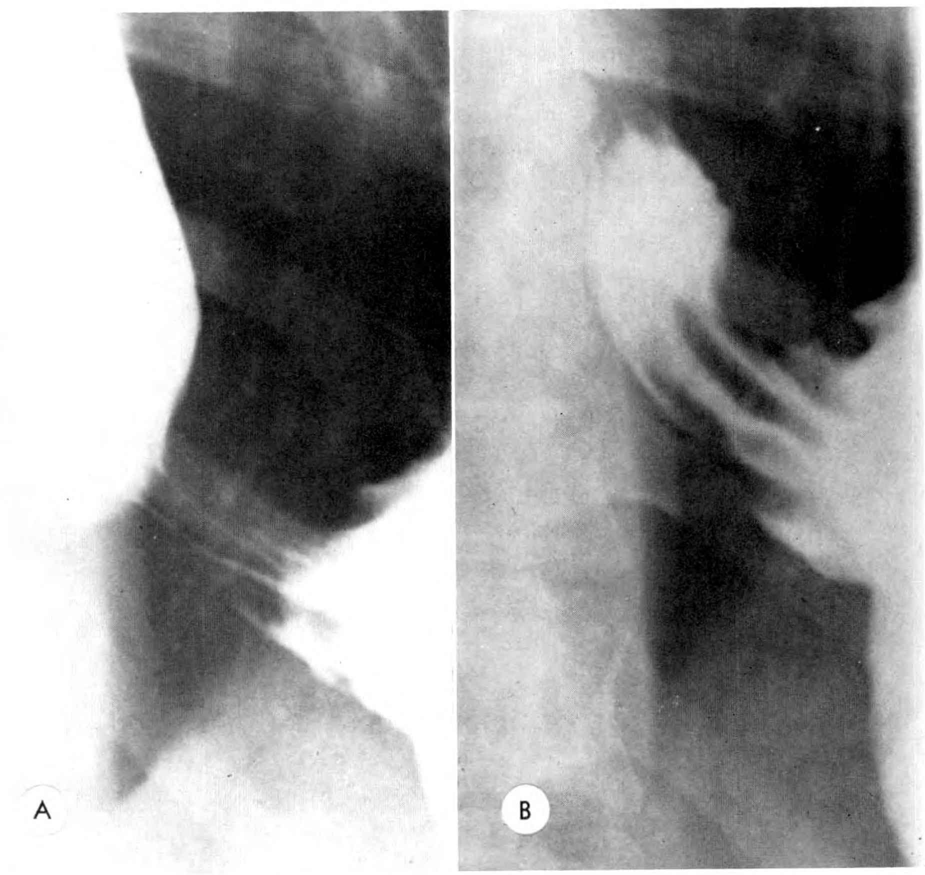


Fig. 12. Esophagogastric junction. (*A*) Inspiration; (*B*) expiration. Note the empty segment during inspiration. The level of the hiatus is at the upper edge of this empty segment.

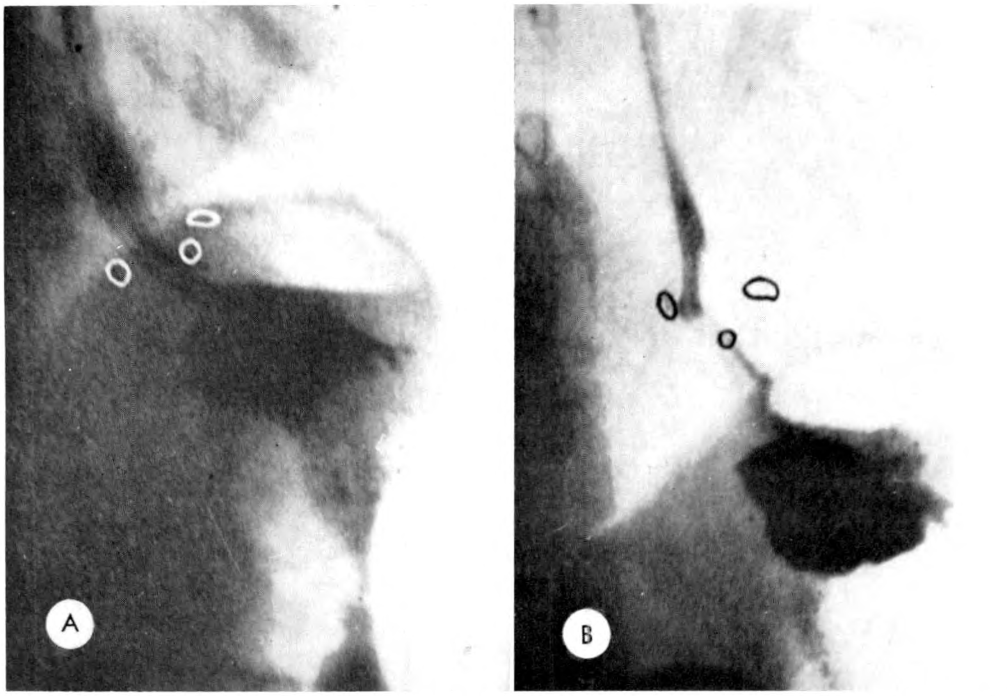

Fig. 13. Position of the hiatus in (*A*) expiration and (*B*) inspiration. Circles indicate clips which have been placed at the hiatus during surgery. (Courtesy of H. Monges, *Gastroenterologia*, 1956, *82*, 232–241, and of S. Karger, Basel/New York.[29])

tion is extremely variable in a normal person. It has become almost fashionable to emphasize its protean location. It is supposed to vary considerably in its position from person to person, and even in a given person it is thought to move up and down with respiration, swallowing, belching and vomiting.

In practice, things are probably not quite that vague and hopeless. In 1953, Palmer[30] demonstrated roentgenologically marked mobility of the esophagogastric mucosal junction after having identified the junction by endoscopically placed metallic clips. Actually, Palmer's illustrations show the clips consistently in the region of the "empty segment." In the light of newer knowledge of the roentgenologic position of the hiatus, it appears at least as likely that his pictures were caused by opening and closing of the "empty segment," resulting in apparent rather than actual motion of the clips. Recent investigators (Creamer *et al.*;[19] Cohen and Wolf[17]) place the mucosal junction during quiet breathing fairly consistently within the empty segment; some of them place it close to its upper end, that is, at the hiatus, others slightly lower down. Of course, islands of gastric mucosa may occur almost anywhere in the esophagus, and in an occasional but rather exceptional case, even a full sheet of atypical gastric mucosa may extend upwards into the esophagus and produce the so-called columnar-lined esophagus of Barrett.[5] In most instances, however, the junction appears to lie somewhere within the empty segment, probably close to the hiatus. Should further investigations confirm the rather constant relationship of the mucosal junction and the hiatal canal in the average normal person—and I believe such confirmation is still needed—then the location of the mucosal junction as it is found in a given person becomes quite important, *e.g.*, when it is found above the diaphragm.

The importance which the lower esophageal ring has as a landmark for this whole

problem is quite obvious. It is the opinion of most, although not all, observers that the ring lies at the esophagogastric mucosal junction. The ring is always found above the diaphragm. Demonstration of a ring, therefore, means that the gastrointestinal tube has been displaced upwards.

Many other questions concerning the ring remain unanswered. What causes the ring to be formed? Various theories have been set forth in the literature. They do not conform to the known facts about the ring. I believe that the formation of the ring is in some way connected with the upward displacement of the intestinal tube, in other words, with the herniation. But why then is a ring present in some and not all hernias? Why is heartburn less common in patients with a ring then in patients with a hernia without a ring? Why is it so rare to see obvious roentgenologic evidence of esophagitis in patients with a ring in contrast to the frequency of esophagitis in hernias without a ring? Does the ring act as a protecting mechanism against reflux? It is difficult to believe that it can. Problems persist.

A closing mechanism at the upper end of the stomach must exist not only for the athlete who hangs upside down from his trapeze but for all of us, particularly if we stoop over. The anatomists of the 17th and 18th centuries found a muscular sphincter at the junction of the esophagus and stomach which appeared to be a satisfactory closing mechanism.

Unfortunately, most modern anatomists cannot find a true sphincteric muscle in man, and much discussion has taken place about a possible closing mechanism. Of the groups particularly interested in this subject, I mention those centered around Ingelfinger (Boston), Code (Mayo Clinic), Wolf (New York), Creamer (London), Barborka (Chicago) and Zaino (New York).

Various mechanisms may play a role:

1. An internal, physiologic sphincter at

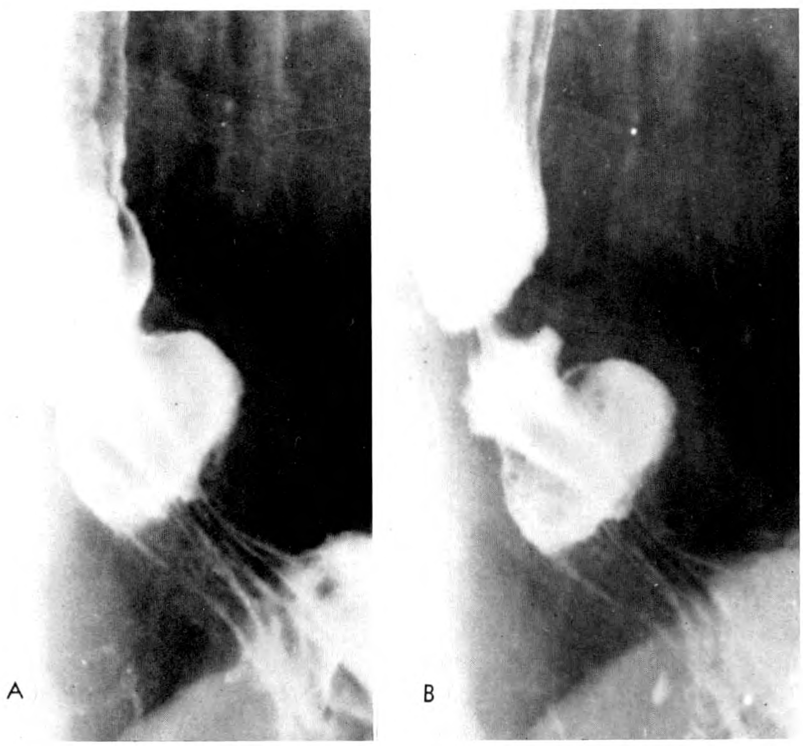


Fig. 14. (*A* and *B*) Small hiatus hernia with sphincteric mechanism at the junction of esophagus and herniated stomach.

the junction of esophagus and stomach. For many years, radiologists have demonstrated such a sphincter, visible only when portions of the stomach are herniated above the diaphragm (Fig. 14, *A* and *B*), but presumably also present, although not demonstrable, when it is in its normal position in the hiatus. Manometric studies have abundantly confirmed the existence of such a functional internal sphincter.[15,17,23,40]

2. A pinch-cock effect of the diaphragm.

3. A flap valve produced by the acute angle between esophagus and the greater curvature of the stomach.

4. A rosette formed by the puckering of the mucosa at the junction of esophagus and stomach.

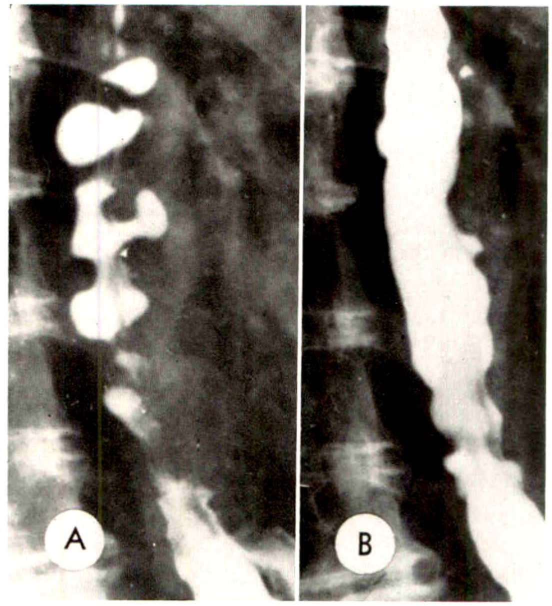


Fig. 16. (*A* and *B*) Grotesque curling.

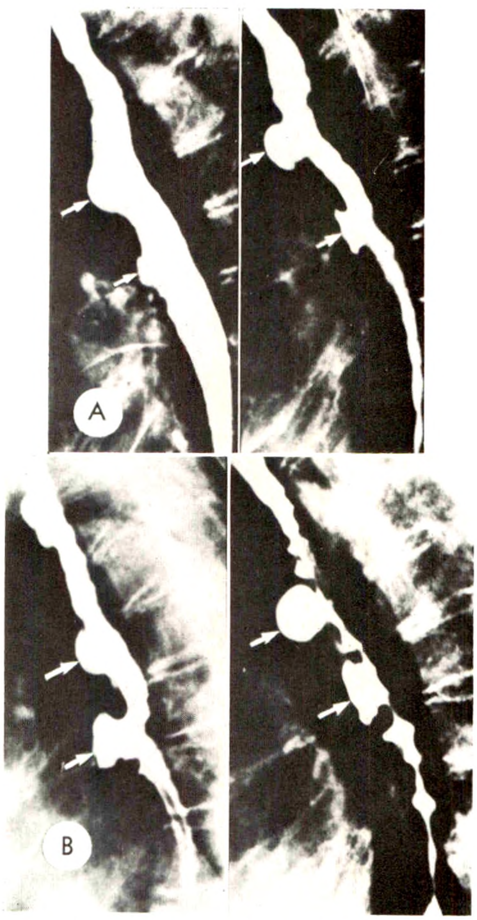


Fig. 15. (*A* and *B*) Extensive curling. Note the areas fixed by adhesions resulting in characteristic adhesion diverticula (arrows). (Courtesy of *Acta radiologica*, Supplement, 18, 1933, p. 68.[33])

5. A closure of the "empty segment" which collapses as it is pushed towards the hiatus by the abdominothoracic gradient.

An analysis of the various mechanisms shows that they all have flaws. It appears likely that an interaction of several factors produces the reflux barrier. Creamer *et al.*[19] propose such a combined action involving the above described mechanisms 1 and 5. They suggest that the walls of the collapsed "empty segment," the "gullet," *i.e.*, the segment between the hiatus and the obvious gastric bag, are held in tight approximation by action of the internal sphincter, and thus produce the reflux barrier. Mann *et al.*[28] suggest a combination of mechanism 1 and 4, the internal sphincter being in their opinion the most important factor.

Actually, in spite of many interesting theories, we still are not certain why the trapeze artist is safe in the upside-down position.

A peculiar phenomenon, or rather a group of phenomena, occurs at times in the middle and/or distal thirds of the esophagus. The result is a variety of bizarre deformities of the esophagus for which many descriptive terms have been created (Fig. 15, *A* and *B*; and 16, *A* and *B*). Functional diver-

ticula, pseudodiverticula, tiered spasm of the esophagus, corkscrew esophagus, rosary esophagus, diffuse spasm of the esophagus and tertiary contractions are some of them. I personally have to plead guilty for having introduced two commonly used words for this phenomenon, the German "Kräuselung"[33] and its rather poor translation into the English language, namely, "curling." For further discussion, I shall use the word "curling" as a descriptive word for all these phenomena.

Common to all phenomena is the fact that they occur during the phase of contraction. An "empty" swallow after a preceding swallow of barium frequently shows the deformity best. The contraction of the whole area seems to occur simultaneously, often changing the shape of the esophagus with lightening speed. The roentgenologic appearance varies considerably from case to case but is more or less repetitious in a given case.

More than 30 years ago, I felt that local abnormalities similar to those described by Fleischner in adhesion diverticula were responsible for these peculiar phenomena.[33] Many papers have since been published by observers throughout the world, and their unanimous opinion is in favor of some form of neuromuscular imbalance and against our theory of local change.[11,15,18,23,38] Some of the authors have assumed a reflux mechanism secondary to other abnormalities such as esophagitis, hiatus hernia, diverticula, duodenal or gastric ulcers, and even cholecystitis, hepatitis and psychosomatic disturbance.

If in the face of this ever-growing literature, I still believe that local anatomic changes are greatly responsible, I am not merely stubborn. Although, at first sight a neuromotor origin of the phenomenon is a very tempting explanation, there is actually very little to support such a theory. Depression of the phenomenon by drugs like atropin[37,39] is no proof of neurologic origin. These drugs simply relax the esophagus and prevent it from contracting properly, and contraction is necessary to bring out the phenomenon.

On the other hand, there are a number of observations which make the presence of local changes likely:

1. Curling is frequently seen in patients who have other obvious areas of esophageal adhesions (Fig. 15, *A* and *B*).

2. Almost any patient who shows curling once will show it again, although not always with each swallow.

3. The larger projections in a given case of curling re-occur at the same level. It is more difficult to ascertain whether the small "teeth" present in curling of old people always occur at the same level.

4. It is impossible to explain simply by contraction the extremely bizarre appearance of the esophagus in some of these patients, *e.g.*, with corkscrew esophagus. Contraction in the presence of local abnormalities, however, could well explain these findings (Fig. 16, *A* and *B*).

5. In 2 instances, I have seen curling occur locally in the area in which an intramural, extramucosal tumor of the esophagus had been shelled out surgically (Fig. 17, *A* and *B;* and 18).

6. I have seen curling develop in a patient after extensive radiation therapy for mediastinal metastases from cancer of the breast. Curling was particularly marked in the area where the compression of the esophagus by the tumor had been present (Fig. 19, *A*, *B* and *C*).

All these reasons speak strongly in favor of local changes. Some of these changes are adhesions. In addition, there are probably localized areas in the wall of the esophagus which are damaged and weakened, as Fleischner has shown to be present in some adhesion diverticula. A combination of inability of the esophagus to contract properly due to some external adherence and "blow outs" caused in the weakened areas during the moment of contraction appears to me to be a likely explanation of the phenomenon.

There are, however, some observations

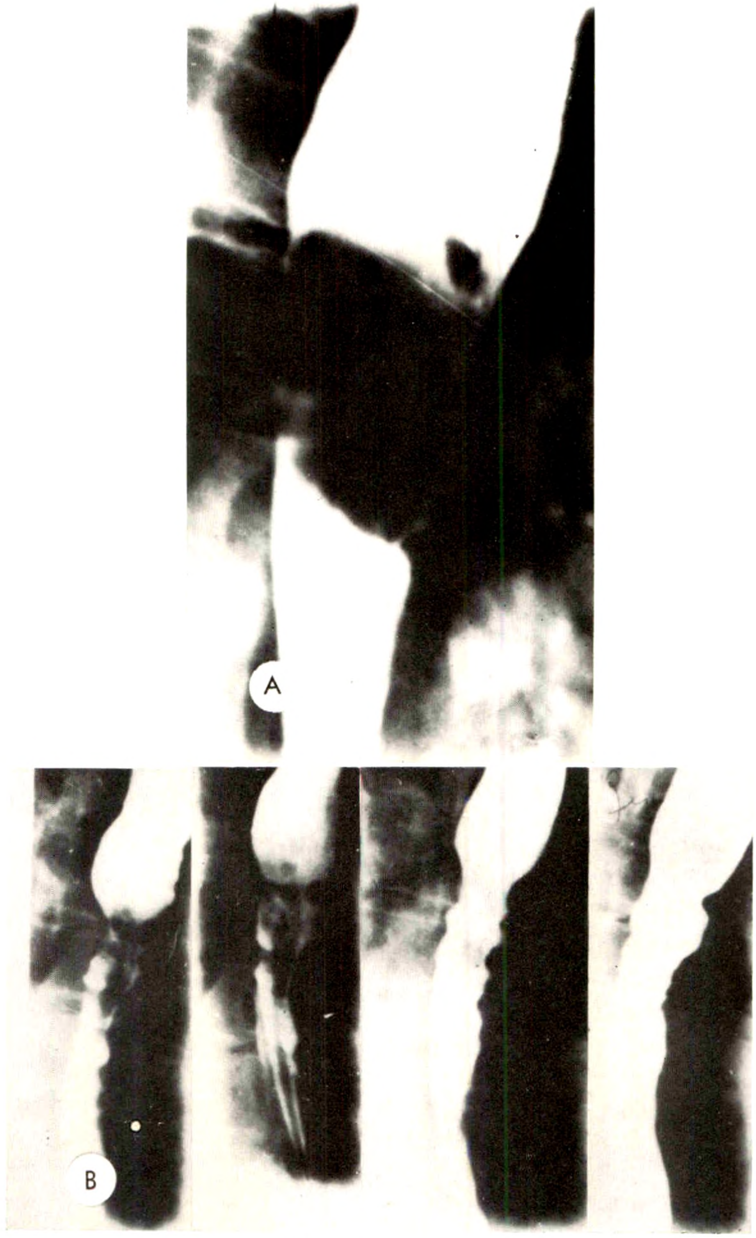


Fig. 17. Localized curling following removal of leiomyoma of the esophagus. (*A*) Preoperative roentgenogram; (*B*) postoperative studies showing curling confined to the area of surgery.

which are difficult to fit into such an explanation:

1. These changes should be present when the esophagus is collapsed. Although this is usually the case, it is not always so. Possibly, this can by explained by the fact that during the resting stage the pressure within the esophagus is not high enough to produce the phenomenon.

2. Zboralske, Amberg and Soergel[47] in their discussion on presbyesophagus, the esophagus of the aged, have reported that curling almost routinely occurs in people above the age of 90. It is hardly possible to

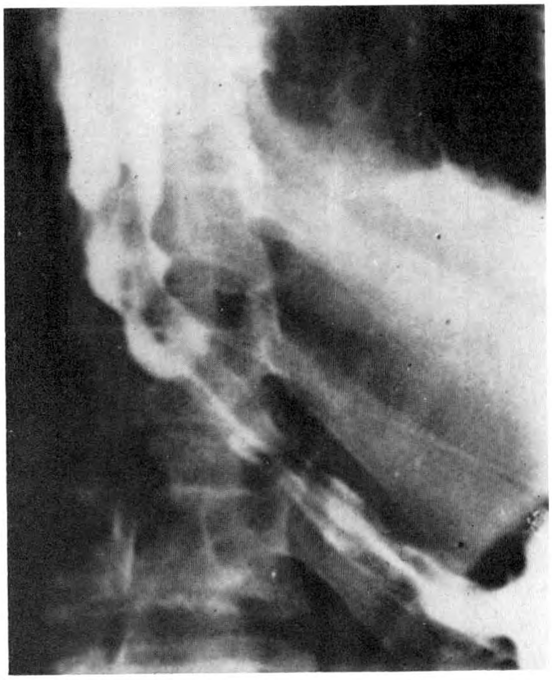

Fig. 18. Localized curling occurring after an intramural bronchogenic cyst of the esophagus had been removed from the same area.

assume that at this age all people have mediastinal scarring and localized weakened areas in the wall of the esophagus. Perhaps the appearance of the esophagus in these old people, particularly the common "small-teeth-curling," is caused by a different mechanism.

3. Finally, anatomic proof for our postulated origin of curling is missing. The fact, however, that some autopsy studies in the literature and some of our own have not shown the predicted changes does not

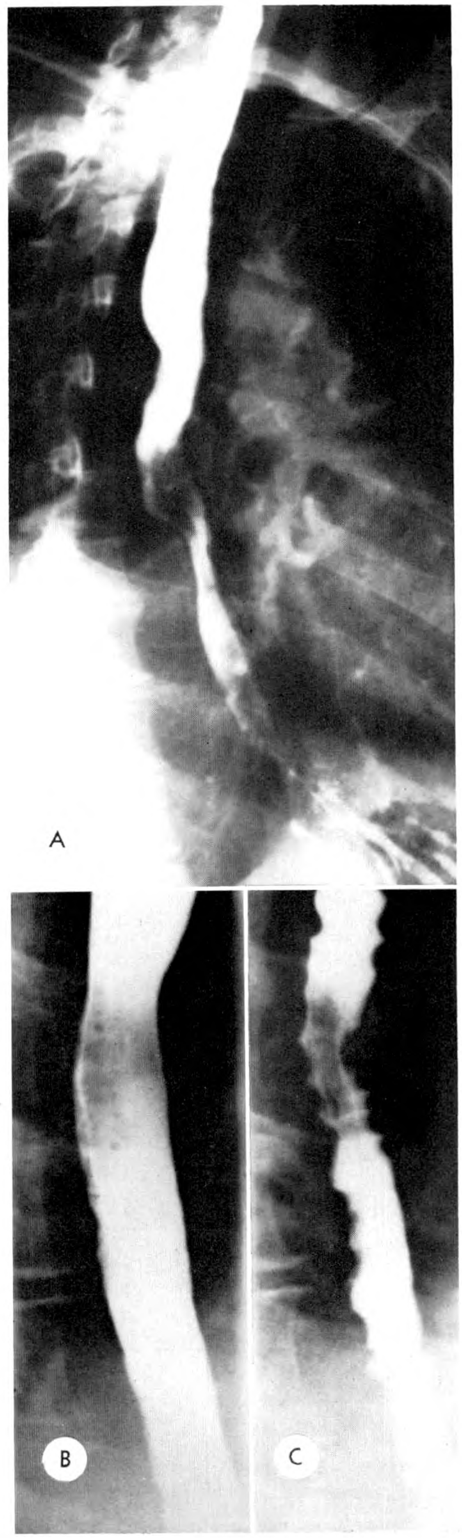


Fig. 19. Localized curling following radiation therapy for mediastinal metastasis from cancer of the breast. (*A*) Compression and probable involvement of the wall of the esophagus by tumor. (*B*) The same area after regression of the tumor following irradiation. (*C*) Curling during contraction localized to this area.

necessarily speak against this theory. Too little is known about the normal relationship of the esophagus to its surroundings, and it is possible that more accurate and more detailed studies may show the very minor changes which we presume to be present.

Does curling cause symptoms? Numerous articles in the literature state that it causes dysphagia and pain in some patients and that the incidence of symptoms increases with the more grotesque forms. Some authors even claim that these marked deformities are always associated with symptoms. Some of our patients had difficulty in swallowing. Was this due to curling? An outside examiner thought so in one patient who had been having episodes of dysphagia for a year (Fig. 20 through 22, inclusive). Nothing abnormal except curling had been found. At first nothing else was seen in our examination. A barium capsule, however, was held up low in the esophagus below the area of curling. More intense attempts to distend the lower esophagus finally succeeded in demonstrating a short segment of obvious narrowing apparently due to esophagitis. Only then was a small hiatus hernia recognized immediately below the narrowed segment. More careful analysis of the patient's history showed that a year ago, she had had a gastric intubation following abdominal surgery. The dysphagia was caused by fibrotic esophagitis, not by curling.

In my own experience, I have been able to demonstrate an area of poor distensi-

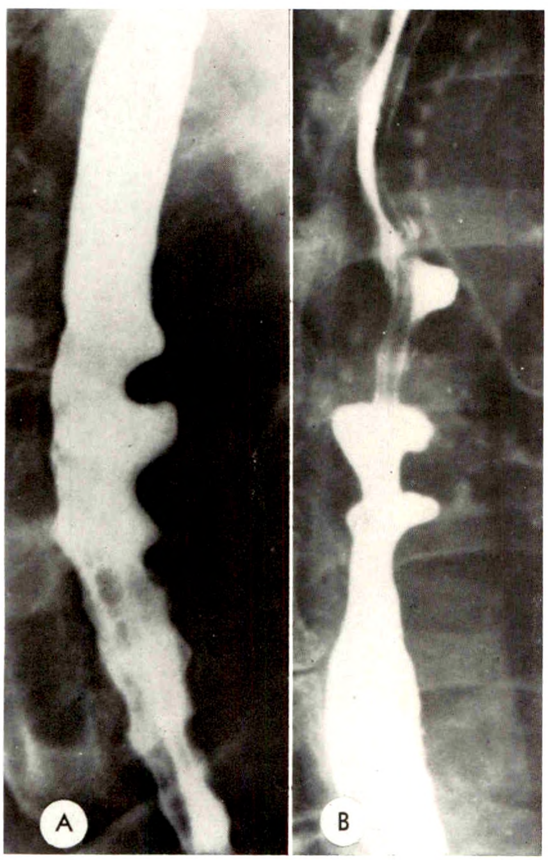


Fig. 20. (*A* and *B*) Extensive curling in a patient with dysphagia (not due to curling).

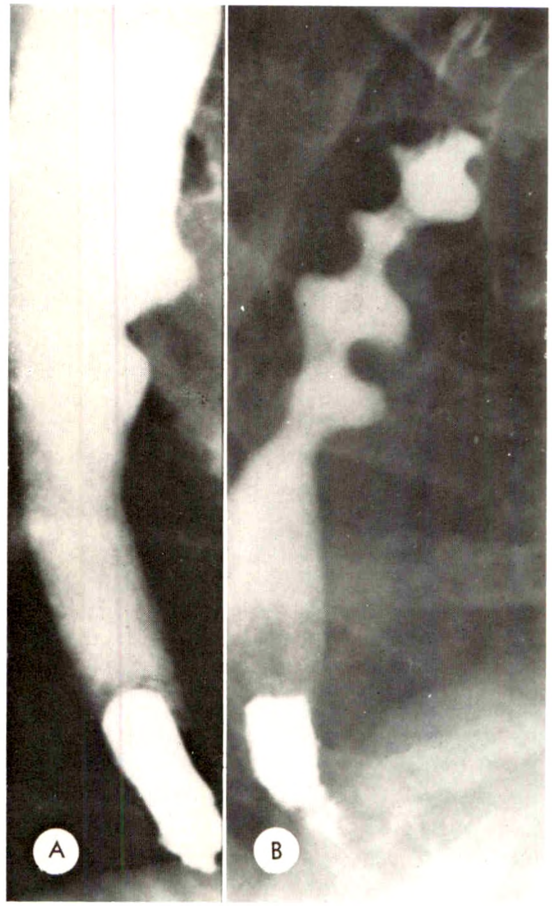


Fig. 21. (*A* and *B*) Same case as in Figure 20. A barium filled capsule is held up below the area of curling and does not pass before it is partially dissolved.

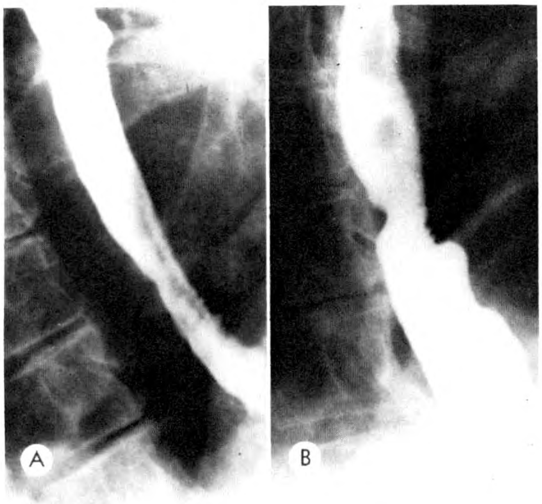


Fig. 22. (*A* and *B*) Same case as in Figure 20 and 21. With proper distention of the distal esophagus, a slightly irregular area of esophagitis with loss of distensibility above a small hiatus hernia is seen. The rigid area of esophagitis rather than the curling explains the patient's dysphagia.

bility in all patients who had curling combined with dysphagia (Fig. 23, *A*, *B* and *C*). The dysphagia in these patients is not due to a mysterious spasm, nor is it due to poor propulsion following uncoordinated contractions. It is simply due to insufficient distensibility of a segment distal to the area of curling. This narrowing is usually caused by esophagitis although this has not been proved in all cases. Occasionally, it may be due to other areas of stenosis as, for instance, a lower esophageal ring. Characteristically, these areas of narrowing may be difficult to demonstrate and will therefore very easily escape the attention of the examiner, particularly since he is fascinated by the curling above.

The coexistence of areas of constriction in the distal end of the esophagus with extensive curling is more frequent than could be explained by chance. Is it possible that when obstruction occurs, the esophagus contracts more vigorously and perhaps differently, resulting in striking degrees of curling when adhesions and/or wall weakness are present? This would explain a number of facts:

1. The frequency of marked curling in cases with narrowing below.

2. The spurts of excessive contraction in

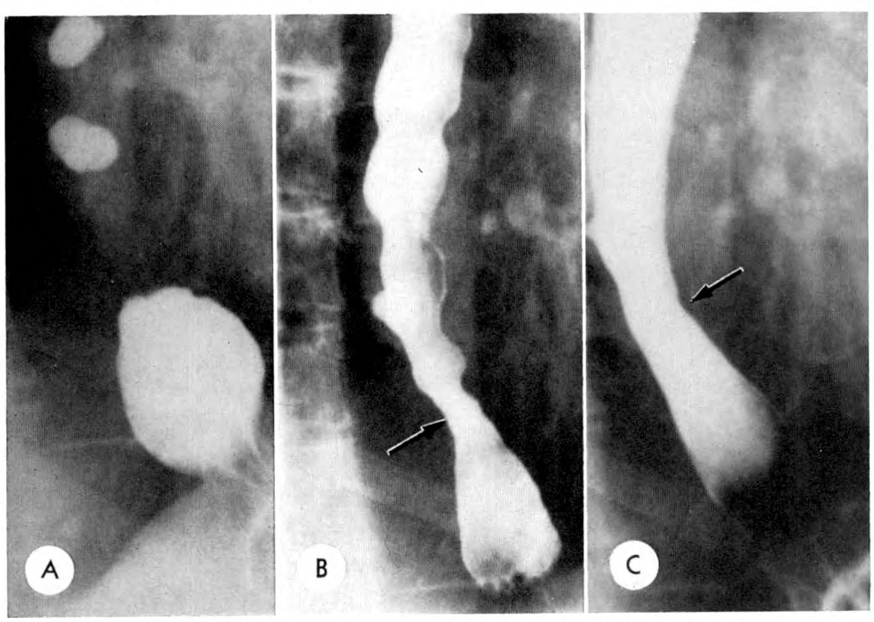


Fig. 23. (*A*, *B* and *C*) Marked curling in a patient with episodes of moderate dysphagia. With proper distention, an area of narrowing probably due to esophagitis is seen in the esophagus (arrow) comparable to the area of esophagitis in Figure 6, *A* and *B*. A barium tablet was held up at this level, indicating that the narrowed rigid area and not the curling caused the dysphagia.

some of these cases as shown manometrically.

3. Hypertrophy of the esophageal wall which has been found by some observers (Johnstone,[24] Barrett[5]). It could be explained on the basis of frequent hypercontraction proximal to areas of narrowing.

I have not been impressed by frequent coexistence of curling and retrosternal pain. In the exceptional case, the pain seemed coincidental rather than causatively connected. Other authors have been more impressed by such a connection, especially in the more extensive deformities like corkscrew esophagus, tiered spasm or diffuse spasm. Code and his co-workers[15] are convinced, as are others, that abnormally forceful contraction of the esophagus is painful.

I do not believe that curling produces the pain. An abnormally strong contraction may cause pain and produce curling in those esophagi which have wall changes as discussed before. A search for an area of diminished distensibility below the region of curling seems indicated in all of these cases.

I frankly admit that much of this is still controversial, and further progress is needed. I can see two approaches which may be helpful: (1) a combination of an interested radiologist, gastroenterologist, thoracic surgeon and pathologist and (2) careful combined cinefluororoentgenographic and manometric studies as they have been started in several institutions.

In the few decades of its existance, roentgenology of the esophagus has accomplished much. It has become the most important method in the diagnosis of its diseases and has given invaluable help in the examination of those organs and structures which are in its neighborhood.

Progress has been made, but many problems remain. Their solution requires the intelligent, painstaking and persistent approach of the examiner and investigator, at least as much as the improvement in technical equipment. For the young radiologist, the comforting thought remains: Much more is to be known than is known.

1180 Beacon Street
Brookline 46, Massachusetts

REFERENCES

1. Adler, D. C., Haverback, B. J., and Meyers, H. I. Cineradiography of esophageal varices. *J.A.M.A.*, 1964, *189*, 77–80.
2. Allison, P. R., Johnstone, A. S., and Royce, G. B. Short esophagus with simple peptic ulceration. *J. Thoracic Surg.*, 1943, *12*, 432–457.
3. Atkinson, M. Mechanisms protecting against gastro-oesophageal reflux: a review. *Gut*, 1962, *3*, 1–15.
4. Bachem, C., and Günther, H. Bariumsulfat als schattenbildendes Kontrastmittel bei Röntgenuntersuchungen. *Zeitschr. f. Röntgenkunde*, 1910, *12*, 369–376.
5. Barrett, N. R. Lower esophagus lined by columnar epithelium. *Surgery*, 1957, *41*, 881–894.
6. Becher, W. Zur Anwendung des Röntgen'schen Verfahrens in der Medizin. *Deutsche med. Wchnschr.*, 1896, *22*, 202–203 and 432.
7. Berg, H. H. Über den Nachweis des Zwölffingerdarmgeschwürs mit Röntgenstrahlen. *Klin. Wchnschr.*, 1923, *2*, 675–682.
8. Berg, H. H. Röntgenuntersuchungen am Innenrelief des Verdauungskanals. Georg Thieme, Leipzig, 1930, pp. 198.
9. Boas, I., and Levy-Dorn, M. Zur Diagnostik von Magen- und Darmkrankheiten mittels Röntgenstrahlen. *Deutsche med. Wchnschr.*, 1898, *24*, 18–19.
10. Botha, G. S. M. Radiological localisation of diaphragmatic hiatus. *Lancet*, 1957, *1*, 662–664.
11. Bromhart, M. Clinical Radiology of the Oesophagus. Translated by S. Kenny. John Wright & Sons, Ltd., Bristol, 1961, pp. 383.
12. Brown, P. American Martyrs to Science through the Roentgen Rays. Charles C Thomas, Springfield, Ill., 1936, pp. 276.
13. Cannon, W. B. Notebook on experiments performed in 1896 and 1897. Harvard Medical Library, Boston, Mass.
14. Ciarfaglini, R., and Iannacone, G. Dynamische Veränderungen des varicösen Oesophagus. *Fortschr. a. d. Geb. d. Röntgenstrahlen u. d. Nuklearmedizin*, 1958, *89*, 551–557.
15. Code, C. F., Creamer, B., Schlegel, J. F., Olsen, A. M., Donoghue, F. E., and Andersen, H. A. An Atlas of Esophageal Motility in Health and Disease. Charles C Thomas, Publisher, Springfield, Ill., 1958, pp. 134.

16. Code, C. F., Kelley, M. L., Jr., Schlegel, J. F., and Olsen, A. M. Detection of hiatal hernia during esophageal motility tests. *Gastroenterology*, 1962, *43*, 521–531.
17. Cohen, B. R., and Wolf, B. S. Roentgen localization of physiologically determined esophageal hiatus. *Gastroenterology*, 1962, *43*, 43–50.
18. Creamer, B., Donoghue, F. E., and Code, C. F. Pattern of esophageal motility in diffuse spasm. *Gastroenterology*, 1958, *34*, 782–796.
19. Creamer, B., Harrison, G. K., and Pierce, J. W. Further observations on gastro-oesophageal junction. *Thorax*, 1959, *14*, 132–137.
20. Fleischner, F. Die Divertikel der Speiseröhre. Haft- oder Adhäsionsdivertikel. *Fortschr. a. d. Geb. d. Röntgenstrahlen*, 1932, *45*, 627–664.
21. Holzknecht, G. Zur Diagnose der Oesophagusstenose. *Deutsche med. Wchnschr.*, 1900, 573–576.
22. Ingelfinger, F. J., and Kramer, P. Dysphagia produced by contractile ring in lower esophagus. *Gastroenterology*, 1953, *23*, 419–430.
23. Ingelfinger, F. J. Esophageal motility. *Physiol. Rev.*, 1958, *38*, 533–584.
24. Johnstone, A. S. Diffuse spasm and diffuse muscle hypertrophy of lower oesophagus. *Brit. J. Radiol.*, 1960, *33*, 723–735.
25. Jutras, A., Levrier, P., and Longtin, M. Étude radiologique de l'oesophage paradiaphragmatique et du cardia. *J. de radiol. et d'électrol.*, 1949, *30*, 373–414.
26. Kraus, F. Über die Bewegungen der Speiseröhre unter normalen und pathologischen Verhältnissen (auf Grund röntgenkinematographischen Untersuchungen). *Deutsche med. Wchnschr.*, 1912, *38*, 393–395.
27. MacMahon, H. E., Schatzki, R., and Gary, J. E. Pathology of lower esophageal ring: report of case with autopsy, observed for nine years. *New England J. Med.*, 1958, *259*, 1–8.
28. Mann, C. V., Greenwood, R. V., and Ellis, F. H. Esophagogastric junction. *Surg., Gynec. & Obst.*, 1964, *118*, 853–862.
29. Monges, H. Considérations sur le rôle du diaphragm dans la physiologie de la continence gastro-ésophagienne et sur la projection radiologique de l'hiatus ésophagien. *Gastroenterologia*, 1956, *82*, 232–241.
30. Palmer, E. D. Attempt to localize normal esophagogastric junction. *Radiology*, 1953, *60*, 825–831.
31. Rumpel, T. Die klinische Diagnose der spindelförmigen Speiseröhrenerweiterung. *Münch. med. Wchnschr.*, 1897, *44*, 383–386.
32. Schatzki, R. Die Röntgendiagnose der Oesophagus- und Magenvarizen und ihre Bedeutung für die Klinik. *Fortschr. a. d. Geb. d. Röntgenstrahlen*, 1931, *44*, 28–39. Also: Roentgen demonstration of esophageal varices; its clinical importance. *Arch. Surg.*, 1940, *41*, 1084–1100.
33. Schatzki, R. Reliefstudien an der normalen und krankhaft veränderten Speiseröhre. *Acta radiol.*, 1933, Suppl. 18, pp. 149.
34. Schatzki, R., and Gary, J. E. Dysphagia due to diaphragm-like localized narrowing in lower esophagus ("lower esophageal ring"). Am. J. Roentgenol., Rad. Therapy & Nuclear Med., 1953, *70*, 911–922.
35. Schatzki, R. Lower esophageal ring; long term follow-up of symptomatic and asymptomatic rings. Am. J. Roentgenol., Rad. Therapy & Nuclear Med., 1963, *90*, 805–810.
36. Schmidt, C. D., Jones, H. D., Hunt, J. C., Code, C. F., Anderson, M. W., and Andersen, H. A. Value of esophageal motility test in evaluation of thoracic pain problems. *Dis. Chest*, 1962, *41*, 303–314.
37. Sheinmel, A., Privíteri, C. A., and Poppel, M. D. Study of effect of certain drugs on curling of esophagus; preliminary report. Am. J. Roentgenol. & Rad. Therapy, 1949, *62*, 807–813.
38. Templeton, F. E. X-Ray Examination of the Stomach: A Description of the Roentgenologic Anatomy, Physiology and Pathology of the Esophagus, Stomach and Duodenum. University of Chicago Press, Chicago, 1944.
39. Teschendorf, W. Die Röntgenuntersuchung der Speiseröhre. *Ergebn. d. med. Strahlenforsch.*, 1928, *3*, 175–288.
40. Vantrappen, G., Liemer, M. D., Ikeya, J., Texter, E. C., Jr., and Barborka, C. J. Simultaneous fluorocinematography and intraluminal pressure measurements in study of esophageal motility. *Gastroenterology*, 1958, *35*, 592–602.
41. Vantrappen, G., Texter, E. C., Jr., Barborka, C. J., and Vanderbroucke, J. Closing mechanism at gastroesophageal junction. *Am. J. Med.*, 1960, *28*, 564–577.
42. Winkelstein, A. Peptic esophagitis; new clinical entity. *J.A.M.A.*, 1935, *104*, 906–909.
43. Wolf, B. S., Marshak, R. H., and Som, M. L. Peptic esophagitis and peptic ulceration of esophagus. Am. J. Roentgenol., Rad. Therapy & Nuclear Med., 1958, *79*, 741–759.
44. Wolf, B. S. Roentgen features of normal and herniated esophagogastric region; problems in terminology. *Am. J. Digest. Dis.*, 1960, *5*, 751–769.
45. Wolf, G. Die Erkennung von Ösophagus-Varizen im Röntgenbild. *Fortschr. a. d. Geb. d. Röntgenstrahlen.*, 1928, *37*, 890–893.
46. Zaino, C., Poppel, M. H., Jacobson, H. G., and Lepow, H. The Lower Esophageal Vestibular Complex. Charles C Thomas, Publisher, Springfield, Ill., 1963, 1–272.
47. Zboralske, F. F., Amberg, J. R., and Soergel, K. H. Presbyesophagus: cineradiographic manifestations. *Radiology*, 1964, *82*, 463–467.

# HABENULAR CALCIFICATION AS AN AID IN THE DIAGNOSIS OF INTRACRANIAL LESIONS*

*By* DONALD L. McRAE, M.D.
MONTREAL, QUEBEC

IN THE investigation of intracranial lesions, ordinary skull roentgenograms are apt to be neglected for several reasons: (a) Plain roentgenograms of the skull are sometimes not done as carefully as they might be, therefore the yield of information from them is disappointing; (b) the impression that pineal measurements are so variable that they are hardly worth doing; (c) angiograms or air studies will be made and will overshadow anything that might be revealed on ordinary skull roentgenograms; and (d) external isotope localization and ultrasonic echograms are being more widely used.

Skull roentgenography is a valuable, nonoperative method of examining the brain and the skull which may reveal information not given by any other method of examination. It should never be omitted in the investigation of intracranial lesions. It should be done with precision and the roentgenograms inspected with care. Measurements of the calcified pineal or calcified habenular commissure or both should always be carried out.

There is some uncertainty about pineal measurements. The pineal gland calcifies irregularly so that it is difficult to find its center, the point from which measurements should be made. Vastine and Kinney[6] did not exactly state how their measurements were made. Their original measurements were modified by Dyke[1] by moving the anterior limit forward. This was probably due to the inclusion of some habenular calcifications. Dyke's modification resulted in a rather large spread of the normal limits. Fray's[2] proportional method and his cranio-angle method seemed to offer greater accuracy but never became popular.

The habenular commissure region is calcified almost as often as the pineal gland. Its shape identifies it uniquely, unlike the shape of the pineal gland. Its apex can be marked accurately. It varies somewhat less in position than does the pineal gland. Stauffer *et al.*[5] and also Smith[4] showed that habenular commissure calcification is found mostly in neuroglial nodules on the ventricular surface of the commissure. Therefore, it can be termed habenular calcification rather than habenular commissure calcification. On many air studies, the calcified nodules can be seen projecting within the air shadow of the posterior part of the 3rd ventricle. Habenular calcification usually appears on lateral skull roentgenograms as a C-shaped calcification open posteriorly, a variable distance anterior to the pineal calcification (Fig. 1). When the patient has an infra-pineal recess in his 3rd ventricle, the C outlines the small projection into the 3rd ventricle between the supra-pineal and infra-pineal recesses. The habenular calcification has a transverse diameter of approximately 4 mm.; therefore, the more closely the central ray of the roentgen-ray beam passes along this diameter, the better the chance of showing it. When stereo lateral roentgenograms of the skull are made, the first roentgenogram is usually made with the central ray of the roentgen-ray beam 1 inch above and 1 inch anterior to the external auditory canal and the second roentgenogram is made with the tube shifted towards the top of the head, 10 per cent of the focal-film distance. The central ray is then about on the same transverse plane as the habenular commissure. It is not uncommon to see a classic habenular calcification on the shift roentgenogram but only a small blob on the true lateral roentgenogram (Fig. 2, *A* and *B*) of a stereo

* Presented at the Sixty-fifth Annual Meeting of the American Roentgen Ray Society, Minneapolis, Minnesota, September 29–October 2, 1964.
From the Montreal Neurological Institute, Montreal, Quebec, Canada.

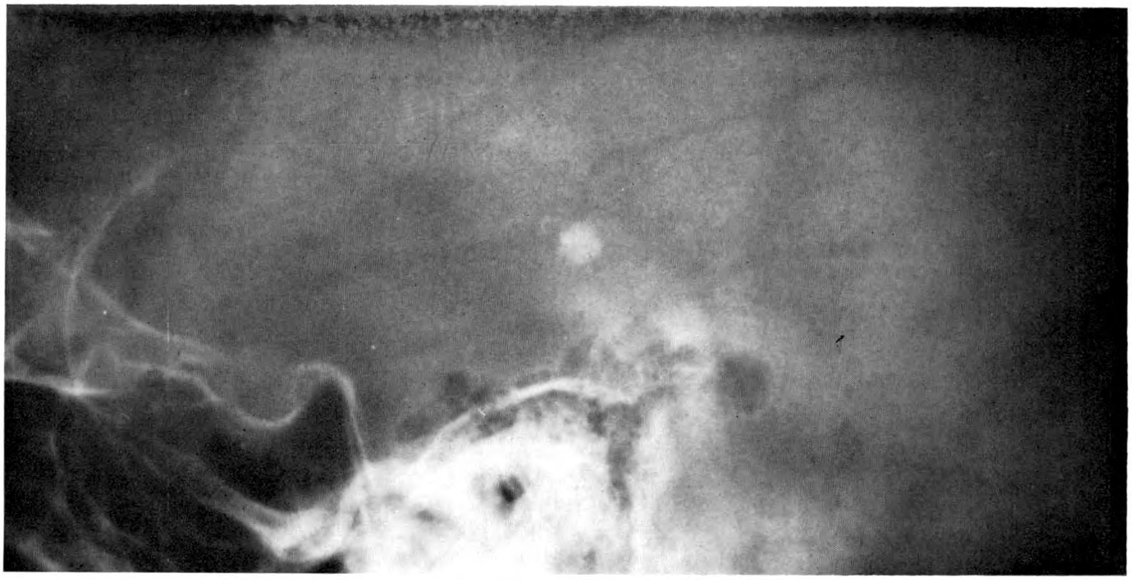

Fig. 1. Habenular calcification and pineal calcification on the lateral skull roentgenogram.

pair. Sometimes, we see habenular calcification only on the shift roentgenogram (Fig. 3, *A* and *B*) of a stereo pair. Occasionally, we see habenular calcification without pineal calcification. Sometimes we see only the upper or lower arm of the C (Fig. 4, *A* and *B*).

For best visualization of intracranial calcification, the density of the roentgenograms should be such that the calcification is in a medium gray area. The roentgenogram must have good contrast. Dense high contrast skull studies are more informative for nearly all purposes than normally exposed films, but often must be viewed in a high intensity illuminator.

The habenular calcification is sometimes visible on anteroposterior roentgenograms even when the pineal gland is not calcified (Fig. 5 *A*). It is necessary to make roentgenograms with the central ray parallel to the long axis of the habenular calcification. The axis of the arms of the habenular calcification is usually parallel to the long axis of the pineal. For best visualization of either or both the pineal and habenular calcification, the angle between their long axes and the Frankfurter horizontal is measured on lateral skull roentgenograms (Fig. 6) and anteroposterior roentgenograms are made with the central ray at that angle. The best average angle is approximately 20°. This projection is termed Ruggles' projection or fronto-occipital projection, 20°. On frontal roentgenograms it is even more necessary to have high density high contrast films since in the Ruggles projection often the pineal-habenular calcification is projected over the shadow of the occipital protuberance.

To establish measurements of the habenular commissure, 100 consecutive sets of skull examinations were chosen. Each set consisted of adult skull roentgenograms showing typical habenular calcification. Each patient had a skull of normal size and also a fairly normal encephalogram. By fairly normal encephalogram is meant one with little or no shift of the midline structures, little or no ventricular asymmetry and ventricles of normal size or only slightly dilated.

The measurement of the anteroposterior diameter of the skull was made in a straight line from the most anterior of the inner table shadows of the frontal bone to the most posterior of the inner table shadows of the supratentorial part of the occipital bone along the line of the habenular calcification. The maximum length was taken. The mea-

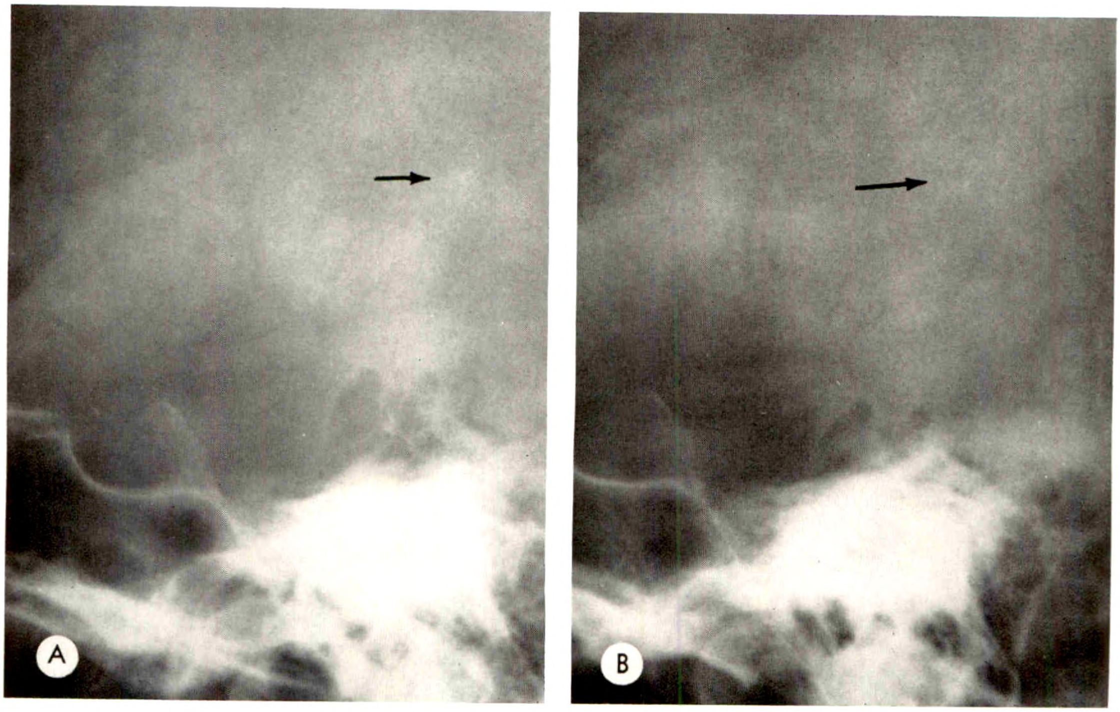


Fig. 2. (*A* and *B*) Stereoscopic lateral skull roentgenograms showing different appearances of the habenular calification.

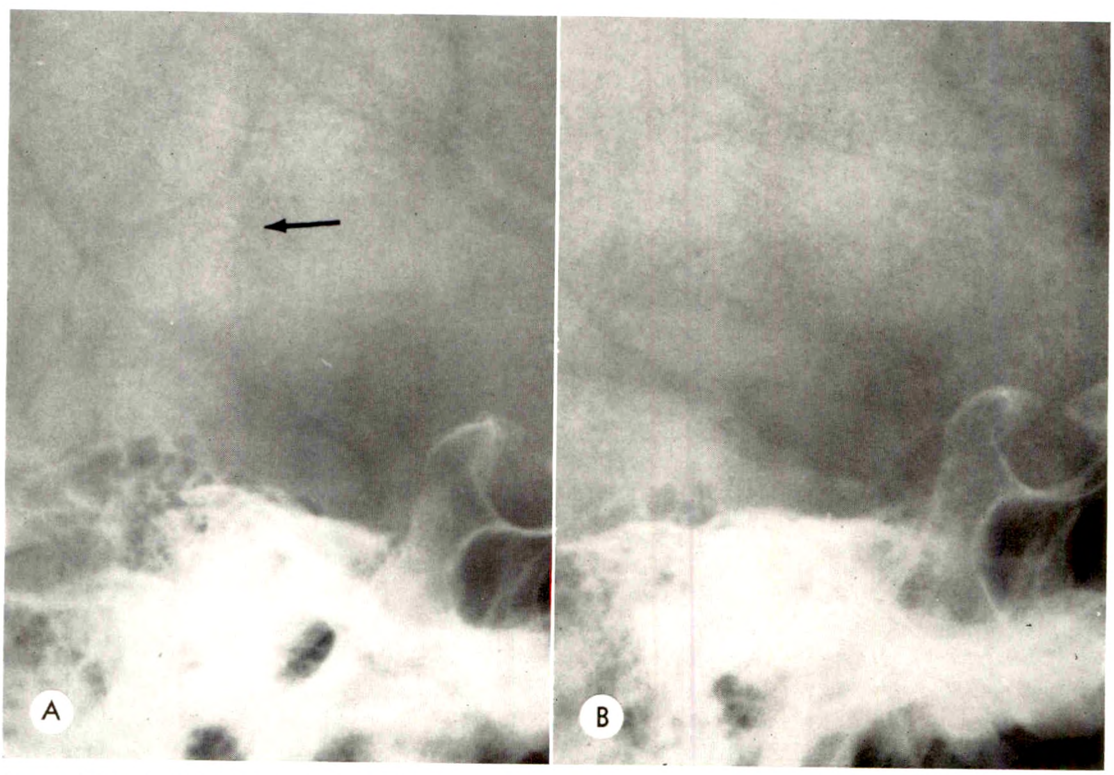


Fig. 3. (*A* and *B*) Stereoscopic lateral skull roentgenograms showing the habenular calcification on only one of the stereo pair.

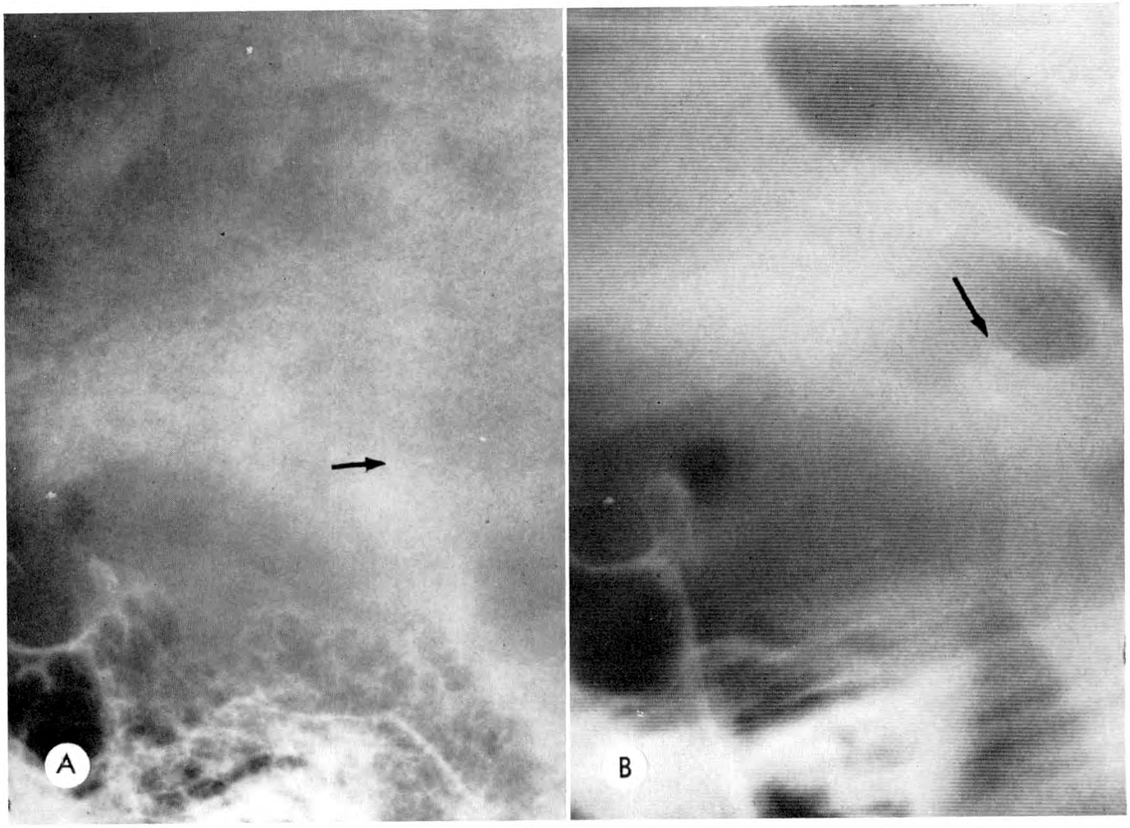


Fig. 4. Linear habenular calcification shown on (*A*) the plain skull roentgenogram and on (*B*) the pneumoencephalogram (autotomogram).

surement from the cranial vault to the foramen magnum was made by taking the lowest of the inner table shadows of the vault of the skull at the vertex and dropping a straight line through the habenular calcification to the foramen magnum line, the line joining its anterior and posterior margins. The measurements from the inner table of the frontal bone to the habenular and from the vault to the habenular were made from the same points on the skull to the apex of the C-shaped habenular calcification. Charts showing the results of the 100 measurements are shown in Figures 7 and 8. It will be noted that the spread of habenular calcifications in an anteroposterior direction is 24 mm. This spread could be decreased to 18 mm. with the loss of only 3 patients. These 3 would then all show false positive anterior displacements. This would still give approximately 95 per cent confidence in a measurement of a habenular commissure in an anteroposterior direction. The spread of normal measurements in a vertical direction is 19 mm. This measurement cannot be reduced without loss of a number of normal cases from both the upper and lower edge of the group.

## DISCUSSION

Displacement of intracranial structures by expanding processes varies with the size of the lesion, its situation and its rate of growth. Positive findings are much more valuable than negative findings.

There are some generalities about displacements of the pineal or habenular calcification that are of value.[1,2,3,6] Expanding lesions lateral to the pineal-habenular region produce early and/or great lateral displacement of these structures with little or no forward or backward displacement. Expanding lesions that are situated anteriorly or posteriorly in the supratentorial part of

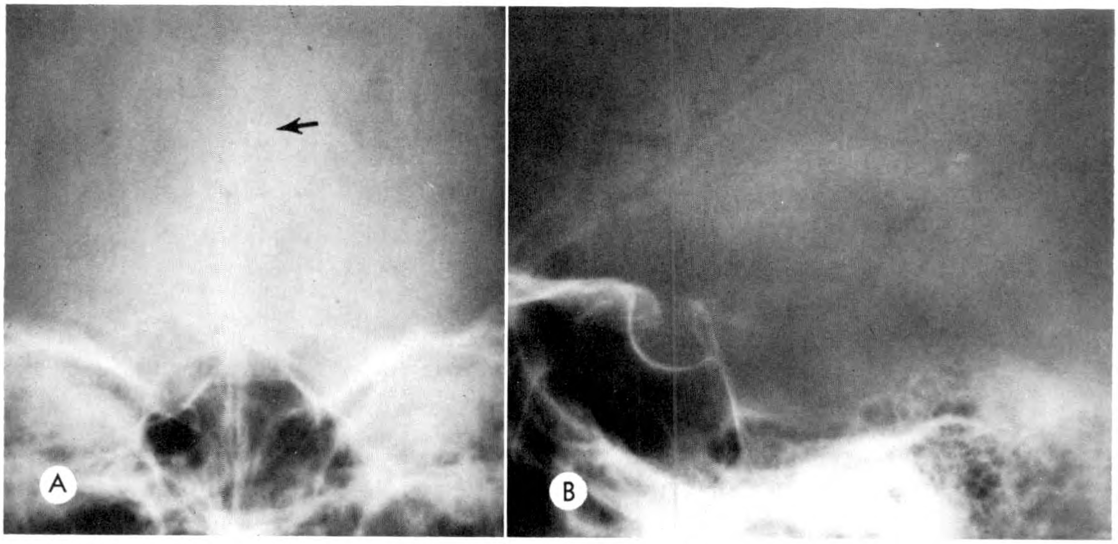


FIG. 5. Habenular calcification without visible pineal calcification shown on both (*A*) frontal and (*B*) lateral skull roentgenograms.

the cranium produce little side to side displacement. They are more apt to produce anterior or posterior displacement. Expanding lesions high in the cranium usually produce downward displacement of the pineal and/or habenular calcification, rarely anterior or posterior displacement. Posterior fossa lesions may produce upward displacement but rarely any anterior or posterior displacement. Sizable supratentorial expanding lesions and also obstructive hydrocephalus of the lateral and 3rd ventricles produce downward displacement of the pineal and habenular calcification, signifying herniation of the brain downwards through the tentorial opening.

No table of measurements will exclude all tumors. In using either pineal measurements or habenular calcification measurements, it is necessary to use some judgment. If the habenular calcification falls outside of the normal limits, then it is very likely displaced. If the habenular calcification is at the anterior, posterior, superior or inferior limits of normal, then displacement should be suspected and further examina-

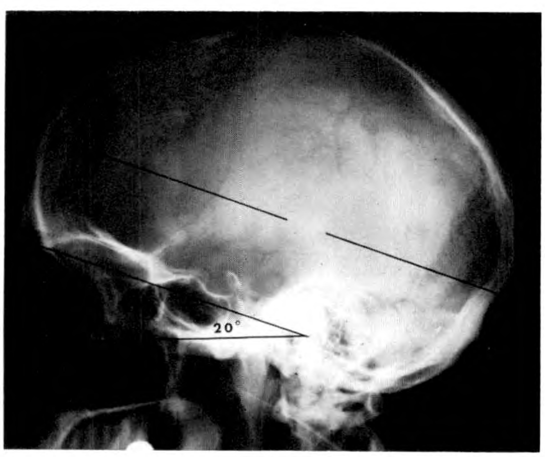


FIG. 6. The average plane of the pineal calcification and habenular calcification.

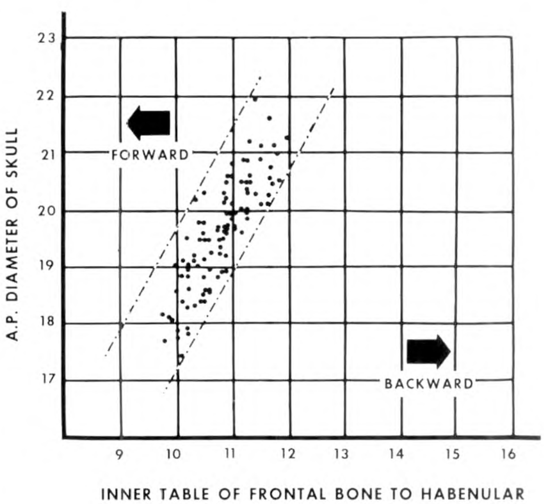


FIG. 7. Chart of the anteroposterior measurements of 100 habenular calcifications in normal patients.

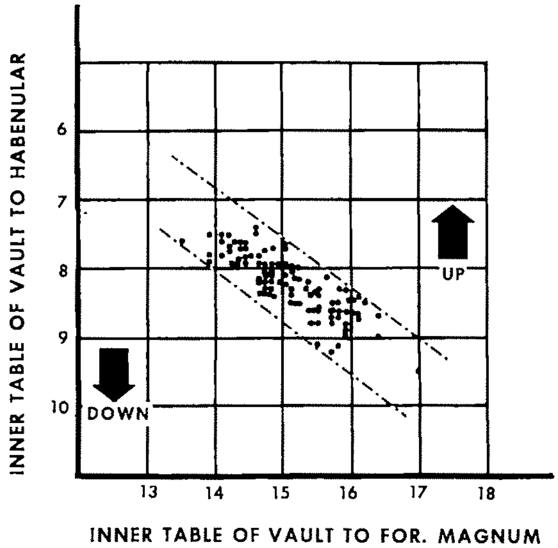


Fig. 8. Chart of vertical measurements of 100 habenular calcifications in normal patients.

tions carried out. If the habenular calcification is in normal position, it does not exclude small tumors, certain medium sized tumors in certain locations or small bilateral expanding lesions.

## SUMMARY AND CONCLUSION

The habenular calcification is uniquely identified by its shape. It varies somewhat less in position than the pineal calcification.

Charts showing the position of the habenular calcification in normal adult skulls have been constructed.

The pineal calcification should be measured by Fray's method or the habenular calcification by the here reported method on all lateral skull roentgenograms.

Montreal Neurological Institute
3801 University Street
Montreal 2, Quebec, Canada

## REFERENCES

1. Dyke, C. G. Indirect signs of brain tumor as noted in routine roentgen examinations: displacement of pineal shadow. Am. J. Roentgenol. & Rad. Therapy, 1930, *23*, 598–606.
2. Fray, W. W. Roentgenological study of pineal orientation: III. Comparison of methods used in pineal orientation. Am. J. Roentgenol. & Rad. Therapy, 1938, *39*, 899–907.
3. Lilja, B. Displacement of calcified pineal body in roentgen pictures as aid in diagnosing intracranial tumors. *Acta radiol.*, 1939, Suppl. 37.
4. Smith, C. G. X-ray appearance and incidence of calcified nodules on habenular commissure. *Radiology*, 1953, *60*, 647–649.
5. Stauffer, H. M., Snow, L. B., and Adams, A. B. Roentgenologic recognition of habenular calcification as distinct from calcification in pineal body: its application in cerebral localization. Am. J. Roentgenol., Rad. Therapy & Nuclear Med., 1953, *70*, 83–92.
6. Vastine, J. H., and Kinney, K. K. Pineal shadow as aid in localization of brain tumors. Am. J. Roentgenol. & Rad. Therapy, 1927, *17*, 320–324.

# THE DILATED CALLOSAL SULCUS SIGN*

*By* HAROLD G. JACOBSON, M.D., ALAN E. ZIMMER, M.D., MANNIE M. SCHECHTER, M.D., *and* JEROME H. SHAPIRO, M.D.
NEW YORK, NEW YORK

IN 1955 SASSAROLI[8] for the first time stressed the importance of the behavior of the callosal sulci over the medial surface of the brain during pneumoencephalography in the presence of obstructing intracranial neoplasms in or near the midline. He reported 4 cases, 3 of which had posterior fossa lesions and 1 an optic nerve glioma. In 2 of the 4 cases with cerebellar tumors, there was no filling of the ventricular system on pneumoencephalography, but the callosal sulci were outlined and dilated. In the remaining 2 cases, the callosal sulci were outlined: in the case with aqueduct stenosis the fourth ventricle filled, and in the other case, with a presumptive diagnosis of optic nerve glioma, an elevated and deformed third ventricle was outlined. In this latter case no ventriculography was performed. In the other 3 cases ventriculography demonstrated the site of obstruction.

In 1958, Schechter, Bull and Carey[9] referred to two new encephalographic signs of pressure hydrocephalus and reported 4 cases. In 3 of the 4 cases, there was no gas in the ventricular system on lumbar encephalography; however, the callosal sulci were outlined and dilated. In a fourth case, a small amount of gas was seen in the fourth ventricle together with dilated callosal sulci. In 1 case there was a cerebellar astrocytoma, in 2 cases aqueduct stenosis, and in a fourth case outlet obstruction of the foramina of the fourth ventricle due to a fibrosing arachnoiditis. In 3 of the 4 cases, the cisterna veli interpositi and ambiens were outlined and dilated. In 1 case the cingulate sulci were grossly enlarged. These authors stressed the importance of recognizing the significance of abnormal dilatation of the sulci of the corpus callosum, the cingulate sulci, and the sulci over the cerebral cortex in obstructing lesions, particularly in the area of the fourth ventricle. They further emphasized that such dilatation did not necessarily indicate brain atrophy. The appearance of the dilated callosal sulci in the frontal views was likened to "rabbit ears" by these authors.

Up to the time of the paper by Schechter *et al.*, other authors[1,2,5,7] had demonstrated examples of the dilated callosal sulcus sign without commenting further on its significance.

Roth,[6] in 1961, reported 6 cases of posterior fossa lesions, in 3 of which there was dilatation of the callosal sulci with no filling of the ventricles. In 1 case the callosal sulci were dilated, as was the cisterna veli interpositi, with only a trace of air in the lateral ventricles. In Roth's fifth case neither the ventricles nor the callosal sulci were outlined, but there was slight dilatation of the cisterna ambiens and veli interpositi. In his sixth case there was good ventricular filling with marked hydrocephalus, but the callosal sulci were dilated and there was encroachment on the cisterna pontis. Roth refers to a "butterfly" pattern which apparently is due to filling of dilated bilateral ambient wings.

The largest series of cases reported to date has been that of Pribram[4] in 1962. He presented a total of 24 cases of which 15 were confirmed as posterior fossa tumors. On pneumoencephalography, ventricular filling was reported to be absent in all cases. In 13 of the 24 cases, the callosal sulci were dilated. The correct diagnosis in this series was made by demonstrating one or more of

* Presented at the Sixty-fifth Annual Meeting of the American Roentgen Ray Society, Minneapolis, Minnesota, September 29–October 2, 1964.
From the Departments of Radiology, Montefiore Hospital, Albert Einstein College of Medicine and St. Vincent's Hospital, New York, New York.

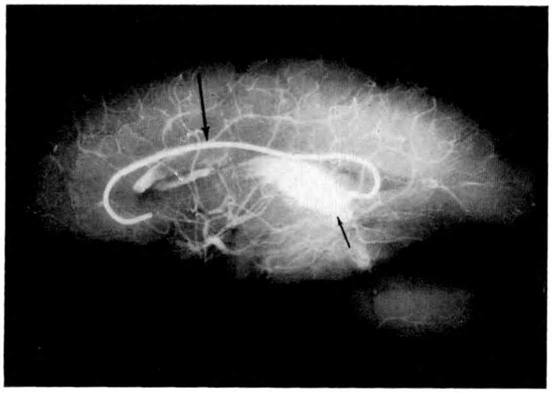

FIG. 1. Roentgenogram of a sagittal section through the brain. The sulcus of the corpus callosum is outlined with solder (large arrow), and the cisterna veli interpositi and a portion of the quadrigeminal cistern (small arrow) are filled with barium paste.

the following findings: hydrocephalus, herniation of the cerebellar tonsils, flattening of the pontine cistern, displacement of the quadrigeminal plate, displacement and dilatation of the vallecula and outlining of the tumor itself.

Pribram stressed the importance of the dilated callosal sulci with failure of ventricular filling in the presence of posterior fossa tumors in the "failed" encephalogram.

## ANATOMY

The pericallosal cistern (Fig. 1) encloses the corpus callosum. This cistern communicates with the cisterna of the lamina terminalis in front, and behind with the cistern of the great vein of Galen and the ambient cistern. Thus, the corpus callosum, in forming the roof of the lateral ventricle, is a true indicator of ventricular dilatation and displacement. The ambient cistern is a twofold cistern, with the cistern proper extending in a fan-wise margin around the brain stem and with the ambient wings lying deep in the fornix. These wings enfold the thalamus and the foramen of Monro in front, cap the pulvinar, and extend forward and medially to the temporal horn, finally ending against the uncus. Each wing communicates with its fellow member above the roof of the third ventricle and below the hippocampal commissure. The membranous roof of the third ventricle is known as the velum interpositum and the potential space above it as the cisterna veli interpositi. On encephalograms, the ambient wings may be seen to curve outward and forward around the thalamus, although they are not commonly visualized. Although Robertson stated that the cisterna veli interpositi is found in all age groups, he attributed no particular significance to its filling. Pribram, on the other hand, felt that when this cistern was distended in the "failed" encephalogram, the presence of a tumor was suggested—an observation previously made by Schechter *et al.* and Roth.

Aside from the aforementioned papers, the importance of dilated callosal sulci in the "failed" pneumoencephalogram has been insufficiently emphasized in the radiologic literature, particularly in the United States. It is, therefore, our purpose in this paper to present a series of cases which demonstrates the importance of a proper evaluation of the "failed" encephalogram, with particular emphasis on the demonstration of dilated callosal sulci in the absence of ventricular filling.

## CLINICAL MATERIAL

We have collected a series of 22 cases from the radiology services of the Montefiore Hospital, Albert Einstein College of Medicine and St. Vincent's Hospital, all in the City of New York.

We have chosen to divide the patterns of the pneumoencephalographic findings into 3 major categories in order to aid in the proper location of the site of obstruction. Category I deals with the classic findings on pneumoencephalograms in which there is no gas in the ventricles, but there is dilatation of the callosal sulci and in some instances the cisternae veli interpositi and ambiens. Category II relates to those cases in which there is only a minimal degree of ventricular filling (generally only the fourth ventricle) but again with dilated callosal sulci. In Category III there is filling of the lateral ventricles associated with dilatation of the callosal sulci; the findings in this

category may closely simulate those of brain atrophy. As noted in Table I there were 17 cases in Category I, 4 cases in Category II, and 1 case in Category III.

Short summaries of each of the 22 cases, including the pneumoencephalographic and ventriculographic findings, together with the results on angiography, when performed, are given in Table II. The operative and/or autopsy findings are included. Illustrative material in 10 of the 22 cases with 8 cases from Category I and 1 each from Categories II and III is presented in Figures 2*A* through 24, inclusive. Figure 25, *A*, *B* and *C* shows a case of cortical and cerebral atrophy without an obstructing lesion.

## DISCUSSION

The significance of the appearance of dilated callosal sulci in the "failed" encephalogram becomes obvious from an evaluation of our material. In this connection, we have noted that where air encephalography fails for technical reasons in the absence of an obstructing lesion, the callosal sulci will generally not appear dilated, regardless of the amount of air injected. Thus, the presence of dilated callosal sulci with nonvisualization or only slight filling of the ventricular system generally indicates an obstructing lesion, usually in the posterior fossa, but occasionally elsewhere at or near the midline. Additionally, we note from Table I that in the Category I patient (17 cases) with the classic pattern of dilated callosal sulci and nonfilling of the ventricular system a posterior fossa obstructing lesion—either a neoplasm or adhesive arachnoiditis—is generally present. Lesions that obstruct the aqueduct or posterior part of the third ventricle will produce examples of Category II (4 cases) in which gas is seen in the fourth ventricle with dilated callosal sulci. Our single case in Category III should serve to illustrate that ventricular filling with dilated callosal sulci may indicate a posterior fossa mass lesion and not brain atrophy alone. Our observations concerning the relationship of the site of the lesion to the category appear to be substantiated in some measure by the cases described in the literature (see Table III), although a definitive appraisal of all the published cases is not possible, greatly limiting our evaluation.

It should be noted that it is possible to demonstrate dilated callosal sulci with no ventricular filling on a pneumoencephalographic study, and on a subsequent examination to find ventricular filling with demonstration of the site of obstruction (see our Case 16).

(*Continued on page 558*)

Table I

| Types of Lesions | *Category I* | *Category II* | *Category III* |
|---|---|---|---|
| A Infratentorial (block at 4th ventricle) | | | |
| Primary cerebellar tumors | 5 | | |
| Cerebellar metastases | 3 | | 1 |
| Cerebellopontine angle tumors | | | |
| Meningioma | 1 | | |
| Neurinoma | 1 | | |
| Fibrosing arachnoiditis or exudate blocking 4th ventricle | 2 | | |
| Tentorial meningioma | 1 | | |
| Mass lesion of undetermined type | 1 | 1 | |
| B Tentorial notch (falco-tentorial junction) (block at aqueduct) | | | |
| Glioma of midbrain and thalamus | 1 | | |
| Meningioma of free margin of the tentorium | | 2 | |
| Cystic cerebellar astrocytoma | 1 | | |
| C Supratentorial (block at interventricular foramina) | | | |
| Falx meningioma | 1 | | |
| Intraventricular glioma | | 1 | |
| Total | 17 | 4 | 1 |

TABLE II

TABULATION OF LESIONS BY CATEGORY

*Category I*

| Case No. | Pneumoencephalography | Ventriculography | Angiography | Surgical or Autopsy Findings |
|---|---|---|---|---|
| Case 1<br>L. G., male, aged 45 | Nonfilling of ventricles on two attempts. Slight dilatation of sulcus of corpus callosum. Narrowed cisterna pontis. Soft tissue mass in right cerebellopontine angle | Moderate hydrocephalus. Aqueduct and 4th ventricle displaced to the left and backward | None | Right cerebellopontine angle tumor-neurinoma of 7th nerve |
| Case 2<br>W. S., male, aged 33 | Nonfilling of ventricular system on two attempts. Dilated sulcus of corpus callosum | Hydrocephalus; 4th ventricle not filled. Positive contrast study demonstrated dilated 4th ventricle and minimally patent ventricular system | Right carotid angiogram demonstrated only hydrocephalus | Two negative posterior fossa explorations. At postmortem examination fibrosing arachnoiditis blocking the outlet foramina of 4th ventricle. Purulent membrane found in lining of 3rd and lateral ventricles |
| Case 3<br>A. G., male, aged 63 | No ventricular filling. Dilated sulcus of corpus callosum, slight narrowing of cisterna pontis. Nonfilling of superior cerebellar cisterns and cerebellar sulci | Large occipital cystic mass communicating with the ventricles (posterior fossa views unsatisfactory) | None | Cystic neoplasm of occipital region communicating with the left lateral ventricle; metastatic adenocarcinoma. Presumptive cerebellar metastasis unproved (no autopsy) |
| Case 4<br>S. S., female, aged 65 | No ventricular filling. Dilated sulcus of corpus callosum | None | Left carotid angiogram demonstrated displacement and draping of both anterior cerebellar arteries posteriorly and around midline mass. Posterior telescoping of internal cerebral vein | Large (100 gm.) bifrontal falx meningioma blocking the interventricular foramina |
| Case 5<br>G. L., female, aged 59 | No filling of ventricles. Dilated sulcus of corpus callosum. Slight dilatation of cisterna ambiens. Narrowed cisterna pontis | Dilated lateral and 3rd ventricles. Aqueduct kinked forward; aqueduct and 4th ventricle displaced to right | None | Fibrocytic meningioma arising from left lateral wall of tentorium |
| Case 6<br>P. B., male, aged 69 | No ventricular filling. Dilated right sulcus of corpus callosum. Slightly dilated cingulate sulcus. Slight encroachment on cisterna pontis | Aqueduct kinked forward and displaced to right | Complete occlusion of origin on the right internal carotid artery. Both anterior and middle cerebral arteries filled on left carotid angiography. Evidence of hydrocephalus prompting pneumoencephalography | Left cerebellar metastasis |
| Case 7<br>G. A., male, aged 3½ | No ventricular filling. Narrowed cisterna pontis. Dilated sulcus of corpus callosum | Aqueduct kinked forward and displaced to left | None | Right cerebellar astrocytoma |
| Case 8<br>J. M., female, aged 51 | No ventricular filling. Dilated sulcus of corpus callosum. Over-filling of the cisterna ambiens. Obliterated cisterna pontis. Postoperative pneumoencephalogram normal except for dilated 4th ventricle | Kinked aqueduct displaced to left | Left vertebral angiogram noncontributory | Right cerebellar metastasis (? from uterine carcinoma) |

Table II (*Continued*)

| Case No. | Pneumoencephalography | Ventriculography | Angiography | Surgical or Autopsy Findings |
|---|---|---|---|---|
| Case 9 M. W., male, aged 22 mo. | Cerebellar tonsils herniated. Dilated sulcus of corpus callosum. Dilated cisterna ambiens. Narrowed cisterna pontis | Aqueduct and ventricles kinked forward and displaced to left | None | Right cerebellar astrocytoma |
| Case 10 J. O., male, aged 41 | No ventricular filling. Dilated sulcus of corpus callosum. Dilated cisterna veli interpositi. Narrowed cisterna pontis | Obstruction with defect in back of 3rd ventricle | Right carotid angiogram noncontributory | Glioblastoma multiforme of midbrain and thalamus involving back of 3rd ventricle |
| Case 11 P. O., male, aged 6 | No ventricular filling. Dilated sulcus of corpus callosum. Narrowed cisterna pontis. Cerebellar tonsil herniation. Filling of cisterna veli interpositi | Marked forward kinking of the aqueduct without definite lateral displacement | None | Medulloblastoma of vermis and left cerebellar hemisphere |
| Case 12 M. N., male, aged 59 | Two pneumoencephalographies. No ventricular filling first attempt; slight second attempt. Dilated sulcus of corpus callosum. Narrowed cisterna pontis. Tumor outlined by air in right cerebellopontine angle | None | Left vertebral angiogram showed elevation of right superior cerebellar artery. Distal basilar artery displaced to left. Slightly depressed right posterior inferior cerebellar artery | Right cerebellopontine angle meningioma |
| Case 13 B., female, aged 16 | No ventricular filling. Narrowed cisterna pontis. Dilated sulcus of corpus callosum. Marked dilatation of cisterna veli interpositi. Dilated, deformed cisterna magna | Slight ventricular dilatation. Aqueduct and 4th ventricle not seen | None | Cerebellar sarcoma |
| Case 14 M. D., female, aged 25 | Dilated sulcus of corpus callosum. Multiple dilated cerebral sulci. No ventricular filling | None | None | Thickened arachnoid above optic chiasm and over convexities of brain. Dilated ventricular system with obstruction of outlet foramina of 4th ventricle by granulomata and arachnoid thickening due to sarcoidosis. Typical sarcoid granulomata found in lungs and hilar lymph nodes at autopsy |
| Case 15 R. K., male, aged 39 | Dilated sulcus of corpus callosum. No ventricular filling | Aqueduct kinked and displaced to left | Vertebral angiogram equivocal | Malignant melanoma; metastasis in right cerebellar hemisphere |
| Case 16 S. W., male, aged 63 | 1st pneumoencephalogram. No ventricular filling, dilated sulcus of corpus callosum. Dilated ambient cisterns. Narrowed cisterna pontis. 2nd pneumoencephalogram. 4th ventricle rotated and displaced forward | None | Vertebral angiography noncontributory | Primary lymphoma in left cerebellar hemisphere |
| Case 17 P. F., male, aged 18 mo. | No ventricular filling. Dilated sulcus of corpus callosum. Cerebellar tonsil herniation. Marked narrowing of cisterna pontis | Large concave defect in back of 3rd ventricle. Aqueduct and 4th ventricle depressed—confirmed by positive contrast study | None | Large bilateral cerebellar astrocytoma which had grown through the tentorial notch |

CENTRAL LIBRARY

TABLE II (*Continued*)

*Category II*

| Case No. | Pneumoencephalography | Ventriculography | Angiography | Surgical or Autopsy Findings |
|---|---|---|---|---|
| Case 18 R. K., male, aged 49 | Dilated sulcus of corpus callosum displaced upward (hydrocephalus). Small amount of air in 4th ventricle | Large lateral ventricles. No filling of 3rd ventricle. Tumor separating frontal horns | None | Fibrillary astrocytoma in right lateral ventricle, 3-4 cm. in diameter, almost occluding it at level of globus pallidus and blocking interventricular foramina |
| Case 19 G. L., female, aged 63 | Slight ventricular filling. Sulcus of corpus callosum tilted. Narrowed cisterna pontis | Marked dilatation of lateral ventricles. Forward kinking of aqueduct | Left carotid angiogram normal | Swollen right cerebellar hemisphere. Negative needle biopsy |
| Case 20 O. V., male, aged 45 | Dilated sulcus of corpus callosum. 4th ventricle filled | Kinked aqueduct | Vertebral angiogram showed splaying of posterior cerebral arteries. Could not opacify great vein of Galen | Meningioma of free margin of tentorium |
| Case 21 J. G., female, aged 20 | Dilated sulcus of corpus callosum. Narrowed cisterna pontis. 4th ventricle filled and depressed | None | Splaying of posterior cerebral arteries | Meningioma of free margin of tentorium |

*Category III*

| Case No. | Pneumoencephalography | Ventriculography | Angiography | Surgical or Autopsy Findings |
|---|---|---|---|---|
| Case 22 B. M., female, aged 47 | Dilated lateral and 3rd ventricles. Dilated sulcus of corpus callosum. Generalized filling of dilated cerebral sulci. 4th ventricle and aqueduct not adequately visualized | Kinked aqueduct | None | Right cerebellar metastasis from breast carcinoma |

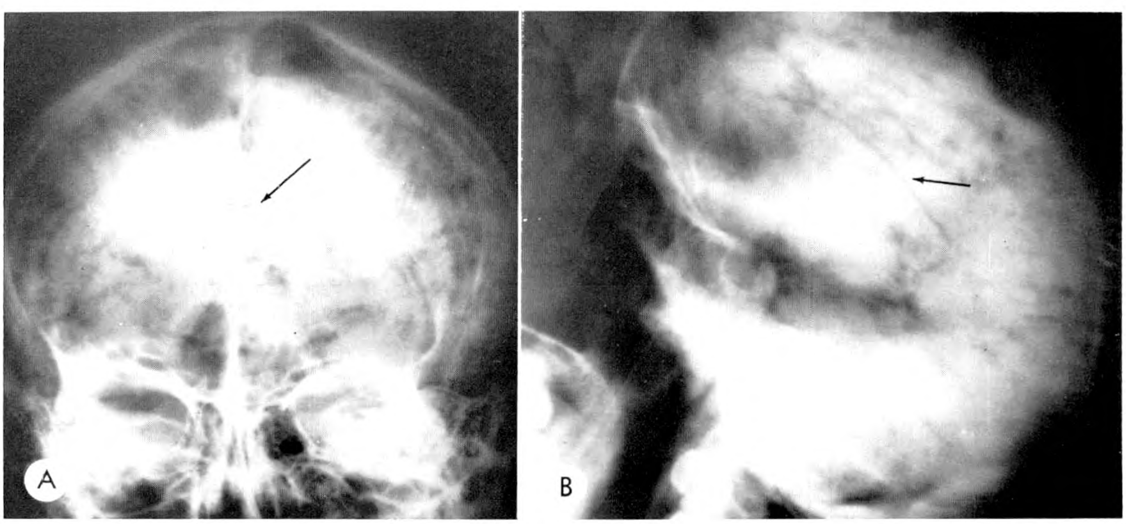


FIG. 2. Case 1. A 45 year old male with a right cerebellopontine angle neurinoma (Category 1). (*A*) Posteroanterior standard and (*B*) lateral erect autotomogram during pneumoencephalography show no filling of the ventricular system. The callosal sulci are outlined and are slightly dilated (arrows).

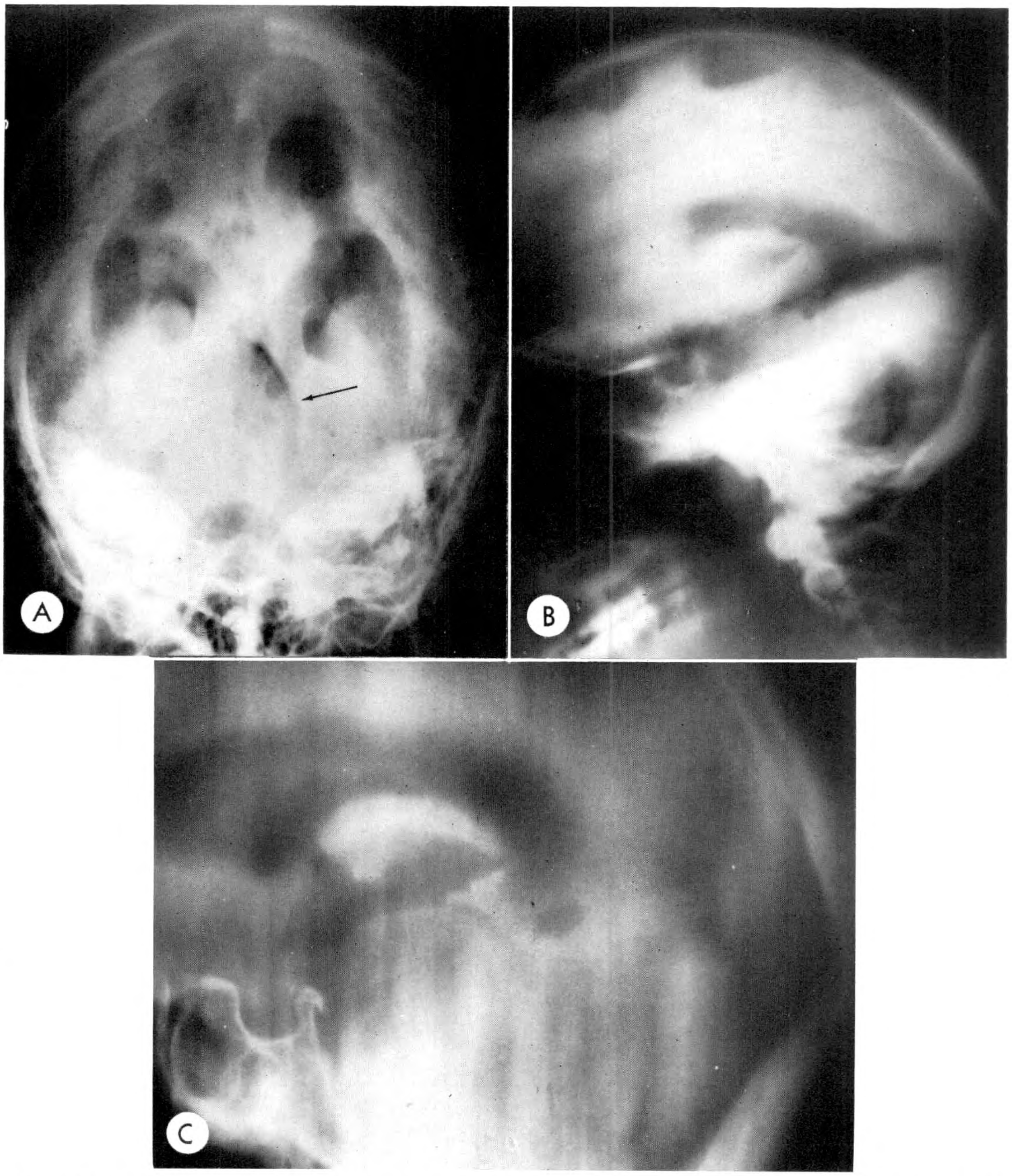


Fig. 3. Case 1. (*A*) A reverse Chamberlain-Towne view during ventriculography shows the fourth ventricle displaced to the left (arrow). (*B*) Brow-down lateral autotomogram during ventriculography shows the fourth ventricle displaced posteriorly. (*C*) A mid-line lateral laminagram shows the aqueduct displaced posteriorly; the fourth ventricle is not delineated. This finding confirms the laterality of the lesion.

This case is typical for Category 1 with the operative findings confirming the diagnosis of a right cerebellopontine angle mass—in this instance a neurinoma.

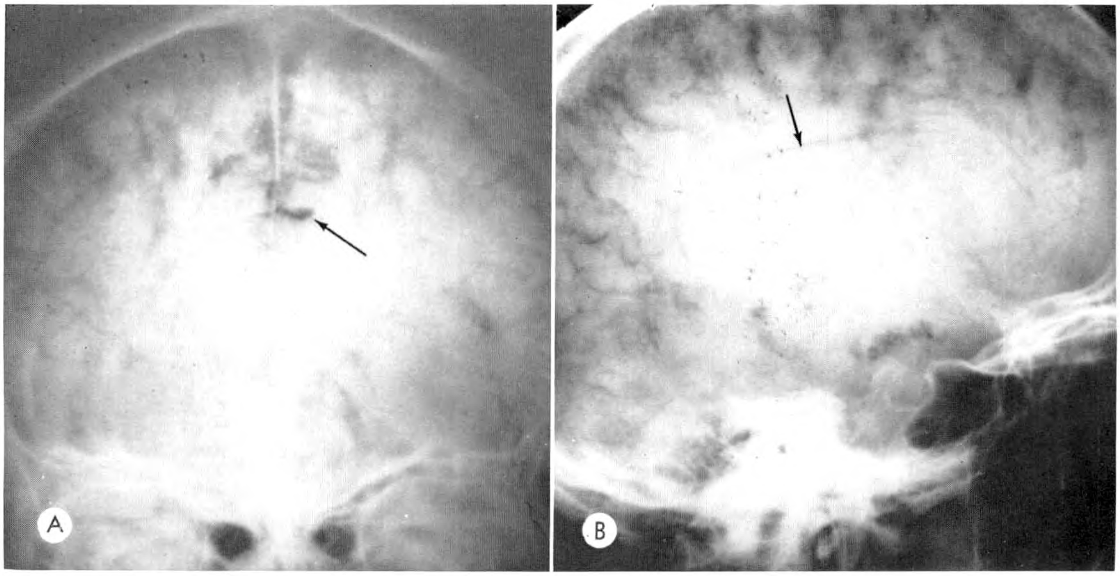

FIG. 4. Case 2. A 33 year old male with outlet obstruction of the fourth ventricle (Category 1). (*A*) Postero-anterior and (*B*) lateral erect pneumoencephalograms show nonvisualization of the ventricles. The callosal sulci are outlined and dilated (arrows), and their position suggests that the lateral fluid-filled ventricles are dilated.

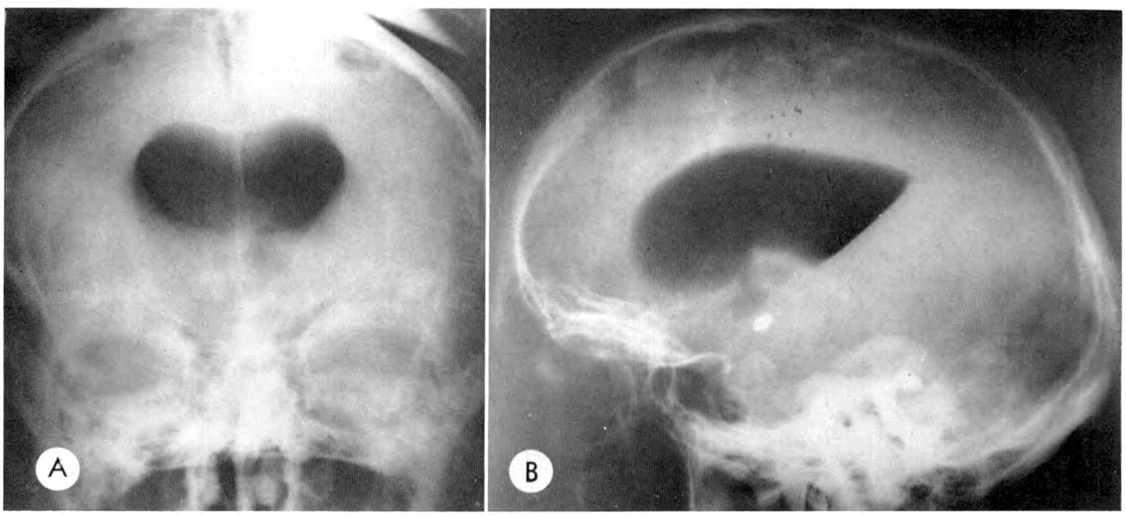

FIG. 5. Case 2. (*A*) Anteroposterior and (*B*) lateral supine brow-up ventriculograms show considerable dilatation of the front half of the lateral ventricles and the frontal horns. The interventricular foramina are dilated, with a small amount of gas in the anterior and upper aspect of the third ventricle. Opaque medium from a previous positive contrast study is seen in the third ventricle, a part of the fourth ventricle, and in the upper portion of the spinal canal. The findings suggest an incomplete outlet obstruction of the fourth ventricle.

At autopsy, a dense fibrosing archnoiditis obstructing the outlet foramina of the fourth ventricle was found, together with a purulent membrane lining the lateral and third ventricles.

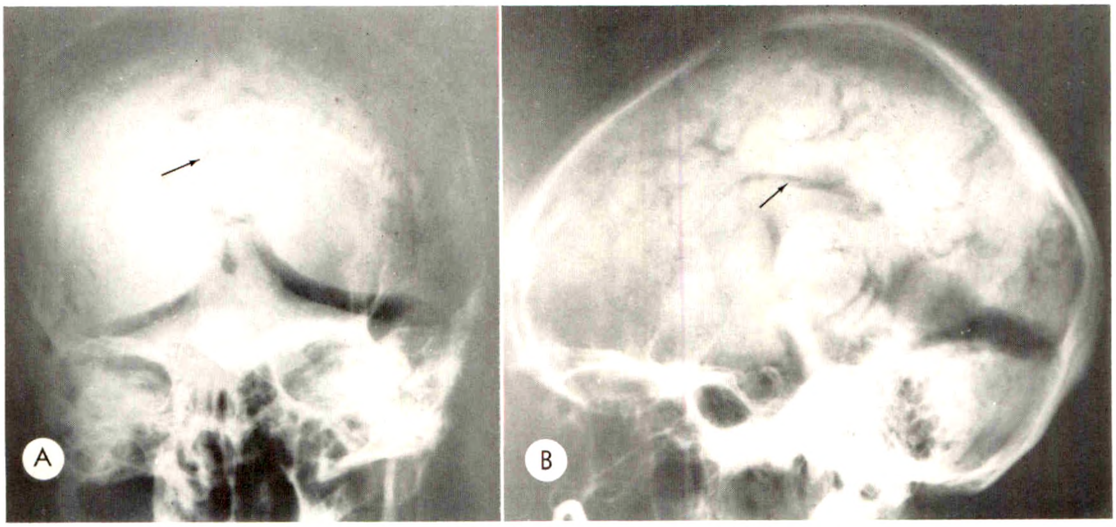


Fig. 6. Case 4. A 65 year old female with a bifrontal falx meningioma (Category 1). (*A*) Posteroanterior and (*B*) lateral erect pneumoencephalograms show an absence of gas in the lateral ventricles. There is dilatation of the callosal sulci (arrows). There is gas seen subdurally under the tentorium on each side.

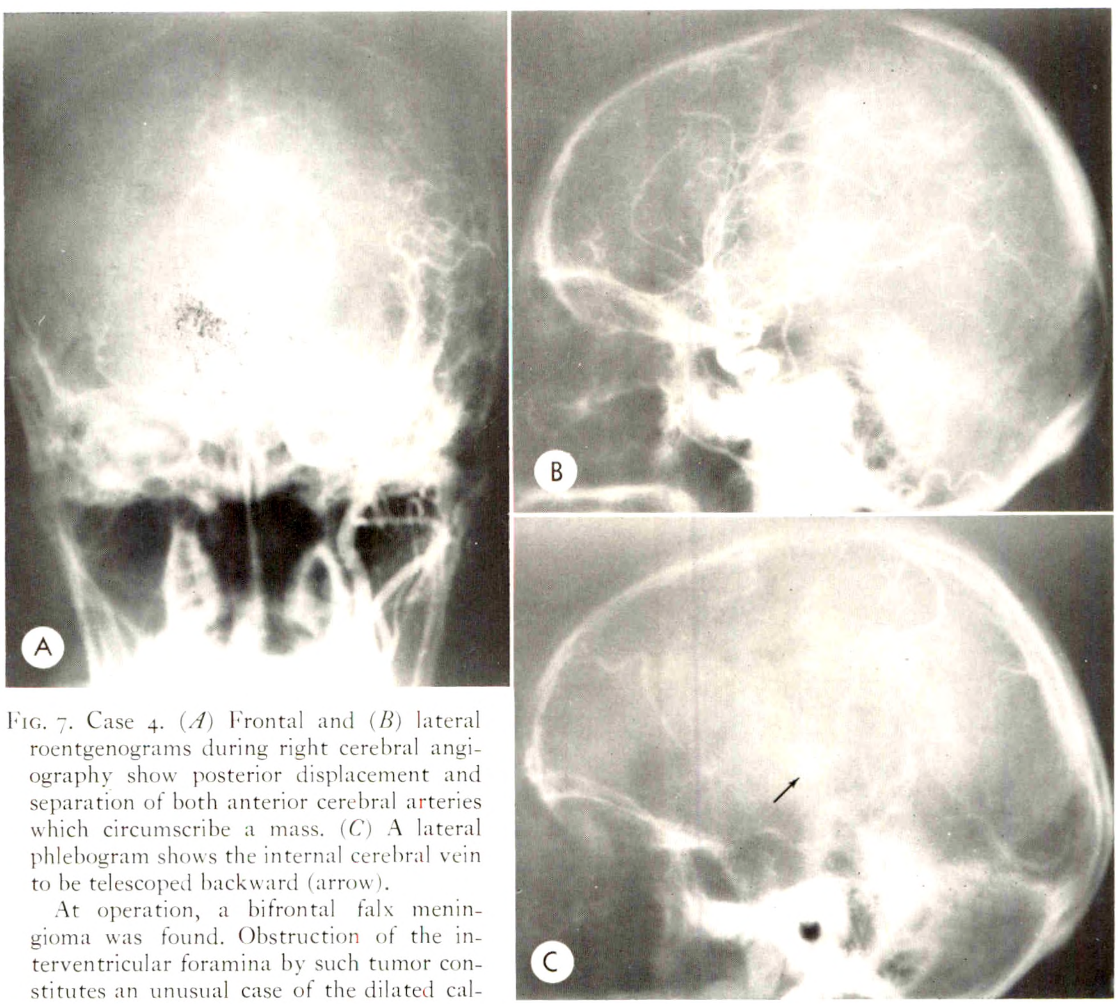


Fig. 7. Case 4. (*A*) Frontal and (*B*) lateral roentgenograms during right cerebral angiography show posterior displacement and separation of both anterior cerebral arteries which circumscribe a mass. (*C*) A lateral phlebogram shows the internal cerebral vein to be telescoped backward (arrow).

At operation, a bifrontal falx meningioma was found. Obstruction of the interventricular foramina by such tumor constitutes an unusual case of the dilated callosal sulcus sign.

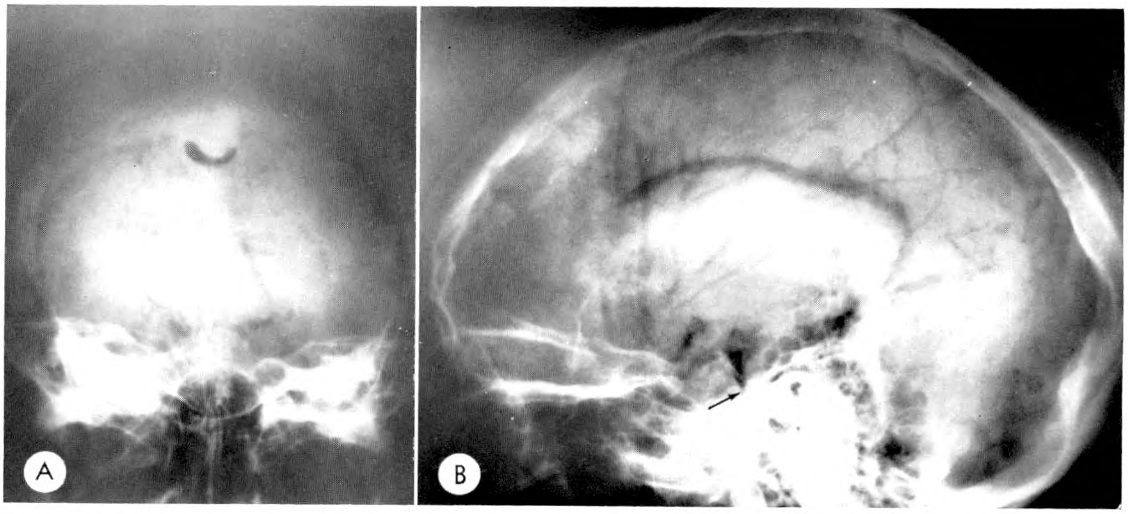


FIG. 8. Case 5. A 59 year old female with metastasis in the right cerebellar hemisphere (Category 1). (*A*) Posteroanterior and (*B*) lateral erect pneumoencephalograms fail to show visualization of the ventricular system. The callosal sulci are outlined and are markedly dilated. The cisterna pontis is encroached upon (arrow).

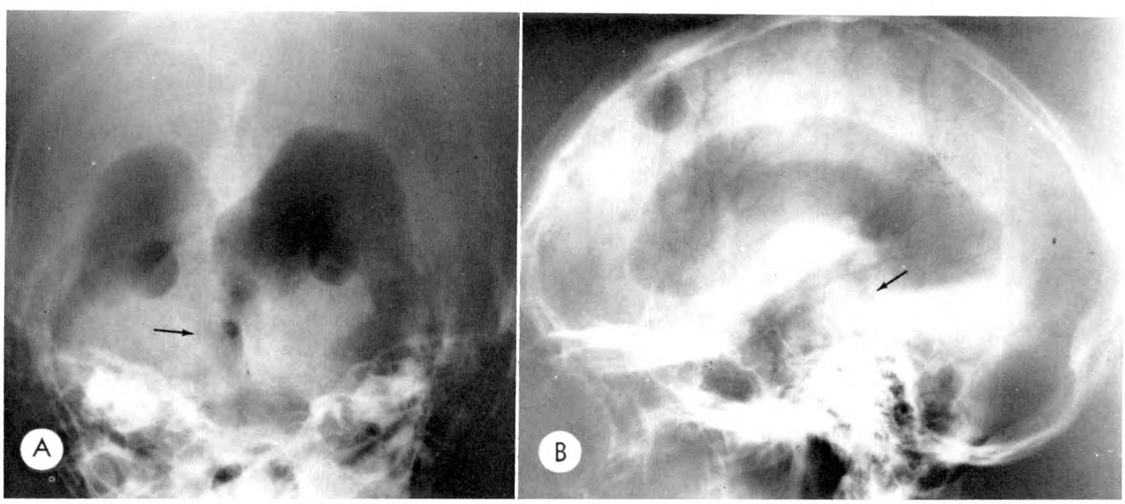


FIG. 9. Case 5. (*A*) A prone reverse Chamberlain-Towne ventriculogram shows marked dilatation of the bodies of the lateral ventricles. The fourth ventricle is faintly defined (arrow) and is displaced slightly to the right. (*B*) A recumbent lateral ventriculogram shows considerable dilatation of the ventricular system. The aqueduct is filled in its upper half (arrow) and is kinked and displaced forward. The fourth ventricle is not clearly identified.

A fibrocystic meningioma arising from the lateral wall of the tentorium on the left side was found at operation, representing another positive example of the dilated callosal sulcus sign.

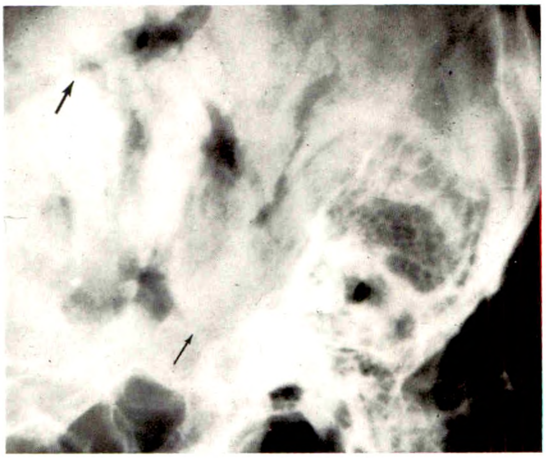

Fig. 10. Case 8. A 51 year old female with a right cerebellar hemisphere metastasis (Category 1). An erect lateral pneumoencephalogram shows gas in the cervical spinal canal; there is no gas in the ventricular system. The callosal sulci are outlined and quite dilated (large arrow). The cisterna pontis is obliterated (small arrow).

Fig. 11. Case 8. A brow-down lateral ventriculogram shows marked dilatation of the posterior half of the ventricular system with gas in the posterior portion of the third ventricle as well as the upper segment of a kinked and anteriorly displaced aqueduct (arrow).

A metastatic lesion in the right cerebellar hemisphere was found at operation, again confirming the importance of the sign.

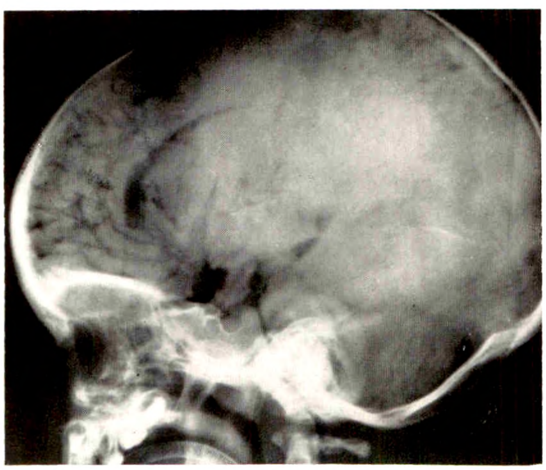

Fig. 12. Case 9. A 22 month old male infant with a right cerebellar hemisphere astrocytoma (Category 1). A brow-up lateral pneumoencephalogram shows no gas in the ventricular system. There is gas in the front half of the dilated callosal sulci. There is encroachment on the cisterna pontis.

Fig. 13. Case 9. A lateral brow-down autotomogram during ventriculography shows considerable dilatation of the posterior half of the lateral ventricle and third ventricle. Gas outlines the aqueduct and a portion of the fourth ventricle with kinking and forward displacement of the aqueduct.

A right cerebellar hemisphere astrocytoma was found at operation.

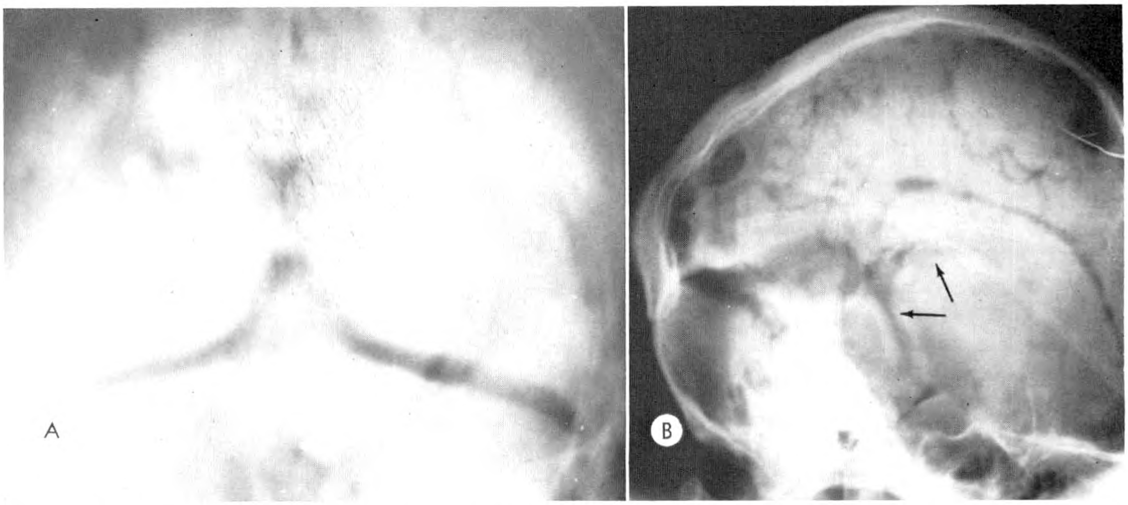


FIG. 14. Case 10. A 41 year old male with a glioblastoma of the thalamus (Category I). Erect half-axial (*A*) posteroanterior and (*B*) lateral pneumoencephalograms show no gas in the ventricular system. The callosal sulci are outlined and are dilated. Gas is seen in the dilated cisternae ambientes and veli interpositi (arrows).

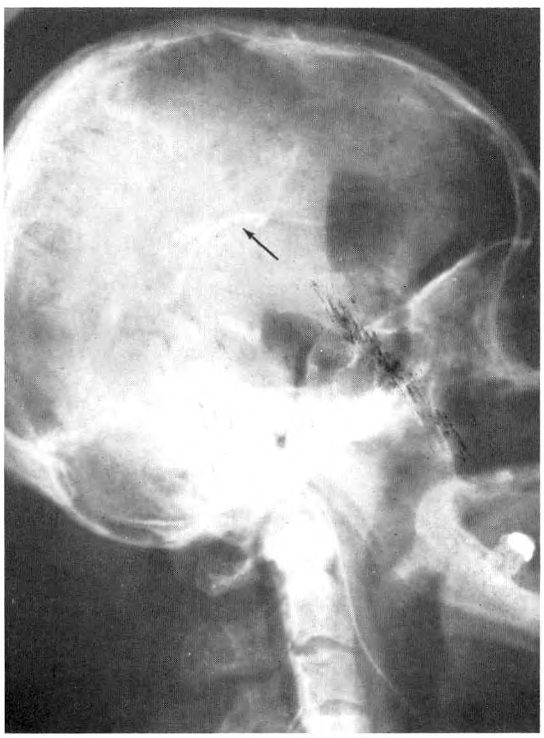

FIG. 15. Case 10. A lateral right-sided carotid angiogram in the venous phase shows the interior cerebral vein to be bowed upward considerably (arrow). Gas is seen in the frontal horns, residual from a ventriculogram.

This case is another example of Category I with a glioblastoma multiforme found at autopsy in the thalamus, growing across the midline and obstructing the posterior portion of the third ventricle and the aqueduct. Note the relationship of the dilated cisterna veli interpositi to the internal cerebral vein.

(*Continued from page 549*)

We have noted examples of the "failed" encephalogram in which there is a small amount of gas in the cisterna pontis encroached upon by an anteriorly displaced pons due to a posterior fossa mass, with nonvisualization of the ventricular system and the callosal sulci. In such instances, cerebellar tonsil herniation, diminished filling of the cerebellar sulci, displacement of the vallecula and, occasionally, outlining of the tumor itself may aid in the correct diagnosis.

We would like to state the following observations and principles that we have derived from the evaluation of our clinical material:

1. The majority of our cases showing a dilated callosal sulcus sign on pneumoencephalography (Categories I and II) comprises lesions in or near the mid-line, for the most part in the posterior fossa. Most of these lesions are cerebellar tumors, either primary or metastatic, cerebellopontine angle tumors, meningiomas arising from

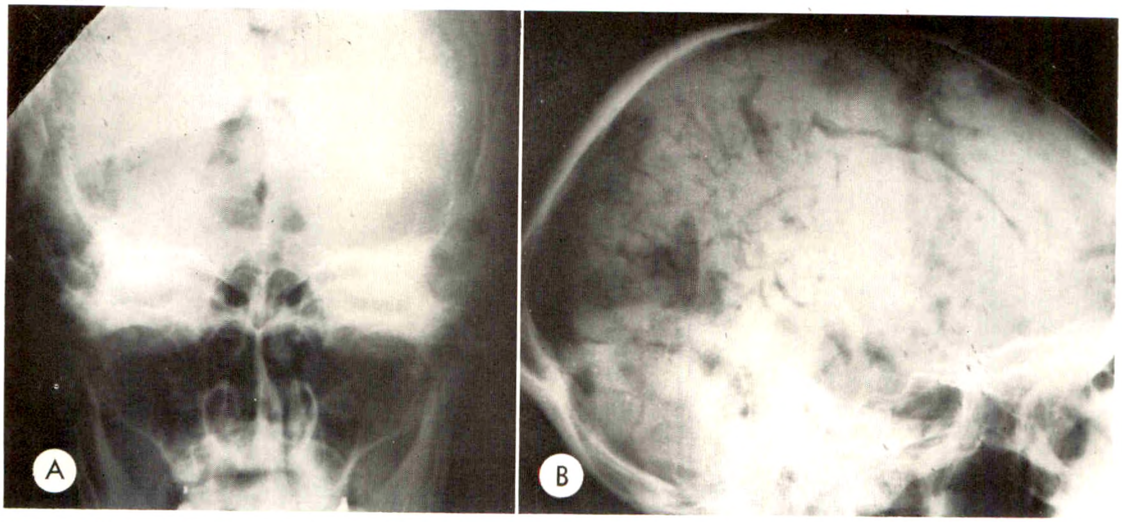


Fig. 16. Case 12. A 59 year old male with a right cerebellopontine angle meningioma (Category 1). (*A*) Posteroanterior and (*B*) lateral pneumoencephalograms show no gas in the ventricular system. The callosal sulci are outlined and are slightly dilated. Subdural gas is seen posteriorly.

Fig. 17. Case 12. A second pneumoencephalogram obtained 3 days later resulted in partial ventricular filling and demonstrates in this autotomogram gas in the posterior portion of the third ventricle and in the aqueduct, which is bowed and displaced backward. Gas is seen in the subdural space.

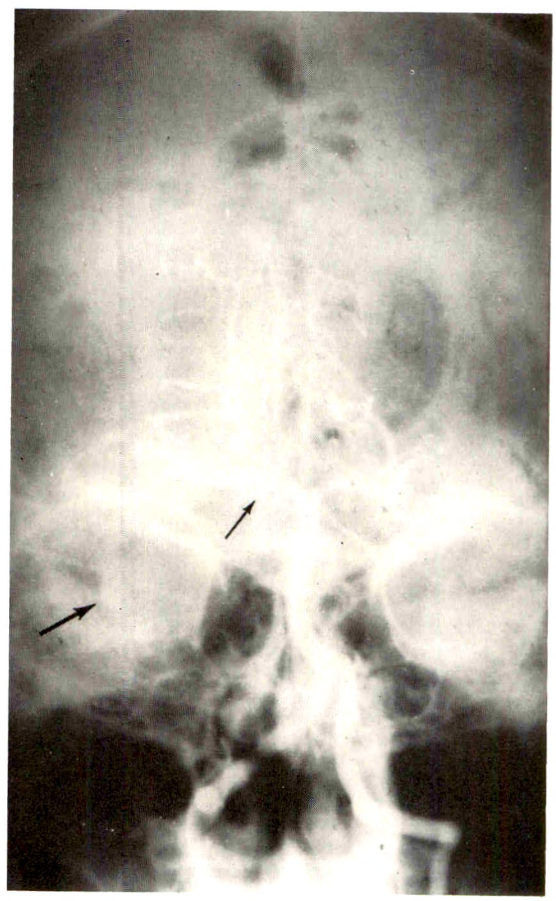

Fig. 18. Case 12. A frontal view during vertebral angiography performed immediately following the second pneumoencephalogram shows elevation of the right superior cerebellar artery (small arrow). The lateral margin of the tumor is faintly outlined by gas (large arrow).

A meningioma of the right cerebellopontine angle was found at operation. This case demonstrates that a pneumoencephalogram may occasionally outline the ventricular system after a "failed" first attempt.

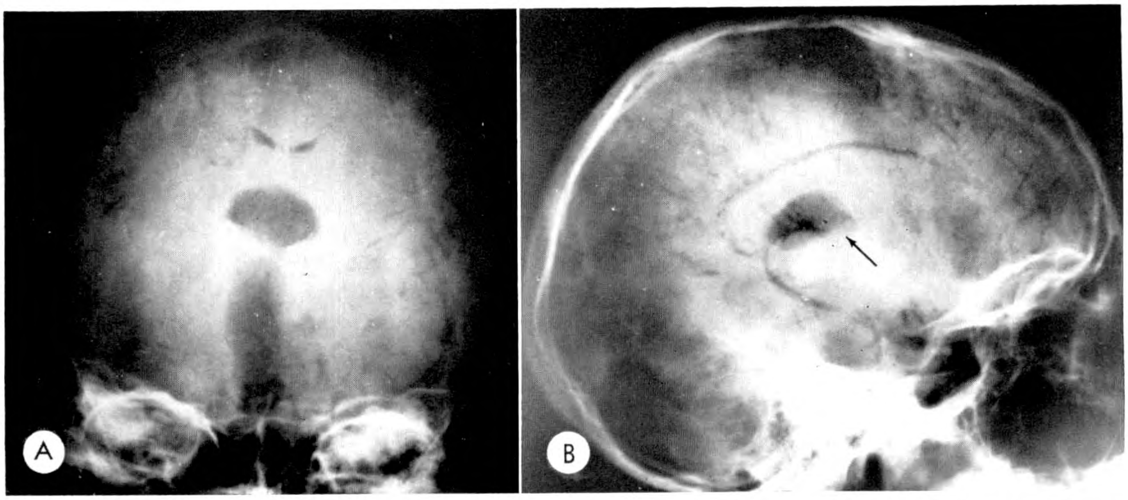


FIG. 19. Case 13. A 16 year old female with a cerebellar sarcoma (Category I). Erect (*A*) frontal and (*B*) lateral pneumoencephalograms show no filling of the ventricular system. The callosal sulci are outlined and dilated. There is a markedly dilated cisterna veli interpositi seen in the mid-line (arrow).

the free margin of the tentorium, aqueduct stenosis and obstructive arachnoiditis of the outlet foramina of the fourth ventricle.

2. In addition to visualization of dilated callosal sulci, one may find dilatation of the cisterna ambiens, cisterna veli interpositi, cingulate sulci and other cerebral sulci.

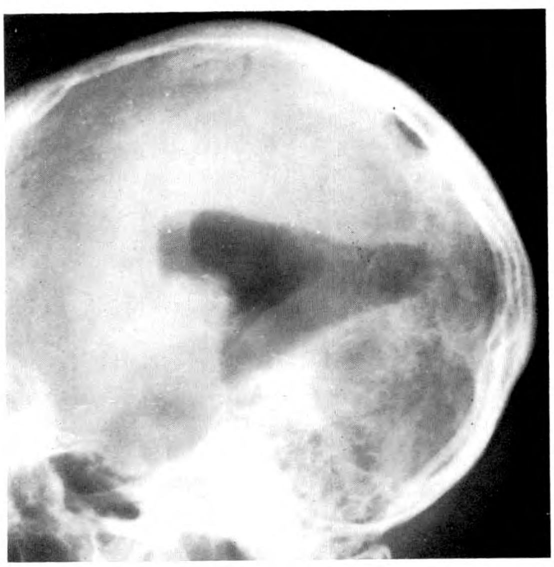

FIG. 20. Case 13. A brow-down lateral ventriculogram shows a dilated ventricular system in its posterior half. The aqueduct and fourth ventricle were never adequately outlined.

A cerebellar sarcoma was found at operation. In addition to the dilated callosal sulcus sign, the striking finding here is a markedly dilated cisterna veli interpositi which may be seen as part of this syndrome.

3. In instances of good filling of the ventricular system when the callosal sulci are dilated, one should not settle for less than adequate and definitive delineation of the aqueduct and fourth ventricle in both frontal and lateral projections in order to exclude an obstructing lesion; in this way a mistaken diagnosis of brain atrophy may be avoided.

4. We would probably have a significantly larger series of cases for all 3 categories, particularly Categories I and II, were the members of our neurosurgical division less conservative in their reluctance to perform or to have performed lumbar pneumoencephalography rather than air ventriculography in patients with suspected fossa mass lesions. In this connection, in all of our cases of posterior fossa tumors and other obstructing lesions discussed in this paper (in a number of whom there was evidence of cerebellar tonsillar herniation), no untoward reactions to lumbar pneumoencephalography were encountered.

## ETIOLOGY

The cause for the occurrence of the dilated callosal sulcus sign in the "failed" pneumoencephalogram is speculative. Sas-

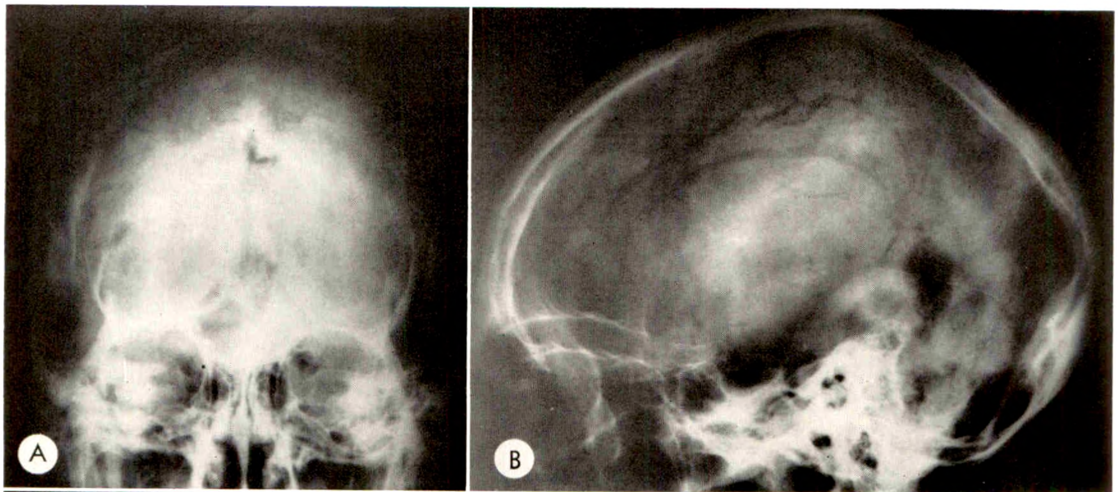


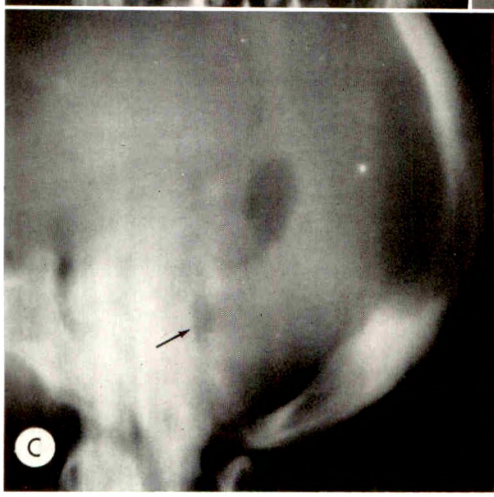


Fig. 21. Case 18. A 49 year old male with an astrocytoma of the right lateral ventricle obstructing the interventricular foramina (Category II). Erect (*A*) frontal and (*B*) lateral roentgenograms together with (*C*) a horizontal lateral laminagram during pneumoencephalography show dilatation mainly of the left callosal sulcus. There is no gas noted in the bodies of the lateral ventricles or the third ventricle. A small amount of gas is seen on the laminagram in the fourth ventricle (arrow).

saroli[8] attempted to explain this air collection on a mechanical basis, stating that the "interhemispheric fissure" was compressed by the intracranial hypertension. He felt that the lips of the sulci by their oblique

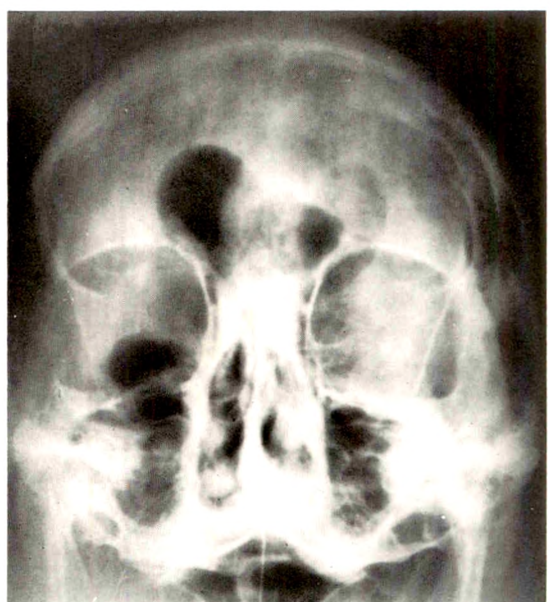

Fig. 22. Case 18. A supine frontal ventriculogram shows a large mass occupying the medial aspect of the right lateral ventricle and extending past the mid-line.

At operation, an astrocytoma was found, occupying the right lateral ventricle and growing across the mid-line to obstruct the interventricular foramina. This case is an example of Category II.

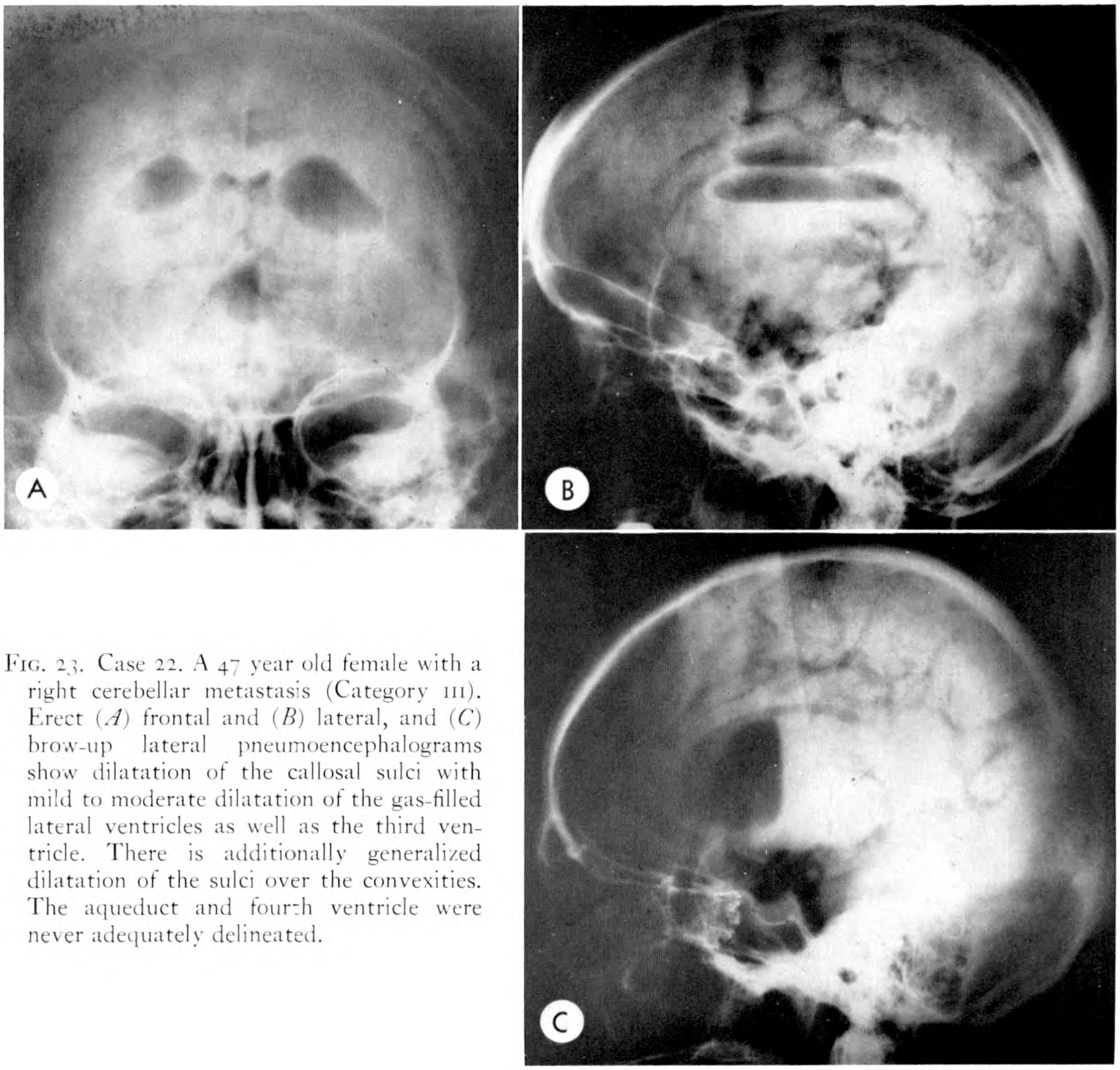


FIG. 23. Case 22. A 47 year old female with a right cerebellar metastasis (Category III). Erect (*A*) frontal and (*B*) lateral, and (*C*) brow-up lateral pneumoencephalograms show dilatation of the callosal sulci with mild to moderate dilatation of the gas-filled lateral ventricles as well as the third ventricle. There is additionally generalized dilatation of the sulci over the convexities. The aqueduct and fourth ventricle were never adequately delineated.

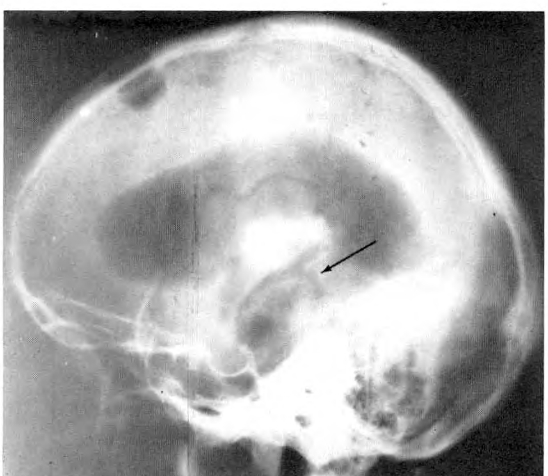

FIG. 22. Case 22. A lateral horizontal ventriculogram shows considerable dilatation of the ventricular system with gas outlining the upper half of the aqueduct which is kinked and displaced anteriorly (arrow).

At surgery, a right cerebellar mass was found due to metastatic carcinoma, primary in the breast. This case is representative of Category III and could easily be confused on the pneumoencephalograms with cerebral and cortical atrophy (see below).

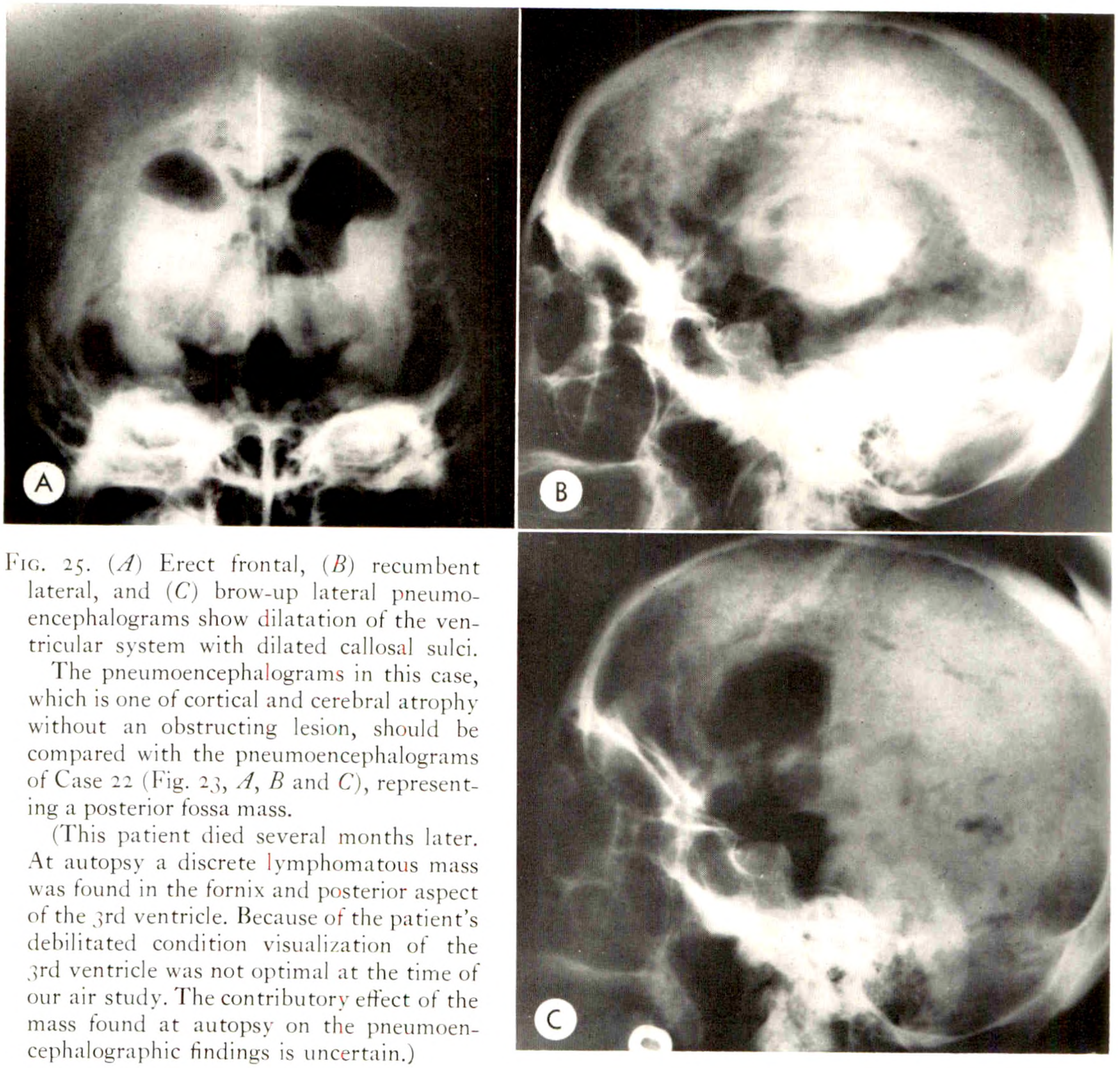


Fig. 25. (*A*) Erect frontal, (*B*) recumbent lateral, and (*C*) brow-up lateral pneumoencephalograms show dilatation of the ventricular system with dilated callosal sulci.

The pneumoencephalograms in this case, which is one of cortical and cerebral atrophy without an obstructing lesion, should be compared with the pneumoencephalograms of Case 22 (Fig. 23, *A*, *B* and *C*), representing a posterior fossa mass.

(This patient died several months later. At autopsy a discrete lymphomatous mass was found in the fornix and posterior aspect of the 3rd ventricle. Because of the patient's debilitated condition visualization of the 3rd ventricle was not optimal at the time of our air study. The contributory effect of the mass found at autopsy on the pneumoencephalographic findings is uncertain.)

configuration became superimposed in a transverse direction and collapsed in a manner that caused air to remain trapped in the sulci.

Roth[6] also discussed a possible cause for the dilated callosal sulci and other sulci in posterior fossa mass lesions during pneumoencephalography. He related these findings to the presence of tentorial herniation or "preherniation," causing an obstruction to the cerebrospinal fluid pathway at the apex of the tentorial notch. It was his opinion that the cerebrospinal fluid was forced from the posterior fossa into the median or paramedian cisternal spaces. The supratentorial spaces, he felt, then eventually underwent selective dilatation because of the transmitted pressure of the cerebrospinal fluid on these spaces. Roth buttressed his hypothesis by a demonstration of schematics and sections through the brainstem dealing with transtentorial herniation.

Schechter *et al.*[9] did not attempt to explain this phenomenon but simply pointed out this constellation of findings as a new sign and stressed that it should not be confused with brain atrophy. These authors, in a study of 100 normal encephalograms and an additional 100 cases showing brain atrophy, emphasized the infrequency of filling of the sulci of the corpus callosum in both groups.

Pribram suggested that dilatation of the cisterna veli interpositi could result from interference with the normal cerebrospinal fluid circulation, although he stated that this finding might occur as a result of distortion or displacement of this structure. However, he advanced no other hypothesis for the dilated callosal sulci.

We have nothing conclusive to offer as to the mechanism for the dilated callosal sulcus sign. The mechanism for these findings in connection with transtentorial herniation as advanced by Roth is a logical one for infratentorial lesions. However, as we have pointed out previously, the dilated callosal sulcus sign may be seen with aque-

TABLE III

| Author | Case or Fig. No. | Diagnosis | Category I | Category II | Category III |
|---|---|---|---|---|---|
| Sassaroli[8] 1955 | Case 1 | Aqueduct stenosis | — | 1 | — |
| | Case 2 | Cerebellar tumor | 1 | — | — |
| | Case 3 | Optic nerve glioma | — | 1 | — |
| | Case 4 | Tumor of 4th ventricle | 1 | — | — |
| Castellano and Ruggiero[1] 1953 | Case 20 | Meningioma of posterior fossa | — | 1 | — |
| Ruggiero[7] 1957 | Case 6 (p. 297) (p. 168) | Left acoustic neurinoma | — | 1 | — |
| Robertson[6] 1957 | Fig. 50 (p. 156) | 4th ventricle tumor | 1 | — | — |
| Schechter *et al.*[9] 1958 | Case 1 | Cerebellar astrocytoma | — | — | 1 |
| | Case 2 | Sheet-like membrane blocking outlet foramina of 4th ventricle | 1 | — | — |
| | Case 3 | Aqueduct stenosis | 1 | — | — |
| | Case 4 | Aqueduct stenosis | — | 1 | — |
| Roth[6] 1961 | Case 1 | Cerebellar astrocytoma | 1 | — | — |
| | Case 2 | Cerebellar astrocytoma | — | 1 | — |
| | Case 3 | Cystic cerebellar astrocytoma | 1 | — | — |
| | Case 4 | No filling of sulcus of corpus callosum | — | — | — |
| | Case 5 | Arachnoidal cyst of cerebellum | — | — | 1 |
| | Case 6 | Cystic tumor of 4th vetricle | 1 | — | — |
| Pribram[4] 1962 | 13/24 | Posterior fossa tumors | 13* | | |
| Taveras and Wood[10] 1964 | Fig. 202 A (p. 1. 264) | Hypothalamic tumor Large pituitary tumor | 1 | — | — |
| | Fig. 202 B (p. 1. 265) | Block of interventricular foramina | 1 | — | — |
| Totals | | | 23 | 6 | 2 (Total 31) |
| Total Present Authors | | | 17 | 4 | 1 (Total 22) |
| Total | | | 40 | 10 | 3 (Total 53 cases) |

* 13 Category 1 cases which are not all illustrated or discussed in Pribram's paper.

duct stenosis and supratentorial lesions. Thus, it may be that the obstructive hydrocephalus found in our cases and in those in the literature results in transmitted pressure to the cerebrospinal fluid around the brain which forces fluid into the callosal sulci, ambient cisterns, and cisterna veli interpositi, resulting in adjacent pressure atrophy with secondary dilatation of these spaces.

Since pneumoencephalography is not always performed in large teaching centers with a trained neuroradiologist available, we feel it necessary to stress the importance of the general radiologist properly evaluating the "failed" pneumoencephalogram, particularly one in which the callosal sulci are outlined and dilated. In considering our material, it is quite obvious that the dilated callosal sulcus sign in a pneumoencephalographic examination constitutes a strong warning to the radiologist that he may be dealing with an obstructing lesion in or near the mid-line and, generally, in the posterior fossa, and that additional studies, such as gas or positive contrast ventriculography, are indicated.

## SUMMARY AND CONCLUSIONS

1. The roentgen findings in the dilated callosal sulcus sign during a "failed" lumbar pneumoencephalogram are described.

2. The literature dealing with this subject and the normal anatomy of the sulci of the corpus callosum, the cisterna veli interpositi, the cisterna ambiens, and adjacent structures is reviewed.

3. We have collected 22 new cases to add to the list of previously reported cases presenting with the dilated callosal sulcus sign.

4. We have established 3 categories of findings, depending on the amount of ventricular filling, and have attempted to relate the location of the lesion to each individual category.

5. It is stressed that failure to outline the ventricular system during lumbar pneumoencephalography with filling of the callosal sulci, cisterna veli interpositi, cisterna ambiens and sulci over the cerebral cortex represents a constellation of roentgen findings highly suggestive of a lesion, usually in the posterior fossa and frequently in or near the mid-line.

6. Such a group of roentgen findings, particularly with a narrowed cisterna pontis, practically demands positive contrast or air ventriculography to exclude such a lesion.

7. The possible reasons for the dilated callosal sulcus sign are presented.

Harold G. Jacobson, M.D.
Department of Radiology
Montefiore Hospital
210th Street and Bainbridge Avenue
New York 67, New York

## REFERENCES

1. Castellano, F., and Ruggiero, G. Meningiomas of posterior fossa. *Acta radiol.*, 1953, Suppl. 104, pp. 54–55.
2. Kautzky, R., and Zulch, K. J. Neurologisch-Neurochirurgische Röntgendiagnostik. Springer-Verlag, Berlin, 1955, p. 103.
3. Liliequist, B. Subarachnoid cisterns: anatomic and roentgenologic study. *Acta radiol.*, 1959, Suppl. 185, pp. 77–79.
4. Pribram, H. F. Encephalography in diagnosis of posterior fossa tumors. *J. Neurosurg.*, 1962, *19*, 269–276.
5. Robertson, E. G. Pneumoencephalography. Charles C Thomas, Publisher, Springfield, Ill., 1957, p. 156 and p. 427.
6. Roth, M. Zisternale pneumographische Erscheinungsbilder bein raumbeschränkenden Prozessen der hinteren Schädelgrube: zum Wirkungsmechanismus der transtentoriellen Herniation. *Fortschr. a. d. Geb. d. Röntgenstrahlen u. d. Nuklearmedizin*, 1961, *94*, 369–393.
7. Ruggiero, G. L. Encéphalographie Fractionée. Masson & Cie, Paris, 1957, p. 189 and p. 297.
8. Sassaroli, S. Sul comportamento dei solchi della faccia mediale degli emisferi nella pneumoencefalografia. *Radiol. med.*, 1955, *41*, 358–364.
9. Schechter, M. M., Bull, J. W. D., and Carey, P. Two new encephalographic signs of pressure hydrocephalus. *Brit. J. Radiol.*, 1958, *31*, 317–325.
10. Taveras, J. M., and Wood, E. H. Diagnostic Neuroradiology. Williams & Wilkins Company, Baltimore, 1964, pp. 1.264–1.265.

# OTOSCLEROSIS: A NEW CHALLENGE TO ROENTGENOLOGY*

*By* GALDINO E. VALVASSORI, M.D.
CHICAGO, ILLINOIS

According to a recent survey, over two million people in the United States are affected by deafness produced by otosclerosis. If one considers that otosclerosis of the labyrinthine capsule is a common finding at autopsy, even in patients who did not complain of hearing trouble, and that otosclerosis has been found in 8 to 15 per cent of white adults,[5] one can obtain a more realistic figure of the number of people affected by this disease.

Otosclerosis is a primary focal disease of the labyrinthine capsule that may in some cases invade the oval window, causing fixation of the stapes, in other cases causing cochlear degeneration, or a combination.[11]

The term "otosclerosis" is actually improper and it was applied by von Tröltsch in 1881, who thought that the fixation of the stapes was produced by sclerosing changes in the tympanic mucosa from a chronic interstitial middle ear catarrh. Politzer, in 1893, recognized that the fixation of the stapes was due to a primary disease of the labyrinthine capsule. Siebenmann, in 1912, proposed the term of otospongiosis in view of the fact that the affected bone is actually less dense than the normal otic capsule. However, the term otosclerosis has become generally accepted and is now applied to all cases of primary disease of the labyrinthine capsule, with or without fixation of the stapes.

## ETIOLOGY

The etiology of otosclerosis is not known. A family tendency due to some kind of hereditary factor has been observed. The frequent association of otosclerosis with osteogenesis imperfecta and the onset or the increase of hearing loss during pregnancy, presumably due to an endocrine factor, constitute possible leads in the research of the obscure etiopathogenesis of this disease. The incidence of otosclerosis is at least twice as great in females as in males. The white race is affected much more frequently than the others. The age of onset of otosclerosis is usually about puberty. The disease slowly progresses to reach a stable condition characterized by a more or less severe hearing loss.

## PATHOLOGY

In order to understand the pathology of otosclerosis, it is necessary to recall that the otic capsule has the unique characteristic of arresting its maturation in a stage of primary ossification. The labyrinthine capsule retains for the entire life the enchondral bone which elsewhere is replaced by the mature haversian osseous tissue. Otosclerosis occurs when this enchondral bone regains its activity so that foci of haversian bone tissue develop in the labyrinthine capsule. These foci may progressively enlarge and extend to the endosteal and periosteal layers of the labyrinthine capsule, producing respectively encroachment upon the lumen of the labyrinth or exostoses-like protrusions into the tympanic cavity. The foci vary from a loose and irregular network of bony trabeculae containing large vascular lacunae, osteoblasts and osteoclasts to a relatively avascular and acellular, much denser type of mature bone. The sites of predilection of the otosclerotic foci in the labyrinthine capsule are the area just in front of the oval window (the fissula ante fenestram) and the borders of the round window. The capsule of the remainder of the cochlea, semicircular canals and internal auditory canal may all be involved, although less frequently. In the majority of

* From the Department of Radiology, The University of Chicago, Chicago, Illinois.

the cases (80 per cent), both ears are involved and often the lesions are quite symmetric.

### TREATMENT

Surgery is, at the present time, the only treatment for patients with otosclerosis uncomplicated by cochlear involvement with sensory-neural loss. Surgical otology has made rapid advances since the introduction of the operating microscope. There are three basic types of surgical procedures for otosclerosis:

(1) Fenestration of the horizontal semicircular canal is based on the principle of establishing a new sound pathway in place of the occluded oval window. This type of procedure, which for many years was the treatment of choice, is now limited to a few cases in which the involvement of the oval window is very extensive.

(2) Stapes mobilization, which tends to restore the normal sound pathways, has been largely abandoned because of the frequent recurrence of the process with refixation of the footplate, presumably due to stimulation of the otosclerotic focus at the time of surgery.

(3) Stapedectomy, which may be partial or total. Total stapedectomy is the procedure of choice today. It consists of removing the stapes and replacing it with a mobile prosthesis made of polyethylene tubing, wire or teflon and wire piston. The prosthesis is connected at one end to the long process of the incus and rests at the other end on the vein graft, fat, gelfoam or other material used to cover the oval window.

### DIAGNOSIS

The diagnosis of otosclerosis has been based until now on the clinical history and on the audiometric tests. The typical history is of progressive conductive hearing loss which began insidiously after puberty. The physical examination is usually negative except in a few cases in which a salmon or flamingo red tint of the promontory is observed (positive Schwartze's sign), indicating a vascular active focus which has reached the mucoperiosteum of the medial wall of the tympanic cavity. The audiometric tests show a conductive hearing loss with a gap between the impaired air conduction and the bone conduction which is normal in cases of pure stapes fixation and more or less depressed in cases of cochlear involvement. Of course, the presence of a good gap between the air and bone conduction is the fundamental requirement for a successful surgical procedure.

### ROENTGENOLOGY IN OTOSCLEROSIS

A review of the literature shows very few reports concerning the problem of otosclerosis. All the observations deal with diffuse labyrinthine otosclerosis, none with otosclerosis limited to the oval window region. The paucity of reports probably is due to the impossibility of showing by conventional roentgenology the small changes which occur in otosclerosis.

J. Beck, in 1915, described an abnormal radiolucency of the cochlea in patients with otosclerosis. Sir Harold Graham Hodgson reported a similar observation in 1928. However, he thought that "the radiographic changes seen in the capsule appear to bear little or no relationship to the severity or otherwise of the symptoms." Guillen, using a unilateral transorbital projection, observed lack of sharpness in the region of the oval window, and thickening of the basilar turn of the cochlea or of the entire labyrinthine capsule in patients with advanced otosclerosis. W. E. Compere,[1] in 1960, noted the following findings in petrous pyramids of patients afflicted with diffuse otosclerosis: (1) local overgrowth of osseous tissue anywhere in the otic capsule; (2) apparent sclerosis of the entire labyrinthine capsule, almost obscuring the labyrinthine system; and (3) hyperostosis of the entire petrous pyramid.

Laminagraphy, when performed with an apparatus which furnishes a sufficiently thin section, together with a satisfactory coefficient of distinctness, has opened to roentgenology a new and challenging field of investigation.

This report is based on the study of over 200 patients with otosclerosis as proved by surgery. In all patients a preoperative examination was performed. In approximately 50 per cent of the patients, a postoperative examination was done; in only 10 per cent of the patients a third follow-up study was performed.

### LAMINAGRAPHY OF THE NORMAL OVAL WINDOW AND ADJACENT LABYRINTHINE CAPSULE

A brief review of the normal roentgenographic appearance is necessary for the understanding of the pathologic findings.

The medial or labyrinthine wall of the middle ear cavity forms an angle open posteriorly for approximately 15° to 25° with the sagittal plane of the skull. The oval or vestibular window follows the same angle with its larger axis pointing about 10° upward anteriorly. It measures 3 to 4 mm. in its anteroposterior diameter and 1.5 to 2.0 mm. in its vertical diameter. Two views are used routinely for the demonstration of the oval window—frontal and semiaxial of the petrous pyramid. In the frontal view (Fig. 1, *A* and *B*), which is obtained with the patient supine and the line from the tragus to the external canthus perpendicular to the table top, the oval window forms a well-defined bony dehiscence in the inferolateral wall of the vestibule below the opening of the ampullar limb of the lateral semicircular canal. The normal footplate of the stapes, which measures 0.2 to 0.4 mm. in thickness, does not cast any shadow because of its obliquity to the roentgen-ray beam. Six sections are obtained in this projection, 1 mm. apart, and the oval window should be clearly detectable in at least two adjacent sections. The semiaxial view is obtained by rotating the patient's head 20° toward the side under examination so that the medial wall of the tympanic cavity, including the oval window, becomes parallel to the direction of the roentgen-ray beam. In such a projection, the normal footplate casts a fine line extending across the oval window opening between the prominent borders of the oval window niche formed by the facial nerve canal superiorly and the promontory inferiorly (Fig. 2, *A* and *B;* and 3). Again 6 sections are obtained, 1 mm. apart, and the oval window is usually visible in 3 adjacent sections.

The round or cochlear window corresponds to the posterior end of the scala tympani and it is located at the bottom of a

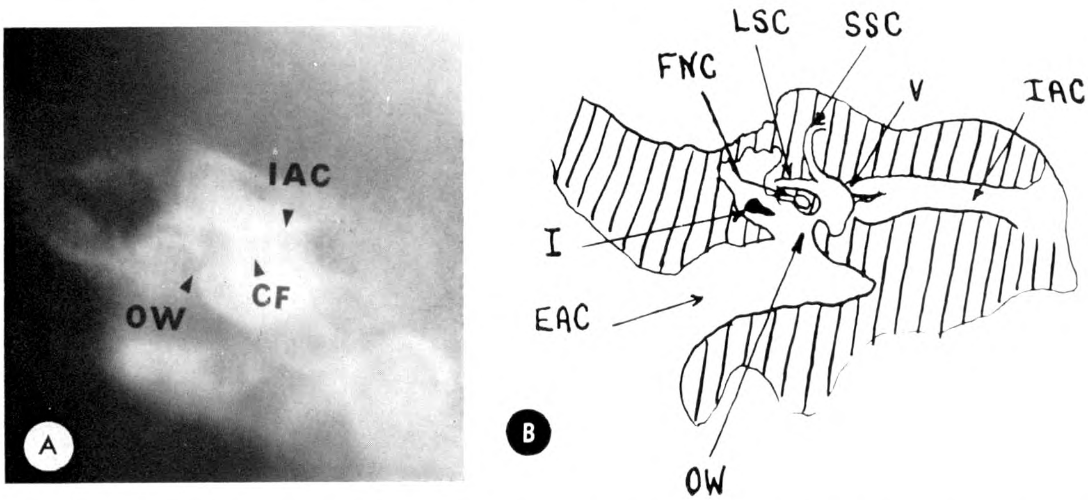


Fig. 1. (*A*) Frontal laminagram and (*B*) tracing of a normal right ear at 5 mm. posterior to the anterior wall of the external auditory canal. CF = crista falciformis; EAC = external auditory canal; FNC = facial nerve canal; I = incus; IAC = internal auditory canal; LSC = lateral semicircular canal; OW = oval window; SSC = superior semicircular canal; V = vestibule.

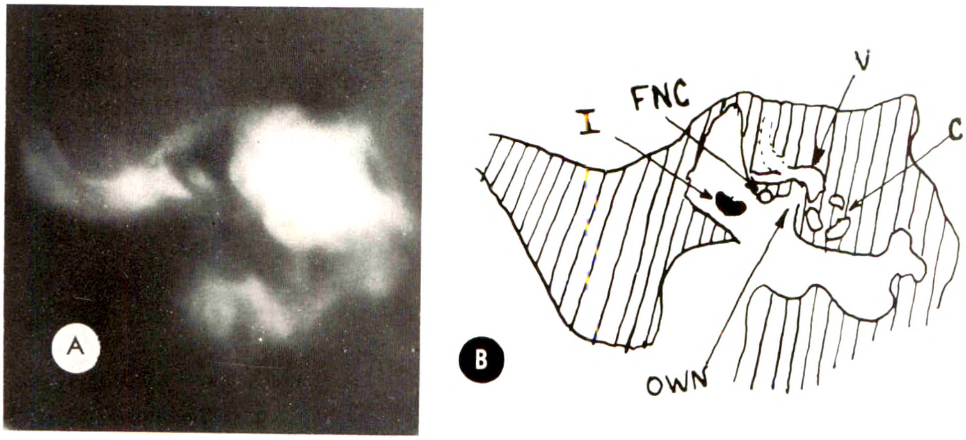


Fig. 2. (*A*) Semiaxial laminagram and (*B*) tracing of a normal right ear at the level of the oval window. C = cochlea; FNC = facial nerve canal; I = incus; OW = oval window; V = vestibule.

depression which is found in the inferior and posterior aspect of the promontory. The round window faces posteriorly, outward and slightly downward. The best view for its demonstration is the Stenvers' projection (Fig. 4, *A* and *B*). In the lateral view the niche leading to the round window is well seen. In the frontal sections the round window appears as a radiolucent area superimposed upon the basilar turn of the cochlea, below and slightly medial to the posterior part of the oval window. Sections taken 1.0 and 2.0 mm. posterior show the round window niche which points upward and slightly medially from a well-defined gap in the outline of the origin of the basilar turn of the cochlea.


Fig. 3. Histologic section of a normal left petrous pyramid obtained in the same plane and at the same level as the laminagram shown in Figure 2*A*. Notice that the appearance of the oval window niche with the footplate of the stapes (S), facial nerve canal (FN) and promontory (P) is identical with that seen in the laminagram.

The normal labyrinthine capsule appears as a sharply defined and homogeneously dense shell outlining the inner ear structures. The density of the capsule enhances the clearness of the lumen of the enclosed cavities, so that the entire system should always be perfectly recognizable (Fig. 10).

### OTOSCLEROSIS OF THE OVAL WINDOW

This is unquestionably the most common site of involvement. The roentgenographic appearance depends upon the type and extent of the process. The type of involvement depends upon the maturation of the otosclerotic focus. In mature otosclerosis one sees in the frontal sections obliteration of the oval window by a bony plate of variable thickness produced by the involved footplate of the stapes (Fig. 5 and 6). In the semiaxial views one sees the thickened footplate of the stapes (Fig. 7). In active otosclerosis or otospongiosis, the usually clear lips of the oval window become unsharp to completely cancelled so that one gets the superficial impression that the window is larger than normal (Fig. 8, *A* and

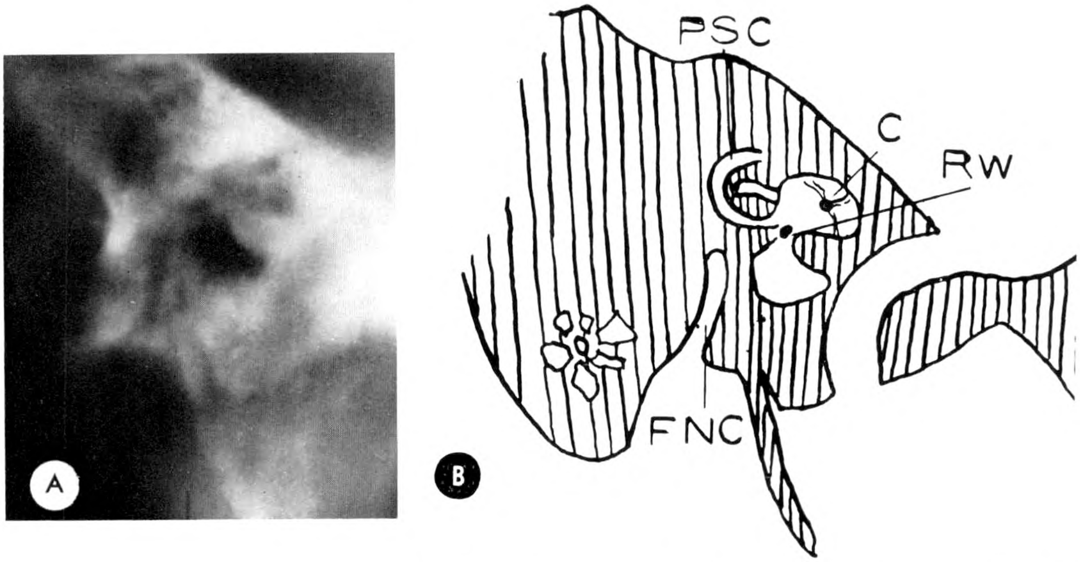


Fig. 4. (*A*) Laminagram and (*B*) tracing in Stenvers' projection at the level of the round window. C = cochlea; RW = round window; FNC = facial nerve canal; PSC = posterior semicircular canal.

*B*). However, a more accurate study of the region reveals almost invariably the presence of a density slightly more opaque than soft tissues containing fine, irregularly scattered calcifications.

The involvement of the oval window is variable in extent. Marginal otosclerosis, involving the periphery of the footplate and the annular ligament, produces narrowing of the oval window (Fig. 5). Central otosclerosis, a focus involving only the footplate of the stapes, appears as a more or less prominent bony structure in the oval window which does not reach at any level the margin of the window (Fig. 7). Complete otosclerosis, a uniform involvement of the entire footplate, appears as a bony plate completely obliterating the oval window (Fig. 6). Otosclerosis with involvement of the oval window niche, as well as of the footplate of the stapes, is well recognizable in the semiaxial projections where the niche appears from partially to totally filled-in (Fig. 9). Otosclerosis causing thick-

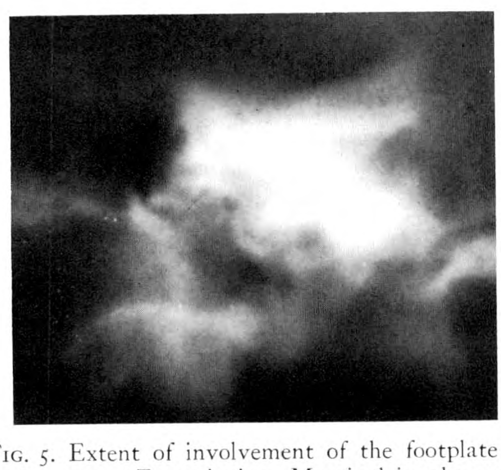

Fig. 5. Extent of involvement of the footplate of the stapes. Frontal view. Marginal involvement. Notice the entire stapes.

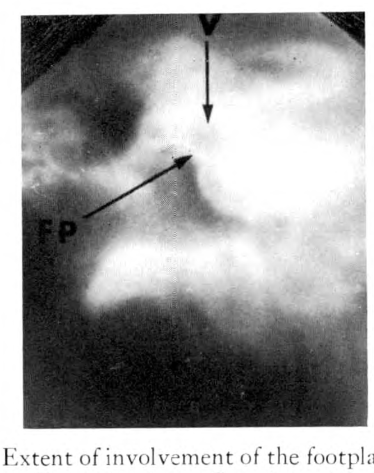


Fig. 6. Extent of involvement of the footplate of the stapes. Frontal view. Complete involvement. FP = footplate; V = vestibule.

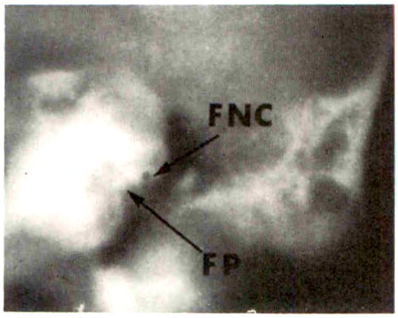


Fig. 7. Extent of involvement of the footplate of the stapes. Semiaxial view. Central involvement. FNC = facial nerve canal; FP = footplate.

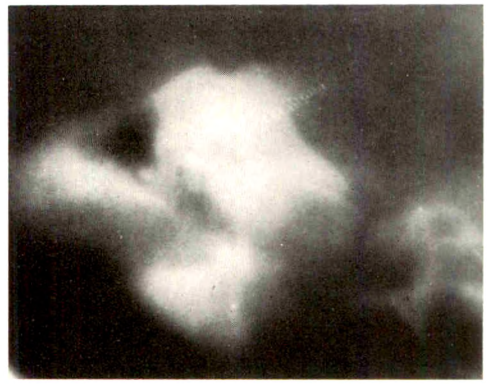

Fig. 9. Extent of involvement of the footplate of the stapes. Semiaxial view. Obliteration of the entire oval window niche.

ening of the footplate heaped up on the inner side produces a marginal obliteration of the vestibule.

### OTOSCLEROSIS OF THE LABYRINTHINE CAPSULE OTHER THAN THE OVAL WINDOW REGION

The involvement of the labyrinthine capsule may or may not be associated with the involvement of the oval window. The extent of involvement of the labyrinthine capsule is variable. The sites of involvement demonstrated roentgenographically are, in order of frequency, the basilar turn of the cochlea, the remainder of the cochlea, the semicircular canals and the internal auditory canal. Our findings are comparable with the histologic study of Nylén,[8] who found in a series of 121 petrous pyramids the following percentage of location: oval window, 90 per cent (50 per cent of which showed stapes fixation); round window, 40 per cent; cochlear capsule, 35 per cent; internal auditory canal, 30 per cent; semicircular canal, 15 per cent; and diffuse, 10 per cent.

The roentgenographic findings depend upon the severity of the involvement,

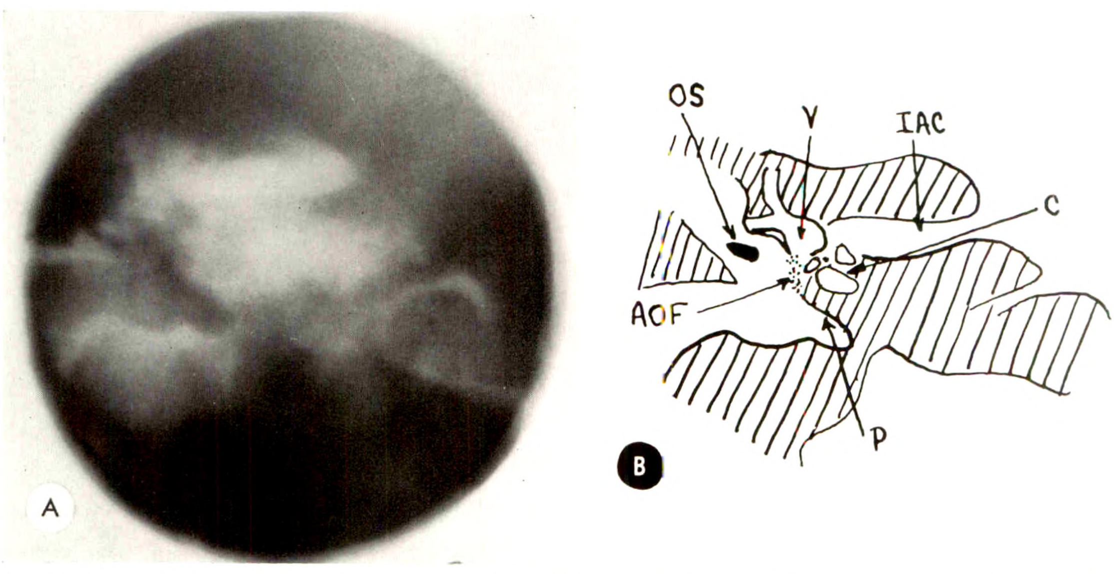


Fig. 8. (*A* and *B*) Otospongiotic involvement. Notice the demineralization of the promontory adjacent to the oval window producing the false impression of enlargement of the oval window. AOF = active otospongiotic focus; C = cochlea; IAC = internal auditory canal; OS = ossicles; P = promontory; V = vestibule.

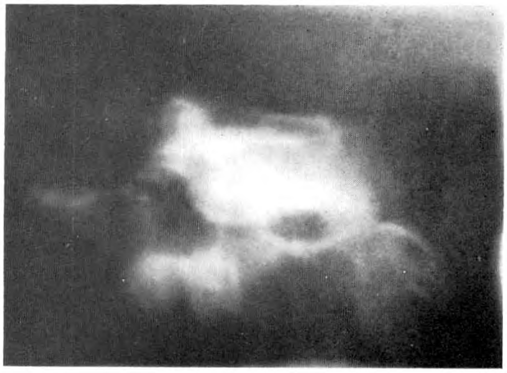

Fig. 10. Normal labyrinthine capsule. Notice the sharpness of the capsule and of the lumen of the basilar turn of the cochlea.

which is not always proportional to the functional impairment. We have observed roentgenographic findings which might represent different features of the same process as it progresses. Some cases show irregularities in the normally smooth and homogeneous line of density cast by the labyrinthine capsule with areas of thickening alternated with others of thinning (Fig. 10 and 11). Small foci of sclerosis may be mixed with the more radiolucent areas (Fig. 12). The roentgenographic appearance is very similar to the changes seen in the skull in Paget's disease. The most extensive type of involvement is characterized by a complete loss in the contrast between the capsule and the lumina of the inner ear structures (Fig. 13). These findings are the result of the combination of changes clearly described by Nylén on histologic sections,

Fig. 12. Otosclerosis of the labyrinthine capsule. Same changes as in Figure 11 with the addition of small foci of sclerosis throughout the basilar turn of the cochlea.

consisting in demineralization of the capsule and obliteration of the lumina of the cochlea, vestibule and semicircular canals by otosclerotic foci.

## DISCUSSION

The importance of the roentgenographic study in otosclerosis is summarized in the following points:

1. *As a Diagnostic Test in Questionable Cases.* Usually, the diagnosis of otosclerosis is made on the basis of the clinical history and audiometric test. Occasionally, the diagnosis of a patient with conductive hearing loss remains uncertain. This is espe-

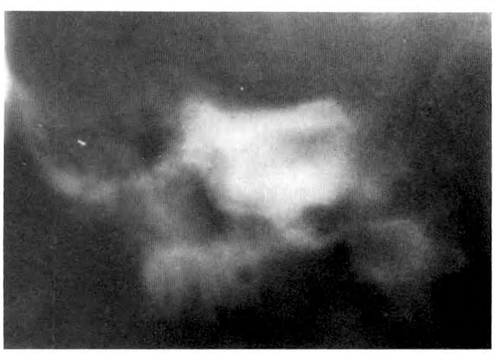

Fig. 11. Otosclerosis of the labyrinthine capsule. Areas of thinning are noticed in the capsule of the promontory.

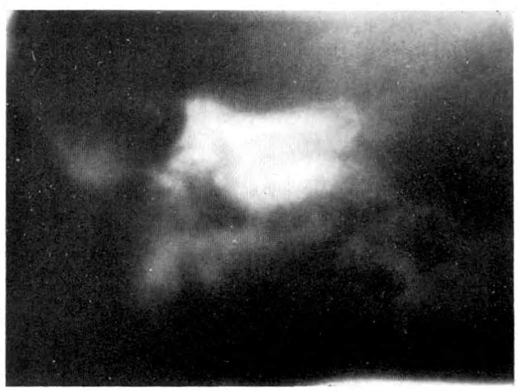

Fig. 13. Otosclerosis of the labyrinthine capsule. Complete loss in the contrast between the capsule and the lumen of the basilar turn of the cochlea.

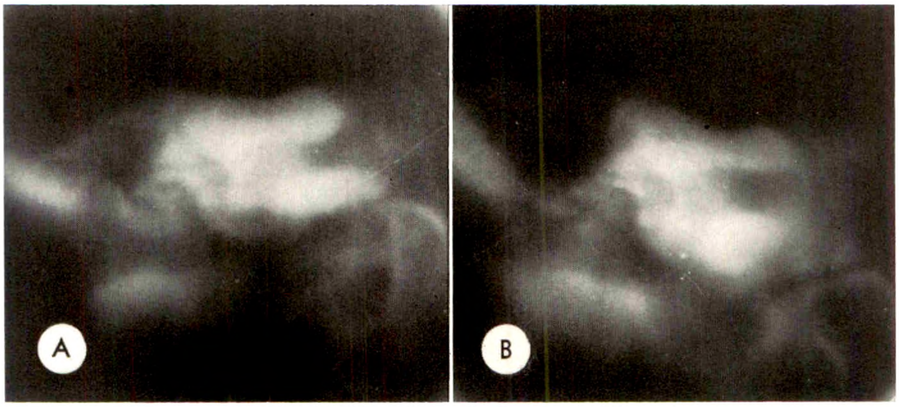

Fig. 14. (*A*) Frontal section shows complete obliteration of the oval window by a very thick footplate of the stapes. (*B*) Same patient after stapedectomy and insertion of a polyethylene strut with vein graft: the oval window appears fully open.

cially true when the picture is complicated by the superimposition of chronic or old inflammatory processes which might have produced the same audiometric findings through other means of involvement. In cases of sensory neural loss of unknown origin, the roentgenographic examination may establish the diagnosis of labyrinthine otosclerosis.

2. *Evaluation of the Type, Degree and Extension of the Process.* This information cannot be obtained by audiometry, the findings of which are not in direct relationship to the severity of the process. The presence of an otospongiotic process, the extension to the labyrinthine capsule and the obliteration of the oval window niche are considered by most of the otosurgeons as contraindication to a surgical procedure. The risk of damaging the membranous labyrinth with a resulting worsening of the hearing and the incidence of recurrence of the process in a very short time after surgery are very high in these instances.

3. *Selection of Side for Corrective Surgery.* Since the involvement by otosclerosis is bilateral in 80 per cent of the cases and since the surgical risk of permanent damage is approximately 1 to 2 per cent, the side selected for corrective surgery has been so

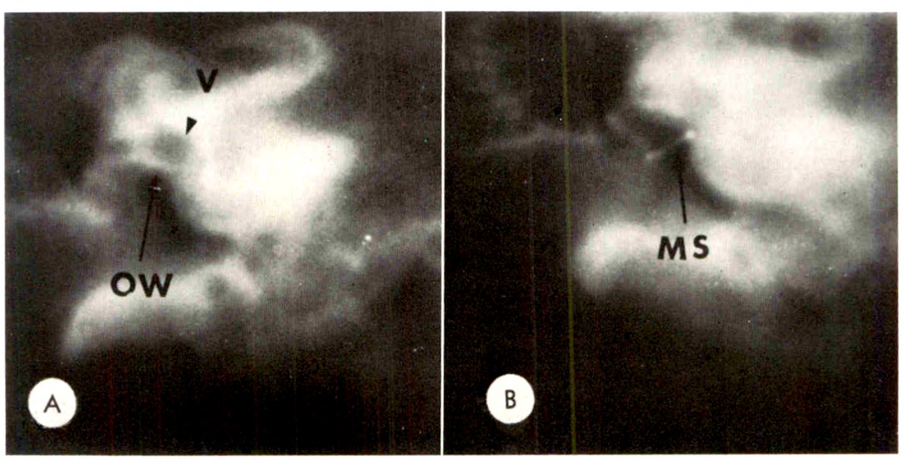


Fig. 15. (*A*) Frontal section shows almost complete obliteration of the oval window by a thick footplate of the stapes. (*B*) Same case after stapedectomy and insertion of a tantalum prosthesis with fat graft shows the oval window reopened and the metallic strut in good position. MS = metallic strut; OW = oval window; V = vestibule.

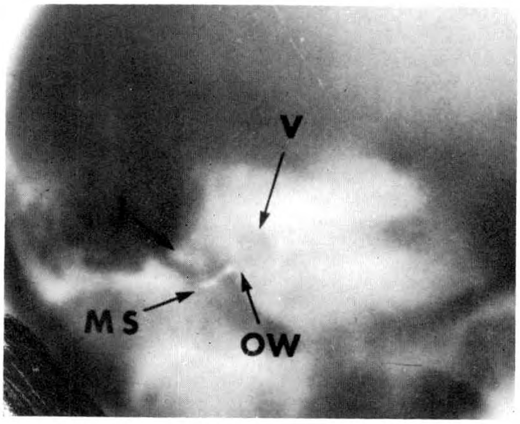


Fig. 16. Same case as in Figure 8, *A* and *B* shows recurrence of the otosclerotic process underneath the vestibular end of the metallic prosthesis 5 months after surgery. I = incus; MS = metallic strut; OW = oval window; V = vestibule.

far the poorest as demonstrated by audiometric tests. In cases with an even hearing loss, the side for surgery is chosen by the patient or by the surgeon without any specific indication. We have proved in several cases that these rules should be completely revised by the introduction of a test which allows for the first time a preoperative visualization of the involved area. In cases of equal deafness, the selection of the side for surgery should be based on the objective findings of the roentgenographic study which might show a significant difference in the involvement between the two sides. In some cases of uneven involvement, the roentgenographic study may show the contraindication of operating on the worst side and may indicate operation, in spite of the surgical risk, on the better side which offers good probability of a successful result.

4. *Demonstration of Possible Abnormalities of the Adjacent Structures.* The facial nerve canal sometimes overhangs upon or covers part of the oval window, especially its superior and anterior segments. With this knowledge, the surgeon might elect to perform a partial rather than a complete stapedectomy in order to avoid damaging the facial nerve.

5. *Evaluation of the Postsurgical Status* (Fig. 14, *A* and *B;* and 15, *A* and *B*). Roentgenography is of value to the otologist in the evaluation of patients who show deterioration of hearing after a transitory improvement following surgery. There are two common reasons for such a relapse. The applied prosthesis might slip out of position at one or both ends with consequent discontinuity of the restored sound pathway. If a metallic prosthesis has been used, this can be demonstrated by the roentgenographic examination. The otosclerotic process can recur with closure of the oval window either underneath the vestibular tip of the prosthesis (Fig. 16) or around it with consequent fixation. We recommend an examination of the operated ear a few weeks after surgery. This examination serves as a baseline for future examinations in the event of deteriorating hearing and permits recognition of even minimal changes.

6. In the event of the discovery of a successful nonsurgical treatment for labyrinthine otosclerosis, the roentgenographic demonstration will become of utmost importance, since there is no other way of visualizing the labyrinthine capsule in living patients.

Department of Radiology
The University of Chicago
950 East 59th Street
Chicago, Illinois 60637

I would like to express my gratitude to Dr. John Lindsay and to the other members of the Department of Otolaryngology of The University of Chicago, without whose cooperation this work would have been impossible.

REFERENCES

1. Compere, W. E., Jr. Radiologic findings in otosclerosis. *A.M.A. Arch. Otolaryng.*, 1960, *71*, 150–155.
2. Compere, W. E., Jr. Radiographic Atlas of the Temporal Bone. Book 1. American Academy of Ophthalmology and Otolaryngology, 1964.
3. François, J., and Barrois, J. J. Anatomie tomographique de l'os temporal normal. *Ann. de radiol.*, 1959, *2*, 71–98.
4. Graham-Hodgson, H. K. In: A Textbook of

X-ray Diagnosis. Volume I. Edited by S. C. Shanks and P. Kerley. H. K. Lewis & Co., Ltd., London, 1957, p. 480.
5. Guild, S. R. Histologic otosclerosis. *Ann. Otol., Rhin. & Laryng.*, 1944, *53*, 246–266.
6. Mündnich, K., and Frey, K. W. Das Röntgenschichtbild des Ohres. Georg Thieme Verlag, Stuttgart, 1959.
7. Nager, F. R., and Fraser, J. S. On bone formation in scala tympani of otosclerotics. *J. Laryng. & Otol.*, 1938, *53*, 173–180.
8. Nylén, B. Histopathological investigations on localization, number, activity and extent of otosclerotic foci. *J. Laryng. & Otol.*, 1949, *63*, 321–327.
9. Portmann, G., Portmann, M., and Claverie, G. La Chirurgie de la Surdité. Librarie Arnette, Paris, 1959.
10. Portmann, M., and Guillen, G. Radiodiagnostic en Otologie. Masson & Cie, Paris, 1959.
11. Shambaugh, G. E., Jr. Surgery of the Ear. W. B. Saunders Company, Philadelphia, 1959.
12. Valvassori, G. E. Laminagraphy of ear: normal roentgenographic anatomy. Am. J. Roentgenol., Rad. Therapy & Nuclear Med., 1963, *89*, 1155–1167.
13. Valvassori, G. E. Discussion of "The Temporal Bone," by M. Portmann. *A.M.A. Arch. Otolaryng.*, 1963, *78*, 347–350.
14. Valvassori, G. E. Radiographic Atlas of the Temporal Bone. Book II. American Academy of Ophthalmology and Otolaryngology, 1964.

# THE CINEROENTGENOGRAPHIC OBSERVATION OF PANTOPAQUE INTRAVASATION DURING MYELOGRAPHY*

*By* BERNARD S. EPSTEIN, M.D., *and* JOSEPH A. EPSTEIN, M.D.
NEW HYDE PARK, NEW YORK

THE inadvertent instillation of pantopaque into the spinal venous circulation is predicated upon the intrusion of the bevel of the lumbar puncture needle into an epidural vein or into the intramedullary basivertebral system (Fig. 1). A review of the literature discloses but 6 reported instances of this occurrence. The observation of the actual entrance of pantopaque into the dorsal venous plexus of the lower lumbar spine during myelography by means of image intensification fluoroscopy and the spot film and cineroentgenographic recording of this phenomenon adds interest to the present case.

## REPORT OF A CASE

P.B., a 49 year old man, complained of increasing difficulty in picking up objects with his right hand for about 2 months. This was associated with numbness and tingling of his forearm and hand. While first occurring during effort, similar disturbances appeared later at rest together with transient mild neck and interscapular pain. About 1 month before admission, similar sensations appeared in his left hand. The patient also had noted progressively diminished sexual capacity for about 4 years. He had had poliomyelitis at the age of 15 months which left him with a short and weakened right lower extremity.

Physical examination disclosed marked weakness and atrophy of the right shoulder girdle and proximal flexor muscles. Some fasciculation was present in his left shoulder and right arm. No pathologic reflexes were elicited. The deep tendon reflexes and the abdominal and cremasteric reflexes were intact.

Roentgenographic examination of his chest, thoracic and lumbosacral spine was normal. Diffuse spondylosis of the cervical vertebrae was present, characterized by marked narrowing of the interspaces between the fourth, fifth, sixth and seventh cervical vertebrae, dorsal spurring and narrowed intervertebral foramina encroached upon by osteophytic overgrowths. The anteroposterior diameter of the cervical canal at the level of the fifth, sixth and seventh interspaces was 1.2 cm. This was regarded as significant narrowing. Myelography was suggested.

The clinical diagnosis was amyotrophic lateral sclerosis. It was agreed that myelographic examination was indicated to rule out a cervical ridge syndrome or a spinal cord tumor.

A lumbar puncture revealed clear colorless cerebrospinal fluid. It was not possible to obtain manometric readings. The total protein content was 30 mg. per cent, chloride content 126 mEq./l. and glucose 86 mg. per cent. The study was followed by an intense headache which subsided in about a week.

Myelography was then performed. A lumbar puncture needle was introduced into the fifth lumbar interspace with the patient in the sitting position. A free flow of clear cerebrospinal fluid was obtained. As part of a study of the cineroentgenographic aspects of myelography, the examination was begun after the patient was placed face down on the fluoroscopic table. The spinal needle was connected to a syringe containing 12 cc. of pantopaque by way of a two-way stopcock and a sterile venotube filled with pantopaque. The injection was instituted with gentle finger pressure after the cineroentgenographic recording was started, the process being monitored by image intensification. The first droplet injected was seen to gather around the needle tip (Fig. 2). Instead of entering the subarachnoid space, the pantopaque assumed a rapidly changing but clearly defined pattern conforming to the intraspinal epidural venous system. The cineroentgenographic recording of the procedure was continued as about 1.5 cc. of pantopaque was injected. The venous channels to the right and left of the needle tip were opaci-

* From the Department of Radiology and the Division of Neurological Surgery, Department of Surgery, The Long Island Jewish Hospital, New Hyde Park, New York.


Fig. 1. Diagrammatic representation of bevel of lumbar puncture needle transfixing the subarachnoid space and an epidural vein. The arrows indicate the flow of blood into the subarachnoid space.

fied. Some of the pantopaque passed caudally as well as cephalad. The pantopaque entering the vessels to the left of the spinal canal then swung sharply to the right to enter the inferior vena cava together with that from the more axial veins and those to the right of the midline. Two spot roentgenograms were obtained. The pantopaque did not progress cephalad for more than one and a half vertebral segments before it emerged from within the canal and entered the inferior vena cava to the right of the vertebral column. Within about 5 seconds the veins were empty, the pantopaque having passed in discrete round and elongated oval globules to the level of the diaphragm where they could no longer be followed. The patient noted nothing unusual either during or after the procedure (Fig. 3, *A* and *B*).

The needle was removed, and with the patient sitting it was reinserted into the third lumbar interspace. A free flow of clear cerebrospinal fluid was obtained and the patient again was placed face down on the fluoroscopic table. The instillation of pantopaque was instituted using the same method of injection under image intensification fluoroscopic control, and 12 cc. readily entered the subarachnoid space. No deformities were seen in the lumbar canal. The passage through the lumbar and thoracic spinal canal was rapid. A partial block was seen at the level of the interspace between the seventh cervical and first thoracic vertebra. The pantopaque then entered narrow lateral channels embracing a widened and flattened spinal cord at the level of the fifth, sixth and seventh cervical vertebrae. After the examination was com-

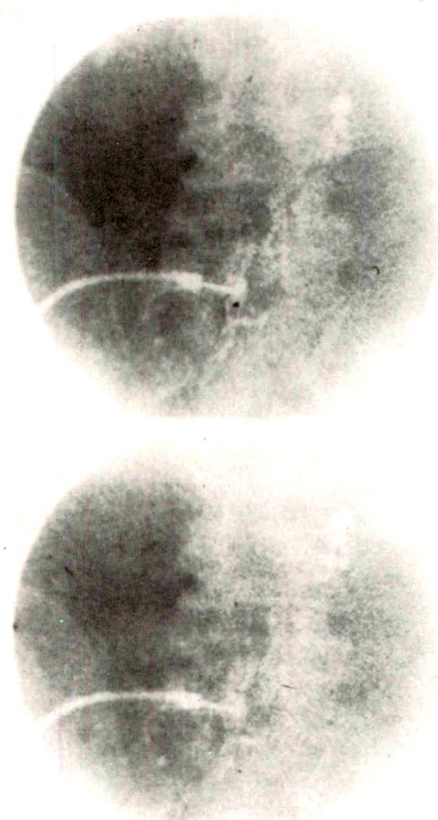

Fig. 2. Two frames from the 16 mm. cineroentgenographic record of the intravasation of pantopaque into the dorsal epidural plexus. A droplet of pantopaque is seen at the needle tip, situated at the lumbosacral interspace. The flow follows the venous pattern. Several droplets to the right of the spinal canal are in the inferior vena cava.

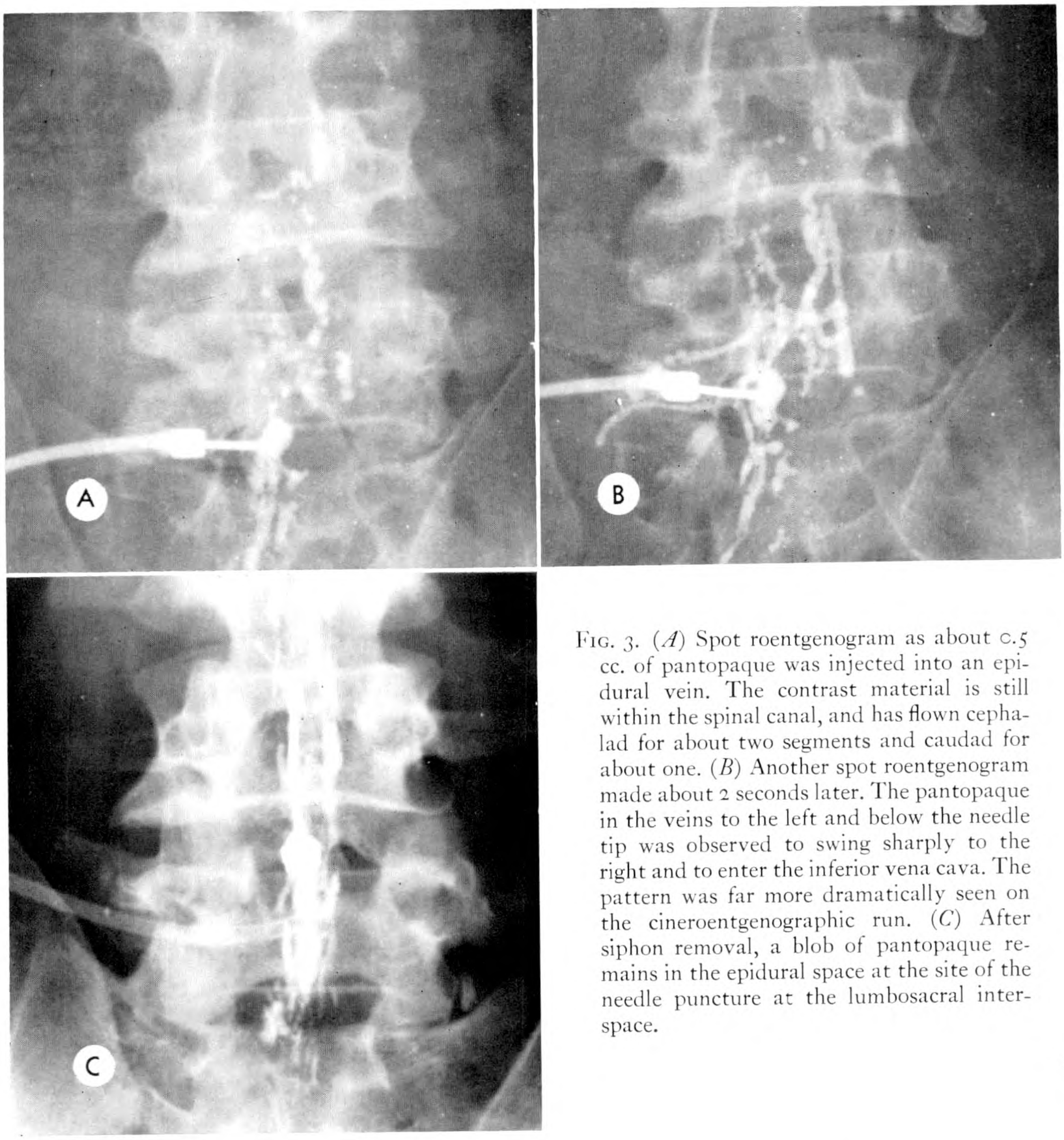


Fig. 3. (*A*) Spot roentgenogram as about 0.5 cc. of pantopaque was injected into an epidural vein. The contrast material is still within the spinal canal, and has flown cephalad for about two segments and caudad for about one. (*B*) Another spot roentgenogram made about 2 seconds later. The pantopaque in the veins to the left and below the needle tip was observed to swing sharply to the right and to enter the inferior vena cava. The pattern was far more dramatically seen on the cineroentgenographic run. (*C*) After siphon removal, a blob of pantopaque remains in the epidural space at the site of the needle puncture at the lumbosacral interspace.

pleted, most of the pantopaque was removed by siphonage (Fig. 3*C*).[2] A fleck persisted in the dorsal epidural space at the lumbosacral level, and some also remained between the thickened nerve roots of the cauda equina.

One hour after myelography roentgenographic examination of the chest was normal. Another chest roentgenogram the next day was unremarkable. The patient had no discomfort or distress after the examination. Surgical removal of the osteophytes by the anterior approach and anterior cervical spine fusion was performed by Dr. I. M. Greenberg.

COMMENT

Intravasation of pantopaque during myelography occurs by way of the dorsal or ventral peridural veins or the intramedullary venous circulation. Inspection of the vascular supply of the cauda equina in fresh specimens indicates that these structures are quite delicate and thin. The arteries follow along the lateral axis of the nerve roots and are easily identified. The veins are more difficult to demonstrate. It is most unlikely that either of these channels can be

pierced or entered by a lumbar puncture needle. Our impression is that bloody cerebrospinal fluid indicates the penetration of an epidural vein, blood entering the subarachnoid space through the needle tract in larger or smaller quantities. If the tip of the needle transfixes the subarachnoid space so that the bevel is situated both in a vein and in the space, a bloody issue of cerebrospinal fluid may be anticipated. This should warn one to discontinue the procedure and reinsert the needle at a higher or lower level. In the present case, the needle tip apparently moved while the patient was being positioned. Image intensification fluoroscopic control of the injection can be credited for the timely discontinuance of the procedure.

It is of interest that in the 7 reported cases, including the present one, clear cerebrospinal fluid was obtained in 3.[5,8] In 1[6] clear cerebrospinal fluid was first obtained, but a bloody tap was encountered when the needle was reinserted for the removal of pantopaque. Intravasation into the basivertebral system was reported by Ginsburg and Skorneck[4] and into the anterior peridural plexus by Todd and Gardner.[8] The latter mentioned that they had obtained clear cerebrospinal fluid at first, but that intravasation occurred when the needle tip was displaced anteriorly later in the examination.

The danger inherent in intravasation into the vertebral venous system is that of pulmonary embolism. In 4 instances[4,6,7,8] cough, chest pressure, weakness and fever were observed. No fatalities have been reported. Steinbach and Hill[7] mentioned that from 4 to 7.5 cc. of pantopaque must enter the venous circulation to produce symptoms. Roentgenographic evidence of pulmonary pantopaque embolism includes transient linear streaks, finely granular and small nodular infiltrates which disappear. It is of interest that considering the absence of valves in the epidural and perivertebral veins no central nervous system changes have been encountered. Perhaps this can be explained by the rapid flow towards the inferior vena cava rather than continuously cephalad, as observed in the present patient. Todd and Gardner[8] noted that in their patient the chest roentgenogram was negative, but that skull studies disclosed numerous linear streaks suggestive of an intracranial venous distribution of contrast medium. In view of the fact that their patient had had a thorotrast myelogram 14 years before pantopaque myelography, it is more likely that the changes noted may have been incident to the first myelogram.[1]

## SUMMARY

Intravasation of pantopaque into the epidural venous circulation was noted when myelography was performed. Cineroentgenographic recording and spot roentgenograms were obtained and the flow of the pantopaque was also observed by means of image intensification fluoroscopy.

Bernard S. Epstein, M.D.
The Long Island Jewish Hospital
270-05 76th Avenue
New Hyde Park, Long Island, New York

## REFERENCES

1. Epstein, B. S. The Spine: A Radiological Text and Atlas. Second edition. Lea & Febiger, Philadelphia, 1962, p. 518.
2. Epstein, B. S. Evacuation of pantopaque from lumbar spinal canal by siphon action. *Radiology*, 1964, *83*, 472–475.
3. Fullenlove, T. M. Venous intravasation during myelography. *Radiology*, 1949, *53*, 410–412.
4. Ginsburg, L. B., and Skorneck, A. B. Pantopaque pulmonary embolism: complication of myelography. Am. J. Roentgenol., Rad. Therapy & Nuclear Med., 1955, *73*, 27–31.
5. Hinkel, C. L. Entrance of pantopaque into venous system during myelography. Am. J. Roentgenol. & Rad. Therapy, 1945, *54*, 230–233.
6. Keats, T. E. Pantopaque pulmonary embolism. *Radiology*, 1956, *67*, 748–750.
7. Steinbach, H. L., and Hill, W. B. Pantopaque pulmonary embolism during myelography. *Radiology*, 1951, *56*, 735–738.
8. Todd, E. M., and Gardner, W. J. Pantopaque intravasation (embolization) during myelography. *J. Neurosurg.*, 1957, *14*, 230–234.

# HEMANGIOMA OF THE MEDIASTINUM*

## REPORT OF A CASE WITH COMPRESSION OF THE SPINAL CORD

*By* HERBERT TOCH, M.D.,† JACK W. C. HAGSTROM, M.D., *and* ISRAEL STEINBERG, M.D.‡
NEW YORK, NEW YORK

PRIMARY hemangiomas of the mediastinum are rare. Indeed, Ellis and his colleagues,[3] in 1955, after reporting a case and reviewing the literature, found only 18 additional cases. To date, about 70 cases of mediastinal hemangiomas have been recorded.[1,2,4,7–10] The case herein reported is unusual because of the presence of secondary osteolysis of the spine which caused compression of the thoracic spinal cord and paralysis of the legs. Laminectomy, preceded by irradiation of the tumor, was curative; the patient died of an unrelated cerebrovascular accident 7 years later.

### REPORT OF A CASE

A 55 year old Caucasian butcher (N.Y.H. No. 730500) was admitted on January 30, 1956 complaining of numbness of the toes, burning of the soles of the feet, intermittent claudication of the lower extremities, and a band-like constricting sensation of the knees and feet of 3 months' duration. Six weeks earlier, a routine roentgenogram of the chest showed a tumor. For the 20 days prior to admission he received a series of daily roentgen treatments to the tumor (dosage unknown) without relief of symptoms. Physical examination of the heart and lungs was normal; the blood pressure was 130/80 mm. Hg. The gait was spastic, a band-like sensory defect from T8–T10 and weakness of the lower extremities were found. The deep tendon reflexes were markedly accentuated, there was ankle clonus bilaterally, and the superficial abdominal reflexes were absent. The lower extremity pulses were palpable except for absence of the left dorsalis pedis and posterior tibial artery pulses.

Roentgenograms of the chest showed a lobu-

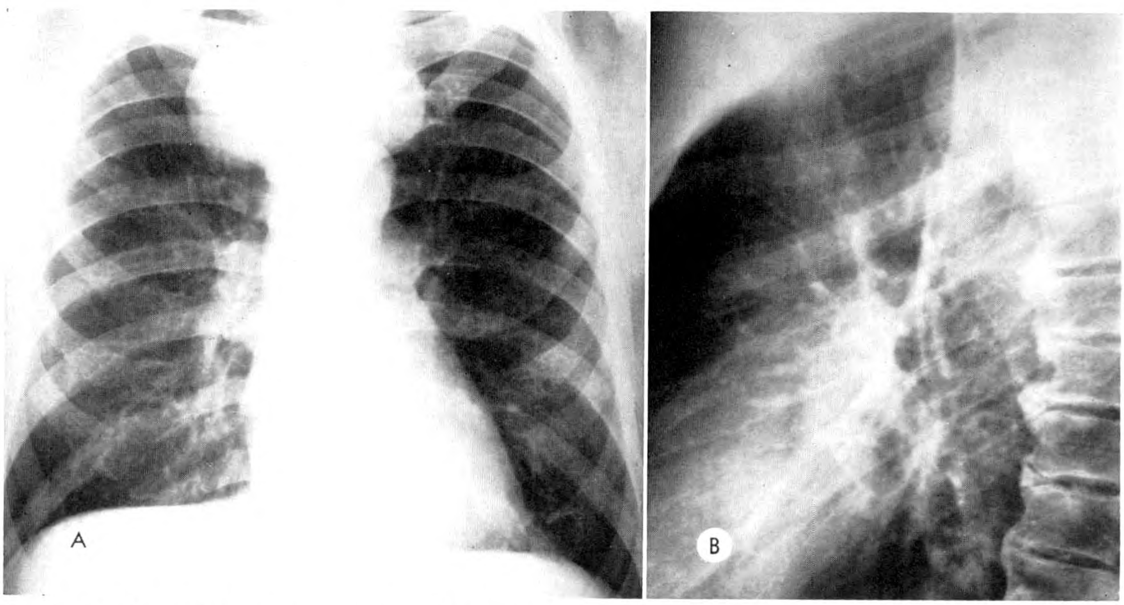


FIG. 1. (*A*) Frontal teleroentgenogram of the chest showing the rounded superior mediastinal tumor. (*B*) Lateral roentgenogram of the chest showing the posterior superior mediastinal location of the tumor.

* From the Departments of Radiology, Medicine, and Pathology, The New York Hospital-Cornell Medical Center, New York, New York.
† Now at New England Deaconess Hospital, Department of Radiology, Boston Massachusetts 02215.
‡ Recipient of Career Scientist Award of The Health Research Council of The City of New York under Contract I-258.

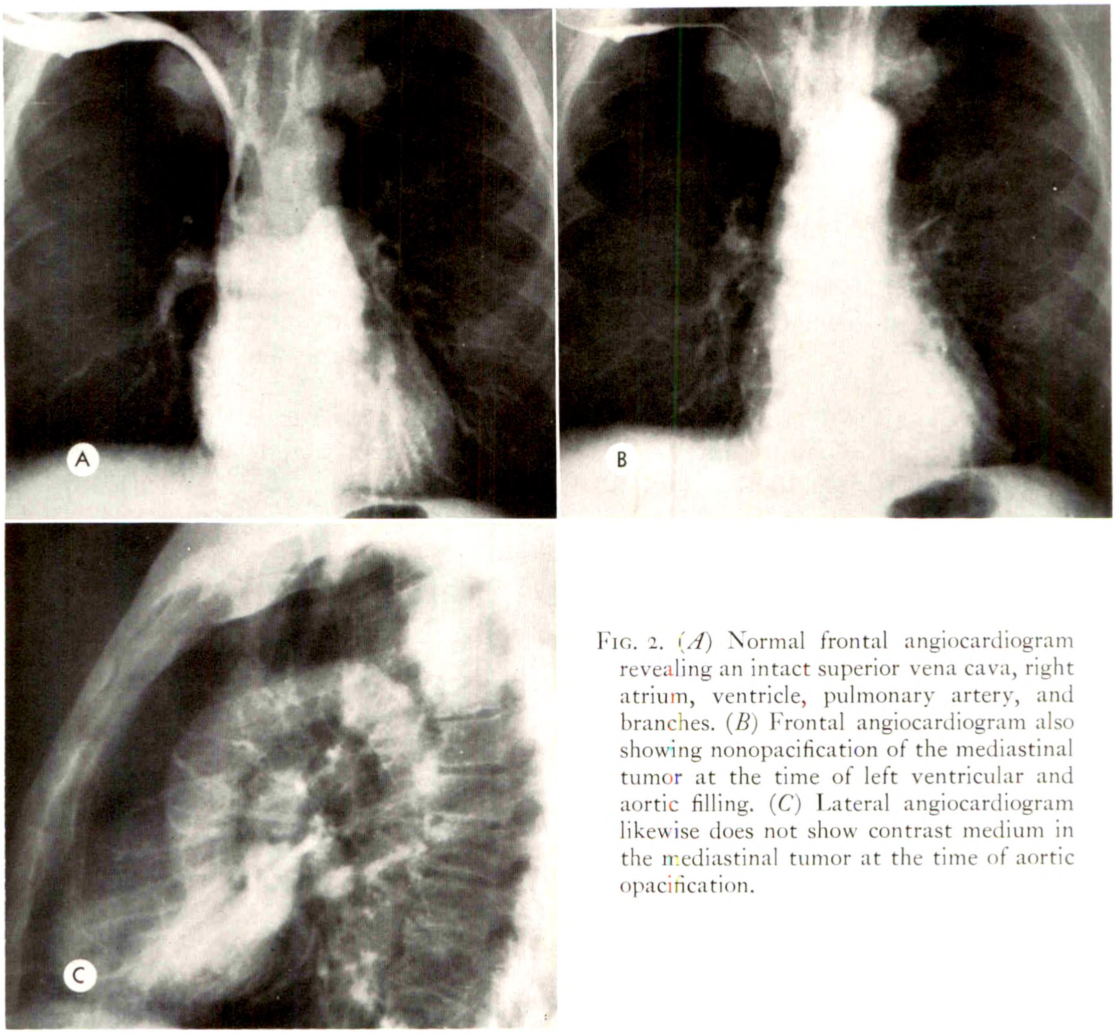


Fig. 2. (*A*) Normal frontal angiocardiogram revealing an intact superior vena cava, right atrium, ventricle, pulmonary artery, and branches. (*B*) Frontal angiocardiogram also showing nonopacification of the mediastinal tumor at the time of left ventricular and aortic filling. (*C*) Lateral angiocardiogram likewise does not show contrast medium in the mediastinal tumor at the time of aortic opacification.

lar posterior superior mediastinal mass (Fig. 1, *A* and *B*). Roentgenograms of the thoracic spine demonstrated irregular areas of sclerosis with radiolucency of the body of the fourth thoracic vertebra. Angiocardiograms, in frontal and lateral views, did not show involvement of the cardiovascular structures (Fig. 2, *A*, *B* and *C*). Because of extrinsic pressure on the spinal cord, a decompression laminectomy of the third, fourth and fifth thoracic vertebrae was performed on February 2, 1956. A thin cuff of extradural tumor tissue was found lying in the recess beneath the right fourth thoracic lamina. This was removed after ample decompression. Histologic examination of the resected specimen showed the tumor to be composed of a multitude of closely crowded endothelium-lined spaces which varied in size and contained blood (Fig. 3). These were admixed with fragments of bone and loose stromal tissue.

Postoperatively, the patient improved rapidly and was discharged on the twentieth day following operation. When seen, on February 1, 1960, he was well and working daily. In June, 1963, he sustained a cerebrovascular accident, developed hemiplegia, became bedridden, and died on November 24, 1963. An autopsy was not performed.

## DISCUSSION

The criteria for diagnosis of a hemangioma of the mediastinum are: a benign neoplasm that is limited to the mediastinum, composed of numerous endothelium-lined vascular channels of varying size, and

encapsulated or locally invasive, but without evidence of metastasis.[3] Although a biopsy of the main tumor mass was not obtained from the patient described above, the portion of the tumor which was removed from the vertebral canal showed it to be a capillary hemangioma with secondary osteolysis (Fig. 3).

The roentgenographic findings in 2 other patients with mediastinal tumors studied at this center resembled those in this case. Histologic study, however, showed them to be mesenchymomas of the mediastinum.[5] In the case of mediastinal hemangioma described above and in those reported in the literature,[3,7] the conventional roentgenograms revealed distinctly rounded borders of the mediastinal mass (Fig. 1, *A* and *B*). The lateral view was essential to clearly delineate the location of the tumor in the mediastinum; *i.e.*, whether it is in the anterior, middle or posterior plane. Apparently, only 25 per cent are in the posterior mediastinum.[7] Angiocardiography, in our case, as well as those reported in the literature, was of no value in making the diagnosis. Despite the vascular nature of the tumor, radiopacity of the mass was not seen. This is probably because the connections between the tumor and afferent vessels have a narrow lumen. Also, the vessels in the tumor are small and have a tendency to thrombose and calcify. These factors thwart opacification. Angiocardiography, however, even though it fails to establish the diagnosis of mediastinal hemangioma, is valuable because it differentiates vascular masses such as aneurysms, buckled veins or arteries, and other vascular anomalies from tumors in the mediastinum.[11]

In the literature, doubt is expressed that radiation therapy is of value for treatment of mediastinal hemangiomas.[3] Surgical exploration and biopsy are advocated in every patient with a mediastinal tumor to verify the diagnosis. If the tumor proves to be a hemangioma and is invasive and not completely resectable, radiation therapy is indicated.

The patient reported above enjoyed good

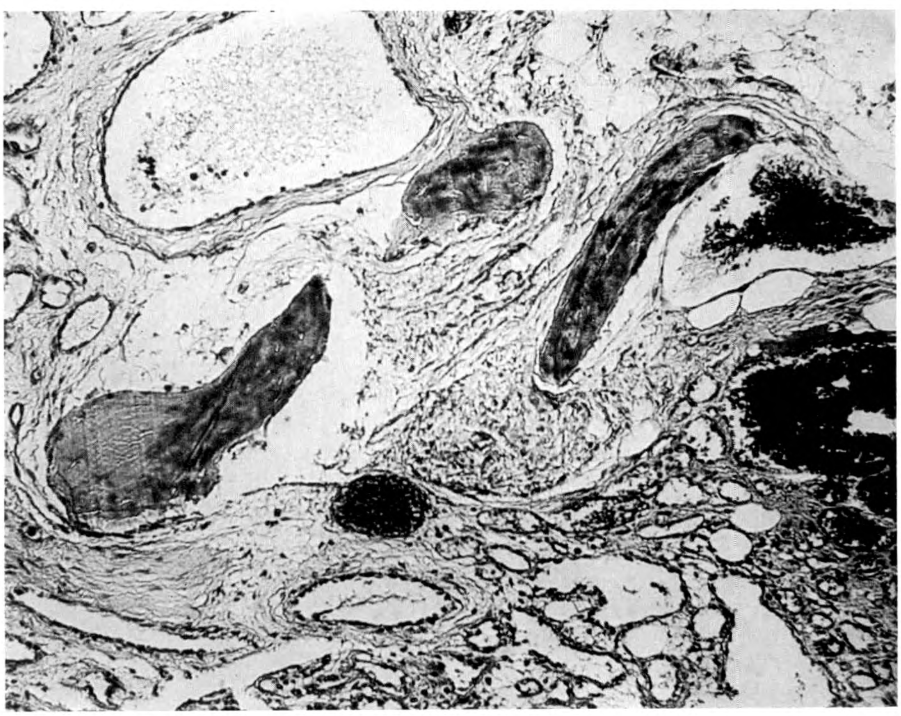

FIG. 3. Photomicrograph of resected epidural capillary hemangioma showing multiple blood-filled, endothelium-lined, vascular channels (hematoxylin and eosin, ×230).

health for a period of 7 years after laminectomy and irradiation of the mediastinal hemangioma. Re-examination of the histologic sections from the patient reported as having a mediastinal hemangioma by Keegan[6] showed a mediastinal mesenchymoma with a prominent vascular component.[5] She, too, is well 14 years following irradiation of the tumor.[5]

## SUMMARY AND CONCLUSIONS

A 55 year old man with paralysis of both lower extremities was improved after irradiation of a posterior mediastinal mass and decompression laminectomy, which alleviated spinal cord compression and secondary hemiplegia. Following this, the patient made an uneventful recovery; death 7 years later was due to an unrelated cerebrovascular accident. Histologic examination of the biopsied portion of the tumor showed it to be an invasive capillary hemangioma with secondary osteolysis of the fourth thoracic vertebra.

Israel Steinberg, M.D.
The New York Hospital—Cornell Medical Center
525 East 68th Street
New York, New York 10021

## REFERENCES

1. BALBAA, A., and CHESTERMAN, J. T. Neoplasms of vascular origin in mediastinum. *Brit. J. Surg.*, 1957, *44*, 545–555.
2. DIXON, W. M., and LAIRD, R. Haemangioma of mediastinum. *Thorax*, 1956, *11*, 45–48.
3. ELLIS, F. H., JR., KIRKLIN, J. W., and WOOLNER, L. B. Hemangioma of mediastinum, review of literature and report of case. *J. Thoracic Surg.*, 1955, *30*, 181–186.
4. FEINBERG, S. B. Posterior mediastinal hemangioma. *Radiology*, 1957, *68*, 90–93.
5. HAGSTROM, J. W. C., and STEINBERG, I. Mediastinal mesenchymoma. To be published.
6. KEEGAN, J. M. Hemangioma of mediastinum: case report. AM. J. ROENTGENOL., RAD. THERAPY & NUCLEAR MED., 1953, *69*, 66–68.
7. LEIFOVICI, D., and ONER, V. Hemangioma of posterior mediastinum: review of literature and report of case. *Am. Rev. Resp. Dis.*, 1962, *86*, 415–419.
8. MEREDITH, J. M., LYERLY, J., JR., BOSHER, L., JR., KAY, S., and OLD, L. Hemangioma of posterior mediastinum with cord compression in midthoracic region: multiple-stage operations with postoperative improvement. *J.A.M.A.*, 1958, *166*, 484–488.
9. PERÄSALO, O. Mediastinal haemangioma. *Thorax*, 1952, *7*, 178–181.
10. ROSENBERG, D. Hemangioma of mediastinum. *Am. J. Surg.*, 1962, *103*, 749–754.
11. STEINBERG, I. Angiocardiographic investigation in differential diagnosis of mediastinal and vascular tumors. *J. Internat. Coll. Surgeons*, 1963, *39*, 10–22.

# FRACTURE OF PARS INTERARTICULARIS OF LUMBAR VERTEBRA*

*By* ABRAHAM MELAMED, M.D.
MILWAUKEE, WISCONSIN

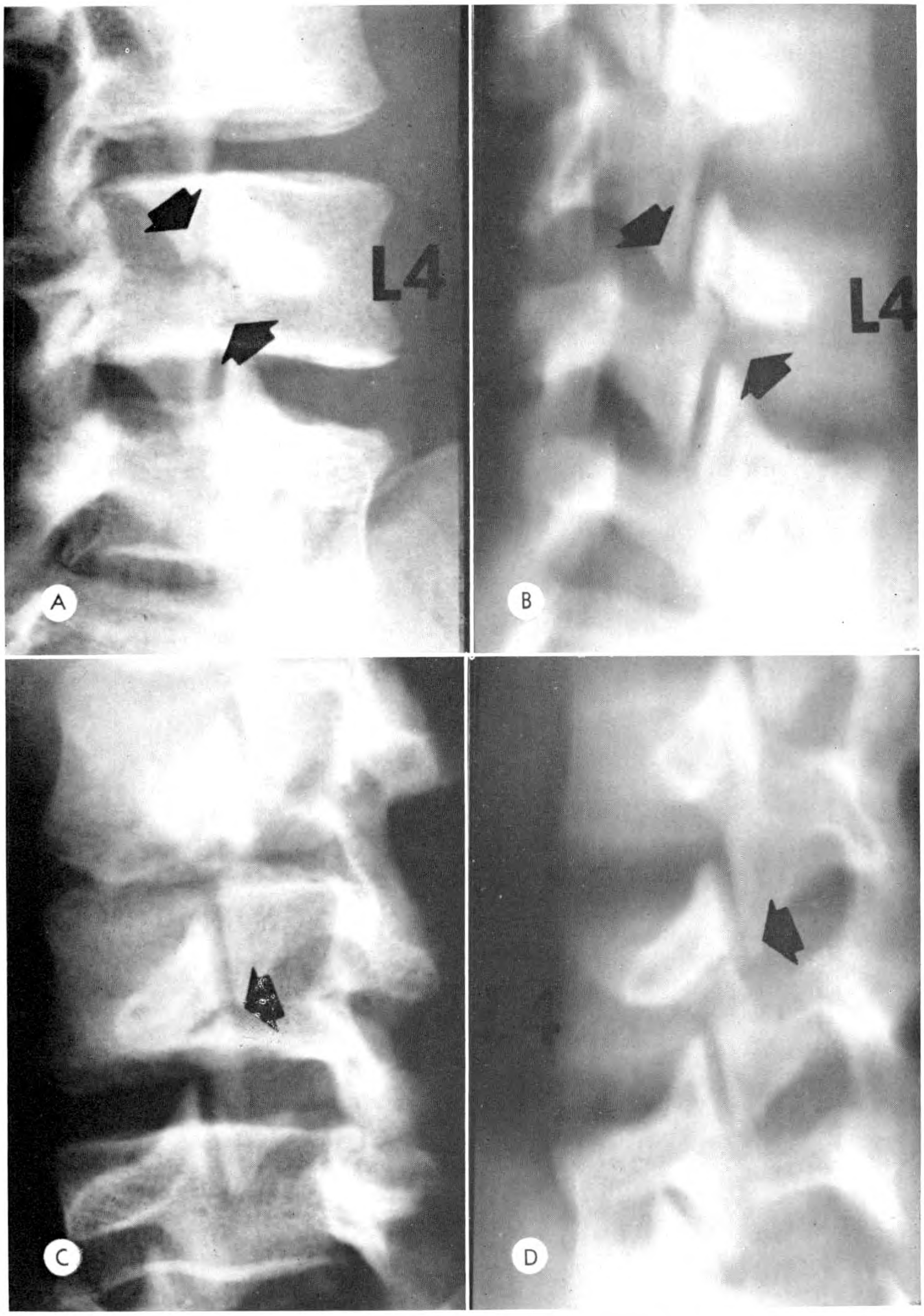


FIG. 1. (*A–D*) Plain roentgenograms and oblique laminagrams obtained in 1958 show fracture lines in both isthmi of L4 vertebra.

* From the Department of Radiology, Evangelical Deaconess Hospital, Milwaukee, Wisconsin.

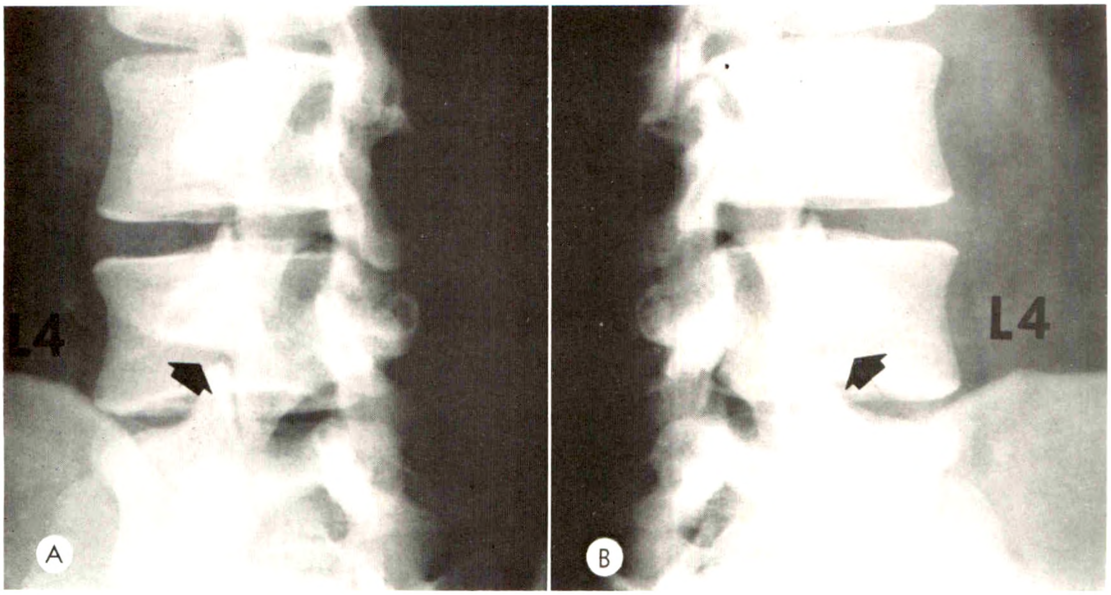


Fig. 2. (*A* and *B*) Oblique roentgenograms obtained in 1964 show complete healing of bilateral pars interarticularis fractures.

There are few proved or recorded cases of spondylolysis due to fracture sustained after severe trauma and which eventually healed. The purpose of this paper is to record a case of bilateral fractures of the partes interarticulares of the fourth lumbar vertebra, in which complete healing was demonstrated 5 years later.

## REPORT OF A CASE

J. H., a 15 year old male, entered Evangelical Deaconess Hospital (service of Dr. T. F. Garland) after two football injuries of the lower back in 1958. Such injuries were sustained 14 and 2 days before admission to the hospital. When he arose from a "pile-up" of football players 2 days before admission, he experienced sharp pain in the lower back region. The back pain resulting from the first football injury was definitely aggravated. The pain was increased by side to side and forward and backward bending. Physical examination showed no abnormality except pain in the lower back on moving in bed. All reflexes were physiologic. No deformity of the back was visible. Roentgenograms of the spine, obtained October 18, 1958, revealed bilateral pars interarticularis defects in the fourth lumbar vertebra without displacement. Oblique views showed jagged fracture lines in both isthmi of the fourth lumbar vertebra (Fig. 1, *A–D*).

After a few days' bed rest in the hospital and being fitted with a back brace, the patient was discharged. He wore the brace for 6 months and never experienced any discomfort or pain after discontinuing the use of the brace.

Roentgenograms obtained on February 10, 1964 (Fig. 2, *A* and *B*) showed no defects in the interarticular portions of the fourth lumbar vertebra. Healing of the fractures sustained in 1958 was complete with dense calcification.

## COMMENT

Roche,[2] in 1948, was probably the first to document the healing of a fracture of the pars interarticularis of a lumbar vertebra. Wiltse,[4] in 1957, described 1 case of fracture through the pars interarticularis which healed solidly. Sullivan and Bickell,[3] in 1960, reported 3 patients with disruption of the pars interarticularis due to severe trauma which healed with immobilization. The disruption in their cases occurred in the lumbar vertebrae immediately above spinal fusions. In 1962, Wiltse[5] described a patient in whom eventual healing of 2 of 3 fractured partes interarticulares was observed. Lambert and Billings'[1] case of traumatic spondylolisthesis with eventual healing was mentioned by Wiltse.[5]

Although there may be some controversy or disagreement concerning the etiology of the average or "typical" case of spondylolysis and spondylolisthesis, the evidence cited above is proof of the fact that some cases of spondylolysis are due to true fractures of the pars interarticularis and that healing of such fractures can and does occur much in the same fashion as in fractures occurring elsewhere.

620 North 19 Street
Milwaukee, Wisconsin 53233

REFERENCES

1. LAMBERT, R. G., and BILLINGS, E. L. Traumatic spondylolisthesis. Paper read at the Annual Meeting of Western Orthopedic Association, Coronado, California, 1960.
2. ROCHE, M. B. Bilateral fracture of pars interarticularis of lumbar neural arch. *J. Bone & Joint Surg.*, 1948, *30A*, 1005–1008.
3. SULLIVAN, C. R., and BICKELL, W. H. Problem of traumatic spondylolysis: report of three cases. *Am. J. Surg.*, 1960, *100*, 698–708.
4. WILTSE, L. L. Etiology of spondylolisthesis. *Clin. Orthop.*, 1957, *10*, 48–58.
5. WILTSE, L. L. Etiology of spondylolisthesis. *J. Bone & Joint Surg.*, 1962, *44A*, 539–560

# INTRATHORACIC RIB*

*By* AARON S. WEINSTEIN, M.D., *and* CHARLES F. MUELLER, M.D.
CINCINNATI, OHIO

INTRATHORACIC rib is evidently an extremely rare anomaly, only 9 cases having been reported previously. Its significance lies in recognizing it as an innocuous thoracic shadow on the chest roentgenogram, one not to be mistaken for other more serious lesions.

This report was prompted by a 23 year old white man, who came to the Cincinnati Veterans Hospital for an evaluation of a pilonidal cyst and with the recent complaint of a cough. Physical examination revealed the pilonidal cyst but was otherwise negative. A posteroanterior chest roentgenogram showed an interesting ribbon-like shadow extending from the right border of the spine inferiorly and laterally to the medial right hemidiaphragm (Fig. 1). Fluoroscopy revealed that it lay intrathoracically, close to the posterior thoracic wall. Laminagraphy demonstrated that the abnormal shadow had a bony cortex and articulated with the spine (Fig. 2, *A* and *B*).

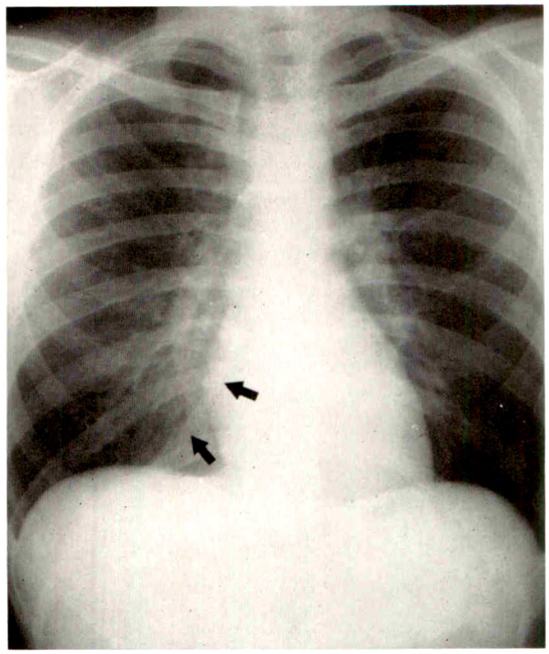

Fig. 1. Routine chest roentgenogram showing a ribbon-like shadow on the right extending from the mid-dorsal spine to the right hemidiaphragm.

## REVIEW OF THE LITERATURE

Despite the frequency of rib anomalies—1 per cent of the normal population[7]—intrathoracic rib is extremely uncommon.

The first description was by Lutz,[2] in 1947. He reported a 25 year old woman who complained of a poorly defined pain in her left side. The chest roentgenogram revealed a peculiar "forking" of the right fourth rib. One branch ended blindly, while the other, an inferior branch, connected to the diaphragm by a band of soft tissue density. There were no other congenital anomalies. Additional surgical and pathologic proof was not mentioned.

Jacobs[1] reported the first autopsy proven case in 1949 in a 43 year old man with far advanced pulmonary tuberculosis. The anomalous rib originated from the right third thoracic vertebral body and coursed laterally and inferiorly, external to the pleura, ending at the eighth rib posterolaterally. The spinal articulation of the normal right third rib was independent of that of the anomalous rib.

In 1953, Marbut and DeGinder[3] reported a 20 year old woman on whom the diagnosis was made roentgenologically. The patient described severe stabbing pain in her right scapula, provoked by exertion and prolonged sitting. She had suffered an injury to her thoracic spine in childhood and subsequently developed intermittent episodes of right chest wall pain which she attributed to the accident. The supernumerary rib articulated with the right anterior margins of the sixth and seventh thoracic vertebral bodies at the interspace

* From the Department of Radiology, Cincinnati Veterans Administration Hospital, and the University of Cincinnati College of Medicine.

and apparently its distal end protruded into lung tissue. The authors theorized that friction between two layers of pleura surrounding the rib accounted for her pain. She was lost to follow-up.

Stevenson and Merendino,[5] in 1956, described a 17 year old girl with two right-sided intrathoracic ribs proven at thoracotomy. They arose from the right sixth and seventh vertebral bodies and coursed posteriorly, laterally and inferiorly. They were covered by parietal pleura and had distal fibrous attachments to the right hemidiaphragm, causing massive tenting of its surface. No mention was made of these ribs penetrating the lung; however, it appeared that they projected into the pleural space while maintaining a pleural covering of their own.

In 1957, Plum *et al.*[4] described a 9 year old asymptomatic girl who, on a routine chest roentgenogram, was suspected of having a mediastinal lesion. Surgical exploration revealed a supernumerary rib arising from the right sixth vertebral margin anterior to the normally articulating right sixth rib.

Also in 1957, Wilk and Hülshoff[9] reported an intrathoracic rib in an asymptomatic 12 year old boy. This was the first left-sided anomalous rib; it originated from the sixth rib as a kind of bifurcation.

Whitlark and Engels,[8] in 1962, reported a 16 year old asymptomatic girl with a left-sided intrathoracic rib and a right-sided aortic arch. The diagnosis was made from the roentgen findings.

The same year Von Ronnen and Jongh[6] introduced the intrathoracic rib to the radiological literature with 2 case pres-

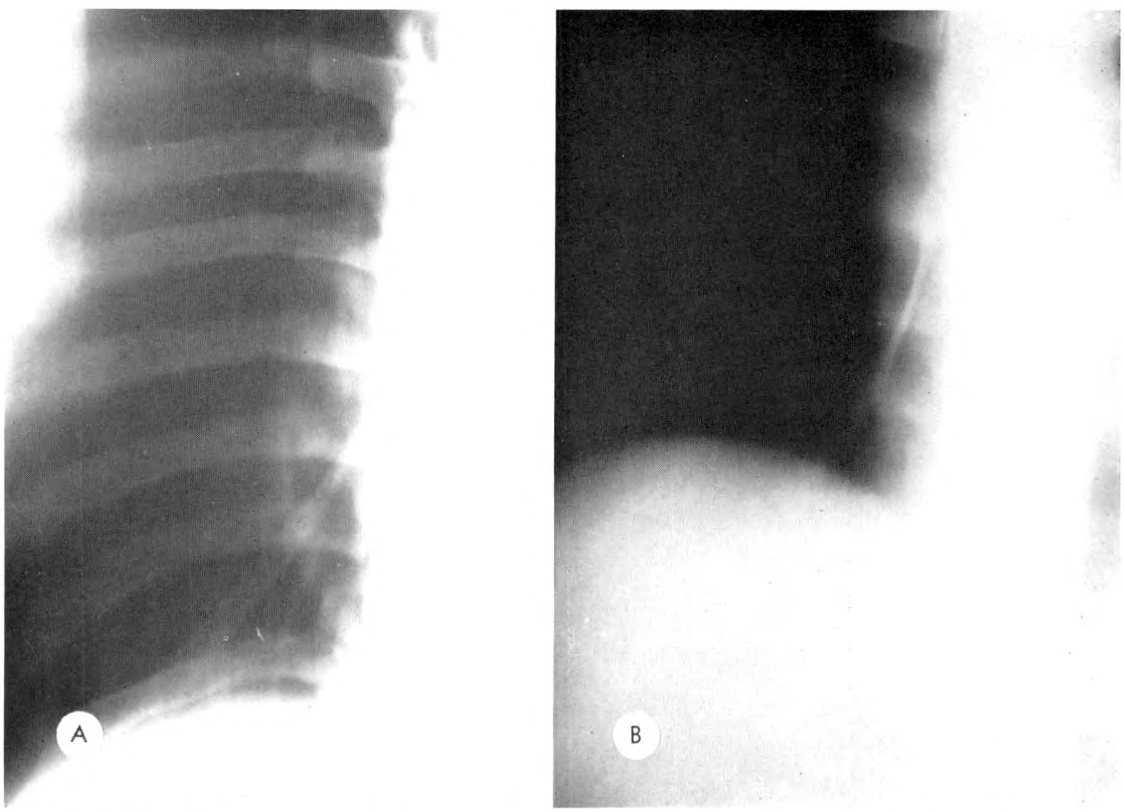


Fig. 2. (*A*) Laminagram in the frontal projection shows the cortex and trabeculation of the supernumerary rib. (*B*) Right anterior oblique laminagram shows the articulation of the intrathoracic rib with the anterolateral surface of the eighth thoracic vertebral body.

entations and a review of the reported cases. Their first patient, an 8 year old girl with ophthalmic scrofula, had an unusual forking of the right rib posteriorly. The inferior branch proceeded almost directly downward for 10 cm. and ended without obvious attachment to or abnormality of the right hemidiaphragm. Operation was not performed. Their second patient, a 5 year old boy, was found on a routine roentgenogram to have a paravertebral thoracic density originating from the area of the right fifth thoracic vertebral body, and apparently ending in the elevated dome of the right hemidiaphragm. Though explored, the anomalous rib was not removed. It was found to have diaphragmatic attachments at its distal end.

## DISCUSSION

That our patient's congenital anomaly should go unrecognized for years despite frequent chest roentgenograms confirms our belief that there is general unfamiliarity with this lesion. The anomaly is undoubtedly quite rare, although lack of awareness of the entity may result in its infrequent recognition and may, in part, account for the paucity of case reports. In all 10 cases so far reported, including our own, the condition has been unilateral, 8 on the right side and 2 on the left. Six of the patients were females and 4 were males. Only 1 case showed two anomalous ribs and both were in the same area; in the rest the aberrant rib was solitary. One patient had a right-sided aortic arch. Three of the 10 patients showed diaphragmatic attachments. The anomalous rib may arise from one of two sites: the posterior inferior margin of an otherwise normal rib or the vertebral body.

Embryologic explanations for intrathoracic rib have been set forth by Lutz[2] and by Stevenson and Merendino.[5] Briefly, they attribute the defect to incomplete fusion between component halves of adjacent sclerotomes. This failure of fusion stimulates the formation of two lateral processes on the affected side, both of which eventually become ribs, one articulating with the transverse process and one with the vertebral body.

Symptoms which might have been related to the supernumerary rib were found in only 1 of the 10 patients. Three of the patients were operated, but in only 2 was the anomalous rib resected. In neither report was a microscopic description included.

Several conditions should be considered in the differential diagnosis. Unlike an anomalous pulmonary vessel, such as the "scimitar shadow" of anomalous pulmonary vein, intrathoracic rib does not branch. Muscle or scar calcification might theoretically appear quite similar, but it would be expected to be palpable clinically and to be less uniform in caliber. Foreign body, especially a surgical drainage tube, can be excluded by the absence of a scar on the skin, and artifact ruled out by a repeat roentgenogram.

In short, if the diagnosis is considered, it is easily established, for the abnormal shadow actually looks like a rib. Since the condition is ordinarily of no clinical significance, resection is unnecessary.

## ROENTGEN DIAGNOSIS

The diagnosis of intrathoracic rib should be suspected from the routine chest roentgenogram and confirmed by further roentgen study. A smooth intrathoracic band-like or ribbon-like density arising from the mid-thoracic region posteromedially and extending laterally and inferiorly toward the hemidiaphragm on the same side is a rather unusual finding deserving further investigation. A cortical margin to the shadow may be visible on the routine roentgenogram. If the superior medial margin of the abnormal shadow articulates with a vertebral body or arises from a rib, the diagnosis of intrathoracic rib is established. Reflection of the diaphragm to-

ward the anomalous rib may occur. Stereoscopic films, fluoroscopy, Bucky roentgenograms and laminagrams demonstrate all the roentgen signs to better advantage and define the intrathoracic location.

SUMMARY

The purpose of this paper is to acquaint radiologists with a rare chest roentgen finding, the intrathoracic rib. The roentgen diagnosis is simply and reliably established if one is aware of the existence of this anomaly.

Charles F. Mueller, M.D.
Department of Radiology
Cincinnati General Hospital
Cincinnati 29, Ohio

The authors wish to express sincere appreciation to Dr. Benjamin Felson, who first made the diagnosis and gave us the impetus to report the findings. The authors are further indebted to him for his aid in reviewing the manuscript. Appreciation is also expressed to Drs. Jan Schwarz and Ernest Hidvegi for their translations of the foreign articles.

REFERENCES

1. Jacobs, S. Supernumerary rib. *Am. Rev. Tuberc.*, 1949, *59*, 76–77.
2. Lutz, P. Ueber eine ungewöhnliche Rippenanomalie, zugleich ein Beitrag zur distalen Rippengabelung. *Wien. klin. Wchnschr.*, 1947, *59*, 846–849.
3. Marbut, W. M., and DeGinder, W. L. Supernumerary intrathoracic rib: case report. *U. S. Armed Forces M. J.*, 1953, *4*, 1507–1510.
4. Plum, G. E., Hayles, A. B., Bruwer, A. J., and Clagett, O. T. Supernumerary intrathoracic rib: case report. *J. Thoracic Surg.*, 1957, *34*, 800–803.
5. Stevenson, J. K., and Merendino, K. A. Two unusual congenital anomalies of thorax: (1) supernumerary ribs and (2) abnormal intrathoracic fascial band: review of literature. *J. Thoracic Surg.*, 1956, *32*, 521–527.
6. Von Ronnen, J., and Jongh, R. Description de deux cas de côte intrathoracique. *Ann. de radiol.*, 1962, *5*, 639–647.
7. White, J. D. Abnormalities of bony thorax. *Brit. J. Radiol.*, 1929, *2*, 351–355.
8. Whitlark, F. L., and Engels, E. P. Supernumerary left intrathoracic rib with right-sided aortic arch. *J.A.M.A.*, 1962, *179*, 968.
9. Wilk, E., and Hülshoff, T. Über eine seltene Rippenanomalie. *Fortschr. a. d. Geb. d. Röntgenstrahlen u. d. Nuklearmedizin*, 1957, *86*, 531–532.

# OSTEOLYSIS: A COMPLICATION OF TRAUMA*

## REPORT OF 2 CASES

By MAJOR FOUAD A. HALABY, MC, and CAPTAIN EUGENE I. DI SALVO, MC
NEW YORK, NEW YORK

OSTEOLYSIS of bone as a complication of trauma is a rare occurrence. Its prognosis and response to therapy are unpredictable. The cause is unknown, although pathologically angiomatosis of a benign histologic pattern replacing the lost bone has been reported. In many of the cases, osteolysis has been massive and distressing in its unrelenting local progress without any respect to local anatomic boundaries.[1,2,3,5,6,7]

In a recent report[6] in the British radiologic literature, osteolysis involving the distal clavicle is described. The author suggests that this condition is more common than previously thought, self-limiting, and a direct result of trauma. This "benign" form may be a process totally different from that seen in the cases of massive osteolysis previously reported.

Two such cases of self-limiting osteolysis which we believe to be a complication of trauma are here reported. One is rather unusual in that chondrolysis was also present.

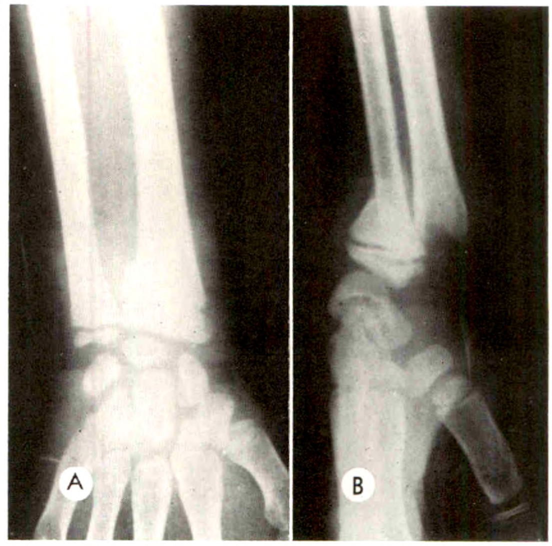

FIG. 1. Case I. (*A*) Posteroanterior and (*B*) lateral roentgenograms of the right wrist show a fracture of the distal shaft of the radius. The ulnar epiphysis appears to be intact.

### REPORT OF CASES

CASE I. J.A., a 15 year old male, came to Rodriguez U. S. Army Hospital on September 9, 1963 with the complaint of slow but progressive ulnar deviation of his right wrist. The history showed that this painless deviation started following a fracture of the radius 8 years earlier, which was diagnosed as a simple fracture with posterior displacement of the distal fragment.

The roentgenogram made on September 9, 1963 (Fig. 4, *A*, *B* and *C*) showed ulnar deviation of the radius with absence of the distal few inches of the ulna. Fortunately, the roentgenograms of the wrist made at the time of the trauma were available for review (Fig. 1, *A* and *B*; and 2, *A* and *B*). Follow-up roentgenograms taken 6 weeks after a routine closed reduction of the fracture were also available and these showed absence of the distal ulnar epiphysis (Fig. 3, *A* and *B*). This was missed on the interpretation at that time, and the patient was without complaint until his present illness.

In 1963, a physical examination revealed only ulnar deviation with fixed contracture of the soft parts; there was no evidence of inflammation.

Comment. This is a rather unusual case in that the distal ulnar epiphysis including the cartilage dissolved. The patient had no complaint at that time nor was any unusual remark made on the patient's chart. The post-reduction roentgenogram showed a normal ulnar epiphysis with osteochon-

* From the Radiology Service and the Orthopedic Section of Surgical Service, Rodriguez U. S. Army Hospital.
This material has been reviewed by the Office of The Surgeon General, Department of the Army, and there is no objection to its presentation and/or publication. This review does not imply any indorsement of the opinions advanced or any recommendation of such products as may be named.

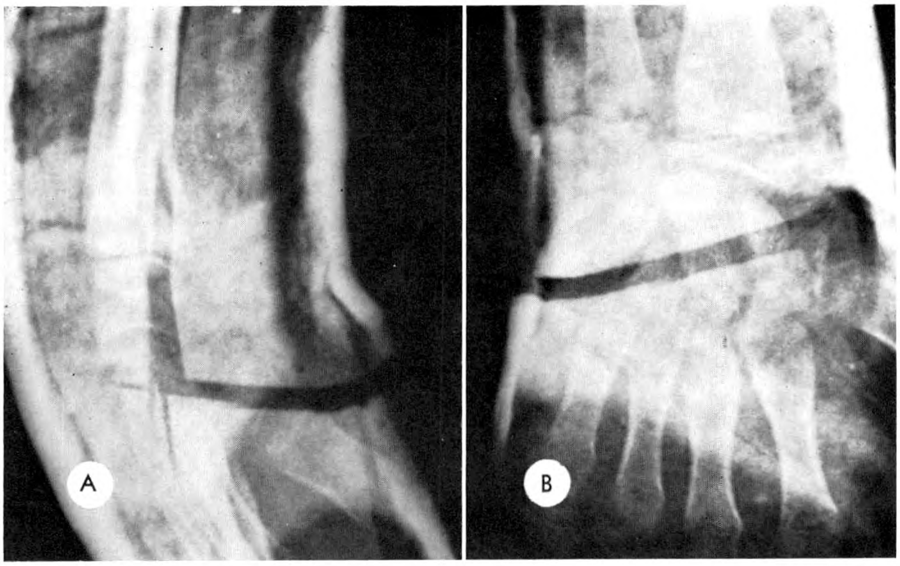


Fig. 2. Case I. (*A*) Lateral and (*B*) posteroanterior roentgenograms taken through plaster cast after reduction demonstrate good position and alignment.

drolysis being complete on the 6 week follow-up study. Treatment since then has consisted of dynamic splinting. The contracture has been corrected. It is anticipated that arthrodesis with fibular grafting will be attempted in the future.

Case II. K.V., a 24 year old U.S. Navy enlisted man, was involved in a motor scooter accident on May 3, 1963. There was no history of loss of consciousness. On examination, he was found to have tenderness of the left acromioclavicular joint with slight elevation of the distal end of the clavicle. He also had limitation of shoulder motion due to pain. A roentgenogram (Fig. 5) showed an acromioclavicular separation measuring 0.7 cm. more than that found on the opposite side. Routine hematology and urinalysis were within normal limits with the exception of a 7 per cent eosinophilia, which was felt to be due to previous intestinal parasites. The patient was treated with adhesive strapping over the clavicle and under the olecranon in the manner of Watson-Jones. He was seen several times in the orthopedic clinic, and, when seen last in December 1963, there were no complaints. A roentgenogram (Fig. 6) of the left shoulder showed osteolysis of the distal end of the clavicle. Physical examination was entirely within normal limits.

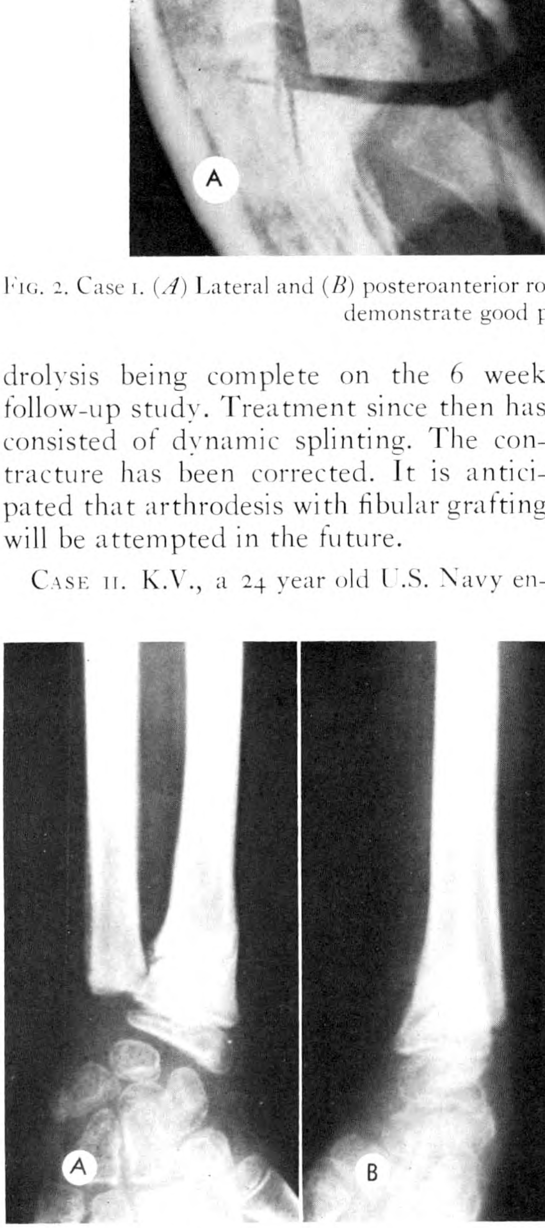


Fig. 3. Case I. (*A* and *B*) Six weeks after reduction there is good healing of the radial fracture and absence of the ulnar epiphysis

Comment. This patient is comparable to those cases reported by Madsen.[6]

## DISCUSSION

The discrepancy between massive osteolysis and the cases reported here as well as those reported by Madsen would suggest that the latter cases may represent a different disease process. For one, these cases of

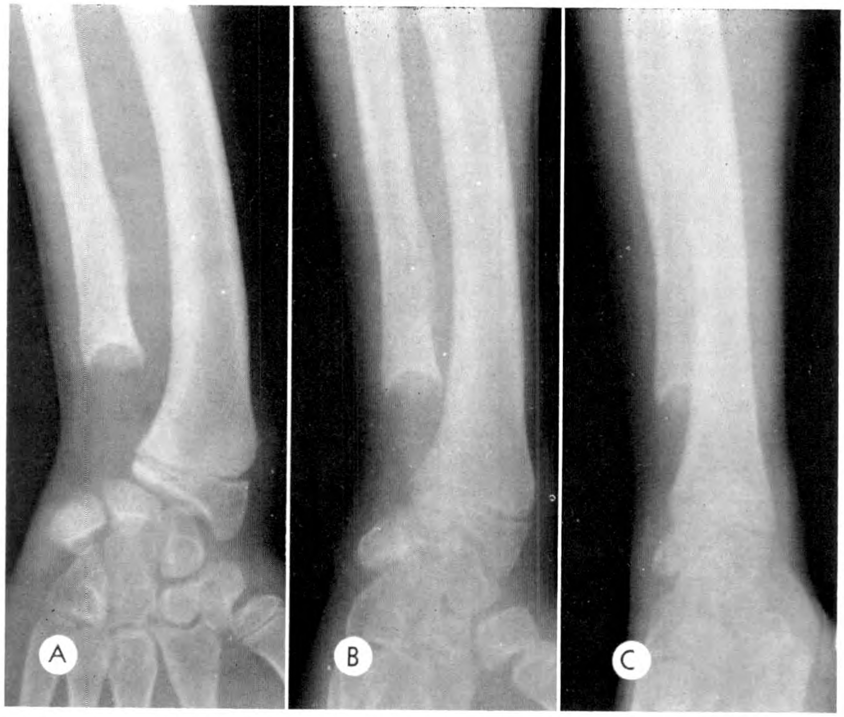


Fig. 4. Case I. (*A*) Posteroanterior, (*B*) oblique and (*C*) lateral roentgenograms 8 years later show osteolysis of the distal portion of the shaft of the ulna and ulnar bowing of the distal radius.

limited osteolysis all occurred following severe trauma, sufficient to cause fracture of bone or rupture of ligaments, whereas in the cases of massive osteolysis there is an inconclusive relation to trauma which usually is mild when present.[3,4] Fractures in massive osteolysis are often the result of the pathologic process rather than the cause of it.

Another differential factor is the self-limited nature of the process in our cases and those reported by Madsen. Our Case I has been followed for 8 years from the onset of the disease with no progression. In none of the cases was more than one bone involved, or a joint crossed.

We feel that the sequence of severe trauma followed by osteolysis represents a cause and effect relationship, although the area involved by osteolysis may not be fractured. The ulnar epiphysis in Case I appeared intact on the original roentgenogram, and no fracture of the clavicle was seen in Case II.

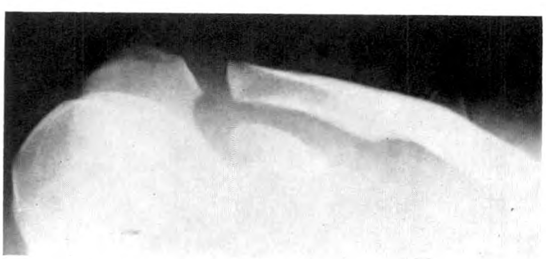

Fig. 5. Case II. Anteroposterior roentgenogram of the shoulder shows acromioclavicular joint separation with no fracture.

Fig. 6. Case II. Anteroposterior roentgenogram of the shoulder 7 months after injury shows osteolysis of the distal portion of the clavicle.

There were no signs, symptoms, or roentgenographic changes implicating autonomic nervous system involvement, or vascular, endocrine or metabolic dysfunction. No biopsy material was available in these cases, and assumption of the presence or absence of angiomatosis would be conjectural.

SUMMARY

Two cases of self-limiting osteolysis secondary to trauma are reported.

Major Fouad A. Halaby, MC
Rodriguez U. S. Army Hospital
A.P.O. 851
New York, New York 10000

REFERENCES

1. Aston, J. N. Case of "massive osteolysis" of femur. *J. Bone & Joint Surg.*, 1958, *40B*, 514–518.
2. Branco, F., and Da Silva Horta, J. Notes on rare case of essential osteolysis. *J. Bone & Joint Surg.*, 1958, *40B*, 519–527.
3. Gorham, L. W., and Stout, A. P. Massive osteolysis (acute spontaneous absorption of bone, phantom bone, disappearing bone): its relation to hemangiomatosis. *J. Bone & Joint Surg.*, 1955, *37A*, 985–1004.
4. Halliday, D. R., Dahlin, D. C., Pugh, D. G., and Young, H. H. Massive osteolysis and angiomatosis. *Radiology*, 1964, *82*, 637–644.
5. Jones, G. B., Midgley, R. L., and Smith, G. S. Massive osteolysis: disappearing bones. *J. Bone & Joint Surg.*, 1958, *40B*, 494–501.
6. Madsen, B. Osteolysis of acromial end of clavicle following trauma. *Brit. J. Radiol.*, 1963, *36*, 822–828.
7. Milner, S. M., and Baker, S. L. Disappearing bones. *J. Bone & Joint Surg.*, 1958, *40B*, 502–513.

# ACRO-OSTEOLYSIS

*By* WILLIAM D. CHENEY, M.D.
LANSING, MICHIGAN

TWO types of acro-osteolysis have been described in the radiologic literature: (1) idiopathic or nonfamilial, and (2) familial. The disease has been considered a rare entity. Idiopathic acro-osteolysis has been reported in both the European and American literature; reports of familial acro-osteolysis have appeared only in the European literature, 72 cases having been recorded to date.[4]

On the basis of a recent study of members of a family exhibiting the characteristics of familial acro-osteolysis, the author believes that there is but one disease entity, and, as stated by some investigators, that the disease is part of a larger degenerative bone process than the term acro-osteolysis would imply.

The term acro-osteolysis is derived from the Greek word "acros" meaning highest or outermost—a combining form denoting "pertaining to the tip or to the extremes or to the extremities"—and the word osteolysis referring to the disintegration of bone. Thus, acro-osteolysis means the disintegration of bone of the tips of the extremities, *i.e.*, specifically the phalanges. As reported by others and noted in this study, the term acro-osteolysis does not in itself encompass all of the features of this disease entity.

## REPORT OF CASES

CASE I (Fig. 1, *A–D*). This white female, aged 57 years, was born and has lived in the upper peninsula of Michigan most of her life. She is the mother of Cases II, III, IV and V. For the past 38 years she has complained of severe intermittent back pain causing considerable incapacitation.

Physical examination revealed finger shortening, primarily at the distal joint level, which has been present for approximately 30 years. Her head is symmetric but the neck is short, the stance is kyphotic, and her height is 55 inches.

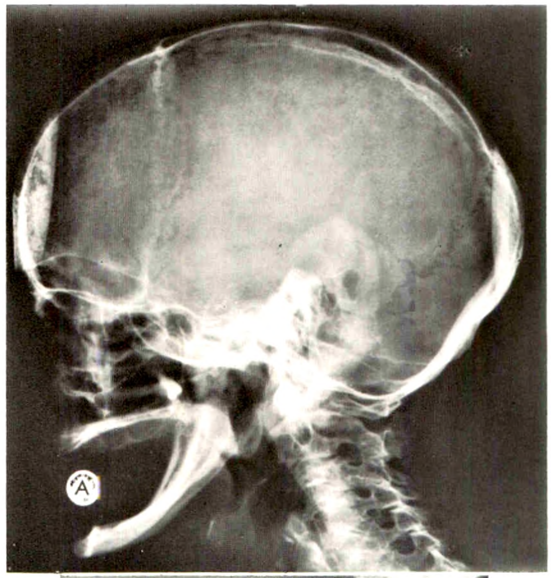


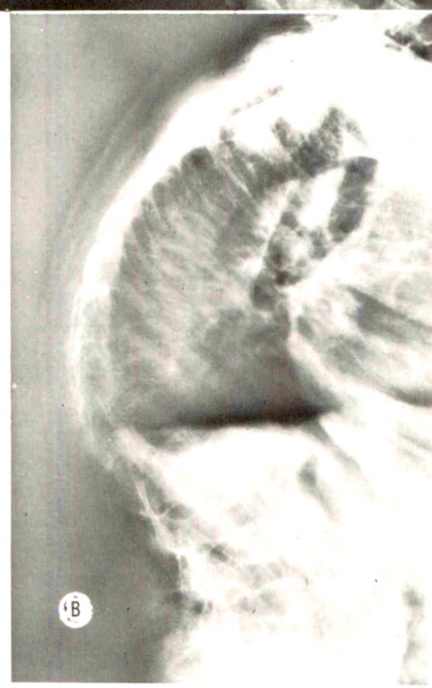


FIG. 1. Case I. (*A*) Skull roentgenogram demonstrates basilar impression. Edentulism is complete except for unerupted maxillary molar. (*B*) Severe kyphosis and demineralization of spine. The intervertebral disk density is greater than the density of the bodies of the lumbar vertebrae.

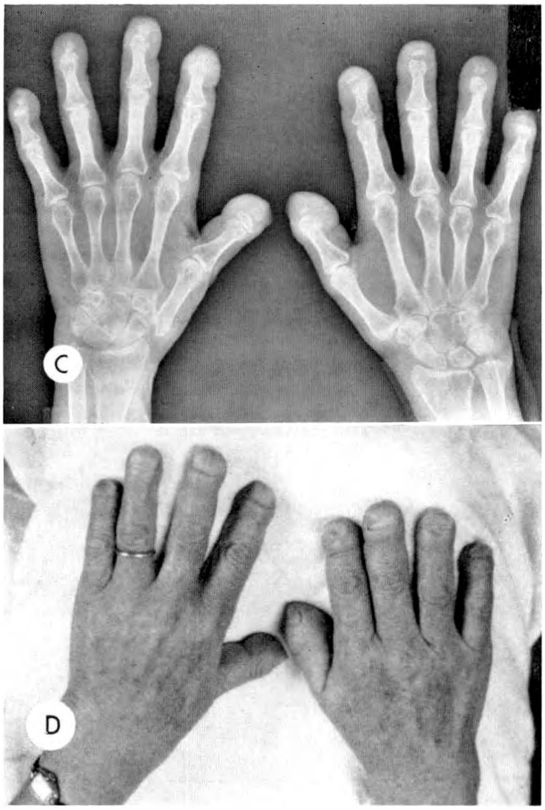


Fig. 1. (*C*) Bilateral osteolysis of the terminal phalanges. (*D*) Soft tissues of the fingers show clubbing, but the fingernails are intact. (Courtesy of Dr. W. Whitehouse, Department of Roentgenology, University of Michigan.)

The family history is negative. Her husband is not a blood relative. Laboratory and chemistry studies are not available.

Roentgen studies made on October 25, 1963 demonstrated marked skeletal decalcification. The sella turcica was shallow and elongated. Basilar impression was present. There was marked atrophy of the alveolar margins of the maxilla and mandible. The patient was completely edentulous except for an unerupted upper molar. The frontal sinuses were absent. An increase in soft tissue volume produced a clubbing effect of all digits. There was a nonreactive but destructive osteolysis involving all terminal phalanges of the right and left hands. There was partial resorption of the proximal end of the metacarpal of the first digit of the left hand. The feet showed marked decalcification, thinning of the cortices of the metatarsals and phalanges, narrowing of the metatarsal and metatarsophalangeal joint spaces bilaterally, and relative shortening of the first digits. The spine showed severe demineralization, compression of the 8th, 9th and 10th dorsal vertebrae and kyphosis centered at the 9th and 10th dorsal vertebrae. The concavity of the superior and inferior margins of most of the vertebrae in the lower thoracic and lumbar spine presented the "fish-bone" contour. Intervertebral disks appeared denser than the vertebrae.

Case II (Fig. 2, *A–G*). This male, aged 35 years, is the second of the 6 siblings. In 1959 he contracted tuberculosis, for which the right upper lobe and a segment of the right middle lobe were resected in August, 1960. It was during this period of hospitalization that his bone lesions were disclosed. For the past 5 years the patient has experienced severe constant back pain with radiation throughout the entire spine. Over a period of several years, he has become shorter in stature. Intermittently, since the age of 10 years, he has had occipital headaches. In childhood he injured his right foot and subsequently noted shortening of the first digit. At the age of 15 years pain occurred in the second digit of each hand. The pain persisted with weakness and progressive shortening of the digits of each hand. The disability has become progressively more severe and has caused him considerable unemployment, although he had previously worked as a welder and as a steel worker.

The patient is of small stature (57 inches) with a short thick neck. The head is elongated and the occiput pointed. His stance is kyphotic. The fingers are broad and short with pain on motion. The interphalangeal joints are hyperflexible. Changes almost identical to those seen in the hands were noted in the feet. Pain is most severe in the right first digit.

Clinical laboratory studies showed normal serum calcium and phosphorus and normal alkaline phosphatase.

Roentgenograms showed decalcification of bone structure. The right and left hands presented osteolytic destructive changes involving the terminal phalanges of all digits. Destructive changes also involved the distal ends of the middle phalanges of the second, third, fourth and fifth digits of both hands. The metacarpophalangeal joints of the first digit showed loss of spacing. Soft tissues at the ends of all digits emphasized the clubbed appearance. Both feet demonstrated osteolytic defects with loss of substance involving the distal phalanges. The short first metatarsal of the right foot seemed to

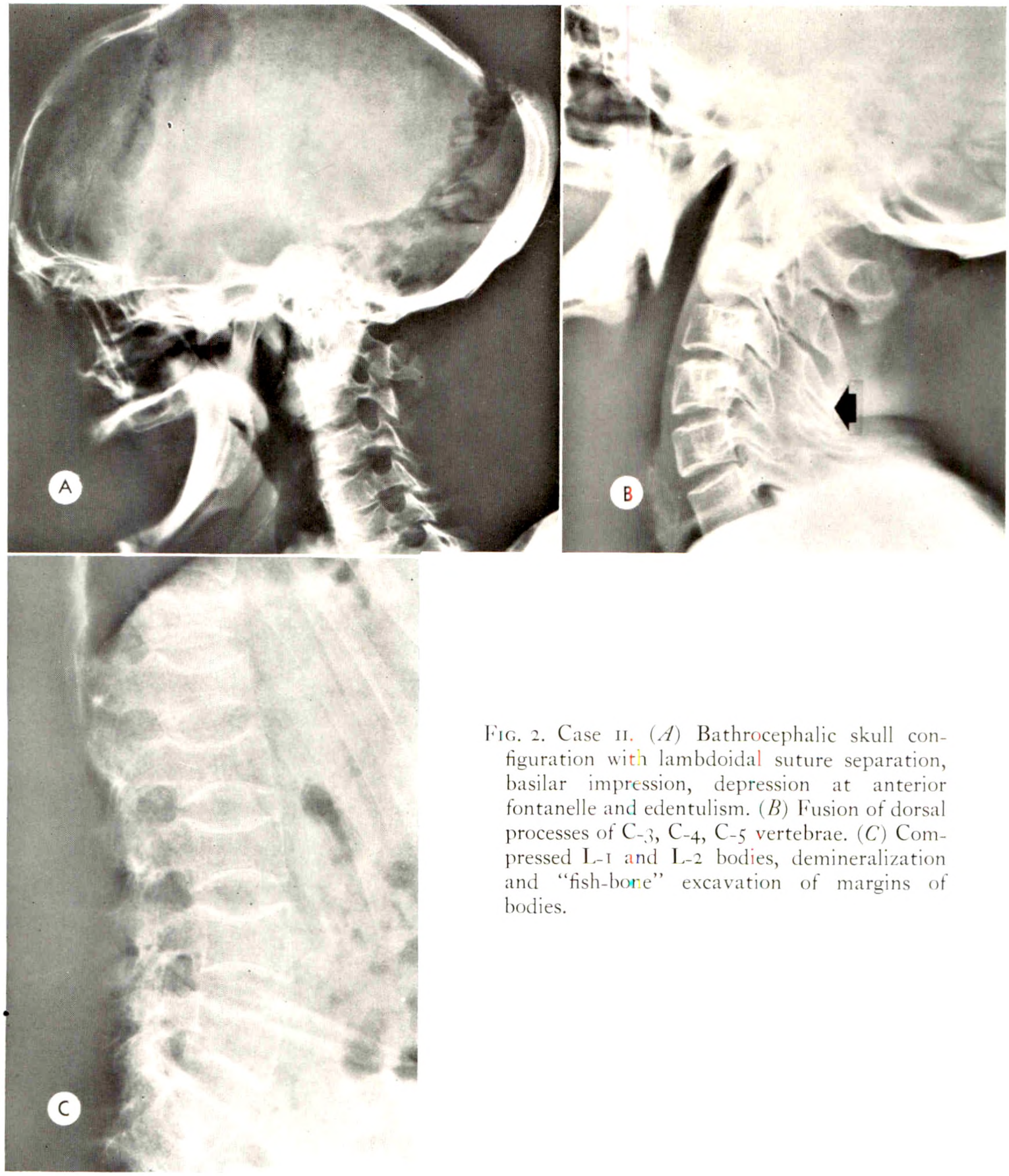


Fig. 2. Case II. (*A*) Bathrocephalic skull configuration with lambdoidal suture separation, basilar impression, depression at anterior fontanelle and edentulism. (*B*) Fusion of dorsal processes of C-3, C-4, C-5 vertebrae. (*C*) Compressed L-1 and L-2 bodies, demineralization and "fish-bone" excavation of margins of bodies.

correlate with the history of childhood injury. Increase in soft tissue volume emphasized the clubbing of all toes.

The skull was elongated, with widening of both coronal and lambdoidal sutures. A depression was seen at the site of the anterior fontanelle. Wormian bone formation was present along the lambdoidal suture line. There was unusual protuberance of the squamosal portion of the occipital bone, producing a bathrocephalic skull configuration. The sella turcica was enlarged and the dorsum sellae was unusually high. Basilar impression was marked. The spinous processes of the 3rd and 4th cervical vertebrae were fused but the bodies were segmented. Complete edentulism and marked atrophy of the alveolar margins of the maxilla and mandible were present. The frontal sinuses were absent.

The lumbar spine showed some degree of

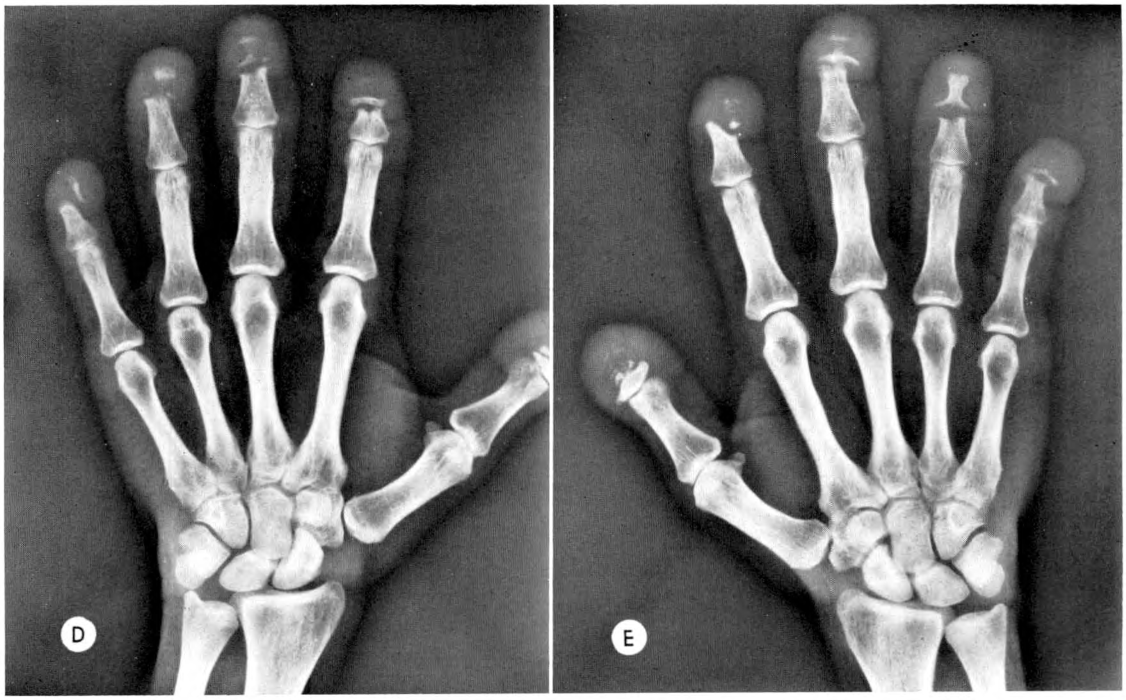


Fig. 2. (*D* and *E*) Severe osteolysis of terminal phalanges of all digits.

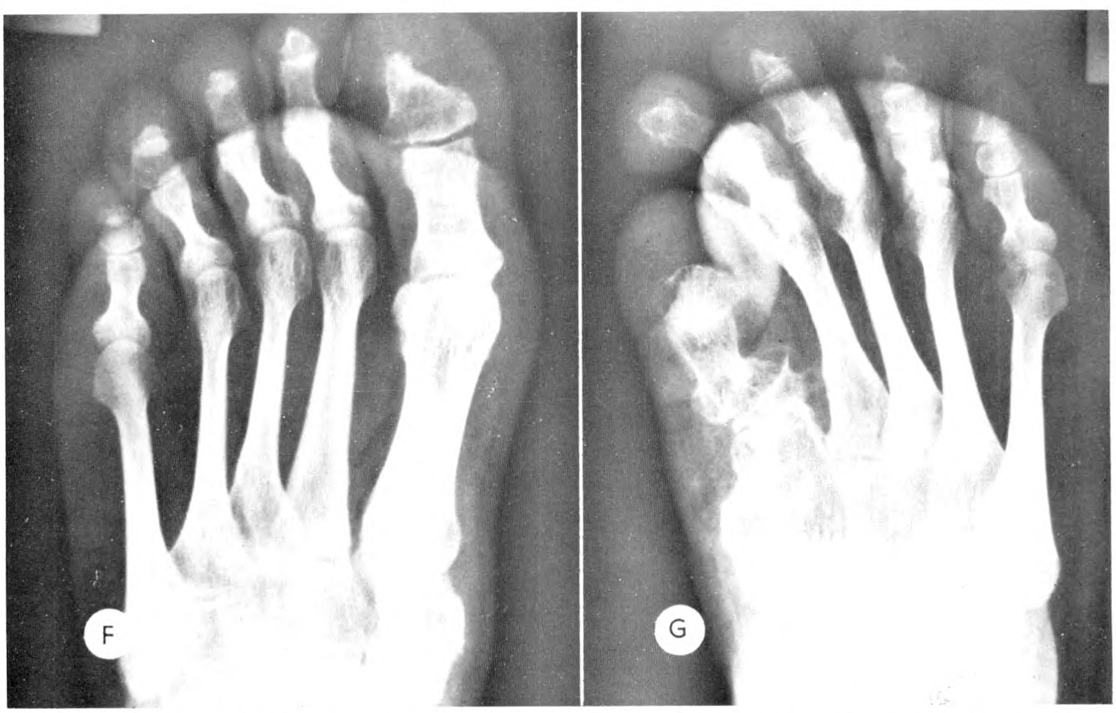


Fig. 2. (*F* and *G*) Clubbing of soft tissues and osteolysis of the terminal phalanges of the feet.

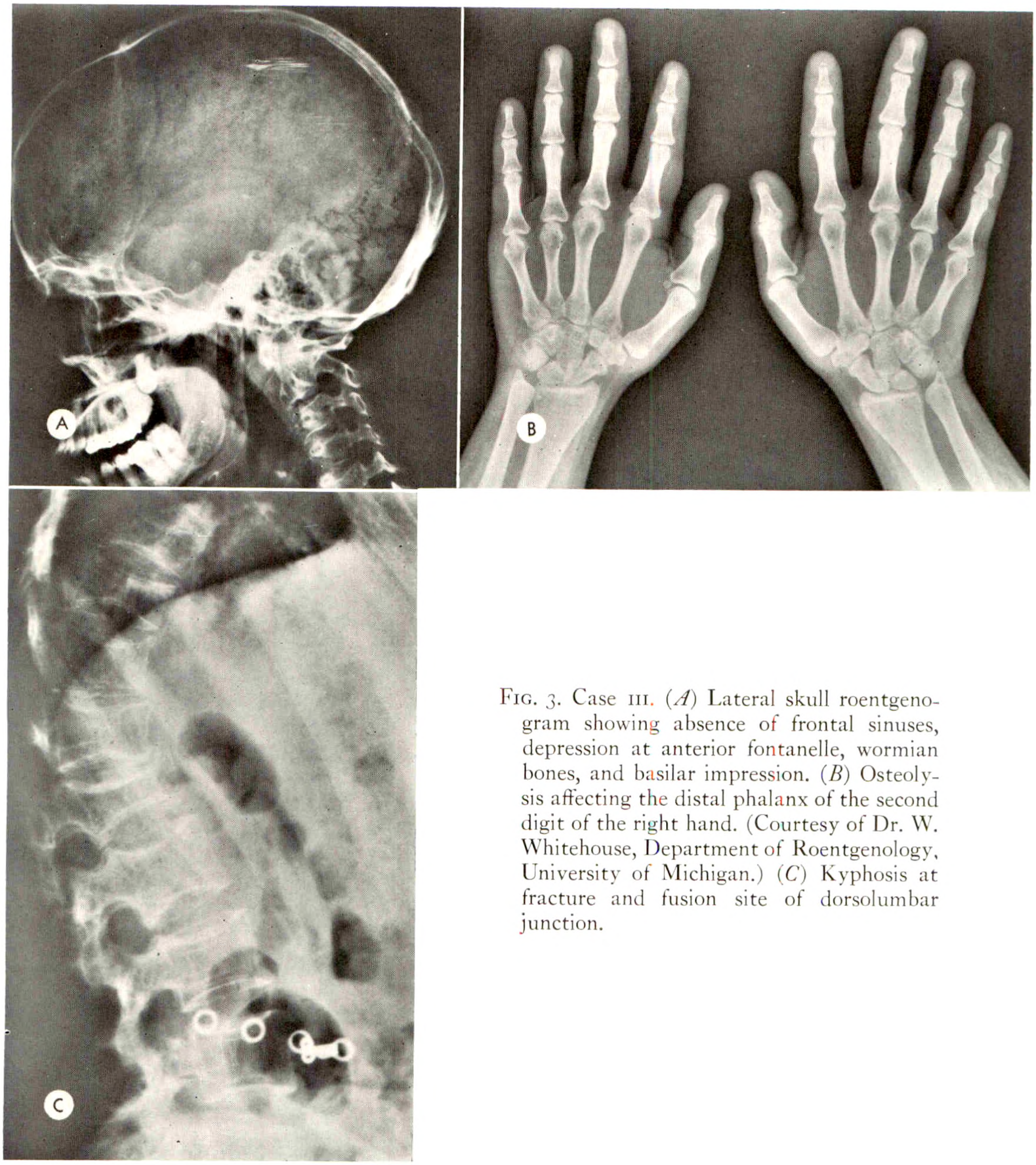


Fig. 3. Case III. (*A*) Lateral skull roentgenogram showing absence of frontal sinuses, depression at anterior fontanelle, wormian bones, and basilar impression. (*B*) Osteolysis affecting the distal phalanx of the second digit of the right hand. (Courtesy of Dr. W. Whitehouse, Department of Roentgenology, University of Michigan.) (*C*) Kyphosis at fracture and fusion site of dorsolumbar junction.

compression of most vertebrae, increase in the width of the intervertebral spacing and a "fish-bone" appearance of the vertebrae. There was slight dorsal kyphotic angulation centered at the 8th thoracic intervertebral space.

Case III (Fig. 3, *A*, *B* and *C*). This female, aged 26 years, is the third of the 6 siblings. She is also short of stature (57 inches) and has experienced back pain for many years. At the age of 10 years, she fractured a lumbar vertebra in a fall. In 1957 she re-injured her lumbar and dorsal spine in an automobile accident, necessitating surgical spinal fusion in the lumbar area. She experiences high cervical and occipital headaches which are triggered by exertion and bending the trunk forward. She has noted no changes in her fingers or toes. She has had no skin manifestations nor fractures of the extremities. The patient has lost 4 inches in height since the age of 16 years.

Physical examination revealed hyperflexible

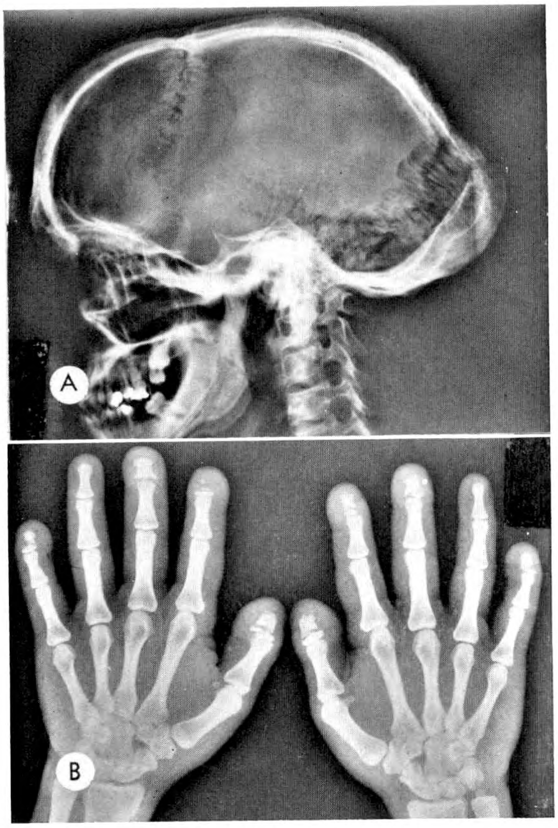


Fig. 4. Case iv. (*A*) Lateral skull roentgenogram showing bathrocephaly, depression at anterior fontanelle, basilar impression and alveolar resorption of mandible and maxilla. (*B*) Osteolysis of distal phalanges of first, second, third, and fifth digits. Fourth digits are not affected.

joints of the hands, particularly the interphalangeal. The digits are shortened and the hands are broadened. The fourth and fifth metacarpals appear to be short. Neurologic examination is normal. The neck is short, but she is not as kyphotic as her older male sibling. The head is generally round and shows no increase in the anteroposterior diameter. Tenderness is noted over the 10th dorsal vertebra.

Extensive laboratory studies including blood calcium and phosphorus were normal. Buccal smear for sex chromatin showed 33 per cent positive cells, a normal female pattern (Courtesy of Department of Genetics, University of Michigan).

Roentgen findings showed minimal fragmentation of the terminal tuft of the distal phalanx of the second digit of the right hand by nonreactive bone osteolysis. Wormian bone formation was seen along the lambdoidal suture line. A depression was seen at the site of the anterior fontanelle and a basilar impression was demonstrated. An unerupted maxillary molar was present. The lamina dura appeared intact around tooth roots. The frontal sinuses were absent.

Evidence of the spinal injury and surgical fusion was noted with compression of the 12th thoracic and 1st lumbar vertebral bodies, bone grafting between the 12th thoracic and 3rd lumbar segments and kyphosis centered at the 1st thoracic intervertebral space. Eburnation and fraying of the adjacent margins of the pubic bones were characteristic for osteitis pubis.

Case iv (Fig. 4, *A–G*). This male, aged 21 years, is the fourth of the 6 siblings. His general health is good. He had fractured his right thumb at the age of 9 years. In January of 1956, at the age of 14 years, he fractured the vertebrae in the mid-back and was placed in a body cast. He has had no specific back pain since, but his back does tire easily. At the age of 15 years, he noticed the onset of tactile soreness in the fingers. He recalls that this started in one of the fingers and gradually spread to the others. The fourth digit in each hand seems to have been spared. He has experienced no weakness of grip. Since the age of 15, he claims to have had fractures in the region of the left elbow, left wrist and right leg. These all healed spontaneously without residual defect. Since the age of 11 years, he has had intermittent severe occipital headaches, triggered by exertion, running or bending forward. The headaches last about 5 to 10 minutes. His height is 60 inches and he is taller than either his older brother or sister. There has been no decrease in height. He is employed as a drill press operator and does not feel physically or socially handicapped.

Physical examination showed a shorter than average male. The fingers are short, broad, slightly clubbed and sore to touch. The nails are intact. All of the joints of the hands show hypermobility. The neck is short and the head is elongated, with a pointed occiput. His posture is good.

Clinical laboratory studies showed a normal serum calcium and phosphorus and normal alkaline phosphatase.

The roentgen findings were similar to those in the older male sibling and characterized by osteolytic nonreactive destructive bone changes

involving digits 1, 2, 3, and 5 of both hands. Clubbing of the fingers due to soft tissue changes was well demonstrated.

The skull was elongated, with pronounced separation of coronal and lambdoidal sutures. A depression was seen at the site of the anterior fontanelle. Wormian bones were seen along the lambdoidal suture line. Marked basilar impression and bathrocephalic configuration of the occipital portion of the skull were demonstrated. The sella turcica was large with an unusually high position of the dorsal clinoid processes. The frontal sinuses were absent. There was an unerupted posterior maxillary molar.

The distal phalanges of both feet were pointed and showed loss of the terminal tufts of the second and third digits.

The spine was generally decalcified. A kyphotic angulation at the 8th dorsal intervertebral space along with slight scoliosis seemed to correlate with the history of back injury. There was compression of the superior plate of the 1st lumbar vertebra and excavation of the superior and inferior margins of the lumbar vertebrae generally, giving the "fish-bone" appearance.

On January 25, 1964, a biopsy was performed (Dr. Harry J. Schmidt). The specimen was obtained from the lateral aspect of the distal phalanx of the left 5th digit. A wedge resection was done, including skin, subcutaneous tissue and bone through the area of the osteolytic process as indicated on roentgenographic study. The microscopic pathologic description (Dr. John F. Dunkel) was as follows: "The slide section consists of skin and bone. The skin is unremarkable. The sections of bone include periosteum. The bone is of the spongy type and displays a striking process of necrosis. This consists of a conversion of multiple foci of bone to a grayish amorphous necrotic material in which are present numerous spicules and very small particles of bone, the bone undergoing the process of necrosis. The process also involves the adjacent adipose tissue of the marrow spaces. Viable bone adjacent to necrotic material displays an absence of the normal endosteal lining. No osteoblasts are seen and no tissue reaction to the necrotic process is evident." The histopathologic changes are shown in Figure 5.

Case v (Fig. 6, *A*, *B* and *C*). This sibling, aged 13 years, has no complaints. She is considered in good health. At the age of 8 years, she fractured the left ankle. The family feels that

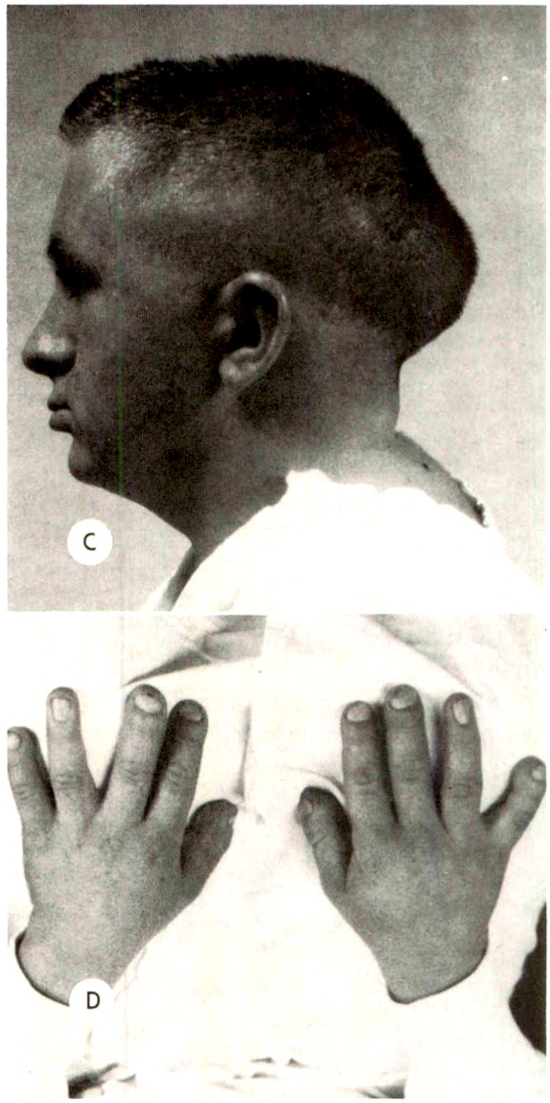


Fig. 4. (*C*) Photograph showing dolichocephaly, receding mandible and short neck. (*D*) Clubbing of fingers; fingernails remain intact.

her hands and fingers show changes similar to those noted in the older brothers prior to the onset of complaints of soreness in their fingers. Her stature is similar to that of her older sister.

Clinical laboratory studies showed a normal serum calcium and phosphorus.

Roentgen study demonstrated no reactive destructive osteolytic bone changes. There was slight fragmentation of the distal phalanx of the 4th digit of the left foot, with "squaring" of the end of the distal phalanx of the 2nd digit of both feet.

The skull demonstrated basilar impression

and a depression at the site of the anterior fontanelle, but no separation of sutures. The general contour of the calvarium was symmetric. The frontal sinuses were absent and there were unerupted teeth. The lamina dura appeared to be intact.

## REVIEW OF THE LITERATURE

In 1950 Harnasch[5] first described an "apparently new type of destructive bone lesion" which he called acro-osteolysis. Bilateral defects were present in the distal phalanges of the fingers and consisted of osteolytic destruction of portions of the shafts and distal ends of the phalanges. Absence of associated reactive bone changes or periosteal thickening was noteworthy. The roentgen changes of the feet consisted of bilateral symmetric destruction of the metatarsophalangeal joints of the 1st digits, with periosteal reaction and similar defects in other phalanges of both feet without periosteal or bone reaction. Bone destruction was noted in the maxillary and mandibular alveolar processes. In the cervical spine, the 5th and 6th vertebral bodies showed an inflammatory process with questionable healing. There was moderate kyphoscoliosis of the lower cervical and upper dorsal spine.

Harnasch considered a differential diagnosis of leprosy, arthritis mutilans, Ainhum disease and various congenital osteolytic and inflammatory conditions such as syringomyelia, etc., but felt that these could be ruled out with reasonable certainty. He regarded these changes as due to imbalance between the sympathetic and parasympathetic systems, manifest by increased sympathetic activity stimulating the osteolytic processes. He postulated that this could occur from overactivity of the eosinophilic cells of the pituitary body.

The case reported by Harnasch was a male, 43 years of age, with no family history of any known bone disease. The patient was a locksmith with recurring attacks of eczema involving the hands, feet, arms and legs and apparently associated with the handling of oils and tar. Over a period of years, the fingers had become shorter and thicker. Numbness of the fingers and toes was noted but actual pain was not present. Unusual mobility of the

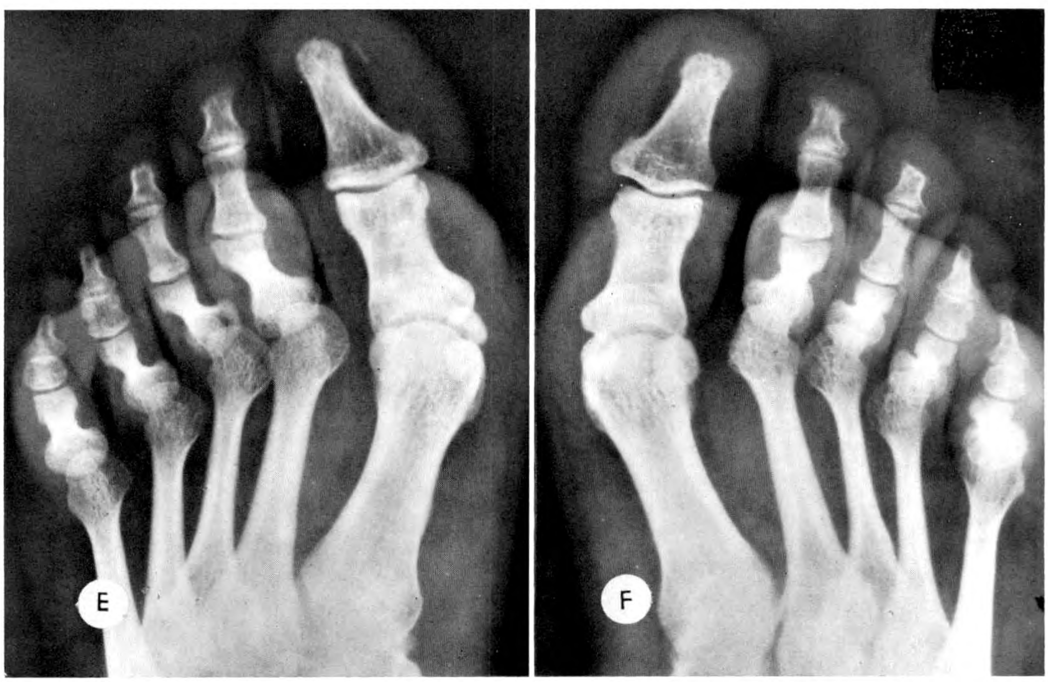


Fig. 4. (*E* and *F*) Osteolysis involving terminal phalanges of toes.

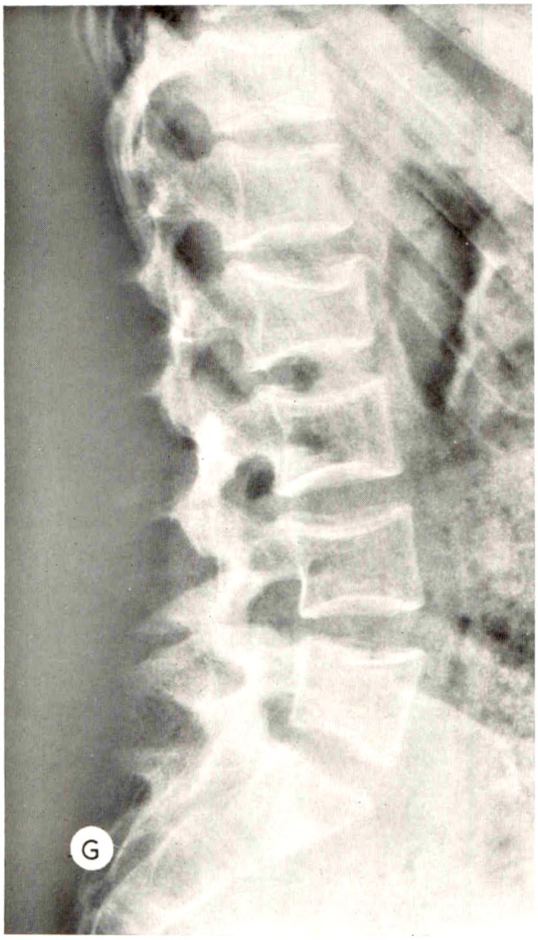

Fig. 4. (*G*) Compression fracture at L-2 and demineralization of vertebrae.

terminal phalanges in all directions was present. The jaw was prognathous. Three years following the original observation, the patient complained of pain in the shoulders and roentgenograms demonstrated destructive lesions of the acromial ends of the clavicles bilaterally, without periosteal or endosteal bone reaction. Harnasch conjectured that these findings represented the antithesis of acromegaly.

In his report of familial acro-osteolysis, Harms[4] stressed the clinical aspects of the disease as beginning with the formation of a swelling along the plantar surface of the foot which gradually develops into a full-blown ulcer of significant size and depth. Involvement of the underlying bone with ejection of bone fragments, followed by spontaneous healing of the ulcer but subject to recurrence after weeks or months, was also described. Comparatively, it is

Fig. 5. Case iv. Microscopic section of bone, taken from the distal phalanx of the 5th digit of the left hand, showing necrosis of bone and marrow without tissue reaction.

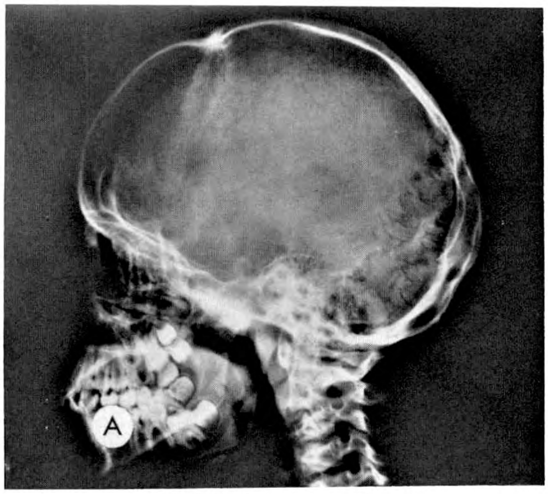

Fig. 6. Case v. (*A*) Premature suture closure causing depression at site of anterior fontanelle. Basilar impression.

interesting to note that in this study no patient demonstrated spontaneous ulcerations anywhere in the skin, yet, all demonstrated osteolytic destructive changes peculiar to acro-osteolysis.

Giaccai[2] and Harms,[4] in reporting acro-osteolysis, pointed out the features differentiating familial and idiopathic acro-osteolysis. Harms[4] stressed the dominant inheritance pattern in familial acro-osteolysis and found agreement with Giaccai[2] regarding the 3:1 male to female incidence. Both emphasized the characteristic clinical appearance of plantar swelling, leading to painful ulcerations with remission and exacerbation at the original or multiple sites. The occurrence of osteomyelitis with sequestration of the metatarsals eventually produces chronic deformity and mutilation of the feet. The phalanges are not so affected, but undergo "concentric bone atrophy" with destruction of the shafts, this latter finding being common to both familial and idiopathic acro-osteolysis. Both authors emphasized the capability of the epiphysis to resist the osteolytic destructive process longer than mature bone. Harms[4] also pointed out that in the idiopathic acro-osteolysis of Harnasch,[5] the fingernails remained intact, plantar ulcers did not occur and there were no tactile or cutaneous sensory disturbances, the opposite being found in familial acro-osteolysis. Prognosis for life is good, but complete recovery is not to be anticipated. Giaccai[2] described idiopathic acro-osteolysis as frequently unilateral and nearly always asso-

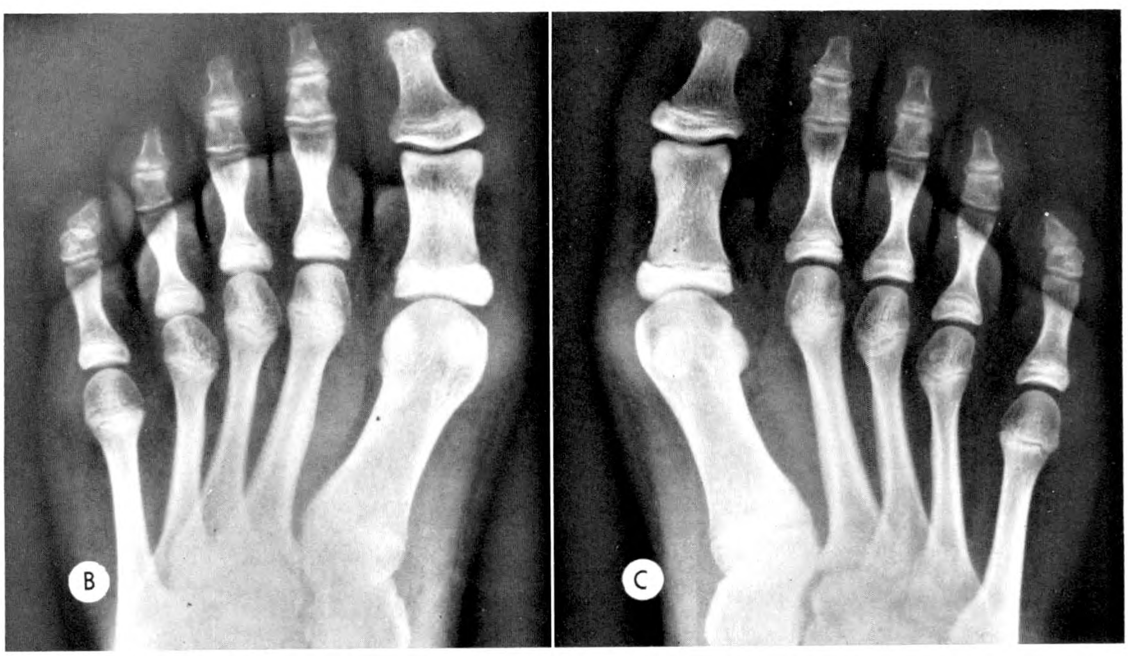

Fig. 6. (*B* and *C*) Early stage of osteolysis of terminal phalanges of digits 2, 4, and 5.

ciated with congenital malformations of the spine and feet. He also felt that idiopathic cases were more common than the familial type.

Further reports of acro-osteolysis have been published by Wieland,[11] Wassner,[10] Greenberg and Street,[3] Papavasiliou, Gargano and Walls[9] and Kleinsorge.[7] There is general agreement as to the characteristic features, *i.e.*, shortened and clubbed digits, at times with tenderness, pain or paresthesias. The principal pathologic change is bone necrosis of distal phalanges without bone reactive changes. Atrophy of mandible or maxilla with an edentulous state was noted by Wassner,[10] Greenberg and Street[3] and Papavasiliou, Gargano and Walls.[9] Dolichocephaly with protuberance of the occipital region, wormian bone formation and absence of tubulation of long bones were reported by Papavasiliou, Gargano and Walls.[9] Looser's zones or possible fractures in metatarsals were reported by Kleinsorge,[7] Greenberg and Street[3] and Papavasiliou, Gargano and Walls.[9] Unstable, hypermobile interphalangeal joints were noted by Greenberg and Street.[3] Wieland[11] reported kyphosis and Wassner[10] observed marked demineralization of the inner aspects of the clavicles. Greenberg and Street[3] obtained a biopsy specimen taken from a lytic area in the first metatarsal and this was reported as "nonspecific fibrosis."

## DISCUSSION

A study of the members of this previously unreported family indicates a hereditary pattern, but the findings more closely follow those of the idiopathic acro-osteolysis as reported by Harnasch,[5] Wieland,[11] Greenberg and Street[3] and Papavasiliou, Gargano and Walls.[9]

The outstanding features of skin ulceration and destruction of nails as emphasized by Harms[4] have not been found in this family. Joint hypermobility and sensory disturbances, particularly painful paresthesias of the fingers, were found. The osteolytic defects involving the phalanges of the hands and feet, the bathrocephalic skull with multiple wormian bones, the bone resorption of the alveolar processes of the maxilla and mandible and the loosening of teeth were all present. It would seem of significance that the female members of this family demonstrated symmetric skull configuration as contrasted to the bathrocephalic type skull of the males. All showed the effect of premature suture closure at the anterior fontanelle. Basilar impression appeared to correlate with headache.

The fingernails have remained intact in the shortened and widened digits. All individuals were uniformly short in stature. Very definite deficient bone strength was demonstrated by the fact that these individuals appeared to be prone to fractures and back injury. "Collapse" of vertebrae and deficiency in collagen components of supporting soft tissues would seem a logical cause for the loss of height, apparently occurring with increasing age. Of significance was the lack of symptoms and signs in early childhood and the beginning of the clinically recognizable changes in the digits occurring in the teens, progressing to generalized osseous involvement with increasing age.

The generalized decalcification of the skeleton in acro-osteolysis would appear to be osteomalacia, although the exact mechanism for the decalcification is not entirely clear.

One might speculate that a process of vascular bone resorption associated with the ingrowth of blood capillaries into bone, the bone being absorbed ahead of the advancing vessels, would offer an explanation for the phalangeal defects. One might further theorize a genetic concept in which the inherent tendencies of the blood capillaries would lead to focal ischemia, directly affecting the bone structure in the phalanges. Certainly, the pathologic histology of the necrotic process demonstrated in microscopic sections does not really clarify the etiology. A type of lesion of small blood vessels producing focal ischemic necrosis, even though such cannot be identified in

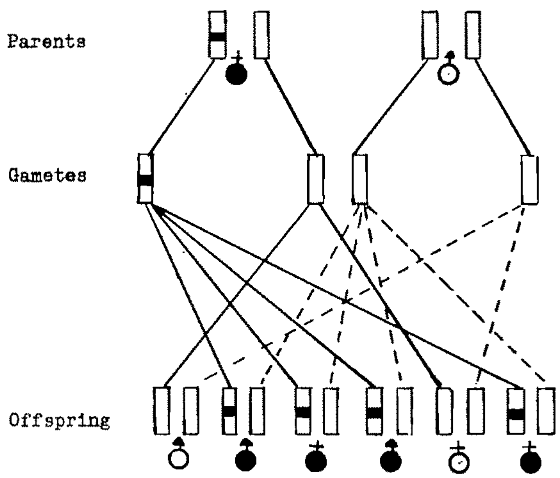


Fig. 7. Dominant inheritance pattern in family. Diagram showing the gamete distribution to produce 2 affected males, 2 affected females, 1 normal male and 1 normal female.

the biopsy material, may be a possibility.

This disease might well be compared with osteogenesis imperfecta tarda in that its clinical manifestations are delayed to a later age. Although the inadequate and abnormal intercellular and cellular substances of bone have the ability to withstand the ordinary wear and strain of life in bone constructive phases, total maturation never seems to occur in focal areas because of vascular insufficiency. The hypermobility of the joints would also indicate a deficiency in the production of collagen components of tendons and ligaments. This would also suggest the inability to transform collagen into its mature adult form. The foregoing concept would allow for the ability of the patient with acro-osteolysis to repair fractures occurring in the earlier stages of life.

## GENETIC CONSIDERATIONS

A factor of great genetic importance is consanguineous marriage. The rarer a specific abnormality is, the greater is the possibility that a thorough study of family history of the affected person would reveal a consanguineous marriage. A study of this family has not uncovered such evidence.

The study, however, confirms the dominant inheritance pattern in this family transmitted from mother to both male and female offspring (Fig. 7). The second generation offspring have not demonstrated the disease entity by roentgen study, but the clinical appearance of at least one individual is suggestive. The abnormal genetic trait appears first in the maternal parent with definite transmission to 2 male and 2 female offspring.

No attempt has been made to determine that acro-osteolysis as a hereditary disorder may be the result of a single genetic defect or a combination of defective genes. If a single gene is responsible, a syndrome of acro-osteolysis represents a bizarre pleiotropic genetic defect. The idiopathic case may be an individual with a dominant trait in homozygous form, the disorder in heterozygous form (in the parents) being so mild as to escape recognition. The idiopathic case would in this situation derive one dominant gene from each parent. If one could assume that the idiopathic or isolated cases of acro-osteolysis reported by others resulted from genetic mutation, the entire entity could be explained on the basis of a genetic concept, in spite of the fact that the entity in possible offspring was neither recognized nor reported. This would help to correlate the rarity of the idiopathic cases, as emphasized by Greenberg and Street[8] and Papavasiliou, Gargano, and Walls.[9]

## SUMMARY

Cases of familial acro-osteolysis, as a dominant inherited disease with roentgen and clinical findings overlapping those previously reported as either familial or idiopathic, are presented and discussed. Basilar impression and bathrocephaly, with variations between the contour of the male and female skulls, and progressive loss of height have been added to the multiplicity of findings.

The age range encountered, spanning the years from early teen age to the sixth decade, would tend to show that there is progressive deterioration of mesenchymal components of bone and bone matrix and

probably of the collagen elements of tendons and ligaments of the joints.

The capability of fractures to heal would seem to indicate the capability of bone forming elements to function in the immature state in spite of ultimate inability to attain the final competent structure of mature bone.

The hereditary pattern is clearly established in this study and substantiates the dominant pattern proposed by others. The genetic concept is used to explain the occurrence of the idiopathic or nonfamilial cases reported, yet to maintain this disease entity within a classification of a large generalized congenital osseous dysplasia, more far reaching in its extent than the term acro-osteolysis would imply.

Department of Radiology
Edward W. Sparrow Hospital
Lansing, Michigan

REFERENCES

1. Aegerter, E., and Kirkpatrick, J. A., Jr. Orthopedic Diseases. W. B. Saunders Company, Philadelphia, 1958.

2. Giaccai, L. Familial and sporadic neurogenic acro-osteolysis. *Acta radiol.*, 1952, *38*, 17–29.

3. Greenberg, B. E., and Street, D. M. Idiopathic non-familial acro-osteolysis. *Radiology*, 1957, *69*, 259–262.

4. Harms, I. Familial acro-osteolysis. *Fortschr. a. d. Geb. d. Röntgenstrahlen*, 1954, *80*, 727–732.

5. Harnasch, H. Acro-osteolysis, new disease picture. *Fortschr. a. d. Geb. d. Röntgenstrahlen*, 1950, *72*, 352–359.

6. Luck, J. V. Bone and Joint Diseases. First edition. Charles C Thomas, Publisher, Springfield, Ill., 1950.

7. Köhler, A., and Zimmer, E. A. Borderlands of the Normal and Early Pathologic in Skeletal Roentgenology. Ninth edition. Grune & Stratton, Inc., New York, 1956.

8. McKusick, V. A. Heritable Disorders of Connective Tissue. C. V. Mosby Company, St. Louis, 1960.

9. Papavasiliou, C. G., Gargano, F. P., and Walls, W. L. Idiopathic nonfamilial acro-osteolysis associated with other bone abnormalities. Am. J. Roentgenol., Rad. Therapy & Nuclear Med., 1960, *83*, 687–691.

10. Wassner, U. J. Additional case of acro-osteolysis with differential diagnosis. *Fortschr. a. d. Geb. d. Röntgenstrahlen*, 1954, *80*, 186–191.

11. Wieland, H. A. Contribution to our knowledge of acro-osteolysis. *Fortschr. a. d. Geb. d. Röntgenstrahlen*, 1952, *77*, 193–198.

# SKELETAL FLUOROSIS AMONG INDIANS OF THE AMERICAN SOUTHWEST

*By* JOHN W. MORRIS, M.D.*
PHOENIX, ARIZONA

SKELETAL fluorosis may be recognized by observing the rather characteristic sclerotic bone changes in individuals exposed to unusually high quantities of fluoride salts. Ingestion of drinking water having a high concentration of fluoride salts is a frequent cause,[1,7,8,9,14,19] but findings may also occur in cryolite workers and in miners working with ores having a high fluoride content.[12]

For the past several years occasional patients at the United States Public Health Service Indian Hospital in Phoenix, Arizona, have been noted to have unusually dense bones, especially of the spine and pelvis, quite similar to the findings of osteopetrosis or "marble-bone disease." Interestingly, these patients came from several specific localities on the Papago and Apache Indian Reservations in Southern Arizona, and this fact prompted an investigation of the drinking water from wells in these areas. Analysis of these waters yielded fluoride concentrations varying from 0.5 parts per million (p.p.m.) to higher than 18 parts per million.[4,15,18] This is considerably in excess of the 1 part per million commonly recommended for the prevention of dental caries.[11] Samples of bone of some of these patients were analyzed for fluoride content, and the excessively high values obtained confirmed the diagnosis of skeletal fluorosis. This communication is concerned with the presentation of these cases and diagnostic data, emphasizing the roentgenographic findings.

## METHOD AND MATERIAL

The United States Public Health Service Indian Hospital at Phoenix, Arizona, is the referral center for field clinics and reservation hospitals of American Indians in California, Nevada, Utah and most of Arizona; and these areas represent the source of the population studied. From 1959 through 1963, 20 American Indian patients with unusually dense bones were discovered. During this 5 year period, there were 9,726 admissions to this hospital, and 84,707 visits to the outpatient clinic. Approximately 40,000 chest roentgenograms were examined, one-third of which were obtained from field units.

The diagnosis of skeletal fluorosis was suspected on the basis of findings on routine chest examinations and studies of the spine and abdomen. The hospital records indicated the patient's residence and other pertinent information. Fluoride content of well water samples was provided by water analysis data compiled by state and federal Public Health Service organizations. Analysis of bone samples for fluoride content was performed by Dr. I. Zipkin of the National Institute of Dental Research, Bethesda, Maryland.

## RESULTS

In our series there were 15 males and 5 females. The ages ranged from 22 to 85 years. Twelve of the 20 cases were over 40 years of age, and 5 exceeded 60 years. Of these 20 patients suspected of having skeletal fluorosis, none had signs or symptoms of bone disease, except one 22 year old Apache male with severe renal rickets resulting from chronic pyelonephritis (A.U.). There was no evidence of any deleterious results of the skeletal changes, with the possible exception of a 58 year old Apache male (F.S.), who, throughout his life, had sustained multiple fractures (Fig. 8 and 9), the cause of which was undetermined, even at necropsy examination. He died of pneumo-

* Surgeon, United States Public Health Service; Chief, Radiology Service, U.S.P.H.S. Indian Hospital, Phoenix, Arizona.

nia. A comparison of tribal distribution of all hospital admissions and patients with skeletal fluorosis is presented in Table I.

From these data it is seen that a disproportionate number of patients with fluorosis are from the Papago tribe. These 16 Papagos live in the general vicinity of Gila Bend, Arizona. The well water fluoride content in this area is quite high. The Gila Bend Water Works gives figures of 7.1 to 7.3 p.p.m. as the fluoride concentration of well water from which they receive their supply. On the Papago reservation about 25 per cent of the wells sampled yielded water of more than 1.5 p.p.m. Water in the southwestern quarter of the reservation, where volcanic rocks are dominant, generally contain greater concentrations of fluoride than waters from other ground-water areas.[4] The 3 Apache patients lived near Bylas, on the San Carlos reservation. Wells in this area contain water with fluoride concentrations of 1.0 p.p.m. to 9.2 p.p.m.[4]

Because of the migrant nature of many of these Indians, it was impossible to determine specifically from which well or wells these patients took their water, but it is clear that all come from areas known to have an excessively high fluoride content in drinking water. Characteristic mottling of the teeth from excessive fluoride ingestion is a frequent observation among these people.

Seven of our 20 patients underwent bone biopsy. The results of the fluoride analysis and the degree of bone changes are tabulated in Table II. The bone changes were subjectively graded from 1 to 4, depending upon the degree of change.

Table I

TRIBAL DISTRIBUTION OF PATIENTS WITH FLUOROSIS COMPARED WITH HOSPITAL ADMISSIONS

| Tribe | All Admissions 1959–1963 | | Skeletal Fluorosis | |
|---|---|---|---|---|
| | No. of Cases | Per Cent | No. of Cases | Per Cent |
| Pima | 3,517 | 36.2 | 1 | 5 |
| Apache | 1,756 | 18.1 | 3 | 15 |
| Navajo | 1,033 | 10.6 | 0 | 0 |
| Papago | 787 | 8.1 | 16 | 80 |
| Hopi | 489 | 5.0 | 0 | 0 |
| Other | 2,144 | 22.0 | 0 | 0 |
| Total | 9,726 | 100.0 | 20 | 100 |

### ROENTGENOGRAPHIC FINDINGS

The roentgenographic manifestations of skeletal fluorosis were first described in 1932 by Møller and Gudjonsson,[12] who in their classic paper reported osseous changes in 30 of 78 cryolite factory workers who had inhaled and swallowed the dust of the fluoride-rich ore. The bones of the spine and pelvis were described as being thick and dense. The contours of the vertebrae were not sharp and the transverse processes appeared plump and thick. Calcification of the spinous ligaments and considerable osteophytosis of the vertebral bodies were present. Occasional calcification of the ischiosacral ligaments was also seen. The ribs appeared to have needle-like calcifications projecting out at the attachments of the intercostal muscles in some cases. The long bones were involved to a lesser extent, but the compact layers of bone appeared thickened and the marrow cavity narrowed. The small bones of the hands and feet were involved to an even lesser extent. The cranium was occasionally involved with some degree of thickening. It was pointed out that the intensity of changes is most marked in the axial skeleton and becomes less toward the periphery. Roholm[14] presents a dynamic description of the changes due to fluorosis and emphasizes that the changes in the extremities and skull were not seen in his cases.

In the present study, it was found that the first and most subtle change appears to be a thickening and roughening of the trabecular pattern of bone, best recognized and earliest seen in the vertebral bodies, especially in the lateral projection (Fig. 1). In cases with a greater degree of involvement, these changes are found also in the pelvis, clavicle and ribs, accompanied by a generalized sclerosis of these bones (Fig. 2),

which at first resembles widespread osteoblastic metastases, but which is not limited to one bone or a discrete area of one bone. These osseous changes are symmetric, diffuse and not well demarcated. The more advanced manifestations are quite obvious and usually are readily apparent on the frontal roentgenogram of the chest (Fig. 3). The ribs are thickened and all visible bones are involved with a diffuse, extensive and generalized sclerotic process. The vertebral bodies, particularly, are extremely dense (Fig. 4) and closely resemble the findings in osteopetrosis, except for the fact that, in skeletal fluorosis, there is a greater degree of osteophytosis than one would expect, and that these osteophytes, too, appear inordinately sclerotic; and, unlike osteopetrosis, the long bones and skull tend to be spared by the sclerotic process. In our series the skull and bones of the hands and feet were not involved. It has been indicated that calcification of the sacrospinous or sacrotuberous ligaments (Fig. 5, 6 and 7) is an important diagnostic feature,[16,17] and this observation was made in 3 of our 20 cases. Calcification of these ligaments may not be symmetric; it appears to progress superiorly, so that the part of the ligament nearest to the sacrum is the last to become opacified.

In addition to osteopetrosis and osteoblastic metastases, the differential diagnosis includes Paget's disease, which is usually not symmetric or as generalized and frequently involves the skull. Differentiation from myelofibrosis may be difficult, but in our cases fluorosis was not associated with anemia or splenomegaly. Osteosclerosis from chronic renal disease associated with secondary hyperparathyroidism may produce similar changes, and indeed may have intensified the findings in one of our patients (A.U.) (Fig. 8). Urticaria pigmen-

Table II

FLUORIDE CONTENT OF BONE OF PATIENTS ANALYZED

| Patient | Age | Sex | Tribe | Residence | Site of Biopsy | Per Cent Ash | Per Cent F Dry Basis | Per Cent F Ash Basis | Estimation of Degree of Roentgenographic Change | | |
|---|---|---|---|---|---|---|---|---|---|---|---|
| | | | | | | | | | Ribs | Pelvis | Vertebrae |
| A.U. | 22 | M | Apache | Bylas | Rib | 55 | .629 | 1.14 | 4+ | 4+ | 4+ |
| | | | | | Ilium | 50 | .649 | 1.08 | | | |
| A.W. | 28 | F | Apache | Bylas | Sternum | 60.6 | .699 | 1.15 | 1+ | 2+ | 2+ |
| | | | | | Rib | 60.6 | .556 | .92 | | | |
| L.V. | 38 | M | Papago | Gila Bend | Sternum | 62 | .149 | .241 | 0 | 1+ | 2+ |
| A.Q. | 60 | M | Papago | Arlington | Sternum | 63.3 | .160 | .253 | 0 | — | 1+ |
| P.J. | 55 | M | Papago | Gila Bend | Sternum | 65.9 | .156 | .237 | 1+ | 1+ | 2+ |
| A.L. | 49 | M | Papago | Gila Bend | Sternum | 61.6 | .126 | .204 | 0 | 1+ | 1+ |
| F.S. | 58 | M | Apache | Bylas | Vertebra | 55.2 | .563 | 1.02 | 2+ | 2+ | 3+ |
| Average values in population drinking water of less than 1.0 part per million (p.p.m.)[20] | | | | | Rib | 56.04 | .045* | .08 ± .01 | 0 | 0 | 0 |
| | | | | | Sternum | 48.59 | .063* | .13 ± .02 | 0 | 0 | 0 |
| | | | | | Vertebra | 49.82 | .050* | .10 ± .01 | 0 | 0 | 0 |
| | | | | | Ilium | 53.51 | .043* | .08 ± .01 | 0 | 0 | 0 |

* Calculated.

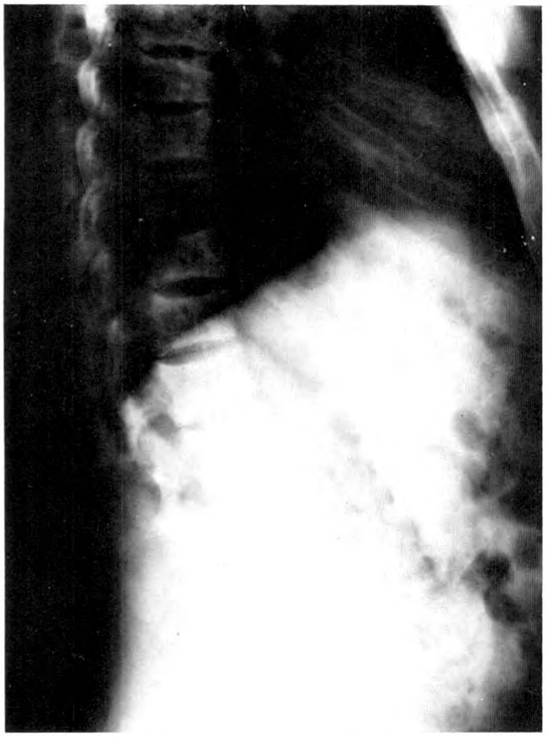

Fig. 1. Lateral roentgenogram best demonstrates the earliest changes of the vertebral bodies.

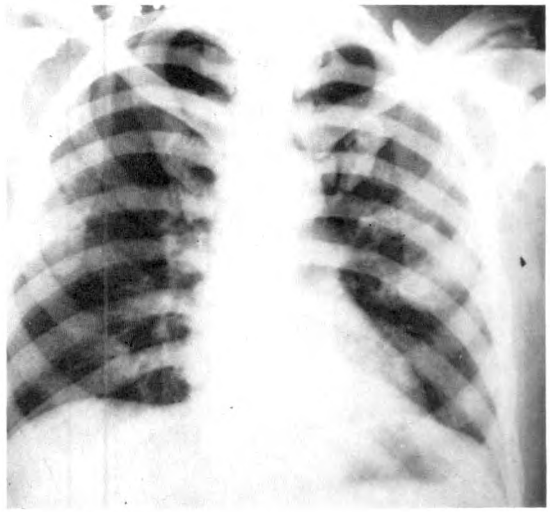

Fig. 2. Posteroanterior chest roentgenogram shows the typical, but not so extensive, changes of sclerosis.

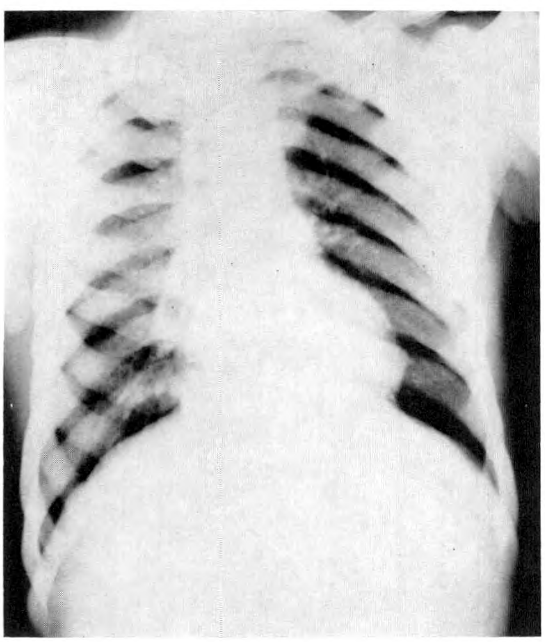

Fig. 3. Typical changes of extensive involvement. The thickened and sclerotic ribs with the coarsened trabecular pattern are characteristic.

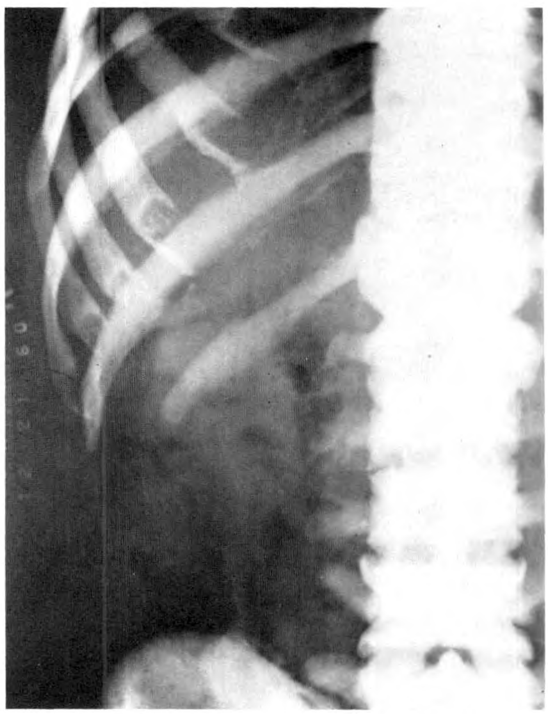

Fig. 4. The extensive osteophytosis and extremely dense vertebral bodies are typical findings.

FIG. 5. The dense lumbar vertebrae are unmistakable. The sacrospinous ligaments are heavily calcified.

tosa may cause sclerotic osseous changes, but only in association with adjacent cutaneous changes.

FIG. 6. Calcified sacrospinous ligaments are considered diagnostic of fluorosis when bone sclerosis is present.

## DISCUSSION

In recent years, it has been pointed out that a certain amount of fluoride in the drinking water is desirable in order to decrease the incidence of dental caries. Most authorities suggest that a fluoride concentration of 1 part per million (1 p.p.m. or .001 mg. per cent) is ideal. The dental profession is cognizant of the fact that considerably higher levels of fluoride (3–4 p.p.m. and higher) may cause a characteristic brownish mottling of the teeth, even before they erupt.[5] In concentrations greater than 4 p.p.m., characteristic sclerotic bone changes are also apt to occur.[5] Hodges *et al.*[6] report no skeletal sclerosis in two Illinois communities where the concentration of fluoride is 3 p.p.m., but mottled enamel was

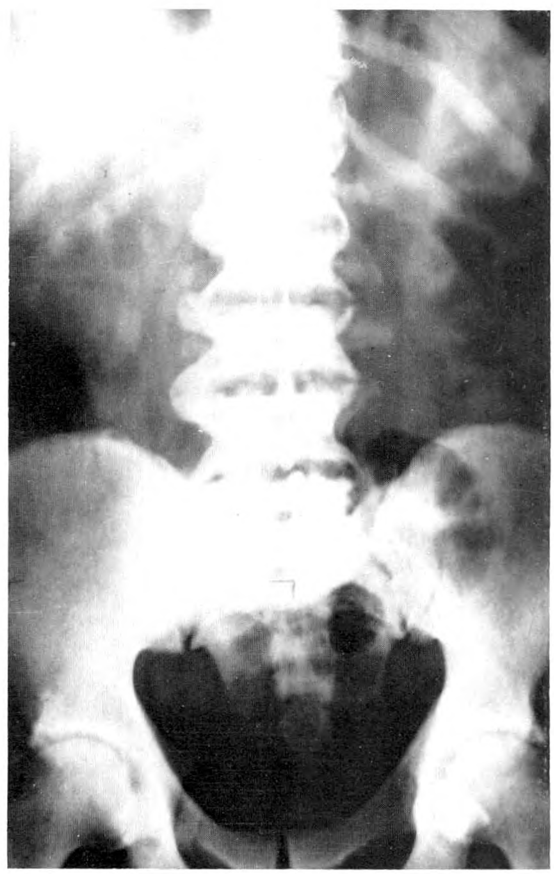

FIG. 7. Extensive sclerosis and osteophytosis of the vertebral bodies and calcification of one sacrotuberous ligament.

observed in the majority of the patients who had been exposed to this water during childhood. Stevenson and Watson[16,17] conclude that osteosclerosis is not roentgenographically apparent when the fluoride concentration is less than 4 p.p.m. However, Azar *et al.*[1] report cases of skeletal fluorosis in Qatari people along the Persian Gulf, who ingest water having a concentration of fluoride of less than 4 p.p.m., but they suggest that local factors such as hot climate and malnutrition may be factors responsible for the manifestations, at this level of fluoride content in the drinking water.

Without doubt, fluorides have been shown to be the ultimate cause of osseous

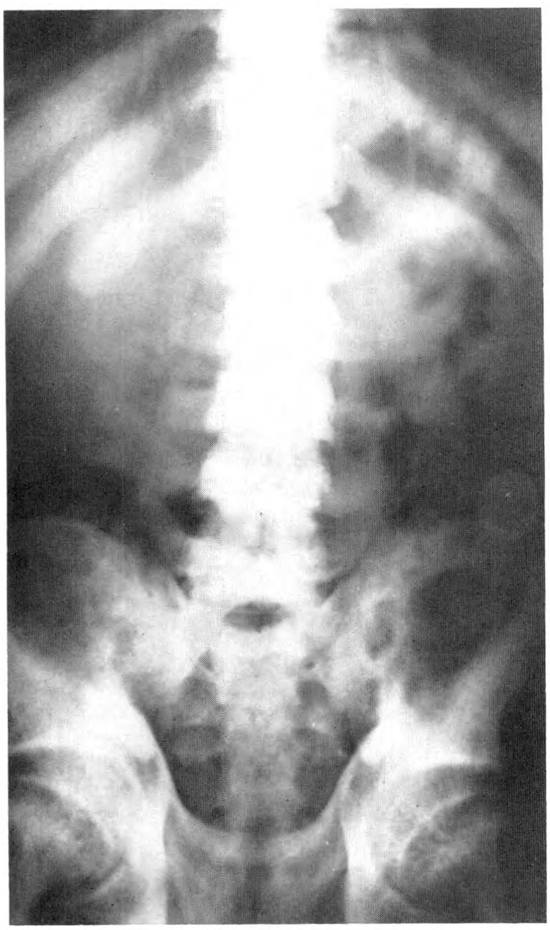

FIG. 8. Typical changes of severe fluorosis complicated by renal rickets, causing bilateral protrusio acetabuli.

FIG. 9. Extensive idiopathic fractures, not related to fluorosis.

and ligamentous changes, but just how these changes come about is not certain. Leone *et al.*,[7,8] after a carefully controlled study, concluded that excessive fluorides in drinking water may produce changes, but they occur in only 10–15 per cent of all those individuals exposed over a period of many years to drinking water with a fluoride concentration of greater than 8 p.p.m. It was noted that roentgenographic changes may not be apparent even when the fluoride content of the bone is 6 times that of normal. It was, therefore, concluded that an increased concentration of fluoride in the drinking water does not uniformly produce the characteristic bone changes. From tabulations of the present study (Table II), it is apparent that the degree of bone

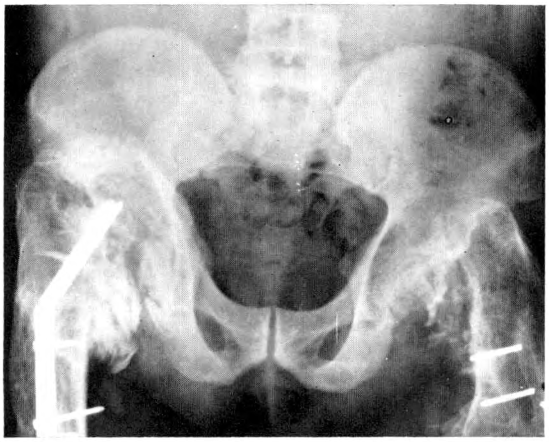

Fig. 10. Extensive idiopathic fractures, not thought to be connected causally with fluorosis (same patient as in Fig. 9).

change does not correlate well with the amount of fluoride present in the bone. It is evident that ingested fluorides may cause osseous sclerosis, but it is an enigma that people from the same area, drinking water from the same source, have considerable variability in the degree of sclerosis, and indeed may have no roentgenographic changes at all, even though it has been shown that fluoride concentrations in bones of a human population has a linear relationship with the concentration of fluorides in the drinking water up to concentrations of 4 p.p.m.[19] Pugh[13] postulates that the sclerotic changes are due, not to the fluoride salts themselves, but to the reactive bone changes in response to their presence. It is, therefore, concluded that the sclerotic bone changes must not be caused directly and entirely by the presence of fluorides in the bone, and that the individual response to the fluorides must, for some reason, be greatly variable. Differences in roentgenographic technique may be partly responsible in some cases, and a carefully controlled study would be necessary to exclude this variable.

Stevenson and Watson[16,17] conclude that osteosclerosis from fluoride concentrations as high as 8 p.p.m. causes no harmful effects. In their series of 23 cases, they were unable to find any unusual incidence of anemia, arteriosclerosis, arthritis, stiffness of the back, renal disease or biliary calculi. Leone[7] states that of 237 people, who for over 30 years drank water with a concentration of 8 p.p.m., no clinically significant, adverse, physiologic or functional effect resulted from the absorption of fluorides, with the exception of dental fluorosis. McCann[10] believes that the human skeletal tissue may have a high degree of physiologic tolerance to the accumulation of skeletal fluorides. As much as .5–.6 per cent in skeletal tissues may not be a physiologic hazard to the individual. Calenoff[3] reports a case of iatrogenic fluorosis in a male who for 6 years medicated himself with considerable quantities of hydrofluoric acid as a tonic. This man presented with extensive osseous changes, but had no symptomatology with reference to fluoride ingestion. Bishop[2] indicates that the extensive osteophytosis may be responsible for back pain occasionally seen, but emphasizes the benign nature of fluorosis. Leone[7] states in a personal communication that he suspects that fluorosis may, in fact, provide some degree of protection against the effects of loss of osseous strength from senile osteoporosis.

Our cases indicate that skeletal fluorosis is a benign condition, since none of our 20 patients had any signs or symptoms relative to the osseous or ligamentous changes, with the doubtful exception of the one patient having multiple and repeated fractures.

## SUMMARY

Presented are 20 cases of Southwestern American Indians having characteristic sclerotic bone changes caused by the ingestion of drinking water containing excessively great quantities of fluoride salts. The changes of skeletal fluorosis are described, and it is pointed out that the degree of change does not seem to correlate well with the concentration of fluoride in the bone. It remains an enigma that there is such variability in the degree of the manifestations among people exposed to the same supply

of drinking water, but it is pointed out that factors such as climate, nutritional status, and habit variations may be responsible. It is concluded that skeletal fluorosis produces no demonstrable physiologic adversities, but it is important to differentiate from serious pathologic conditions which it may simulate.

Section of Radiology
United States Public Health Service Indian Hospital
Phoenix, Arizona

The author wishes to express thanks to Dr. Maurice L. Sievers, Surgeon, Director Grade, U.S.P.H.S. and Dr. James Marquis for their help in accumulating case material, and to Dr. Marcy Sussman, Dr. Ted Leigh, and Dr. Nicholas Leone, Surgeon, Director Grade, U.S.P.H.S. for their constructive criticism enabling this paper to be completed.

## REFERENCES

1. Azar, H. A., Nucho, C. K., Bayyuk, S. I., and Bayyuk, W. B. Skeletal sclerosis due to chronic fluoride intoxication: cases from endemic area of fluorosis in region of Persian gulf. *Ann. Int. Med.*, 1961, *55*, 193–200.
2. Bishop, P. A. Bone changes in chronic fluorine intoxication: roentgenographic study. Am. J. Roentgenol. & Rad. Therapy, 1936, *35*, 577–585.
3. Calenoff, L. Osteosclerosis from intentional ingestion of hydrofluoric acid. Am. J. Roentgenol., Rad. Therapy & Nuclear Med., 1962, *87*, 1112–1115.
4. Heindl, L. A., and Cosner, O. J. Hydrologic data and drillers' logs, Papago Indian Reservation, Arizona. U. S. Geological Survey, Open File Report, 1960.
5. Hodge, H. C. Notes on effects of fluoride deposition on body tissues. *A.M.A. Arch. Indust. Med.*, 1960, *21*, 350–352.
6. Hodges, P. C., Fareed, O. J., Ruggy, G., and Chudnoff, J. Skeletal sclerosis in chronic sodium fluoride poisoning. *J.A.M.A.*, 1941, *117*, 1938–1939.
7. Leone, N. C. Effects of absorption of fluoride. *A.M.A. Arch. Indust. Med.*, 1960, *21*, 324–325.
8. Leone, N. C., Stevenson, C. A., Hilbish, T. F., and Sosman, M. C. Roentgenologic study of human population exposed to high-fluoride domestic water: ten-year review. Am. J. Roentgenol., Rad. Therapy & Nuclear Med., 1955, *74*, 874–885.
9. Linsman, J. F., and McMurray, C. A. Fluoride osteosclerosis from drinking water. *Radiology*, 1943, *40*, 474–484.
10. McCann, H. G. Effects of absorption of fluorides. VII. Comparison of physiologic and pathologic characteristics of fluoride content of skeletal tissues of two persons of similar experience, except for exposure to fluoride. Part 2. Fluoride content of skeletal tissues. *A.M.A. Arch. Indust. Health.*, 1960, *21*, 336–337.
11. McClure, F. J., and Zipkin, I. Physiological effects of fluoride as related to water fluoridation. In: Dental Clinics of North America. W. B. Saunders Company, Philadelphia, 1958, pp. 441–458.
12. Møller, P. F., and Gudjonsson, S. V. Massive fluorosis of bones and ligaments. *Acta radiol.*, 1932, *13*, 269–304.
13. Pugh, D. G. Roentgenologic Diagnosis of Diseases of Bones. Williams & Wilkins Company, Baltimore, 1958.
14. Roholm, K. Fluorine Intoxication: A Clinical Hygienic Study. H. K. Lewis & Co., London, 1937.
15. Skibitzke, H. D., and Yost, C. B. Location of sites for irrigation wells near Chiu Chiuschu, Papago Indian Reservation, Pinal County. U. S. Geological Survey, Open File Report, 1951.
16. Stevenson, C. A., and Watson, A. R. Fluoride osteosclerosis. Am. J. Roentgenol., Rad. Therapy & Nuclear Med., 1957, *78*, 13–18.
17. Stevenson, C. A., and Watson, A. R. Roentgenologic findings in fluoride osteosclerosis: summary of report. *A.M.A. Arch. Indust. Health*, 1960, *21*, 340.
18. Yost, C. B. Geophysical and geological reconnaissance to determine groundwater resources of Chiu Chiuschu Area, Papago Indian Reservation, Arizona. U. S. Geological Survey, Open File Report, 1953.
19. Zipkin, I., McClure, F. J., Leone, N. C., and Lee, W. A. Fluoride deposition in human bones after prolonged ingestion of fluoride in drinking water. Public Health Report, 1958, *73*, 732–740.
20. Zipkin, I., McClure, F. J., and Lee, W. A. Relation of fluoride content of human bone to its chemical composition. *Arch. Oral Biol.*, 1960, *2*, 190–195.

# OSTEOPETROSIS*

## A CASE PRESENTATION

By GEORGE LOTT, LT MC USNR,† and EDWARD KLEIN, LCDR USN‡
GREAT LAKES, ILLINOIS

OSTEOPETROSIS, a developmental abnormality of the skeleton of unknown etiology, is characterized by generalized increased bone density. The entity was first described by Albers-Schönberg in 1904 and termed "marble bones." Later, in 1926, the condition was designated as osteopetrosis by Karshner.[4]

The disease is hereditary and shows a strong familial tendency.[2,3,5,6] There are no indications of race or sex predilections. Consanguinity of the parents has been reported to be present not infrequently in osteopetrotic descendants.[2,6]

McPeak[5] was one of the first to describe two different types of osteopetrosis based on their clinical course. In the malignant variety, the onset is at birth or shortly thereafter. There may be, in addition to marbling of the bones, hydrocephalus, severe anemia, ocular disturbances, hepatosplenomegaly, frequent fractures and the resulting deformities. These infants are usually underdeveloped and survive only a few years.

The second type is the benign form in which the onset is later in life. Here, there may be a history of fractures from minor trauma or the patient may be entirely asymptomatic. Anemia is not common and hepatosplenomegaly is rare. In the following case, osteopetrosis was an incidental finding during a routine study.

### REPORT OF A CASE

D.K., a 37 year old white housewife, had twisted her right ankle one week prior to being seen in the out-patient department. The ankle remained tender and slightly swollen. Roentgenograms of the ankle showed no fracture; however, an unusual sclerotic pattern was noted in the distal tibia and fibula as well as in all the tarsal bones (Fig. 5 and 6). The patient was unaware of these findings and consented to a skeletal survey (Fig. 1 through 8).

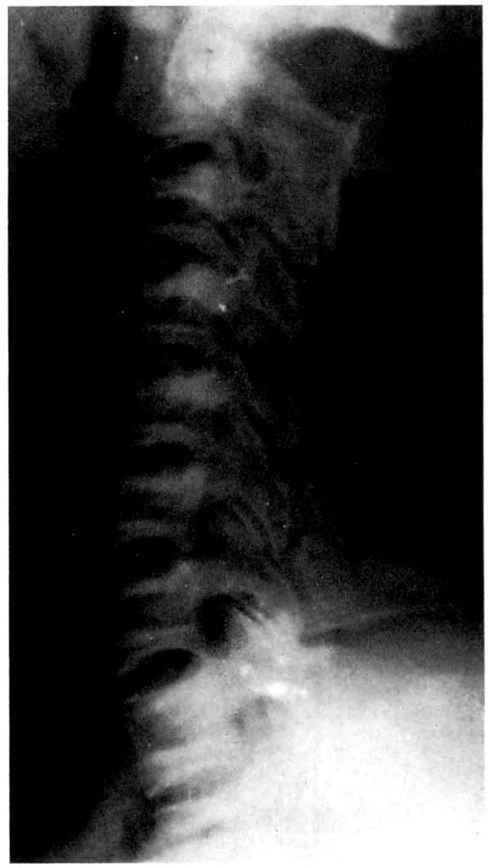

Fig. 1. Lateral view of the cervical spine shows the typical "sandwich vertebrae" characteristic of osteopetrosis.

The family history was not obtainable as the patient was an adopted child. Past history revealed that she was hospitalized as a child (age 7 years) for polyneuritis and suspected lead poisoning. Detailed study for lead ingestion,

* From the Department of Radiology, US Naval Hospital, Great Lakes, Illinois.
The opinions expressed are those of the authors and do not necessarily represent the views of the Navy Department.
† Resident in Radiology, Veterans Administration Hospital, Hines, Illinois, currently serving in US Navy.
‡ Staff Radiologist.

however, was negative. Roentgenograms at that time were considered suggestive of osteosclerosis. These films cannot be located; however, they were interpreted as follows: "Films of the extremities show a broad zone of increased density at the ends of the long bones which shades off gradually for a considerable distance into the diaphysis. The bones in general appear to be increased in density." It was the impression of the house officers that the patient did have plumbism but also that marble bone disease should be a consideration. She recovered from this episode uneventfully. She had no other significant childhood or adult illnesses.

Indicated laboratory studies, including a complete blood cell count, sedimentation rate, urinalysis, serum calcium and phosphorus, alkaline phosphatase, blood smear and 24 hour urine examination for calcium, were all within normal limits. Roentgenograms of the patient's children were normal.

A detailed examination of the present roentgenograms suggested that the disease process began when the patient was 4 or 5 years of age and ceased somewhere between the ages of 10 and 12. Bone formed before and after this period was normal. Retention of original bone was most striking in the epiphysis. It appeared that bone laid down in the epiphysis remained without reconstruction. The metaphysis of the long bones showed that remodeling had occurred but sufficient findings were present by which it was possible to roughly identify the time when the disease began and ceased. The lack of sclerosis in the carpal bones as compared to the tarsal bones suggested that considerable reconstruction had taken place in the former.

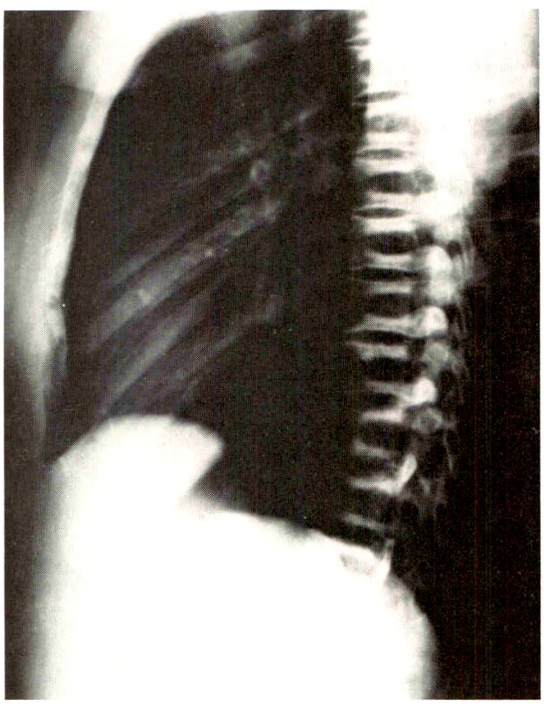

Fig. 2. Roentgenogram of the thoracic spine clearly shows the "sandwich vertebrae."

Fig. 3. Roentgenogram of the lumbar spine shows findings similar to those in Figure 1 and 2.

Physical examination of the patient was not remarkable with the exception of pain and limitation of motion of the left shoulder. Roentgenograms revealed rather large calcium deposits within the rotator cuff.

Surgical correction was advised for the peritendinitis calcarea of the shoulder and the patient consented to undergo bone biopsy at the time of surgery. Specimens were taken from the humeral head and distal tibia.

The Department of Pathology at the Navy

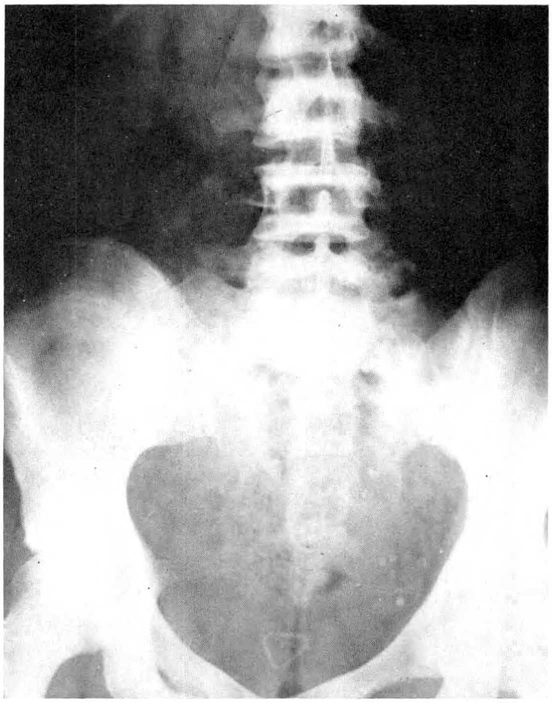

Fig. 4. Roentgenogram of the pelvis demonstrates laminated ring-like densities of the iliac bones. These alternating lines of increased and decreased density point to the fact that the disease process is subject to remissions and exacerbations.

Hospital, San Diego, California, as well as the Armed Forces Institute of Pathology, diagnosed the biopsy findings as osteopetrosis.

DISCUSSION

Osteopetrosis is a rare condition in that there are only 257 cases reported in the literature. The roentgenographic changes in the malignant variety are seen *in utero* or soon after birth and show uniform sclerosis or marbling of the entire skeleton, narrowing of the medullary spaces and failure of normal remodeling of the metaphyseal portion of the long bones.

In the benign variety the long bones show sclerosis in the metaphysis and at the site of the previous epiphysis. This sclerosis gradually fades in the diaphysis, in which there may be a lesser degree of involvement. The pelvis is commonly involved and may show concentric sclerotic rings giving the appearance of a "bone within a bone." In the spine, as seen on the lateral view, there is a "sandwich vertebrae" appearance due to dense superior and inferior portions with normal bone in the middle.

The carpal and tarsal bones may also show a "bone within a bone" appearance which is characteristic of benign osteopetrosis.[2]

Fig. 6. Foot roentgenogram shows to advantage the "bone within a bone" effect best seen in the cuboid.

Fig. 5. Lateral roentgenogram of the ankle shows dense sclerotic deposits in the distal tibia, talus and os calcis.

The bones of the hands are not commonly involved; however, they may show various degrees of increased density which may be associated with thickening of the shafts and, occasionally, syndactyly.[8]

In the skull, there may be sclerosis of the base and narrowing of the foramina, resulting in neurologic symptoms.[6] Clubbing of the anterior and posterior clinoids is common. In the malignant variety there may be, in addition to the above, sclerotic changes involving the vault, orbits, maxillae and mandibles with obliteration of the mastoid cells and sinuses.

In the authors' experience, the "sandwich vertebrae" and "bone within a bone" appearance when present in adults are pathognomonic of benign osteopetrosis.

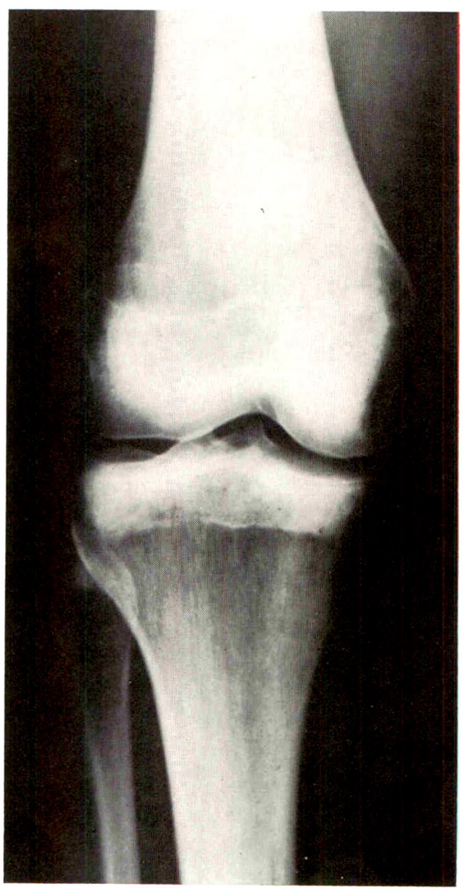

Fig. 7. Note the persistence of dense transverse lines in the distal femur and proximal tibia. This is attributed to deficient bone resorption. Also note metaphyseal sclerosis.

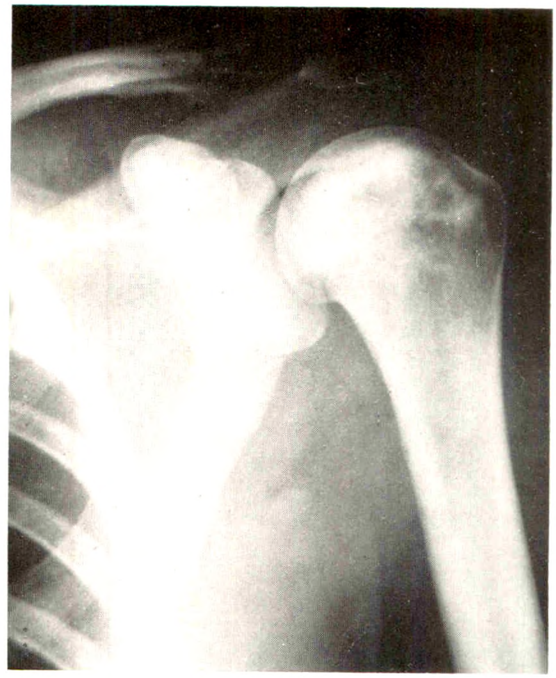

Fig. 8. Unresorbed juvenile bone persists in the humeral head. Several sclerotic nidi are seen in the coracoid process, clavicle and ribs.

In most cases of osteopetrosis, the roentgenographic differential diagnosis is not difficult. In heavy metal poisoning, transverse bands of increased density are present in the metaphyseal regions of growing tubular bones. The astragalus and the sphenoid are not involved. When exposure to the toxin ceases, the densities gradually fade. In adults, the roentgenologic diagnosis of heavy metal poisoning cannot be made.[7]

In fluorosis, the growth centers are involved; however, the skull is spared. There is mottling of the teeth and ligamentous calcifications. In addition to the above findings, a history of increased fluorine intake and chemical analysis of the bones will clarify the diagnosis.

Early in myelosclerosis the bones may show patchy areas of increased density. As the condition progresses, the density becomes diffuse and involves the entire skeleton with the exception of the skull. Trans-

verse bands of increased density are not seen. This condition is also characterized by progressive anemia and splenomegaly. The bone marrow examination which shows myelofibrosis is diagnostic.

Other entities which must be considered are lymphoblastomas, metastatic osteoblastic carcinoma, Paget's disease, osteopathia striatum, Englemann's disease, infantile cortical hyperostosis, melorheostosis and osteopoikilosis. For discussion of the above, the reader is referred to Hinkel's excellent article.[3]

## SUMMARY

A case of benign osteopetrosis is presented. Following a brief review of the literature, the roentgenographic characteristics and differential diagnosis are discussed.

George Lott, M.D.
Department of Radiology,
Veterans Administration Hospital
Hines, Illinois

## REFERENCES

1. Hasenhuttle, K. Osteopetrosis; review of literature and comparative studies on case with a twenty-four-year follow-up. *J. Bone & Joint Surg.*, 1962, *44A*, 359–370.
2. Hinkel, C. L., and Beiler, D. D. Osteopetrosis in adults. Am. J. Roentgenol., Rad. Therapy & Nuclear Med., 1955, *74*, 46–64.
3. Hinkel, C. L. Developmental affections of skeleton characterized by osteosclerosis. *Clin. Orthop.*, 1957, *9*, 85–106.
4. Karshner, R. G. Osteopetrosis. Am. J. Roentgenol. & Rad. Therapy, 1926, *16*, 405–419.
5. McPeak, C. N. Osteopetrosis; report of eight cases occurring in three generations of one family. Am. J. Roentgenol. & Rad. Therapy, 1936, *36*, 816–829.
6. Montgomery, R. D., and Standard, K. L. Albers-Schönberg's disease; changing concept. *J. Bone & Joint Surg.*, 1960, *42B*, 303–312.
7. Pugh, D. G. The Roentgenographic Diagnosis of Diseases of Bones. Williams & Wilkins Company, Baltimore, 1960.
8. Truswell, A. S. Osteopetrosis with syndactyly; morphological variant of Albers-Schönberg's disease. *J. Bone & Joint Surg.*, 1958, *40B*, 208–218.

# GAUCHER'S DISEASE*

## ROENTGENOLOGIC BONE CHANGES OVER 20 YEAR INTERVAL

*By* JAMES A. ROURKE, M.D.,† *and* D. JAMES HESLIN, M.D.‡
BOSTON, MASSACHUSETTS

GAUCHER'S disease is an uncommon metabolic disturbance characterized by abnormal deposition of cerebrosides in the cells of the reticuloendothelial system. A positive diagnosis depends upon the identification of Gaucher's cells in biopsy aspirate from the sternal marrow[5] or, more reliably, from the spleen. Neither Gaucher's cells nor abnormal cerebrosides can be isolated from the circulating blood.

Although the disorder is a systemic one, symptoms and roentgen manifestations vary widely, depending upon the predominant sites of involvement and upon the stage of the disease process.

### CLINICAL FEATURES

Gaucher's disease occurs predominantly, but not exclusively, in people of Jewish ancestry. Cases have been reported in Indians, Filipinos, Mexicans, Japanese, and Negroes. The sex incidence is equal. The disease is described as occasionally familial, since approximately one-third of the reported cases have involved several members of a family in a single generation.[18] Occurrence in siblings is unusual.[4] Two forms are recognized, an infantile or acute form, which usually terminates fatally within 18 months, and a chronic form, characterized by a progressive, insidious course, consistent with a relatively long life span.

Approximately one-third of cases of Gaucher's disease are seen in infancy. At this age, symptoms are referable chiefly to the nervous and respiratory systems. There is a close resemblance to Niemann-Pick disease except that there are no macular changes. Commonly, the first abnormality noted is abdominal enlargement from hepatosplenomegaly. Usually, after 6 months, there is evidence of apathy, anorexia with mental regression, and, occasionally, spasticity.[17] No instance of macroscopic bone change was discovered in this age group in a review of the literature, nor are anemia, thrombocytopenic purpura, or skin pigmentation encountered.

Of the chronic cases, 50 to 60 per cent show symptoms in the first decade of life, with vague feelings of weakness and fatigue and abdominal discomfort which may continue over long periods of time. There is sometimes a slow and unexplained progressive weight loss. The skin of the exposed parts, particularly the face, neck, and pretibial surfaces, takes on a yellowish-brown hue and eventually the patients look chronically ill. A triangular conjunctival thickening somewhat resembling pingueculae develops in approximately one-third of the cases.[2] The patients show a bleeding tendency, usually in the nature of gingival bleeding, epistaxis, and hematuria, and often bruise easily.

Bouts of pain and limitation of motion of joints are a result of osseous involvement; the hip and knee joints are the most commonly involved, followed by the ankle and shoulder. The symptoms and roentgen changes in the hips are indistinguishable from those of Legg-Perthes' disease. Pathologic fractures occur in from 5 to 10 per cent of cases in childhood, usually involving the hips, ribs, and vertebrae, but are uncommon in adult life.[22]

Splenomegaly is almost invariably found. Enlargement of the liver occurs in 70 to 80 per cent of cases but is usually of considerable less degree than that of the spleen. Approximately 80 per cent of cases will

* From the Department of Radiology, Massachusetts General Hospital, Boston, Massachusetts.
† Assistant in Radiology, Harvard Medical School; Assistant in Radiology, Massachusetts General Hospital.
‡ Clinical Fellow in Radiology, Massachusetts General Hospital. Presently: St. Michael's Hospital, Toronto, Ontario, Canada.

show hematologic abnormality,[10] frequently a pancytopenia; anemia, leukopenia, and thrombocytopenia may be found in varying combinations. Elevation of serum phosphatase is almost invariable.[21] Superficial lymphadenopathy is unusual.

A purely osseous form of the disease without hepatosplenomegaly has been described by Pick,[15] and Harrison and Louis[6] reported a case with extensive bone changes and pathologic fractures without splenomegaly. An atypical example was reported by Petit and Schleicher[14] in a 79 year old Jewish male who showed no clinical findings or gross changes either roentgenographically or at autopsy, but did show microscopic infiltration of Gaucher's cells in the bone marrow, spleen, and lymph nodes of the porta hepatis.

The typical roentgenographic finding of a trumpet-shaped deformity of the distal femora with thinning of the cortices and subsequent rarefaction and condensation of spongiosa is characteristic but not pathognomonic and presents in only those cases in which there is gross bone involvement. In general, the more delayed the onset of symptoms, the better the prognosis seems to be.

## PATHOLOGIC MANIFESTATIONS

In the adult, the predominant sites of involvement are spleen, liver, bone marrow, and deep lymph nodes.[15] The spleen will usually show massive involvement with Gaucher's cells, with coarse bands of collagen tissues which may calcify. In the liver, Gaucher's cells are found only in the capillaries in infants and children, whereas in the adult they are seen also in the portal spaces and sinusoids. The deep lymph nodes will show infiltration with Gaucher's cells and also pigment deposition.

The marrow infiltrates of Gaucher's cells are usually associated with atrophy of marrow cells and fibrosis. The destruction of bone as a rule results from multiplication of Gaucher's cells packing the intramedullary spaces, and pressure atrophy and ischemic necrosis. The process is slow and appositional bone is laid down on the outer cortical surfaces of the involved areas, giving them an expansive appearance.

Thannhauser believes that the disorder is due to a defect in the reticular cell enzyme system leading to increased synthesis and storage of cerebrosides.[15]

Two cases of Gaucher's disease in siblings, seen at the Massachusetts General Hospital, with an evaluation of the roentgenographic bone changes over a 20 year interval are reported.

## REPORT OF CASES

Case I (M.B.). The diagnosis of Gaucher's disease was made in this patient in 1942, and the bone changes were followed over a period of 21 years. The history was obtainable, however, over a much longer time.

The first admission to the hospital was in 1932 at the age of 24, because of digestive complaints of 2 years' duration. Abnormal findings were a peculiar pigmentation of the face and ankles and a blood pressure of 145/80; gastric analysis showed some hyperacidity; a complete gastrointestinal series was negative, as were a cholecystogram and chest roentgenogram. Studies of the pelvis (not now available) disclosed changes in the right hip consistent with "old epiphyseal displacement."

A history was elicited of recurrent painful joint swelling involving primarily the knee, ankle, wrist, and phalangeal joints over a period of 20 years. All episodes had subsided spontaneously. At the age of 11 years, the patient had been thought to have had tuberculosis of the right hip joint and was treated in a cast for a period of 6 months and considered cured.

In 1939, the patient was seen with gingival bleeding, attributed to dietary restrictions. At this time, pigmentation of the ankles and ankle edema were noted, and scurvy was suspected. Anemia and leukopenia were also detected; the anemia was not relieved by iron, but there was a fairly good response to a combination of iron and vitamin C, and the gingival bleeding subsided with large doses of vitamin C, orally and parenterally.

The 1942 admission followed the patient's rejection for military service because of ankle edema and hepatosplenomegaly. Physical examination now showed a yellowish tint to the skin and sclerae, gingival recession, caries and

pyorrhea, and restriction of hip and ankle motion bilaterally. Laboratory findings were: a red blood cell count of 4.2 million, hemoglobin 9.8 gm., and a white blood cell count between 3,000 and 5,000. Stools were negative and blood chemistries including calcium, phosphorus, and phosphatase were normal. Gastric analysis showed free acid, fasting.

Roentgenograms of the skeleton disclosed flask-shaped deformities of the lower end of the femora and destructive changes in the hip joints. A gastrointestinal series was negative. Sternal biopsy showed Gaucher's cells.

The patient was re-admitted on July 24, 1963, at the age of 55, because of weakness and limitation of motion in the hip and shoulder joints. In the 21 year interval since previous admission, he had worked steadily but suffered increasingly severe episodes of arthritis involving primarily the hips, knees, ankles, and shoulders; the joints became hard, red, swollen, and painful, but the process always subsided spontaneously in a few days to a few weeks. There was, however, a progressive limitation of motion of all involved joints. During the past year the patient had taken 20 aspirin tablets a day. His thighs had become increasingly weak and he had had to resort to the use of a cane for ambulation. For 9 years, he had been treated for hypertension. The blood pressures were between 160/100 and 180/115.

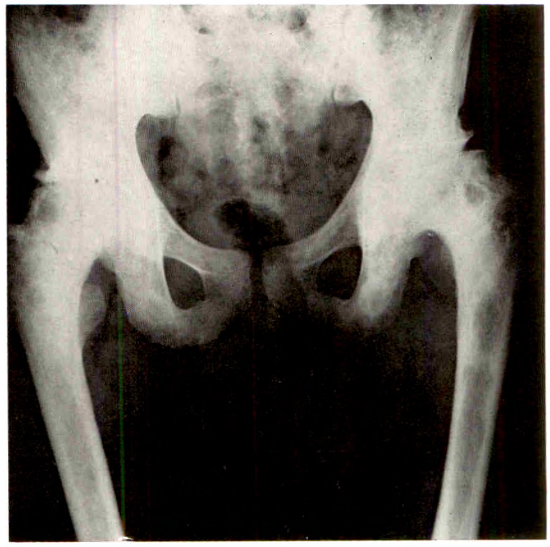

Fig. 2. Case 1. *July 2, 1942:* Mushrooming and destruction of femoral heads with irregular pitting of subchondral cortices and varus deformity hypertrophic changes. Rarefactions, scleroses, coarsening of trabecular structure throughout femora and pelvis.

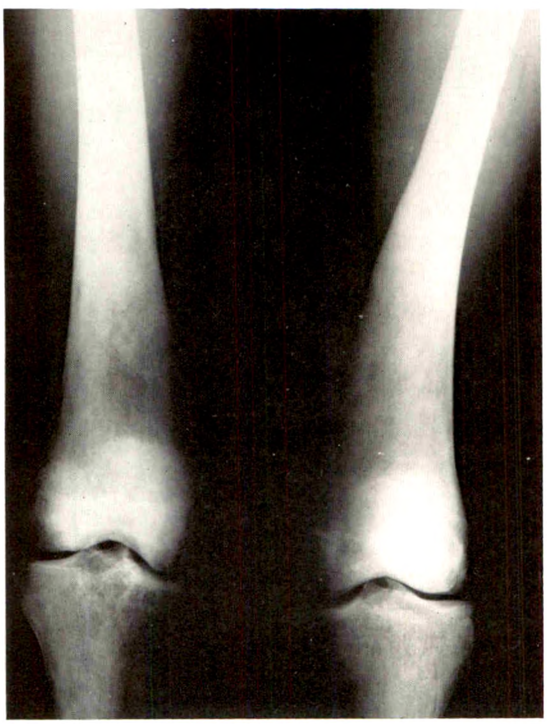

Fig. 1. Case 1. *July 2, 1942:* Fusiform expansion of distal femora with thinning of cortices, coarsening of spongiosa, patchy areas of sclerosis and rarefaction. Similar changes in proximal tibiae with depression and sclerosis of medial tibial plateau.

On physical examination the skin over the head, neck, forearms, and legs was darkly pigmented with swelling and some scaling of the ankles. Other observations included bilateral pingueculae, brownish discoloration of the tongue, increased anteroposterior dimension of the chest, normal heart and lungs, hepatosplenomegaly with the spleen to the level of the iliac crest and liver margin down 8 cm. in the mid-clavicular line. There was marked limitation of motion in the hip, knee, ankle, and shoulder joints, as well as forward flexion of the spine.

Laboratory findings were as follows: urine negative, hematocrit 38 per cent, white blood cell count 2,300 with normal differential. Thrombocytopenia was present. Blood chemistries were negative except for an albumin-globulin ratio of 2.1/4.3 and uric acid of 7.0 mg. The possibility of gout was entertained.

The skeletal survey showed changes consistent with advanced Gaucher's disease (see

Fig. 3. Case i. *July 2, 1942:* Lateral view of the thoracic spine. Stature of centra maintained. Superior and inferior end-plates irregular; hypertrophic spurring. Diffuse rarefaction with coarse trabecular structure.

Roentgen Findings, below). The patient left the hospital against advice.

Case ii (G.B.). In 1942, when a diagnosis of Gaucher's disease was made in Case i, the older sister had similar but less severe joint symptoms. Consequently, roentgenograms were taken of the sister's pelvis and femora, which showed broadening of the femoral heads with trumpet-shaped deformities of the distal femora, consistent with Gaucher's disease. She had also hepatosplenomegaly, skin pigmentation, and recurrent gingival bleeding, and complained of bruising easily and of repeated episodes of joint pain. She stated that symptoms seemed to be alleviated following ingestion of large amounts of orange juice.

In 1963, the sister was asked to return for follow-up roentgenographic examination, at which time she reported that her father had died at the age of 52 of pneumonia and her mother at the age of 34 of Hodgkin's disease. She mentioned that her father and several of her cousins on the paternal side of the family had a peculiar yellowish discoloration of the skin.

## ROENTGEN FINDINGS

The roentgenographic appearance in Gaucher's disease will vary with the age of the patient and the degree of skeletal or visceral involvement. In the acute infantile form, there are rarely, if ever, any macroscopic skeletal changes. In the chronic form bone changes usually appear in the first or second decade of life, although they may be delayed until adult life. Depending upon the duration of involvement, the earliest roentgen changes in the hip joint may be those of an aseptic necrosis with typical sclerosis, flattening and fragmentation of the femoral head[1,20,23] and, depending upon the age of the patient, may be mistaken for Legg-Perthes' disease, traumatic arthritis, or slipped capital femoral epiphysis.

Regardless of the age of the patient, the most typical change is the trumpet-shaped deformity of the distal femora (the Erlenmeyer flask deformity or Fischer's sign), with relatively diffuse rarefaction, with or without patchy areas of destruction of spongiosa and with or without bone condensations (Fig. 5 and 14). Similar changes may be seen in the proximal tibiae. Our Case i showed advanced changes in the pelvis, hips, distal femora, proximal tibiae, even at the age of 24 (Fig. 1 and 2). The sister, Case ii, at the age of 28 showed the more typical early skeletal changes (Fig. 12 and 14).

The roentgenographic appearance is predominantly one of radiolucency, although sclerosis, due to the formation of reactive new bone, is common. Bones primarily involved are femora, vertebrae, ribs, sternum, and flat bones of the pelvis. The long tubular bones of the lower extremities are involved more often than those of the upper

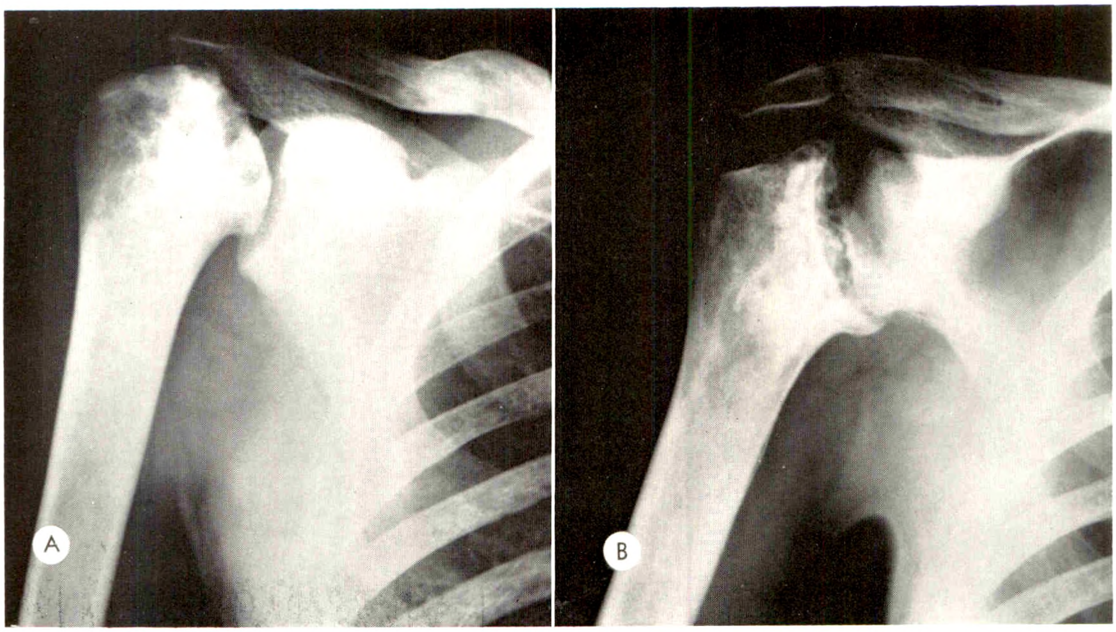


FIG. 4. Case I. (*A* and *B*) *July 2, 1942:* Anteroposterior views of shoulders. Irregular destruction of glenoid aspects of humeral heads, more advanced on left, with varus deformity on left, and with extensive patchy condensations and rarefactions. Left glenoid fossa involved. (The print of the left shoulder is reversed.)

FIG. 5. Case I. *July 25, 1963:* Marked expansion of distal femora and proximal tibiae with severe destruction of articular cartilage. More extensive rarefaction and sclerotic change; periosteal reaction in lateral aspect of distal left femur.

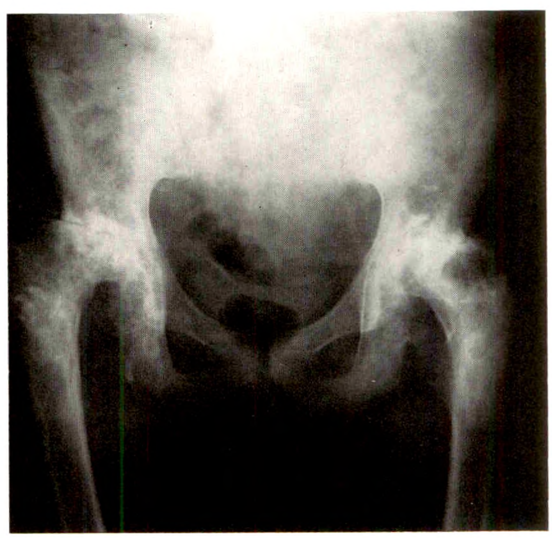

FIG. 6. Case I. *July 25, 1963:* Greater destruction and flattening of femoral heads with marked destruction of articular cartilage of hip joints. Bones extensively rarefied, with large focal areas of destruction. Cortices thin but intact. Marked periosteal reaction in medial aspect of right femoral neck.

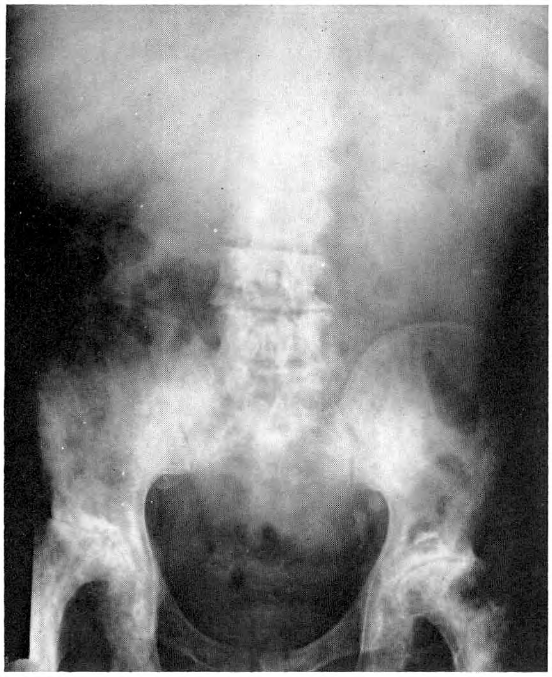

Fig. 7. Case 1. *April 9, 1964:* Thoracolumbar spine. Slight right convex scoliosis of lumbar spine. Diffuse demineralization with coarse spongiosa and patchy areas of sclerosis.

extremities. The medullary canals are widened, trabeculae are sparse, and the cortices are thin. In early stages, there is no epiphyseal destruction, periosteal reaction, or cortical destruction. In addition to thinning of the cortices, there is loss of definition between the cortex and medulla. Appositional periosteal new bone is laid down to provide bone support. Additional periosteal new bone may be formed as a result of subperiosteal hemorrhage, or pathologic fracture. It is felt that in many instances the typical bone pain is the result of small foci of subperiosteal hemorrhage. The increased fragility of the involved bones, leading to pathologic fractures in childhood, is the result of progressive endosteal

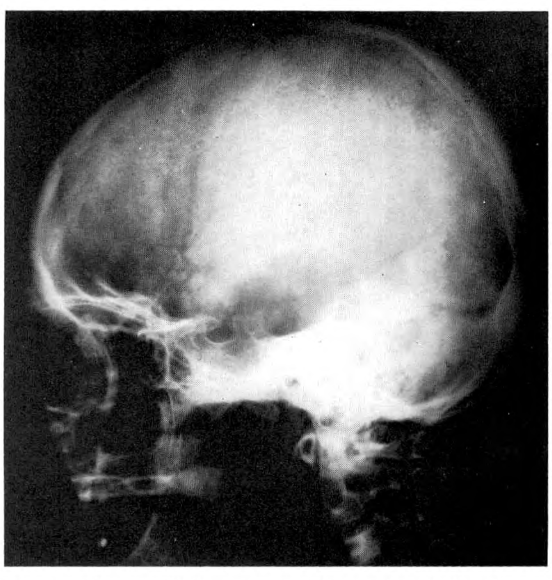

Fig. 9. Case 1. *July 29, 1963:* Diminished density of skull with faint patchy rarefactions.

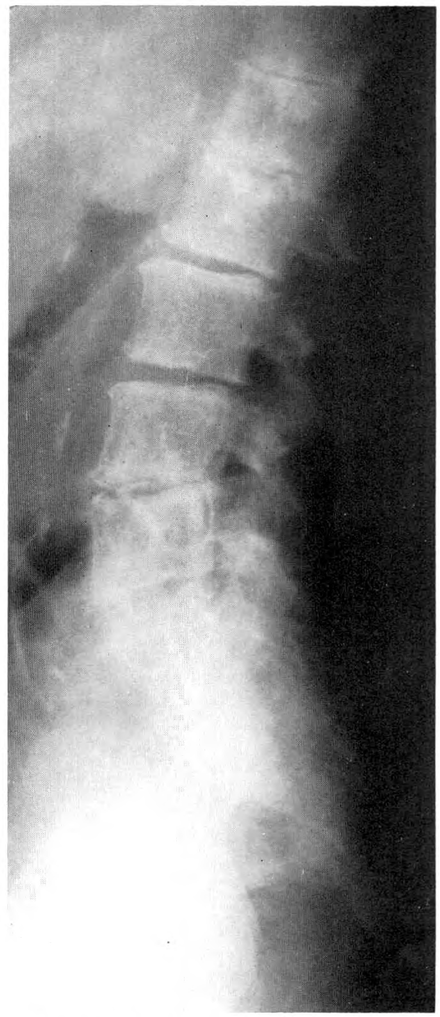

Fig. 8. Case 1. *April 9, 1964:* Kyphosis of lower thoracic-upper lumbar region with slight anterior wedging of multiple centra. Marked narrowing of multiple intervertebral joints. Hepatosplenomegaly. Ribs broadened and rarefied.

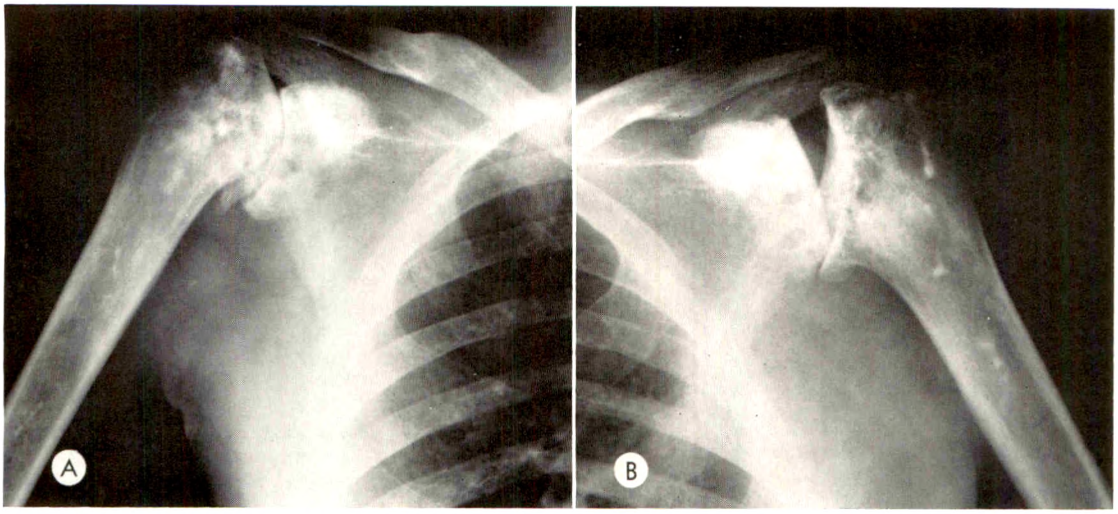

Fig. 10. Case I. (*A* and *B*) *July 25, 1963:* Anteroposterior views of shoulders. Broadening of subarticular surfaces of humeri, with deeper cupping of the left humeral surface. Destruction of joint cartilage on right; hypertrophic spurring, more extensive patchy sclerosis on the right, with some confluence of rarefactions bilaterally and spotty sclerosis of humeral shafts. More involvement of scapulae.

erosion with cortical thinning rather than due to a deficiency of bone matrix, as there is prompt callus formation and early union.[6]

The spine, when involved, usually shows diffuse rarefaction with loss of spongiosa and reduction of height of the vertebral body with or without local condensation and degenerative changes (Fig. 3). Compression fractures of the vertebral bodies may occur in advanced stages; however, the intervertebral joints are well preserved. Gibbus is unusual[22] unless there has been extreme collapse of the centra, but there is usually some degree of kyphosis.

The skull rarely shows a significant de-

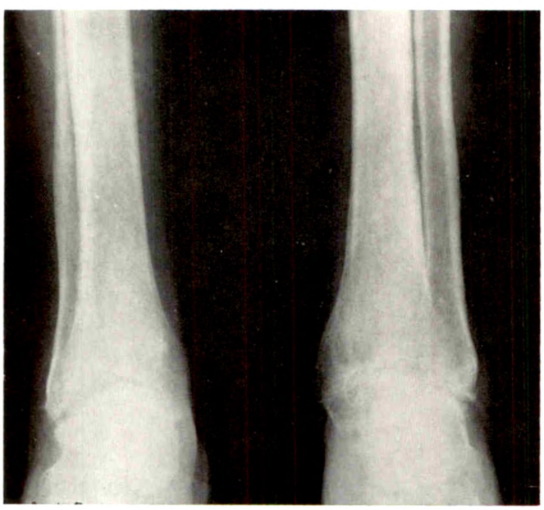

Fig. 11. Case I. *July 25, 1963:* Periosteal reaction in tibiae and fibulae producing appositional new bone resulting in thickened cortices. Patchy areas of destruction of spongiosa. Marked destructive joint changes with excavation of tibial and fibular subchondral margins and substantial asymmetric narrowing of joints.

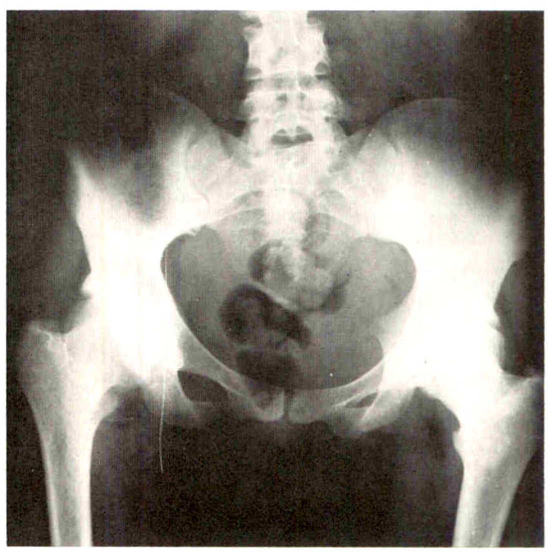

Fig. 12. Case II. *July 26, 1942:* Anteroposterior view of pelvis. Varus deformity, some expansion of femoral heads, and some patchy rarefaction with coarsening of trabecular pattern.

FIG. 13. Case II. *September 30, 1964:* Anteroposterior view of pelvis. Narrowing of hip joints with hypertrophic spurring, further expansion of femoral heads, patchy areas of sclerosis and rarefaction throughout heads and proximal femora. Mottled sclerosis contiguous to sacroiliac joints. Osteopenia, confluence of rarefied areas in left greater trochanteric region.

gree of involvement. The shoulder joints are commonly involved and frequently show marked destruction of the humeral head, as in Case I (Fig. 4, *A* and *B*). Scleroses and rarefactions are frequently seen in the pelvis, ribs, sternum, and scapulae. The skull and phalanges may be involved quite late in the disease process.

The 2 patients described in this article showed roentgenographic skeletal changes over a period of 20 to 22 years. In Case I all typical changes of Gaucher's disease were observed involving the femora, tibiae, pelvis, spine, and shoulder joints. The more recent roentgenograms reveal a diffuse diminution of density of the skull with patchy rarefactions (Fig. 9). There is considerably greater destruction and reactional new bone in the pelvis (Fig. 6), long bones (Fig. 5), spine (Fig. 7 and 8), and shoulders (Fig. 10, *A* and *B*); the ankles (Fig. 11) are also involved. Case II showed advancement of the disease in the femora (Fig. 13), tibiae,

FIG. 14. Case II. *September 26, 1942:* Expansion of distal femoral metaphyses with patchy areas of condensation and rarefaction, thinning of cortices.

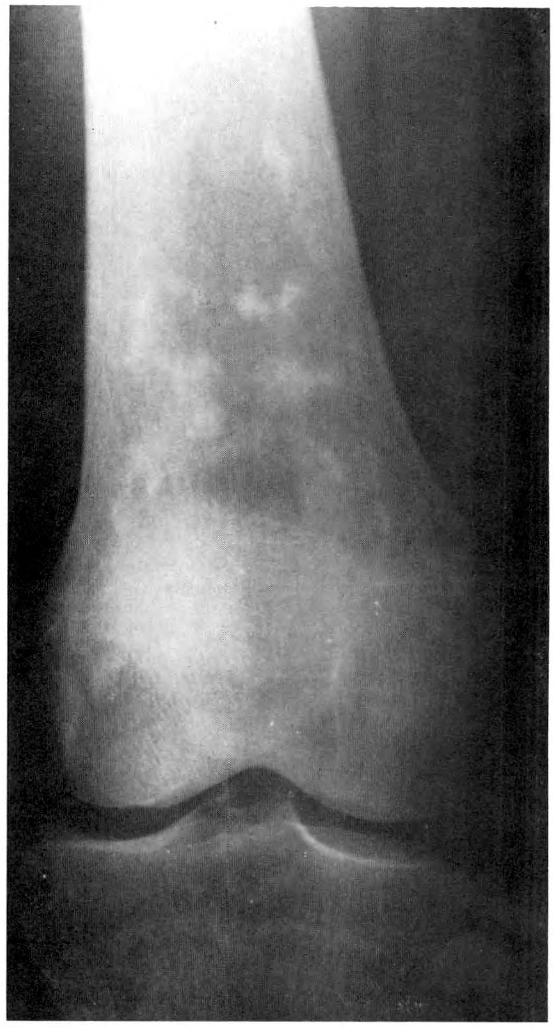

FIG. 15. Case II. *September 30, 1964:* Configuration of distal femora unchanged. Moderate increase in number of condensations, accentuated as result of osteopenia.

and pelvis (Fig. 15), but the changes were not nearly as extensive as in her brother's case, and there were no typical alterations in the spine, ribs, vertebrae, or skull.

Occasional reference has been made in the literature to extensive rarefaction and cyst-like areas of destruction of the mandible.[9,18] In the lateral skull roentgenogram of Case 1 in 1942, these changes can be detected upon close observation.

### DISCUSSION

No pathognomonic roentgenologic changes are found in Gaucher's disease with macroscopic bone involvement, although the almost invariable occurrence of club-shaped deformity of the distal femora is of great assistance in suggesting the diagnosis.

Aseptic necrosis of the femoral head is common and usually occurs in pre-adolescent years. It has been postulated that the advanced degenerative changes in the hips of adults with Gaucher's disease are due to continued weight-bearing during childhood and that, as in Legg-Perthes' disease, the femoral head may be reconstituted if weight-bearing is held in abeyance for a relatively long time.[1,13] Our first case, however, in which the patient as a child was maintained in a cast for 6 months on a diagnosis of tuberculosis of the hip, fails to support this contention.

The skeletal changes may be simulated by Cooley's anemia, but in the latter disease the outstanding changes are in the short tubular bones of the hands and feet.[16] Sickle-cell anemia would also deserve consideration. In general, the bone changes in that condition resemble those of Cooley's anemia, with patchy areas of condensation as the result of bone infarction,[16] but there may be expansion of the distal femora with thinning of the cortices producing the typical Erlenmeyer flask deformity indistinguishable from that of Gaucher's disease. Advanced cases of sickle-cell disease usually produced marked collapse of vertebral bodies with biconcave configurations, whereas, as in Case 1, the stature of the centra in Gaucher's disease is usually fairly well maintained in spite of advanced change. Other possible sources of confusion are multiple cavernous angiomata affecting the bone, as reported by Parsons and Ebbs;[13] the rare instance of Niemann-Pick disease with survival into childhood; syphilis; leukemia; and Hodgkin's disease.

Splenomegaly is not necessary for a diagnosis of Gaucher's disease,[12] but, although the spleen may not be enlarged, there usually is extensive splenic infiltration with Gaucher's cells. In the usual case, splenic enlargement precedes the bone changes,[3] and bone pain is the first indication of skeletal involvement. Cases have been reported, however, in which there were typical changes for many years prior to the onset of bone pain.[8] Pathologic fractures may occur in the absence of splenomegaly.[6]

There may be long lapses in clinical symptomatology in spite of continuing bone changes, but in most instances there is progressive and inexorable bone involvement with relatively persistent clinical symptoms and periodic "crises" of bone pain and exacerbation of symptoms.

There is no specific therapy for Gaucher's disease.[19] Diet has little influence on the course, although, as in the present cases, massive doses of vitamin C may be influential in preventing some of the hemorrhagic manifestations. Splenectomy may be performed when the spleen becomes massive and causes abdominal discomfort, but the usual indication for so radical a measure is correction of hypersplenism and reversal of severe pancytopenia.[19] It would appear that splenectomy neither accelerates, prevents, nor delays the onset of bone changes.

Radiation therapy may be applied to an uncomfortably enlarging spleen and will produce temporary regression in the size of the organ and hypersplenic state as well as partial or complete alleviation of abdominal discomfort. Radiation therapy has also been employed in treatment of the bone lesions with mitigation of symptoms for variable periods; it probably should be applied to localized areas in which there is

extensive skeletal destruction associated with unremitting bone pain.[6]


SUMMARY

Gaucher's disease is an uncommon metabolic disturbance characterized by abnormal deposition of cerebrosides in the reticuloendothelial system. The proliferating cell mass is responsible for the visceral and skeletal changes. The condition may be detected at any age. When it develops in infancy, the course is malignant and characterized by neurologic abnormalities. In the chronic form, the condition is compatible with relatively long life. Roentgenographic bone manifestations, particularly a club-shaped deformity of the distal femora, although not pathognomonic, may be suggestive of the disease. The only positive method of diagnosis is biopsy of involved structures, with a finding of the characteristic Gaucher's cell.



James A. Rourke, M.D.
Department of Radiology
Massachusetts General Hospital
Boston 14, Massachusetts


REFERENCES


1. Arkin, A. M., and Schein, A. J. Aseptic necrosis in Gaucher's disease. *J. Bone & Joint Surg.*, 1948, *30-A*, 631–641.
2. Cushing, E. H., and Stout, A. P. Gaucher's disease: with report of case showing disintegration and joint involvement. *Arch. Surg.*, 1926, *12*, 539–560.
3. Davies, F. W. T. Gaucher's disease in bone. *J. Bone & Joint Surg.*, 1952, *34-B*, 454–459.
4. Gordon, A. Osseous Gaucher's disease: report of two cases in siblings. *Am. J. Med.*, 1950, *8*, 332–341.
5. Groen, J., and Garrer, A. H. Adult Gaucher's disease, with special reference to variations in its clinical course and to value of sternal puncture as aid to its diagnosis. *Blood*, 1948, *3*, 1221–1237.
6. Harrison, W. E., Jr., and Louis, H. J. Osseous Gaucher's disease in early childhood: report of case with extensive bone changes and pathological fractures without splenomegaly. *J.A.M.A.*, 1964, *187*, 997–1000.
7. Holt, L. E., Jr., McIntosh, T., and Barnett, H. L. Pediatrics. Appleton-Century, Inc., New York, 1962.
8. James, N. E. Gaucher's disease: report of case. *J. Bone & Joint Surg.*, 1952, *34-B*, 464–465.
9. Levine, S., and Solis-Cohen, L. Gaucher's disease. Am. J. Roentgenol. & Rad. Therapy, 1943, *50*, 765–769.
10. Medoff, A. S., and Bayrd, E. D. Gaucher's disease in 29 cases: hematologic complications and effect of splenectomy. *Ann. Int. Med.*, 1954, *40*, 481–492.
11. Melamed, S., and Chester, W. Osseous form of Gaucher's disease: report of case. *Arch. Int. Med.*, 1938, *61*, 798–807.
12. Morgans, M. E. Gaucher's disease without splenomegaly. *Lancet*, 1947, *2*, 576–578.
13. Parsons, L. G., and Ebbs, J. H. Generalized angiomatosis presenting clinical characteristics of storage reticulosis, with some observations on reticulo-endothelioses. *Arch. Dis. Childhood*, 1940, *15*, 129–158.
14. Petit, J. V., and Schleicher, E. M. "Atypical" Gaucher's disease. *Am. J. Clin. Path.*, 1943, *13*, 260–266.
15. Pick, L. Classification of diseases of lipoid metabolism and Gaucher's disease. *Am. J. M. Sc.*, 1933, *185*, 453–469.
16. Pugh, D. G. Roentgenologic Diagnosis of Disease of Bone. Williams & Wilkins Company, Baltimore, 1960.
17. Reed, J., and Sosman, M. C. Gaucher's disease. *Radiology*, 1942, *38*, 579–583.
18. Reich, C., Seife, M., and Kessler, B. J. Gaucher's disease: review, and discussion of twenty cases. *Medicine*, 1951, *30*, 1–20.
19. Smith, C. H. Indications for splenectomy in pediatric patient. *Am. J. Surg.*, 1964, *107*, 523–530.
20. Todd, R. McL., and Keidan, S. E. Changes in head of femur in children suffering from Gaucher's disease. *J. Bone & Joint Surg.*, 1952, *34-B*, 447–453.
21. Tyson, M. C., Grossman, W. I., and Tuchman, L. R. Gaucher's disease (with elevated serum acid phosphatase level) masquerading as cirrhosis of liver. *Am. J. Med.*, 1964, *37*, 156–158.
22. Welt, S., Rosenthal, N., and Oppenheimer, B. S. Gaucher's splenomegaly (with especial reference to skeletal changes). *J.A.M.A.*, 1929, *92*, 637–644.
23. Wood, H. L.-C. Gaucher's disease with pseudocoxalgia: report of case. *J. Bone & Joint Surg.*, 1952, *34-B*, 462–463.

# NODULAR RHEUMATOID VERTEBRAL LESIONS VERSUS ANKYLOSING SPONDYLITIS*

*By* A. GLAY, M.D., F.R.C.P.(C),† *and* G. RONA, M.D., F.R.C.P.(C)‡
MONTREAL, QUEBEC

INVOLVEMENT of the vertebral bodies by rheumatoid nodules is a rare occurrence. Baggenstoss *et al.*[1] in 1952 reported 4 cases of destructive vertebral lesions in patients with rheumatoid disease, but granulomatous rheumatoid nodules were found in the vertebrae (T12 and L3) in only 1 of these, whereas the other 3 cases were patients with ankylosing spondylitis. Lorber *et al.*[10] reported an autopsied case in 1961 with rheumatoid nodules in the vertebral bodies (T7 and T8) and 2 other cases with peripheral joint involvement in which the roentgenograms demonstrated wedging of the vertebral bodies from T5 to T9. In a study of the vertebral lesions in rheumatoid diseases, Seaman and Wells[17] described 2 cases of long standing peripheral rheumatoid arthritis in which roentgenograms showed destructive vertebral lesions of a type different from those found in the 11 cases of ankylosing spondylitis included in their study.

Thus, a review of literature disclosed 5 cases of peripheral rheumatoid arthritis associated with destructive disko-vertebral lesions.

To these, we should like to add 3 cases from our material. All 3 had long lasting peripheral rheumatoid arthritis and during the course of their illness developed destructive vertebral lesions. The one patient who died was found to have rheumatoid nodules in the vertebrae. The other 2 patients are alive, but their clinical histories and roentgenographic findings are so similar to the autopsied case that it appeared worthwhile to report them in the same paper.

## REPORT OF CASES

CASE 1. A 73 year old widow in previously good health had a rather sudden onset of rheumatoid arthritis, severe and progressive enough that she was treated with cortisone. Three years later a fracture of the left femoral neck was repaired by insertion of a Smith-Petersen nail. At that time, clinical examination disclosed involvement of elbows, wrists, hands, knees, and feet by rheumatoid arthritis. Another three years later (age 79) she was re-admitted because of severe back and left abdominal pain of 3 months' duration. The pains became worse 6 weeks prior to admission following a fall; lying down relieved the pain to some extent, but never completely. The patient had lost 30 pounds in weight during her prolonged illness and was emaciated and weak.

Physical examination disclosed advanced deformities of the peripheral joints. Large nodules were palpable in both buttocks. (One of these was removed and showed the histologic structure of a typical rheumatoid nodule.) The blood pressure was 110/60 and pulse 72/min. The white blood cell count was 7,450 with normal differential and the hematocrit 36 per cent. The serum protein was 5.3 gm. Blood serology was negative.

Roentgenograms revealed destructive lesions of both acromioclavicular joints (Fig. 1). Those of the thoracolumbar spine (Fig. 2 and 3) showed collapse of T12, L2 and L3. She expired after a short stay in hospital.

At autopsy, the following were the pertinent gross findings: deformity of the fingers of both hands was present with ulnar deviation, fibrous ankylosis, and muscle wasting. Rubbery movable nodules, varying in size from 1.0 to 3.0 cm., were found over the left wrist, right olecranon, and sternoclavicular joints. There was collapse of the bodies of T12 and L3 vertebrae. Sectioning of these showed a grayish amorphous tissue replacing the normal cancellous structure. This

* From the Departments of Radiology† and Pathology,‡ St. Mary's Hospital, Montreal, Quebec, Canada.

FIG. 1. Case I. Posteroanterior roentgenogram showing destructive rheumatoid arthritis involving the acromioclavicular joints.

tissue blended with the superior end plate and intervertebral disk. The periosteum was thickened over T12 and the upper lumbar vertebrae.

Histologic examination revealed amyloid deposit in the follicles of the spleen, glomerular capillaries, and adrenal cortex. The subcutaneous nodules consisted of central homogeneous eosinophilic areas with some calcification and palisading histiocytes at the periphery. Sections of the involved vertebrae showed destruction of the bone spicula and replacement of the marrow by granulation tissue, revealing extensive areas of confluent hyaline change with necrosis and cavity formation (Fig. 4). At the periphery of these cavities, there was a proliferation of palisading histiocytes and giant cells (Fig. 5). Between the nodules, scar tissue with round cell infiltration was present and in this the blood vessels showed thickening by hyalinization, intimal proliferation, and thrombosis. The medullary cavity adjacent to the granulomata showed thin, widely spaced spicula and mucoid transformation of the marrow (Fig. 6).

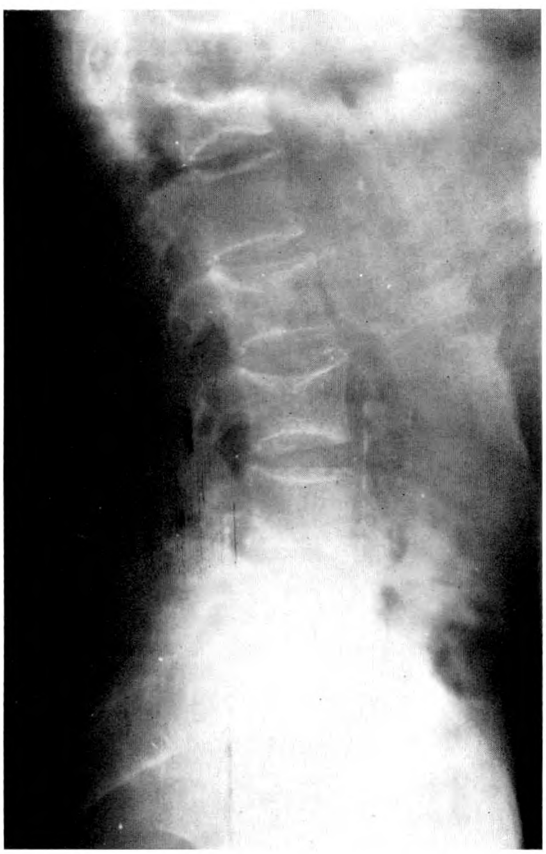

FIG. 2. Case I. Lateral roentgenogram of lumbar spine shows collapse of T12, L2 and L3. Note the concavity of the superior end plates of the involved lumbar vertebrae and the absence of syndesmophytes.

CASE II. R.J., a 67 year old white male, was first admitted to St. Mary's Hospital in 1963 for evaluation. Rheumatoid arthritis had begun 50 years before with initial involvement of the wrist joints and then steady progression to most other peripheral joints. Steroid therapy had been given since 1949 with but little effect on the relentless progress of the disease. He had led a bed-wheel-chair existence for the 10 years before admission.

FIG. 3. Case I. Close-up of T12. Note the granular pattern of the vertebral body and the opaque layer along the superior end plate.

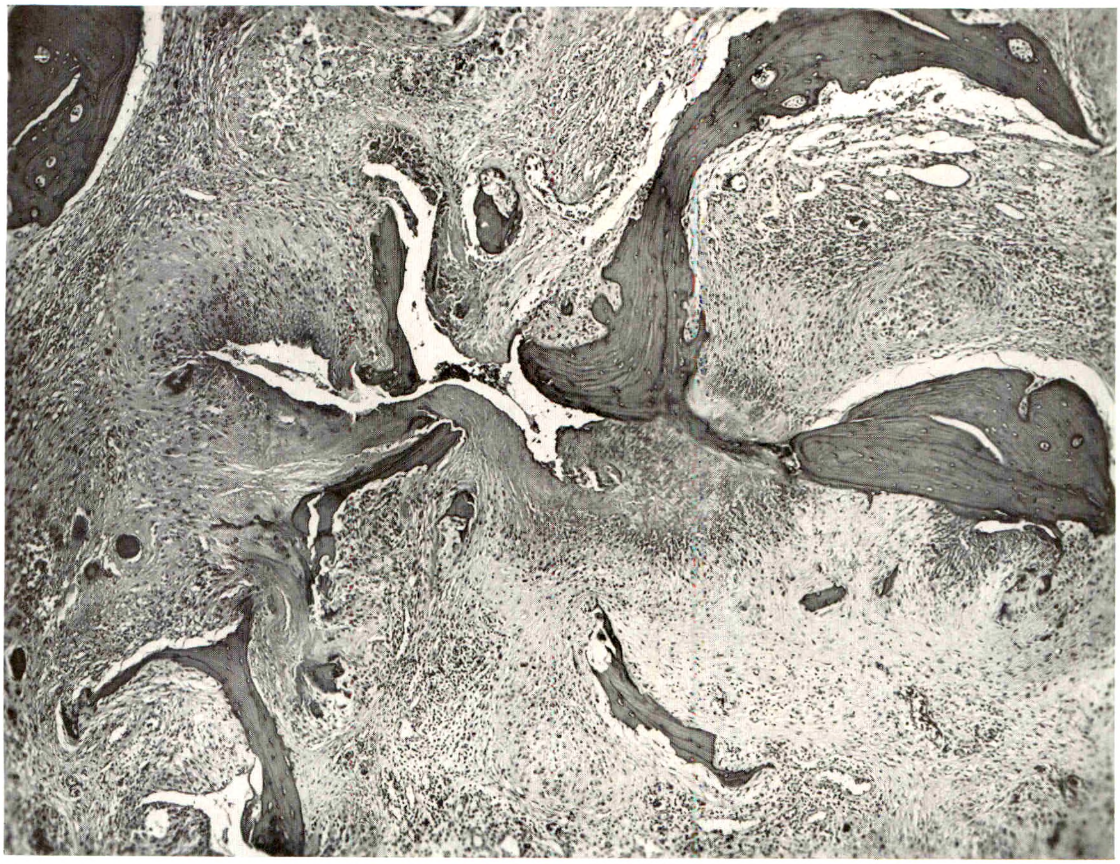

Fig. 4. Case i. The granulation tissue with central cavity formation encroaches upon the bone spicula and replaces the marrow. There is scarring at the periphery with diffuse round cell infiltration (H&E×59).

Physical examination revealed widespread joint deformities involving all 4 limbs. The hemoglobin was 12.4 gm. and the erythrocyte sedimentation rate 115 mm./per hr. The latex fixation test was negative. Roentgenograms of the thoracolumbar spine disclosed diffuse osteoporosis, bilateral protrusio acetabuli, and collapsed vertebrae (Fig. 7 and 8).

Case iii. S.H., a 58 year old white woman, had progressive rheumatoid arthritis with deformities of 10 years' duration. The disease had been resistant to all forms of treatment, including corticosteroids. During her admission in 1964, the hemoglobin was 16.8 gm., white blood cell count 19,250, and the sedimentation rate 15 mm. (Westergreen). The latex fixation test was positive. Roentgenograms showed diffuse osteoporosis, bilateral protrusion of the acetabula, and a pathologic fracture of the left femur (Fig. 9). Roentgenograms of the spine (Fig. 10 and 11) disclosed a degree of collapse of the bodies of T9–T12 and L2–L5.

## DISCUSSION

In the reviewed articles,[1,10,17] cases of ankylosing spondylitis and cases of destructive vertebral lesions produced by rheumatoid nodules were considered together under the same heading. The latter type of lesions, we would like to suggest, should be separated from ankylosing spondylitis. There is still controversy as to whether peripheral rheumatoid arthritis and ankylosing spondylitis are different expressions of the same basic disease process or completely different entities.[13] Recent studies indicate that the history, heredity pattern,[2,14] serologic findings and morphology of the two diseases are different.[5,8] Roentgenologic findings would also be more in keeping with the latter view.[15]

Almost invariably, ankylosing spondylitis begins in the sacroiliac joints which, in

the course of the disease, become fused. From here, the process gradually makes its way cephalad. It is essentially an inflammatory lesion of the small intervertebral joints. This is followed closely by a process of repair manifested by fibrosis and ankylosis. The classic picture of fusion of the sacroiliac joints, squaring of the vertebral bodies, and the bamboo appearance of the spine due to syndesmophytosis are too well known to merit more than passing mention here. That ankylosing spondylitis may be associated with destructive disko-vertebral lesions has been amply demonstrated.[1,3,6,9–11,15–18] The destructive process affects primarily the articular apparatus, and secondarily, involves the bone of the articular process or the vertebral body in the immediate vicinity of the disk or joint alteration. Thus, ankylosing spondylitis is primarily a disease of the intervertebral joints without specific lesions of the cancellous bone or bone marrow.

In the cases in which rheumatoid granulomas were found in the vertebrae, the process involved the vertebral body without primary relation to the joint. The granulomas destroyed the trabeculae of the cancellous bone, extended to the end plates, and led to destruction of the bone and intervertebral disks. Grossly, the granulomas appeared as white grayish nodules. As a result of growth, coalescence and necrosis of these nodules, the spicula of the vertebral body were replaced and destroyed, leading to weakening of the bony structure, and finally, collapse of the vertebral body (under influence of gravity and muscle pull). In this context the lesions produced in the vertebrae by rheumatoid nodules could be regarded as spondylitis, analagous to the spondylitis associated with infectious dis-

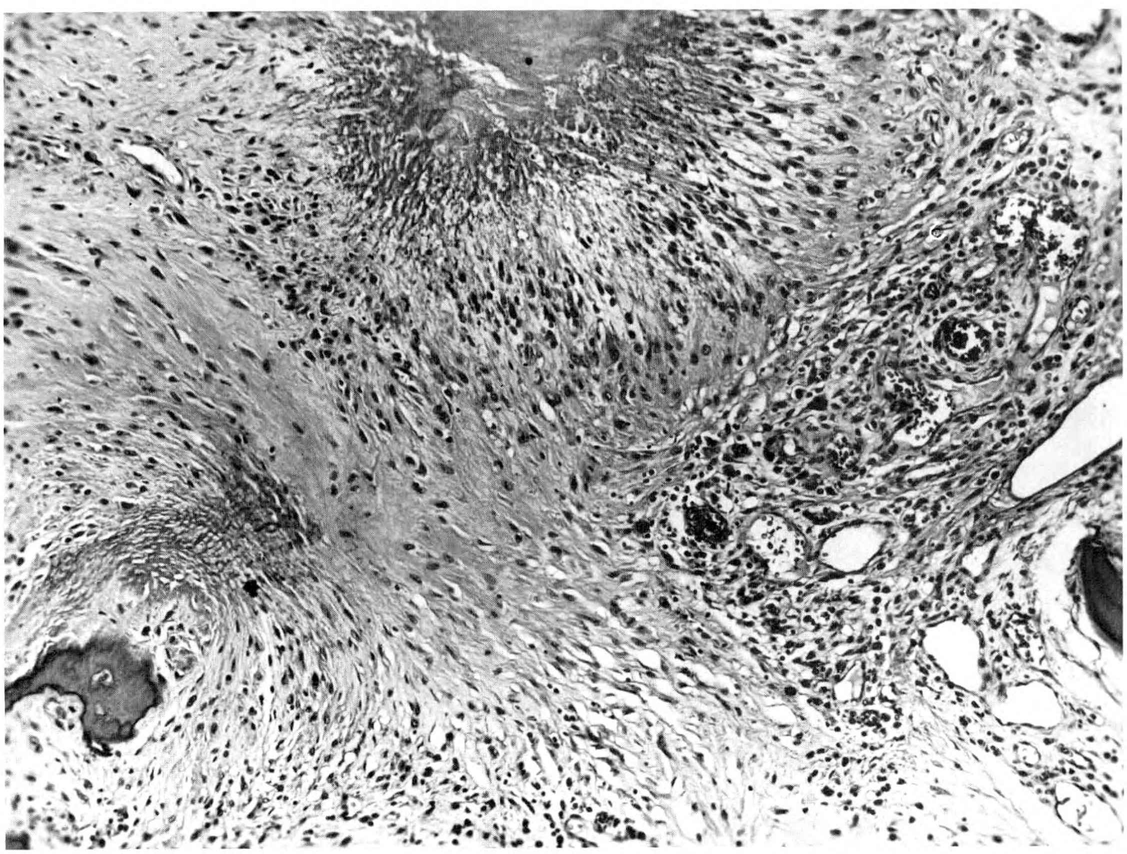

FIG. 5. Case I. Palisading histiocytes around foci of hyaline necrosis (H&E×129).

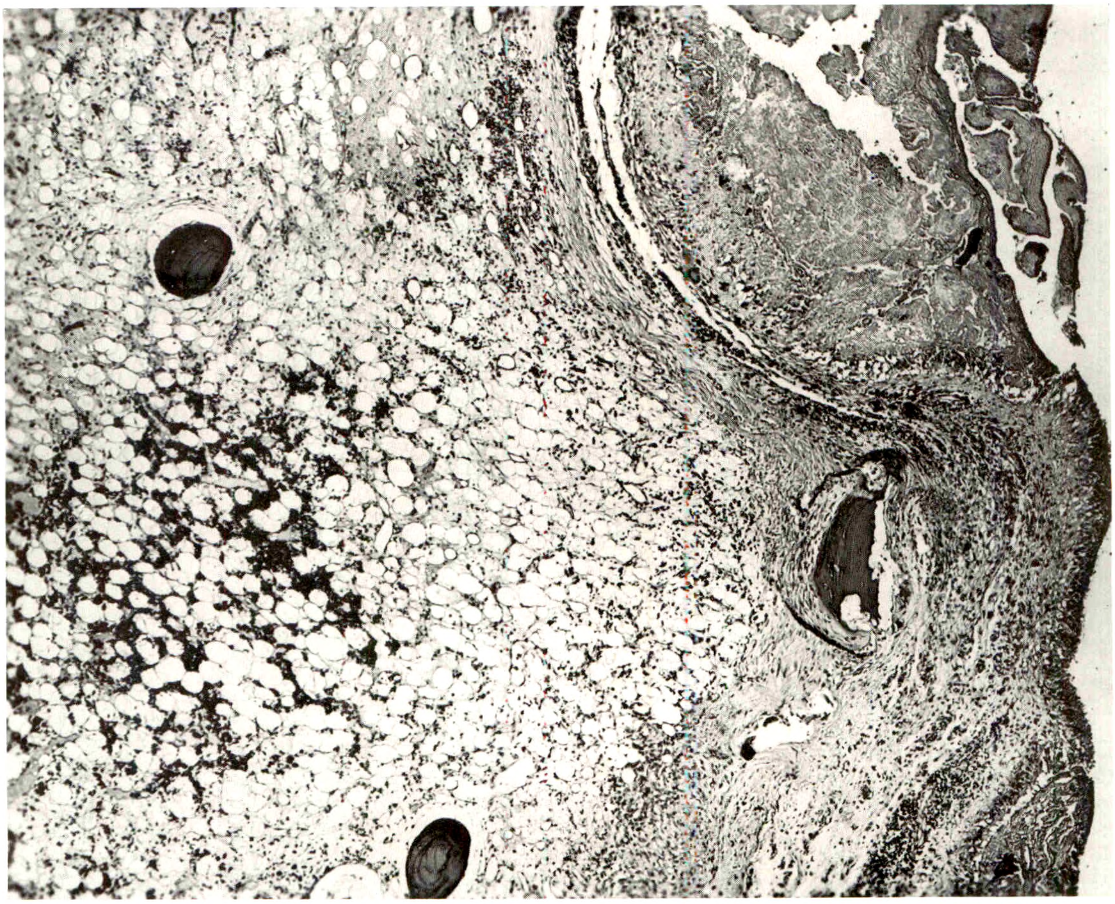

Fig. 6. Case i. Osteoporosis close to the collapsed vertebral body (H&E×56).

eases produced by tuberculosis, brucellosis, salmonella, or pyogenic cocci. It might conceivably be termed nodular or granulomatous spondylitis accompanying rheumatoid arthritis.

In cases of peripheral rheumatoid arthritis, the diffuse osteoporosis usually found in the bones adjacent to involved joints may also be found in the spine. Roentgenographically, the involved vertebrae have a ground-glass appearance with poor definition of the trabeculation. Occasionally, the cancellous structure shows a fine stippled and granular pattern (Fig. 3). In some vertebrae, subchondral bands of increased density are seen. They are mostly located below the superior end plate (Fig. 3 and 8). Usually, several vertebrae are involved. The degree of destruction and collapse of the vertebral bodies varies; there may be only slight depression of one or both end plates (Fig. 11), or the body may be reduced in height to as little as one-fourth of normal (Fig. 8). The latter may produce a gibbus deformity. The anterior portion of the collapsed vertebra can project forward partially (Fig. 11), or totally (Fig. 10). The body may become wedge-shaped (Fig. 8 and 10), or assume the shape of a biconcave lens (Fig. 3). Against the background of the osteoporotic vertebral body, the end plates stand out as fine pencilled lines of increased density. Depending upon the degree of destruction, the vertebral surfaces will be either depressed or irregularly indented (Fig. 8). As a rule, there are no syndesmophytes. Osteophytic spurs are not a part of the picture unless there is superimposed degenerative change. The pedicles, neural arches, articular processes, and apophyses

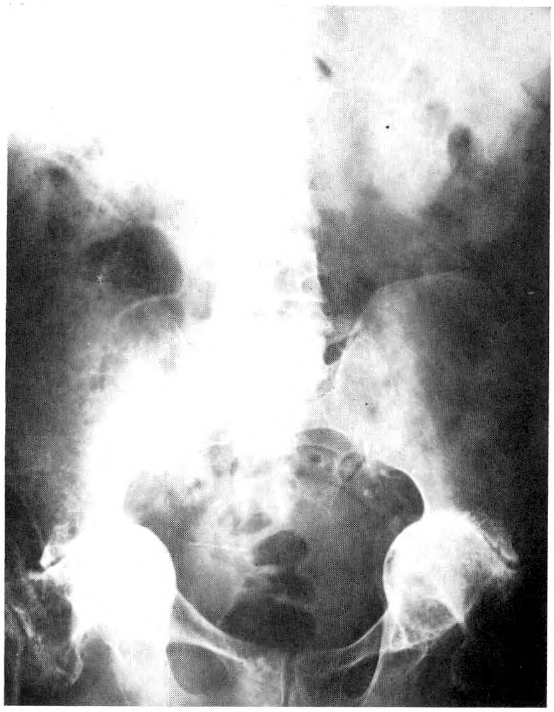

Fig. 7. Case II. Anteroposterior roentgenogram of lumbar spine and pelvis. The sacroiliac joints remain open. Bilateral protrusio acetabuli.

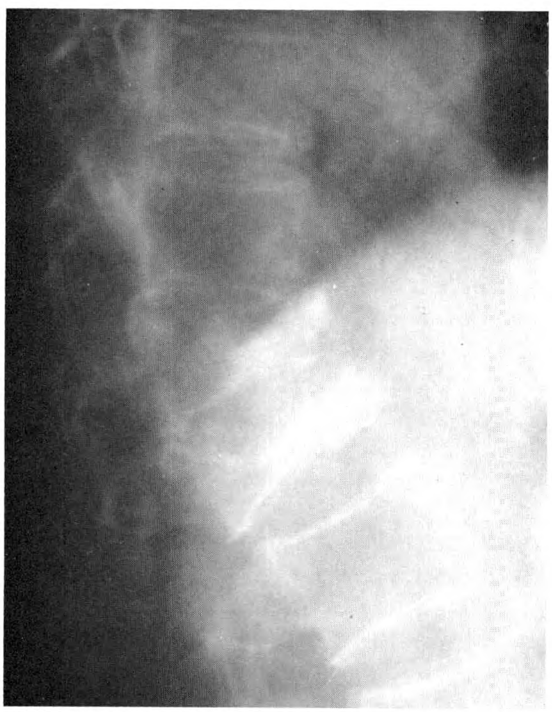

Fig. 8. Case II. Close-up of lateral thoracolumbar spine roentgenogram showing marked collapse of T12 and L1 with gibbus formation. Irregular depression of superior end plate of T12 and smooth concavity of L1. Anterior projection of the collapsed vertebrae.

show no evidence of destruction. The disk spaces are preserved and may be of normal width or expanded, depending on the degree of collapse of the bodies. The sacroiliac joints remain open. Finally, there are no fusiform paravertebral soft tissue shadows to suggest abscess formation. Any vertebra may be involved, but the lesions occur most frequently at the thoracolumbar junction.

The roentgen appearance of this type of destructive lesion is so strikingly different from that seen in ankylosing spondylitis that the two conditions should hardly be considered together in the differential diagnosis. On the other hand, any vertebral lesion associated with collapse of the vertebral bodies may pose differential diagnostic problems. Traumatic vertebral lesions are separated by the history and the normal structure of the vertebra. Eosinophilic granuloma, the substratum of vertebra plana, occurs in much younger patients. Here again, generalized osteoporosis is not

Fig. 9. Case III. Anteroposterior roentgenogram of the pelvis showing diffuse osteoporosis, bilateral protrusio acetabuli and spontaneous fracture of the left femur.

present. Infectious spondylitis produces destruction of the disk and may be complicated by formation of abscesses. Primary (plasmacytoma) or secondary tumors (carcinoma, lymphoma) may be more difficult to eliminate. The demonstration of foci of destruction in other skeletal segments or of the primary lesion will facilitate the diagnosis.

Senile osteoporosis, Cushing's disease, and corticosteroid therapy may create diagnostic difficulties. However, late association of destructive vertebral changes in a known case of peripheral rheumatoid arthritis is strongly suggestive of nodular rheumatoid vertebral lesion, and, in doubtful cases, biopsy will assist in establishing the correct diagnosis.

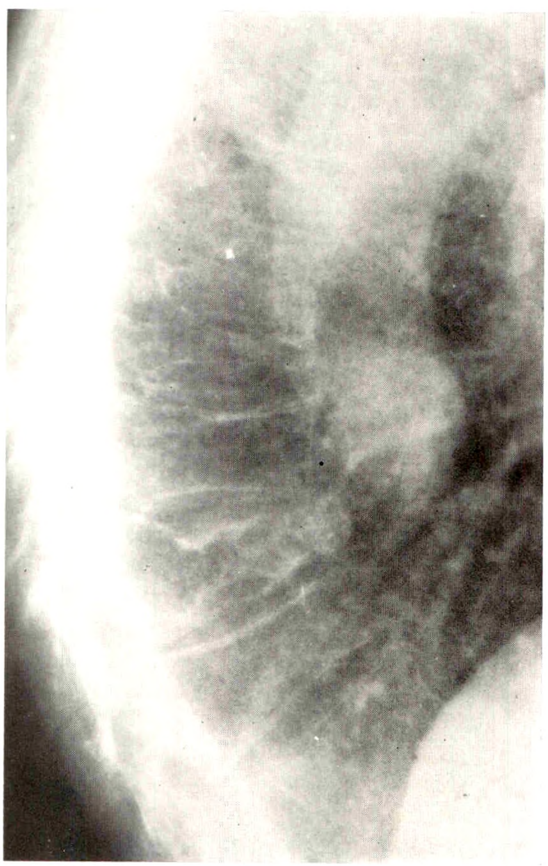

FIG. 10. Case III. Lateral roentgenogram of the thoracic spine showing diffuse osteoporosis and variable collapse of the vertebral bodies at T9–T12. Note irregularities of the end plates and anterior projection of T11.

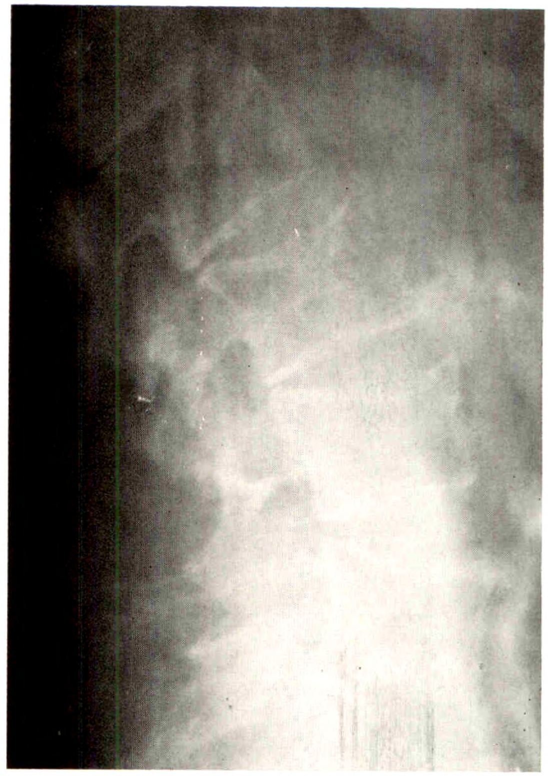

FIG. 11. Case III. Lateral roentgenogram of the lumbar spine showing partial collapse of L2–L5 and concavity of superior end plates.


SUMMARY

Granulomatous rheumatoid spondylitis is defined by the presence of rheumatoid nodules in the marrow of vertebral bodies. The process leads to necrosis of the bone substance and collapse of the vertebral bodies. Three such cases, including one with autopsy findings, are reported together with a review of the literature. The striking differences in the roentgen appearance and the clinical behavior of rheumatoid nodular and ankylosing spondylitis indicate that the two diseases are different entities.

The differential roentgen diagnosis of collapsed vertebrae produced by granulomatous rheumatoid lesions and other morbid processes is briefly discussed.



A. Glay, M.D.
Department of Radiology
St. Mary's Hospital
3830 Lacombe Avenue
Montreal 26, Quebec, Canada

REFERENCES

1. Baggenstoss, A. H., Bickel, W. H., and Ward, L. E. Rheumatoid granulomatous nodules as destructive lesions of vertebrae. *J. Bone & Joint Surg.*, 1952, *34A*, 601–609.
2. Blecourt, J. J. de., Polman, A., Blecourt-Meindersma, T. de. Heredity factors in rheumatoid arthritis and ankylosing spondylitis. *Ann. Rheumat. Dis.*, 1961, *20*, 215–220.
3. Boland, E. W., and Shebesta, E. M. Rheumatoid spondylitis: correlation of clinical and roentgenographic features. *Radiology*, 1946, *47*, 551–561.
4. Calabro, J. J. Therapeutic approach to rheumatoid spondylitis. *G.P.*, 1960, *22*, 88–95.
5. Cruickshank, B. Histopathology of diarthrodial joints in ankylosing spondylitis. *Ann. Rheumat. Dis.*, 1951, *10*, 393–404.
6. Forestier, J., and Faidherbe, P. Spondylite et spondylarthrite. *J. de radiol., d'électrol. et de méd. nucléaire*, 1949, *30*, 569–570.
7. Franklin, E. C. Immune globulins in man. *Pediat. Clin. North America*, 1963, *10*, 857–877.
8. Graham, W. Is rheumatoid spondylitis a separate entity? *Arthritis & Rheum.*, 1960, *3*, 88–90.
9. Guest, C. M., and Jacobson, H. G. Pelvic and extrapelvic osteopathy in rheumatoid spondylitis: clinical and roentgenographic study of ninety cases. Am. J. Roentgenol. & Rad. Therapy, 1951, *65*, 760–768.
10. Lorber, A., Pearson, C. M., and Rene, R. M. Osteolytic vertebral lesions as manifestation of rheumatoid arthritis and related disorders. *Arthritis & Rheum.*, 1961, *4*, 514–532.
11. Louyot, P., Graucher, A., Mathieu, J., and Miquel, C. Les lésions destructives disco-vertébrales de la spondylarthrite ankylosante. *Ann. méd.*, 1962, *1*, 250–262.
12. Martel, W., and Page, J. W. Cervical vertebral erosions and subluxations in rheumatoid arthritis and ankylosing spondylitis. *Arthritis & Rheum.*, 1960, *3*, 546–556.
13. Mason, R. M. Ankylosing spondylitis. *Brit. J. Ven. Dis.*, 1959, *35*, 71–76.
14. McKusick, V. A. Genetic factors in diseases of connective tissues; survey of present state of knowledge. *Am. J. Med.*, 1959, *26*, 283–302.
15. Romanus, R., and Yden, S. Destructive and ossifying spondylitic changes in rheumatoid ankylosing spondylitis (pelvo-spondylitis ossificans). *Acta orthop. scandinav.*, 1952, *22*, 88–99.
16. Romanus, R., and Yden, S. Diskography in ankylosing spondylitis. *Acta radiol.*, 1952, *38*, 431–439.
17. Seaman, W. B., and Wells, J. Destructive lesions of vertebral bodies in rheumatoid disease. Am. J. Roentgenol., Rad. Therapy & Nuclear Med., 1961, *86*, 241–250.
18. Wholey, M. H., Pugh, D. G., and Bickel, W. H. Localized destructive lesions in rheumatoid spondylitis. *Radiology*, 1960, *74*, 54–56.

# POSTERIOR DISLOCATION OF THE SHOULDER*

*By* J. H. ARNDT, M.D., *and* A. D. SEARS, M.D.
DALLAS, TEXAS

ONE hundred and twenty-three years after Sir Astley Cooper's[5] optimistic observation, "It is an accident which cannot be mistaken . . . ," half or more of posterior dislocations of the shoulder cases are missed or misdiagnosed. In 3 of the larger modern series, the correct diagnosis was made initially in but 18 of 50 cases reported.[9,13,15] In the remainder, there was a delay of days, months, or years before the diagnosis was made. McLaughlin[10] described 13 cases that were unrecognized for an average period of 8 months before the correct diagnosis was made. Delayed or inappropriate treatment results in unnecessary morbidity and continuing damage to the joint structures. Early diagnosis of the posterior dislocation may obviate a surgical repair, frequently required for the neglected injury.[7,8,12]

The frequency with which this diagnosis is missed is largely the result of 4 factors: (1) the injury is rare, accounting for only 2–4 per cent of all shoulder dislocations;[11,12] (2) the appearance of the anteroposterior roentgenogram may be deceptively normal; (3) the clinical findings may be subtle, obscured by soft tissue injury or simulate the much more common condition termed "frozen shoulder" or "periarthritis;"[6,8,10,13,17] and (4) various fractures may accompany a posterior dislocation, and the patient's symptoms may be attributed to these by the unwary physician.[14,16,18]

Our interest in acute traumatic posterior dislocation of the humerus was stimulated when 2 such cases were seen within a 10 day period. A search of hospital records produced a third case. A fourth case was graciously provided by the Radiology Department of Methodist Hospital of Dallas, Texas.

Unlike anterior or inferior dislocations,

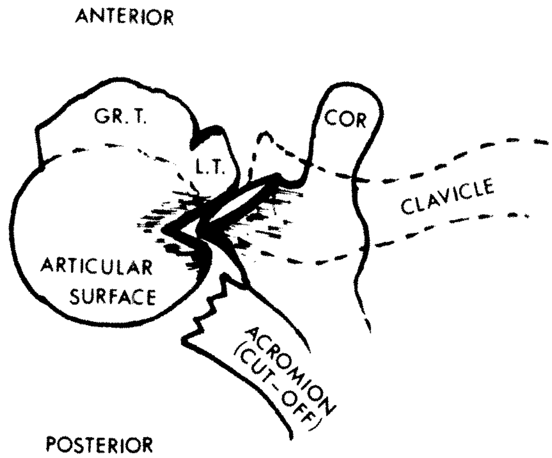


FIG. 1. Notching of the humeral head obscures the rim sign. The sketch illustrates a posteriorly dislocated and notched humerus as seen from above. The defect between the lesser tuberosity (L.T.) and the articular surface is produced by the ridged posterior glenoid rim, which it straddles. If the groove is deep enough, the rim sign will be obliterated. Notching accounted for all but 4 of the false negative rim signs encountered in the reviewed case material (see text).

approximately one-half of the cases of posterior dislocation of the humerus result from convulsive episodes.[10,11,12] The remainder are produced by a direct blow to the anterior surface of the humeral head or a force transmitted along a flexed, adducted and internally rotated humerus. The displaced articular surface of the humeral head comes to rest behind the glenoid, facing posteriorly. The humerus is then locked in internal rotation. The soft anterior surface of the anatomic neck hinges on the posterior rim of the glenoid (Fig. 1). Compression fracture with flattening of this nonarticular surface frequently occurs during the dislocation (Fig. 3; and 4 *A*).[10]

If the dislocation is unrecognized or mistakenly treated as a "frozen shoulder," the hard posterior glenoid rim eventually

* From the Department of Radiology, Baylor University Medical Center, Dallas, Texas.

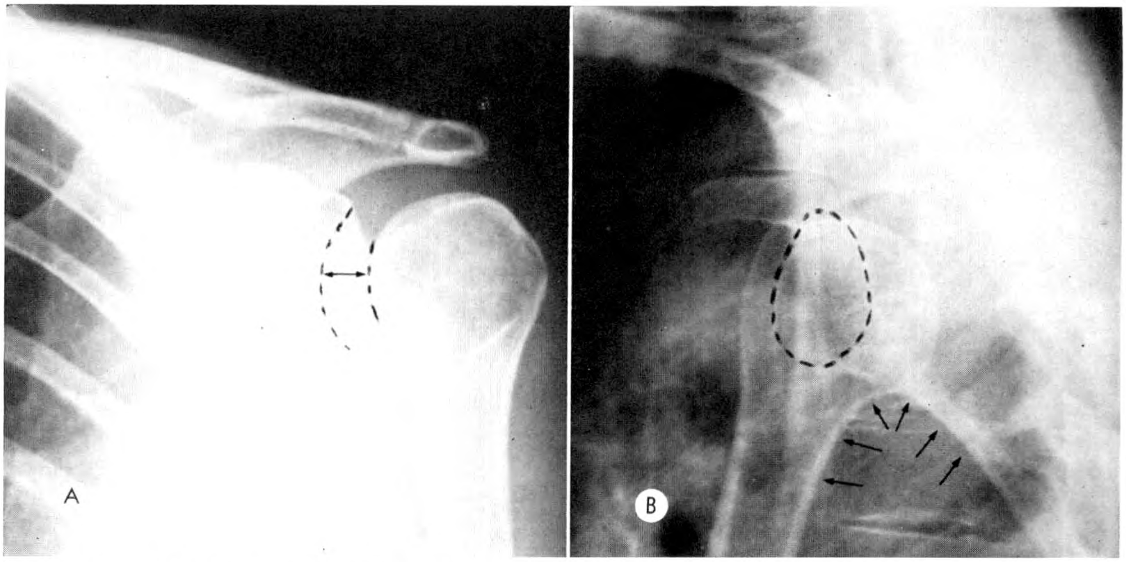


Fig. 2. Case I. Positive rim sign. (*A*) The humerus is in internal rotation, yet the space between the medial margin of the humeral head and the anterior rim of the glenoid fossa (↔) measured 11 mm. (*B*) Transthoracic lateral roentgenogram. Rounded articular surface of humerus faces posteriorly and does not engage the glenoid fossa (dotted oval). Apex of scapulohumeral arch is narrowed (arrows). Compare with Figure 4*B*.

erodes a deep notch in the humeral head (Fig. 1).[9,12,13,17] This notch may also be produced during the initial injury, particularly if there is a direct blow to the head of the humerus. Whatever its cause, the notch

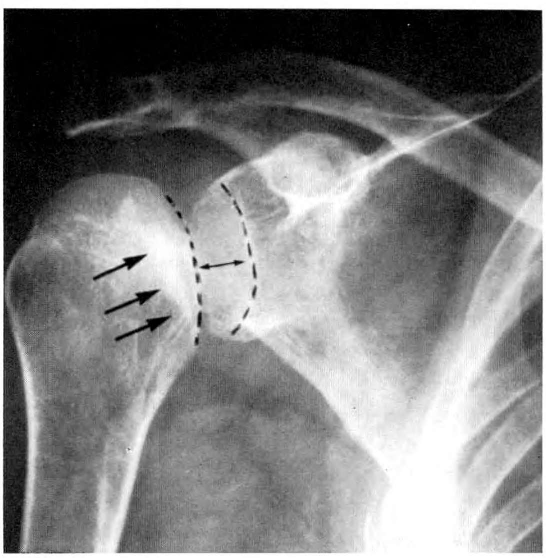

Fig. 3. Case II. Positive rim sign. The joint space measured 13 mm. (↔). Compression fracture of internally rotated humeral head evidenced by flattening of medial profile and dense zone of compressed spongy bone (arrows).

obscures helpful diagnostic features on the anteroposterior roentgenogram.

Once considered, a posteriorly displaced humerus may be readily demonstrated on transthoracic lateral or transaxillary (vertical) roentgenograms. Stereoscopic studies have been utilized with variable success because the posterior displacement of the humerus is usually slight.[16] Since few departments obtain these views in every case of shoulder pathology, an evaluation of the clues provided by the anteroposterior roentgenogram seems worthwhile.

A similar and striking abnormality was observed on the anteroposterior roentgenogram of our 4 cases. There was an apparent increase in the space between the anterior rim of the glenoid fossa and the medial aspect of the humeral head (Fig. 2 through 5, inclusive). These spaces measured 11, 11, 12, and 13 mm., respectively. We have termed this widened appearance a "positive rim sign." It may be present in posterior dislocation because the normal glenoid fossa faces as much anteriorly as it does laterally.[19] Since the dislocated humeral head rests against the posterior glenoid

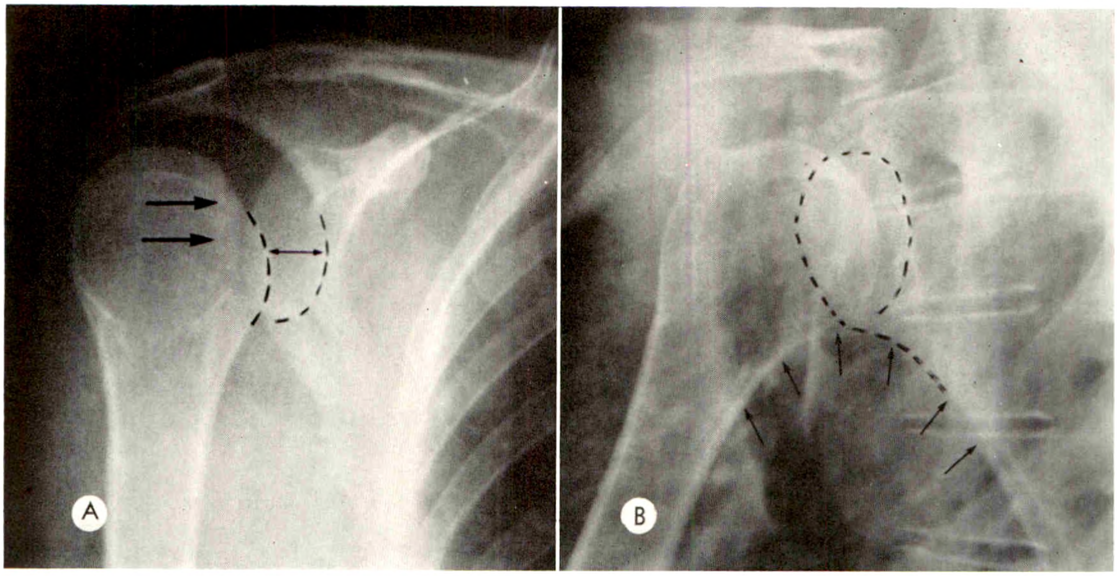


FIG. 4. Case III. (*A*) Positive rim sign. Joint space (↔) measured 12 mm. Compression fracture of internally rotated humeral head (arrows) is evident. (*B*) Postreduction transthoracic lateral roentgenogram demonstrates the restored glenohumeral relationship and the normal broad scapulohumeral arch. Compare with Figure 2*B*.

rim, the space between the anterior rim and the head appears increased.

Measurement of the joint space on the anteroposterior roentgenogram (36–40 inches target film distance) of 100 normal shoulders revealed that these may vary from less than 0 to a maximum of 6 mm., depending upon the degree of rotation of the humerus (Fig. 6, *A*, *B* and *C*). Children with incompletely ossified epiphyses were excluded. When the humerus is in extreme internal rotation, the lesser tuberosity overlaps the anterior rim of the glenoid and the space is less than 6 mm. (Fig. 6*C*). Since the posteriorly dislocated humerus is usually held in marked internal rotation, a measurement of more than 6 mm. is significant.

## MATERIAL

In order to determine the frequency and reliability of the "rim sign," the anteroposterior roentgenograms of 48 reported cases of posterior dislocation of the shoulder were reviewed. Selection was random, the only requirement being a reasonably adequate reproduction of the anteroposterior roentgenogram. Only those cases in which the space between the anterior rim of the glenoid fossa and the medial margin of the humerus was obviously widened were considered to have a "positive rim sign."

## RESULTS

The rim sign was positive in all 4 of our

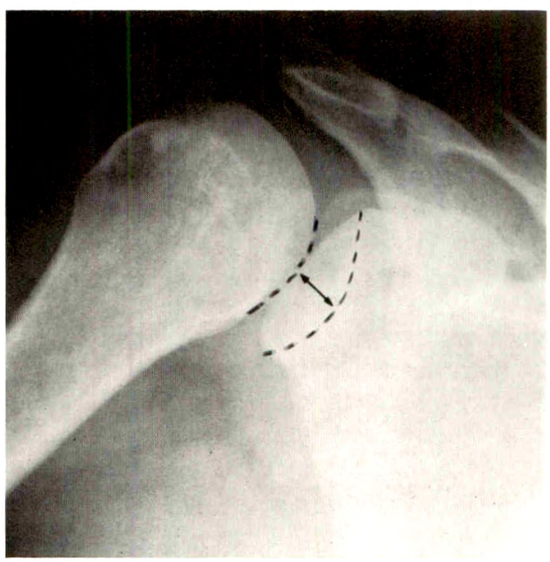

FIG. 5. Case IV. Positive rim sign. Joint space (↔) measured 11 mm. No compression of humeral head is seen. Compare with Figure 6, *B* and *C*.

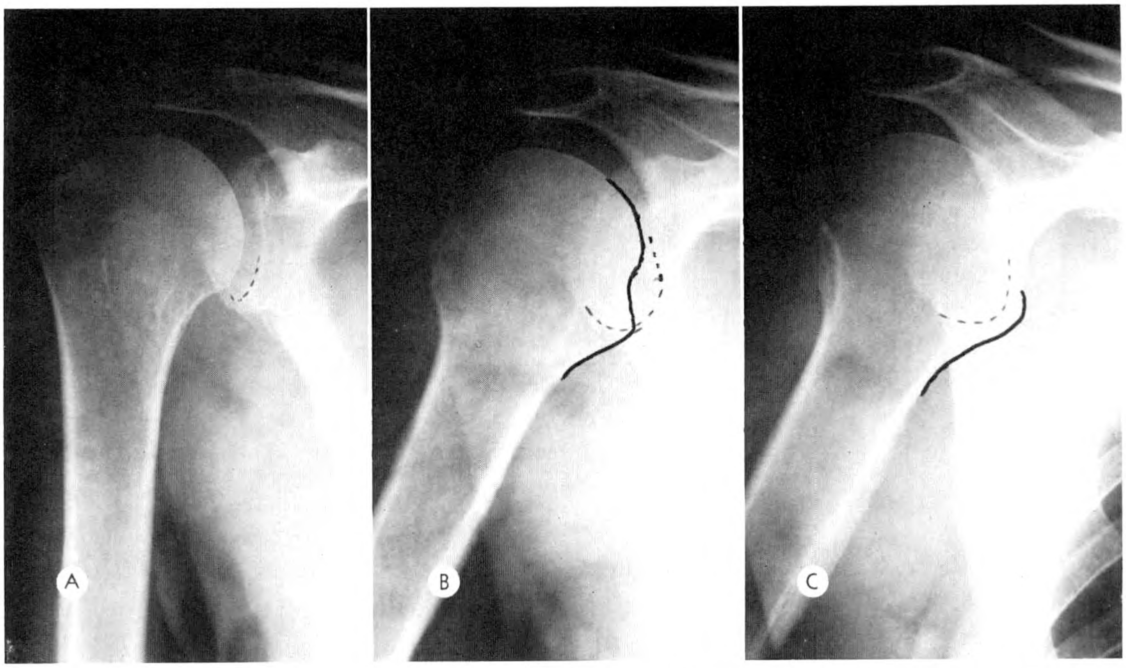


FIG. 6. Normal shoulder with humerus in (*A*) external rotation, (*B*) moderate internal and (*C*) marked internal rotation. Note the relationship of the medial profile of the humeral head and the anterior rim of the glenoid fossa (dotted line) as the degree of internal rotation is increased. In the normal shoulder the separation of these two surfaces is never more than 6 mm. regardless of rotation or projection.

cases. In Case 11, the dislocation was unsuspected clinically. The sign was considered positive in 31 of the 48 roentgenograms reviewed in the literature (64.6 per cent). In 10 of the cases misdiagnosed at the time of injury, a positive rim sign was evident.

Since a positive rim sign is the result of lateral displacement of the humeral head, any mass or fluid accumulation within the shoulder joint can produce this appearance. Ligamentous laxity, as seen in flaccid paralysis, can also widen the joint space. In such cases, malrotation of the humerus would not be expected.

Conversely, a positive rim sign could be obscured by poor centering of the roentgen beam or by rolling the supine patient into a posterior oblique position. Since ablation of the sign by the latter mechanism would require that the injured shoulder be "down," this possibility seems unlikely. Variation in projection was not considered a significant factor in any of the cases reviewed.

False negative rim signs were present in 17 cases (35.4 per cent). In 4 of these there was exaggerated medial displacement of the humeral head, secondary to comminuted fracture of the head or neck. This "excessive overlap" should lead one to suspect a concomitant dislocation. In the remaining 13 cases, notching of the humeral head by the glenoid lip obscured the rim sign (Fig. 1). It was not possible to ascertain whether the notching occurred during the initial injury or resulted from trauma associated with the unrecognized dislocation. In 7 instances, however, there was a delay in diagnosis of from 2 days to 6 months. The interval between injury and diagnosis was not given in the other 6 cases.

It is, therefore, probable that roentgenograms obtained at the time of injury are most likely to demonstrate a positive rim sign. The longer the interval between injury and roentgenography, the less helpful the sign is likely to be.

## OTHER ROENTGEN MANIFESTATIONS

Previously described anteroposterior roentgen manifestations of posterior dis-

location of the humerus were also evaluated and include the following:

1. *Absence of a Half-Moon Overlap.* Bonadeo[3] was the first to observe an absence of the shadow formed by the overlap of the humerus and the posterior rim of the glenoid. This was reaffirmed by Nobel[12] who stated, "Normally, the medial part of the head of the humerus overlaps the glenoid fossa to form a shadow shaped like a half-moon which reaches down to the inferior border of the fossa. In posterior dislocation this half-moon shadow may disappear, and the lower part of the glenoid fossa may be empty." (Normal half-moon overlap is seen in figure 6*A*.) Subsequent authors have expressed doubt about the reliability of this observation since overlap may be present with a dislocated humerus, or absent in a normal shoulder depending on projection.[11,13]

In 16 of the 48 cases of dislocation reviewed, overlap was absent. The rim sign was also positive. In the remaining 32 cases a normal or diminished overlap was present. In 14 of this group, the rim sign was considered positive. Both the rim sign and the absence of overlap are obviously based on the same phenomenon. It is our feeling that the rim sign is more eye-catching, and, since actual measurements may be made, will better lend itself to objective interpretation.

2. *Velpeau or "Reverse" Velpeau Position.* The humeral head may be higher (Velpeau position) or lower than normal ("reverse" Velpeau position) in its relationship to the glenoid fossa.[9,12] A Velpeau position was evident in 14 cases and a "reverse" Velpeau position in 7 of the 48 cases reviewed. It should be noted that a Velpeau position may be present in normal shoulders.

3. *Internal Rotation.* The posteriorly dislocated humeral head is usually held in internal rotation. In 7 of the cases reviewed, it appeared to be in a neutral position. If the humerus appears to be externally rotated, a traumatic posterior dislocation may be excluded.

4. *Flattening of the Medial Aspect of the Humeral Head.* This defect was observed in 22 of the 48 roentgenographic reproductions studied as well as in 2 of our cases (Fig. 3; and 4*A*). McLaughlin[9] feels that this represents a true compression fracture of the anterior surface of the humerus which presents as the medial profile because of marked internal rotation. He cautions against attributing the patient's symptoms to this "relatively insignificant injury."

5. *Linear Fractures of the Humeral Head.* Posterior dislocation of the shoulder was associated with a major fracture in 10 instances. In 7 of the 10, the diagnosis of the dislocation was delayed. Axillary or transthoracic views were not obtained initially.

*Diagnostic Accuracy.* Twenty-nine of the 48 cases studied presumably presented diagnostic problems. The dislocation was not detected at the time of injury in 21 (72 per cent) of these. Seven additional cases were chronic recurrent dislocations and presented no diagnostic problem. The diagnostic accuracy was not recorded in 12.*

## REPORT OF CASES

Case i. J.K.G., a 52 year old female, leaned forward on her outstretched arm while gardening and felt her left shoulder "pop out." She had experienced several similar episodes in the past. Physical examination revealed pain upon motion of the arm and a depression of the soft tissue contour of the anterior surface of the shoulder. Anteroposterior roentgenograms demonstrated a positive rim sign. Transthoracic lateral views revealed loss of the normal arch formed by the humerus and scapula (Fig. 2, *A* and *B*).[6]

Case ii. C.A.S., a 56 year old female, sustained spine and rib fractures, cerebral concussion and pulmonary contusion in an automobile accident. She complained of pain upon motion of the left shoulder. Anteroposterior roentgenograms revealed a compression fracture of the medial surface of the humeral head and a positive rim sign (Fig. 3). Transthoracic lateral views (not reproduced) confirmed a posterior dislocation. Reduction was delayed

* A detailed report of the individual case analyses may be obtained from the authors on request.

until the patient could tolerate a general anesthesia. One week after injury, successful closed manipulation was accomplished. Redislocation could be produced by internal rotation.

Case iii. L.N., a 42 year old female, complained of pain and limitation of motion of the right shoulder following an automobile accident. A posterior dislocation was suspected clinically and confirmed roentgenographically. A positive rim sign was evident on the anteroposterior view (Fig. 4*A*). A transthoracic lateral view demonstrated a loss of the humeroscapular arch but was not of sufficient technical quality for reproduction. The postreduction transthoracic view is included for comparison (Fig. 4*B*).

Case iv. J.C.D., a 34 year old male, sustained fractures of the mandible and patella in an automobile accident. A hematoma over the right shoulder and limitation of motion of the arm were noted. An anteroposterior roentgenogram demonstrated a positive rim sign (Fig. 5). No other views were obtained. During manipulation under anesthesia the "head was felt to slip back into the glenoid fossa."

## SUMMARY AND CONCLUSIONS

Posterior dislocation of the shoulder is a rare injury, missed or misdiagnosed in over one-half of the cases reviewed. This is partly accounted for by reliance upon anteroposterior roentgenograms for detection of shoulder pathology.

In the normal adult shoulder, the measurement on roentgenograms of the joint space does not exceed 6 mm., regardless of projection. An apparent increase in the width of this space has been termed a "positive rim sign." We have found it a useful sign of posterior dislocation. All 4 of the cases reported demonstrated a positive rim sign. The joint space measurements were 11, 11, 12, and 13 mm., respectively.

The rim sign was positive in 64.6 per cent of cases reviewed from the literature. It is probable that it is positive in an even greater percentage of *acute* dislocations. In the neglected injury, however, and in those cases associated with comminuted fractures of the humeral head-neck region, the sign is of less value. Axillary or transthoracic lateral roentgenograms should be obtained in all cases in which there is uncertainty as to the glenohumeral relationship.

Jerome H. Arndt, M.D.
St. Paul Hospital
5909 Harry Hines Boulevard
Dallas, Texas

The authors wish to express their gratitude to Dr. Brooks Chapman for his efforts in obtaining the roentgenograms of Case iv and to Drs. R. H. Millwee, R. E. Hodges, H. S. McCreary, and Joe Hawkins for allowing us to use them.

## REFERENCES

1. Arden, G. P. Posterior dislocation of both shoulders: report of case. *J. Bone & Joint Surg.*, 1956, *38-B*, 558–563.
2. Basmajian, J. V. In: Primary Anatomy. Fourth edition. Williams & Wilkins Company, Baltimore, 1960, p. 87.
3. Bonadeo, A. A. Sobre un caso de luxación posterior recidivante de la articulación escápulohumeral. *Rev. ortop. y traumatol.*, 1933, *3*, 188–208.
4. Cooper, A. On dislocation of os humeri upon dorsum scapulae, and upon fractures near shoulder-joint. *Guy's Hosp. Rep.*, 1839, *4*, 265–284.
5. Cooper, A. A Treatise on Dislocations and Fractures of the Joints. 1842, p. 391. New edition edited by B. B. Cooper. J. & A. Churchill, Ltd., London.
6. Dorgan, J. A. Posterior dislocation of shoulder. *Am. J. Surg.*, 1955, *89*, 890–900.
7. Hill, N. A., and McLaughlin, H. L. Locked posterior dislocation simulating "frozen shoulder." *J. Trauma*, 1963, *3*, 225–234.
8. Jones, V. Recurrent posterior dislocation of shoulder: report of case treated by posterior bone block. *J. Bone & Joint Surg.*, 1958, *40-B*, 203–207.
9. McLaughlin, H. Posterior dislocation of shoulder. *J. Bone & Joint Surg.*, 1953, *34-A*, 584–590.
10. McLaughlin, H. L. Locked posterior subluxation of shoulder: diagnosis and treatment. *S. Clin. North America*, 1963, *43*, 1621–1622.
11. Neviaser, J. S. Posterior dislocation of shoulder; diagnosis and treatment. *S. Clin. North America*, 1963, *43*, 1623–1630.
12. Nobel, W. Posterior traumatic dislocation of shoulder. *J. Bone & Joint Surg.*, 1962, *44-A*, 523–538.

13. O'CONNOR, S. J., and JACKNOW, A. S. Posterior dislocation of shoulder. *A.M.A. Arch. Surg.*, 1956, *12*, 479–491.
14. RENDICH, R. A., and POPPEL, M. H. Roentgen diagnosis of posterior dislocation of shoulder. *Radiology*, 1941, *36*, 42–45.
15. TAYLOR, R. G., and WRIGHT, P. R. Posterior dislocation of shoulder: report of six cases. *J. Bone & Joint Surg.*, 1952, *34-B*, 624–629.
16. THOMAS, M. A. Posterior subacromial dislocation of head of humerus. AM. J. ROENTGENOL. & RAD. THERAPY, 1937, *37*, 767–773.
17. WILSON, J. C., and MCKEEVER, F. M. Traumatic posterior (retroglenoid) dislocation of humerus. *J. Bone & Joint Surg.*, 1949, *31-A*, 160–172.
18. WOOD, J. P. Posterior dislocation of head of humerus and diagnostic value of lateral and vertical views. *U. S. Naval Med. Bull.*, 1941, *39*, 532–535.

# BAKER'S CYST AND THE NORMAL GASTROCNEMIO-SEMIMEMBRANOSUS BURSA

*By* JOHN L. DOPPMAN, M.D.*
BETHESDA, MARYLAND

A POPLITEAL cyst is a firm fluid-filled mass presenting at the back of the knee. Adams[1] first described the entity in 1840, referring to it as "dropsy of the knee." Baker[2] in 1877 presented 10 cases, noted the frequent association of popliteal cysts with intrinsic pathology of the knee joint, and contributed his name as the most enduring and widely used of many eponyms. The initial symptom is usually one of painless swelling behind the knee: occasionally mild aching and stiffness of the joint are associated. Clinical examination reveals a tense cystic mass best palpated with the knee fully extended and usually presenting on the medial aspect of the flexor surface of the knee just below the transverse crease.[18] Treatment, if symptomatic, involves excision of the cyst with particular attention to closing any communication between the popliteal cyst and the knee joint space proper.

Roentgenography has little to offer the clinician in the diagnosis of popliteal cysts, and only a single reference to this subject in the American radiologic literature of the past 20 years could be found. Kuhn and Hemphill[12] described the plain roentgen findings of a soft tissue swelling behind the knee and by pneumoarthrography demonstrated several air containing popliteal cysts posterior to and communicating with the knee joint. In the course of cineroentgenographic studies of knee joint motion following routine arthrography, the author has demonstrated similar cysts in approximately 50 per cent of persons without clinical evidence of Baker's cysts. The possibility of confusing these apparently normal communicating bursae with popliteal cysts has prompted the following presentation. In addition, some observations on the hydrodynamics of joint fluid during knee flexion and extension are discussed.

## ANATOMY

Wilson *et al.*[16] described 6 primary bursae behind the knee. The only posterior bursa consistently communicating with the knee joint lies between the medial head of the gastrocnemius and the semimembranosus muscles. This bursa, referred to as the gastrocnemio-semimembranosus bursa (G-S bursa), was found to communicate with the knee joint space in 17 out of 30 cadaver dissections. Of the multiple bursae about the knee, only 2, the suprapatellar (100 per cent) and the gastrocnemio-semimembranosus (about 50 per cent) consistently communicate. The neck of the G-S bursa enters the upper posteromedial corner of the knee joint space opposite the posterior articular surface of the medial femoral condyle. The wall of the bursa consists of fibrous tissue lined with synovia continuous with the synovial membrane of the knee joint.[11]

Although some authors[8,15] attempt to subdivide popliteal cysts into (1) hernias of the posterior joint capsule and (2) abnormally distended communicating posterior bursae, most authorities[7,11,13,16] support the latter theory and define Baker's cyst as an abnormal distention of the gastrocnemio-semimembranosus bursa with or without a demonstrable knee joint communication. Burleson *et al.*[3] demonstrated such a communication in 50 out of 83 surgically excised cysts (65 per cent); Gristina and Wilson[7] showed a similar incidence of communication in a series of 90 operated cases.

## ROENTGENOGRAPHIC FINDINGS

In a cineroentgenographic study of knee joint motion following routine arthrogra-

* Now at Department of Radiology, Hospital of St. Raphael, New Haven, Connecticut.

phy, filling of the G-S bursa was noted in about 50 per cent of cases when the knee was sharply flexed. Although none of these patients had clinically evident Baker's cysts, the size of the distended G-S bursa was often striking (Fig. 1). Such filling on flexion appeared to involve 2 processes: (1) the relaxation and opening of the neck of the bursa as the enclosing gastrocnemius and semimembranosus tendons slackened with knee flexion; and (2) the compression of the suprapatellar bursa between the quadriceps tendon and the anterior surface of the lower femur, forcing joint fluid (or contrast agent) into the posterior compartment of the knee and out into the G-S bursa (Fig. 2, *A* and *B*). When no communication between the knee joint and the G-S bursa exists (about 50 per cent of our cases), the entire posterior joint compartment bulges (Fig. 3, *A* and *B*). This see-saw movement of joint fluid on knee flexion and extension is dramatically demonstrated on cine studies with the G-S bursa often appearing to "pop open" as increasing flexion compresses and empties the suprapatellar bursa. This squeezing of the suprapatellar bursa between the quadriceps muscle and the femoral shaft during flexion is probably a more important mechanism than the relaxation of the hamstring tendons. This was demonstrated by contrast filling of the knee joint of a mid-thigh amputation specimen. Since the quadriceps group was not proximally anchored, sharp flexion of the knee caused no compression of the suprapatellar bursa and no posterior migration of the joint fluid. When the suprapatellar bursa was manually compressed with the knee flexed, the G-S bursa readily filled.

Occasionally, in the presence of a torn posterior capsule, contrast material will extravasate into the fascial planes behind the knee, particularly on sharp flexion. Such extravasation may be demonstrated long after the initial injury, suggesting that capsular tears are slow to heal. The appearance of the contrast medium is linear and streaky, with a tendency to track inferiorly, close to the posterior tibial surface (Fig. 4,

FIG. 1. Note the large gastrocnemio-semimembranosus (G-S) bursa communicating via a narrow neck with the posterior knee joint space. No joint effusion and no clinical evidence of a Baker's cyst were present.

*A* and *B*); a typical G-S bursa is smoothly outlined and globular and usually extends directly posteriorly or even slightly craniad. Most important in differential diagnosis, the G-S bursa will empty as the flexed knee is extended; extravasated contrast will remain extra-articular once it has escaped the confines of the synovial space (Fig. 4 *C*).

Contrast filling of the G-S bursa has on at least one occasion helped to explain the location of a loose body far posterior in the popliteal space (Fig. 5, *A* and *B*).

## DISCUSSION

It seems obvious that since the normal knee joint contains only a small quantity of lubricating fluid, flexion and extension movements have little influence on its distribution. In the presence of a joint effusion, or its iatrogenic counterpart, about 15 cc. of water soluble contrast agent, the fluid preferentially accumulates in the suprapatellar bursa with the knee in extension or moderate flexion (the routine position for lateral knee roentgenography). When the knee is sharply flexed, the joint


Fig. 2. (*A*) Contrast agent accumulates in the suprapatellar bursa with the knee fully extended. Note the absence of any posterior bursal filling. (*B*) Flexion of the knee compresses and empties the suprapatellar bursa. The posterior joint compartment and an "average-sized" G-S bursa are now contrast filled. Extension of the knee would restore the appearance in *A*.


Fig. 3. (*A* and *B*) Flexion of the knee empties the suprapatellar bursa but the G-S bursa evidently does not communicate. The entire posterior knee joint compartment bulges.

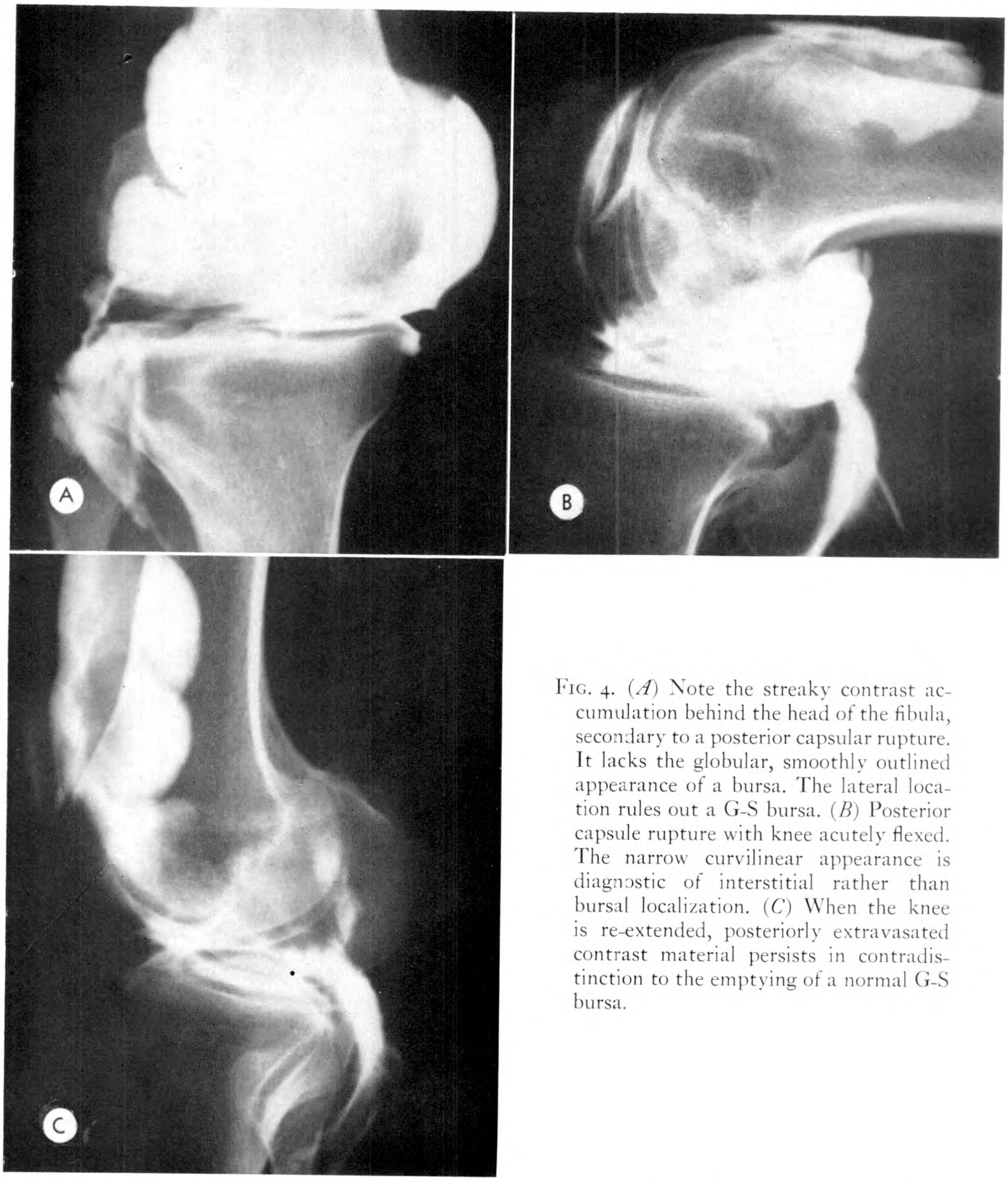


Fig. 4. (*A*) Note the streaky contrast accumulation behind the head of the fibula, secondary to a posterior capsular rupture. It lacks the globular, smoothly outlined appearance of a bursa. The lateral location rules out a G-S bursa. (*B*) Posterior capsule rupture with knee acutely flexed. The narrow curvilinear appearance is diagnostic of interstitial rather than bursal localization. (*C*) When the knee is re-extended, posteriorly extravasated contrast material persists in contradistinction to the emptying of a normal G-S bursa.

fluid is forced out of the suprapatellar bursa into the posterior compartment of the knee and (in 50 per cent of the population) into the communicating gastrocnemio-semimembranosus bursa. This tidal movement of joint fluid has several roentgenologic implications.

1. The diagnosis of a joint effusion roentgenographically depends upon the demonstration of the soft tissue outline of a distended suprapatellar bursa. Progressive knee flexion will empty this bursa and although the gastrocnemio-semimembranosus bursa when communicating will become distended, we agree with Lewis[14] that it is a difficult structure to define roentgeno-

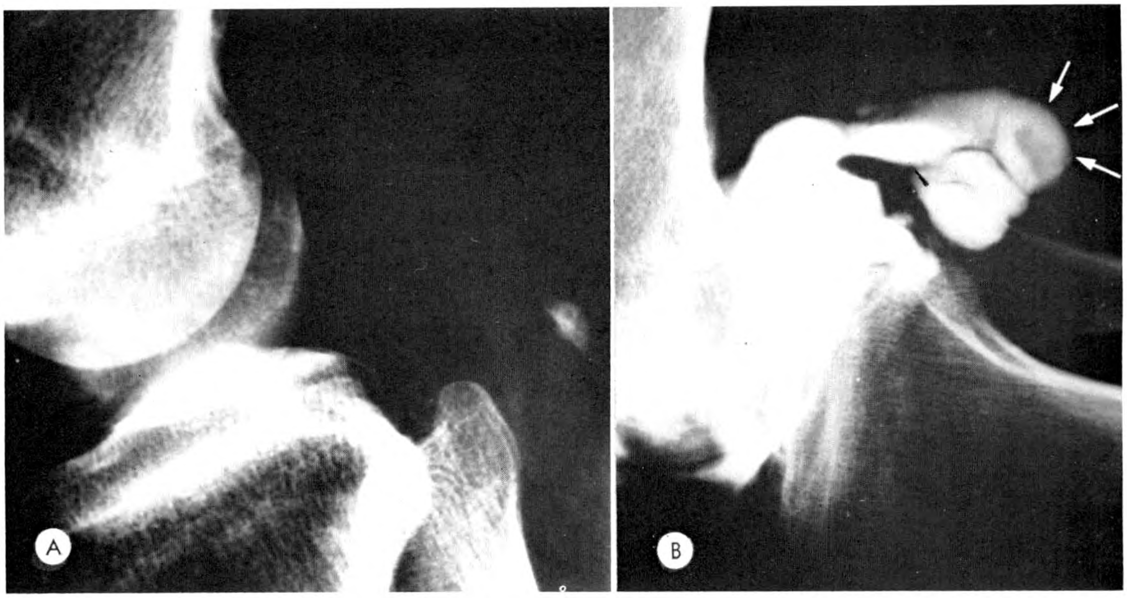


Fig. 5. (*A*) Patient had multiple joint mice and a small calcification far posterior in the popliteal space. (*B*) Popliteal calcification demonstrated as a filling defect or loose body in the contrast filled G-S bursa.

graphically because "in most instances it is superimposed upon the heads of the gastrocnemius muscles with whose shadow it blends almost perfectly." Thus, the diagnosis of a small joint effusion is best made with the knee fully extended, not partially flexed.

2. The size of the gastrocnemio-semimembranosus bursa is anatomically determined. There are large and small ones just as there are large and small suprapatellar bursae.[5] The filling of a large G-S bursa during arthrography is not diagnostic of a clinically significant Baker's cyst. It indicates only a large communicating gastrocnemio-semimembranosus bursa. To qualify

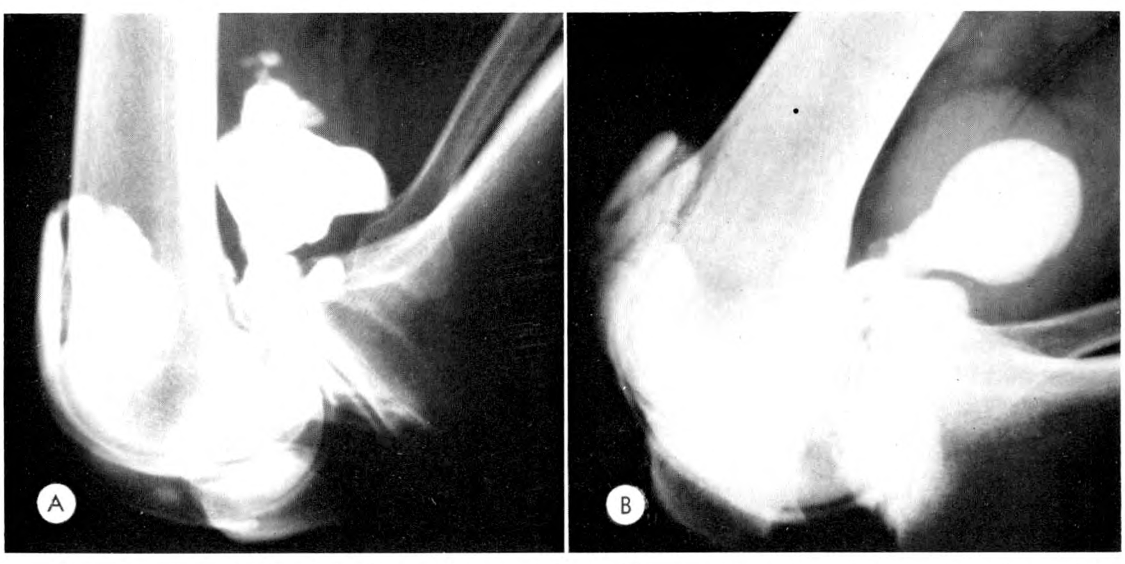


Fig. 6. (*A*) Easily palpable Baker's cyst in association with a torn lateral meniscus and moderate joint effusion are demonstrated. (*B*) Roentgenogram shows a dry knee with "large normal" G-S bursa but no clinical findings of Baker's cyst.

as a disease process, the bursa must be chronically distended, due either to knee joint pathology with associated effusion or to primary bursal disease. The roentgenographic similarity between *A* and *B* of Figure 6 is striking. The patient depicted in Figure 6 *A* had an easily palpable Baker's cyst and 50 cc. of joint fluid was aspirated before arthrography. The patient in Figure 6 *B* had a dry knee and no clinical evidence of a Baker's cyst.

3. Although some Baker's cysts do not communicate with the knee joint and are due to primary bursal trauma (particularly in children[7]), most popliteal cysts are secondary to intrinsic knee disorders and probably arise as "decompression chambers" in the presence of chronic knee effusions. This concept has been especially emphasized by Haggart.[8,9] When a Baker's cyst is associated with intermittent swelling of the knee itself, the primary knee pathology, *i.e.*, torn meniscus, rheumatoid arthritis, villonodular synovitis, must be dealt with; otherwise, simple excision of the cyst will usually lead to recurrence. This is particularly true of the large Baker's cysts occasionally encountered in rheumatoid arthritis.[6,10] These giant cysts may extend well below the mid-calf, are often confused clinically with an acute thrombophlebitis, and appear to wax and wane with the activity of the primary synovial disease. They may disappear spontaneously with remission of the joint disease only to recur, even following excision, with reactivation of the rheumatoid process.

Because of this frequent association, the surgical treatment of so called primary Baker's cysts should be undertaken only after careful arthrography has excluded unsuspected disease of the menisci, cruciate ligaments or synovial membrane.

Several orthopedic authors[13,15] state that the gastrocnemio-semimembranosus bursa communicates with the joint space when the knee is fully extended but closes off with flexion of the knee. Hoffman[11] has suggested and we have demonstrated on cineroentgenographic studies that the reverse is true, *viz.*, the bursal neck opens on flexion but tends to seal off when the knee is extended, perhaps accounting for the tenseness of the cyst and the inability to decompress it in the usual examining position of full knee extension.

Caughey and Bywaters[4] have recently measured joint fluid pressure in the presence of chronic knee effusions. Resting pressures varied from 5–30 mm. Hg and were not significantly elevated by inflating a blood pressure cuff above the knee. However, quadriceps contraction resulted in marked intra-articular pressure elevations (up to 300 mm. Hg), particularly when the back of the knee was braced and reflux into the G-S bursa was prevented. These pressure changes reflect hydrodynamically the same changes that we have demonstrated roentgenographically. In the presence of joint fluid, compression of the suprapatellar bursa against the femoral shaft either by active quadriceps contraction or knee flexion markedly elevates intra-articular fluid pressure and may distend a communicating gastrocnemio-semimembranosus bursa into a clinically evident Baker's cyst.

## SUMMARY

Baker's cysts are distended gastrocnemio-semimembranosus bursae often arising secondary to primary knee joint pathology with chronic effusion. They usually communicate with the knee joint proper and tend to fill as flexion of the knee or quadriceps contraction displaces joint fluid out of the suprapatellar bursa. The filling of a large G-S bursa on arthrography does not justify the diagnosis of clinically significant Baker's cyst.

Small joint effusions are most readily visualized on lateral roentgenograms of the fully extended knee.

Department of Diagnostic Radiology
The Clinical Center
National Institutes of Health
Bethesda, Maryland

## REFERENCES

1. Adams, R. Chronic rheumatic arthritis of knee joint. *Dublin J. M. Sci.*, 1840, *17*, 520.

2. Baker, W. M. Formation of synovial cysts in leg in connection with disease of knee joint. *St. Bartholomew's Hosp. Rep.*, 1877, *13*, 245.
3. Burleson, R. J., Bickel, W. H., and Dahlin, D. C. Popliteal cyst: clinico-pathologic survey. *J. Bone & Joint Surg.*, 1956, *37A*, 1265–1274.
4. Caughey, D. E., and Bywaters, E. G. Joint fluid pressure in chronic knee effusions. *Ann. Rheum. Dis.*, 1963, *22*, 106–109.
5. Doppman, J. L. Association of patellofemoral erosion and synovial hypertrophy: diagnostic entity. *Radiology*, 1964, *82*, 240–245.
6. Good, A. E. Rheumatoid arthritis, Baker's cyst and "thrombophlebitis." *Arth. & Rheum.*, 1964, *7*, 56–64.
7. Gristina, A. G., and Wilson, P. D. Popliteal cysts in adults and children; review of 90 cases. *A.M.A. Arch. Surg.*, 1964, *88*, 357–363.
8. Haggart, G. E. Posterior hernia of knee joint; cause of internal derangement of knee. *J. Bone & Joint Surg.*, 1938, *20*, 363–373.
9. Haggart, G. E. Synovial cysts of popliteal space: clinical significance and treatment. *Ann. Surg.*, 1943, *118*, 438–444.
10. Harvey, J. P., Jr., and Coros, J. Large cysts in lower leg originating in knee occurring in patients with rheumatoid arthritis. *Arth. & Rheum.*, 1960, *3*, 218–228.
11. Hoffman, B. K. Cystic lesions of popliteal space. *Surg., Gynec. & Obst.*, 1963, *116*, 551–558.
12. Kuhn, H. H., and Hemphill, J. E. Baker's cysts: posterior herniation of knee joint. *Radiology*, 1944, *42*, 237–240.
13. Lewin, P. The Knee and Related Structures: Injuries, Deformities, Diseases, Disabilities. Lea & Febiger, 1952, pp. 914.
14. Lewis, R. W. The Joints of the Extremities: A Radiographic Study. Charles C Thomas, Publisher, Springfield, Ill., 1955, pp. 108.
15. Meyerding, H. W., and VanDemark, R. E. Posterior hernia of knee (Baker's cyst, popliteal cyst, semimembranosus bursitis, medial gastrocnemius bursitis and popliteal bursitis). *J.A.M.A.*, 1943, *122*, 858–861.
16. Wilson, P. D., Eyre-Brook, A. L., and Francis, J. D. Clinical and anatomical study of semimembranosus bursa in relation to popliteal cyst. *J. Bone & Joint Surg.*, 1938, *20*, 963–984.

# COCCIDIOIDOMYCOSIS* (DIAGNOSIS OUTSIDE THE SONORAN ZONE)

## THE ROENTGEN FEATURES OF ACUTE MULTIPLE PULMONARY CAVITIES

*By* EDWARD W. KLEIN, LCDR MC USN,† *and* JOHN P. GRIFFIN, LCDR MC USN‡
GREAT LAKES, ILLINOIS

COCCIDIOIDES IMMITIS, probably the most infectious of all fungi capable of producing serious systemic disease, is endemic in select areas of the Western hemisphere. The climatic Lower Sonoran Life Zone constitutes the endemic area in the United States.[8] The zone is characterized by an arrid or semi-arrid climate, high mean January and July temperatures, an alkaline soil, few frosts and a hot season which is generally followed by rain (5 to 20 inches annually). The southwestern and central portions of California, southern Nevada, the southwestern corner of Utah, southern Arizona, southern New Mexico, western Texas and contiguous areas in Mexico constitute the Lower Sonoran Zone in North America. Physicians residing in these areas are constantly alert to this infection; however, little thought is given to this mycotic disease by physicians residing distant from these areas.

Two major factors have become apparent in recent decades which dictate that we, outside the Lower Sonoran Zone, become more aware of the incidence of this disease removed from its endemic area. The first and by far the most important factor to consider is that of rapid transcontinental travel and its various ramifications. Since World War II, due to increase in vacation and leisure time, travel to the Sonoran Zone has become increasingly more popular. The scenic and climatic wonders available in this area will undoubtedly reflect themselves in increasing numbers of visitors. It has been estimated that 2½ million people, each year, visit the national forests and parks on the eastern edge of the San Joaquin Valley of California.[5] In addition to these large numbers of people who, by their presence in endemic areas, make themselves susceptible to *C. immitis*, there are many military bases in the area. The constant transferring and discharging of military personnel from these areas would result in cases of coccidioidomycosis appearing in all corners of this country. It is most probable that a very short residency in, or even travel through, (Blank[3] in Miami, Florida, presented a case of a patient who motored through southern California about 2 weeks prior to her illness) the Lower Sonoran Zone may result in infection. In our experience, particular interest should be given to those individuals who have been exposed to windy and dusty conditions in these areas. Such conditions exist and are encountered in construction work and, particularly, during military maneuvers.

The second factor to consider in coccidioidomycosis discovered outside the endemic zone is that of infection from fomites. Albert and Sellers[1] recently reviewed the literature on fomite transmission and presented a case which occurred in a waste cotton mill worker who handled gin flues from Tulare, California. These authors reviewed 24 other such cases. Soil transported from San Diego County, American Indian artifacts, clothing, and San Joaquin cotton are implicated fomites.

Thus, *Coccidioides immitis* finds its way outside the Lower Sonoran Zone. Harrell and Honeycutt[6] recently highlighted this

* The opinions expressed are those of the authors and do not necessarily represent those of the Navy Department.
† Staff Radiologist, U. S. Naval Hospital, Great Lakes, Illinois.
‡ Staff, Medical Department, U. S. Naval Hospital, Great Lakes, Illinois.

traveling fungus disease as did Izenstark[7] in his monograph entitled "Modern Travel and Coccidioidomycosis." Most authors consider that the radiologist should be at the forefront in suggesting the diagnosis.

The roentgenographic pattern of coccidioidal infection retains a variability that defies easy classification. Birsner[2] attempted to clarify the problem in the radiologic literature. In the more recent literature, however, little attention has been given to the roentgenographic features of this disease. In particular, minimal interest has been given to the fleeting primary cavities of the acute infection. Fiese[5] states that serial roentgenograms, made during the course of primary coccidioidal pneumonia, sometimes demonstrate an area of transient excavation in the midst of consolidative pulmonary tissue. This is more often than not an accidental discovery without symptoms or sequelae. No mention is made of multiple excavations of the primary type. Winn[13,14] and Smith *et al.*[11] have directed their attention to the chronic or secondary cavitary form of the disease. While the acute transitory cavity is of little significance clinically, it may be of immense value from the roentgenographic point of view. The presence of small, diffuse foci of granulomatous tissue which show such areas of transient excavation should alert the radiologist to the possibility of coccidioidomycosis. The additional presence of a cutaneous toxic erythema should heighten this suspicion. Roentgenographic differentiation from pulmonary cavitation due to tuberculosis may be difficult. Tuberculous cavitation usually occurs during the adult form (re-infection type), whereas coccidioidal cavitation of the transient type develops during the primary pulmonary infection. We have also noted that involvement of the anterior segments of the upper lung is strongly in favor of coccidioidomycosis when attempting to differentiate the disease from tuberculosis.

The authors recently and independently became suspicious of the possibility of coccidioidomycosis in 2 patients, who experienced an acute illness while visiting the Great Lakes area, from their military base in California. It is our opinion that their case reports will be of interest to radiologists everywhere.

REPORT OF CASES

Case I. R. T. is a 21 year old Private, U. S. Marine Corps, who noted the sudden onset of anorexia, malaise, feverishness, dry cough and burning substernal pain with respiration on December 22, 1963. These symptoms progressed with particularly aggravating nocturnal paroxysms of cough and, 4 days later, he noted the onset of a minimally pruritic rash, first on the upper then the lower extremities and finally spreading to the chest area. On December 27, 1963, he was admitted to a private hospital with the above symptoms and the additional complaint of backache. Examination there revealed a temperature of 104° F., inflammation of the nasal and pharyngeal mucous membranes, patches of rales and rhonchi over both lung fields and a generalized maculopapular eruption. Chest roentgenograms showed scattered, ill-defined, nodular densities throughout both lungs. His course was that of continuing high fever with chills and night sweats, despite adequate antibiotic therapy. He was transferred to the U. S. Naval Hospital, Great Lakes, Illinois, on December 31, 1963, for further evaluation. Additional history revealed that he had been born in Alabama, but had resided in Illinois for the 10 years preceding his induction into the Marine Corps on July 31, 1963. He had not traveled west of St. Louis until he reported for basic training at the Marine Corps Recruit Depot, San Diego, California. In October, 1963, he was transferred to Camp Pendleton, California, where he underwent extensive field training. Here, he experienced repeated and prolonged exposure to the rocky and sandy soils of rural San Diego County. He returned to Illinois on December 20, 1963, for holiday leave. Past history of significant respiratory disease was unremarkable and he related no history of allergic symptomatology or of drug hypersensitivity reaction. He was unaware of recent contact with contagious disease in either his family or his fellow marines. Physical examination at the time of arrival at this hospital revealed an alert Negro male, in no acute dis-

Fig. 1. Case 1. Posteroanterior erect chest roentgenogram demonstrating clearly defined multiple nodular densities. The borders are slightly irregular and early cavitation is apparent in several of the nodules. Bilateral hilar lymphadenopathy is present. Minimal peribronchial infiltrates are present in the lower lung fields.

Fig. 3. Case 1. Laminagram of the chest showing the typical "doughnut" cavities which are multiple and diffusely located. Hilar lymphadenopathy is apparent.

tress, but with a fever of 102° F. There was no remarkable tachycardia and, other than minimal nasopharyngitis, the remainder of the examination, including that of the lung fields, was normal. There were no residua of the previously described rash. His hospital course was characterized by remittent fever in the range of 102° F. maximum for the first week, followed by low-grade fever for an additional 10 days. Paroxysms of coughing, occasionally productive of minimal amounts of mucoid sputum, resolved gradually over a 2 week period. Only symptomatic treatment and a short course of penicillin orally were employed at this facility. Serial roentgenographic studies are described below (Fig. 1 through 4).

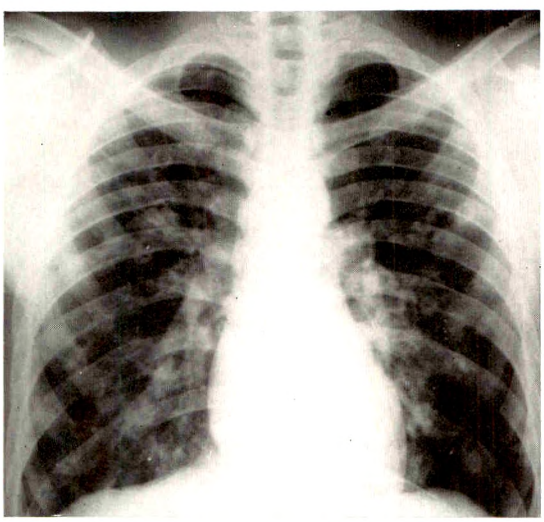

Fig. 2. Case 1. The majority of nodules have undergone cavitary degeneration. Peribronchial infiltration persists in the lower lung fields.

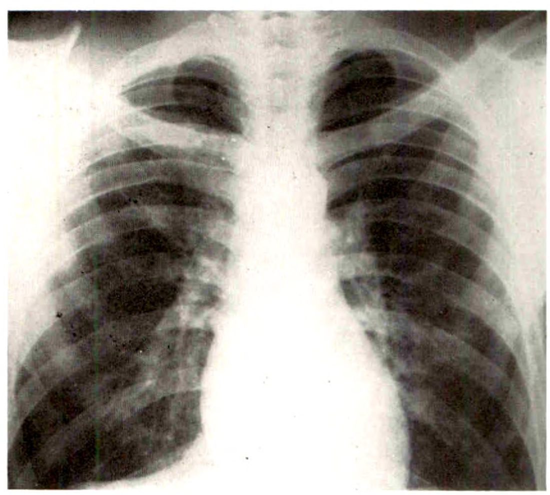

Fig. 4. Case 1. The majority of the cavities have resolved, placing them in the category of acute fleeting cavities of coccidioidomycosis (28 days). Further studies showed resolution of all of the cavities.

Laboratory data revealed an admission white blood cell count of 13,600, with 66 per cent neutrophils and 3 per cent band forms. During his fifth week of hospitalization, a peripheral blood morphology revealed 15 per cent monocytes and 10 per cent eosinophils (confirmed by a total eosinophilic count of 532 per cu. mm). Sputum cultures revealed no bacterial pathogens. Abundant fungal growth from multiple sputum specimens was noted on Sabouraud's medium at room temperature; the colonies were composed of white mycelial forms with some arthrospores; however, these organisms were lost in passage before more specific identification could be accomplished. Aerobic and anaerobic blood cultures showed no growth. Erythrocytic sedimentation rate was elevated to 51 mm. (Wintrobe). Serum protein electrophoresis obtained during convalescence revealed a minimal elevation of alpha-2 and gamma globulin components.

Intermediate strength purified protein derivative of tuberculin skin test was negative, while a histoplasmin test revealed 1.5 cm. induration at 48 hours. Coccidioidin skin test (1:100), initially negative on two occasions, converted to positive in the fourth week of hospitalization here. Acute and convalescent sera for fungal serology showed complement fixation titers of 1:4 and 1:4 for *Histoplasma capsulatum*, 1:2 and negative for *Blastomyces dermatitidis*, and 1:16 with zoning for *Coccidioides immitis*. A repeat study (2 months later) revealed the presence of complement fixing antibodies for *Coccidioides immitis* in a titer of 1:16.

The patient experienced a slow, but progressive, improvement without evidence of dissemination of his disease, and was returned to a full duty status with minimal residual pulmonary infiltration.

CASE II. A. S. is an 18 year old Private, U. S. Marine Corps, who noted the sudden onset of feverishness, anorexia, malaise, dry cough and paravertebral myalgia on December 14, 1963. These symptoms persisted and were followed by the appearance of a generalized rash 4 days later. This was associated with prostration and aggravation of nonproductive cough, particularly at night. He was evaluated at a Veterans Administration Hospital where a dermatologist noted skin lesions consistent with erythema multiforme and, on December 20, 1963, he was transferred to the U. S. Naval Hospital, Great Lakes, Illinois, for further evaluation. Additional history revealed that the patient had resided in Chicago, Illinois, from birth to his induction into the Marine Corps on August 8, 1963. He had not previously traveled west of Iowa nor south of Illinois until he arrived at the Marine Corps Recruit Depot, San Diego, California, for his basic training. In late October, he was transferred to Camp Pendleton, California, where he had undertaken extensive field training in the rural area of San Diego County. On December 13, 1963, he departed for Chicago on holiday leave. There was no significant past history of medical disease and the family history was noncontributory. He related no history of allergic symptomatology or drug reaction. Physical examination, at the time of admission to this facility, revealed a well-nourished Caucasian male, in no acute distress, but with a fever of 101.2° F. Bilateral anterior cervical lymph nodes, measuring 1.0 cm., were present in conjunction with injection and lymphoid hyperplasia of the pharynx. The lungs were clear to auscultation. An erythematous macular eruption with slightly raised serpiginous borders and somewhat depressed centers was noted over the arms, hands, legs, chest, abdomen and back. The patient's hospital course was characterized by an intermittent fever to a maximum of 103° F., gradually resolving over a 9 day period. His rash resolved within 4 days of admission, but cough persisted for some 2 weeks. He was treated with tetracycline antibiotics, intramuscular ACTH gel and antihistaminics.

Serial roentgenographic studies are described below (Fig. 5 through 8).

Laboratory data revealed an admission white blood cell count of 11,100 with 88 per cent neutrophils and 4 per cent band forms. In the third week of hospitalization, his white blood cell count was 10,200 with 46 per cent neutrophils, 10 per cent monocytes and 20 per cent eosinophils (confirmed by a total eosinophil count of 1,820 per cu. mm.). Erythrocytic sedimentation rate was 40 mm. (Wintrobe) and C-reactive protein was positive. Serum protein electrophoresis, obtained during convalescence, revealed a relative increase in alpha-2 and gamma globulins.

Purified protein derivative of tuberculin (intermediate strength), histoplasmin and blastomycin skin tests were negative, while coccidioidin 1:100 revealed 15 mm. induration at 48 hours. Serial determinations of fungal serology were made with the initial specimen obtained during the third week of hospitalization. Complement fixation tests for *Blastomyces dermati-*

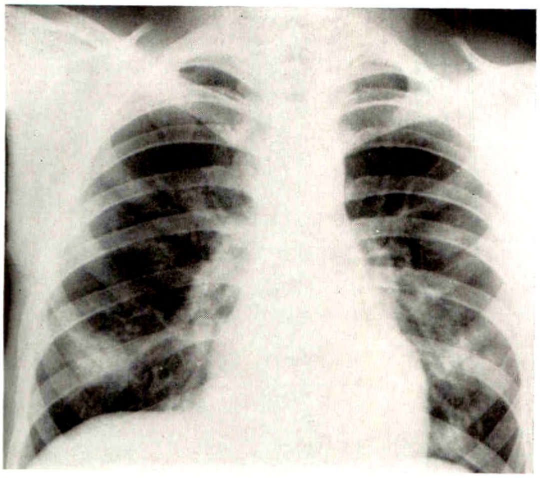

Fig. 5. Case II. Erect posteroanterior roentgenogram of the chest shows bilateral irregular nodular infiltrations. No cavities are discernible. Hilar lymphadenopathy is present.

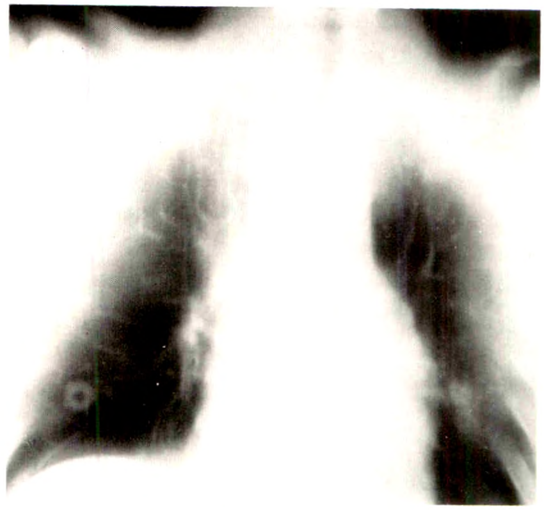

Fig. 7. Case II. Laminagram 23 days from original study shows that several of the cavities have resolved.

*tidis* were negative and those for *Histoplasma capsulatum* revealed a peak titer of 1:4. Complement fixing antibodies for *Coccidioides immitis* were obtained in significant titers of 1:32 and 1:16. Two months later a 1:4 titer for complement fixing antibodies for *Coccidioides immitis* was reported.

The patient experienced a slow, but progressive, improvement without definite evidence of dissemination of his disease and was returned to a full duty status with the solitary residual cavitation described.

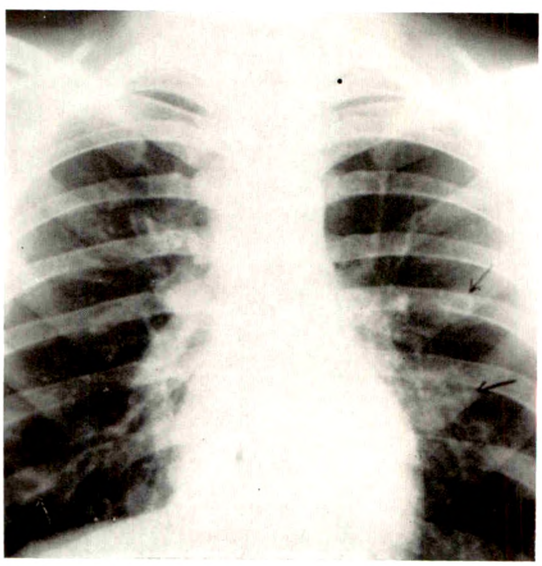

Fig. 6. Case II. Fourteen days after Figure 5, cavitary degeneration is apparent.

## DISCUSSION

The symptomatology in the acute primary infection of coccidioidomycosis is usually that of a respiratory illness with chest pain and a minimally productive cough associated with rather striking systemic symptoms of fever, diffuse myalgia,

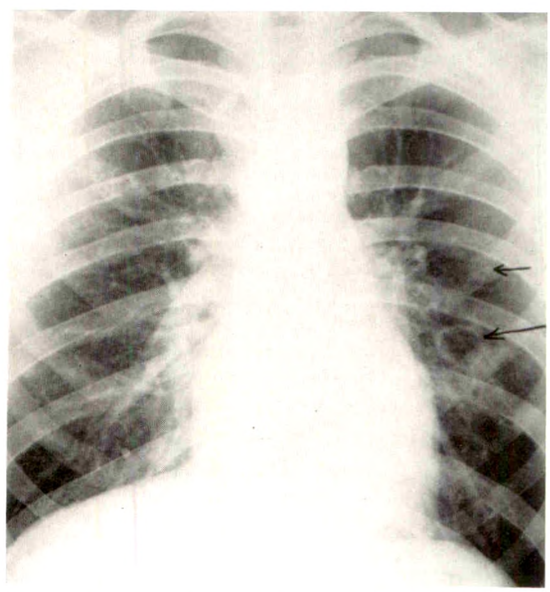

Fig. 8. Case II. Four months after initial study, it is noted that all cavities have resolved with the exception of the large, thin-walled, chronic or latent cavity in the left mid-lung field. A smaller resolving cavity is also seen above the larger one.

anorexia and often prostration.[4,5,9,15] However, it is estimated that some 60 per cent of primary infections are clinically inapparent.[12] Patterned cutaneous lesions, which are of great assistance in suggesting the diagnosis, are found in only about 5 per cent of males afflicted with this disease. These eruptions, taking the clinical form of erythema nodosum or erythema multiforme, are usually seen in the second or third week of the illness corresponding with the appearance of dermal hypersensitivity as manifest by the positive coccidioidin skin test.[15] An earlier generalized fine erythematous macular rash appears in about 10 per cent of patients within several days of the onset of symptoms and resolves within 1 week; this eruption occurs prior to the appearance of dermal hypersensitivity and is considered to represent only a nonspecific toxic erythema.[5] Case I in this paper exhibited this type of rash prior to the appearance of a positive skin test, while Case II, although exhibiting a rapid development of hypersensitivity, demonstrated an erythema multiforme eruption after the appearance of a positive coccidioidin skin test.

The diagnosis of coccidioidomycosis can be established by the identification of *C. immitis* in the sputum or bronchial washings. Coccidioidin, however, when used intelligently, is the most valuable single tool generally available for the diagnosis of coccidioidal infections. This material is employed not only for the quite specific and very sensitive skin test, but is also used as the antigen for the precipitin and complement fixation tests. In actual experience, the serologic tests are more practicable in diagnosis than isolation of the fungus from the sputum, since about 90 per cent of cases of symptomatic primary infection will reveal some serologic confirmation.[5] Some authors consider a complement fixation titer of 1:32 or greater as a criterion of dissemination.[4] However, Case II showed a titer of 1:32 in the face of progressive clinical improvement and serial determinations, probably of more value than a single numerical criterion, confirmed the lack of dissemination with a fall in titer to 1:4. The complement fixation titer in this disease is presumably a direct measure of specific antibody response. Studies by Reed and his associates[10] have shown a significant correlation of this titer with the absolute and relative concentrations of gamma globulin. Both cases reported here demonstrated relative increases in gamma globulin components on serum protein electrophoresis. These cases also demonstrated relative increases in alpha-2 globulin components, which these authors have correlated with the high sedimentation rates and have related to acute inflammatory activity.

Probably the most important consideration in the clinical course is the detection of dissemination of the disease, since potentially curable therapy is now available for this problem in the form of amphotericin B. Colwell and Tillman[4] have drawn attention to the desirability of early recognition of dissemination and have listed criteria for suspicion of this event to include: (1) systemic symptoms of more than 1 week in a Negro patient, and (2) roentgenographic evidence of paratracheal lymphadenopathy. The authors were justifiably concerned with the fulfillment of both of these manifestations in Case I, in conjunction with the striking roentgenographic evidence of diffuse pulmonary cavitation. However, with intensive supportive care there was, fortunately, a progressive clinical improvement in conjunction with a continued lack of serologic evidence of dissemination and amphotericin B therapy became unnecessary.

## SUMMARY

1. Coccidioidomycosis is endemic within the climatic Lower Sonoran Zone in the United States.

2. Method of spread "Outside the Sonoran Zone" is discussed.

3. Awareness of the disease "Outside the Sonoran Zone" is stressed, especially regarding the radiologist's participation.

4. Two cases are presented which dem-

onstrated acute multiple transient pulmonary cavities.

Edward W. Klein, LCDR MC USN
Department of Radiology
U. S. Naval Hospital
Great Lakes, Illinois 60088

REFERENCES

1. Albert, B. L., and Sellers, T. F., Jr. Coccidioidomycosis from fomites. *A.M.A. Arch. Int. Med.*, 1963, *112*, 253–261.
2. Birsner, J. W. Roentgen aspects of five hundred cases of pulmonary coccidioidomycosis. Am. J. Roentgenol., Rad. Therapy & Nuclear Med., 1954, *72*, 556–573.
3. Blank, H. Why a chest film of a patient with erythema multiforme? *J.A.M.A.*, 1962, *179*, 151.
4. Colwell, J. A., and Tillman, S. P. Early recognition and therapy of disseminated coccidioidomycosis. *Am. J. Med.*, 1961, *31*, 676–691.
5. Fiese, M. J. Coccidioidomycosis. Charles C Thomas, Publisher, Springfield, Ill., 1958.
6. Harrell, E. R., and Honeycutt, W. M. Coccidioidomycosis: traveling fungus disease. *A.M.A. Arch. Dermat.*, 1963, *87*, 188–196.
7. Izenstark, J. L. Modern travel and coccidioidomycosis. *South. M. J.*, 1963, *56*, 745–751.
8. Maddy, K. T., Crecelius, H. G., and Cornell, R. G. Where can coccidioidomycosis be acquired in Arizona? *Arizona Med.*, 1961, *18*, 184–194.
9. O'Leary, D. J., and Curry, F. J. Coccidioidomycosis: review and presentation of 100 consecutively hospitalized patients. *Am. Rev. Tuberc.*, 1956, *73*, 501–518.
10. Reed, W. B., Heiskell, C., Holeman, C. W., and Carpenter, C. M. Serum protein profiles in coccidioidomycosis. *J. Invest. Dermat.*, 1963, *40*, 147–158.
11. Smith, C. E., Beard, R. R., and Saito, M. T. Pathogenesis of coccidioidomycosis with special reference to pulmonary cavitation. *Ann. Int. Med.*, 1948, *29*, 623–655.
12. Smith, C. E., Pappagianis, D., Levine, H. B., and Saito, M. Human coccidioidomycosis. *Bact. Rev.*, 1961, *25*, 310–320.
13. Winn, W. A. Pulmonary cavitation associated with coccidioidal infection. *Arch. Int. Med.*, 1941, *68*, 1179–1214.
14. Winn, W. A. Pulmonary mycoses; coccidioidomycosis and pulmonary cavitation: study of 92 cases. *Arch. Int. Med.*, 1951, *87*, 541–550.
15. Winn, W. A. Diagnosis and treatment of coccidioidomycosis. *Arizona Med.*, 1962, *19*, 211–217.

# BRONCHIOLAR EMPHYSEMA*

By DAVID BRYK, M.D., and KEN MORI, M.D.
BROOKLYN, NEW YORK

BRONCHIOLAR emphysema is an unusual type of diffuse pulmonary disease characterized by progressive respiratory insufficiency. Other terms used for this entity are: muscular cirrhosis of the lungs,[2,7] bronchiolectasis,[3] and cystic pulmonary cirrhosis.[2] There have been about 20 cases previously reported in the literature.[1–7]

The purpose of the authors is to report another case which was followed for 8 years and came to autopsy, and to emphasize the differential pathologic and roentgen features.

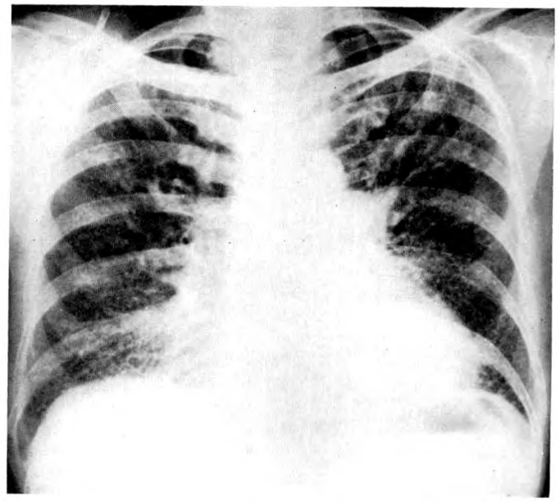

FIG. 1. Posteroanterior view of the chest showing fine diffuse interstitial infiltrations, more prominent in the lower lobes. The vessels in the upper lobes are prominent. The heart shows right ventricular enlargement.

## REPORT OF A CASE

S.M. was a white female whose first respiratory complaint developed in 1937 at the age of 41, when she had an episode of left chest pain. She was told that this was pleurisy. In 1945, she began to have episodes of dyspnea which were intermittent, occurring day or night. She also developed frequent upper respiratory infections with rhinorrhea and cough. These were treated by antibiotics.

She was first seen in the Maimonides Hospital in 1955 at the age of 59. The cause of admission was an episode of respiratory infection characterized by fever, dyspnea, heaviness in the chest, sneezing and cough productive of yellowish sputum. Clubbing of the fingers was present. Fine crackling rales were heard at both lung bases. The roentgenologic report described patchy and linear infiltrations in both lung fields.

In 1957, because of worsening symptoms, she was started on steroids which were continued until death in 1963.

In 1959, she was re-admitted due to another episode of fever, cough and increased dyspnea. She had lost considerable weight. Marked clubbing of the fingers and toes was now present. There was a suggestion of cyanosis at times. Rales and rhonchi were heard in the lungs. There was a systolic murmur at the base of the heart. P2 was greater than A2. An electrocardiogram showed right ventricular preponderance.

She was re-admitted in 1961 because of increasing dyspnea even at rest. Productive cough was more persistent. Examination revealed distended neck veins, liver enlargement and pedal edema. Cyanosis was marked. The patient became extremely cachectic. Right heart failure became intractable and she expired in October, 1963, 27 years after the initial respiratory difficulty and 8 years after the first admission to Maimonides Hospital.

*Roentgen Findings.* The roentgenograms from 1959 to 1963 were available for review. The pattern was that of fine interstitial pulmonary infiltrates. These were bilateral and symmetric with more prominent involvement of the lower lobes (Fig. 1). In the region of the costophrenic angles, the infiltrates were linear, horizontal and parallel, resembling Kerley B lines (Fig. 2). These indicated the lymphangitic distribution of the infiltrates. Between the infiltrates were small oval equal-sized lucencies producing a pattern of fine honeycombing.

There was complete obliteration of the vascu-

* From the Departments of Radiology and Pathology, Maimonides Hospital of Brooklyn, Brooklyn, New York.

lar markings in the lower lobes. The vessels in the upper lobes were prominent, presumably due to shunting of blood through the upper lobes.

The serial roentgenograms from 1959 to 1963 showed no significant change over this 4 year period, except for progressive cardiac enlargement. The cardiac enlargement was due to progressive hypertrophy and dilatation of the right ventricle secondary to the pulmonary abnormalities.

*Autopsy Findings.* Each lung weighed 550 gm. Each showed diffuse rigidity, maintaining a cone shape as if fixed *in situ*. The left lung revealed distinct depressions caused by the aortic arch, descending aorta, and left subclavian artery (Fig. 3). On the medial aspect of the right lung, both venae cavae produced depressions. The pleura presented a whitish diffuse thickening and a coarse granular appearance produced by partially aerated, cystic spaces. Anthracotic pigment and prominent vascular channels were present in the depressed dividing septa. Bullae were most prominent in the lower

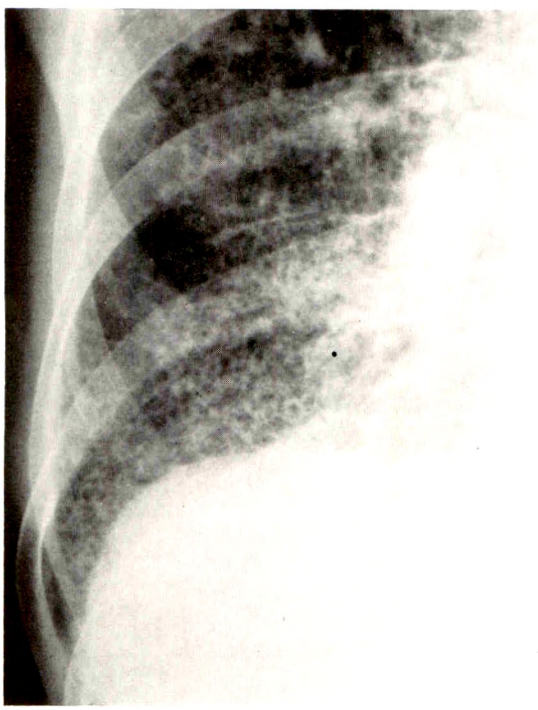

Fig. 2. Localized view of the right lower lung demonstrating the fine uniform interstitial pattern with the intervening lucencies producing a pattern of fine honeycombing. The thickened horizontal parallel interstitial septa are seen in the costophrenic angles.

Fig. 3. Medial view of the left lung specimen in the fresh state showing diffuse rigidity. The aortic arch produces a distinct groove.

segments and at the anterior and inferior edges. Both apices were resilient and free of bullae.

On section, both lower lobes, the right middle lobe and the lower segments of both upper lobes presented whitish pale cut surfaces studded with microcystic spaces measuring up to 0.5 cm. in diameter (Fig. 4). A majority of the spaces were filled with whitish tenacious mucus. The intervening pulmonary parenchyma was rigid, whitish, fibrotic and avascular. The anthracotic pigment was distributed in a network fashion against the whitish background. The bronchial branches contained viscid mucus and disclosed moderate thickening of their walls. Both apices were free except for scattered streaky fibrotic strands. The pulmonary arterial tree showed moderate to marked intimal plaque formation.

Microscopically (Fig. 5), all the cystic spaces were lined by tall columnar ciliated epithelium except when desquamated by acute and chronic inflammation. The cystic spaces contained inflammatory leukocytes, mucus, brown pig-

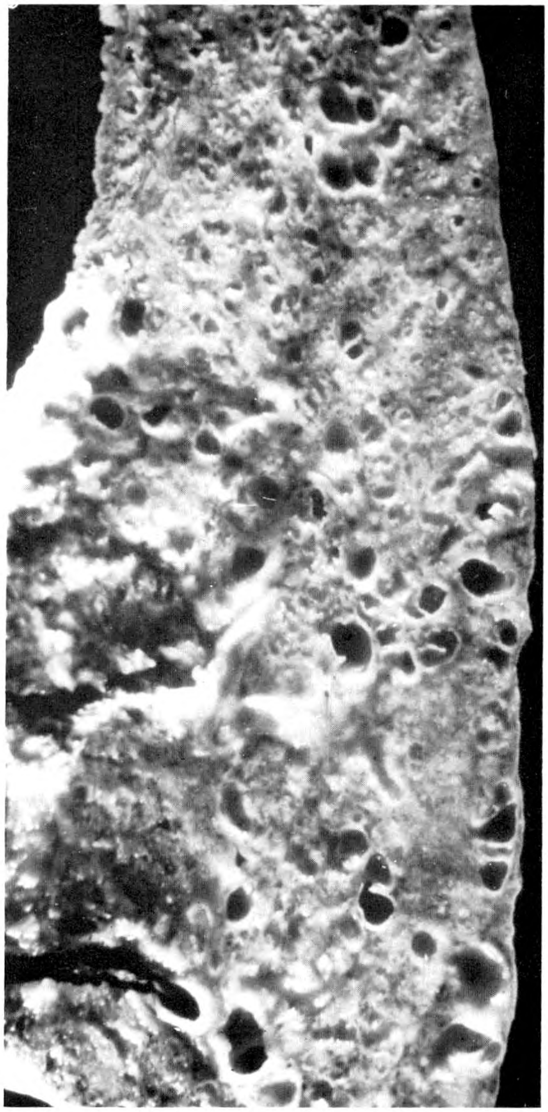

Fig. 4. Cross section of the fixed lung specimen showing the multiple small cystic spaces.

mented macrophages, and foam cells. The septa showed chronic inflammatory cells, fibrous tissue, a small number of capillaries and a large amount of smooth muscle. No alveolar structures were recognized except in the apical regions. The heart, weighing 390 gm., was enlarged and globular. The apex was formed by the right ventricle, which was markedly dilated and hypertrophied. The trabeculae carneae of the right ventricle were as prominent as the papillary muscles of the left ventricle. The thickness of the right ventricular wall measured 0.8 cm. while that of left 1.3 cm. Coronary atheromatosis was mild.

DISCUSSION

The case presented above clearly fulfills the clinical and pathologic critera of the entity of bronchiolar emphysema. The pathologic findings, as noted at autopsy, of rigid hobnail lungs with cystic spaces on cut section (honeycomb lung) and, on microscopic study, dilated terminal bronchioles with hyperplasia of smooth muscle, are characteristic of this entity.[5,7] The involvement is usually diffuse and symmetric but there may be asymmetry in involvement, with partial sparing of the upper lobes, as in our case, or of the lower lobes.[3]

Pathologically, differentiation must be made from focal lesions producing an identical histologic picture which are found incidentally at autopsy in patients dying of other diseases. These lesions are usually found at the periphery of the lung and in a random asymmetric distribution. They are usually considered to be the result of focal inflammation of undetermined etiology.[8] The diagnosis of bronchiolar emphysema can, therefore, only be made when the involvement is diffuse.

Other diseases which pathologically resemble bronchiolar emphysema are tuberous sclerosis and scleroderma. Tuberous sclerosis is probably a systemic hamartomatous condition. The honeycomb lung in tuberous sclerosis therefore tends to contain adipose tissue and hemangiomatous structures rather than only smooth muscle. In addition, tuberous sclerosis involves other organs. The reported cases of the so-called "forme fruste" of tuberous sclerosis involving only the lung are probably cases of bronchiolar emphysema.

Scleroderma may involve the lungs and give a pathologic picture of honeycomb lung. The proliferative connective tissue in scleroderma, however, is collagen rather than smooth muscle.

The roentgenographic picture in bronchiolar emphysema is not specific. The changes described can be seen in sarcoidosis, tuberous sclerosis, pulmonary eosinophilic granuloma, lymphangitic carcinoma, scleroderma, and pneumoconiosis. How-

FIG. 5. Microscopic section (H&E stain, ×250) shows the cystic spaces lined by tall columnar epithelium. The septa are thickened, containing smooth muscle, fibrous tissue and inflammatory cells.

ever, the fineness of the infiltrations, the smallness and uniform size of the lucencies and the chronicity of the process may suggest the diagnosis.

The infiltrations are due to thickening of the interstitial tissues by fibrous tissue, chronic inflammatory cells and smooth muscle hyperplasia. The lucencies are apparently due to the dilated terminal bronchioles. Of interest in the present case is the greater involvement of the lower lobes and the prominent vasculature in the upper lobes. The latter finding is apparently due to shunting of the pulmonary blood flow to the upper lobes secondary to obliteration of the lower lobe vascular channels by the disease process.

The etiology of bronchiolar emphysema

is unknown. One widely accepted theory propounded by Siebert and Fisher[7] is that there is a pre-existing dysplasia of the terminal respiratory units.

## SUMMARY

An additional case of bronchiolar emphysema, a rare diffuse pulmonary disease, is reported. The disease produces slow progressive pulmonary insufficiency over a period of many years. Pathologically, the entity is fairly clear-cut. The roentgen picture is that of fine diffuse uniform infiltrations with intervening small uniform cysts. This picture is not specific for this entity but in a patient with a slowly progressive interstitial pulmonary process with these features, the diagnosis of bronchiolar emphysema should be considered.

David Bryk, M.D.
Maimonides Hospital of Brooklyn
4802 Tenth Avenue
Brooklyn, New York

## REFERENCES

1. Gonzalez-Angulo, A. Diffuse bilateral peribronchiolar and interstitial muscular hyperplasia associated with bronchiolar dilatation (bronchiolar emphysema). *Am. Rev. Resp. Dis.*, 1962, *86*, 256–260.
2. Hirshfield, H. J., Krainer, L., and Coe, G. C. Cystic pulmonary cirrhosis (bronchiolar emphysema); (muscular cirrhosis of the lungs). *Dis. Chest*, 1962, *42*, 107–110.
3. Jerry, L. M., and Ritchie, A. C. Bronchiolar emphysema; report of a necropsied case of diffuse bronchiolectasis and review of literature. *Canad. M.A.J.*, 1964, *90*, 964–970.
4. McAdams, G. B. Bronchiolar emphysema; report of case. *A.M.A. Arch. Int. Med.*, 1961, *108*, 279–283.
5. Ravines, H. T. Bronchiolar emphysema of lungs: report of case. *A.M.A. Arch. Path.*, 1960, *69*, 554–556.
6. Schaffner, F., Editor. Clinico-pathological conference: Severe dyspnea for 15 years. *J. Mt. Sinai Hosp.*, 1959, *26*, 324–338.
7. Siebert, F. T., and Fisher, E. R. Bronchiolar emphysema; so-called muscular cirrhosis of lungs. *Am. J. Path.*, 1957, *33*, 1137–1161.
8. Spencer, H. Pathology of Lung; Excluding Pulmonary Tuberculosis. Macmillan Company, New York, 1962, pp. 428, 460.

# THE PULMONARY VESSELS IN THE DIAGNOSIS OF LOBAR COLLAPSE

By H. J. CRANZ, M.D., and H. F. W. PRIBRAM, M.D., D.M.R.D.
IOWA CITY, IOWA

INCREASING attention has been paid to the pulmonary vessels in the diagnosis of mitral stenosis and left ventricular failure,[2,3,9,15,16] yet little or no attention has been paid to their changes in pulmonary collapse. A detailed search of the literature shows that although the classic signs of lobar collapse have been well described,[1,4,7,11–14] no analysis of the changes in the major pulmonary vessels has been attempted. Some authors have alluded to changes in the vascular pattern of the hilus but without analyzing these in detail.[4,14]

The pulmonary vessels can be identified and the diagnosis of pulmonary collapse may be made on this basis alone, when other and better known signs are absent. It has been stated[16] that "satisfactory assessment of the radiographic pattern of the pulmonary arteries, particularly its major branches, and to a lesser extent its minor branches, is possible on adequate chest radiographs." Herrnheiser[5] described the composition of the hilus and concluded that the normal hilar shadows are chiefly produced by vessels. He also noted that vessel architecture was remarkably constant and that there was no basic difference between the right and left hilus—the lingula on the left corresponding to the middle lobe on the right. Simon[14] also noted the constancy of the vessels and stressed that the pulmonary arteries change their appearance in cases of atelectasis.

It is our purpose to elaborate on the usefulness of precise analysis of the hilar shadows, as this is of particular value in the diagnosis of left lower lobe collapse. It is known that collapse of the left side of the lung is more difficult to recognize because of the presence of the heart shadow. The lower lobe, in particular, may be invisible and hidden in the paravertebral gutter. It may not be demonstrable in any of the standard projections. On the right side the situation is different due to the absence of the heart shadow and the prominence of the main lower lobe artery.

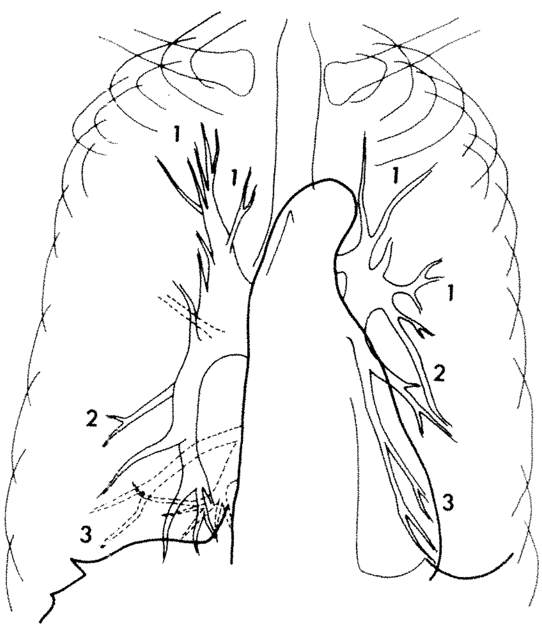


FIG. 1. Tracing of normal posteroanterior chest roentgenogram to demonstrate distribution of normally recognizable vascular shadows. (1) Vessels to upper lobes; (2) vessels to middle lobe and lingula; (3) vessels to lower lobes. Dotted lines: veins.

### ANATOMIC CONSIDERATIONS

The pulmonary arteries follow the major bronchi from the hilus to the periphery. The pulmonary veins have an independent course to the left atrium at a lower level than the pulmonary arteries.[5,8] The vessels as seen on a normal chest roentgenogram have been traced to show their radiation from the hilus into the lung field (Fig. 1). The veins, shown with dotted lines, normally run in a more horizontal direction and cross the arteries. However, it is not always possible to distinguish arteries from veins.

The hilus resembles a "Y" lying horizontally with the fork facing outwards. The pulmonary artery and its main branches are usually well seen on the right but less well seen on the left. A slightly overpenetrated roentgenogram or one taken with the air gap technique[6] may show the vessels better. Figure 1 shows the upper lobe vessels (1) having a regular distribution and pattern. One or two vessels to the middle lobe or lingula may be outlined (2). The main pulmonary artery extends downwards in an even sweep on both sides, giving off a variable number of branches to the lower lobes (3).

## ROENTGENOLOGIC FINDINGS

### COLLAPSE OF THE LEFT UPPER LOBE

In the posteroanterior chest roentgenogram, a density extends superiorly for a variable degree from the left hilus. The number and caliber of the vessels are reduced as compared to the same region of the right lung. The left hilus may be elevated. Neither the usually well visible upper lobe arteries nor the vessels to the lingula can be identified. The main pulmonary artery to the left lower lobe often takes a more lateral course than normal. Herniation of the right lung through the superior mediastinum anteriorly may be present and identifiable.[14] In the lateral view the collapsed upper lobe may be visible as a shadow of varying width, running parallel to the sternum and adjacent to it.

Thus, the salient features of the left upper lobe collapse are the slight elevation of the left hilus, the fanning out and reduction in the number of the visible vessels, their reduced caliber and the absence of the lingular branches. In the lateral view an anterior mass may be identifiable.

### COLLAPSE OF THE LEFT LOWER LOBE

The reduction in size and number of the visible vascular structure may be minimal or not apparent. The artery to the apical posterior segment of the upper lobe maintains its normal course. The anterior segmental artery of the upper lobe is deflected to a varying degree and runs horizontally or downwards across the mid-lung field. The hilus may be slightly depressed or in normal position but appears reduced in size. The vessels of the lingula are strongly deflected downwards and are seen extending parallel to the left heart border. Care must be taken not to confuse these structures with the normal main pulmonary artery to the left lower lobe. As a rule their origin from the upper portion of the left hilus can be determined, disclosing their identity. The collapsed left lower lobe may or may not be visible as a paravertebral mass behind the heart on the left side. If visible, it has to be distinguished from the shadow of the descending aorta.

## REPORT OF CASES

CASE 1. W.C., a male aged 72 years, had bronchogenic carcinoma with almost complete collapse of the left upper lobe (proved at thoracotomy). Posteroanterior and left lateral chest roentgenograms were made on June 23, 1959 (Fig. 2 and 3). A slight reduction of the volume of the left hemithorax was seen in the posteroanterior view. The trachea was midline. The lung field and pulmonary vascular markings on the right were normal. The left hilus was elevated. A homogeneous density extended from the left hilus into the left mid-lung field. The vascular markings were diminished throughout. The main hilar vessels were spread apart and had lost their orderly distribution. The lower lobe branches of the pulmonary artery were fanned out. The size of all vascular shadows in the left lung was reduced when compared with the normal right side. A radiolucent area extending laterally from the aortic knuckle to the left apex represented the herniation of the right lung into the left chest. In the lateral view (Fig. 3) a line of increased radiodensity extended parallel to the anterior chest wall from the manubrium to the diaphragm. This was the anteriorly displaced major fissure and the upper lobe, sandwiched between the anteriorly herniated right lung and the overinflated left lower lobe.

*Comment.* The salient features of this case were the elevation of the left hilus, diminution in size and number of all pulmo-

nary vascular markings, particularly of the main trunks, which extended from the left hilus into the left lung field on the postero-anterior view. The mass extending from the hilus (shown in magnification in Fig. 4) suggested partial collapse, and was readily identified in the left lateral view by its anterior location and the anteriorly displaced greater fissure.

Case II. M.E., a female aged 39 years, had an adenoma of the left upper lobe bronchus with almost complete collapse of the upper lobe (proved at operation). Posteroanterior and lateral chest roentgenograms were made on August 14, 1963 (Fig. 5 and 6). The posteroanterior view again showed the trachea to be in the midline, and the diffuse haziness extending from the left hilus into the left mid-lung field. The left hilus was somewhat elevated and a radiolucency was seen extending laterally from the aortic knuckle into the left upper lung field. These features represented again the partially collapsed left upper lobe and the herniation of

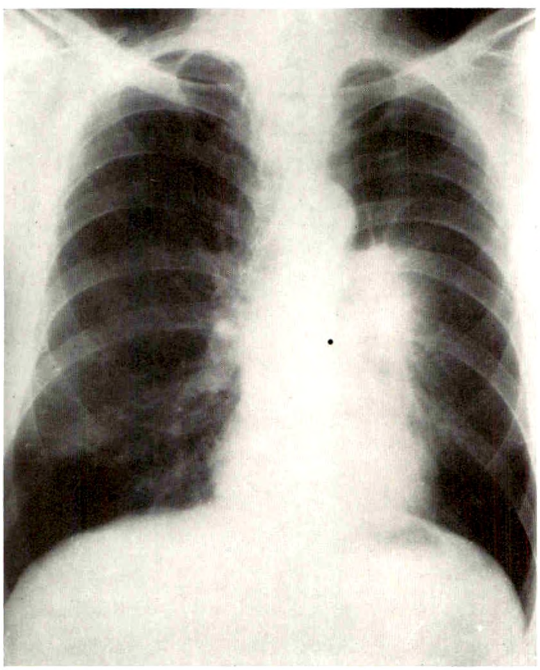

Fig. 2. Case I. Posteroanterior chest roentgenogram (June 23, 1959) shows slight reduction in volume of the left hemithorax. A homogeneous density extends from the left hilus. The vascular markings are diminished throughout the left lung field. The main vascular shadows are reduced in size and number and are spread out.

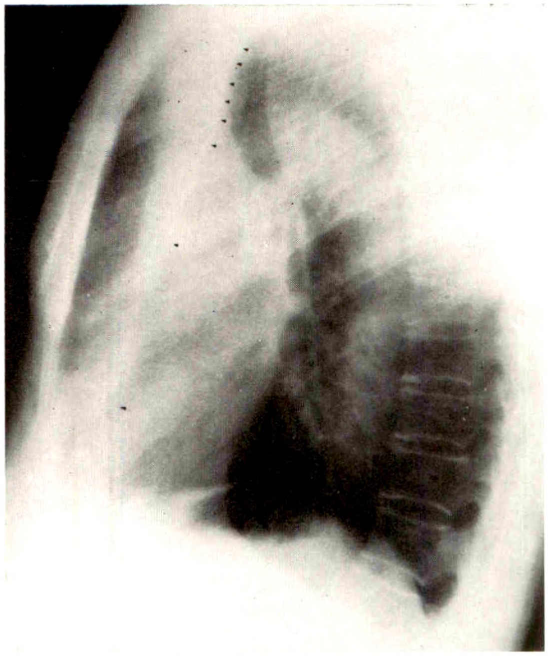

Fig. 3. Case I. Left lateral view of chest shows a line of increased density (arrows) running parallel to the anterior chest wall. Radiolucency directly underneath sternum represents herniated right lung. The left upper lobe is sandwiched between chest wall and herniated right upper lobe anteriorly and overexpanded left lower lobe posteriorly.

the right lung into the left hemithorax. The main pulmonary artery on the left could not be identified. The visible vascular markings were fanned out. These findings were particularly striking, when compared to the normal right side. The normal size and distribution of vascular shadows on the left side were completely lost (Fig. 7, magnified view of left side). In the lateral view (Fig. 6), a faint line of radiopacity could be seen running more or less parallel to the anterior chest wall from the apex of the lung to the diaphragm (arrows). This again represented the anteriorly collapsed and compressed upper lobe with the anteriorly displaced major fissure.

*Comment.* The main features of these roentgenograms were the gross distortion of the main pulmonary vascular shadows in their distribution and their size as compared to the normal right hilar shadows. The appearance of the parahilar mass on the left in the posteroanterior view and of an anterior mass in the left lateral view

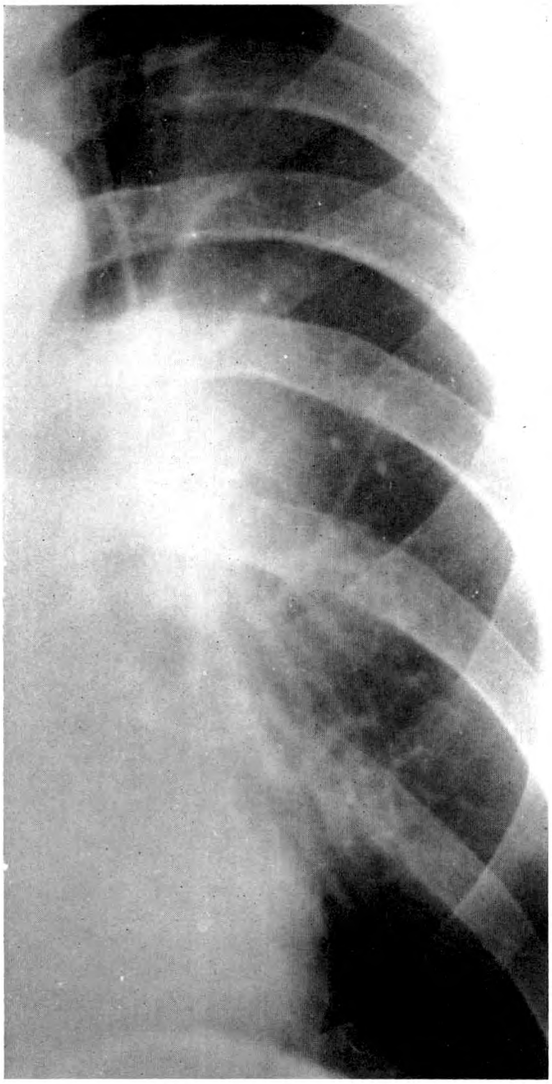

FIG. 4. Case I. Enlarged view of left hilus shows to advantage the reduced number and caliber and size of the vascular shadows.

helped confirm the diagnosis of the left upper lobe collapse.

CASE III. C.M., a male aged 27 years, had a left lower lobe collapse (proved at operation). A roentgenogram (Fig. 8) September 3, 1963 showed the trachea to be midline. There was moderate overdistention of the right lung. The pulmonary vessels on the right appeared to be normal. The left costophrenic angle was obliterated following empyema. The pulmonary vascular markings on the left side were diminished throughout. The hilus appeared in its usual position. The main pulmonary artery to the left lower lobe could not be identified. The anterior segmental branch of the upper lobe was displaced downwards. The lingular branches were recognizable and were seen parallel to the left heart border; the inferior branch was superimposed on the heart border, the superior branch somewhat lateral to it. A paravertebral density was noted behind the heart shadow. These features are all shown to better advantage in the magnified view (Fig. 10). The lateral view was normal (not shown). A bronchogram 2 days later (Fig. 9) showed good filling of the major bronchi on the left side. Downward displacement of the anterior bronchus of the left upper lobe was apparent. Downward and medial displacement of the two lingular branches was striking. The inferior lingular branch was superimposed on the lateral border of the heart shadow. The initial portion of the left lower lobe bronchus and its subdivisions were visualized and marked crowding and bronchiectatic changes were apparent. The findings indicated almost complete collapse of the left lower lobe.

*Comment.* The pertinent feature of this case again was a completely normal left

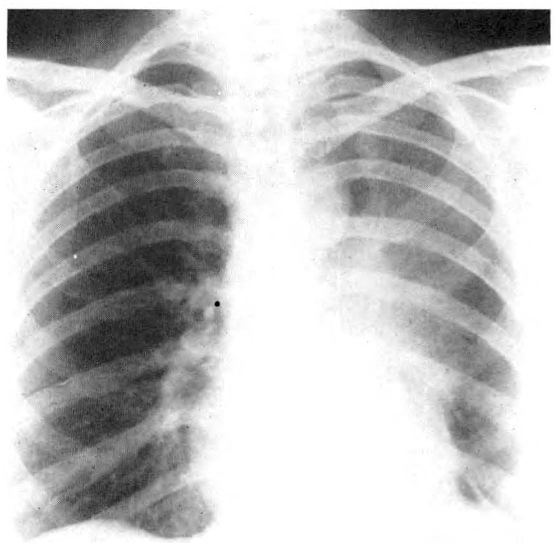

FIG. 5. Case II. Posteroanterior chest roentgenogram (Aug. 14, 1963) shows haziness extending from left hilus into left lung field. The main pulmonary arteries cannot be identified. The vascular shadows fan out from the hilus and are much reduced in size, number and caliber. The radiolucent area lateral to and above the aortic knuckle represents herniation of the right upper lobe through the anterior mediastinum.

Fig. 7. Case ii. Enlarged view of left hilus shows density extending from left hilus. Reduction of vascular shadows in size, number and caliber is well demonstrated. Herniation of right upper lobe indicated by radiolucent area adjacent to the left of aortic knob.

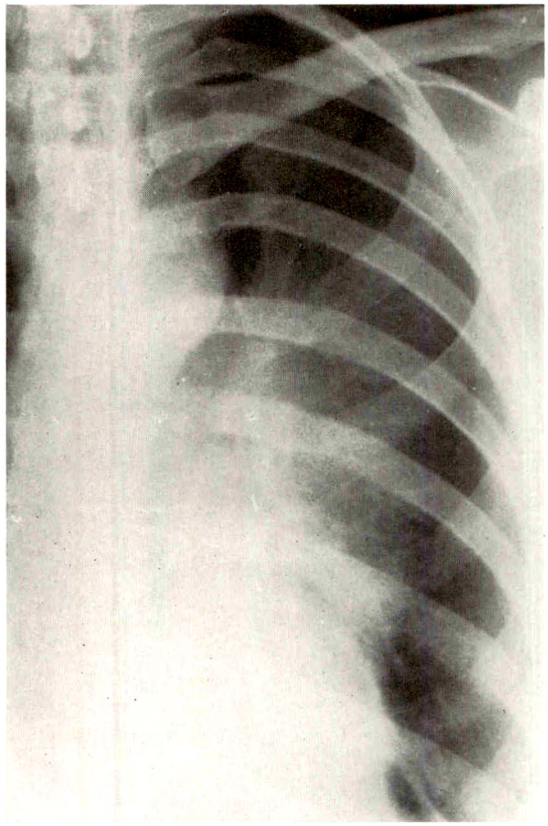

lateral view of the chest (not reproduced). In the posteroanterior view distortion of the vascular shadows, reduction in size and number and the take off of the lingular branches from the upper portion of the left hilus were apparent. The lingular branches were markedly deflected downwards and medially.

Case iv. B.E., a male aged 21 years, had complete collapse of left lower lobe. A posteroanterior chest roentgenogram made on January 22, 1963 (Fig. 11) showed the trachea to be midline. The right lung field and pulmonary vessels were normal. The left lung field showed minimal increase in radiolucency. The left hilus was somewhat lower than the right. A general

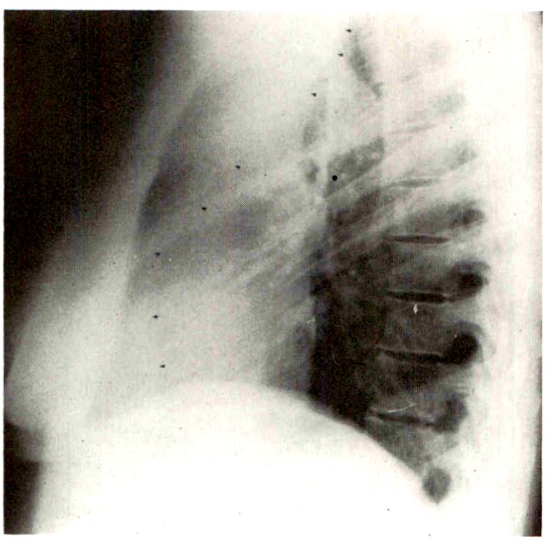

Fig. 6. Case ii. Left lateral chest roentgenogram showing partial collapse of left upper lobe. There is a faint line of radiodensity running almost parallel to the anterior chest wall (arrows). This represents the partially collapsed and anteriorly displaced left upper lobe.

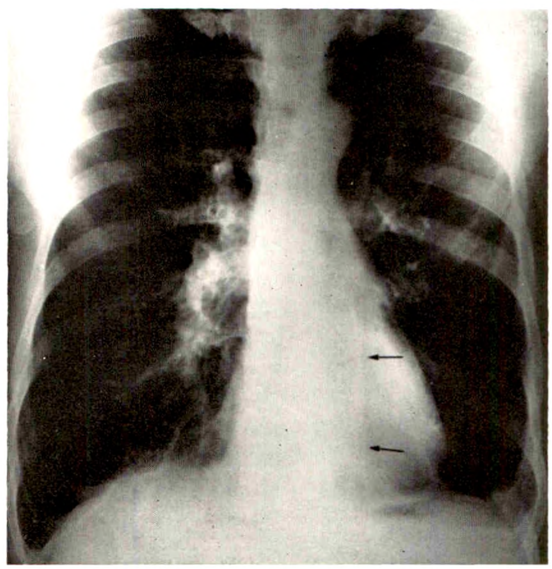

Fig. 8. Case iii. Posteroanterior chest roentgenogram (Sept. 3, 1963) shows the right side to be normal. Trachea is midline. Left hilus is in normal position. There is reduction of vascular markings in the left lower lung field mainly. Major vessels are spread out. The anterior segment of the left upper lobe is displaced downwards. A paravertebral density (arrows) is seen behind the heart.

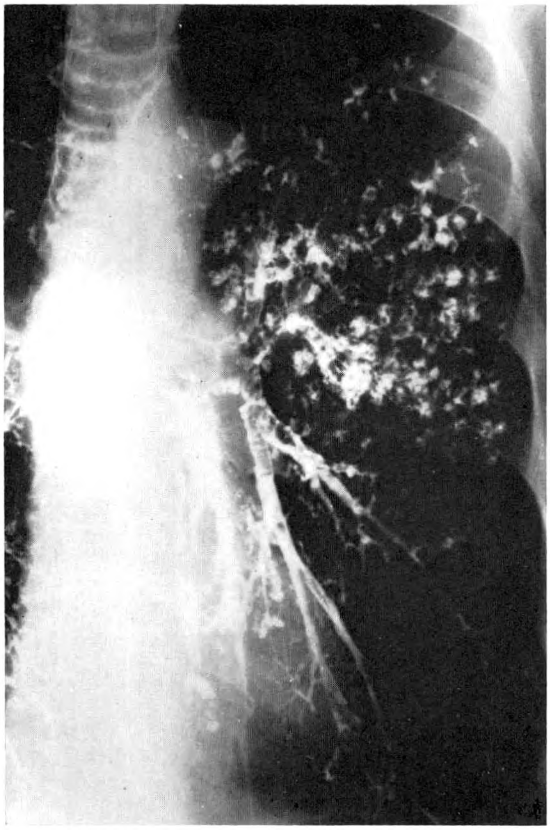

FIG. 9. Case III. Bronchogram shows good filling of all major bronchi on the left. The lingular branches are markedly displaced downwards, running parallel to the left heart border. The left lower lobe bronchus and main subdivisions are outlined. Marked bronchiectatic changes and almost complete collapse of the left lower lobe are evident.

decrease in vascular markings was apparent. A close analysis of the vessels extending from the left hilus showed the upper lobe vessels to be spread out and the artery to the anterior segment of the upper lobe running horizontally and then downwards (Fig. 12, enlarged view). The superior lingular branch extended downwards almost parallel to the left heart border. The inferior lingular branch could be seen behind the heart shadow. The main lower lobe pulmonary artery was not visible. There was a paravertebral mass on the left (arrows). The lateral view was normal (not shown). A bronchogram on January 23, 1963 (Fig. 13) showed good filling of the upper lobe bronchi on the left with spreading of the bronchi and, in particular, downward displacement of the branches to the anterior segment of the upper lobe. The lingular bronchus was markedly depressed and its superior branch ran almost parallel to the cardiac border, while the inferior lingular branch was seen behind the heart shadow. The main lower lobe bronchus and the beginning of its segmental branches were visualized in the paravertebral mass and complete left lower lobe collapse was apparent.

*Comment.* The salient features in this case were the fanning out of the main pulmonary vascular shadows of the left hilus. The lingular branches could be identified in

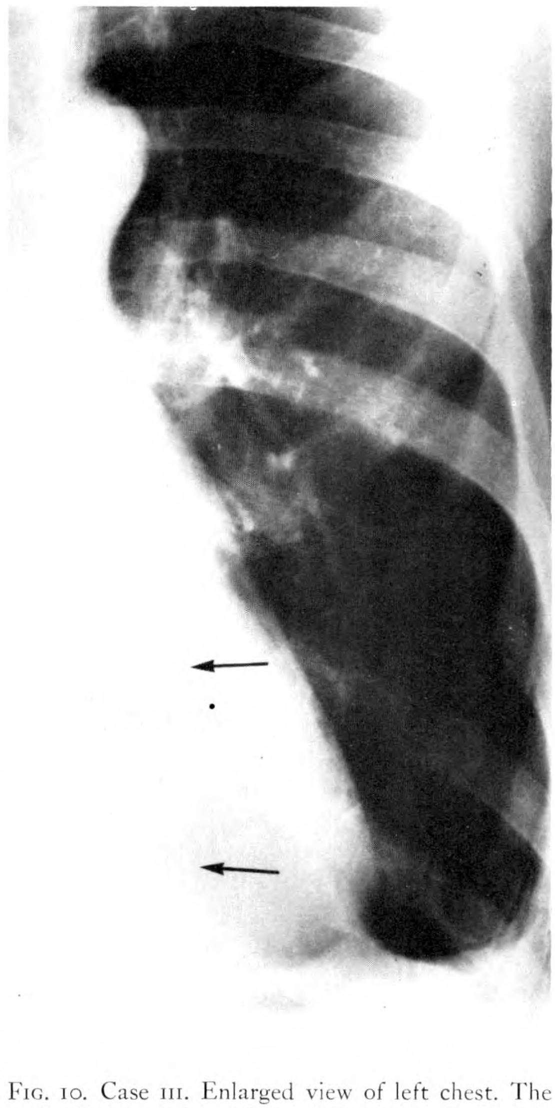

FIG. 10. Case III. Enlarged view of left chest. The lingular branches of the pulmonary artery are seen parallel to the left heart border, originating from the upper portion of the hilus. A paravertebral mass (arrows) is faintly visible behind the heart shadow.

the posteroanterior view and corresponded to the lingular bronchi, seen in the bronchogram. They were markedly depressed, running parallel to the heart border. Their origin from the upper pole of the depressed hilus was apparent. The diagnosis of left lower lobe collapse can be made from the posteroanterior chest roentgenogram alone, if these features are recognized. The left lateral chest roentgenogram was perfectly normal.

## DISCUSSION

The value of precise and detailed analysis of the pulmonary vessels as shown on routine posteroanterior and lateral chest roentgenograms has been described. Unsuspected lobar collapse occurs most frequently in the left lower lobe. The left lower lobe, when completely collapsed may be hidden behind the heart shadow and may not be demonstrable on any of the routine chest roentgenograms.

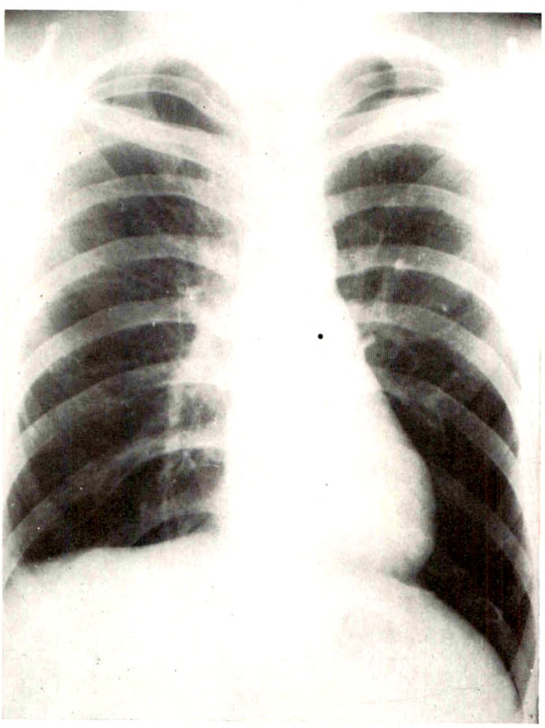

Fig. 11. Case iv. Posteroanterior chest roentgenogram (Jan. 22, 1963) shows reduction in number of vascular shadows, mainly in left lower lung field. A paravertebral mass on the left is barely visible behind heart shadow.

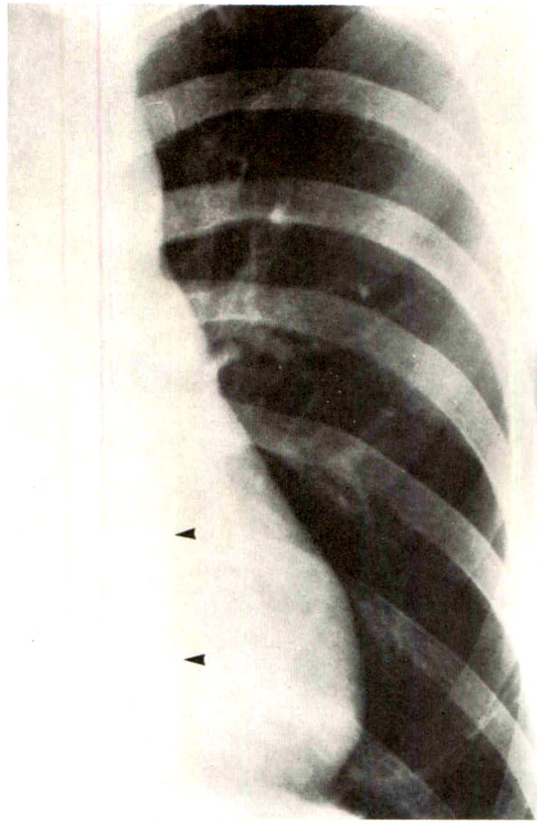

Fig. 12. Case iv. Enlarged view of the left hilar region. The spreading of the left upper lobe vessels is well visible. The lingular vessels are depressed. The paravertebral mass is indicated by two arrows.

On the plain posteroanterior chest roentgenogram, the pulmonary arteries can usually be well identified. One should look for any difference in the general vascular pattern between the right and the left hilus and lung. Such a difference may at times be minimal, as shown in our Case iv. The relative position of the hili is then observed. Such changes may be difficult to evaluate. A detailed analysis of the hilar vessels is then made, tracing each vessel separately as to origin and course. Changes in their distribution, course, number and caliber may be the only finding.

The upper lobe vessels distribute to the posterior apical segment and to the anterior segment. This latter segmental artery usually has a horizontal or slightly upwards arching course into the upper lung field. In Case iii and iv, both showing almost com-

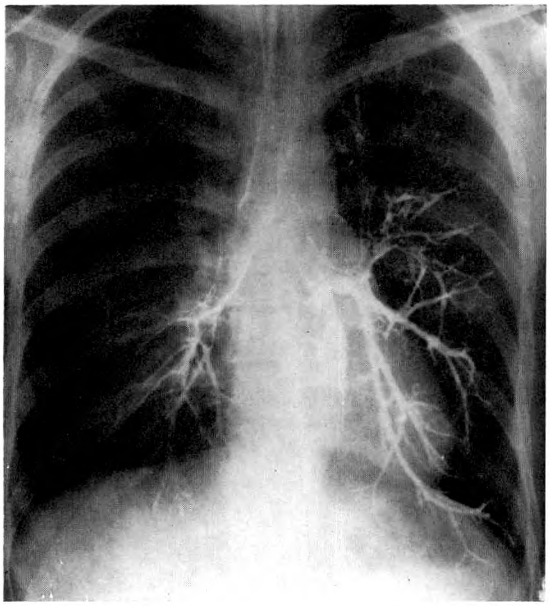

FIG. 13. Case IV. Bronchogram (Jan. 23, 1963) shows good filling of bronchi in left lung. The anterior segmental bronchus of the upper lobe is markedly deflected downward. The two lingular bronchi are deviated downwards and medially, running parallel to the left heart border. The proximal portion of the left lower lobe bronchus and its main subdivisions are visualized. Almost complete collapse of the left lower lobe is apparent.

plete collapse of the left lower lobe, this artery was strongly deflected downwards, indicating the lower lobe collapse. Similarly, deflection inferiorly and medially of the lingular branches of the pulmonary artery is noted in lower lobe collapse. These two arteries come to lie partly behind the heart shadow and take a course parallel to the left heart border. The usually characteristically arching lower lobe artery cannot be identified in lower lobe collapse. Care must be taken not to mistake the lingular branches for the main lower lobe artery in lower lobe collapse. This differentiation can be made, if one is able to recognize, that the lingular arteries originate from the upper part of the left hilus.

In collapse of the upper lobe, an apparent mass is very often identified, extending from the left hilus. The hilar vessels are elevated and are fanned out. The reduction in number of vessels per surface unit is particularly striking if compared to the normal right side. Again, it is difficult to identify the main pulmonary artery branches. However, it is exactly this difficulty in exact identification which should alert the observer to the possibility of existing lobar collapse.

SUMMARY

The detailed appearance of the vascular shadows in the left hilus in cases of lobar collapse of the left upper or lower lobe has been discussed. It has been pointed out that the normal vascular shadows of the pulmonary artery and its main branchings can be identified in adequate posteroanterior chest roentgenograms. The only sign of presence of lobar collapse may be a disturbance in the usual pattern of the pulmonary arteries and the impossibility to identify the various branches properly.

H. F. W. Pribram, M.D.
Department of Radiology
University of Iowa
Iowa City, Iowa

The authors express their sincere thanks to Mr. M. Meeuse of the photography department of the University of Alberta Hospital for his help in preparing the photographic prints.

REFERENCES

1. BESSLER, W., and TORRANCE, D. Recognition of pulmonary lobe atelectasis in roentgen picture. *Schweiz. med. Wchnschr.*, 1960, *90*, 1372–1378.
2. DOYLE, A. E., GOODWIN, J. F., HARRISON, C. V., and STEINER, R. E. Pulmonary vascular patterns in pulmonary hypertension. *Brit. Heart J.*, 1957, *19*, 353–365.
3. ESCH, D., and THURN, P. Zur Diagnose der pulmonalen Hypertonie im gewöhnlichen Röntgenbild. *Fortschr. a. d. Geb. d. Röntgenstrahlen u. d. Nuklearmedizin*, 1959, *90*, 434–435.
4. FELSON, B. Fundamentals of Chest Roentgenology. W. B. Saunders Company, Philadelphia, 1960, pp. 85–91.
5. HERRNHEISER, G. Anatomic-roentgenological analysis of normal hilar shadow. AM. J. ROENTGENOL. & RAD. THERAPY, 1942, *48*, 595–612.
6. JACKSON, F. I. Air-gap technique, and improvement by anteroposterior positioning for chest

roentgenography. Am. J. Roentgenol., Rad. Therapy & Nuclear Med., 1964, *92*, 688–691.

7. Krause, G. R., and Lubert, M. Gross anatomico-spatial changes occurring in lobar collapse: demonstration by means of three-dimensional plastic models. Am. J. Roentgenol., Rad. Therapy & Nuclear Med., 1958, *79*, 258–268.
8. Lavender, J. P., and Doppman, J. Hilum in pulmonary venous hypertension. *Brit. J. Radiol.*, 1962, *35*, 303–313.
9. Lavender, J. P., Doppman, J., Shawdon, H., and Steiner, R. E. Pulmonary veins in left ventricular failure and mitral stenosis. *Brit. J. Radiol.*, 1962, *35*, 293–302.
10. Lubert, M., and Krause, G. R. Further observations on lobar collapse. *Radiol. Clin. North America*, 1963, *1*, 331–346.
11. Lubert, M., and Krause, G. R. Patterns of lobar collapse as observed radiographically. *Radiology*, 1951, *56*, 165–182.
12. Michelson, E., and Salik, J. O. Vascular pattern of lung as seen on routine and tomographic studies. *Radiology*, 1959, *73*, 511–526.
13. Robbins, L. L., and Hale, C. H. Roentgen appearance of lobar and segmental collapse of lung: preliminary report. *Radiology*, 1945, *44*, 107–114.
14. Simon, G. Principles of Chest X-ray Diagnosis. Second edition. F. A. Davis Company, Philadelphia, 1962, pp. 45–61.
15. Simon, M. Pulmonary vessels: their hemodynamic evaluation using routine radiographs. *Radiol. Clin. North America*, 1963, *1*, 363–376.
16. Steiner, R. E. Radiological appearances of pulmonary vessels in pulmonary hypertension. *Brit. J. Radiol.*, 1958, *31*, 188–200.

# ROENTGENOGRAPHIC ASPECTS OF HEMORRHAGIC PULMONARY-RENAL DISEASE (GOODPASTURE'S SYNDROME)*

*By* R. G. SYBERS, M.D., Ph.D., J. L. SYBERS, M.D., H. A. DICKIE, M.D., *and* L. W. PAUL, M.D.
MADISON, WISCONSIN

IN 1919 GOODPASTURE[5] reported the case of a young man who had repeated hemoptysis as a complication of influenza. At necropsy, gross pulmonary hemorrhage and glomerulonephritis were demonstrated. Stanton and Tange[14] in 1958 reported 9 cases of pulmonary hemorrhage associated with glomerulonephritis and suggested the term, Goodpasture's syndrome.

Since that time there has been a sufficient number of cases reported presenting this disease complex (hemorrhagic pulmonary-renal disease or Goodpasture's syndrome) to warrant its being regarded as a specific clinical entity. Saltzman, West and Chomet[13] in 1962 reviewed the literature and collected 36 published cases of this syndrome and added 3 of their own. Subsequently, others[1,2,6,7,8,9,11,15] have added several additional cases to the literature. It is the purpose of the authors to present 3 cases with specific emphasis on the roentgenographic findings in the lungs. In each of these cases, there were repeated episodes of pulmonary hemorrhage with subsequent development of renal symptoms.

## REPORT OF CASES

Case I. A 27 year old white male was hospitalized because of marked dyspnea. He had a history of productive cough with hemoptysis for at least 1 year with the development of painless hematuria 1 month prior to admission. A chest roentgenogram (Fig. 1) 3 days prior to admission demonstrated bilateral nodular densities throughout the lung fields, ranging in size from a few millimeters to 1 cm. in diameter. The nodular infiltrate was most pronounced in the central lung fields with a slight tendency for sparing of the apices. Physical examination re-

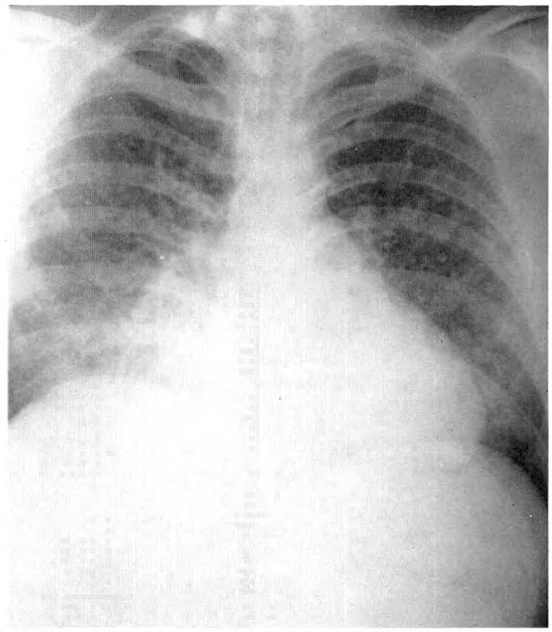

Fig. 1. Case I. *August 18, 1963:* Three days prior to admission.

vealed a pale, weak, white male. His temperature was 98.8° F., pulse was 94/min., and respirations were 22/min. The blood pressure was 140/80. Auscultation of the lungs revealed a few fine rales bilaterally.

Laboratory studies were as follows: hemoglobin 6.4 gm./100 ml., hematocrit 20 per cent. The white blood cell count and differential blood cell count were normal. Urinalysis showed hematuria and proteinuria. The blood urea nitrogen was 97 mg./100 ml. Antistreptolysin-O titer was negative. Admission chest roentgenogram (Fig. 2) revealed the persistence of a fine granular reticular pattern, but the nodular densities had cleared considerably. Intravenous pyelography was done and there was no excretion of the contrast material during the first 15 minutes. A chest roentgenogram (Fig.

* From the Department of Radiology, University Hospitals, University of Wisconsin, Madison, Wisconsin.

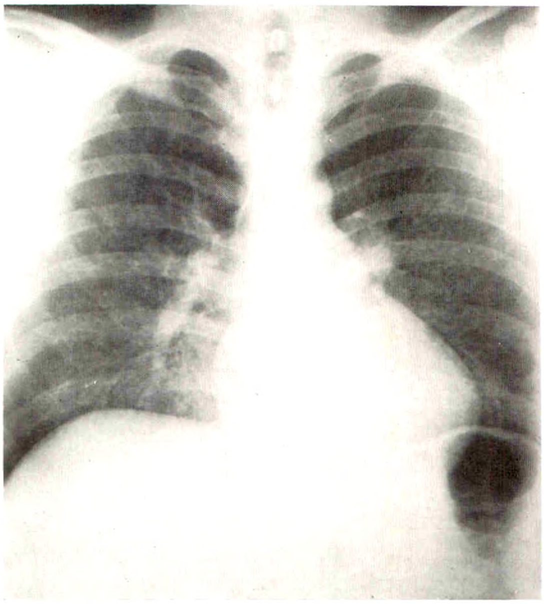

Fig. 2. Case i. *August 21, 1963:* On admission.

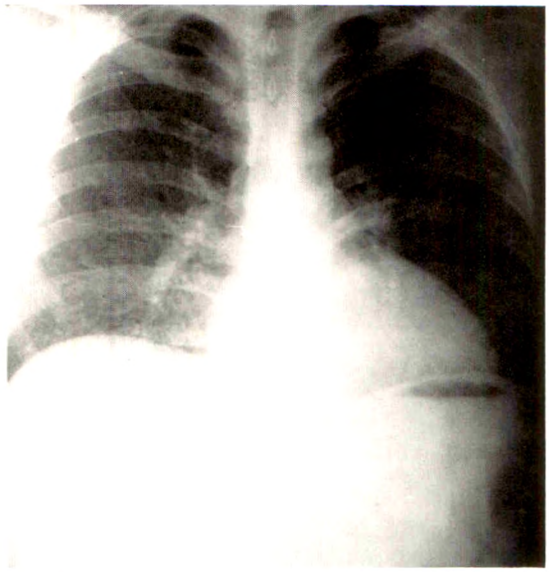

Fig. 3. Case i. *August 22, 1963:* Second hospital day.

3) the following day showed further clearing with complete disappearance of the small nodular densities previously noted. Only the fine granular reticular infiltrate remained.

The patient was started on steroid therapy. However, his renal problem continued to worsen and peritoneal dialysis was instituted on the 7th hospital day. His condition gradually deteriorated and he expired on the 18th hospital day. A chest roentgenogram (Fig. 4) just prior to his death demonstrated the typical findings of pulmonary edema and congestion compatible with an azotemic lung.

At autopsy, the right lung weighed 1,070 gm., the left 870 gm. The pleural surfaces of both lungs were smooth and transparent. Crepitance was decreased throughout the lungs and there was noted a slight nodularity in some areas. The bronchi contained a thin frothy fluid. On cut surface the parenchyma was reddish-brown in color and there was extrusion of thin bloody fluid. Microscopically, there was noted patchy atelectasis and moderate to marked pulmonary edema. There were fresh intra-alveolar hemorrhages and many hemosiderin-filled macrophages in the alveoli. Also noted were focal areas of fibrosis and thickening of the alveolar septa. There was no evidence of arteritis.

The kidneys each weighed 375 gm. In each, the capsule was smooth and the cortex was pale with small areas of focal congestion. Microscopically, there was noted a marked proliferation of the epithelial cells of Bowman's capsule involving all glomeruli. Some of the glomeruli showed hyalinization with complete obliteration of the glomerular tuft. The tubules were dilated and contained hyaline casts, red blood cells and red blood cell casts. The interstitial tissues showed a marked degree of edema with chronic inflammatory cells. There was no evidence of arteritis.

Case ii. A 19 year old white male was hospitalized because of the sudden occurrence of gross hemoptysis and dyspnea. A chest roentgenogram (Fig. 5) 3 days following the acute

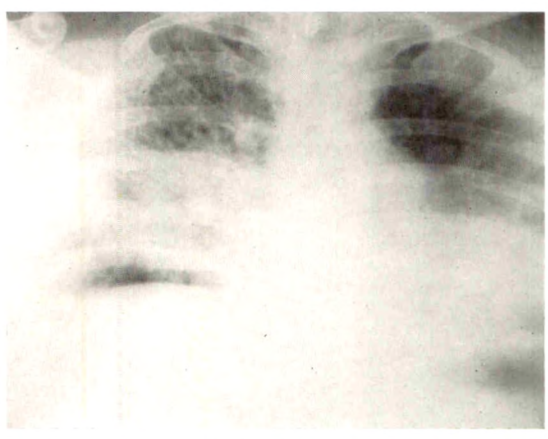

Fig. 4. Case i. *September 9, 1963:* Just prior to death.

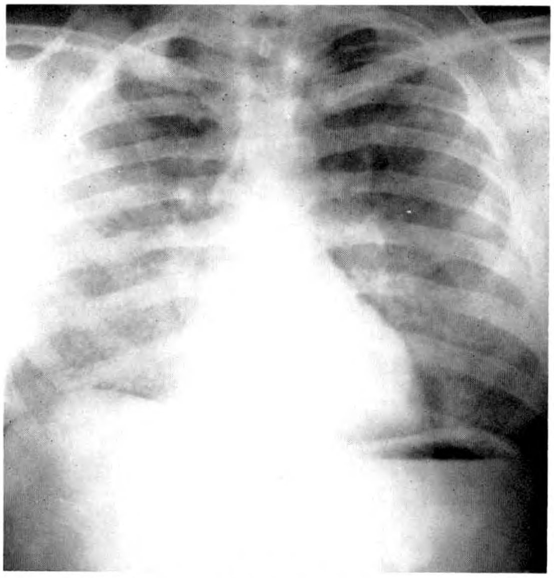

FIG. 5. Case II. *August 26, 1959:* Three days following initial acute episode of hemoptysis.

episode of hemoptysis revealed a bilateral pulmonary infiltrate with soft nodular densities measuring from a few millimeters to 1 cm. in diameter, in this case slightly more prominent in the right mid lung field and right lower lobe. Physical examination at the time of admission 1 week later revealed a well developed 19 year old male in no acute distress. His temperature was 98.6° F., pulse was 96/min., respirations were 20/min., and the blood pressure was 130/85. Auscultation of the chest revealed a few fine rales bilaterally.

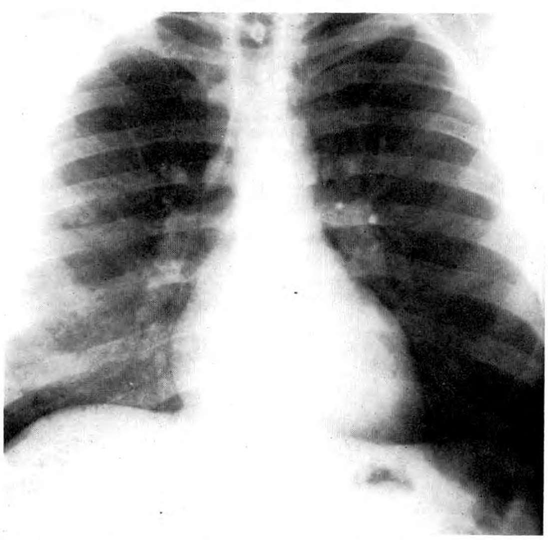

FIG. 6. Case II. *September 2, 1959:* On admission.

Laboratory studies were as follows: hemoglobin 7.3 gm./100 ml., hematocrit 27 per cent. Urine studies were within normal limits except for a slight trace of protein .02 gm. per cent. The white blood cell count and differential blood cell count were normal. A chest roentgenogram (Fig. 6) at the time of admission showed considerable clearing of the nodular infiltrate with a fine granular infiltrate remaining in the right lower and middle lung fields. He was started on iron therapy with some improvement clinically and on the 12th hospital day his chest was clear and he was discharged.

Two weeks later he was re-admitted to the hospital following another acute episode of hemoptysis at which time hematuria was also present. On physical examination his temperature was 100° F., pulse was 108/min., respirations were 29/min., and the blood pressure was 190/90. Auscultation of the chest again revealed the presence of a few rales at the right base.

Laboratory studies were as follows: hemoglobin 8.6 gm./100 ml., hematocrit 28 per cent. The white blood cell count and the differential blood cell count were normal. Urinalysis showed albumin 0.1 gm. per cent and there were many red blood cells and red blood cell casts in the urine. A repeat urinalysis on the following day showed a 0.2 gm. per cent albumin and again gross hematuria. Blood urea nitrogen was 18 mg./100 ml. Renal function studies revealed 15 per cent excretion of phenolsulfonphthalein in 3 specimens. Urine cultures and blood cultures were negative. Lupus erythematosus preparations were negative on 3 occasions. The admission chest roentgenogram (Fig. 7) showed a recurrence of the nodular infiltrate in the right lower lobe. Intravenous pyelography revealed the right kidney to be definitely enlarged with diminished function. There was no evidence of a kidney on the left. A scalene muscle biopsy was normal. A progress chest roentgenogram (Fig. 8) on the 19th hospital day revealed considerable clearing of the infiltrate in the right lower lobe. The patient's renal problem, however, continued to worsen and the blood urea nitrogen rose to 78 mg./100 ml. On the 20th hospital day the patient expired in pulmonary edema.

At autopsy, the lungs were congested with multiple pulmonary hemorrhages and edema. Microscopically, many of the alveoli were filled with macrophages containing hemosiderin, red

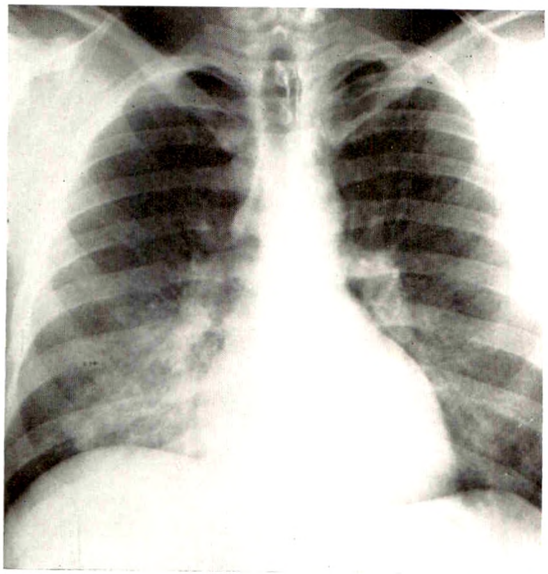

Fig. 7. Case II. *October 6, 1959:* Re-admission following recurrence of hemoptysis.

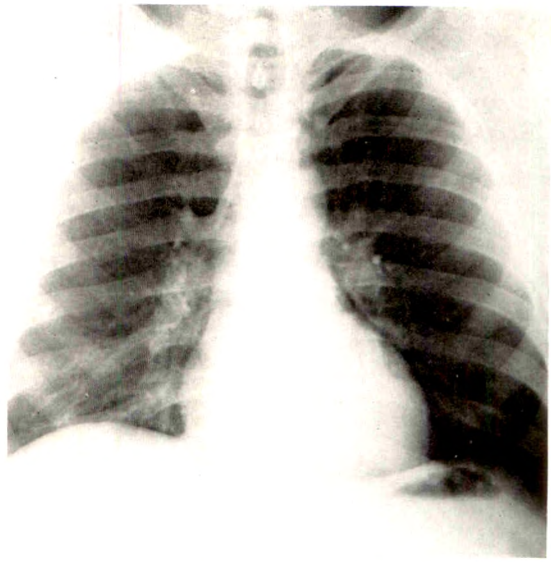

Fig. 8. Case II. *October 16, 1959:* Progress roentgenogram 10 days following second admission.

blood cells and small round cells. In some regions there were thickening and fibrosis of the intra-alveolar septa.

There was a single kidney on the right which weighed 700 gm. The capsule was smooth, revealing a pale cortex with numerous petechial hemorrhages. Microscopically all the glomeruli were involved with a pronounced cellular proliferation of the epithelial cells of Bowman's capsule. Many of the glomeruli had undergone partial to complete fibrosis. Many of the tubules were dilated and contained red blood cell casts and hyaline casts. There was no evidence of vasculitis.

Case III.* A 21 year old white male was hospitalized with marked dyspnea which had been progressive for 3 months following a bout of influenza. History revealed that he had a productive cough with intermittent hemoptysis for 3 years. Physical examination revealed a well developed white male who was pale but in no acute distress. His temperature was 98.6° F., pulse was 120/min., respirations were 24/min., and the blood pressure was 140/70. Examination of the chest revealed a few inspiratory rales at the right base.

Laboratory findings were as follows: hemoglobin 5.7 gm./100 ml., hematocrit 16.5 per cent, reticulocyte count 7.1 per cent. Bleeding time and clotting time were normal. Serum iron was 0.045 mg. per cent. Fasting blood sugar, blood urea nitrogen, serum electrolytes and serum proteins and A/G ratio were normal. Repeated sputum examination showed cells laden with hemosiderin. Skin tests for tuberculosis and fungi were negative. The admission chest roentgenogram (Fig. 9) revealed a fine granular hazy infiltrate involving both lungs most marked in the central areas with less prominence at the bases and apices.

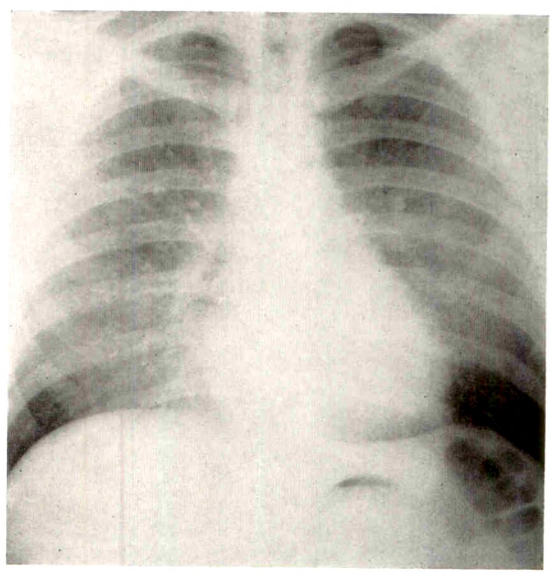

Fig. 9. Case III. *December 13, 1961:* On admission. (Reproduced with permission of *Arch. Int. Med.*)

* For a detailed discussion of the medical aspects of Case III, refer to Azen, E. A. and Clatanoff, D. V. Prolonged survival in Goodpasture's syndrome. *Arch. Int. Med.*, 1964, 114, 453–460.

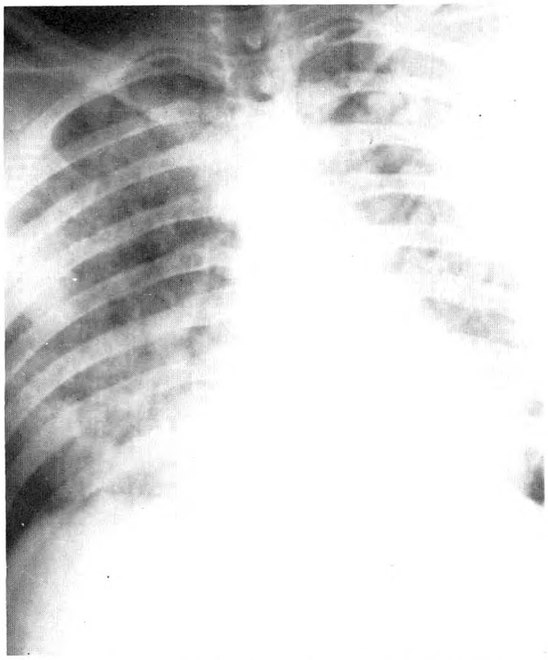

FIG. 10. Case III. *December 31, 1961:* Bedside roentgenogram during acute episode of hemoptysis.

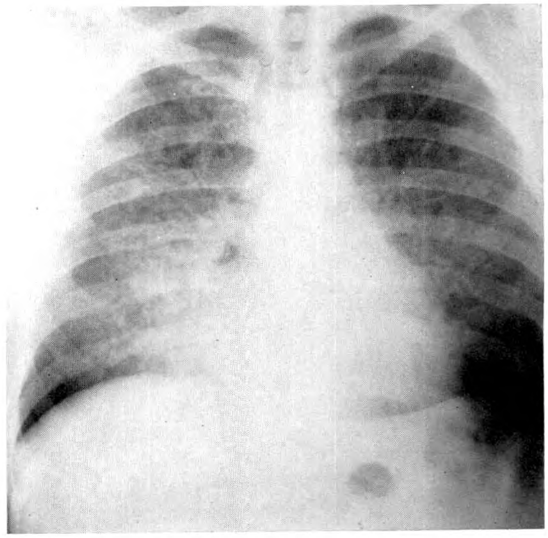

FIG. 12. Case III. *February 3, 1962:* Second admission following recurrent hemoptysis.

The patient was started on a course of iron therapy and after 2 weeks of treatment improved clinically so that he was allowed to leave the hospital on a 2 day pass. However, within 24 hours he developed acute respiratory distress with hemoptysis, fever and chills, and returned to the hospital. His blood pressure was 114/56, pulse was 136/min., respirations were 42/min., and temperature was 99.8° F. There were inspiratory rales over both lungs. A chest roentgenogram (Fig. 10) taken at the bedside showed multiple conglomerate nodular densities measuring up to a centimeter and a half in diameter throughout both lung fields. Because of a sharp drop in hematocrit, the patient received 4 units of whole packed cells and was started on steroid therapy. His clinical condition gradually but steadily improved and a chest roentgenogram (Fig. 11) 4 days later demonstrated considerable clearing of the nodular densities. He was continued on steroid therapy and a few days later was discharged from the hospital.

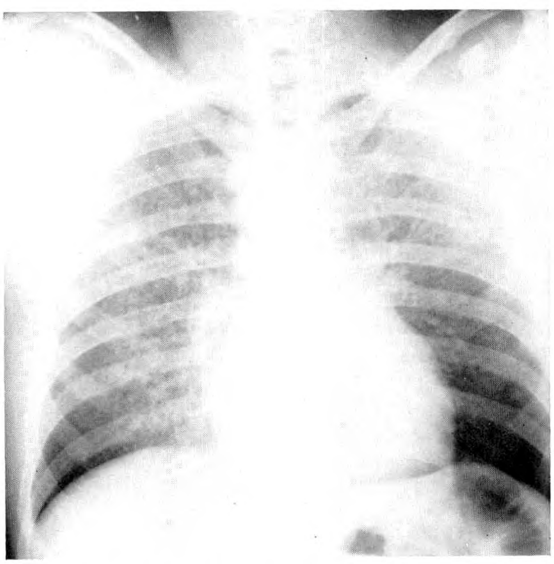

FIG. 11. Case III. *January 4, 1962:* Progress roentgenogram 4 days following acute episode of hemoptysis.

Three weeks following his discharge from the hospital, he was re-admitted because of recurrent hemoptysis. Physical examination at this time revealed rales over both lungs.

Laboratory findings were as follows: hemoglobin 10 gm./100 ml., blood urea nitrogen 37 mg. per cent. Urinalysis showed a trace of protein and many red blood cells. The phenolsulfonphthalein excretion test showed delayed excretion. Lupus erythematosus preparations were negative on several occasions. An intravenous pyelogram was interpreted as normal. A chest roentgenogram (Fig. 12) at the time of this admission showed a recurrence of the bilateral nodular infiltrate.

While in the hospital, the patient was maintained on steroid therapy. A renal biopsy was done which showed changes of early prolifera-

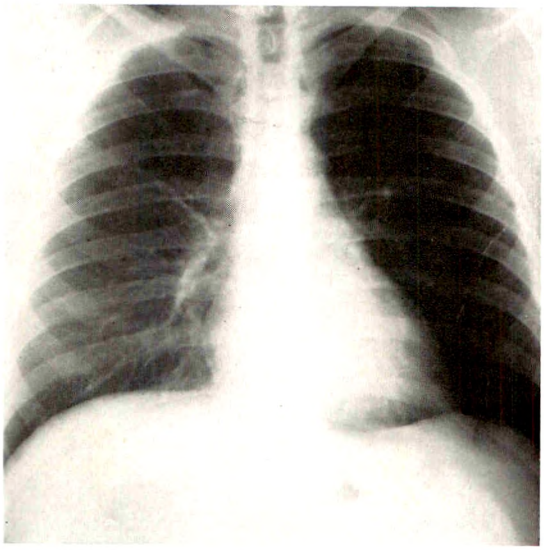

Fig. 13. Case III. *February 16, 1962:* Progress roentgenogram 2 weeks following second admission.

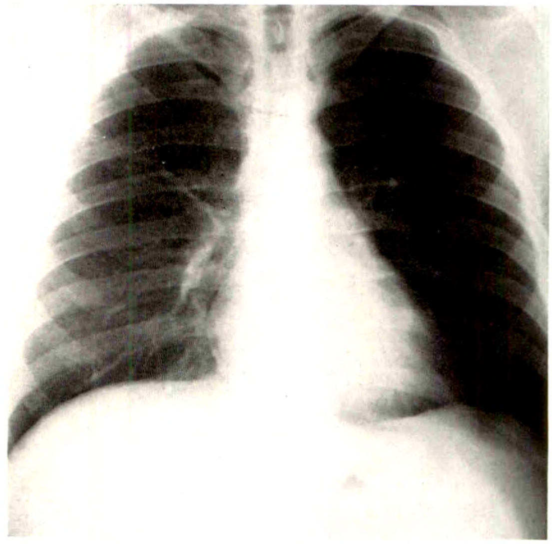

Fig. 14. Case III. *February 22, 1963:* One year following last episode of hemoptysis. (Reproduced with permission of *Arch. Int. Med.*)

tive and membranous glomerulitis. A progress chest roentgenogram (Fig. 13) 2 weeks after admission showed complete clearing of the pulmonary infiltrate and the patient was discharged from the hospital. Since that time, the patient has been continued on steroid therapy and the pulmonary disease appears to be under control. A second renal biopsy in November, 1962, 9 months following the initial renal biopsy, showed no progression of the renal disease. He has been followed at regular intervals in the outpatient clinic and chest roentgenograms (Fig. 14) have remained clear. Although microscopic hematuria has persisted, there has been no other clinical evidence to indicate progression of the renal disease.

## DISCUSSION

Although hemorrhagic pulmonary-renal disease is recognized as a distinct clinical entity, the underlying disease process has yet to be clarified.

Parkin *et al.*[10] and others[7] have suggested that the changes seen may be secondary to a generalized hypersensitivity reaction which produces an acute necrotizing alveolitis resulting in repeated episodes of pulmonary hemorrhage.

Various drugs (including penicillin) and antigens have been implicated as possible causative agents. In 1963 Lundberg[8] suggested that a pre-existing nephritogenic streptococcal infection might have served as an etiologic factor in the case he reported.

The similarity between the pulmonary manifestations of hemorrhagic pulmonary-renal disease and idiopathic pulmonary hemosiderosis has led to the suggestion that the two conditions may actually represent different manifestations of the same pathologic process (Rusby and Wilson,[12] Canfield *et al.*[2]).

The relationship of Goodpasture's syndrome to polyarteritis nodosa is confusing because many of the cases reported have demonstrated the typical changes of polyarteritis at autopsy. It has, in fact, been questioned whether or not Goodpasture's syndrome is ever anything other than a manifestation of vasculitis.[3] However, it is generally felt that the presence of vasculitis is atypical.

Clinically, the cases reported have been remarkably similar. The patients almost always are young adult males with a history of repeated episodes of hemoptysis and subsequent development of glomerulonephritis which is rapidly fatal. The diagnosis depends on an accurate clinical history correlated with roentgenographic and laboratory findings. In the absence of specific

therapy, steroids have been widely used and the results were often disappointing.[11] However, there are 3 reported cases (not including the 1 in this report) in which steroids have been beneficial in arresting the disease process.[6,12,15] In these cases steroid therapy was instituted before severe renal disease was manifest clinically. It is the feeling of those authors who propose steroid therapy that with earlier diagnosis and earlier initiation of treatment more long term survivors may be expected in the future.[2,4,6,15]


SUMMARY

Three cases of hemorrhagic pulmonary-renal disease are presented with correlation between the clinical course and the roentgenographic changes in the lung. The roentgenographic appearance of the lungs is basically the same as that observed with idiopathic pulmonary hemosiderosis. During the acute episodes of hemoptysis, there are ill-defined multiple nodular densities bilaterally which disappear within a few days. Characteristically, the pattern is one of perihilar distribution with a tendency to spare the apices and bases. Chest roentgenograms taken between the acute episodes show an increase in the interstitial markings characterized by a finely granular appearing reticular accentuation throughout the lungs.

In spite of the rapidly fatal course of the disease in the past, it is felt that early recognition of this condition and prompt institution of steroid therapy may offer a more hopeful prognosis to these patients in the future.



Robert G. Sybers, M.D.
Department of Radiology
Emory University
Atlanta, Georgia



REFERENCES

1. Brannan, H. M., McCaughey, W. T. E., and Good, C. A. Roentgenographic appearance of pulmonary hemorrhage associated with glomerulonephritis. Am. J. Roentgenol., Rad. Therapy & Nuclear Med., 1963, *90*, 83–88.
2. Canfield, C. J., Davis, T. E., and Herman, R. H. Hemorrhagic pulmonary-renal syndrome; report of three cases. *New England J. Med.*, 1963, *268*, 230–234.
3. Case records of Massachusetts General Hospital, case 9-1964. *New England J. Med.*, 1964, *270*, 414–421.
4. Fairley, K. F., and Kincaid-Smith, P. Goodpasture's syndrome. *Brit. M. J.*, 1961, *2*, 1646.
5. Goodpasture, E. W. Significance of certain pulmonary lesions in relation to etiology of influenza. *Am. J. M. Sc.*, 1919, *158*, 863–870.
6. Joseph, M. Nephritis with lung haemorrhage. *Lancet*, 1963, *1*, 1160.
7. Leff, I. L., and Fazekas, G. Hemorrhagic and interstitial pneumonitis with nephritis. *Ann. Int. Med.*, 1962, *56*, 296–302.
8. Lundberg, G. D. Goodpasture's syndrome; glomerulonephritis with pulmonary hemorrhage. *J.A.M.A.*, 1963, *184*, 915–919.
9. McCaughey, W. T. E., and Thomas, B. J. Pulmonary hemorrhage and glomerulonephritis; relation of pulmonary hemorrhage to certain types of glomerular lesions. *Am. J. Clin. Path.*, 1962, *38*, 577–589.
10. Parkin, T. W., Rusted, I. E., Burchell, H. B., and Edwards, J. E. Hemorrhagic and interstitial pneumonitis with nephritis. *Am. J. Med.*, 1955, *18*, 220–236.
11. Randall, R. E., Jr., Glazier, J. S., and Liggett, M. Nephritis with lung haemorrhage. *Lancet*, 1963, *1*, 499.
12. Rusby, N. L., and Wilson, C. Lung purpura with nephritis. *Quart. J. Med.*, 1960, *29*, 501–511.
13. Saltzman, P. W., West, M., and Chomet, B. Pulmonary hemosiderosis and glomerulonephritis. *Ann. Int. Med.*, 1962, *56*, 409–421.
14. Stanton, M. C., and Tange, J. D. Goodpasture's syndrome: (pulmonary haemorrhage associated with glomerulonephritis). *Australasian Ann. Med.*, 1958, *7*, 132–144.
15. Walker, J. M., and Joekes, A. M. Survival after haemoptysis and nephritis. *Lancet*, 1963, *2*, 1199–1201.

# THE DIAGNOSIS OF TUMORS OF THE THORAX WITH INCLINED TOMOGRAPHY*

By THEODOR LAUBENBERGER
HOMBURG (SAAR), GERMANY

THE aim of the author is to acquaint radiologists with the combined use of inclined frontal tomography and inclined sagittal tomography in the diagnosis of tumors of the thorax.

On tomograms of the lungs, the trachea and the bronchi are the best standards for purposes of orientation. In most cases it is possible to demonstrate these hollow organs in their entire length on a single tomogram with ordinary tomographic technique; however, with inclined tomography exposures can be made in all planes. Frain *et al.*,[6–9] and Tempini and Pazienza[21] proposed planes in which the trachea and the main branches of the bronchi are completely demonstrated; these were termed by Kováts and Zsebök[14] the characteristic planes. It has been our experience that, using the characteristic planes of the lungs, more information about intrathoracic pathology can be gained with inclined tomography than with conventional tomography. In the characteristic frontal plane (Fig. 1*B*), the roentgen ray cuts through the trachea and the main branches of the bronchial tree. In the characteristic right and left sagittal planes, the beam cuts beginning at the trachea through the main bronchus and the branches of the lower lobe bronchi of the respective side (Fig. 1, *A* and *C*).

Frain *et al.*, who developed the inclined frontal tomography, and other French authors, who also employed the method, performed their investigations with the Radiotome (Massiot) and Pantomix (C.G.R.). We made use of the Siemens-Transversal-Planigraph and constructed a device by which proper inclination of the film could be obtained (Fig. 2, *A* and *B*).

Frey[10] used a similar method; Szenes[22] inclined the film in the planigraph; Kováts and Zsebök,[14] and Voigt[24] suggested equalizing the inclination angle of the frontal tracheobronchial plane by positioning the patient. The desired planes should parallel the movement of the tomograph.

## TECHNIQUE

The examination is carried out with the patient in a sitting position. Figure 2 is a diagram of the procedure. During roentgenographic exposure the tube is fixed so that the path of roentgen rays is horizontal. A 220 cm. focus-film-distance and 55 cm. object-film-distance are used. A coordinated contrarotating movement is obtained between the patient and the film. The geometric scheme of the arrangement is shown in Figure 3. The body plane, which is the same distance from the center of the revolving chair as the film from the center of the film holder, is drawn in a heavier line than the rest of the figure. The supposed point $p$ ($p_1$, $p_2$, $p_3$ are various phases of the movement) of the plane is constantly projected on the same spot on the film during rotation. Every point which is outside the plane will be blurred.

The desired plane is adjusted by changing the distance of the film from the center. During a constant rotating speed, the tomographic angle is determined by the duration of roentgenographic exposure. For the examination of the lungs, we generally choose an angle of 60 degrees. For frontal tomograms the inclination angle—that formed by the trachea and the vertical body axis—is determined by the profile roentgenogram of the thorax and the film is inclined at the film-holder accordingly. The lateral inclination angles—those formed by the main and lower lobe bronchi and the median plane—are determined by the

* From the Department of Radiology of the University of the Saarland. Director: Professor Dr. F. Sommer.

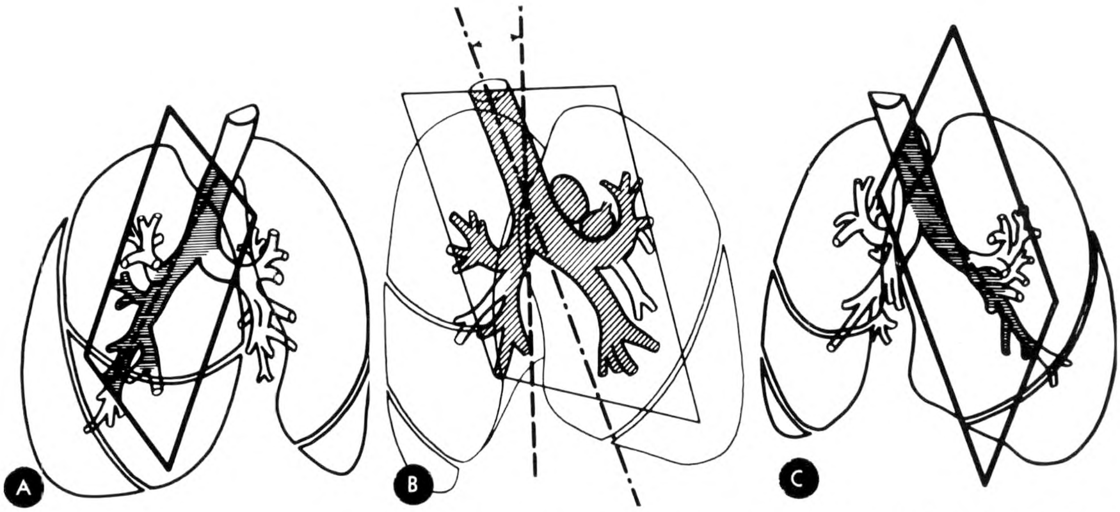


Fig. 1. Diagrams showing (*A*) the right characteristic sagittal plane, (*B*) the characteristic frontal plane, and (*C*) the left characteristic sagittal plane. (*A* and *B* reproduced with permission of *Fortschr. a. d. Geb. d. Röntgenstrahlen u. d. Nuklearmedizin.*[20])

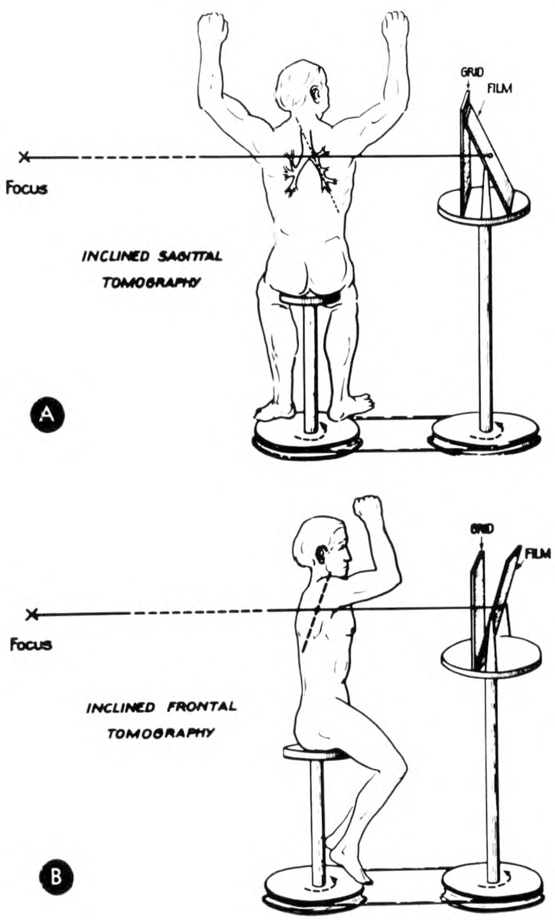


inclined frontal tomogram. The postero-anterior thorax roentgenogram cannot be used because of the geometric distortion of the tracheobronchial plane. Studies have shown a difference of more than 10 degrees between the inclination angles of the normal chest roentgenogram and those on the inclined frontal tomograms.

## ADVANTAGES

1. Inclined tomography may be performed while the patient is sitting or standing.

2. The patient and film are rotated using the Vallebona[23] and Bozzetti[2] principle. Greater areas of the body, therefore, are blurred than in conventional tomography. For example, the spine is completely blurred and a better study of the vessels and of the enlarged lymph nodes of the mediastinum is obtained.

3. The sweeping angle can be varied from 0–180 degrees with an automatic switch.

Fig. 2. Sketches of the positioning for (*A*) inclined sagittal tomography and (*B*) inclined frontal tomography.

4. With the film-holder the inclination of the film can be regulated.

5. Generally, a single tomogram using a characteristic plane reveals most changes of the bronchial tree, vessels and lymph nodes. In comparison with the conventional method, the radiation dose to a patient is greatly reduced.

## DISCUSSION

### INCLINED FRONTAL TOMOGRAPHY

For a characteristic inclined frontal tomogram an inclination of 15 to 20 degrees to the vertical body axis is used. The trachea, main bronchi and their branches, the apical and posterior segmental bronchi of the upper lobe bronchi, and the lateral and posterior segmental bronchi of the lower lobe bronchi are visualized. However, only a short part of the lingula bronchus is included and the middle lobe bronchus is blurred, since it is outside the plane (Fig. 4*B*).

A great advantage of this method is ready-demonstration of enlarged lymph nodes in the case of bronchial carcinoma with metastatic formation. With the conventional planigraphic method there is little possibility of visualizing enlarged lymph nodes in the mediastinum since the dense spine lying behind them cannot be blurred sufficiently. Other useful applications are the differentiation of vessels in various layers and the identification of pathologic changes. Thus, in a characteristic inclined frontal tomogram, deviations of hollow organs, changes in the tracheal and bronchial walls, enlarged lymph nodes of the mediastinum and interbronchial areas, changes of the pulmonary vessels and shadows caused by infiltrations of the lungs can be recognized. Figure 5 shows a trachea displaced by a calcified struma nodosa. The aorta and the arteria pulmonalis are cut on orthograde; and they are broadened and their walls are partly calcified.

### INCLINED SAGITTAL TOMOGRAPHY

In the characteristic inclined sagittal tomograms, the trachea, main bronchi and

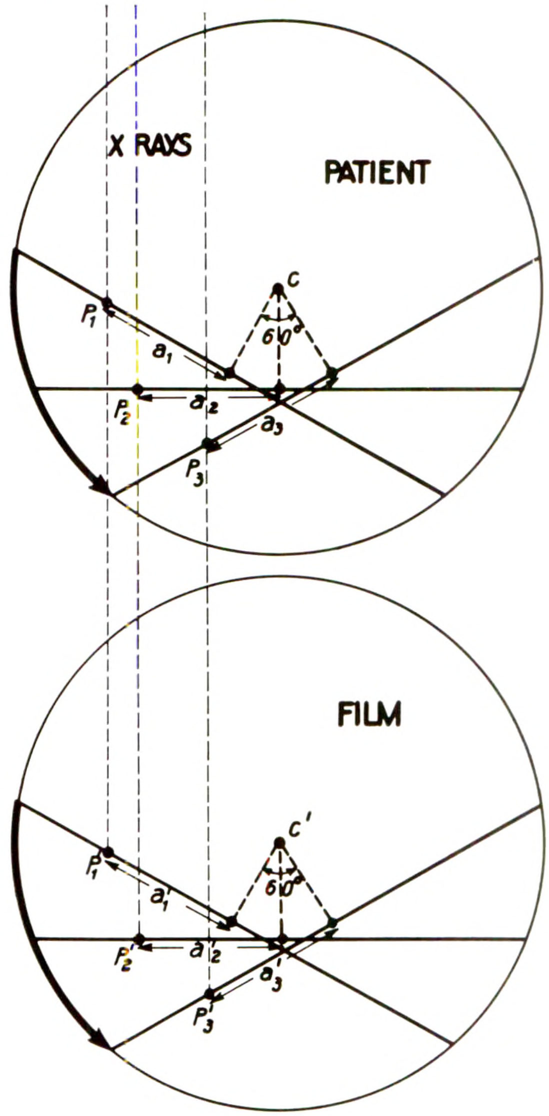


FIG. 3. Geometric scheme of the procedure.

the lower lobe bronchi are cut (Fig. 4, *A* and *C*). The inclination of the left characteristic sagittal plane to the vertical body axis is 35 to 50 degrees and of the right 25 to 35 degrees. The left main bronchus is a little shortened because of a small geometric distortion. The upper lobe bronchi are outside the plane and cannot be demonstrated. The trunci and many of the branches of the inferior vena and arteria pulmonalis can be visualized.

Pathologic changes of the bronchi are discovered more readily than with other

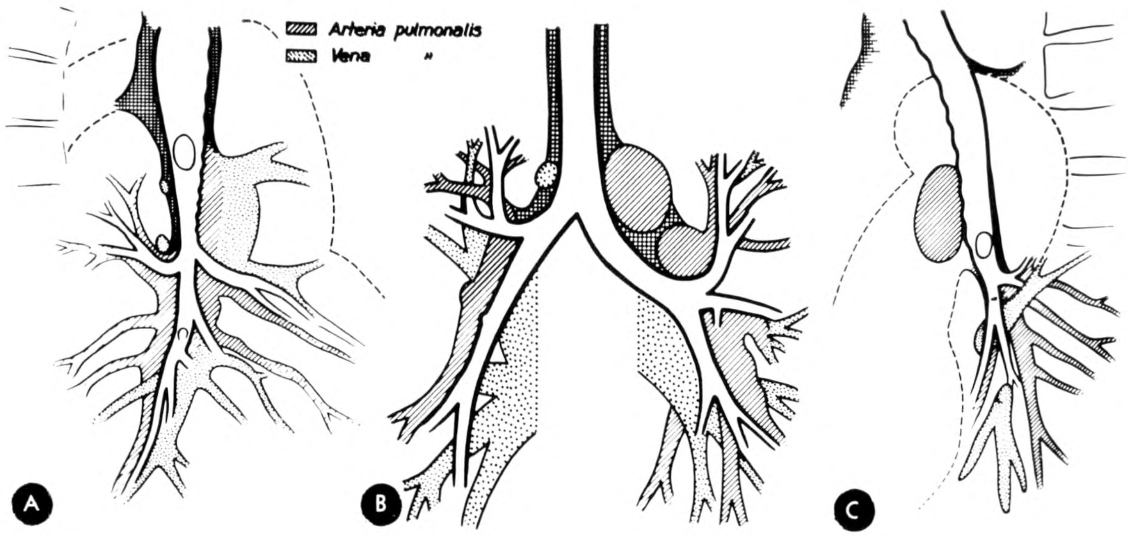


Fig. 4. Drawings showing (*A*) the right inclined sagittal plane, (*B*) the inclined frontal plane, and (*C*) the left inclined sagittal plane. (*A* and *B* reproduced with permission of *Fortschr. a. d. Geb. d. Röntgenstrahlen u. d. Nuklearmedizin.*[20])

methods. Usually, neoplasias and their secondary manifestations, atelectasis, obstructive pneumonia, and dislocation of bronchi or vessels are demonstrated on a single tomogram.

### COMBINED METHOD

Figure 6, *A* and *B* is a study obtained with a combination of inclined frontal and inclined right sagittal tomography. The distal part of the bronchus intermedius is obstructed and the dense tissue of a bronchial carcinoma is demonstrated on the inclined frontal tomogram. The full extent of the tumor and the secondary atelectasis of the posterobasal and the anterobasal segments are seen on the inclined right sagittal tomogram. The lower lobe bronchi and segmental bronchi as well as the proximal part of the middle lobe bronchus are narrowed; their walls are thickened by the infiltrating tumor.

Figure 7, *A* and *B* shows in the left posterobasal segment a tumor causing displacement of the normal structures. On the inclined frontal tomogram, the proximal part of the lower lobe bronchus is visible but the distal part lies outside the plane. The interaortopulmonary space is broadened by enlarged lymph nodes. The left inclined sagittal tomogram shows the situation more clearly. A spherical tumor in the posterobasal segment spreads the subsegmental bronchi of the posterior segment.

It is known that in tomography more detailed information about dense tumor masses can be obtained by using a large sweeping angle. Figure 8, *A* and *B* was

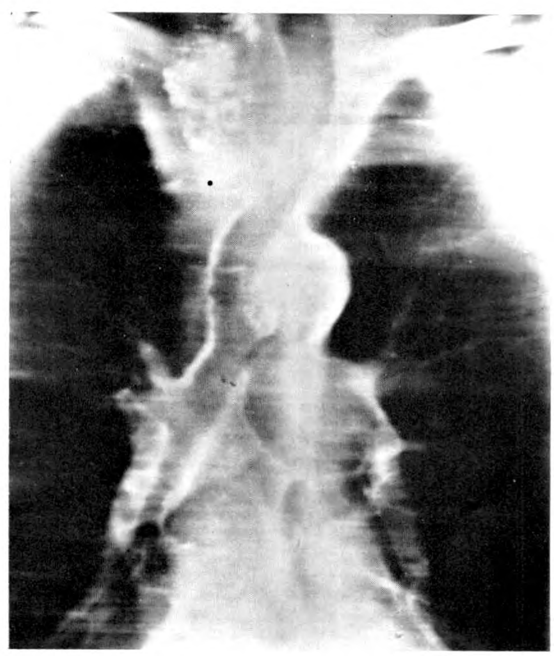

Fig. 5. Inclined frontal tomogram of a 64 year old patient with a calcified struma nodosa and sclerosis of the pulmonary vessels.

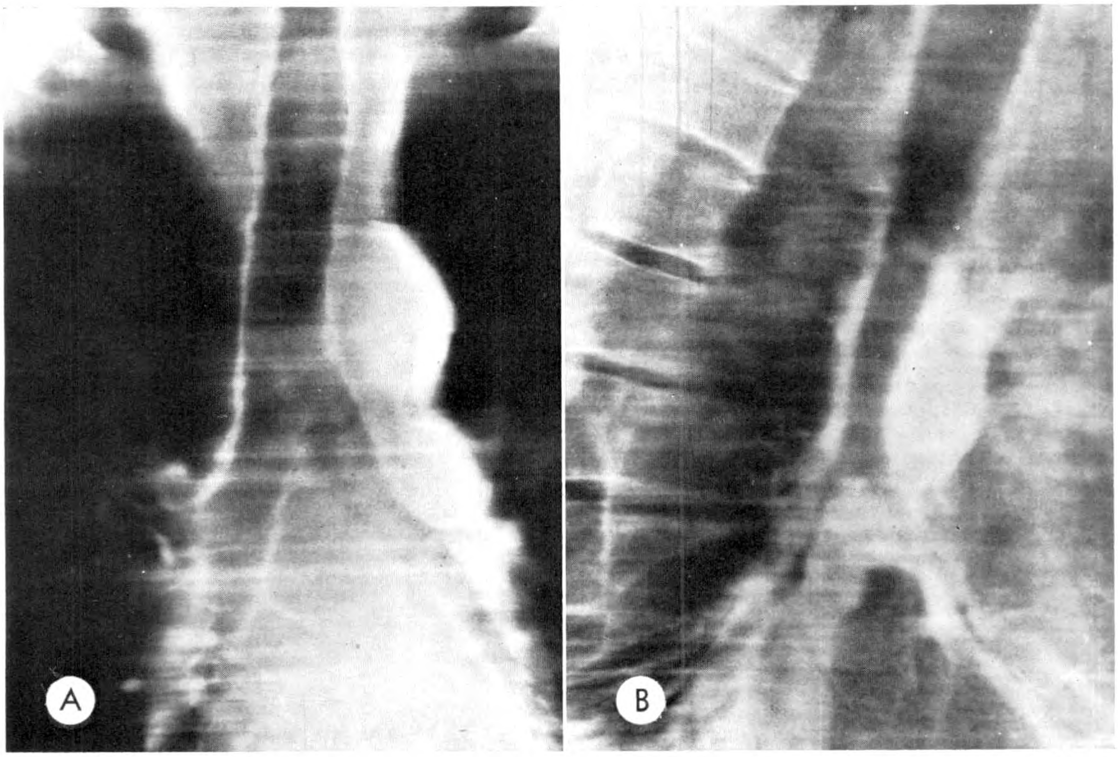


Fig. 6. A 40 year old patient with a squamous epithelium carcinoma of the branching area of the right lower lobe bronchus. (*A*) Inclined frontal tomogram; (*B*) right inclined sagittal tomogram.

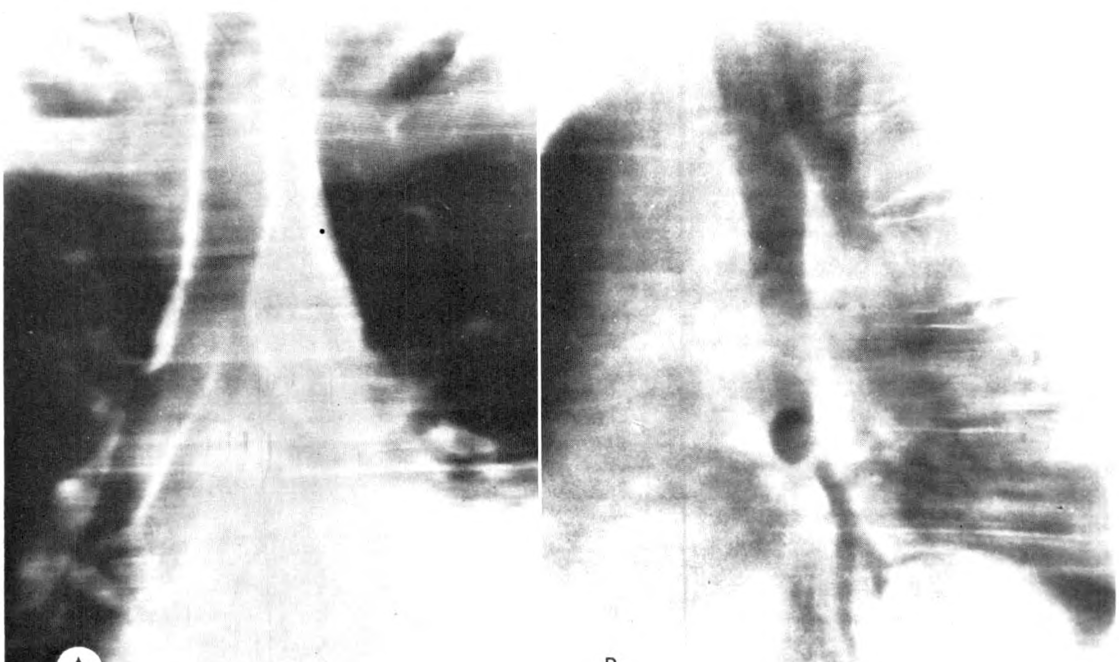


Fig. 7. A 56 year old patient with an undifferentiated epithelium carcinoma in the left posterobasal segment. (*A*) Inclined frontal tomogram; (*B*) left inclined sagittal tomogram.


Fig. 8. A 59 year old patient with a large cylindrocellular carcinoma of the right upper lobe bronchus. (*A*) Inclined frontal tomogram; (*B*) right inclined sagittal tomogram.

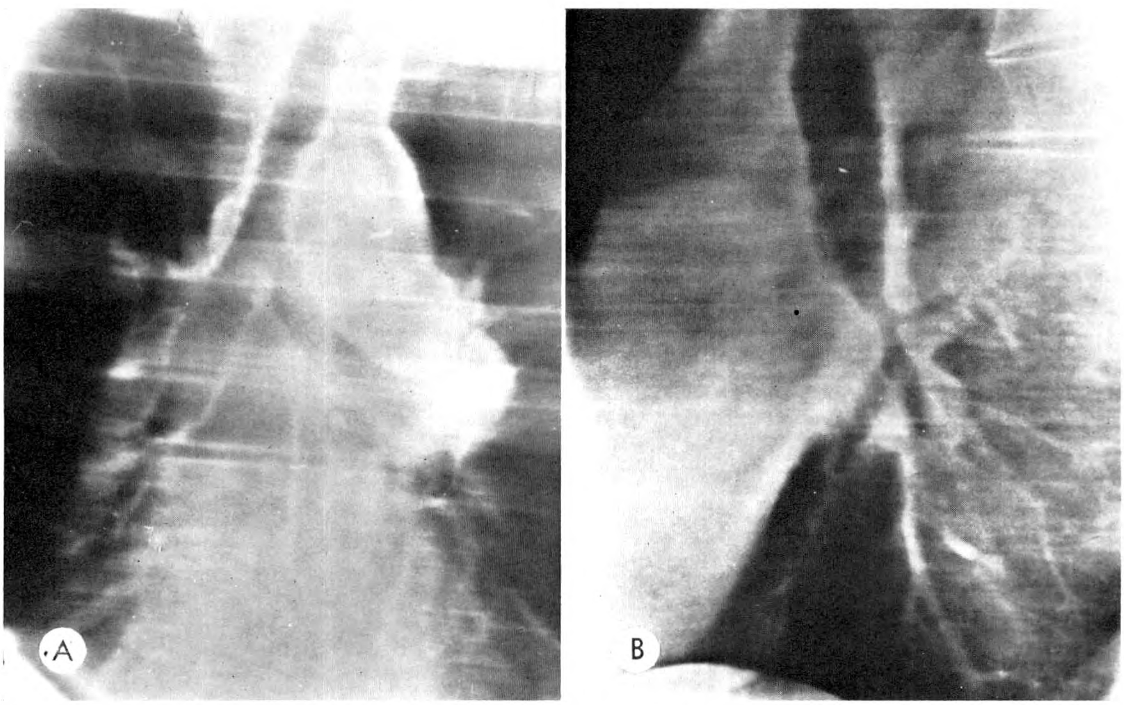


Fig. 9. A 62 year old patient with a squamous cell carcinoma of the left upper lobe with intramural infiltration of the wall of the left lower lobe bronchus. (*A*) Inclined frontal tomogram; (*B*) left inclined sagittal tomogram.

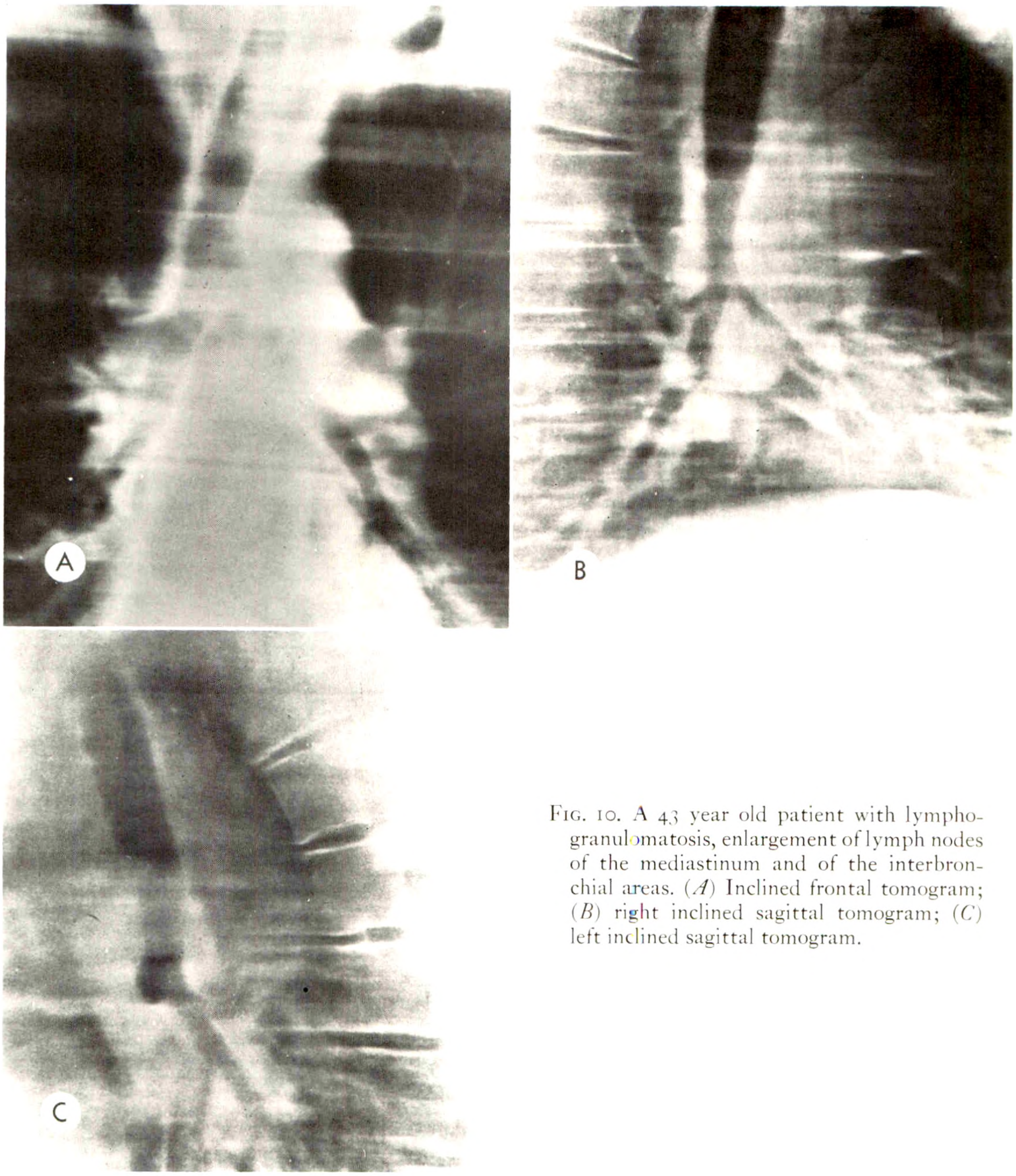


Fig. 10. A 43 year old patient with lymphogranulomatosis, enlargement of lymph nodes of the mediastinum and of the interbronchial areas. (*A*) Inclined frontal tomogram; (*B*) right inclined sagittal tomogram; (*C*) left inclined sagittal tomogram.

made with an angle of 60 degrees and shows a large bronchial carcinoma of the right lung. The narrowed bronchi and the wall infiltration are distinctly visible.

Wall infiltrations of the bronchi with stenosis are also well demonstrated. Figure 9*A*, an inclined frontal tomogram, shows the shadow of a bronchial carcinoma at the branching of the upper lobe bronchi. In Figure 9*B*, an inclined left sagittal tomogram, it is evident that the tumor has already infiltrated the wall of the lower lobe bronchus.

Enlarged lymph nodes in various areas are easily seen on inclined tomograms. Figure 10 shows the tomograms of a patient with lymphogranulomatosis. The inclined frontal tomogram (*A*) demonstrates en-

larged lymph nodes of the paratracheal, interaortopulmonary, intertracheobronchial and parts of the interbronchial areas. Most of the interbronchial areas are better visible on the inclined right (*B*) and left (*C*) sagittal tomograms.

SUMMARY

The technique of inclined tomography, for the diagnosis of tumors of the thorax is described. Its advantages as compared to conventional tomography are discussed and illustrative examples are given.

Strahleninstitut
Universitätskliniken
665 Homburg (Saar)
Germany

REFERENCES

1. Boyden, E. A. Segmental Anatomy of the Lungs: a Study of the Patterns of the Segmental Bronchi and Related Pulmonary Vessels. McGraw-Hill Book Company, Inc., New York, 1955.
2. Bozzetti, G. La realizzazione practica della stratigrafia. *Radiol. med.*, 1935, *22*, 257–267.
3. Brock, R. C. The Anatomy of the Bronchial Tree: with Special Reference to the Surgery of Lung Abscess. Oxford University Press, London, 1946.
4. Ellis, F. H., Jr., Grindlay, J. H., and Edwards, J. E. The bronchial arteries: II. Their role in pulmonary embolism and infarction. *Surgery*, 1952, *31*, 167–179.
5. Esser, C. Topographische Ausdeutung der Bronchien im Röntgenbild. Georg Thieme Verlag, Stuttgart, 1957.
6. Frain, C., Roujeau, J., Marlois, R., and Talamas. Étude tomographique de l'arbre trachéo-bronchique. *J. franç. méd. et chir. thorac.*, 1954, *8*, 519–522.
7. Frain, C., Even, R., Roujeau, J., Marlois, R., and Talamas. Exploration tomographique en frontale oblique de l'arbre trachéo-bronchique. *J. de radiol., d'électrol. et de méd. nucléaire*, 1955, *36*, 154–158.
8. Frain, C., and Gaucher, Mme. Tomographie thoracique en frontale oblique et exploration vasculaire (note préliminaire). *J. de radiol., d'électrol. et de méd. nucléaire*, 1957, *38*, 848–851.
9. Frain, C., and Duquesne. L'arbre trachéo-bronchique en tomographie oblique. *J. de radiol., d'électrol. et de méd. nucléaire*, 1962, *43*, 297–403.
10. Frey, E. Tumordiagnostik des Mediastinums durch frontale Schrägtomographie. *Fortschr. a. d. Geb. d. Röntgenstrahlen u. d. Nuklearmedizin*, 1962, *97*, 441–448.
11. Gebauer, A., Muntean, E., Stutz, E., and Vieten, H. Das Röntgenschichtbild. Georg Thieme Verlag, Stuttgart, 1959.
12. Grossmann, G. Tomographie. *Fortschr. a. d. Geb. d. Röntgenstrahlen*, 1935, *51*, 61–80, 191–208.
13. Herrnheiser, G. Röntgenanatomie der Lunge. *Fortschr. a. d. Geb. d. Röntgenstrahlen*, 1951, *74*, 623–648.
14. Kováts, F., and Zsebök, Z. Röntgenanatomische Grundlagen der Lungenuntersuchung. Akademia Kiadó, Budapest, 1959.
15. Laubenberger, T. Eine neue Konstruktion zur Anfertigung von Neige-Frontalschichten mit dem Siemens-Transversal-Planigraphen. *Röntgen Blätter*, 1963, *16*, 249–255.
16. Link, R., and Strnad, F. Tumoren des Bronchialsystemes unter besonderer Berücksichtigung bronchoskopischer und röntgenologischer Untersuchungsmethoden. Springer-Verlag, Berlin, 1956.
17. Marlois, R. Exploration tomographique de l'arbre trachéobronchique à l'aide d'un balayage horizontal. Thèse, Paris, 1956.
18. Markovits, P., and Desprez-Curely, J. P. Inclined frontal tomography in examination of mediastinum. *Radiology*, 1962, *78*, 371–380.
19. Sommer, F., and Laubenberger, T. Die geneigte Frontaltomographie des Thorax. *Radiologe*, 1963, *3*, 347–351.
20. Sommer, F., and Laubenberger, T. Die geneigte Sagittalschichtuntersuchung des Thorax. *Fortschr. a. d. Geb. d. Röntgenstrahlen u. d. Nuklearmedizin*, 1964, *101*, 85–89. (Abstr. Year Book of Radiology, 1965–1966 Series. Year Book Medical Publishers Inc., Chicago, Ill.)
21. Tempini, G. B., and Pazienza, C. L'esame stratigrafico del torace secondo piani obliqui rispetto ai piani frontali. *Radiol. med.*, 1953, *39*, 36–48.
22. Szenes, T. Verfahren zur Herstellung schräger Röntgenschichtaufnahmen. *Acta med. hung.*, 1959, *13*, 329–339.
23. Vallebona, A. Axial transverse laminagraphy. *Radiology*, 1950, *55*, 271–273.
24. Voigt, O. Eine einfache Technik zur Anfertigung von Tracheobronchotomogrammen mit normalen Schichtgeräten. *Röntgen Blätter*, 1964, *17*, 33–42.

# ERRORS IN DIAGNOSTIC RADIOLOGY*

## ON THE BASIS OF COMPLACENCY

*By* MARCUS J. SMITH, M.D.
SANTA FE, NEW MEXICO

"... *let every student of nature take this as a rule; that whatever his mind seizes and dwells upon with particular satisfaction is to be held in suspicion* ..."

—Francis Bacon

ALTHOUGH much excellent work has been done in assessing the accuracy of diagnostic examinations[9] and the nature of perceptual error,[28] very little has been accomplished in exploring what Garland referred to as the "unexplained human equation in diagnostic procedures." In this presentation an attempt is made to evaluate the human error in a very specific, nonteaching radiologic practice, with both small hospital and office services. Included are a description of the method of obtaining material, a broad classification of all (known) errors in 6 general categories, and a detailed description, with comments, of the varied manifestations of the first of these categories—errors attributed to the attitude of complacency.

### METHODS

The two major sources of knowledge of errors were clinicians and radiologists. Clinicians often volunteered information but more often had to be queried as to the outcome of a specific case. Of the volunteered data, it was of interest to note that most came from those referring physicians who were in the habit of looking at roentgenograms of their own patients. Surprisingly little information was revealed by postmortem examinations.

Of the information supplied by radiologists, most was from a personal file of long duration, also containing errors noted by regional radiologists. More recently, an incomplete form of double reading was used, based on the daily changing of location of radiologists. This method permitted considerable cross-checking of interpretations and proved to be very productive in uncovering radiologic errors. A review of the last 100 recorded errors showed that 72 per cent were revealed by this process. Two minor sources of information were the occasional perceptive technician in a rural installation and (fortunately rare) the disgruntled patient returning from "elsewhere."

The study does not provide a figure for total error, since a complete follow-up and continuous double reading were not feasible. However, a supplementary study was obtained, in which there was double reading of 300 consecutive office examinations. Disagreements totalled 30 per cent of all interpretations. Since most errors were found by dual reading, the guarded assumption was made that total error is probably close to this figure, and not too dissimilar to statistics presented for errors in many varied radiologic and nonradiologic procedures.[7,10,24,30] It should be emphasized that the impressions and statistics presented in this paper cannot and should not be extended to any radiologic practice elsewhere.

Several impressions obtained during this period seem worth recording. One is relevant to the group discussions by radiologists that often follow the discovery of an error. These discussions encourage study and constructive thinking in areas not customarily scrutinized. Another concerns the accelerated findings of errors when it is known that such an interest exists. It also

* Presented at the Sixty-fifth Annual Meeting of the American Roentgen Ray Society, Minneapolis, Minnesota, September 29–October 2, 1964.

seems probable that the actual pursuit of errors of others improves one's own critical and discriminating abilities; it also produces occasional feelings of insecurity about personal ability, and resignation to the unhappy prevalence of error.

## CLASSIFICATION

A classification of the causes of error was attempted. All errors were basically those of commission or omission. Furthermore, all of them could be placed into a false negative group (under-reading), a false positive group (over-reading), or a false emphasis group (misinterpretation). This grouping did not help in understanding the nature of the enemy, and other classifications were sought. The Seven Deadly Sins seemed quite practical, but were discarded since no instance of (radiologic) error could be attributed to the Sin of Lechery.

In searching the literature, the early classification of medical errors by Browne was found, as reported by Bean,[3] then the four Idols, or false notions of men, of Bacon,[1] and in more recent years, the extensive listing by Bean. None of these classifications was ideal, probably because most errors, like diseases, have no single cause, and an ideal grouping should be one in which the categories are mutually exclusive. With credit to the three B's, the somewhat oversimplified but workable classification seen in Table I was then devised. (Bean's contributions will be noted in discussion of the separate classes.) This classification is based on the arbitrary and subjective assignment of each instance of error into one or another of the 6 subheadings. The subheadings are self-explanatory and are the presumed basic causes of errors. Class I errors are the subject of the present paper. It is hoped that the errors assigned to Classes II to VI will be the subjects of future communications.

Table I

| Class | Cause of Error | Bacon[1] | Browne (reported by Bean[3]) |
|---|---|---|---|
| I | Complacency | Idols of Cave | Authority<br>Popular Conceits |
| II | Faulty Reasoning | Idols of Theater | Misapprehension |
| III | Lack of Knowledge | | Human Nature |
| IV | Faulty Perception | Idols of Tribe | Credulity |
| V | Poor Communication | Idols of Market Place | |
| VI | Unknown<br>Miscellaneous | | Endeavors of Satan |

## CLASS I: ERRORS CAUSED BY COMPLACENCY

The meaning of "complacency" is best expressed in the following sentence by Fowler:[8] "He is complacent who is pleased with himself or his state, or with persons and things as they affect him." It is suggested that the following 10 types of errors all derive from complacency and its corollary, the settled mind. It should also be pointed out that they are predominantly examples of over-reading (false positive) and misinterpretation.

### I. THE UNJUSTIFIED INFERENCE THAT A LEGITIMATE ROENTGEN ABNORMALITY IS THE CAUSE OF THE PATIENT'S DISTRESS

Occasionally, the disorder that has been found is the lesser part of the patient's disease or is not at all related to his important problem. In this situation the clinician is diverted from his real goal of finding out "not only what the patient has got, but what the patient is suffering from."[18]

Figure 1 shows the esophageal diverticulum of a 60 year old man who complained of tightness in his throat, weakness, a 14 pound weight loss, and a moderately severe anemia. Could the diverticulum cause the anemia? The radiologist thought that this was possible, either as the source of chronic bleeding or in some manner similar to the Plummer-Vinson syndrome. On admission for extirpation, other clinical features were recognized and bone marrow smears were compatible with pernicious anemia. The significant clinical condition had almost

been obscured by the overly presumptuous radiologic opinion.

*Comment.* Improvement in this category would seem to lie in thorough interdepartmental or consultant discussions. Such conferences are rare in our practice as a result of the heavy pressure of routine work. Our impression is that many clinicians, also harried and restricted by boundaries of schedule and demands of patients, are uncritical acceptors of roentgenologic reports.

2. APPARENT ALTERATIONS OF NORMAL ANATOMY INTERPRETED AS DISEASE STATES

Of the innumerable anatomic variants that border on the normal, the most disturbing at the postgraduate level are in the duodenum, stomach and low back.

In the lumbar spine, the local radiologists and orthopedists cannot agree among themselves as to the presence or significance of the orientation or contour of facets, acuteness of the lumbosacral angle, dimensions of the lumbosacral interspace, and to a lesser extent, variations of spinous and transverse processes. In the roentgenogram shown in Figure 2, the radiologist reported "relative narrowing of the lumbosacral interspace." Eventual treatment of this patient would then depend on the aggressiveness of the consultant, or employment could be denied if this were part of a pre-employment study. Some authors put much credence in these findings,[14,25] while others deny their significance.[15,22,24] That all of these findings are present in varying percentages of normal subjects supports the contention that they represent variants of little or no importance. Industrial and medical-legal pressures favor over-reading, as do the equivocal statements in text books. Too few fundamental correlative studies are available.

Over-reading of the normal mucosa of the stomach and duodenum leads to the erroneous diagnoses of gastritis and duodenitis. One hundred consecutive gastro-intestinal examination reports were reviewed and gastritis was found reported in

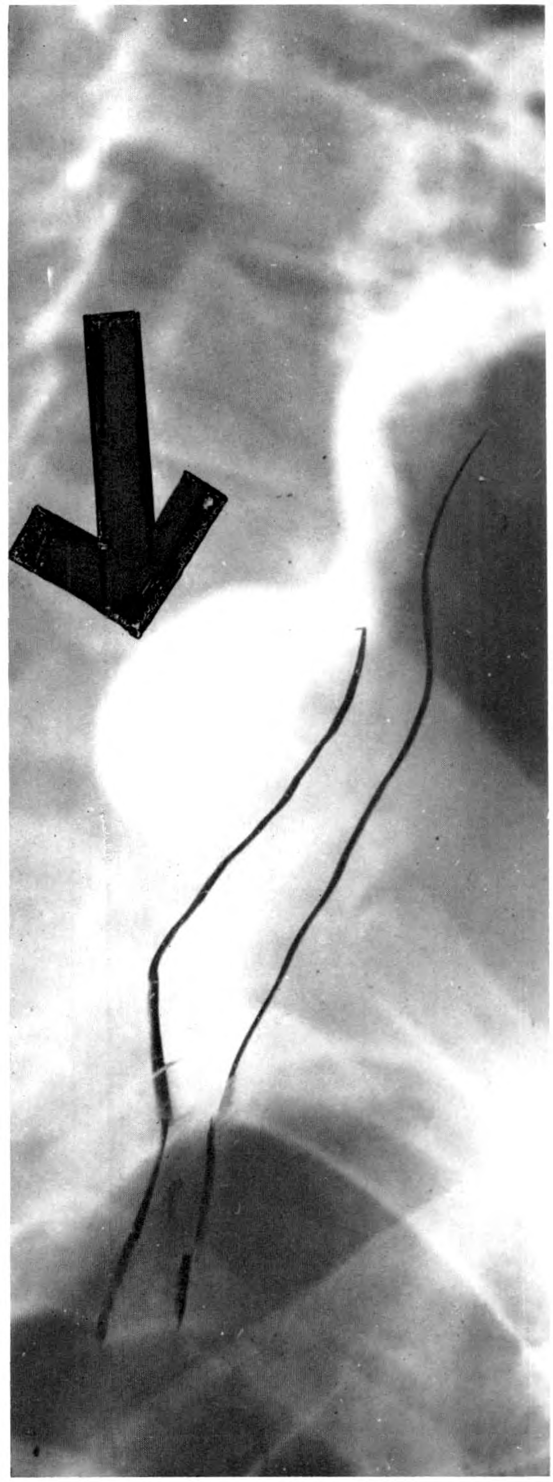

Fig. 1. Esophageal diverticulum presumed to be cause of anemia. (Reproduced with permission from the *Rocky Mountain M. J.*, May, 1961.)

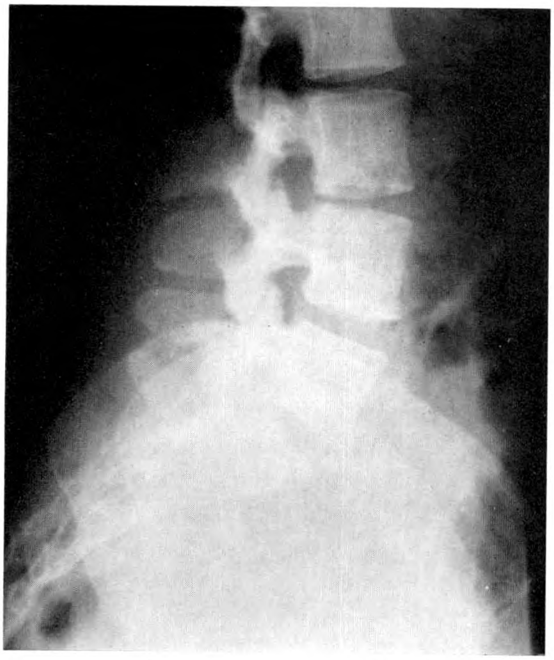

Fig. 2. Lateral view of lumbosacral spine reported as "narrowed lumbosacral interspace."

17 per cent and duodenitis in 13 per cent. In contrast, authorities such as Bockus[5] and Templeton[27] feel that the roentgenologic findings in both of these conditions are indistinct and that these diagnoses should rarely be made. In Figure 3, *A* and *B* the diagnoses of both gastritis and duodenitis were made roentgenologically. The patient died of a coronary thrombosis 1 month after his examination, and at autopsy, the stomach and duodenum were entirely normal. Figure 4, *A* and *B* shows a 73 year old man who was thought to have duodenitis. His symptoms persisted and 3 weeks later a re-examination showed an esophageal ulcer (Fig. 4 *C*), missed originally, and a normal duodenum.

*Comment.* There has been some reduction in over-reading of minor low-back alterations, but little change in attitude toward gastritis and duodenitis. It is of value to review etiologic studies, such as Templeton's. Another, by Ghormley,[11] evaluated 2,000 patients with low back pain and sciatica. He did not even list the lumbosacral angle in this study, feeling that it was of doubtful significance.

### 3. THE LABELLING OF PHYSIOLOGIC VARIATIONS AS ABNORMAL

These errors arise with disturbing persistence in interpretation of children's chest

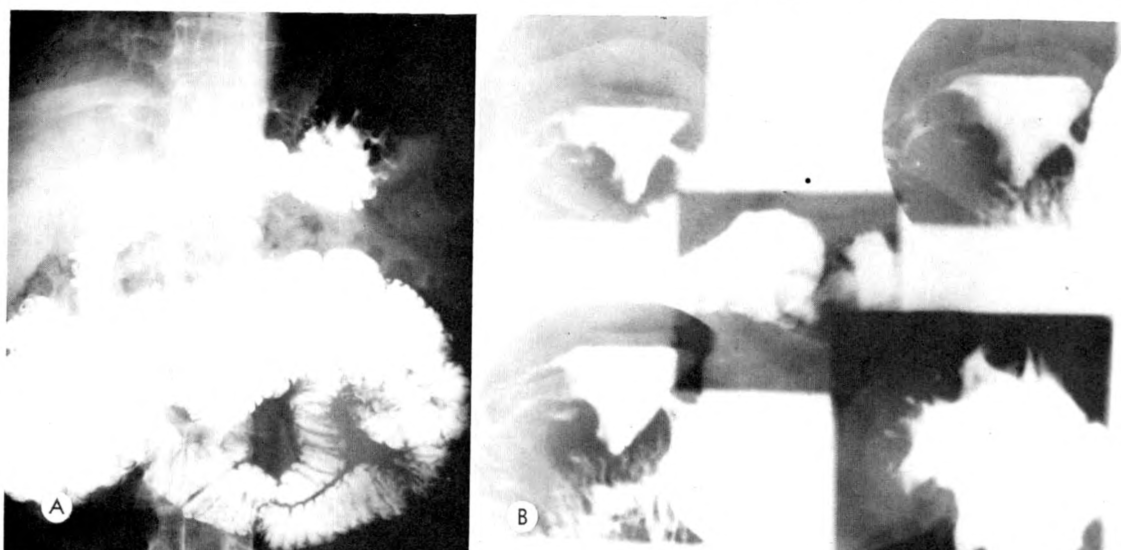


Fig. 3. Roentgenologic diagnoses of gastritis and duodenitis. (*A*) No specific deformity is seen on this roentgenogram of the upper gastrointestinal tract. (*B*) Spot roentgenograms of the duodenal bulb showed anatomic variation of the postbulbar mucosa. Spot roentgenogram of the gastric fundus (lower right corner) showed "prominent" mucosa. At autopsy, 1 month later, no abnormality was found in the stomach or duodenum.

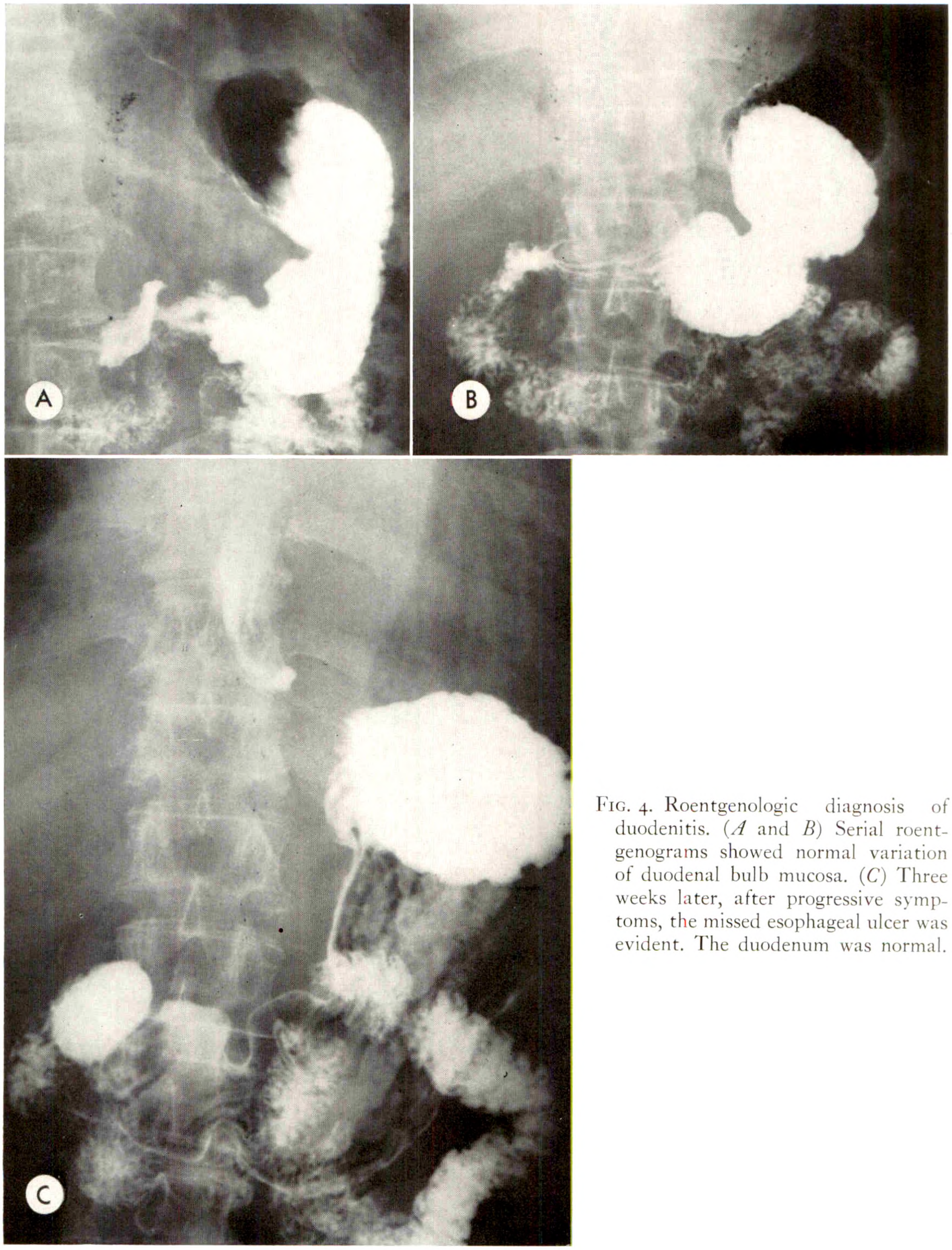


Fig. 4. Roentgenologic diagnosis of duodenitis. (*A* and *B*) Serial roentgenograms showed normal variation of duodenal bulb mucosa. (*C*) Three weeks later, after progressive symptoms, the missed esophageal ulcer was evident. The duodenum was normal.

roentgenograms, in differentiating senescence (physiologic aging) from senility, and, perhaps most seriously, in the pseudo-ulcer diagnoses of the duodenal bulb. As in the preceding category, a sense of satisfaction is derived from attaching a label to a roentgenographic finding; perhaps this is based on the gratification of identifying

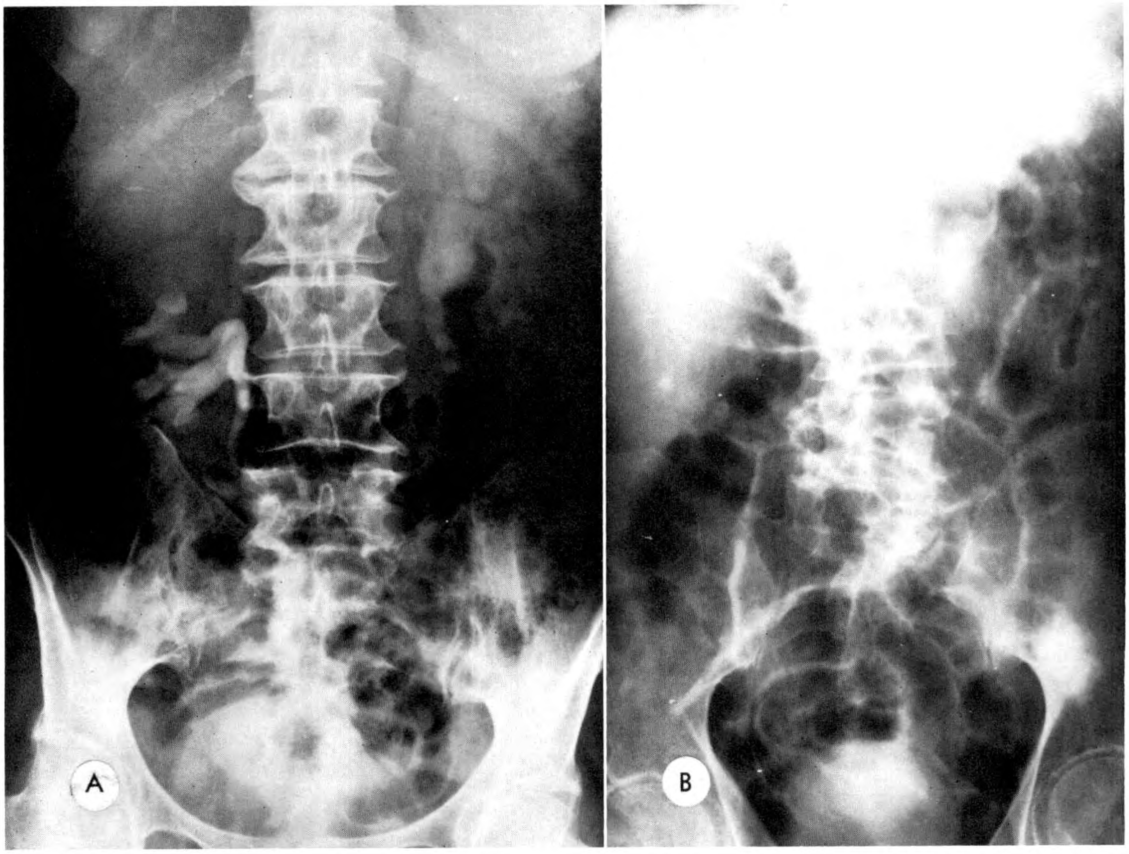


Fig. 5. Over-reading of senescent changes. (*A*) Spurs of lumbar spine called "osteoarthritis." "Cystitis" unjustly inferred from this late pyelogram. (*B*) Fifteen minute pyelogram of another elderly patient. Diagnosis of "cystitis" was made because of thickening of bladder wall.

with the clinician or patient.

Some of the wear-and-tear changes in the aged, occasionally over-read as diseases, are seen in Figure 5, *A* and *B*. Indicating that osteophytes are evidence of osteoarthritis is a common occurrence, while it is well known that they are representative of protective senescent processes.[17] Attaching undue significance to the usual visible medial vascular sclerosis also is commonplace, without regard to the presence or absence of peripheral vascular obstruction. An attempt should be made[2] to distinguish medial from intimal vascular calcification. In both of these patients in Figure 5, *A* and *B*, the diagnosis of "cystitis" was made by two different radiologists after noting or presuming the presence of a thickened bladder wall or increased trabeculations. However, these signs are only evidence of hypertrophy of the bladder muscles.[22] Similarly noted has been the over-diagnosing of senile osteoporosis, senile emphysema (Fig. 6) and bronchitis from single roentgenograms and without clinical reference.

In babies one of the common and persistent errors occurs in evaluating the chest. If the roentgenogram is made in expiration, the apparent cardiomegaly is still a bugbear, although it is a well-known phenomenon, and the central lung area haziness is often misinterpreted as inflammatory disease. Figure 7*A* was so misinterpreted in this patient; in Figure 7*B*, made later the same day, the normal appearance in inspiration is clearly evident. In Figure 8*A*, the radiologic report read: "cardiomegaly, increased lung markings, bronchitis and probably pneumonia." In Figure 8*B* of the same baby made 2 weeks later, it becomes

quite clear that the previous roentgenogram was made in expiration and that the multiple diagnoses were unwarranted.

In the duodenum, peristaltic waves, physiologic variations of filling interpreted as spasm or irritability, and indentations by neighboring structures, such as the gallbladder, are frequently misinterpreted as evidence of duodenal ulcer, using such qualifying adjectives as "minimal," "presumptive," or "possible." The implication to the clinician is that there is an obscure ulcer or a pseudoulcer syndrome.[4] Figure 9, *A–D* shows a duodenum reported as being ulcerated by 3 different radiologists on 4 examinations. At a subsequent emergency operation, a bleeding esophageal varix was found as was a normal duodenum. Figure 10, *A* and *B* shows the bulb of another patient in whom the diagnosis of duodenal ulcer was returned after 3 roentgenologic examinations, on improper criteria. At operation, the bulb was normal, and localized collagen disease of the jejunum was found.

*Comment.* Reports of 100 gastrointestinal series were studied and showed that duodenal ulceration was intimated in 8 per cent and an additional 5 per cent of cases were labeled ulcer without demonstration of a crater. Part of the error is in assuming that physiologic variations can be secondary signs of duodenal ulcer. Many of these errors would not occur if one really believes

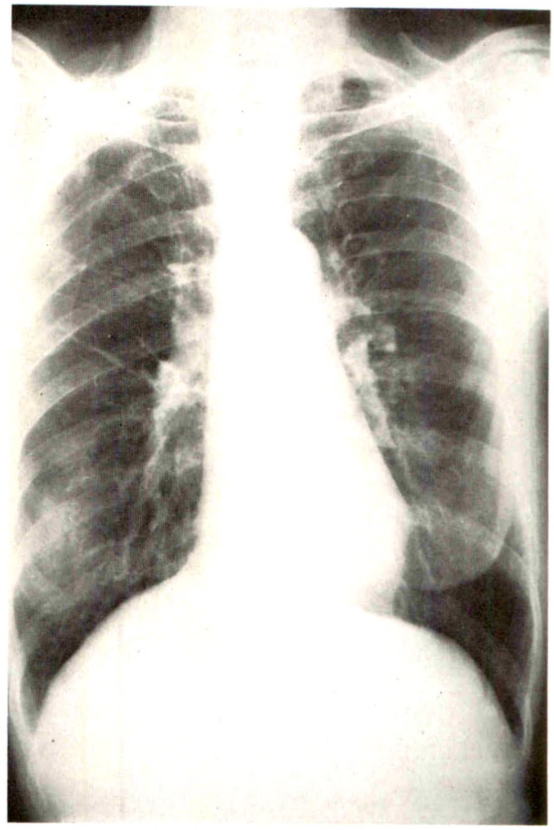

FIG. 6. Roentgenologic diagnosis of senile emphysema, based on this single roentgenogram. There was no investigation of diaphragmatic motion, size of chest or status of the patient.

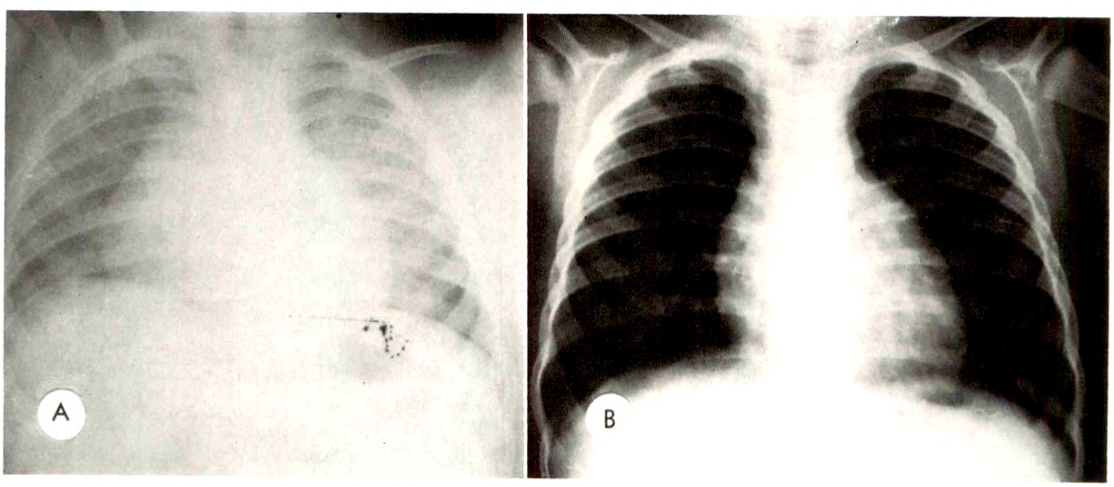


FIG. 7. (*A*) Expiration chest roentgenogram. (*B*) Inspiration chest roentgenogram of the same patient, made the same day.

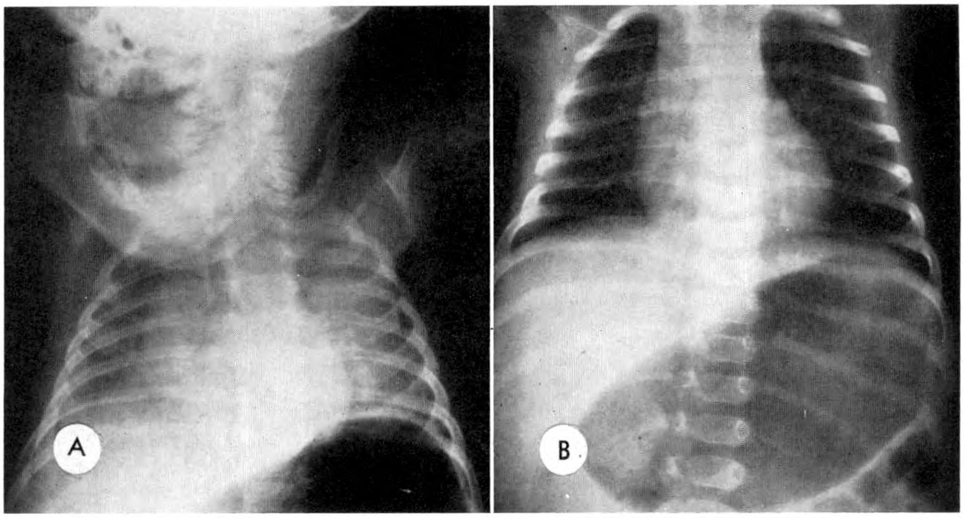

FIG. 8. (*A*) Expiration chest roentgenogram. (*B*) Inspiration chest roentgenogram of same patient, 2 weeks later.

that secondary signs of duodenal ulcer are of little value, as pointed out by many authorities, and particularly in a recent critical study by Stein *et al.*[26]

Dual reading also helps to eliminate some of these errors. One hundred consecutive gastrointestinal examinations were so studied and patients were recalled for re-

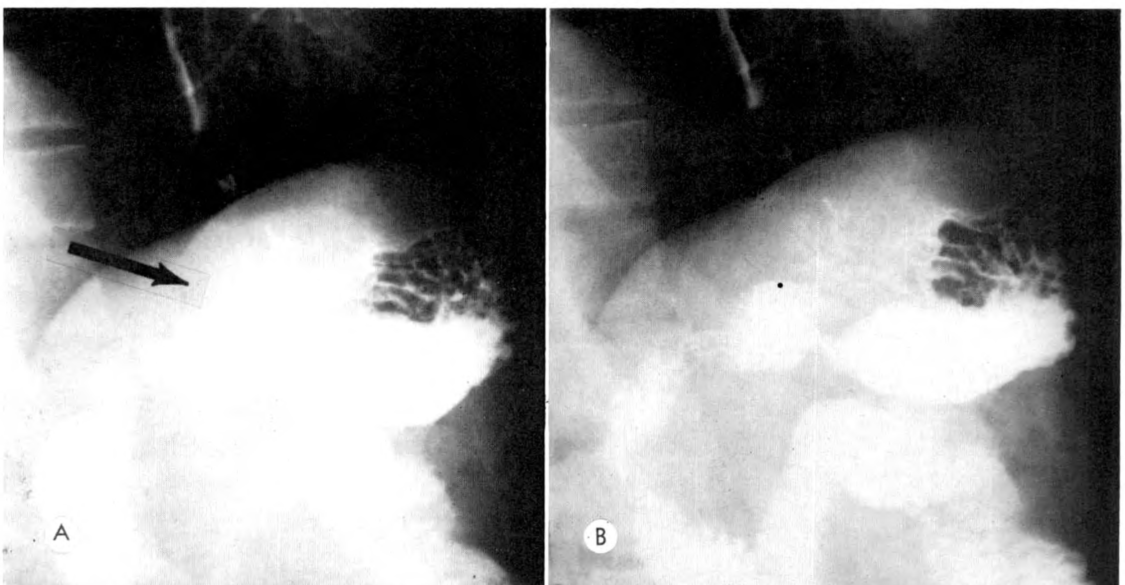

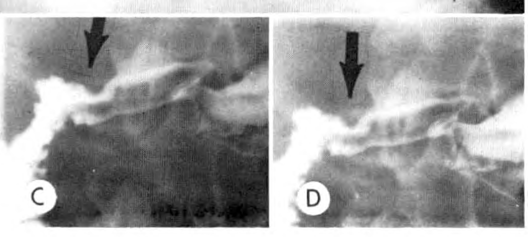

FIG. 9. (*A* and *B*) Serial roentgenograms of the duodenal bulb. (*C* and *D*) Spot roentgenograms of same patient show indentation (arrows) of apical portion of bulb, interpreted as evidence of duodenal ulcer. The patient was explored for bleeding and an esophageal varix was found The duodenum was normal.

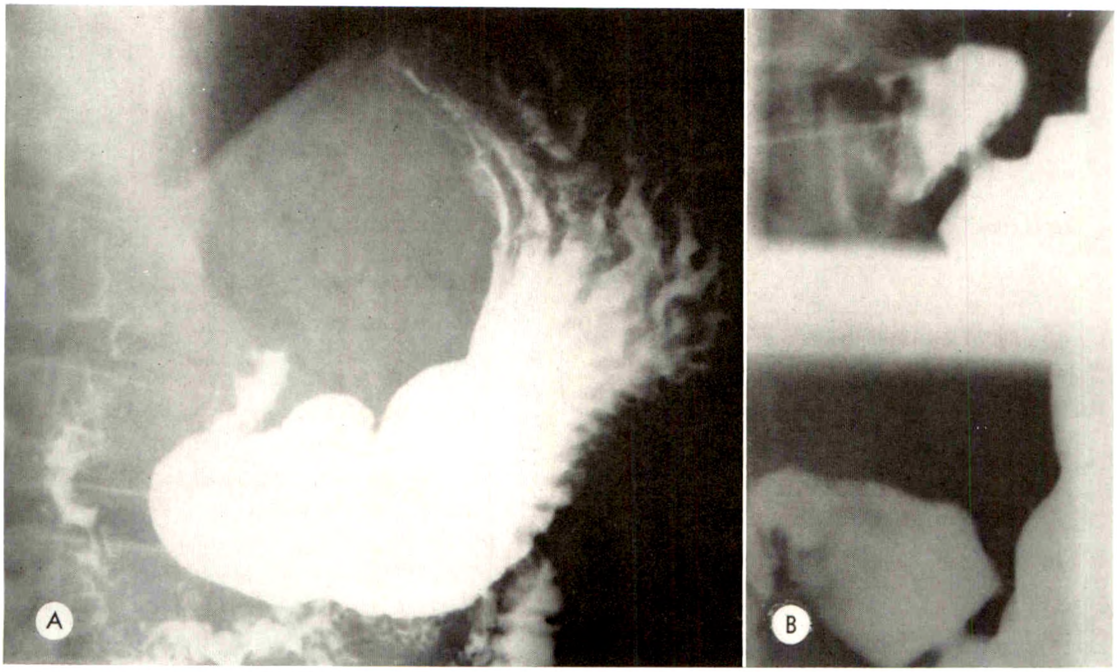


Fig. 10. Over-reading of physiologic variations. (*A*) Apparent "spasm" of the bulb led to erroneous diagnosis of duodenal ulcer. (*B*) Same patient, but different examination. "Spasm" still reported, despite distensibility. Barium trapped in a fold was interpreted as evidence of ulcer. Three examinations were recorded as duodenal ulcer. At operation, the duodenum was normal and collagen disease of the jejunum was found.

peat procedures when one observer expressed dissatisfaction. Subsequently, 12 per cent of the reports were revised. Dual reading has had only a minor and episodic effect on the over-reading of bronchitis and pneumonia in babies, and little effect on the evaluation of senescent changes. Additional procedures that will help clarify some of the physiologic changes have been helpful. For example, inspiration and expiration roentgenograms of the chest in babies have excluded some pseudopneumonias and air contrast studies of the bulb have eliminated some pseudoulcers.

#### 4. HOBBY-RIDING, A SPECIAL FORM OF OVER-READING NORMALS

If a disease or organ is subjected to overzealous investigation, "one can recognize the smallest abnormality to that organ, the slightest manifestation of that ailment, while swallowing the camel of some greater derangement."[18] Or, one can have a morbid preoccupation with a specialized technique and succeed in finding disease where none exists. It is suspected, but not proved, that our records show too many hiatus hernias, esophageal rings, and urethritides demonstrated by special studies.

*Comment.* No inroads were made into this problem. One's own methods seem sacred, and attempted criticism of the techniques of others lead to resentment, which has hampered the present investigation.

#### 5. MYTHICAL MALADIES

Bean[3] used this phrase to describe nonexistent disease, such as autointoxication and status lymphaticus. Clendening and Hashinger[6] coined the word "factition"—a "habit doctors have of talking about a pathologic condition which does not exist in nature . . . a kind of faery pathology . . . a blind man looking in a dark room for a black cat which wasn't there." Reviewing the radiologic literature of 50 years ago, several mythical maladies were encountered. For example, a patent ileocecal valve was considered evidence of "alimentary toxemia."

TABLE II

POSSIBLE MYTHICAL (AND SEMANTIC) CONDITIONS*

| |
|---|
| Roentgenologic Diagnosis |
| Pylorospasm (adult, no ulcer) |
| Prominent pyloric muscle (adult) |
| Slow filling of duodenal bulb |
| Rapid motility at 6 hours |
| Ten per cent gastric retention at 6 hours |
| Ptosis, colon |
| Ileocecal valve, prominent lips |
| Ileocecal valve, trabeculated |
| Kink of ureter (no hydronephrosis) |
| Relaxed lumbar apophyseal joints |
| Minimal acute lumbosacral angle |
| Thickened lung markings |
| Slight prominence, pulmonary conus |

* From review of 200 consecutively numbered reports.

One hundred cases were cured by surgery.

It is impossible to know what our factitious maladies or conditions are today, but one suspects that there are some. A review of 200 consecutive roentgenologic reports produced the information seen in Table II. Undoubtedly some of these diagnoses and conclusions are of "faery pathology." A kink of the ureter without hydronephrosis[21] is not a disorder. The term "pylorospasm" when used by the impatient fluoroscopist, is mythical. One doubts whether any use of the term "pylorospasm" is justified.

*Comment.* Unfortunately, it takes historical perspective for the recognition of mythical maladies. One such condition, prolapsed gastric mucosa, is being relegated from a malady to a physiologic state.[16] How many others exist today is uncertain.

### 6. PREJUDICE

These errors arise from a sense of satisfaction with one's conclusions, investigations and opinions. They are the result of a biased point of view and lead inexorably to the failure to consider all possibilities. (Prejudice is not the only cause of such failure. Reasoning error and observer attitude,[9] such as pessimism or optimism, also can be responsible.) Gruver and Freis[18] studied diagnostic errors in 1,106 autopsied cases. Of the 6 per cent misdiagnosed, bias was felt to be responsible for 16 per cent.

The prejudiced observer makes his diagnosis on first seeing the patient, or the roentgenogram, or on first hearing the history. He cannot change his mind and remains silently unconvinced in the face of irrefutable data. It is particularly evident in the approach to diagnostic procedures on the senile patient.

An example of prejudice is shown in Figure 11, *A* and *B*. The observer had interpreted a roentgenogram (Fig. 11*A*) demonstrating a large zone of destroyed bone from a metastatic breast lesion. When the stomach was examined, he called the gross crater in the duodenal bulb (Fig. 11*B*) a "deformity" but did not use the word ulcer. The patient's peptic symptoms progressed and an additional examination 2 weeks later by a different radiologist again showed an ulcer crater. Treatment was then instituted and the patient's ulcer symptoms were alleviated. In the discussion, the original observer said that he felt that any disease the patient had was insignificant in comparison to her known cancer. He refused to acknowledge any other possibilities, and felt that the gastrointestinal examination should not have been ordered.

### 7. RECENCY

This stepchild of prejudice tends to make objective interpretations impossible. If the last gastric ulcer was malignant, there is more suspicion of the next one. This important and well-known psychologic attitude has influenced the interpretation of pulmonary lesions, particularly in the differentiation of pulmonary infarcts from pneumonia.

*Comment.* Attempts to discuss prejudice and the factor of recency have been unsuccessful, provoking resentment and hostility and have disturbed the atmosphere of friendly discussions.

### 8. PROVINCIALISM

The feeling of superiority to the referring general practitioner or the doctor in a smaller town or institution elsewhere is productive of some errors. Such errors arise

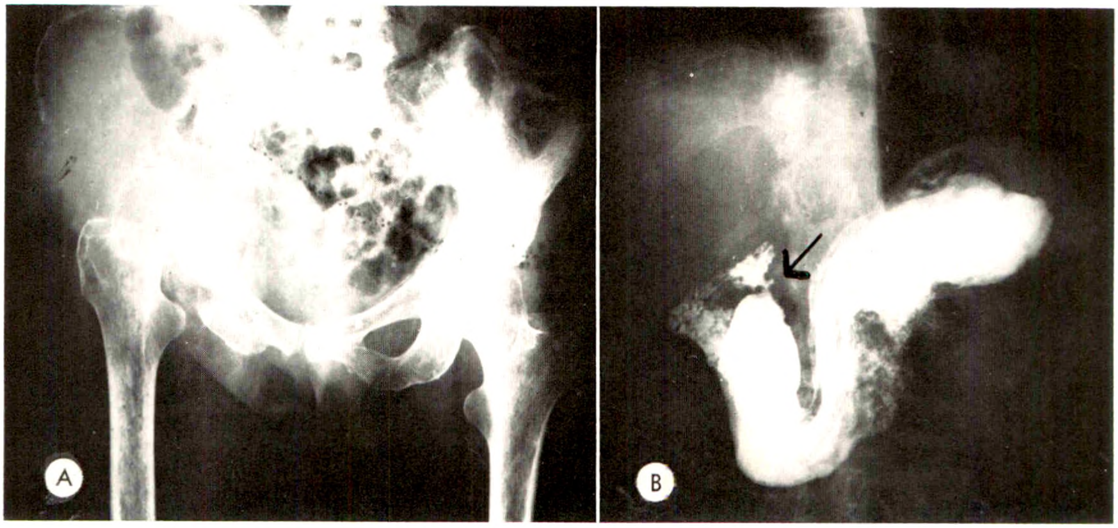


Fig. 11. Example of prejudice in a patient with metastatic carcinoma of the breast. (*A*) The pelvis shows a large zone of bone destruction. (*B*) Later, the observer would not call the overt crater (arrow) in the duodenum evidence of an ulcer because of his knowledge of the patient's condition and prognosis. He felt that the gastrointestinal examination was unnecessary.

from the attempt to prove the referring agency wrong. Also, a feeling of satisfaction with one's own knowledge and efforts makes it seem unnecessary to obtain someone else's roentgenograms or roentgenographic reports.

Figure 12, *A* and *B* shows a gallbladder considered normal. However, the radiologist did not call for the roentgenograms or report of a previous gallbladder study performed 3 years earlier in a regional office that showed characteristic, large, nonopaque calculi. Continued presence of the stones was later shown. (Error was compounded in this case by the use of high kilovoltage technique,[29] making the stones difficult to see.)

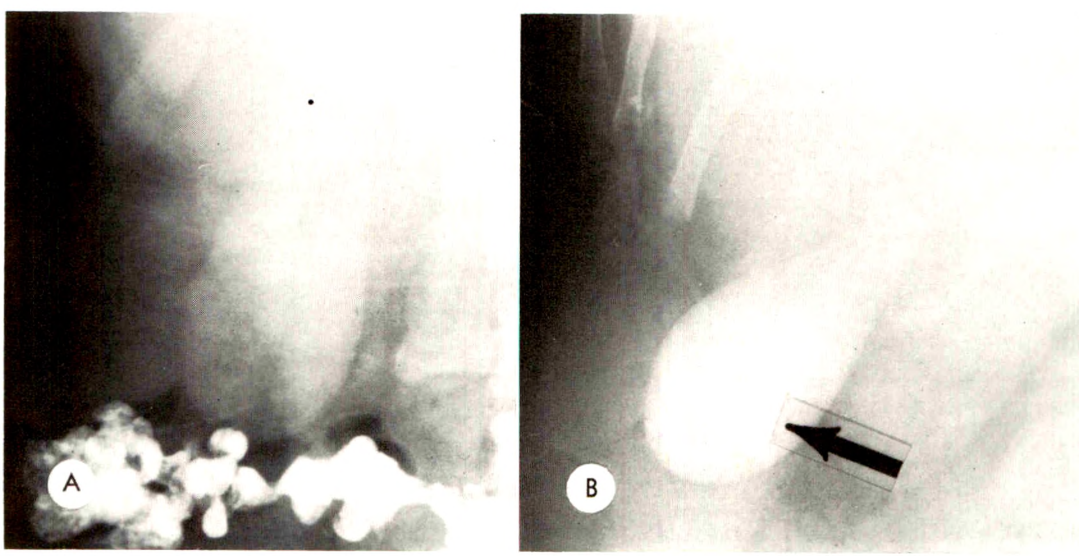


Fig. 12. Example of provincialism. (*A*) The gallbladder was considered normal. The radiologist did not call for roentgenograms made 3 years previously (*B*) on which gallstones were evident. The continued presence of stones was later confirmed.

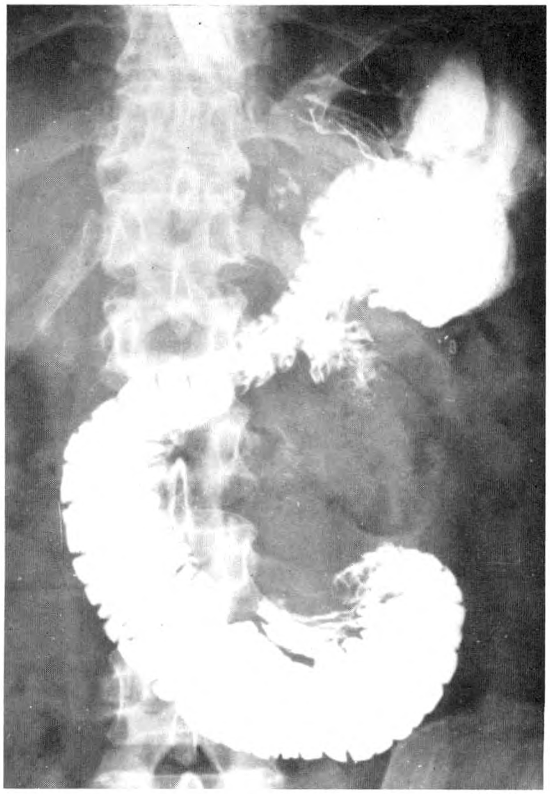

Fig. 13. Disregard of the obvious. An obstructed efferent loop was presumptuously alleged to be on the basis of hypoproteinemia.

*Comment.* Combating provincialism is possible by acknowledging the referring physician's diagnosis and discussing findings with him, even by long-distance telephone. Also, a diligent effort to obtain previous reports or roentgenograms would obviate many errors.

9. DISREGARD OF THE OBVIOUS

This is also a manifestation of the attitude that we are superior to, and should see more in our roentgenograms, than a nonradiologist. "Common diseases most commonly occur," but fear of equating with those less technologic makes us observe our roentgenograms more obliquely.

Figure 13 shows an obstructed jejunal loop considered by the radiologist to be caused by edema since the patient had a low serum protein level. Fluid and protein therapy failed to relieve the obstruction and, at operation, an adhesion was found. The radiologist's flight from the obvious was abetted by incomplete recall of Golden's treatise[12] on the role of hypoproteinemia in ileus.

*Comment.* There has been no improvement in this category.

10. CLINICAL MYOPIA

The notion that one needs to know no more than what is revealed by one's own methods leads to three different types of error. Gross misinterpretation derives from the failure to elicit significant clinical data before dictating reports. Later, the clinician may be blamed for not sending more information on the miniature requisitions, but why ignore the availability of the telephone, the patient's chart or the patient? Sometimes, the vital information may be absent, but more often the omission stems from the radiologist's deadly sitting habit and failure to circulate among clinicians and patients. Clinical myopia is fundamentally another of the Deadly Sins—the Sin of Sloth.

Another type of error in this category occurs after reading roentgenograms in which there is uncertainty as to the presence or absence of a finding, for example, a questionable fracture line. Immediate correlation with the patient will usually allow a decision to be made, often with avoidance of a false-positive report. This happens daily in an office practice in which an attempt is made to check each patient before discharging him. There are few accounts of the effect of clinical knowledge on the accuracy of film interpretation. Schreiber,[23] in a recent paper, indicates that the total performance of chest film readers is improved by a knowledge of clinical findings, with a decrease in the number of false-positive conclusions.

A third type of error caused by clinical myopia occurs following the report of a "negative" examination. It is well known that such statements should be qualified to indicate need for special or serial studies at appropriate intervals when there is suspicion of tuberculosis, osteomyelitis, aseptic necrosis and other situations.[20] Yet the radiologist who has not correlated with the

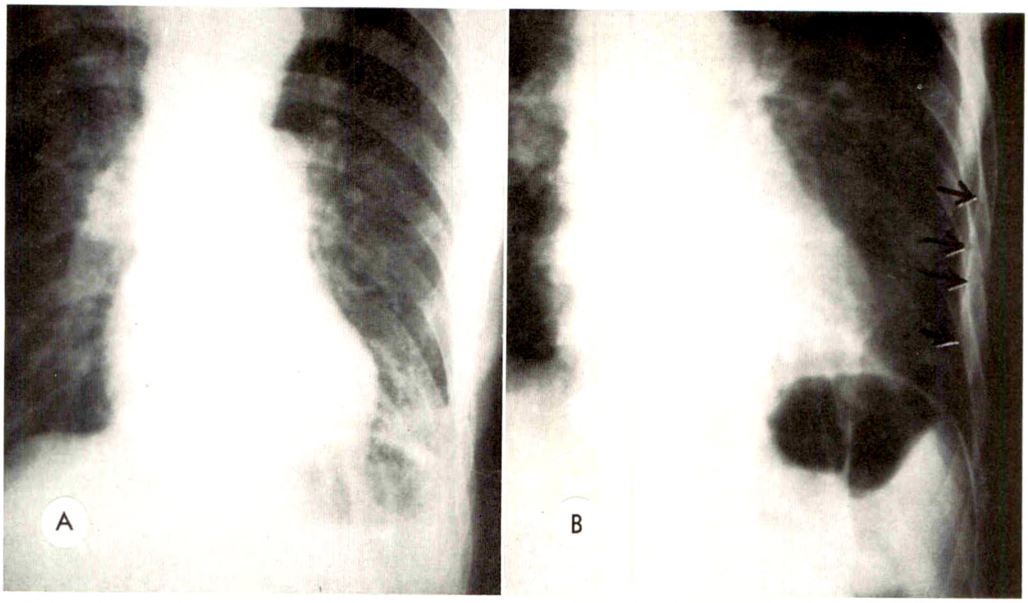


Fig. 14. Clinical myopia. (*A*) Abnormal changes at base of left lung read as "pneumonia," without knowledge of history of trauma. (*B*) A day later, the rib fractures were clearly evident and were also discernible on the original roentgenogram. The pulmonary lesion most likely represented a hematoma.

clinical findings can mislead the clinician with his arbitrary pronouncements.

Figure 14*A* shows fractured ribs and pulmonary hematoma. Without clinical information, the roentgenogram was read as showing pneumonia; the rib fractures (Fig. 14*B*) were not perceived. They would have been seen if the history had been known. Figure 15*A* shows the normal pelvis of a 7 year old boy who complained of right hip pain. The pain persisted and a limp developed. One year later another roentgenogram (Fig. 15*B*) showed changes of Legg-Perthes disease. Had the observer known the history, his awareness of the latent period for roentgenographic changes would have prevented a peremptory "negative" report, and earlier re-evaluation would have resulted.

*Comment.* Some progress has been made in correcting clinical myopia. Osler[19] advised that "wide contact with men in other departments may serve to correct the inevitable tendency to a narrow and per-

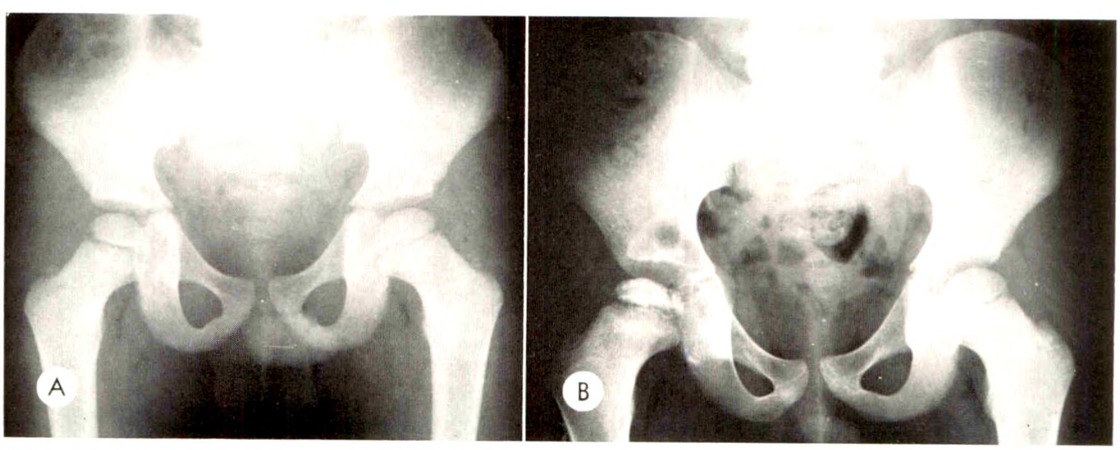


Fig. 15. (*A*) Roentgenogram of pelvis read as normal without the knowledge of symptoms—pain in the hip and limp. (*B*) A year later, the changes of Legg-Perthes disease were apparent. Had the clinical findings been known originally, the long delay before diagnosis might have been avoided.

verted vision in which the life of the anthill is mistaken for the world at large." Some radiologists attempt clinical correlation more vigorously than others. The hospital milieu seems to breed better correlation than the private office. There is now a policy of liberal consultation with other radiologists, but there are still other colleagues who are seen only at county medical society meetings. One also has grave doubts about the efficacy of pointing out that a radiologic report needs correlating with the clinical findings; the radiologist should make this effort, if it is possible.

## IMPRESSIONS AND CONCLUSIONS

1. Diagnostic disagreements occur in about one-third of all film readings.
2. About two-thirds of all errors are found by modified dual-reading techniques.
3. The search for and discussion of errors probably improves the critical ability.
4. Errors of complacency are primarily those of over-reading and misinterpretation.
5. More emphasis should be placed on the teaching of normal anatomic and physiologic variants, particularly in the low back and upper gastrointestinal tract.
6. It is felt, at this time, that such diagnoses as gastritis, duodenitis, cystitis and bronchitis should not ordinarily be made from conventional studies.
7. Special diagnostic procedures that permit differentiation and discrimination of physiologic changes are conducive to reducing errors.
8. Periodic double reading also aids such discrimination. In addition, it will emphasize areas of interpretative disagreement.
9. Some of our diagnoses are probably of mythical conditions.
10. Efforts to obtain previous roentgenograms, reports, and opinions from other radiologists and clinicians will eliminate some errors.
11. Before dictating a report, it is well to ask: "What does the patient manifest?" "What other data are needed?" "What else might this mean?"

## SUMMARY

More than 70 per cent of errors in a rural diagnostic radiology practice were uncovered by modified dual-reading methods. The incidence of disagreements in interpretations is about 30 per cent.

A general classification of all errors is presented; shortcomings of the classification are mentioned.

The present paper concerns errors caused by complacency; ten subgroups are described with examples. These are: (1) attributing unjustified significance to positive findings; (2, 3) erroneous labelling of anatomic and physiologic variants as diseases; (4) hobby-riding; (5) reporting of mythical maladies; (6) prejudice; (7) the factor of recency; (8) provincialism; (9) searching for the rarity; and (10) clinical myopia.

It is believed that this study has been somewhat helpful in reducing the incidence of errors arising in categories 2, 3, 5, 8 and possibly 10.

P.O. Box 1812
Santa Fe, New Mexico

The assistance of Drs. Elliott I. Wyloge and Charles F. Veverka is gratefully acknowledged, as well as the cooperation and advice of Drs. Murray M. Friedman, Carol K. Smith, Richard M. Angle and George E. Humphrey.

## REFERENCES

1. Bacon, F. The New Organon and Related Writings. Liberal Arts Press, New York, 1960, pp. 47–66.
2. Barnum, E. N. Roentgenographic differentiation of peripheral arteriosclerosis. Am. J. Roentgenol., Rad. Therapy & Nuclear Med., 1952, *68*, 619–626.
3. Bean, W. B. Natural history of error: pseudodoxia endemica. *A.M.A. Arch. Int. Med.*, 1960, *105*, 184–193.
4. Bockus, H. L. Gastroenterology. Volume I. W. B. Saunders Company, Philadelphia, 1944, pp. 431–432.
5. Bockus, H. L. Gastroenterology. Volume II. W. B. Saunders Company, Philadelphia, 1944, pp. 82–84.
6. Clendening, L., and Hashinger, E. H. Methods of Diagnosis. C. V. Mosby Company, St. Louis, 1947, p. 14.

7. Cooley, R. N., Agnew, C. H., and Rios, G. Diagnostic accuracy of barium enema study in carcinoma of colon and rectum. Am. J. Roentgenol., Rad. Therapy & Nuclear Med., 1960, *84*, 316–331.
8. Fowler, H. W. A Dictionary of Modern English Usage. Oxford University Press, London, 1960, p. 87.
9. Garland, L. H. On scientific evaluation of diagnostic procedures. *Radiology*, 1949, *52*, 309–328.
10. Garland, L. H. Studies on accuracy of diagnostic procedures. Am. J. Roentgenol., Rad. Therapy & Nuclear Med, 1959, *82*, 25–37.
11. Ghormley, R. K. Etiologic study of back pain. *Radiology*, 1958, *70*, 649–653.
12. Golden, R. Some problems in abnormal intestinal physiology associated with peritoneal adhesions and ileus. Am. J. Roentgenol. & Rad. Therapy, 1946, *56*, 555–568.
13. Gruver, R. H., and Freis, E. D. Study of diagnostic errors. *Ann. Int. Med.*, 1957, *47*, 108–120.
14. Henry, G. W., Larsen, I. J., and Stewart, S. F. Roentgenologic criteria for appraising human back as economic asset or liability. Am. J. Roentgenol., Rad. Therapy & Nuclear Med., 1958, *79*, 658–672.
15. Levin, E. J., and Felson, B. Asymptomatic gastric mucosal prolapse. *Radiology*, 1951, *57*, 514–520.
16. Meschan, I., and Farrer-Meschan, R. M. F. Important aspects of roentgen study of normal lumbosacral spine. *Radiology*, 1958, *70*, 637–648.
17. Nathan, H. Osteophytes of vertebral column: anatomical study of their development according to age, race, and sex with considerations as to their etiology and significance. *J. Bone & Joint Surg.*, 1962, *44A*, 243–268.
18. Ogilvie, W. H. Surgery: Orthodox and Heterodox. Charles C Thomas, Publisher, Springfield, Ill., 1949, p. 122.
19. Osler, W. Aequanimitas with Other Addresses to Medical Students, Nurses and Practitioners of Medicine. Third edition. Blakiston Company, New York, 1942, p. 419.
20. Rigler, L. G. Possibilities and limitations of roentgen diagnosis. Am. J. Roentgenol. & Rad. Therapy, 1949, *61*, 743–761.
21. Rolnick, H. C. Practice of Urology. Volume 1. J. B. Lippincott Company, Philadelphia, 1949, p. 290.
22. Rolnick, H. C. Practice of Urology. Volume 1. J. B. Lippincott Company, Philadelphia, 1949, p. 562.
23. Schreiber, M. H. Clinical history as factor in roentgenogram interpretation. *J.A.M.A.*, 1963, *185*, 399–401.
24. Sosman, M. C. Specificity and reliability of roentgenographic diagnosis. *New England J. Med.*, 1959, *242*, 849–855.
25. Stack, J. K. Role of radiologist in management of low back pain. *Radiology*, 1958, *70*, 666–671.
26. Stein, G. N., Martin, R. D., Roy, R. H., and Finkelstein, A. K. Evaluation of conventional roentgenographic techniques for demonstration of duodenal ulcer craters. Am. J. Roentgenol., Rad. Therapy & Nuclear Med., 1964, *91*, 801–807.
27. Templeton, F. E. X-ray Examination of the Stomach. University of Chicago Press, Chicago, 1944, p. 274.
28. Tuddenham, W. J. Problems of perception in chest roentgenology: facts and fallacies. *Rad. Clin. North America*, 1963, *1*, 277–289.
29. Virtama, P. Influence of certain physical factors on radiographic demonstration of cholesterol gallstones. *Acta radiol.*, 1961, *56*, 193–201.
30. Yerushalmy, J. Reliability of chest radiography in diagnosis of pulmonary lesions *Am J. Surg.*, 1955, *89*, 231–240.

# EXPERIMENTAL DETERMINATION OF FLOW EQUATION IN CATHETERS FOR CARDIOLOGY*

By D. E. WILLIAMSON†
MIAMI, FLORIDA

INCREASED use of high pressure injectors in angiocardiography has necessitated a means of predicting the flow of moderately viscous fluids at high velocities through long narrow catheters. In a typical application, the pressures and catheter lumens used are such that highly turbulent flow results. Under these conditions, it is clear that the classic Poiseuille formula is of little use, since this formula applies to laminar flow exclusively.

The problem is to devise a means of predicting the time required to inject a given bolus of radiopaque material with the known parameters of catheter diameter, length, and injection pressure. Whereas high accuracy is not required, it is clear that a choice between various published flow formulae could result in more error than seems necessary. For instance, the differences in the exponents used by Darcy[1] and those used by Blasius[2] could result in a 15 per cent difference over the range of pressures in common use.

Whereas at the beginning of this investigation it was not certain that sufficiently consistent data could be obtained, the results have been most gratifying and it is believed that the accuracy of such a determination has been demonstrated. In the process of arriving at a useful formula, it is shown that viscosity and density have little effect, and that as a practical matter these parameters as well as the friction coefficient can be included in a constant.

## EQUIPMENT

Since the primary purpose here was to obtain empirical results, the equipment used is essentially identical with that which would be used in a catheterization laboratory. Pressures were produced by a standard Cordis Injector. This is basically a high pressure syringe with a capacity of 40 ml., whose plunger is operated by a constant torque electric motor operated through a ball-nut and screw to convert rotary into linear motion. Within the speed limitations of this device, pressure in the syringe is controlled by varying the voltage on the torque motor by means of a variable transformer.

Because this device is basically designed as a very low-duty-cycle instrument, overload currents in the motor and consequent heating are of little consequence in normal operation. For repeated tests, however, the variable transformer calibration is unreliable due to the increase in resistance of the motor windings caused by heating. For this reason, pressure must be monitored by means of a pressure transducer built into the nosepiece of the syringe, pressure being read on a cathode ray oscilloscope with a triggered sweep. The pressure transducer used in this work was the U. S. Gauge, PT143-1500B-10W Rahm Pressure Transducer. As injection times for the full 40 ml. of solution generally run greater than 1 second, this device has adequate response for the purpose.

Catheters were standard production of United States Catheter and Instrument Corporation and were mainly the NIH or RA design. In these catheters, the distal end is closed, with 6 round or oval openings placed in laterally opposed pairs within the last 1.5 cm. Open end catheters as well as stainless steel hypodermic tubing was also used. It was determined experimentally

* Data for this study were taken in collaboration with the U. S. Catheter & Instrument Corporation, Glens Falls, New York.
† Director of Engineering, Cordis Corporation, Miami, Florida.

that there was no difference between the injection rate from an open end catheter and one of the NIH design. The inside surface of these catheters is the surface of the extruded nylon tubing which forms the inner layer. Variations in lumen diameter from those given by the manufacturer did not appear to significantly influence the results, and no effort was made to measure individual catheters.

Time of injection was measured by means of a Standard Electric Time Corporation Sl timer with a dc clutch. The timer clutch was operated from a spare set of contacts on the torque motor relay. This relay is closed by manually depressing a switch to start the injection, and is opened by a limit switch at the end of the injection.

The fluids used were the actual contrast media, and included hypaque 50 and 75, angio-conray, ditriokon, and renografin 60 and 76.* The temperature of these solutions was maintained at 38° C. by means of a thermostatically controlled heater in the injector syringe, injections being made into an Erlenmeyer flask kept in a water bath of the same temperature. Temperature control at both ends of the catheter is necessary to prevent cooling from convection at the flask and also to provide cooling when data are being taken rapidly due to the energy delivered to the fluid during injection. This point will be discussed later.

It is interesting to note that it is essential to constrain the catheter so that no "whipping" is possible. Unless this precaution is taken, erratic results are obtained.

## DATA

Altogether 102 curves were obtained, each curve representing 6 to 12 points covering the range of injection pressures from 100 to 800 psi. Each curve represented a single catheter length, diameter and contrast medium. Catheters of lengths 80, 100, 125 and 150 cm. were used. Catheter sizes from 5F to 9F were tested, this giving a range of lumens from 0.85 to 2.0 mm. diameter. The style of the tip, as mentioned above, was either open end or NIH.

Data for each catheter-contrast medium combination were plotted as individual data points, using distinct black dots on log-log graph paper. An example of the consistency of the data is shown in Figure 1. In this figure, lines have been drawn through the data points, the lines all having the slope represented by the equation developed as the result of this investigation. This illustrates the uniformity of results and the validity of determining a single equation to represent a wide variety of conditions. The scatter of points near the low pressure end of some curves is caused by the greater difficulty both in maintaining a low injection pressure and in reading the resulting pressure accurately.

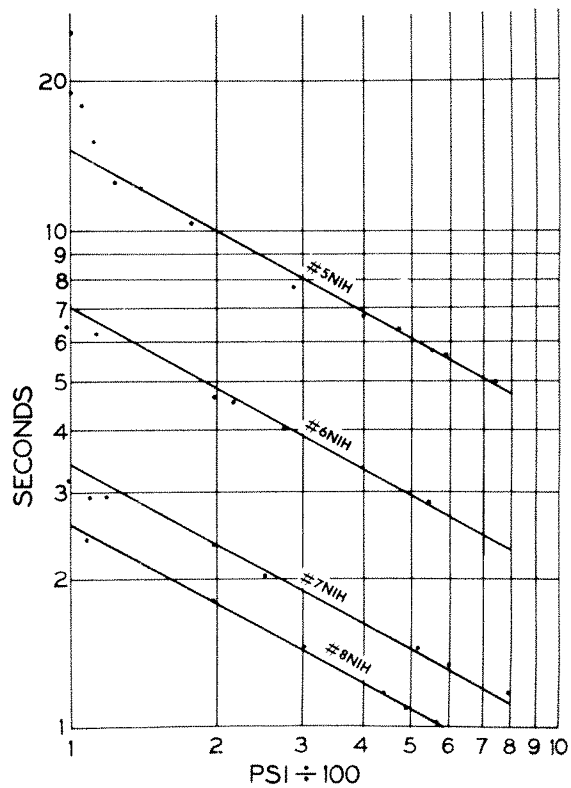


FIG. 1. Representative time versus pressure curves. These data show relation for 125 cm. catheter using renografin (60 per cent). The straight lines have the "average slope" as described in the text.

* Ditriokon and Angio-Conray, manufactured by Mallinckrodt Chemical Works; Hypaque by Winthrop Laboratories; Renografin by E. R. Squibb & Sons.

### REDUCTION OF DATA

The formulae of Darcy and Blasius have been applied by other investigators[2] and are as follows:

$$\text{Darcy} \qquad t = \frac{f^{1/2}\rho^{1/2}l^{1/2}V}{p^{1/2}d^{5/2}}, \tag{1}$$

$$\text{Blasius} \qquad t = \frac{c\rho^{4/7}\eta^{1/7}l^{4/7}}{p^{4/7}d^{2-5/7}}, \tag{2}$$

where $t$ = time for flow of volume $V$; $f$ = friction factor; $\rho$ = density of fluid; $l$ = length of tube; $p$ = pressure drop in length; $d$ = diameter of lumen; $c$ = constant; and $\eta$ = viscosity.

We propose to examine, however, the applicability of the formula

$$t_{40} = \frac{Kl^h}{p^c d^b}, \tag{3}$$

with the expectation that the friction factor will be essentially constant and that the normal variations of density and viscosity for the fluids used will contribute a negligible effect. This was indeed found by Lehman and Debbas[8] who show an almost constant injection rate for fluids of viscosity between 3 and 9 centipoises.

It was apparent, however, from examining the data such as shown in Figure 1 that most of the curves had the same slope when plotted on log-log paper. Some of the curves, nevertheless, showed a different slope, falling more rapidly with increasing pressure and apparently representing a different kind of fluid flow. A small intermediate group of curves showed the high slope for low pressures, flattening out to the above mentioned average at the high pressures. It was further observed that these curves represented data taken with the smallest of the catheters used and with the most viscous of the contrast media. Since the technique of high pressure injection is for the purpose of introducing a large quantity of fluid in a small time, it was decided to first focus attention on those data (which were greatly in the majority) which represented most accurately that type of operation.

Any straight line, such as one of those shown in Figure 1, can be represented by the formula

$$t_{40} = \frac{T_1}{p^a}, \tag{4}$$

where $T_1$ represents the time duration of the injection at unit pressure. We thus plot pressure as abscissa in hundreds of psi, thereby establishing unity pressure at the left side of the graph. The value of $T_1$ for a particular graph can be simply read off and recorded for future use. Our interest at the moment is in determining the exponent $a$, which will relate pressure and time for all the graphs.

The average slope of the data points was determined, and from this the value of the pressure exponent was found to be 0.544. Straight lines having this average slope were then drawn on each of the curves, fitting the data points as well as possible, for the purpose of determining the value of $T_1$ for the particular conditions of catheter size, length and contrast medium.

The values of $T_1$ from all the curves can now be tabulated, grouped both according to catheter length and catheter diameter. It can be seen from the equation

$$T_1 = \frac{Kl^h}{d^b},$$

that $T_1$ is a function of both length and diameter. Unfortunately, the range of lengths used (from 80 to 150 cm.) is not sufficient to obtain a good determination for the coefficient $h$. If, however, the values of $T_1$ are plotted against catheter length for the 8 catheter diameters represented, it can be seen that the slopes of these eight lines are essentially the same. A clue as to the expected coefficient may be had from examining equations 1 and 2, in which the parameter "pressure drop per unit length" is used. It would, therefore, be most reasonable to expect that the coefficient of length would be the same as the coefficient of pressure drop, or namely 0.544. If this line

is drawn on the graph of $T_1$ versus catheter length, it is found to fit all of the data very well, only one data point departing more than the 5 per cent from these average lines. For this reason, it was decided to use $h=0.544$ in the equation.

For the determination of the exponent $b$ which relates $T_1$ to lumen size, the values of $T_1$ were plotted against lumen for catheter lengths 100, 125 and 150 cm. Here again, the range of diameters is insufficient for an accurate independent determination, so the slopes represented by both the Darcy and Blasius formulae were tried. As a result of this, it was determined that the exponent 5/2 fits the data very well, whereas the exponent 2–5/7 did not fit.

"Best fit" straight lines through these data gave 3 curves representing the equation $T_1=C/d^{5/2}$ for 3 catheter lengths. Since the value of $K$ in equation 5 has not been determined, the entire numerator was replaced by $C=Kl^{0.544}$ for this step in the determination. When these values of $C$ were plotted against catheter length and the "best fit" straight line of the given slope was drawn, the value of the constant $K$ could be determined. The final equation now reads

$$t_{40} = \frac{0.77l^{0.544}}{p^{0.544}d^{2.5}}.$$

## DISCUSSION

As was mentioned previously, over a large range of viscosities there was no detectable effect on injection rate. The lowest viscosity used was for hypaque M (50 per cent), which is rated by the manufacturer at 2.16 centipoises at 37.5° C. The highest viscosity material used in these studies was renografin (76 per cent) with a viscosity of 9.1 centipoises. With this material and with hypaque (75 per cent), curves of greater slope were obtained when using a small (No. 5 and No. 6) catheter. The values of the pressure coefficient "$a$" in these cases was 0.822 for the No. 5 and 0.755 for the No. 6 catheter.

Several examples were found of curves which exhibited a high slope at low pressures and an "average" slope at high pressures, with a short plateau about 50 psi wide joining the two slopes. These curves and the plateau were reproducible. Calculation of the Reynolds number for 4 of these cases gave values between 2,560 and 2,920, which is certainly in the range expected for transition from laminar to turbulent flow. It must be pointed out, however, that since the "high slope" did not yield a pressure exponent of unity, it cannot, at least on this basis, be considered laminar within the meaning of the Poiseuille formula.

Another effect which operates in the favor of consistent and average results at high pressures with the more viscous media is the increase in temperature of the contrast medium as it is forced at high velocity through the catheter. Some idea of the temperature rise can be obtained by estimating the amount of power delivered to the fluid by the electric drive motor, making suitable correction for efficiency and mechanical friction losses in the system. According to this calculation, a 40 ml. injection in 1 second should raise the temperature of the fluid by approximately 3° C. Only one fairly crude measurement was taken to verify the existence of the effect, and did indeed detect a temperature rise about equal to half the calculated value.

## CONCLUSION

It has been shown that a useful formula relating injection time to only 3 variables can be obtained. This is subject to only the limitation that pressures, viscosities and tube diameter be such as to ensure turbulent flow.

Using these data, the simple nomogram was constructed which is shown in Figure 2. Starting with catheter size and length, a point is established on the turning axis $T_1$, which actually represents the value of that parameter. From this point, a line drawn through the injection pressure scale is extended to indicate injection time in seconds

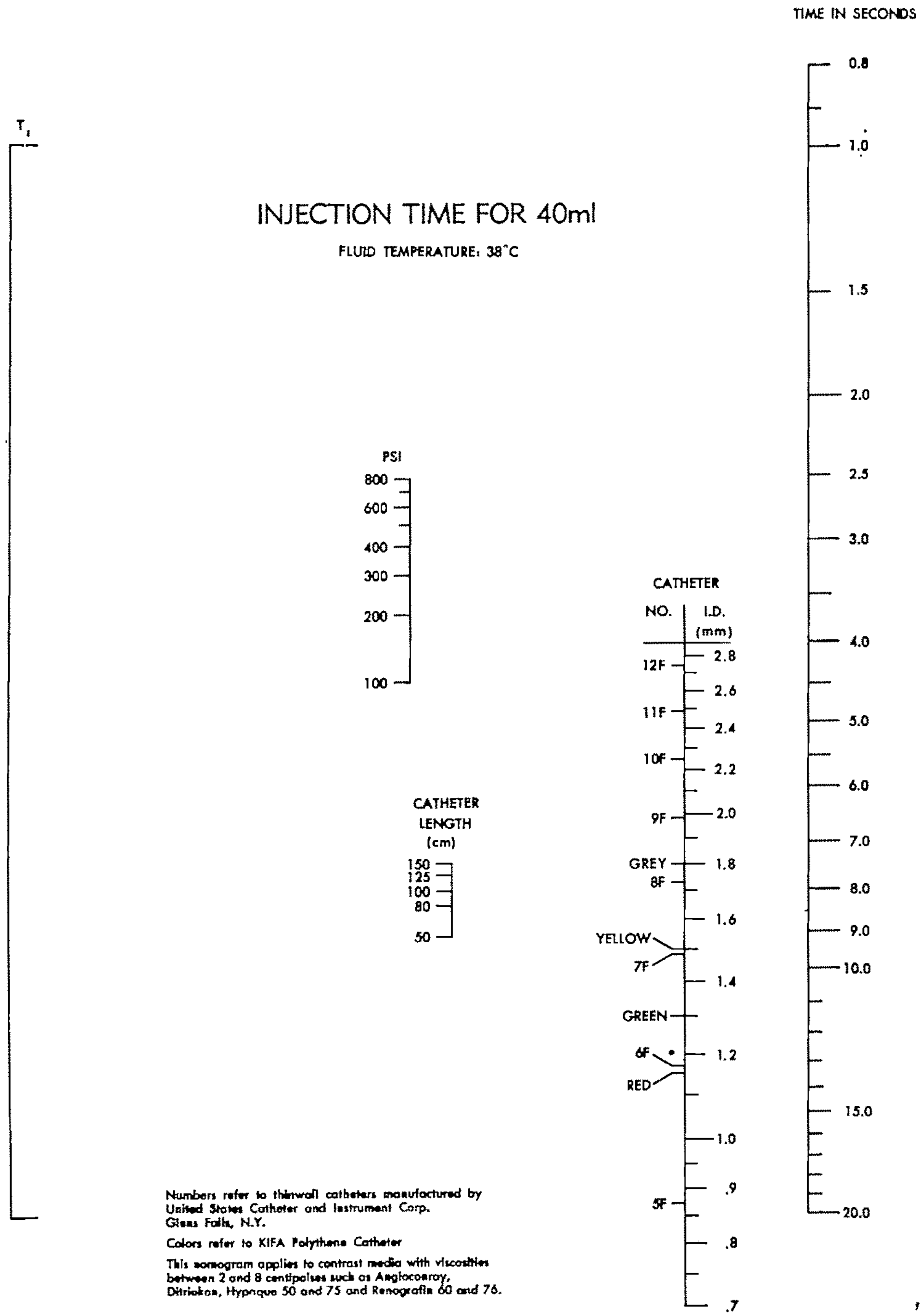


Fig. 2. Injection time nomogram for 40 ml. syringe at 38°C.

for 40 ml. The nomogram represents all the data used with an accuracy of better than ±10 per cent, this accuracy being realized largely due to the experimental determination of the constant and the exponent of pressure.

## SUMMARY

A large amount of experimental data has been obtained relating rate of flow with pressure in small diameter tubes. The flow was measured in tubes between 0.85 and 2.0 mm. diameter and 80 to 150 cm. in

length, over a pressure range from 100 to 800 psi. Variations in viscosity between 2 and 8 centipoises have no effect. The flow rate is shown to be proportional to pressure to the 0.544 power.

Cordis Corporation
241 N. E. 36th Street
Miami, Florida 33137

REFERENCES

1. Crane Company, Chicago, Ill. Flow of fluids through valves, fittings, and pipe. Technical paper No. 410.
2. COOLEY, R. N., and BEENTJES, L. B. Inquiry into physical factors governing flow of contrast substances through catheters. AM. J. ROENTGENOL., RAD. THERAPY & NUCLEAR MED., 1963, *89*, 308–314.
3. LEHMAN, J. S., and DEBBAS, J. M. Evaluation of cardiovascular contrast media. *Radiology*, 1961, *76*, 548–564.
4. LAMB, H. Hydrodynamics. Dover Publications, New York, 1945.
5. STREETER, V. L. Fluid Mechanics. McGraw-Hill Book Company, Inc., New York, 1962.

# A MANIFOLD FOR A CLOSED ANGIOGRAPHIC SYSTEM

By FRED SHIPPS, M.D.
PORTLAND, OREGON

THE proposed use of a manifold in all angiographic procedures is a step in the direction of patient safety. We have often observed that those who repeatedly open into a sterile intravascular system invite injection of contaminants (bacteria and other foreign materials). Even the most experienced operators leave catheters or needles in patients for prolonged periods of time because of delays and film processing. This practice may lead to blood clotting within these instruments and hence to the threat of embolization. It is our opinion that a closed angiographic system should be used at all times to prevent contamination and to provide constant flushing of the catheter or needle during waiting periods. Where such a system increases preparatory work, it pays off in operator convenience and patient safety during the procedure.

## DESCRIPTION

The manifold (Fig. 1) and a functional drawing (Fig. 2) are shown. Other important components of the closed system, not illustrated, include a bottle of saline, an intravenous type bottle containing the contrast agent, two intravenous sets and a syringe to pressurize the intravenous bottles. The M5 manifold not only overcomes the problems of injector reloading and catheter flushing but offers several advantages over using antiquated fittings originally designed for intravenous therapy. An effective lumen size of .106 inch diameter provides low resistance to flow during injection. The fittings and valves will hold to 1,000 p.s.i. The teflon valve seats do not bind and do not require grease lubricants that are of potential hazard when applied too generously. The improved male taper tip locks more securely for high pressure work and avoids unwanted pressure drops to transducers. Unscrewing the knurled nut in the taper lock applies leverage to disengage the connection. A hemostat is never required as a wrench.

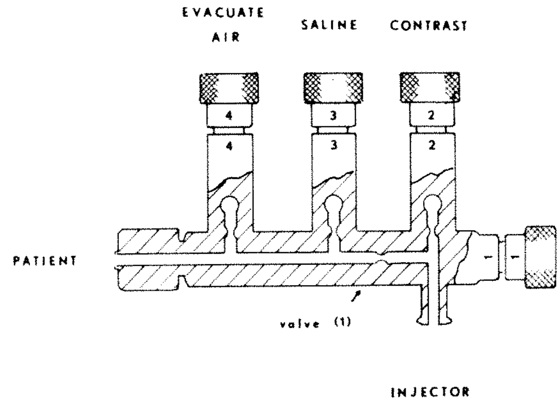


FIG. 1. The M5 angiographic manifold.

## OPERATION

Setting up the system and purging it of air is of paramount importance. The operational drawing of the manifold (Fig. 2) is labeled to show the functions of the five ports. It is set up as follows: With the body valve (#1) closed and valve #2 open, the injector is loaded from an inverted and pressurized intravenous bottle containing contrast material. By closing valve #2 and opening valve #1, the air is evacuated from the injector syringe. Closing valve #1 again completes purging of the injector portion of the system. Next the saline intravenous set

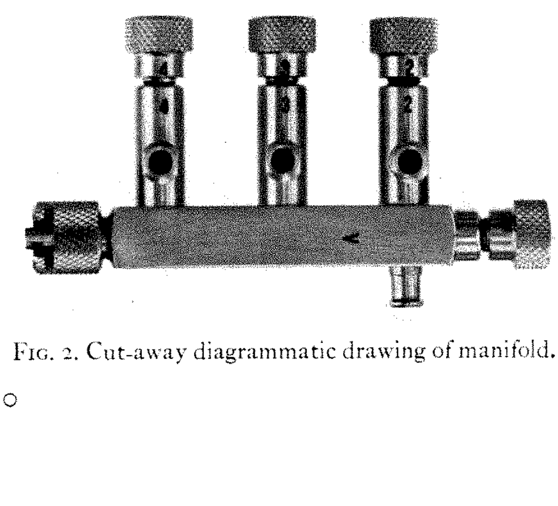

FIG. 2. Cut-away diagrammatic drawing of manifold.

is connected to port #3, port #4 is pressurized and flushed and the connecting tube is attached to the patient end of the manifold. After connection to the patient's catheter, or needle, back bleeding or aspiration is done via port #4. Now the system is purged and closed. The injector may be reloaded and the patient's catheter flushed simultaneously. Injection position is valve #1 open two turns and the others closed. Port #4 may be used for a transducer. In multiple simultaneous injections ports #3 and #4 may be used.

The manifold can be easily completely disassembled for cleaning and autoclaving. This is simply accomplished by unscrewing each valve handle four and one-half turns. They are numbered for identification in reassembly. Alignment of the numbers indicates visually the closed position of the valves.

SUMMARY

A closed angiographic system designed to encourage certain safety features in angiographic technique has been described. The M5 manifold incorporated in the system offers several other advantages over older fittings originally designed for intravenous therapy.

Good Samaritan Hospital
1915 Northwest Twenty-Second Avenue
Portland 10, Oregon

# OPTICAL TRANSFER FUNCTIONS OF THE FOCAL SPOT OF X-RAY TUBES

*By* KUNIO DOI
CHIGASAKI, JAPAN

An IMAGING system, like radiography, is best evaluated as to the characteristics of "blur" by its optical transfer function. One of the advantages of this procedure is that the over-all transfer function in a whole imaging system can be obtained easily by the multiplication or the addition of its elements.

The optical transfer function, introduced and developed in optics, is most simply described as a Fourier transform of an image of an infinitely narrow slit or a pinhole, the frequencies being spatial and usually called spatial frequencies.

The over-all transfer functions of a radiographic system in several cases were calculated from its components.[3,5,6,8] Some of the components were directly measured and others were calculated from the spread functions, which were assumed to have some simple form. Until now, optical transfer functions obtained experimentally were mainly the screen-film combinations.[1,4,7,9]

In this study optical transfer functions of the focal spot of the x-ray tube were measured photoelectrically using the fluorescent screen and an anisotropic spread function. These and the field characteristics of the focal spot are discussed.

The geometry of this radiographic system is shown in Figure 1. The x-ray image on an image plane is formed as a shadow of the object under x-ray exposure. If the spatial extent of the object is $o(x',y')$ at an object plane and the spread function of the focal spot corresponding to a pinhole as the object is $f(x,y)$ at the image plane, then the x-ray image $i(x,y)$ at the image plane is given as a convolution integral:

$$i(x, y) = \int_{-\infty}^{\infty}\int_{-\infty}^{\infty} f(x - x', y - y') \cdot o(x', y')dx'dy'. \qquad (1)$$

When this relation is expressed in spatial frequency domain, Fourier transforms $I(\nu,\tau)$, $F(\nu,\tau)$ and $O(\nu,\tau)$ of corresponding spread functions $i(x,y)$, $f(x,y)$ and $o(x,y)$ are simply connected as follows:

$$I(\nu, \tau) = F(\nu, \tau)\cdot O(\nu, \tau). \qquad (2)$$

Then the optical transfer function of the focal spot of the x-ray tube is clearly defined in two dimensional form as:

$$F(\nu, \tau) = \int_{-\infty}^{\infty}\int_{-\infty}^{\infty} f(x, y) \cdot \exp\{-2\pi i(\nu x + \tau y)\}dxdy. \qquad (3)$$

When the point spread function $f(x,y)$ is isotropic, the optical transfer function is more simply represented by one dimensional form from the line spread function which can be deduced from the point spread function. If $f(x,y)$ is not isotropic, one dimensional optical transfer functions should be determined for every direction. This seems to be the usual case for the focal spot of an x-ray tube.

## MEASURING SYSTEM OF OPTICAL TRANSFER FUNCTIONS

The optical transfer functions are photoelectrically measured by an area type masking method which is well known in lens testing. A direct scanning apparatus is built for a Fourier transformer of radiographic images using the x-ray fluorescent screen as a converter of an x-ray image to a light image.

When a metal slit as the object is placed between the focal spot and the fluorescent screen, the line spread function of the focal spot of the x-ray tube is reproduced on the fluorescent screen with the form of light emission according to the so-called pinhole effect.

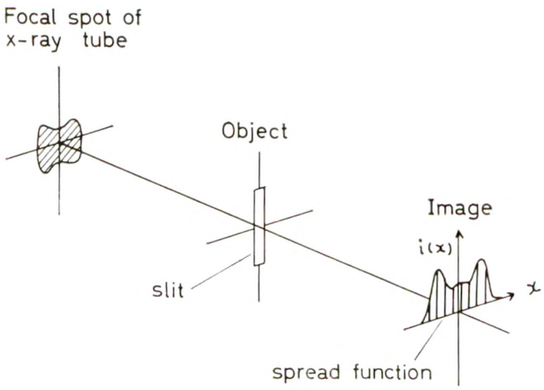


Fig. 1. Illustration of the relation between a focal spot of the x-ray tube, an object and an image.

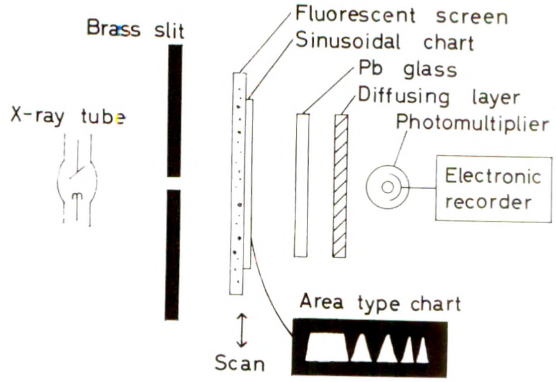


Fig. 2. Schematic diagram of the direct scanning apparatus for the measurement of optical transfer functions of the x-ray fluorescent screen and the focal spot of the x-ray tube. The position of the slit can be varied between the x-ray tube and the fluorescent screen.

The principle of this method is explained as follows. If $f(x)$ is the line spread function of the radiographic image and $x'$ is the displacement of the area type sinusoidal chart from the line spread function, then the transmitted light $T(x')$ is given by

$$T(x') = \int_{-\infty}^{\infty} f(x)\{1 + \cos 2\pi\nu(x' - x)\}\,dx,$$

where the x-ray image converter has an ideal property about its blur.

If $f(x)$ is symmetric, the Fourier transform is easily given by only Fourier cosine transform. Usually, this should be valid for the fluorescent screen and the focal spot. Then the Fourier transform $F(\nu)$ in normalized form is given by

$$F(\nu) = \frac{T_{\max} - T_{\min}}{T_{\max} + T_{\min}},$$

where $T_{\max}$ and $T_{\min}$ correspond to the maximum and the minimum of the light transmitted through the chart, respectively.

Practically, since the fluorescent screen is used as the x-ray image converter which has its optical transfer function $Fl(\nu)$, the optical transfer functions obtained by this method include both components from the focal spot and the fluorescent screen connected by multiplication. However, they can be easily separated by simple division, if $Fl(\nu)$ is obtained by itself. $Fl(\nu)$ is, of course, measurable from the line spread function of the fluorescent screen by slit exposures, when the slit is placed close to the fluorescent screen by the same measuring equipment.

The schematic diagram of the direct scanning apparatus is shown in Figure 2 and the photograph of it in Figure 3.

In Figure 2 the brass slit, 6 mm. thick and 100 $\mu$ wide, is used for x-ray exposures on the fluorescent screen which lies in close contact with the sinusoidal chart. The sinusoidal chart is made by photographic means using high resolution type photographic emulsion. This, in turn, lies in close contact with the scanning part, which can be moved perpendicular to the x-ray exposure axis with a speed of 0.5 mm./sec.

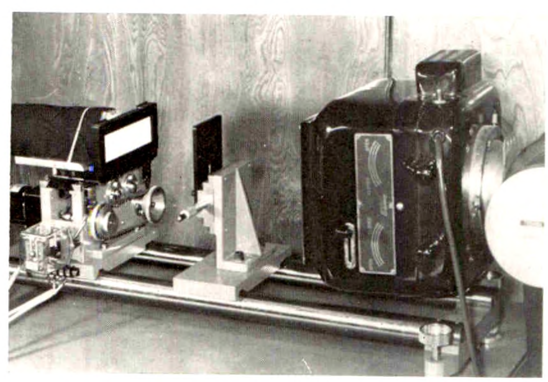

Fig. 3. Photograph of the direct scanning apparatus.

During the movement of the scanning part, the light emission from the fluorescent screen transmitted through the chart is collected by a photomultiplier behind a lead glass and a diffusing layer.

The finite slit, x-ray quantum fluctuations, and build-up and decay characteristics of the phosphor are considered to introduce errors in the experiment. However, their influence on the experiment is estimated as negligible in the range of spatial frequency below 2.0 lines/mm.[2]

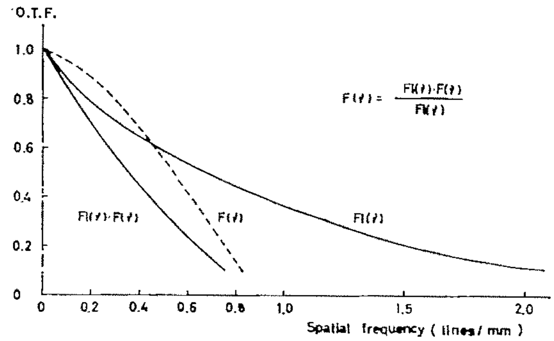


FIG. 5. Measurement of the optical transfer function of the focal spot of the x-ray tube. X-ray tube voltage, 70 kvp.; magnification ratio, 0.5; screen, F-2 (Kyokko).

### OPTICAL TRANSFER FUNCTION CURVES OF THE FOCAL SPOT

Figure 4 shows the electronic record of photo-currents for the optical transfer function measurement by the direct scanning apparatus.

Periodic sinusoidal variations of photo-currents correspond to the spatial frequencies on the chart. At low frequencies, periods of the sinusoidal waves are increasing by geometric progression, and at high frequencies, several sinusoidal waves for each frequency are repeatedly arranged in order to prevent the end effect.

Figure 5 illustrates the separation of the optical transfer function of the focal spot $F(\nu)$ from two experimentally obtained curves $Fl(\nu)$ and $Fl(\nu) \cdot F(\nu)$ by simple division at the magnification ratio of 0.5. Since the magnification ratio is easily changed only by the geometry of the experimental arrangement, it is convenient to define the

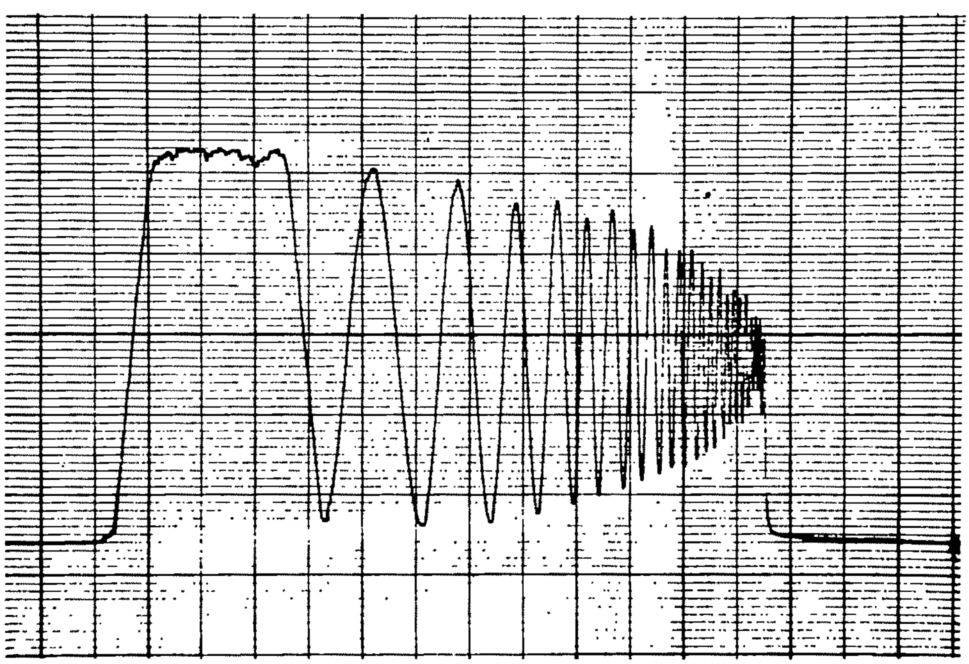

FIG. 4. Electronic record of photo-currents for the optical transfer function measurement obtained by the direct scanning apparatus.

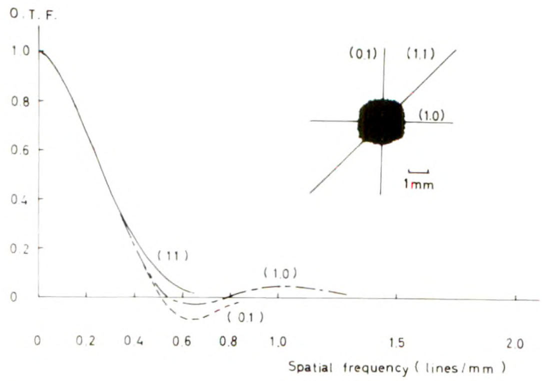


Fig. 6. Optical transfer functions of the focal spot along three directions. Magnification ratio, 1.0.

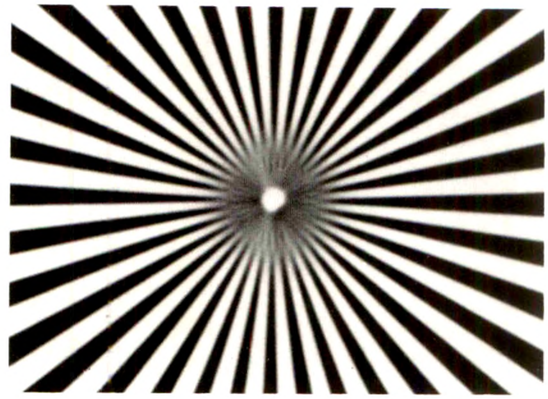

Fig. 7. Photograph of the Siemens star.

optical transfer function of the focal spot at the magnification ratio of 1.0.

Usually, the point spread function of the focal spot of an x-ray tube is not isotropic; this means that different optical transfer functions along some directions exist.

Figure 6 shows optical transfer functions measured at three directions about the focal spot of the x-ray tube described by nominal focal spot sizes of 2.0×2.0 mm.[2]. From this figure, it is seen that they have negative components along (1.0) and (0.1) directions, but not along (1.1) direction, where the component is approximately given by a Gaussian function rather than a sampling function.[6,8]

However, at low frequencies, the optical transfer functions at these three directions are almost the same; therefore, it seems that the problem of the image transfer in practical radiography may be treated by only the component given by the Gaussian function at low frequency range.

### COMPARISONS OF SPREAD FUNCTIONS BETWEEN CALCULATIONS AND EXPERIMENT

The measured optical transfer function curves can be compared with a photograph of the focal spot using a Siemens star made of lead.* In Figure 7 spurious resolutions can be observed at two directions: (1.0) and (0.1). On the other hand, no spurious resolutions are seen at the (1.1) direction. This corresponds quite well to the optical transfer function curves shown in Figure 6.

A quantitative comparison of the line spread functions of the focal spot is given in Figure 8. The solid line shows the line spread function of (0.1) direction calculated from the inverse Fourier transform which is carried out by numerical integrations. Experimental points are obtained from the slit image of the focal spot by photographic means. The exposed and processed slit images are traced by a microphotometer, and the normalized line spread function is obtained by the characteristic curve of the film.

Comparison of the calculated and the

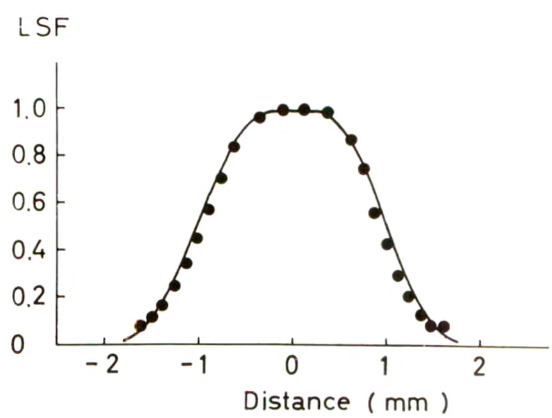


Fig. 8. Comparison of the line spread function between calculation and measurement.

* This test object was made by electro-deposition of lead to a copper plate which was pretreated by the photo-etching method. After the electro-deposition, the copper plate was dissolved by hydrogen chloride solution. The obtained lead object is about 200 μ thick.

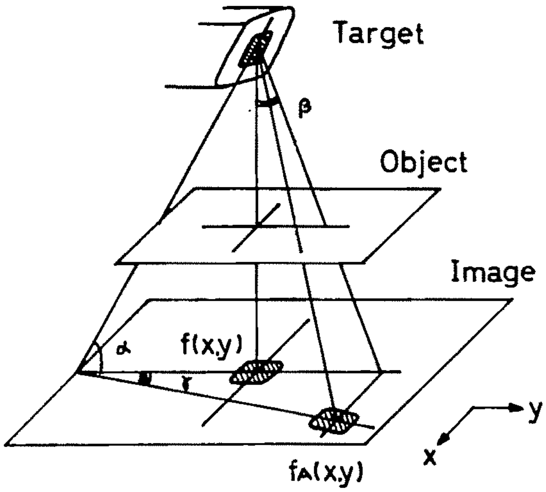


Fig. 9. Illustration of the spatial position of the target, the object plane and the image plane.

measured values, as shown in Figure 8, indicates good accuracy.

FIELD CHARACTERISTICS OF THE FOCAL SPOT

Since the target plane of the x-ray tube is positioned at an angle $\alpha$ with both of the object plane and the image plane, as in Figure 9, because of the geometry of the x-ray tube, the point spread functions of the focal spot on the image plane strongly depend on the field position of the image plane. This property should be called "field characteristics" as has been named in optics. The optical transfer functions of the focal spot which depend on the field characteristics can be determined at some specified positions by the geometric method.

GEOMETRIC CONSIDERATIONS

If $x,y$ are coordinates in image plane and $f(x,y)$ is the point spread function of the effective focal spot at the center of the radiation field, the field characteristics can be determined by obtaining the point spread function $f_A(x,y)$ at an arbitrary position as at angles $\beta$ and $\gamma$ shown in Figure 9 and 10. From these figures it is apparent that $f_A(x,y)$ is determined from $f(x,y)$, taking into account the change of the projected size of the focal spot along the y-axis and the conversion of the rectangular coordinates to the oblique coordinates.

If $R$ and $r$ are the distances of target-object and object-image, respectively in Figure 10, the effective focal spot size $E$ is given by

$$E = (r/R)F \cos \alpha,$$

using the actual focal spot size $F$, where the asymmetry of $E$ caused by the projection is negligible in practical cases. Then focal spot size $E'$ at the arbitrary position is given by

$$E' = E(1 + \tan \alpha \tan \beta).$$

Therefore, in general form $f_A(x,y)$ is given by

$$\begin{aligned} f_A(x,y) &= f\{x + y(1 + \tan\alpha\tan\beta)\tan\gamma, \\ &\qquad y(1 + \tan\alpha\tan\beta)\} \\ &= f\{x + k_1 y, k_2 y\} \qquad k_2 > 0. \end{aligned}$$

If $f^*(x)$ and $f^{**}(y)$ are the line spread functions of the effective focal spot along $x$ and $y$ directions respectively, the optical transfer functions $F^*(\nu)$ and $F^{**}(\tau)$ corresponding to $x$ and $y$ directions are given by

$$\left\{\begin{aligned} f^*(x) &= \int_{-\infty}^{\infty} f(x,y)dy \\ F^*(\nu) &= \int_{-\infty}^{\infty} f^*(x) \exp\{-2\pi i\nu x\}dx \end{aligned}\right. \tag{4}$$

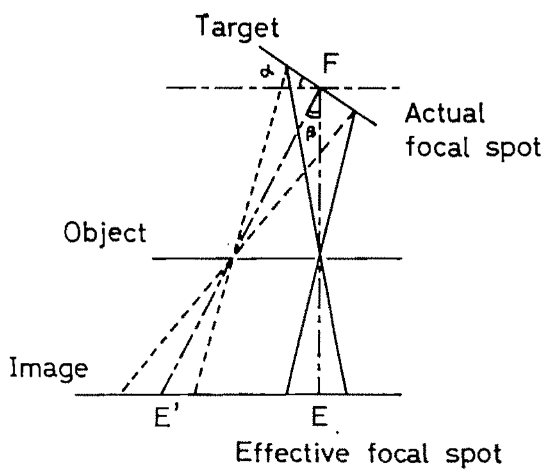


Fig. 10. Illustration of the variation of the focal spot size on the image plane.

$$\begin{cases} f^{**}(y) = \int_{-\infty}^{\infty} f(x, y)dx \\ F^{**}(\tau) = \int_{-\infty}^{\infty} f^{**}(y) \exp\{-2\pi i \tau y\} dy. \end{cases} \quad (5)$$

Similarly, the optical transfer functions $F_A^*(\nu)$ and $F_A^{**}(\tau)$ at the arbitrary position can be calculated using Equation 3.

At first $f_A^*(x)$ is given by

$$f_A^*(x) = \int_{-\infty}^{\infty} f(x + k_1 y, k_2 y)dy$$

from Equation 4. At $k_1 = 0$ it becomes

$$f_A^*(x) = (1/k_2)f^*(x).$$

Then in normalized form, the optical transfer function is given by

$$F_A^*(\nu) = F^*(\nu).$$

This means that at $k_1 = 0$, *i.e.*, $\gamma = 0$ the optical transfer functions along the x-axis are constant. Along the y-axis from Equation 5, we have

$$f_A^{**}(y) = \int_{-\infty}^{\infty} f(x + k_1 y, k_2 y)dx = f^{**}(k_2 y),$$

and then we obtain

$$F_A^{**}(\nu) = F^{**}(\nu/k_2). \quad (6)$$

This means that the optical transfer functions along the y-axis at the arbitrary position can be calculated using $k_2$ from the optical transfer functions of the effective focal spot.

## COMPARISONS OF CALCULATION AND MEASUREMENT

Figure 11 shows a comparison of the optical transfer function curves between calculated and measured values. The solid lines at $F(\nu/0.59)$ and $F(\nu/1.41)$ are calculated from $F(\nu)$ in Figure 6 using Equation 6. Experimental points are obtained at $k_2 = 0.59$ and 1.41 correspondent to $\beta = \pm 8.5$ degrees, assuming $\alpha = 70$ degrees.

From the good agreement in Figure 11, it is shown that field characteristics of the focal spot can be determined by the method described above.

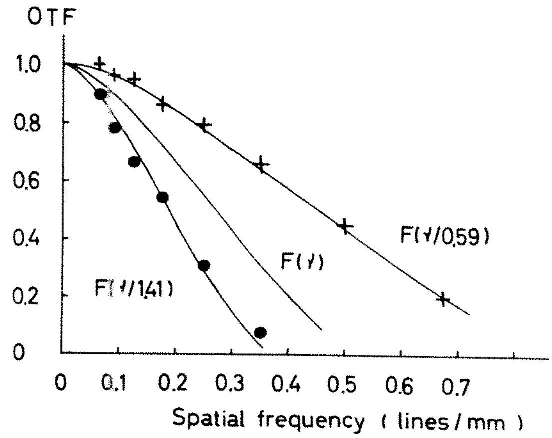


FIG. 11. Comparison of the field characteristics between calculations and measurements.

Field characteristics, as noted in Figure 11, show considerable extent, and so the results may give a practical suggestion to clinical radiography.

In chest diagnosis it has been recommended that the apex of the lung, most affected by the disease should be placed at the target side. This means that the field position which shows high quality in optical transfer function curves is applied to the area of the disease.

## SUMMARY

Optical transfer functions of the focal spot of the x-ray tube were measured photoelectrically using the x-ray fluorescent screen. The light image on the fluorescent screen was Fourier transformed optically by the area type masking method, using the direct scanning apparatus. This apparatus can be applied to a Fourier transformer of radiographic images. Optical transfer functions of the focal spot which gave negative components along some directions were qualitatively corresponding to the photograph of the Siemens star showing spurious resolutions. The line spread function calculated from the optical transfer function data agreed with the one obtained by the photographic method. Field characteristics of the focal spot

caused by the geometry of the x-ray tube were obtained theoretically and experimentally, and good agreement between these two treatments showed that field characteristics can be determined by simple calculations in some specified fields.

Kyokko Research Laboratories
Dai Nippon Toryo Co., Ltd.
6181 Chigasaki, Japan

The author gratefully expresses his thanks to Dr. K. Sayanagi, Canon Camera Co., for invaluable discussions; Dr. H. Ohzu, Waseda University, for fruitful advice; and to Dr. T. Toryu and Mr. H. Sakamoto for helpful discussions and encouragement throughout the work.

1. Doi, K. Measurement for optical transfer functions of x-ray intensifying screens. *Oyo Buturi*, 1964, *33*, 50–52.
2. Doi, K., and Sayanagi, K. Optical transfer function in radiography: Part 1. X-ray fluorescent screen. *Oyo Buturi*, 1964, *33*, 721–726.
3. Doi, K., Kaji, A., Takizawa, T., and Sayanagi, K. Application of optical transfer function in radiography. In: Proceedings of ICO Conference on Photographic and Spectroscopic Optics. Tokyo Meeting, 1964. To be published.
4. Hofert, M. Messung der Kontrastübertragungsfunktion von Röntgenverstärkerfolien. *Acta radiol.*; *Diag.*, 1963, *1*, 1111–1122.
5. Holm, T. Some aspects of radiographic information. *Radiology*, 1964, *83*, 319–327.
6. Morgan, R. H. Frequency response function: valuable means of expressing informational recording capability of diagnostic x-ray systems. Am. J. Roentgenol., Rad. Therapy & Nuclear Med., 1962, *88*, 175–186.
7. Morgan, R. H., Bates, L. M., Gopalarao, U. V., and Marinaro, A. Frequency response characteristics of x-ray films and screens. Am. J. Roentgenol., Rad. Therapy & Nuclear Med., 1964, *92*, 426–440.
8. Oosterkamp, W. F., and Albrecht, C. Evaluation of fluoroscopic screens and x-ray image amplifiers. In: Technological Needs for Reduction of Patient Dosage from Diagnostic Radiology. Charles C Thomas, Publisher, Springfield, Ill., 1963, pp. 251–273.
9. Rossmann, K. Spatial fluctuations of x-ray quanta and recording of radiographic mottle. Am. J. Roentgenol., Rad. Therapy & Nuclear Med., 1963, *90*, 863–869.

Vol. 94, No. 3

# RADIOLOGIC AND ALLIED PROCEDURES FROM THE POINT OF VIEW OF INFORMATION CONTENT AND VISUAL PERCEPTION*

By HYMER L. FRIEDELL, M.D., and EARLE C. GREGG, Ph.D.
CLEVELAND, OHIO

THE activities of the diagnostic radiologist have been vitally concerned with display systems which furnish information on the configuration and structure of internal organs and tissues. This display is translated into normal and pathologic anatomy and eventually into diagnostic medical entities.

In order to do this, a record is examined almost entirely by visual means and must be made intelligible. It is this latter phase that has primarily concerned the radiologist and can be broadly designated as pattern recognition. Pattern recognition is, undoubtedly, a complex problem, but in its simplest aspect it requires detection, storage, and conversion of some original signal into light, so that it may be recognized by the eye. The record (or stored information) is usually a spatial distribution of the intensity of the original signal which, in turn, may be presented directly to the eye, so that there may be eventual comprehension.

The purpose of this discussion is not to review in any way the complex procedures involved in cerebration carried out by the radiologist, but rather to point out that the problems of pattern production and ultimate recognition with which the radiologist concerns himself have identical counterparts in many other systems using a variety of signals.

Figure 1 illustrates a simple series array of components and/or simple operations that can be said to constitute an over-all system. While many systems are much more complex with feedback loops and other higher order intricacies, the series arrangements illustrated are representative of a class of devices common to diagnostic equipment with a final presentation of a spatial array of data.

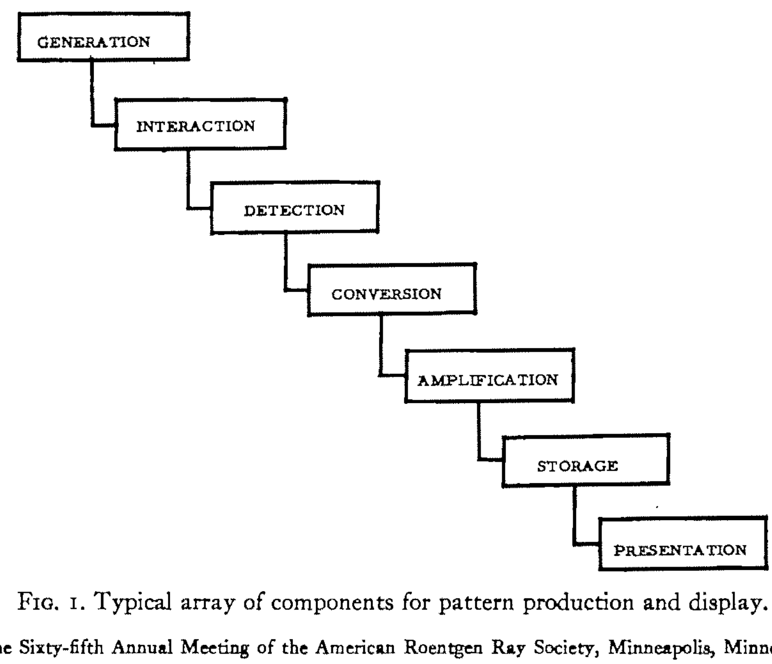


Fig. 1. Typical array of components for pattern production and display.

* Presented at the Sixty-fifth Annual Meeting of the American Roentgen Ray Society, Minneapolis, Minnesota, September 29-October 2, 1964.

Table I illustrates a breakdown of a number of different diagnostic techniques into the sequence of operations shown in Figure I. Table II is a listing of those factors which limit and interfere with the capability of the system to handle and transmit information.

It has always been fruitful to examine any display of a complex pattern from the point of view of available information. Recently, theoreticians have begun to apply information theory to various systems and to operations involving the transmission of such information.[1,7,8] While few results of direct practical importance have resulted to date, a number of interesting concepts have arisen that may affect future techniques of handling and presenting information.

Three general terms are used which are helpful in discussing the over-all problem. These are: (1) information capacity, (2) information content, and (3) information index.

(1) Information capacity has a particular mathematical definition and is a measure of the maximum number of "bits" of information that may be handled by a system.*

The information capacity of a photographic film is defined as the maximum number of bits per unit area that can be recorded on a film and read off with zero error.[4] For whatever it is worth, the information capacity of photographic film is about $10^6$ bits per cm.$^2$ It should be emphasized that this is for film only and does not represent the over-all information capacity of a system that usually contains other more severely limiting elements prior to the film recording. An interesting point of comparison is that one complete standard television frame in the United States has an information capacity which approximately equals 1 cm.$^2$ of film.

(2) Information content as used in this discussion is a subjective term which describes the intrinsic value of the display to the observer. It is really a measure of the probability that a particular message is not merely a random sequence of events but rather a real and significant conveyance of some order. It can be calculated for certain simple messages but for others we only have intuitive measures. For example, if a particular roentgenogram showed a uniform darkening and little or no structure, it could have been the result of random motion of x-ray target, patient or film, fogging due to unknown exposure, or a satisfactory roentgenogram of a homogeneous medium. In all these cases, the film would still have its original high information capacity, but the information content would depend upon many values determined by circumstances and the choices available to the observer.†

It is desirable to require that any system for pattern recognition should have an information capacity larger than necessary for the particular problem at hand. However, a problem which often arises—and not in the least trivial—is to determine the minimum information capacity required for a particular pattern display, or more specifically, for a particular diagnosis. There is little doubt that the enormous information capacity of film is wasted in most diagnoses.

In pattern recognition we become directly concerned with signal intensity levels (contrast) and the ability to discriminate discrete points, lines, or areas (resolution). Contrast and resolution are clearly related to information capacity, but in a manner which has not yet been precisely determined. A further important parameter is contour recognition which is the next order of complexity in cerebration after detection. Our innate ability to recognize geometric shapes and areas is of definite aid in

* One "bit" of information is the information gained by a decision of "yes" or "no" when the prior probabilities of "yes" or "no" are equal. The information capacity of a telephone channel is measured in bits per second while that for photographic film is bits per square centimeter.

† Some investigators have argued that the final information content of a roentgenogram is simply two "bits" of information, namely, "yes" (normal) or "no" (abnormal). However, it must be kept in mind that this is really a decision based on perhaps $10^7$ bits of information and is by no means a measure of the necessary information capacity of the system.

TABLE I

GENERAL SYSTEMS OF SIGNAL PRODUCTION AND HANDLING

| System | Generation | Interaction | Detection | Conversion | Amplification* | Storage* | Presentation* |
|---|---|---|---|---|---|---|---|
| Radiography | X-ray tube | Interaction with atoms (absorption) | Film | X-rays to photographic density | Selection of film gamma (contrast sensitivity) | Film storage. Deposition and fixing of exposed grains | Light transmission |
| Radiography with Intensifying Screens | X-ray tube | Interaction with atoms (absorption) | Films plus fluorescent screen | X-rays to light and subsequent photographic density | Selection of film gamma (contrast sensitivity) | Film storage. Deposition and fixing of exposed grains | Light transmission |
| Fluoroscopy | X-ray tube | Interaction with atoms (absorption) | Fluorescent screen | X-rays to light | Screen efficiency | Temporary in eye and phosphor | Direct viewing |
| **Fluoroscopy with Image Amplification | X-ray tube | Interaction with atoms (absorption) | Image amplifier tube or equivalent | (1) X-rays to light to electrons to light (2) X-rays to light to electrons (3) X-rays to electrons | Electrical and change in area | Temporary in eye and phosphor | Direct viewing |
| Radioisotope Scanning | Distribution of radioisotopes | | Scintillation detector | Gamma photons to light to electrical pulses | Secondary emission and electronic | (1) Tape (2) Film (3) Digital print-out | (1) Print-out (2) Film (3) T.V. monitor |
| Ultrasound | Charge activated quartz crystal (transducer) (reciprocal Piezo electric effect) | Reflection at interface and relative absorption differences | Acoustically sensitive crystal | Sound converted to electrical pulse (Piezo electric effect) | Electronic | Film or tape | Film, print-out mechanisms, or T.V. monitors |
| Thermography | Spatial array of temperature | | Temperature sensing devices | Heat to electrical signal | Electronic | Film Tape | Direct visualization Digital print-out |

* A logic operation, or mathematical manipulation of the data, is a recognized engineering technique and may be introduced in many ways, but is usually applied to the amplification, storage or presentation steps.

** Cinefluorography stores the image of the phosphors or the electrical signal on film or tape for subsequent analysis.

TABLE IIa

DISTURBING FACTORS IN PATTERN PRODUCTION

*Roentgenography*

| Generation | Interaction | Detection | Conversion | Amplification | Storage | Presentation |
|---|---|---|---|---|---|---|
| 1. Geometric distortion due to size of focal spot<br>2. Random uncertainties of size and intensity of focal spot (noise) | 1. Scattering (edge unsharpness)<br>2. Motion of object<br>3. Undefined 3-dimensional orientation and structure of object | 1. Uncertainties in size and x-ray absorption of screen phosphor crystals*<br>2. Uncertainties in size and sensitivity of developable grains<br>3. Stray radiation | 1. Effect on photographic processing of:<br>(1) heat<br>(2) chemicals<br>(3) pressure<br>(4) charge<br>2. Uncertainties in light emission and absorption by screen phosphor crystals* | Spatial variations in contrast sensitivity of film | Long time deterioration due to incomplete fixation and oxidation | 1. Improper or incomplete range of light intensity for viewing<br>2. Nonuniformity of illumination |

* Present only with intensifying screens.

TABLE IIb

DISTURBING FACTORS IN PATTERN PRODUCTION

| Generation | Interaction | Detection | Conversion | Amplification | Storage | Presentation |
|---|---|---|---|---|---|---|
| *Fluoroscopy* | | | | | | |
| 1. Geometric distortion due to the size of focal spot<br>2. Random uncertainties of size and intensity of focal spot (noise) | 1. Scattering (edge unsharpness)<br>2. Motion of object (noise)<br>3. Undefined 3-dimensional orientation and structure of object | 1. Uncertainties in size and x-ray absorption of screen phosphor crystals<br>2. Stray radiation | 1. Uncertainties in light emission and absorption by screen phosphor crystals | Variations in conversion efficiency with time | Eye fatigue | 1. Incomplete dark adaptation<br>2. Improperly lighted fluoroscopy room<br>3. Eye fatigue |
| *Fluoroscopy with Image Amplification* | | | | | | |
| 1. Geometric distortion due to size of focal spot<br>2. Random uncertainties of size and intensity of focal spot (noise) | 1. Scattering (edge unsharpness)<br>2. Motion of object (noise)<br>3. Undefined 3-dimensional orientation and structure of object | 1. Uncertainties in size and x-ray absorption of screen phosphor crystals<br>2. Stray radiation | 1. Uncertainties in light emission and absorption by screen phosphor crystals<br>2. Uncertainties in efficiency of photo-emissive surface<br>3. Uncertainties in charge leakage | 1. Uncertainties in size and efficiency of output phosphor signals<br>2. Variations in electrical size reduction<br>3. Internal electrical noise<br>4. Bandpass limitations of associated electrical circuits | 1. Bandpass limitations of tape*<br>2. Tape artefacts (noise)*<br>3. Film graininess (noise)*<br>4. Eye fatigue | 1. Limited resolution and dynamic range of viewed phosphors<br>2. Projector vibrations*<br>3. Eye fatigue |

* Cinefluorography with image amplifiers.

### Table IIc

DISTURBING FACTORS IN PATTERN PRODUCTION

*Ultrasound*

| Generation | Interaction | Detection | Conversion | Amplification | Storage | Presentation |
|---|---|---|---|---|---|---|
| 1. Crystal size and geometry (acoustic "break-up")<br>2. Uncertainty of source intensity | 1. Uncertainties of interface orientation<br>2. Motion<br>3. Irregularities in density of medium<br>4. Irregularities in structure | 1. Internal losses in crystal absorption<br>2. Loss of resolution due to finite crystal size | Electronic noise | Electronic noise | Film uncertainties | Uneven light intensity |

### Table IId

DISTURBING FACTORS IN PATTERN PRODUCTION

*Radioisotope Scanning*

| Generation and Interaction | Detection | Conversion | Amplification | Storage | Presentation |
|---|---|---|---|---|---|
| 1. Motion of patient<br>2. Metabolic alteration of radioisotope distribution<br>3. Geometric uncertainties due to location of radioisotope distribution<br>4. Paucity of signal (quantum noise) | 1. Scattered radiation<br>2. Extraneous background radiation<br>3. Leakage through detector shielding | 1. Electronic noise<br>2. Stray light | Electronic noise | 1. Uneven development and film graininess<br>2. Mechanical lag in mechanical print-out systems<br>3. Artifacts in tape | Nonlinearity due to limited dynamic range |

### Table IIe

DISTURBING FACTORS IN PATTERN PRODUCTION

*Thermography*

| Generation and Interaction | Detection | Conversion | Amplification | Storage | Presentation |
|---|---|---|---|---|---|
| Irregularities of surface heat distribution<br><br>Stray thermal radiation<br>Body motion | 1. Alterations in temperature sensitivity<br><br>2. Size of sensor (resolution)<br>3. Variations in effective optical aperture | Electrical noise in conversion of heat to electrical signal | Electronic noise | Film uncertainties | Uneven light intensity |

diagnosis. Contour enhancement* is of definite value in making more rapid appraisals of the nature of the pattern.[3,5] It undoubtedly reduces the number of bits of information necessary for a given pattern recognition or diagnosis, but, as yet, its significance has not been reduced to precise assessment.

(3) Information index is a parameter that has been proposed as a more practical measure of the information capacity of systems utilizing visual presentations. This index is simply defined as the product of the contrast sensitivity (the fractional intensity change required for just recognizing a change) and the resolution (the reciprocal of the minimum resolvable distance in cm. between two lines). It can be shown that for statistically limited processes, this index is equal to one-fifth of the square root of the number of photons per sq. cm. (see appendix). Table III shows such indices for various diagnostic techniques under the usual conditions for the techniques involved. It is obvious that additional extraneous signals (noise), geometric unsharpness, and other forms of distortions prior to the final recording will lower these indices by affecting either or both the contrast sensitivity and resolution.

* *i.e.*, Xerography, logEtronic systems and the method of unsharp masks are techniques concerned with contour enhancement.

The data given in Table III are approximate and will vary with technique, x-ray spot size, choice of film, etc. However, the values are reasonably representative. It should be pointed out that film alone has a much higher index than implied in the first row. The lowering is due to the technique employed (spot size, etc.).

The column labeled R is the ratio of information index to patient dose. It should be remembered that, for the same information index, the patient exposure will be increased and R correspondingly decreased for thicker body sections and the use of grids because of their increased absorption of the radiation prior to detection. The values listed in Table III are for typical conditions of observation and may not be calculated for other conditions unless these

Table III

COMPARISON OF INFORMATION CAPACITY OF VARIOUS SYSTEMS

| System | Skin Dose (r) | Information Index | R |
|---|---|---|---|
| Radiography (film only) | .5 | 800 | 1,600 |
| Radiography (film, plus screen) | .01 | 500 | 5,000 |
| Fluoroscopy | .02 (0.2 sec.) | 80 | 4,000 |
| Cinefluorography | 2 (per frame) | 170 | 85 |
| Fluoroscopy with Image Amplifier | .008 (0.2 sec.) | 130<br>350 (noiseless) | 16,000 |
| Cinefluorography with Image Amplifier | .025 (per frame) | 100 | 4,000 |
| Radioisotope Scanning (single bore collimator) | 5 (internal organ dose) | 20 (liver) | 4 |
| Ultrasonography | — | 50 | — |
| Thermography | — | 75 | — |

characteristics are known. Such data will be presented later.

While the value of R is rather high for fluoroscopy both with and without an image amplifier, it must be pointed out that the dose is calculated for the averaging time of the eye (0.2 sec.) and there is no information storage involved. Thus, for these two cases, a comparison with other techniques can only be made if one assumes that the brain has perfect memory for all the information delivered in a 0.2 second view. Actually, the total exposure dose for a given diagnosis is much higher in these two cases which results in a considerable lowering of R.* Further, a comparison of R for one frame of cinefluorography (with an image amplifier) with the R value for film plus screen shows that the latter is still a superior method even when considering patient dose. One must be careful in utilizing R as any basis for comparison since a certain minimum value of information (index) must be achieved for any given diagnosis. Also, the index itself may not be the most desirable measure since obviously resolution may be of more or less importance for a given diagnosis than assumed here.

The radiologist has been well aware of the importance of maximizing contrast and resolution within the limits of a given exposure dose and has been responsible for the development of many techniques for their improvement. One has only to consider high speed, fine grain films, use of intensifying screens, grids for elimination of scatter, small focal spot x-ray tubes, proper patient positioning and control, use of large ranges of kilovoltage to make optimum the detectability of the defect under study, and, finally, introduction of electron optical devices and other electronic aids. All of these techniques have involved compromises that ultimately lead to optimizing the amount of information possible per exposure dose even though the total amount of information relative to the old technique may be actually decreased. It must be recognized that in most cases resolution is sacrificed for a greater gain in sensitivity while in a few instances the opposite choice is made. The addition of fluorescent screens to film is an example of the former, while the use of grids illustrates the latter choice.

The increased use of electronic devices, however, has emphasized another parameter, namely, "noise" which is simply a random signal produced at all times within the system and which is independent of the real signal bearing the information. True noise (white or random) can be either electrical or mechanical (thermal) in nature. Electrical noises are generated within the circuit components themselves (*i.e.*, tubes, transistors, etc.) while thermal (or mechanical) noises are due to random motion of the molecules of interest or to the distribution of grain size in the final film. Generally, graininess of the film and thermal motions have a much smaller impact on information capacity than the effect of mechanical motion of the patient, x-ray spot or other geometric uncertainties that produce unsharpness. While one may treat patient or x-ray spot motion as "noise," their temporal variations are significantly different from white noise and may be eliminated (filtered) by shortening the time of observation.

Another manifestation of noise is that which exists in the signal itself and is due to the random nature of the very processes that give rise to the radiation.[6] This is known as quantum noise in the case of particulate radiations and is usually unimportant in most roentgenograms due to the large number of photons available. However, it is the limiting factor in radioisotope scanning, as will be shown later. It is important to keep in mind that while some extraneous disturbances may affect resolution and others the contrast, noise, in general, can affect both, depending on the

* If a given fluoroscopic diagnosis would take 2 seconds, R would be reduced by a factor of 10. This illustrates the value of a memory unit for storage and more leisurely evaluation of the data. Since the eye has a region of sharp focus of only 5 cm.$^2$ at a 25 cm. viewing distance, a crude number expressing the influence of storage versus "glancing" on information capacity would be the area of the film in cm.$^2$ divided by 5.

display and detection systems. In all cases, increased noise will result in decreased information capacity or information index. It is obvious that one must strive to bring the signal to noise ratio $(S/N)$* to a maximum and that any manipulation of the signal will only introduce more noise. This may result in either an increased or decreased over-all ratio depending on the manner in which it is done. However, nothing can be done about the statistical variations (quantum noise) in the input signal itself.

The influence of system noise (as contrasted with signal noise) has been minimized in communication systems by several techniques:

(1) Negative feedback which introduces at the system input a signal opposite in phase to that appearing at the output and hence cancels out those signals arising internally in the system.

(2) A signal modulation which increases the *a priori* knowledge as to the time of occurrence of the real signal.

(3) Repeated observations of the same signal at different times (computor of average transients or CAT). While the amount of signal is necessarily increased, the signal to noise ratio also increases as the square root of the number of observations.

(4) Filtration, if the system noise or signal has known temporal variations.

(5) Simply increasing the input signal if the source of noise is not signal dependent. This is essentially the same as (3).

In roentgenography, where patient dosage is the limiting factor, it is obvious that one cannot simply increase the exposure dose or total delivered energy. Since this total delivered energy is proportional to the total number of photons, we see that it is also a measure of the information available for a given resolution. While for rate independent devices we will still have the same information capacity available at the detector whether the dose is delivered in a short or long time, the question remains as to how much noise is introduced during the time of observation. Neglecting patient motion, it is obvious that if a detector is recording for a period that is long compared to any signal pulse length, the noise observed during this time will be independent of pulse length and the signal to noise ratio will remain constant. If, on the other hand, the detector is gated "on" only when the signal is on, then we see and record less noise as the signal pulse is made shorter and correspondingly more intense to preserve a constant energy. This results in an increased signal to noise ratio. This process of gating is really a special form of modulation as described above. While some x-ray sources are pulsed (primarily for stopping motion), the authors are not aware of any associated electronic equipment in radiology that is also gated to improve the signal to noise ratio.

Regarding total energy or total number of photons as a measure of information under the circumstances of changing a viewing technique with constant dose, let us consider a typical roentgenogram of the abdomen with a laminagram of the same region. One parameter that we do not know and have not specified in our previous discussion, since we were dealing with two dimensional displays, is the value of resolution in depth. Such resolution is obviously not present in a typical roentgenogram and the superposition of internal organs will introduce large geometric uncertainties.

Now, in making a laminagram, where one sees a layer with a certain resolution in depth, the "out-of-focus" layers appear as a uniform film blackening (under ideal conditions) and, hence, reduce the contrast

* By signal to noise ratio is meant the square root of the ratio of total signal energy to total noise energy received over the time of observation, or, equivalently, the ratio of the average signal to the rms value of its fluctuations. For a statistically varying signal (quantum noise), the variation in any group of particles occurring at random and containing $M$ particles on the average is proportional to $\sqrt{M}$. Thus, the relative magnitude of the fluctuations is $\sqrt{M}/M = 1/\sqrt{M}$ and the signal to noise ratio is $S/N = M/\sqrt{M} = \sqrt{M}$.

Rose[4] and others have shown that the minimum observable contrast difference of a given area relative to background must be 3 to 5 times the rms fluctuations for minimum observable contrast. This means, in essence, that the information index as used here is 1/5 the signal to noise ratio where $S$ and $N$ are evaluated for each sq. cm. of image.

sensitivity of the "in-focus" picture. Thus, in achieving depth resolution (or, the elimination of superposed geometric uncertainties), we have to sacrifice contrast sensitivity, implying that the maximum information available is a constant determined only by the total number of photons. While this has not been expressed analytically to date, the general conclusion is that for a given number of photons, an increase in information about one aspect of a record means a loss in others. To further pursue this aspect, electronic scanning devices have the inherent ability to change contrast, "erase" unwanted backgrounds (*i.e.*, filter out the steady-state components), and to enhance contours. While these techniques do not change the available information capacity,* they undoubtedly allow easier and more rapid diagnoses by the eye. Whether or not these ultimately allow a smaller system information capacity for a given diagnosis remains to be seen.

Before discussing the application of Figure 1 to various diagnostic techniques in radiology, let us first examine the final visual presentation. No computor or analyzing device has been constructed today that even remotely approaches the capability of the eye-brain system. This system has an enormous range of amplitude sensitivities, ability to recognize complex forms, integrates and organizes quickly a large variety and number of bits of information and has a long time memory bank for detection of alterations from some established norm. All this without reference to judgment which often allows the elimination of unnecessary and undesired information.

While it may be concluded that the eye-brain system is superior to anything available to date, it must be recognized that the information must be presented in such a manner as to enhance the efficiency of this system. Here the intensity of the illumination must be sufficient to sharply increase the contrast sensitivity and visual acuity since at low intensities of light the rods are utilized instead of cones with loss in resolution. If one plots the product of visual acuity and contrast sensitivity of the eye as a function of illumination level, the relationship shown in Figure 2 is obtained. This product may be considered to be an information index for the eye similar to that defined previously for instruments.** This graph shows quite clearly that the apparent information index of the eye-brain system varies rapidly with illumination level. One can now introduce devices that will increase the illumination level of the display—at the expense of the information capacity of the system, to be sure. However, the increase in information capacity of the eye-brain system at high illumination levels usually more than compensates for any reduction.

Unlimited gain, however, is inadvisable since there is no advantage in increasing the information capacity of the eye beyond that of the prior system. In fact, it may make the inherent noise more obvious. Rose[6] has shown that the quantum efficiency of the eye over a great range of illumination levels is about 5 per cent which means that the eye is already detecting 5 per cent of the total information incident on it. Thus, any light amplifier can only increase the 5 per cent to 100 per cent which is a net gain of 20. This limitation on gain, however, should not be confused with the enormous increase in convenience accruing from viewing at high light levels such as very short adaptation times, minimizing viewing disturbances, etc. A very good example of the above discussion is the use of image amplifier tubes in fluoroscopy.

As shown in Table III when a typical fluorescent screen is viewed at very low light levels, the measured information index is 80, or just about that of the eye as

* It is to be noted that increase in amplification (contrast) will not change the signal to noise ratio if the noise is introduced prior to amplification since both are amplified equally. In most electronic devices, the principal source of noise is usually in the input, or, for devices of the sort described here, in the signal itself. While it is recognized that the eye itself will limit the processes at very low illumination levels and "light amplification" is of definite value, the above statement is made for the usual case of the non-threshold limited eye.

** It is to be noted that this definition is for the statistically limited retina and is presumably the condition under which the data of Figure 2 were obtained.

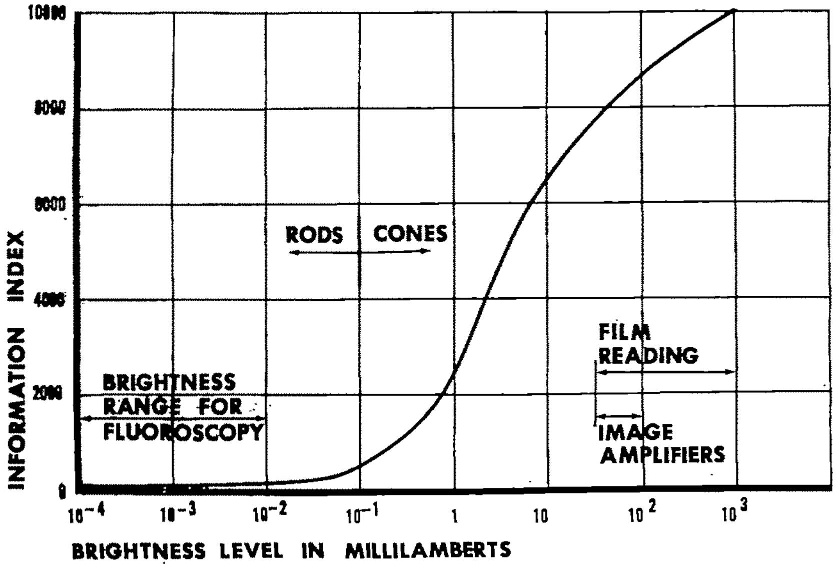


Fig. 2. Characteristics of the dark-adapted eye. The Information Index is simply the reciprocal of the product of contrast sensitivity and the resolution (in cm.) at 25 cm. viewing distance. If the dark adapted eye is exposed to bright light, the values of information index will be lowered by a factor greater than 2,000.

shown in Figure 2. Introduction of a typical image amplifier with a gain of 1,000 in brightness only increases the measured index to 130. For a typical fluorescent screen, about $10^7$ x-ray photons per square cm. are absorbed and converted into light during the integration time of the eye. At this point, the signal to noise ratio is $\sqrt{10^7}$, or about $3\times10^3$. Now each x-ray photon creates about 5,000 light photons which produces a total photon density of $5\times10^{10}$ per sq. cm. While the signal to noise ratio of this is $2\times10^5$, it is important to remember that these photons are coming off in groups of 5,000 so the original signal to noise ratio is controlling. Due to the pupil diameter of the eye and its quantum efficiency, a reduction of about $5\times10^6$ occurs in the light reaching the retina. This is $10^5$ per apparent sq. cm. of image with a $S/N=300$. By our previous definition, this is an information index of 60 which is a reasonable comparison with the measured value. This illustrates the fact that the primary limitation in direct visual fluoroscopy is due to the fluctuations in the converted photon density at the retina because of poor collecting optics and a low quantum efficiency as expected.

Let us now consider the image amplifier. In order to preserve resolution, the input phosphor is generally made thin and only about $3\times10^6$ x-ray photons are converted into light with an $S/N=1.7\times10^3$. Accepting the usually listed values of photon gain per cm.[2] (avg. 2,000) and including the efficiency, etc., of the eye, we end up with about $.7\times10^{10}$ photons per apparent sq. cm. of image with an $S/N=.8\times10^5$. The eye is no longer the limiting process. Instead the original converted x-ray photons with a signal to noise ratio of 1,700 occupy this role. In this chain of events we assumed noiseless amplification and under these circumstances we obtain an index of 340 *versus* a measured 130. It is interesting that if we now introduce noise in the light-photoemission-acceleration-light chain in the image amplifier we need only a signal to noise ratio of 650 to explain the discrepancy. This is a very low noise factor for electron tubes under these circumstances (some television tubes have a $S/N=50$) and shows the extreme care that must be

taken in construction. More recent tubes may have an even higher value than reported in Table I.

The above calculations show several significant points. Of fundamental importance is the fact that the curve for the eye shown in Figure 2 cannot be used when the limiting statistical fluctuations are produced prior to detection at the retina even though the apparent brightness is very high. The controlling index is the minimum value in the chain of events including the eye. A second point is that the efficiency of the x-ray conversion to light is very important when light amplification is used. Present day fluorescent screens only convert about 25 per cent of the incident x-ray photon flux so an improvement of 4 is possible. The last point is that, in any over-all system, each and every step must be fully appraised in both conversion efficiency and signal to noise ratio.

It is to be noted in all this discussion that the information index does not depend upon the resolution but only upon the number of photons per $cm.^2$. This arises from the basic definition which shows (appendix) that as the area of visual integration increases, the required contrast difference for detection decreases and the product $cr$ remains constant. Actually, data on the eye show that for large areas, one needs a smaller contrast difference (3 instead of 5) for identification which would make the index a little higher. In practice, however, resolution is a very important parameter for any diagnosis and probably should be specified separately. The discussion herein assumes that the resolution is at all times adequate for the problem at hand.

While steps outlined in Table I for various x-ray diagnostic procedures are all familiar to the diagnostic radiologist, it is important to re-emphasize that all steps in the processes introduce noise and geometric distortions and that each must be judged in terms of its effect on the over-all information per patient dose. These are shown in Tables IIa through IIe for various systems.

To further pursue this general approach let us transfer our attention to radioisotope scanning. Here a collimated detector is used to determine and present the distribution of radioisotopes in a particular organ or tissue structure. In this particular instance, the signal interaction may be considered to be the distribution of the radioisotopes since this is the primary alteration which determines the observed pattern. The detector is a scintillation counter in which the gamma ray signal is absorbed in a crystal and converted into light. This light signal in turn is converted into an electric charge which is amplified by a photo-multiplier tube and associated electronics and presented for display on film or printed out in spatial array on paper. There may be an intervening storage system, such as tape or film with eventual presentation on film or televison monitors. It is important to observe that distortion of the pattern arises from the nature of the detecting collimator and is indentical in its effect to the influence of the size of the focal spot in x-rays. The scattered radiation is also a source of unsharpness, while noise arises in the scintillation counter from leakage and background, the photo-multiplier system, and finally, the storage system. In this particular system, the principal source of noise is quantum in nature due to the small particle flux emanating from the radioactive source itself.

As mentioned, this limitation results from patient dose considerations only. A typical roentgenogram which results in a patient dose of perhaps 0.1 r utilizes a flux about $10^7$ photons/$cm.^2$. The statistical fluctuation in this is 0.003 per cent and the resolution is 0.3 mm. On the other hand, a typical liver scan with a single bore collimator produces a patient dose of 5 r, a resolution of 1 cm. and a detected photon density of about 300 per sq. cm. The statistical fluctuation in this is 6 per cent. The difference in information index per patient dose is tremendous as is shown in Table III. These differences are due primarily to the poor collection efficiency of the detector

and the fact that the source continues emitting after the scintigram is made.

To put it conversely, if roentgenograms were made with a very large focal spot equal to the size of the projected collimator bore used for isotope scans and the x-ray photon flux was reduced to the order of 300 per sq. cm., the resultant roentgenograms would be essentially the same as scanograms.

Perhaps we have belabored this unnecessarily, but we wish to point out that all physical instruments systematically used for pattern recording and display may be analyzed on the above basis. Any method or system which records a pattern of internal organs and structures and uses visual presentation must clearly be of prime importance to the radiologist. At the present time, he has confined himself primarily to x-rays, since the signal interaction with tissues is of a unique character and the large amount of information that can be stored on film provides an exceptionally valuable display which can be received and managed by the eye-brain system. There are, however, other promising systems, such as ultrasonic echo mapping and temperature mapping (thermography) which permit the visualization of internal structures in a different way.

Ultrasonic echo mapping is based on the fact that sound waves are reflected at any boundary separating two volumes of different acoustic impedance. Since the resolution is determined by the wave length of the sound wave, high frequency sound (ultrasound) is used. By pulsing the sound source and detecting the reflected sound (echos) at a later time determined by the distance to the boundary, a two dimensional picture can be made of the reflecting boundaries.

The shape and orientation of the boundary, the difference in impedance, and the absorption of the intervening tissues determine the intensity of the reflection. Patient dose is limited by the thermal rise of critical tissues due to the absorption of the ultrasound.

Thermography is simply a collimated detector sensitive to the temperature of a given observed surface so arranged to scan an object and present a picture of the detected surface temperatures. Its use lies in the fact that disturbances in depth apparently can change the near surface temperature of the skin. While patient dose is of no concern here (unless one is observing the response to an insult), observing time is distinctly limited by patient discomfort and environmental changes.

These systems, as shown in Tables IId and IIe, just as in the roentgenographic process, have inherent noise, geometric unsharpness, utilize storage, permit the manipulation of the stored information, and ultimately produce a visual display. The challenge presented to the diagnostic radiologist with these new devices is that he has indeed major contributions to make, because of his years of intensive involvement with the radiation signal which has been manipulated to provide a display pattern of internal structures and their eventual translation into disease processes. We believe that now it is becoming increasingly important for the radiologist to dissect out the various elements involved in the final translation of the signal into the visual display and the manner in which this visual display is best handled.

Already there are in the background proposals for utilizing the radiation signal following its interaction in the body in ways other than those which we have traditionally known. It is conceivable that the photons might be translated directly into electrical signals and eventually displayed in a system which does not utilize the photographic process. If this were indeed possible, enormous improvement in handling, storing, and transmission of the x-ray image could be realized. However, as has been pointed out earlier, every step involved in the conversion of the original signal reduces the information capacity. It may prove sensible to accept a more limited level of information in order to introduce important advantages in the manipulation,

detection, storage, and display of the roentgen image.

There is ample evidence to indicate that already there is far more information detected and stored in a roentgenogram on film than is necessary for most diagnoses.

The future of visualization of internal structures is indeed promising, since the basic concepts are common to all systems, no matter what the origin of the signal. Radiology, with nearly 70 years of experience, is in a highly advantageous position to make effective contributions.

Hymer L. Friedell, M.D.
Department of Radiology
Western Reserve University
Cleveland, Ohio 44106

## APPENDIX

From present day concepts of information and information content, it is obvious that any precise message—like the letter $S$—has an infinite information content. If we now look at "noise" as a message with a gaussian distribution of probabilities, it follows that any one sampling will not represent the desired average value, but rather will only have a certain probability that it is the average value. From this viewpoint, then, it can be shown that the information content of a small sampling area $A$ of a spatial distribution of gaussian noise with an average density of $S$ per unit area and a variance of $\sqrt{SA}$ in each area $A$ is $Cga = log_2 \sqrt{SA}$ bits. Since there are $A^{-1}$ areas per unit area, we have $Cg = A^{-1} log_2 \sqrt{SA}$ bits per unit area. Now, if we consider $S$ to be the "amplitude" of information theory, the signal power is $S^2$ and if we add noise with an rms variation of $N_A$ in each area $A$, the usual formula for the information capacity of a channel becomes

$$Cc = A^{-1} \log_2 \left(1 + \frac{K^2S^2}{N_A{}^2}\right)^{1/2}$$

$$\cong A^{-1} \log_2 \left(\frac{KS}{N_A}\right) \text{bits/unit area}$$

$$\text{for } K^2S^2/N_A{}^2 \gg 1.$$

This formula holds only if the system is mean square limited and has no intersymbol interference. Intersymbol interference occurs when signal from adjacent test areas "floods" over into the actual test area. $K$ is a constant that essentially determines the risk of error involved. It is interesting that if we consider the added channel noise to be the noise in the signal itself and $K = 1$, then $N_A = \sqrt{S/A}$ and $Cg \cong Cc$. It is important to note that the above formulation for $N_A$ results from the fact that the rms deviations in the average number $S$ become larger as the test area becomes smaller.

Consider now the information index as defined by Hay[2] where it is assumed that for a test area (square, of sides $d = 1/r$ where $r$ is the resolution) to be just seen, it must differ in number of events from adjacent test areas of the same size by at least 4 to 5 times the rms variations in these same adjacent areas. If $S$ is the average number of events per unit area (cm.$^2$), then $N_A{}^1 = Sd^2$ and $\Delta N_A{}^1 \geq 5\sqrt{Sd^2}$.

Defining the contrast sensitivity $c = N_A{}^1/\Delta N_A{}^1$, we see $cr = \frac{1}{5}\sqrt{S}$.

Now, if we add noise with an rms variation of $N$ per unit area, we see that the total rms fluctuation in the adjacent background test areas is

$$\sqrt{Sd^2 + N^2d^2}$$

and

$$cr = \frac{1}{5} \frac{S}{\sqrt{S + N^2}} \cong \frac{1}{5} \frac{S}{N} \qquad \text{for } N^2 > S.$$

It is very important to note that the index is concerned with the number of events and their fluctuations in each test area while the information capacity is concerned with the influence of the fluctuations in the test area on the determination of the average number of events per unit area. Along this line, the contrast sensitivity as defined and used in the "index" increases with the test area which is a property of the threshold limited eye. Thus, we see again that the "index" is a measure of the optimum performance of a system

including the eye while the "capacity" is concerned only with the capabilities of the system prior to the eye. By the above relations, however, it is possible to calculate the information content of a gaussian message as seen by the threshold limited eye-brain system. This can be considered to be the information "capacity" $C_B$ of the eye. We obtain

$$C_B = A^{-1}\log_2 [1 + A(cr)^2]^{1/2}$$
$$\cong 4r^2 \log_{10} (1 + c^2)^{1/2} \qquad \text{for } K^{-1} = 5.$$

This formulation shows an increase in information capacity with increasing resolution and contrast sensitivity.

Using data for the eye at 25 cm. viewing distance and high illumination levels (100 millilamberts), we compute $C_B = 1.9 \times 10^5$ bits/cm.$^2$ of apparent image at 25 cm. which is about $\frac{1}{8}$ that of film and 800 times that of one television frame. This final eye-brain image capacity obviously depends upon both the resolution and the illumination level and represents the upper limit to any visual interpretation of a message.

If extraneous noise of power $N^2$ per unit area is introduced into the system, it is possible to show

$$C_B = C_C = A^{-1}\log_2\left(1 + \frac{K^2S^2A}{S + N^2}\right)^{1/2}$$
$$\cong A^{-1}\log_2 (KSA^{1/2}/N) \qquad \text{for } N^2 > S.$$

This expression is obviously the information capacity of the over-all eye-brain system when the limitations (noise) are introduced prior to the eye. In this case it is assumed that the eye has sufficient illumination so that it is not threshold limited. For cases where the noise is signal dependent, the formulation must be modified slightly. Enlargements and applications of these concepts to other systems such as scintiscanning will be given in another paper.

REFERENCES

1. Bell, D. A. Statistical Methods in Electrical Engineering. Chapman & Hall, Ltd., 1953.
2. Hay, G. A. Quantitative aspects of television techniques in diagnostic radiology. *Brit. J. Radiol.*, 1958, *31*, 611–618.
3. Jacobson, B., and MacKay, R. S. Radiological contrast enhancing methods. Volume VI. In: Biological and Medical Sciences. Academic Press, Inc., New York, 1958.
4. Jones, R. C. Information capacity of photographic film. *J. Opt. Soc.*, 1961, *51*, 1159.
5. Kovasznay, L. S. G., and Joseph, H. M. Image processing. *Proc. I. R. E.*, 1955, p. 560.
6. Rose, A. Quantum effects in human vision. In: Biological and Medical Sciences, Volume 5. Academic Press, Inc., New York, 1957, p. 211.
7. Shannon, C. E., and Weaver, W. The Mathematical Theory of Communication. University of Illinois Press, 1963.
8. Woodward, P. M. Probability and Information Theory. McGraw-Hill Book Company, Inc., New York, 1953.
9. Symposium on Photoelectric Image Devices. Volume XII. Advances in Electronics and Electron Phy\$ics. Academic Press, Inc., 1960.

# STEREOSCOPIC ILLUSTRATIONS*

By JOSHUA A. BECKER, M.D.†
PHILADELPHIA, PENNSYLVANIA

THE problem of the perfect presentation of a stereoscopic image on the printed page has not been adequately solved. Various processes have been devised and used in the publication of stereoscopic material.

The list of these includes:

1. *Crossed eye presentation.* The viewer crosses his eyes and, using the appropriate stereoscopic pair of films, he will fuse the images into a three dimensional view.

2. *Stereopticon.* This is a mechanical device to present a separate image to each eye. The old type used in the early 1900s has been replaced by the stereoscopic viewer of today equipped with adjustable optics and a battery light source.

3. *Anaglyphic process.* In this method the stereoscopic images are printed, superimposed, either in two colors or in the polaroid process. The images are separated with appropriate colored glasses; *i.e.*, red and green or polaroid glasses.

4. *Lenticulated paper.* This is a patented printing process that has recently been introduced. Its expense and fidelity are problems that limit its present use.

For the observer to see in depth, two images are required, each with a different perspective; *i.e.*, equivalent to that produced by 2 inches of separation in the viewing of the scene: the interpupillary distance. This is obtained in roentgenology by shifting the roentgen-ray tube and exposing two films—the right eye and left eye roentgenograms. These two images permit us to identify the depth relationships.

Photographers have used the following simple method in the illustration of 3 dimensional objects: with optimal black and white reproduction, a stereoscopic image can be seen with the aid of a 2×3 inch pocket mirror.

Starting with the stereoscopic roentgenograms, the illustration is processed in the following manner:

1. The left eye film is reproduced in the usual manner for the preparation of printed illustration.

2. The right eye roentgenogram is turned over, reversing the left and right side, and is, therefore, a mirror image of itself.

3. This right eye mirror image is now used to produce the plate for the illustration.

4. The final prints of the right and left images should be large enough, so that, with the head approximately 1 foot from the page, either image will fill the field of view of one eye.

5. These illustrations are placed 2 inches apart on the page.

For viewing, the small mirror is placed along the right side of the nose, the mirror side towards the right eye (Fig. 1, *A* and *B*). The mirror should almost block the left eye image from the right eye. The mirror is angulated to reflect the right eye image, and the head is moved from side to side until the two images are of equal size. Then, the mirror is again angulated until the right eye image is superimposed on the left eye image. The observer should then stare slightly to the left, and the image will be seen stereoscopically.

We have been impressed with the aid that stereoscopic studies can give in certain instances (Fig. 2, *A* and *B*); we hope that others who are similarly inclined may use this technique to illustrate their findings.*

Temple University Hospital
3401 N. Broad Street
Philadelphia, Pennsylvania 19140

* A similar method for stereoscopic viewing of roentgenograms was published in this Journal by E. S. Kerckes, 1956, *75*, 140.

* From the Department of Radiology, Temple University School of Medicine and Hospital, Philadelphia, Pennsylvania.
† Scholar in Radiologic Research of the James Picker Foundation.

(*For illustrations, please turn page*)

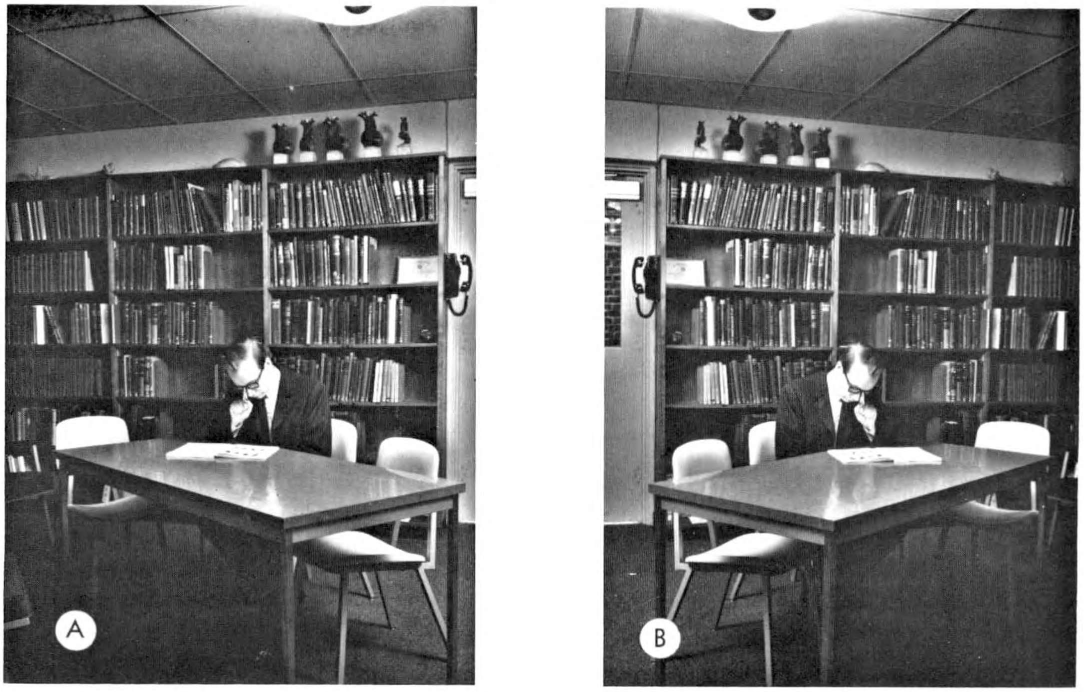


Fig. 1. (*A*) Left eye. (*B*) Right eye. The subject (viewing the journal on table) can easily be separated from the bookcase behind him; note how clearly several hairs on his head are seen when the scene is viewed stereoscopically.

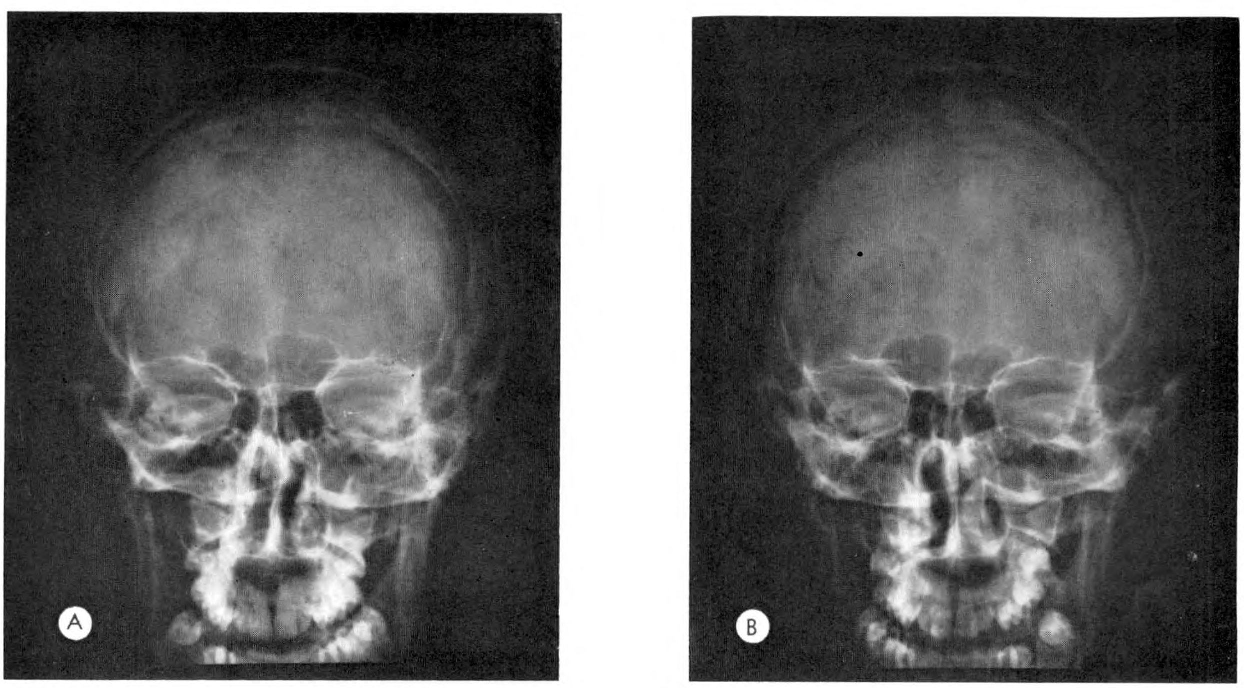


Fig. 2. (*A*) Left eye. (*B*) Right eye. This is a posteroanterior projection—the orbits are the most distant structures. The sphenoid ridges and petrous can be seen as separate portions of the skull, although they are superimposed on the two dimensional roentgenogram.

# MEDICAL THERMOGRAPHY*

*By* J. GERSHON-COHEN, M.D., D.Sc. (Med.), *and* J. D. HABERMAN, M.D.
PHILADELPHIA, PENNSYLVANIA

THERMOGRAPHY is a form of heat portrayal which can be used effectively in medicine. Since heat is a form of energy confined to the infrared portion of the electromagnetic spectrum, thermography might be referred to as another radiologic discipline. Infrared radiation is part of the same electromagnetic spectrum which comprises roentgen rays and gamma rays, the basis of roentgenologic and radiologic practice. Thermography might therefore some day assume importance similar to roentgenology, although concerned with a different portion of the electromagnetic spectrum.

Every object whose temperature is above absolute zero spontaneously emits electromagnetic energy in the infrared part of the spectrum. The total amount of energy emitted is proportional to the fourth power of the object's temperature and is expressed in "degrees Kelvin"—*i.e.*, 32°F. = 0°C. = 273°K. Thus the total radiant energy emitted by every object may be expressed by the formula $R \sim ET^4$, where emissivity or $E$ varies from zero to unity and describes the physical and chemical characteristics of the object's surface. For a perfect mirror which reflects 100 per cent of the energy striking it, $E$ would be equal to 0; for a perfectly opaque object, where all the energy striking it is absorbed and none is reflected or transmitted, $E$ would be equal to 1. For a highly polished mirror $E$ is about 0.02, whereas for human skin $E$ approaches 1.

Energy emitted by man falls within a broad band of wave lengths stretching from about 3 $\mu$ to beyond 20 $\mu$, with a maximum at about 10 $\mu$. Although these wave lengths are invisible (visible light extends from about 0.4 $\mu$ for violet to 0.8 $\mu$ for red), they may be collected optically, amplified electronically, and utilized in much the same fashion as light. To instruments sensitive to this infrared part of the spectrum all objects appear incandescent in their own self-emitted "light," and may therefore be detected, measured, or photographed.[1]

The detection and study of self-emitted infrared rays thus provide us with a powerful diagnostic method and make possible a direct approach to nondestructive testing. The potentialities of this method are obviously great, and its total scope in medicine is as yet undetermined.[2]

Almost 100 years have elapsed since Wunderlich demonstrated the value of recording body temperature in the diagnosis, prognosis, and treatment of illness.[12] With the introduction of the prototype of the present-day clinical mercury thermometer, thermometry was put on a practical basis and rapidly achieved universal acceptance. An oral thermometer measures only the temperature of the mouth, yet it has served so effectively to reflect the temperature of the body that such readings are mandatory on every patient's hospital chart.

Since skin is a perfect absorber of heat, it is also a perfect emitter, and the emanating infrared rays can be detected and recorded with thermisters, thermocouples, thermopiles, and more sophisticated apparatus often referred to as thermographs.[6,11] Thermography is a method which measures these infrared emissions so as to obtain an accurate determination of surface temperatures of the body. Contact

* Presented at the Sixty-fifth Annual Meeting of The American Roentgen Ray Society, Minneapolis, Minnesota, September 29–October 2, 1964.

From the Division of Radiology, Albert Einstein Medical Center, Philadelphia, Pennsylvania. Supported in part by USPHS Grant No. CA-07084 (02) RAD from the National Cancer Institute, Bethesda, Maryland, and by the Samuel S. Shubert Foundation, Inc., through the good offices of Mr. Lawrence Shubert Lawrence, Jr., New York, New York.

Some of this material was presented in the George E. Pfahler Oration given at the Twenty-eighth Annual Postgraduate Institute of the Philadelphia County Medical Society, April 2, 1964, in Philadelphia, Pennsylvania.

with the skin, necessitated by thermocouples, is avoided. Other advantages are rapidity of recording, integration of measurements of small skin areas rather than point contact recordings, and avoidance of thermal loading.

In the apparatus we are now using,* the infrared radiation emitted from a patient falls upon a scanning mirror and is then focused upon a sensitive thermister heat detector. By means of a rotating chopper, the incoming energy is compared 200 times per second with the energy being emitted by an ambient controlled temperature reference. After the infrared radiation has been converted by the thermister to an electrical signal and after the signal has been suitably amplified and processed, proportional output is used to control the intensity of a glow modulator tube which emits visible light. This light is reflected from a mirror attached to the back of the scanning mirror and then focused upon the film of a camera. A quantitative two-dimensional record of the infrared emission from the subject is thus obtained directly from the density of the photographic film. The hot areas are portrayed in light shades of gray and the cool areas in darker tones. To facilitate calibration, 10 sensitivity ranges of known values are reproduced on each thermogram, forming a quantitative "thermal gray scale." The sensitivity of the apparatus may be varied so that the full dynamic capability of the film may be utilized for any one of the 10 ranges of temperature difference.

With a portable radiometer recently made available, direct surface temperature readings over a suspect area can now be made and compared with those of its opposite symmetric image. This instrument also makes possible selection of proper settings on the thermograph in order to take advantage of the full dynamic range of the film emulsion. Optimal contrast is thus achieved in the same way that the selection of proper kilovoltage governs procurement of optimal contrast on roentgenograms.

* Barnes Engineering Co., 30 Commerce Road, Stamford, Conn.

The infrared apparatus may be focused from 3 feet to infinity and can encompass 10 angular degrees vertically and 20 angular degrees horizontally. The full scan of the patient can be obtained in 4 minutes. The picture or thermogram contains approximately 60,000 bits of temperature information with an optical resolution of about one angular mil. This resolution can record detail as small as $\frac{1}{8}$ inch at a distance of 10 feet.[1,2]

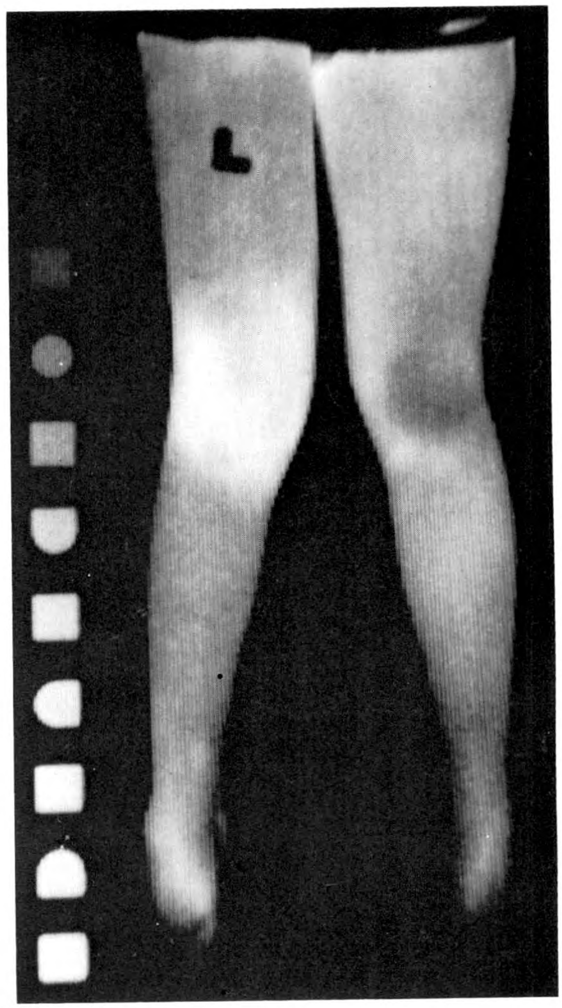

Fig. 1. Acute rheumatoid arthritis. Thermogram made 4 days after the onset of pain, swelling, and tenderness of the left knee and ankle reveals increased skin temperature (>2°C.) over these joints. The course of this attack could be followed objectively by repeated examinations similar to our current one employing the oral thermometer, but in this case, the oral temperature was normal.

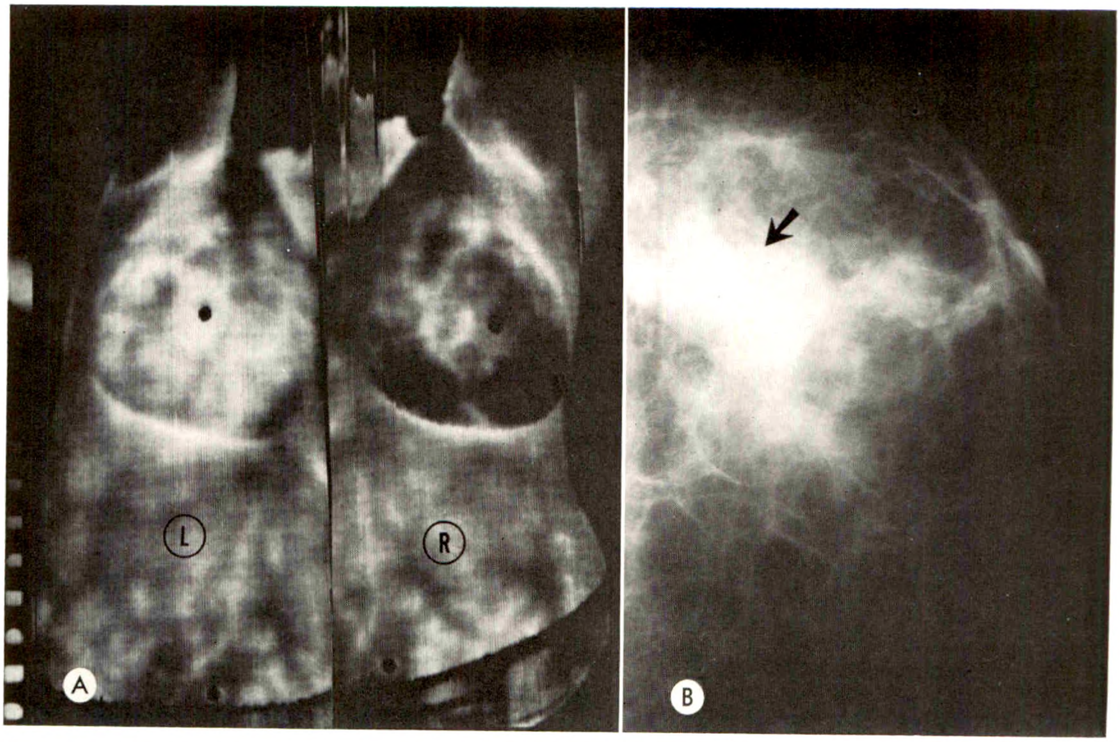


Fig. 2. Infiltrating duct carcinoma of left breast. (*A*) Thermogram reveals 2.5°C. skin temperature elevation over lesion in left breast, as compared with similar area of the right breast. (*B*) Mammogram of lesion. The presence of surrounding sclerosing adenosis was also reported by the pathologist. The patterns of elevated temperatures over both breasts have intrinsic diagnostic implications of physiologic and pathologic states, which will require further study and analysis, also suggested by the findings shown in Table I.

## CLINICAL APPLICATIONS

Using our present apparatus, the unclothed patient is exposed to an ambient temperature of 70°F. for 15 or 20 minutes. The patient is permitted to lie comfortably in a prone position during the examination, since the radiation coming from the body can be reflected into the camera from a mirror above the patient angled at 45°. The front rather than the rear surface of the mirror is silvered so as to permit optimal reflection of the infrared rays.

If the breasts are to be examined, the arms are raised so as to prevent cross radiation of the axillae from the arms to the chest wall. The shade of gray on the thermogram over the suspected lesion is compared with a similar area of the contralateral breast with reference to a standardized thermal gray scale. This is done with a recently developed densitometer and an automatic X-Y plotter by which the thermogram is analyzed with objective precision instead of by the unaided eye.[5] Differences in temperature are thus determined and when found to be locally elevated, an abnormal physiologic or pathologic process may be suspected such as might characterize a rapidly growing neoplasm, inflammation, or an unusually active physiologic process.

Among more than 3,000 examinations, elevation of skin temperature has been found over such diverse conditions as primary and metastatic cancers, fractures, contusions, myositis, tendonitis, herniated disks, abscesses, arthritis, and various forms of peripheral vascular disease. Among patients with breast cancer, more than 95 per cent have been found to exhibit localized skin temperature elevations. Not all local skin temperature elevations of the breast are due to cancer (Table I).

The reading of thermograms is ap-

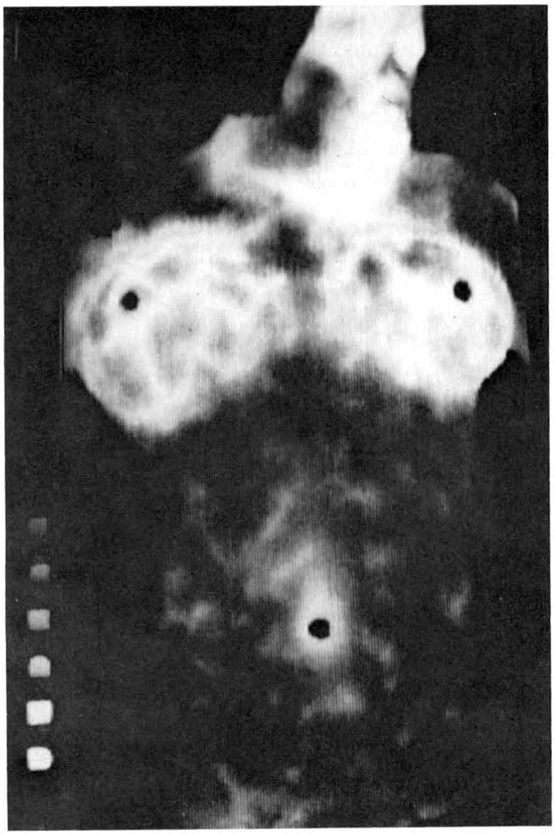

FIG. 3. Breasts and position of placenta during 8th month of pregnancy. Skin temperature of both breasts is >1.5°C. above average normal temperature. Elevated temperature over lower abdomen, >1.0°C., marks confirmed position of the placenta in upper anterior portion of uterus. Umbilicus and nipples are identified by aluminum markers placed in position before thermographic examination.

proached in many respects like that of clinical thermometry but with an important difference. An elevated oral temperature of itself does not establish a diagnosis. In contrast, a localized elevation of skin temperature as revealed by a thermogram circumscribes the area of study. Since the thermogram records thousands of temperature variations in meaningful shades of gray to form a pictorial map, not unlike a conventional roentgenogram, familiarization with these variations and their significance leads to recognition of valuable diagnostic criteria much like that involved in the interpretation of roentgenograms.

Finally, thermography, like thermometry, is among the first steps to be taken in the examination of a patient; but since thermography pinpoints the area to be investigated further, arrival at a final diagnosis is hastened. Examples of the varied uses of thermography are illustrated in Figures 1 through 5.

## DISCUSSION

Localized skin temperature elevations have long been recognized to be present over inflammatory processes, but Lawson,[7] and Williams, Williams, and Handley[10] reported elevation of skin temperature over malignant tumors. Carried out under controlled conditions, thermography unearths a wealth of information concerning metabolic activity of structures within the body.[3,4]

Thermography must not be confused with infrared *photography*, which depends upon waves reflected by the surface of the object photographed. The short infrared rays used in infrared photography must come from a hotter extrinsic source. On the other hand, the infrared radiation used in thermography lies in that portion of the spectrum to which sensitive photographic emulsions are not available. By converting the long infrared rays in the thermograph to light waves, however, ordinary photographic films may be exposed.

TABLE I

DISEASES OF THE BREAST ASSOCIATED WITH LOCALIZED SKIN TEMPERATURE ELEVATIONS

| Diagnosis | No. of Cases | Elevation >1°C. | Elevation <1°C. |
|---|---|---|---|
| Normal | 90 | 16 | 74 |
| Cancer | 91 | 88 | 3 |
| Adenosis and Mazoplasia Cystica | 62 | 8 | 54 |
| Secretory Disease | 23 | 8 | 15 |
| Fibroadenoma | 19 | 9 | 10 |
| Cysts | 17 | 3 | 14 |
| Epithelial Hyperplasia | 13 | 6 | 7 |
| Plasma Cell Mastitis | 4 | 3 | 1 |

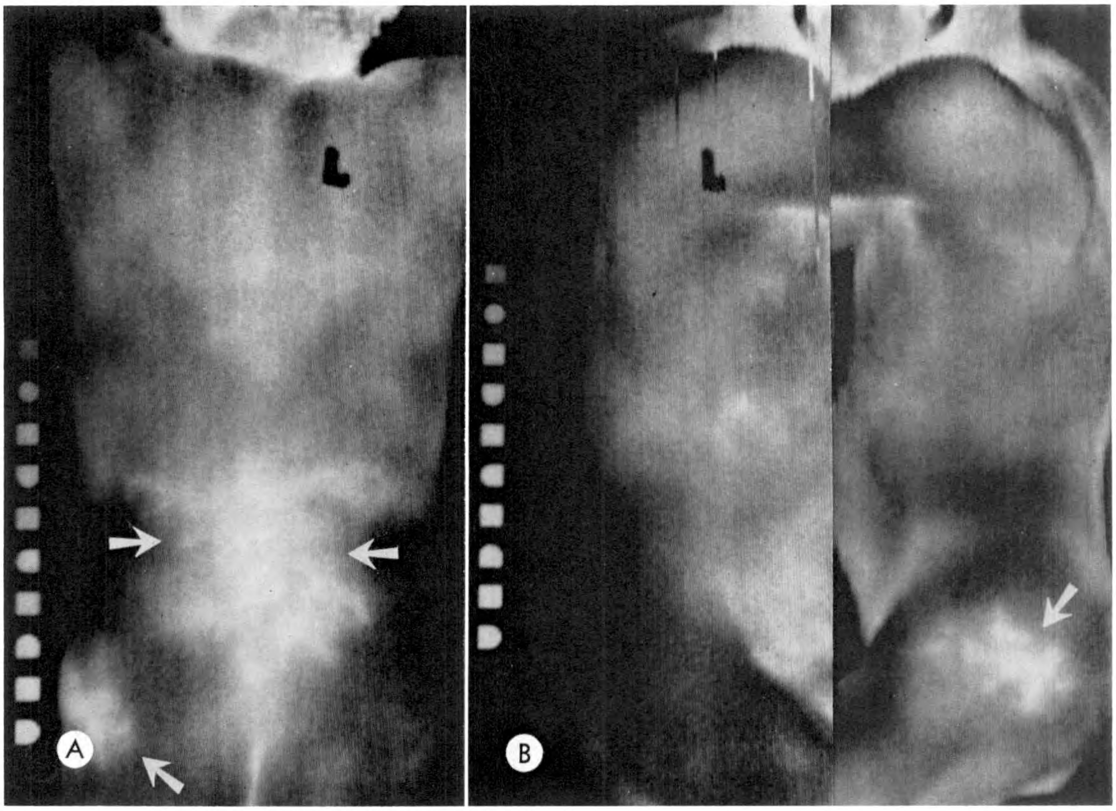


FIG. 4. Metastatic prostatic carcinoma to lumbar vertebrae and right pelvis. (*A*) Skin temperature over lumbar area and right pelvis is elevated, >2.0°C. Compare light (warmer) gray tones over lateral right pelvis with darker (cooler) similar areas of the left pelvis. (*B*) Right lateral thermogram reveals mosaic pattern of temperature elevations over metastatic lesions in ilium and ischium.

It would be natural to suppose that the skin temperature elevation over pathologic processes would stem chiefly from the associated increased vascularity, but observations already made indicate that the cause resides more in the cellular activity of the lesions.[8] The increased number of cells involved in an inflammatory or malignant process or in an area of increased cellular metabolic activity seems to be largely responsible for the elevation of local temperature. The absorption and radiation of heat from these lesions by the overlying skin make thermography possible.

Research and development of infrared detectors have advanced considerably in the last 3 decades. Infrared sensing devices in the nose cones of rockets guide them toward a hot target with phenomenal accuracy. Improvements in the sensitivity and response time of photo-conductors and the improvement of signal-to-noise ratio achieved with cooling the detectors have made it possible to detect the heat of a match at 20 miles with a response time on the order of microseconds. With such rapidly expanding knowledge, application of these new techniques to medical problems should result in ever more sensitive and efficient apparatus.[9] It is hopefully anticipated that technical advances in thermography will help to accelerate its use in the diagnosis, prognosis, and treatment of a wide variety of diseases.

## SUMMARY

Thermograms are images of body surface temperatures which record changes over localized metabolic, inflammatory, or malignant disturbances in and below the

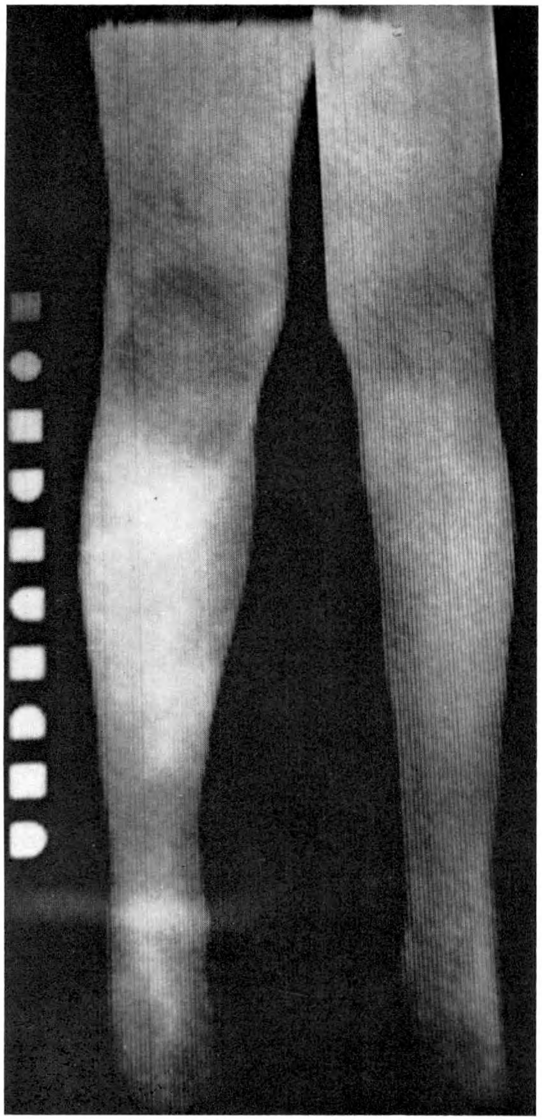

Fig. 5. Thrombophlebitis, left leg, associated with a pattern of skin temperature elevations varying up to>2.0°C. over upper leg and ankle as compared with opposite side. To follow progress of disease, serial thermograms can be obtained similar to oral temperature charting during the course of an illness.

skin surface. Some applications of this technique to medicine have already been made in the study of fractures, trauma to the soft tissues, arthritis, localized inflammations, primary and secondary malignancy of the soft tissues and bones, and in peripheral vascular disease.

In conjunction with mammography, thermography has yielded much helpful data in diagnosis and treatment of breast diseases. Physiologic activity within the breasts and placental localization during pregnancy have produced positive thermographic findings. With widespread application of this discipline and with improvements in apparatus and techniques, it is expected that thermography will broaden its scope of clinical usefulness in biology and medicine.

J. Gershon-Cohen, M.D.
Albert Einstein Medical Center
York and Tabor Roads
Philadelphia, Pennsylvania 19141

We are grateful to R. Bowling Barnes, Ph.D., President, Barnes Engineering Co., Stamford, Conn., for his expert help and counsel.

REFERENCES

1. Astheimer, R. W., and Wormser, E. M. High-speed infrared radiometers. *J. Optic. Soc. Amer.*, 1959, *49*, 179–183.
2. Barnes, R. B. Thermography of human body. *Science*, 1963, *140*, 870–877.
3. Barnes, R. B., and Gershon-Cohen, J. Thermomastography. *J. Albert Einstein M. Center*, 1963, *11*, 107–112.
4. Barnes, R. B., and Gershon-Cohen, J. Clinical thermography. *J.A.M.A.*, 1963, *185*, 949–952.
5. Brueschke, E. E., Haberman, J. D., and Gershon-Cohen, J. Relative densitometric analysis of thermograms for more precise temperature determinations. *Ann. N. Y. Acad. Sci.*, 1964, *121*, 80–89.
6. Hardy, J. D. Radiation of heat from human body. III. Human skin as black-body radiator. *J. Clin. Invest.*, 1934, *13*, 615–620.
7. Lawson, R. N. Implications of surface temperatures in diagnosis of breast cancer. *Canad. M. A. J.*, 1956, *75*, 309–310.
8. Lawson, R. N. Personal communications.
9. Williams, K. L., Cade, C. M., and Goodwin, D. W. Electronic heat-camera in medical research. *J. Brit. I. R. E.*, 1963, *25*, 241–250.
10. Williams, K. L., Williams, F. J., and Handley, R. S. Infra-red thermometry in diagnosis of breast disease. *Lancet*, 1961, *2*, 1378–1381.
11. Wormser, E. M. Properties of thermister infrared detectors. *J. Optic Soc. Amer.*, 1953, *43*, 15–21.
12. Wunderlich, C. A. On the Temperature in Diseases: a Manual of Medical Thermometry. Translated from the second German edition by W. B. Woodman. The New Sydenham Society. London, 1871.

Vol. 94, No. 3

# ABSTRACT CARD CLASSIFICATION AND RETRIEVAL SYSTEMS FOR RADIOLOGIC LITERATURE*

*By* RICHARD E. ERNST, M.D.
ST. LOUIS, MISSOURI

As a result of the rapidly expanding volume of medical literature published each year, it is becoming progressively more difficult and time-consuming to find specific information in the journals. For this reason, a practical radiology abstract classification and filing system based on the use of edge-punched cards has been developed to be used as an adjunct to the established methods of searching the literature.

While at times it is important to thoroughly investigate the literature, more frequently in the practice of radiology it is sufficient to recall a recently read article for review. This article provides not only the latest information but a bibliography of additional references which can be utilized if necessary. However, the time and effort required for even a limited search of the recent literature, using the cumulative indices, the volume indices, and the tables of contents of several different journals, can prove discouraging.

Many radiologists have tried to simplify the problem of recall by using abstract cards to record summaries of articles they have read. Such a card file provides a quick reference to specific current information of personal interest. While there is merit in such a card file, as it expands, the usual limited number of filing categories, lack of a simple method for cross-indexing, and difficulty in easily updating it by separating older abstracts from more recent ones seriously limit its value.

Numerous classifying and indexing systems have been developed for roentgenologic examinations.[1,3,4,7] Others have been designed for radiation therapy records.[5,8] However, in only a few of the medical specialties has consideration been given to the need for a practical abstract card classification and retrieval system. In 1945, Duncan *et al.*[2] devised such a system for anesthesiology literature based on the use of edge-punched cards. Ochs[6] in 1957 developed a similar system for neurophysiology.

We have designed an abstract card classification and retrieval system for radiologic literature that retains the advantages inherent in a personal card file but minimizes the disadvantages. This system utilizes edge-punched cards, thus permitting rapid and efficient sorting of the abstracts by semimechanical means without the need for expensive equipment or specialized training.

## EQUIPMENT

The card used with this system is an inexpensive, standard 3-3/10 inch by 7-1/2 inch edge-punched card of convenient size for handling and filing (Fig. 1). Holes punched around the periphery of each card are assigned specific numbers and functions of the classification system. Each hole is coded by notching away that portion of the card between the hole and the edge. This notching allows the coded cards to be separated from the unnotched cards when a sorting needle is inserted in one of the holes of a group of cards. Since the notched cards have nothing to support them on the needle, they fall away from the group, leaving the unnotched cards on the sorting needle.

Two coding methods are used: direct code and numerical code. In the direct code a single number and function are assigned to each hole. Notching a hole codes the number and function assigned to that hole. The numerical code is a space-saving device that uses only four holes to code a set of numbers from 1 through 9. These four holes are assigned numerical values of 7, 4, 2 and 1. By notching either a single hole or a

* From the Department of Radiology, De Paul Hospital, St. Louis, Missouri.

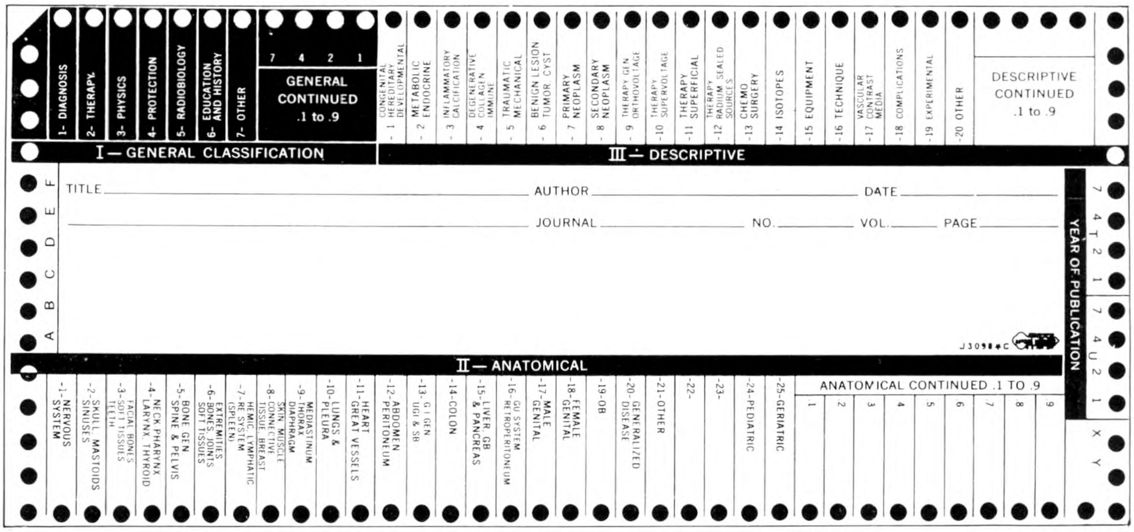


Fig. 1. Reproduction of the standard 3-3/10 inch by 7-1/2 inch index card printed with the basic classification. (This printed key sort card is available through Royal McBee—No. J3098*C.)

combination of two holes, any number from 1 through 9 can be expressed by the sum of the numerical value(s) of the hole(s) notched in each set. A set of four holes can thus be used to code as many as 9 items.

The direct code is the simpler of the two methods to understand and is, therefore, used whenever possible. Because of the limited number of holes around the periphery of each card, it is necessary to resort to the space-saving numerical code for less frequently used data. For example, the last two digits of the publication year of each abstracted article are coded along the left border of the card, using two sets of the numerical codes. The numerical code is also used to provide additional space on the card for coding certain minor subdivisions of the basic classification system.

The basic classification has been printed directly on each card. This system minimizes the need for reference to additional charts when coding, notching, and later sorting the cards, thus simplifying these procedures and greatly decreasing chances for error.

## CLASSIFICATION SYSTEM

The purpose of the classification system is to provide a simple and practical means of separating the radiologic literature into categories of related subject matter and to permit rapid retrieval of the needed information.

Every effort has been made to provide adequate separation of information, while preserving simplicity and practicability. Occasionally, there will be ambiguity in classifying and coding certain articles. We believe, though, that this difficulty is more than offset by the rapidity and flexibility with which the bulk of information can be retrieved, the objectives of this system being to permit the radiologist to quickly locate a relatively small number of related abstract cards on any particular subject which he can then further evaluate by manual-visual sorting for the exact information he desires.

The basic classification system consists of three major fields: Field I—General, Field II—Anatomic, and Field III—Descriptive; with each field divided into a number of related subject headings as shown in Table I.

Classification under Field I permits the primary separation of the literature into a limited number of large, generally well-defined categories. Classification under Field II describes the anatomic character (if

Table I

BASIC CLASSIFICATION SCHEME INDICATING THE SUBJECT HEADING FOR EACH OF THE THREE MAJOR FIELDS*

I. *General*

1. Diagnosis
2. Therapy
3. Physics
4. Protection
5. Radiobiology
6. Education and history
7. Other

II. *Anatomic*

1. Nervous system
2. Skull, mastoids, and sinuses
3. Facial bones, soft tissues, and teeth
4. Neck, pharynx, larynx, and thyroid
5. Bone, general, spine and pelvis
6. Extremities, bones, joints, and soft tissues
7. Hemic, lymphatic, reticuloendothelial systems, and spleen
8. Skin, muscle, connective tissue, and breast
9. Mediastinum, thorax, and diaphragm
10. Lungs, and pleura
11. Heart, and great vessels
12. Abdomen, peritoneum
13. Gastrointestinal system (general), upper gastrointestinal system and small bowel
14. Colon
15. Liver, gallbladder, and pancreas
16. Genitourinary system, retroperitoneum
17. Male genital
18. Female genital
19. Obstetrics
20. Generalized disease
21. Others
22.
23.
24. Pediatric
25. Geriatric

III. *Descriptive*

1. Congenital, hereditary and developmental
2. Metabolic, endocrine
3. Inflammatory, calcification
4. Degenerative, collagen, immune
5. Traumatic, mechanical
6. Benign lesion, tumor, cyst
7. Primary neoplasm
8. Secondary neoplasm
9. Therapy, general, orthovoltage
10. Therapy, supervoltage
11. Therapy, superficial
12. Therapy, radium, sealed sources
13. Chemotherapy, surgery
14. Isotopes
15. Equipment
16. Technique
17. Vascular (contrast media)
18. Complications
19. Experimental
20. Other

* This information is printed on each of the edge-punched cards.

any) of the material. Arbitrarily, two of the subject headings under Field II are used to provide separation of pediatric and geriatric information from the general literature because of the special problems related to these facets of radiology. Field III provides the necessary further separation of the abstracts according to the usual needs of the radiologist. These subject headings, therefore, define the nature of the disease processes, the type of diagnostic and therapeutic measures used, techniques and complications, as well as basic experimental work.

Provision has been made for possible further expansion of the classification in order to adapt the system to the needs of each individual user. Each abstract card contains space for numerical coding of up to 9 minor subdivisions under each of the subject headings of Field I and Field III. Space has also been provided for direct coding of up to 9 minor subdivisions under each of the subject headings of Field II.

The minor subdivisions of Field II are given in Table II. Minor subdivisions of Field I and Field III are left to the requirements of each radiologist.

## METHOD OF USE

In practice, an abstract is classified by appropriate coding, if possible, under each of the three major fields. When there is a question as to which of several possible subject headings is to be used in coding an individual abstract, it should be coded

TABLE II

MINOR SUBDIVISIONS OF THE SUBJECT HEADINGS
FIELD II—ANATOMIC

1. *Nervous system*
   1. Meninges
   2. Ventricles and midline structures
   3. Brain, general
   4. Brain, supratentorial (carotid artery and branches)
   5. Brain, subtentorial (vertebral artery and branches)
   6. Cranial nerves
   7. Spinal cord
   8. Peripheral nerves
   9.
2. *Skull, mastoids, and sinuses*
   1. Cranial vault
   2. Base of skull (sella turcica)
   3. Ear and temporal bone
   4. Accessory sinuses
   5.
   6.
   7.
   8.
   9.
3. *Facial bones, soft tissues and teeth*
   1. Facial bones (nose, zygoma)
   2. Mandible and teeth
   3. Eye and orbit
   4. Oral cavity
   5. Salivary glands
   6. Soft tissues
   7.
   8.
   9.
4. *Neck, pharynx, larynx, and thyroid*
   1. Soft tissues
   2. Pharynx
   3. Larynx
   4. Thyroid, parathyroid
   5.
   6.
   7.
   8.
   9.
5. *Bone (general), spine and pelvis*
   1. Generalized bone disease
   2. Spine, general
   3. Cervical spine
   4. Thoracic spine
   5. Lumbar spine
   6. Sacrococcygeal spine
   7. Pelvis, sacroiliac, and hip joints
   8.
   9.
6. *Extremities, bones, joints, and soft tissue*
   1. Upper extremities (soft tissues and vessels)
   2. Shoulder girdles and long bones
   3. Carpals, metacarpals, and phalanges
   4. Lower extremities (soft tissues and vessels)
   5. Long bones (excluding hips)
   6. Tarsals, metatarsals, and phalanges
   7.
   8.
   9.
7. *Hemic, lymphatic, reticuloendothelial systems (spleen)*
   1. Hemic, general
   2. Bone marrow
   3. Lymphatic
   4. Reticuloendothelial system
   5. Spleen
   6.
   7.
   8.
   9.
8. *Skin, muscle, connective tissue, and breast*
   1. Skin
   2. Muscle
   3. Connective tissue
   4. Breast
   5.
   6.
   7.
   8.
   9.
9. *Mediastinum, thorax, and diaphragm*
   1. Mediastinum, general (middle)
   2. Mediastinum (anterior)
   3. Mediastinum (posterior)
   4. Bony thorax and sternum
   5. Diaphragm
   6.
   7.
   8.
   9.
10. *Lungs and pleura*
    1. Respiratory system, general
    2. Trachea
    3. Bonchi and lungs
    4. Pleura
    5.

Table II—(*Continued*)

6.
7.
8.
9.

11. *Heart and great vessels*
 1. Heart
 2. Pericardium
 3. Lesser circulation
 4. Aorta and great vessels
 5. Vena cava
 6. Azygos system
 7.
 8.
 9.

12. *Abdomen and peritoneum*
 1. Abdominal cavity
 2. Peritoneum
 3.
 4.
 5.
 6.
 7.
 8.
 9.

13. *Gastrointestinal (general), upper gastrointestinal system and small bowel*
 1. Gastrointestinal, general
 2. Esophagus
 3. Stomach
 4. Duodenum
 5. Jejunum and ileum
 6.
 7.
 8.
 9.

14. *Colon*
 1. Cecum
 2. Ascending colon
 3. Transverse colon
 4. Descending colon
 5. Sigmoid colon
 6. Rectum
 7. Appendix
 8.
 9.

15. *Liver, gallbladder, and pancreas*
 1. Liver
 2. Gallbladder, bile ducts
 3. Portal system
 4. Pancreas
 5.
 6.
 7.
 8.
 9.

16. *Genitourinary system, retroperitoneum*
 1. Genitourinary system, general
 2. Kidneys
 3. Renal pelvis and ureters
 4. Bladder
 5. Urethra
 6. Retroperitoneum (adrenals)
 7.
 8.
 9.

17. *Male genital system*
 1. Reproductive system, general
 2. Scrotum
 3. Testicles, epididymis
 4. Seminal vesicles and ducts
 5. Prostate
 6. Penis
 7.
 8.
 9.

18. *Female genital system*
 1. Reproductive system, general
 2. Ovaries
 3. Uterus and adnexae
 4. Cervix uteri
 5. Vagina
 6. External genitalia
 7.
 8.
 9.

19. *Obstetrics*
 1. Obstetrics, general
 2. Pelvimetry and placental localization
 3. Fetal determination
 4.
 5.
 6.
 7.
 8.
 9.

20. *Generalized disease*
 1.
 2.
 3.
 4.
 5.
 6.
 7.
 8.
 9.

Table II—(*Continued*)

| | |
|---|---|
| 21. *Other* | 5. |
| 1. | 6. |
| 2. | 7. |
| 3. | 8. |
| 4. | 9. |
| 5. | 23. |
| 6. | 1. |
| 7. | 2. |
| 8. | 3. |
| 9. | 4. |
| 22. | 5. |
| 1. | 6. |
| 2. | 7. |
| 3. | 8. |
| 4. | 9. |

under that subject heading most nearly describing the gist of the article. If this cannot be determined, two or more subject headings under the same field may be coded and the card notched accordingly. This particular abstract card can then be retrieved from the file by sorting for any of the subject headings previously notched. In a similar manner, cross-references are easily provided simply by notching the additional appropriate subject headings on the card. The last two digits of the date of each abstract are appropriately coded on the card so that later, depending on the rate of growth of the card file, the older cards can easily be separated, thus keeping the file current and of manageable size.

Retrieval of specific abstract cards is usually accomplished by sequential sorting under each of three major fields. However, in order to obtain a varying degree of selectivity, sorting may be limited to only one or two fields. At times, it may be of advantage to sort for a combination of subject headings in a single field. In this manner, it is possible to "browse" through the abstract cards in search of specific information.

Since cards may be filed in a random manner and still be located by the sorting technique, the risk of losing a card through misfiling is eliminated. There is, however, an advantage in filing cards according to the subject headings under Field I. In this manner the cards are presorted according to these subject headings by their position in the file. Proof of correct filing can then be quickly obtained by noting the alignment of the coding notches of the cards under each subject. Therefore, by initially selecting the appropriate group of cards, the subsequent sorting procedures can be limited to Field II and Field III.

## SUMMARY

A practical abstract classification and card file system based on the use of edge-punched cards has been developed to be used as an adjunct to the conventional means of literature retrieval. Providing an additional avenue of approach to the increasing volume of radiologic literature and facilitating information retrieval should simplify and enhance the use of reference journals in the practice of radiology. The main advantages to this system are simplicity and flexibility with low initial and subsequent cost. Such a card file would represent a readily available and individualized record of each radiologist's evaluation of the literature he has read.

Beaumont Medical Building
3720 Washington Boulevard
St. Louis 8, Missouri

REFERENCES


1. DONALDSON, S. W. Code system for cross indexing records. AM. J. ROENTGENOL. & RAD. THERAPY, 1925, *13*, 81–87.
2. DUNCAN, G. W., HANLEY, H. G., and MORTON, H. J. V. Filing of abstracts and case-records. *Lancet*, 1945, No. 249, 379–380.
3. HODGES, F. J., and LAMPE, I. Filing and cross-indexing roentgen ray records; demonstration of simple and efficient method. AM. J. ROENTGENOL. & RAD. THERAPY, 1939, *41*, 1007–1018.
4. Index for Roentgen Diagnoses. Second edition. American College of Radiology, 1961.
5. LAMPE, I. Filing and cross-indexing of radiation therapy records. *Radiology*, 1945, *45*, 168–175.
6. OCHS, S. Elementary discussion of design of a punch card system exemplified by one for neurophysiology. *Texas Rep. Biol. & Med.*, 1957, *15*, 911–915.
7. SANTE, L. R. Indexing system for cataloguing of pathological films. *Radiology*, 1926, *7*, 149–163.
8. SCHULTZ, M. D., and WANG, C. C. Simple method of follow-up, disease indexing, and filing of radiation therapy records. *Radiology*, 1962, *79*, 842–847.

# THE AMERICAN JOURNAL OF ROENTGENOLOGY RADIUM THERAPY AND NUCLEAR MEDICINE

*Editor:* TRAIAN LEUCUTIA, M.D.
*Assistant to the Editor:* KENNETH L. KRABBENHOFT, M.D.
*Associate Editors:* HARRY HAUSER, M.D., RUSSELL H. MORGAN, M.D., EDWARD B. D. NEUHAUSER, M.D., WENDELL G. SCOTT, M.D.
*Consulting Editorial Board:* See front cover.
*Published by:* CHARLES C THOMAS, Publisher, 301–327 East Lawrence Avenue, Springfield, Illinois.

*Issued monthly. Annual subscription: United States, Mexico, Cuba, Central and South America, and Canada $15.00; other countries, $17.00. Current single numbers, $1.50. Advertising rates submitted on application. Editorial office, 110 Professional Building, Detroit 1, Michigan. Office of publication, 301–327 East Lawrence Avenue, Springfield, Illinois. Information of interest to authors and readers will be found on page ii.*



AMERICAN ROENTGEN RAY SOCIETY

*President:* H. O. Peterson, Minneapolis, Minn.; *President-Elect:* J. P. Medelman, White Bear Lake, Minn.; *1st Vice-President:* C. B. Peirce, Montreal, Que., Canada; *2nd Vice-President:* H. C. Sehested, Fort Worth, Tex.; *Secretary:* C. A. Good, Mayo Clinic, Rochester, Minn.; *Treasurer:* S. W. Brown, 1467 Harper Street, Augusta, Ga.

*Executive Council:* H. O. Peterson, J. P. Medelman, C. B. Peirce, C. A. Good, S. W. Brown, C. B. Holman, R. R. Greening, J. F. Roach, H. G. Reineke, J. C. Cook, R. M. Caulk, E. E. Barth, T. Leucutia, E. F. Van Epps, S. F. Ochsner, J. S. Dunbar, H. M. Stauffer, T. F. Leigh, Chairman, Emory University Clinic, Atlanta, Ga. 30322

*Program Committee:* C. A. Good, J. F. Roach, T. Leucutia, R. R. Greening, H. O. Peterson, J. P. Medelman, Chairman, White Bear Lake, Minn.

*Publication Committee:* J. A. Campbell, M. M. Figley, R. N. Cooley, J. F. Holt, J. F. Roach, Chairman, Albany, N. Y.

*Finance and Budget Committee:* J. S. Dunbar, H. M. Stauffer, R. E. Parks, T. M. Fullenlove, C. B. Holman, Chairman, Rochester, Minn.

*Committee on Scientific Exhibits:* R. G. Lester, J. O. Reed, R. R. Greening, Chairman, Philadelphia, Pa.

*Advisory Committee on Education and Research:* A. Raventos, A. R. Margulis, E. C. Lasser, F. J. Bonte, H. G. Reineke, Chairman, Cincinnati, Ohio.

*Representatives on the American Board of Radiology:* C. A. Good, Rochester, Minn.; C. A. Stevenson, Spokane, Wash.; J. F. Roach, Albany, N. Y.

*Director of Instruction Courses:* H. O. Peterson, Minneapolis, Minn.; *Assoc. Director:* D. G. Mosser, Minneapolis, Minn.

*Manager of the Annual Meeting:* J. C. Cook, 110 Professional Building, Detroit, Mich. 48201

*Editor:* T. Leucutia, 110 Professional Building, Detroit, Mich. 48201

*Representative on the Board of Chancellors of the American College of Radiology:* Seymour F. Ochsner.

*Sixty-sixth Annual Meeting:* Washington Hilton Hotel, Washington, D. C., Sept. 28–Oct. 1, 1965.

AMERICAN RADIUM SOCIETY

*President:* Justin J. Stein, Los Angeles, Calif.; *President-Elect:* Milton Friedman, New York, N. Y.; *1st Vice-President:* Manuel Garcia, New Orleans, La.; *2nd Vice-President:* Richard J. Jesse, Houston, Tex.; *Secretary:* John L. Pool, New York, N. Y.; *Treasurer:* Juan A. del Regato, Penrose Cancer Hospital, 2215 North Cascade Ave., Colorado Springs, Colorado 80907.

*Executive Committee:* Gilbert H. Fletcher, Chairman, Houston, Tex.; Charles G. Stetson; Joseph H. Farrow; Justin J. Stein; John L. Pool; Milton Friedman; Manuel Garcia; Richard H. Jesse; Juan A. del Regato.

*Scientific Program Committee:* Justin J. Stein, Chairman; Glenn E. Sheline; Robert C. Hickey; Lewis W. Guiss; Harvey P. Groesbeck, Jr.; Roald N. Grant; Milton Friedman; Joseph H. Farrow, Ex officio.

*Committee on Arrangements:* R. Lee Foster, Chairman, The Medical Center, 1313 North 2nd Street, Phoenix, Ariz. 85004; Clifford L. Ash; James M. Ovens; Jerome M. Vaeth.

*Publication Committee:* Harry Hauser, Chairman, Cleveland, Ohio; Wendell C. Hall, Hartford, Conn.; Martin Van Herik, Rochester, Minn.

*Public Relations Committee:* James M. Ovens, Chairman, Phoenix, Ariz.; John Day Peake; R. C. Burr.

*Janeway Lecture Committee:* William S. MacComb, Chairman, Houston, Tex.; Clifford L. Ash; A. N. Arneson.

*Representatives on the American Board of Radiology:* Donald S. Childs, Jr., Rochester, Minn.; Justin J. Stein, Los Angeles, Calif.; Bernard P. Widman, Philadelphia, Pa.

*Representative on the National Council on Radiation Protection and Measurements:* Herbert M. Parker, Richland, Wash., Liaison Member.

*Representative on the Board of Chancellors of the American College of Radiology:* Charles G. Stetson.

*Forty-eighth Annual Meeting—Golden Anniversary of the American Radium Society:* Camelback Inn, Phoenix, Ariz., April 13–16, 1966.

# EDITORIALS

## THE SIXTY-SIXTH ANNUAL MEETING OF THE AMERICAN ROENTGEN RAY SOCIETY

The American Roentgen Ray Society will hold its Annual Meeting, the Sixty-sixth, at the Washington-Hilton Hotel in Washington, D. C., September 28, 1965, to October 1, 1965. That occasion will mark the sixth time in the last fifteen years that the Society has chosen the City of Washington as its meeting place. And, the choice is no coincidence in regard either to the city or to the hotel. The Washington meetings have invariably been eminently successful from all standpoints. It is foreseen that this meeting will be no exception.

Washington is ideally situated as far as all means of transportation are concerned. It is reached directly by air from even the distant points of both hemispheres.

Washington has more than the usual attractions of large cities. The location was selected by General Washington in 1791, and the city is unique in that it was deliberately created to provide a seat for the National Government. It is laid out with the Capitol as the focal point. Avenues radiate from this center like the spokes of a wheel. It is a magnificent city with broad tree-lined streets and great public buildings housing the many federal bureaus. It abounds in national monuments and shrines. Its historical and art collections rank among the world's finest. But, its significance above all is ideological—the Capital of the United States since 1800, where one may still feel the presence of and be able to visit some of the homes of the enterprising men of ideas and ideals who founded and preserved our Nation.

The Society is fortunate that the new Washington-Hilton Hotel was planned and built at the time when it became apparent that the meetings had outgrown their former comfortable and pleasant locale. The Washington-Hilton is an exciting downtown hotel with the atmosphere of a resort. It towers high on a hill in the embassy area of the Capital. The grounds and interior structures are spacious. They are brilliantly designed and executed for both beauty and business-like efficiency.

Dr. and Mrs. Edgar M. McPeak head the Committees on Local Arrangements. Their plans are complete for four days (Monday through Thursday) of interesting social activities and reflect the time and effort that went into the planning.

The Ladies' Program includes cocktails and dinner for all members and guests on Monday, September 27, at the Flagship Restaurant, followed by a two hour sightseeing tour of the city. This particular affair is usually considered to be arranged for the "golf-widows." However, discrimination is not a policy of the Society so gentlemen may accompany their ladies to this or other appropriate events sponsored by the Ladies' Committee. On Tuesday, September 28, there will be a tour to the Woodrow Wilson House, Decatur House and Woodlawn Plantation in Virginia, with luncheon at the Lazy Susan Inn. Wednesday and Thursday mornings will afford opportunities for Private White House Tours. At noon on Wednesday, there will be a Luncheon and Fashion Show in the West Ballroom of the Washington-Hilton Hotel. On Thursday, at 6:30 P.M., the Annual Banquet will take place. A Ladies' Hospitality Room will be open in the Cabinet Room of the Hilton from 8:00 A.M. to 12:30 P.M., Monday through Thursday, September 27–30.

Registration desks will be open from 2:00

P.M. to 5:00 P.M. on Sunday, September 26. They will then be open daily from 8:00 A.M. to 5:00 P.M. throughout the week except that registration will close at 1:30 P.M. on Friday, October 1. Registration for all in attendance will be in the Concourse connecting the Hilton International Ballroom and the Exhibit Hall.

The annual Golf Tournament is scheduled for Monday, September 27. Dr. Ralph Caulk, a past-President of the Society, has again consented to act as Chairman of the Golf Committee. Dr. Caulk has demonstrated his great aptitude in arranging the Tournament on several previous occasions. Play will take place at the Manor Country Club, Norbeck, Maryland. Many of you will remember that this is a most interesting course in a delightful setting. Arrangements have been made for bus transportation to and from the Club and for lunch, golf and dinner there. In the evening following the dinner, among other pleasant and momentous diversions, there will be presentation of awards; most notably, the Willis F. Manges Trophy for the Net Score winner and the Exhibitors' Trophy for the Gross Score winner.

On Tuesday, September 28, at 8:30 A.M., the President of the Society, Dr. Harold O. Peterson, will call the Annual Meeting to order in the Hilton International Ballroom. The President of the Medical Society of the District of Columbia, Dr. Paul R. Wilner, will give the Address of Welcome. President Peterson, assisted by Dr. Ted F. Leigh, Chairman of the Executive Council, will then install Dr. John Paul Medelman as the new President of the Society. The Scientific Sessions will begin at the conclusion of the Inaugural Address of the newly installed President.

The Program Committee has selected forty-eight papers for presentation. The preliminary program is published elsewhere in this issue of the JOURNAL. The program is intended to be a combination of the introduction of new knowledge and skill with re-evaluation and further exposition of more or less familiar material. As in the past, the Scientific Sessions will adjourn early enough to allow time for attendance at the Instruction Courses and study of the Technical and Scientific Exhibits.

Dr. Harold O. Peterson is again Director of the Instruction Courses and Dr. Donn G. Mosser is the Associate Director. They are bringing together an outstanding faculty. The program with a description of the courses and instructions for registration will be published in the August issue of this JOURNAL. Dr. Peterson is more than satisfied with the number, size and comfort of the rooms available for presentation of the Courses.

The Scientific Exhibits and the Technical Exhibits will both be located in the tremendous Exhibit Hall of the Hilton, across the Concourse from the site of the Scientific Sessions. This is a great advantage for all concerned and will result in easy accessibility and convenience for examining and displaying the material. Dr. R. F. Greening, Chairman of the Scientific Exhibit Committee is gratified by the number and quality of the exhibits that are to be shown. Several exhibits amplify essays to be presented at the meeting.

Likewise, Dr. James C. Cook, Manager of the Annual Meeting, and Mr. Clifford L. Sherratt, Honorary Member, are enthusiastic about the Technical Exhibits which—I am informed—will be the largest and most outstanding in the history of the Society. The Exhibits contribute immeasurably to the success of the meeting and it appears that they will be record making this year. It is stimulating to gain knowledge of the great theoretic advance in the science of radiology and then to see its practical application almost simultaneously in both Departments of the Exhibits. This is particularly true in our times of spectacular expansion of the radiologic world. It is most important for the members and guests, individually and collectively, to give serious attention to the Exhibits.

Dr. Clyde A. Stevenson will deliver the Caldwell Lecture at 8:30 P.M. on Tuesday, September 28. Dr. C. Allen Good, Secre-

tary of the Society, head of the Section of Diagnostic Roentgenology of the Mayo Clinic and Professor of Radiology at the Mayo Graduate School of Medicine, will introduce the lecturer on this notable occasion.

Dr. Stevenson, Scientific Exhibit Gold Medalist of the American Medical Association, is Director of the Department of Radiology of the Sacred Heart Hospital in Spokane, Washington. He deservedly commands great respect for his accomplishments in Radiology and especially for his dedication to the clinical aspects of the Science in its relation to the whole field of Medicine. His subject will be "Clinical Roentgenology of the Colon." The Caldwell Medal will be presented to him at the conclusion of his Lecture.

The American College of Radiology will present a Panel Discussion on "Some Current Problems of the American College of Radiology" on Wednesday, September 29, at 1:30 P.M. Dr. Jackson E. Livesay will be the Moderator. Panelists will be Drs. W. D. Buchanan, Richard E. Ottoman and Earl R. Miller.

The Annual Banquet will be held in the International Ballroom on Thursday, September 30, at 7:30 P.M. It will be preceded by a cocktail party beginning at 6:30 P.M., in the International Ballroom East. Dr. McPeak and his Committee have made arrangements for a splendid evening of music during the Banquet, for entertainment and for dancing later. Tickets for the Banquet may be purchased at the Main Registration Desk in the Concourse.

The Officers of the American Roentgen Ray Society cordially invite all radiologists, their guests and their families to attend this Sixty-sixth Annual Meeting in the fascinating city of Washington.

J. P. Medelman, M.D.
*President-Elect*

110 Birchwood Avenue
White Bear Lake, Minnesota 55110

# JOHN T. FARRELL, Jr., M.D.
## 1897–1965

Dr. John Thompson Farrell, Jr., Philadelphia radiologist, died on April 30, 1965 of coronary occlusion. He was born October 7, 1897 in Providence, Rhode Island, the son of John T. Farrell, M.D., and Louise Smith Farrell. He graduated from Hobart College in 1918 and from Jefferson Medical College in 1922. He served internships at Rhode Island Hospital, Providence, Rhode Island and White Haven Sanatorium, White Haven, Pennsylvania. Dr. Farrell married Miriam Ott in 1926. He leaves his widow, two brothers and two sisters.

In 1925 Dr. Farrell returned to Jefferson and became associated with the late Willis

F. Manges who was his preceptor in Radiology. After Dr. Manges' death in 1936, he established his own practice.

At Jefferson Dr. Farrell rose through successive promotions to the rank of Professor of Roentgenology. From 1941 to 1948 he was radiologist to the Lankenau Hospital, Philadelphia. Up to the time of his death, he was Clinical Professor of Radiology to the Graduate School of Medicine of the University of Pennsylvania, Consultant in Radiology to the Mercy-Douglass Hospital and engaged in private practice.

Dr. Farrell was always interested in organized medicine. He was President of the Philadelphia County Medical Society in 1956 after he served on its Board of Directors for 2 years. He served on numerous committees of the Society and was a member of the House of Delegates since 1943. He was also President of the Pennsylvania State Medical Society in 1958.

He was a Diplomate of the American Board of Radiology and a member of the American College of Radiology, American Roentgen Ray Society, Radiological Society of North America (Vice President in 1934), Philadelphia Roentgen Ray Society (President in 1930), Pennsylvania Radiological Society (President in 1944), American College of Physicians, College of Physicians of Philadelphia, Laennec Society, Medical Club of Philadelphia, Theta Delta Chi and Nu Sigma Nu.

Dr. Farrell was on the Board of Directors of Pennsylvania Blue Shield and Philadelphia Blue Cross.

He was the author of numerous papers on diagnostic and the therapeutic phases of roentgenology. His "Roentgen Diagnosis of the Gastrointestinal Tract" was published in 1946.

Dr. Farrell possessed an engaging personality. Because of his sincere love for people, he made friends easily. He was honest in his work and in his association with his medical colleagues. Few will forget his untiring efforts in the defense of the high principles and ethics of Radiology. Many will remember his determined labors for the improvement of hospital-radiologist contractual relationships. Dr. Farrell's appreciation of right and wrong was clear and definite. He was easily upset by anything he considered to be unjust. His kindness, consideration and thoughtfulness were some of his endearing traits.

In an article "To Succeed" written for the Philadelphia Inquirer a few years ago, Dr. Farrell summarized the meaning of success—"In my opinion, to succeed is to get from one's work a sense of heart felt satisfaction—not necessarily from the exact realization of early hopes or the acclaim of one's fellows, but from the feeling that with thoughtful industry and by playing the game fairly according to the rules, one has strived to reach that far star set in the sky of ambition."

Mario A. Cinquino, M.D.

1518 South Broad Street
Philadelphia, Pennsylvania 19146

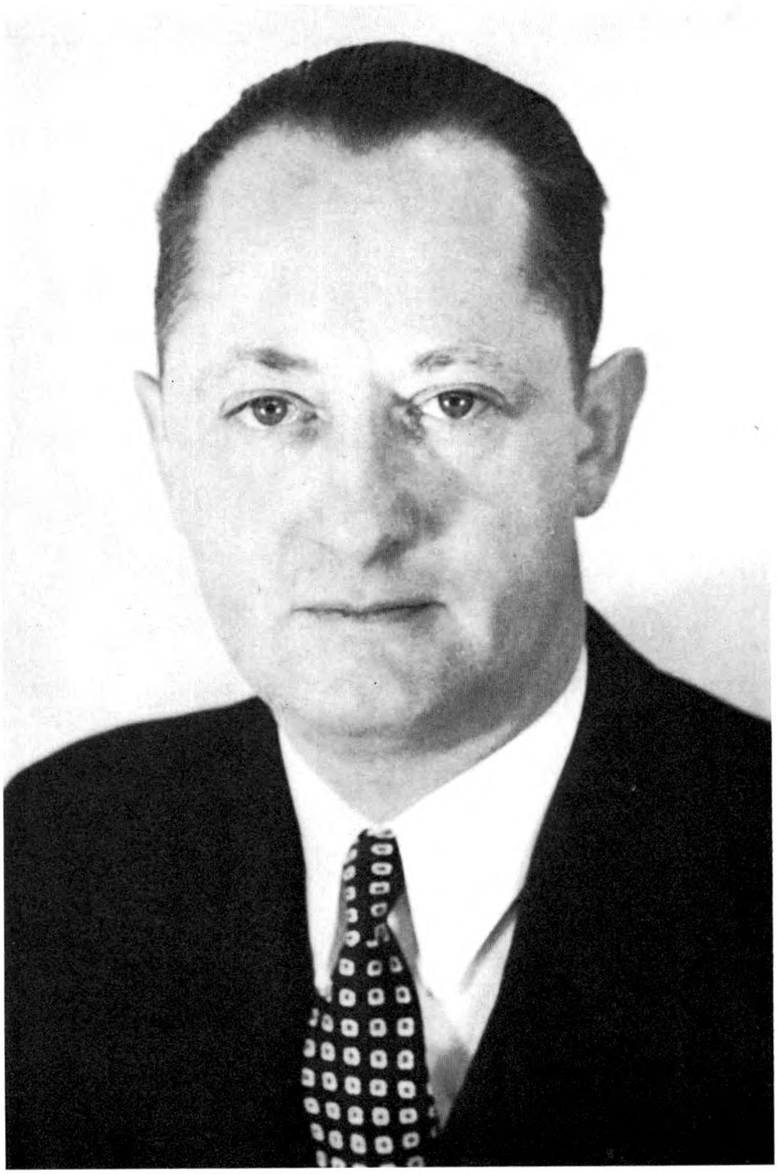

# ERNST ALBERT POHLE, M.D.
## 1895–1965

*Memorial Resolution of the Faculty of the University of Wisconsin, April 5, 1965* U. W. (Madison Campus) Faculty Document 15

PROFESSOR ERNST ALBERT POHLE died February 10, 1965, as a result of injuries sustained in a fall at his home. Professor Pohle was a native of Germany, having been born in Wiesbaden on December 31, 1895, the son of Reinhold and Lisette (Hannappel) Pohle. He received his M.D. degree from the University of Frankfort on Main in 1921. Following his graduation, he worked in Dessauer's laboratory in Frankfort and it was here that he developed his interest in radiation

therapy. Methods of measuring radiation quantity were unsatisfactory at the time and Dr. Pohle became interested in developing a more precise method. It was this that first brought him to the United States on a lecture tour. In 1923 he came to this country to stay and soon became a naturalized citizen. He served as radiologist to the Mt. Sinai Hospital in Cleveland until 1925. At that time he was invited by the late Dr. Preston Hickey to join the faculty of the University of Michigan as Assistant Professor. He was subsequently promoted to Associate Professor. While at Michigan, he received a Ph.D. degree in biophysics in 1928.

He came to the University of Wisconsin in 1928 as the first Professor of Radiology and Chairman of the Department of Radiology in the Medical School. He held the post of Chairman until 1957 and that of Professor until his retirement in 1961.

Dr. Pohle was active in both basic and clinical research. Some of his best known work concerned the effects of x-radiation on the healing of wounds. Since little was known about such effects, his experimental work served as a guideline in the treatment of patients during the immediate postoperative period. He also did basic research on the effects of radiation on normal tissues, particularly the heart. He was the author of numerous publications dealing with the theoretical and clinical aspects of radiation therapy. He served as editor of three textbooks, "Theoretical Principles of Roentgen Therapy," "Clinical Roentgen Therapy," and "Clinical Radiation Therapy." Because of his wide contacts both here and abroad, he was able to assemble a group of outstanding contributors to these volumes which received wide acceptance.

At Wisconsin, he installed the first radon plant in the area for the manufacture of radon seeds which were widely used at the time in the treatment of a variety of malignant conditions. Later he was responsible for the installation of the first million volt roentgen ray machine in this State.

He trained over 40 residents and, in appreciation, they recently subscribed a substantial sum of money for the development of a special area in the proposed new William S. Middleton Memorial Medical Library to be given over to radiology and related subjects.

Dr. Pohle was a charter member of the Wisconsin Radiological Society and served as its President for two consecutive terms. He was a diplomate of the American Board of Radiology, a member of the American Roentgen Ray Society, the Radiological Society of North America, the American Radium Society, the Dane County and Wisconsin Medical Societies, the American Medical Association, the American Association for the Advancement of Science and Sigma Xi. He was a Fellow of the American College of Radiology. He was an honorary member of the American Society of X-Ray Technicians, the Detroit Roentgen Ray and Radium Society and the Radiological Society of Panama.

Dr. Pohle was a lover of nature and an avid sportsman during his active years. Much of his leisure was spent in roaming the fields and woods of Wisconsin.

Dr. Pohle served with the German Army during World War I. In this country he became a Commander in the Medical Corps of the United States Naval Reserve.

Dr. Pohle was married to the former Marie C. Graubaum in 1923. He is survived by his wife; two daughters, Mrs. Charles L. Pember of Columbus, Wisconsin, and Mrs. Donald V. Hooper, Milwaukee; and four grandchildren.

MEMORIAL COMMITTEE:
John H. Juhl
Kenneth E. Lemmer
Ovid O. Meyer
Lester W. Paul,
*Chairman*

Department of Radiology
University of Wisconsin
Medical Center
1300 University Avenue
Madison, Wisconsin 53706

# PRELIMINARY PROGRAM

## SIXTY-SIXTH ANNUAL MEETING OF THE AMERICAN ROENTGEN RAY SOCIETY

The Sixty-sixth Annual Meeting of the American Roentgen Ray Society will be held in the new Washington-Hilton Hotel, Washington, D. C., Tuesday through Friday, September 28 to October 1, 1965.

The Executive Council will meet Sunday, September 26, 9:00 A.M. in the Georgetown Room A.

On Monday, September 27, the Annual Golf Tournament for Members and Guests—competing for the Willis F. Manges' Trophy and the Exhibitors' Trophy—will be held at the Manor Country Club in Norbeck, Maryland, followed by the Annual Golf Dinner at 7:30 P.M. at that Club.

The Scientific Sessions will be held in the morning from 8:30 A.M. to 12:30 P.M., Tuesday through Friday in the Hilton International Ballroom. The Caldwell Lecture will be given by Dr. Clyde A. Stevenson on Tuesday evening at 8:30 P.M. in the Hilton International Ballroom.

The Instruction Courses will be held in the afternoon from 3:00 P.M. to 4:30 P.M. on Tuesday, Wednesday and Thursday and from 1:30 P.M. to 3:00 P.M. on Friday. The detailed plan of the Instruction Courses will be published in the August issue of the Journal.

The Scientific Exhibits will be set up in the Exhibit Hall of the Hilton. They will open daily at 8:30 A.M., and will close at 8:00 P.M. Tuesday; 9:00 P.M. Wednesday; 7:30 P.M. Thursday and 12:30 P.M. Friday.

The Technical Exhibits will also be located in the Exhibit Hall of the Hilton. They will open daily at 8:30 A.M. and will close at 6:00 P.M., Tuesday through Thursday. They will close on Friday at 12:30 P.M.

The Annual Banquet will be held Thursday evening at 7:30 P.M. in the Hilton International Ballroom, preceded by a Cocktail Party beginning at 6:30 P.M. in the Hilton International Ballroom East.

The Program Committee, under the Chairmanship of President-Elect John Paul Medelman, has arranged the following program for the Scientific Sessions.

*Tuesday, September 28, 1965*
*Hilton International Ballroom*

8:30 A.M. Call to Order, Sixty-sixth Annual Meeting: Harold O. Peterson, M.D., Minneapolis, Minn., President. Address of Welcome: Paul R. Wilner, M.D., President of the Medical Society of the District of Columbia.

Installation of President-Elect, John Paul Medelman, M.D., St Paul, Minnesota, by Harold O. Peterson, M.D., President, Minneapolis, Minnesota, and Ted F. Leigh, M.D., Chairman of the Executive Council, Atlanta, Georgia.

Inaugural Address: President John Paul Medelman, M.D.

9:10 A.M.

Presiding: John Paul Medelman, M.D.
St Paul, Minnesota

1. Electric Shock Hazards in Departments of Radiology. William F. Barry, Jr., M.D., Durham, N. C., C. Frank Starner, B.S.E.E. (by invitation), Durham, N. C., Robert E. Whalen, M.D. (by invitation), Durham, N. C., and Henry D. McIntosh, M.D. (by invitation), Durham, N. C.
2. Carbon Dioxide Cine-angiocardiography in the Diagnosis of Pericardial Disease. A. Franklin Turner, M.D. (by invitation), Los Angeles, Cal., Harvey I. Meyers, M.D. (by invitation), Los Angeles, Cal., George Jacobson, M.D., Los Angeles, Cal., and William Lo, M.D. (by invitation), Los Angeles, Cal.
3. Roentgen Diagnosis of Renal Mass Lesions. Glen G. Cramer, M.D. (by invitation), Minneapolis, Minn., Eugene Gedgaudas, M.D. (by invitation), Minneapolis, Minn., and Kurt Amplatz, M.D., Minneapolis, Minn.
4. Diagnosis of Suprarenal Mass Lesions by Retroperitoneal Gas Studies and Arteriography. Erich K. Lang, M.D. (by invitation), Indianapolis, Ind., Myron Nourse,

M.D. (by invitation), Indianapolis, Ind., Jack Mertz, M.D. (by invitation), Indianapolis, Ind., John Beeler, M.D., Indianapolis, Ind., Donald C. McCallum, M.D. (by invitation), Indianapolis, Ind., and William Niles Wishard, M.D. (by invitation), Indianapolis, Ind.

5. Meatal Stenosis and Distal Ureteral Obstruction in Girls: Radiologic Signs and Their Reliability. J. S. Dunbar, M.D., Montreal, Quebec, Canada, and M. B. Nogrady, M. D. (by invitation), Montreal, Quebec, Canada.

6. Excretory Urography in Renovascular Hypertension: Rapid Sequence Filming and Osmotic Diuresis. David M. Witten, M.D. (by invitation), Rochester, Minn., James C. Hunt, M.D. (by invitation), Rochester, Minn., Sheldon G. Sheps, M.D. (by invitation), Rochester, Minn., Lawrence F. Greene, M.D. (by invitation), Rochester, Minn., and David C. Utz, M.D. (by invitation), Rochester, Minn.

7. A Comparative Study of $I^{131}$ Renografin Split-Function Clearances Simultaneously Performed with Inulin and PAH in Patients. I. Meschan, M.D., Winston-Salem, N.C., F. C. Watts, B. S. (by invitation), Winston-Salem, N. C., William H. Boyce, M.D. (by invitation), Winston-Salem, N. C., E. J. Lathem, M.D. (by invitation), Winston-Salem, N. C., H. E. Schmid, M.D. (by invitation), Winston-Salem, N. C., and Ted Roper, M.D. (by invitation), Winston-Salem, N. C.

8. Placental Localization: A Comparison of Radiopharmaceutical and Thermographic Methods. Philip M. Johnson, M.D., New York, N. Y., and David C. Bragg, M.D. (by invitation), New York, N. Y.

9. Television Fluoroscopic Control of Intrafetal Transfusion with Television Tape and Kinescopic Recording. Walter M. Whitehouse, M.D., Ann Arbor, Mich., Lawrence R. Griewski, M.S.E.E. (by invitation), Ann Arbor, Mich., Bruce A. Work, M.D. (by invitation), Ann Arbor, Mich., Robert Jaffe, M.D. (by invitation), Ann Arbor, Mich., and Colin Campbell, M.D. (by invitation), Ann Arbor, Mich.

10. Technetium $99^m$ Radioisotope Scanning with the Scintillation Camera. Alexander Gottschalk, M.D. (by invitation), Chicago, Ill.

11. Radioisotope Scanning with a System for Total Information Storage and Controlled Retrieval. Hymer L. Friedell, M.D., Cleveland, Ohio, Earle C. Gregg, Ph.D. (by invitation), Cleveland, Ohio, and Abbas M. Rejali, M.D. (by invitation), Cleveland, Ohio.

*Tuesday Evening, September 28, 1965*
*Eight-thirty o'clock*

*Hilton International Ballroom*

THE CALDWELL LECTURE

Clinical Roentgenology of the Colon

By

Clyde A. Stevenson, M.D.

Director, Department of Radiology, Sacred Heart Hospital, Spokane, Washington.

*Introduction:* C. Allen Good, M.D., Head of the Section of Diagnostic Roentgenology, Mayo Clinic; Professor of Radiology, Mayo Graduate School of Medicine, Rochester, Minnesota.

*Wednesday, September 29, 1965*
*Hilton International Ballroom*

8:30 P.M.

Presiding: Carleton B. Peirce, M.D.
Montreal, Quebec, Canada

12. Gastric Ulcers after Seventy. J. R. Amberg, M.D., Milwaukee, Wis., and F. F. Zboralske, M.D. (by invitation), San Francisco, Cal.

13. Radiological Evaluation of Gastric Freezing. Harold O. Peterson, M.D., Minneapolis, Minn., M. J. Gilson, M.D. (by invitation), Minneapolis, Minn., C. Hewel, M.D. (by invitation), Minneapolis, Minn., and E. Gedgaudas, M.D. (by invitation), Minneapolis, Minn.

14. The Vermiform Appendix. Thomas C. Beneventano, M.D. (by invitation), New York, N. Y., Clarence J. Schein, M.D. (by invitation), New York, N. Y., and Harold G. Jacobson, M.D., New York, N. Y.

15. The Potential of Polyps of the Intestine. J. Arnold Bargen, M.D. (by invitation), Temple, Tex.

16. Gastrointestinal Findings in Patients with Cystic Fibrosis. Herman Grossman, M.D. (by invitation), New York, N. Y., Walter E. Berdon, M.D. (by invitation), New

York, N. Y., and David H. Baker, M.D., New York, N. Y.

17. The Radiant Energy Received by Patients in Diagnositic X-ray Practice. Russell H. Morgan, M.D., Baltimore, Md., and Judith Gehret (by invitation), Baltimore, Md.
18. New and Simple Techniques for Demonstration of the Jugular Foramen. Jane M. Strickler, M.D. (by invitation), Boalsburg, Pa.
19. The Roentgenological Evaluation of Orbital Blow-Out Injury. Gerhard F. Fueger, M.D. (by invitation), Baltimore, Maryland, William A. Britton, M.D. (by invitation), Montreal, Quebec, and Albert T. Milauskas, M.D. (by invitation), Baltimore, Maryland.
20. Late Consequences of Pulmonary Irradiation. George Cooper, Jr., M.D., Memphis, Tenn., and David Teats, M.D. (by invitation), Charlottesville, Va.
21. The Significance of the R, the Rad, the Rem and Related Units. Marvin M. D. Williams, Ph.D., Rochester, Minn.
22. End Results of Radiotherapy in Laryngeal Cancer Based upon Clinical Staging by the T.N.M. System. Ralph M. Caulk, M.D., Washington, D. C.
23. Squamous Cell Carcinoma of the Tonsillar Area and Palatine Arch. Gilbert H. Fletcher, M.D., Houston, Tex., and Robert D. Lindberg, M.D. (by invitation), Houston, Tex.
24. The Etiology of Treatment Failures in Early Stage Carcinoma of the Cervix. Ralph M. Scott, M.D., Louisville, Ky., Herbert E. Brizel, M.D. (by invitation), Louisville, Ky., and Craig Wetzelberger, M.D. (by invitation), Louisville, Ky.

*Wednesday, September 29, 1965*
*Hilton International Ballroom*

1:30 P.M.

Presiding: John Paul Medelman, M.D.
St Paul, Minnesota

Panel: Some Activities of the American College of Radiology.

*Moderator:* Jackson E. Livesay, M.D., Flint, Michigan.

*Panelists:* W. D. Buchanan, M.D., South Bend, Indiana. Richard E. Ottoman, M.D., Los Angeles, California. Earl R. Miller, M.D., San Francisco, California.

*Thursday, September 30, 1965*
*Hilton International Ballroom*

8:30 A.M.

Presiding: Herman C. Sehested
Fort Worth, Texas

25. A New Method of Percutaneous Catheterization. Donald T. Desilets, M.D. (by invitation), Los Angeles, Cal., and Richard B. Hoffman, M.D. (by invitation), Los Angeles, Cal.
26. Portal Venography by Selective Arterial Catheterization. Robert A. Nebesar, M.D. (by invitation), Boston, Mass., and James J. Pollard, M.D. (by invitation), Boston, Mass.
27. Right Aortic Arch; Plain Film Diagnosis and Significance. James R. Stewart, M.D. (by invitation), Rochester, Minn., Owings W. Kincaid, M.D., Rochester, Minn., and Jack L. Titus, M.D. (by invitation), Rochester, Minn.
28. Coronary Artery Calcification: Its Incidence and Significance in Patients over Forty. John P. Tampas, M.D. (by invitation), Burlington, Vt., and A. Bradley Soule, M.D., Burlington, Vt.
29. Evaluation of Arteriography in the Study of Cephalic Vessels. K. L. Krabbenhoft, M.D., Detroit, Mich., J. O. Reed, M.D., Detroit, Mich., G. A. Kling, M.D. (by invitation), Detroit, Mich., and F. P. Shea, M.D. (by invitation), Detroit, Mich.
30. Diagnosis of Embolic Occlusions of Small Branches of the Intracerebral Arteries. B. Albert Ring, M.D., Burlington, Vt., and Winston M. Eddy, M.D. (by invitation), Burlington, Vt.
31. Positive Contrast Medium (iophendylate) Diagnosis of Tumors of the Cerebellopontine Angle (Particularly Acoustic Neuromata. Robert L. Scanlan, M.D., Los Angeles, Cal., and Brian H. Jarchow, M.D. (by invitation), Los Angeles, Cal.
32. Ultrasound Brain Scanning. Ray A. Brinker, M.D. (by invitation), St Louis, Mo., and Juan M. Taveras, M.D., St Louis, Mo.
33. Bone Abnormalities in Congenital Neurosensory Deafness As Shown by Plesiosectional Tomography. Henry J. Woloshin, M.D. (by invitation), Philadelphia, Pa., Marc S. Lapayowker, M.D. (by invitation), Philadelphia, Pa., Max L. Ronis, M.D. (by invitation), Philadelphia, Pa., and Mar-

garet J. McGann, R. T. (by invitation), Philadelphia, Pa.

34. Radiation Therapy in the Control of Persistent Thyroid Carcinoma. Glenn E. Sheline, M.D., San Francisco, Cal., Maurice Galante, M.D. (by invitation), San Francisco, Cal., and Stuart Lindsay, M.D. (by invitation), San Francisco, Cal.
35. Bilateral Wilms' Tumor Including Report of a Patient Surviving Nine Years after Treatment. Justin J. Stein, M.D., Los Angeles, Cal., and Willard E. Goodwin, M.D. (by invitation), Los Angeles, Cal.
36. Radiotherapy for Renal Adenocarcinoma. Philip T. Hudgins, M.D. (by invitation), Houston, Tex., and Vincent P. Collins, M.D., Houston, Tex.

*Friday, October 1, 1965*
*Hilton International Ballroom*

8:30 A.M.

Presiding: Ted F. Leigh, M.D.
Atlanta, Georgia

37. Comparative Mammography Study. James V. Rogers, M.D., Atlanta, Ga., and R. Waldo Powell, M.D. (by invitation), Atlanta, Ga.
38. Double Contrast Arthrography of the Knee. Robert H. Freiberger, M.D., New York, N. Y., Paul J. Killoran, M.D. (by invitation), New York, N. Y., and Gonzala Cardona, M. D. (by invitation), New York, N. Y.
39. Relationship of Disk Disorders and Abdominal Symptoms. John B. Coleman, M.D. (by invitation), St Paul, Minn.
40. Comparison of Gas and Positive Contrast in Evaluation of Cervical Spondylosis. Gabriel Wilson, M.D. (by invitation), Los Angeles, Cal., William Hanafee, M.D., Los Angeles, Cal., Paul Crandall, M.D. (by invitation), Los Angeles, Cal., and Lawrence Rosen, M.D. (by invitation), Los Angeles, Cal.
41. Reevaluation of the "Fish-Vertebra" Sign in Sickle Cell Hemoglobinopathy. Jack Reynolds, M.D. (by invitation), Dallas, Tex.
42. Blastomycosis. Robert D. Sloan, M.D., Jackson, Miss., and Nancy M. Burrow, M.D. (by invitation), Jackson, Miss.
43. The Angiographic and Pneumoencephalographic Findings in Holoprosencephaly. L. H. Zingesser, M.D. (by invitation), New York, N. Y., and M. M. Schechter, M.D. (by invitation), New York, N. Y.
44. Roentgen Evaluation of Aspiration As a Cause of Recurrent or Chronic Pneumonias in Infancy and Childhood. Olga M. Baghdassarian, M.D. (by invitation), Baltimore, Md., and John J. Vanhoutte, M.D. (by invitation), Baltimore, Md.
45. Asymptomatic Segmental Disturbances in Aeration in Asthmatic Children. Fred A. Lee, M.D. (by invitation), Pittsburgh, Pa., and Bertram R. Girdany, M.D., Pittsburgh, Pa.
46. Radiographic Findings of the Rubella Syndrome in Newborn Infants. Edward B. Singleton, M.D., Houston, Tex., and Arnold J. Rudolph, M.D. (by invitation), Houston, Tex.
47. The Cervical Spine in Mongolism. William Martel, M.D., Ann Arbor, Mich., and Jack M. Tischler, M.D. (by invitation), Ann Arbor, Mich.
48. Periosteal Bone Growth in Normal Infants. Chas. E. Shopfner, M.D., Kansas City, Mo.

# NEWS ITEMS

## TENTH BRAZILIAN CONGRESS OF RADIOLOGY

The Tenth Brazilian Congress of Radiology will be held, under the auspices of the Brazilian College of Radiology and the Portuguese Society of Radiology and Nuclear Medicine, in Rio de Janeiro, Brazil, September 12–18, 1965. This will be the First Portuguese-Brazilian Congress of Radiology and also the Third Annual Meeting of the Brazilian Radiological Society.

An excellent scientific program is arranged. The social activities will include part of the official program of the commemoration of the Fourth Centennial of the Foundation of Rio de Janeiro.

For further information contact Dr. Abercio Arantes Pereira, General Secretary of the Tenth Brazilian Congress of Radiology, Al. Churchill 97, Sala 508, Rio de Janeiro, Gb., Brazil.

A special chartered flight is planned for this meeting. Those interested please write to Mr. Maurice Ellis, District Manager of Verig Airlines, Du Pont Plaza Center, Miami, Florida.

## ASSOCIATION OF UNIVERSITY RADIOLOGISTS

At the annual meeting of the Association of University Radiologists, held at the University of Washington in Seattle, Washington on May 14 and 15, 1965, the following officers were elected:

*President:* Dr. Sidney W. Nelson, Professor and Chairman, Department of Radiology, Ohio State University Medical School, Columbus, Ohio.

*President-Elect:* Dr. Alexander R. Margulis, Professor and Chairman, Department of Radiology, University of California, San Francisco Medical Center, San Francisco, California.

*Secretary-Treasurer:* Dr. Morton M. Kligerman, Professor and Chairman, Department of Radiology, Yale University Medical School, New Haven, Connecticut.

The next annual meeting of the Association of University Radiologists will be held at the University of Arkansas, in Little Rock, on May 13 and 14, 1966.

## LA SOCIÉTÉ CANADIENNE-FRANÇAISE DE RADIOLOGIE

At the recent meeting of La Société Canadienne-Française de Radiologie the following officers were elected:

L. Philippe Bélisle, M.D., *Président;* Jean-Louis Léger, M.D., *1er Vice-Président;* Luc Audet, M.D., *2ième Vice-Président;* Jacques Lespérance, M.D., *Secrétaire général;* Raymond Bélanger, M.D., *Trésorier;* Hubert Grégoire, M.D., *Assistant-Secrétaire,* Montréal; René Drouin, M.D., *Assistant-Secrétaire,* Québec; and Robert Lessard, M.D., *Conseiller.*

The Third Annual Convention will be held in Montreal, Quebec, Canada, December 8–11, 1965.

## THE ROCKY MOUNTAIN RADIOLOGICAL SOCIETY

The Twenty-seventh Midsummer Radiological Conference of the Rocky Mountain Radiological Society will be held in Denver, Colorado, at the Brown Palace Hotel from Thursday through Saturday, August 19–21, 1965.

An excellent Scientific Program has been arranged. The Guest Speakers are: George D. Davis, M.D., Mayo Clinic, Rochester, Minn.; Harold G. Jacobson, M.D., Montefiore Hospital, New York, N.Y.; and Manuel Viamonte, Jr., M.D., University of Miami School of Medicine, Miami, Fla. On August 20, there will be a Commemorative Program honoring Dr. Benjamin Felson, with 26 former associates of Dr. Felson participating.

The social activities will include on Friday evening the Annual Banquet at the Brown Palace Hotel, followed by dancing, and on Saturday evening a trip to Central City in the Rockies with a social hour, dinner and a play at the famous Central City Opera House.

For further information contact Dr. John H. Freed, Secretary-Treasurer, 4200 East Ninth Ave., Denver, Colorado 80220.

# BOOK REVIEWS

*Books sent for review are acknowledged under: Books Received. This must be regarded as a sufficient return for the courtesy of the sender. Selections will be made for review in the interest of our readers as space permits.*

Diagnostic Urology. Edited by James F. Glenn, M.D., F.A.C.S., Professor of Urology and Chief, Division of Urologic Surgery, Duke University Medical Center, Durham, N. C. Cloth. Pp. 415, with 287 illustrations. Price, $13.50. Hoeber Medical Division, Harper & Row, Publishers, Inc., 49 East 33rd Street, New York 16, N. Y., 1964.

This is a compact book divided into 20 chapters containing 287 illustrations compiled by 23 authors. It is printed on good quality paper in clear distinct type which makes it relatively easy to read. According to the editor, it is an exposition of diagnostic methods intended as a handy reference for medical students, interns, residents, urologists, and others. The chapter material has been selected in sequential order, beginning with the basic urologic techniques, proceeding to physiologic studies in general and developing the diagnostic procedures used in special subdivisions of the practice of urology. The roentgenographic reproductions are of good quality and well chosen.

Chapter 3 concerns standard techniques of urography by excretory and retrograde methods. This includes considerable detail pertaining to roentgenographic technique which is elementary to the trained radiologist and may be inadequate for the beginner in x-ray technology. On the other hand, some notable omissions to this chapter are recent techniques, including the urea washout test and the intravenous drip method of urography for those patients who have impaired renal function. Another technique not mentioned is the use of direct fluoroscopic control during retrograde pyelography in selected cases.

Chapters 8 (Renal Metabolic Studies); 10 (Radio-Isotope Renography); 11 (Renal Radioisotope Function and Scanning); 12 (Aortography); and 13 (Lymphangiography and Venography) are well written and pertinent to the practicing urologist and radiologist. These chapters should be of particular value to radiologic students.

In general, this is an excellent textbook for urologists. Its usefulness to the radiologist is limited to reference purposes, and particularly to selected topics.

George W. Chamberlin, M.D.

Two Centuries of Medicine: A History of the School of Medicine, University of Pennsylvania. By George W. Corner, M.D., Sc.D., Ll.D. Cloth. Pp. 363, with some illustrations. J. B. Lippincott Company, Philadelphia 5, Pa., 1965.

The School of Medicine of the University of Pennsylvania has a special place in American Medicine. It was in 1765 that John Morgan, with the aid of William Shippen, founded this school as a part of Benjamin Franklin's College of Philadelphia, which later became the University of Pennsylvania. It thus is the Nation's oldest medical school—older than the Nation itself.

To honor the 200th Anniversary of this historical event, Dr. George W. Corner, a noted medical historian and Executive Officer of the American Philosophical Society, at the University's request, has written this comprehensive yet exciting volume. As stated by Dr. I. S. Ravdin in the Foreword, "In this volume he has brought to life again the men who, over the years since its founding, have played a part in the progress of our School of Medicine." Those years were filled with men's ideas, growth and change, service and greatness, magnificently kaleidoscoped by the author into 16 chapters of attainment and achievement.

Among the giants, venerated and awed, who were responsible for this epochal success, Dr. Henry K. Pancoast occupies a significantly illustrious position. It was, in recognition of the importance of his untiring pioneering investigations in the field of the new but rapidly expanding science of radiology in clinical medicine, that in 1911 a Professorship of Roentgenology (since changed to Radiology) was created, of which he was the first holder. In narrating the contributions of Arthur W. Goodspeed, Assistant Professor of Physics, of Professor J. William White, who applied

Roentgen's discovery to surgical diagnosis, and particularly of Charles Lester Leonard, the famous "skiagrapher" of the hospital, which paved the way for this appointment, the author states, "The early history of radiology in the University of Pennsylvania is a tale of extraordinary talent and enterprise." And again, "Getting an excellent group of young men about him, Pancoast created a radiologic laboratory of international reputation."

In 1913 Dr. Pancoast was elected President of the American Roentgen Ray Society. His eminent successor, Dr. Eugene P. Pendergrass, in 1965, is the Director of the Bicentennial Observance of the Foundation of the University of Pennsylvania's School of Medicine—and through it of the Foundation of Medical Education in the United States.

T. Leucutia, M.D.

## BOOKS RECEIVED

Cellular Radiation Biology. A Symposium Considering Radiation Effects in the Cell and Possible Implications for Cancer Therapy. A Collection of Papers Presented at the Eighteenth Annual Symposium on Fundamental Cancer Research, 1964. Published for the University of Texas M. D. Anderson Hospital and Tumor Institute. Cloth. Pp. 618, with many figures. Price, $16.00. The Williams and Wilkins Company, Baltimore 2, Md., 1965.

Studies in the Pathology of Radiation Disease. By N. A. Krayevskii. Translated by A. Lieberman. English translation edited by Hermann Lisco and Malcolm Walker. Cloth. Pp. 219, with 113 illustrations. Price, $15.00. A Pergamon Press Book, distributed by The Macmillan Company, 60 Fifth Avenue, New York 11, N.Y., 1965.

Tumors of Bone and Soft Tissue. A Collection of Papers Presented at the Eighth Annual Clinical Conference on Cancer, 1963 at The University of Texas M. D. Anderson Hospital and Tumor Institute, Houston, Texas. Cloth. Pp. 448, with many illustrations. Price, $13.00. Year Book Medical Publishers, Inc., 35 East Wacker Drive, Chicago 1, Ill., 1965.

Progress in Atomic Medicine. Volume 1. Edited by John H. Lawrence, M.D., D.Sc., F.A.C.P., Director, Donner Laboratory and Donner Pavilion, University of California, Berkeley, Calif. Cloth. Pp. 233, with some illustrations. Price, $9.75. Grune & Stratton, Inc., 381 Park Avenue South, New York 16, N.Y., 1965.

Progress in Radiation Therapy. Volume III. Edited by Franz Buschke, M.D., Professor of Radiology, University of California School of Medicine; Chief of the Section of Therapeutic Radiology, University of California Hospitals, San Francisco, Calif. Cloth. Pp. 242, with some illustrations. Price, $14.50. Grune & Stratton, Inc., 381 Park Avenue South, New York 16, N.Y., 1965.

Rheumatic Fever: Diagnosis, Management and Prevention. By Milton Markowitz, A.B., M.D., Assistant Pediatrician-in-Chief, Sinai Hospital of Baltimore; Associate Professor of Pediatrics, Johns Hopkins University School of Medicine; Pediatrician-in-Charge, Rheumatic Fever Clinic, Harriet Lane Home Service, Children's Medical and Surgical Center, The Johns Hopkins Hospital; and Ann Gayler Kuttner, B.S., Ph.D., M.D., Associate Professor of Pediatrics, Emeritus, New York University, Bellevue Medical Center; Visiting Scientist, Streptococcal Disease Laboratory, Sinai Hospital of Baltimore; with a special chapter on Community Health Services by Leon Gordis, A.B., M.D., Field Officer, Heart Disease Control Program, U. S. Public Health Service; Fellow in Pediatrics, Sinai Hospital and The Johns Hopkins Hospital. Volume II in the Series, Major Problems in Clinical Pediatrics. Alexander J. Schaffer, Consulting editor. Cloth. Pp. 242, with some illustrations. Price, $7.50. W. B. Saunders Company, West Washington Square, Philadelphia, Pa., 1965.

Radiation Protection. Recommendations of the International Commission on Radiological Protection. I.C.R.P. Report No. 5. Report of Committee V on the Handling and Disposal of Radioactive Materials in Hospitals and Medical Research Establishments, 1964. Published for The International Commission on Radiological Protection. Paper. Pp. 50, with some tables. Price, $3.50. A Pergamon Press Book, distributed by The Macmillan Company, 60 Fifth Avenue, New York 11, N.Y., 1965.

Dorland's Illustrated Medical Dictionary. Twenty-fourth edition. Paper. Pp. 1,724. Price, $13.00, deluxe edition $17.00. W. B. Saunders Company, West Washington Square, Philadelphia, Pa., 1965.

Annual Review of Medicine. Volume 16. Edited by Arthur C. DeGraff, New York University College of Medicine. Associate editor, William P. Creger, Stanford University School of Medicine. Cloth. Pp. 473. Price, $8.50. Annual Reviews, Inc., 231 Grant Avenue, Palo Alto, Calif., 1965.

Die Strahlenpneumonitis: Experimentelle Grundlagen, Klinik und Therapie. By Professor Dr. med. W. Eger, Path. Institut der Univ. Göttingen; and Priv.-Doz. Dr. med. A. Gregl, Röntgeninstitut der Univ. Göttingen. Cloth. Pp. 152, with 75 illustrations. Hippokrates-Verlag Stuttgart, Germany, 1965.

# SOCIETY PROCEEDINGS

## MEETINGS OF RADIOLOGICAL SOCIETIES*

United States of America

American Roentgen Ray Society
*Secretary*, Dr. C. Allen Good, Mayo Clinic, Rochester, Minn. Annual meeting: Washington Hilton Hotel, Washington, D. C., Sept. 28–Oct. 1, 1965.

American Radium Society
*Secretary*, Dr. John L. Pool, 444 East 68th Street, New York, N. Y. 10021. Annual meeting: Camelback Inn, Phoenix, Ariz., April 13–16, 1966 (Golden Anniversary).

Radiological Society of North America
*Secretary-Treasurer*, Dr. Maurice Doyle Frazer, 1744 South Fifty-eighth St., Lincoln, Neb. Annual meeting: Palmer House, Chicago, Ill., Nov. 28–Dec. 3, 1965.

American College of Radiology
*Executive Director*, William C. Stronach, 20 N. Wacker Drive, Chicago 6, Ill. Annual meeting: Drake Hotel, Chicago, Ill., Feb. 1–5, 1966.

Section on Radiology, American Medical Association
*Secretary*, Dr. Clyde A. Stevenson, Sacred Heart Hospital, West 101 Eight Ave., Spokane 4, Wash. Annual meeting: Chicago, Ill., June 26–30, 1966.

American Board of Radiology
*Secretary*, Dr. H. Dabney Kerr. Correspondence should be directed to Kahler Hotel Building, Rochester, Minn.

The Fall 1965 examination will be held at the Statler Hilton Hotel, Dallas, Texas, December 5–10, inclusive. The deadline for filing applications for this examination was June 30, 1965.

The Spring 1966 examination will be held at the Terrace Hilton Hotel, Cincinnati, Ohio, June 6–10, inclusive. The deadline for filing applications for this examination is December 31, 1965.

The Fall 1966 examination will be held at the Washington Hilton Hotel, Washington, D.C., December 5–9, inclusive. The deadline for filing applications is June 30, 1966.

American Association of Physicists in Medicine
*Secretary*, Leonard Stanton, Hahnemann Medical College, 230 N. Broad St., Philadelphia, Pa. 19102. Annual meeting to be announced.

American Club of Therapeutic Radiologists
*Secretary*, Dr. J. A. del Regato, Penrose Cancer Hospital, Colorado Springs, Colo.

Eleventh International Congress of Radiology
*Secretary-General*, Professor Dr. Med. Arduino Ratti, via Moscova, 44–1, Milan, Italy. Address inquiries to Professor Dr. Med. Luigi Turano, President-Elect, Istituto di Radiologia, Università di Roma, Rome, Italy. Meeting: September 22–28, 1965.

Ninth Inter-American Congress of Radiology
*Counselor for the United States*, Dr. Philip J. Hodes, Jefferson Medical College Hospital, 11th and Walnut Streets, Philadelphia 7, Pennsylvania.
Meeting: Montevideo, Uruguay, 1967.

Alabama Radiological Society
*Secretary*, Dr. Walter Brower, Birmingham, Ala. Meets time and place of Alabama State Medical Association.

American Nuclear Society
*Treasurer*, Raymond Maxson, 86 E. Randolph St., Chicago, Ill. Annual meeting to be announced.

Arizona Radiological Society
*Secretary-Treasurer*, Dr. George Gentner, 3435 W. Durango, Phoenix, Ariz. Two regular meetings a year. Annual meeting at time and place of State Medical Association and interim meeting six months later.

Arkansas Radiological Society
*Secretary*, Dr. Charles W. Anderson, 1108½ Poplar, Pine Bluff, Ark. Meets every three months and also at time and place of State Medical Association.

Association of University Radiologists
*Secretary-Treasurer*, Dr. Morton M. Kligerman, Dept. of Radiology, Yale University Medical School, New Haven, Conn. Annual meeting: University of Arkansas, Little Rock, Ark., May 13–14, 1966.

Atlanta Radiological Society
*Secretary*, Dr. Donald R. Rooney, Burnt Hickory Road, Marietta, Ga. Meets monthly except during three summer months, on third Tuesday, at the Academy of Medicine, Atlanta, Ga., at 8:00 P.M.

Bavarian-American Radiologic Society
*Secretary*, Dr. Roy R. Deffebach, Major, MC, Radiology Service, 5th General Hospital, APO 154, New York, N. Y. Meets quarterly.

Blockley Radiological Society
*Secretary*, Dr. Bernard J. Ostrum, 2412 North 52nd St., Philadelphia, Pa.

Bluegrass Radiological Society
*Secretary-Treasurer*, Dr. Arthur Lieber, University of Kentucky, University Hospital, Lexington, Kentucky. Meets quarterly.

Brooklyn Radiological Society
*Secretary*, Dr. Edward Feely, St. Johns Episcopal Hospital, 480 Herkimer St., Brooklyn, N. Y. Meets first Thursday of each month, October through June.

Buffalo Radiological Society
*Secretary*, Dr. Berkeley Zinn, 85 Wehrle Dr., Buffalo 25, N. Y. Meets second Monday evening each month, October to May inclusive.

California Radiological Society
*Secretary*, Dr. L. Henry Garland, Suite 1739, 450 Sutter St., San Francisco, Calif. Meets annually during meeting of California Medical Association.

Catawba Valley Radiological Society
*Secretary*, Dr. Emmett R. White, P. O. Box 303, Rutherford College, N. C. Meets every Tuesday, Dept. of Radiology, Valdese General Hosp., Valdese, N. C. at 12:00 P.M.

Central New York Radiological Society
*Secretary-Treasurer*, Dr. Edward W. Carsky, Crouse-Irving Hospital, 820 S. Crouse Ave., Syracuse, N. Y. Meets first Monday each month, October through May.

Central Ohio Radiological Society
*Secretary-Treasurer*, Dr. Harold W. Long, 81 S. Fifth St., Columbus 15, Ohio. Meets third Thursday in October, and second Thursday in November, January, March and May at Fort Hayes Hotel, Columbus, Ohio.

Central Society of Nuclear Medicine
*Secretary*, Dr. Robert S. Landauer, Radiation Center Bldg., 1903 West Harrison St., Chicago 12, Ill.

Chicago Roentgen Society
*Secretary-Treasurer*, Dr. Robert D. Moseley, Jr., Dept. of Radiology, Univ. of Chicago, 950 E. 59th St., Chicago 37, Ill. Meets second Thursday of each month, October to April except December at the Pick-Congress Hotel at 8:00 P.M.

Cleveland Radiological Society
*Secretary-Treasurer*, Dr. James Christie, 10515 Carnegie Avenue, Cleveland, Ohio. Meetings at 7:00 P.M. on fourth Monday of October, November, January, February, March and April.

Colorado Radiological Society
*Secretary*, Dr. David J. Stephenson, 8300 West 38th Ave., Wheat Ridge, Colo. Meets third Friday of each month at Denver Athletic Club from September through May.

*** Secretaries of societies are requested to send timely information promptly to the Editor.**

CONNECTICUT VALLEY RADIOLOGIC SOCIETY
*Secretary*, Dr. William W. Walthall, Jr., 130 Maple St., Springfield, Mass. Meets in April and October.

DALLAS-FORT WORTH RADIOLOGICAL SOCIETY
*Secretary*, Dr. R. E. Collier, 3500 Gaston Ave., Dallas, Tex. Meets monthly, third Monday, at Southwest International Airport at 6:30 P.M.

DETROIT ROENTGEN RAY AND RADIUM SOCIETY
*Secretary*, Dr. Robert L. Willis, Harper Hospital, Detroit 1, Mich. Meets monthly, first Thursday, October through May, at David Whitney House, 1010 Antietam, at 6:30 P.M.

EAST BAY ROENTGEN SOCIETY
*Secretary*, Dr. William G. Faraghan, 450 30th St., Oakland 9, Calif. Meets first Thursday each month at University Club, Oakland, Calif.

EAST TENNESSEE RADIOLOGICAL SOCIETY
*Secretary*, Dr. C. H. Kimball, 2200 Harris Circle, Cleveland, Tenn. Meets in January and September.

EASTERN RADIOLOGICAL SOCIETY
*Secretary*, Dr. James F. Martin, North Carolina Baptist Hospital, Winston-Salem, N. C.

FLORIDA RADIOLOGICAL SOCIETY
*Secretary*, Dr. Andre S. Capi, 3471 N. Federal Highway, Fort Lauderdale, Fla. Meets twice annually, in the spring with the annual State Society Meeting and in the fall.

FLORIDA WEST COAST RADIOLOGICAL SOCIETY
*Secretary-Treasurer*, Dr. Garth R. Drewry, Tampa General Hospital, Tampa 6, Fla. Meets in January, April, July and October.

GEORGIA RADIOLOGICAL SOCIETY
*Secretary*, Dr. David Robinson, P.O. Box 394, Savannah, Ga. Meets in spring and fall with Annual State Society Meeting.

GREATER MIAMI RADIOLOGICAL SOCIETY
*Secretary-Treasurer*, Dr. Oliver P. Winslow, Jr., Baptist Hospital of Miami, Inc., 8900 S. W. 88th St., Miami 56, Fla. Meets monthly, third Wednesday at 8:00 P.M. at Jackson Memorial Hospital, Miami, Fla.

GREATER ST. LOUIS SOCIETY OF RADIOLOGISTS
*Secretary-Treasurer*, Dr. Mark D. Eagleton, 950 Francis Place, St. Louis, Mo.

HOUSTON RADIOLOGICAL SOCIETY
*Secretary*, Dr. D. A. Van Velzer, Texas Medical Center Library, Jesse H. Jones Library Bldg., Houston 25, Tex. Meets fourth Monday of each month, except June, July, August and December, at the Doctors' Club, 8:00 P.M., Houston, Tex.

IDAHO STATE RADIOLOGICAL SOCIETY
*Secretary*, Dr. George H. Harris, Bannock Memorial Hospital, Pocatello, Idaho. Meets in the spring and fall.

ILLINOIS RADIOLOGICAL SOCIETY
*Secretary*, Dr. George A. Miller, Carle Hospital Clinic, Urbana, Ill. Meets in the spring and fall.

INDIANA ROENTGEN SOCIETY, INC.
*Secretary*, Dr. Richard A. Silver, 1815 N. Capitol Avenue, Indianapolis, Ind. Meets first Sunday in May and during fall meeting of Indiana State Medical Association.

IOWA RADIOLOGICAL SOCIETY
*Secretary*, Dr. L. L. Maher, 1419 Woodland Ave., Des Moines, Iowa. Luncheon and business meeting during annual session of Iowa State Medical Society. The scientific section is held in the autumn.

KANSAS RADIOLOGICAL SOCIETY
*Secretary-Treasurer*, Dr. Robert C. Lawson, 310 Medical Arts Bldg., 10th and Home, Topeka, Kan. Meets in spring with State Medical Society and in winter on call.

KENTUCKY CHAPTER, AMERICAN COLLEGE OF RADIOLOGY
*Secretary-Treasurer*, Dr. Robert H. Greenlaw, Dept. of Radiology, Univ. of Kentucky Med. Ctr., Lexington, Ky. Meetings will be semiannually.

KENTUCKY RADIOLOGICAL SOCIETY
*Secretary-Treasurer*, Dr. Joan R. Hale, 402 Heyburn Building, Louisville, Ky. Meets monthly on second Friday at Sheraton Hotel, Louisville, Ky.

KINGS COUNTY RADIOLOGICAL SOCIETY
*Secretary*, Dr. Stanley Dannenberg, 1917 Bedford Ave., Brooklyn 25, N. Y. Meets Kings County Med. Soc. Bldg. monthly on fourth Thursday, October to May, 8:45 P.M.

KNOXVILLE RADIOLOGICAL SOCIETY
*Secretary*, Dr. Clifford L. Walton, Blount Professional Bldg., Knoxville 20, Tenn. Meetings are held the third Monday of every other month at the University of Tennessee Memorial Research Center and Hospital.

LONG ISLAND RADIOLOGICAL SOCIETY
*Secretary*, Dr. Perry R. Mandel, Nassau Hospital, Mineola, L. I., N. Y. Meets second Tuesday of the month in February, April, June, October and December.

LOS ANGELES RADIOLOGICAL SOCIETY
*Secretary*, Dr. Austin R. Wilson, 540 N. Central Ave., Glendale, Calif. 91203. Meets second Wednesday of month in November, January, April and June at Los Angeles County Medical Association Building, Los Angeles, Calif.

MAINE RADIOLOGICAL SOCIETY
*Secretary*, Dr. J. T. Chen, 7 Cherry Hill Terrace, Waterville, Me. Meets in June, September, December and April.

MARYLAND RADIOLOGICAL SOCIETY
*Secretary*, Dr. Henry Startzman, Medical Arts Building, Baltimore, Md.

MEMPHIS ROENTGEN SOCIETY
*Secretary-Treasurer*, Dr. Vernon I. Smith, Jr., Suite 203, 1085 Madison Ave., Memphis, Tenn. 38104. Meets first Monday of each month at John Gaston Hospital.

MIAMI VALLEY RADIOLOGICAL SOCIETY
*Secretary*, Dr. William D. Roberts, 2197 Los Arrow Dr., Dayton 9, Ohio. Meets second Friday of fall and winter months.

MID-HUDSON RADIOLOGICAL SOCIETY
*Secretary-Treasurer*, Dr. Alexander W. Friedman, Mid-Hudson Medical Group, Fishkill, N. Y. Meets 7:00 P.M., first Wednesday of each month September to May.

MILWAUKEE ROENTGEN RAY SOCIETY
*Secretary-Treasurer*, Dr. Harold F. Ibach, 2400 W. Villard Avenue, Milwaukee 9, Wis. Meets monthly on fourth Monday, October through May, at University Club.

MINNESOTA RADIOLOGICAL SOCIETY
*Secretary-Treasurer*, Dr. Edward A. Peterson, St. Paul, Minn. Meets twice annually, fall and winter.

MISSISSIPPI RADIOLOGICAL SOCIETY
*Secretary-Treasurer*, Dr. Dan T. Keel, Jr., 504 Chippewa St., Brookhaven, Miss. Meets third Thursday of each month at the Heidelberg Hotel, Jackson, at 6:00 P.M.

MISSOURI RADIOLOGICAL SOCIETY
*Secretary-Treasurer*, Dr. M. Shoss, Cape Girardeau, Mo.

MONTANA RADIOLOGICAL SOCIETY
*Secretary*, Dr. Clark Grimm, Great Falls, Montana. Meets at least once a year.

NEBRASKA STATE RADIOLOGICAL SOCIETY
*Secretary*, Dr. Richard Bunting, The Radiologic Center, Nebraska Methodist Hospital, Omaha 31, Neb. Meets third Wednesday of each month at 6 P.M. in Omaha or Lincoln.

NEVADA RADIOLOGICAL SOCIETY
*Secretary*, Dr. William G. Arbonies, Department of Radiology, St. Mary's Hospital, Reno, Nev.

NEW ENGLAND ROENTGEN RAY SOCIETY
*Secretary*, Dr. Jack R. Dreyfuss, Zero Emerson Place, Boston, Mass. 02114. Meets third Friday of each month, October through April, at The Longwood Towers, 20 Chapel Street, Brookline, Mass., at 4:30 P.M.

NEW HAMPSHIRE ROENTGEN RAY SOCIETY
*Secretary*, Dr. Paul Y. Hasserjian, 1470 Elm St., Manchester, N. H. Meets four to six times yearly.

NEW MEXICO ASSOCIATION OF RADIOLOGISTS
*Secretary-Treasurer*, Dr. Justin J. Wolfson, Department of Radiology, Bernalillo County-Indian Hospital, Albuquerque, New Mexico.

NEW MEXICO SOCIETY OF RADIOLOGISTS
*Secretary*, Dr. William G. McPheron, Hobbs, New

Mexico. Four annual meetings, three held in Albuquerque, N. M., and one held at time and place of New Mexico State Medical Society annual meeting.

New York Roentgen Society
*Secretary*, Dr. Harry Z. Mellins. Meets monthly on third Monday at the New York Academy of Medicine at 4:30 P.M.

North Carolina Radiological Society
*Secretary*, Dr. E. H. Schultz, North Carolina Memorial Hospital, Chapel Hill, N. C. Meets in the spring and fall each year.

North Dakota Radiological Society
*Secretary*, Dr. Robert J. Olson, 1240 8th Ave., Williston, N. D. Meets at time of State Medical Association meeting. Other meetings arranged on call of the President.

North Florida Radiological Society
*Secretary*, Dr. Charles H. Newell, 800 Miami Road, Jacksonville 7, Fla. Meets quarterly in March, June, September and December.

Northeastern New York Radiological Society
*Secretary*, Dr. Anthony J. Tabacco, 621 Central Ave., Albany 6, N. Y. Meets in Albany area on second Wednesday of October, November, March and April.

Northern California Radiological Society
*Secretary*, Dr. John M. Johannessen, Mercy Hospital, Sacramento, Calif. Meets fourth Monday of Sept., Nov., Jan., March and May at the Sutter Club in Sacramento.

Northwestern Ohio Radiological Society
*Secretary*, Dr. Vito J. Zupa, Mercy Hospital, Department of Radiology, Toledo, Ohio.

Ohio State Radiological Society
*Secretary*, Dr. M. M. Thompson, Jr., 316 Michigan St., Toledo 2, Ohio. Annual meeting to be announced.

Oklahoma State Radiological Society
*Secretary*, Dr. Robert Sukman, 1200 N. Walker, Oklahoma City, Okla. Meets in January, May and October.

Orange County Radiological Society
*Secretary-Treasurer*, Dr. Herbert H. Benson, 100 East Valencia-Mesa Dr., Fullerton, Calif. Meets fourth Tuesday of every month in Orange County Medical Association Building.

Oregon Radiological Society
*Secretary-Treasurer*, Dr. James A. Schneider, St. Vincent Hospital, Portland 10, Ore. Meets on second Wednesday of month at 7:00 P.M. at the University Club, Portland, Ore.

Orleans Parish Radiological Society
*Secretary*, Dr. Joseph V. Schlosser, Charity Hospital, New Orleans 13, La. Meets second Tuesday of each month.

Pacific Northwest Radiological Society
*Secretary*, Dr. Willis Taylor, Seattle, Washington. Annual meeting to be announced.

Pennsylvania Radiological Society
*Secretary-Treasurer*, Dr. Frederick R. Gilmore, Clearfield Hospital, Clearfield, Pa. Annual meeting to be announced.

Philadelphia Roentgen Ray Society
*Secretary*, Dr. C. Jules Rominger, Misericordia Hospital, 54th St. and Cedar Ave., Philadelphia, Pa. 19143. Meets first Thursday of each month at 5 P.M., from October to May in Thompson Hall, College of Physicians.

Pittsburgh Roentgen Society
*Secretary*, Dr. Robert N. Berk, 3305 Fifth Ave., Pittsburgh 13, Pa. Meets second Wednesday of month, October through June at Park Schenely Restaurant.

Radiological Society of Connecticut
*Secretary-Treasurer*, Dr. Orlando F. Gabriele, 1450 Chapel St., New Haven 11, Conn. Meetings are held bimonthly.

Radiological Society of Greater Cincinnati
*Secretary*, Dr. Harold N. Margolin, 6159 Tulane Road, Cincinnati, Ohio. Meets first Monday of each month at Cincinnati Academy of Medicine.

Radiological Society of Greater Kansas City
*Secretary*, Dr. J. Stewart Whitmore, 1010 Rialto Bldg., Kansas City, Mo. Meets last Friday of each month.

Radiological Society of Hawaii
*Secretary*, Dr. Russell E. Graf, P.O. Box 294, USA Tripler General Hospital, Honolulu, Hawaii. Meets third Monday of each month at 7:30 P.M.

Radiological Society of Kansas City
*Secretary*, Dr. Arthur B. Smith, 800 Argyle Bldg., Kansas City, Mo. Meets third Thursday of each month.

Radiological Society of Louisiana
*Secretary*, Dr. Andrew F. Giesen, Ochsner Clinic, New Orleans 15, La. Meets annually during Louisiana State Medical Society meeting.

Radiological Society of New Jersey
*Secretary*, Dr. E. Arthur Kratzman, 912 Prospect Ave., Plainfield, N. J. Meets in Atlantic City at time of State Medical Society meeting and in October or November in Newark, N. J.

Radiological Society of Rhode Island
*Secretary-Treasurer*, Dr. Harvey B. Lesselbaum, Miriam Hospital, Providence, R. I.

Radiological Society of the State of New York
*Secretary-Treasurer*, Dr. John W. Colgan, 273 Hollywood Ave., Rochester 18, N. Y.

Radiological Society of South Dakota
*Secretary-Treasurer*, Dr. Donald J. Peik, 303 S. Minnesota Ave., Sioux Falls, S. D.

Radiological Society of Southern California
*Secretary-Treasurer*, Dr. John L. Gwinn, Children's Hospital of Los Angeles, 4614 Sunset Blvd., Los Angeles, Calif. 90027. Meets three times a year, usually October, February, and May.

Redwood Empire Radiological Society
*Secretary*, Dr. Lee F. Titus, 164 W. Napa St., Sonoma, Calif. Meets second Monday every other month.

Richmond County Radiological Society
*Secretary*, Dr. W. F. Hamilton, Jr., University Hospital, Augusta, Ga. Meets first Thursday of each month at various hospitals.

Rochester Roentgen Ray Society, Rochester, N. Y.
*Secretary*, Dr. Irving B. Joffe, Rochester General Hospital, 1425 Portland Ave., Rochester 21, N. Y. Meets at 8:15 P.M. on the last Monday of each month, September through May, at Strong Memorial Hospital.

Rocky Mountain Radiological Society
*Secretary*, Dr. John H. Freed, 4200 East Ninth Ave., Denver 20, Colo. Annual meeting to be announced.

San Antonio-Military Radiological Society
*Secretary*, Dr. Hugho F. Elmendorf, Jr., 730 Medical Arts Bldg., San Antonio 5, Tex. Meets third Wednesday each month in Fort Sam Houston Officer's Club at 6:30 P.M.

San Diego Radiological Society
*President-Secretary*, Charles P. Hyslop, 7901 Frost St., San Diego 22, Calif. Meets first Wednesday of each month at the University Club.

San Francisco Radiological Society
*Secretary*, Dr. Malcolm Jones, University of California Hospital, San Francisco 22, Calif. Meets quarterly at the San Francisco Medical Society, 250 Masonic Ave., San Francisco 18, Calif.

Section on Radiology, California Medical Association
*Secretary*, Dr. William H. Graham, 630 East Santa Clara St., San Jose, Calif.

Section on Radiology, Medical Society of the District of Columbia
*Secretary-Treasurer*, Dr. Martin A. Thomas, 1150 Connecticut Ave., Washington 36, D. C. Meets at Medical Society Library, third Wednesday of January, March, May and October at 8:00 P.M.

Section on Radiology, Southern Medical Association
*Secretary*, Dr. Andrew F. Giesen, Jr., White-Wilson Clinic, Fort Walton Beach, Fla. Annual meeting: Houston, Texas, Nov. 1–4, 1965.

Section on Radiology, Texas Medical Association
*Secretary*, Dr. George F. Crawford, St. Elizabeth Hospital, Beaumont, Tex. Meets annually with the Texas Medical Association.

SHREVEPORT RADIOLOGICAL CLUB
*Secretary*, W. R. Harwell, 608 Travis St., Shreveport, La. Meets monthly on third Wednesday at 7:30 P.M., September to May inclusive.

SOCIETY FOR PEDIATRIC RADIOLOGY
*Secretary*, Dr. John L. Gwinn, Children's Hospital, Los Angeles 27, Calif. Annual meeting: Washington Hilton Hotel, Washington, D. C., September 27, 1965.

SOCIETY OF NUCLEAR MEDICINE
*Secretary*, Mr. C. Craig Harris, Oak Ridge National Laboratories, Oak Ridge, Tenn. *Administrator*, Mr. Samuel N. Turiel, 430 N. Michigan Ave., Chicago 11, Ill. Annual meeting to be announced.

SOUTH BAY RADIOLOGICAL SOCIETY
*Secretary*, Northern Section: Dr. John H. Callaghan, 2900 Whipple Ave., Redwood City, Calif.; Southern Section: Dr. Carleton J. Wright, 2015 Clarman Way, San Jose, Calif. Meets second Wednesday of each month.

SOUTH CAROLINA RADIOLOGICAL SOCIETY
*Secretary*, Dr. George W. Brunson, 1406 Gregg St., Columbia, S. C. Annual meeting (primarily business) in conjunction with the South Carolina Medical Association meeting in May. Annual fall scientific meeting at time and place designated by the president.

SOUTH DAKOTA RADIOLOGICAL SOCIETY
*Secretary*, Dr. Donald J. Peik, 1417 S. Minnesota Ave., Sioux Falls, S. Dak. Meets in spring with State Medical Society and in fall.

SOUTHERN RADIOLOGICAL CONFERENCE
*Secretary-Treasurer*, Dr. Marshall Eskridge, Mobile Infirmary, P.O. Box 4097, Mobile, Ala. Annual meeting: Grand Hotel, Point Clear, Ala., Jan. 28–30, 1966.

SOUTHWESTERN RADIOLOGICAL SOCIETY
*Secretary*, John M. McGuire, 904 Chelsea, El Paso, Tex. Meets last Monday of each month at 6:30 P.M. in the Paso del Norte Hotel.

TENNESSEE RADIOLOGICAL SOCIETY
*Secretary*, Dr. B. M. Brady, St. Joseph Hospital, Memphis, Tenn. Meets annually at the time and place of the Tennessee State Medical Association meeting.

TEXAS RADIOLOGICAL SOCIETY
*Secretary*, Dr. Herman C. Sehested, 815 Medical Arts Bldg., Fort Worth 2, Tex. Annual meeting: Driscoll Hotel, Corpus Christi, Jan. 28–29, 1966.

TRI-STATE RADIOLOGICAL SOCIETY
*Secretary*, Dr. John H. Marchand, Jr., Methodist Hospital, Henderson, Ky. Meets third Wednesday of Oct., Jan., March and May, 8:00 P.M., Elks Club in Evansville, Ind.

UNIVERSITY OF MICHIGAN DEPARTMENT OF ROENTGENOLOGY STAFF MEETING
Meets each Monday evening from September to June, at 7:00 P.M. at University Hospital, Ann Arbor, Mich.

UPPER PENINSULA RADIOLOGICAL SOCIETY
*Secretary*, Dr. A. Gonty, Menominee, Mich. Meets quarterly.

UTAH STATE RADIOLOGICAL SOCIETY
*Secretary*, Dr. Carlisle C. Smith, Salt Lake General Hospital, 2033 S. State St., Salt Lake City, Utah. Meets fourth Wednesday in January, March, May, September and November at Holy Cross Hospital.

VERMONT RADIOLOGICAL SOCIETY
*Secretary*, Dr. John R. Williams, 160 Allen St., Rutland, Vt.

VIRGINIA RADIOLOGICAL SOCIETY
*Secretary*, Dr. John M. Ratliff, Mary Immaculate Hospital, Newport News, Va.

WASHINGTON STATE RADIOLOGICAL SOCIETY
*Secretary*, Dr. Owen Marten, 930 Terry Avenue Seattle, Wash. Meets quarterly.

WEST VIRGINIA RADIOLOGICAL SOCIETY
*Secretary*, Dr. Karl J. Myers, The Myers Clinic-Broaddus Hospital, Philippi, W. Va. Meets concurrently with Annual Meeting of West Virginia State Medical Society; other meetings arranged by program committee.

WESTCHESTER RADIOLOGICAL SOCIETY
*Secretary*, Dr. Peter P. Brancucci, Westchester Academy of Medicine, Section on Radiology, Purchase, N. Y. Meets on third Tuesday of January and October and on two other dates.

WISCONSIN RADIOLOGICAL SOCIETY
*Secretary*, Dr. Charles Benkendorf, 408 St. Francis St., Green Bay, Wis. Meets twice a year, May and September.

## CUBA, MEXICO, PUERTO RICO AND CENTRAL AMERICA

ASOCIACIÓN DE RADIÓLOGOS DE CENTRO AMERICA Y PANAMÁ. Comprising: Guatemala, El Salvador, Honduras, Nicaragua, Costa Rica and Panamá.
*Secretary-General*, Dr. Roberto Calderón, Calle Central Oeste No. 218, Managua, Nicaragua, Central America. Meets annually in a rotating manner in the six countries.

SOCIEDAD DE RADIOLOGÍA DE EL SALVADOR
*Secretary*, Dr. Rafael Vaga Gómez.

SOCIEDAD DE RADIOLOGÍA DE GUATEMALA
*Secretary*, Dr. Carlos E. Escobar, 9ª. Calle A 0-05, Zona 1, Guatemala.

SOCIEDAD DE RADIOLOGÍA Y FISIOTERAPÍA CUBANA
*Secretary*, Dr. Miguel A. García Plasencia, Hospital Curie, 29 y F, Vedado, Habana, Cuba. Meets monthly at Curie Hospital.

SOCIEDAD COSTARRICENSE DE RADIOLOGIA
*Secretary*, Dr. James Fernández Carballo, Apartado VIII, San José, Costa Rica.

SOCIEDAD MEXICANA DE RADIOLOGÍA, A.C.
Calle del Oro No. 15, México 7, D. F.
*Secretary-General*, Dr. E. Alvarez Hernández.
Meets first Monday of each month.

ASOCIACIÓN PUERTORRIQUEÑA DE RADIOLOGÍA
*Secretary*, Dr. R. B. Díaz Bonnet, Suite 504, Professional Bldg., Santurce, Puerto Rico.

SOCIEDAD RADIOLÓGICA PANAMEÑA
*Secretary*, Dr. L. Arrieta Sánchez, Apartado No. 6323, Panamá, R. de P. Meets monthly in a department of radiology of a local hospital chosen at preceding meeting.

SOCIEDAD RADIOLÓGICA DE PUERTO RICO
*Secretary*, Dr. Jorge Carreras Girard, Suite 504, Professional Bldg., Santurce, Puerto Rico. Meets second Thursday of each month at 8:00 P.M. at the Puerto Rico Medical Association Bldg. in San Juan.

## BRITISH COMMONWEALTH OF NATIONS

ASSOCIATION OF RADIOLOGISTS OF THE PROVINCE OF QUEBEC
*Secretary*, Dr. R. Robillard, Notre-Dame Hospital, 1560 Sherbrooke St., East, Montreal, Que., Canada. Meets four times a year.

BRITISH INSTITUTE OF RADIOLOGY
*Honorary Secretary*, Dr. R. D. Hoare, 32 Welbeck St., London, W. 1, England. Meets monthly from October until May.

CANADIAN ASSOCIATION OF PHYSICISTS, DIVISION OF MEDICAL AND BIOLOGICAL PHYSICS.
*Honorary Secretary-Treasurer*, Paul M. Pfalzner, Dept. of Therapeutic Radiology, University of Western Ontario, London, Ont., Canada. Annual meeting to be announced.

EDMONTON AND DISTRICT RADIOLOGICAL SOCIETY
*Secretary*, Dr. J. T. Mason, 540 Tegler Bldg., Edmonton, Alberta, Canada. Meets second Tuesday of each month, October to May.

FACULTY OF RADIOLOGISTS
*Honorary Secretary*, Dr. J. N. Pattinson, 47 Lincoln's Inn Fields, London, W.C.2, England. Annual meeting to be announced.

FACULTY OF RADIOLOGISTS, ROYAL COLLEGE OF SURGEONS IN IRELAND
*Registrar*, Dr. H. O'Flanagan, F.R.C.P.I., D.P.H., 123 St. Stephens Green, Dublin 2, Ireland.

SECTION OF RADIOLOGY OF THE ROYAL SOCIETY OF MEDICINE (CONFINED TO MEDICAL MEMBERS)
Meets third Friday each month at 4:45 P.M. at the Royal

Society of Medicine, 1 Wimpole St., London, W. 1, England.

Canadian Association of Radiologists
*Honorary Secretary-Treasurer*, Dr. D. J. Sieniewicz, *Associate Honorary Secretary-Treasurer*, Dr. Maurice Dufresne, 1555 Summerhill Ave., Montreal 25, Que., Canada. Annual meeting to be announced.

Montreal Radiological Study Club
*Secretary*, Dr. Leonard Rosenthall, Montreal General Hospital, Montreal, Que., Canada. Meets first Tuesday evening, October to April.

Section of Radiology, Canadian Medical Association
*Secretary*, Dr. C. M. Jones, Inglis St., Ext. Halifax, N. S.

Société Canadienne-Française de Radiologie
*Secretary General*, Dr. Jacques Lespérance, 1656 Sherbrooke East, Montreal, Que., Canada. Meets every third Tuesday from October to April. Annual meeting: Montreal, Que., Canada, Dec. 8–11, 1965.

Toronto Radiological Society
*Secretary*, Dr. Wallace M. Roy, St. Joseph's Hospitals, 30 The Queensway, Toronto 3, Ont., Canada. Meets second Monday of each month, September through May.

College of Radiologists of Australasia
*Honorary Secretary*, Dr. E. A. Booth, c/o British Medical Agency, 135 Macquarie St., Sydney, N.S.W., Australia.

South America

Asociación Argentina de Radiología
*Secretary*, Dr. Lidio G. Mosca, Avda. Gral. Paz 151, Córdoba, Argentina. Meetings held monthly.

Ateneo de Radiologia
*Secretary*, Dr. Victor A. Añaños, Instituto de Radiologia, Santa Fe 3100, Rosario, Argentina. Meets monthly on second and fourth Fridays at 7:00 p.m. in the Hospital Nacional de Centenario, Santa Fe 1300, Rosario.

Colégio Brasileiro de Radiologia
*Secretary-General*, Dr. Tede Eston de Eston, Caixa Postal 5984, São Paulo, Brazil.

Sociedad Argentina de Radiologia
*Secretary*, Dr. Armando B. de Onaindia, Santa Fe 1171, Buenos Aires. Meetings are held monthly.

Sociedad Bolivana de Radiología
*Secretary*, Dr. Javier Prada Méndez, Casilla 1596, La Paz, Bolivia. Meets monthly. General assembly once every two years.

Sociedade Brasileira de Radiologia
*Secretary*, Dr. Nicola Caminha, Av. Mem. de Sa, Rio de Janeiro, Brazil. General Assembly meets every two years in December.

Sociedade Brasileira de Radioterapia
*Secretary*, Dr. Oscar Rocha von Pfuhl, Av. Brigadeiro Luiz Antonio, 644, São Paulo, Brazil. Meets monthly on second Wednesday at 9:00 p.m. in São Paulo at Av. Brigadeiro Luiz Antonio, 644.

Sociedad Chilena de Radiología
*Secretary*, Dr. J. P. Velasco, Avenida Santa María 0410, Santiago, Chile. Meets fourth Friday of each month.

Sociedad Colombiana de Radiologia
*Secretary*, Dr. Armando Uribe, Hospital Miltar Central, Apartado aéreo No. 5804, Bogotá, Colombia. Meets last Thursday of each month.

Sociedad Ecuatoriana de Radiología y Fisioterapía
*Secretary*, Dr. Luis Blum, P.O. Box 3712, Guayaquil, Ecuador.

Sociedad Paraguaya de Radiología
*Secretary*, Dr. Miguel González Addone, 15 de Agosto 322, Asunción, Paraguay.

Sociedad Peruana de Radiologia
*Secretary*, Dr. Vicente Ubillus, Apartado 2306, Lima, Peru. Meets monthly except during January, February and March, at Asociación Médica Peruana "Daniel A. Carrión," Villalta 218, Lima.

Sociedad de Radiologica del Atlantico
*Secretary*, Dr. Raul Fernandez, Calle 40 #41–110, Baranquilla, Colombia. Society meets monthly at the Instituto de Radiologia.

Sociedad de Radiología, Cancerología y Física Médica del Uruguay
*Secretary-General*, Dr. Ernesto H. Cibils, Av. Agraciada 1464, piso 13, Montevideo, Uruguay.

Sociedade de Radiologia de Pernambuco
*Secretary*, Dr. Manoel Medeiros, Instituto de Radiologia da Faculdade de Medicina da Universidade do Recife, Caixa Postal 505, Pernambuco, Brazil.

Sociedad de Roentgenologia y Medicina Nuclear de la Provincia de Córdoba
*Secretary-General*, Dr. Carlos A. Oulton, Santa Rosa 447, Córdoba, Argentina.

Sociedad Venezolana de Radiología
*Secretary-General*, Dr. Rubén Merenfeld, Apartado No. 9362 Candelaria, Caracas, Venezuela. Meets monthly third Friday at Colegio Médico del Distrito Federal, Caracas.

Continental Europe

Österreichische Röntgen-Gesellschaft
*President*, Dr. Konrad Weiss, Mariannengasse 10, Vienna 9, Austria. Meets second Tuesday of each month in Allgemeine Poliklinik. Annual meeting to be announced.

Société Belge de Radiologie
*General Secretary*, Prof. Simon Masy, Louvain, Belgium. Meets in February, March, May, June, September, October, November and December.

Société Européenne de Radiologie Pédiatrique
*Permanent Secretary*, Dr. Jaques Sauvegrain, Hôpital des Enfants-Malades, 149, rue de Sèvres, Paris 15e, France. *General Secretary*, Dr. Ole Eklöf, P.O. Box, Stockholm 60, Sweden. Annual meeting to be announced.

Société Française d'Électroradiologie Médicale, and its branches: Société du Sud-Ouest, du Littoral Méditerranéen, du Centre et du Lyonnais, du Nord, de l'Ouest, de l'Est, et d'Alger et d'Afrique du Nord. Central Society meets third Monday of each month, except during July, August and September, rue de Seine 12, Paris, France.
*Secretary-General*, Dr. Ch. Proux, 9 rue Daru, Paris 8e, France.

Československá Společnost pro Roentgenologii a Radiologii
*Secretary*, Dr. Robert Poch, Praha 12, Srobárova 50, Czechoslovakia. Meets monthly except during July, August, and September. Annual general meeting.

Deutsche Röntgengesellschaft
*Secretary*, Professor Dr. med. H. Lossen, Universitäts-Röntgeninstitut, Lagenbeckstr. 1, Mainz, Germany.

Società Italiana di Radiologia Medica e di Medicina Nucleare
*Secretary*, Dr. Ettore Conte, Ospedale Mauriziano, Torino, Italy. Meets annually.

Nederlandse Vereniging voor Radiologie
*Secretary*, Dr. H. F. O. Stricker, Schalklaar, Netherlands.

Scandinavian Roentgen Societies
The Scandinavian roentgen societies have formed a joint association called the Northern Association for Medical Radiology, meeting every second year in the different countries belonging to the Association.

Sociedad Española de Radiología y Electrología Médicas y Medicina Nuclear
*Secretary*, Dr. D. Aureo Gutierrez Churruca, Esparteros, No. 9, Madrid, Spain. Meets monthly in Madrid.

Schweizerische Gesellschaft für Radiologie und Nuklearmedizin (Société Suisse de Radiologie et de Médecine Nucléaire)
*Secretary*, Dr. Max Hopf, Effingerstrasse 47, Bern, Switzerland.

Asia

Indian Radiological Association
*Secretary*, Dr. R. F. Sethna, Navsari Building, Hornby Road, Bombay 1, India.

Indonesian Radiological Society
*Secretary*, Professor Sjahriar Rasad, Taman Tjut Mutiah 1, Diakarta, Indonesia.

# ABSTRACTS OF RADIOLOGICAL LITERATURE

## INDEX TO ABSTRACTS

## ROENTGEN DIAGNOSIS

### Abdomen

Walker, Frank C., and Curtis, Graham T. Irreversible changes of ulcerative colitis. *Brit. M. J.*, Feb. 13, 1965, *1*, 414–416. (From: Department of Surgery and Department of Radiology, Royal Victoria Infirmary, Newcastle upon Tyne, England.)

In 40 cases of ulcerative colitis the authors have compared the roentgenologic features with the actual specimen removed by panproctocolectomy. It was concluded that irreversible stages of the disease were represented roentgenographically by pseudopolyposis, stricture, carcinoma, confluent lacunar sepsis, loss of mucosal haustrations, acute toxic dilatation, and certain reticular patterns.

Months or years of full medical treatment did not cause regression of the disease as observed by roentgenologic examination, although temporary remission of clinical symptoms did occur.

The authors believe that there must be a stage where the disease is restricted to the mucosa or submucosa and the changes are reversible. However, valid distinguishing features have not yet been reported. The recognition of a stage at which damage to the colon becomes irreversible suggests that surgery should not be unduly delayed, and that when the disease has been present for 10 or more years the carcinoma hazard is such as to justify a prophylactic colectomy.—*Arch H. Hall, M.D.*

Gillis, D. A., and Grantmyre, Edward B. The meconium-plug syndrome and Hirschsprung's disease. *Canad. M. A. J.*, Jan. 30, 1965, *92*, 225–227. (From: Departments of Surgery and Radiology, The Children's Hospital, Halifax, Nova Scotia, Canada.)

The meconium-plug syndrome is a distinct and relatively common entity characterized by obstruction of the distal colon or rectum by an inspissated meconium plug. It is unrelated to meconium ileus and cystic fibrosis and must be differentiated in the neonatal period from ileal and colonic atresia and Hirschsprung's disease. Bariam enema examination is usually diagnostic and therapeutic. Infants commonly present with signs of low intestinal obstruction and the plain roentgenograms are not diagnostic.

The authors report 2 cases in which the patients presented with a meconium-plug syndrome and subsequently were discovered to have Hirschsprung's disease.

The first of these patients died having aganglionosis of the entire colon. The second survived following surgical correction of a low aganglionic segment.

The authors feel that Hirschspurng's disease should be considered in all cases presenting with meconium-plug syndrome.—*Donald S. Linton, Jr., M.D.*

Flemma, Robert J., Capp, Paul M., and Shingleton, William W. Percutaneous transhepatic cholangiography. *A.M.A. Arch. Surg.*, Jan., 1965, *90*, 5–10. (From: Departments of Surgery and Radiology, Duke University Medical Center, Durham, N. C. 27706.)

The authors describe their experience with 63 cases in which percutaneous transhepatic cholangiography was attempted. Successful cholangiograms were obtained in 54 of the 63 attempts. The procedure was only performed in patients with a normal prothrombin time, prepared for possible surgery, who had received 24-hour course of tetracyline and streptomycin.

The examination is carried out in the radiology department under local anesthesia. An 18 gauge aortogram needle is introduced 12 cm. into the liver. The styloid is removed, and suction applied to the needle, which is slowly withdrawn until bile is aspirated. Then under fluoroscopic control 20 to 60 cc. of 50 per cent sodium diatrizoate (hypaque) is injected into the biliary tree and spot roentgenograms are taken.

Further details of the technique including needle placement and direction, and modifications if no bile is aspirated are discussed. The contrast material is aspirated at the end of the examination if a completely obstructed common duct is demonstrated.

Indications for percutaneous cholangiography are: (1) to investigate jaundice of obscure etiology; (2) to locate the level of extrahepatic obstruction, and distinguish carcinoma of the head of the pancreas from choledocholithiasis with ampullary impaction; and (3) to delineate the exact pathologic anatomy in cases of suspected benign stricture.

In the presence of extrahepatic obstruction visualization of the bile ducts is relatively easy. Twenty of 22 patients with carcinoma of the head of the pancreas had three distinctive findings: (1) a convex downward configuration of the contrast medium in the common duct; (2) complete obstruction; and (3) a greatly dilated common duct. Differentiation was possible from choledocholithiasis where the findings were: (1) convex upward configuration of contrast medium in the common duct; and (2) partial obstruction with some contrast material entering the duodenum.

In a group of 12 patients with benign strictures of the biliary tree, a high percentage had multiple anomalies—all demonstrated by percutaneous cholangiography. Knowledge of this anatomic detail saved considerable operating time.

In the 10 patients with a normal ductal system with nonvisualization of the system, no subsequent evidence of obstructive disease could be shown. Although the point is still debatable, it has been shown that nonvisualization of the biliary tree is

very frequently associated with hepatocellular disease without an obstructive component.

The complications of this procedure are: (1) bile leakage; (2) septicemia; and (3) hemorrhage. The total incidence of bile leakage in the literature is 3.5 per cent. In the authors' experience, leakage occurred only in patients completely obstructed by carcinoma of the head of the pancreas. This was recognized within minutes and the necessary operative procedure carried out without increase in morbidity and no mortality.

Major advantages of this procedure are: (1) laparotomy may be obviated with demonstration of a normal biliary tree; (2) differentiation may be possible between obstruction due to carcinoma of the head of the pancreas and choledocholithiasis; and (3) the exact anatomy of a benign stricture can be identified, facilitating the operative procedure.—*Alan G. Greene, M.D.*

Edmunds, Robert, Rucker, Charles, and Finby, Nathaniel. Intravenous cholangiography: used in postcholecystectomy biliary tract disease. *A.M.A. Arch. Surg.*, Jan., 1965, *90*, 73–75. (Address: Dr. Edmunds, Amsterdam Avenue and 113th Street, New York, N. Y. 10025.)

The records of 124 postcholecystectomy patients investigated by intravenous cholangiography were reviewed. In 101 asymptomatic patients the common duct varied from 4 mm. to 13 mm. in diameter; the average diameter was 8.5 mm. In the 23 symptomatic patients, the common duct diameter varied from 5 mm. to 20 mm.; the average diameter was 10.3 mm. In 7 of these symptomatic patients, with evidence of biliary obstruction (either by history or by elevated serum bilirubin) the average duct diameter was 12.0 mm.

The authors feel that a common bile duct with a diameter greater than 10 mm. is probably abnormal, and that in patients with persistent biliary tract symptoms after cholecystectomy and an abnormal common duct by intravenous cholangiography a second operation should be considered.—*Alan G. Greene, M.D.*

Harrow, Benedict R., and Sloane, Jack Allen. Acute renal failure following oral cholecystography: a unique nephrographic effect. *Am. J. M. Sc.*, Jan., 1965, *249*, 26–35. (From: Section of Urology, University of Miami School of Medicine, Miami, Florida.)

Reported cases of acute renal failure following the administration of oral cholecystographic agents have continued to become increasingly more common. Concern over this increased incidence, especially after orabilex administration, has resulted in its withdrawal from the market by the Food and Drug Administration. The authors add 6 new cases to 22 previously reported in the literature. In 5 cases the renal failure followed bunamiodyl soduim (orabilex) administration and in 1 case it was observed after Iodoalphionic acid (priodax) administration.

The common denominator in the majority of cases presented was doubled, repeated and excessive dosage. The attempt to force gallbladder visualization in patients with severe obstructive jaundice was also felt to be a factor. Twnety-six of the total 28 patients had severe liver or gallbladder disease. The authors believe that pre-existing renal disease, however, is not as clearly implicated as a predisposing factor since the majority of the cases had normal renal function prior to the reported episodes.

The mechanism of renal damage is not completely understood. In most discussions, the renal changes have been ascribed to a direct action of the contrast media on kidney tubules causing an acute tubular necrosis. Possibility of crystalluria damaging the tubules or toxic action on the renal blood vessels with constriction of preglomerular vessels has also been suggested. The latter has been suggested to explain one case in which the nephrogram persisted for 30 hours on an intravenous pyelogram performed following oral cholecystography. This patient had had normal renal function on admission.

Although orabilex has been the agent more frequently cited, cases of acute renal failure following priodax and telepaque administration have been reported. It has also been shown that all common cholecystographic agents can cause temporary renal impairment and azotemia.

The authors express the opinion that the evidence is not conclusive that orabilex is more toxic than those agents previously used because of its higher rate of intestinal absorption. Further investigation into this problem is warranted. In the over-all view, these are among the safest drugs available today and double doses should continue to be used in appropriate clinical problems. Attempts to force gallbladder visualization in patients severely jaundiced should be avoided.—*Alan G. Greene, M.D.*

## Genitourinary System

Marshall, Sumner. A test of renal function: excretion of contrast medium as measured by urinary specific gravity. *Brit. J. Urol.*, Dec., 1964, *36*, 519–525. (From: Division of Urology, University of California School of Medicine, San Francisco 22, Calif.)

The author uses the determination of urine specific gravity as a test of renal function. Base line specific gravity determinations were done on 30 catheterized patients who had varying degrees of renal function. The specific gravity was then tested on 15 or 30 minute urine samples through a 2 hour period following the injection of 30 ml. of 50 per cent sodium diatrizoate (hypaque). Measurements were made by

hydrometer. The increase of specific gravity was compared with the percentage of phenolsulphonphthalein (PSP) excretion at 30 and 60 minutes and also with serum creatinine levels.

The author observed a specific gravity increase within 15 minutes which persisted throughout the following 2 hours. A statistically significant correlation was observed between the increase and the other tests of renal function, although closer correlation was present between the PSP and the specific gravity than with the serum creatinine.

Variation in urine volume did not affect the specific gravity nor did the amount or concentration of injected contrast material. The test is easily performed and requires only a hydrometer and two specimen bottles, one for a pre-injection base line determination and one for a urine sample taken before the post voiding roentgenogram. A specific gravity rise of 0.025 or greater indicates normal renal function.—*John A. Tobin, M.D.*

Hotchkiss, Robert S., and Sammons, B. P. Selective renal angiography. *J. Urol.*, Feb., 1965, *93*, 309–318. (From: Departments of Urology and Radiology, New York University Medical Center, New York, N. Y.)

The authors report 6 patients with urinary tract disease not disclosed by the usual excretory and retrograde pyelography. In each instance, selective renal arteriography or aortography established a definitive diagnosis. These diagnoses included a small clear cell carcinoma, clear cell carcinoma in multicystic renal disease, papillary carcinoma of the renal pelvis, renal carcinoma with anomalous blood supply, silent hydronephrosis, and bilateral adrenal pheochromocytomas.

Selective renal angiography requires only 8 cc. of opaque medium per kidney. The renal arteries are identified by the use of the image amplifier and television reception, after injection of radiopaque material into the aorta. The catheter is placed selectively into the artery to be studied.

In a series of over 700 renal angiographies performed by the authors, no serious complications were noted.

This article points out that in addition to the value of selective renal angiography for the study of hypertension, it is also valuable in obscure or complicated renal disease.—*George W. Chamberlin, M.D.*

Steyn, J., and Logie, N. J. Medullary sponge kidney. *Brit. J. Urol.*, Dec., 1964, *36*, 482–486. (From: Aberdeen Royal Infirmary, and University of Aberdeen, Aberdeen, Scotland.)

Medullary sponge kidney is usually seen in adults. Cystic dilatation of the collecting tubules is confined to the renal pyramids and may be either unilateral or bilateral. The diagnosis is made from the roentgenologic appearance, which reveals filling of the cystic spaces in the pyramids with contrast medium during intravenous pyelographic examination. The differential diagnosis is from renal tuberculosis, renal papillary necrosis, solitary calyceal cysts, and nephrocalcinosis. Often calcium concretions are present in the cysts at the apices of the pyramids.

The purpose of this paper is to report the result of renal function studies in 3 cases of medullary sponge kidney. Glomerular function was normal as determined by creatinine clearance studies. Tubular function was probably impaired as indicated by hypercalciuria in approximately one-third of cases or an inability to concentrate urine as seen in approximately one-half of the reported cases. The response to the acid load test of Wrong and Davies, however. was unimpaired.

The disease itself is not progressive, but calculus formation or renal sepsis may modify the renal function considerably.—*Charles Hewel, M.D.*

Owen, Kenneth. Renal ischemia and hypertension. *Brit. J. Surg.*, Oct., 1964, *51*, 731–735. (From: St. Mary's Hospital, London, W.2, and St. Paul's Hospital, London, W.C.2, England.)

Renal ischemia is now well recognized as a cause of hypertension experimentally and clinically.

The author limits his discussion to obstructions of the main vessels. In his series of 41 cases, the two most common causes were: (1) atheroma of the renal artery, usually causing stenosis near the origin of the artery and most commonly found in men, the age range being 38 to 70 years; (2) fibromuscular hyperplasia, usually producing a beaded appearance in the middle of the artery, most commonly in females in the age range of 2 to 57 years. Definitive diagnosis is by renal angiography but intravenous pyelography and renography were the most valuable screening tests.

The author points out that the typical intravenous pyelographic finding is of a smaller kidney and pelvis on the ischemic side with the increased density of contrast medium which occurs because of maintained tubular function concentrating a diminished glomerular filtrate on the affected side to a greater degree than on the other side. In suspected cases, split function studies, renal biposy, renal vascular flow and pressure studies are helpful in final confirmation.

The author feels that surgery should be considered for hypertension not responding to medical treatment and discusses in detail the surgical techniques of thrombo-endarterectomy, splenic and renal artery anastomosis, by-pass graft from aorta to renal artery, and hypothermia.

The results were regarded as good when the blood pressure returned to normal levels after surgery without hypotensive drugs, and improved when the blood pressure dropped significantly although not to

normal levels, or was controllable at normal levels with drugs which were ineffective preoperatively. Of the 37 survivors of operation, 15 had a good result, 11 were improved and 10 showed no change. In most of the successful cases, a gradual drop in blood pressure was noted, taking up to 6 months for return to normal.

Reasons for failure were coincidence of atheroma and essential hypertension, late development of stenosis in a contralateral artery, persistence of hyperaldosteronism and disease in the renal artery branches. —*James R. Knapp, M.D.*

Kauffman, H. Myron, Jr., Cleveland, Richard J., Dwyer, James J., Lee, H. M., and Hume, David M. Prolongation of renal homograft function by local graft radiation. *Surg., Gynec. & Obst.*, Jan., 1965, *120*, 49–58. (From: Department of Surgery and the Lewis L. Strauss Surgical Research Laboratory, Medical College of Virginia, Richmond, Va.)

Therapy which will prolong functional survival of renal homografts has been limited to irradiation and/or immuno-suppressive drugs. The authors feel that it would be desirable to inhibit the host response to the homografts selectively rather than suppress the entire system indiscriminately.

Lymphocyte and plasma cell infiltration into the interstitium of the homotransplanted kidney is one of the earliest and most characteristic histologic changes of rejection. In order to assess the effect of radiation upon the lymphoid cells migrating to the grafts, which are presumed to be capable of producing antibodies against the transplant, the authors irradiated the grafts locally in a series of mongrel dogs which had received kidney homografts. Significant prolongation of functional survival was achieved without either hematopoietic depression or generalized immune system suppression.

Sequential doses of 150 r every other day for a total of 900 r, were effective in prolonging survival only if the first dose was given the day of the transplant. If the first dose of the radiation was delayed until the second or third day after the transplant or if increments of only 100 r were used, no significant prolongation of function over the control group was seen. Lowering of elevated blood urea nitrogen and attenuation of round cell infiltration was occasionally observed.—*James R. Knapp, M.D.*

Marshall, Sumner, Lapp, Maurice, and Schulte, John W. Lesions of the pancreas mimicking renal disease. *J. Urol.*, Jan., 1965, *93*, 41–45. (From: Division of Urology, Department of Surgery, University of California Medical Center, San Francisco, Calif.)

The authors present 13 brief case reports of adult patients who had subjective symptoms or roentgenographic signs which suggested the possibility of left renal disease, but in all of whom the lesions were in the body or tail of the pancreas. Uro-genital symptoms were present in 11 of the 13; 3 had hematuria. Eleven patients showed downward displacement of the left kidney on the intravenous urograms; 4 had calyceal distortion; and 7 exhibited anterior displacement of the stomach on the roentgenogram.

Because of the intimate relationship of the tail of the pancreas to the left kidney, any mass in this area could encroach directly upon the left urinary tract. The roentgen findings of extrinsic pressure on the kidney can be confusing. Careful evaluation of the roentgenograms taken with the patient in various positions, including the erect and lateral projections, are necessary to differentiate intrarenal from extrarenal disease when associated with pancreatic mass lesions.

The authors include 1 table and 7 figures to illustrate the findings in their article.—*George W. Chamberlin, M.D.*

Giannardi, G. F., Pelu, G., and Gasparri, F. L'indagine radiologica dell'anastomosi ureterale dopo interventi di derivazione urinaria. (Radiologic investigation of the ureteral anastomosis after surgical interventions for urinary diversion.) *Radiol. med.*, Nov., 1964, *50*, 1132–1143. (Address: Dott. Gianfranco Giannardi, Via Cuoco, 5, Firenze, Italy.)

Incompetence or stenosis of the ureteral orifice is the most common postoperative complication after urinary diversion. In either case there is an obstacle to the normal urinary flow through the ureter with secondary ureteral hypertension which will eventually produce severe damage to the kidneys.

The authors have reviewed the roentgen findings observed in intravenous and retrograde urograms of 104 patients who had total pelvic exenteration because of malignant lesions of the internal genital organs.

The types of urinary diversion were: ureterorectostomy in 33 patients, ureterocolocystoplasty in 12, ureterosigmoidostomy in 8, ureterocolostomy in 48, and ureteroileostomy in 3.

Discussed are the incompetence and stenosis of the ureteral anastomosis and the related changes in the whole urinary tract.

From the analysis of their case material, the authors found that ureteral stenosis was usually followed by severe and irreversible changes in the urinary system, while ureteral reflux was better controlled and tolerated.—*A. F. Govoni, M.D.*

Hyman, Richard M., and Yulis, George B. An improved technique for male urethrocystography. *J. Urol.*, Jan., 1965, *93*, 62–63.

(From: Departments of Urology, The French and Morrisania Hospitals, New York, N. Y.)

The disadvantages of the Brodny clamp for the roentgen demonstration of the male urethra are well known to those who have used this procedure. It necessitates some degree of roentgen exposure to the hands of the examiner and the clamp is often uncomfortable to the patient.

The following method is used by the authors: After a preliminary roentgenogram of the lower urinary tract has been obtained, the bladder is filled to slightly less than its capacity with any opaque medium. The catheter is then withdrawn and a second roentgenogram is taken. An 8F Foley pediatric catheter with a 3 cc. balloon is inserted into the fossa navicularis. The balloon is inflated with 2 cc. of water and gentle traction is applied in order to completely occlude the urethral lumen. An extension of several feet of sterile, ordinary rubber tubing of small caliber is connected to the catheter so that the examiner can remain well out of the field of roentgen-ray exposure. A 20 per cent aqueous solution of sodium skiodan is a satisfactory medium. An injection is made with an ordinary 2 ounce bulb syringe using even pressure throughout the exposure. Roentgenograms are taken with the patient in the supine and in the usual bicycle riding position.

In more than 300 patients, the authors have obtained excellent urethrocystograms with rare exceptions. They do not recommend the use of any appreciable thickening of the 20 per cent skiodan and have found this liquid radiopaque medium somewhat more advantageous than the more viscid media. The usual care and gentleness in the performance of the injection and the avoidance of an examination too soon after previous instrumental trauma are recommended.

The advantages of the authors' method are its simplicity, its inherent inexpensive nature, and its safety both to the patient and to the operator.—*George W. Chamberlin, M.D.*

Fraley, Elwin E., Clouse, Melvin, and Litwin, S. Bert. The uses of lymphography, lymphadenography and color lymphadenography in urology. *J. Urol.*, Feb., 1965, *93*, 319–325. (From: Departments of Urology, Radiology and Surgery, Massachusetts General Hospital, Boston, Mass.)

The authors have studied 24 urologic patients, 6 of whom had idiopathic retroperitoneal fibrosis and 16 a malignant lesion or complication following radical surgery. The technique of performing the lymphography is the standard procedure which has been previously published.

In 5 of the 6 patients who had retroperitoneal fibrosis, there were significant lymphographic abnormalities. These abnormalities included extensive collateral circulation with blockage of the more cephalic portions of the lumbar lymph nodes and lymph channels. There was also evidence of displacement of both the lymph vessels and the lymph nodes by the fibrotic process which surrounds the ureters.

Lymphography is of value in the preoperative diagnosis of retroperitoneal fibrosis since this condition is rarely amenable to diagnosis by the usual routine urologic procedures. In addition, the use of chlorophyll dye to stain the lymphatics has been of assistance in the surgical dissection of the involved areas. Various types of malignant metastases, some of which were previously undiagnosed by clinical and other laboratory studies, were disclosed by the use of lymphography and color lymphadenography.

The authors include 8 illustrations.—*George W. Chamberlin, M.D.*

## Nervous System

Daniel, P. M. Observations on the pathology of metastatic tumours in the nervous system. *Proc. Roy. Soc. Med.*, Dec., 1964, *57*, 1151–1153. (From: Department of Neuropathology, Institute of Psychiatry, Maudsley Hospital, London, England.)

Cancer of the lung, breast, kidney, and melanomas are those which most commonly metastasize to the nervous system. The most frequent sites for metastases are the cerebral hemispheres followed by the cerebellum and the brain stem. Metastases within the spinal cord are somewhat rare, although not uncommonly seen in the subarachnoid space. Metastases, both large and small, usually originate in the grey matter and are quite often well defined and easily shelled out completely by the neurosurgeon, in this way being quite unlike gliomas.

Two forms of involvement of the nervous system by carcinomata are relatively little known. These are carcinomatosis of the meninges, "carcinomatous meningitis," and the so-called "carcinomatous encephalitis." Clinically, the most striking feature of the former is extremely severe headache. An early sign may be blindness due to pressure on the optic nerves. In "carcinomatous encephalitis," dementia may be the presenting symptom. In the meningitic form, the tumor grows along the meninges, and in the encephalitic form, the small vessels of the brain are cuffed by a layer of tumor cells. In both of these conditions, it is sometimes possible to make the diagnosis by identifying tumor cells in the cerebrospinal fluid. It is thought that these tumor cells interfere with the passage of oxygen and metabolites to and from the cerebral tissue.

Finally, there are forms of degeneration of the nervous system which may occur in association with carcinoma of various organs (especially carcinoma of the lung). The sensory neuropathy, first described by Denny-Brown in 1948, in which severe loss of

nerve cells in the posterior root ganglia leads to extensive sensory loss, is probably less rare than is generally thought. Cerebellar degeneration is also not uncommonly associated with carcinoma. There is severe loss of Purkinje cells of the cerebellum, with degeneration of parts of the white matter. There is believed to be a myopathy associated with carcinoma, but this is not so clear cut pathologically as are the neuropathies and cerebellar lesions.

At present, the real causes of these degenerations of the nervous system associated with carcinoma are unknown but it seems most likely that they are due to some metabolic disturbance, presumably secondary to carcinoma.—*Charles Hewel, M.D.*

Windeyer, Brian. Metastases in the central nervous system: treatment by radiotherapy and chemotherapy. *Proc. Roy. Soc. Med.*, Dec., 1964, *57*, 1153–1159. (From: The Middlesex Hospital, London, England.)

Metastasis in the central nervous system may be the final stage in the evolution of generalized malignant disease. Occasionally this may be the first sign of recurrence after previous successful therapy. Infrequently this may give the presenting sign in the case of a previous undiagnosed cancer.

Symptoms from intracranial disease may include headache, vomiting, failing vision, nystagmus, paralysis, behavioral changes and progressive coma.

Therapy of intracranial metastases is essentially palliative in nature. Such therapy may be of inestimable value to the patient as it would be possible to give relief of painful and distressing symptoms. Moreover, it would be possible to produce prolongation of life as illustrated by the author's cases.

If the amount of brain destruction is extensive, treatment should not be undertaken. If there are other extensive metastases elsewhere, radiotherapy to the brain is not indicated unless to relieve pain.

Metastases involving the spinal cord may present with pain or with neurologic symptoms. The onset may be slow or sudden. There may or may not be associated bone involvement. Rapidly developing paraplegia may be the first sign in Hodgkin's disease.

The author believes that laminectomy designed to relieve pressure should be done and this should be followed immediately by radiotherapy. Additional chemotherapy should be employed only in the presence of wide-spread disease of known radiosensitivity.

Wide-spread and terminal disease with longstanding paraplegia is a contraindication to therapy.

Intra-arterial perfusion of intracranial tumors has not been proven useful in the author's experience. Hormone therapy may be efficacious in metastases for cancer of the breast.—*K. K. N. Chary, M.D., F.F.R.*

O'Connel, J. E. A. The place of surgery in intracranial metastatic malignant disease. *Proc. Roy. Soc. Med.*, Dec., 1964, *57*, 1159–1164. (From: St. Bartholomew's Hospital, London, England.)

The author reviews the neurosurgical problem of metastatic intracranial disease and presents 6 illustrative cases. These are: (1) dural metastases (1 case); (2) leptomeningeal metastases (2 cases); and (3) metastases within the nervous tissues (3 cases).

Dural metastases may simulate a subdural collection. Leptomeningeal metastases clinically may present with meningeal irritation and examination of cerebrospinal fluid cytology or meningeal biopsy will establish the diagnosis. No definite neurosurgical treatment is possible for these conditions. Metastases within the nervous tissue are managed individually according to the problem and disease, and in selected cases neurosurgery can provide worthwhile palliation.—*Yosh Maruyama, M.D.*

Geile, G., and Puff, K.-H. Problems in the clinical diagnosis of median intervertebral disc prolapses. *German Med. Monthly*, Dec., 1964, *9*, 505–509. (From: Neurological Section, the Neuroradiological Section, and the General Section of the Neurological Department and Polyclinic, University Hamburg-Eppendorf, Hamburg, Germany.)

Median prolapse of intervertebral disk has few clinical manifestations. There may be reflex stiffness of the back and transient pain radiating to either side. However, these lesions can give rise to compression of the cauda equina which leads to grave danger if the patient undergoes chiropractic or similar medico-mechanical treatment. Operative therapy is indicated, consisting of laminectomy and removal of the disk; postoperatively the patients do well.

During a period of 4 years the authors found a total or subtotal block, using abrodil myelography, in 47 patients. Only 6 of these patients had a caudal syndrome due to massive prolapse; the remaining 41 usually presented with a history of recurrent lumbago. Pain radiating into the legs was not definitely segmental and alternated from one leg to another. Most of the patients had had symptoms for 5 to 10 years; only 10 patients had pain for less than 3 years. The cases of total prolapses with cauda equina signs belonged in the latter group.

Atypical sciatica may hide a relatively asymptomatic median disk prolapse; therefore, myelography is indicated. A characteristic pattern is seen in a total block with a distinct, horizontal, irregular break-off. Often small traces of the contrast medium are noted caudal to the lesion, indicating subtotal block. Unlike lateral prolapses which frequently involve the fifth lumbar disk, median prolapses usually affect the fourth, third, and second disks, respectively.

A case, with illustrations, is reported in detail to emphasize the uncertainty of the clinical diagnosis

and the diagnostic importance of myelography in median disk prolapses.—*W. J. Carmoney, Jr., M.D.*

## SKELETAL SYSTEM

DELBARRE, F. Les manifestations ostéo-articulaires de l'hémochromatose. (Osteo-articular manifestations of hemochromatosis.) *Presse méd.*, Nov., 1964, *72*, 2973–2978. (From: Clinique de Rhumatologie de la Faculté de Médecine de Paris et du Centre de Recherches sur les Maladies ostéo-articulaires, Hôpital Cochin, 27, rue du Faubourg-Saint-Jacques, Paris-14, France.)

Gastroenterologists, cardiologists and endocrinologists have long been concerned with hemochromatosis, but recently it has aroused the interest of the specialists treating osteo-articular diseases as well.

In 1960, the author reported on the osteoporosis encountered in this disease and his attention was sharpened by the fact that many patients had consulted for pains and even fractures. The coexisting articular signs were noted but, on account of the patients' ages, arthrosis was the usual diagnosis. Recently, Schumaker (1964) mentioned the possible occurrence of a particular arthropathy.

The author reviews his cases and describes three types of manifestations: (1) *osteoporosis*, (2) *chrondrocalcinosis*-like changes and (3) *arthropathy*.

He then briefly reports 3 typical cases. The first presented a painful and deforming arthritic process localized in both hands, predominantly in the left one. The process involved mostly the proximal interphalangeal joints and, to a lesser degree, the metacarpophalangeal joints. Discrete osteoporosis was also noted. In the second case, a right coxopathy was present, associated with minimal osteophytosis. Both knees showed meniscal calcifications and a marked osteoporosis was noted. The third case showed a pronounced osteoporosis, with a picture of chondrocalcinosis and arthralgia involving both knees, left elbow, and right cubito-carpal joint.

(1) *Osteoporosis* is present in about 25 per cent of the cases, and, after being latent for a long period, it becomes evident late in the disease. This is why it should be searched for by biochemical tests and biopsy, especially in cases up to 40 years of age, before more severe clinical manifestations appear. The bone biopsy reveals a picture of common osteoporosis which cannot be accounted for on a senile, nutritional, or diabetic basis. A high testosterone treatment (50 mg./24 hours) corrects the metabolic anomalies. During the treatment, calciuria progressively decreases and the provoked hypercalciuria shows that more calcium is retained. The relief is temporary, as long as the patient is being treated, and hypercalciuria reappears in the following months. The most probable cause is the hypoandrogenic hormonal status.

(2) *Chondrocalcinosis*-like deposits are seen in the shoulders, elbows, wrists, and most frequently, the knee menisci. They may or may not be accompanied by pains. They are identical to idiopathic chondrocalcinosis, but without the painful bouts reminiscent of gout. Comparable findings have been described in Wilson's disease. This last entity could result from a load of heavy metal in cartilage, as in hemochromatosis where an abnormal ferric deposit has been found in contact with bone trabeculae.

(3) *Arthropathy* is characterized by pain and articular swelling, with periodic exacerbations, and affects the knees, hips, ankles, symphysis pubis, and particularly the proximal interphalangeal joints. The biopsy reveals synovial infiltration with hemosiderin deposits. Roentgenologic examination demonstrates a narrowing of the joint, intra-osseous punched-out areas adjacent to the joint, and subchondral bone condensation, osteophytosis being minimal in spite of the long duration of the disease. —*H. P. Lévesque, M.D.*

BUNDENS, WARNER D., JR., BRIGHTON, CARL T., and WEITZMAN, GERALD. Primary articular-cartilage calcification with arthritis (pseudogout syndrome). *J. Bone & Joint Surg.*, Jan., 1965, *47-A*, 111–122. (From: Orthopaedic Service, United States Naval Hospital, Philadelphia, Pa.)

Calcification of knee menisci has been recognized for many years. Occasionally calcification of articular cartilage has been reported in association with meniscus calcification. Extensive review of the foreign and English literature reveals calcified articular cartilage reported under various names; *i.e.*, chondrocalcinosis polyarticularis, diffuse articular chondrocalcinosis, pseudogout syndrome, etc.

The authors report 4 cases of their own and tabulate the findings of 65 cases reported in the literature. The entity is noted about twice as often in men, has two peaks of incidence at 40–69 years (the larger), and 20–29 years, with both acute and chronic onsets. The knee joint was the most commonly involved. Calcification also may occur in the triangular ligament of the wrist, the fibrocartilage of the annulus fibrosus, but calcification of interphalangeal joint cartilage has not been reported.

Acute attacks last from 1 to 3 weeks, and therapy with colchine, phenylbutazone, or aspirin relieves them. Aspiration of joint fluid alone may abort an acute episode. Use of intra-articular procaine and hydrocortisone is not successful. Calcified articular cartilage may also be found in asymptomatic patients. Occasionally, patients present with multiple recurrent episodes of pain and joint effusion without roentgenologic evidence of calcified cartilage.

Diagnosis can only be proven by examination of the joint fluid, which is opaque, has low viscosity

and gives a loose, friable clot with glacial acetic acid. Intraleukocytic, weakly birefringent, crystals were identified as calcium pyrophosphate by roentgen-ray diffraction.

The authors agree with others that the calcification is primary and not secondary to degenerative processes. The multiple frequently asymmetric joint involvement, the occasional familial incidence, the even distribution of calcium throughout the intermediate layer of articular cartilage, the lacunar or perilacunar location of the initial calcium deposition and the finding of calcium pyrophosphate (not calcium phosphate) crystals in articular cartilage support this view. They believe that the disease is a disorder of calcium metabolism. If the deposition of calcium is rapid, acute symptoms develop; if the deposition is slow, possibly no symptoms may be observed. Regardless of the speed of deposition, the crystals cause chondrocyte death which eventually leads to cartilage degeneration.

The authors suggest another name for this malady: primary articular cartilage calcification with arthritis.—*W. J. Carmoney, Jr., M.D.*

Maroteaux, Pierre, and Lamy, Maurice. L'opigophrénie polydystrophique (mucopolysaccharidose H.-S.) (Polydystrophic oligophrenia [mucopolysaccharidosis H.-S.].) *Presse méd.*, Nov., 1964, *72*, 2991–2996. (From: Clinique de Génétique Médicale, 149 rue de Sèvres, Paris-15, France.)

In Hurler's disease, two mucopolysaccharides are eliminated in great quantities in the urine: chondroitin sulfate-B and heparin-sulfate. In 1961, K. Meyer, studying gargoylism, noted the exclusive presence of heparin-sulfate in 2 of his patients. The present article is a report based on 7 similar cases, and the authors refer to this entity as polydystrophic oligophrenia, since mental degradation predominates, and because of its relationship to Hurler's polydystrophy. The exclusive elimination of heparin sulfate in the urine differentiates this anomaly from Hurler's disease.

*Clinically*, the disease is usually noted around the second or third year, sometimes later. Often the parents have noted a disturbance in the child's character, stagnation and even regression of his psychomotor development. The child appears normal in the first stage, then, more or less rapidly, the normal evolution stops and previous acquisitions, especially speech, fade away. A severe idiocy develops. During the first years, physical development is normal and even excessive; later on, moderate statural retardation is noted. Among the typical features are a voluminous skull with prominent frontal bosses and increased orbital ridges; the face is enlarged with orbital hypertelorism. The base of the nose is flattened, the lips are thick, macroglossia is noted. The eyebrows are heavy, meeting on the medial line, and the hair is hirsute with a low implantation. The appearance resembles Hurler's disease, but the typical gargoyle aspect is not realized. There is no lumbar kyphosis, the skin is usually thickened, hepatomegaly is frequent, splenomegaly rare. Deafness occurs rather frequently. Abnormal cells, similar to those in gargoylism, are found in the blood (Gasser's cells) and in the bone marrow (Buhot's cells).

*Roentgenographically*, the skull shows a thickening of the vault at the expense of the diploe and there is an increased density of its base. There is no scaphocephaly, as in gargoylism. In the vertebral spine, the dorsal and lumbar bodies appear ovoid, grossly hexagonal. Sometimes they show a minimal anterior spur and a slight flattening. True anterior aplasia of one or two vertebrae is not encountered; hence, there is no important kyphosis. In the pelvis, the iliac wings are short and square. The acetabulum is slightly irregular in structure and orientation, it is of normal size and appears too large for the femoral heads. The diaphyses of long bones are slightly enlarged, with density sometimes increased. The epiphyses are rather small. The metaphysis is not everted as in achondroplasia. A discrete obliquity of the distal extremity of the radius and cubitus is present. Sometimes, a conical deformity of these metacarpal extremities is noted; these are massive, but do not show the "*sugar-loaf*" deformity seen in gargoylism. The ribs are sometimes enlarged. These roentgenographic features are comparable to those of Hurler's disease, but the slight difference noted in the pelvis and at the base of the skull should point to the correct diagnosis.

*Genetically*, the mode of transmission is recessive, and the percentage of consanguinity is more than 25 per cent in the reported series.

*Biochemical Studies.* The urinary output of mucopolysaccharides (determined with a modification of Di Ferrante and Rich's method) was around 30 mg./liter in 4 patients; it was higher in the others. No parallelism has been found between these values and the severity of the disease. In polydystrophic oligophrenia, the only abnormal fraction corresponds to a heparin-sulfate. In Hurler's disease, in addition to the heparin-sulfate, more than two-thirds of excreted mucopolysaccharides are chondroitin-sulfate B. In Morquio's disease, the abnormal fraction is a kerato-sulfate. In polydystrophic nanism, there is exclusive excretion of chondroitin-sulfate B.—*H. P. Lévesque, M.D.*

Gjørup, Poul A. Dorsal hemivertebra. *Acta orthop. scandinav.*, 1964, *35*, 117–125. (From: Finsen Institute and Radium Centre, Copenhagen, Denmark.)

A dorsal hemivertebra means a vertebra in which the anterior half of the ossification center in the body has failed to develop. A cleft vertebra, having

many features in common with dorsal hemivertebra, is a bipartite vertebra which is gradually pushed backward because of the distribution of pressure at that site in the spine and takes on a wedge shape with the pointed end foreward.

In the lateral projection both will show identical appearances, *i.e.* a more or less wedge-shaped body with subluxation backward in relation to the adjacent vertebrae. Anteroposterior roentgenograms, however, will distinguish which vertebral malformation is present. In such a roentgenogram the cleft vertebra presents as 2 symmetric triangles on each side of the midline with the smallest angle facing each other and separated by a gap of varying size. The cleft vertebra is increased in width as compared with adjacent vertebrae and often coexists with other vertebral malformations.

The true dorsal hemivertebrae are most often localized at or near the thoracolumbar junction and may present as the only deformity or as a link in more widespread disease, such as achondroplasia, cretinism, or chondrodystrophy.

Three case reports are presented to emphasize the fetarues of dorsal hemivertebrae as well as the differential diagnosis.

A detailed roentgenographic investigation of unusual vertebral malformations is urged to avoid unnecessary treatment, and to advise patients at an early stage regarding future occupation.—*Francis Shea, M.D.*

Harty, Michael. The significance of the calcar femorale in femoral neck fractures. *Surg., Gynec. & Obst.*, Feb. 1965, *120*, 340–342. (From: Anatomy Department, Graduate School of Medicine, University of Pennsylvania, Pa.)

The author describes the calcar femorale as a thin laminated vertical plate of condensed bone which is entirely within the medullary canal of a femur. It is attached to the thick medial cortex of the femoral shaft and laterally extends toward the gluteal tuberosity. Proximally the calcar is continuous with the posterior cortex of the neck and distally it blends with the postero-medial aspect of the diaphysis. The author states that the calcar represents the persistence and expansion of the epiphyseal plate of the lesser trochanter.

The calcar is found in the anteroposterior projection in femoral neck fractures where the shaft has rotated externally.—*Donald S. Linton, Jr., M.D.*

Emnéus, H., and Hedström, Ö. Overgrowth following fracture of humerus in children. *Acta orthop. scandinav.*, 1964, *51*, 51–58. (From: Orthopaedic Clinic, Lund, Sweden.)

It has long been known that the rate of growth of a long bone after a fracture is temporarily increased if the epiphyseal cartilage is intact. This has also been observed in osteomyelitis, and it is widely accepted that the overgrowth is due to increased blood supply to the epiphyseal cartilage. This phenomenon has been studied in human beings and animals, especially in the lower limbs.

The authors' study consists of 70 fractures of the humerus in which 63 demonstrated overgrowth. Twenty-one cases had a 3 year follow-up with repeated measurements; in 16 of these cases the increased rate of growth ceased after 18 months, and in 4 it continued longer. Only in 1 case was no difference found between the rate of growth of fractured and unfractured bones. The increased rate of growth was not found to vary with the level of the fracture.—*James R. Knapp, M.D.*

Johnson, Lanny L., and Kempson, Richard L. Epidermoid carcinoma in chronic osteomyelitis: diagnostic problems and management; report of ten cases. *J. Bone & Joint Surg.*, Jan., 1965, *47-A*, 133–145. (Address: Dr. Johnson, 600 South Kingshighway, St. Louis, Mo. 63110.)

Epithelial proliferation is frequent in sinus tracts of chronic osteomyelitis. A benign hyperplastic or metaplastic change is most common. This change may clinically and histologically simulate a malignant lesion. Epidermoid carcinoma is a rare complication of chronic osteomyelitis.

Ten patients with chronic osteomyelitis complicated by epithelial proliferation, arising in sinus tracts, were studied to determine the signs, symptoms, and course of this disease. A follow-up of 1½–10 years after the original diagnosis of carcinoma was obtained in all the patients by personal communication or examination.

Epidermoid carcinoma has been reported to arise most frequently in sinus tracts of chronic osteomyelitis involving the tibia. One-half as many cases have been described in the femur. Carcinoma has developed in chronically draining sinus tracts from the calcaneus, metatarsals, skull and metacarpals. The patients are usually between 40 and 70 years of age when the malignant change occurs.

Signs and symptoms associated with epidermoid carcinoma are some combination of the following: an increased discharge or the onset of a foul odor from the sinus; increased pain; bleeding; and the presence of a mass. Roentgenograms show osseous destruction or fractures. Often these signs and symptoms are considered a part of the patient's infection and the possibility of carcinomatous change is not considered.

Carcinoma was not suspected clinically in 6 patients, despite significant symptoms; in 5 there was a final pathologic diagnosis of cancer, and 2 of the tumors metastasized. In each case inadequate surgical procedures were performed prior to the original diagnosis of a malignant lesion. In all, the

definitive procedure was amputation. Postoperatively, enlargement of the inguinal lymph nodes aroused suspicion of metastases in 2 patients. A groin dissection was performed in both. In 1 patient the lymph nodes contained metastatic epidermoid carcinoma.

Seven of the patients in this series are alive and well 1–10 years after definitive therapy. The longest follow-up was 10 years; the shortest, $1\frac{1}{3}$ years.

The authors believe that patients with atypical pseudoepitheliomatous hyperplasia should be treated by amputation for the following reasons: (1) in some instances an epidermoid carcinoma will be missed because the tumor is so well differentiated that a definite histologic diagnosis of carcinoma cannot be made; and (2) almost all patients with this form of hyperplasia will have extensive osseous destruction and a nonfunctional limb.

Epidermoid carcinoma in chronic osteomyelitis should be treated with amputation at an adequate level for malignant lesions. Inadequate local excision or inadequate amputation may result in recrudescence. Regional lymph nodes should be biopsied at the time of amputation. If the lymph node biopsy shows metastatic carcinoma, a lymph node dissection should be done.—*Stephen N. Tager, M.D.*

## Blood and Lymph System

Kate, N. Y., and Tatlow, W. F. Tissington. Two cases of vertebral-basilar aneurysm. *Canad. M. A. J.*, Feb. 27, 1965, *92*, 471–474. (Address: Dr. Tatlow, 3446 Gray Avenue, Montreal, Quebec, Canada.)

Two patients with aneurysms of the vertebral-basilar artery are reported.

The first patient presented with symptoms of right hemifacial spasm. After rapid progression of symptoms, a vertebral angiography was performed and this demonstrated a saccular aneurysm of the posterior cerebral artery. There was distortion of the vessels in the region, suggesting a space-occupying lesion, probably due to bleeding. Her condition weakened and she died 3 months later.

The second patient presented with complaints of progressive staggering and gradual loss of hearing on the left. He had had difficulty of swallowing as well as slurring of speech, blurring of vision, and diplopia. Pneumoencephalograms showed a mass lesion in the region of the pons, particularly on the left. He was given deep roentgen-ray therapy. Six months later he was re-admitted with similar complaints to those before. Pneumoencephalograms again showed the mass which now was larger than at the first examination. The patient became worse and died. At autopsy a large bilocular aneurysm was found, producing pressure on the pons.

The authors point out that with present methods visualization and vertebral angiography the possibility of such lesions should be considered and that attempts should be made to demonstrate them. —*George L. Sackett, Jr., M.D.*

Nandy, Kalidas, and Blair, Charles B., Jr. Double superior venae cavae with completely paired azygos veins. *Anat. Rec.*, Jan., 1965, *151*, 1–10. (From: Department of Anatomy, Emory University, Atlanta, Ga.)

The authors report a case of double venae cavae with bilaterally symmetric azygos veins. This was noted as an incidental finding on a routine autopsy.

They reviewed the literature and found 216 cases of double superior venae cavae and 7 cases of double azygos veins previously reported.

The embryology is discussed.—*George L. Sackett, Jr., M.D.*

Chiappa, S., Galli, G., Luciani, L., and Severini, A. Considerations on the restoration of the lymphatic circulation after pelvic lymphadenectomy. *Surg., Gynec. & Obst.*, Feb., 1965, *120*, 323–334. (From: Istituto di Radiologia dell'Università di Milano and the Divisione Ginecologica dell'Istituto Nazionale per lo studio e la cura dei tumori di Milano, Milan, Italy.)

Eighteen patients were studied by direct lymphangiography following total hysteroadnexectomy with pelvic lymphadenectomy. The time interval following operation varied from several months to 9 years. Two patients had both pre- and postoperative studies made.

Two general patterns were observed following radical pelvic lymphadenectomy. The first was that in which no lymphatics were opacified in the course normally seen for the iliac channels. In these there was always opacification of a prominent collateral pathway. The second type consisted of those in which opacifiable lymph vessels and even lymph nodes were still present. Occasionally, these vessels became very large, presumably due to increased flow. The were invariably reduced in number.

The deep inguinal lymph nodes were almost always grossly enlarged and more numerous than normal. In addition, small inter-connecting channels were identified between the deep inguinal lymph nodes which remained opacified over a prolonged period. The vessels of the lower extremities were usually normal in appearance but had reduced flow as manifested by retention for several days.

The collateral channels were smaller than normal and tended to form plexuses. Anastomoses over the pubic and sacral region were commonly visualized. Collaterals also ran laterally along the iliac wing toward the aortic lymph nodes. These latter channels can be indentified occasionally in normal per-

sons. The smaller plexuses in the pelvis commonly opacified on the delayed lymphangiograms.

In these patients there was no evidence clinically of local tumor recurrence nor of lymphedema. Several had had intracavitary irradiation in addition to radical surgery.

The authors discuss the phenomenon of lymph vessel regeneration which probably has little bearing on the postoperative appearance. Most vessels visualized were thought to represent vessels left in place or previously existing and not normally opacified and, therefore, representing normal collateral pathways. The possibility of lympho-venous connections is also discussed.

The article is an excellent technical discussion and should be read in the original by those interested.—*Donald S. Linton, Jr., M.D.*

## General

COLQUHOUN, J. Intramural gas in hollow viscera. *Clin. Radiol.*, Jan., 1965, *16*, 71–86. (From: University Hospitals and Western Reserve University, Cleveland, Ohio.)

Intramural gas in hollow viscera is a rare phenomenon, but it may be recognized roentgenologically. The subject is here discussed under the following headings: (1) cystic pneumatosis (non-infective); (2) interstitial emphysema (non-infective); and (3) gas-forming infections (infective).

(1) *Cystic pneumatosis* consists of cyst-like collections of gas in the walls of the hollow vicsera, in their peritoneal attachments and in the retroperitoneal tissues. It is most frequently seen in the intestinal tract, usually referred to as 'pneumatosis cystoides intestinalis' (P.C.I.). It is generally accepted that the cysts are distended tissue spaces. The most commonly affected regions are the terminal ileum, cecum, splenic flexure and descending colon. Etiologically, ulceration alone does not appear to be sufficient to cause P.C.I. The association with obstructive lesions suggests that increased intraluminal pressure is an important factor in forcing gas into or through the mucosa. Cystic pneumatosis of the intestine is the most common variety of intramural gas. On barium studies the gas cysts are seen closely applied to loops of bowel and may indent the lumen of the bowel in many places. The cysts become flattened when the bowel is distended, and assume a more spherical shape after evacuation of the enema. The cysts often disappear spontaneously. In such cases it is possible that a temporary interstitial pulmonary emphysema is the cause. Keyting and his associates in 1961 presented experimental proof that in cases of P.C.I. where no gastrointestinal lesion could be found the primary lesion is interstitial pulmonary emphysema, and that the interstitial air tracks along the blood vessels to the lung root, and then by way of the aortic sheath to the mesenteric vessels and bowel wall. Cystic pneumatosis of the stomach and of the vagina have been reported very rarely.

(2) The term '*interstitial emphysema*' is restricted by the author to those conditions in which gas is found in the walls of hollow viscera in non-cystic collections and without associated infection by gas-forming organisms. These conditions are rare and are usually found in the stomach or large bowel. Where the stomach is involved, single or double linear radiolucent streaks a few millimeters wide are seen parallel to the border of the stomach and separated from the lumen by a band of water density, also a few millimeters wide. In involvement of the colon roentgen examination may disclose (a) sharply defined linear radiolucent streaks outlining parts of the bowel, (b) ill-defined streaks adjacent to the bowel in toxic megacolon, or (c) bands of tiny punctate radiolucencies in the bowel wall associated with chronic obstruction. Cystic pneumatosis differs from non-infective interstitial emphysema in that there are wider radiolucent bands with scalloped internal margins.

(3) The micro-organisms capable of producing gas most commonly involved in human *gas-forming infections* are *E. coli*, *Cl. welchii* and *Aer. aerogenes.* In emphysematous gastritis, the stomach is contracted and the gas appears as a group of frothy or mottled radiolucencies in the left upper abdomen. It is characterized by sudden onset of severe epigastric pain with abdominal tenderness and rigidity, marked prostration, toxemia, high fever and rapid, thready pulse. In emphysematous cholecystitis, at first gas may be seen only in the gallbladder lumen, but later it appears in and adjacent to the gallbladder wall. Emphysematous entero-colitis may be seen in which gas in the bowel wall is associated with mucosal infection. In the rare condition of gas gangrene of the uterus, peritonitis and ileus are likely. The uterus is enlarged and contains irregular collections of gas. Dark stripes or patches of gas may be seen in the uterine wall. Emphysematous entero-colitis and gastritis have the worst prognosis, emphysematous cholecystitis and gas gangrene of the uterus being only slightly less serious. Emphysematous cystitis is much less dangerous and responds quickly to treatment.—*Samuel G. Henderson, M.D.*

GLADYSZ, BOLESLAW, and GORNA, HANNA. Etude sur la perception du contraste de l'image tomographique. (Study of contrast perception of the tomographic image.) *J. de radiol., d'électrol. et de méd. nucléaire*, Aug.–Sept., 1964, *45*, 469–476. (From: Institut de Radiologie de l'Académie de Médecine à Poznan, Poland.)

If the optical features of a tomogram are observed with the naked eye or analyzed with a densitometer, two different phenomena may be noted: objective

and subjective contrast. Many obscure and as yet unexplained problems are related to these two phenomena. The present work aims at throwing some light on these problems in relation to tomographic images.

A special method was devised in order to study contrast of a roentgenogram and a tomogram from the viewpoint of radiologic interpretation.

*Objective contrast* was investigated with a microdensitometer which gives constant results that can be read on a logarithmic scale. An image element corresponds to a field of homogeneous optical density, independently of its size and shape. Two elements form the detail of an image. The density of elements as small as 10 microns can be measured with this densitometer. Thus, the objective contrast of each point in a tomogram can be expressed in numerical values, and this is called local contrast.

To study *subjective contrast*, tomographic films were submitted to experienced radiologists, who had to determine on a previously traced line each contour of the image. Then, along the same line, a densitometer curve was drawn, and in this way it was possible to analyze which physical factors of the objective contrast corresponded to the perception of local subjective contrast.

In the present stage of their investigation, the authors cannot yet reach clear-cut conclusions. They ascertained, however, that various types of tomographic images are characterized by a particular gamut of contrasts. Moreover, when the contrasts of conventional roentgenograms are compared to those of tomograms of the same anatomic regions, it may be seen that tomograms show a lower gradient and narrower contours. The subjective improvement of contrasts on the tomograms is based on a steeper gradient only in cases where gas contrast or artificial opacification is used. Otherwise, good discernment and perception of individual details on tomograms depend on the particular arrangement of local contrasts.—*H. P. Lévesque, M.D.*

Bell, G. R., and Smart, M. J. *In vivo* angiography of the Pacific salmon (oncorhynchus). *J. Canad. A. Radiologists*, Dec., 1964, *15*, 200–210. (From: Fisheries Research Board of Canada, Biological Station, Nanaimo, British Columbia, Canada.)

Increasing industrial and domestic pollution of our waters have necessitated investigation into the effects of pollutants on economically important fish, such as the Pacific salmon.

Modern radiographic methods were utilized to investigate the physiology and pathology of the Pacific salmon. After anesthetizing the fish by adding M.S.222 (tricaine methane sulphonate [Sandoz]) to their water, a needle was inserted into the dorsal aorta through the roof of the mouth. A polyethylene tubing, connected to the needle, was attached to a hole drilled through the nasal cartilage. The fish were allowed to recover from anesthesia and were transported to the X-ray office in large containers, where after re-anesthesia 3–4 cc. hypaque was injected through the tubing in order to demonstrate the vascular tree.

The method is helpful in finding routes of injection and sampling to measure blood volume, blood pressure, blood lactate hemoglobin, and serum enzyme levels. These tests are used in experiments designed to study mechanisms of detoxication of pollutants.—*W. J. Carmoney, Jr., M.D.*

## RADIATION THERAPY

Ciampelli, L. Trattamento radiologico dell'acromegalia. (Radiologic treatment of acromegaly.) *Radiol. med.*, Dec., 1964, *50*, 1241–1256. (Address: Istituto di Radiologia dell'Università, Firenze, Italy.)

Between 1945 and 1962 the author treated 48 cases of acromegaly with radiation therapy. Twelve were eliminated from this report because of incomplete clinical and roentgenologic information. Of the remaining 36, 2 were operated on some time after the roentgen treatment.

The technique of irradiation was in 12 patients: 160 kv., 4 ma., filter 0.5 mm. Cu and 1 mm. Al, 40 cm. target skin distance, 4 fields (2 temporal, 1 frontal and 1 occipital). In 11 patients the technical factors were changed to; 250 kv., 30 ma., filter Thoreus III with a half value layer of 2.8 mm. Cu, target skin distance of 50 cm., 2 opposite temporal fields. More recently, 13 cases were treated by cobalt 60 teletherapy through 2 opposite temporal fields with a source skin distance of 80 cm. The tumor dose varied between 5,000 and 8,000 r in one or more courses with an average of 700 r weekly.

The patients were followed up to 16 years, with a minimum of 8 months. The majority of cases were followed up for more than 5 years.

Positive roentgen findings in the sella turcica were present in 31 cases. The changes were not modified by radiation therapy.

Somatic changes were noted more or less in all patients and remained unchanged in 30 patients; in 3 cases the improvement was moderate and in 3 more cases there was a return to an almost normal facies.

Headaches were present in 33 cases, from minimal to severe. Following radiation therapy, in 10 patients there was no improvement, in 8 the headaches were makerdly reduced in intensity and disappeared in the remaining 8 cases.

Visual disturbances were noted in 24 patients. These disappeared in 9 cases, improved in 5 and remained stationary in 8, while progressing in severity in 1 case.

Amenorrhea and altered libido were present in 8 women and 4 men. At the end of the treatment,

there was marked improvement in 2 women with return to normal menstrual cycle, while in 3 there was only moderate improvement. In only 1 man was there return of the normal libido.

A few interesting cases are reported in detail.

Concluding, the author recommends radiation therapy as the treatment of choice in acromegaly. Surgery should be used in individuals in whom there is danger of loss of vision and there is evidence of increased intracranial pressure and, when after radiation therapy, the disease continues to progress. Cobalt therapy should now be adopted because of its many advantages over conventional roentgen therapy. A tumor dose of 3,500 r in 5 to 6 weeks is considered satisfactory.—*A. F. Govoni, M.D.*

PEREZ-TAMAYO, R., and KRAMER, S. Rhabdomyosarcomas of the head and neck in children: place of radiotherapy. *Radiol. clin.*, 1964, *33*, 307–318. (From: Division of Radiation Therapy, Department of Radiology, Jefferson Medical College Hospital, Philadelphia, Pa.)

The literature on the place of radiotherapy in the treatment of rhabdomyosarcoma of the head and neck is confusing largely because of the failure to distinguish between radiosensitivity and radiocurability.

Five cases are presented to show that regressions, sometimes spectacular, can occur following even modest tumor doses indicating the rather pronounced radiosensitivity of rhabdomyosarcoma. However, in all but 1 case disseminated metastases and death occurred soon after therapy proving the lack of radiocurability of this disease.

The authors suggest that irradiation followed by surgery would be the best form of therapy for rhabdomyosarcoma of the head and neck.—*Henry J. Klos, M.D.*

VAETH, J. M., and PURCELL, T. R. Radiation response of diffuse pleural mesothelioma: a case report. *Radiol. clin.*, 1964, *33*, 319–327. (Address: Dr. Vaeth, Department of Radiology, University of California Medical Center, San Francisco, Calif. 94122.)

Radiation therapy has not been regarded favorably in the treatment of pleural mesothelioma. On the basis of the favorable response to irradiation in 1 case, the authors suggest that a more vigorous use of this form of treatment is indicated in this uncommon neoplasm.

After subtotal removal of a right pleural mesothelioma in a 24 year old male, a recurrence in the right lower thoracic cavity cleared with a midplane dose of 6,100 r in 63 days given with a 1 mev. roentgen-ray machine. Later recurrences in the lung and supraclavicular region responded to midplane doses on the order of 5,000 r given with 250 kv. equipment in 52 to 56 days.

Total survival after surgery was 49 months and after the first roentgen therapy, 38 months.—*Henry J. Klos, M.D.*

TALBERT, LUTHER M., PALUMBO, LEONARD, SHINGLETON, HUGH, BREAM, C. A., and MCGEE, JOHN A. Urologic complications of radical hysterectomy for carcinoma of the cervix. *South. M. J.*, Jan., 1965, *58*, 11–17. (From: Department of Obstetrics and Gynecology and Department of Radiology, University of North Carolina School of Medicine, Chapel Hill, N. C.)

The purpose of this paper is to review the changes that occur in the urinary tract following radical hysterectomy for carcinoma of the cervix.

Since 1952, 112 radical hysterectomies had been done for carcinoma of the cervix at the North Carolina Memorial Hospital. Most patients received preoperative radium therapy.

On intravenous pyelography, all patients had "considerable dilatation" of the upper urinary tract within the first week postoperatively and maximal dilatation at 3 weeks. Those who eventually had normal urinary tracts were "well on the way to a normal appearance" by 3 months. A graph is printed showing the variation in normals postoperatively based on measurement of the circumference of the renal pelvis.

Five patients (4.5 per cent) developed ureteral strictures and they all had marked dilatation of the upper urinary tract at 3 months. Nine patients (8 per cent) developed ureteral fistulas, usually detected 2 weeks postoperatively. Although some hydronephrosis developed with these fistulas, autonephrectomy usually occurred before dilatation was pronounced.

Three patients (2.5 per cent) developed vesicovaginal fistulas bringing the total of urologic complications to 15 per cent.—*Henry J. Klos, M.D.*

FOR SUPERIOR X-RAY DIAGNOSIS

# INTROPAQUE

## BARIUM SULFATE, U.S.P. 91%

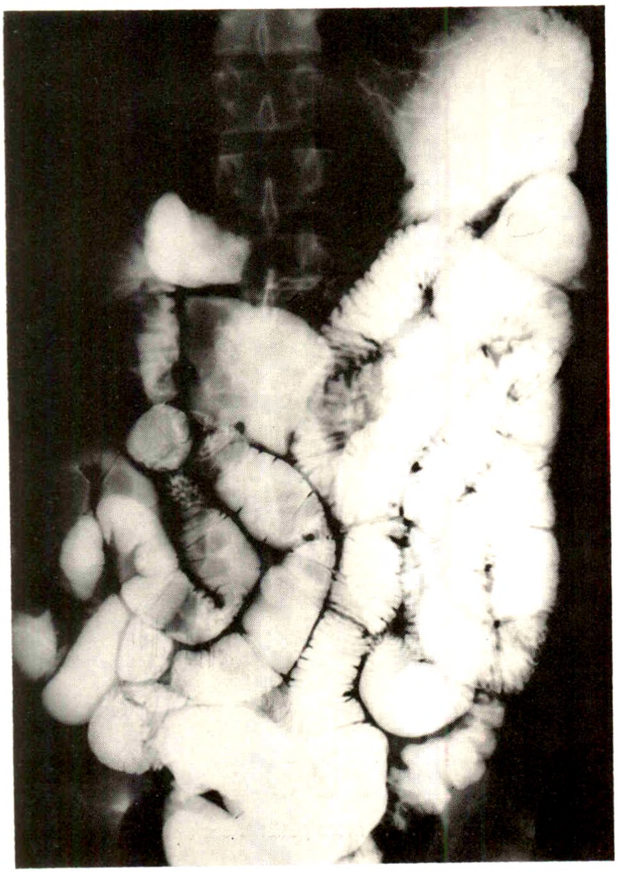

- INTROPAQUE deposits a smooth, lasting coating and does not form lumps.
- INTROPAQUE has optimum density and good adhesive qualities.
- INTROPAQUE will not dry or flake in the colon for an hour or more.
- INTROPAQUE has maximum opacity allowing for easy penetration.
- INTROPAQUE is a non-foaming, stable formula allowing excess suspension to be used another day.
- INTROPAQUE has a remarkable ability to overcome pylorospasm.

This formula was developed to satisfy multiple criteria for an ideal suspension. We invite you to try a sample and see how it performs for you.

Distributed by
General Electric Company
X-Ray Department
Milwaukee, Wisconsin

General Electric Company
X-Ray Department
P. O. Box 1472
Lafayette, Indiana

Please send me a free sample of Intropaque

Name__________

Address__________

City_____ Zip Code_____ State_____

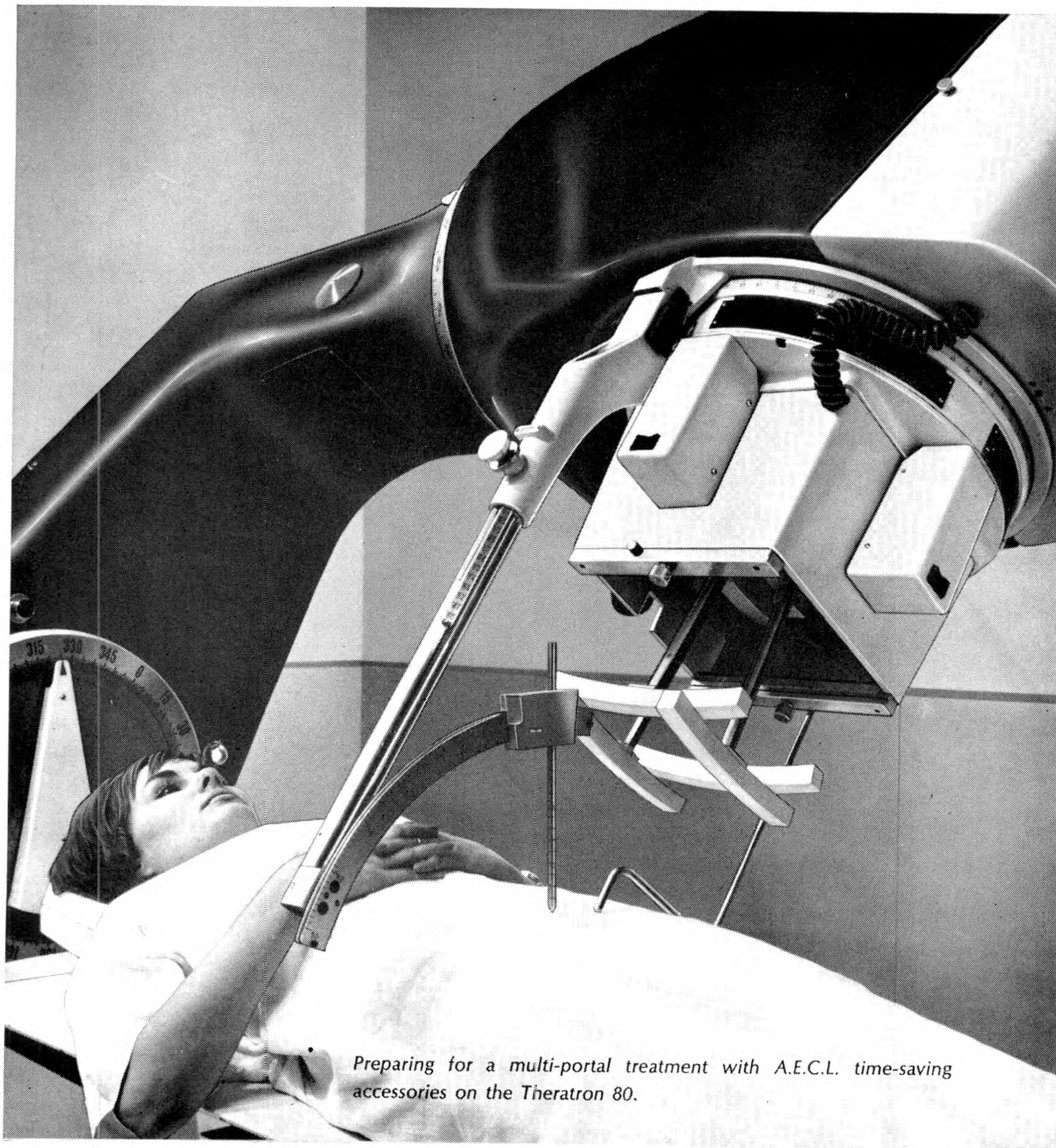

*Preparing for a multi-portal treatment with A.E.C.L. time-saving accessories on the Theratron 80.*

STAND 36
ELEVENTH
INTERNATIONAL CONGRESS
OF RADIOLOGISTS
Rome, Italy
Sept. 22-28, 1965

# THE MINUTES YOU SAVE

*mean less strain on the patient . . . more patients each day — a more efficient clinic*

*The established efficiency and effectiveness of A.E.C.L.'s teletherapy equipment, supplemented with a full range of accessories developed to meet the rigorous demands of modern teletherapy, assures the precise application of each treatment to the exacting requirements of the radiotherapist.*

*Sales and service representation in over 100 countries.*

**ATOMIC ENERGY OF CANADA LIMITED**
Commercial Products • P.O. Box 93 • Ottawa • Canada

64-2M

# INDEX TO ADVERTISERS



•

**We try to present an accurate index. Occasionally this may not be possible because of a last-minute change or an omission.**

# —NOW AVAILABLE—

## CONSOLIDATED INDICES

# VOLUME VI

embracing

***The American Journal of Roentgenology, Radium Therapy and Nuclear Medicine***

**Volumes 79-88 (1958-1962)**

Covers some 8,000 pages of original papers, editorials, biographical sketches, and abstracts of both domestic and foreign journals published in THE AMERICAN JOURNAL OF ROENTGENOLOGY, RADIUM THERAPY AND NUCLEAR MEDICINE for the years 1958-1962.

Fills a very definite need and will be welcomed by those who have occasion to consult the Journal during this five-year period. Increases the usefulness of your set of journals a hundred-fold.

**A Limited Quantity Has Been Printed**

**Order Your Copy NOW**

**CHARLES C THOMAS · PUBLISHER**
301-327 East Lawrence Avenue
Springfield · Illinois

Send me the volumes I have checked below on ten days free inspection approval. I will send a remittance within thirty days for the ones I decide to keep. (Purchasers outside U.S.A. should send cash with order.)

Volume II (1938-1942), $10.00
Volume III (1943-1947), $22.50
Volume IV (1948-1952), $23.50
Volume V (1953-1957), $25.00
Volume VI (1958-1962), $23.50
*Volume I (1903-1937) out of print.

name ....................................
address ....................................
city ............................ zone .......
state ....................................

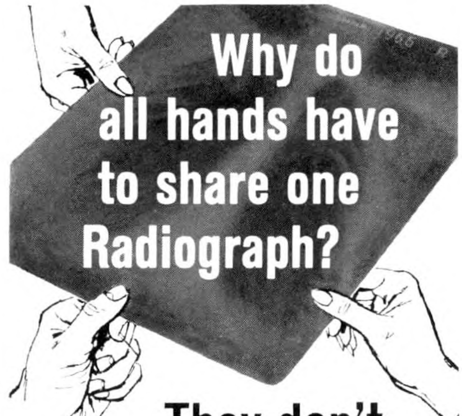


## They don't

Not when radiograph duplicate films can be made so quickly and easily on a Blu-Ray Radiograph Duplicating Printer.
Why else do you need one? Because it's an ideal tool for producing subtraction masks used in the subtraction technique (with Kodak Commercial Film — Estar thick base). Also because it makes radiograph duplicate films that . . . provide copies for therapy mapping; furnish records for transferrals; are excellent OR aids for surgeons; furnish economical research and teaching aids; and stop the waste of do-it-yourself solarization.

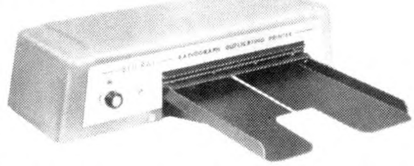

Any valuable radiograph film should be duplicated. Today it's easy.

**SEND COUPON FOR A FREE TRIAL**

BLU-RAY

**Reproduction Engineering Corporation**
**6507 Westbrook Road, Essex, Connecticut**

Please send literature and arrange for a free trial of a Blu-Ray Radiograph Duplicating Printer. I understand there is no obligation.

NAME....................
Title....................
Institution....................
Address....................
City....................
State.................... Zip No. ..........
Telephone....................

# The British Journal of Radiology

FOUNDED 1896

*A monthly publication covering the fields of*

RADIODIAGNOSIS, RADIOTHERAPY, RADIOBIOLOGY, RADIOLOGICAL PHYSICS, RADIATION PROTECTION AND NUCLEAR MEDICINE

*This Journal is the official organ of*

THE BRITISH INSTITUTE OF RADIOLOGY

The British Journal of Radiology is the oldest radiological journal in the world, having started in 1896 as *The Archives of Clinical Skiagraphy.*

In addition to the presentation of selected papers which have been read at meetings of the Institute, original contributions from workers actively engaged in radiology in all parts of the world are published. By publishing material embracing new developments in both clinical and academic fields of radiology, this Journal is designed to serve the reader who wishes to keep abreast of the advancing and widening front of radiological science and practice today.

An increasing proportion of editorial space is being used to publish original contributions in radiodiagnostic physics and technology, cellular and human radiation biology, the techniques for clinical investigation using labelled compounds and in other rapidly growing fields on the fringe of radiology.

The size has been increased to an average of 80 pages pêr month, 9½″ x 7″, while maintaining the number and excellent quality of the illustrations, for which this Journal has become justly famous.

No effort is being spared to make THE BRITISH JOURNAL OF RADIOLOGY a publication of the highest possible excellence both as regards matter and form of presentation.

*obtainable from*

THE BRITISH INSTITUTE OF RADIOLOGY
32 WELBECK STREET, LONDON, W.1
*and from leading booksellers all over the world*

Price £6.16.6d (U.S. $20.50) per annum.

**27 YEARS** of integrity have helped us to become America's largest buyers of

# USED X-RAY FILM

- We purchase all makes and sizes from any point in the nation, and pay the freight cost.
- We remit in advance if desired, or promptly after receipt and tally of the value.
- Write for prices today. We will send shipping labels, and direct your film to our nearest plant.

## DONALD McELROY, INC.

53 W. Jackson Blvd., Chicago 4, Ill.

---

*Subscribe today to*

THE JOURNAL OF THE CANADIAN ASSOCIATION OF RADIOLOGISTS

published quarterly: March, June, September and December. It is the **official organ** of **The Canadian Association of Radiologists.**

Price $5.00 per annum in Canadian or equivalent funds.

The Canadian Association of Radiologists,
1555 Summerhill Avenue,
Montreal 25, Quebec, Canada

Please enter my subscription to the JOURNAL OF THE CANADIAN ASSOCIATION OF RADIOLOGISTS, for which my cheque is enclosed.

Name ....................................................
(Please print)

Address ....................................................
(Please print)

City ................................ Province or State .................. Country ....................

# 16 ANSWERS TO YOUR PROBLEMS IN ROENTGENOLOGY

*Offering New Techniques . . . New Procedures*

☐ **A TEXTBOOK OF ELEMENTARY RADIOGRAPHY FOR STUDENTS AND TECHNICIANS** *by* **Donald deForest Bauer,** *Klamath Valley Hosp., Klamath Falls, Ore.* 260 pp., 6 il., 5 tables, $8.50.

☐ **MEDICAL RADIOGRAPHIC TECHNIC** *(3rd Ed.). Rewritten by* **William L. Bloom, Jr., John L. Hollenbach,** *and* **James A. Morgan,** *all of the Technical Service Dept., General Electric Company, Milwaukee, Wis. Originally under the editorial supervision of* **Glenn W. Files** *(1897-1945).* '65, 368 pp. (7 × 10), 510 il., 7 tables, $11.00.

☐ **RADIOTHERAPY OF BENIGN DISEASE** *by* **Stephen B. Dewing,** *Hunterdon Medical Center, Flemington, N.J. With a guest chapter contributed by* **Ralph Wier Grover,** *Nassau County Tuberculosis Sanatorium, Farmingdale, N.Y.* '65, 320 pp., $9.75

☐ **PRACTICAL GAMMA SPECTROMETRY** *by* **A. J. Duivenstijn,** *Eindhoven, and* **L. A. J. Venverloo,** *Veldhoven. Both of the Netherlands. Translated by* **G. du Cloux,** *Waitington, England.* '63, 154 pp., 87 il., $7.50

☐ **MAMMOGRAPHY** *by* **Robert L. Egan,** *The Methodist Hospital of Indiana, Indianapolis, Indiana.* '64, 480 pp. (8½ × 11), 355 il., 42 tables (Amer. Lec. Roentgen Diagnosis edited by Lewis E. Etter), $25.50

☐ **ROENTGENOGRAPHY AND ROENTGENOLOGY OF THE MIDDLE EAR AND MASTOID PROCESS** *by* **Lewis E. Etter,** *Univ. of Pittsburgh. With the Collaboration of* **Lawrence C. Cross** *and* **Merle J. Stuart,** *both of Western Psychiatric Institute and Clinic. All of Pittsburgh, Pa.* '65, 168 pp. (8½ × 11), 157 il., $9.75

☐ **THE EARLY RADIOLOGICAL DIAGNOSIS OF DISEASES OF THE PANCREAS AND AMPULLA OF VATER: Elective Exploration of the Ampulla of Vater and the Head of the Pancreas by Hypotonic Duodenography** *by* **Paul Jacquemet,** *Lyon Faculty of Medicine, Lyon, France;* **Domingo Liotta,** *Baylor Univ., Houston, Texas; and* **Pierre Mallet-Guy,** *Lyon Faculty of Medicine. Translated by* **Lee D. Cady,** *Baylor, Univ.* About 230 pp. (7 × 10), about 392 il. In Press

☐ **ATLAS OF CARDIOVASCULAR KYMOGRAPHY** *by* **Giovanni Juliani** *and* **Cesare Quaglia,** *both of Univ. of Turin, Torino, Italy. Translated from Italian by* **John L. Maurice.** '65, 224 pp. (8½ × 11), 164 il., $12.75

☐ **CLINICAL ROENTGENOLOGY OF COLLAGEN DISEASES** *by* **Charles M. Nice, Jr.,** *Tulane Univ., New Orleans, La.* About 176 pp., about 134 il. (Amer. Lec. Roentgen Diagnosis). In Press.

☐ **RADIOISOTOPES AND THEIR INDUSTRIAL APPLICATIONS** *by* **Henri Piraux,** *Compagnie Francaise Philips, Paris, France. Translated by* **L. B. Firnberg,** *Amersham-on-the-Hill, England.* '64, 288 pp., 210 il. (12 in full color), 22 tables, $14.50

☐ **DOSEMETERS FOR X-RAY DIAGNOSIS** *by* **K. Reinsma,** *Philips' Industrial Division for X-Ray and other Medical Equipment, Eindhoven, The Netherlands.* '62, 100 pp., 40 il., 16 tables, $4.50

☐ **THE ROENTGENOLOGICAL FEATURES OF SICKLE CELL DISEASE AND RELATED HEMOGLOBINOPATHIES** *by* **Jack Reynolds,** *Univ. of Texas, Dallas, Texas.* About 320 pp., about 80 il. In Press.

☐ **UTEROSALPINGOGRAPHY IN GYNECOLOGY: Its Application in Physiological and Pathological Conditions** *by* **Samuel Rozin,** *Hebrew University-Hadassah Medical School, Jerusalem, Israel.* About 410 pp. (8½ × 11), 369 il., 2 tables. In Press

☐ **MYELOGRAPHY** *by* **Vincenzo Valentino,** *Univ. of Naples, Naples, Italy.* '65, 292 pp. (8½ × 11), 276 il. (3 color plates), $19.50

☐ **MEDICAL X-RAY TECHNIQUE** *(2nd Ed.) by* **G. J. van der Plaats,** *St. Annadal Hosp., Maastricht, The Netherlands. Translated by* **Gerald E. Luton,** *Eindhoven, The Netherlands.* '65, 508 pp., 323 il., $14.50

☐ **PROGRESS IN ANGIOGRAPHY** *compiled and edited by* **Manuel Viamonte, Jr.** *and* **Raymond E. Parks,** *both of Univ. of Miami, Miami, Fla. (With 20 Contributors)* '64, 576 pp. (6¾ × 9¾), 893 il., 12 tables, $29.50

**CHARLES C THOMAS · PUBLISHER** 301-327 East Lawrence Avenue **SPRINGFIELD · ILLINOIS**

# Radiologia Clinica

International Radiological Review

*Redactores:* F. BUSCHKE, San Francisco, Cal.; R. SARASIN, Genève; A. ZUPPINGER, Bern

One volume of six parts is issued annually and costs U.S. $15.50 (postage included).

*Contents Vol. 33, No. 5*

BUSCHKE, F. (San Francisco, Cal.): Introduction to the New Radiation Therapy Section of Radiologia Clinica

HOHL, K. (St. Gallen): Heutiger Stand der Therapie und Prognose der Lymphogranulomatose

BLOEDORN, F. G. and WIZENBERG, M. J. (Baltimore, Md.): Preoperative Irradiation

SCHREIBER, A. (Zürich): Spätschaden nach Radiumbehandlung eines gelenknahen Hauthämangioms

PEREZ-TAMAYO, R. and KRAMER, S. (Philadelphia, Pa.): Rhabdomyosarcomas of the Head and Neck in Children: Place of Radiotherapy

VAETH, J. M. and PURCELL, T. R. (San Francisco, Cal.): Radiation Response of Diffuse Pleural Mesothelioma: A Case Report

*Contents Vol. 33, No. 6*

Competition 1965 / Dr. HEINZ KARGER Memorial Foundation

MAURER, H.-J.; SCHREIBER, H. W. und KOCH, W. (Bonn): Splenoportographie und Chirurgie des Pfortaderhochdrucks

BECKER, H. W. und BECKER, C. (Halle): Mesotheliome der Pleura im Röntgenbild

ROČEK, V.; BENDA, K.; VOLEJNÍK, J. und DUŠEK, J. (Olomouc): Das röntgenologische Bild der Mukoviscidose (Fibrosis cystica pancreatis)

LEICHNER-WEIL, S. (Budapest): Das Vorkommen von Schaltknochen an den Schädelaufnahmen von Epileptikern

Ask for specimen copies

---

ORDER FORM

S. Karger AG, Arnold-Böcklin-Strasse 25, Basel (Switzerland)

Please enter my subscription to RADIOLOGIA CLINICA, Vol. ......

Name ............................ Address ..........................

..............................................................

---

**To be ordered through your agent or:**

**Albert J. Phiebig, P.O. Box 352, White Plains, N.Y.**

**Original radiograph—reproduced upper left—was made on Kodak Blue Brand Medical X-ray Film.**

**Copy of original radiograph—reproduced lower right—was made on Kodak Radiograph Duplicating Film.**

# Two Radiographs of the same chest?

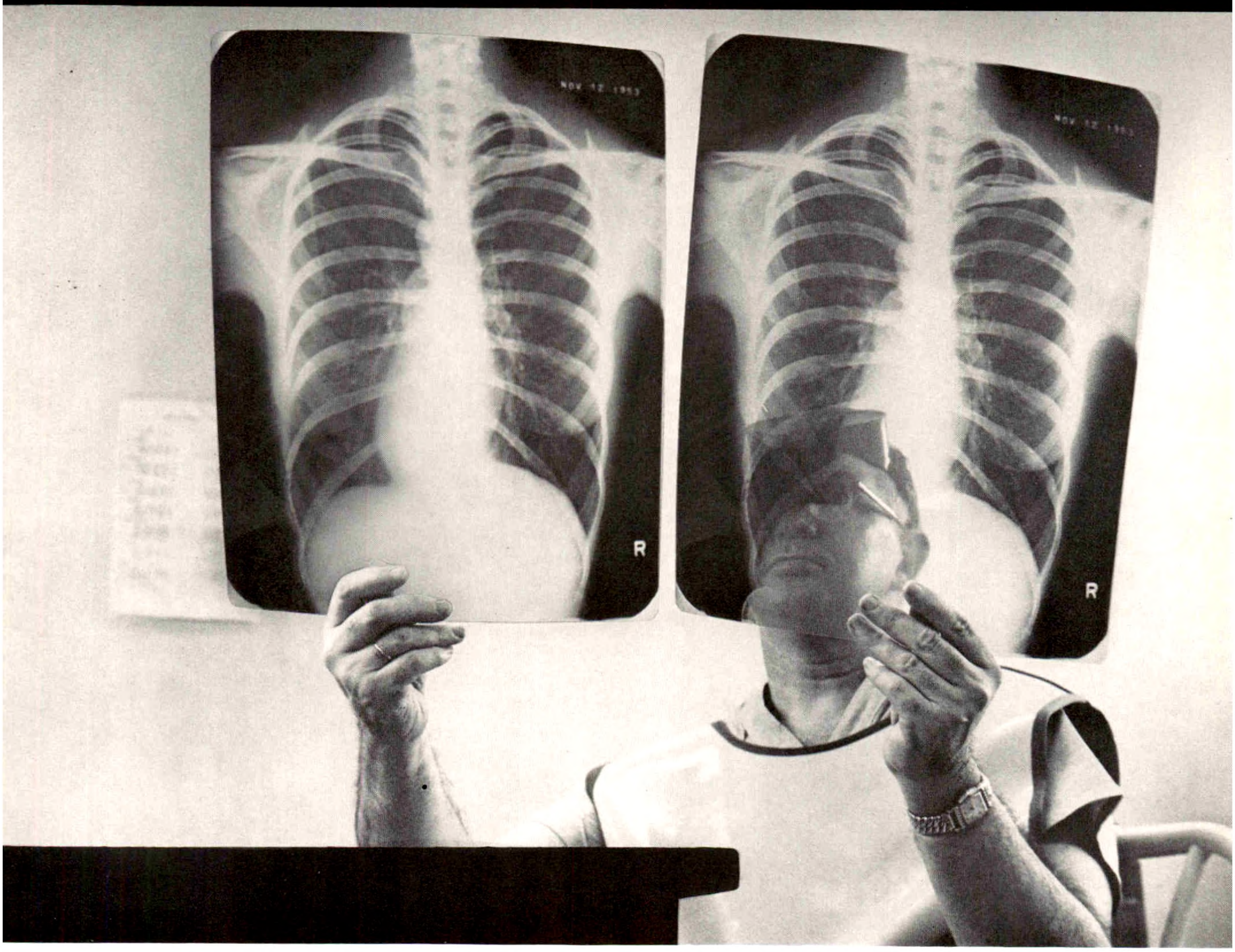


**No—they are both copies of the same radiograph— made possible by the new KODAK Radiograph Duplicating Film**

How many times have you wanted duplicates of a radiograph—and *not* been able to get them? Now you can—with ease and speed—thanks to KODAK Radiograph Duplicating Film. It lets you produce an unlimited number of duplicates of excellent quality, for instant use.

Now you can send same-size, same-tone duplicates of significant radiographs with reports to referring physicians. Duplicates can accompany patients' records when they move to other localities. Duplicates can be used for therapy mapping. Duplicates can be invaluable in teach-

KODAK Radiograph Duplicating Film can be exposed in seconds in a simple printing frame or in automatic exposure equipment. Process it right along with other Kodak medical x-ray film in a KODAK X-OMAT Processor . . . or manually with conventional x-ray film processing equipment.

Ask your Kodak X-ray Dealer or Kodak X-ray Technical Sales Representative for more information and a demonstration.

**EASTMAN KODAK COMPANY**

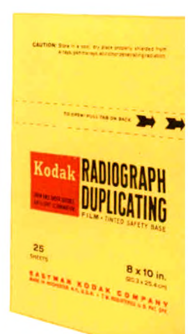

FOUNDED IN 1906 AS THE AMERICAN QUARTERLY OF ROENTGENOLOGY

# THE AMERICAN JOURNAL OF ROENTGENOLOGY RADIUM THERAPY AND NUCLEAR MEDICINE

OFFICIAL ORGAN OF
THE AMERICAN ROENTGEN RAY SOCIETY
THE AMERICAN RADIUM SOCIETY

CALCUTTA UNIVERSITY CENTRAL LIBRARY

TRAIAN LEUCUTIA, Editor
KENNETH L. KRABBENHOFT, Assistant to the Editor

ASSOCIATE EDITORS

HARRY HAUSER    RUSSELL H. MORGAN    EDWARD B. D. NEUHAUSER
WENDELL G. SCOTT

CONSULTING EDITORIAL BOARD

PAUL C. AEBERSOLD
OSCAR V. BATSON
JOHN CAFFEY
ROSS GOLDEN
PAUL C. HODGES
HOWARD B. HUNT
JOHN H. LAWRENCE
REED M. NESBIT
EUGENE P. PENDERGRASS
U. V. PORTMANN
LAURISTON S. TAYLOR
OWEN H. WANGENSTEEN
SHIELDS WARREN

*Issued Monthly for the American Roentgen Ray Society by*
CHARLES C THOMAS · PUBLISHER · SPRINGFIELD · ILLINOIS

VOLUME 94    AUGUST, 1965    NUMBER 4

Sixty-sixth Annual Meeting, American Roentgen Ray Society
Washington-Hilton Hotel, Washington, D.C.
September 28-October 1, 1965
INSTRUCTION COURSES
For Preliminary Program see July issue

INDEX NUMBER

Want to get the sharpest, clearest radiographs possible in cerebral, aortic, renal and other small area angiography?

(As well as quick operating room films for radium insertions, operative cholangiography, and hip nailings)

Get this.

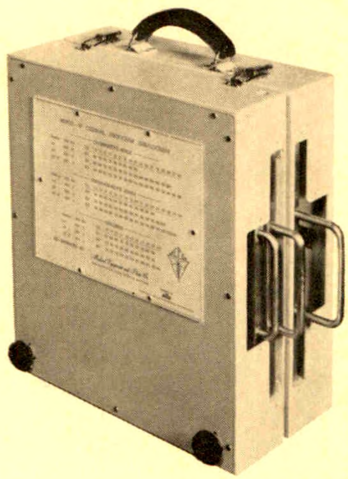

The Mepco IV serialograph.

It never breaks down.
It never gets jammed.
It never magnifies.
It can be used in the operating room or the X-Ray Department, with portable as well as fixed X-Ray tubes, and with Polaroid® as well as standard 10″ x 12″ cassettes. And it's economical, both in purchase price and use.
**Get the picture?**

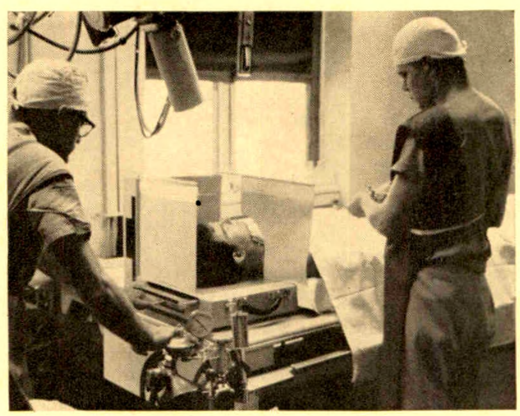

*Mepco IV*

For information, call or write:
Medical Equipment and Photo Company
12300 Washington Avenue
Rockville, Maryland
Phone (301) 427-3850

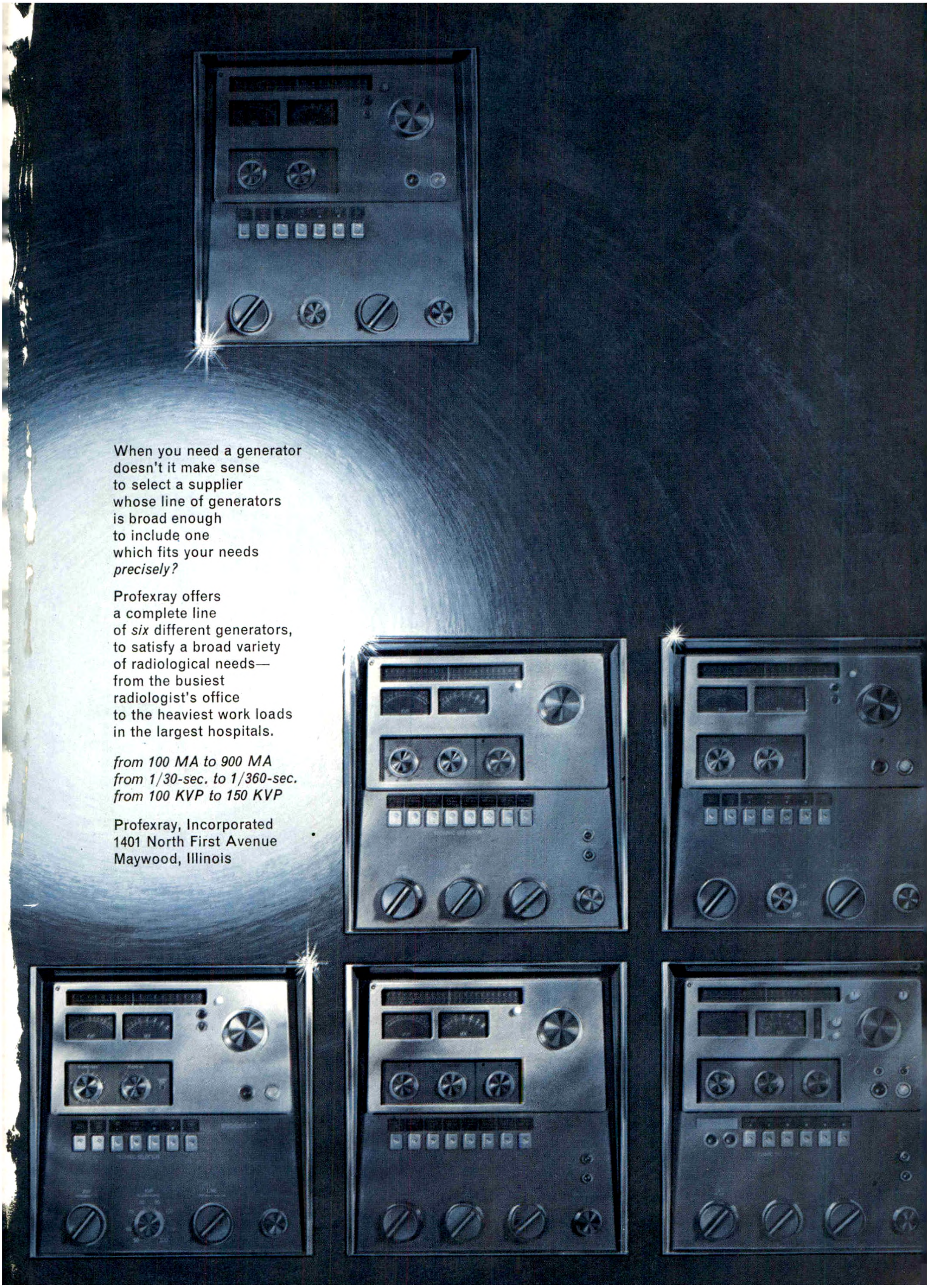
When you need a generator doesn't it make sense to select a supplier whose line of generators is broad enough to include one which fits your needs *precisely?*
Profexray offers a complete line of *six* different generators, to satisfy a broad variety of radiological needs—from the busiest radiologist's office to the heaviest work loads in the largest hospitals.
*from 100 MA to 900 MA*
*from 1/30-sec. to 1/360-sec.*
*from 100 KVP to 150 KVP*
Profexray, Incorporated
1401 North First Avenue
Maywood, Illinois

# GENERAL INFORMATION

Manuscripts offered for publication and other correspondence relating to the editorial management and books for review should be sent to Dr. Traian Leucutia, Editor, 401 Professional Building, Detroit, Michigan 48201. Contributions may be sent in foreign languages and will be translated if found acceptable. Original articles are published with the understanding that they are contributed exclusively to THE AMERICAN JOURNAL OF ROENTGENOLOGY, RADIUM THERAPY AND NUCLEAR MEDICINE.

A certain number of illustrations will be supplied free of cost; but special arrangements must be made with the Editor and Publisher for excess illustrations and elaborate tables.

Fifty reprints are furnished without charge to authors. Additional reprints may be purchased according to a scale of prices that accompanies galley proofs. As soon as each issue is printed, the type is destroyed except for reprint orders *in hand*. Reprint orders *must* be returned with corrected galley proof to the Editorial Office if additional reprints are desired.

Correspondence regarding subscriptions, advertisements, and other business relating to THE AMERICAN JOURNAL OF ROENTGENOLOGY, RADIUM THERAPY AND NUCLEAR MEDICINE should be addressed to Charles C Thomas, Publisher, 301–327 East Lawrence Avenue, Springfield, Illinois. (All requests to be submitted in writing.)

---

Manuscripts should be typewritten, with double spacing, and good margins (not on thin paper) and the *original* should be sent to the Editor. The author should keep a carbon copy, as the original is not returned. The name of the author should appear on each sheet of manuscript. Tabular materials should be typed on separate sheets; likewise bibliographical lists, footnotes, etc.

Drawings and charts for reproduction should be made in black (*never* in blue). Photographic prints of plates or slides on glossy paper produce the best half-tones.

All photographs and drawings intended for illustrations should be numbered, the top plainly indicated, and an abbreviated title of the paper placed on the back of *each one*.

Legends for illustrations should be typewritten in a single list, double spaced, with numbers corresponding to those on the photographs and drawings, instead of attaching each legend to its corresponding figure.

Care in preparation of bibliographies will save much time and correspondence. Each reference in a bibliography should include the following information in the order indicated: Name of the author with initials; title of the article; name of the periodical; year, volume and pages. It is requested that the authors use the following as model:

1. Olcott, C. T., and Dooley, S. W. Agenesis of lung of infant. *Am. J. Dis. Child.*, 1943, *65*, 766–780.

The month should be given if the reference is to an issue of the current year. An alphabetical arrangement of the authors is requested.

The author should always place his full address somewhere on his manuscript This is very important and is often omitted

---

For information regarding membership in the American Roentgen Ray Society, address the Chairman of the Executive Council, Dr. Ted F. Leigh, Emory University Clinic, Atlanta, Georgia 30322.

For information regarding the program of the annual meeting of the American Roentgen Ray Society, address the President-Elect, Dr. J. P. Medelman, 110 Birchwood Avenue, White Bear Lake 10, Minnesota.

For information regarding membership in the American Radium Society, address the Secretary, Dr. John L. Pool, 444 East 68th Street, New York, New York 10021.

For information regarding the program of the annual meeting of the American Radium Society, address the President, Dr. Justin J. Stein, U.C.L.A. Medical Center, Los Angeles, California 90024.

---

THE AMERICAN JOURNAL OF ROENTGENOLOGY, RADIUM THERAPY AND NUCLEAR MEDICINE is owned, maintained by, and in the interests of the American Roentgen Ray Society, Inc. It is issued monthly by Charles C Thomas, Publisher, 301–327 East Lawrence Avenue, Springfield, Illinois. THE AMERICAN JOURNAL OF ROENTGENOLOGY, RADIUM THERAPY AND NUCLEAR MEDICINE does not hold itself responsible for any statements made or opinions expressed by any contributors in any article published in its columns.

Delivery is not guaranteed. Replacements are not guaranteed nor promised, but will be attempted if extra single copies are available and only if requested within 30 days from first of month following publication (17th of month) for domestic subscribers and 60 days for foreign subscribers.

Annual subscription price is as follows: United States, U. S. Possessions, U. S. Trusteeships, Pan-American Union, and Canada, $15.00; other countries $17.00. Prices for back volumes quoted on application. Extra single copies of back issues, if available, $1.50, postpaid. Current subscriptions may begin with any issue. Remittance should be sent to CHARLES C THOMAS, PUBLISHER, 301–327 East Lawrence Avenue, Springfield, Illinois, U.S.A.

ADDRESS CHANGE—When a change of address is necessary please allow at least 60 days notice and preferably 90 days. When ordering a change of address, send the Publisher both the old and new address.

Entered as Second-class at Springfield, Illinois under the Act of March 3, 1879. Printed in U.S.A.

Second-class postage paid at Springfield, Illinois and at additional mailing offices.

Copyright © 1965, by AMERICAN ROENTGEN RAY SOCIETY, Inc. No part may be duplicated or reproduced without permission of both the Publisher and the Editor.

# THE AMERICAN JOURNAL OF ROENTGENOLOGY, RADIUM THERAPY AND NUCLEAR MEDICINE

Vol. 94 AUGUST, 1965 No. 4

CONTENTS



(*Continued on page iv*)

# the new **MEL SL75** offers many outstanding advantages- here are just some of them

- X-Ray output 400 rads/minute in air fully flattened at 100cm.
- Compact X-Ray head with full facilities and all-round control – 18 inch clearance to isocentre.
- Electron output available.
- Alternative treatment couch designs.
- Exocentrically mounted drum for high stability and smooth rotation with freedom from wear.
- Steel tube accelerator guide support for rigid mouting free from torsional deformation.
- The high efficiency electroformed accelerating guide is Ion pumped for high vacuum and reliability.
- Powered by low cost 2MW tuneable magnetron.
- Treatment controls completely separate from accelerator controls.

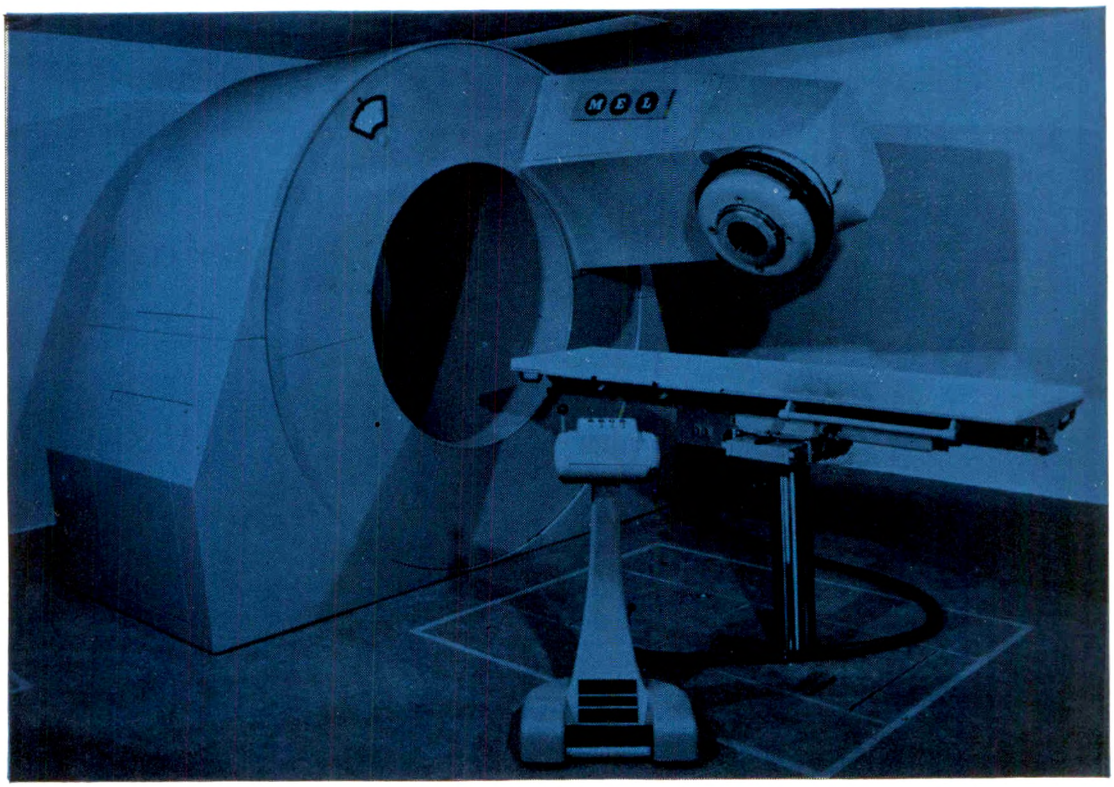

MEL

This equipment is sold in the USA through
**North American Philips Co Inc**
100 East 42nd Street New York 17 NY
Write now for details and fully illustrated booklet

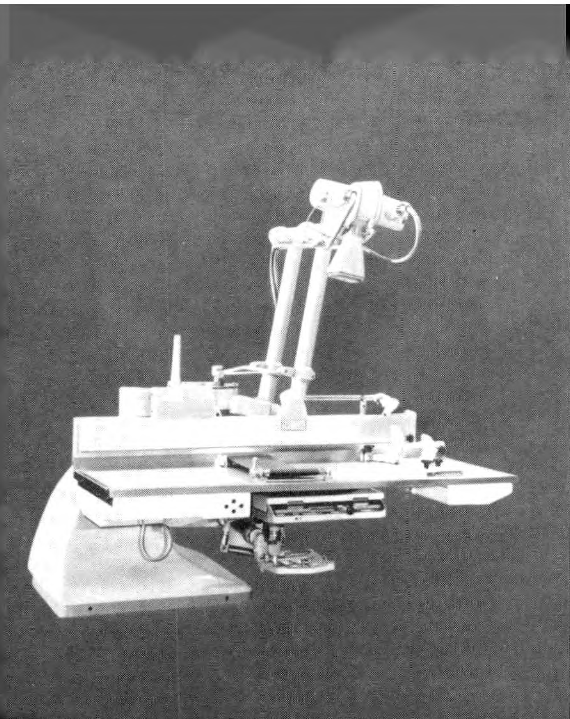

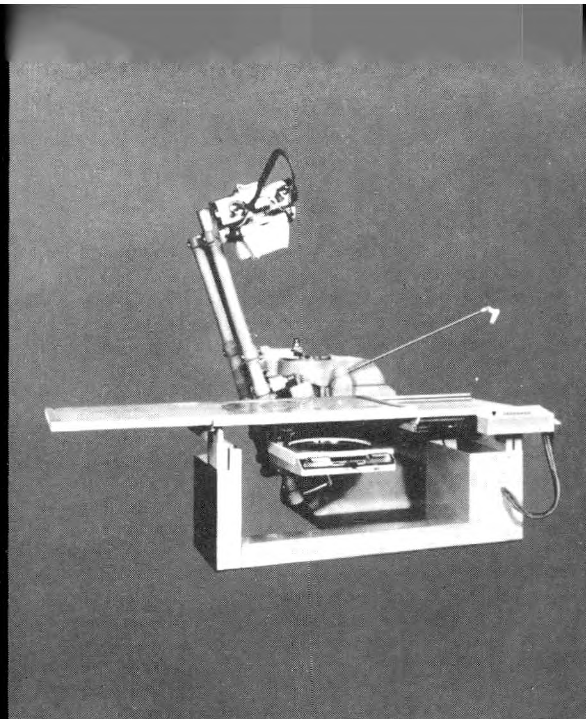

# Both these Norelco tomographic units do anything any other unit will do...

linear,

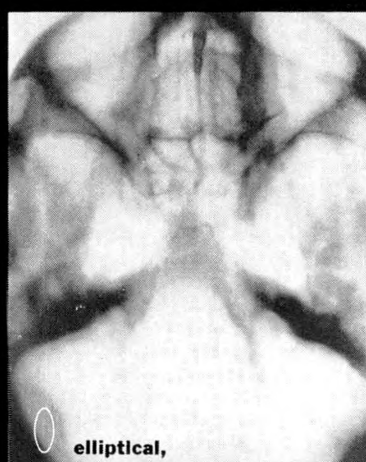

elliptical,

circular,

The clearest tomograms of thinnest possible layers are provided by the trajectory and exceptional length (451cm) of the Norelco Polytomes' hypocycloidal movements.

Of course, linear, elliptical and circular movements, with wide choice of swing angle and orientation, are provided for examinations where conventional movements are preferred. Zonography (small-angle circular tomography), producing cuts of several cm thickness, is also possible at any angle from 0° to 20°.

Focus, tomographic layer and film remain at fixed mutual distances, thereby preserving constant enlargement factors of 1.3, with secondary holder for magnification of 1.6. Removable Grid: 10:1, 110 lines.

## but *only* the Norelco units do this

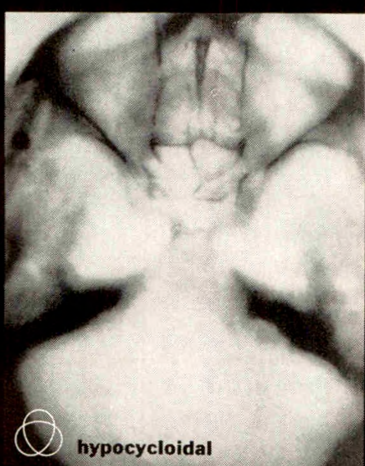


MANUFACTURED FOR NORELCO BY MASSIOT PHILIPS

The Universal Polytome (*above, left*) tilts, permitting tomography in any position from horizontal to vertical. Longitudinal tabletop movement is provided. Conventional Bucky exposures are possible with the Horizontal Polytome (*above, right*), which is equipped with a floating tabletop providing a generous range of longitudinal and transverse travel. Both models are equipped with a lightbeam positioning device, compression band, headclamps, footrest and stool.

Our systems engineers will be pleased to give you detailed information. Write or call North American Philips Company, Inc., Professional Products Division, Medical Department, 100 East 42nd Street, New York, N.Y. 10017. In the Chicago area: 749 Howard Street, Evanston, Illinois.

IN CANADA: PHILIPS ELECTRONIC EQUIPMENT LTD., TORONTO 17, ONTARIO

Norelco®

*Comfortable protection**...

# HALSEY FLEXI-PLY

## *Lead Vinyl Aprons*

***They flex with every body movement because they're made of multiple layers of thin, soft, lead vinyl...***

Broad shoulder and back panels assure optimum weight distribution. Note how the tie straps provide snug, easy fit without any pull on the shoulders.

**Halsey Flexi-Ply Aprons clean easily, and are exceptionally resistant to tearing, cracking, abrasion.**

## HALSEY LEAD-RUBBER APRONS

Available in conventional apron and in coat type; lined or unlined. Conventional type can be had in standard weight (0.5 mm lead equivalent), heavy weight (0.75 mm lead equivalent) and light weight (0.35 mm lead equivalent). Coat type is available in standard and light weights.

These aprons are all 36″ long; extra-long aprons can be supplied on special order.

*Write for complete apron listing or ask your dealer*

**FLEXI-PLY APRONS**

| | |
|---|---|
| **0.5 mm lead equivalent** | |
| Regular (38″ long) | No. 181-A-R |
| Long (42″ long) | No. 181-A-L |
| Extra-long (48″ long) | No. 181-A-XL |
| **0.25 mm lead equivalent** | |
| Regular (38″ long) | No. 180-A-R |
| Long (42″ long) | No. 180-A-L |

HALSEY

HALSEY X-RAY PRODUCTS, INC.
1425-37th STREET, BROOKLYN, N.Y. 11218

# another CINELIX installation

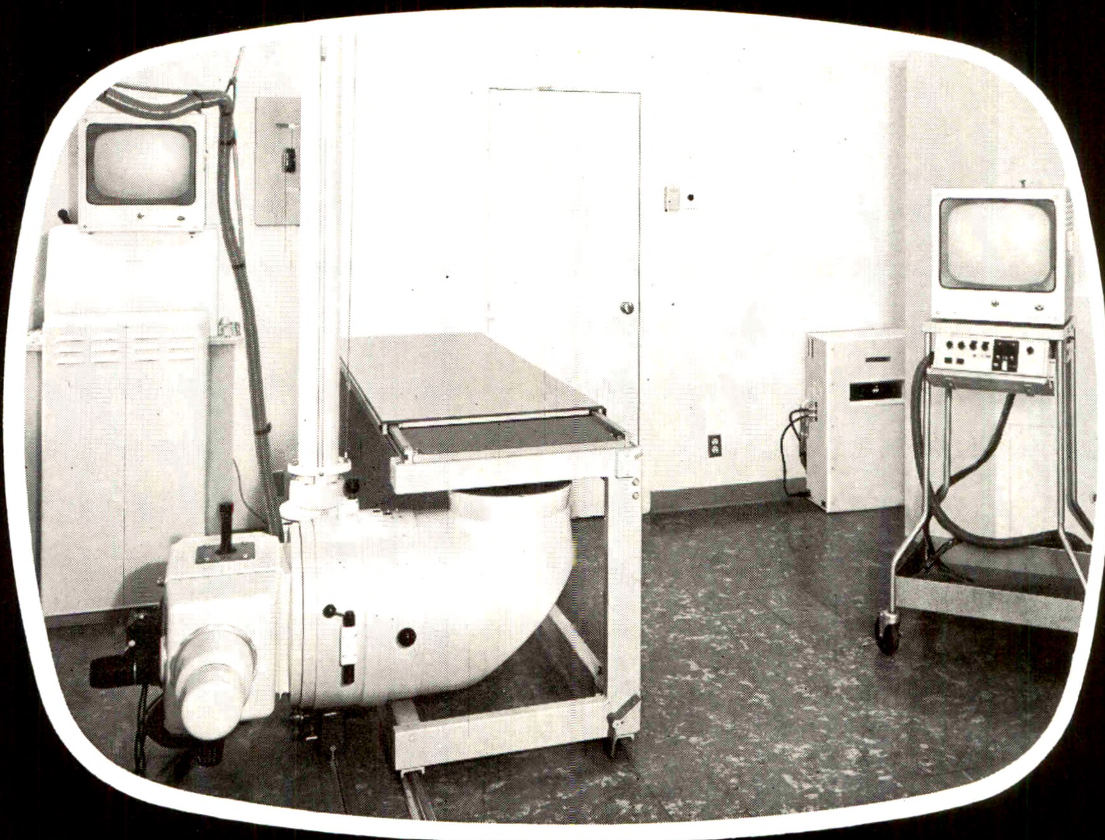

a new concept in image intensification

providing extremely high contrast response and resolution

## CINELIX 12½″

### ELECTRO-OPTICAL IMAGE INTENSIFIER

- Interchangeable screen
- Standard type Image Orthicon Tube
- Inexpensive upkeep guaranteed
- Small light intensifier tube
- Engineered to absorb new developments economically
- Electron-optical magnification and other features

*Accessory equipments available*

Electrocardioscope for superimposing E.K.G. onto the film | 100mm Spot Film Camera

*For more information contact your local X-Ray supply house or:*

AD

MEDICAL MARKETING DIVISION

**AEROJET DELFT**

CORPORATION

Skyline Drive, Engineers Hill, Plainview, L.I., New York 11803

516 OVerbrook 1-2310

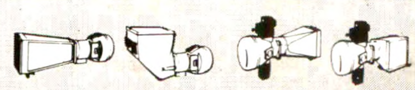

*Odelca P-F Cameras and Accessories*

the ULTIMATE in table design!

# Standard
# ULTIMA-105

HEAVY DUTY
RADIOGRAPHIC-FLUOROSCOPIC

## X-RAY TABLES

FOR THE PATIENT:
the ultimate in comfort

FOR THE RADIOLOGIST: the ultimate in efficiency and convenience... less work and less effort to do it!

**FUNCTIONAL CONVENIENCE:** Maximum accessibility to the table. There's NO FRONT LEG, covered up or exposed, to keep the radiologist away from the table and spot film device. He can work comfortably right up against the inward slope of the table body (just 14 inches away from the center) without back-breaking bending and strain, resulting in more ease and much less effort.

• Choice of manual, semi-automatic or fully automatic Spot Film Device. It is quickly, easily "parked" out of the way, leaving table top free and clear. Movement is smooth and light because of the weight-saving counterbalance method. Low profile of tower and spot film device in "parked" position eliminates interference with shock-proof radiographic cables.

• Table operates on a single fulcrum. Tilts 90° vertical, and full 15° Trandelenburg. Automatic horizontal stop is standard equipment. Provides coast-free tilting from foot switch on base or hand switch on spot device. A retractable step for patient's convenience is standard. Features power driven moving table top (optional).

• Magnetic locks for all movements of the fluoroscopic and spot film staging. Switch control at operator's fingertips or automatic operation by the spot device action.

**FUNCTIONAL EFFICIENCY:** The manually operated multiple plane fluoroscopic collimator is the proven best method of coning in radiography. It is now adapted for fluoroscopy as standard equipment, at no extra cost.

You get the built-in protection of a fluoroscopic collimator, completely enclosed body and automatic bucky slot cover at no extra cost.

**FUNCTIONAL BEAUTY:** a truly handsome table with clean, simple lines that is all new from the ground up. No unnecessary gadgets or decoration to increase cost or decrease function. It is handsome in a dignified way. Smooth surfaces are easy to clean and keep clean. Smart two-tone colors: light sand-tone on the body to emphasize working area; dark hammer-tone on base that continues to look good after years of cleaning, spillage or just plain abuse. This table is the finest exampe of Standard's more than 50 years of experience in the field!

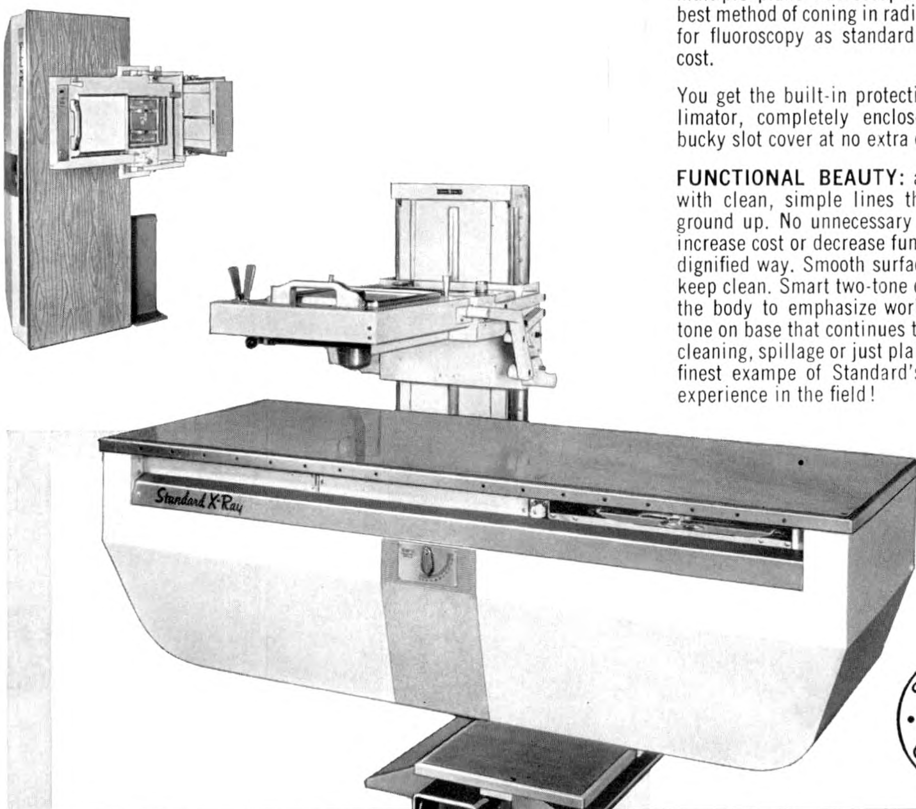


STANDARD X-RAY CO. CHICAGO

• See your "Standard" Dealer or write for Descriptive Literature.

**Standard X-RAY COMPANY**
1932 N. Burling St., Chicago 14, Ill.

## For Greatly Improved Scanning

# TECHNETIUM (Tc 99m)

## Delivered EVERY Monday

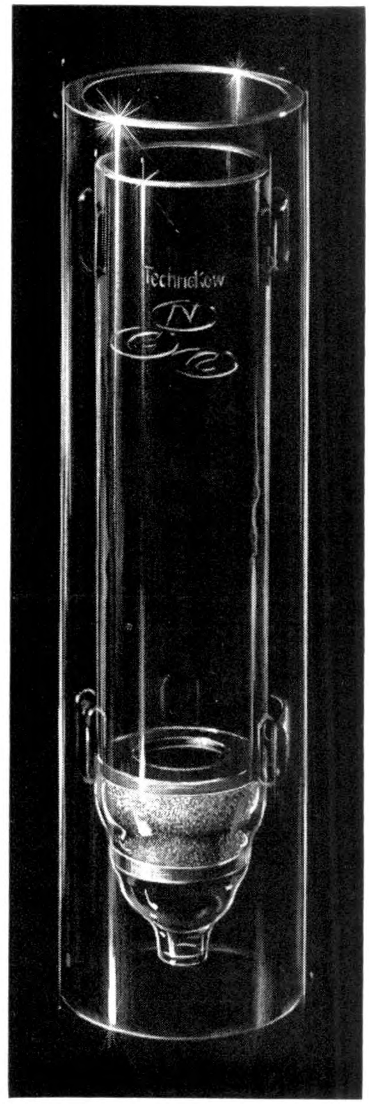

- an ideal scanning agent with easily collimated 140 kev gamma.
- 6 hour half-life minimizes patient exposure.
- permits dosage up to 10 mc, allowing greatly reduced scanning time with any scanner.
- can be administered orally or by intravenous injection.
- delivered EVERY Monday in NCC TecheneKowtm source generator.

*America's First Commercial Supplier of Technetium (Tc 99m)*

**REFERENCES:**

Harper, P.V., Beck, R., Charleston, D., and Lathrop, K.A.: "Optimization of a Scanning Method Using Tc99m." Nucleonics, 22:1, 50-54, January 1964.

Harper, P.V., Lathrop, K.A., and Richards, P.: Tc99m as a Radiocolloid. J. Nuclear Med. 5:5, 382, May 1964.

Smith, E.M.: Radiochemical Purity, Internal Dosimetry and Calibration of Tc99m J. Nuclear Med. 5:5, 383, May 1964.

*Write for complete information today*

NUCLEAR CONSULTANTS CORPORATION
Box 6172, Lambert Field, St. Louis, Missouri 63145

Chicago
Cleveland
Houston
Los Angeles
New York
San Francisco
Washington, D.C.

6502

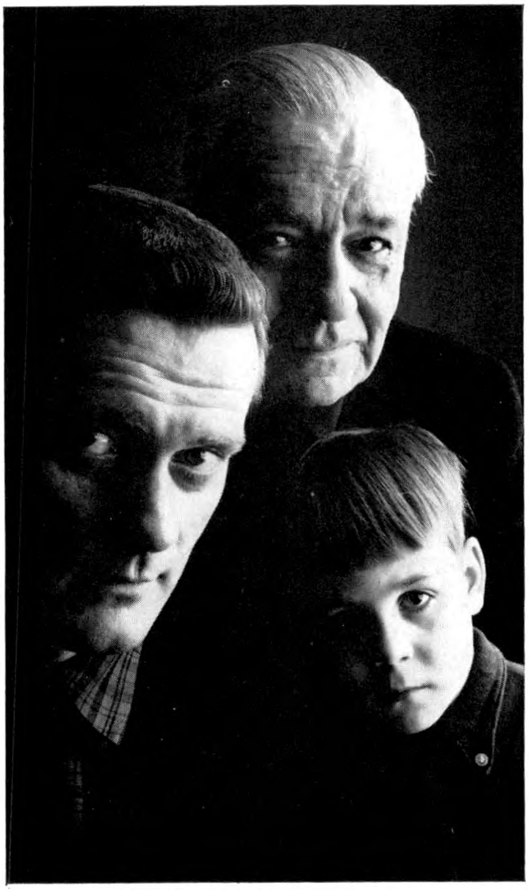

## Is there a stroke in his future?

About 2 million people in this country are incapacitated by cerebrovascular disease. About 190,000 people die each year from this disease—nearly 12% of the total national mortality. With an increasingly aging population, these statistics will undoubtedly get worse —unless something is done about it.

Stroke is a major form of cerebrovascular disease. Is there a stroke in your patient's future? Perhaps. In many individuals one may observe clues and suspect signs which may lead to a diagnosis of such a potential hazard early enough to prevent it by appropriate medical or surgical therapy.

A radio-diagnostic procedure that has become more and more accepted, both for its safety and its precision, is the indirect injection of the carotid and vertebral-basilar arterial system with radiopaque contrast media by means of brachial cannulation or catheterization. Injection of contrast medium is followed by opacification of the carotid and cerebral vascular tree. Lesions that could lead to stroke are thereby highlighted, and the specialist can make suitable recommendations.

Physicians trained in these, and in other new radiologic procedures that have been developed to a fine degree of accuracy and safety, are now able to provide invaluable assistance for the patient with a special problem.

WINTHROP LABORATORIES, New York, N.Y. 10016

Winthrop PIONEERS IN PRODUCTS FOR RADIOLOGIC DIAGNOSIS

# Not every physician is a radiologist...

...and not every patient requires radiologic examination. But we think it is useful to remind physicians in other fields that revolutionary advances in radiologic diagnosis have been made during recent years. Through early diagnosis, and prompt therapy, many lives have been saved that might otherwise have been lost.

Winthrop Laboratories is happy to publish "reminder" advertisements like the above, directed to physicians who are not specialists in radiology. It is our hope that these messages will continue to remind practitioners of the important services a specialist can provide.

WINTHROP LABORATORIES, New York, N.Y. 10016

Winthrop PIONEERS IN PRODUCTS FOR RADIOLOGIC DIAGNOSIS

*ITS NEW FEATURES AND CONVENIENCES HAVE MADE IT A UNIVERSAL SUCCESS!*

# HYDRADJUST*

## UROLOGICAL X-RAY TABLE

NEW features of the HYDRADJUST Table are too numerous to be listed in their entirety but important among them are—

- Wide range elevation—29″ to 57″.
- Extreme 88° upright tilt, particularly useful in voiding studies. (Note small photo below.)
- Disposable sterile drain bag—folds against end of table to give the urologist "elbow room."
- Accommodates image intensification units.
- "Floating" Table Top.

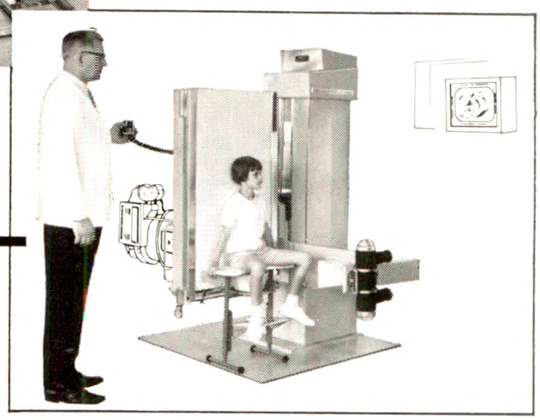

**SEE IT IN ACTION AT VARIOUS UROLOGICAL AND RADIOLOGICAL CONVENTIONS**

***ECONOMY TABLE FOR OFFICE AND CLINIC USE, ETC.***

The Hugh H. Young Tubular-Base Table, with fixed height and manually operated tilt, has long been the table of choice in private offices and small clinics.

**WRITE FOR BROCHURE OR SEE YOUR X-RAY SUPPLIER FOR FURTHER INFORMATION.**

**LIEBEL-FLARSHEIM COMPANY** L-F **CINCINNATI, OHIO 45215**

**DIVISION OF RITTER CORPORATION**

*Trademark, Liebel-Flarsheim Division of Ritter Corporation

# E-Z-EM™ PREPACKAGED

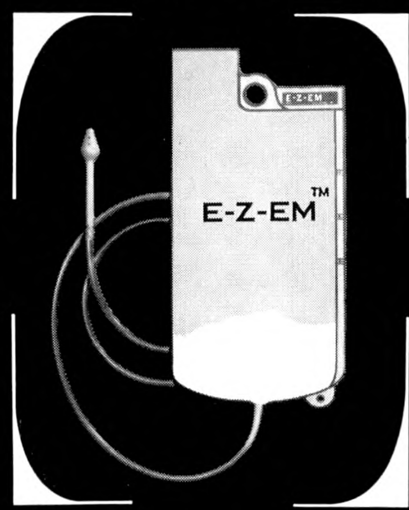


# FOR MAXIMUM CONTROL

**E-Z-EM* Disposable Barium Enema System is prepackaged for Maximum EASE... SPEED... CLEANLINESS... CONSISTENCY.**

**YOUR SPECIFIC TECHNIQUE IS ASSURED AND CONTROLLED**

Standardized and prepackaged based on **your** needs. Instant dispersing colloidal barium **(BARI-EM™)** or any barium formulation you desire.

**IMPROVED DIAGNOSTIC TECHNIQUES AND VERSATILITY**

Sealed system makes possible single stage, double contrast examination. Carbon dioxide may be used for increased patient comfort. (Sealed system can be used as a disposable bedpan for old and arthritic patients precluding problems due to poor sphincter control.)

**MAXIMUM CONVENIENCE**

Retrograde filling system eliminates waste and mess. Completely assembled — just add water and mix in bag.

**ELIMINATES CROSS PATIENT CONTAMINATION**

No danger of faulty sterilization. It's disposable! Entire unit is discarded after each procedure.

**Order today through your local x-ray supply dealer or write for literature and free sample.**

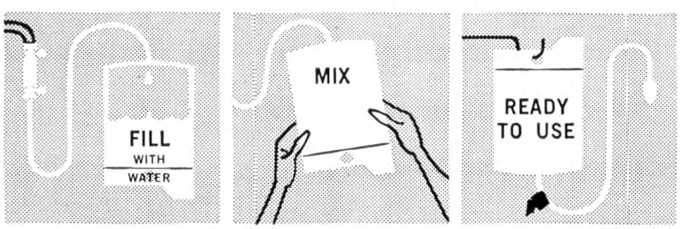


1 Connect to water tap with tubing. Add small amount hot water. Mix. Add water to desired density.

2 Mix thoroughly for about 30 seconds. Disconnect from water tap. Bleed air and water from system.

3 Add air or $CO_2$ if double contrast exam is desired. Clamp tubing with hemostat. Administer enema.

**"THE SYSTEM OF CHOICE"**

# E-Z-EM

32 South Street,
Port Washington, L. I., N. Y..
516 - PO 7-4743

* Patent Pending

1. Meyers, P. H.: J.A.M.A. 173: 1589, August 6, 1960. 2. Nathan, M. H.: Am. J. Roentgenol., Rad. Ther. and Nuclear Med. 81: 650, 1959. 3. Steinbach, H. L., et al.: J.A.M.A. 174: 1207, Oct. 29, 1960 4. Pochaczevsky, R., et al.: Radiology 77: 831, (Nov.) 1961.

**Ask about Sol-O-Pake,™ the pleasant tasting barium formulation for upper GI's.**

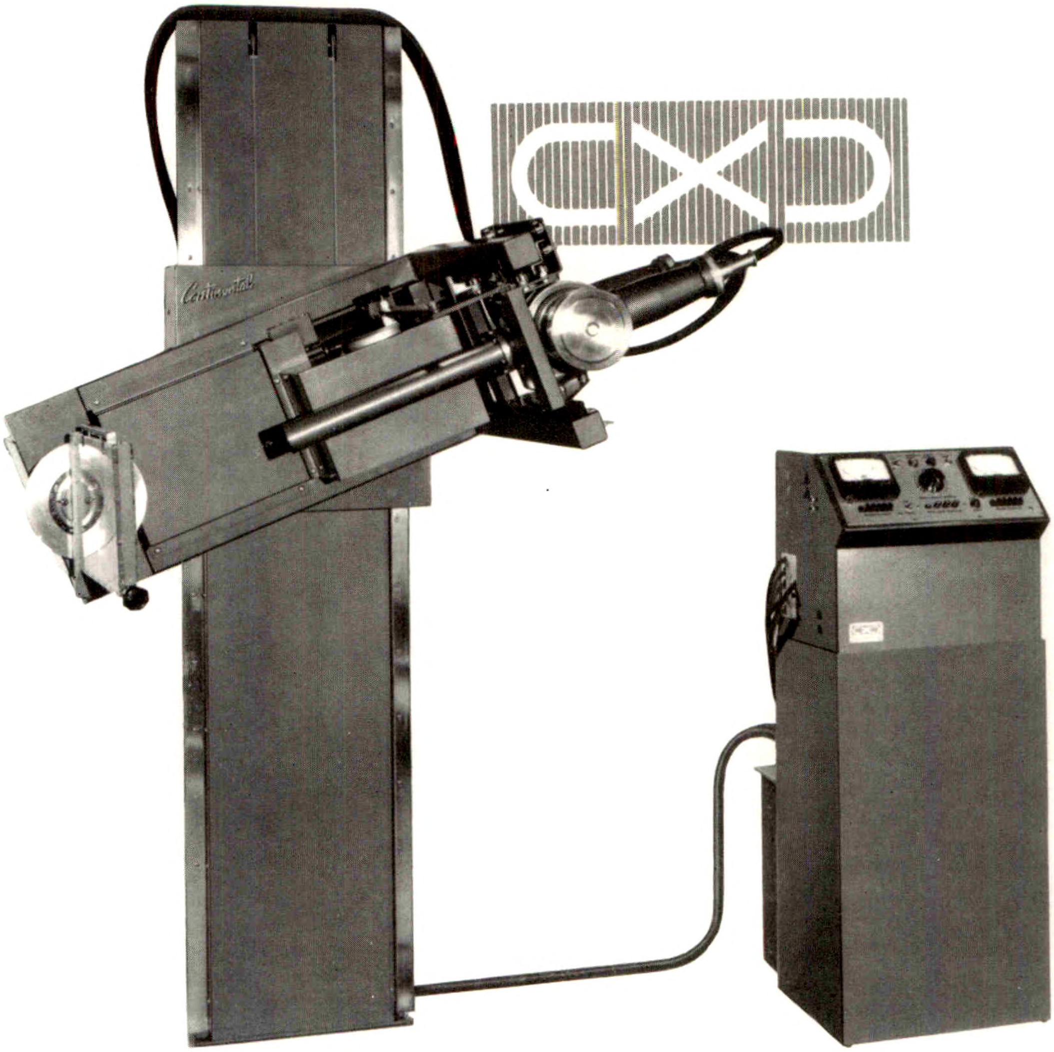

# COMPERE TEMPORAL BONE RADIOGRAPHY

Quality radiographs of the temporal bone are usually very difficult to obtain. The Compere Head Unit permits these desired views to be produced easily because of:

1. Reduced anatomy-to-film spacing.
2. Compact cassette holder that permits positioning close to the head, above the patient's shoulder.
3. Precision, double-collimated Micro-Cones.
4. Fractional focus X-ray tube.
5. Simple, repeatable positioning techniques.

Routine skull and sinus views can also be taken easily.

Completely automatic stereo exposure sequence mechanism simplifies the taking of stereo pairs. These views augment temporal bone radiographic diagnosis, either through stereo viewing or by means of separately viewing the two radiographs taken at different angles.

CONTINENTAL **X-RAY** CORPORATION

1536 NORTH CLYBOURN AVENUE, CHICAGO, ILLINOIS 60610

FOR SUPERIOR X-RAY DIAGNOSIS

# INTROPAQUE

## BARIUM SULFATE, U.S.P. 91%

- ▶ INTROPAQUE deposits a smooth, lasting coating and does not form lumps.
- ▶ INTROPAQUE has optimum density and good adhesive qualities.
- ▶ INTROPAQUE will not dry or flake in the colon for an hour or more.
- ▶ INTROPAQUE has maximum opacity allowing for easy penetration.
- ▶ INTROPAQUE is a non-foaming, stable formula allowing excess suspension to be used another day.
- ▶ INTROPAQUE has a remarkable ability to overcome pylorospasm.

This formula was developed to satisfy multiple criteria for an ideal suspension. We invite you to try a sample and see how it performs for you.

General Electric Company
X-Ray Department
P. O. Box 1472
Lafayette, Indiana

Please send me a free sample of Intropaque

Name____________

Address____________

City______ Zip Code______ State______

Distributed by
General Electric Company
X-Ray Department
Milwaukee, Wisconsin

THE AMERICAN JOURNAL OF ROENTGENOLOGY RADIUM THERAPY AND NUCLEAR MEDICINE

VOL. 94 AUGUST, 1965 No. 4

# DIFFERENTIAL LOCALIZATION OF ISOTOPES IN TUMORS THROUGH THE USE OF INTRA-ARTERIAL HYDROGEN PEROXIDE*

BASIC SCIENCE

*By* JAMES W. FINNEY, M.A., GEORGE A. BALLA, M.D., RICHARD E. COLLIER, M.D., JACK WAKLEY, B.S., HAROLD C. URSCHEL, M.D., *and* JOHN T. MALLAMS, M.D.

DALLAS, TEXAS

ONE of the basic radiobiologic concepts dealing with the lethality of ionizing radiation is concerned with the oxygen concentration in a tissue at the time of its exposure to radiation. It has been shown that the slope of the radiosensitivity curve increases steeply as the oxygen concentration increases above anoxia, and at high oxygen concentration reaches a maximum sensitivity, which is difficult to exceed by increasing the amount of oxygen present. Due to the innate anoxic character of neoplastic tissue and the fact that the greatest increase of radiosensitivity is seen at the lower oxygen levels, the oxygen effect is more pronounced in some tumor tissue than in the corresponding or adjacent normal tissue. Therefore, it is probable that the radiotherapeutic ratio can be favorably influenced by increasing the oxygen in the region of the tumor. Various groups have used hyperbaric oxygen to achieve this result in the treatment of malignant tumors.[2,3] Our group has used intra-arterial hydrogen peroxide in a regional system to achieve the same result.[1,5,7,8,9] It has been noted that by adding hydrogen peroxide to blood or other biologic fluids, these media become "supersaturated" with oxygen and carry several atmospheres equivalent total oxygen content.[6]

Radioisotopes were used by this group early in the study of the physiologic effects of intra-arterial hydrogen peroxide. It has been observed that when certain isotopes were given intra-arterially following the intra-arterial infusion of hydrogen peroxide, the isotope localized preferentially in the area of the malignant tumor in the infused field.[4] These studies were extended and conducted in rats, using the Walker 256 carcinosarcoma; in rabbits, using the VX-2 carcinoma; and in humans having a variety of malignancies. The following is a

* Presented at the Sixty-fifth Annual Meeting of the American Roentgen Ray Society, Minneapolis, Minnesota, September 29–October 2, 1964. From the Charles A. Sammons Research Division, Baylor University Medical Center, Dallas, Texas.

Supported in part by the Abbott Laboratories, the Putman Estate, Fort Worth, Texas, The Moody Foundation, A.C.S. Grant No. T-284, and the U. S. National Institutes of Health Grant No. CA 07127-01.

preliminary report of the results obtained to date.

## ANIMAL EXPERIMENTS

The animal studies were conducted in both rats and rabbits. Fifteen rats received liver implants of Walker 256 carcinosarcoma. Two groups of rabbits were studied using VX-2 carcinoma implants; 10 were implanted in the liver and 36 received bilateral hindlimb implants. In both groups of animals receiving hepatic implants, the aorta was exposed at the level above the renals and below the celiac axis. A PE-50 catheter was introduced through a purse-string suture and passed retrograde to the level of the diaphragm. The animals were infused with 0.24 per cent hydrogen peroxide in Ionosol-T* (5 ml. in the rat and 10 ml. in the rabbit) at the rate of 0.5 to 1.5 ml./minute. The rats were given 5 $\mu$c of radioiodinated human serum albumin, the rabbits were given 15 $\mu$c and the isotope was flushed through with hydrogen peroxide solution (2 ml. of solution was used for the rats and 5 ml. for the rabbits). The control groups were exposed to the same procedure using Ionosol-T without hydrogen peroxide for the infusion. The animals were scanned externally at 24, 48, and 72 hours. They were then sacrificed, the livers were removed and sections were taken from "normal" liver, liver adjacent to tumor, and tumor tissue, and the activity was determined in a well-type counter. The ratio of isotope in the tumor when compared to normal tissue was from 2:1 to 4:1, and the same relative ratio held for both rats and rabbits. Animals receiving Ionosol-T only with $I^{131}$ labeled human serum albumin showed no significant difference in isotope concentration between normal and malignant tissue. The second group of rabbit experiments consisted of 36 animals bearing bilateral hindlimb implants of the VX-2 carcinoma. The tumors were allowed to reach a size of 4 cm. in diameter, at which time the animals were prepared for aseptic surgery. A midline incision was made and the aorta was exposed approximately 5 cm. above the bifurcation of the aorta into the iliacs. A PE-50 catheter was introduced into the aorta through a purse-string suture and passed into the right iliac artery. The limb was infused with 10 ml. of 0.24 per cent hydrogen peroxide in Ionosol-T solution at 0.5 to 1.5 ml./minute followed by 15 $\mu$c of radioiodinated human serum albumin, which was then flushed through with 5 ml. of hydrogen peroxide solution. The catheter was then partially withdrawn and passed into the left iliac artery and the procedure was repeated, using Ionosol-T instead of hydrogen peroxide solution. The catheter was removed, the artery repaired and the animal closed. Alternate animals were infused, with alternate legs being infused first so that the first animal received hydrogen peroxide and iodine first in the right leg, the next animal received carrier solution and iodine first in the left leg. The results obtained from the experiments carried out on this group showed no significant difference with respect to limb infusion sequence. The animals were scanned at 24, 48, 72, 96, and 120 hours following the injection of isotope and hydrogen peroxide solution. Typical scans are shown in Figures 1 and 2. It will be noted that the isotope concentrated primarily in the right limb (the limb which received hydrogen peroxide and isotope). Again the ratio of isotope in the tumor as compared to normal tissue was from 2:1 to 4:1. The ratio of isotope in the tumor of the hydrogen peroxide infused limb compared to the tumor in the control infused limb was from 1.5:1 to 4:1.

It was felt that for a more definitive and quantitative study of increased isotope uptake of malignant tissues under the influence of hydrogen peroxide, a more adequate model system was desirable. For this study the Hela S-3 tissue culture cell line was chosen. The cells were mixed to a final concentration of 2 million cells/ml. in a Hanks balanced salt solution containing 25 units of catalase/ml. Two sets of studies

* Abbott Laboratories.

were conducted, one with $I^{131}$ labeled human serum albumin, the other with [3-(chloromercuri) -2- methoxypropyl] -urea-$Hg^{203}$. Each series consisted of a controlled set with isotope and no hydrogen peroxide and an experimental set to which was added 0.5 per cent hydrogen peroxide in a 1:10 final concentration and isotope. It was found that approximately 70 per cent more $I^{131}$ labeled human serum albumin and 30 per cent more [3-(chloromercuri)-2-methoxypropyl]-urea-$Hg^{203}$ were taken up by the tumor cells under the influence of hydrogen peroxide than the tumor cells with no hydrogen peroxide (control). These are preliminary results from the system using tissue culture cells as the model but seem sufficiently indicative to mention in this publication.

## STUDIES IN HUMANS

The diagnostic potential using this procedure has been explored on a preliminary basis in humans with known malignancies who were being treated with hydrogen peroxide intra-arterially and external irradiation or chemotherapy. To date, 40 patients have been investigated with satis-

Fig. 1. External photoscan of rabbit #360 bearing identical bilateral hindlimb VX-2 carcinomas. The right tumor area was infused intra-arterially with hydrogen peroxide and $I^{131}$ labeled human serum albumin. The left tumor area was infused intra-arterially with carrier solution and isotope. The animal was scanned 24 hours after the infusion. Note the increased isotope uptake in the right tumor area.

Fig. 2. External photoscan of rabbit #340 taken 72 hours after treatment identical with animal #360.

factory results. Figures 3 and 4 are representative of the results obtained. This individual had an adenocarcinoma of the pancreas. Figure 3 is a scan taken following the intra-arterial infusion of 200 cc. of Ionosol-T, 250 $\mu c$ of $I^{131}$ which was flushed through with 50 cc. of Ionosol-T. It will be noted that no localization of isotope occurred. Figure 4 shows the same patient, this time after being infused with 200 cc. of 0.48 per cent hydrogen peroxide in Ionosol-T, 250 $\mu c$ of $I^{131}$ labeled human serum albumin, and flushed through with 50 cc. of the peroxide solution. In this scan the tumor is easily visualized. Further data on this

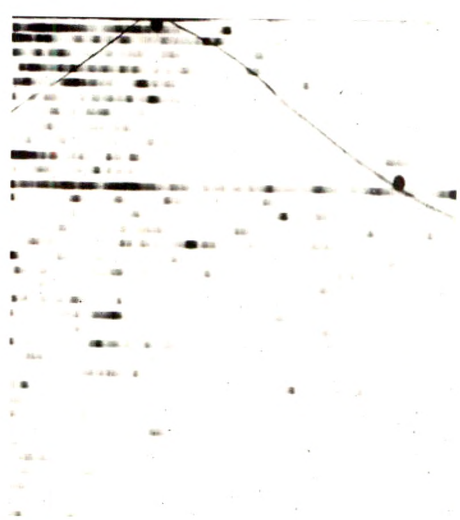

Fig. 3. Photoscan of patient T. T. (carcinoma of the pancreas) taken after the intra-arterial infusion of $I^{131}$ labeled human serum albumin and Ionosol-T. The scan was repeated at 24 hours without change.

Fig. 4. Photoscan of patient T. T. taken 48 hours after the intra-arterial infusion of 0.48 per cent hydrogen peroxide and $I^{131}$ labeled human serum albumin. Note the concentration of the isotope in the pancreas.

technique can be found in the article which follows. The case is used here simply to demonstrate the increased uptake of isotope under the influence of intra-arterial hydrogen peroxide.

In a number of cases, tissue sections have been obtained in 1 to 4 days following the scan procedure and autoradiographs were prepared. The sections were taken from biopsy or surgical specimens. Frozen sections were placed on chrome alum coated slides, stripped with Kodak AR-10 film, placed in a light-tight container and allowed to develop. Figures 5 through 10 are autoradiographs obtained in this fashion. Figures 5 and 6 show sections taken from a primary carcinoma of the breast metastatic to the brain. The patient was scanned using the hydrogen peroxide-[3-(chloromercuri)-2-methoxypropyl]-urea-$Hg^{203}$ procedure as described before and went to surgery the following day, at which time the tissue was obtained for the autoradiographs. As can be seen, there is a heavy concentration of isotope over both the nucleus and cell membranes.

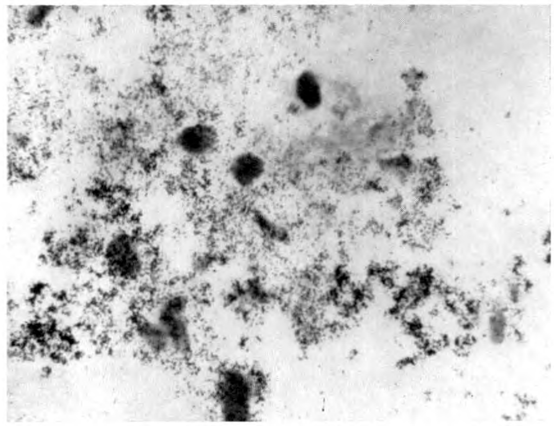

Fig. 5. Autoradiograph of tissue taken from a patient following a brain scan with hydrogen peroxide and [3-(chloromercuri)-2-methoxypropyl]-urea-$Hg^{203}$ for diagnosis and localization of a brain lesion metastatic from a primary carcinoma of the breast.

Figures 7 and 8 are autoradiographs prepared from a glioblastoma multiforme, Grade IV, taken 2 days following a hydrogen peroxide-[3-(chloromercuri)-2-methoxypropyl]-urea-$Hg^{203}$ scan conducted in the above fashion. Again, it will be noted that there is a relatively heavy concentration of isotope in the area of the nucleus and cell membrane. Figures 9 and 10 are autoradiographs prepared from tissue obtained from a patient with an invasive

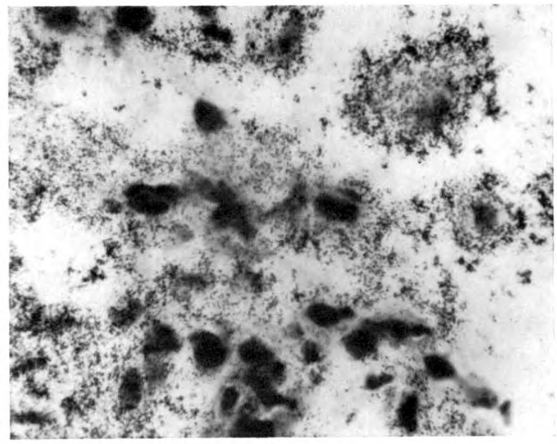

Fig. 6. Another field of the same tissue as shown in Figure 5.

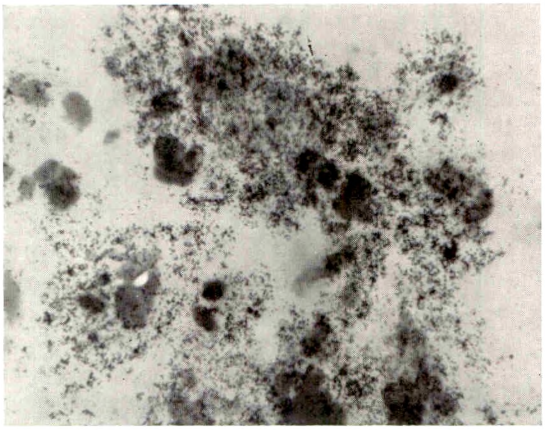

Fig. 7. Autoradiograph prepared from a glioblastoma multiforme, Grade IV, taken 2 days following a hydrogen peroxide-[3-(chloromercuri)-2-methoxypropyl]-urea $Hg^{203}$ scan.

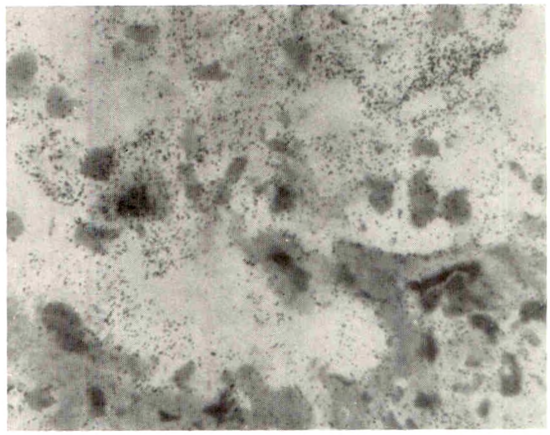

Fig. 9. Autoradiograph prepared from tissue obtained from a patient with an invasive squamous cell carcinoma of the cervix 1 day following a hydrogen peroxide-$I^{131}$ labeled human serum albumin scan. Very little isotope is associated with the fibrous tissue.

squamous cell carcinoma of the cervix 1 day following a hydrogen peroxide-$I^{131}$ labeled human serum albumin scan conducted as previously mentioned. It will be noted in these figures that the concentration of the isotope in the tumor area is characterized by predominant concentration in the area of the cell wall and very little concentration of isotope in the area over the nucleus. In Figure 9 it will be noted that very little isotope is associated with the fibrous tissue in this photomicrograph.

Autoradiographs prepared from the Hela cell isotope experiment demonstrate quite a similar phenomenon relative to the distribution of the $I^{131}$ labeled human serum albumin and the [3-(chloromercuri)-2-methoxypropyl]-urea-$Hg^{203}$. It is of interest to note that the cells in the heavy isotope concentrated area are in various stages of degeneration.

The mechanisms for the isotope localization are still for the most part matters of speculation. Studies are in progress to define more clearly the physiology and biochemistry involved.

## SUMMARY

It has been shown that both $I^{131}$ labeled

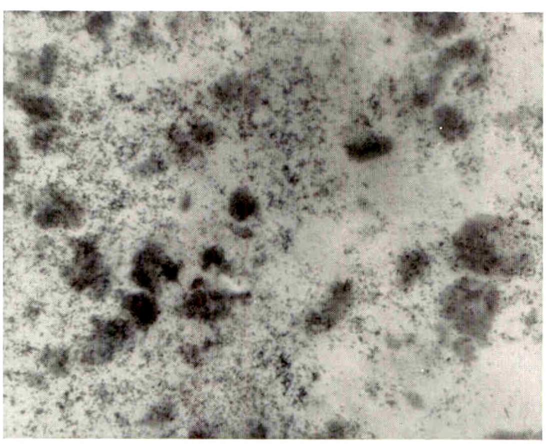

Fig. 8. Another view of the same tissue as shown in Figure 7.

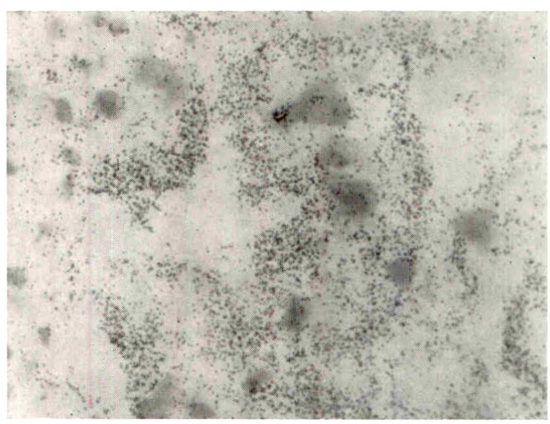

Fig. 10. Another field of the same tissue as shown in Figure 9.

human serum albumin and [3-(chloromercuri)-2-methoxypropyl]-urea-$Hg^{203}$ will localize preferentially in the area of malignant tumor tissue when given intra-arterially during the intra-arterial infusion of dilute hydrogen peroxide in either tumor bearing animals or human beings. Autoradiographic data indicate the intracellular geographic distribution of the isotope. It is our opinion at this time that much further investigation is necessary, but that there is potential applicability in both diagnosis and treatment of malignant tumors.

James W. Finney
Charles A. Sammons Research Division
Baylor University Medical Center
Dallas, Texas

The authors acknowledge the assistance and advice of Dr. J. E. Miller, Radiology Department; Dr. D. F. Rowan, Microbiology Department; Dr. G. J. Race, Pathology Department; Mr. E. Lambert, Mrs. E. McCormick, Mr. B. Jay, Mr. H. Pingree, Miss G. Davis, Mrs. J. Copeland, Mrs. N. Petty, Mrs. M. Bratton, and Miss M. Schneider.

REFERENCES

1. Balla, G. A., Finney, J. W., and Mallams, J. T. Method for selective tissue oxygenation utilizing regional intra-arterial infusion technics. *Am. Surgeon*, 1963, *29*, 496–498.
2. Churchill-Davidson, I. Oxygen effect in radiotherapy. *Cancer Prog.*, 1960, 164–179.
3. Churchill-Davidson, I., Sanger, C., and Thomlinson, R. H. High-pressure oxygen and radiotherapy. *Lancet*, 1955, *1*, 1091–1095.
4. Finney, J. W., Collier, R. E., Balla, G. A., Tomme, J. W., Wakley, J., Race, G. J., Urschel, H. C., D'Errico, A. D., and Mallams, J. T. Preferential localization of radioisotopes in malignant tissue by regional oxygenation. *Nature*, 1964, *202*, 1172–1175.
5. Finney, J. W., Balla, G. A., and Mallams, J. T. Method for achieving increased available oxygen through regional intra-arterial infusion. *Proc. Am. A. Cancer Res.*, 1959–1962, *3*, 318.
6. Jay, B. E., Finney, J. W., Balla, G. A., and Mallams, J. T. Supersaturation of biologic fluids with oxygen by decomposition of hydrogen peroxide. *Texas Rep. Biol. & Med.*, 1964, *22*, 106–109.
7. Mallams, J. T., Balla, G. A., Finney, J. W., and Aronoff, B. L. Regional oxygenation and irradiation: head and neck. *A.M.A. Arch. Otolaryng.*, 1964, *79*, 155–159.
8. Mallams, J. T., Finney, J. W., and Balla, G. A. Use of hydrogen peroxide as source of oxygen in regional intra-arterial infusion system. *South. M. J.*, 1962, *55*, 230–232.
9. Mallams, J. T., Balla, G. A., and Finney, J. W. Regional intra-arterial hydrogen peroxide infusion and irradiation in treatment of head and neck malignancies: progress report. *Tr. Am. Acad. Ophth.*, 1963, *67*, 546–553.

# DIFFERENTIAL LOCALIZATION OF ISOTOPES IN TUMORS THROUGH THE USE OF INTRA-ARTERIAL HYDROGEN PEROXIDE*

## CLINICAL EVALUATION

*By* R. E. COLLIER, M.D., G. A. BALLA, M.D., J. W. FINNEY, M.A., A. D. D'ERRICO, M.D., J. W. TOMME, M.D., J. E. MILLER, M.D., *and* J. T. MALLAMS, M.D.
DALLAS, TEXAS

THE use of increased oxygenization to enhance the effect of radiation therapy has been well established. This has been done either by use of a hyperbaric oxygen chamber or with the intra-arterial infusion of hydrogen peroxide with a resulting supersaturation of the tissues and the achievement of several atmospheres equivalent total oxygen content in the blood and other biologic fluids.[6] This latter technique has been used by us for enhancement of radiation therapy in the treatment of malignant disease.[3–5] During the biologic studies involved in this work, it became apparent that certain isotopes when given intra-arterially after the intra-arterial infusion of hydrogen peroxide would locate preferentially in the malignant tumor being infused.[4] This is discussed in the preceding article. The present part deals with the clinical application of the hyperoxygenization intra-arterial isotope technique.

In the past, the localization of tumor has been limited to uptake of radioactive iodine in thyroid carcinoma, by concentration of a radioactive isotope in brain tumors or by a "cold" area in an organ outline obtained by using an appropriate isotope.

The technique to be described here represents a departure from the scan with inference of tumor by detection of cold spot. Instead, the tumor is caused to concentrate the isotope and becomes a "hot" spot, as is seen in the uptake of radioactive iodine by thyroid carcinoma or the detection of brain neoplasms by using mercury 203.

We think the uptake in the tumor is caused by an altered cell permeability secondary to supersaturation with oxygen of the blood supplying the area. This latter is achieved by the intra-arterial infusion of hydrogen peroxide through a catheter that has been properly positioned to bathe the area with the super-oxygenated blood.

The technique of placement of the intra-arterial catheter for hydrogen peroxide infusion has been described by Balla *et al.*[1,2] The catheter is inserted either surgically or through a percutaneous puncture using a Cournard needle. The catheter is placed in the abdominal aorta via the femoral artery with the tip in the mid-thoracic aorta for abdominal and pelvic scans. For head and neck scans the catheter is inserted in the common carotid artery; 250 cc. of a concentration of either 0.24 or 0.48 hydrogen peroxide in Ionosol-T* is infused in about 30 to 45 minutes. During the last 50 cc., 100 $\mu c$ of radioiodinated human serum albumin is injected directly into the infusion tubing, and then flushed in with the remaining hydrogen peroxide Ionosol-T solution. Concentration of radioactive iodine in the thyroid is blocked by the use of Lugol's solution the day prior and for 2 to

* Abbott Laboratories. Sterile, pyrogen-free electrolyte replacement solution containing dextrose, sodium chloride, sodium lactate anhydrous monosodium phosphate, potassium chloride and sodium bisulfite in water.

* Presented at the Sixty-fifth Annual Meeting of the American Roentgen Ray Society, Minneapolis, Minnesota, September 29–October 2, 1964.
From the Division of Cancer Research, Charles A. Sammons Department of Radiation Therapy and Nuclear Medicine, Baylor University Medical Center, Dallas, Texas, and supported in part by the Abbott Laboratories, the Putman Estate, Fort Worth, Texas, The Moody Foundation, A.C.S. Grant No. T-284 and U. S. National Institutes of Health Grant No. CA 07127-01.

Table I

LESIONS STUDIED

| | |
|---|---|
| Squamous cell carcinoma of cervix | 8 |
| Metastatic adenocarcinoma of colon | 5 |
| Undifferentiated adenocarcinoma of stomach | 1 |
| Squamous cell carcinoma of pharynx, hard palate, antrum | 4 |
| Papillary follicular carcinoma of thyroid | 1 |
| Pulmonary metastasis, adenocarcinoma | 1 |
| Adenocarcinoma of pancreas | 4 |
| Adrenal cortical carcinoma | 1 |
| Transitional cell carcinoma of bladder | 2 |
| Liposarcoma | 2 |
| Carcinoma of ureter | 1 |
| Diffuse abdominal carcinomatosis, probable origin in ovary | 2 |
| Leiomyosarcoma of uterus | 1 |
| Fibrosarcoma | 1 |
| Rhabdomyosarcoma | 1 |
| Hepatoma | 1 |

3 days after infusion. Patients have been scanned at 24, 48 and 72 hours.

Various types of tumors have been scanned (Table I). These range from adenocarcinoma of the gastrointestinal tract, squamous cell carcinoma of the cervix to soft tissue sarcomas. Table II is a summary of the results. All cases were proven pathologically. In most cases the extent of the tumor had been determined previously by surgical exploration before the scans were made. A total of 37 cases has been scanned. There have been 3 negative scans, 3 questionably positive scans and 1 scan which was apparently false-positive for metastatic tumor in the pelvis but was positive for primary rhabdomyosarcoma in the thigh. There has been a total of 31 positive scans including this latter case.

Table II

SUMMARY OF SCANNING RESULTS

| | |
|---|---|
| Positive | 30 |
| Questionably Positive | 3 |
| 2—pancreas | |
| 1—antrum | |
| Negative | 3 |
| 1—thyroid | |
| 2—pulmonary metastasis | |
| False Positive | 1 |
| Rhabdomyosarcoma; pelvic lymph nodes negative at surgery but scan interpreted as positive. Primary lesion in thigh was positive on scan | |

The negative scans were cases of a metastatic carcinoma of the thyroid, pulmonary metastasis from an adenocarcinoma and 1 case with a pleural effusion due to adenocarcinoma. The pathologist thought that its origin might have been the ovary but a pelvic scan was completely negative. Clinically, there was nothing palpable in the pelvis. The patient with the negative scan and recurrent carcinoma of the thyroid had tumor in the right lower cervical chain and supraclavicular lymph nodes. This carcinoma of the thyroid had been treated by several surgical procedures and multiple doses of radioactive iodine and radiation therapy and at the time the patient was scanned there was no longer concentration of radioactive iodine in the tumor. The localization of the catheter was checked with fluorescein, but only a poor fluorescence was obtained and it was thought that the failure of the isotope localization in this instance was due to inadequacy of the blood supply to the tumor with the resulting inability to get the super-oxygenated blood and isotope into the area. We have been unsuccessful in demonstrating uptake in pulmonary lesions. The catheters have been placed in the thoracic aorta and presumably there has been not enough blood supply to the area from the bronchial arteries to get sufficient oxygenization and isotope concentration.

The questionable positive cases were an adenocarcinoma of the pancreas, a diffuse adenocarcinoma of the abdomen with the primary site in the ovary and a squamous cell carcinoma of the maxillary antrum. These cases were called questionably positive because they were not as clear-cut as some of the other cases. It was felt that there was some concentration of the isotope in the tumors involved but the complete dense outline that is generally seen was not present.

Fig. 1. Recurrent squamous cell carcinoma of the cervix.

Fig. 2. Radioactive rose bengal liver scan of a metastatic carcinoma of the colon.

## MATERIAL

Figure 1 is a typical example of a good tumor outline or localization. This patient had a recurrent carcinoma of the cervix following previous treatment with radiation. The tumor concentration is apparent in the midportion of the pelvis suprapubicly. This was not the urinary bladder or radioactive urine as a urine specimen was checked after the scanning procedure and was found to be nonradioactive. In addition, the patient was rescanned after voiding and the configuration and localization of the activity was the same.

Figure 2 is a typical radioactive iodine rose bengal scan of a patient with metastatic carcinoma of the colon involving the liver. A large "cold" area involving the inferior margin of the liver was noted. This was palpable clinically and extended to the umbilicus. Figure 3 is the intra-arterial hydrogen peroxide and radioiodinated human serum albumin scan showing concentration of the isotope in the metastasis; the extent and localization of the metastatic lesion are readily visualized.

Figure 4*A* shows concentration of the isotope in a leiomyosarcoma of the uterus at 48 hours after infusion of hydrogen peroxide and isotope. Figure 4*B* shows the same patient scanned 6 days later with persistent tumor concentration and localization of the isotope.

Figure 5*A* is a scan of a patient with a liposarcoma involving the thigh. Figure 5*B* was made at 7 days and still shows good outline of the tumor. This patient had a benign lipoma inferior to the liposarcoma and there was no evidence of uptake over

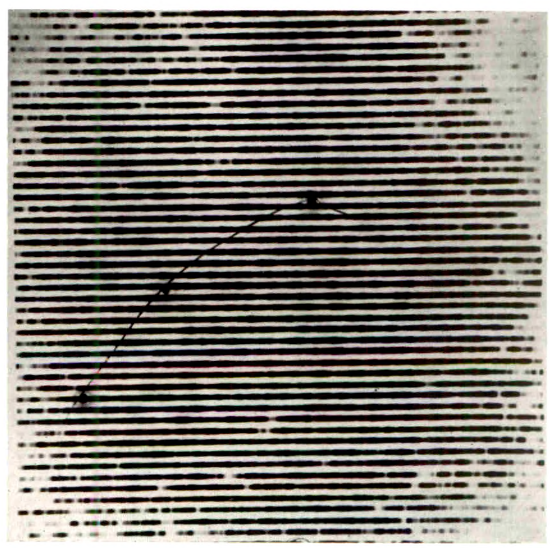

Fig. 3. Scan of same patient as in Figure 2 using hydrogen peroxide radioiodinated human serum albumin.

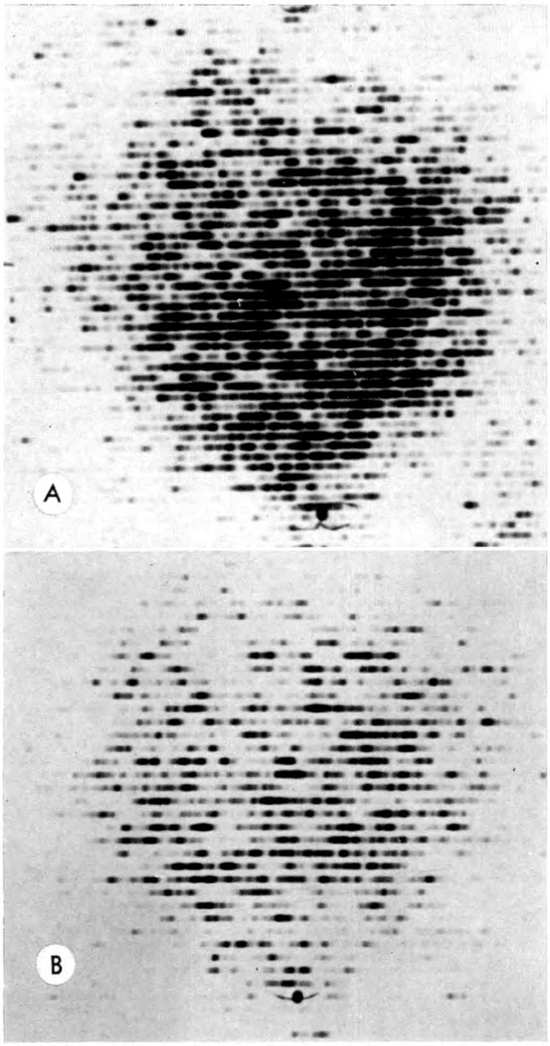


Fig. 4. (*A*) Leiomyosarcoma of the uterus. (*B*) Same patient 6 days later, persistent tumor concentration of isotope.

this lesion. This was the only benign tumor we have been able to study.

Figure 6*A* shows a patient with a recurrent carcinoma of the cervix. The tumor can be seen in the pelvis but the radioactivity above the umbilicus is quite heavy and may represent tumor localization also. However, at 48 hours (Fig. 6*B*) this is beginning to diminish while the pelvic tumor remains the same and is more easily visible.

Figure 7*A* is a 24 hour scan of a patient with recurrent carcinoma of the cervix. The amount of radioactivity in the upper abdomen could be due to metastatic lymph nodes. Figure 7*B* is a scan at 72 hours and there is beginning decrease of the radioactivity in the upper abdomen. By 96 hours (Fig. 7*C*) the differential is sufficient to rule out upper abdominal tumor while the pelvic lesion is still visible. Figure 8*A* shows a carcinoma of the pancreas at 24 hours; Figure 8*B* at 60 hours. The latter shows scanty but definite uptake in the tumor while the liver and other tissues are washed out and are no longer visible. The scans of the upper abdomen have shown enough background activity that unless an area persists on the late scan it should not be considered positive. Scans have also shown outlines of multiple areas of involvement. Figure 9 shows a patient with a recurrent fibrosarcoma of the thigh. The primary tumor itself is well-outlined but in addition metastatic lymph nodes along the iliac chain are seen. These were not palpable or suspected

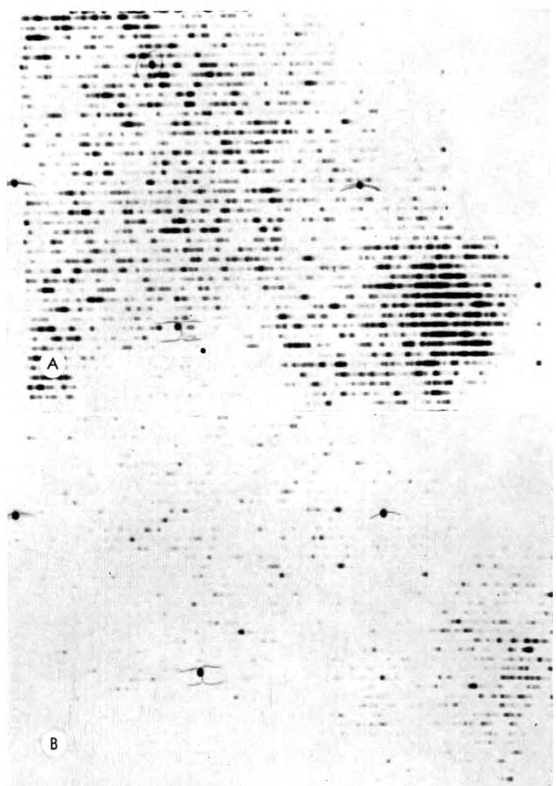


Fig. 5. (*A*) Liposarcoma of thigh. (*B*) Same patient 7 days later showing persistent outline of tumor.

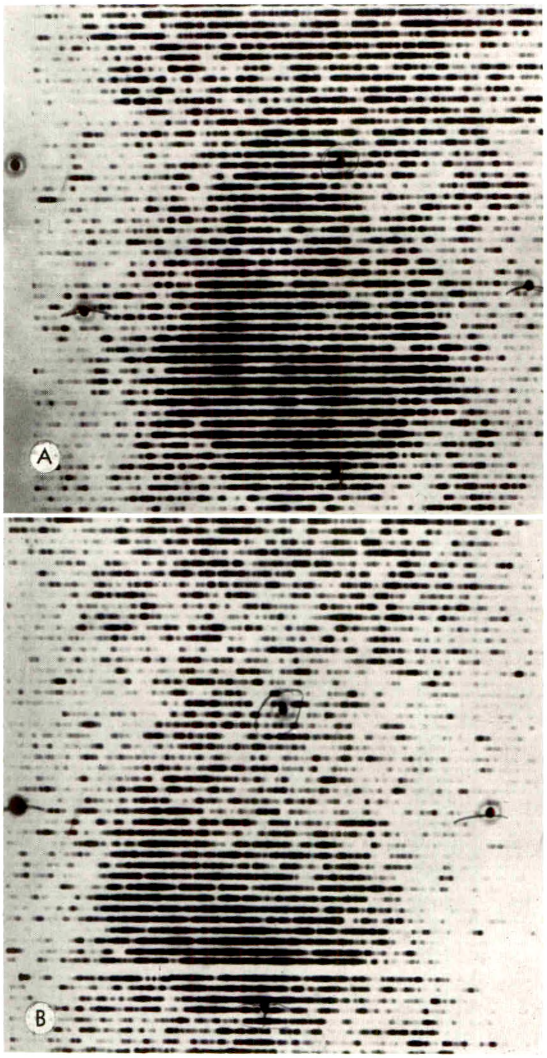

Fig. 6. (*A*) Recurrent carcinoma of the cervix, question of localization in tumor above umbilicus. (*B*) Only pelvic tumor seen; area above umbilicus is not neoplasm.

clinically and the patient's subsequent therapy could be better planned in view of the scan.

Figure 10 shows a recurrent extensive carcinoma of the bladder. A collection of radioactivity in the lower left corner of the scan is due to some leakage of the isotope around the injection site. This can occur especially if the injection is done percutaneously. However, the area of concentration on the right corresponds to bone metastasis involving the ischial tuberosity as was seen on the pelvic roentgenogram.

Figure 11*A* is a scan of the pelvis and lower abdomen in a patient with extensive carcinoma of the ovary. She had completed a course of combined radiation therapy and chemotherapy. Pretreatment scans were not made. Following the scanning procedure, the patient was re-explored with the hope of resection but was still found to be inoperable. A specimen for biopsy was removed from the omentum and the scan of the removed tissue (Fig. 11*A*, insert) shows concentration of the isotope in the tumor area. A subsequent scan 4 months later (Fig. 11*B*) shows persistence of the pelvic carcinoma with extension to the right paracolic gutter. In addition, tumor can be seen just inferior to the umbilicus.

Figure 12 is a scan superimposed on the roentgenogram of a patient with recurrent carcinoma of the cervix. The patient had been explored and clips were placed around the lesion to outline it. The localization of radioactivity on the scan correlates quite well with the findings on the roentgenogram. Figure 13*A* is a scan of a rhabdomyosarcoma of the thigh. Although the localization is spotty, the scan is positive. Figure 13*B* shows the pelvic scan at 48 hours. We interpreted this as a positive scan showing tumor in lymph nodes since the spotty uptake simulated the appearance in the tumor. This patient was explored and multiple pelvic lymph nodes were removed. These, however, showed only reactive hyperplasia. Unfortunately, the tissue was fixed before we could obtain radioautographs to determine if localization of the radioactivity of the isotope in these lymph nodes was actually present. This was the one false-positive scan mentioned earlier.

## DISCUSSION

The main prerequisite for tumor concentration is an adequate blood supply as demonstrated by the one true negative scan of the thyroid carcinoma, the blood supply of which had been compromised by previous therapeutic procedures. The more vascular tumor will obviously concentrate

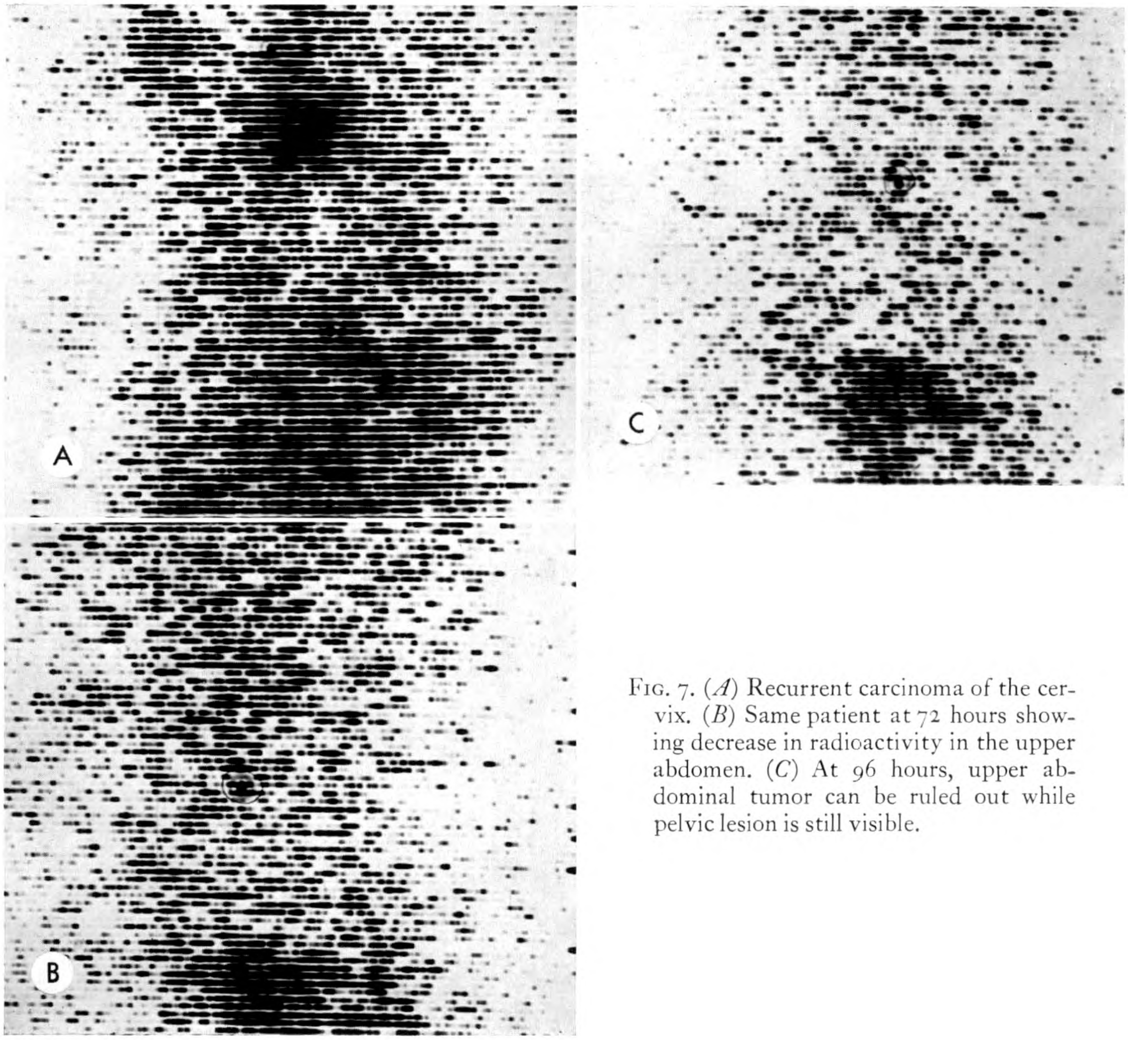

Fig. 7. (*A*) Recurrent carcinoma of the cervix. (*B*) Same patient at 72 hours showing decrease in radioactivity in the upper abdomen. (*C*) At 96 hours, upper abdominal tumor can be ruled out while pelvic lesion is still visible.

the isotope better while the less vascular ones may show a spotty uptake, as is seen in Figure 13*A*.

We have found that 48 to 72 hours is the best time for scanning. After 72 hours there is usually re-entry of the isotope into the general circulation. However, as shown in Figures 4*B* and 5*B*, persistent concentration in tumor does occur. Since the time of scanning is not critical, scans in multiple projections can be made to better demonstrate the extent of the malignant tumor.

By doing 48 hour and 72 hour scans, we have been able to differentiate tumor concentration from radioactivity due to circulating isotope. Since the isotope remains in the tumor for at least 72 hours, the tumor remains visible on the scans while the circulating isotope is diminished, thus the outline of the tumor is more easily seen. This is demonstrated in Figures 6, *A* and *B*; 7, *A*, *B* and *C*; and 8, *A* and *B*.

In general, all cases discussed represent extensive recurrent or extensive primary malignant neoplasm. However, the technique of oxygen enhanced isotope tumor localization is applicable to the early cancer patient. It is possible to accurately outline the extent of a malignant neoplasm and to detect the presence of clinically unsuspected metastasis. The subsequent therapy can then be more correctly prescribed. This is demonstrated by the case in Figure 9. The presence of pelvic metastases

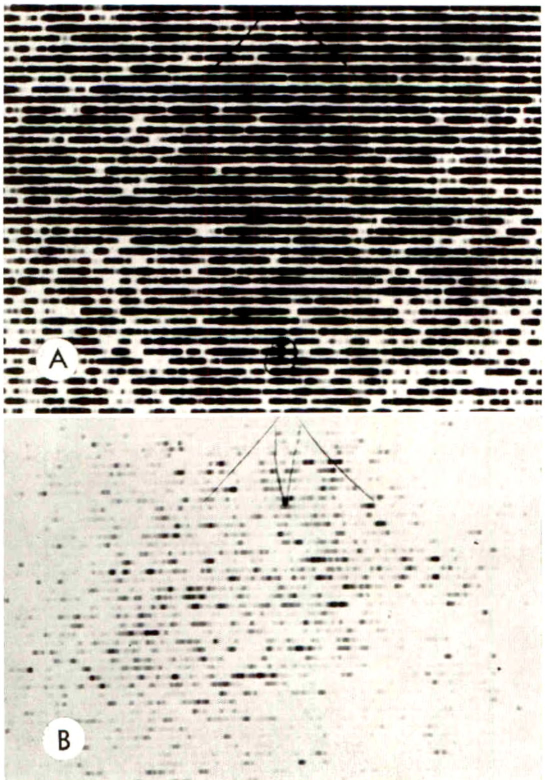


FIG. 8. (*A*) Carcinoma of the pancreas at 24 hours. (*B*) Scan at 60 hours showing residual concentration in tumor.

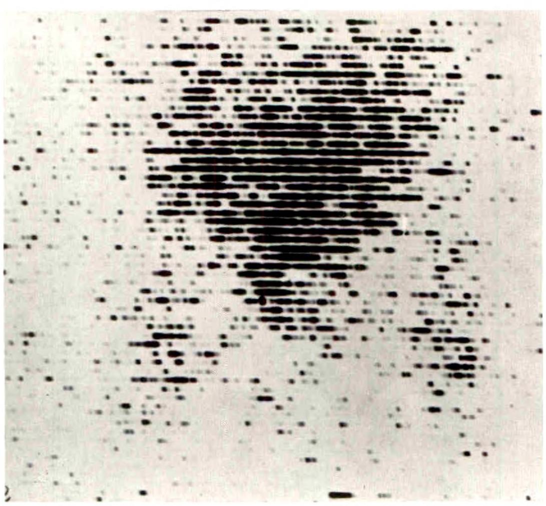

FIG. 10. Extensive recurrent carcinoma of the bladder with metastasis in the right ischium.

FIG. 9. Recurrent fibrosarcoma of the thigh with metastasis in the left iliac lymph node chain.


FIG. 11. (*A*) Extensive carcinoma of the ovary. Insert. Scan of a biopsy specimen removed after *A* was made. (*B*) Four months later showing persistence of pelvic carcinoma with extension to right paracolic gutter.

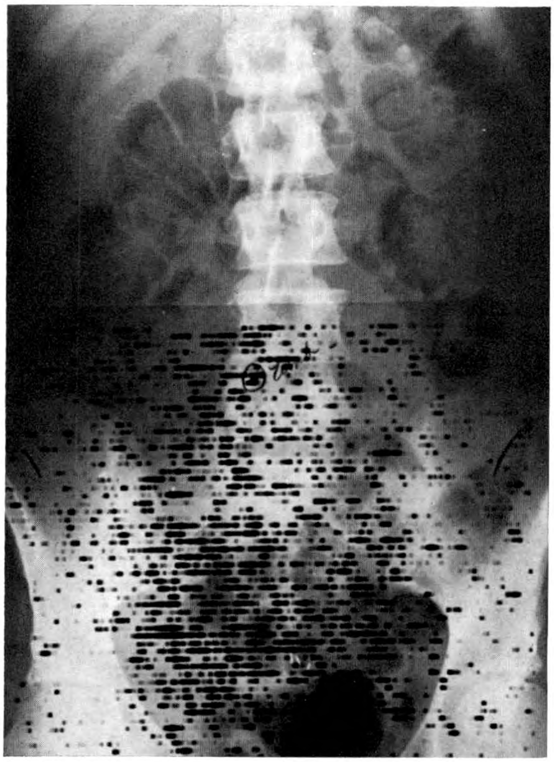

Fig. 12. Recurrent carcinoma of the cervix. The clips outline the lesion surgically.

was unsuspected and their demonstration on the scan spared the patient an inadequate surgical procedure which had been planned previously. The one benign tumor scanned, a lipoma, did not concentrate the isotope while the adjacent liposarcoma did (Fig. 5, *A* and *B*). We have not scanned any other benign tumors but, if this differentiation persists, the technique will be an extremely useful diagnostic method, especially in the area of ovarian tumors where the present means of diagnosis are poor.

We have also been successful in utilizing this technique in the localization of brain tumors. Since the timing of the scan is not critical and the radiation dose to the body, especially to the kidneys, is quite small as compared to the mercury compounds, this technique may be exceedingly useful.

The technique also opens up an avenue of studying cellular metabolism. Labeled compounds can be deposited in the cell and then their subsequent metabolic pathway and fate can be studied. This might be applicable especially in the study of labeled chemotherapeutic agents.

This technique of oxygen potentiation of isotope tumor concentration also has therapeutic possibilities. Due to the differential concentration of the isotope in the tumor, it should be possible to deliver enough radiation to the tumor to destroy it as one does thyroid cancer with radioactive iodine. Various isotopes and isotope labeled compounds are now being considered for this by our group and a pilot study is being outlined.

## SUMMARY

1. A new technique of tumor localization with intra-arterial injection of hydrogen

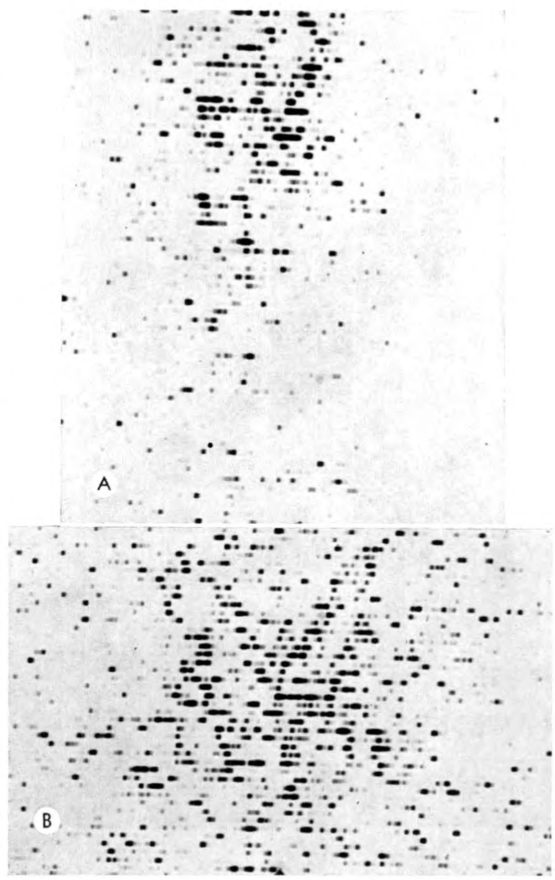



Fig. 13. (*A*) Rhabdomyosarcoma of thigh. (*B*) Pelvic scan interpreted as positive but lymph nodes were negative at surgical exploration.

peroxide and radioiodinated serum albumin has been described.

2. The time of the scan is not critical. The best tumor outline is obtained at 48 and 72 hours.

3. Thirty-seven cases have been scanned as a pilot study. There were 30 positive scans, 3 questionably positive scans, 3 negative scans and 1 false-positive scan.

4. Various pathologic types of tumors have been demonstrated including sarcomas, adenocarcinomas and squamous cell carcinomas. There does not seem to be any specificity as regard to cell type and the ability to concentrate the isotope in the tumor with the technique described.

5. The technique is of value in outlining tumor size and extent of involvement so that proper therapy can be planned.

6. It can be used to follow the results of therapy such as radiation or chemotherapy.

7. The possibilities of the application of the technique in the treatment of malignant tumors and the study of the cellular metabolism have been considered.

R. E. Collier, M.D.
Charles A. Sammons Research Division
Baylor University Medical Center
Dallas, Texas

REFERENCES

1. Balla, G. A., Finney, J. W., Aronoff, B. L., Byrd, D. L., Mallams, J. T., and Davis, G. Use of intra-arterial hydrogen peroxide to promote wound healing. I. Regional intra-arterial therapy: technical surgical aspects. *Am. J. Surg.*, 1964, *108*, 621–624.
2. Balla, G. A., Finney, J. W., Mallams, J. T., Aronoff, B. L., Byrd, D. L., and Davis, G. Use of intra-arterial hydrogen peroxide to promote wound healing. II. Wound healing: clinical. *Am. J. Surg.*, 1964, *108*, 625–629.
3. Balla, G. A., Finney, J. W., and Mallams, J. T. Method for selective tissue oxygenation utilizing continuous regional intra-arterial infusion technics. *Am. Surgeon*, 1963, *29*, 496–498.
4. Finney, J. W., Collier, R. E., Balla, G. A., Tomme, J. W., Wakley, J., Race, G. J., Urschel, H. C., D'Errico, A. D., and Mallams, J. T. Preferential localization of radioisotopes in malignant tissue by regional oxygenation. *Nature*, 1964, *202*, 1172–1173.
5. Finney, J. W., Balla, G. A., and Mallams, J. T. Method for achieving increased available oxygen through regional intra-arterial infusion. *Proc. Am. A. Cancer Res.*, 1959–1962, *3*, 318.
6. Jay, B. E., Finney, J. W., Balla, G. A., and Mallams, J. T. Supersaturation of biologic fluids with oxygen by decomposition of hydrogen peroxide. *Texas Rep. Biol. & Med.*, 1964, *22*, 106–109.
7. Mallams, J. T., Balla, G. A., and Finney, J. W. Regional intra-arterial hydrogen peroxide infusion and irradiation in treatment of head and neck malignancies: progress report. *Tr. Am. Acad. Ophth.*, 1963, *67*, 546–553.
8. Mallams, J. T., Balla, G. A., Finney, J. W., and Aronoff, B. L. Regional oxygenation and irradiation: head and neck. *A.M.A. Arch. Otolaryng.*, 1964, *79*, 155–159.

# SULFUR 35 STUDIES IN HUMAN CHONDROSARCOMA*

*By* J. ROBERT ANDREWS† *and* PAUL HOLLAND‡
WASHINGTON, D. C.

IN A previously published, detailed study of a single case of inoperable human chondrosarcoma, we were able to show that radioactive sulfur 35 is deposited in relatively high concentration in viable zones of human chondrosarcoma, that it is retained there for an extended period of time, that hematologic depression is the limiting factor in the amount of $S^{35}$ which may be administered, and that the radiation dose in the chondrosarcoma from the beta radiation of $S^{35}$ may be as great as several thousand or more rads for the amount of $S^{35}$, administered intravenously, which is tolerated.[3] This study suggested that the administration of large doses of $S^{35}$ might be beneficial, in terms of tumor growth restraint, in the management of patients with inoperable chondrosarcoma and it was decided, therefore, to extend the study to a group of such patients. The present report is, then, a review of our experience with 10 patients with inoperable chondrosarcomas.

The patients selected for study had histologically verified chondrosarcomas and were judged to be inoperable by both the referring physicians and the Surgery Branch of the National Cancer Institute. Several of the patients in whom it was feasible to perform multiple biopsies were given tracer doses (10 mc) of $S^{35}$ so that radiochemical and radiation dosimetric studies could be made of specimens of urine, blood, and selected tissues (chondrosarcoma, rib cartilage, or skin).

The $S^{35}$ was administered as carrier-free sulfate, $H_2SO_4$, in HCl and NaCl solution adjusted to a pH of 4.5 to 5.5. Pyrogen and sterility tests were performed on all doses and there were no immediate reactions following the $S^{35}$ administration. The methods for the dosimetric assay of the biologic materials were described in the previously published study.[3] In several instances the uptake of $S^{35}$ in tumor and normal tissues was monitored and its disappearance followed by measuring the Bremsstrahlung with a standard scintillation crystal and rate-meter placed externally over the sites of interest. In those instances where external beam radiotherapy was applied in addition to the $S^{35}$, this was administered by means of a 2 mev. Van de Graaff x-ray machine.

The influence of autologous bone marrow transfusion on the rate of hematologic recovery was studied in 6 patients. In these instances, bone marrow was removed from each patient by multiple aspirations, performed under general anesthesia, from sites not involved by chondrosarcoma. The marrow so collected was diluted with an equal volume of heparinized (10 u/ml.) tissue culture medium, NCTC 109,* and stored at 4° C. in plastic bags which, in turn were wrapped in aluminum foil. Immediately prior to replacement by intravenous administration, the marrow suspension was warmed to 37° C. Cell counts were made at the time of marrow withdrawal and again at reinfusion. At the time of reinfusion, eosin dye exclusion and cell division in tissue culture medium tests were performed and 75 per cent to 85 per cent of the cells were found to be viable.†

* Mc Quillin, W. T., Evans, V. G., and Earle, W. R. The adaptation of additional lines of NCTC Clone 929 (Strain L) cells to chemically-defined, protein-free medium. *J. Nat. Cancer Inst.*, 1957, *19*, 885–907.

† We are indebted to the Tissue Bank of the National Naval Medical Center for these studies and for many of the bone marrow collection, storage, and processing procedures.

* From the Radiation Branch, National Cancer Institute, and the Clinical Center Blood Bank, National Institutes of Health, United States Public Health Service, Department of Health, Education, and Welfare.
† Professor of Radiology and Director of Radiotherapy, Georgetown University Medical Center, erstwhile Chief, Radiation Branch, National Cancer Institute.
‡ Staff Physician, Clinical Center Blood Bank, National Institutes of Health.

The response of patients to either $S^{35}$ therapy or combined $S^{35}$ and x-ray therapy was determined by judgment as to whether or not there had been a change in the anticipated course of the disease rather than by measurable parameters. In no instance was there considered to be a deleterious effect save for the temporary depression of hematopoiesis.

The case report summaries of these 10 patients are presented below. Where appropriate for the stressing of certain features of this study, these reports have been expanded in detail.

### CASE REPORT SUMMARIES

Case 1. J.B. D1-13-15.* This case was reported in full in the original study.[3]

Case 2. F.U. 04-50-11. This 48 year old Negro male fractured his left hip at the age of 40; pain commenced 4 years later. Shortly thereafter, he had an internal fixation of an ununited fracture. One year later and 3 years prior to admission he was reoperated upon for nonunion; a biopsy revealed chondrosarcoma and a left hemipelvectomy was performed. Three months prior to admission, pain commenced in the left lower quadrant and roentgenographic examination showed invasion of the left ilium and sacrum. Physical examination revealed a diffuse, firm mass in the left lower quadrant extending to the hemipelvectomy scar.

Bone marrow containing $3\times10^9$ nucleated cells was removed and immediately following this procedure 500 mc of $S^{35}$ was given intra-arterially by retrograde catheter in the lower thoracic aorta. In the next 3 days midplane tumor exposures of 2,000 r, total, of 2 mev. x-rays were given through large fields and on the fourth day following marrow aspiration the marrow was replaced intravenously. Twelve days later 1,500 ml. of fluid drained spontaneously from the massive tumor. There was some decrease in pain but the condition of the patient remained essentially unchanged until 13 months later when he died as a result of uncontrolled tumor. It was concluded that this patient was not benefited.

* These numbers are the Clinical Center admissions and case records numbers.

Case 3. B.C. 02-16-11. This 82 year old Caucasian male was struck by a plow at the age of 22, receiving multiple fractures of his right rib cage. He developed a small, nontender mass on his right chest which was asymptomatic until 5 years prior to admission when it suddenly increased in size. It was partially removed 3 times and was determined to be a chondrosarcoma.

Physical examination revealed a $4\times6$ cm. irregular mass in the right upper anterior rib cage together with swelling and induration of the shoulder. Roentgenographic examination of the chest showed contiguous and adjacent intrathoracic lesions.

An initial dose of 387.7 mc of $S^{35}$ was administered intravenously with an additional dose of 334.8 mc 65 days later. Small increments of exposure of 2 mev. x-rays to a total exposure of 3,000 r were given in the interval. The tumor remained stabilized for several months following this treatment but subsequently became widely disseminated and the patient died 12 months after the treatment. It was concluded that this patient was benefitted.

The location and the character of the tumor made it amenable to the procurement of multiple biopsies for radioactivity assay procedures. Figure 1 shows these assays of tumor tissue, skin, blood, and urine for a pre-therapy

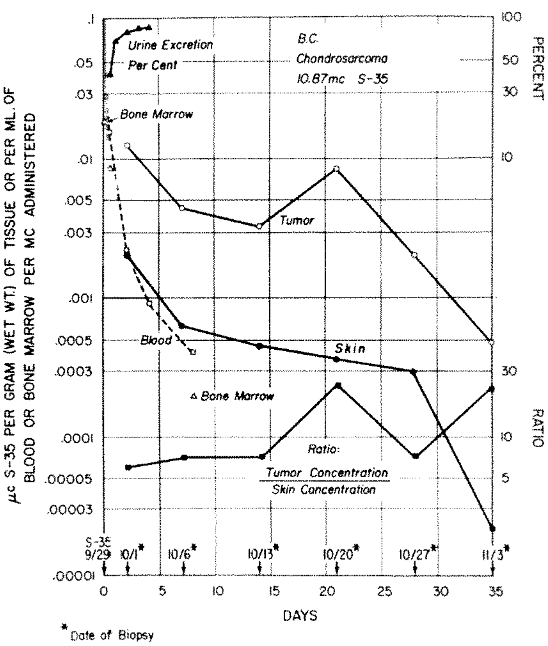


Fig. 1. Case 3. $S^{35}$ assay of tissue, blood and urine.

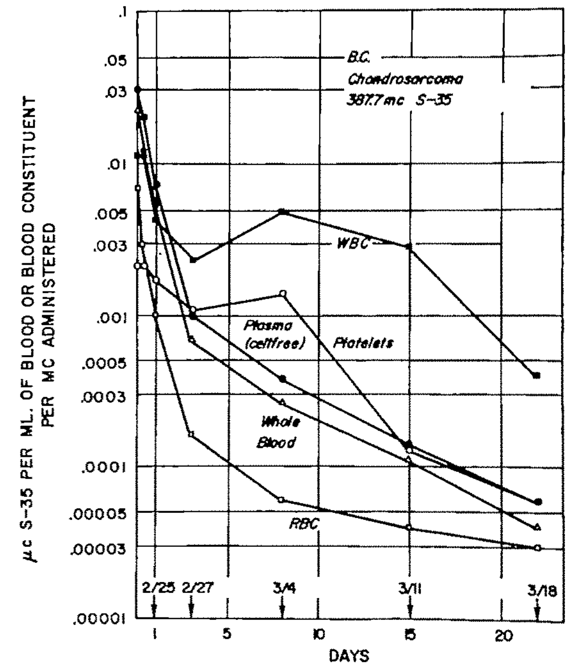


FIG. 2. Case 3. $S^{35}$ assay of blood and blood constituents.

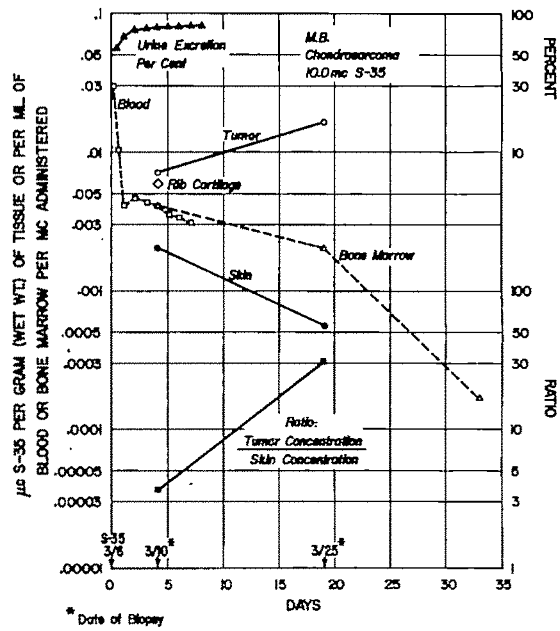


FIG. 3. Case 4. $S^{35}$ assay of tissue, blood, and urine.

tracer dose of $S^{35}$ and Figure 2 shows similar assays for various components of the blood following the therapeutic dose of $S^{35}$.

CASE 4. M.B. 00-82-56. This 53 year old Caucasian female noted pain in her right hip 4 months prior to admission. She was found to have erosion of the right ilium by roentgenographic examination and a massive pelvic and abdominal tumor by physical examination. A partial resection of the presenting tumor was effected by laparotomy but gross intra-abdominal tumor was palpable on admission.

Pre-treatment radioactivity assays are shown in Figure 3 following a tracer dose of 10 mc of $S^{35}$, administered intravenously. The patient received two doses of 333 mc, each, of $S^{35}$, administered intravenously, on two separate occasions 10 days apart and followed by a mid-tumor exposure of 6,000 r of 2 mev. x-rays delivered in small fractions. The course of the hematologic depression and recovery is shown in Figure 4. Following this treatment, the patient made a total recovery from a state of partial invalidism; pain disappeared and there was a substantial reduction in the size of the palpable intra-abdominal and pelvic mass. This state persisted to the time of death, almost 3 years later, from uncontrolled diabetes, severe electrolyte imbalance, and congestive heart failure. It was concluded that this patient received great benefit from the treatment.

CASE 5. T.T. 02-49-85. This 44 year old Caucasian male had noted the onset of fullness in his left buttock three years prior to admission. Surgical exploration revealed a chondrosarcoma which recurred 2 years later and was then treated with external roentgen irradiation. The patient subsequently underwent left hemipelvectomy followed by a third surgical procedure for recurrence. Physical examination on admission to the Clinical Center showed a 10×12 cm. mass on the medial aspect of the right thigh.

Bone marrow containing $10\times10^9$ nucleated cells was aspirated, following which the patient was given 487.6 mc of $S^{35}$ intravenously. The autologous marrow was returned intravenously 4 days later. The course of the hematologic depression and recovery is shown in Figure 5. The patient's pain increased and his condition continued to deteriorate until death 6 months later. The patient was not benefited by the treatment.

CASE 6. E.P. 03-14-55. This 22 year old Caucasian male developed right sciatica 1 year before admission. A biopsy revealed a chondrosarcoma of the hip and pelvis and he under-

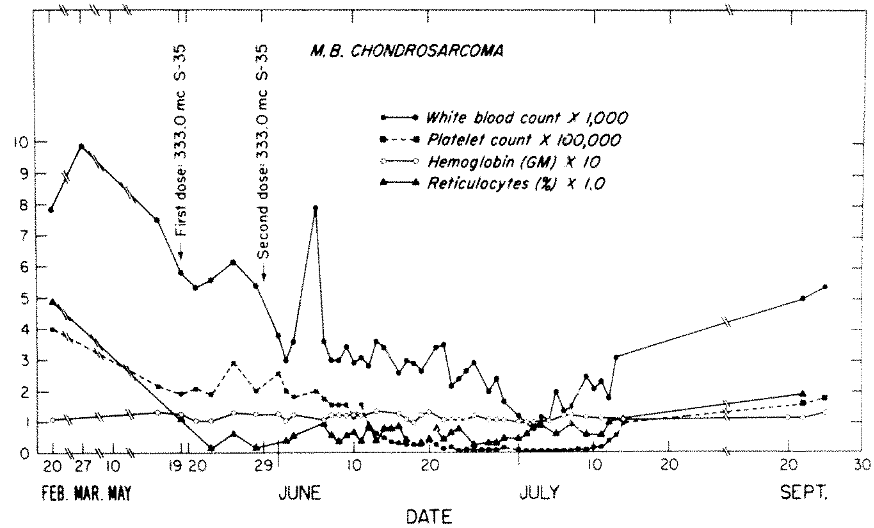


FIG. 4. Case 4. Hematological data.

went right hemipelvectomy. Pain and the tumor mass recurred.

The patient was given 350 mc of $S^{35}$ intravenously by catheter. The $S^{35}$ was administered slowly over a period of several hours during which time the patient was maintained in a hypothermic state with orthopedic tourniquet isolation of the extremities. The radioactive sulfur was administered in this manner to determine whether or not the hematologic depressant effect could be minimized by such a procedure. The course of the hematologic depression and recovery, as shown in Figure 6, manifested no departure from the general pattern of such and this kind of procedure was not studied further.

The tumor mass increased in size and the patient developed a urethrocutaneous fistula. The patient deteriorated rapidly and died 7 months later with massive local extension and metastases. The patient was not benefited by the treatment.

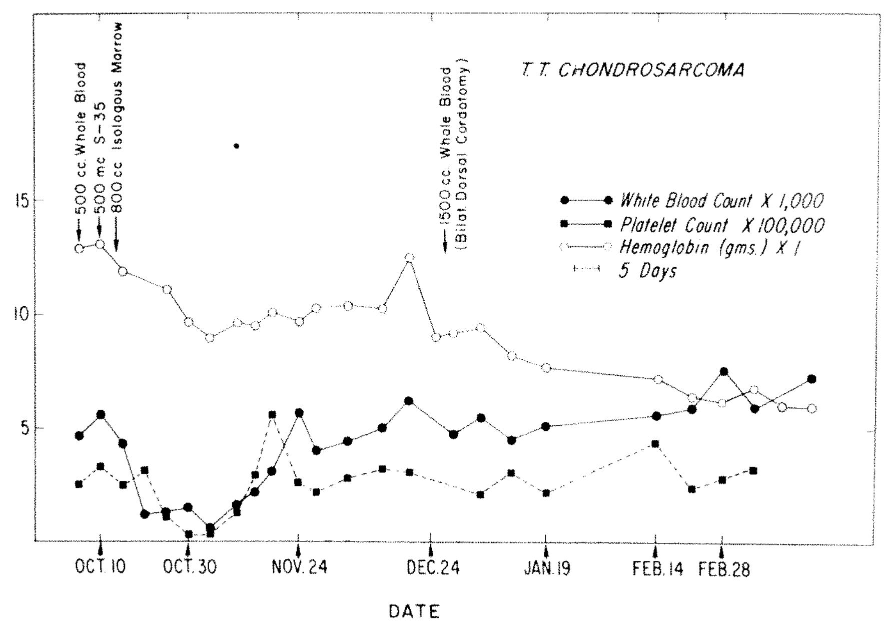


FIG. 5. Case 5. Hematological data.

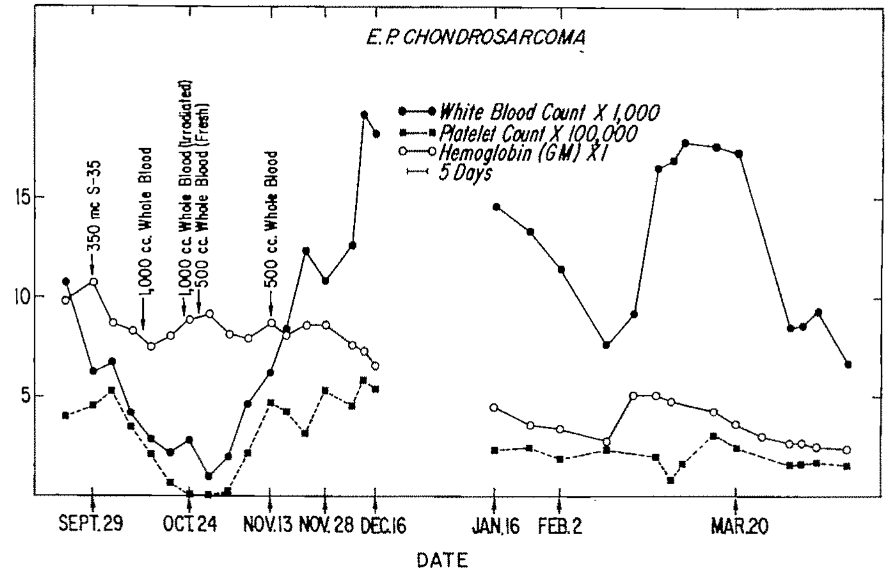


Fig. 6. Case 6. Hematological data.

Case 7. L.J. 04-91-99. This 47 year old Caucasian male developed a small nodule on the manubrium at the age of 42 years, which suddenly enlarged 2 years prior to admission. It was excised and found to be a chondrosarcoma. One year prior to admission, the mass recurred, necessitating wider excision, and a right pleural effusion developed. On admission, the sternal mass had again recurred, measuring $11 \times 12$ cm., and there were contiguous intrathoracic masses.

Bone marrow containing $13 \times 10^9$ nucleated cells was aspirated and 485 mc of $S^{35}$ was administered intravenously. This was followed by a tumor exposure of 1,000 r of 2 mev. x-rays administered in a single sitting. Four days after the sulfur administration, the autologous bone marrow was returned intravenously. Additional external irradiation of 1,000 r was given later.

Tumor growth apparently ceased; the patient returned home and resumed his normal activities in the metal trades, feeling much improved. One year later, the presenting external tumor had shown no increase in size but metastases had developed. The patient was readmitted to the Clinical Center for consideration of a second course of treatment. During this second admission there was an acute episode of severe and prostrating abdominal cramping pain with leukocytosis and, as shown by roentgenographic examination, cholelithiasis. At laparotomy the gallbladder, containing stones, and a portion of small bowel, which was nonvascular and which appeared nonviable, were resected. Histologic examination of the resected bowel showed invasion of the mesenteric veins by chondrosarcoma. The patient died a few months later. It was concluded that the patient did derive benefit from the treatment.

Case 8. G.H. 05-11-98. This 18 year old Caucasian female experienced the onset of pain in her right thigh 9 months prior to admission. A mass was subsequently noted and destruction of the proximal right femur was demonstrated on roentgenograms. Surgical resection of the affected femur was attempted. Physical examination on admission revealed a 20 cm. in diameter, tense and very tender mass in the proximal thigh.

Bone marrow containing $15 \times 10^9$ nucleated cells was aspirated and 500 mc of $S^{35}$ was administered intravenously. The patient then received a tumor exposure of 2,000 r of 2 mev. x-rays in the succeeding 3 days and on the fourth day the autologous marrow was returned intravenously. Several transfusions of whole blood and of platelets were given during the course of the hematologic depression and recovery. Six months after treatment the patient was much more comfortable, the tumor mass was smaller, and it was felt that a useful pallia-

tive effect had been achieved. Pulmonary metastases had, however, appeared and 4 months later the patient died with massive pulmonary metastases and massive local recurrence of tumor. It was felt that this patient benefited from the treatment.

Case 9. R.M. 05-15-13. This 17 year old Caucasian male noted pain in and subsequent swelling of the left hip approximately $2\frac{1}{2}$ years prior to admission. He underwent three surgical procedures for resection and attempted prosthetic repair of the hip prior to admission to the Clinical Center. Physical examination revealed moderate soft tissue swelling of the left buttock. Roentgenographic examination demonstrated extensive recurrence of the chondrosarcoma in the region of the hip joint and the soft parts of the adjacent pelvis.

Bone marrow containing $15 \times 10^9$ nucleated cells was aspirated and 482 mc of $S^{35}$ was administered intravenously. Seven days after the marrow was aspirated, it was returned by intravenous infusion. A tumor exposure of 4,000 r of x-irradiation was given in the following 24 days. Eight months later the patient was in good general condition with no local recurrence of palpable tumor and he underwent another surgical procedure for the prosthetic reconstruction of his hip. Cartilaginous masses lying in the soft parts were removed during this procedure. It was concluded that this patient was benefited by the treatment.

Case 10. C.L. 04-72-64. This 35 year old Caucasian male developed dysuria and urinary retention 5 years prior to admission. A large mass of chondrosarcoma arising from the neural arches of L-3 through S-1 was excised. The mass recurred and invaded the abdomen. Physical examination revealed an enlarged liver and a $15 \times 17 \times 7$ cm. mass in the right lower back area.

Bone marrow containing $11 \times 10^9$ nucleated cells was aspirated and 450 mc of $S^{35}$ was administered intravenously. Five days later the autologous marrow was returned by intravenous infusion. Six months later the patient had less pain and was able to carry on some of his farming activities including the driving of a tractor. A few months later the tumor recurred, grew rapidly, and the patient died with massive, ulcerative tumor. It was concluded that this patient was benefited by the treatment.

## DISCUSSION

It has not been proved that the administration of $S^{35}$ to patients with chondrosarcoma results in the restraint of tumor growth or in other beneficial responses related to $S^{35}$ radiation effects. The experiences with patients, as cited in the case report summaries, suggest that such responses may occur, but the scientific evidence that $S^{35}$ has a growth-restraining effect on cartilage is indirect. This evidence was developed in a previous study[13] where it was shown that severe damage, the histologic manifestations of which are similar to those due to x-irradiation, to the growing cartilage of rodents results from less than lethal doses of $S^{35}$. Further, the movement of sulfate into and through the chondrocyte and from the chondrocyte into the matrix is an active transport phenomenon,[5,8,10] and not simply a passive diffusion process. Where there are radioactive atoms within a cell, there will be some probability of cell lethal effect. The cell lethal effects of ionizing radiations are associated with interference, by these radiations, with the reproductive capacity of cells and it is thought that all the somatic cells of the normal of neoplastic tissues of a given species are, essentially, of equal, or nearly equal, inherent radiosensitivity. Apparent differences in radiosensitivity may be explained on the bases of the oxygen effect and the different cell population growth and replacement kinetics of different tissues, both normal and neoplastic. A discussion of these postulates appears in Reference 4.

External beam 2 mev. x-ray therapy was administered to these patients in addition to the $S^{35}$. It has been the recent practice to administer the radiotherapy in one or a few large doses for 3 reasons. One is that it was thought desirable to administer all the radiation, both that due to $S^{35}$ and that due to the external beam irradiation, prior to the return of the patient's bone marrow. Secondly, certain of our experimental studies have shown that external beam irradiation results in prolongation of the half-time of $S^{35}$ in cartilage[7] and presum-

ably, therefore, in a greater radiation effect due to the longer presence of $S^{35}$. Lastly, it is a well-known radiobiologic phenomenon that a given dose of ionizing radiation is more effective if delivered in one or a few large increments over a short period of time than if delivered in many small increments over a long period of time.

The responses of certain patients, as described in the case report summaries, suggest that the radiation effects were beneficial; some patients showed either no improvement or actual progression of the disease after treatment. Since chondrosarcoma patients have such a variable course, it is difficult to assess accurately the value of $S^{35}$ with or without external irradiation. However, no clinical radiation effects on the kidneys, skin, hair, joint cartilages or tissues other than the hematopoietic ones have been observed.

The human dosimetry of $S^{35}$ is difficult to study both because of the clinical problems associated with biopsy of chondrosarcoma and because of other tissue sampling problems. The clinical problems are those of discomfort to the patient, anesthetic risk, hemorrhage, and infection. The sampling problems are due to the fact that large human chondrosarcomas are not homogeneous in their anatomic characteristics; some zones are more cellular than others and some zones are either cystic, hemorrhagic, or necrotic. It is impossible, therefore, to make a consistently valid radioactivity assay of human chondrosarcoma biopsy tissue and many attempts fail. The disappearance of $S^{35}$ from the blood and its excretion in the urine are, initially, very rapid, as shown in Figures 1 and 3. In addition, $S^{35}$ appears in the perspiration and saliva. These aspects of sulfate metabolism pose stringent problems in radiation protection if area contamination and personnel exposure are to be avoided. A detailed account of the radiation safety practices employed is not germane to this particular study, but a careful consideration of them is certainly germane if similar work is to be undertaken and a detailed account of these practices, in respect to these reported patients and procedures, has been published.[6]

The limiting factor in the dose of $S^{35}$ which can be administered to the human is its hematopoietic depressant effect. The degree of this effect and its temporal characteristics are shown in Figures 4, 5 and 6 for 3 representative patients. The time of maximum platelet and white blood cell depression was about the 28th day, the platelet count falling to an average of 48,000 per mm.$^3$ and the white blood cell count to 1,700 at that time. In no instance was death due to this depressant effect and, with the exception of Case 3, there was hematopoietic recovery, usually within 40 days after the $S^{35}$ was administered.

There is no known direct way to measure the radiation dose delivered to the stem cells of the hematopoietic system by an internally administered radioisotope. There are, however, published data on the human hematopoietic effects of externally administered ionizing radiation, either as the deliberate application of measured doses or as an accidental exposure to estimated doses. Some of these data are compiled in Table 1. In the case series here reported of $S^{35}$ and external x-ray beam irradiated patients, there was no mortality due to radiation effects. Petechiae of very slight degree appeared in 3 of the 10 patients, no other hemorrhagic phenomena were manifest and the maximum depression of the platelets occurred on about the 28th day. These observations and their comparison with the data of Table 1 suggest that the hematopoietic depressant effect of the internally administered $S^{35}$ was less than that due to a dose of some 300 rads from external radiation sources.

Patients in whom similar doses of $S^{35}$ were administered but in whom the autologous bone marrow procedure was not employed showed essentially the same patterns of hematopoietic depressant effect and recovery as those in whom the autologous bone marrow procedure was employed. Our interpretation of these observations is not that the procedure is an ineffec-

Table I

HUMAN HEMATOPOIETIC RESPONSES TO TOTAL BODY IRRADIATION

| Reference No. | Type of Irradiation | Dose | Time of Maximum Platelet Depression (days) |
|---|---|---|---|
| 9 | External beam, planned | 200–250 rads, 4–6 days later, 150–230 rads<br>400 rads | 20<br><br>20 |
| 1 | External beam, planned | 400 rads | (lymphocytes) 5 |
| 11 | External beam, planned | 250, or more rads<br>350 rads | 20<br>(50% mortality) |
| 2 | Fission, accidental | 236–365 rads | 25<br>(5 cases)<br>Petechiae 2/5<br>Hematuria 3/5<br>Bleeding gums 2/5<br>Epilation 5/5 |
| 12 | Fission, accidental | 350–640 rads<br>640 rads | 25<br>(death at 18th day) |
| This Report | $S^{35}$ series (10 cases) | Estimated as less than 300 rads | To average count of 48,000 at 28 (range: 6,000 to 173,000)<br><br>White blood cell count to average count of 1,700 at 28 (range: 600–3,700)<br>Petechiae, 3/10<br>(no mortality) |

tive one but that, simply, either the population of the hematopoietic stem cells was not reduced by the doses of $S^{35}$ administered to levels sufficiently low for the effects of the procedure to become manifest, or insufficient numbers of marrow cells were employed. It is assumed, if the dose of $S^{35}$ were large enough, that the exhaustion of hemopoietic stem cells would be absolute and that, under such circumstances, the effects of the procedure could become manifest. What the upper limit of a dose of $S^{35}$ might be under such circumstances has not been determined. In some of the patients, it was considered that clinical indications existed for the replacement of certain formed circulating blood elements and under such circumstances the appropriate replacement therapy was effected.

## CONCLUSIONS

1. The conclusions tentatively drawn in the first report[3] have been confirmed and the work has been extended.

2. Data have been developed on the human hematopoietic and chondrosarcoma dosimetry of large doses of $S^{35}$ administered intravenously.

3. Sulfur 35 is deposited in relatively high concentration in viable zones of human chondrosarcoma and is retained there for an extended period of time.

4. The dose-limiting factor in the possible therapeutic administration of $S^{35}$ is the depletion effect on the hematopoietic tissues.

5. The combined administration of $S^{35}$ and external beam x-irradiation has resulted in beneficial clinical responses in

some patients with inoperable chondrosarcoma.

J. Robert Andrews
Georgetown University Medical Center
3800 Reservoir Road, N.W.
Washington, D. C.

REFERENCES

1. ANDREWS, G. A. Discussion, diagnosis, treatment and prognosis of human radiation injury from whole-body exposure. Symposium on Physical Factors and Modification of Radiation Injury. *Ann. New York Acad. Sc.*, 1964, *114*, 349–355.
2. ANDREWS, G. A., SITTERSON, B. W., KRETCHMAR, A. L., and BRUCER, M. Criticality accident at Y-12 plant. In: Diagnosis and Treatment of Acute Radiation Injury. Proceedings of a Scientific Meeting sponsored by the International Atomic Energy Agency and the World Health Organization, Geneva, 1960. International Documents Service, New York, 1961, pp. 27–48.
3. ANDREWS, J. R., SWARM, R. L., SCHLACHTER, L., BRACE, K. C., RUBIN, P., BERGENSTAL, D. M., GUMP, H., SIEGEL, S., and SWAIN, R. W. Effects of one curie of sulfur 35 administered intravenously as sulfate to a man with advanced chondrosarcoma. AM. J. ROENTGENOL., RAD. THERAPY & NUCLEAR MED., 1960, *83*, 123–134.
4. ANDREWS, J. R. Physical, biological, and clinical aspects of fast neutron and other high-LET radiations and implications for fast neutron beam radiotherapy. In: Cellular Radiation Biology. Proceedings of Eighteenth Annual Symposium on Fundamental Cancer Research sponsored by the University of Texas, M.D. Anderson Hospital and Tumor Institute, Texas Medical Center, Houston, March 2–4, 1964. Williams & Wilkins, Baltimore, 1965.
5. BOSTRÖM, H. On metabolism of sulfate group of chondroitinsulfuric acid. *J. Biol. Chem.*, 1952, *196*, 477–481.
6. BROWN, J. M., JR., HOWLEY, J. R., MCINTOSH, Y., DRIVER, D., and DICKINSON, M. B. Contamination problems associated with administration of massive doses of sulfur-35 to patients. *Health Physics*, 1964, *10*, 557–561.
7. CORREA, J. N., SWARM, R. E., WALKER, C. D., and ANDREWS, J. R. Effect of external irradiation on incorporation and retention of $S^{35}$ in mouse chondrosarcoma. Presented before the Annual Meeting of the Radiation Research Society, Philadelphia, 1965. To be published.
8. CURRAN, R. C., and GIBSON, T. Uptake of labelled sulfate by human cartilage cells and its use as test for viability. *Proc. Roy. Soc. Med.*, 1956, *144*, Ser. B., 572–576.
9. DEALY, J. B., JR., and TUBIANA, M. Hematological responses to inhomogeneous and homogeneous whole-body irradiation. Symposium on Physical Factors and Modification of Radiation Injury. *Ann. New York Acad. Sc.*, 1964, *114*, 268–283.
10. DZIEWIATOWSKI, D. D. Isolation of chondroitin sulfate-$S^{35}$ from articular cartilage of rats. *J. Biol. Chem.*, 1951, *189*, 187–190.
11. MATHÉ, G., AMIEL, J. L., and SCHWARZENBERG, L. Treatment of total-body irradiation injury in man. Symposium on Physical Factors and Modification of Radiation Injury. *Ann. New York Acad. Sc.*, 1964, *114*, 368–392.
12. PENDIC, B. Zero-energy reactor accident at Vinca. In: Diagnosis and Treatment of Acute Radiation Injury. Proceedings of a Scientific Meeting jointly sponsored by the International Atomic Energy Agency and the World Health Organization, Geneva, 1960. International Documents Service, New York, 1961, pp. 67–81.
13. RUBIN, P., BRACE, K. C., GUMP, H., SWARM, R., and ANDREWS, J. R. The radiotoxic effects of $S^{35}$ in growing cartilage. *Radiology*, 1957, *69*, 711–719.

# DISTRIBUTION OF PULMONARY VENTILATION DETERMINED BY RADIOISOTOPE SCANNING*

## A PRELIMINARY REPORT

By FELIX J. PIRCHER, M.D.,† JOEL R. TEMPLE, M.D.,‡ WILLIAM J. KIRSCH, M.D.,§ and ROBERT J. REEVES, M.D.†

DURHAM, NORTH CAROLINA

RADIOISOTOPE scanning has been used successfully to define size, shape and location of certain organs and to demonstrate whether disease may involve them diffusely or locally.[13,24] For certain organs, "visualization" may be accomplished by more than one technique. The liver, for example, may be "visualized" with radioiodinated rose bengal, which is retained by the polygonal cells, or with radiocolloidal gold, which is retained in the reticuloendothelial cells because both types of tissue are distributed diffusely throughout the liver and are usually equally affected by disease. This is not true for the two main compartments of the lung: the space perfused with pulmonary artery blood and the space ventilated with air. They are known to be affected unequally and differently by disease processes. Recently, a method was described that maps the capillary bed of the pulmonary circulation, visualizes the lungs, and demonstrates perfusion defects.[7,21,25] Regional pulmonary ventilation has been measured by bronchospirometry,[10] fluorodensimetry,[2,12,17,23] and by external counting using radioactive gases.[3,8,11,26] The technique described here employs scanning of the chest after inhalation of $I^{131}$ labeled human serum albumin aerosol for mapping the ventilated space of the lungs.

### METHODS AND MATERIALS

Experiments were carried out in 5 healthy mongrel dogs without evidence of lung disease clinically or on chest roentgenograms. Their weight ranged from 20 to 26 pounds. They were anesthetized with intravenous pentobarbital and were intubated with a cuffed endotracheal tube. The endotracheal tube was connected to a Bird micronebulizer which was driven by a Bird Mark VII respirator. One millicurie of $I^{131}$ labeled human serum albumin in a 6 per cent solution and in a volume of 1 to 2 ml. was placed in the nebulizer. While in the prone position, the animals breathed spontaneously with the respirator. Automatic cycling was not used. The exhaled air was trapped in a plastic bag. The average time necessary to nebulize and inhale the dose was approximately 15 minutes. Immediately following inhalation, scans were made over the posterior aspect of the chest with the dog in the prone position.

After a recovery period of 1 week, during which the chest counts returned to background levels, cork balls which contained a radiopaque marker were placed in 1 to 3 bronchi, causing their complete obstruction. Scanning was then performed again by the same method.

Ventilation scans were also made of 4 normal men, ages 20 to 25 years, who had no evidence of pulmonary disease by history or by chest roentgenograms. In addition, ventilation scans were made of 25 patients with a variety of lung diseases. For each human subject the nebulized dose of radioiodinated human serum albumin was 2 mc contained in a 1 to 4 ml. volume. The isotope material was administered via the

* Duke University Medical Center, Durham, North Carolina.
Aided in part by Grant #T-215 of the American Cancer Society, in part by Grant #112 of the United Medical Research Foundation Fund, and in part by a Fellowship from the American Heart Association 62F73.
† Department of Radiology.
‡ Research Fellow, American Heart Association, Department of Internal Medicine.
§ Department of Pathology.

Bird micronebulizer and Bird Mark VII respirator. The subjects were seated in a straight-backed chair and breathed the aerosol through a mouthpiece attached to the micronebulizer. Nasal respiration was blocked with a nose clip. Pressure settings on the respirator were kept as low as possible, in the range of 5 to 10 cm. of water, and the flow rate was adjusted so that respiration was as comfortable as possible. The exhaled air was trapped in a plastic bag. The inhalation time varied with the volume of the dose and averaged 10 minutes. The scans were made over the posterior aspect of the chest with the subject in the prone position. Thyroid uptake of radioactive iodine was blocked with Lugol's solution administered in doses of 10 drops three times a day for 5 days.

The dose of nebulized material retained by the lungs was calculated for the normal subjects by determining the number of counts, both after inhalation and after the intravenous injection of 500 $\mu$c of $I^{131}$ labeled macro-aggregated human serum albumin. The retention of aggregates in the lung was calculated in per cent of the injected dose and expressed in microcuries. The number of microcuries retained in the lungs from the inhalation was then calculated as the product of lung counts from inhalation times microcuries of retained aggregates divided by lung counts from the aggregates. Measurement of whole body retention and distribution of the inhaled isotope was made with the whole body scanner and counter.[18]

## RESULTS

A total of 11 studies were performed in the 5 dogs. Each animal had an initial scan which showed pulmonary dimensions comparable with the chest roentgenogram and a distribution of scan densities that was in concurrence with the predicted ventilated space (Fig. 1*A*). One of the test animals developed pneumonia after the initial scan. The ventilation scan was then repeated. It showed a decrease in scan densities in areas that corresponded with the areas of consolidation in the chest roentgenogram (Fig. 1*B*). In the remaining 4 animals, perfusion scans were made after the lung counts had returned to background levels. The ventilation and perfusion scans were found to be nearly indistinguishable in appearance. In addition, ventilation scans were repeated in 3 of these 4 animals after regional bronchial obstruction was accomplished. These scans showed decreased or no densities in the affected areas, indicating failure of the nebulized material to reach the area distal to the obstruction (Fig. 2, *A* and *B*). The animals were sacrificed and autopsied at

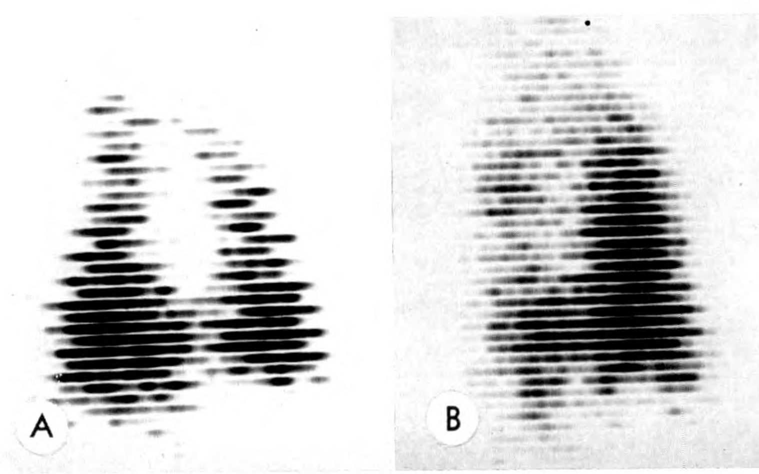


Fig. 1. (*A*) Normal ventilation scan of Dog 1. (*B*) Ventilation scan of Dog 1 with suppurative bronchopneumonia involving the right upper and middle lobe.

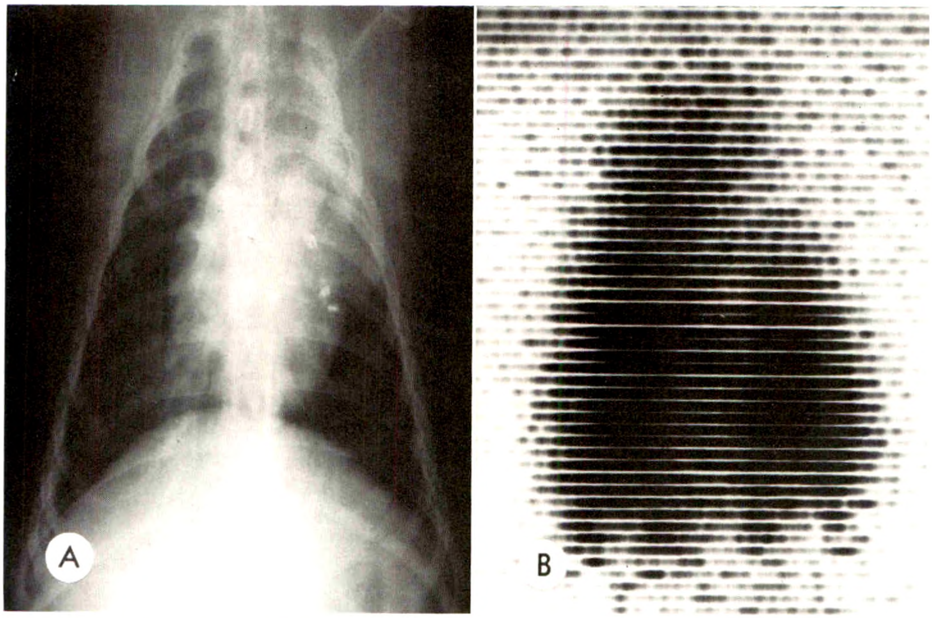


Fig. 2. (*A*) Chest roentgenogram of Dog 5 after block of left upper lobe bronchus (note density in left upper lung field and position of radiopaque marker). (*B*) Ventilation scan of same dog showing decreased radioactivity in the atelectatic area.

varying intervals. Their lungs showed areas of atelectasis and bronchopneumonia distal to the areas of the block. The remaining uninvolved portions of the lungs showed no signs of allergic or foreign body reaction. The last dog received iodine 125 labeled human serum albumin in nebulized form. The animal was sacrificed after the completion of the scan and the lungs were removed. The lungs were fixed by intratracheal insufflation with formaldehyde fumes. Then sections of the lungs were prepared for autoradiography. The macroscopic preparation showed a diffuse distribution of radioactivity (Fig. 3, *A* and *B*). The microscopic preparations showed radioactivity in the entire bronchial tree and in the alveoli (Fig. 3, *C* and *D*).

The ventilation scans obtained from the normal subjects showed good definition of size, shape and location of the lungs and a distribution of scan densities compatible with the expected ventilated space (Fig. 4, *A* and *B*). The group of subjects with lung disease included 6 patients with tuberculosis who showed a great variety of roentgenographic changes; 3 patients had tumors; 1 patient exhibited right-sided pleural effusion and right lower and middle lobe pneumonia; and 15 patients had chronic bronchitis and emphysema. The distribution of scan densities in the area of the lungs of these patients showed irregularities of varying degrees. A preliminary evaluation of these irregularities suggests that a decrease or absence of scan densities is found in areas of pulmonary fibrosis, neoplastic involvement, emphysematous changes and atelectases. Furthermore, it was noted that in patients with tuberculosis there was good agreement between scan abnormalities and chest roentgenographic findings (Fig. 5, *A* and *B*); that neoplastic lesions appear to impair ventilation more extensively than suggested by roentgenographic findings (Fig. 6, *A* and *B*); that pleural effusion may reduce ventilation of an entire lung appreciably and diffusely (Fig. 7, *A* and *B*); and, finally, that patients with bronchitis and emphysema may have marked reduction of ventilation in an irregularly localized pattern, not demonstrated by roentgenograms (Fig. 8, *A* and *B*).

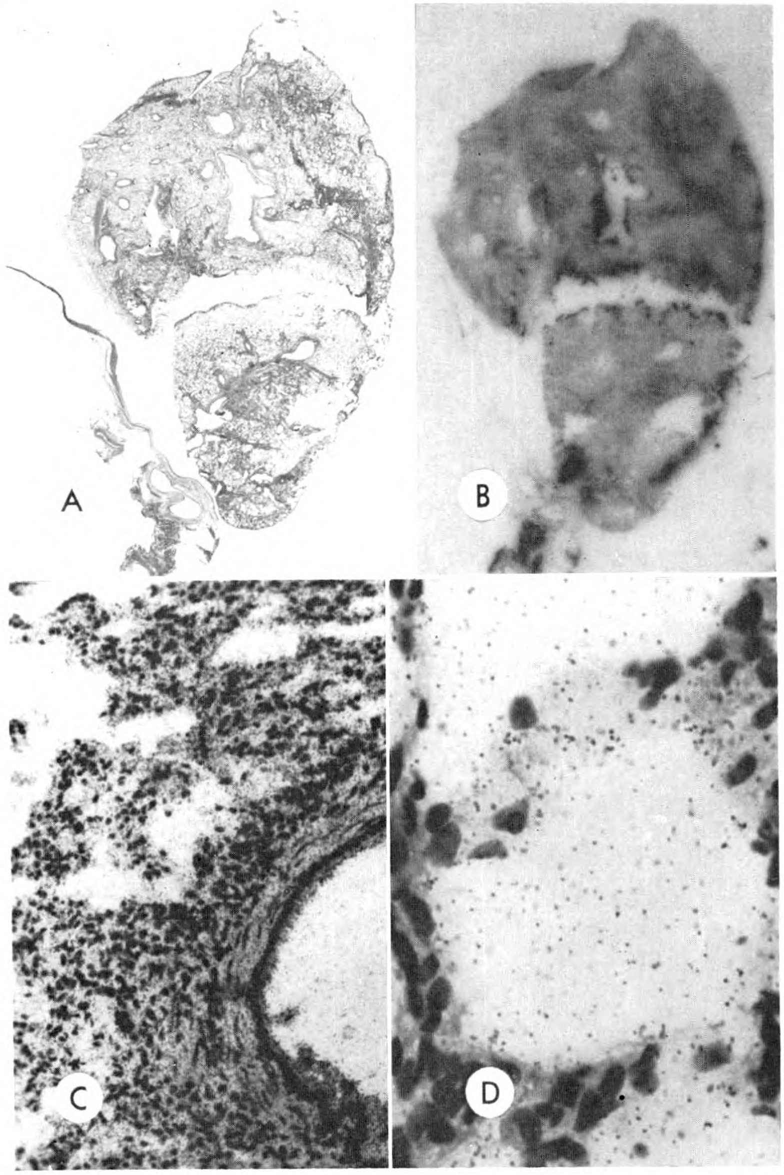


Fig. 3. (*A*) Lung section of Dog 4. (*B*) Macro-autoradiograph showing diffuse distribution of radioactivity ($I^{125}$). (*C* and *D*) Micro-autoradiograph of part of the same section showing radioactivity within the bronchial tree and alveoli.

Outside the areas of the lungs, retention of varying degree was noticed in the area of the trachea and bronchi in 2 of the 4 normal subjects and in 14 of the 25 patients, in 3 of whom there was prominent retention. Radioactivity was also noticed in the mouth and in the stomach of all 29 subjects. Data on retention and distribution of the inhaled radioactivity have been collected and computed for the 4 normal subjects. The retention in their lungs was found to vary from 190 to 320 $\mu$c, averaging 14.6 per cent of the total dose. The average effective half life of the retained dose in the lungs was found to be 18.5 hours. The retention in the mouth averaged 5 per cent of the total dose. The radioactivity in the stomach ranged from 20 to 190 $\mu$c at the end of inhalation. Blood activity levels reached a peak of 2 per cent of the total dose between

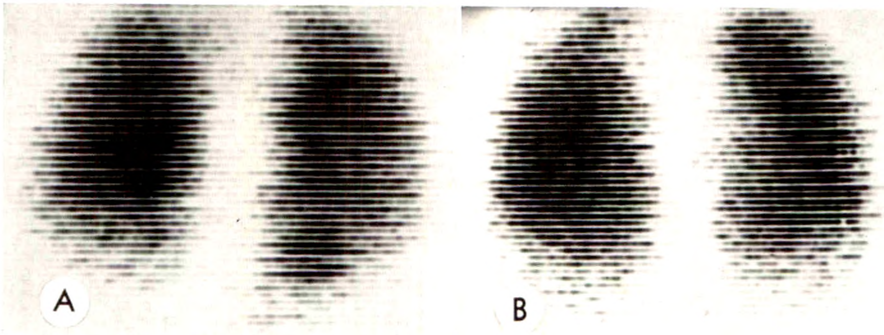


FIG. 4. (*A*) Ventilation and (*B*) perfusion scans of a normal subject.

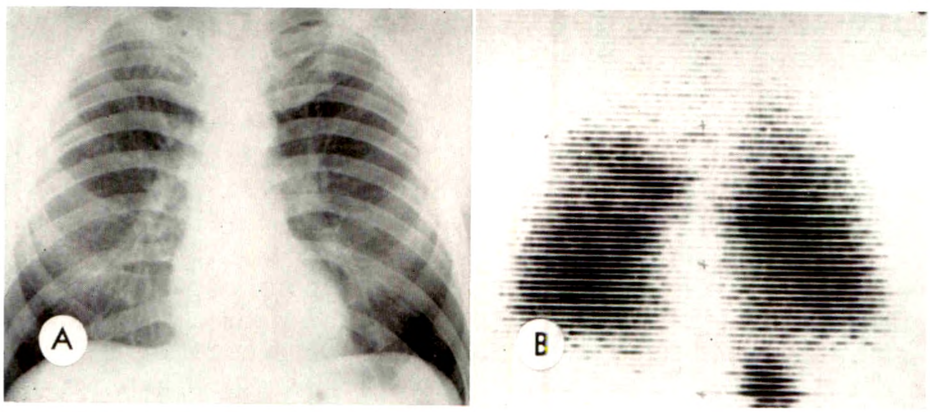


FIG. 5. (*A*) Chest roentgenogram of a patient with scarring in the right upper lung field and at the base of the right upper lobe; bronchovascular thickening in left apex. (*B*) Ventilation scan of the same patient with decreased radioactivity in both apical regions, more extensive on the right, and in the lateral aspect of the upper half of the right lung.

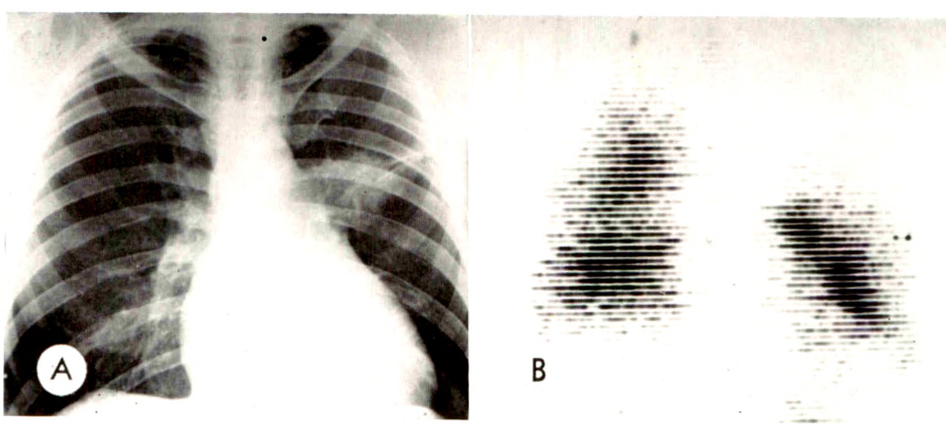


FIG. 6. (*A*) Chest roentgenogram of a patient with a mass lesion in the left upper lung field, probably carcinoma, and decreased vascularity on both sides. (*B*) Ventilation scan of the same patient, showing no ventilation of upper third of left lung and irregular distribution of radioactivity throughout both lungs.

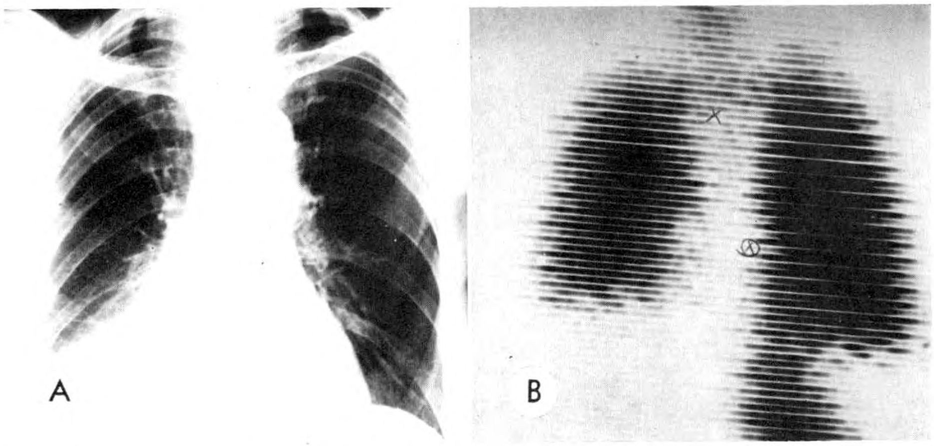

FIG. 7. (*A*) Chest roentgenogram of a patient with right sided pleural effusion and right lower medial lung field pneumonia. (*B*) Ventilation scan of the same patient showing diffusely decreased ventilation of entire right lung (in prone position), marked decrease in radioactivity in the area of the pneumonia and retention of radioactivity in the stomach.

6 and 24 hours. After 2 days, 90 per cent of the radioactive iodine in the plasma was protein bound.

## DISCUSSION

Other methods have been used for the measurement of regional pulmonary ventilation, but they have certain disadvantages. Bronchospirometry requires skill and experience, is associated with significant patient discomfort, is performed under unphysiologic conditions and its measurement is limited at best to individual lobes. Fluorodensimetry is limited in its spacial resolution by the size and the number of available external detectors. This is also true for external counting using radioactive gases. Radioactive gases, although quite valuable in determining regional ventilation perfusion ratios, are of limited use because of their rapid diffusion into the blood, making them unsuitable for scanning of the air compartment of the lung. The technique described has the advantage

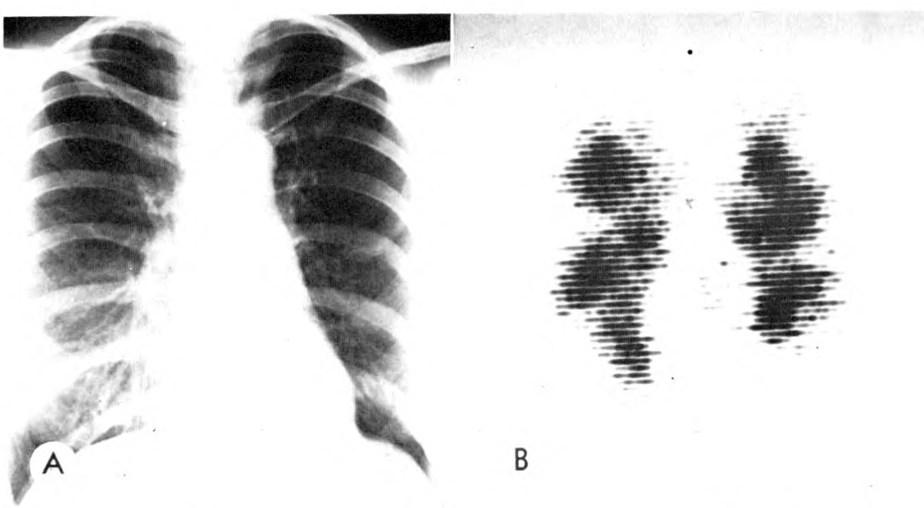

FIG. 8. (*A*) Chest roentgenogram of a patient with asthma, read as negative. (*B*) Ventilation scan of the same patient showing marked decrease of ventilation in a localized, irregular pattern.

of providing continuity of recording over the entire area of the lungs with a spacial resolution approaching 2 cm.[13,24] It requires a radioactive material that has a gamma emission suitable for scanning, is nontoxic, can be distributed relatively evenly throughout the ventilated space, remains *in situ* long enough to permit scanning, and is eliminated at a reasonable rate in order to reduce the radiation dose to the organ. Nebulized $I^{131}$ labeled human serum albumin meets most of these requirements. It has a gamma emission suitable for scanning. Serum albumin is nontoxic and nonantigenic in man and is eliminated from the bronchial tree at a reasonable rate by expectoration and absorption. Its effective half life in the lungs averages 18 hours. Nebulized radioiodinated human serum albumin appears to be distributed diffusely in the lungs, when compared with the intravascular distribution of macroaggregated serum albumin as seen in perfusion scans, and as suggested by autoradiographic studies.

The production of aerosol particles and their pulmonary distribution and retention has been extensively studied in connection with inhaled dust as an industrial hazard, radioactive contamination of the air, chemical warfare and aerosol therapy.[5,16,19] Agreement among investigators is poor with reference to penetration and deposition of aerosol particles in the lungs. Many factors are known to influence deposition: particle size,[9,14,27] particle composition,[6] electrical charge of particles,[15] respiratory rate,[1] air flow rate and air turbulence.[4] The Bird micronebulizer used in our experiments is an air-liquid jet nebulizer and produces, according to the manufacturer, floating particles ranging from 0.01 to 4 $\mu$ in diameter.[4] We have found that low flow rates with the Bird respirator gave best results, and that high flow rates produced large airway deposition which is recognizable on scans. Scratches and other blemishes on the internal parts of the nebulizer also cause deposition in major airways, presumably by producing larger particles. The dimensions of the lungs as defined by the ventilation scan are the same or slightly larger than by the perfusion scan, and compare favorably with the lung size on chest roentgenograms.

The average pulmonary retention of the radioactive material in the 4 normal subjects was 14.6 per cent of the total dose and the average half life was 18.5 hours in the lungs and 20 hours in the whole body. Using Quimby's formula for absorbed beta dose[20] and an average beta energy of iodine 131 of 0.3 mev. for the lungs and 0.44 mev. for the whole body,[22] the dose to the lungs was calculated to be 5 rads and the whole body dose 80 millirads. Corrections were not made in the calculations for variance of gamma ray absorption in the various parts of the body. Efforts are being made to reduce the trapping of labeled serum albumin in the stomach because it contributes substantially and undesirably to the whole body burden. The rate of pulmonary absorption of inhaled serum albumin and the rate of its elimination by expectoration remain to be determined.

SUMMARY

A method for the determination of the distribution of pulmonary ventilation by scanning has been described. Iodine 131 labeled human serum albumin solution is nebulized and inhaled. An average of 14.6 per cent of the total dose is retained in the lungs. The retained tracer material permits mapping of the ventilated space by scanning. Studies were performed on dogs, normal subjects and patients who had a variety of lung diseases. The results indicate that areas with defective or impaired ventilation can be detected and localized. This information should be of value in the diagnosis and management of patients who have marginal pulmonary function.

Robert J. Reeves, M.D.
Department of Radiology
Duke University Medical Center
Durham, North Carolina

We wish to express our thanks to Dr. Forrest Bird for the donation of equipment and for his

advice, to Dr. William F. Barry and Dr. A. P. Sanders for their advice and suggestions, and to Mrs. Nina Goble for the many expertly done scans.

REFERENCES

1. ALTSHULER, B., YARMUS, L., PALMES, E. D., and NELSON, N. Aerosol deposition in human respiratory tract. I. Experimental procedures and total deposition. *A.M.A. Arch Indust. Hyg.*, 1957, *15*, 293–303.
2. ANDREWS, A. H., JR., JENSIK, R., and PFISTERER, W. H. Fluoroscopic pulmonary densitography. *Dis. Chest*, 1959, *35*, 117–126.
3. BALL, W. C., JR., STEWART, P. B., NEWSHAM, L. G. S., and BATES, D. V. Regional pulmonary function studied with xenon-133. *J. Clin. Invest.*, 1962, *41*, 519–531.
4. BIRD, F. M. Bird Corporation, Palm Springs, California. Personal communication.
5. DAUTREBANDE, L. Microaerosols: Physiology, Pharmacology, Therapeutics. Academic Press, Inc., New York, 1962.
6. DAUTREBANDE, L., and WALKENHORST, W. Deposition of microaerosols in human lung with special reference to alveolar spaces. *Health Physics*, 1964, *10*, 981–993.
7. DWORKIN, H. J., HAMILTON, C., SIMECK, C. M., and BEIERWALTES, W. H. Lung scanning with colloidal RISA. *J. Nuclear Med.*, 1964, *5*, 48–57.
8. DYSON, N. A., HUGH-JONES, P., NEWBERY, G. R., SINCLAIR, J. D., and WEST, J. B. Studies of regional lung function using radioactive oxygen. *Brit. M. J.*, 1960, *1*, 231–238.
9. FINDEISEN, W. Über das Absetzen kleiner, in der Luft suspendierter Teilchen in der menschlichen Lunge bei der Atmung. *Arch. ges. Physiol.*, 1935, *236*, 367–379.
10. JACOBAEUS, H. C., FRENCKNER, P., and BJÖRKMAN, S. Some attempts at determining volume and function of each lung separately (bronchospirometry): preliminary report. *Acta med. scandinav.*, 1932, *79*, 174–207.
11. KNIPPING, H. W., BOLT, W., VENRATH, H., VALENTIN, H., LUDES, H., and ENDLER, P. Eine neue Methode zur Prüfung der Herz- und Lungenfunktion. *Deutsche med. Wchnschr.*, 1955, *80*, 1146–1147.
12. KOURILSKY, R., and MARCHAL, M. Le cancer primitif du poumon et la cinédensigraphie. Fourth International Congress on Diseases of the Chest, Cologne, 1956.
13. KRISS, J. P. Radioisotope scanning in medical diagnosis. *Ann. Rev. Med.*, 1963, *14*, 381–406.
14. LANDAHL, H. D. On removal of air-borne droplets by human repiratory tract. I. Lung. *Bull. Math. Biophys.*, 1950, *12*, 43–56.
15. MERCER, T. T. Aerosol production and characterization: some considerations for improving correlation of field and laboratory derived data. *Health Physics*, 1964, *10*, 873–887.
16. MITCHELL, R. I. Retention of aerosol particles in respiratory tract: review. *Am. Rev. Resp. Dis.*, 1960, *82*, 627–639.
17. ODERR, C., KIRKLEY, D., and GOLDSTEIN, M. Fluorodensimetry as used to detect regional impairment of lung function. *Bull. Tulane Med. Fac.*, 1962, *21*, 61–64.
18. PIRCHER, F. J., HORN, E. G., REEVES, R. J., and BUFFALOE, T. Design and properties of whole body scanner at Duke. To be published.
19. Proceedings of the Hanford Symposium on Inhaled Radioactive Particles and Gases, Richland, Washington, May 4–6, 1964. *Health Physics*, 1964, *10*, 861–1259.
20. QUIMBY, E. H., and FEITELBERG, S. Radioactive Isotopes in Medicine and Biology: Basic Physics and Instrumentation. Second edition. Lea & Febiger, Philadelphia, 1963, p. 113.
21. QUINN, J. L., III, WHITLEY, J. E., HUDSPETH, A. S., and WATTS, F. C. Approach to scanning of pulmonary infarcts. *J. Nuclear Med.*, 1964, *5*, 1–8.
22. Report of ICRP Committee on Permissible Dose for Internal Radiation, 1959. *Health Physics*, 1960, *3*, 125, 151.
23. SMALL, M. J., MILLER, W. N., LEINER, G. C., STRAUSS, H. D., and ABRAMOWITZ, S. Radiopulmonography: simple method for simultaneous estimation of individual lung function. *J. Nuclear Med.*, 1961, *2*, 249–252.
24. WAGNER, H. N., JR., MCAFEE, J. G., and MOZLEY, J. M. Medical radioisotope scanning. *J.A.M.A.*, 1960, *174*, 162–165.
25. WAGNER, H. N., JR., SABISTON, D. C., JR., IIO, M., MCAFEE, J. G., MEYER, J. K., and LANGAN, J. K., Regional pulmonary blood flow in man by radioisotope scanning. *J.A.M.A.*, 1964, *187*, 601–603.
26. WEST, J. B., and DOLLERY, C. T. Distribution of blood flow and ventilation-perfusion ratio in lung, measured with radioactive $CO_2$. *J. Appl. Physiol.*, 1960, *15*, 405–410.
27. WILSON, I. B., and LAMER, V. K. Retention of aerosol particles in human respiratory tract as function of particle radius. *J. Indust. Hyg. Toxicol.*, 1948, *30*, 265–280.

# TECHNETIUM 99m NORMAL BRAIN SCANS AND THEIR ANATOMIC FEATURES

*By* MILO M. WEBBER, M.D.
LOS ANGELES, CALIFORNIA

BRAIN scanning is based on the fact that certain substances normally do not diffuse into the substance of the normal brain, but pass through, staying within the blood vascular system. A number of such substances, tagged with radioactive tracers, have been described. Notable ones include diiodofluorescein, serum albumin, chlormerodrin, and pertechnetate. These substances, after finding their way into the blood stream, can be used to outline the normal structures of the head. The brain is seen as an area of a lack of activity.

Areas of uptake within the brain itself reflect a breakdown of the blood-brain barrier secondary to tumor, infarction, or infection. Areas of increased vascularity within the brain also appear as areas of increased uptake and may be secondary to tumor.

This paper concerns itself with the normal pattern of activity seen with brain scanning done with pertechnetate, one of the most recently used brain scanning agents.

Technetium is an artificial element which is truly a product of the atomic age. It was discovered in 1937 by Segré and Perrier,[3] while bombarding molybdenum with either neutrons or deuterons.

It is a member of the manganese series and as such is a very near neighbor to the halogens. In its most readily available form, pertechnetate ion, it behaves remarkably similar to perchlorate and the iodide ion, with respect to its ability to be concentrated in the salivary glands, gastric mucosa, thyroid and other areas of the human body.

Because of the fact that the element is artificial and of relatively short half life, little has been written regarding its chemical compounds and its chemical toxicity. However, due to the very small amount of actual technetium required in clinical procedures (less than .002 $\mu$g.), it has generally been tacitly assumed that chemical toxicity can not become a problem. This appears to be borne out in clinical applications thus far. Radiation toxicity can be estimated by calculation of radiation dose delivered to the patient when the brain is examined by the use of 10 mc of $Tc^{99m}$. This calculation has been performed by many[1,4] and estimated doses are in the order of 100 mr total body dose. Target organ doses are in the order of: thyroid, 1 rad; gastric mucosa, .8 rad; liver, .7 rad; and large bowel, 1 rad for intravenous administration. The daughter product $Tc^{99}$ is present in an amount of about $10^{-6}$ $\mu$c from a dose of 10 mc $Tc^{99m}$. This is considered a negligible amount.

## METHOD

Technetium is now available from many commercial sources as well as Brookhaven National Laboratory in the form of a column of alumina upon which is adsorbed $Mo^{99}$ in the form of molybdate. By eluting this column with 0.1 *N* HCl, pertechnetate ion may be separated from the molybdate with minimal contamination by $Ru^{103}$ and $I^{131}$.

The eluate is caught in a vial filled with appropriate amounts of pyrogen-free 0.1 *N* NaOH and pyrogen-free physiologic phosphate buffer. The pH is checked by placing a drop on narrow range pH paper. The bottle is capped and autoclaved. Oral administration has been used, which avoids pyrogen-free sterile technique, but which yields slightly less activity within the brain and a higher dose to the gastrointestinal tract.

In this laboratory brain scanning is

started approximately 15 minutes after injection. Longer times have been advocated by some;[1] others suggest immediate scanning.[2] The question of the appropriate time to scan does not appear to be a settled issue. Optimum time may perhaps be a function of cerebral circulation times, extent of break-down of the blood-brain barrier, and/or nature of the tumor, and ability of kidneys to excrete the pertechnetate ion.

The accompanying scans were obtained with a Nuclear Chicago Photo Dot scanner which was set at the $Tc^{99m}$ peak of 140 kev. It uses a 3 inch diameter$\times$2 inch thick thallium activated NaI crystal.

We have attempted to achieve the best possible pictorial representation consistent with patient comfort and time limitations. A scan speed of 45–60 cm./min. is what is usually employed. Spacing of $\frac{1}{8}$ inch, scanning in both directions, and 20–30 per cent background cut-off are used, depending on activity differentials noted.

Using this technique, approximately 15 minutes is required per view. In most instances this is well tolerated by the patient. It represents about one-third of the time required for $Hg^{203}$ chlormerodrin and/or RISA scanning. Collimators with greater resolution capabilities have been tried from time to time with no other change in the procedure. The 37 hole collimator for example yields pictures which appear coarse and blotchy. Unless $2\frac{1}{2}$ or more times the dose is given or $2\frac{1}{2}$ or more times as slow a speed is used, the information composing the scan suffers from a statistical variation which can and usually does negate any increased resolution benefit arising from the use of the 37 hole collimator. The same holds true of the 61 hole collimator except that a factor of 6 or more applies.

A comparison of the type of pictorial representation of the head with $Hg^{203}$ and with $Tc^{99m}$ is revealing. When both are employed in the usual amounts, the irregular blotchy black and white pattern of the $Hg^{203}$ scan is a reflection of the marked statistical variation at the low count rates encountered. The $Tc^{99m}$ scan has an even, uniform appearance, largely devoid of the statistical changes. Because of this feature, it now becomes possible to appreciate certain anatomic landmarks which were, to a large extent, hidden with previous scanning agents.

It now behooves the interpreter of brain scans to attempt to evaluate all aspects of the image. It is granted that, at present, there is much speculation as to the significance of certain features of the image. What is presented here, therefore, represents partially unproven opinion and partially fact. In the future, as experience accumulates, the comments expressed in this paper will most certainly have to be modified.

## ANATOMIC CONSIDERATION OF NORMAL BRAIN SCANS

Figure 1, *A* and *B* shows a typical front view of the head with the collimator focal plane at a distance of approximately 4 cm. beneath the skin surface. The scan is labeled as to significance of the various portions. The characteristic pattern is formed by the skull outline representing activity within the diploë, meninges, and superficial arteries. The midline activity represents midline vascularity, including the anterior cerebral arteries.

Figure 2, *A* and *B* shows a side view of the skull with, again, the focal plane about 4 cm. beneath the skin surface. This means that all structures on either side of this plane will be enlarged and shown with less resolution than if they were located on the plane. The typical pattern of activity of the diploë, superior sagittal sinus, confluence of the sinuses, and lateral sinuses is shown. Activity in the lower middle area represents the activity in the cavernous sinus and overlying temporalis muscle.

Figure 3, *A* and *B* shows a posterior view of the skull. The confluence of the sinuses is clearly apparent as are the sagittal and lateral sinuses which contribute to it. At times, an area of decreased density can be seen in the confluence which represents the occipital protuberance.

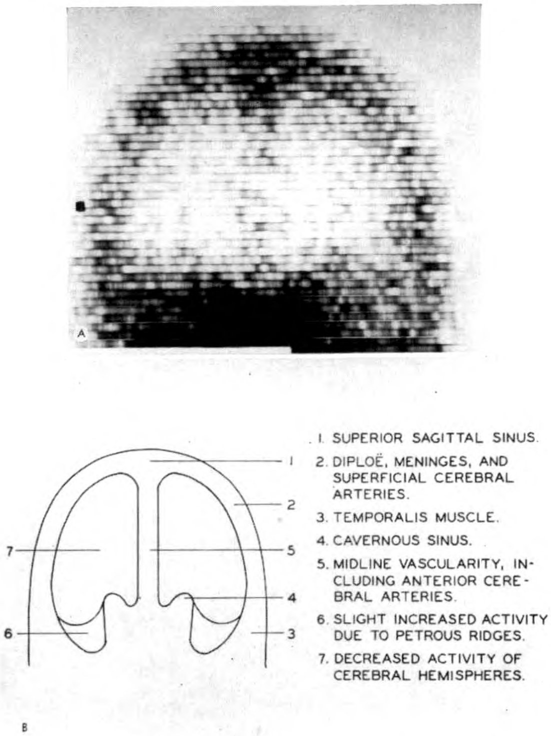


FIG. 1. (*A* and *B*) Typical front view of head with the collimator focal plane at a distance of approximately 4 cm. beneath the skin surface.

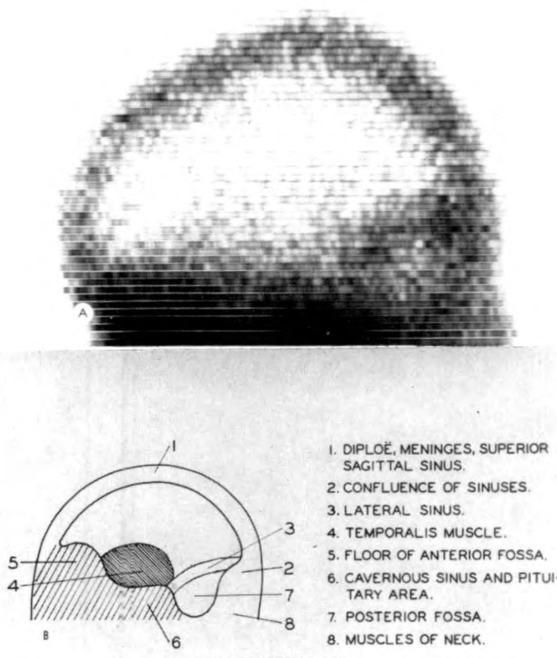


FIG. 2. (*A* and *B*) Side view of skull with the focal plane about 4 cm. beneath the skin surface.

Figure 4, *A* and *B* is the lateral view of the skull of a small child. Here the focal distance factors may be much more important because of the smaller diameter of the head.

The area marked by 4 indicates increased activity which cannot be clearly explained. It may be that this represents choroid plexus. Anomalous drainage of the venous system may also cause lateralization of increased activity. This observation has been made by us in 2 children who have no angiographic evidence of abnormality in this region.

Figure 5, *A* and *B* shows a lateral view of the skull with an area of increased activity, which apparently is due to venous lakes found in this same area on the lateral skull roentgenograms.

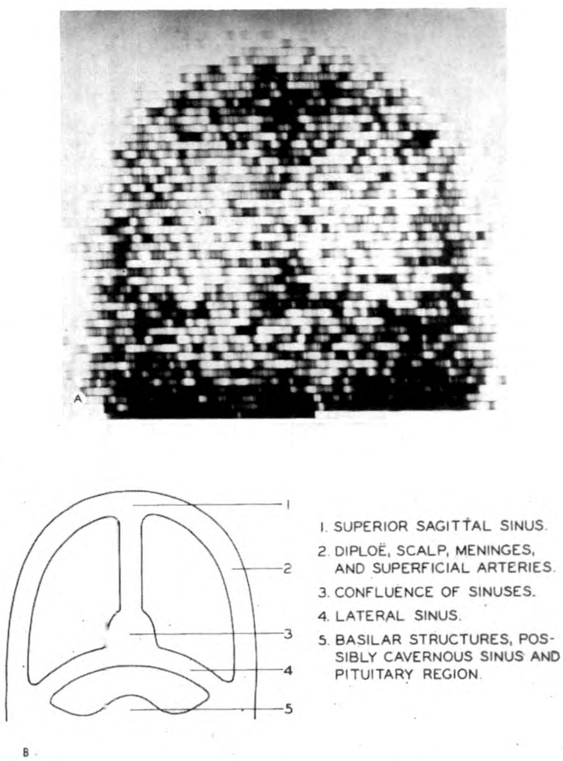


FIG. 3. (*A* and *B*) Posterior view of skull.

SUMMARY

The advent of greater apparent detail brain scanning using Tc$^{99m}$ makes it neces-

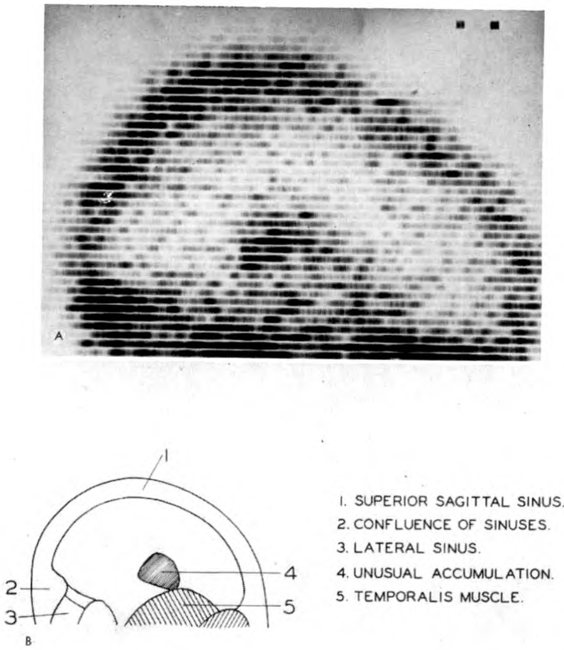


Fig. 4. (*A* and *B*) Lateral view of the skull of a small child; right side up.

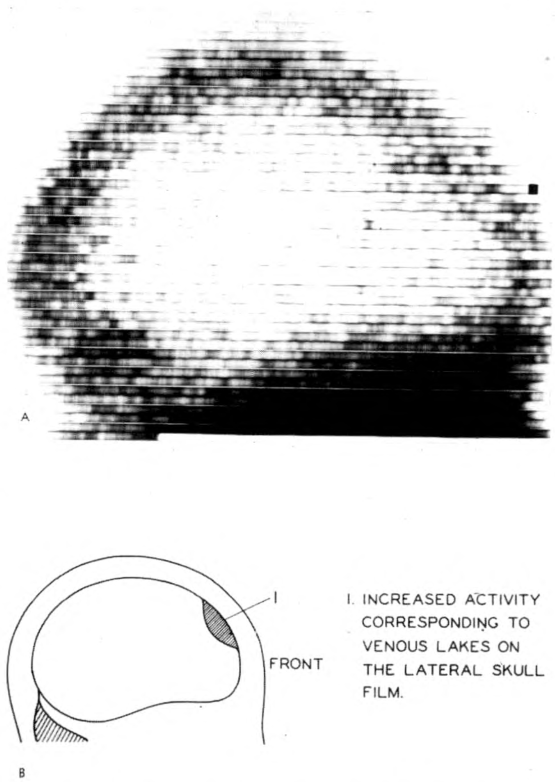


Fig. 5. (*A* and *B*) Lateral view of skull showing an area of increased activity.

sary to explain more of the detail of the pictures obtained. An anatomic consideration of normal brain scans is presented.

Department of Radiology
Center for the Health Sciences
University of California
Los Angeles, California 90024

The author thanks Frank Connon for his help with the illustrations.

REFERENCES

1. Harper, P. V., Beck, R., Charleston, D., and Lathrop, K. A. Optrinization of a scanning method using $Tc^{99m}$. *Nucleonics*, 1964, *22*, 50–54.
2. Hillig, B. J., Fink, R. A., Beck, R. N., Harper, P. V., and Charleston, D. B. Brain scannings using $Tc^{99m}$ and a new rapid scanning technique. Presented at Annual Meeting of Radiological Society of North America, Chicago, 1964.
3. Lange, N. A. Handbook of Chemistry. McGraw-Hill Book Company, Inc., New York, 1961, p. 86.
4. McAfee, J. G., Fueger, C. F., Stern, H. S., Wagner, H. N., Jr., and Migita, T. $Tc^{99m}$ pertechnetate for brain scanning. *J. Nuclear Med.*, 1964, *5*, 811–827.

# CORRELATION OF BRAIN SCANS AND ANGIOGRAPHY IN INTRACRANIAL TRAUMA*

*By* ALBERT J. GILSON, M.D., *and* FREDIE P. GARGANO, M.D.
MIAMI, FLORIDA

THE general usefulness of brain scanning in the diagnosis and management of patients with intracranial neoplastic lesions has gained wide acceptance as a clinical method.[2,4,5] The potential value of this procedure has not been fully exploited in the screening of patients sustaining trauma to the head. The systematic use of routine brain scanning in our clinic has been of major importance in detecting intracranial lesions of traumatic etiology. It is the purpose of this presentation to indicate the lesions of traumatic etiology we have found amenable to brain scanning, to present the salient diagnostic features of these lesions as found on the scan and to correlate the scans with conventional angiographic techniques.

## CLINICAL MATERIAL AND METHOD

A series of 73 patients with positive neurologic findings and suspected intracranial lesions following acute trauma was studied over a 14 month period. Only patients with questionable lesions were examined. Those patients in acute distress or with classic evidence of pathology were handled as emergencies by classic diagnostic and therapeutic techniques. Three commercially available scanning instruments were utilized for all diagnostic radioisotopic procedures. The majority of the scans was performed with two Nuclear-Chicago Pho-Dot scanners utilizing a 19 hole focusing collimator. The scan speed was set at 32 cm. per minute. The spectrometer of this instrument was modified in our laboratory so that the window width was continuously variable between 5 and 15 per cent of the full scale energy. Five per cent was selected for all brain scans utilizing either mercury 197 or mercury 203 neohydrin. A Picker Magnascanner was the third clinical instrument utilized. A 19 hole focusing collimator was employed at a scan speed of 28 cm. per minute. For mercury 203 neohydrin, the spectrometer window was set at 250–300 kv. Utilizing mercury 197 neohydrin, the spectrometer was set to include energies between 60–90 kv.

Scanning techniques were preceded by a renal blocking dose of 1 cc. mercuhydrin as suggested by Blau and Bender.[1] In adults mercury 203 neohydrin was utilized. In an attempt to minimize the total radiation dose delivered to the total body as well as the renal system, mercury 197 neohydrin was utilized in all patients below 16 years of age.[3]

Scanning commenced 2 hours after injection of the radioisotopic compound. Usually, two projections were sufficient for diagnosis. An anteroposterior view was used initially. Based on this view, a lateral examination was made on the side suggesting pathologic localization of the radiomercury. Additional views were employed when deemed necessary.

## RESULTS

Of the 73 patients studied, 28 patients had positive localizing lesions. Of these 28 patients, 22 subsequently underwent arteriography and 18 had surgical procedures. The 6 patients not undergoing arteriography clinically suffered from cerebral contusions and were followed and eventually discharged without further treatment. Of the 18 patients who underwent surgery, 1 had a chronic epidural hematoma, 14 had

* Presented at the Sixty-fifth Annual Meeting of the American Roentgen Ray Society, Minneapolis, Minnesota, September 29–October 2, 1964.
From the Department of Radiology, Jackson Memorial Hospital and University of Miami Medical School, Miami, Florida.

subdural hematomas, 2 had intracerebral hematomas and 1 had massive anterior cerebral infarction secondary to surgical transection of the nutrient artery. To our knowledge there have been no false negative scans. No patient with a negative scan was later found to have an intracranial lesion on follow-up examination. There was 1 case which was reported as a contusion on the brain scan and which was later diagnosed as unilateral subdural hematoma at arteriography. There were 2 false positives which were interpreted as subdural lesions on the basis of the scan but had negative arteriograms. These cases were felt to be contusions in retrospect.

ILLUSTRATIVE CASES

*Normal Brain Scan.* Because of the wide variation of brain scans produced by different scanning apparatus as well as individual techniques and preferences, an example of a normal scan from our laboratory is shown in Figure 1. The anteroposterior view demonstrates symmetry of the right and left portions of the scan, which in the normal state should approach mirror images. The area occupied by the brain appears as a relatively clear or low count rate area. The vascular structures of the scalp are seen as areas of increased density outlining the shape of the head. We feel that a sufficient count rate should be obtained such that the over-all outline of the head is presented without the necessity for "drawing in" the outline of the skull. Excess suppression will cause missed lesions; many times the count rate obtained from the subdural membrane will not be appreciably greater than the scalp activity.

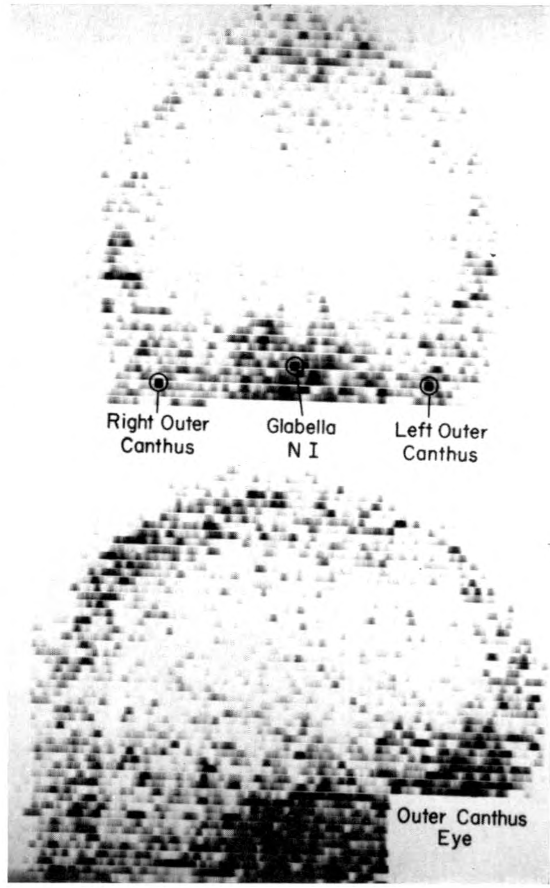


Fig. 1. Normal brain scan.

*Unilateral Subdural Hematoma* (Fig. 2, *A* and *B*). Although there may be exceptions, patients harboring blood clots on the surface of the brain, either epidural or subdural, present an anterior scan showing a massive uptake of radioactive material along the affected lateral portions of the brain. There is a definite asymmetry between the affected and contralateral normal peripheral area. This crescentic area of increased activity is characteristic of subdural hematoma and to our knowledge does not occur to this degree in any other abnormality detectable by brain scanning. The lateral scan frequently appears normal or may have a diffusely increased area of activity which has no specific site localization.

*Bilateral Subdural Hematoma* (Fig. 3; and 4, *A* and *B*). Patients with bilateral chronic subdural hematoma can pose additional problems due to symmetry of the abnormality on the brain scan. These lesions, however, demonstrate bilateral crescentic thickening of the normally thin areas of peripheral activity. The lateral scan in chronic bilateral subdural hematoma is somewhat characteristic as evidenced by

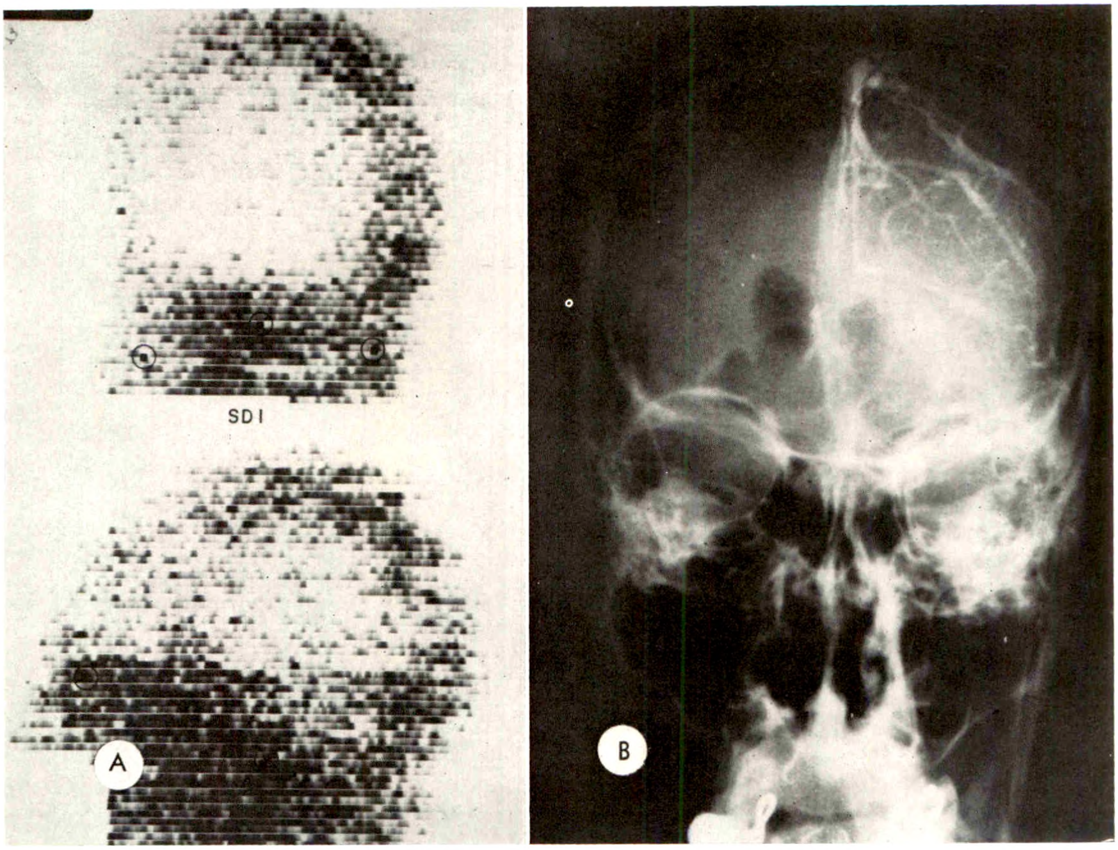


Fig. 2. Case i. (*A* and *B*) Left subdural hematoma.

the abnormally high concentration of activity diffusely scattered in the normally

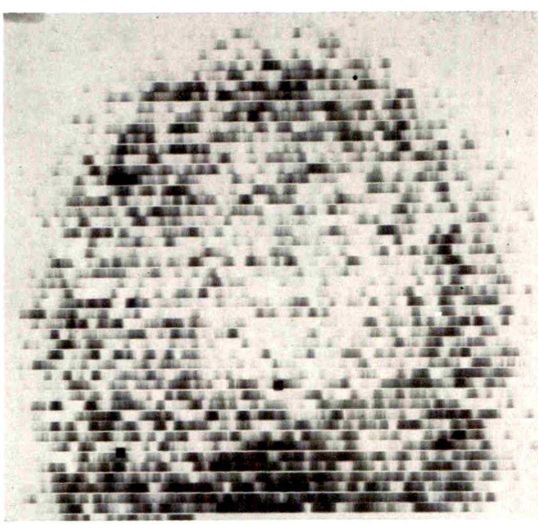

Fig. 3. Case ii. Bilateral subdural hematoma.

clear cerebral areas. In some cases a combined lesion as, for example, a subdural hematoma with an associated intracerebral hematoma, can be suspected on the basis of the lateral scan.

*Epidural Hematoma* (Fig. 5; and 6, *A* and *B*). To date, we have not had sufficient cases of epidural hematoma to assign any specific diagnostic features to the process. At this time, we feel that the epidural hematoma is indistinguishable from the subdural hematoma by scan. The differential diagnosis between the two lies primarily in the arteriographic and postoperative findings.

*Intracerebral Hematoma* (Fig. 7; and 8, *A* and *B*). The intracerebral hematoma is quite distinctive in character from the other abnormalities presented in this paper. Its location is usually well within the sub-

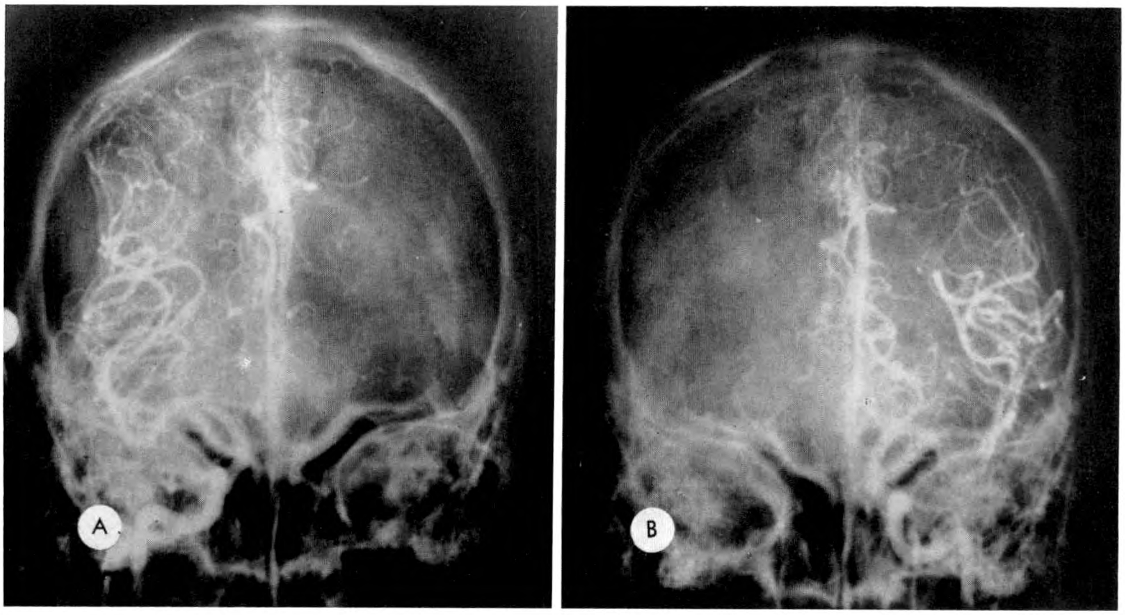


Fig. 4. Case II. Bilateral subdural hematoma. (*A*) Right and (*B*) left carotid arteriograms.

stance of the cerebral cortex and it is more localized in appearance. It can be differentiated from tumor and infarction by its variable distribution and irregular pattern.

*Cerebral Contusion* (Fig. 9, *A* and *B*). In contrast to the subdural hematoma, the cerebral contusion generally presents a more localized area of radioactive uptake on both the anterior and lateral scans. The majority of our contusions have appeared in the lateral aspects of the temporal lobe and a significant number have been on the side opposite to the direct trauma indicating contrecoup injuries. Generally, a contused area of the brain appears to resolve within 6 to 10 weeks, with the scan reverting to normal.

*Cerebral Infarction* (Fig. 10, *A* and *B*; 11, *A* and *B*; and 12, *A* and *B*). The cerebral infarct has two distinctive characteristics

Fig. 5. Case III. Left epidural hematoma.

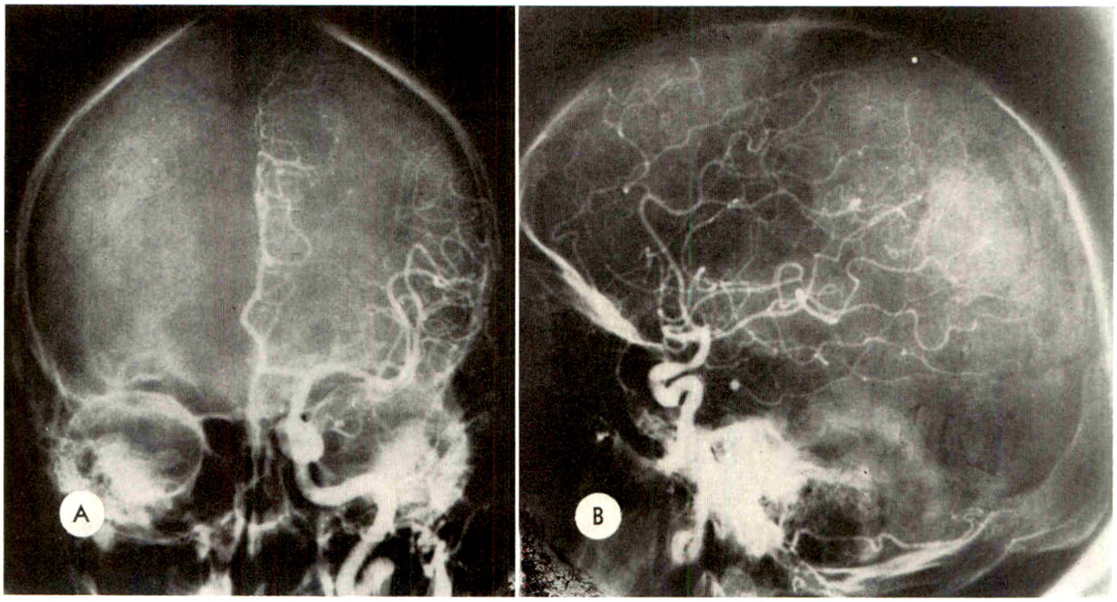


Fig. 6. Case iii. Left epidural hematoma. (*A* and *B*) Left carotid arteriograms.

that set this lesion apart from those previously mentioned: (1) the affected area has an unusually intense pickup of the radioactive compound; (2) the area of radioisotopic concentration follows a familiar geographic distribution coinciding with an area of the brain served by a principal nutrient artery. In the case presented, Figure 10*A* demonstrates the preoperative findings. A metastatic tumor in the area of the anterior fossa is noted. At the time of surgery, the anterior cerebral artery was transected in the process of removing this lesion. Figure 10*B* shows the brain scan 12 hours postoperatively; the infarct is clearly demonstrated on the scan. Figures 11, *A* and *B*, and 12, *A* and *B* are the pre- and postoperative arteriograms. It can be seen that the postoperative arteriograms show lack of filling of the anterior cerebral artery on the affected side.

### KINETICS OF RADIOISOTOPIC LOCALIZATION

It is assumed that localization of radioactive compounds by intracranial neoplasm results from a selective breakdown of the normal blood-brain barrier in the area of pathology. This barrier breakdown then

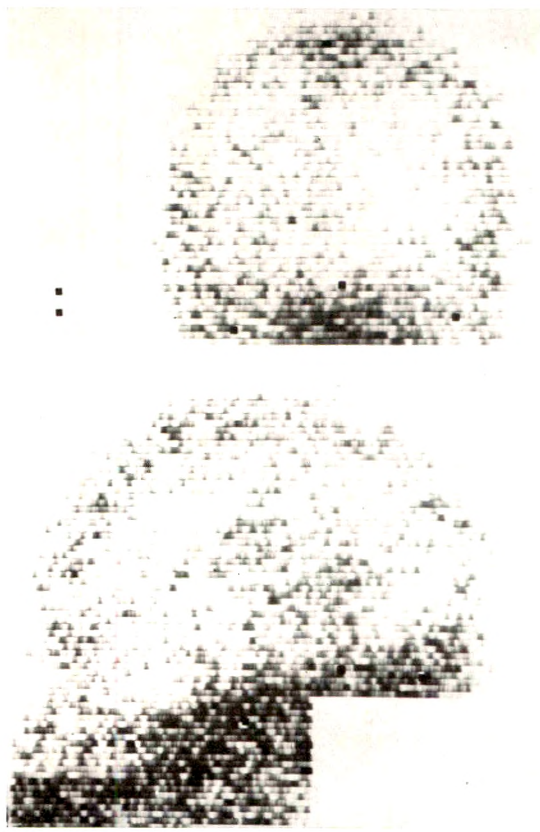

Fig. 7. Case iv. Intracerebral hematoma.

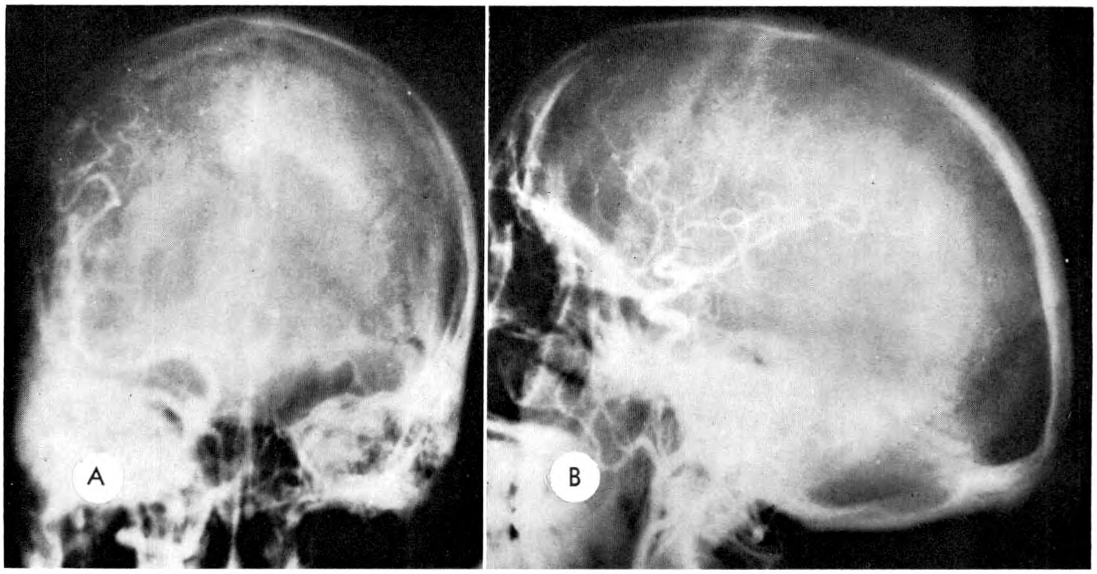


FIG. 8. Case IV. Intracerebral hematoma. (*A* and *B*) Right carotid arteriograms.

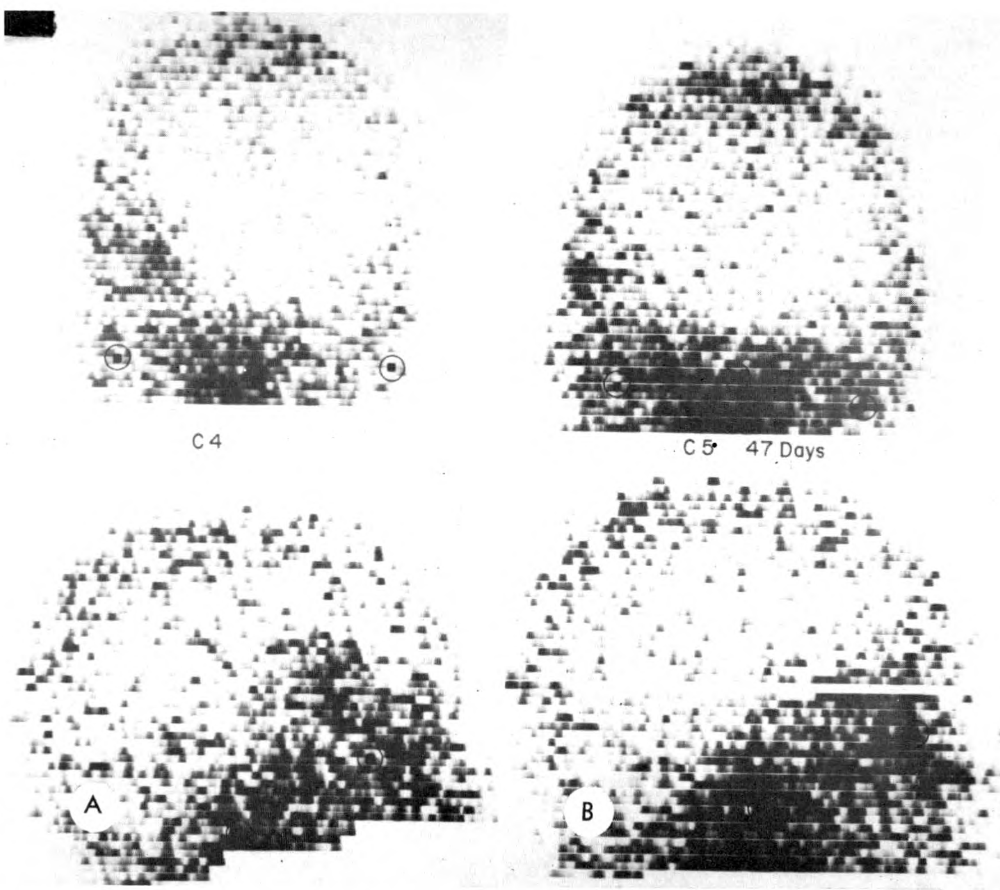


FIG. 9. Case V. Left cerebral contusion. (*A*) Scan made 24 hours post trauma. (*B*) Scan made 47 days later. Note marked resolution of lesion.

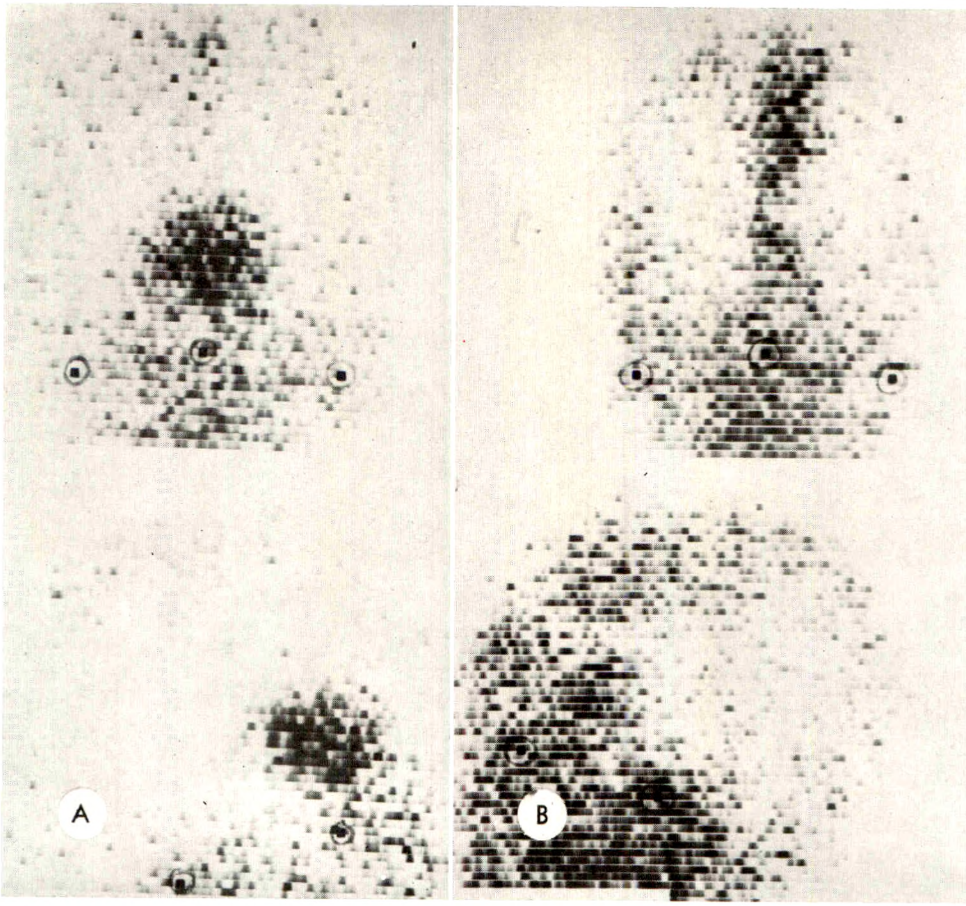


Fig. 10. Case vi. (*A*) Preoperative brain scan. Note large metastatic lesion in area of anterior fossa. (*B*) Right postoperative brain scan. Note large localization in area served by anterior cerebral artery.

permits the entry of normally rejected compounds into the cerebral tissues. The entry of radiomercury into the areas of contusion, infarction and intracerebral hematoma probably follows a similar pathogenesis. Collection of radioactivity in subdural hematoma appears to follow a somewhat different route. We have collected samples of subdural fluid and subdural membrane at the time of surgery and exposed them to assay for radioactive content. In all cases the subdural membrane has yielded a most significant accumulation of radioactivity with the subdural fluid itself being relatively free of radioactivity. Mealey[6] has carried this work further under laboratory conditions and produced excellent experimental data which confirm the above. It would seem then that subdural lesions with definite membrane formation are most amenable to detection by the brain scanning.

SUMMARY

The radioisotopic cerebral scan is a valuable adjunctive method in the diagnosis and measurement of intracranial lesions secondary to trauma. The scan does not, however, replace any of the accepted diagnostic radiographic techniques. The principal advantage of the scan lies in its capability to serve as an innocuous screening procedure on patients with equivocal neurologic findings. By initially screening our patients with brain scans, we were able to limit our final series of patients undergoing angiography to roughly half of the original group. At this stage of develop-

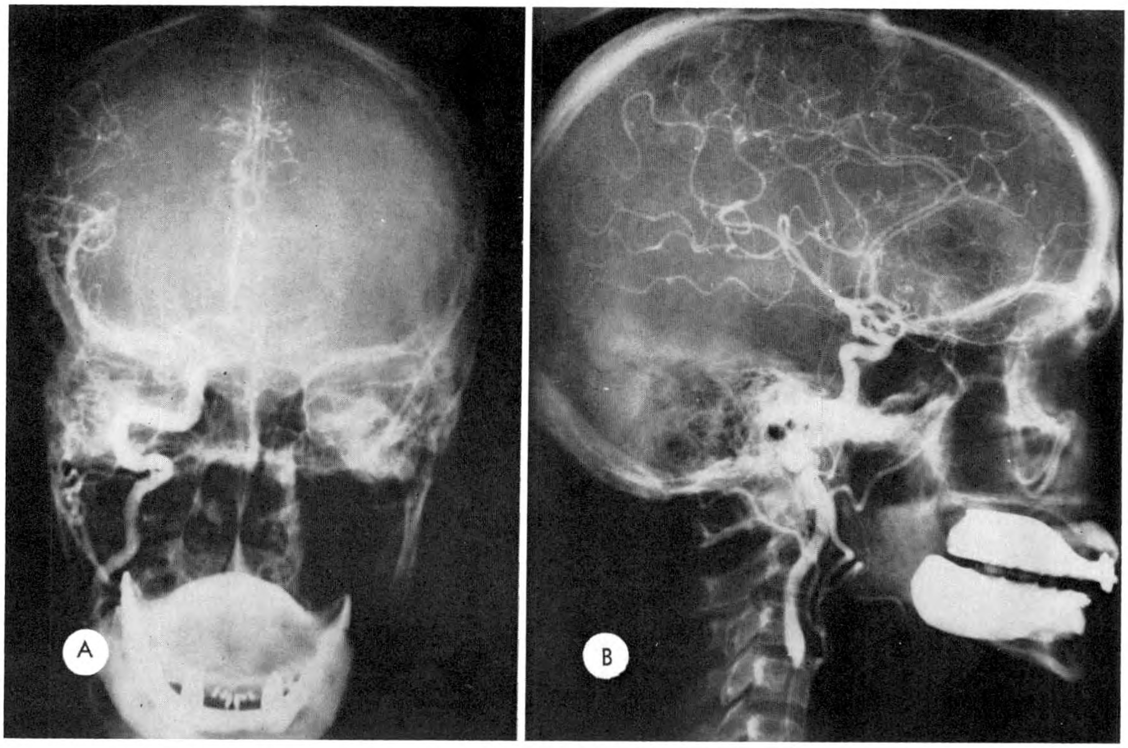


FIG. 11. Case VI. (*A* and *B*) Preoperative right carotid arteriograms. Note filling of left anterior cerebral artery. The metastatic anterior fossa lesion is well demonstrated.

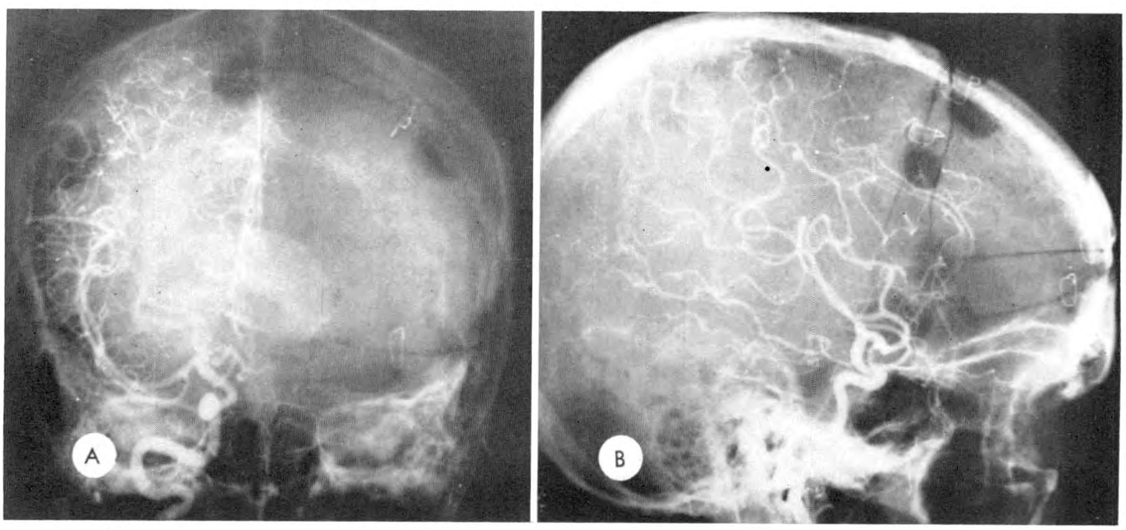


FIG. 12. Case VI. (*A* and *B*) Postoperative right carotid arteriograms following surgical transection and liga tion of left anterior cerebral artery.

ment we strongly feel that, once a lesion has been detected by scanning, further, more established diagnostic procedures, such as angiography, should be performed and indeed are of great importance.

Albert J. Gilson, M.D.
Department of Radiology
University of Miami
School of Medicine
Miami, Florida 33136

REFERENCES

1. BLAU, M., and BENDER, M. A. Radiomercury ($Hg^{203}$) labeled neohydrin: new agent for brain tumor localization. *J. Nuclear Med.*, 1962, *3*, 83–93.
2. GOODRICH, J. K., TUTOR, F. T., and WEBSTER, C. L., JR. Isotope encephalogram. *Mississippi State M. A. J.*, 1963, *4*, 277–283.
3. KING, E. R., and SHARPE, A. R. Visualization of internal organs and tumors by radioisotope photoscanning. *Postgrad. M. J.*, 1963, *34*, 47–57.
4. MCAFEE, J. G., and TAXDAL, D. R. Comparison of radioisotope scanning with cerebral angiography and air studies in brain tumor localization. *Radiology*, 1961, *77*, 207–222.
5. MCCLINTOCK, J. T., and DALRYMPLE, G. V. Value of brain scans in management of suspected intracranial lesions. *J. Nuclear Med.*, 1964, *5*, 189–192.
6. MEALEY, J., JR. Radioisotopic localization in subdural hematomas: experimental study with arsenic-74 and radioiodinated human serum albumin in dogs. *J. Neurosurg.*, 1963, *20*, 770–776.

# MEASUREMENT OF THE MASS OF THE THYROID GLAND *IN VIVO**

*By* J. MYHILL, T. S. REEVE, *and* P. M. FIGGIS
SYDNEY, AUSTRALIA

MEASUREMENT of the mass of the thyroid gland is important for two reasons. Firstly, in definitive treatment with iodine 131, the outcome depends on the radiation dose to the gland, and the least accurately determined factor in the calculation of this dose at the present time is that of the thyroid mass. Secondly, some of the quantitative physiologic findings in the study of nontoxic goiters may be purely mass effects, in contradistinction to specific changes of function, and this could be clarified by a measurement of the thyroid mass.

Three methods of measurement are in use. The mass is most commonly estimated by palpation[12,13] but this is rather subjective and inaccurate. A method of "pneumothyroid" has been developed[3,4] which seems to be capable of comparatively high accuracy, but is a specialized and time consuming procedure. In the third method, attempts are made to calculate the mass of the thyroid by using data obtained from a radioisotope scan. Radioactive iodine is administered to the patient and the thyroid is scanned at a later time to determine its size and shape. Various geometric parameters may be measured on this scan, such as the heights of the lobes, the width of the gland, and the area of the gland; and these parameters may be used in a formula to predict the thyroid mass. This approach involves two major problems; firstly, determining accurately from the scan the borders of the thyroid, and secondly, finding the formula which most accurately predicts the three dimensional volume (or mass) of the thyroid gland from information obtained in one plane only, or, depending on the technique, from two planes.

Reports in the literature concerning the estimation of the mass of the thyroid gland are summarized in Table I, which gives the formulae used, the values of the parameters in each formula, the number of glands analyzed and two measures of the accuracy of prediction. These measures are the difference in grams between the predicted and true mass, and the percentage difference between the predicted and true mass. Data are presented from Williams *et al.*[13] comparing palpation estimates with the true mass, and from 6 groups[1,2,5–8] using the radioisotope scanning technique. A listing of thyroid weights and geometric parameters was not available for the pneumothyroid technique to allow calculation of the differences between predicted and measured masses. This technique is therefore not included in Table I.

The standard deviation of the per cent error is seen to vary greatly, averaging 20 per cent for the isotope methods.

The work described in this paper was undertaken to evaluate thyroid mass estimation by radioisotope scanning using simple equipment and a simple technique.

## MATERIAL

Twenty-five patients who had thyroidectomy for thyrotoxicosis or nontoxic goiter were subjected to sufficient measurements to include in some part or other of the study. Of these, 5 were males and 20 were females; 4 had diffuse thyrotoxic goiter, 2 had multinodular thyrotoxic goiter, 3 had diffuse nontoxic goiter, 13 had multinodular nontoxic goiter, and 3 had not been classified. Table II is a summary of these cases.

The thyroid scans were made using a

* From the Thyroid Investigation Clinic, the Institute of Medical Research, the Royal North Shore Hospital of Sydney, and the Department of Surgery, the University of Sydney, Sydney, Australia.

TABLE I

THYROID GLAND MASS ESTIMATION

| Authors | Formula* | Values of Parameters | No. of Glands Analyzed | $M_{predicted} - M$ (gm.) | | $\frac{M_{predicted} - M}{M}$ (per cent) | |
|---|---|---|---|---|---|---|---|
| | | | | Mean | S.D. | Mean | S.D. |
| Allen and Goodwin[1] | $M = k.A.h.$ | $k = 0.323$ | 10 | −0.44 | 3.9 | −0.76 | 12.0 |
| Goodwin *et al.*[5] | $V = k.AL$ | $k = 0.32$ | 4 | 4.80 | 4.7 | 5.92 | 2.6 |
| Kelly[7] | $M = H_{max} \times A^2 \times k$ (mass of lobe) | $k = 0.32$ | 15<br>15† | 23.12<br>0.81 | 23.4<br>4.0 | 49.05<br>8.43 | 40.8<br>30.6 |
| Libby[8] | $M = k.A^2h_{ave}$ | $k = 0.23$ | 15 | −0.26 | 16.0 | 6.41 | 29.3 |
| Himanka and Larsson[6] | $V = k(\sqrt{A})^3$ | $k = 0.33$ | 44† | 0.16 | 6.3 | 0.09 | 19.4 |
| Burkinshaw[2] | $M/h = k_1W^2 - k_2$ | $k_1 = 0.238$<br>$k_2 = 1.817$<br>if $h$ is average height of two lobes | 9 | −5.52 | 17.0 | −5.8 | 19.8 |
| Williams *et al.*[13]‡ | Palpation estimate | | 41 | 0.22 | 15.4 | 4.3 | 22.2 |

* Parameters taken from radioisotope scans of the thyroid, except where otherwise indicated.
† Visual outlines used.
‡ Palpation estimates. Observed weight of thyroid gland was not corrected for thyroid tissue left in neck.

simple automatic scintillation scanning machine* by methods previously reported by Myhill *et al.*[10]

## METHOD

Iodine-131 was administered to the patient 1 or 2 days before thyroidectomy and an *in vivo* thyroid scan was made, generally the afternoon before the operation was scheduled. At operation, great care was exercised to remove the thyroid gland, or such part of it as was judged necessary to be removed, in one complete piece. The technique of the operation has been previously described.[11] The thyroid was weighed and then carefully set upon a glass plate in the same position as it was in the patient's neck. An anteroposterior photograph of the gland was taken and a scan was made. Two days later, the thyroid tissue remaining in the patient's neck was also scanned *in vivo.* Figure 1, *A–D* shows the *in vivo* scan before operation, the estimated outline of the gland, the photograph of the excised gland, and the scan of the gland of Patient 24.

Firstly, using the corrected gland mass and the corrected gland dimensions taken from the photographs, an attempt was made to predict the gland mass from the photographic dimensions. The corrections referred to here are, of course, those necessitated by the fact that not all of the thyroid gland was removed in most cases. Surgeons' estimates of the amount of thy-

* N.R.D. Instrument Co., St. Louis, Mo.

Table II

PATIENT MATERIAL*

| Serial No. | Age | Sex | Thyroid State | Goiter Type† | Clinical Goiter Size Grading‡ | Thyroid Mass Surgically Removed (gm.) | Estimated§ Total Thyroid Mass (gm.) |
|---|---|---|---|---|---|---|---|
| 3 | 54 | F | Euthyroid | N | +2 | 29 | 34.7 |
| 33 | 54 | M | Euthyroid | N | +1 | 25 | 40.0 |
| 16 | 36 | F | Euthyroid | N | +2 | 38 | 42.2 |
| 12 | 29 | F | Hyperthyroid | — | 0 | 37 | 42.3 |
| 14 | 32 | F | Euthyroid | N | +2 | 33 | 44.0 |
| 36 | 53 | F | Euthyroid | N | +1 | 48 | 56.5 |
| 22 | 38 | F | Euthyroid | N | +1 | 53 | 60.0 |
| 34 | 34 | F | Hyperthyroid | D | +2 | 54 | 61.7 |
| 32 | 32 | F | Hyperthyroid | D | +3 | 58 | 64.4 |
| 18 | 37 | F | Euthyroid | N | +3 | 58 | 70.6 |
| 35 | 19 | F | Hyperthyroid | D | +2 | 82 | 96.5 |
| 19 | 29 | F | Hyperthyroid | N | +3 | 85 | 100.0 |
| 20 | 65 | F | Euthyroid | N | +3 | 99 | 104.2 |
| 7 | 63 | F | Euthyroid | N | +3 | 100 | 105.3 |
| 2 | 48 | M | Euthyroid | D | +3 (intra) | 117 | 117.0 |
| 24 | 29 | M | Hyperthyroid | N | +3 | 106 | 151.4 |
| 1 | 44 | M | Euthyroid | N | +3 (intra) | 155 | 155.0 |
| 4 | 68 | F | Euthyroid | N | +4 (intra) | 172 | 181.1 |
| 13 | — | M | Euthyroid | N | +3 | 195 | 195.0 |
| 27 | 53 | F | Euthyroid | N | +3 (intra) | 168 | 202.4 |
| 28 | 51 | F | Euthyroid | D | +3 (intra) | 177 | 208.2 |
| 37 | 48 | F | Euthyroid | D | +3 | 201 | 236.4 |
| 10 | — | F | Hyperthyroid | D | +2 | 252 | 252.0 |
| 21 | 70 | F | Euthyroid | — | +3 (intra) | 252 | 265.3 |
| 39 | 64 | M | Euthyroid | N | +1 (intra) | 98 | — |

* A total of 35 patients were studied, but in 11 of these the surgeon did not feel that an accurate estimate of tissue left *in situ* was possible.

† N = multinodular, D = diffuse.

‡ Size in neck graded as 0, +1, +2, +3 or +4, see text; "intra" signifies intrathoracic goiter.

§ Weighed excised gland plus surgeon's estimate of amount left *in situ*.

roid tissue left and where it was left were used as correction factors to the weighed excised gland and measured photographic dimensions of the excised gland.

Secondly, the outlines of the scans of the excised glands were determined visually, by simply drawing in a line which appeared to be the border of the thyroid gland on the scan. The dimensions of the excised glands as determined from these drawings on the scans were then compared with the dimensions on the photographs. This afforded some measure of the accuracy of determining the borders of the thyroid gland from the radioisotope scan.

Finally, the dimensions of the whole thyroid gland before operation, as determined visually from the radioisotope scan, were used in formulae in an effort to predict the total *in vivo* mass; this was then compared with the corrected weighed mass.

## RESULTS

### THYROID CLINICAL SIZE GRADING

The thyroid glands were graded empirically into a rough classification as follows: 0 = no enlargement of the thyroid, or with only the isthmus palpable; +1 = lateral lobes clearly palpable but not visible; +2 = moderate and visible enlargement of

the thyroid; +3 = considerable palpable and visible enlargement of the thyroid; and +4 = gross enlargement. The size grading and the corrected gland mass are compared in Table III, where it is seen that there is a consistent increase in the average mass with increasing clinical size grading.

#### PHOTOGRAPHIC PREDICTION OF GLAND MASS

In this comparison and the several described below, a number of different formulae was examined for predicting gland mass from the dimensions of the gland when viewed frontally. These formulae fell into two classes: (1) simple proportionality formulae and (2) regression equations. The first class is really a special case of the second class, namely, when the constant in the regression equation is zero. The formulae are listed in detail in the Appendix.

As an illustration of the method of presenting the results, the case of formula (7) will be considered. Here the constant $K_5$ is defined for each thyroid gland as being the result of dividing the mass of the gland by the three halves power of the frontal area. The constant is averaged over several glands and then the predicted mass for each gland is calculated by using this average constant. The difference for each gland between the actual mass and the predicted mass is examined, as is also the percentage difference relative to the true mass.

The comparison between true mass and predicted mass as derived from the dimensions measured on the photographs is shown in Table IV. For the small glands, the mass was predicted with an average standard deviation of 40 per cent and for the large glands 25 per cent.

#### COMPARISON OF DIMENSIONS FROM PHOTOGRAPHS AND SCANS

The thyroid frontal area, height of left lobe, height of right lobe, and width were measured for each thyroid on the photograph and on the thyroid outline drawn on the radioisotope scan. These measurements are compared in Table V, where it is seen that there is no significant difference between the dimensions derived from the photographs and those derived from the scans.

Table III

COMPARISON OF CLINICAL SIZE GRADING WITH GLAND MASS AT THYROIDECTOMY

| Clinical Goiter Size Grading | No. of Cases | Thyroid Mass (gm.) | | |
|---|---|---|---|---|
| | | Mean | S.D. | S.E. |
| 0 | 1 | 42.3 | — | — |
| +1 | 3 | 52.2 | 10.68 | 6.17 |
| +2 | 6 | 88.52 | 83.10 | 33.92 |
| +3 | 8 | 128.4 | 192.7 | 68.82 |
| Intrathoracic (+3, +4 in neck) | 6 | 188.2 | 50.54 | 20.63 |

#### PREDICTION OF THYROID MASS FROM RADIOISOTOPE SCAN

The prediction of thyroid mass by simple proportionality formulae is evaluated in Table VI and the prediction by regression formulae in Table VII.

From Table VI it can be seen that the type of formula used made no difference in the accuracy of the prediction. For the small glands, the standard deviation of the differences was about 10 gm. and the standard deviation of percentage differences was about 25 per cent. This applied irrespective of the formula used. For the large glands the standard deviation of the differences was about 45 gm. and the standard deviation of the percentage differences was about 33 per cent. Thus, the smaller glands are more accurately estimated, but the accuracy of the estimation is in either case rather poor.

Table VII shows that for small glands, the standard deviation of the percentage difference averages 20 per cent, while that for large glands is 30 per cent. Once again, the small glands are estimated with a lower standard deviation, and predictions from the regression formulae are slightly better than those from the simple proportionality formulae, though the improvement is not marked.

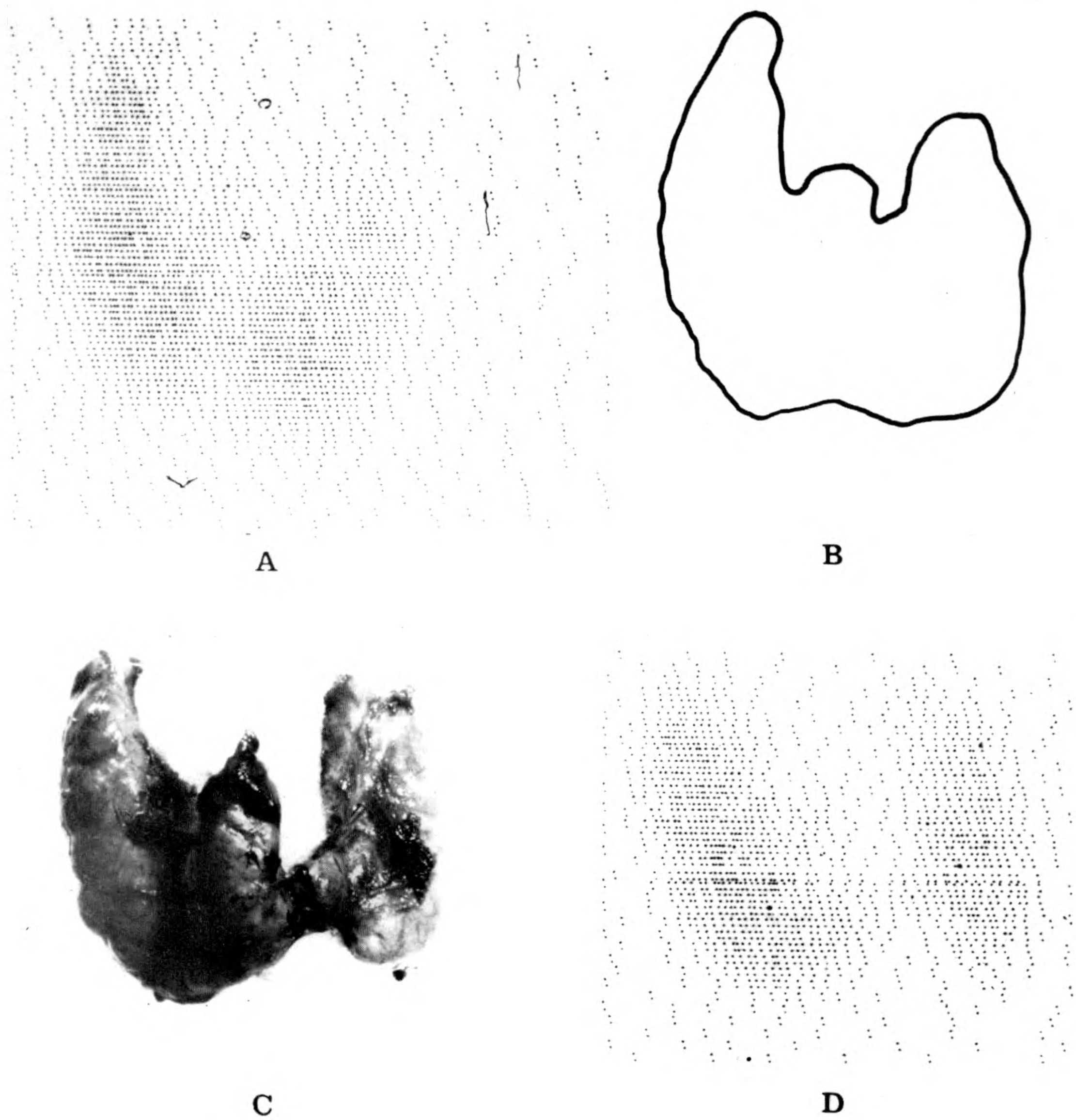


Fig. 1. Patient 24. (*A*) Radioisotope scan of thyroid gland *in vivo* before operation. (*B*) Outline of the gland as estimated from the scan. (*C*) Photograph of the excised gland positioned on glass plate. (*D*) Scan of the excised gland.

## DISCUSSION

While there is a definite correlation between predicted and true mass, no one formula has evidenced any distinct superiority, nor is the accuracy obtained by any of them very great. With a standard deviation of the percentage differences equal to 25 per cent, we may expect the true mass to lie within plus or minus 50 per cent of the predicted mass 95 per cent of the time. This amount of error, while large, is an improvement over simple clinical grading of goiter size, since, for example, the masses of goiters graded as +3 varied from 60 to 240 gm. The improvement in mass prediction by the scanning method over a simple clinical grading may thus be represented by a factor of about 2.

TABLE IV

COMPARISON BETWEEN MASS PREDICTED FROM PHOTOGRAPHS OF EXCISED THYROID GLANDS AND WEIGHTS OF GLANDS PLUS SURGEON'S ESTIMATED CORRECTIONS

| | No. of Glands | Differences* | | | | | | | | | Per Cent Differences† | | | | | | | | |
|---|---|---|---|---|---|---|---|---|---|---|---|---|---|---|---|---|---|---|---|
| | | No. of Formula Used for Calculation (see Appendix) | | | | | | | | | | | | | | | | | |
| | | (1) | (2) | (3) | (4) | (5) | (6) | (7) | (8) | (9) | (1) | (2) | (3) | (4) | (5) | (6) | (7) | (8) | (9) |
| Size +1 or +2 | 6 | | | | | | | | | | | | | | | | | | |
| Mean | | 15.1 | 5.3 | 5.0 | 6.1 | 4.8 | 5.4 | 2.1 | 9.9 | 13.2 | 31.0 | 12.9 | 12.5 | 12.9 | 10.8 | 12.2 | 4.9 | 22.5 | 31.4 |
| S.D. of individual difference | | 12.1 | 12.5 | 15.7 | 15.1 | 14.7 | 15.5 | 10.9 | 21.5 | 26.1 | 31.8 | 33.6 | 40.5 | 34.1 | 34.6 | 37.3 | 25.9 | 52.7 | 70.9‡ |
| Size +3 | 13 | | | | | | | | | | | | | | | | | | |
| Mean | | −7.9 | 4.0 | 3.0 | 2.5 | 3.0 | 1.7 | 6.2 | −1.2 | 3.9 | −6.7 | 1.2 | −0.9 | 1.5 | 1.1 | −0.8 | 2.2 | 9.0 | 10.7 |
| S.D. of individual difference | | 24.8 | 44.7 | 47.6 | 35.3 | 43.4 | 44.9 | 49.5 | 39.8 | 41.0 | 17.2 | 21.7 | 21.6 | 39.1 | 21.9 | 21.8 | 24.5 | 26.8 | 33.5 |
| All sizes | 19 | | | | | | | | | | | | | | | | | | |
| Mean | | −6.6 | 4.4 | 3.6 | 3.6 | 3.6 | 2.9 | 4.9 | 2.3 | 1.3 | 5.2 | 4.9 | 3.3 | 5.1 | 4.2 | 3.4 | 3.1 | 8.0 | 12.0 |
| S.D. of individual difference | | 32.0 | 37.1 | 39.8 | 38.1 | 36.3 | 37.6 | 40.8 | 34.7 | 37.1 | 28.3 | 24.6 | 28.4 | 28.5 | 26.0 | 26.0 | 24.4 | 37.3 | 49.0 |

* The mean difference under (1) is $\frac{1}{n}\sum_{i=1}^{n}(\overline{K}_1 A_i - M_i)$, where $n$ = number of glands, $\overline{K}_1$ is the mean $K_1$ $\left(i.e., \frac{1}{n}\sum_{i=1}^{n}\frac{M_i}{A_i}\right)$, $A_i$ is the area of the $i^{th}$ gland and $M_i$ is the mass of the $i^{th}$ gland. The other mean differences are similarly defined.

† The mean per cent difference under (1) is $\frac{100}{n}\sum_{i=1}^{n}\frac{(\overline{K}_1 A_i - M_i)}{M_i}$, where the symbols have the same meaning, and the other relative differences are similarly defined.

‡ It was observed in retrospect that one gland had been poorly positioned on the glass plate in such a manner that it lay considerably flatter than when *in situ*. The measured width, relative to its mass, was thus much greater than normal and the discrepancy introduced in the predicted mass was much greater when formulae employing the square of the width (formulae 8 and 9) were employed, as would be expected.

There is some possibility of improving the methods by using a slit collimator which would scan the gland in two mutually perpendicular directions. The borders of the gland would be expected to be more accurately defined by this method. This was the method used by Burkinshaw,[2] though, as yet, there is no commercially available scanning machine which incorporates a collimator of this type. However, the standard deviation by this method was still 20 per cent.

Since estimated masses derived from photographic dimensions also give large standard deviations, the error must result mainly from the variety of shapes observed in thyroid glands rather than the isotope technique.

By estimating the mass of the thyroid gland by a scanning method, some of the uncertainty in the calculation of millicurie dosage in iodine 131 therapy can be removed.[9] It will be interesting to see what effect this has on a rational dosage system for $I^{131}$ therapy of thyrotoxicosis and whether the delayed incidence of hypothyroidism can be correlated with the radiation dose.

Table V

COMPARISON OF DIMENSIONS FROM PHOTOGRAPHS AND SCANS

| | No. of Glands | Mean Difference (scan minus photograph) | S.E. of Mean | t* | P (approx.) |
|---|---|---|---|---|---|
| Size +1 or +2 | 6 | | | | |
| Area, cm.² | | 2.4 | 1.9 | 1.23 | 0.25 |
| Height left, cm. | | −0.2 | 0.27 | 0.73 | 0.45 |
| Height right, cm. | | −0.18 | 0.30 | 0.61 | 0.55 |
| Width, cm. | | 0.07 | 0.11 | 0.61 | 0.55 |
| Size +3 | 13 | | | | |
| Area, cm.² | | −1.7 | 2.0 | 0.82 | 0.45 |
| Height left, cm. | | −0.26 | 0.21 | 1.27 | 0.25 |
| Height right, cm. | | −0.03 | 0.18 | 0.18 | 0.85 |
| Width, cm. | | 0.04 | 0.26 | 0.15 | 0.85 |

* Testing the significance from zero of the mean differences, using the Student t-test.

Table VI

EVALUATION OF PREDICTION OF GLAND MASS FROM SCAN BY SIMPLE PROPORTIONALITY FORMULAE*

| | No. of Glands | Differences (gm.) | | | | | | | | | Relative Differences (%) | | | | | | | | |
|---|---|---|---|---|---|---|---|---|---|---|---|---|---|---|---|---|---|---|---|
| | | No. of Formula Used for Calculation (see Appendix) | | | | | | | | | | | | | | | | | |
| | | (1) | (2) | (3) | (4) | (5) | (6) | (7) | (8) | (9) | (1) | (2) | (3) | (4) | (5) | (6) | (7) | (8) | (9) |
| Size +1 or +2 | 9 | | | | | | | | | | | | | | | | | | |
| Mean | | −0.29 | 4.6 | 5.5 | 2.4 | 2.2 | 3.8 | 3.5 | 2.0 | 2.7 | 3.3 | 6.5 | 7.3 | 4.4 | 4.0 | 5.8 | 5.2 | 4.8 | 5.0 |
| S.D. | | 9.8 | 14.9 | 15.4 | 9.4 | 11.2 | 11.5 | 11.0 | 9.9 | 10.4 | 21.1 | 26.8 | 27.7 | 22.1 | 23.8 | 24.3 | 23.7 | 23.9 | 23.7 |
| S.E. | | 3.3 | 5.0 | 3.1 | 3.1 | 3.7 | 3.8 | 3.6 | 3.3 | 3.5 | 7.0 | 8.9 | 9.2 | 7.4 | 7.9 | 8.1 | 7.9 | 8.0 | 7.9 |
| Size +3 | 11 | | | | | | | | | | | | | | | | | | |
| Mean | | −3.8 | −1.0 | 0.9 | −1.9 | −0.1 | −2.1 | −2.5 | −1.5 | −0.9 | 10.0 | 8.2 | 9.5 | 9.3 | 9.7 | 8.7 | 7.9 | 9.4 | 10.8 |
| S.D. | | 46.8 | 43.9 | 41.7 | 45.4 | 44.4 | 44.5 | 41.9 | 50.1 | 51.2 | 35.4 | 29.9 | 30.9 | 33.1 | 31.3 | 31.6 | 30.6 | 33.5 | 35.3 |
| S.E. | | 14.1 | 13.2 | 12.6 | 13.7 | 13.4 | 13.4 | 12.6 | 15.1 | 15.4 | 10.7 | 9.0 | 9.3 | 10.0 | 9.4 | 9.5 | 9.2 | 10.1 | 10.6 |

* The differences are calculated in the same manner as in Table IV.

While we believe that thyroidectomy or an antithyroid drug is the indicated treatment for most patients with thyrotoxicosis, it nevertheless seems worthwhile to expend some effort in making the alternative form of therapy (dosage with iodine-131) as satisfactory as possible by measuring the thyroid mass with the radioisotope scanning technique and using this information to more accurately assess the correct therapy dose.


SUMMARY

A method of measuring the mass of the thyroid gland *in vivo* by radioisotope scanning has been investigated in a series of 25 patients.

By comparing the scans of excised thyroid glands with the photographs of these glands, it was found that the frontal dimensions of a gland could be satisfactorily predicted from the scan of the gland. However, the thyroid mass could only be pre-

### Table VII

EVALUATION OF PREDICTION OF GLAND MASS FROM SCAN BY REGRESSION FORMULAE*

| | No. of Glands | Differences (gm.) | | | | | | | | | Relative Differences (%) | | | | | | | | |
|---|---|---|---|---|---|---|---|---|---|---|---|---|---|---|---|---|---|---|---|
| | | No. of Formula Used for Calculation (see Appendix) | | | | | | | | | | | | | | | | | |
| | | (10) | (11) | (12) | (13) | (14) | (15) | (16) | (17) | (18) | (10) | (11) | (12) | (13) | (14) | (15) | (16) | (17) | (18) |
| Size +1 or +2 | 9 | | | | | | | | | | | | | | | | | | |
| Mean | | 0.54 | 0.83 | 0.63 | 0.20 | 0.02 | −0.12 | −0.06 | −0.03 | −0.02 | 4.0 | 4.7 | 4.3 | 3.4 | 2.4 | 2.3 | 1.5 | 2.1 | 1.9 |
| S.D. | | 10.7 | 10.4 | 9.4 | 9.6 | 9.4 | 8.3 | 8.5 | 8.7 | 8.4 | 21.6 | 19.5 | 21.8 | 20.6 | 20.6 | 18.6 | 19.8 | 18.8 | 19.4 |
| S.E. | | 3.6 | 3.5 | 3.1 | 3.2 | 3.2 | 2.8 | 2.8 | 2.9 | 2.8 | 7.2 | 6.5 | 7.2 | 6.9 | 6.9 | 6.2 | 6.6 | 6.3 | 6.5 |
| Size +3 | 11 | | | | | | | | | | | | | | | | | | |
| Mean | | 0.31 | 0.40 | −1.30 | −0.77 | 0.25 | −0.022 | 0.43 | −0.29 | 0.63 | 7.5 | 7.5 | 10.8 | 11.2 | 7.5 | 9.8 | 9.4 | 8.0 | 8.2 |
| S.D. | | 43.5 | 43.2 | 51.0 | 51.1 | 40.6 | 41.5 | 45.3 | 43.3 | 42.2 | 28.0 | 28.2 | 33.2 | 33.7 | 28.4 | 30.1 | 30.0 | 28.7 | 28.9 |
| S.E. | | 13.1 | 13.0 | 15.4 | 15.4 | 12.2 | 42.5 | 13.6 | 13.0 | 12.7 | 8.4 | 8.5 | 10.0 | 10.2 | 8.6 | 9.1 | 9.0 | 8.6 | 8.7 |

* The differences are those between the actual masses and those predicted by the regression formulae in the Appendix.

dicted from either the photograph or the scan with an average standard deviation of 30 per cent of the true mass.

The limit of accuracy would seem to be imposed by the variety of shapes observed in thyroid glands, the shape sometimes depending to a large extent upon the size of the gland.

The estimation of the mass by radioisotope scanning is more accurate than that obtained by palpation.

J. Myhill
The Royal North Shore Hospital of Sydney
Crows Nest, N.S.W., Australia

## APPENDIX

### FORMULAE FOR THE PREDICTION OF THYROID GLAND MASS *

1. *Simple Proportionality Formulae.*

The following nine constants were calculated for each gland.

$$(1)\quad K_1 = \frac{M}{A}$$

$$(2)\quad K_{2a} = \frac{M}{AH_{\max}}$$

$$(3)\quad K_{2b} = \frac{M}{AH_{\text{ave}}}$$

$$(4)\quad K_3 = \frac{M}{AW}$$

$$(5)\quad K_{4a} = \frac{M}{A\sqrt{H_{\max}W}}$$

$$(6)\quad K_{4b} = \frac{M}{A\sqrt{H_{\text{ave}}W}}$$

$$(7)\quad K_5 = \frac{M}{(A)^{3/2}}$$

$$(8)\quad K_{6a} = \frac{M}{H_{\max}W^2}$$

$$(9)\quad K_{6b} = \frac{M}{H_{\text{ave}}W^2}$$

Here, $M$ = mass of the thyroid, $A$ = frontal area, $W$ = width viewed frontally, $H_{ave}$ = average height of the lobes, $H_{max}$ = maximum height of the lobes.

The average constant was calculated in each case, and the predicted mass obtained as $M_1 = K_{1ave}A_1$ for the predicted mass of the first gland using the first constant, and similarly for other glands and constants.

2. *Regression Formulae.*

The following formulae were fitted by regression analysis to the observed values of $M, H, W$, and $A$, thus yielding the values of the constants $\alpha$, $\beta$, $\gamma$ and $\delta$.

$$(10)\quad \frac{M}{H_{\max}} = \alpha_1 A + \beta_1$$

$$(11)\quad \frac{M}{H_{\text{ave}}} = \alpha_2 A + \beta_2$$

$$(12)\quad \frac{M}{H_{\max}} = \alpha_3 W^2 + \beta_3$$

$$(13)\quad \frac{M}{H_{\text{ave}}} = \alpha_4 W^2 + \beta_4$$

$$(14)\quad M = \gamma_1 A + \delta_1$$

$$(15)\quad M = \gamma_2 AW + \delta_2$$

$$(16)\quad M = \gamma_3 A\sqrt{H_{\max} W} + \delta_3$$

$$(17)\quad M = \gamma_4 A\sqrt{H_{\text{ave}} W} + \delta_4$$

$$(18)\quad M = \gamma_5 (A)^{3/2} + \delta_5$$

Using the observed values of $H$, $W$ and $A$ and the calculated values of the constants, the predicted masses were calculated.

REFERENCES


1. Allen, H. C., Jr., and Goodwin, W. E. Scintillation counter as instrument for *in vivo* determination of thyroid weight. *Radiology*, 1952, *58*, 68–79.
2. Burkinshaw, L. Method of measuring mass of thyroid gland *in vivo*. *Acta radiol.*, 1958, *49*, 308–320.
3. Clode, W., Sobral, V., Baptista, A. M., Perez-Fernandez, M. A., Martins, L. M., Botelho, L., Freire da Cruz, M., and Magalhães Colaço, F. Importance of determination of weight of thyroid gland and clinical biologic factors in treatment of hyperthyroidism with I-131. Am. J. Roentgenol., Rad. Therapy & Nuclear Med., 1959, *81*, 65–73.
4. Franco, V. H., and Quina, M. G. Pneumo-thyroid: new procedure for determining mass of thyroid gland for radioiodine treatment of hyperthyroidism. *Brit. J. Radiol.*, 1956, *29*, 434–439.
5. Goodwin, W. E., Cassen, B., and Bauer, F. K. Thyroid gland weight determination from thyroid scintigrams with postmortem verification. *Radiology*, 1953, *61*, 88–92.
6. Himanka, E., and Larsson, L.-G. Estimation of thyroid volume: anatomic study of correlation between frontal silhouette and volume of gland. *Acta radiol.*, 1955, *43*, 125–131.
7. Kelly, F. J. Observations on calculation of thyroid weight, using empirical formulae. *J. Clin. Endocrinol. & Metabol.*, 1954, *14*, 326–335.
8. Libby, R. L. Empirical formulae for estimation of thyroid weight. Comment on Kelly's article. *J. Clin. Endocrinol. & Metabol.*, 1954, *14*, 1265–1268.
9. Myhill, J., Oddie, T. H., Rundle, F. F., Hales, I. B., and Thomas, I. D. System of radioiodine therapy for thyrotoxicosis and non-toxic goitre involving measurement of thyroidal radio-sensitivity. *J. Clin. Endocrinol. & Metabol.*, 1961, *21*, 817–825.
10. Myhill, J., Hales, I. B., Reeve, T. S., Thomas, I. D., and Oddie, T. H. Radioisotope scanning in thyroid disease. *M. J. Australia*, 1964, *2*, 6–11.
11. Reeve, T. S. Thyroidectomy in treatment of thyrotoxicosis. *J. Coll. Radiol. Australasia*, 1964, *8*, 104–106.
12. Soley, M. H., Miller, E. R., and Foreman, N. Graves' disease: treatment with radioiodine (I-131). *J. Clin. Endocrinol.*, 1949, *9*, 29–35.
13. Williams, R. H., Towery, B. T., Jaffe, H., Rogers, W. F., Jr., and Tagnon, R. Radioiodotherapeusis. *Am. J. Med.*, 1949, *7*, 702–717.

# A DIAGNOSTIC PITFALL WITH RADIOIODINE SCANNING*

By EDWIN G. ZALIS, CAPTAIN, MC, RICHARD E. ELLISON, CAPTAIN, MC, and O'NEILL BARRETT, Jr., MAJOR, MC
SAN FRANCISCO, CALIFORNIA

THE radioiodine scintiscan is an important diagnostic tool in evaluating thyroid disease. It has been especially helpful in demonstrating functioning metastatic carcinoma to lymph nodes, lung and bone.[1] It is the purpose of the authors to direct attention to a possible pitfall in scintiscan interpretation.

## REPORT OF A CASE

A 35 year old Oriental woman was discovered to have a thyroid nodule during the third trimester of pregnancy. One month post partum she was referred for evaluation to the Radioisotope Clinic. A firm, 1 cm. nodule was noted at the junction of the left lobe and the isthmus. A scintiscan demonstrated the nodule to be nonfunctioning, and exploratory surgery was recommended. Ten days later surgery was performed, and a tumor involving the isthmus of the left lobe of the thyroid gland with extension outside the gland was found. The recurrent laryngeal nerve was involved, and many firm, stone-hard, fixed lymph nodes involving the left jugular chain and carotid sheath were present. A total thyroidectomy was performed.

The histologic diagnosis was papillary adenocarcinoma of the thyroid. Postoperatively, the patient was treated with external radiation therapy and received a tumor dose of 4,000 rads through an 8 by 12 cm. anterior neck port, over a 6 week period. Subsequently, she was referred to the Isotope Clinic for postoperative evaluation. She was given 387 $\mu$c of $I^{131}$ orally for a neck and chest scintiscan. The 24 hour $I^{131}$ uptake was 1.7 per cent and the scintiscan demonstrated well localized uptake of the radioiodine just to the left of the midline in the approximate area of the thyroid gland (Fig. 1). This was thought to represent residual thyroid tissue. The scintiscan over the chest demonstrated considerable activity over both lung fields, considered to be compatible with diffuse pulmonary metastases. A chest roentgenogram was obtained to determine whether lesions were demonstrable roentgenographically. On overlaying the scintigram on the chest roentgenogram, it was apparent that the areas of increased activity over the lung fields corresponded to the breast shadows on the roentgenogram (Fig. 2). It was suspected that the breasts were the source of the radioactivity.

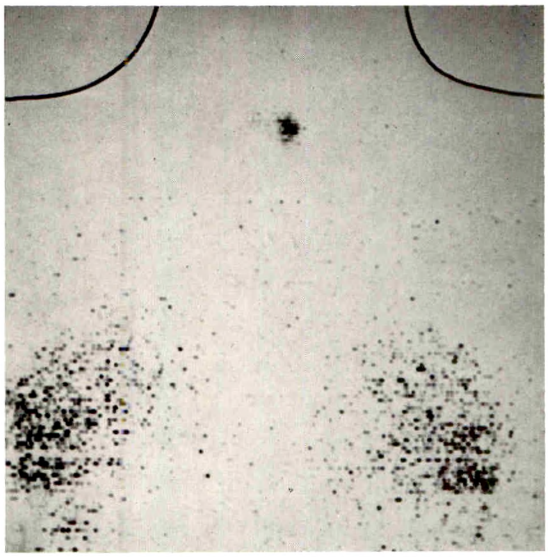

Fig. 1. Radioiodine scintiscan of the neck and chest which demonstrates considerable activity over both lung fields as well as localized activity in the area of the thyroid gland.

On further questioning, it was learned that the patient was still actively lactating. A repeat scintiscan was performed with the patient in the supine position with her breasts bound in the middle of the chest. Figure 3 is a superimposition of the scintigram over the roentgenogram taken in this position. This maneuver demonstrated a shift of the radioactivity from the area of the lung to the area of the breasts in the midline. No activity in the lung fields was noted. These maneuvers established that the previously noted activity throughout the lung parenchyma was, in reality, from the breasts

* From the Department of Medicine and Radiology Service, Letterman General Hospital, San Francisco, California.

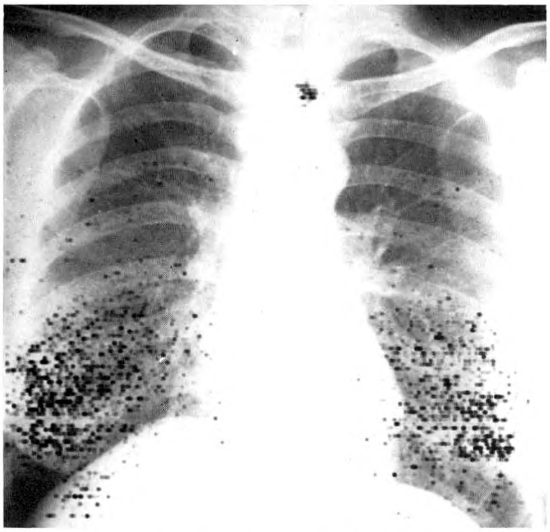

Fig. 2. An overlay of the scintiscan shown in Figure 1 on a posteroanterior erect roentgenogram of the chest which demonstrates that the areas of increased activity correspond to the breast shadows.

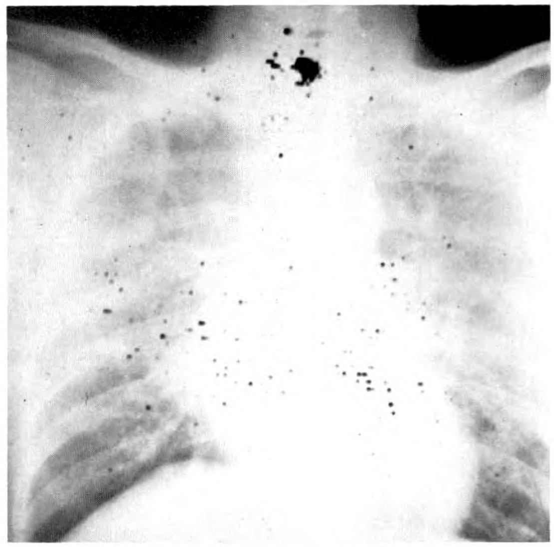

Fig. 3. An overlay of a repeat scintiscan on a supine chest roentgenogram. Both the scintiscan and the roentgenogram were obtained with the patient's breasts bound in the midline of the chest. This maneuver demonstrates a shift of the radioactivity to the area of the breasts in the midline.

which were actively secreting $I^{131}$. This was confirmed by counting the activity of a 3 cc. sample of breast milk which was observed to have 237,323 cpm at the time of the repeat scintiscan. In the absence of demonstrable functioning metastases, no radioactive iodine therapy was given. She was continued on a daily dose of 180 mg. of desiccated thyroid for TSH suppression.

## DISCUSSION

Iodine is known to be secreted in breast milk in a physiologically significant amount.[2] Likewise, radioiodine used for diagnostic thyroid studies has been demonstrated to be excreted in human maternal milk.[3,4,5]

In this case, a radioiodine scintiscan was made during lactation. The resultant concentration of radioactivity in the breasts led to an initial false interpretation of its localization and metastatic carcinoma of the lungs was suspected. Correct interpretation was made after repeating the scan with displacement of the breasts as described above. This possible source of confusion should be considered when making a chest scintiscan.

O'Neill Barrett, Jr., Major, MC
Department of Medicine
Letterman General Hospital
San Francisco, California 94129

## REFERENCES

1. Beierwaltes, W. H., Johnson, P. C., and Solari A. J. The Clinical Use of Radioisotopes. W. B. Saunders Company, Philadelphia, 1957, pp. 131–191.
2. Elmer, A. W. Iodine Metabolism and Thyroid Function. Oxford University Press, London, 1938, pp. 103–110.
3. Miller, H., and Weetch, R. S. Excretion of radioactive iodine in human milk. *Lancet*, 1955, *2*, 1013.
4. Noble, M. J. D., and Rowlands, S. Utilization of radio-iodine during pregnancy. *J. Obst. & Gynaec. Brit. Emp.*, 1953, *60*, 892–894.
5. Nurnberger, C. E., and Lipscomb, A. Transmission of radioiodine ($I^{131}$) to infants through human maternal milk. *J.A.M.A.*, 1952, *150*, 1398–1401.

# THE PREOPERATIVE DIAGNOSIS OF SPLEEN CYSTS BY SCINTISCANNING

## REPORT OF A CASE

*By* JOSEPH A. VOLPE, CAPTAIN, MC,* *and* GERALD L. DeNARDO, MAJOR, MC†
DENVER, COLORADO

CYSTS of the spleen are rare lesions, occurring less frequently than cystic disease in any other abdominal viscera.[6] The diagnosis may not be considered in the evaluation of the patient with splenomegaly. In most cases the patient is asymptomatic or symptomatology is vague. The palpable abdominal mass is nonspecific and the routine laboratory data are nondiagnostic. Many of the splenic cysts have been incidentally discovered at surgery.

Diagnosis has depended upon the demonstration of calcification of the cyst.[10,12] However, Qureshi *et al.*[10] noted that only 50 of 421 cases of splenic cysts found in the literature contained calcium. Schechter *et al.*[11] reported that only 1 case in 10 contains calcium. Displacement of the stomach to the right and downward displacement of the splenic flexure on barium study or downward displacement of the left kidney on excretory urography suggest splenic enlargement.

Recently, the technique of radioisotope scintiscanning of the spleen has permitted a more precise method for evaluation of its size and contour. Several milliliters of the patient's erythrocytes are labeled with radioactive chromium ($Cr^{51}$), then heat-treated and reinjected into the patient. Such erythrocytes have an increased mechanical and osmotic fragility and are selectively sequestered in the spleen. A scintiscan of the spleen can be obtained because of the gamma photon of the radioactive chromium.[7,8,15] The following case illustrates the usefulness of this technique in the preoperative diagnosis of cysts of the spleen.

### REPORT OF A CASE

A 14 year old Caucasian female was admitted to Fitzsimons General Hospital after a left upper quadrant mass was discovered during a routine physical examination. She was asymptomatic and had no history of abdominal trauma, pregnancy, bleeding tendency, serious infections or jaundice. She was an enthusiastic horseback rider but denied any injuries.

Physical examination was normal except for a firm, nontender mass palpable in the left upper quadrant of the abdomen, 5 cm. below the left costal margin. This mass descended with inspiration and was interpreted to be an enlarged spleen.

Routine laboratory tests, hematologic studies and the chest roentgenogram were normal. A barium enema study revealed downward displacement of the transverse colon. An excretory urogram suggested an extrinsic mass which displaced the left kidney downward (Fig. 1). No calcium could be identified in the area of the mass.

Anterior, posterior and left lateral scintiscans of the spleen were made using the methods described by Wagner *et al.*[13] and by Johnson and Herion.[8] There was increased concentration of radioactivity in the liver, indicating impairment of splenic function. The majority of the spleen was replaced by a large ovoid lesion, the tip of which corresponded to the palpable abdominal mass. Only a small rim of functioning splenic tissue was present as manifested by concentration of radiochromium (Fig. 2, *A*, *B* and *C*). An anterior liver scintiscan using colloidal gold ($Au^{198}$) disclosed the left lobe of the liver to be small with a concave border further outlining the splenic mass (Fig. 3). On the basis of the spleen and liver scintiscans, a large splenic cyst was presumed to be present.

Celiac and selective splenic arteriography was performed under local anesthesia by the

* Resident, Internal Medicine, Fitzsimons General Hospital.
† Chief, Radioisotope Section, Fitzsimons General Hospital; Assistant Clinical Professor of Radiology, University of Colorado School of Medicine.

Fig. 1. Excretory urogram. The left kidney (arrow) is displaced downward by a large extrarenal mass.

percutaneous catheterization of the left axillary artery. The branches of the splenic artery were stretched around a large mass which corresponded in size and location to that identified on the splenic scintiscan. The radiopaque material pooled in the inferior portion of the spleen. The left hepatic artery was small (Fig. 4, *A* and *B*).

At exploratory laparotomy, a large cystic mass occupied the entire upper, medial and posterior portion of the spleen and was adherent to the diaphragm. A splenectomy was performed. The patient recovered uneventfully and was discharged on the seventh postoperative day.

The spleen weighed 1,360 gm. and contained a 10×7.5×6.5 cm. cyst at its superior and middle portion (Fig. 5, *A* and *B*). When opened, the cyst was trabeculated and filled with a brownish-red liquid. Microscopic sections of the inferior tip of the spleen revealed normal splenic architecture. The cyst wall was composed of dense hyalinized fibrous connective

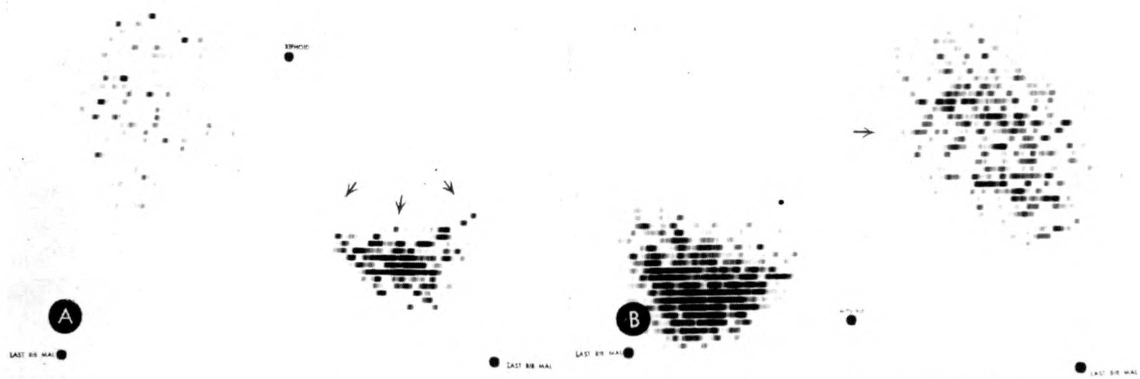



Fig. 2. Radiochromium spleen scintiscans. (*A*) *Anterior*. A small rim of functioning splenic tissue concentrates radioactivity (arrows). (*B*) *Posterior*. An increased concentration of radioactivity in the liver is demonstrated (arrow) indicating impaired function of the spleen. A larger amount of splenic tissue is seen on this view. (*C*) *Left lateral*. The rim of splenic tissue is better defined. The upper border is concave and attenuated (arrows) suggesting a large ovoid lesion.

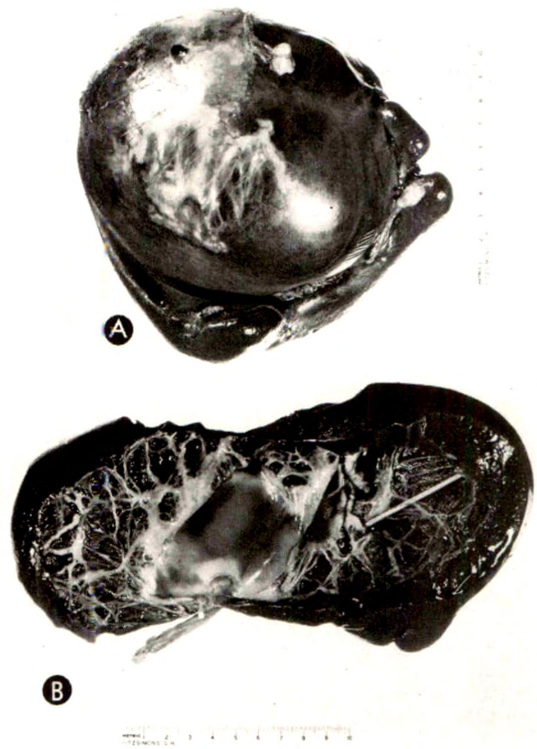

Fig. 5. Gross specimens. (*A*) Posterior view of the spleen demonstrating the large cystic mass. (*B*) Opened cyst with trabeculated wall.

Fig. 3. Colloidal radiogold liver scintiscan. The liver and spleen are visualized. The concave upper border of the functioning splenic tissue is demonstrated (arrows). The left lobe of the liver is also concave, further defining the splenic mass.

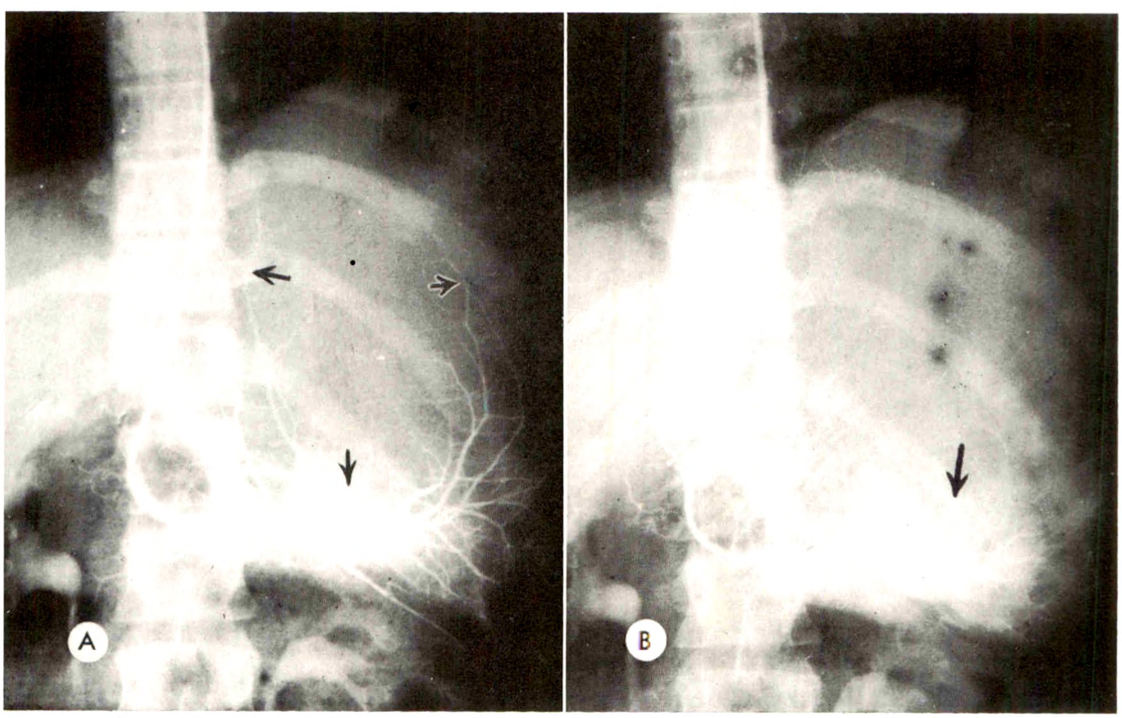

Fig. 4. Splenic arteriograms. (*A*) The branches of the splenic artery (arrows) are stretched around the large mass. (*B*) The radiopaque material pools in the inferior portion of the spleen (arrow).

tissue. No epithelial lining was identified. There was a considerable amount of scattered calcium in the cyst wall. The appearance was characteristic of a hemorrhagic cyst of the spleen.

## DISCUSSION

This case report demonstrates the usefulness of spleen and liver radioisotope scintiscans and splenic arteriograms in the differential diagnosis of abdominal masses.

Abnormalities of the left kidney, pancreas, left lobe of the liver, omentum, gastrointestinal tract and retroperitoneal area may present as a left upper quadrant abdominal mass. Splenomegaly due to systemic diseases, such as the leukemias, lymphomas, reticuloses and infectious diseases, may also present in this fashion. The history, physical examination, clinical laboratory tests and roentgenographic study of the gastrointestinal tract and kidneys usually indicate the source of the mass.

Solitary lesions of the spleen may be solid or cystic. Solid lesions consist of primary tumors of the spleen including hemangiomas, lymphangiomas, fibromas, dermoids, hamartomas and sarcomas.

Cysts of the spleen have been classified by Fowler.[4,5] The only parasite that produces cysts in the spleen is *Echinococcus granulosus* and this is a rare location for such cysts. Nonparasitic cysts are classified as primary or true cysts which contain a cellular lining, and secondary or false cysts without a cellular lining. Primary cysts are congenital, traumatic, inflammatory or neoplastic. Secondary cysts are usually associated with trauma to a previously diseased or normal spleen.[11] The trauma may have been quite remote in time and in many no history of injury is obtained.

Splenic scintiscanning and arteriography assume major diagnostic importance with solitary space occupying lesions. Cysts of the spleen have been diagnosed preoperatively by percutaneous puncture of the cyst and by splenoportography.[2,8] However, these procedures are hazardous especially if the cyst should be a hydatid cyst. In contrast, splenic scintiscanning is without morbidity.

As demonstrated by our case as well as by a patient reported by Wagner *et al.*,[13] a large cyst is readily apparent on the scintiscan as an area which fails to concentrate any radioactivity. The border is sharply circumscribed. Small or multiple cysts may be difficult to differentiate from multiple abscesses of the spleen. However, abscesses usually have an irregular border on scintiscans, and the clinical picture will differentiate the two.[9,13]

Solid tumors of the spleen have not been studied adequately by scintiscanning techniques. Benjamin *et al.*[1] have reported a case of hemangioma of the spleen with a scintiscan pattern similar to that in our patient. Other cases have not been reported. Presumably, some solid tumors may be distinguished from cysts on scintiscans because they do not completely replace the splenic tissue. Splenic arteriography may assist further in the differentiation of solid from cystic lesions. The angiogram in our case revealed complete avascularity of the mass, suggesting a cystic lesion. A solid lesion such as a hamartoma is usually vascular and shows vascular lakes within the tumor.[14]

## SUMMARY

A patient is reported in whom the diagnosis of a splenic cyst was established prior to surgery. Radioisotope scintiscans of the spleen and liver and splenic arteriography permitted this preoperative diagnosis. The differential diagnostic considerations and the advantages of radioisotope study are discussed.

Gerald L. DeNardo, Major, MC
Fitzsimons General Hospital
Denver, Colorado 80240

## REFERENCES

1. Benjamin, B. I., Mohler, D. N., and Sandusky, W. R. Hemangioma of spleen. *A.M.A. Arch. Int. Med.*, 1965, *115*, 280–284.
2. Eban, R. E. Splenic cyst with pre-operative diagnosis. *Brit. J. Radiol.*, 1959, *32*, 821–823.

3. Ellis, H. Splenic cyst diagnosed by splenography. *Brit. J. Radiol.*, 1958, *31*, 331–332.
4. Fowler, R. H. Cystic tumors of spleen. *Internat. Abstr. Surg.*, 1940, *70*, 213–223.
5. Fowler, R. H. Collective review: nonparasitic benign cystic tumors of spleen. *Internat. Abstr. Surg.*, 1953, *96*, 209–227.
6. Hoffman, E. Non-parasitic splenic cysts. *Am. J. Surg.*, 1957, *93*, 765–770.
7. Johnson, P. M., Herion, J. C., and Mooring, S. L. Scintillation scanning of normal human spleen using sensitized radioactive erythrocytes. *Radiology*, 1960, *74*, 99–101.
8. Johnson, P. M., and Herion, J. C. Technical considerations in scintillation scanning of human spleen. *Radiology*, 1961, *76*, 438–443.
9. Parrish, R. A., Jr., and Sherman, H. C. Surgical significance of splenic abscess. *Am. Surgeon*, 1964, *30*, 712–716.
10. Qureshi, M. A., Hafner, C. D., and Dorchak, J. R. Nonparasitic cysts of spleen. *A.M.A. Arch. Surg.*, 1964, *89*, 570–574.
11. Schechter, D. C., Owens, J. C., and Palmieri, A. J. Hemorrhagic cyst of spleen; report of two cases. *Am. J. Surg.*, 1962, *104*, 777–784.
12. Soler-Bechara, J., and Soscia, J. L. Calcified echinococcus (hydatid) cyst of spleen. *J.A.M.A.*, 1964, *187*, 62–63.
13. Wagner, H. N., Jr., McAfee, J. G., and Winkleman, J. W. Splenic disease diagnosis by radioisotope scanning. *A.M.A. Arch. Int. Med.*, 1962, *109*, 673–684.
14. Wexler, L., and Abrams, H. L. Hamartoma of spleen; angiographic observations. Am. J. Roentgenol., Rad. Therapy & Nuclear Med., 1964, *92*, 1150–1155.
15. Winkleman, J. W., Wagner, H. N., Jr., McAfee, J. G., and Mozley, J. M. Visualization of spleen in man by radioisotope scanning. *Radiology*, 1960, *75*, 465–466.

# ISOTOPE LOCALIZATION AND SCANNING OF THE PLACENTA

*By* EDWARD W. KLEIN, LCDR, MC, USN,* *and* HERBERT G. HOPWOOD, JR., LCDR, MC, USN†
GREAT LAKES, ILLINOIS

BROWNE and Veall first reported the use of sodium 24 for localization of the human placenta in 1950. Since that time, numerous techniques have been developed using iodine 131 and iodine 132 tagged human serum albumin as tracer material. Paul *et al.*,[9,10] in recent years, have advocated the utilization of $Cr^{51}$ tagged erythrocytes which has the advantage of lower radiation exposure to both the mother and fetus.

The benefits derived from accurate placental localization in placenta previa are well documented.[3,7,8,11–14] Radioisotope localization of the placenta is based upon the premise that the placenta represents a large blood pool wherein the isotope may accumulate and be detected. With this procedure it has been clearly shown that the radiation dosage to the maternal abdomen and gonads, as well as the fetal whole body radiation, is reduced far below levels which are received by the appropriate roentgen placentography.[3,5,7,13] The exact radiation dosage to the fetal thyroid is in a state of controversy. The placenta has been shown to be relatively impermeable to RISA;[3,6,7,14] thus, the majority of fetal thyroidal irradiation results from the gamma radiations emitted in the maternal circulation and placenta. Metabolic degradation of RISA, plus small amounts of contaminant, results in concentration of inorganic $I^{131}$ in the fetal thyroid itself. The combined exposure resulting from a 5 $\mu$c dosage has been calculated to give a maximum dose to the fetal thyroid of 2,500 millirads. This estimated dose is calculated without blocking the fetal thyroid with Lugol's solution or potassium iodide. Weinberg *et al.*[14] estimate the dose to the fetal thyroid at 26 millirads for a 5 $\mu$c injection, utilizing an effective half life of 4.7 days. The utilization of Lugol's solution, at least 24 hours prior to the administration of the isotope, is widely used to block the fetal and maternal thyroid uptake of $I^{131}$. This specifically minimizes irradiation of the gland. The total maternal radiation for an average patient, again utilizing 5 $\mu$c, is less than 44 millirads. For the fetus, the total body radiation is, as stated previously, almost entirely from gamma rays emanating from the maternal circulation and is estimated in the vicinity of 5 millirads.[14]

The procedure of placental localization is shown to be uniformly reliable and most authors report an accuracy of greater than 90 per cent.

## TECHNIQUE

We have adopted the technique outlined by Visscher and Baker,[13] with excellent results. The patients are given 20 drops of Lugol's solution, orally, 2 to 6 hours before examination. Routinely, 5 $\mu$c of RISA is injected intravenously. A 10 minute period is allowed for the isotope to mix thoroughly in the maternal circulation. During this time, the abdominal surface over the gravid uterus is divided into 12 approximately equal sections. This is done by measuring the length of the fundus above the symphysis and dividing this area into 4 equal horizontal parts. Each horizontal part is then divided into thirds. The xiphoid is also marked and used as a reference point. A 2 or 1 inch scintillation detector, without collimation, is placed flush with the skin surface. Successive counts are taken over

* Staff Radiologist. Director Radioisotope Department, U. S. Naval Hospital, Great Lakes, Illinois.
† Department of Obstetrics and Gynecology. Presently at U. S. Naval Hospital, Bethesda, Maryland.
The opinions expressed are those of the authors and do not necessarily represent the views of the Navy Department.

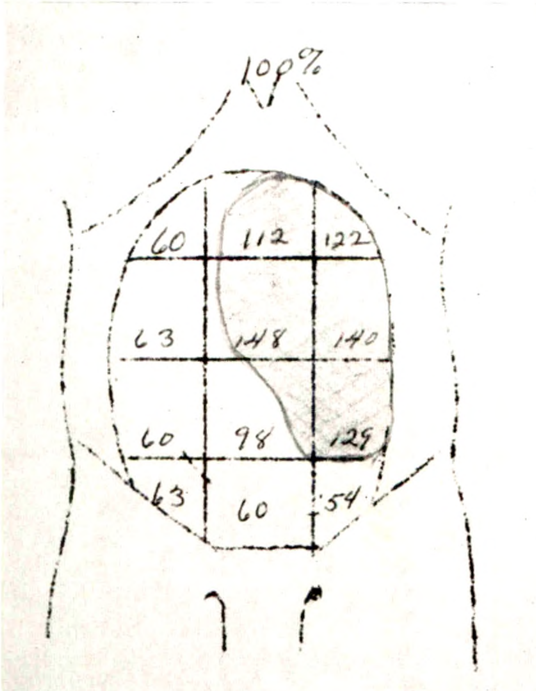


FIG. 1. Example of placental counts obtained. The average of the highest percentage (148 per cent) and the lowest (54 per cent) is 101 per cent. Therefore, the significant counts will be above this number. The placenta in this case is localized to the upper left uterine segment anteriorly.

the xiphoid and over the center of each section. Pre-set counts are taken (minimum of 2,560 counts) over the xiphoid and over each section. With the xiphoid count taken as 100 per cent, counts over the 12 sections are expressed as a percentage.

Interpretation of the results, as a rule, is not difficult. Numerous formulae have been used to determine which of the percentage counts are significant. The average of the highest and lowest counts has been shown to be of value in two ways. The percentage counts above this average are usually grouped together over the placental site and constitute the significant counts. The average figure is also of value in determining whether or not the placenta is on the anteroposterior wall of the uterus. If this value is above 70, the placenta is most likely to be found on the anterior wall and, if below 70, on the posterior wall. Occasionally, all the counts appear to be base-

FIG. 2. Photograph taken during the scanning procedure. The mechanical bed is lowered or raised as needed with each passage of the probe.

line, and the placenta is then diagnosed by exclusion as being on the posterior mid-line wall of the fundus. A typical case is shown in Figure 1.

PLACENTAL SCANNING

At the present time, the authors quite well realize that placental scanning offers no significant advantage over the conventional method of isotope localization. We feel, however, that in the future, with improved instrumentation, placental scanning, with direct visualization of the placenta, may very well replace the present system of isotope localization. We have attempted to demonstrate placentas by scanning 2 patients with suspected placenta previa. Both patients were in good condition, presenting no contraindication to scanning. The placentas were localized, as outlined above, with 8 $\mu c$ of RISA. Both placentas were shown to be previa and photoscans were attempted. Utilizing a Nuclear Chicago Dual Scanner with a 19 hole course focusing collimator, the patient was scanned over the area of suspected placental localization. The factors utilized were pulse height discrimination centering about the 364 kev. window of $I^{131}$. Scanning speed was 18 cm. per minute, 10–30 per cent maximum count acceptance. With this technique, a mechanical bed is mandatory (Fig. 2). The attendant takes care of the

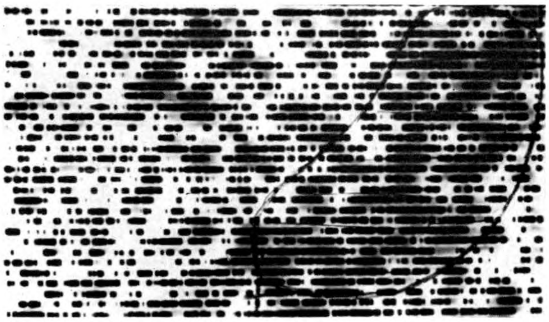

Fig. 3. Case I. Placental scan outlining the placenta as a large area of isotope concentration in the lower left pelvis extending over the region of the os.

patient throughout the scanning and lowers or raises the bed with each passage of the probe, thus maintaining a fairly constant focal distance. The two resulting photoscans gave a fair outline of the placentas. Both patients underwent cesarean section and, at the time of surgery, the visualized placentas were localized to the area shown on the photoscan (Fig. 3; and 4). These 2 cases are presented in detail.

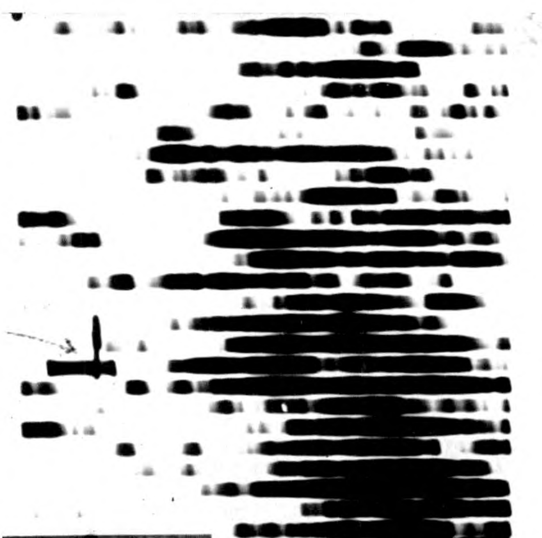

Fig. 4. Case II. Placental scan shows a well defined area of isotope concentration in the lower right pelvis extending well across the midline. (Arrow on the left points to right iliac crest, arrow on the right points to symphysis pubis.) At surgery, a placenta previa centralis was found.

## REPORT OF CASES

Case I. B.M., a 30 year old gravida 12, para 4, abortion 7, was admitted at 38 weeks' gestation to the Obstetrical Service of the U. S. Naval Hospital, Great Lakes, Illinois, with the complaint of painless vaginal bleeding. Pelvic examination was deferred, but clinical impression was of a term size infant in unengaged breech position. The patient's vaginal bleeding spontaneously stopped and after 24 hours of observation, during which time she received Lugol's iodine 10 drops every 3 hours, a placental localization using RISA was performed. The impression both by isotope localization and placental scan (Fig. 3) was that the placenta was localized to the left lateral wall of the uterus, extending well into the minor pelvis. The patient spontaneously went into labor while in the hospital and a double set-up examination performed in the operating room revealed a placenta previa. Upon performing a classic cesarean section, the placenta was shown to extend onto the left lateral wall, covering 95 per cent of the internal cervical os. The postoperative course of both mother and infant was uneventful, and both appear in excellent health.

Case II. M.P., a 30 year old gravida 6, para 3, abortion 1 (stillborn twins), was admitted to the Obstetrical Service of the U. S. Naval Hospital, Great Lakes, Illinois, at 32 weeks' gestation with the complaint of painless vaginal bleeding. Pelvic examination was deferred, but clinical impression was of a $7\frac{1}{2}$ month size uterus with the fetus in transverse lie, face looking at the internal cervical os. The patient spontaneously ceased bleeding, was primed with Lugol's iodine, and using 8 $\mu$c RISA, a placental localization and photscan were performed. The placentogram defined the implantation as extending from the right lower uterine wall across the pelvic mid-line. The placental scan confirmed this (Fig. 4). The patient was observed in the hospital and spontaneously went into labor and began bleeding heavily through the vagina. A double set-up examination was performed in the operating room; placenta previa was detected. A low cervical transverse cesarean section was done and a placenta previa centralis was found. Unfortunately, the infant died within 48 hours due to prematurity. The mother's postoperative course was uneventful.

SUMMARY

1. Isotope localization (placentogram) of the placenta is reviewed. RISA placentography has proven to be of equal or greater accuracy than roentgen studies. It is safe, expeditious and inexpensive. Second trimester localization has been reported as accurate.

2. Radiation exposure to mother and fetus from a 5 $\mu$c dose is significantly less than that received from roentgen placentography.

3. A method of this procedure is outlined.

4. Placental scanning in 2 patients is discussed and the case histories are presented.

Edward W. Klein, LCDR, MC, USN
Department of Radiology
U. S. Naval Hospital
Great Lakes, Illinois

REFERENCES

1. Cavanagh, D., Gilson, A. J., and Powe, C. E. Isotopic placentography: an evaluation based upon a study of 50 patients. *South. M. J.*, 1961, *54*, 1340–1346.
2. Coale, G. B., III, Richey, L. E., and McGanity, W. J. Localization of placenta with intravenous aortography. *Am. J. Obst. & Gynec.*, 1962, *83*, 1150–1156.
3. Croll, M. N., Shuman, L. H., Stanton, L., and Czarnecki, C. Radioisotope placentography: bedside procedure. *J. Nuclear Med.*, 1963, *4*, 417–425.
4. Cronin, W. T. Placenta localization with $I^{131}$ HSA. *St. Vincent Hosp. Med.*, 1962, *4*, 19–22.
5. Durfee, R. B., and Howieson, J. L. Localization of placenta with radioactive iodinated serum albumin. *Am. J. Obst. & Gynec.*, 1962, *84*, 577–581.
6. Heagy, F. C., and Swartz, D. P. Localizing placenta with radioactive iodinated human serum albumin. *Radiology*, 1961, *76*, 936–944.
7. Hibbald, B. M. Placental localization using radio-iodinated serum albumin (R.I.S.A.). *J. Obst. & Gynaec. Brit. Emp.*, 1961, *68*, 481–489.
8. Merchant, R. V., and Moran, J. P. Routine use of isotope localization of placenta using I-131. *Obst. & Gynec.*, 1964, *23*, 72–75.
9. Paul, J. D., Jr., Gahres, E. E., Albert, S. N., Terrell, W. D., Jr., and Dodek, S. M. Placenta localization using $Cr^{51}$-tagged erythrocytes. *Obst. & Gynec.*, 1963, *21*, 33–39.
10. Paul, J. D., Jr., Gahres, E. E., Rhoads, J. C., and Dodek, S. M. Cr-51 placenta localization and blood loss determination in placenta previa accreta. *Obst. & Gynec.*, 1964, *23*, 259–261.
11. Swartz, D. P., Platt, M. A., and Heagy, F. C. Radioisotope (I-131) studies of placental location and circulation. *Am. J. Obst. & Gynec.*, 1963, *85*, 338–344.
12. Thaieigsman, J. H., and Schulman, H. Placenta localization using radioactive I-131 tagged human serum albumin. *Obst. & Gynec.*, 1964, *23*, 747–763.
13. Visscher, R. D., and Baker, W. S., Jr. Isotope localization of placenta in suspected cases of placenta previa. *Am. J. Obst. & Gynec.*, 1960, *80*, 1154–1160.
14. Weinberg, A., Shapiro, G., and Bruhn, D. F. Isotopic placentography; evaluation of its accuracy and safety. *Am. J. Obst. & Gynec.*, 1963, *87*, 203–209.

# FAT ABSORPTION STUDIES AND SMALL BOWEL X-RAY STUDIES IN PATIENTS UNDERGOING $Co^{60}$ TELETHERAPY AND/OR RADIUM APPLICATION*

*By* R. J. REEVES, M.D., P. J. CAVANAUGH, M.D., K. W. SHARPE, B.A., W. A. THORNE, M.D., C. WINKLER, M.D., *and* A. P. SANDERS, Ph.D.

DURHAM, NORTH CAROLINA

THIS paper concerns a group of patients who received cobalt 60 teletherapy to the pelvis and intrauterine radium application. The variations observed in fat absorption from the gastrointestinal tract and the results of the small bowel x-ray examinations made during the course of therapy are analyzed.

Since the initial work by Walsh[13] in 1897, many studies have been performed on the various effects of radiation on the gastrointestinal tract. Among these are reports by Warren *et al.*[14,15] and Martin and Rogers,[7] describing the anatomic changes; Goodman *et al.*,[3] Wallace,[12] and Conard[2] reported on alterations in motility. Reeves *et al.*[8,9] discussed the effects on the fat absorption in one group of patients undergoing conventional x-ray therapy and in a second group of patients undergoing $Co^{60}$ teletherapy.

Goodrich and Hickman,[4] in a study of 48 patients with a diagnosis of carcinoma of the cervix, found that a very low incidence of depression to abnormal levels occurred during therapy, at the completion of therapy and at 8 weeks after therapy with $Co^{60}$ irradiation.

## METHODS

In the present series 38 patients receiving cobalt 60 teletherapy to the pelvis, or cobalt 60 teletherapy to the pelvis plus intrauterine radium application, were studied during the course of treatment. Fat absorption techniques as described by Baylin *et al.*,[1] Sanders *et al.*,[11] and Isley *et al.*[5,6] were utilized for determining the absorption of fat from the gastrointestinal tract. Each patient had two tests per week unless his condition or other circumstances dictated otherwise. In one of the tests both the blood levels and the fecal recovery were measured after an $I^{131}$ labeled neutral fat test meal, and in the second test only the fecal recovery was measured. Control studies were made prior to the initiation of radiation therapy. In addition, x-ray examinations of the small bowel patterns and transit time were carried out at different times during the course of radiation therapy. Both the small bowel x-ray studies and the fat absorption studies were correlated with the radiation dosage to the midline of the patient.

## RESULTS

The relationship between the abnormal results and the midline radiation dosage is shown in Figure 1 for both the small bowel x-ray and the fat absorption studies. As in the previous series of cobalt 60 teletherapy patients,[9] the majority of the abnormal findings in this series occurred at a midline exposure dose of 2,000 to 3,000 r, between the second and third week of therapy. There appears to be absolutely no correlation between the findings of abnormal small bowel x-ray patterns and abnormal fat absorption studies.

Table 1 is a summary of the results of the fat absorption studies. Of 31 patients with blood level determinations, 77 per cent showed abnormal studies some time during the course of therapy. Of a total number of 142 blood level studies in the 31 patients, 64

* From the Department of Radiology, Duke University Medical Center, Durham, North Carolina.
Supported in part by Grant No. C2602 (C4-C6) U.S.P.H.

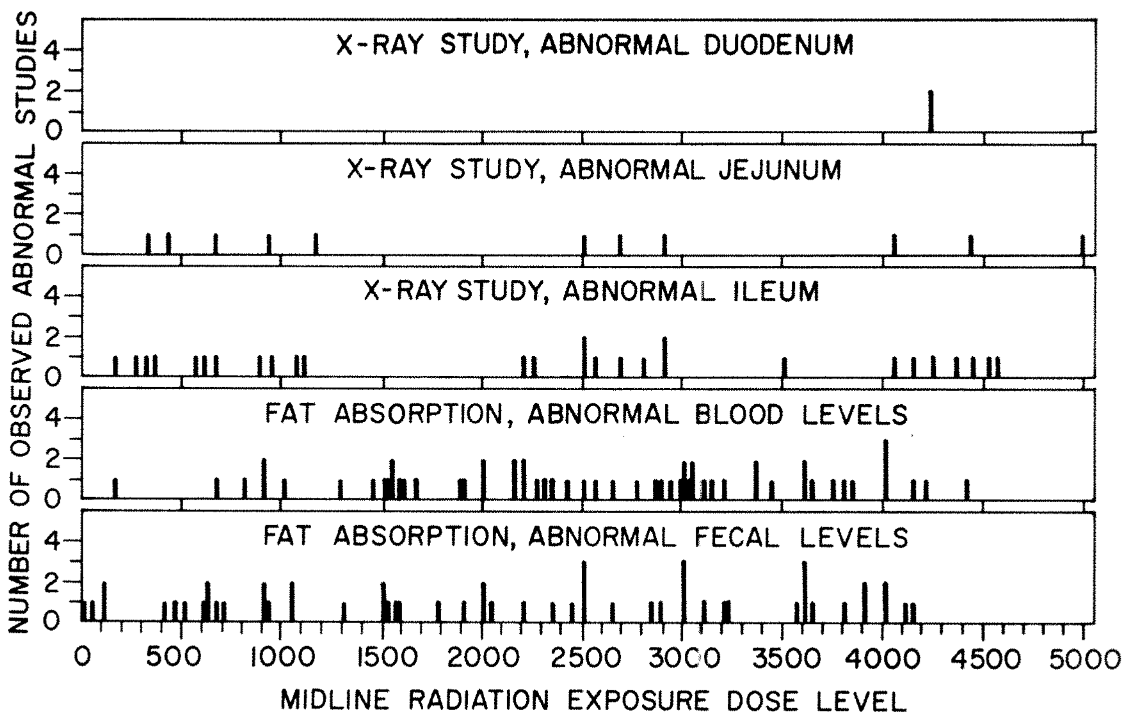


Fig. 1. Correlation between abnormal findings and midline exposure dose level (r).

(45 per cent) gave abnormal results. The fecal determinations were carried out in 33 patients; 15 showed abnormal studies sometime during the course of therapy. There were 168 fecal level determinations in this group of patients, 54 of which gave abnormal results.

Table II shows the results of the small bowel x-ray studies in the 33 patients; 18 exhibited an abnormal pattern at one time or another during the course of therapy. Of a total of 83 studies made, 27 demonstrated abnormal ileal patterns, 10 abnormal jejunal patterns, and 2 abnormal duodenal patterns.

Table III shows the results of the motility studies in those patients having both cobalt 60 teletherapy and intracavitary radium application. Of the 24 cases studied, 15 had changes in motility at the end of the therapy: 5 showed an increased transit time and 10 hypermotility.

Table I

Fat Absorption Studies in $Co^{60}$ Teletherapy Patients

| | Blood Level Determination | Fecal Level Determination |
|---|---|---|
| No. of patients studied | 31 | 33 |
| No. showing abnormal studies | 24 (77%) | 15 (46%) |
| Total no. of studies | 142 | 168 |
| No. of abnormal studies | 64 (45%) | 54 (32%) |

## Discussion

Regaud *et al.*[10] reported in 1912, that the

Table II

Small Bowel X-ray Studies during $Co^{60}$ Teletherapy

| | |
|---|---|
| No. of patients | 33 |
| No. of studies | 83 |
| Abnormal ileal* | 27 |
| Abnormal jejunal | 10 |
| Abnormal duodenal† | 2 |
| No. of patients showing abnormal patterns | 18 |

* Mucosal edema, puddling, segmentation, dilatation.
† Purse string.

Table III

CASES STUDIED AFTER BOTH $CO^{60}$ TELETHERAPY PLUS INTRACAVITARY RADIUM APPLICATION

| | |
|---|---|
| No. of cases | 24 |
| No change in motility | 9 |
| Increased transit time | 5 (21%) |
| Hypermotility | 10 (42%) |
| No. with changed pattern | 15 (63%) |

small bowel of the dog is more sensitive to radiation than the stomach, and that the duodenum and jejunum are more sensitive than other regions of the gastrointestinal tract. It is generally believed that the small bowel sensitivity to radiation decreases as one progresses from the duodenum to the ileum. The x-ray examinations of the small bowel performed in these patients showed the highest incidence of abnormal patterns in the ileum. This may be due to the fact that the ileum is in the direct field of the radiation.

Jejunal and ileal changes as observed in the x-ray studies seemed to appear at relatively the same radiation dosage level, with the higher incidence of abnormal patterns occurring in the ileum. No correlation was seen between the abnormal x-ray findings of small bowel patterns and abnormal fat absorption studies. There was a much higher incidence of abnormal fat absorption during the course of radiation therapy than abnormal small bowel x-ray patterns. This suggests that the fat absorption study is a more sensitive indicator of changes occurring in the gastrointestinal tract due to ionizing radiation than are the x-ray studies. This is to be expected since small functional changes could affect fat absorption and be reflected in these results. Subtle changes within cells which could affect function would not be visible by gross x-ray examination.

The studies of gastrointestinal motility in patients who had received both cobalt 60 teletherapy plus intracavitary radium application showed that of the 24 patients, 10 had increased motility, 5 had an increased transit time, and 9 of the patients showed no changes. These studies were performed at the end of the radiation therapy program. Realizing that the full extent of the effects on tissue from irradiation may not appear until many months after therapy, it is our plan to follow these patients at periodic intervals. An effort will be made to determine the incidence and degree of intestinal malabsorption.

## SUMMARY AND CONCLUSIONS

Fat absorption studies and small bowel x-ray studies were performed on 33 patients undergoing cobalt 60 teletherapy, 24 of whom were also studied following intrauterine radium application.

1. Seventy-seven per cent of all patients showed abnormal fat absorption blood levels, and 46 per cent of the patients studied showed abnormal fecal recovery of fat at one time or another during the course of therapy.

2. Small bowel x-ray studies showed that 18 of the 33 patients had abnormal ileal, jejunal or duodenal patterns during the course of therapy.

3. Twenty-seven of the 83 studies performed in the 33 patients showed abnormal ileal patterns, 10 studies showed abnormal jejunal patterns, and 2 studies showed abnormal duodenal patterns.

4. There was no correlation between abnormal small bowel x-ray findings and abnormal fat absorption studies.

5. At the end of treatment, small bowel x-ray studies performed in those cases receiving both cobalt 60 teletherapy and intracavitary radium application, showed that of 24 patients, 10 demonstrated hypermotility patterns, 5 showed increased transit time, and 9 showed no changes in motility.

6. Fat absorption studies are a more sensitive indicator of changes in the gastrointestinal tract due to ionizing radiation than are small bowel x-ray studies.

7. Insufficient time has elapsed for the determination in these patients of any

delayed changes in the gastrointestinal tract due to the radiation.

R. J. Reeves, M.D.
Department of Radiology
Duke University Medical Center
Durham, North Carolina

REFERENCES

1. Baylin, G. J., Sanders, A. P., Isley, J. K., Shingleton, W. W., Hymans, J. C., Johnston, D. H., and Ruffin, J. M. I-131 blood levels correlated with gastric emptying determined radiographically. II. Fat test meal. *Proc. Soc. Exper. Biol. & Med.*, 1955, *89*, 54–56.
2. Conard, R. A. Effect of x-irradiation on intestinal motility of rat. *Am. J. Physiol.*, 1951, *165*, 375–385.
3. Goodman, R. D., Lewis, A. E., Schuck, E. A., and Greenfield, M. A. Gastrointestinal transit. *Am. J. Physiol.*, 1952, *169*, 236–241.
4. Goodrich, J. K., and Hickman, B. T. Oleic acid $I^{131}$ intestinal absorption in pelvic cobalt 60 irradiation. Am. J. Roentgenol., Rad. Therapy & Nuclear Med., 1962, *87*, 69–75.
5. Isley, J. K., Jr., Sanders, A. P., Baylin, G. J., Ruffin, J. M., Shingleton, W. W., Anlyan, W. G., and Sharpe, K. W. Modification of $I^{131}$ triolein test of fat absorption utilizing capsule test meal. *Gastroenterology*, 1958, *35*, 482–484.
6. Isley, J. K., Jr., Sanders, A. P., Baylin, G. J., Sharpe, K. W., Hymans, J. C., Ruffin, J. M., Shingleton, W. W., and Wilson, J. R., Jr. Use of $I^{131}$ labeled oleic acid in study of gastrointestinal function. *Proc. Soc. Exper. Biol. & Med.*, 1957, *94*, 807–809.
7. Martin, C. L., and Rogers, F. T. Intestinal reaction to erythema dose. Am. J. Roentgenol. & Rad. Therapy, 1923, *10*, 11–19.
8. Reeves, R. J., Sanders, A. P., Isley, J. K., Jr., Sharpe, K. W., and Baylin, G. J. Fat absorption from human gastrointestinal tract in patients undergoing radiation therapy. *Radiology*, 1959, *73*, 398–401.
9. Reeves, R. J., Sanders, A. P., Sharpe, K. W., Thorne, W. A., and Isley, J. K., Jr. Fat absorption from human gastrointestinal tract in patients undergoing teletherapy. Am. J. Roentgenol., Rad. Therapy & Nuclear Med., 1963, *89*, 122–126.
10. Regaud, C., Nogier, T., and Lacassagne, A. Sur les effets redoutables des irradiations étendues de l'abdomen et sur les lésions du tube digestif déterminées par les rayons de Roentgen. *Arch. d'électric méd.*, 1912, *21*, 321–334.
11. Sanders, A. P., Sharpe, K. W., Baylin, G. J., Isley, J. K., Shingleton, W. W., Hymans, J. C., Ruffin, J. M. and Reeves, R. J. Radioiodine recovery in feces following an $I^{131}$ labeled fat test meal. Am. J. Roentgenol., Rad. Therapy & Nuclear Med., 1956, *75*, 386–389.
12. Wallace, W. S. Intestine in radiation sickness. I. Gross effect on small intestine of protracted deep pelvic irradiation. *J.A.M.A.*, 1941, *116*, 585–586.
13. Walsh, D. Deep tissue traumatism from roentgen ray exposure. *Brit. M. J.*, 1897, *2*, 272–273.
14. Warren, S. L., and Whipple, G. H. Roentgen ray intoxication. I. Unit dose over thorax negatives—over abdomen lethal. Epithelium of small intestine sensitive to x-rays. *J. Exper. Med.*, 1922, *35*, 187–202.
15. Warren, S. L., and Whipple, G. H. Roentgen ray intoxication. I. Bacterial invasion of blood stream as influenced by x-ray destruction of mucosal epithelium of small intestine. *J. Exper. Med.*, 1923, *38*, 713–723.

# AN ANALYSIS OF FACTORS AFFECTING OPTIMAL AXIS PLACEMENT AND 80% ISODOSE VOLUME DIMENSIONS IN TELECOBALT ARC THERAPY*

*By* J. E. TURNER, M.D., R. M. JOHNSON, M.S., *and* S. M. WHITFIELD, R.T.
CHICAGO, ILLINOIS

THE purpose of this study is to provide for the radiotherapist the following information concerning arc therapy tissue-dose distributions in convenient form: (1) location of the maximum dose generated; (2) size, shape, and centering of the volume enclosed by the 80%-of-maximum isodose surface—hereafter called the "effectively treated volume;" and (3) percentage of the maximum dose arriving at the rotational axis. The data of this study are not transferable to other techniques, and apply only to those telecobalt machines having a source diameter of 2 cm., a source-to-collimator distance of 33 cm., and a rotational radius of 75 cm.

## PRECEDENTS

Isodose charts and dosage systems for various arc therapy techniques have been published for other source-axis-distances by Jacobson *et al.*[6] and by Dahl. *et al.*[4] Charts for other energies have been published by Nielsen,[10] Trump *et al.*,[13] Dahl *et al.*,[4] Johns *et al.*,[7] Stern,[12] and Turner.[15] Dosage systems for telecobalt at radius 75 cm. have been published by Braestrup and Mooney,[1] Johns *et al.*,[8] Tsien,[14] Roberts,[11] and Kornelson.[9]

None of these systems is specifically designed to show systematically how to adjust the axis position within the patient so as to center, to best advantage, the effectively treated volume to the tumor center for a useful variety of arc techniques at a radius of 75 cm.

## DEFINITIONS

Nominal field sizes (widths and lengths) are defined as the distance between the 60% isodose lines as measured 75 cm. from the source—*i.e.*, at the position of the rotational axis.

The basic conditions of this study assume irradiation of a water-equivalent cylinder of 15 cm. radius and infinite height. This cylinder's cross-section is divided into 10-degree segments, labeled counter-clockwise. The 0-degree direction is arbitrarily designated "anterior;" the 180-degree direction is designated "posterior;" the 90-degree and 270-degree directions are designated, respectively, "left" and "right lateral."

The arcs described in this study are arbitrarily centered anteriorly on the 0-degree radius, extending to either side of this radius an equal number of degrees. In other words, the 0-degree radius is the bisector of all arcs described. All arcs are initially centered upon the axis of rotation.

*Examples.* A 120-degree arc extends 60 degrees to the left and to the right of the bisecting 0-degree (anterior) radius, while a 300-degree arc extends 150 degrees to the left and to the right of the bisecting 0-degree (anterior) radius. Both of these arcs, and all other arcs of this study are initially centered in the center of the cylindrical phantom at a source-axis-distance (rotational radius) of 75 cm.

Data are illustrated and tabulated for nominal axis-field widths and lengths of 4, 6, 8, 10, 12, and 15 cm., and for arc spans of 120, 180, 240, 300, and 360 degrees.

## MATERIALS AND METHODS

This study used theratron-B isodose charts, furnished by Atomic Energy of Canada, Ltd., normalized to 100 per cent of

* From the Therapeutic Radiology Service, Veterans Administration Research Hospital, Chicago, Illinois, and Department of Radiology, Northwestern University Medical School, Chicago, Illinois.

tumor/air dose ratio* at the axis of rotation. Depth dose values, in percentage of tumor/air dose ratio, were read off for 247 points within a half-circle representing half of the central transverse section through a water-equivalent cylinder of 15 cm. radius and infinite height. Bilateral symmetry was assumed. The 247 points lay at the intersections of concentric circles of radii 1, 2, 3, 4, 5, 6, 8, 10, 12, 14, (16, 18, and 20)† cm. with radial lines drawn at 10-degree intervals from 0-degrees through 180-degrees. For data involving field widths, charts for nominal field sizes 4×10, 6×10, 8×10, 10×10, 12×12, and 15×15 cm. were used. It was found that variation of nominal field length between 4 cm. and 15 cm. changed the position of the 80% isodose line at the axis position by only 2 mm. Conversely, it was found that variation of nominal field width had negligible influence upon the nominal field length as determined by the 80% isodose lines.

The average tissue dose at each of the 247 points was calculated for each of the 30 arc techniques presented. The dose along the 180-degree and 0-degree radial lines was graphed to find the location and magnitude of the maximum dose with respect to the axis position and axis dose. The 80%-of-maximum dose value was found, and its anterior and posterior positions along the arc bisector tabulated. The midpoint between these 80% points was then found and recorded. The 80% value was then sought by interpolation along the 30, 60, 90, and 150-degree radii and the positions charted. The 80% points for each arc technique were then joined with the aid of a French curve to produce a closed boundary. In some problems, extra points were used to aid in interpolating the position of the posterior boundary of the 80% zone. From these data Figures 1 through 25 and Table I were prepared.

As shown by Roberts[11] and by Du Sault,[5] the 80% contours can be shifted within the patient's outline as far as 5 cm. anteriorly, posteriorly, or laterally with only 3 mm. deviation in shape. As the center of the 80% zone is moved *toward* a given skin surface, the nearest portion of the 80% line tends to *approach the center* slightly. As the center of the 80% zone is moved *away* from a given skin surface, the nearest portion of the 80% line tends to *move away from the center* slightly.

To determine the *lengths* of the various effectively treated volumes, isodose charts depicting all 36 combinations of nominal field widths and lengths for 4, 6, 8, 10, 12, and 15 cm. were used. The effective field lengths were determined by the intersections of (1) the line representing 80% of the maximum dose generated by each arc technique with (2) a line drawn through the center of the effectively treated volume's cross-section. From these data Table II was prepared.

### DISCUSSION OF FACTORS

1. *Location of the maximum dose generated.* An arc of 0 degrees (*i.e.*, a stationary field) produces a maximum dose lying 5 mm. beneath the skin surface at the center of the skin field. An arc of 360 degrees produces a maximum dose zone centered at the rotational axis. Logically, an arc of less than 360 degrees generates a maximum dose zone somewhere between the axis and the skin, along the bisector of the arc (in this study—along the 0-degree radius). In practice, the location of this maximum dose varies from 0.1 cm. to 6.4 cm. out along the 0-degree radius. The shorter the arc and the wider the field, the farther out the maximum dose occurs.

2. *Size, shape, and center of the 80%-of-maximum isodose zone* (effectively treated volume). This study is designed to present, for rapid selection, effective treatment volumes of known size and shape to be centered to the tumor's center, *allowing the maximum dose to fall where it will*, since the maximum dose and the center of the effective treatment volume do not coincide for

* The tumor/air dose ratio, as defined by Johns *et al.*[7] equals the tissue dose at the rotational axis per r in air arriving at the axis position.

† These values were extrapolated.

TABLE I

THE AXIS PLACEMENT GUIDE

Source Diameter 2 cm., Source-Collimator-Distance 33 cm., Source-Axis-Distance 75 cm.

| Figure | Field Width | Arc° | 80%-of-Maximum Isodose Line: Center | Total Anteroposterior | Total Transverse | Shape | Major Axis of Cross-Section | Dose Maximum in % of TAR*: Location | Magnitude | Reciprocal: "f" factor† |
|---|---|---|---|---|---|---|---|---|---|---|
| 1 | 4 | 120 | +0.9 | 4.4 | 3.2 | Oval | Anteroposterior | +1.0 | 104 | .96 |
| 2 | 4 | 180 | +0.5 | 4.0 | 4.0 | Circle | None | +0.5 | 100 | 1.00 |
| 3 | 4 | 240 | +0.4 | 3.4 | 4.4 | Oval | Transverse | +0.2 | 100 | 1.00 |
| 4 | 4 | 300 | +0.1 | 3.5 | 4.2 | Oval | Transverse | +0.0 | 100 | 1.00 |
| 5 | 6 | 120 | +1.6 | 6.3 | 5.0 | Oval | Anteroposterior | +2.0 | 111 | .90 |
| 6 | 6 | 180 | +0.8 | 5.4 | 6.2 | Oval | Transverse | +1.4 | 106 | .94 |
| 7 | 6 | 240 | +0.6 | 5.3 | 6.8 | Oval | Transverse | +1.0 | 103 | .97 |
| 8 | 6 | 300 | +0.3 | 5.5 | 6.8 | Oval | Transverse | +1.0 | 101 | .99 |
| 9 | 8 | 120 | +2.8 | 7.0 | 6.6 | Oval | Anteroposterior | +3.5 | 119 | .84 |
| 10 | 8 | 180 | +1.3 | 6.7 | 8.0 | Oval | Transverse | +2.3 | 111 | .90 |
| 11 | 8 | 240 | +0.8 | 7.2 | 9.0 | Oval | Transverse | +2.0 | 106 | .94 |
| 12 | 8 | 300 | +0.4 | 7.9 | 9.0 | Oval | Transverse | +2.0 | 102 | .98 |
| 13 | 10 | 120 | +4.2 | 7.6 | 8.0 | Hemi-oval | Transverse | +4.8 | 128 | .78 |
| 14 | 10 | 180 | +2.5 | 6.6 | 9.0 | Oval | Transverse | +3.5 | 121 | .83 |
| 15 | 10 | 240 | +1.0 | 9.0 | 11.8 | Oval | Transverse | +3.0 | 109 | .92 |
| 16 | 10 | 300 | +0.4 | 10.4 | 11.8 | Oval | Transverse | +3.2 | 104 | .96 |
| 17 | 12 | 120 | +5.4 | 8.5 | 9.6 | Hemi-oval | Transverse | +6.2 | 135 | .74 |
| 18 | 12 | 180 | +3.3 | 8.5 | 12.8 | Oval | Transverse | +4.8 | 120 | .83 |
| 19 | 12 | 240 | +1.8 | 10.3 | 14.0 | Oval | Transverse | +4.5 | 110 | .90 |
| 20 | 12 | 300 | +0.7 | 12.7 | 14.8 | Oval | Transverse | +3.5 | 104 | .96 |
| 21 | 15 | 120 | +7.4 | 9.1 | 11.2 | Hemi-oval | Transverse | +6.7 | 146 | .68 |
| 22 | 15 | 180 | +4.7 | 8.9 | 15.4 | Hemi-oval | Transverse | +6.2 | 126 | .79 |
| 23 | 15 | 240 | +3.0 | 11.3 | 16.8 | Hemi-oval | Transverse | +6.1 | 115 | .87 |
| 24 | 15 | 300 | +0.9 | 15.5 | 17.8 | Oval | Transverse | +6.1 | 106 | .94 |
| 25 | 4 | 360 | 0.0 | 3.8 | 3.8 | Circle | None | 0.0 | 100 | 1.00 |
| 25 | 6 | 360 | 0.0 | 6.0 | 6.0 | Circle | None | 0.0 | 100 | 1.00 |
| 25 | 8 | 360 | 0.0 | 8.6 | 8.6 | Circle | None | 0.0 | 100 | 1.00 |
| 25 | 10 | 360 | 0.0 | 11.4 | 11.4 | Circle | None | 0.0 | 100 | 1.00 |
| 25 | 12 | 360 | 0.0 | 14.0 | 14.0 | Circle | None | 0.0 | 100 | 1.00 |
| 25 | 15 | 360 | 0.0 | 17.4 | 17.4 | Circle | None | 0.0 | 100 | 1.00 |

* TAR = tumor/air dose ratio.
† f = tumor dose correction factor.

arcs shorter than 360 degrees. At the same time, the location of the maximum dose is tabulated, so that if it falls in an undesirable area within the patient, the therapist may select another, more favorable technique.

Once the tumor's center has been localized, the patient, for 360 degree rotation, is positioned for treatment so that the tumor's center coincides with the axis of rotation. For treatment with arcs shorter than 360 degrees, the patient is positioned so that the axis of rotation does *not* lie at the tumor's center, but rather, *deep* to the tumor's center by the number of centimeters specified in Table I: The Axis Placement Guide.

In usual practice (for treatment of a tumor in the trunk of a supine patient), the rotational axis is first placed at the tumor's center by alignment of guide lights to anterior and lateral skin markings which

Table II

EFFECTIVE FIELD LENGTH

(80% of maximum)

| | | | | | | |
|---|---|---|---|---|---|---|
| Nominal field length (cm.) | 4.0 | 6.0 | 8.0 | 10.0 | 12.0 | 15.0 |
| Effective field length (cm.) | 2.9 | 4.8 | 6.7 | 8.5 | 10.6 | 13.4 |

represent projections of the tumor's center. This alignment is correct for 360-degree rotation, but for arcs of less than 360 degrees, one proceeds as follows: The treatment table is raised so that the lateral guide light coincides with a second, more posterior skin mark which, by projection, depicts the distance from the center of the 80% zone to the appropriate new axis position.

Figures 1 through 24 show the 80% zone as calculated in the second position above—namely, with the axis of rotation properly displaced deep to the tumor center by the distance CA. Figure 25 involves no axis displacements, since this shows the 80% zones for 360-degree rotation only.

In Table I the 80% zones generated are described in 3 shapes: circles, ovals, and hemi-ovals. The hemi-ovals are flattened roughly parallel to the transverse dimension of the body and lie almost entirely anterior to the axis of rotation. The hemi-ovals result when short arcs are used with wide fields. Circles result when 360-degree rotations are used. Ovals result when most other arc techniques are used.

In considering field lengths, we have stated before that the *nominal* field dimensions are outlined by the 60% isodose lines at a distance of 75 cm. from the source. For any of the transverse plane diagrams (Fig. 1 through 25), the field length dimension extends into and out of the plane of the paper.

In contrast to the *nominal* field length defined above, one may define an *effective* field length, which is the distance between the 80%-of-maximum isodose lines as measured on a line extending in and out of the paper and passing through C, the center of the 80%-of-maximum isodose zone (effectively treated volume).

Table II presents these *effective* field lengths, which have the following characteristics: they are 15% to 27% shorter than the corresponding nominal field lengths; they are independent of field width; and they are independent of arc span (120° through 360°).

To use the tables, combine the information from Tables I and II as indicated by the corresponding superscripts in the examples below.

(a) Describe the effectively treated volume generated by a nominal 15×15 cm. field, using 360-degree rotation.

The volume is an oblate spheroid measuring 17.4 cm. anteroposteriorly,[I] 17.4 cm. transversely,[I] and 13.4 cm. longitudinally,[II] centered at the axis of rotation.[I]

(b) Describe the effectively treated volume generated by a nominal 6×12 cm. field, using a 180-degree arc.

The volume is a flattened ovoid measuring 5.4 cm. anteroposteriorly,[I] 6.2 cm. transversely,[I] and 10.6 cm. longitudinally,[II] centered 0.8 cm. superficial (anterior) to the rotational axis.[I]

Data for nominal field widths, nominal field lengths, and arc spans not explicitly appearing in Tables I and II may be approximated by graphical interpolation.

3. *The dose at the axis expressed as a percentage of the maximum dose.* For arcs of 360 degrees, the positions of the maximum dose and the axis of rotation coincide, but for all arcs of less than 360 degrees, the axis receives less than the maximum dose. In this study, this reduced dose at the axis is tabulated in the form of a decimal fraction of the maximum dose, and is presented as the *tumor dose correction factor:* designated **f.** Examples follow to show where this factor should and should not be used.

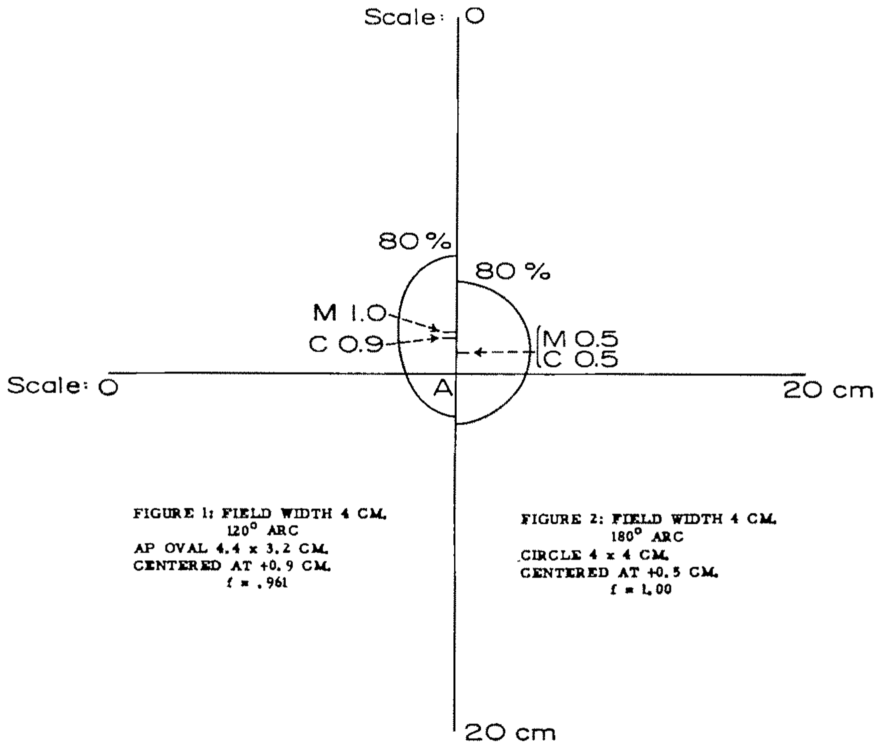


In these figures and all to follow:

A = position of the rotational axis (at intersection of vertical and horizontal line).

M = position of the maximum dose generated in cm. anterior to the axis.

80% = boundary of the 80%-of-maximum (effectively treated) area.

C = position of the center of the 80%-of-maximum (effectively treated) area in cm. anterior to the axis.

The total length of either the vertical or horizontal baseline is 20 cm., reduced for publication. All figures are drawn to the same scale. Figures 1–24 are presented in pairs, different arc techniques being presented on the left and on the right of the bisecting vertical line.

(a) Calculation of the axis tissue-dose rate. Once the axis position for the individual patient has been determined, the therapist obtains the appropriate cross-section body contour and measures the distances from the skin to the axis along the radii included within the treatment arc. The tumor/air dose ratios corresponding to these distances are obtained from dosage tables (Johns *et al.*[8] or *Brit. J. Radiol., Supplement 10*[2]) and an average tumor/air dose ratio ($TAR$) value is determined. The machine output, or intensity ($I$) in r per minute in air at 75 cm. is noted and the axis tissue-dose rate is calculated as follows:

$$d = I \times TAR \times f, \qquad (1)$$

where

$d$ = tissue-dose rate at the axis in rad per minute,

$I$ = machine output (intensity) at the axis in r (air) per minute,

$TAR$ = dose at axis in rad per r (air) delivered to the axis position,

$f$ = conversion factor from r to rad.

Numerical example: The machine output is 60 r/min. in air at source-axis-distance 75 cm. The average $TAR$, as determined from the patient's body contour, is .258. What is the axis tissue-dose rate ($d$)?

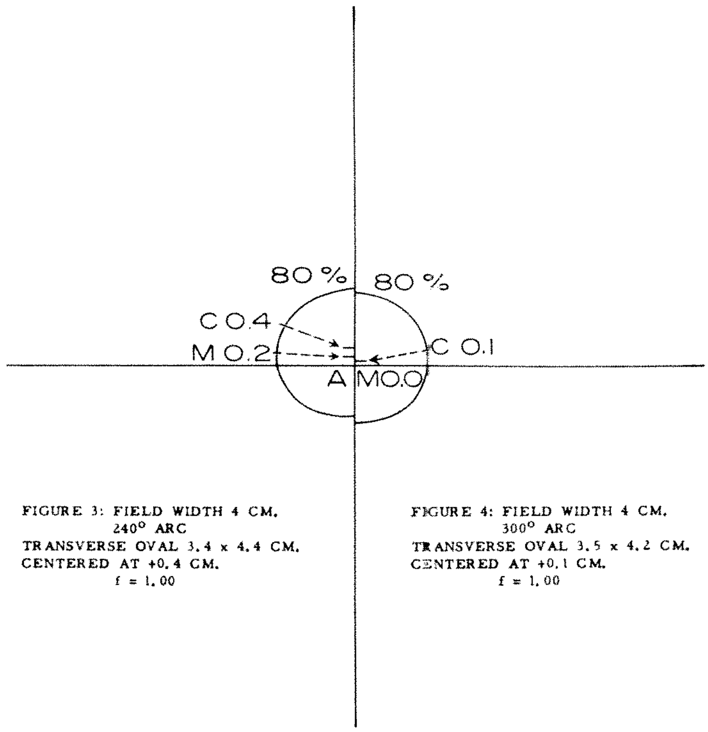


FIGURE 3: FIELD WIDTH 4 CM.
240° ARC
TRANSVERSE OVAL 3.4 x 4.4 CM.
CENTERED AT +0.4 CM.
f = 1.00

FIGURE 4: FIELD WIDTH 4 CM.
300° ARC
TRANSVERSE OVAL 3.5 x 4.2 CM.
CENTERED AT +0.1 CM.
f = 1.00

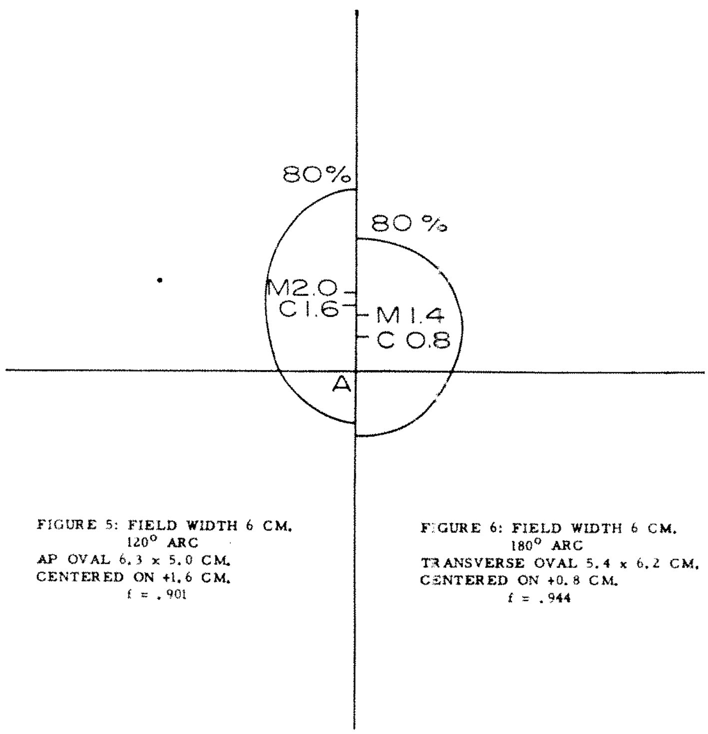


FIGURE 5: FIELD WIDTH 6 CM.
120° ARC
AP OVAL 6.3 x 5.0 CM.
CENTERED ON +1.6 CM.
f = .901

FIGURE 6: FIELD WIDTH 6 CM.
180° ARC
TRANSVERSE OVAL 5.4 x 6.2 CM.
CENTERED ON +0.8 CM.
f = .944

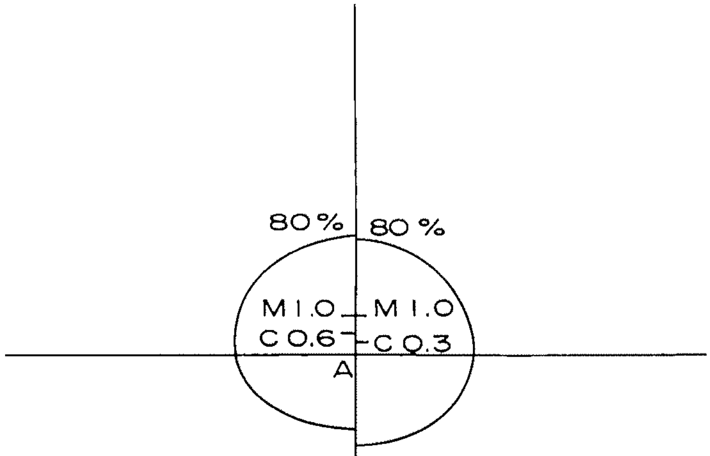


FIGURE 7: FIELD WIDTH 6 CM.
240° ARC
TRANSVERSE OVAL 5.3 x 6.8 CM.
CENTERED AT +0.6 CM.
$f = .971$

FIGURE 8: FIELD WIDTH 6 CM.
300° ARC
TRANSVERSE OVAL 5.5 x 6.8 CM.
CENTERED AT +0.3 CM.
$f = .990$

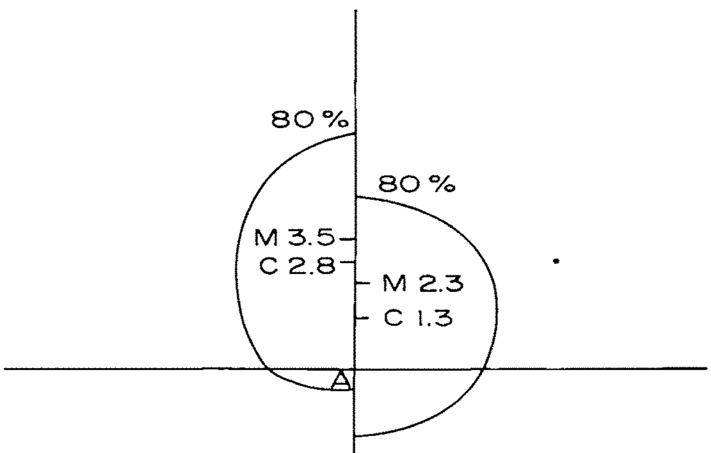


FIGURE 9: FIELD WIDTH 8 CM.
120° ARC
AP OVAL 7.0 x 6.6 CM.
CENTERED AT +2.8 CM.
$f = .840$

FIGURE 10: FIELD WIDTH 8 CM.
180° ARC
TRANSVERSE OVAL 6.7 x 8.0 CM.
CENTERED AT +1.3 CM.
$f = .901$

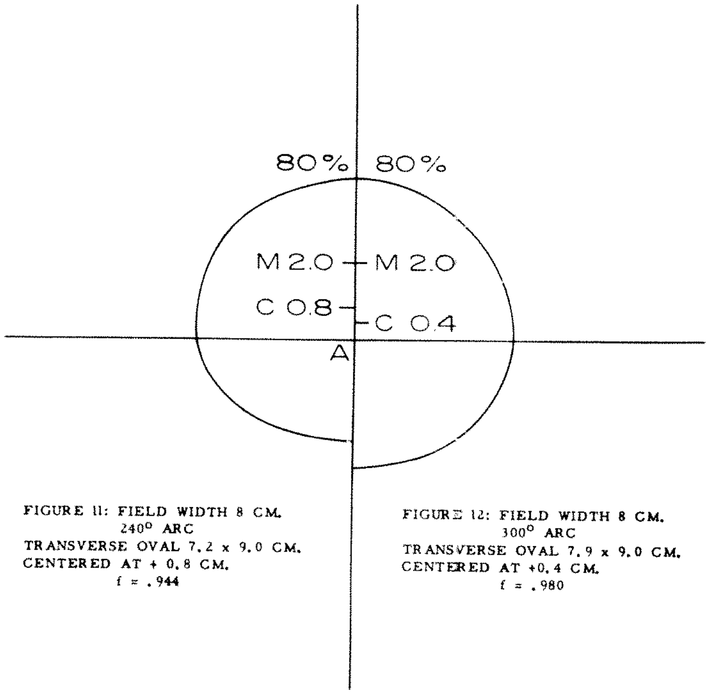


FIGURE 11: FIELD WIDTH 8 CM. 240° ARC TRANSVERSE OVAL 7.2 x 9.0 CM. CENTERED AT + 0.8 CM. f = .944

FIGURE 12: FIELD WIDTH 8 CM. 300° ARC TRANSVERSE OVAL 7.9 x 9.0 CM. CENTERED AT +0.4 CM. f = .980

(1) $d = I \times TAR \times f = 60 \times .258 \times .97$
$= 15$ rad per min.

This dose rate ($d$) will be used in all the examples to follow.

(b) Calculation of treatment time for 360-degree rotation. In this case, the maximum dose and the axis dose coincide in magnitude and location. The tumor dose correction factor, **f**, since it equals 1.00, *need not be used.* The calculation is as follows:

$$t = \frac{TD_a}{d}, \qquad (2)$$

where

$t$ = treatment time (minutes),
$TD_a$ = desired tumor dose at the axis in rad,
$d$ = tissue-dose rate at the axis in rad per minute as determined by equation (1) above.

Numerical example: What treatment time is required to deliver a tissue dose ($TD_a$) of 225 rad to the axis?

(2) $t = \frac{TD_a}{d} = \frac{225 \text{ rad}}{15 \text{ rad/min.}} = 15$ min.

(c) Calculation of treatment time for arcs of less than 360 degrees. In these cases the axis dose is less than the maximum dose and is expressed as a decimal fraction of the maximum dose in the form of the tumor dose correction factor, **f**, as follows:

$$TD_a = \mathbf{f} \times TD_m, \qquad (3)$$

where

$TD_a$ = dose at the axis in rad,
**f** = tumor dose correction factor,
$TD_m$ = maximum dose in rad.

Numerical example: An arc of 120 degrees is to be used with an axis-field width of 12 cm. The tumor dose correction factor for this combination is $\mathbf{f} = .74$. A dose of 225 rad is desired as the *maximum* dose. What is the treatment time required?

(3) $TD_a = \mathbf{f} \times TD_m = .74 \times 225 = 166.5$ rad

(2) $t = \frac{TD_a}{d} = \frac{166.5 \text{ rad}}{15 \text{ rad/min.}} = 11.1$ min.

(Check: The ratio of the answers from problems c and b: $11.1/15.0 = .74$)

(d) Calculation of treatment time for 90%-of-maximum tissue dose. In these cases a tissue-dose homogeneity of $\pm 11\%$ can be obtained by specifying the tumor

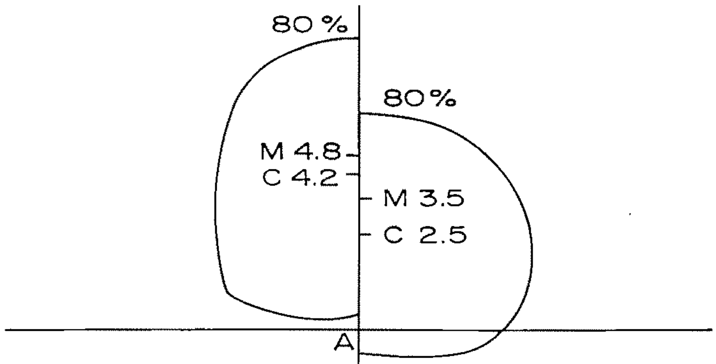


FIGURE 13: FIELD WIDTH 10 CM.
120° ARC
TRANSVERSE SEMI-OVAL 7.6 x 8.0 CM.
CENTERED AT +4.2 CM.
f = .782

FIGURE 14: FIELD WIDTH 10 CM.
180° ARC
TRANSVERSE OVAL 6.6 x 9.0 CM.
CENTERED AT +2.5 CM.
f = .826

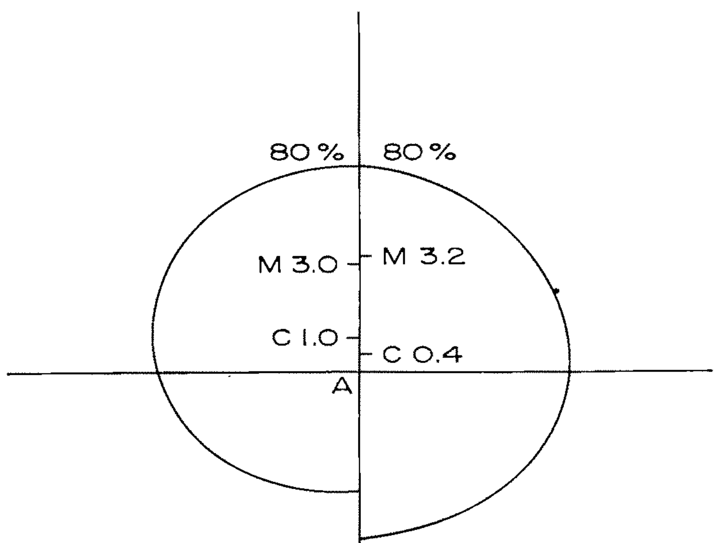


FIGURE 15: FIELD WIDTH 10 CM.
240° ARC
TRANSVERSE OVAL 9.0 x 11.8 CM.
CENTERED AT +1.0 CM.
f = .918

FIGURE 16: FIELD WIDTH 10 CM.
300° ARC
TRANSVERSE OVAL 10.4 x 11.8 CM.
CENTERED AT +0.4 CM.
f = .961

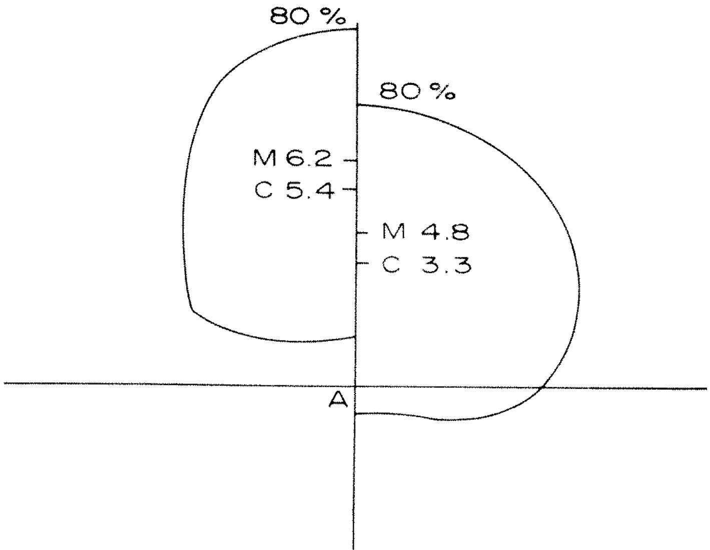


FIGURE 17: FIELD WIDTH 12 CM.
120° ARC
TRANSVERSE SEMI-OVAL 8.5 x 9.6 CM.
CENTERED AT +5.4 CM.
f = .741

FIGURE 18: FIELD WIDTH 12 CM.
180° ARC
TRANSVERSE OVAL 8.5 x 12.8 CM.
CENTERED AT +3.3 CM.
f = .834

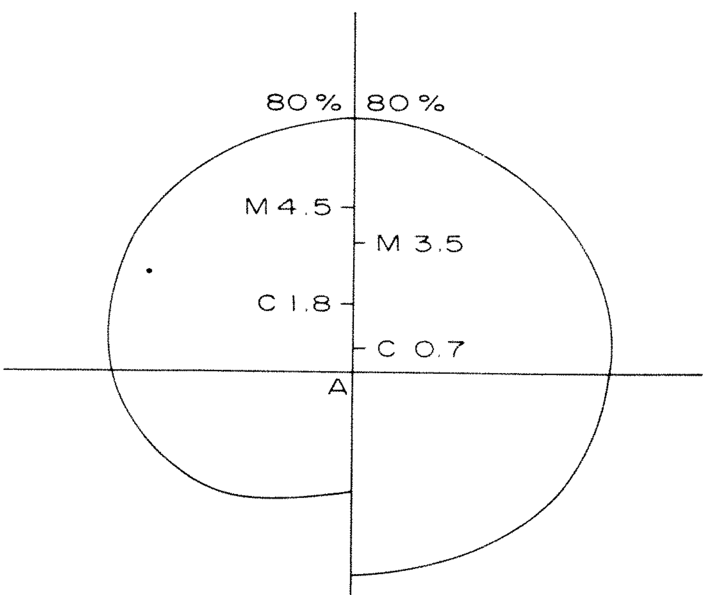


FIGURE 19: FIELD WIDTH 12 CM.
240° ARC
TRANSVERSE OVAL 10.3 x 14.0 CM.
CENTERED AT + 1.8 CM.
f = .901

FIGURE 20: FIELD WIDTH 12 CM.
300° ARC
TRANSVERSE OVAL 12.7 x 14.8 CM.
CENTERED AT +0.7 CM.
f = .961

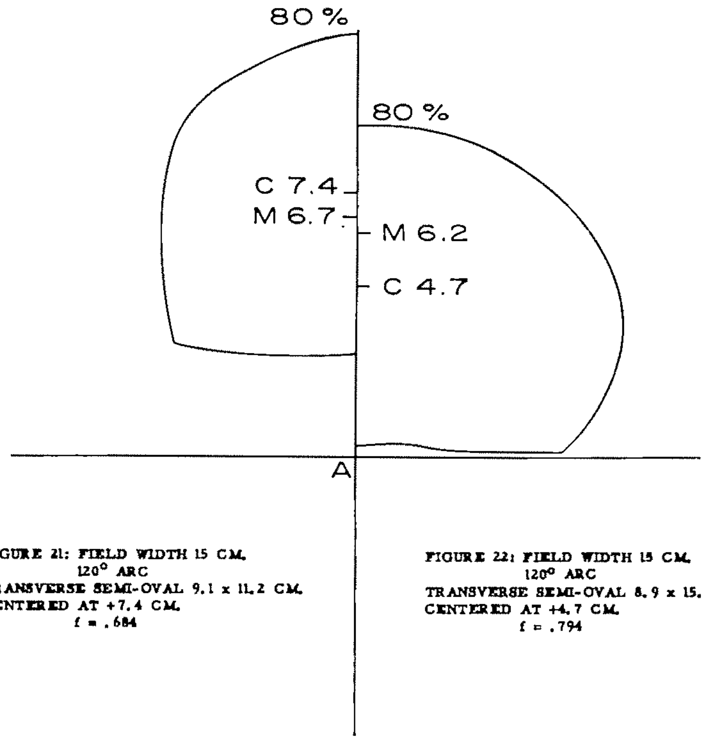


FIGURE 21: FIELD WIDTH 15 CM.
120° ARC
TRANSVERSE SEMI-OVAL 9.1 x 11.2 CM.
CENTERED AT +7.4 CM.
f = .684

FIGURE 22: FIELD WIDTH 15 CM.
120° ARC
TRANSVERSE SEMI-OVAL 8.9 x 15.4 CM.
CENTERED AT +4.7 CM.
f = .794

dose as 90% of the maximum tissue dose generated—*i.e.*, as $TD_s$. The appropriate equations are as follows:

(i) For 360-degree rotation:

$$TD_a = TD_m = 10/9\ TD_s \qquad (4)$$

and

$$TD_e = 8/9 TD_s, \qquad (5)$$

where

$TD_a$ = dose at the axis in rad,
$TD_m$ = maximum dose in rad,
$TD_s$ = tumor dose specified at $9/10\ TD_m$,
$TD_e$ = tissue dose at *edge* of 80% enclosure (edge of effectively treated volume).

Numerical example: Let the tumor dose for specification at 90%-of-maximum be 225 rad. Then

(4) $TD_a = TD_m = 10/9 TD_s = 10/9 \times 225$ rad $= 250$ rad.

(5) $TD_e = 8/9 TD_s = 8/9 \times 225$ rad $= 200$ rad.

Now find the treatment time required for $TD_s = 225$ rad.

(2) $$t = \frac{TD_a}{d} = \frac{10/9 TD_s}{d} = \frac{10/9 \times 225}{15}$$

$$= \frac{250}{15} = 16.67 \text{ min.} = 16 \text{ min. } 40 \text{ sec.}$$

(ii) For arcs shorter than 360 degrees:

$$TD_m = 10/9 TD_s \qquad (4')$$

and

$$TD_e = 8/9 TD_s$$

(as defined in the previous problem d—i). (5)

Once again, if $TD_s$ is to be 225 rad, then $TD_m = 250$ rad and $TD_e = 200$ rad.

Numerical example: If a 120-degree arc and an axis-field width of 12 cm. are used, requiring a tumor dose correction factor of $\mathbf{f} = .74$, what treatment time is required for a $TD_s$ of 225 rad?

(3) $TD_a = \mathbf{f} \times TD_m = .74 \times 250 = 185$ rad,

(2) $$t = \frac{TD_a}{d} = \frac{185}{15}$$

$$= 12.33 \text{ min. or } 12 \text{ min. } 20 \text{ sec.}$$

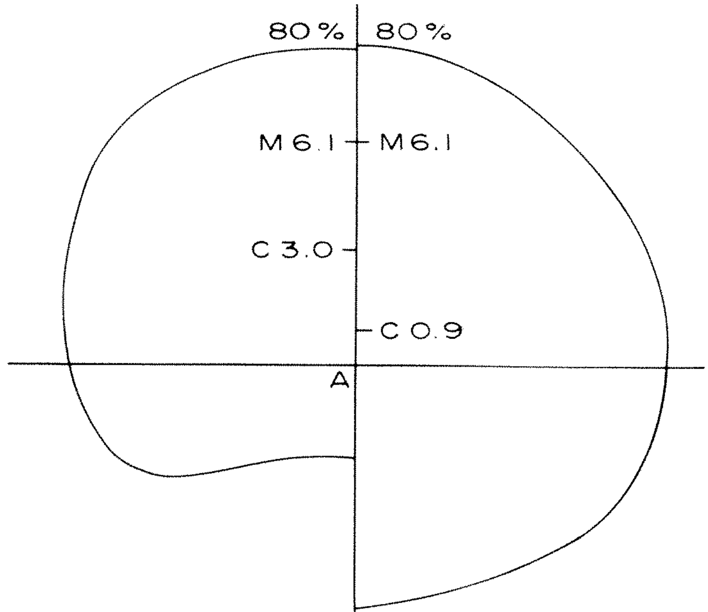


FIGURE 23: FIELD WIDTH 15 CM.
240° ARC
TRANSVERSE OVAL 11.3 x 16.8 CM.
CENTERED AT +3.0 CM.
f = .870

FIGURE 24: FIELD WIDTH 15 CM.
300° ARC
TRANSVERSE OVAL 15.5 x 17.8 CM.
CENTERED AT +0.9 CM.
f = .944

FIGURE 25: SIX FIELD WIDTHS
360° ROTATION
CIRCLES OF SPECIFIED DIAMETER
CENTERED AT AXIS
f = 1.00

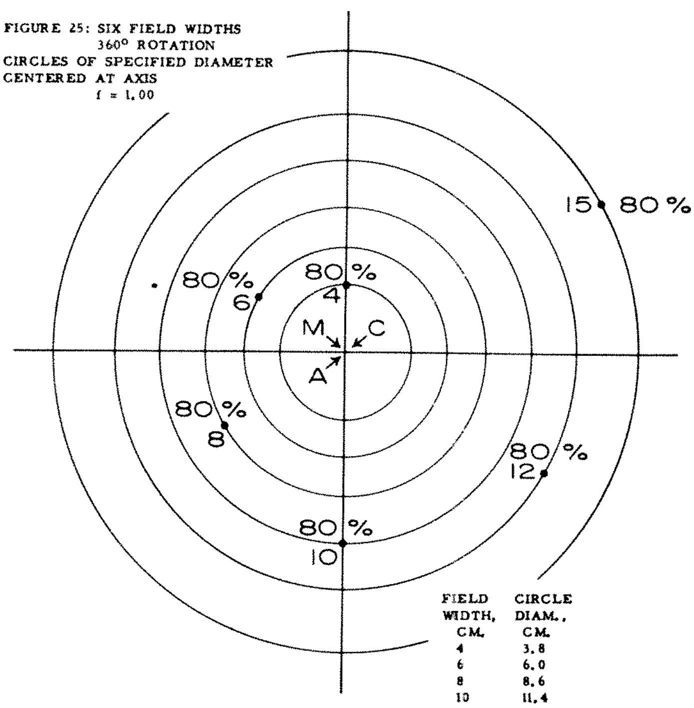


| FIELD WIDTH, CM. | CIRCLE DIAM., CM. |
|---|---|
| 4 | 3.8 |
| 6 | 6.0 |
| 8 | 8.6 |
| 10 | 11.4 |
| 12 | 14.0 |
| 15 | 17.4 |

(Check: The ratio of the answers from the preceding problems, d-ii and d-i: 12.33/16.67 =.74.)

SUMMARY

1. By means of 25 diagrams and 2 tables this study presents: (a) the location and magnitude of the maximum dose generated by various telecobalt arc therapy techniques; (b) the anteroposterior, transverse, and longitudinal dimensions of the volume enclosed by the 80%-of-maximum isodose surface (designated the "effectively treated volume"); and (c) An Axis Placement Guide which indicates where to locate the rotational axis so as to place the tumor's center at the center of the effectively treated volume.

2. The data above are presented for 36 nominal axis-field sizes (width or length 4, 6, 8, 10, 12, and 15 cm.) and for arc spans of 120, 180, 240, 300, and 360 degrees.

3. The data are not transferable—applying only to telecobalt machines having a source diameter of 2 cm., a source-to-collimator distance of 33 cm., and a rotational radius of 75 cm.

4. Sample equations and problems show how to calculate tumor doses and treatment times when the rotational axis does (for arcs of 360 degrees) and does not (for arcs of less than 360 degrees) coincide with the location of the maximum dose generated.

J. E. Turner, M.D.
416 South Second Street
Geneva, Illinois 60134

The authors acknowledge with thanks the able assistance of the following: Lee Douglas, Rosemary Callahan and Dorothea Brooks of the typing and calculating departments of Statistical Tabulating Corporation, who performed the dosage calculations and typed the manuscript; Jane Gordon, medical illustrator, who prepared the 25 drawings; Fred Hartmann, medical photographer, who photographed the drawings, and Dr. William T. Moss, who provided constructive criticisms of the manuscript.

REFERENCES

1. Braestrup, C. B., and Mooney, R. T. Physical aspects of rotating telecobalt equipment. *Radiology*, 1955, *64*, 17–28.
2. *British Journal of Radiology*, Supplement 10. Depth dose tables for use in radiotherapy. British Institute of Radiology, 1961, London, p. 58.
3. Dahl, O., and Vikterlof, K. J. Dose distributions in arc therapy in 200 to 250 KV range. *Acta radiol.*, 1958, Suppl. 171.
4. Dahl, O., Hultberg, S., Thoraeus, R., Vikterlof, K. J., and Walstam, R. Kilocurie cobalt-60 therapy at Radiumhemmet. Appelsberg Boktrycheri, Uppsala, Sweden, 1959.
5. Du Sault, L. A. Simplified method of treatment planning. *Radiology*, 1959, *73*, 85–94.
6. Jacobson, L. E., Koeck, G. P., Hillsinger, W. R., and Schwarz, M. E. $Co^{60}$ isodose curves for 240° rotation, showing displacement of center of dose from center of rotation. *Radiology*, 1961, *77*, 66–76.
7. Johns, H. E., Whitmore, G. F., Watson, T. A., and Umberg, F. H. System of dosimetry for rotation therapy with typical rotation distributions. *J. Canad. A. Radiologists*, 1953, *4*, 1–14.
8. Johns, H. E., Morrison, M. T., and Whitmore, G. F. Dosage calculations for rotation therapy: with special reference to cobalt 60. Am. J. Roentgenol., Rad. Therapy & Nuclear Med., 1956, *75*, 1105–1116.
9. Kornelson, R. O. Predetermined dose distributions for cobalt-60 circumaxial rotation. *J. Canad. A. Radiologists*, 1957, *8*, 42–44.
10. Nielsen, H. Rotatory irradiation. *Acta radiol.*, 1952, *37*, 318–328.
11. Roberts, J. E. Limiting factors of moving-field dosimetry. Roentgens, Rads and Riddles, 1956. U. S. Atomic Energy Commission, Washington, D. C., pp. 29–38.
12. Stern, B. E. Instrumental and technical notes: dose calculation for moving field therapy. *Brit. J. Radiol.*, 1956, *29*, 518–519.
13. Trump, J. G., Wright, K. A., Evans, W. W., Hare, H. F., and Lippincott, S. W., Jr. Two million volt roentgen therapy using rotation. Am. J. Roentgenol. & Rad. Therapy, 1951, *66*, 613–623.
14. Tsien, K. C. Study of basic external radiation treatment techniques with aid of automatic computing machines. *Brit. J. Radiol.*, 1958, *31*, 32–40.
15. Turner, J. E. Fast tissue-dosage system for 200-KV arc therapy. *Radiology*, 1963, *81*, 1028–1038.

# A FAST MOVING-FIELD TELECOBALT TISSUE-DOSAGE METHOD FOR ADDING MACHINE, TABULATING MACHINE, OR ELECTRONIC COMPUTER*

*By* J. E. TURNER, M.D.,† R. M. JOHNSON, M.S., *and* S. M. WHITFIELD, R.T.
GENEVA, ILLINOIS

THE goal of this study is to provide for the use of radiologists the basic data for assembling a library of "instant" radiation dose distribution charts for multiple fixed-field and moving-field techniques, covering most of the clinical problems encountered in cobalt 60 teletherapy. These data are presented in a form which permits 3 types of calculation: (1) by ordinary adding machine, (2) by automatic tabulating machine, and (3) by electronic computer. The first method enables a technician to calculate the tissue dose at any of 469 points in the cross-section of the patient within 40 to 60 seconds per point. The second method permits tabulation of the tissue dose at all 469 points in 4 to 30 minutes. The third method provides tabulation and print-out, as isodose lines, a whole cross-sectional distribution in 3 to 120 seconds.

The depth dose data presented are normalized to 100 per cent of tumor/air dose ratio[6] at the center of rotation (Table I), but the dosage distributions can be normalized, if desired, to the maximum dose generated (Fig. 1). Full cross-sectional tissue dose distributions developed from the data charts will be found to be largely independent of patient's size and shape,[2,10] providing wide and rapid application.

The physical factors used for this study are: cobalt 60 source diameter 2 cm., source-collimator-distance 33 cm., and source-center-distance 75 cm. These data cannot be applied to machines with different factors.

Before applying the data in this study, radiologists should determine the field sizes on their individual machines according to the recommendations of Hall.[3]

## REVIEW OF PREVIOUS DOSIMETRY METHODS

Johns *et al.*,[6] in 1953, introduced the concept of tumor/air dose ratio (tissue dose at axis per r in air at axis) to describe the central tissue dose for rotational and common-centered multiple fixed-field radiotherapy. Braestrup and Mooney,[1] in 1955, evolved a manual telecobalt dosimetry system requiring the averaging of 12 isodose chart readings at 30° intervals for each point of interest in the patient's anatomic cross-section. These readings were expressed as per cent of tumor/air dose ratio. The system requires a tedious number of readings, and the wide 30° interval (as opposed to a 10° interval or continuous integration) produces inaccuracies toward the periphery of the cross-section. Braestrup and Mooney illustrated the relative lack of sensitivity of the central tissue dose to variations of body contour.

Jones and Gregory, cited by Roberts,[10] evolved a pre-read, pre-calculated manual dosage system for rotational telecobalt therapy, requiring 2 hours to obtain a complete cross-sectional dosage distribution. They showed that the patient's cross-sectional contours, varying up to 5 cm. in radius from the radius of a circle of equivalent area, shifted the 80 per cent (of tumor/air dose ratio) isodose line only 3 mm. This paved the way for preparation of universal dosage charts, by du Sault,[2] in 1959, which can be centered anywhere up to 5 cm. from the center of a patient's cross-section with-

* From the Therapeutic Radiology Service, Veterans Administration Research Hospital and Department of Radiology, Northwestern University Medical School, Chicago, Illinois. This study was supported in part by a grant from the American Cancer Society, Illinois Division.

† Present address: Community Hospital, 416 South Second Street, Geneva, Illinois 60134.

## Table I

TUMOR/AIR DOSE RATIO (TAR) SHEET, FIELD WIDTH 6 CM. AT AXIS, COBALT 60, SOURCE-AXIS-DISTANCE 75 CM., TUMOR DOSE AT AXIS OF ROTATION PER 100 r IN AIR AT AXIS

| Angle of Beam Entry° | | Radial thickness of patient (cm.) 5.0 | 6.0 | 7.0 | 8.0 | 9.0 | 10.0 | 11.0 | 12.0 | 13.0 | 14.0 | 15.0 | 16.0 | 17.0 | 18.0 | 19.0 | 20.0 |
|---|---|---|---|---|---|---|---|---|---|---|---|---|---|---|---|---|---|
| 0 | ← | 86 | 82 | 78 | 74 | 70 | 66 | 62 | 59 | 56 | 53 | 50 | 47 | 44 | 41 | 39 | 37 |
| 10 | | 86 | 82 | 78 | 74 | 70 | 66 | 62 | 59 | 56 | 53 | 50 | 47 | 44 | 41 | 39 | 37 |
| 20 | | 86 | 82 | 78 | 74 | 70 | 66 | 62 | 59 | 56 | 53 | 50 | 47 | 44 | 41 | 39 | 37 |
| 30 | | 86 | 82 | 78 | 74 | 70 | 66 | 62 | 59 | 56 | 53 | 50 | 47 | 44 | 41 | 39 | 37 |
| 40 | | 86 | 82 | 78 | 74 | 70 | 66 | 62 | 59 | 56 | 53 | 50 | 47 | 44 | 41 | 39 | 37 |
| 50 | | 86 | 82 | 78 | 74 | 70 | 66 | 62 | 59 | 56 | 53 | 50 | 47 | 44 | 41 | 39 | 37 |
| 60 | | 86 | 82 | 78 | 74 | 70 | 66 | 62 | 59 | 56 | 53 | 50 | 47 | 44 | 41 | 39 | 37 |
| 70 | | 86 | 82 | 78 | 74 | 70 | 66 | 62 | 59 | 56 | 53 | 50 | 47 | 44 | 41 | 39 | 37 |
| 80 | | 86 | 82 | 78 | 74 | 70 | 66 | 62 | 59 | 56 | 53 | 50 | 47 | 44 | 41 | 39 | 37 |
| 90 | | 86 | 82 | 78 | 74 | 70 | 66 | 62 | 59 | 56 | 53 | 50 | 47 | 44 | 41 | 39 | 37 |
| 100 | | 86 | 82 | 78 | 74 | 70 | 66 | 62 | 59 | 56 | 53 | 50 | 47 | 44 | 41 | 39 | 37 |
| 110 | | 86 | 82 | 78 | 74 | 70 | 66 | 62 | 59 | 56 | 53 | 50 | 47 | 44 | 41 | 39 | 37 |
| 120 | | 86 | 82 | 78 | 74 | 70 | 66 | 62 | 59 | 56 | 53 | 50 | 47 | 44 | 41 | 39 | 37 |
| 130 | | 86 | 82 | 78 | 74 | 70 | 66 | 62 | 59 | 56 | 53 | 50 | 47 | 44 | 41 | 39 | 37 |
| 140 | | 86 | 82 | 78 | 74 | 70 | 66 | 62 | 59 | 56 | 53 | 50 | 47 | 44 | 41 | 39 | 37 |
| 150 | | 86 | 82 | 78 | 74 | 70 | 66 | 62 | 59 | 56 | 53 | 50 | 47 | 44 | 41 | 39 | 37 |
| 160 | | 86 | 82 | 78 | 74 | 70 | 66 | 62 | 59 | 56 | 53 | 50 | 47 | 44 | 41 | 39 | 37 |
| 170 | | 86 | 82 | 78 | 74 | 70 | 66 | 62 | 59 | 56 | 53 | 50 | 47 | 44 | 41 | 39 | 37 |
| 180 | | 86 | 82 | 78 | 74 | 70 | 66 | 62 | 59 | 56 | 53 | 50 | 47 | 44 | 41 | 39 | 37 |
| 190 | | 86 | 82 | 78 | 74 | 70 | 66 | 62 | 59 | 56 | 53 | 50 | 47 | 44 | 41 | 39 | 37 |
| 200 | | 86 | 82 | 78 | 74 | 70 | 66 | 62 | 59 | 56 | 53 | 50 | 47 | 44 | 41 | 39 | 37 |
| 210 | | 86 | 82 | 78 | 74 | 70 | 66 | 62 | 59 | 56 | 53 | 50 | 47 | 44 | 41 | 39 | 37 |
| 220 | | 86 | 82 | 78 | 74 | 70 | 66 | 62 | 59 | 56 | 53 | 50 | 47 | 44 | 41 | 39 | 37 |
| 230 | | 86 | 82 | 78 | 74 | 70 | 66 | 62 | 59 | 56 | 53 | 50 | 47 | 44 | 41 | 39 | 37 |
| 240 | | 86 | 82 | 78 | 74 | 70 | 66 | 62 | 59 | 56 | 53 | 50 | 47 | 44 | 41 | 39 | 37 |
| 250 | | 86 | 82 | 78 | 74 | 70 | 66 | 62 | 59 | 56 | 53 | 50 | 47 | 44 | 41 | 39 | 37 |
| 260 | | 86 | 82 | 78 | 74 | 70 | 66 | 62 | 59 | 56 | 53 | 50 | 47 | 44 | 41 | 39 | 37 |
| 270 | | 86 | 82 | 78 | 74 | 70 | 66 | 62 | 59 | 56 | 53 | 50 | 47 | 44 | 41 | 39 | 37 |
| 280 | | 86 | 82 | 78 | 74 | 70 | 66 | 62 | 59 | 56 | 53 | 50 | 47 | 44 | 41 | 39 | 37 |
| 290 | | 86 | 82 | 78 | 74 | 70 | 66 | 62 | 59 | 56 | 53 | 50 | 47 | 44 | 41 | 39 | 37 |
| 300 | | 86 | 82 | 78 | 74 | 70 | 66 | 62 | 59 | 56 | 53 | 50 | 47 | 44 | 41 | 39 | 37 |
| 310 | | 86 | 82 | 78 | 74 | 70 | 66 | 62 | 59 | 56 | 53 | 50 | 47 | 44 | 41 | 39 | 37 |
| 320 | | 86 | 82 | 78 | 74 | 70 | 66 | 62 | 59 | 56 | 53 | 50 | 47 | 44 | 41 | 39 | 37 |
| 330 | | 86 | 82 | 78 | 74 | 70 | 66 | 62 | 59 | 56 | 53 | 50 | 47 | 44 | 41 | 39 | 37 |
| 340 | | 86 | 82 | 78 | 74 | 70 | 66 | 62 | 59 | 56 | 53 | 50 | 47 | 44 | 41 | 39 | 37 |
| 350 | | 86 | 82 | 78 | 74 | 70 | 66 | 62 | 59 | 56 | 53 | 50 | 47 | 44 | 41 | 39 | 37 |

TABLE OF RECIPROCALS (1/N)

| n | 1/n | n | 1/n | n | 1/n | n | 1/n | n | 1/n | n | 1/n |
|---|---|---|---|---|---|---|---|---|---|---|---|
| 6 | 0.167 | 11 | 0.0909 | 16 | 0.0625 | 21 | 0.0476 | 26 | 0.0385 | 31 | 0.0323 |
| 7 | 0.143 | 12 | 0.0833 | 17 | 0.0588 | 22 | 0.0455 | 27 | 0.0370 | 32 | 0.0313 |
| 8 | 0.125 | 13 | 0.0769 | 18 | 0.0556 | 23 | 0.0435 | 28 | 0.0357 | 33 | 0.0303 |
| 9 | 0.111 | 14 | 0.0714 | 19 | 0.0526 | 24 | 0.0417 | 29 | 0.0345 | 34 | 0.0294 |
| 10 | 0.100 | 15 | 0.0667 | 20 | 0.0500 | 25 | 0.0400 | 30 | 0.0333 | 35 | 0.0286 |
| | | | | | | | | | | 36 | 0.0278 |

Record skin-to-axis distances by means of underscoring lines drawn on a transparent sheet placed upon the TAR sheet for the field size selected. Draw each underscoring line to correspond to the proper skin-to-axis distance (labels across top of sheet) and angle of beam entry (labels down left-hand column of sheet). Draw a horizontal arrow toward the 0° label. To find average TAR, add and average the individual TAR values (not the labels) underscored.

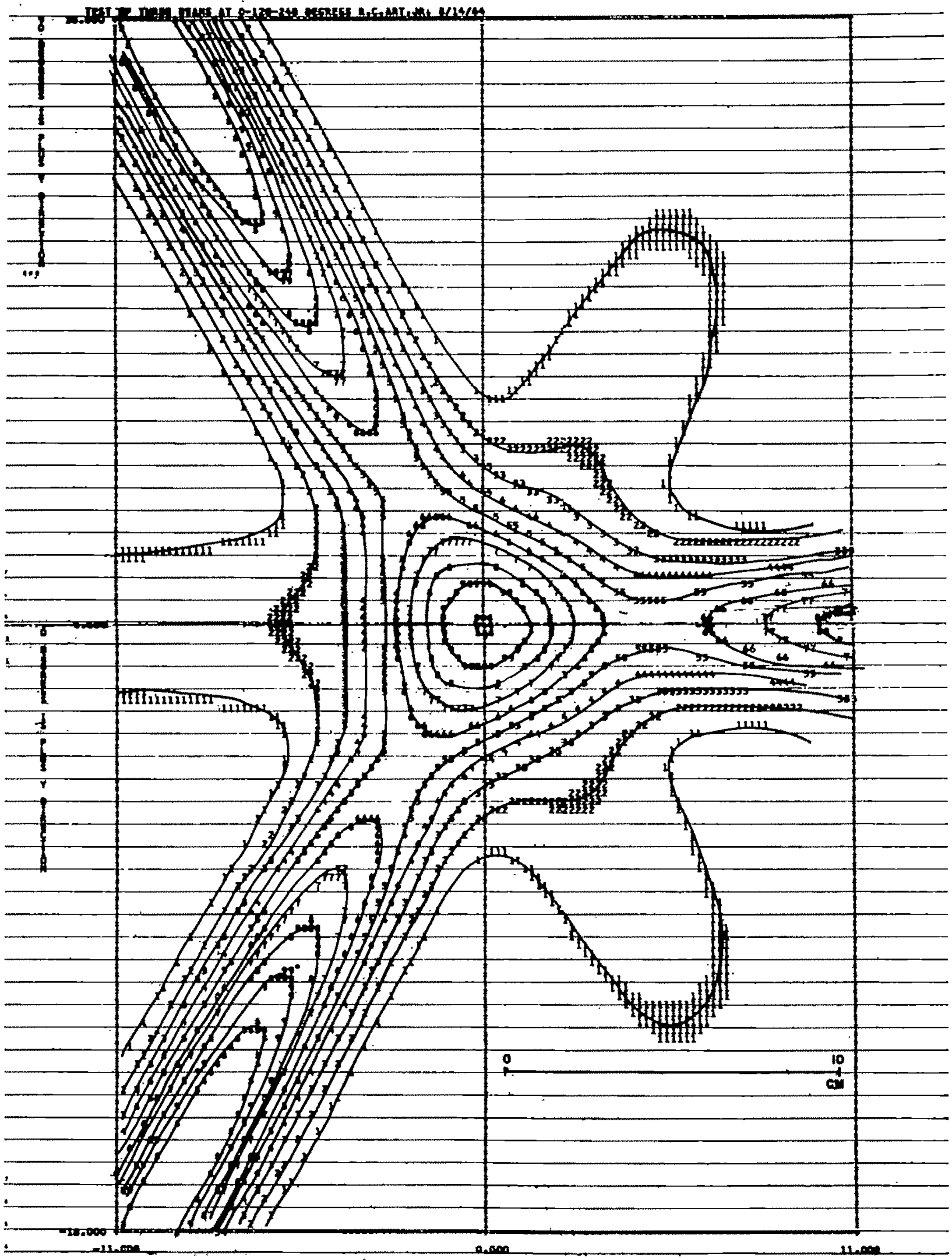

FIG. 1. Computer print-out for 3 beams, each 4 cm. wide, entering at 0°, 120° and 240°. The digits comprising the isodose lines represent tenths of the maximum dose generated. The symbol $ represents this maximum dose. Print-out scale of ½ inch = 2 cm. produces 27 per cent magnification, which can be reduced to actual life size by projection: 0° beam enters at right. When figure is turned counterclockwise 90°, it represents the dosage distribution in a slab of tissue 22 cm. thick and 36 cm. wide.

out significantly disturbing the dose distribution.

In 1957 Kornelson[8] evolved a precalculated dosage system for opposed arcs to be applied from the lateral aspects of the trunk. This approach, however, jeopardizes the laterally situated lungs, kidneys, and femurs. In 1961, Jacobson *et al.*[5] published isodose charts for 240° arcs at radii of 55 cm. and 95 cm. (but not at 75 cm.) showing where best to place the axis of rotation relative to the patient's tumor center. Tsien[13,14] and Sterling *et al.*[11] showed the applicability of tabulating machines and computers to dosage problems whereby complete cross-sectional dosage distributions could be calculated and printed out in 3 to 15 minutes per problem. The rotational problems in these programs were designed from the skin surface toward the center, *i.e.*, dependent in each problem upon the individual contour of the patient.

## MATERIALS AND METHODS

Tissue doses, expressed in per cent of tumor/air dose ratio were read for each point on a polar grid (every 10° on concentric circles of radius 1, 2, 3, 4, 5, 6, 8, 10, 12, 14, 16,* 18* and 20* cm.) from a set of Atomic Energy of Canada, Ltd., Theratron B Isodose Charts for 6 nominal axis-field sizes (4×10, 6×10, 8×10, 10×10, 12×12, and 15×15 cm.). The data for field width 6 cm. are presented in Table II. Tumor/air dose ratios, arranged in compatible format, are exemplified in Table I.

## ADDING MACHINE SYSTEM

A set of 12 tables comprises all the data required for adding machine computation.†

## TABULATING MACHINE SYSTEM

The following suggestions are offered for processing the data for use in automatic tabulating machines:

1. Tissue doses can be punched onto 6 sets of 36 decks of 36 IBM cards each (total 7,776 cards) and arranged so that the radiologist may obtain, at will, print-outs of the tissue doses at 469 points for a choice of any or all of 36 angles of treatment beam direction for any or all of the 6 field sizes (Fig. 2). Field length has negligible effect upon tissue dose distribution in the transverse plane of rotation, and it is felt that the 6 field widths selected cover most of the field sizes a radiologist would use.

2. The print-out data for the desired dose distributions can be transferred to polar charts and isodose lines interpolated and drawn.

3. The isodose lines can then be retraced on other polar charts so that the original data (469 three digit entries) will not show on the final isodose charts.

4. The final 146 charts can be photographed onto 35 mm. film from which 2×2 inch slides can be made. These slides can be projected life size onto patient's body cross-section contours for direct application to clinical teletherapy problems.

* Values extrapolated.

† Available from author.

## COMPUTER SYSTEM

Sophisticated computers can operate from 6 sets of 36 punch cards. The answers for the dosage problems can be printed out as (a) listings, (b) Cartesian distributions, or (c) properly interpolated isodoses composed of either small numerals (*e.g.*, 99999 = 90% isodose line) or actual contour lines depending on the degree of sophistication of the computer. Projection slides of (c) can be prepared for clinical use.

*Description of Punch Cards.* A typical punch card for use with the tabulating machine method is shown in Figure 3. Explanation of abbreviations is as follows:

RT = Radiation technique, designated by number. Our technique No. 1 is for cobalt 60 with source diameter 2 cm., source-collimator-distance 33 cm., and source-center-distance 75 cm.

FW = Field width (60% isodose line) as measured at the axis.

BDD = Beam direction, degrees, as depicted on a polar chart labeled

| | | | | | | | | | | | | | | | | | |
|---|---|---|---|---|---|---|---|---|---|---|---|---|---|---|---|---|---|
| 1 | 4 | | 360 | 100 | 109 | 120 | 129 | 141 | 153 | 165 | 196 | 232 | 262 | 318 | 376 | 440 | 514 |
| | | 90 | | 100 | 89 | 58 | 25 | | | | | | | | | | |
| | | | | 200 | 198 | 178 | 154 | 141 | 153 | 165 | 196 | 232 | 262 | 318 | 376 | 440 | 514 |
| 1 | 4 | | 350 | 100 | 108 | 118 | 129 | 132 | 140 | 146 | 150 | 139 | 119 | 99 | 57 | | |
| | | 90 | | 100 | 88 | 56 | 26 | | | | | | | | | | |
| | | | | 200 | 196 | 174 | 155 | 132 | 140 | 146 | 150 | 139 | 119 | 99 | 57 | | |
| 1 | 4 | | 340 | 100 | 107 | 111 | 113 | 108 | 94 | 80 | 38 | | | | | | |
| | | 90 | | 100 | 88 | 58 | 28 | | | | | | | | | | |
| | | | | 200 | 195 | 169 | 141 | 108 | 94 | 80 | 38 | | | | | | |
| 1 | 4 | | 330 | 100 | 106 | 103 | 91 | 71 | 50 | 30 | | | | | | | |
| | | 90 | | 100 | 88 | 60 | 32 | | | | | | | | | | |
| | | | | 200 | 194 | 163 | 123 | 71 | 50 | 30 | | | | | | | |
| 1 | 4 | | 320 | 100 | 106 | 93 | 69 | 43 | 24 | | | | | | | | |
| | | 90 | | 100 | 89 | 66 | 40 | 25 | | | | | | | | | |
| | | | | 200 | 195 | 159 | 109 | 68 | 24 | | | | | | | | |
| 1 | 4 | | 310 | 100 | 100 | 81 | 50 | 20 | | | | | | | | | |
| | | 90 | | 100 | 90 | 71 | 50 | 36 | 21 | | | | | | | | |
| | | | | 200 | 190 | 152 | 100 | 56 | 21 | | | | | | | | |
| 1 | 4 | | 300 | 100 | 96 | 70 | 36 | | | | | | | | | | |
| | | 90 | | 100 | 91 | 78 | 60 | 50 | 35 | 24 | | | | | | | |
| | | | | 200 | 187 | 148 | 96 | 50 | 35 | 24 | | | | | | | |
| 1 | 4 | | 290 | 100 | 92 | 64 | 30 | | | | | | | | | | |
| | | 90 | | 100 | 91 | 81 | 70 | 61 | 50 | 41 | 26 | | | | | | |
| | | | | 200 | 183 | 145 | 100 | 61 | 50 | 41 | 26 | | | | | | |
| 1 | 4 | | 280 | 100 | 90 | 60 | 27 | | | | | | | | | | |
| | | 90 | | 100 | 92 | 83 | 76 | 70 | 62 | 56 | 44 | 34 | 27 | | | | |
| | | | | 200 | 182 | 143 | 103 | 70 | 82 | 58 | 44 | 34 | 27 | | | | |
| 1 | 4 | | 270 | 100 | 89 | 58 | 25 | | | | | | | | | | |

FIG. 2. Illustration shows 1st page of print-out listing of depth doses at all 469 points in the polar grid in per cent of 2×TAR (the number of beams×TAR) since the tabulating machine only adds—it cannot divide, average or normalize. Dosage distribution is from 2 beams, 4 cm. wide, entering at 0° and 90°.

counterclockwise from the 0° position. The patient's anterior surface faces this 0° position. These beam directions are indicated by the labels in the left hand column of the TAR sheet. They are printed on the right margin of corresponding punch cards and used for filing.

PPD = Point position, degrees. This is used to designate location of dosage points upon concentric circles within the patient, as depicted by the polar chart, and as depicted by the left hand column of depth dose sheets. PPD also equals 360° minus BDD (see Appendix II for details).

O = The rotational axis.

1–20 = The labels for the ring numbers (or radii, in centimeters, of concentric circles) within the patient corresponding to the top horizontal line across the depth dose sheet. This, together with the point position in degrees (PPD), completes designation of dosage points (according to polar co-ordinates) within the patient as depicted on the polar chart.

SEQU = Sequence. The cards for the entire technique are punched in sequence from 0001 through 7776. In case they are spilled they can be reassembled in proper order by a mechanical collator.

*Content of Punched Cards.* Each depth dose sheet contains 36 lines of data (re-

TABLE II

DEPTH DOSES (PERCENTAGE OF TUMOR/AIR DOSE RATIO) DELIVERED TO POINTS 10° APART ON VARIOUS CIRCLES OF RADIUS R INSIDE THE PATIENT

FIELD WIDTH 6 CM. AT AXIS, COBALT 60, SOURCE-AXIS-DISTANCE 75 CM.

| Point Location Degrees | Radius (R) of concentric circle within patient (cm.) 1.0 | 2.0 | 3.0 | 4.0 | 5.0 | 6.0 | 8.0 | 10.0 | 12.0 | 14.0 | 16.0 | 18.0 | 20.0 |
|---|---|---|---|---|---|---|---|---|---|---|---|---|---|
| 360 | 109 | 119 | 129 | 139 | 150 | 163 | 190 | 222 | 252 | 308 | 366 | 424 | 488 |
| 350 | 109 | 118 | 127 | 138 | 149 | 161 | 182 | 196 | 190 | 161 | 202 | 158 | 102 |
| 340 | 108 | 117 | 125 | 133 | 131 | 126 | 92 | 42 | 20 | | | | |
| 330 | ← 107 | 115 | 119 | 111 | 97 | 74 | 25 | | | | | | |
| 320 | 106 | 112 | 103 | 87 | 60 | 33 | | | | | | | |
| 310 | 105 | 103 | 87 | 62 | 32 | | | | | | | | |
| 300 | 103 | 100 | 74 | 48 | 22 | | | | | | | | |
| 290 | 102 | 91 | 62 | 36 | | | | | | | | | |
| 280 | 100 | 87 | 56 | 30 | | | | | | | | | |
| 270 | 99 | 84 | 52 | 29 | | | | | | | | | |
| 260 | 98 | 82 | 51 | 29 | | | | | | | | | |
| 250 | 96 | 82 | 65 | 33 | | | | | | | | | |
| 240 | 95 | 83 | 60 | 40 | 21 | | | | | | | | |
| 230 | 94 | 84 | 66 | 48 | 29 | | | | | | | | |
| 220 | 93 | 84 | 71 | 58 | 42 | 29 | | | | | | | |
| 210 | 92 | 85 | 76 | 68 | 54 | 44 | 26 | | | | | | |
| 200 | 92 | 84 | 78 | 72 | 64 | 57 | 42 | 29 | 20 | | | | |
| 190 | 91 | 84 | 77 | 72 | 66 | 61 | 52 | 44 | 36 | 30 | 24 | 19 | |
| 180 | 91 | 84 | 77 | 72 | 66 | 61 | 52 | 44 | 38 | 33 | 28 | 24 | 21 |
| 170 | 91 | 84 | 77 | 72 | 66 | 61 | 52 | 44 | 36 | 30 | 24 | 19 | |
| 160 | 92 | 84 | 78 | 72 | 64 | 57 | 42 | 29 | 20 | | | | |
| 150 | 92 | 85 | 76 | 68 | 54 | 44 | 26 | | | | | | |
| 140 | 93 | 84 | 71 | 58 | 42 | 29 | | | | | | | |
| 130 | 94 | 84 | 66 | 48 | 29 | | | | | | | | |
| 120 | 95 | 83 | 60 | 40 | 21 | | | | | | | | |
| 110 | 96 | 82 | 65 | 33 | | | | | | | | | |
| 100 | 98 | 82 | 51 | 29 | | | | | | | | | |
| 90 | 99 | 84 | 52 | 29 | | | | | | | | | |
| 80 | 100 | 87 | 56 | 30 | | | | | | | | | |

Transfer the transparency from the TAR sheet to the depth dose sheet for the field size selected. With ruler and pencil, extend all underscoring lines across the full width of the paper. Points for dose-finding within the patient are designated by radius of concentric circle (with labels at tops of the vertical columns) and position in degrees on each circle (horizontal lines with labels at left). Point the arrow at the degree position desired and consult the appropriate vertical column. Adding and averaging underscored depth dose figures for selected points (or for all points) gives the average depth dose at each point in per cent of TAR.

TABLE II (*Continued*)

| Point Location Degrees | Radius (R) of concentric circle within patient (cm.) 1.0 | 2.0 | 3.0 | 4.0 | 5.0 | 6.0 | 8.0 | 10.0 | 12.0 | 14.0 | 16.0 | 18.0 | 20.0 |
|---|---|---|---|---|---|---|---|---|---|---|---|---|---|
| 70 | 102 | 91 | 62 | 36 | | | | | | | | | |
| 60 | 103 | 100 | 74 | 48 | 22 | | | | | | | | |
| 50 | 105 | 103 | 87 | 62 | 32 | | | | | | | | |
| 40 | 106 | 112 | 103 | 87 | 60 | 33 | | | | | | | |
| 30 | 107 | 115 | 119 | 111 | 97 | 74 | 25 | | | | | | |
| 20 | 108 | 117 | 125 | 133 | 131 | 126 | 92 | 42 | 20 | | | | |
| 10 | 109 | 118 | 127 | 138 | 149 | 161 | 182 | 196 | 190 | 161 | 202 | 158 | 102 |
| | 109 | 119 | 129 | 139 | 150 | 163 | 190 | 222 | 252 | 308 | 366 | 424 | 488 |
| | 109 | 118 | 127 | 138 | 149 | 161 | 182 | 196 | 190 | 161 | 202 | 158 | 102 |
| | 108 | 117 | 125 | 133 | 131 | 126 | 92 | 42 | 20 | | | | |
| | 107 | 115 | 119 | 111 | 97 | 74 | 25 | | | | | | |
| | 106 | 112 | 103 | 87 | 60 | 33 | | | | | | | |
| | 105 | 103 | 87 | 62 | 32 | | | | | | | | |
| | 103 | 100 | 74 | 48 | 22 | | | | | | | | |
| | 102 | 91 | 62 | 36 | | | | | | | | | |
| | 100 | 87 | 56 | 30 | | | | | | | | | |
| | 99 | 84 | 52 | 29 | | | | | | | | | |
| | 98 | 82 | 51 | 29 | | | | | | | | | |
| | 96 | 82 | 65 | 33 | | | | | | | | | |
| | 95 | 83 | 60 | 40 | 21 | | | | | | | | |
| | 94 | 84 | 66 | 48 | 29 | | | | | | | | |
| | 93 | 84 | 71 | 58 | 42 | 29 | | | | | | | |
| | 92 | 85 | 76 | 68 | 54 | 44 | 26 | | | | | | |
| | 92 | 84 | 78 | 72 | 64 | 57 | 42 | 29 | 20 | | | | |
| | 91 | 84 | 77 | 72 | 66 | 61 | 52 | 44 | 36 | 30 | 24 | 19 | |
| | 91 | 84 | 77 | 72 | 66 | 61 | 52 | 44 | 38 | 33 | 28 | 24 | 21 |
| | 91 | 84 | 77 | 72 | 66 | 61 | 52 | 44 | 36 | 30 | 24 | 19 | |
| | 92 | 84 | 78 | 72 | 64 | 57 | 42 | 29 | 20 | | | | |
| | 92 | 85 | 76 | 68 | 54 | 44 | 26 | | | | | | |
| | 93 | 84 | 71 | 58 | 42 | 29 | | | | | | | |
| | 94 | 84 | 66 | 48 | 29 | | | | | | | | |
| | 95 | 83 | 60 | 40 | 21 | | | | | | | | |
| | 96 | 82 | 65 | 33 | | | | | | | | | |
| | 98 | 82 | 51 | 29 | | | | | | | | | |
| | 99 | 84 | 52 | 29 | | | | | | | | | |
| | 100 | 87 | 56 | 30 | | | | | | | | | |
| | 102 | 91 | 62 | 36 | | | | | | | | | |
| | 103 | 100 | 74 | 48 | 22 | | | | | | | | |
| | 105 | 103 | 87 | 62 | 32 | | | | | | | | |
| | 106 | 112 | 103 | 87 | 60 | 33 | | | | | | | |
| | 107 | 115 | 119 | 111 | 97 | 74 | 25 | | | | | | |
| | 108 | 117 | 125 | 133 | 131 | 126 | 92 | 42 | 20 | | | | |
| | 109 | 118 | 127 | 138 | 149 | 161 | 182 | 196 | 190 | 161 | 202 | 158 | 102 |

peated for the convenience of adding machine users). One punched card depicts one line; thus 36 cards are required to reproduce the information on a single depth dose sheet. Assuming BDD = 0, the depth dose sheet or a print-out listing of the corresponding 36 punched cards would give the depth doses at 469 points within the patient *resulting from a single stationary beam entering at 0°*. There are, however, 36 such beam directions to consider. In the adding machine system, these are indicated by the

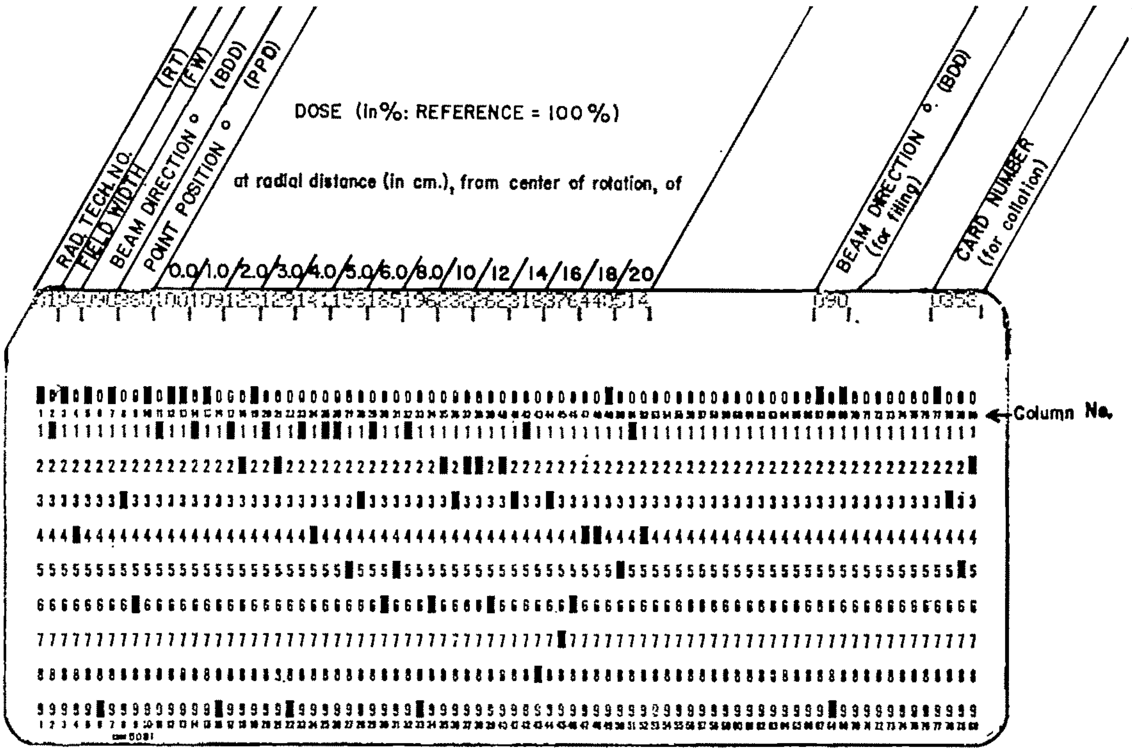


FIG. 3. Sample punch card for one line of one depth dose sheet. Column label abbreviations are explained in the text.

underscoring lines on the tracing-paper dose-finder (see Adding Machine Procedure). In the tabulating machine system, these beam directions are indicated by preparing 36 decks of punch cards differing only in that the BDD figure differs by 10° for each deck. From these 36 decks are selected only those decks which correspond to the directions of beam entry involved for each separate dosage problem.

OUTLINE OF COMPUTER PROGRAM (IBM 709)

1. Depth dose data from 216 punch cards are converted from polar to Cartesian co-ordinates.

2. These data can be punched onto other cards or stored in the computer's memory tape.

3. The depth dose readings for each beam size are fitted with a fourth order exponential equation. The resulting coefficients of the equations are punched on 3 IBM cards per beam and used as input data for later calculations.

4. The beam directions for which summated data are to be obtained are supplied to the computer.

5. The computer is instructed to add up the data at 80 points in each square inch, find the maximum value within a variable-sized rectangle centered at the rotational axis, take this maximum value at 100, and normalize all other data to this value.

6. The print-out is in isodose curves for 10, 20, 30, 40, 50, 60, 70, 80 and 90 per cent of the maximum value. Values lying within $\pm 1$ per cent of these decile lines are printed wherever they occur (*e.g.*, $80 \pm 1$ per cent is printed as a series of eights—the character for the 80% isodose line). The scale is $\frac{1}{4}$ inch on the print-out sheet equal to 1 cm. inside the patient.

REVIEW OF PHYSICAL FACTOR DEFINITIONS

1. A half-value layer of 11.1 cm. of lead is used.

2. The distance from the cobalt 60 source to the center of rotation (SCD) is held constant at 75 cm.

3. (a) Treatment field dimensions are expressed in terms of field size as measured at the axis. In practice, this involves placing a ruler or sheet of graph paper on the treatment table 75 cm. from the source and adjusting the light localizer shutters (patient absent) until the desired field dimensions are outlined. The patient is then positioned without changing the field size.
   (b) One can also pre-set the field size at 75 cm. by marking appropriate scales on the collimator shutters, or by placing an appropriately engraved transparent plastic insert in the flange below the shutters. Some commercial machines have the field size at the axis already engraved on the collimator scales.
   (c) If the patient's skin field is relatively perpendicular to the treatment beam, this can be drawn in ink on the patient's skin at a source-skin-distance of 75 cm. The patient is then moved so that a source-center-distance of 75 cm. results.

4. Intensity (roentgen output) is expressed as r per minute in air at a source-center-distance of 75 cm. The ionization chamber occupies the axis position, and measurement is made with the collimator shutters adjusted for the desired axis-field size, as in 3 above.

5. Tissue doses are expressed in terms of 100 r in air as measured at the axis position.

6. The tissue dose at the axis is measured by placing progressively thicker cylinders of unit density material around the ionization chamber, the position of which is never changed from 75 cm. source-center-distance.

7. The tissue dose at the axis of rotation per 100 r in air at the axis is known as the tumor/air dose ratio.

8. Placement of the axis of rotation to coincide with the tumor center is rarely appropriate and then only in some cases of 360° rotation. Single arcs generate a carcinocidal dose zone whose center falls up to 6 cm. superficial to the axis; hence, centering should be made according to the axis placement guide (see Table III) designed for use with the method.

9. For an arc of given span, more "fields" are available for crossfiring the tumor if they are narrow; fewer if they are wide. Therefore, central axis percentage depth

Table III

THE AXIS PLACEMENT GUIDE

SOURCE DIAMETER 2 CM., SOURCE-COLLIMATOR-DISTANCE 33 CM., SOURCE-AXIS DISTANCE 75 CM.

| Field width at 75 cm. | Arc (degrees) | Axis displacement (cm.) |
|---|---|---|
| 4 | 120 | 0.9 |
| 4 | 180 | 0.5 |
| 4 | 240 | 0.4 |
| 4 | 300 | 0.1 |
| 6 | 120 | 1.6 |
| 6 | 180 | 0.8 |
| 6 | 240 | 0.6 |
| 6 | 300 | 0.3 |
| 8 | 120 | 2.8 |
| 8 | 180 | 1.3 |
| 8 | 240 | 0.8 |
| 8 | 300 | 0.4 |
| 10 | 120 | 4.2 |
| 10 | 180 | 2.5 |
| 10 | 240 | 1.0 |
| 10 | 300 | 0.4 |
| 12 | 120 | 5.4 |
| 12 | 180 | 3.3 |
| 12 | 240 | 1.8 |
| 12 | 300 | 0.7 |
| 15 | 120 | 7.4 |
| 15 | 180 | 4.7 |
| 15 | 240 | 3.0 |
| 15 | 300 | 0.9 |

Displace the rotational axis the indicated number of cm. deep to the tumor's center in order to place center of 80% isodose area at tumor's center.

dose in arc therapy is greater for narrow fields and less for wide fields, since the dose gain from utilizing a large number of "fields" within a given arc span more than offsets the dose loss due to reducing the width and area of each field.

10. In this dosimetry system, rotation is imitated by assuming entry of stationary beam at 10° intervals.

## PROCEDURE

### I. FINDING THE AVERAGE TUMOR/AIR DOSE RATIO

1. Obtain the patient's body cross-section contour on transparent material.

2. If moving beam techniques are to be used, consult the axis placement guide (see Table III) to determine proper position of axis with reference to patient's skin outline. Choose field size and angles of beam entry to be used.

3. Place patient's outline transparency upon a polar chart with axis of rotation at the center of the chart (Fig. 4). (The polar chart should consist of concentric circles whose radii vary by 1 cm. from 1 through 20 cm. Radii should be drawn in every 10 degrees around the circle.)

4. Now place a piece of tracing paper over the tumor/air dose ratio sheet for the field size selected.

5. For proper registry, trace the following two lines: (a) the horizontal line underscoring the skin-to-axis distances near the top of the page, and (b) the vertical line joining the periods which follow the "angle of beam entry" labels down the left hand side of the sheet (see Table I).

6. Draw a short horizontal arrow toward the 0° label (see Table I).

7. Returning to the patient's outline on the polar chart, note the distances from skin-to-axis along each angle of beam entry.* Record these distances by finding their position on the tumor/air dose ratio sheet and by underlining the corresponding values.

8. Adding and averaging the underscored values gives the average tumor/air dose ratio unique to this patient's cross-section.

The above steps (1 through 8) must usually be done for each patient regardless of whether one uses the adding machine, tabulating machine or computer system. For most cases of 360° rotation, one may obtain a pre-averaged TAR value from the tables of Haynes and Froese.[4]

### II. ADDING MACHINE PROCEDURE FOR FINDING THE PERCENTAGE DEPTH DOSE AT OFF-AXIS POINTS

1. Remove tracing paper from tumor/air dose ratio sheet.

2. Give it to a technician with instructions to extend the underscoring lines all the way across the paper with a ruler (see Table II).

3. The technician places the tracing paper on the depth dose sheet for the field width selected. The format of the depth dose sheet is a selection of 468 points for dose-finding: 36 points (indicated by degree labels in the left hand column) on each of 13 concentric circles (indicated by radius labels in the top horizontal line) within the patient.

4. To find depth doses at any selected point, place arrow at degree value, find radius value, add and average the underscored figures in that column. This should require 40 to 60 seconds per point. It is recommended that a tally sheet be made in the format of the depth dose sheet for recording the answers.

5. Suggested manipulation of data comprises:

(a) Selected points ("add and multiply" method): This is done faster with a desk calculator capable of multiplication than with a simple adding machine. The percentage depth dose values are first added. The averaging of values can be done by multiplying the sum by the reciprocal (1/n) of the number of underscoring lines (n). This procedure is faster than dividing the sum by n. If some additional normalizing factor other than 100 per cent of tumor/air dose ratio is desired, that factor can be multiplied by 1/n and used as a single multiplier

* Skin to axis distances along untreated radii are ignored.

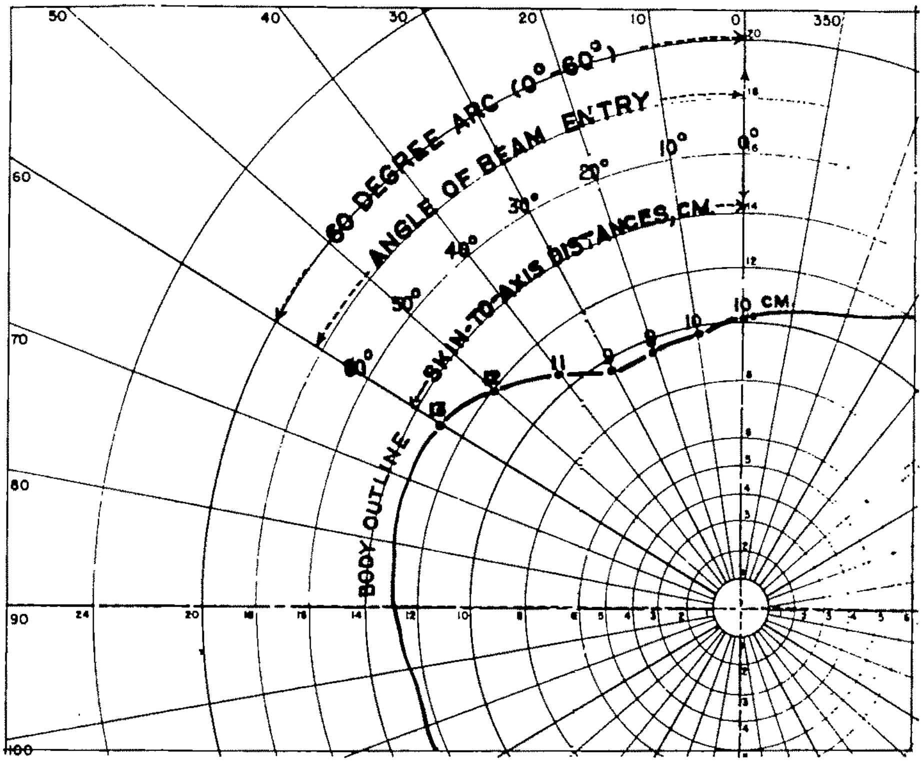


FIG. 4. Place transparency depicting patient's outline and axis position upon polar chart. Read off skin-to-axis distances every 10° along treatment arc.

to average and normalize the summated figures in a single step. In no case should more than one sum and one multiplication be necessary for finding the percentage depth dose at a given point.*

(b) Complete cross-section dose distributions ("add-select-decimate-interpolate" method): This can be done with a simple adding machine.

*Add:* The underscored figures are added as before.

*Select:* The axis tissue dose, the maximum tissue dose generated, or some other selected figure is designated as a reference value.

*Decimate:* One-tenth of the reference value is added to itself, subtotaling, 8 times to obtain the values of each tenth of the whole reference value. This list of tenths shows the values to be located by interpolation in order to obtain isodose curves from 10% through 90% of the reference value. Perhaps only 3 curves: 80%, 50%, and 20% would be germane to the treatment plan. Only those percentage depth dose values lying on either side of the percentage depth dose value to be located need be entered on the polar chart.

*Interpolate:* Points representing the positions of the interpolated dose points are recorded on the polar chart and joined, thus producing isodose curves.

* As long as there is no mixing of field sizes or "weighting" of exposures.

III. ACCOUNTING MACHINE PROCEDURE

1. The average tumor/air dose ratio is found by an adding machine or manually for each patient as in I.

2. Finding the percentage depth dose at off axis points.

(a) Select from the punch card file the 36-card decks corresponding to the desired field width and angles of beam entry.

(b) Place the decks in the collator so

that the cards will be resorted by point position (corresponding to the left hand column and arrow in the adding machine method).

(c) Feed the collated decks into an IBM 402 or 407 tabulating machine.

(d) A print-out will be obtained in 4 to 30 minutes showing summated percentage depth dose values in the same format as the depth dose sheet of the adding machine method. Save this print-out sheet to furnish values directly for selected points in terms of percentage of tumor/air dose ratio or for selected points to be normalized to some other value (as in II 5(a) above), or for complete cross-sectional dose distributions (as in II 5(b) above).

(e) The punch cards are returned to the collator to be re-sorted by angle of beam entry and then filed.

### IV. ELECTRONIC COMPUTER PROCEDURE

1. The average tumor/air dose ratio is found by adding machine or manually for each patient as in I.
2. Select from the file the $2\times 2$ inch slides corresponding to the desired treatment plan.
3. Establish axis position with reference to the patient's contour drawing as indicated in the axis placement guide (Table III).
4. Apply the projected dosage data directly to the contour drawing.

### THE BASIC LIBRARY

The punch cards in file can be used to obtain 146 basic dose distributions which can be made available in 3 forms: (1) duplicate files of punch cards for those who wish to conduct other dosage schemes in addition to the basic 146; (2) print-out sheets for those who wish to interpolate isodose curves for themselves; and (3) $2\times 2$ inch slides of the 146 basic distributions.

An outline description of the 146 problems is as follows:

I. Distributions for all 6 field width sets (4, 6, 8, 10, 12 and 15 cm.)
   A. Stationary beams: two directions, 0 and 90, 120, 150 and 180-degrees.
   B. Stationary beams: three directions, 0, 140, 220; 0, 130, 230; 0, 120, 240; and 0, 90, 270-degrees.
   C. Stationary beams: four directions, 0, 90, 180, 270; 30, 150, 210, 330; 40, 140, 220 and 320-degrees.
   D. Stationary beams at 180° opposition with 0:180 "loaded" dose-wise 2:1.
   E. Arcs of 120, 180, 240, 300 and 360-degrees.
   F. Opposed anterior and posterior arcs of span 100, 120 and 140 degrees each.

II. Special problems: Only for the field widths specified.
   A. Three beams of mixed widths for total pelvis.
      (1) 0, 120 and 240-degrees at field width 15, 12 and 12 cm., respectively.
      (2) 0, 130 and 230-degrees at field width 15, 10 and 10 cm., respectively.
      (3) 0, 140 and 220-degrees at field width 15, 8 and 8 cm., respectively.
   B. Two arcs (anterolateral and posterolateral) bilaterally for parametria for field widths 4 and 6 cm.
      (1) 80° arcs.
      (2) 100° arcs.
   C. One anterior arc for internal mammary lymph node chain in field width 6 and 8 cm.
      (1) 80° arc.
      (2) 100° arc.
   D. Six beam directions with double dose loading on the 0 and 180° beam directions for esophagus (to deliver 4,000 r tumor dose anteriorly and posteriorly; 2,000 r tumor dose through 4 oblique fields).
      (1) Field width 8 cm. only: $2\times 0$, 50, 130; $2\times 180$, 230, 310-degrees.
      (2) Field width 6 cm. only: $2\times 0$,

40, 140; 2×180, 220, 320-degrees.

### OPTIONAL NORMALIZATIONS

The radiologist may elect to refer tissue doses to a dose at the axis other than that of 100% of tumor/air dose ratio. Other convenient doses of reference are—tissue dose rate at the axis in rads per minute, 100 rads tissue dose, the daily tissue dose, and the total tissue dose contemplated for the course. Tissue doses can be normalized to these values by use of the following conversion factors:

| Dose of reference at axis (*A*) | Conversion factor (**f**) |
|---|---|
| Machine output in r/minute in air | Output×tumor/air-dose ratio (*TAR*) |
| 100 rads tissue dose | 100/*TAR* |
| Daily tissue dose (*TD*) | Daily *TD*/*TAR* |
| Total tissue dose (*TD*) | Total *TD*/*TAR* |

The tissue dose ($D$) obtained from the dose-finding transparency, multiplied by the conversion factor (**f**) can now be expressed as $D'$ in terms of A, the new dose of reference at the axis, *i.e.*, $D \times \mathbf{f} = D' (a)$.

Details of normalization to the maximum dose generated is the subject of a future report.[16]

### SUMMARY

1. A fast tissue dose system for multifield and rotational telecobalt therapy is presented for source diameter 2 cm., source-collimator-distance 33 cm., and source-center-distance 75 cm. The data cover field widths of 4, 6, 8, 10, 12 and 15 cm., as measured at the axis (60 per cent isodose line).

2. Tissue doses at any of 469 points within the patient may be calculated: (a) by adding machine in 40 to 60 seconds per point; (b) by automatic tabulating machine in 4 to 30 minutes for the entire 496 point distribution; or (c) by computer for a library of 146 of the 469-point dosage distribution in 90 minutes.

3. Tumor/air dose ratio and percentage depth dose sheets are presented for the adding machine system. Sample punch card and print-out formats are presented for the tabulating machine and computing systems.

4. Depth dose data presented are normalized to 100% of tumor/air dose ratio at the axis of rotation, but other normalizations are possible.

5. The cross-sectional distributions developed from the data are largely independent of patient's size and shape.

6. A basic library of 146 dosage distributions is described. This library can be made available in the form of (a) duplicate punch cards (b) print-out sheets and (c) 2×2 inch slides.

James E. Turner, M.D.
416 South Second Street
Geneva, Illinois 60134

The authors are pleased to acknowledge the valuable assistance of Richard Art, Jr., programming consultant at the Northwestern University Computer Center; Dr. William C. Krumbein, Professor of Geology, whose contour line equation project was adapted for radiation dosimetry; and Fred Hartmann who photographed the tables and illustrations.

Credit is also due to the following personnel at Statistical Tabulating Corporation of Chicago: Mr. Robert O'Brien, methods engineer, who helped design the format of the tabulating machine punch cards; Hazel Nelson, who typed the dosage tables; Dorothea Brooks, who typed the manuscript; and Rosemary Callahan, who calculated many dosage distributions by the adding machine method.

### APPENDIX I

Simplifying Assumptions Made:

1. Rotation is imitated by assuming entry of stationary beam at 10° intervals.

2. The tumor/air dose ratios corresponding to the various radial thicknesses of patient's tissue overlying the axis (in treated sectors) are averaged to obtain a mean tumor/air dose ratio value. This value reflects the variations in the patient's cross-sectional contour from that of a 15 cm. radius cylinder. This mean value is more accurate than the single tumor/air dose ratio value corresponding to the patient's average radial thickness.

3. The percentage depth dose figures for axis depth beyond 15 cm. were extrapolated and hence are less accurate than those for depths less than 15 cm.

4. The percentage depth dose figures for entry of stationary beams at 10° intervals become less accurate toward the periphery of the body cross-section than would figures for entry at 1° intervals or for continuous entry. They are more accurate, however, than figures for beam entry at 30° or 20° intervals. This situation will cause skin and near-surface doses to be estimated higher than the actual dose.

5. Additional correction for variation of body contour from a cylinder, namely the Jones-Gregory $e \pm \mu d$ factor was considered unnecessary for this system.

6. No correction was made for variation of body surface curvature from that of a cylinder perpendicular to each 10° beam. This would tend to affect the percentage depth dose values lying near the edges of each beam.

7. No correction was made for the "shoulder" of the tumor/air dose ratio versus depth curve: linearity is assumed. Estimates of skin dose made as percentage of tumor/air dose ratio from the sheets presented will thus be slightly higher than the actual dose.

8. The tumor/air dose ratio sheets present values for axis field sizes $4\times10$, $6\times10$, $8\times10$, $10\times10$, $12\times12$ and $15\times15$ cm. These values differ from those of other field lengths but the same field width. The most extreme example is the tumor/air dose ratio value for a $4\times4$ cm. field at axis depth 16 cm. The charted value in Figure 1 is 6.5 per cent higher than the true value. If desired, tumor/air dose ratio sheets in the format of Figure 1 can be prepared for individual field sizes using the data presented in the *British Journal of Radiology*, Supplements 5 and 10.

9. Off-axis percentage depth dose values vary negligibly with field lengths from 4 to 15 cm. The position of the 80% isodose line varies 1 mm. and the 20% isodose line 3 mm. as a maximum.

10. No correction is made for dose variations due to reversal of beam movement at either end of an arc.

These simplifying assumptions have been quantitated by several authors, as follows:

| Assumption No. | Author |
|---|---|
| 1, 3, 4, 6, 9 | Summers *et al.*[12] (1964) |
| 2 | Johns *et al.*[6] (1953) |
| 5 | Roberts[10] (1956) |
| 7 | Du Sault[2] (1959) |
| 10 | Nutall[9] (1956) |

## APPENDIX II

Explanation of Angle Labeling Formats:

The angle labels of the depth dose sheets are entered in sequence from 360° through 10°—*i.e.*, proceeding clockwise around the circle. This format is used because a patient revolving clockwise before a radiation beam carries with him all points for dosage calculation in a clockwise direction with reference to the beam. The beam, however, is entering the patient's skin in successive positions counterclockwise with reference to the patient's starting position.

This situation allows the dosage-planner two choices: (a) Either two sets of angle labels must be printed on the polar chart—one clockwise for the patient's dosage points and the other counterclockwise for angles of beam entry; or (b) a single set of angle labels printed on the polar chart must proceed in one direction for beam entry, while the angle labels printed on depth dose sheets for the patient's dose-points must proceed in the opposite direction. The latter alternative was chosen. (The counterclockwise labeling was retained on the TAR sheets because the axis of rotation does not lie on any angle-labeled radius. Hence, dosage considerations for the axis are not affected by choice of either clockwise or counterclockwise angle labeling.)

## REFERENCES


1. Braestrup, C. B., and Mooney, R. T. Physical aspects of rotating telecobalt equipment. *Radiology*, 1955, *64*, 17–28.
2. Du Sault, L. A. Simplified method of treatment planning. *Radiology*, 1959, *73*, 85–94.

3. Hall, E. J. On specification of field size for telecobalt units. Am. J. Roentgenol., Rad. Therapy & Nuclear Med., 1964, *92*, 207–212.
4. Haynes, R. H., and Froese, G. Averaged tumor-air ratios for 360-degree cobalt-60 rotation therapy. *Radiology*, 1958, *70*, 507–515.
5. Jacobson, L. E., Koeck, G. P., Hillsinger, W. R., and Schwarz, M. E. Cobalt 60 isodose curves for 240° rotation, showing displacement of center of dose from center of rotation. *Radiology*, 1961, *77*, 66–76.
6. Johns, H. E., Whitmore, G. F., Watson, T. A., and Umberg, F. H. System of dosimetry for rotation therapy with typical rotation distributions. *J. Canad. A. Radiologists*, 1953, *4*, 1–14.
7. Johns, H. E., Morrison, M. T., and Whitmore, G. F. Dosage calculations for rotation therapy: with special reference to cobalt 60. Am. J. Roentgenol., Rad. Therapy & Nuclear Med., 1956, *75*, 1105–1116.
8. Kornelson, R. O. Predetermined dose distributions for cobalt-60 circumaxial rotation. *J. Canad. A. Radiologists*, 1957, *8*, 42–44.
9. Nutall, A. K. Dose distributions in arc therapy. *Brit. J. Radiol.*, 1956, *29*, 119–120.
10. Roberts, J. E. Limiting factors of moving-field dosimetry. In: Roentgens, Rads, and Riddles. U. S. Atomic Energy Commission, Washington, D. C., 1956, pp. 29–38.
11. Sterling, T. D., Perry, H., and Bahr, G. K. Practical procedure for automating radiation treatment planning. *Brit. J. Radiol.*, 1961, *34*, 726–733.
12. Summers, R. E., Concannon, J. P., and Leone, D. P. Study of simplified methods for construction of complete isodose distributions in rotational cobalt teletherapy: trunk: horizontal 360° central rotation. *Radiology*, 1964, *83*, 231–242.
13. Tsien, K. C. Application of automatic computing machines to radiation treatment planning. *Brit. J. Radiol.*, 1955, *28*, 432–439.
14. Tsien, K. C. Study of basic external radiation treatment techniques with aid of automatic computing machines. *Brit. J. Radiol.*, 1958, *31*, 32–40.
15. Turner, J. E. Fast tissue-dosage system for 200-KV arc therapy. *Radiology*, 1963, *81*, 1028–1038.
16. Turner, J. E., Johnson, R. M., and Whitfield, S. M. Analysis of factors affecting optimal axis placement and 80% isodose volume dimensions in telecobalt arc therapy. Am. J. Roentgenol., Rad. Therapy & Nuclear Med., 1965, *94*, 852–864.

# A COMPUTER PROGRAM FOR ROTATIONAL TREATMENT PLANNING*

By WALTER MAUDERLI, D.Sc., and L. T. FITZGERALD, M.S.
GAINESVILLE, FLORIDA

IN EXTERNAL radiation therapy utilizing a rotational method, the calculation of the dose distribution throughout the entire cross section of the patient is so laborious that it is rarely done as completely as would be desired except in model cases. It is usual to calculate 4 of 5 points of interest in a patient; this ordinarily requires about 3 to 4 hours of time. With the widespread introduction and general availability of high-speed digital computers, it is now feasible to calculate the dose at many hundreds of points and plot isodose curves automatically for individual patients. The purpose of the authors is to describe a computer program for completely automated rotational treatment planning with automatic plotting of isodose curves within the body cross section.

## DATA PREPARATION

In contrast to medical diagnostic programs where the logic of the program may be different from the method actually used by the physician, the logic of the computer calculation is identical with that employed by personnel utilizing a manual calculation. A body contour is obtained and transferred to paper. From clinical knowledge and roentgenograms, the tumor is localized and indicated on the paper. Twenty-four lines are drawn from the center of the tumor to the body contour at 15° intervals. The lengths of these lines together with the desired field size, method of rotation (turning angle) and type of output desired (either a print out to scale or a plot of body cross section and isodose curves) are then given to the programmer for punching onto IBM cards.

In order to carry out manual calculations, one must employ radiation field data which are ordinarily given to the treatment planner in the form of isodose curves. The computer also must have these data, but it must be expressed in digital form, *i.e.*, the isodose curves must be "digitized."

The digitization is easily accomplished by placing a translucent sheet of graph paper with ½ inch divisions over the isodose curves. The dose value is then found at each of the ½ inch points on the graph paper by interpolation. Only one-half of the isodose curve need be digitized since the field is assumed to be symmetric. These digitized data are punched onto IBM cards. A still better method, of course, is to measure the field data in digital form. A depth dose scanning device has been built in this department for such a purpose.[2]

## METHOD

In rotational treatment planning, one usually determines the depth dose at several points within the patient cross section. In order to have a picture of the dose distribution, it is necessary to place the calculated dose values at their proper locations within the cross section. Likewise, when the depth dose values are calculated for many points by the computer, it is desirable to have a print out of the dose values in the proper scale. Computer printers are presently set up to print 10 characters per inch so a convenient spacing between points would be ½ inch. By locating the calculated dose value at each point at the center of the maximum of three digits needed (*e.g.*, 100 or 052), we may easily print values to scale with the dose value points ½ inch apart in horizontal and vertical directions.[6] This spacing of lines and points results in a grid on which points are located in a system of rectangular coordinates. This grid is called

* From the Department of Radiology, J. Hillis Miller Health Center, Gainesville, Florida.

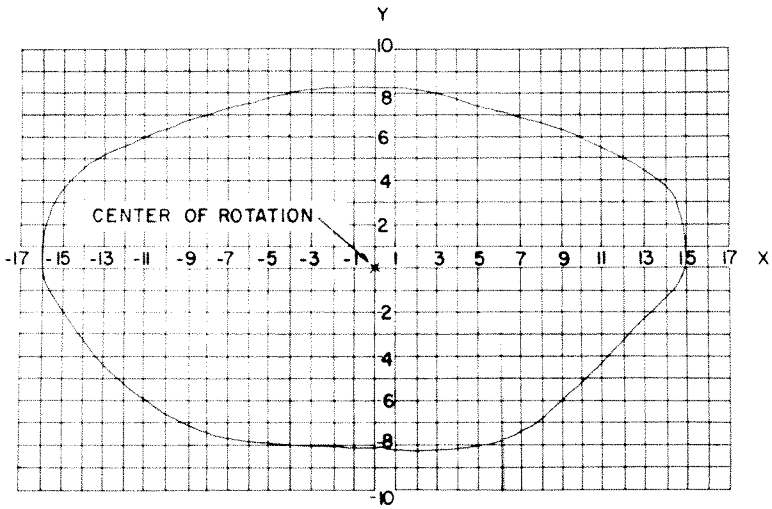


Fig. 1. Illustration of dose grid and location of patient contour.

the dose grid, $M$, and is illustrated in Figure 1. To allow for any size cross section, the dose grid is taken to be $39\times39$ units (1 unit $=\frac{1}{2}$ inch). The point with the coordinates (0, 0) is located at the center of the dose grid, which in turn is placed at the rotational center (see Fig. 1). The computer is programmed to calculate the depth dose at each point of $M$ within the cross section and to print the results in the $\frac{1}{2}$ inch scale discussed previously.

With multiple field therapy, each point of the cross section receives a particular dose rate which remains unchanged throughout the course of treatment. However, in rotational therapy, the radiation dose rate at each point varies as the patient (or therapy unit) revolves. Theoretically, to find the depth dose at a point, one would have to consider the contribution of an infinite number of stationary fields. However, the depth dose value at any point can be closely approximated by considering 24 fields spaced around the cross section and entering at 15° intervals. Each field has a weight of 1/24.

The computer sums the 24 fields in a manner described below. The first of the 24 fields is superimposed on the dose grid at 0° and the depth dose due to this field is found by interpolation at every point of the dose grid which lies within the superimposed field. The second field is then superimposed on the dose grid at 15° and again the depth dose is found at every point of the dose grid within the field and is added to the dose already found at these points from the first field. This process is continued for all 24 fields with the contribution from each field added to the contribution of all previous fields. The $n$th field enters at an angle of $(n-1)\cdot 15°$ for $n=1, 2, \cdots, 24$.

The above described summing procedure has been previously used for dose calculations with multiple stationary field therapy but has not been used with rotational therapy. The biggest problem encountered in extending this approach to rotational therapy was the correction of each field for nonperpendicular entry.

In digitizing the field data, we assumed that the radiation field was symmetric with respect to the beam axis. This assumption is valid only when the entire field edge (border line between air and phantom) lies on the skin or when bolus material is added. In rotational therapy the use of bolus material would be impractical. Hence, it is necessary to correct the digital symmetric field data for patient contour variations. This correction is done automatically by the computer for each of the 24 fields. The computer method for this correction is briefly described below.

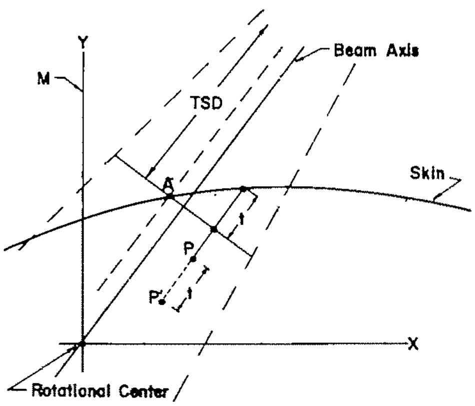


FIG. 2. Illustration of the correction method in case of nonperpendicular radiation beam entry.

With rotational therapy the beam axis always passes through the center of rotation and the target-to-center of rotation distance remains constant. The skin line may cut the radiation field edge at any point. (This is illustrated in Figure 2 where point $A$ is the intersection point of skin and the field edge.) Figure 2 shows a general case to illustrate the corrections needed in the case of too much tissue or too little tissue absorption. When using the symmetric field data, all points on the left side of the line through the target and point $A$ have values too low since there is too little tissue; all data points on the right side of the mentioned line have values too high since there is additional tissue. The computer program takes into account the fact that the depth dose at point $P$ is actually less than is given there by the symmetric beam data obtained from the isodose curves because of additional tissue of thickness $t$. (The distance $t$ is positive if there is additional tissue and negative if there is less tissue.) The correction process for point $P$ is done in two steps:

(1) The depth dose value at point $P'$ at distance $t$ below $P$ ($t>0$) or above $P$ ($t<0$) is found.

(2) This value is multiplied by a factor to correct for the inverse-square change introduced by the shifting from $P$ to $P'$.

Step 1 finds the correct dose value from the standpoint of tissue absorption, but this dose value is not correct from the standpoint of target distance due to the shifting from point $P$ to $P'$. Step 2 corrects the dose value found in Step 1 for the proper distance from the target. This method of inverse-square correction is well known. The correction factor is

$$\left(\frac{S+d+t}{S+d}\right)^2,$$

where $S$ is the target-skin distance, $d$ is the depth of point $P$ and $t$ is the thickness of tissue. Notice if $t=0$ (skin line and field edge coincide) that the dose value remains unchanged after the two step correction procedure. For convenience in computation, the shifting from $P$ to $P'$ is done along a line parallel to the beam axis. The shifting from $P$ to $P'$ should rather be done on a line through $P$ and the target; however, for target distances exceeding 100 cm., the error may be neglected, especially for points well within the radiation field.

With this process, every point of the given perpendicular (symmetric) field data is corrected so that the depth dose distribution is obtained for the nonperpendicular field. When the field has been corrected, it is superimposed on the dose grid $M$ and the dose due to this field is found at each point of $M$, within the field by interpolation.

These dose values are added to the depth dose from any previous fields. Since each of the 24 fields enters the body at a different angle, each field must individually be corrected for nonperpendicular entry by following the above two correction steps. The total dose at each point of the dose grid is the sum of the contributions of each of the 24 corrected fields.

It is convenient to express the maximum dose in the dose grid as 100%. The computer scans the dose grid $M$ to find the maximum value and divides the dose value at each point by this maximum and multiples by 100. In this way a 100% scale for the points is obtained. The dose grid is printed out to scale and the patient contour

is transferred to the print-out sheet.

If a plot of isodose curves is desired the computer is instructed to scan each scaled point in the dose grid and interpolate to find the coordinates of all 40% points. A Cal-Comp digital *x-y* plotter draws a curve through the points. The coordinates of the 50%, 60%, 70%, 80%, 90%, and 95% points are found in a similar manner and a curve is drawn through them. An *X* is drawn at 100% points and the patient contour is drawn in by the plotter.

## RESULTS AND DISCUSSION

With the print out to scale, one may immediately see the entire dose distribution within the cross section. However, more useful is the plot of isodose curves within the body. With this plot no additional manual plotting is necessary as is the case with the print out to scale. Figure 3 shows a typical print out to scale of the dose distribution resulting from a course of rotational therapy with a 2 mev. Van de Graaff unit with a distance of 110 cm. from the target to the center of rotation. Figure 4 illustrates a plot of the isodose curves and patient contour for the same case directly as it comes from the computer.

Various methods for automation of treatment planning have been previously described by Dalrymple and Perez-Tamayo,[1] Siler and Laughlin,[3] Tsien,[8,9] and others.[4,5,7] In 1963, Sterling, Perry and Weinkam[6] suggested a simple method of expressing dose distributions and a method of direct print out to scale of treatment plan results. However, to see the complete isodose distribution, one still has to manually draw in isodose curves. Sterling and his group applied this approach with multiple convergent and nonconvergent fields. The calculations for rotational treatment planning, as might have been expected, were

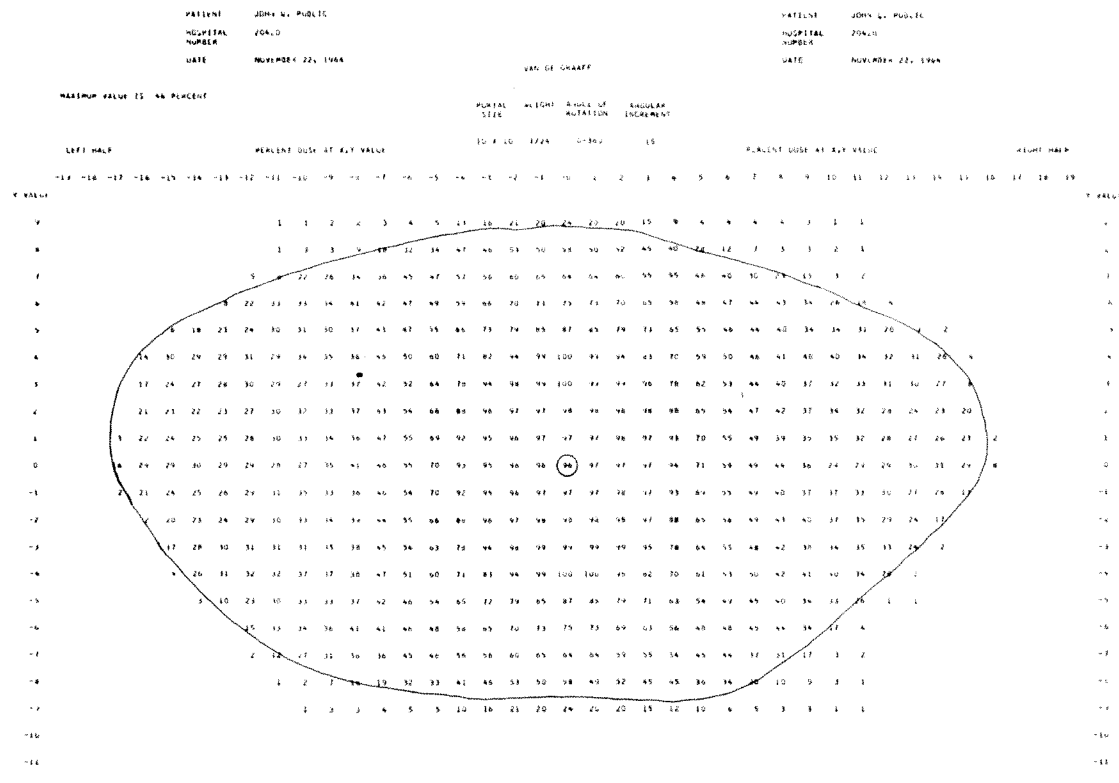

Fig. 3. Print out to scale of depth dose distribution for a 2 mev. Van de Graaff unit and a target-axis distance of 110 cm.

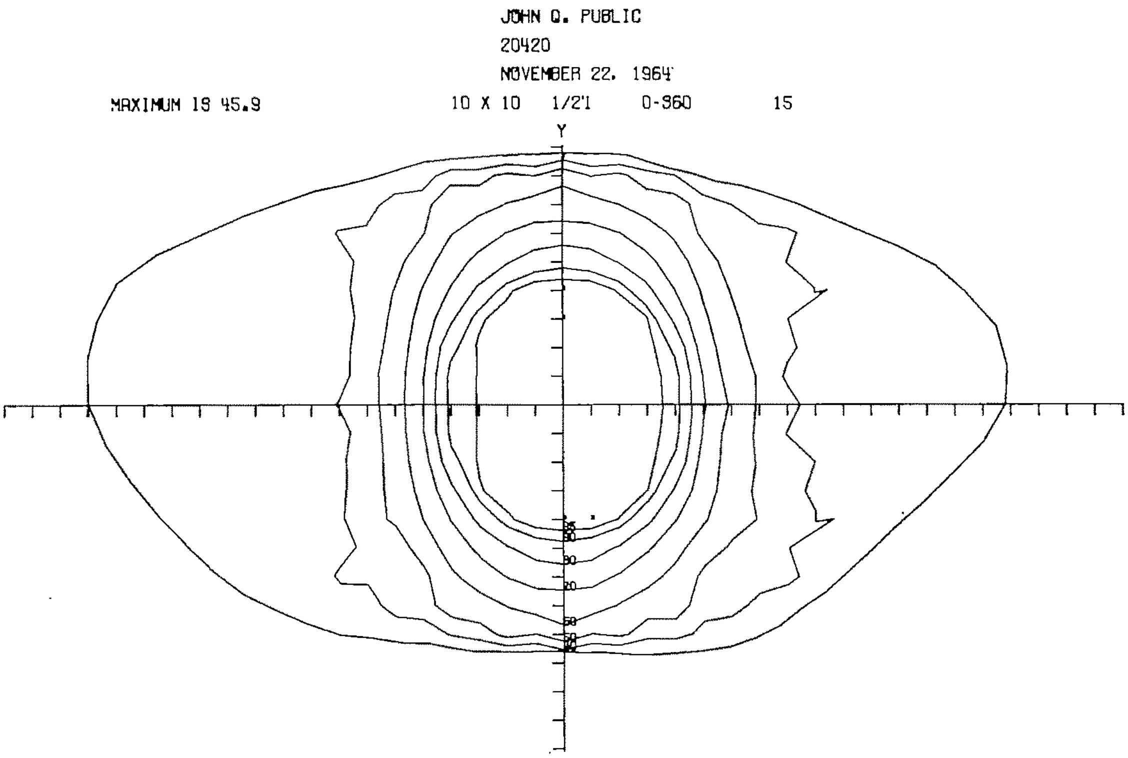


Fig. 4. Plot of patient contour and isodose curves.

considerably more complex. Our paper is the first account, to our knowledge, of a computer program for completely automated rotational treatment planning with automatic plotting of isodose curves within the body cross section.

The use of digital computers for rotational planning has been hindered by (1) the complexity of the mathematical calculations necessary for the estimation of depth dose with nonperpendicular beam entries, and (2) the necessity for connecting points of equal dose by lines drawn in by hand in case of a digital print out. The program in this paper has overcome these two obstacles. As suggested by Perez-Tamayo, it is now possible to prepare libraries of different body contour treatment plans with different field sizes for use in institutions without access to a computer. At institutions where a computer is available, many treatment plans may be prepared for individual problems of a unique nature.

The program, together with detailed mathematical formulation of the corrections for nonperpendicular beam entry and flow sheets for the IBM 709, has been prepared and is available on request. Execution time for the IBM 709 is about $4\frac{1}{2}$ minutes. The method is currently being used on all patients requiring rotation.

## SUMMARY

A method has been described for the automatic computation of a rotation treatment plan and the automatic plotting of isodose curves within the body cross section. The procedure is in routine use.

## APPENDIX

When considering the mathematical approach used for nonperpendicular beam entry corrections, it is convenient to represent the digital field data on a rectangular grid system with $\frac{1}{2}$ inch between adjacent points. The field edge (border line between air and phantom) serves as abscissa and the

central axis of the beam as ordinate. The digital field data are obtained from isodose curves for a particular target-skin distance (TSD) or from direct measurements with a depth dose plotting device.[2] The treatment distance (target-to-axis of rotation) is denoted by TAD. The abscissa of each field superimposed on the dose grid is tangent to a circle about the axis of rotation whose radius is the difference between the TSD and the TAD.

For generality, consider the $n$th field, where $n=1, 2, \cdots, 24$. The entry angle of the $n$th treatment field is $(n-1)\cdot\Delta\phi$, where $\Delta\phi=15°$. The coordinates $(X_0, Y_0)$ of the origin of the $n$th field in the dose grid coordinate system are:

$$X_0 = D\cdot\cos\,[(n-1)\cdot\Delta\phi]$$
$$Y_0 = D\cdot\sin\,[(n-1)\cdot\Delta\phi], \tag{1}$$

where $D$ is the difference between the TSD and the TAD.

Let $(x, y)$ be the coordinates of any point in the $n$th field coordinate system as shown in Figure 5. Let $t$ be the distance from the field abscissa to the skin line at the point $(x, 0)$. The coordinates of the point $(x, 0)$ with respect to the dose grid coordinate system are:

$$X = x\cdot\cos\,[(n+5)\cdot\Delta\phi] + X_0$$
$$Y = x\cdot\sin\,[(n+5)\cdot\Delta\phi] + Y_0, \tag{2}$$

where $X_0$ and $Y_0$ are defined in Equation 1.

A line is constructed through $(X, Y)$ parallel to the beam axis. This line is given in point-slope form by:

$$Y_G - Y - m\cdot(X_G - X) = 0, \tag{3}$$

where $(X_G, Y_G)$ is any point on the line and $m$ is the slope of the line (slope of central axis) in the dose grid system. In case the slope is infinite, the equation of the line is:

$$X_G - X = 0. \tag{3a}$$

Consider the equation

$$T = Y_G - Y - m\cdot(X_G - X). \tag{4}$$

The value of $T$ is zero for points on the line. For points not on the line, $T$ is not zero and

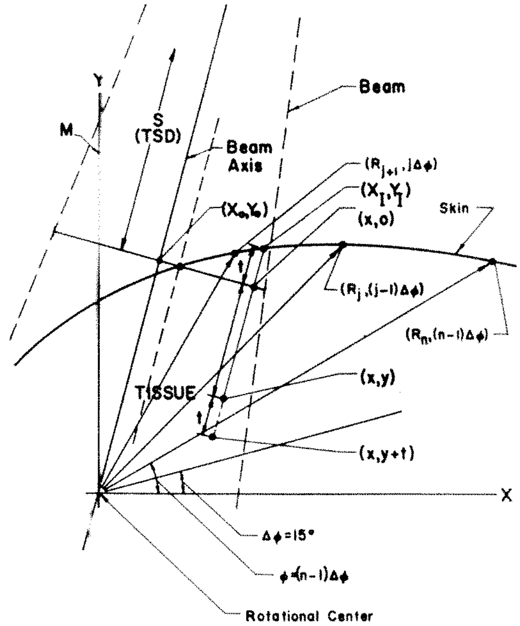


Fig. 5. Detailed geometry for a radiation beam with nonperpendicular skin entry.

the sign of $T$ is different for points on opposite sides of the line.

In order to find the value $t$ (thickness of of tissue), the computer must determine between which two points on the patient contour the line through the point $(X, Y)$ passes. To find these points, the computer tests the sign of $T_n$ for points on the contour to determine when a sign change occurs, where

$$T_n = R_n\cdot\{\sin\,[(n-1)\cdot\Delta\phi] - m \cdot\cos\,[(n-1)\cdot\Delta\phi]\} + m\cdot X - Y \tag{5}$$

and $R_n$ is the distance from the center of rotation to the $n$th contour point.

A change in the sign of $T_n$ indicates that the two last tested points lie on opposite sides of the line through the point $(X, Y)$. This line must, therefore, intersect the contour somewhere between these two points.

Suppose when testing, the computer finds that the signs of $T_j$ and $T_{j+1}$ are different. Then the line passes between the contour points with polar coordinates $(R_j, (j-1)\cdot\Delta\phi)$ and $(R_{j+1}, j\cdot\Delta\phi)$. The rectangular coordinates of these points are:

$$\begin{aligned} X_j &= R_j \cdot \cos\ [(j-1)\cdot\Delta\phi] \\ Y_j &= R_j \cdot \sin\ [(j-1)\cdot\Delta\phi] \\ X_{j+1} &= R_{j+1} \cdot \cos\ [j\cdot\Delta\phi] \\ Y_{j+1} &= R_{j+1} \cdot \sin\ [j\cdot\Delta\phi]. \end{aligned} \tag{6}$$

The line through the two contour points whose coordinates in the dose grid system are in Equation 6 is intersected with the line given by Equation 3. The coordinates in the dose grid system of the point of intersection of these two lines are:

$$X_I = \frac{(X_{j+1} - X_j)\cdot(Y - Y_j - m\cdot X) + X_j\cdot(Y_{j+1} - Y_j)}{Y_{j+1} - Y_j - (X_{j+1} - X_j)\cdot m}. \tag{7}$$

$$Y_I = Y + m\cdot(X_I - X).$$

In the case $m$ is infinite, the point of intersection is given by:

$$X_I = X$$

$$Y_I = \frac{(X - X_j)\cdot(Y_{j+1} - Y_j)}{X_{j+1} - X_j} + Y_j. \tag{7a}$$

The distance between $(X, Y)$ and $(X_I, Y_I)$ is $t$.

$$t = \sqrt{(X_I - X)^2 + (Y_I - Y)^2}. \tag{8}$$

The sign of $t$ is determined by comparing the respective distances of the points $(X, Y)$ and $(X_1, Y_1)$ from the origin.

To correct the dose at the point $(x, y)$ in the radiation field, find the dose at depth $y+t$ by linear interpolation and multiply by

$$\left(\frac{S+y+t}{S+y}\right)^2,$$

where $S$ is the target-abscissa distance. The value $t$ is used in the correction of all data points on the line through $(x, 0)$, which are parallel to the beam axis. When one column of field data is corrected, the value of $t$ for the next point on the field abscissa is found and that column is corrected. When all data points for the field in question have been corrected for nonperpendicular beam entry, the field is superimposed on the dose grid and the depth dose contribution from this field is found at each point of the dose grid by linear interpolation. The total dose is found by the summing of all 24 fields, each corrected in the manner described above.

The same method of nonperpendicular entry correction can also be applied to stationary nonconvergent fields.

Presently, we are investigating the effect of body inhomogeneities upon the depth dose distribution. In the future, corrections for inhomogeneities shall be added to the computer program now in use.

Walter Mauderli, D.Sc.
Department of Radiology
J. Hillis Miller Health Center
Gainesville, Florida

This investigation was supported in part by the 1963 and 1964 National Institutes of Health General Research Support Grant and an institutional grant from the American Cancer Society.

All programs were run on the IBM 709 Computer made available through the Computing Center, University of Florida, Gainesville, Florida.

REFERENCES

1. Dalrymple, G. V., and Perez-Tamayo, R. Numerical method for determination of moving field isodose curves for treatment planning in radiotherapy. *Comm. ACM.*, 1963, *6*, 625–626.
2. Mauderli, W., and Hazard, B. Depth-dose scanning device. *Radiology*, 1965, *84*, 130–131.
3. Siler, W., and Laughlin, J. S. Computer method for radiation treatment planning. *Comm. ACM.*, 1962, *5*, 407–408.
4. Sterling, T. D., Perry, H., and Bahr, G. K. Practical procedure for automating radiation treatment planning. *Brit. J. Radiol.*, 1961, *34*, 726–733.
5. Sterling, T. D., Perry, H., and Weinkam, J. J. Automation of radiation treatment planning. II. Calculation of non-convergent field dose distribution. *Brit. J. Radiol.*, 1963, *36*, 63–67.

6. STERLING, T. D., PERRY, H., and WEINKAM, J. J. Automation of radiation treatment planning. III. Simplified system of digitising isodoses and direct print-out of dose distribution. *Brit. J. Radiol.*, 1963, *36*, 522–527.
7. STERLING, T. D., PERRY, H., and KATZ, L. Automation of radiation treatment planning. IV. Derivation of mathematical expression for per cent depth dose surface of cobalt 60 beams and visualisation of multiple field dose distributions. *Brit. J. Radiol.*, 1964, *37*, 544–550.
8. TSIEN, K. C. Application of automatic computing machines to radiation treatment planning. *Brit. J. Radiol.*, 1955, *28*, 432–439.
9. TSIEN, K. C. Study of basic external radiation treatment techniques with aid of automatic computing machines. *Brit. J. Radiol.*, 1958, *31*, 32–40.

# A SIMPLE, INEXPENSIVE, MANUALLY-OPERATED ISODOSE PLOTTER

*By* J. EUGENE ROBINSON, Ph.D., *and* R. S. McDOUGALL, B.Sc.
BALTIMORE, MARYLAND

ONE of the most essential pieces of equipment in a modern Radiotherapy Center is an isodose plotter. Although most manufacturers supply a limited number of isodose curve charts with their radiotherapy equipment, they cannot supply information to fit the special needs of individual departments. There are many descriptions in the literature of isodose plotting systems. Most of the ones described are technically sophisticated, automated plotters. In general, because of complexity, they are expensive and difficult to construct; and, perhaps more important in the long run, they are not easy to maintain. In this paper, a plotting system is described which fulfills most requirements and yet is inexpensive to build and has proved to be essentially maintenance free.

The basic requirements for an isodose plotting system are: (a) remote drive of the radiation detecting probe; (b) a marking system to indicate probe position; (c) a measuring phantom which simulates radiation absorption and scattering of the patient; and (d) appropriate radiation detectors.

## POSITIONING MECHANISM

Plotting systems are conventionally centered around an X-Y drive system which moves a detector in the radiation beam and duplicates this motion at a plotting table in the control area. The mechanism which we have designed is operated by two pairs of selsyn motors. The X-Y pair on the plotting table (Fig. 1) is manually driven by means of the two black knobs (seen in the illustration) and a pulley-and-string system coupled to the supporting blocks of the motors. The knobs are radiator valve handles and the string is silk fishing line coated with rosin. The blocks are supported by linear bearings which move along precision-ground steel rods, one-half inch in diameter. As the knobs are manually rotated, the supporting blocks are pulled along. This linear motion is translated into rotary motion of the selsyn armatures by means of a pinion attached to the shaft of the armature and a fixed rack attached to the plotting table frame. The companion system which drives the ionization chamber in the water phantom operates in a complementary manner. Since the armature of the driving selsyn is rotated as it is pulled along a rack on the plotting board, the armature of the receiving selsyn is rotated and a pinion, mounted on its shaft, rolls along a rack mounted on the phantom assembly and drives the detector in the phantom. The support is again made by linear bearings. The mechanical assembly at the water phantom is mounted on an angle-brass frame-work which is easily removed from the water tank when the equipment is placed in storage.

The drive system moves so smoothly on its support bearings that there is little or no "electrical spring" or slippage between the selsyn motor pairs. This has been tested by establishing an index between positions of detector in the phantom and marker at the plotting table and violently driving the system over its complete range of travel. Reproducibility of indexing was found to be better than one-tenth of a millimeter.

## MARKING SYSTEM

The marking system is somewhat unique. A "Model T" Ford spark coil is used to step up the voltage from a 6-volt battery. When a foot switch is pressed, the potential generated is sufficient to produce a spark between the marking pointer and conduc-

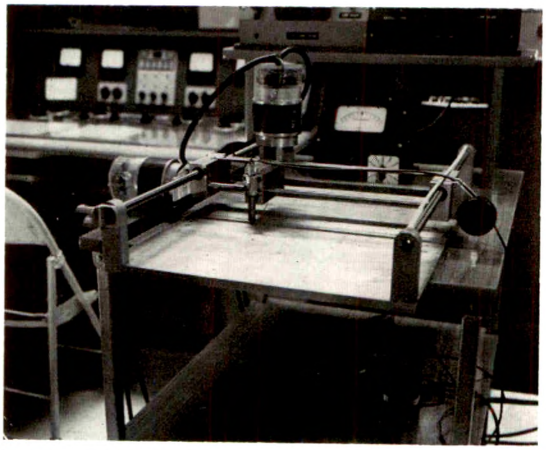

Fig. 1. Plotting table assembly.

tive recording paper* placed on the plotting table. The sparking potential and height of the pointer can be adjusted to yield a clear mark of any convenient size.

## WATER PHANTOM

The measurement phantom (Fig. 2) was constructed from $\frac{3}{8}$th inch lucite. The joints were bonded with ethylene dichloride and mechanically secured with brass screws. One side of the tank, rather than being solid, has a thin rubber dam or window. The dam is made from rubber sheeting secured by plexiglass clamping blocks. This dam (0.2 mm. thick) presents a thin window so that a radiation detector can be moved close to the surface. An ionization chamber probe with a small right-angle bend was constructed to make radiation measurements at or near the phantom surface. The probe can be forced against the rubber dam so that half the chamber is covered by water and half exposed. This makes it possible to make radiation measurements at or near the surface without submerging the whole probe and cable assembly.

The system was developed, in part, for dosimetry measurements with a betatron. Since there are random fluctuations in radiation output with such a machine, it is convenient, when determining isodose curves, to use the difference in output from

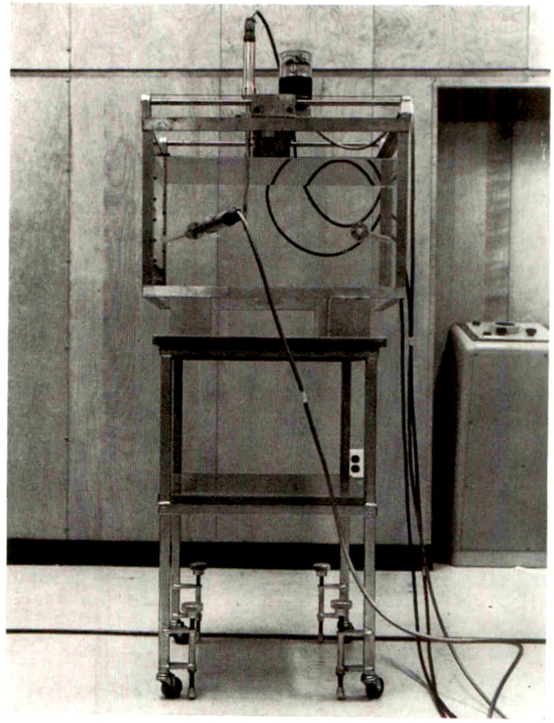

Fig. 2. Water phantom.

a fixed monitor probe and a search probe. The phantom tank has a lucite tube angling in from one side to accommodate the monitor probe. The monitor then can be placed in the radiation beam inside of the phantom without the necessity of waterproofing the cable and probe assembly. The tube is mounted on a boss on the side of the tank so that it can readily be removed or replaced.

## IONIZATION CHAMBER AND PROBE ASSEMBLY

The ionization chamber and probe assembly which were constructed are shown in Figures 3 and 4. The chamber is made from muscle-equivalent conducting plastic,† with an internal diameter of 3.5 mm., a wall thickness of 1 mm. and an active length of 15 mm. The open end is internally threaded to screw onto a teflon support plug. The central collecting electrode is aluminum, with the base end threaded for mounting onto the support plug. A thin brass washer makes electric contact be-

* Teledeltos Picker Nuclear.

† St. Procopius College, Lisle, Illinois.

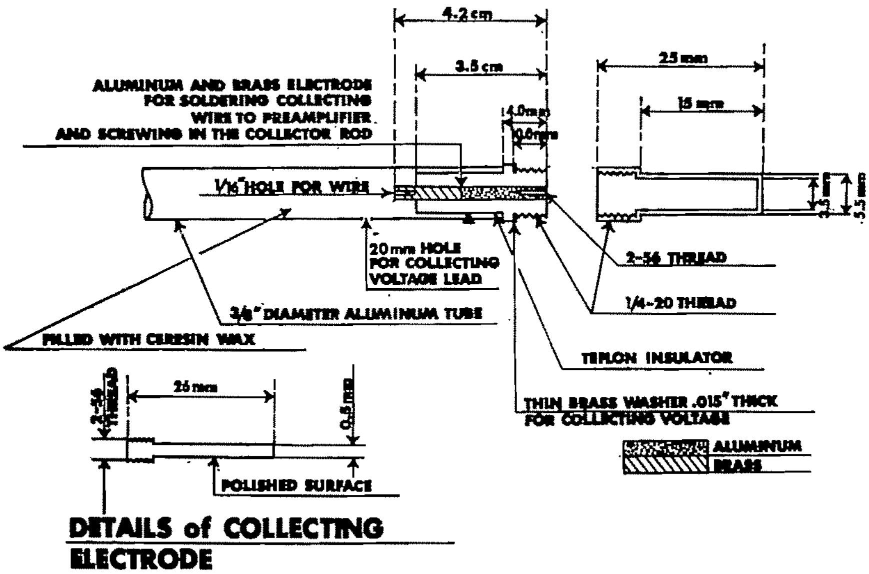


FIG. 3. Details of ionization chamber for measuring isodose curves in water.

tween the chamber wall and the collecting voltage lead.

The stem which supports the chamber is made of ⅜th inch aluminum tubing. One end is threaded and screws into a 1 inch diameter thin-wall aluminum tube, which acts as a pre-amplifier housing. A 32 pitch rack is mounted on the side of the support stem. This rack meshes with a pinion on the search probe support block and is used for manually raising and lowering the chamber in the phantom. A seven-pin "Amphenol" connector is mounted internally on the end of the pre-amplifier assembly to make the necessary electrical connections for the chamber and pre-amplifier. The pre-amplifier is a modular assembly, rigidly mounted in a lucite tube and is "potted" in ceresin wax.

The plotting system is used for measurements over a wide range of dose rates. To span this range, replicate pre-amplifier modules have been constructed containing various values for the high-meg measuring resistors. Exact duplicates have been made for those values most commonly used; and, since the modules are "plug-in" units, they can be rapidly replaced in event of malfunction. In the same way, all parts of the ionization chamber and probe assembly have been duplicated and can be replaced in the matter of minutes.

## AMPLIFIERS

The amplifiers are of the electrometer type and are battery operated. They are

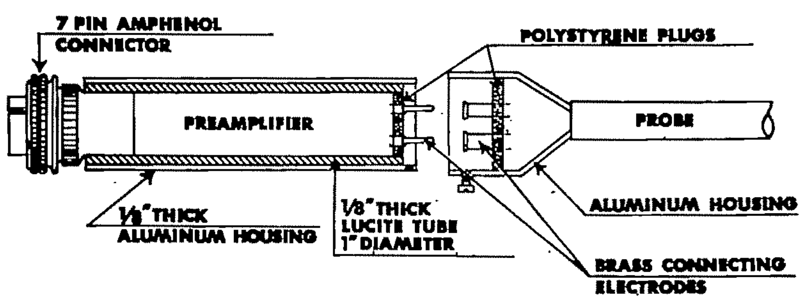


FIG. 4. Pre-amplifier assembly.

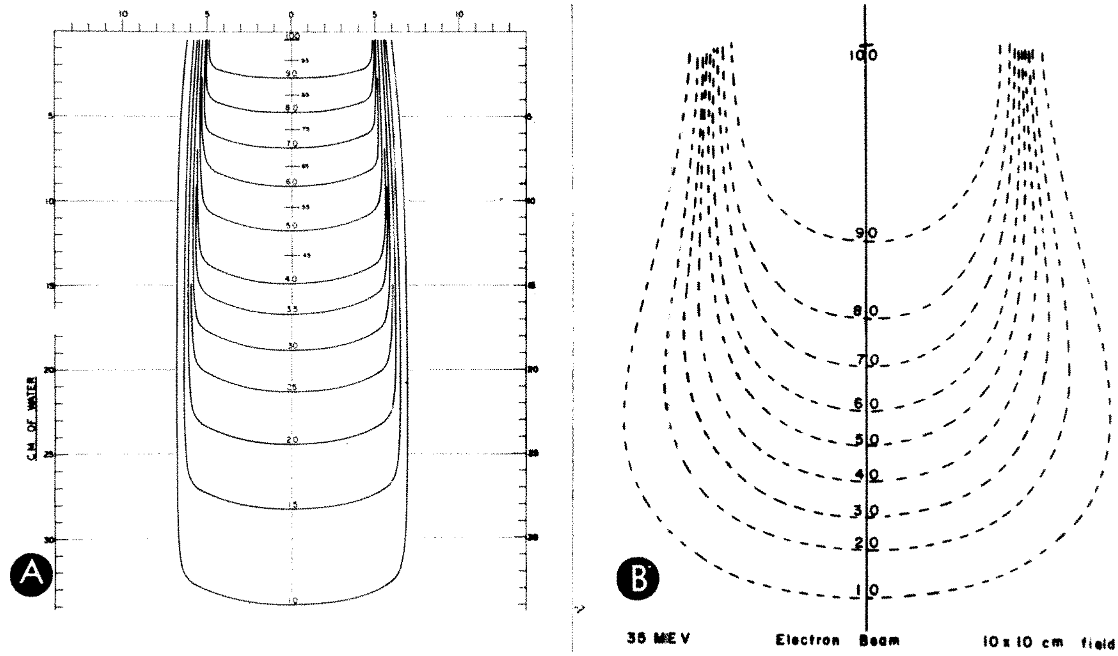


Fig. 5.(*A*) Cobalt 60 isodose curves, 10×10 cm. field, 80 cm. S.S.D.; (*B*) betatron 35 mev. electron beam isodose curves, 10×10 cm. field.

conventional in design, being basically those described by Steele,[5] which are in turn a modification of those described by Moody.[3] They have been reliable; have a negligible drift after a short warm-up period, and have a reasonably linear response.

## ISODOSE PLOTTING PROCEDURE

A "ratio circuit" and sensitive null voltmeter are used in isodose plotting. The circuit compares the ratio of voltage developed by the movable search probe to a known definite fraction of that developed by the stationary reference probe. The "ratio circuit" for measuring isodose curves in 10 per cent steps is a resistor chain made of 10 10-K precision resistors and an eleven-position switch. In practice, the reference probe is placed in the fringe of the radiation beam and the search probe is moved to the point in the beam which gives maximum ionization current. Then a potentiometer in the out-put circuit of the search probe is adjusted until the voltage (as indicated by the null voltmeter) is just equal to that from the stationary reference probe. To locate a 90 per cent point, the switch is set to compare the voltage from the search probe to 90 per cent of the voltage out-put from the reference probe. The search probe is then moved from the radiation source until a null is indicated by the voltmeter (a 90 per cent isodose point), and the position is marked. It is faster for us to "search" for other adjacent 90 per cent points, rather than move the probe over a regular grid pattern. The same procedure is followed for other isodose points.

In many cases it is desirable to measure isodose levels other than the standard 10 per cent steps. To make this possible, special resistor chains and switches have been incorporated in the system. These make it possible to measure isodose points differing by either 2 or 5 per cent and isodose curves which are normalized to 100 per cent at the axis of rotation. With the system, one can conveniently shift from measuring rotational isodose curves, standard 10 per cent steps, and fine details in areas of interest for a particular isodose curve.

### GENERAL PERFORMANCE

Figures 5, *A* and *B;* and 6, *A, B* and *C* illustrate general performance of the plotting system. Figure 5 *A* is a plot of a 10×10 cm. field from a cobalt 60 teletherapy unit, 5 *B* is a plot of an electron beam isodose curve for an energy of 35 mev. Figure 6 *A* is a comparison of central axis dose curves for 300 kv.p. (H.V.L. of 4 mm. Cu) roentgen rays, Figure 6 *B* for cobalt 60, and Figure 6 *C* for betatron electrons at 35 mev. The comparison bases for the 300 kv.p. and cobalt 60 units are published values in *The British Journal of Radiology*, Supplement No. 10. Those for the betatron are comparisons between the measured plotter values and those determined by chemical dosimetry with ferrous sulfate. There is excellent agreement between the values determined with the described plotting system and standard accepted values.

### SUMMARY

The construction and operation of a simple, manually-operated isodose plotter are described. The estimated cost of the equipment (excluding labor) is less than three hundred dollars. In operation, in the determination of several hundred isodose curves during the past 18 months, there have been no mechanical failures. Accuracy in positioning is more than adequate; and comparison with standard published values for central axis dose indicates sufficient accuracy for most clinical applications. The speed and ease of operation are such that routine isodose curves can be measured in 20–25 minutes.

J. Eugene Robinson, Ph.D.
Department of Radiology
University of Maryland
School of Medicine
Baltimore, Maryland 21201

Acknowledgement must be given to the ex-

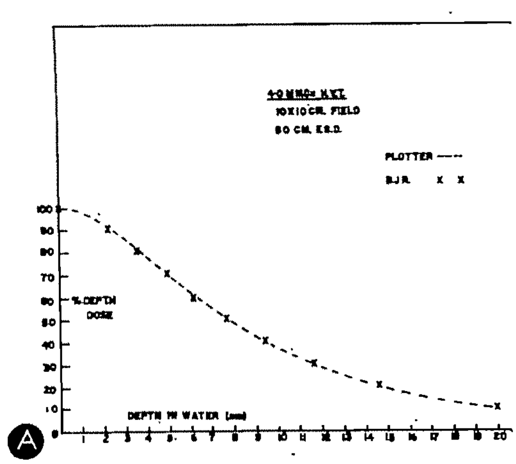

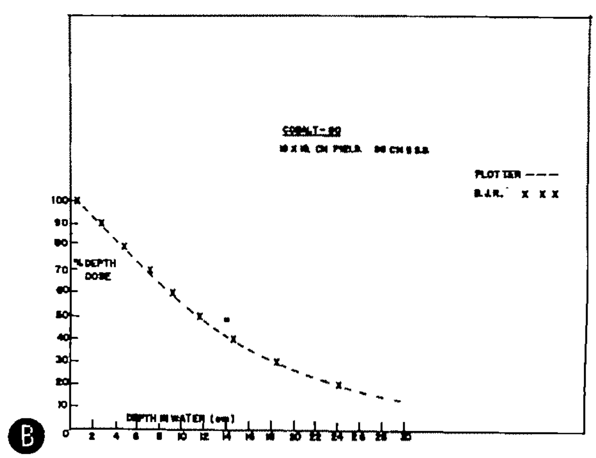

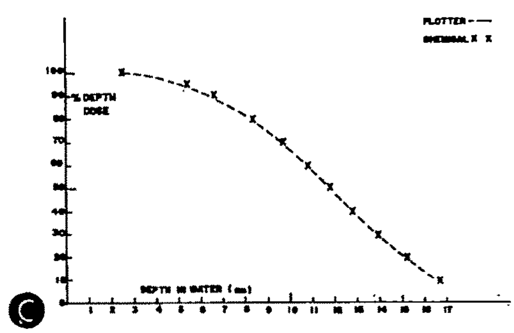

FIG. 6. (*A*) Central axis depth dose, 4.0 mm. Cu H.V.L., 10×10 cm. field, 50 cm. F.S.D.; (*B*) central axis depth dose, cobalt 60, 10×10 cm. field, 80 cm. S.S.D.; (*C*) central axis depth dose, 35 mev. electrons, 10×10 cm. field.

cellent machine work and suggestions by Mr. R. Schroeder and Mr. W. Matney, Machinists in the Department of Radiotherapy, University Hospital, Baltimore, Maryland. Partial financial support for this development work has been under American Cancer Society Grant, No. T-124C and NIH Grant, No. VS01.

REFERENCES

1. BERMAN, M., LAUGHLIN, J., YONEMITSU, M., and VACIRCA, S. Automatic isodose plotter. *Rev. Sc. Instrum.*, 1955, *26*, 328–333.
2. MAUCHEL, G. A., and JOHNS, H. E. Automatic isodose plotter. *Nucleonics*, 1954, *12*, No. 12, 50–51.
3. MOODY, N. F. Improved D. C. amplifier for portable ionization chamber measurements. *Rev. Sc. Instrum.*, 1951, *22*, 236–239.
4. SHALEK, R. J., SINCLAIR, W. K., and CALKINS, J. C. Relative biological effectiveness of 22-Mevp x-rays, cobalt-60 gamma rays, and 200-kvcp x-rays. II. Use of ferrous sulfate dosimeter for x- and gamma-ray beams. *Radiat. Res.*, 1962, *16*, 344–351.
5. STEELE, R. E. Four MEVP X-Ray Dosimetry. M. L. Report No. 475, Jan., 1958. Hansen Laboratories of Physics, Stanford University, Stanford, California.
6. TROUT, E. D., KELLEY, J. P., and LUCAS, A. C. Isodose curves for intracavitary roentgen therapy. AM. J. ROENTGENOL., RAD. THERAPY & NUCLEAR MED., 1954, *72*, 94–111.

# STATISTICS IN PHOTOSCANNING*

*By* W. C. DEWEY *and* RICHARD LAROBADIERE
HOUSTON, TEXAS

IT IS possible to determine the distribution of isotopes *in vivo* by scanning with a collimated scintillation probe and displaying the information by exposing film with a modulated light source.[1,2,4,7,10] In the photoscanning methods the intensity of the light is roughly proportional to the counting rate. Therefore, the optical density on the film represents the counting rate over the source, and variations in optical density should represent variations in counting rate. However, it is necessary to determine when variations in optical density represent real changes in counting rate as distinguished from statistical variations in an average counting rate obtained from a constant source of radioactivity. This can be determined only by considering the integration process associated with photoscanning.

In photoscanning there are two integrating effects. One form of integration is associated with the storage of electrical charge by the resistance-capacitance circuit in the rate meter, and the other integrating effect is associated with the exposure of the film. Both integrating effects were considered in order to determine the relationship between the rate meter time constant, scanning speed, light spot size, counting rate, and the standard deviation of the fluctuations in optical density observed on the photoscan. It was then possible to determine the best set of parameters in order to detect radioactive targets located in a radioactive environment.

## MATERIALS AND METHODS

### DESCRIPTION OF PHOTOSCANNER

A commercial scanning system was used in which a 2 inch×2 inch crystal was coupled to a continuous light source, the intensity of which increased with an increase in counting rate. The pulses from the photomultiplier tube were fed through a pulse-height analyzer and then through a scaling circuit (1, 2, 4, or 8) to a rate meter; the output voltage of the rate meter controlled the intensity of the light bulb. The light arrangement consisted of a Sylvania Type 48-D telephone switchboard lamp set into a small cylinder on the carriage. The top of the bulb, frosted for diffusion of light, was 1.6 cm. below a 5×10 mm. rectangular opening in the diaphragm which in turn was 1.8 cm. below a lens of 1.35 cm. focal length. One of several circular disks, each with a different sized aperture (2, 3, or 4 mm. in diameter) in its center, was placed immediately over the lens in order to regulate the amount of light reaching the film. The rectangle in the diaphragm was focused on the plane of the film which was 5.3 cm. above the lens.

### CALIBRATION OF PHOTOSCANNER

The photoscan system was calibrated by scanning at different speeds while constant counting rates were fed into the rate meter (Fig. 1). The counting rates were obtained by feeding a 60 cycle test signal through the scaling circuit, out of which one pulse was obtained for every 1, 2, 4, 8, 16, or 32 input pulses. All films (Kodak Bluebrand X-Ray) were processed in the same manner, and the optical density measurements were made with an Ansco-MacBeth densitometer.

### STATISTICAL ANALYSIS OF PHOTOSCAN LINES

A small vial of $I^{131}$ was used to provide the randomly distributed impulses (an average of 450 counts/min.) necessary for the formation of the photoscan lines on the film used for the statistical analysis. The vial was securely mounted in a lead single-bore collimator attached to the probe. The

* From the Department of Physics, The University of Texas, M. D. Anderson Hospital and Tumor Institute, Texas Medical Center, Houston, Texas.

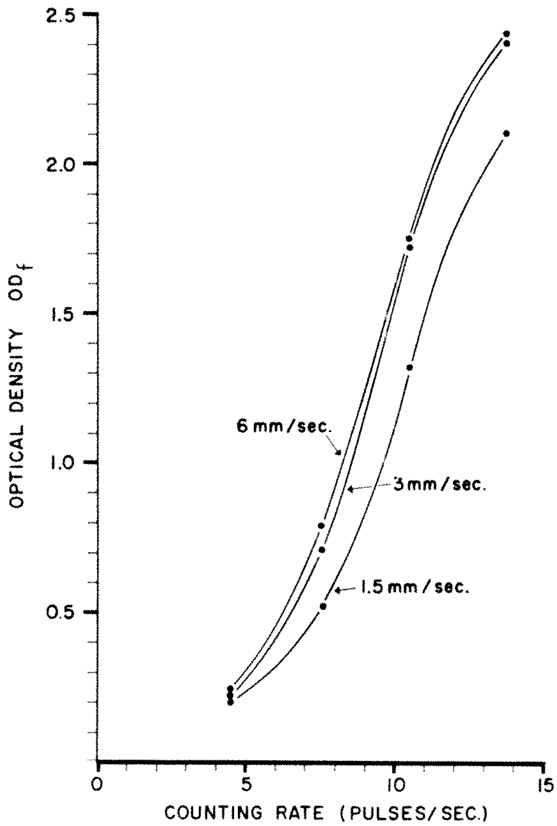


Fig. 1. Optical density obtained on the photoscan as a function of counting rate and, as indicated, at different scanning speeds. As described under *Methods*, the light apertures were changed for the different scanning speeds. Although it is not shown, the slopes could also be changed.

counts or impulses from the source were first recorded by a magnetic tape recorder connected to the output of the scintillation probe. Then, for the photoscan lines the impulses recorded on magnetic tape were used. At the time of replay, the output of the rate meter circuit, which controls the light intensity, was connected to a rectilinear recorder. Analysis of the graphical record ensured that the entire system was stable, and that fluctuations in light output were caused only by normal statistical variation.

Photoscan lines used for the statistical analysis were made with three scanning speeds, 1.5, 3.0, and 6.0 mm. per second, and with each of four time constants, 0.5, 0.8, 1.8 and 3.6 seconds. The time constants were measured by oscilloscope rise time. A sufficient number of lines was obtained in order to provide about 50 optical density measurements, with a separation of at least 3 time constants ($3RC$) between points of reading, for each of the 12 sets of parameters used. For each optical density reading, the counting rate was determined from data in Figure 1.

Separating the points of reading by three time constants was justified as follows. The time, $T$, required for the charge on the capacitance in the rate meter circuit to change from an equilibrium value for one counting rate to within one standard error of the equilibrium value of a new counting rate is given by:[5]

$$T = \frac{RC}{2} \ln 2RC\,R_{NT}. \qquad (1)$$

For the counting rate $R_{NT}$ of 450 cpm. or 7.5 counts/sec. and a 3.6 second time constant, $T$ equals 7.2 sec. or $2RC$. For the same counting rate and a 0.5 second time constant, $T$ equals 0.5 second or $1RC$. Alternatively, the time required for the rate meter to change by 95 per cent of the difference between the two counting rates is given by:

$$(T_f - T_i) = RC \ln (0.05) = 3RC. \qquad (2)$$

Therefore, measuring optical densities at points separated by at least 3 time constants is reasonable in order to ensure statistical independence of each reading, *i.e.*, with no significant overlapping of integrating effect. Thus, for a scanning speed of 1.5 mm. per second and a time constant of 3.6 seconds, the distance between two consecutive points should be greater than $3\times3.6\times1.5=16.2$ mm. For the speed of 1.5 mm./sec. the optical densities were read at intervals of 18, 9, 5, and 5 mm. for the time constants of 3.6, 1.8, 0.8 and 0.5 sec., respectively. Examples are shown in Figure 2. For the speed of 3.0 mm./sec. the intervals were 36, 18, 9 and 5 mm., and for 6.0 mm./sec. the intervals were 72, 36, 18, and 9 mm.

The fractional standard deviation of the

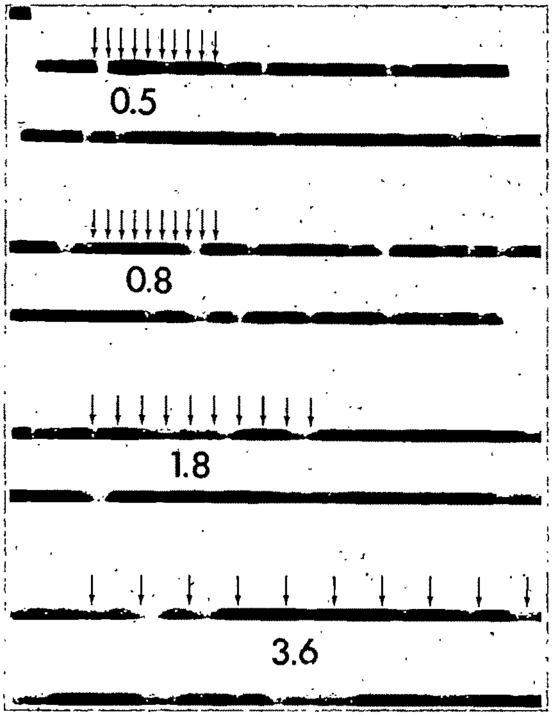


FIG. 2. Examples of photoscan lines obtained at a scanning speed of 1.5 mm./sec. and used for the determination of statistical fluctuations in the counting rate, *i.e.*, the value of $\sigma(t)$ in Equation 3 and plotted in Figure 7. The input to the photoscanner was provided from a magnetic tape which had recorded pulses from a constant radioactive source at an average counting rate of 450 counts/min. (7.50 counts/sec.). The rate meter time constant, $RC$, in seconds is indicated for each pair of lines. The optical density was read at intervals ($>3RC$) as indicated by the arrows, and each optical density reading was converted to counting rate by using Figure 1. The exposure produced by a flash of the light when it was stationary is shown by the rectangle in the upper left corner. The distribution of optical density measurements across such a spot is shown in Figure 5.

counting rate experimentally determined for each set of scanning parameters was calculated as follows:[8]

$$\sigma(t) = \frac{N}{\Sigma y}\sqrt{\frac{(\Sigma y^2) + (\Sigma y)^2/N}{N - 1}}, \qquad (3)$$

in which $y$ represents the individual reading in counting rate as converted from optical density in Figure 1, and $N$ represents the number of individual readings used for the particular set of parameters. Note that the fractional standard deviation is the standard deviation divided by the average counting rate, $\Sigma y/N$.

## STATISTICAL CONSIDERATIONS IN PHOTOSCANNING

### THEORETICAL CONSIDERATIONS

The light spot passing over a point on the film averages the output from the rate meter over a period of time, depending on the speed and effective length of the light spot. As described by Schiff and Evans[9] for a continuous observation over an interval of time, $t$, the fractional standard deviation, $\sigma(t)$, in the counting rate is:

$$\sigma(t) = \frac{\sqrt{1 + 2t/RC}}{(1 + t/RC)}\,\frac{1}{\sqrt{2RC\,R_{NT}}}, \qquad (4)$$

in which $RC$ is the time constant of the rate meter in seconds, and $R_{NT}$ is the average counting rate (counts/sec.). This expression contrasts with the fractional standard deviation for a single observation which is equal to the second part of Equation (4), *i.e.*, $1/\sqrt{2RC\,R_{NT}}$. In deriving Equation 4, the counting rates observed over small increments of time during the period, $t$, were weighted equally and averaged; *i.e.*, the counting rate observed on a recorder would be averaged over a time interval, $t$. The photoscanner replaces the recorder and records the counting rate for a period of time, $t$, as the light spot traverses a point on the film. As seen in Figure 1, the film exposure produced by the light passing over a point on the film gives an optical density, $OD_f$, which is approximately linearly related to counting rate. Ideally, to meet the conditions of Equation 4, the accumulation of film exposure or optical density as the light traverses a point on the film should be linearly related with time (Fig. 3). Therefore, in order to determine $t$ for the photoscan, the accumulation of light exposure or optical density must be studied as a function of light movement or time.

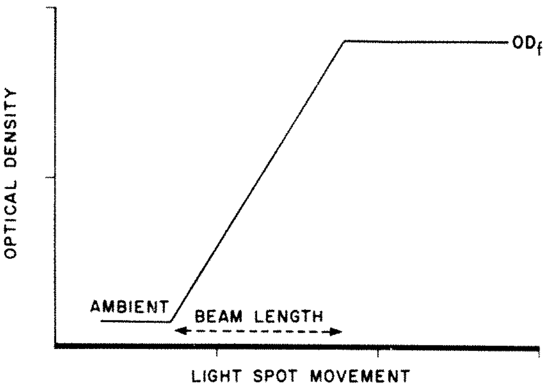


FIG. 3. Idealized plot of the accumulation of light exposure at a point on the film (expressed as optical density) as a function of the movement of the light spot across this point. Movement of the light spot can be specified in terms of distance or time (time = distance/scanning speed). The effective length of the light spot is indicated as the distance or time required for the optical density to increase from ambient to the maximum value, $OD_f$.

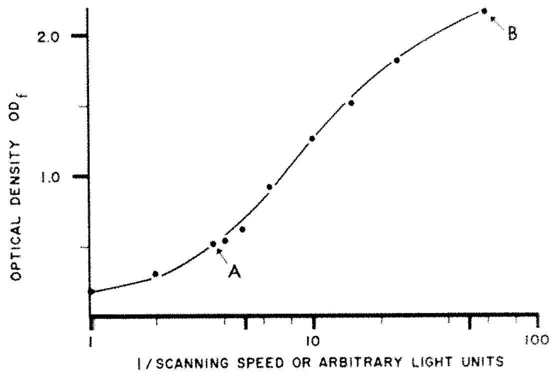


FIG. 4. Optical density obtained on the photoscan as a function of the inverse of scanning speed, when the light output was held constant (14 mamps. with a 2 mm. aperture). The points designated A and B were actually measured at speeds of 1.54 and 0.08 mm./sec., respectively. Since the amount of light exposing the film is inversely proportional to scanning speed, the abscissa also represents light units (actual units not measured) exposing the film. Other curves (not shown) were determined with different light outputs, and they were shifted to the right or left by constant amounts.

DETERMINATION OF THE EFFECTIVE LENGTH OF THE LIGHT SPOT

First, it was necessary to determine the relationship between optical density and light exposure. This was accomplished by setting the light at a given output and scanning at different speeds. Since light exposure is proportional to the inverse of scanning speed, the optical density, $OD_f$, was plotted as a function of 1/speed or arbitrary light units (Fig. 4). If the light output was set at different values, a family of parallel curves (not shown) was obtained, in which the curves were shifted on the abscissa by a fixed amount.

Secondly, the distribution of light output was determined by holding the light stationary and flashing it once for a short period of time; two typical plots are shown in Figure 5, in which optical density was measured at intervals of 0.5 mm. along the film spot. The optical densities in Figure 5 were converted to arbitrary light units (not

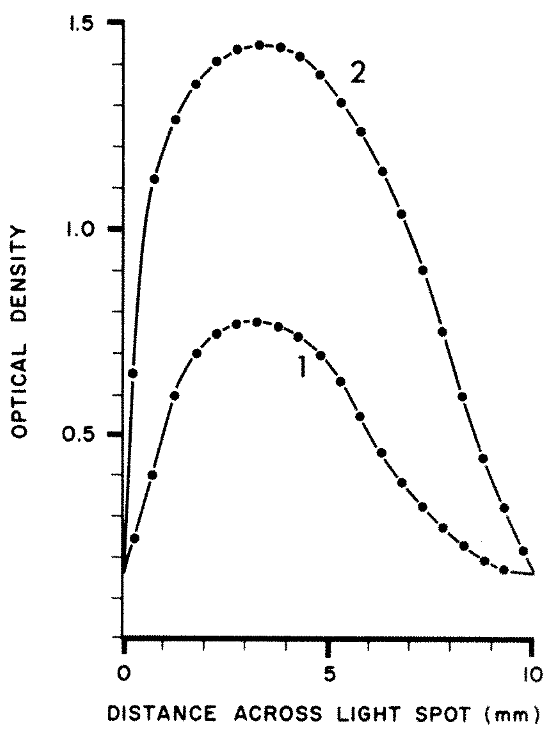


FIG. 5. Variation in optical density as measured across the area of the film exposed by two different light spots (curves 1 and 2). For each spot the light was stationary and was flashed once. An example of such a spot is shown in Figure 2. The effective length of the light spot was determined from the data in Figure 6; for these data the light spot was moved from right to left.

shown) by reading $OD$ as a function of light output in Figure 4.

Thirdly, the accumulation of light output, as the light passed over a point on the film, was determined by summing the light units at 0.5 mm. intervals. The accumulated optical density was then determined by using Figure 4 to convert accumulated light exposure to optical density. Since the light units were arbitrary, the maximum optical density which is reached, $OD_f$, can be chosen by multiplying all light units in Figure 4 by an appropriate factor. Curves showing optical density as a function of light movement are shown in Figure 6 for several different values of $OD_f$. These curves are relatively independent of which optical density distribution in Figure 5 was used.

As mentioned previously, in the ideal case the accumulation of optical density should occur in a linear manner (Fig. 3); *i.e.*, each unit of distance along the light spot should be weighted equally. The idealized plots are shown by the dotted lines; the method of constructing these straight lines is defined in the legend. The effective beam lengths of the light spot, 3 mm. for a final optical density ($OD_f$) of 2.0 and 7 mm. for a final optical density of 0.7, were determined from the straight lines by the intervals of distance required for increasing from ambient to the final optical density.* The effective beam lengths can be compared with the apparent length of 9–10 mm. (see Fig. 2 and 5). The effective time, $t$, in Equation 4 is equal to:

$$t = \text{effective beam length/scanning speed.} \quad (5)$$

* The effective length was determined from Figure 6 for the light source, illustrated in Figure 5, moving from right to left. When the effective length was determined for the light source moving in the opposite direction, it changed by no more than 3 per cent.

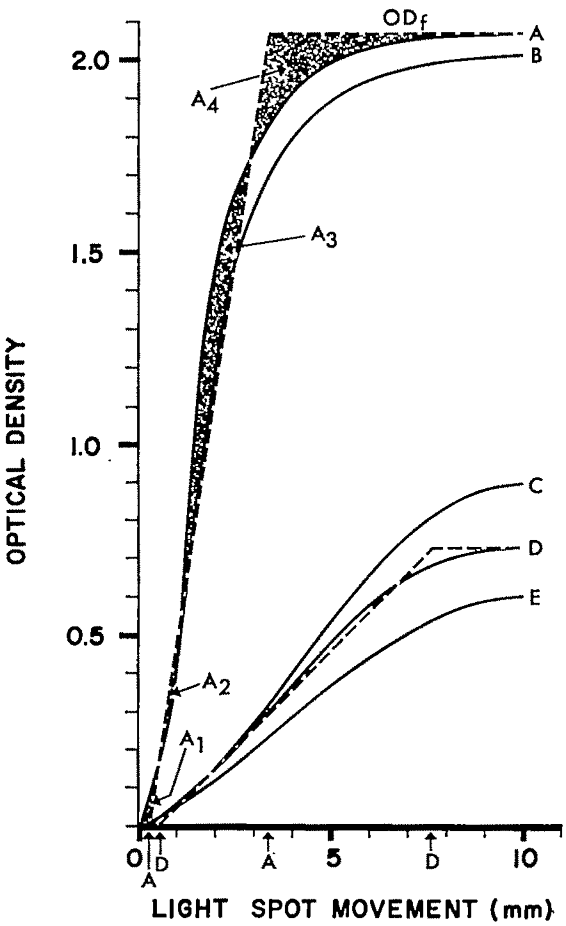


FIG. 6. The accumulation of light exposure at a point on the film (expressed as optical density) as a function of the movement of the light spot across this point. To obtain these curves, light exposure as a function of distance across the light spot (expressed in arbitrary light units) was first obtained by using data in Figures 4 and 5; a summation of this curve (not shown) then gave the cumulative light exposure at a point as a function of light spot movement. The cumulative light exposure was then converted to optical density by using the data in Figure 4; in making this conversion the number of light units was multiplied by a constant factor in order to determine the final value of optical density, $OD_f$, reached when the light spot had traversed the point. Curves A and D were obtained from curve 1 in Figure 5, and curves B, C, and E were obtained from curve 2 in Figure 5. The idealized curve (discussed in Figure 3) was constructed as a dotted line for curve A, for example, by making area $A_1$ equal to area $A_2$ and area $A_3$ equal to area $A_4$. The effective length of the light spot, which depends on the final optical density, is equal to the distance between the two A's on the abscissa (3 mm.) for curve A or between the two D's (7 mm.) for curve D. The effective lengths can be compared with the apparent length, about 9–10 mm. (see Fig. 2 and 5).

COMPARISON OF THEORETICAL CALCULATIONS WITH EXPERIMENTAL RESULTS

The validity of using Equation 4 to describe the fractional standard deviation in the counting rate was established experimentally by taking the information stored on magnetic tape, an average counting rate of 450 cpm. or 7.5 pps., and playing it back at different scanning speeds and rate meter time constants. The fractional standard deviation was experimentally determined from the photoscan lines as described under *Methods* (see Equation 3). The film exposure was controlled by combinations of speed and light aperture sizes, such that the average optical density was 0.7. Therefore, as seen in Figure 6, the effective beam length was estimated as 7 mm. Results in Figure 7 indicate that the theoretical Equation 4 describes quite well the fractional standard deviation observed. (The theoretical values for $RC=0$ were obtained from the limits of Equation 4 as $RC$ approached zero.) Note that as the speed decreases the fractional standard deviation differs greatly from that showing the integrating effect of the rate meter only, *i.e.*, $1/\sqrt{2RC\,R_{NT}}$. This difference is particularly apparent at the shorter time constants, 0.5–1.0 sec., and clearly illustrates the integrating effect obtained from accumulation of light by the film during the interval of time required for the light spot to pass over a point on the film.

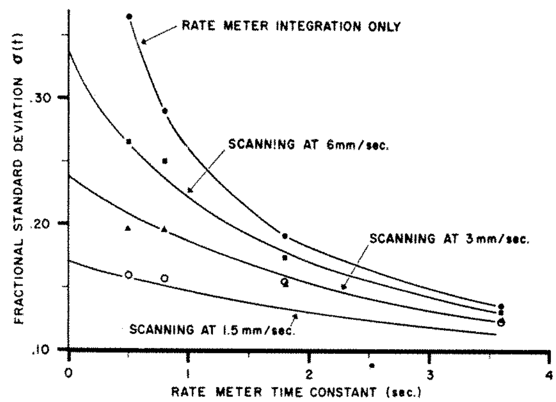


FIG. 7. The fractional standard deviation in the counting rate obtained on the photoscan as a function of the rate meter time constant for different scanning speeds. The points were obtained experimentally for an average counting rate of 7.50 counts/sec. by measuring the optical density on the film at 50 independent points and converting to counting rate (see Equations 1, 2, and 3 and Fig. 1 and 2). The average optical density was 0.7, for which the effective beam length was about 7 mm. (Fig. 6). The curves were calculated from Equations 4 and 5 for a counting rate ($R_{NT}$) of 7.5 counts/sec. and an effective beam length of 7 mm. Note that the integrating effect of the film becomes very important for low scanning speeds and short time constants, *i.e.*, 1.5 mm./sec. and 0.5 sec., respectively.

It is important to note that the curves in Figure 7 are for an average optical density of 0.7 which has an effective beam length of 7 mm. As illustrated in Figure 6, the effective beam length and, therefore, the effective integration time (Equation 5) should decrease as the average optical density increases. Therefore, for a greater optical density, the standard deviation should increase although the counting rate and rate meter time constant are held constant. To verify this, the same magnetic tape recording was used as before, 450 cpm., and scanning lines were obtained with a 0.5 second time constant and a scanning speed of 1.5 mm./sec. In one set of lines an average $OD_f$ of 2.07 was obtained by using a 3 mm. light aperture, and in another set of lines an average $OD_f$ of 1.13 was obtained by using a smaller 2 mm. light aperture. For the $OD_f$ of 2.07 the experimental and theoretical fractional standard deviation of 0.22 was greater than the value of 0.16 obtained for an $OD_f$ of 1.13 (Table 1). This confirms that the effective time in Equations 4 and 5 is dependent on the average $OD_f$ obtained in the area of the scan to be considered.

## PRACTICAL APPLICATIONS

### MEMORY LAG AND RELATIVE INCREASE IN COUNTING RATE OVER THE TARGET AS RELATED TO THE FRACTIONAL STANDARD DEVIATION IN THE COUNTING RATE

In order to evaluate the effect of the scanning parameters on the probability of detecting the target area located within a background of radioactivity, scans were

TABLE I

FRACTIONAL STANDARD DEVIATION IN THE COUNTING RATE OBTAINED FOR DIFFERENT OPTICAL DENSITIES ($RC=0.5$ SEC., SCANNING SPEED = 1.5 MM./SEC., 7.50 PULSES/SEC.)

| Average Optical Density | Effective Beam Length (mm.) | Effective Time "$t$" (sec.) | Fractional Standard Deviation* | |
|---|---|---|---|---|
| | | | Theoretical | Experimental |
| 1.13 | 7 | 4.67 | 0.157 | 0.155 |
| 2.07 | 3 | 2.0 | 0.218 | 0.219 |

* Defined and calculated with Equations 3, 4, and 5.

made of a 2 cm. target cube placed 7 cm. below the face of the collimator and at the center of a 12 cm. cube. The two cubes were filled with solutions of iodine 131 having different concentrations of radioactivity. The photoscan settings gave average optical densities of 0.5 over the nontarget area and 0.9 over the target area, which provided an effective beam length of about 7 mm. (Fig. 6). A 19 hole focusing collimator[4] with an 8 cm. focal distance was used in all cases in order to provide the same resolution (0.90 cm.) for all scans. The following values were measured:

$$R_T = \text{counting rate over the target;} \quad (6)$$

$$R_{NT} = \text{nontarget counting rate} \quad (7)$$

(obtained at a point 3 cm. from the edge of the large cube);

$$\Delta R = R_T - R_{NT}. \quad (8)$$

The value $n$, which is related to the probability of detecting a target[4] is equal to:

$$n = \frac{\Delta R/R_{NT}}{\sigma(t)}, \quad (9)$$

in which $\sigma(t)$ is the fractional standard deviation in the counting rate $R_{NT}$, calculated from the scanning parameters entered in Equations 4 and 5.

A "memory lag" existed between the collimator-detector system and the recording light because of the time required for the capacitance in the rate meter circuit to charge or discharge as the counting rate changed[7,10] (see Equations 1 and 2). An empirical relationship between "memory lag" and scanning speed was obtained by scanning a square 3 cm. container and noting the displacement of the adjacent scanning lines. The lag was determined for different amounts of radioactivity which gave counting rates over the container varying from 4 to 40 pulses per second. The lag, which was independent of counting rate, was empirically equal to:

$$\text{Lag (mm.)} = 1.29 \times \text{scanning speed (mm./sec.)} \times \text{time constant (sec.)}. \quad (10)$$

In time units the lag equals 1.29 $RC$. The displacement of adjacent scanning lines caused by "memory lag" was compensated for on all scans by automatically changing the length of the rod connecting the detector and the light, each time the scanning direction was reversed.

Photoscans of the 2 cm. target located at the center of the 12 cm. cube are shown in Figure 8, and photocopies,[8] which eliminated most of the exposure on the film produced by radioactivity in the nontarget area, are shown in Figure 9. In Studies B and C the concentration of radioactivity in the small cube was five times greater than that in the large cube, and in Study A the concentration of radioactivity was 7.7 times higher in the small cube. The concentrations used and counting rates obtained (334–902 cpm. over the nontarget area with increases of 33–61 per cent over the target) are indicated in the legend of Figure 8. In all studies the background (when the cubes were removed) varied between 50 and 60 counts/min. The cubes were scanned at different speeds with various rate meter time constants in order to provide different values for $n$ and "memory lag," as indicated in Figures 8 and 9. In Study A, when $n$ was equal to 3.8 or 5.2 with a "memory lag" of 2.0 mm., the target was detected quite clearly. Reducing the spacing between the lines from 8 mm. to 4.5 mm. also improved the detection of the target. Fluctuations over the nontarget area interfered slightly with the detection of the target when $n$ decreased to 2.4 with a lag of 2 mm.

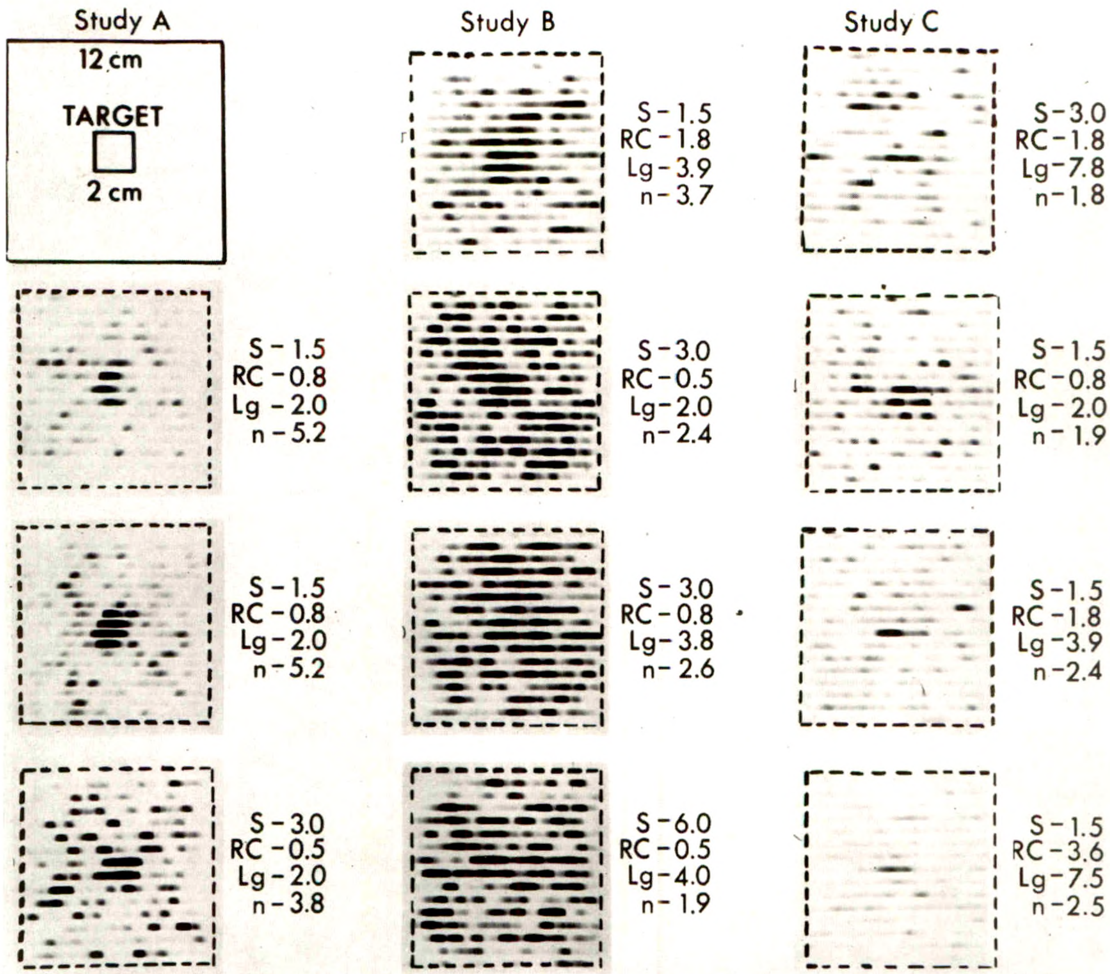


FIG 8. Photoscans of a 2 cm. cube (target) containing $I^{131}$ and placed at the center of a 12 cm. cube containing a lower concentration of $I^{131}$. Pertinent data are as follows (see Equations 7 and 8):

| | μc/ml. in 2 cm. cube | μc/ml. in 12 cm. cube | Ratio of concentrations | Average OD over target | $R_{NT}$ cpm. | $\Delta R/R_{NT}$ |
|---|---|---|---|---|---|---|
| Study A | 0.223 | 0.029 | 7.7 | 0.95 | 749 | 0.61 |
| Study B | 0.18 | 0.036 | 5.0 | 0.91 | 902 | 0.35 |
| Study C | 0.067 | 0.013 | 5.0 | 0.69 | 334 | 0.33 |

From Figure 6 the effective length of the light spot was determined to be 7.0 mm. Other scanning conditions, speed ($S$) in mm./sec., rate meter time constant ($RC$) in sec., memory lag ($Lg$) in mm. (see Equation 10), and $n$ (see Equations 4, 5, and 9) are specified for each span. Note (see Fig. 9 also) that in order to clearly distinguish the increase in counting rate over the target from fluctuations over the nontarget area, $n$ should exceed 3, and the memory lag should be less than 4 mm.

in Study B, and when $n$ decreased to 1.9 with a lag of 2 mm. in Study C. Therefore, when a small lag of 2 mm. was used and $n$ was greater than about 2, the target was detected quite clearly. For even better detection the value of $n$ should approach values greater than 3.

The effect of "memory lag" was demonstrated in Study B by comparing the scan of $n = 2.4$ and lag $= 2.0$ mm. with the scan of

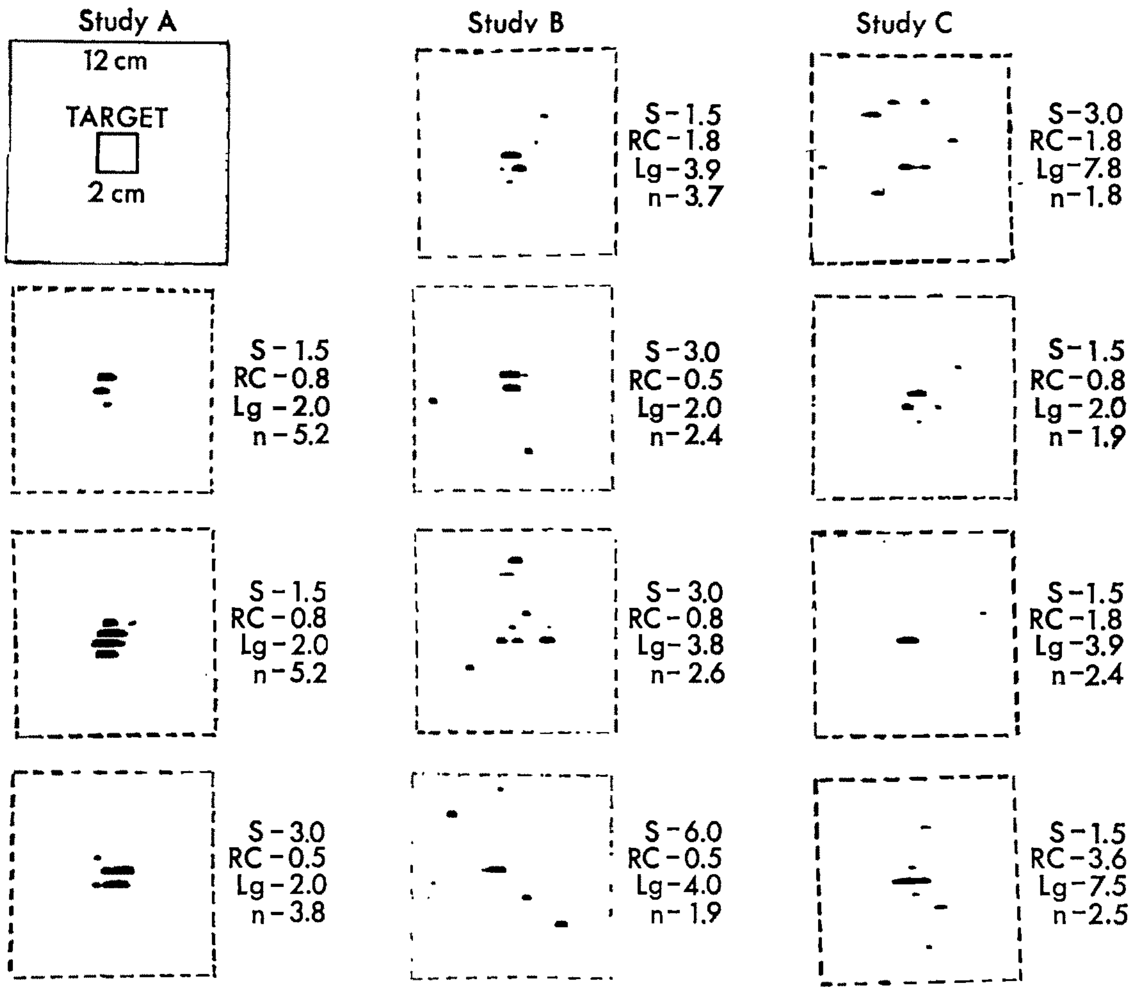


Fig. 9. Photocopies of the photoscans in Figure 8. The photocopies were made in order to erase as much of the film density over the nontarget area as possible without erasing the density over the target area.

$n = 2.6$ and lag $= 3.8$ mm., in which the lag of 3.8 mm. reduced the quality of target detection. However, the effect of lag is illustrated more clearly in Study C, in which the speed was kept constant at 1.5 mm./sec. while the time constant was increased, thereby increasing the lag. (Note from Equation 10 that the memory lag can be decreased by decreasing either the scanning speed or the time constant.) Although the value of $n$ increased from 1.9 with a lag of 2.0 mm. to 2.5 with a lag of 7.5 mm., the detection of the target was impaired as the lag increased. Thus, if the lag approached one-fourth to one-half the width of the target, the probability of detecting the target was reduced because of insufficient time for the capacitance to charge as the probe passed over the target. It appears that the "memory lag" should be reduced to less than 4 mm., *i.e.*, about 2 mm. for the 20 mm. target. That is, the memory lag should be about one-tenth the target width for good detection (then, $3RC$ are required to traverse one-fourth of the target). If the memory lag is greater than one-tenth the target width, the value of $n$ will have to be increased in order to provide adequate detection of the target. For example, in Study B the target was detected quite well with a lag of 4 mm. when the value of $n$ was increased to 3.7.

SELECTION OF SCANNING PARAMETERS

Referring to Figures 7, 8 and 9, some general conclusions can be reached concerning parameters to be used in photoscanning. One of the most difficult problems to be considered is that of brain tumor detection, for which counting rates of less than 500 counts per minute are often obtained,[2] and the ratio of concentration in the tumor to that in the normal brain ranges from 5 to 30.[6] As shown by the data in Figure 8, the counting rate over the tumor may be only 30–60 per cent higher than that over the normal brain. If sufficient time is available for the scan, a slow speed of 1.5 mm./sec. should be used with a 1 second time constant. This will reduce the fractional standard deviation to 15 per cent or less (for 450 cpm. as shown in Figure 7) and will reduce the memory lag to about 2 mm. (Equation 10), which is sufficient for a 2 cm. tumor. Under these conditions, shown in the cube studies in Figures 8 and 9, a 2 cm. tumor located at the center of the brain and having a concentration of radioactivity 5 times greater than the normal brain would have an $n$ value greater than 2; this means that the tumor should be detected. At this speed of 1.5 mm./sec., increasing the time constant from 1 to 2 sec., for example, would decrease the fractional standard deviation only slightly from 15 to 13 per cent (Fig. 7), but would not improve the detection of the tumor because the memory-lag would increase from 2 to 4 mm. It is also clear that if the scanning speed were increased to values greater than 1.5 mm./sec., the time constant would have to be reduced because of the "memory lag" effect. At 3 mm./sec., a time constant of 0.5 sec., or possibly 0.8 sec., would be acceptable. Although increasing the time constant from 0.5 to 2 seconds would decrease the fractional standard deviation from about 20 to 15 per cent, the increase in "memory lag" from 2 mm. to 8 mm. would not be acceptable. At 6 mm./sec. a time constant of about 0.25 second should provide the best results with a compromise between the fractional standard deviation (29 per cent) and the "memory lag" (2 mm.).

In summary, it appears that for good target detection, $n$ should be equal to or greater than 3, and a "memory lag" effect of no more than 2 mm. should be used, *i.e.*, a "memory lag" effect of about one-tenth the target width.

SUMMARY

In photoscanning the effects of scanning speed, counting rate, light-spot size, and rate meter time constant on the quality of target detection were studied both theoretically and experimentally. Equations were developed in order to determine the best set of parameters for detecting radioactive targets located in a radioactive environment. In order to adequately detect the target, the change in counting rate which occurs as the detector passes over the target should be 2 to 3 times larger than the standard deviation of the counting rate obtained adjacent to the target.

W. C. Dewey
Department of Physics
The University of Texas
M. D. Anderson Hospital and Tumor Institute
Houston, Texas

This work was supported in part by Institutional Grant IN-43-A-12 provided by the American Cancer Society and by Grant C-5831 from the National Cancer Institute, U. S. Public Health Service.

REFERENCES

1. Bender, M. A. Photoscanning detection of radioactive tracers *in vivo*. *Science*, 1957, *125*, 443–444.
2. Bender, M. A., and Blau, M. Versatile, high-contrast photoscanner for localization of human tumors with radioisotopes. *Internat. J. Appl. Rad. & Isotopes*, 1959, *4*, 154–161.
3. Dewey, W. C., Heidelberg, J. G., and Moore, E. B. Use of photocopying process for erasing background of photoscans and accentuating small differences in optical density. *J. Nuclear Med.*, 1962, *3*, 51–62.
4. Dewey, W. C., and Sinclair, W. K. Criteria for evaluating collimators used in *in vivo* distribution studies with radioisotopes. *Internat. J. Appl. Rad. & Isotopes*, 1961, *10*, 1–16.

5. ELMORE, W. C., and SAND, M. Electronics Experimental Techniques. First edition. McGraw-Hill Book Company, Inc., New York, 1949, p. 250–252.
6. KRAMER, S., BURTON, L. K., and TROTT, N. G. Radioactive isotopes in localisation of brain tumours. *Acta radiol.*, 1956, *46*, 415–424.
7. MACINTYRE, W. J., and HOUSER, T. S. Method for visualization of configuration and structure of liver. Part B. Counting rate cut-off circuit for increased contrast in automatic scanning. AM. J. ROENTGENOL., RAD. THERAPY & NUCLEAR MED., 1957, *77*, 471–475.
8. OSTLE, B. Statistics in Research. Iowa State College Press, Ames, Iowa, 1954, pp. 117–149.
9. SCHIFF, L. I., and EVANS, R. D. Statistical analysis of counting rate meter. *Rev. Sci. Inst.*, 1936, *7*, 456–462.
10. WINKLER, C. Use of increase of contrast in automatic photoscanning for visualization of organs and tumors by means of radioactive isotopes. *Proceedings of the Second U. N. Internation. Conference on Peaceful Uses of Atomic Energy*, 1958, *26*, 252–257.

# RADIUM ALIGNMENT APPLICATOR

By WALTER P. SCOTT
JACKSONVILLE, FLORIDA

AFTER many years of experience and experimentation with the various types[3] of so-called loose and rigid applicator systems used in the treatment of carcinoma of the uterine cervix, it is felt that the basic Paris system of tandem and colpostats is most reliable, having proven itself over the decades with good clinical results and minimal complications. The practical advantages are numerous: relatively inexpensive, disposable, adaptable to most all pelvic situations (9 sizes), flexible, light, comfortable to the patient, requiring minimal packing (an indwelling catheter is often not necessary), easily loaded, easily applied, and easily removed. However, the sum of all these can be outweighed by the complication of malposition. Quite often, there is significant deviation of the tandem, displacement and/or rotation of the colpostats, or all three factors; consequently, the axis of the radium elements within the colpostats is not perpendicular to the axis of the tandem. The theoretic and practical aspects of malposition are well illustrated by Louis, Raventos, and Hale[2] in a paper on space-dose relationship which showed that rigid applicators were associated with a more posterior and inferior location of points A and B than unrigid containers. Also, these points were more inferior and posterior in older patients, patients with advanced disease, and patients whose vaginal size required the use of smaller applicators. Sherman[4] has documented a series of radiation failures principally resulting from malposition of applicators and the M. D. Anderson group[1] has presented these problems with consideration of means towards their correction.

The stainless steel applicator to be described retains all advantages of the reliable Paris system, eliminates the possibility of malposition, permits postoperative correction without re-application, and allows a safe distance during the actual application. Furthermore, it remains inexpensive, mechanically simple, light in weight, and easily maintained. Being fixed, yet flexible, it combines the advantages of both the rigid and the loose systems and allows actual fitting of the patient with the appropriate applicators prior to loading—thus rendering a modified after-loading technique.

### RADIUM SYSTEM (Fig. 1 and 2)

The radium system* consists of the stainless steel alignment applicator (1–5) and attachments (A–C). The basic parts of the alignment applicator are:

1. Handle. One end bored and equipped with a set-screw for the shaft and a keyway for the large nut.
2. Threaded shaft with bevelled point.
3. Large nut with key.
4. Small nut.
5. Tandem base-adapter. Four small holes allow it to be grasped and controlled with a tenaculum. The adapter segment fits both metal and plastic tandems. A longer adapter segment would allow the attachment of a central colpostat. The attachments are as follows:
   a. Colpostats. Cross bar perforated with a $\frac{1}{8}$ inch hole.
   b. Plastic tandem ($3\frac{1}{4}\times\frac{1}{4}$ inch). This may be cut down to size with scissors.
   c. Metal tandems ($4\times\frac{1}{4}$ inch, $3\times\frac{1}{4}$ inch, and $2\times\frac{1}{4}$ inch).

The shaft passes freely through a small $\frac{1}{8}$ inch hole in the colpostat's flexible crossbar which is then secured to the shaft by the nuts on either side. By maintaining the correct tension with these nuts, the cross-

* Stainless steel tandems and alignment applicator: Radium Chemical Co., New York. Plastic tandem: Meca-Vigor, 88 Rue de la Folie Mericourt, Paris. Colpostats: Laboratoires Bruneau, 17 Rue de Berri, Paris.

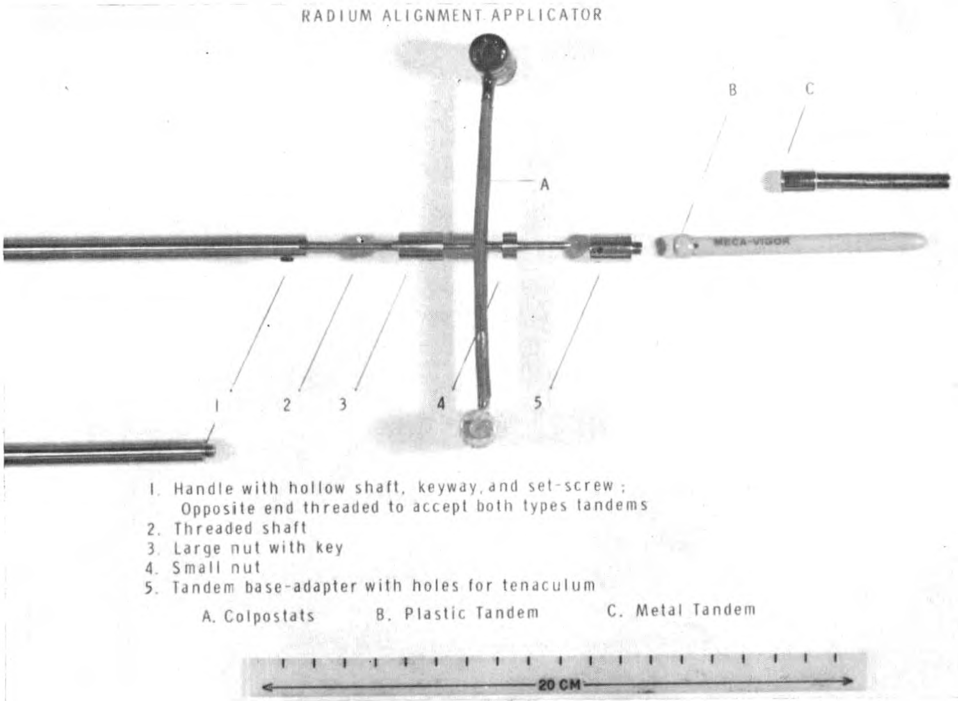


Fig. 1. Radium alignment applicator.

bar can be made to move up and down the shaft (by screwing the latter counter-clockwise and clockwise, respectively) in order to properly position the colpostats within the vaginal vault and fornices. Since the crossbar is covered with rubber, the shaft revolves without loosening the nuts. The handle is attached to the external end of the shaft by tightening a set-screw with an Allen wrench. When the set-screw is

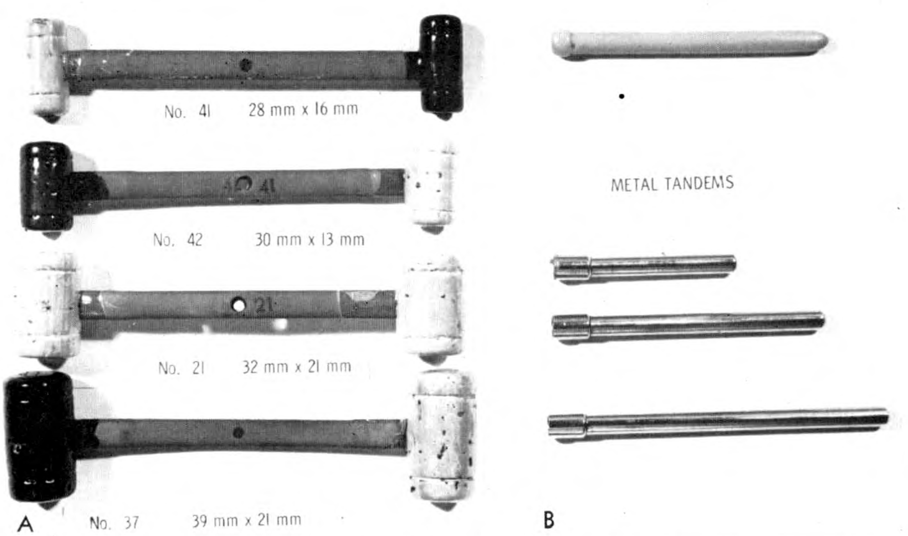


Fig. 2. Selection of attachments. (*A*) Four commonly used disposable colpostats. (*B*) A disposable plastic tandem at the top, and 3 metal tandems below.

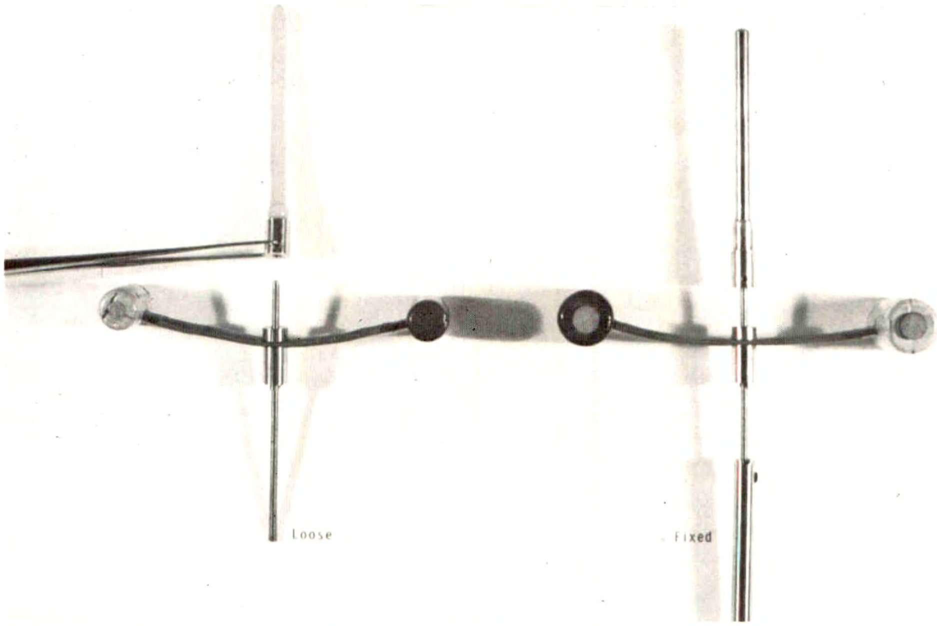


Fig. 3. Alignment applicator system—loose and fixed. (Note: attachments vary in size for purposes of demonstration.)

loosened, the handle is free to pass down the shaft and engage the key of the large nut.

ONE METHOD OF APPLICATION (Fig. 3)

1. Establish the correct tandem length and colpostat size.
2. With the large and small nuts, secure the crossbar of the colpostats to the tip of the shaft. Attach handle to other end of shaft.
3. Load tandem, screw on tandem base-adapter, and insert into cervico-uterine canal with aid of a tenaculum.
4. Load colpostats and insert into vaginal fornices.
5. Screw shaft forward so that the bevelled point will engage the tandem base-adapter.
6. Screw point of shaft into tandem base-adapter, pack away rectum and bladder, and detach handle.

The colpostats are removed by unscrewing the shaft (with handle attached) from the tandem base-adapter and extracting first, the shaft with its fixed colpostats and then, the tandem. Used colpostats and tandems of this alignment system may be cleaned, sterilized, and serve for subsequent fittings to establish the correct size.

The following cases illustrate some features of the alignment applicator. Unfortunately the quality of the lateral roentgenograms is limited by the supine technique with the mobile unit in obese patients.

ILLUSTRATIVE CASES

Case I (Fig. 4, *A* and *B*). A 50 year old Negro female with Stage I squamous cell carcinoma of the cervix. The lateral roentgenogram (Fig. 4*A*) shows anterior displacement of the tandem and posterior rotation of the colpostats resulting in parallel arrangement of the radium elements. Consequently, maximum rectal and minimal cervical doses would be expected. Figure 4*B* shows correction with the alignment applicator.

Case II (Fig. 5, *A* and *B*). A 49 year old white female with Stage I squamous cell carcinoma of the cervix. In the lateral roentgenogram (Fig. 5*A*) posterior deviation of the tandem and anterior displacement of its base in relation to the colpostats are demonstrated. Figure 5*B* shows correction with the alignment applicator.

Case III (Fig. 6, *A–D*). A 53 year old Negro female with Stage II squamous cell carcinoma

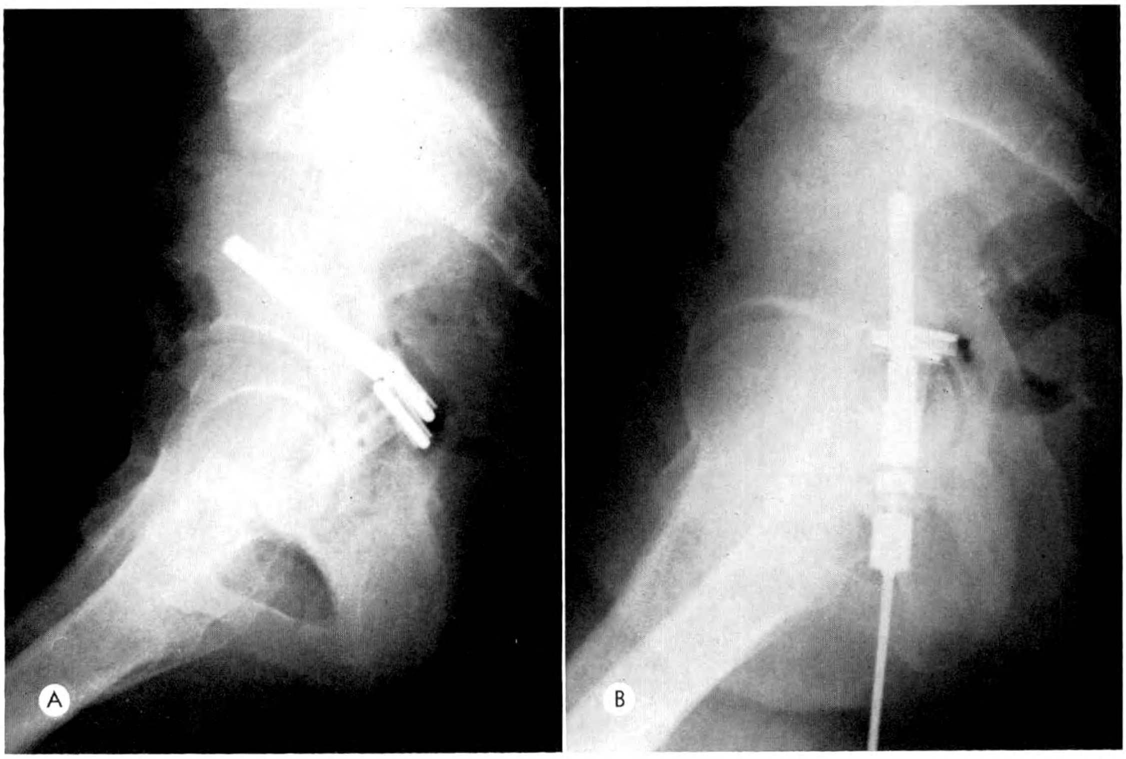


Fig. 4. Case i. (*A*) Initial application showing malposition. (*B*) Correction with alignment applicator.

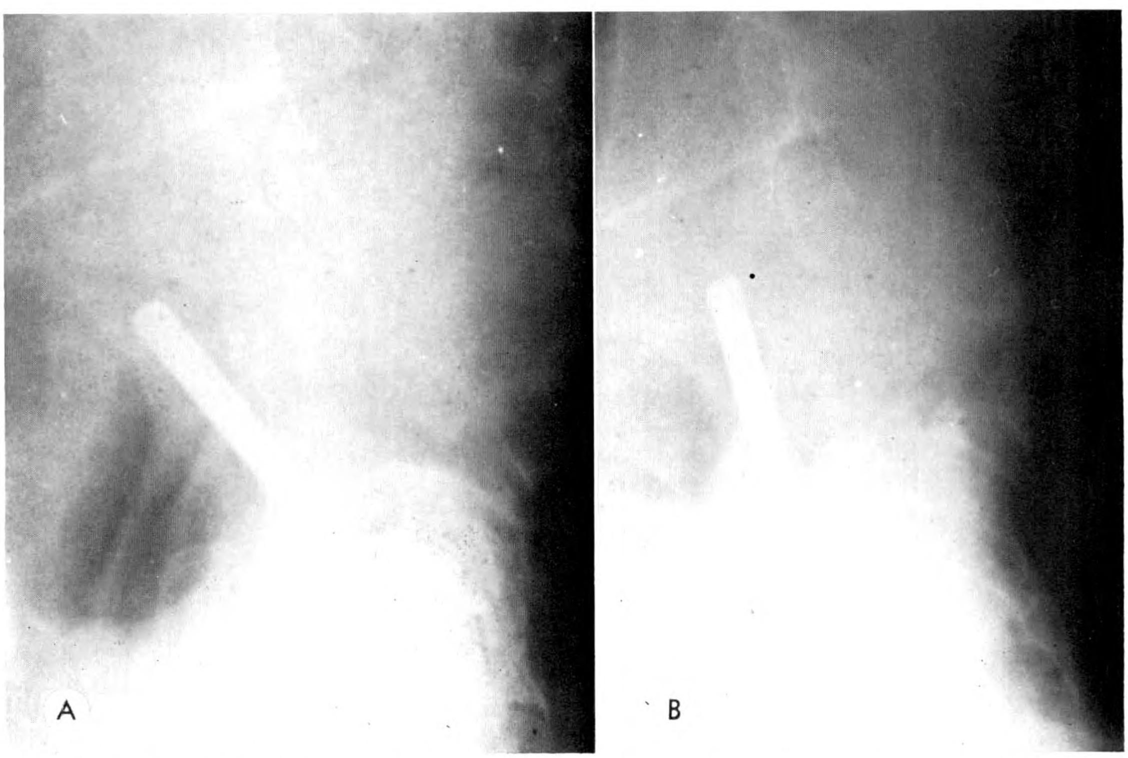


Fig. 5. Case ii. (*A*) Initial application showing malposition. (*B*) Correction with alignment applicator.

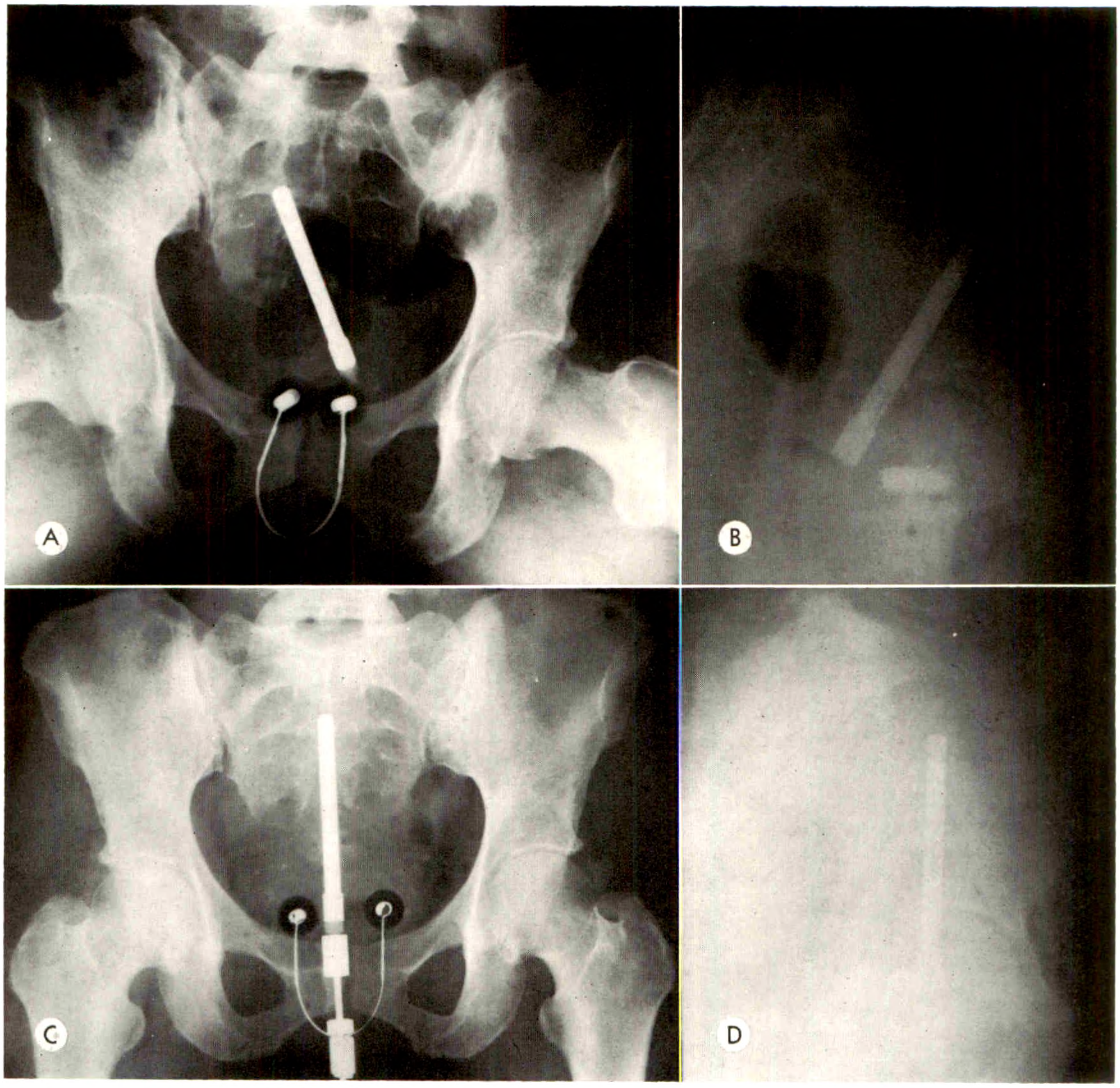


Fig. 6. Case III. (*A* and *B*) Initial application showing malposition. (*C* and *D*) Correction with alignment applicator.

of the cervix. Roentgenograms of the pelvis (Fig. 6, *A* and *B*) show right lateral deviation of the tandem, displacement posterior and to the right of its base, and clockwise rotation of the colpostats. Figure 6, *C* and *D* reveals correction with the alignment applicator.

Comment. In Cases I, II, and III the original model of the applicator fashioned of brass was used. It is interesting to note (Case I) that when the cervix is relatively long and the fornices deep, the colpostats rotate posteriorly. In the following 2 cases the newer model made of stainless steel was employed.

Case IV (Fig. 7, *A–H*). A 30 year old white female with Stage I squamous cell carcinoma of the cervix, who received her initial application with a double crossarm tandem applicator. The roentgenograms (Fig. 7, *A* and *B*) showed antero-lateral deviation and slight clockwise rotation of the system. The roentgenograms of the second application (Fig. 7, *C* and *D*) showed posterior rotation of the colpostats which was subsequently corrected with the alignment ap-

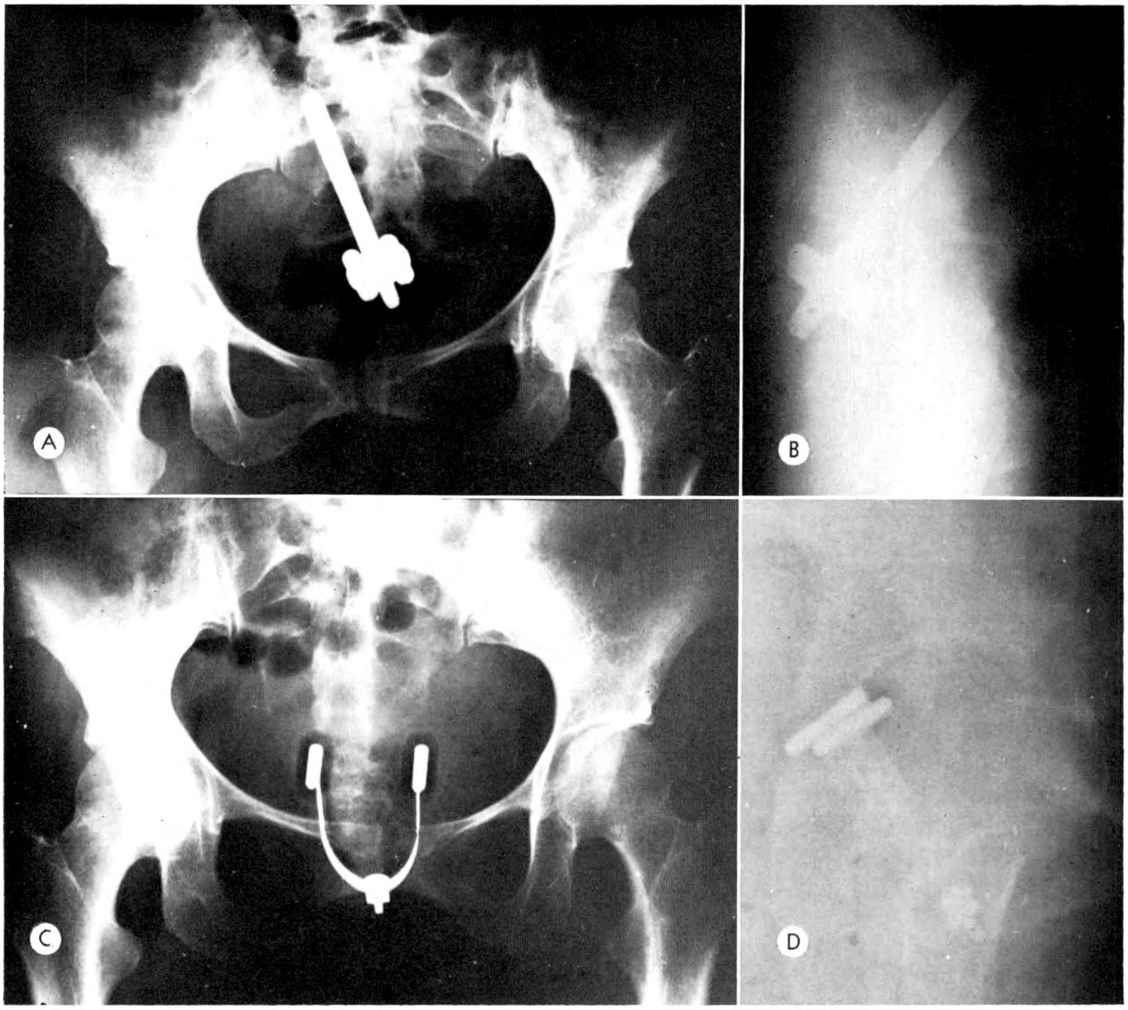


Fig. 7. Case iv. (*A* and *B*) Initial application showing malposition of double crossarm applicator. (*C* and *D*) Application of colpostats showing malposition.

plicator, using an empty tandem (Fig. 7, *E* and *F*). Although the position was greatly improved, the slight posterior displacement of the system was further corrected (Fig. 7, *G* and *H*) without re-application by merely manipulating the shaft. The large nut can be so well tightened down on the crossbar that the system is rendered virtually rigid.

Comment. These corrective procedures were done without anesthesia, excessive packing, and insertion of an indwelling catheter. Although the system described makes use of the Paris type colpostat, it is quite feasible for the alignment applicator to accommodate any type of joined colpostats, particularly the modified Manchester ovoids.

Case v (Fig. 8, *A–E*). A 57 year old white female with Stage ii b squamous cell carcinoma of the cervix. Roentgenograms of the pelvis illustrate antero-(right) lateral deviation of the tandem and rotation of the colpostats (Fig. 8, *A* and *B*). In addition, the colpostats are not fully expanded and the entire rigid system lies low in the vaginal vault out of contact with the cervix. Figure 8, *C* and *D* shows correction with the alignment applicator system and Figure 8*E* shows even further improvement with time due to the expanding nature of the spring crossbar.

SUMMARY

A mechanically simple and inexpensive applicator is described which retains the

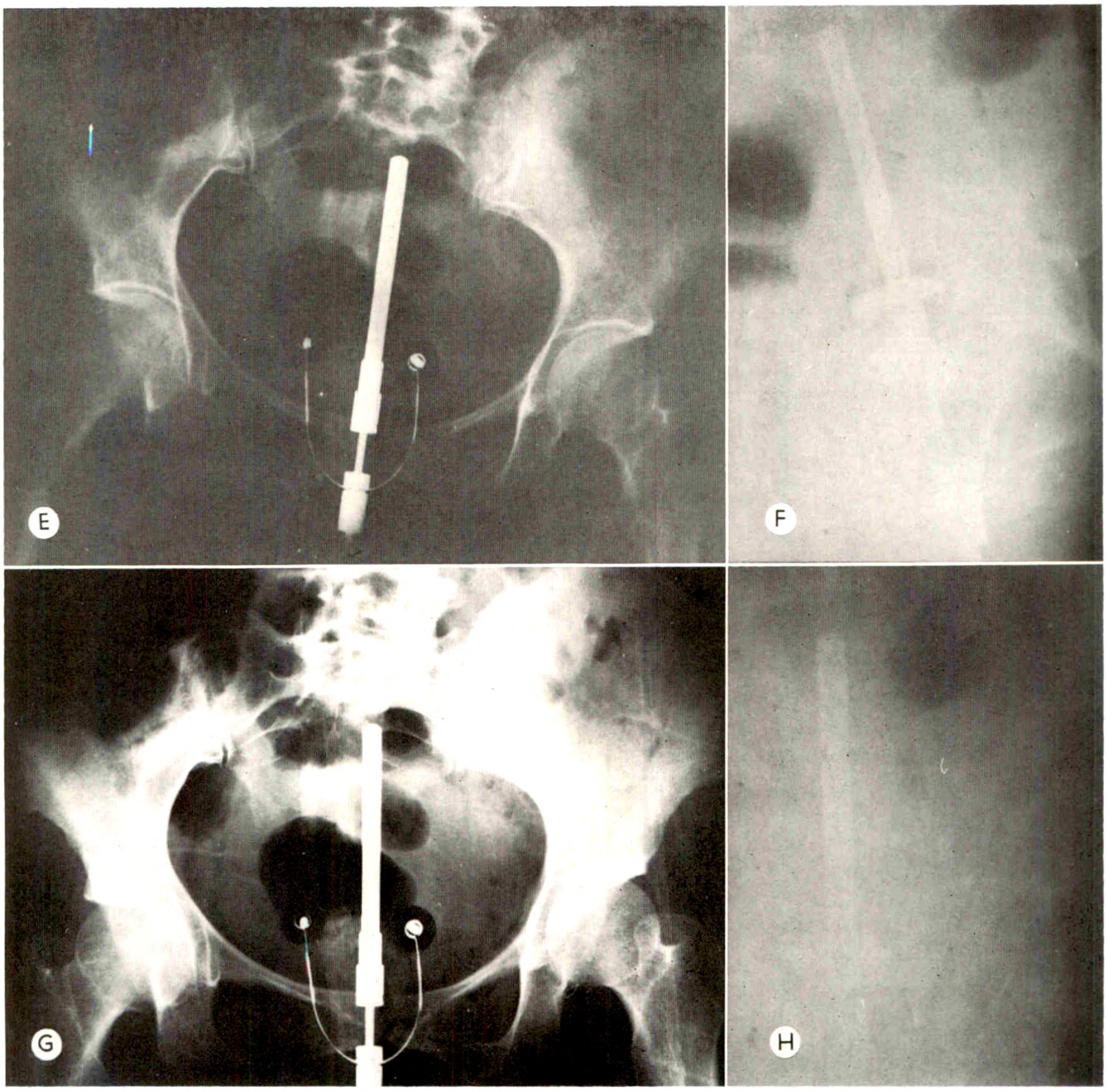


FIG. 7. (*E* and *F*) Correction with alignment applicator. (*G* and *H*) Further improvement in position with alignment applicator without re-application.

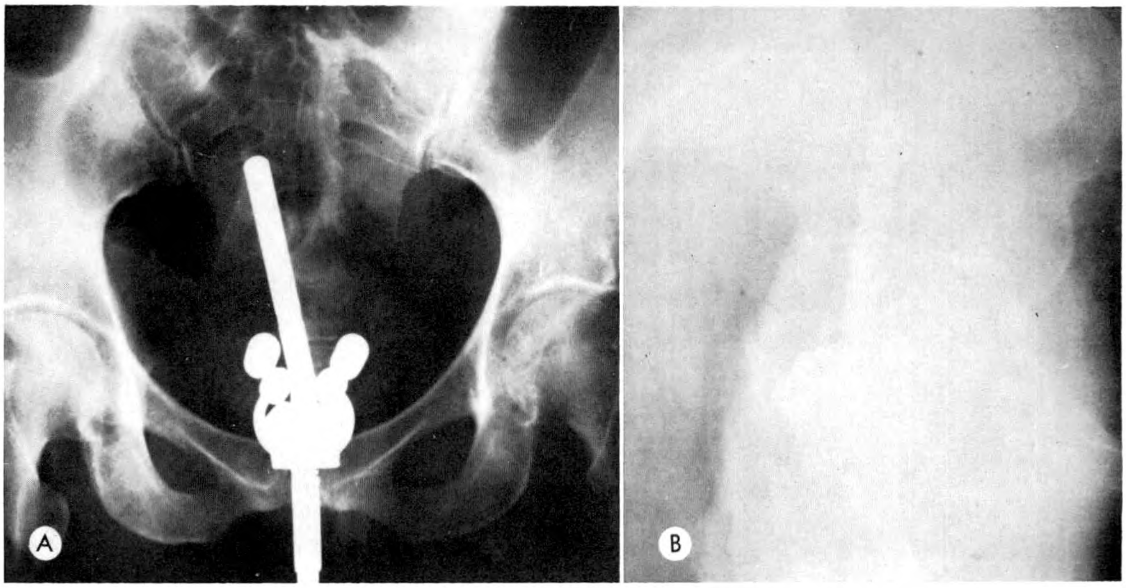


FIG. 8. Case v. (*A* and *B*) Initial application showing malposition of rigid applicator.

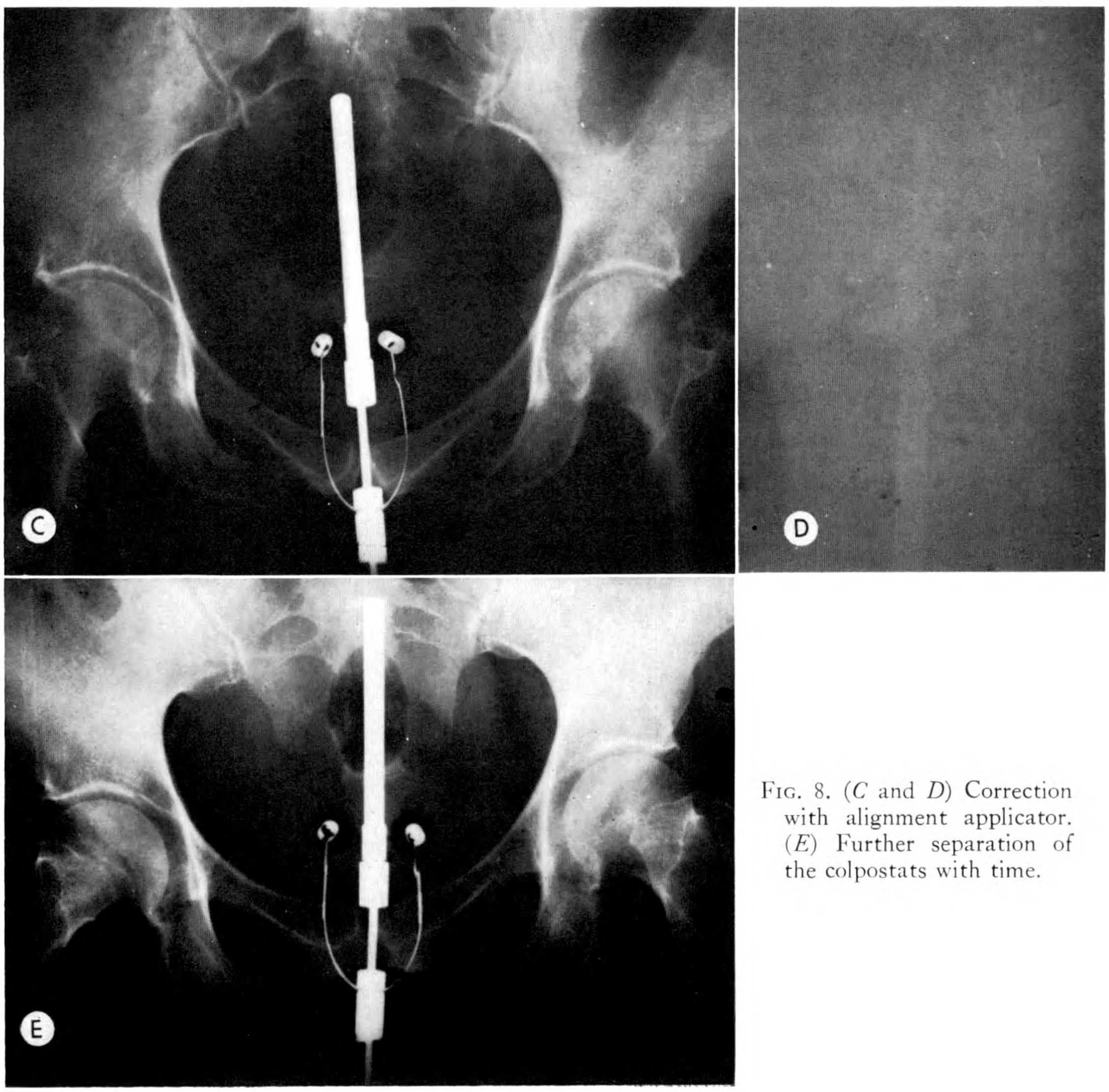


FIG. 8. (*C* and *D*) Correction with alignment applicator. (*E*) Further separation of the colpostats with time.

innumerable good points of the loose tandem-colpostat system; it converts it into a rigid yet flexible system by first fitting the patient with the appropriate tandem and colpostats, and then aligning them at right angles to one another. Particularly in difficult plevic anatomic situations the loose system has advantages over the rigid system, and therefore, this simple method, ensuring proper alignment, will result in the optimal application for the situation.

Duval Medical Center
2000 Jefferson Street
Jacksonville 8, Florida

REFERENCES

1. FLETCHER, G. H., STOVALL, B. A., and SAMPIERE, V. Carcinoma of the Uterine Cervix, Endometrium and Ovary. Year Book Medical Publishers, Chicago, 1962, pp. 80–116.
2. LOUIS, G. C., JR., RAVENTOS, A., and HALE, J. Space dose relationships for points A and B in radium therapy of cancer of uterine cervix. AM. J. ROENTGENOL., RAD. THERAPY & NUCLEAR MED., 1960, *83*, 432–446.
3. SHERMAN, A. I. Cancer of the Female Reproductive Organs. C. V. Mosby Company, St. Louis, 1963, pp. 98–118.
4. SHERMAN, A. I. Study of radiation failures and role of radioresistance in treatment of cancer of cervix. AM. J. ROENTGENOL., RAD. THERAPY & NUCLEAR MED., 1961, *85*, 466–478.

# FLEXIBLE SCINTILLATION RADIATION MEASUREMENT PROBE*

By CARL R. BOGARDUS, Jr., M.D.,† and MICHEL TER-POGOSSIAN, Ph.D.
ST. LOUIS, MISSOURI

THE direct measurement of radiation dosage from radioactive implants is a valuable aid in treatment planning. In cases of interstitial or intracavitary implants, it is of importance to be able to check the radiation dosage at key points during the implant in order to optimize the treatment plan. Most of the scintillation type instruments available at this time embody a rigid probe.[2] The probe we have developed surmounts this problem.

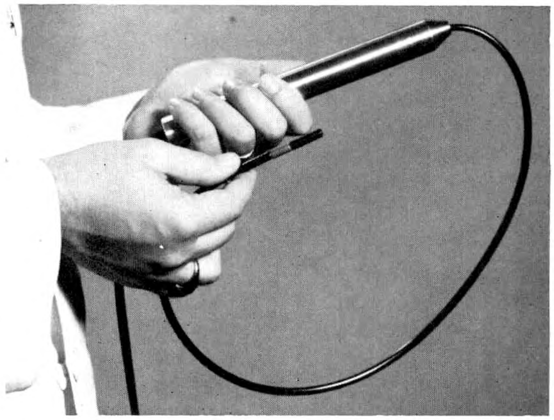

Fig. 1. Photograph of the flexible probe, demonstrating the relative size of components and flexibility of the light guide.

## DESIGN OF THE FLEXIBLE PROBE

The cylindrical probe tip is 6 mm. in diameter and is continuous with a 76 cm. flexible glass fiber light guide (American Optical Co.). The photomultiplier tube is mounted on the cable as shown in Figure 1. This is sufficiently far from the radiation area to reduce direct radiation photocathode stimulation to a negligible value, thus eliminating the need for heavy shielding or background correction. The phototube is mounted in plastic inside a cylindrical aluminum case: 2.5 cm. in diameter and 23 cm. long. The probe is waterproof and so may be cold sterilized.

The scintillator used in the probe is a hand cut and polished cylindrical thallium activated cesium iodide crystal 4 mm.×4 mm. The crystal is mounted with a piece of polystyrene foam in the hard rubber tip of the probe. The foam serves both to protect the crystal and to keep it forced against the tip of the lightpipe. A good optical coupling is assured by the use of silicone optical fluid. CsI (Tl) was selected for its high fluorescence efficiency. Anthracene was first considered as the crystal to use due to its established tissue equivalence for higher energy photons.[2] However, numerous measurements were carried out which demonstrated no significant difference between anthracene and thallium activated cesium iodide for this system with clinical applications of cobalt 60 (Fig. 2). All the measurements were carried out in water using a 7.2 mc source of cobalt 60 (15 mm. active length with a .6 mm. steel filtration) which was calibrated against a 10 mg. radium source. Up to 5 cm. distance from the source, there was no significant difference in readings. At 10 cm. there was 2.0 per cent difference. With other systems such as radium with its wide energy spectrum, $Ir^{192}$ or $Cs^{137}$ with lower energy gamma rays, there might have been a significant difference between the two crystals. If an isotope with lower energy radiation than cobalt 60 is used, we feel that anthracene would be the crystal of choice.

The lightpipe is a noncoherent glass fiber guide made of fibers .003 inch in diameter.[3] Each fiber has a core of 1.62 index glass and has been clad with a 1.52 index glass to

* From the Edward Mallinckrodt Institute of Radiology, Washington University School of Medicine, St. Louis, Missouri.
† Present address: Division of Radiation Therapy, University of Oklahoma, Oklahoma City, Oklahoma.

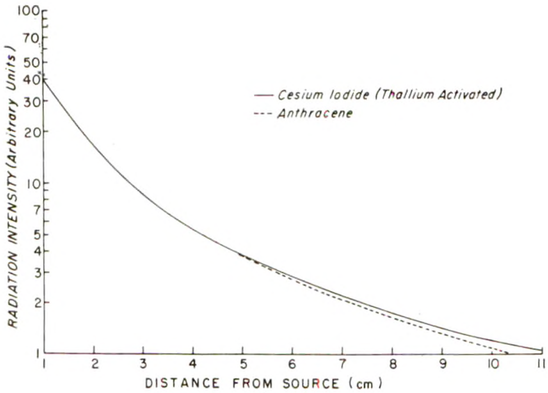


FIG. 2. Graph comparing cesium iodide (Tl) and anthracene.

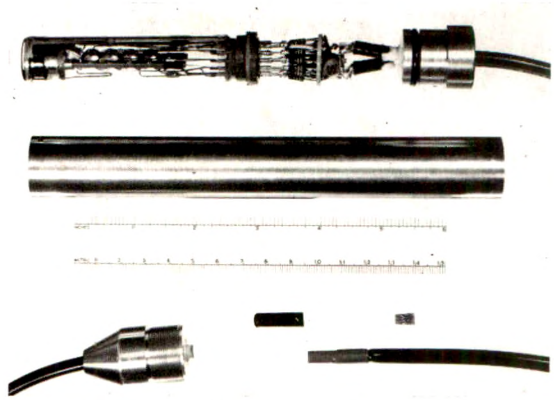

FIG. 3. Disassembled view of photo tube unit and crystal tip.

serve as optical insulation and thus protect the reflective surface of the core. This combination of indices provides a numerical aperture of .55. The published light half value length is 213 cm.[3] This theoretically gives a transmission efficiency of 78 per cent in the 76 cm. length we are using. The glass light guide has a very low fluorescence factor as compared to quartz or lucite. We measured the cobalt 60 gamma photon stimulated light emission from various lightpipes without crystals, and found that lucite gave 8 times the amount of light, and quartz gave 16 times as much light as the fiber optic light guide under the same conditions.

The low fluorescence of the light guide is very important when attempting to measure dosages on the posterior aspects of implants. In many of these cases, the light guide may be in a much higher field of radiation than the crystal. This could cause an appreciable error if the light guide itself was highly fluorescent.

We have found this light guide to be flexible and not affected by average usage and handling. It is easily cold sterilized by immersion and its plastic sheath is not affected by standard instrument sterilization fluids.

The photomultiplier used is a 152 AVP manufactured by Amperex. It is an end-window tube with an over-all gain of $5 \times 10^6$ at 1,800 v. The dark current is less than .1 $\mu$a. at an anode sensitivity of 30 a./1 m.[1] A voltage divider network of ten $\frac{1}{4}$ watt resistors and two capacitors is built in a compact form at the base of the tube (Fig. 3). We built a number of different networks. The most satisfactory resistance range is one in which the bridge current is from .5 ma. up to .7 ma. The voltage between the photocathode and dynode 1 must be at least 180 volts and the operational voltage between dynodes at about 120 volts (Fig. 4).

With a 7.2 mc cobalt 60 source at 3 cm. for calibration; conduction begins at about 1,000 v., calibration is reached at approximately 1,400 v., and a reading of 10 times calibration is reached at 1,800 v.

Two cables leave the unit; one is a negative high voltage input, the other is the signal output connected to a microammeter. The output impedance is of the order of 10 megohms. A two stage vacuum tube voltmeter readout is used. The scale may be

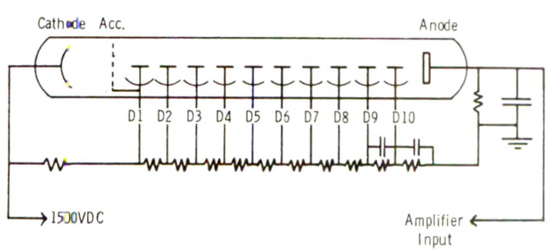


FIG. 4. Schematic diagram of photomultiplier and its network.

read in arbitrary units or calibrated directly in roentgens by the use of a standard radium source.

### CLINICAL USE

In clinical use the described probe has, by virtue of its light weight and flexibility, proven itself superior to others we have previously used. In the oral cavity, it is easy to reach the base of the tongue and other areas which had previously been difficult to monitor. The length and flexibility make it easy to insert into the esophagus, larynx, nasopharynx, and other areas of difficult access during external radiation therapy. In this way, we are able to monitor the dosage in these areas and compare these readings to calculated doses.

In carcinoma of the cervix, we are able to reach behind applicators and into other areas around implants which would be difficult to reach otherwise. It is easy to reach all areas of the bladder, and we have found it easy to reach high into the sigmoid and monitor areas previously inaccessible.

Carl R. Bogardus, Jr.
Division of Radiation Therapy
The University of Oklahoma Medical Center
800 Northeast 13th Street
Oklahoma City, Oklahoma 73104

### REFERENCES

1. Amperex Cat. No. NPC 7–63.
2. Belcher, E. H. Radiation dosimetry with scintillation detectors. *Brit. J. Radiol.*, 1953, *26*, 455–464.
3. Siegmund, W. P. Fiber Optics: Principles, Properties, and Design Considerations. American Optical Co., Southbridge, Mass., 1962.

VOL. 94, No. 4

# CAN CANCER REALLY BE CURED WITH RADIATION THERAPY?*

*By* CHARLES L. MARTIN, M.D., JAMES A. MARTIN, M.D.,
*and* ROBERT A. WILSON, M.D.
DALLAS, TEXAS

IT WOULD seem a recurring paradox in many areas that, as experience accumulates, some truths become progressively more difficult to define. As a fundamental motive in clinical radiotherapy the word "cure" has long had basic significance and would appear to be a straightforward absolute, meaning simply to heal and restore health. In relation to cancer therapy it has been necessary to modify the word in terms of time, or resort rather euphemistically to such terms, as "permanent control" or "tumor sterilization." Some would prefer to bypass the semantic trial altogether and resort to the noncommittal word "survival" which is comfortable usage but easily misleading. Without considerable explanation for example, a "3 year survival" would apply equally to the incurable, barely alive, and the curable, alive and vigorous.

Excluding those neoplasms which are at present incurable and those which have a high rate of late recurrence, there remains a significant group which can be eradicated with reasonable predictability. Primary cancer of the uterine cervix, mouth, pharynx, larynx and skin is potentially radiocurable and the 5 year evaluation has been considered an accurate end-point. In recent years, however, some disturbing results from prolonged follow-up studies repeatedly reveal small proportions of "late recurrences" in patients previously thought well, as time-defined. Quite obviously, a fatal recurrence of the original neoplasm even after 20 years signals a treatment failure, absolute and irrevocable. One's faith in the term "5 year cure" thus becomes incompletely deserved, and the point becomes one of practicality. Should we cling to the designation as a useful although slightly inaccurate device, or should we discard it altogether since it is no longer more than almost right?

Soon after the turn of the century, the foundation for the radiotherapy section of our clinic was laid by James M. Martin when he became convinced that skin cancer could, in truth, be cured by fractionated low voltage roentgen-ray therapy. His earliest work was begun with gas tubes energized by static machines and rather empirical dosages were related to minimum skin erythema standards rather than physical units. Built on this foundation, his report of 15 years' experience in treating skin cancer presented before this society in 1923[10] was certainly artistry as well as science. The senior author of this paper entered practice with James M. Martin in 1920 and soon shared the conviction that, contrary to some prevailing opinions, cutaneous cancer could indeed be cured by radiotherapy. A fundamental optimism thus ingrained years ago is intrinsically difficult to discard. Perhaps our attitude also reflects subjective identification with lay cynicism for cautious medical pessimism.

"They answered, as they took their Fees,[2]
There is no cure for this disease."

It has been our conviction over the years that each patient, in order to qualify as cured, must have a properly authenticated lesion and must remain observed alive and with no evidence of residual, recurrent or metastatic disease throughout the designated time period. Should a patient develop

* Presented at the Sixty-fifth Annual Meeting of the American Roentgen Ray Society, Minneapolis, Minnesota, September 29–October 2, 1964.

and succumb to a new and different neoplasm before the end of that time, the initial treatment effort can only be labeled a failure. Should that tragedy occur after the primary criteria in time are fulfilled (often it would seem at intervals approximating multiples of 7 years), the initial lesion was likely cured. Combined with the fact of late recurrences, it is evident that these requirements preclude an unbounded faith in evaluation methods based on numerical predictions beyond short-term observations.

## MATERIAL

In an attempt to explore the validity of these precepts we have analyzed personal experience with 481 consecutive cases of cancer of the cervix admitted to our clinic between 15 and 26 years ago. Since this lesion tends to remain localized in the pelvis for relatively long periods of time and can usually be eradicated by adequate radiotherapy when not too advanced, it was chosen for this study. Seven cases were deleted since they were histologically classed as noninvasive lesions, and an eighth was dropped since it proved to be primary adenocarcinoma of the endometrium. In the present context no valid conclusions may be drawn from those patients inadequately treated and 18 in that category were eliminated from study. Most of these received heavy radiation therapy elsewhere thus precluding further treatment of any magnitude as potentially disastrous. Two, however, died abruptly before treatment could be given, one from severe hemorrhage and the other as an anesthetic accident.

Of the 455 cases left by exclusion, no attempts to subdivide by clinical staging were made. Two or more examiners may well disagree as to classification, especially in the late Stage II and many of the Stage III and Stage IV cases. If Stage IV patients were limited to those with positive biopsy reports on tissue removed from the rectum or bladder as recommended by the Memorial Hospital group in New York, we doubt that any of them would actually have been cured. An attempt was made to stage the cases treated in 1948 and 1949 in a previous article[11] using the League of Nations method, and the distribution of material in other years has been similar. For the purposes intended in this study accurate clinical staging is not considered a necessity.

In all cases the primary treatment approach was with radium therapy, using multiple capsules augmented by small doses of roentgen rays for the early lesions and low-intensity needle implants for large primary lesions and extensions into the vaginal walls and parametria. These techniques were not altered during the period of study and uniformity was enhanced by the fact that all treatments were administered and all follow-up examinations of the patients that could return were conducted by the senior author. External orthovoltage roentgen-ray therapy was used as a secondary procedure for the advanced cases and recurrences. This method is advantageous because the treatment time for most cases does not exceed 7 or 8 days (an economic boon to our patients, many of whom are less than wealthy) and a low incidence of treatment sickness and radiation sequelae is obtained. These methods have been described elsewhere in considerable detail.[12,13,14,17]

None of the patients treated 15 or more years ago received our relatively more recent combined method of low-intensity radium needle implantation in the parametria augmented by moderate amounts of orthovoltage roentgen-ray therapy,[15] patterned after our successful method used in the treatment of metastatic cervical lymph nodes.[16] This procedure has reopened a small series of ureters significantly obstructed by parametrial invasion and may enhance our 5 year salvage in the future.

## ANALYSIS

As a matter of order, the word "survival" may be used in analysis until conclusions regarding cure and its meaning are obtained. The 5 year survivals are tabulated

TABLE I

FIVE YEAR SURVIVAL OF 455 CASES OF CANCER OF CERVIX ADEQUATELY TREATED

| Year Treated | Cases Admitted | Cases Adequately Treated | Surviving 5 Years |
|---|---|---|---|
| 1938 | 35 | 33 | 17=51.5% |
| 1939 | 39 | 39 | 19=48.7% |
| 1940 | 31 | 29 | 15=51.7% |
| 1941 | 34 | 32 | 15=46.8% |
| 1942 | 32 | 28 | 11=39.2% |
| 1943 | 45 | 44 | 20=50.0% |
| 1944 | 41 | 41 | 19=46.3% |
| 1945 | 47 | 46 | 21=45.6% |
| 1946 | 45 | 41 | 20=48.7% |
| 1947 | 48 | 44 | 19=43.1% |
| 1948 1949 | 84 | 78 | 43=55.1% |
| Total | 481 | 455 | 221=48.5% |

for each year (Table I) except for the 1948 and 1949 cases which are grouped together, as in a previously published report in which the 5 year salvage of 55.1 per cent was the best obtained in the present study. The over-all 5 year survival rate for the entire group treated in 1938 through 1949 was 221 out of 455, or 48.5 per cent.

Decker and Van Herik[3] of the Mayo Clinic report a 5 year survival of 49.0 per cent using all forms of treatment and note an average figure of 48.5 per cent combining reports from Stockholm, Manchester, St. Louis and Copenhagen. Makowski and his group[9] at the University of Minnesota use large doses of roentgen rays and radium, thereby accepting an increased liability to both early and late sequelae, but claim a 5 year survival rate of 58.8 per cent. It should be noted that these authors have felt it necessary to include noninvasive lesions within their Stage I category and this likely enhances the salvage figure. Fletcher, Rutledge and Chau[5] claim a very high 5 year survival rate of 63 per cent, attributed largely to the addition of supervoltage therapy to their radium techniques. This figure, however, is reached through a life-table method of biometric projection and cannot be compared, using the data given, with the direct percentage methods given here. Using comparable methods of analysis, it is evident that the salvage presented in our series is similar to that obtained in many other clinics.

Of major concern, of course, is the fate of 78 patients known dead or untraced after passing the 5 year end-point in apparent good health. This information is tabulated in Table II with a separate tabulation in Table III of those 18 patients who developed "late recurrences," and succumbed to their disease. It is of interest to note that

TABLE II

DEAD OR LOST AFTER 5 YEAR CHECKUP

| Years after Treatment | Inter-current Disease | Lost | Cancer of Cervix |
|---|---|---|---|
| 26 | 4 | 4 | 2 |
| 25 | 7 | 1 | 2 |
| 24 | 4 | 1 | 0 |
| 23 | 3 | 1 | 0 |
| 22 | 4 | 0 | 1 |
| 21 | 4 | 0 | 0 |
| 20 | 3 | 1 | 2 |
| 19 | 3 | 3 | 2 |
| 18 | 5 | 0 | 2 |
| 17 | 2 | 0 | 4 |
| 16 15 | 9 | 1 | 3 |
| Total | 48 | 12 | 18 |

TABLE III

OUTCOME OF EIGHTEEN 5 YEAR SURVIVORS WHO DIED OF CANCER OF CERVIX

| Treated | Actual Survival (yr.) | Treated | Actual Survival (yr.) |
|---|---|---|---|
| 1938 | 11–21 | 1944 | $6\frac{1}{2}$–13 |
| 1939 | $5\frac{2}{3}$–7 | 1945 | $5\frac{1}{2}$–$6\frac{1}{2}$ |
| 1940 | 0 | 1946 | 6–11 |
| 1941 | 0 | 1947 | $5\frac{3}{4}$–8–9–13 |
| 1942 | 6 | 1948 | $5\frac{1}{3}$–6–12 |
| 1943 | 0 | 1949 | |

half of this group of 18 died between the fifth and seventh year, and almost all of them, or 17 out of 18, expired before the fourteenth year. If this sampling were of sufficient size one might be justified in saying that any patient treated with this technique who remains alive and well 13 years, may be classed as cured with no more error than a fraction of 1.0 per cent. However, combining this experience with that of others,[1] it is difficult to know at what point in time before 15 years one should place a critical end point.

It is apparently common experience in all long-term follow-up studies to detect at least one instance of an extraordinarily late recurrence. In this study, one patient died of recurrent disease 21 years after treatment although she was examined at 12 years and seemed perfectly well at that time. Graham, Sotto and Paloucek[6] report the death of a patient with an adenocarcinoma of the cervix 26 years after presumed successful radiotherapy of primary squamous cell carcinoma (or in retrospect, a possible adenoacanthoma). Their suggested explanation on the basis of prolonged weak irradiation produced by a deteriorating radon seed is conjectural at best. Of several similar reports it would appear that the record is held by Latour and Fraser[8] with a recurrence appearing at 34 years, followed in close second position by Howkins and Andrew[7] with one at 30 years. It is also of interest that some material would indicate a pattern of late recurrence in surgically treated cases similar to that obtained after primary irradiation.[6]

Other causes of death as listed in Table II involve 48 patients labeled as dead of intercurrent disease. Table IV includes 10 who died of other types of cancer. As additional evidence that these were new rather than metastatic lesions is the fact that only 3 patients succumbed prior to the 13 year end point beyond which death from recurrence of cervical cancer virtually ceased. Of the remaining 38, 29 died of cardiovascular disease, 2 of gallbladder disease, 2 of unknown causes and 1 each of hip fracture, postoperative hemorrhage, pneumonia, cirrhosis of the liver and suicide.

The 143 patients known to be well and free of any evidence of cancer of the cervix at 15 to 26 years after treatment are listed in Table V. As an exercise, this table also includes a reverence for "13 years" and demonstrates how the cure rate at 15 to 26 years can be elevated from 31.4 per cent to 37.5 per cent if one considers those lost or dead of intercurrent disease after 13 years as "probably cured."

## COMPLICATIONS

Current medical literature directs considerable emphasis toward treatment

TABLE IV

DEATH FROM OTHER TYPES OF CANCER AT MORE THAN 5 YEARS AFTER SUCCESSFUL TREATMENT OF CANCER OF CERVIX

| Point of Origin | Survival after Cervix Treatment (yr.) |
|---|---|
| 2—Colon | 16–14 |
| 1—Fundus | 15 |
| 1—Breast | 22 |
| 1—Kidney | 21 |
| 1—Hand | 18 |
| 1—Liver | 7 |
| 1—Stomach | 9 |
| 1—Face | 20 |
| 1—Cecum | 13 |

Table V

cases of cancer of cervix well 15 to 26 years

| Treated Years Ago | Known Alive and Well (Sept. 1964) | Dead or Lost after 13 Years (no cancer) | | Probably Cured |
|---|---|---|---|---|
| | | Intercurrent Disease (yr.) | When Lost (yr.) | |
| 26 | 7 of 33=21.2% | 15⅓<br>16<br>19<br>20 | 15<br>16<br>21 | 14=51.5% |
| 25 | 9 of 39=23.0% | 15<br>19<br>19<br>22 | 0 | 13=33.3% |
| 24 | 10 of 29=34.4% | 15<br>20<br>21<br>21 | 0 | 14=48.2% |
| 23 | 11 of 32=34.3% | 19 | 0 | 12=37.5% |
| 22 | 6 of 28=27.3% | 16<br>17<br>18 | 0 | 9=32.1% |
| 21 | 18 of 44=40.9% | 14<br>16<br>16 | 0 | 21=49.0% |
| 20 | 13 of 41=31.7% | 14 | 0 | 14=34.1% |
| 19 | 13 of 46=28.2% | 17 | 0 | 14=30.4% |
| 18 | 13 of 41=31.7% | 14 | 0 | 14=34.1% |
| 17 | 13 of 44=29.5% | 14⅓ | 0 | 14=31.8% |
| 16<br>15 | 30 of 78=38.4% | 15<br>14 | 0 | 32=41.0% |
| Total | 143 of 455=31.4% | 25 | 3 | 171=37.5% |

methods and biomathematics, but the frequency and magnitude of complications are at times difficult to extract. Some years ago among men of wisdom there were those who perceived radiation damage with grave misgiving and wondered if the risks of treatment might be more offensive than the disease.[4] It is apparent that the tissue-sparing effect of new techniques has proved relative and tissue tragedy has not been banished. Indeed, there are some reports giving the impression that some increase in the complication rate coincidental with an increase in voltage capability assumes a place as acceptable in the name of pure physics. It is the authors' conviction that sequelae can be reduced toward zero, and that the conversion of a potentially curable patient into a radionecrotic terminal event is both tragic and reprehensible.

In the series presented here, the incidence of significant radiation complication is low. Three cases of hemorrhagic proctitis and 2 of radiation cystitis regressed with local treatment only and are considered, in retrospect, to be the result of technical faults subsequently corrected. One case of ureterovaginal fistula was apparently the result of a direct although inadvertent ureteral puncture with a radium needle inserted per vaginam. A surgical report from another town reveals that one patient (a 24 year survivor) required a bypass procedure to correct small bowel fibrosis occurring 18 years after radiotherapy. Another case of ulcerative cecal disease with symptoms antedating most of the treatment is of obscure etiology, even to the microscopist. Irradiation produced no cases of rectosigmoid obstruction, none of acute small bowel necrosis and obstruction, no episodes of severe vault necrosis, no detected cases of ureteral stricture and was not responsible for the death of any patient. All of 11 rectovaginal and vesicovaginal fistulae occurred directly through necrotic tumor and, although complications of the disease, are not considered errors of irradiation. One case of peritonitis and one of thermal burn from the "indifferent" electrode of the electrocautery unit are certainly complications of treatment but not of irradiation. Thus a total of 8 significant radiation sequelae constitutes a rate of 1.8 per cent and is considered reducible.

## CONCLUSIONS

The title question regarding radiocurability of cancer need not actually be debated except as a rhetorical stimulant. Multiple reports in the scientific literature proclaim that curability in certain lesions adequately treated is an accomplished fact. The observation that approximately 91 per cent of our cervical carcinoma cases alive and well at 5 years were cured, is additional testimony for the affirmative. The application of this fact to the status of any individual patient on the other hand becomes a practical question. Omnipresence of the rare late, late, late recurrence of cervical cancer would seem in the strictest sense to condemn each seemingly well patient to a prolonged sentence as survivor rather than victor. Such an attitude toward the curable lesions is certainly one of misplaced emphasis. It would seem wiser to relocate emphasis in other ways. It is evident for instance that in cervical carcinoma, cure at 5 years is a reasonable accuracy, but equally evident that adequate observation should exceed that limit to at least 10 and perhaps 15 years. Each additional uneventful year in the patient's life enhances the truth value of the word "cure." In a second instance, it is evident from the case study presented here that significant radiation sequelae can be minimized and largely eliminated while preserving a cure rate comparable to that in other centers. Perhaps a large portion of cautious pessimism should be re-directed toward an attitude which considers significant radiation damage, even at a minimum, as inescapable.

Charles L. Martin, M.D.
The Martin X-Ray & Radium Clinic
3501 Gaston Avenue
Dallas, Texas 75246

## REFERENCES

1. Arneson, A. N., and Williams, C. F. Long-term follow-up observations in cervical cancer. *Am. J. Obst. & Gynec.*, 1960, *80*, 775–790.
2. Belloc, H. Cautionary Verses. Henry King. Alfred A. Knopf, New York, 1959, pp. 13–16.
3. Decker, D. G., and Van Herik, M. Survival in invasive carcinoma of cervix five to ten years after radiation therapy. Am J. Roentgenol., Rad. Therapy & Nuclear Med., 1961, *85*, 488–496.
4. Ewing, J. Therapy Symposium Discussion. Am. J. Roentgenol. & Rad. Therapy, 1932, *28*, 343–348.
5. Fletcher, G. H., Rutledge, F. N., and Chau, P. M. Policies of treatment in cancer of cervix uteri. Am. J. Roentgenol., Rad. Therapy & Nuclear Med., 1962, *87*, 6–21.
6. Graham, J. B., Sotto, L. S. J., and Paloucek, F. P. Carcinoma of the Cervix. W. B. Saunders Company, Philadelphia, 1962.
7. Howkins, J., and Andrew, J. D. Reappearance of cervical carcinoma thirty years after treatment with radium. *J. Obst. & Gynaec. Brit. Emp.*, 1955, *62*, 870–871.

8. Latour, J. P. A., and Fraser, W. D. Problem of late local recurrence of carcinoma of cervix. *Canad. J. Surg.*, 1960–1961, *4*, 508–511.
9. Makowski, E. L., McKelvey, J. L., Flight, G. W., Stenstrom, K. W., and Mosser, D. G. Results of irradiation therapy of carcinoma of cervix. *J.A.M.A.*, 1962, *182*, 637–642.
10. Martin, J. M. Fifteen years' experience with fractional dose method of treating cutaneous malignancies. Am. J. Roentgenol. & Rad. Therapy, 1923, *10*, 726–733.
11. Martin, C. L. Approximation technique in treatment of cancer of cervix with irradiation. Am. J. Roentgenol., Rad. Therapy & Nuclear Med., 1957, *77*, 388–396.
12. Martin, C. L. Advances in treatment of carcinoma of cervix. *Texas J. Med.*, 1938, *34*, 471–475.
13. Martin, C. L. Elimination of irradiation injuries in treatment of cancer of cervix. Am. J. Roentgenol. & Rad. Therapy, 1943, *49*, 494–503.
14. Martin, C. L. New developments in irradiation therapy of cancer of uterine cervix. *Texas J. Med.*, 1948, *44*, 587–593.
15. Martin, C. L. Ureteral obstruction in Stage III cancer of cervix relieved by low intensity radium needle implantation. Am. J. Roentgenol., Rad. Therapy & Nuclear Med., 1961, *85*, 479–487.
16. Martin, C. L. Treatment of cervical lymph node metastases with irradiation alone. *Radiology*, 1950, *55*, 62–67.
17. Martin, C. L., and Martin, J. A. Low Intensity Radium Therapy. Little, Brown & Company, Boston, 1959.

# THE IMPORTANCE OF TOMOGRAPHY FOR THE INTERPRETATION OF THE LYMPHOGRAPHIC PICTURE OF LYMPH NODE METASTASES*

*By* Dr. T. de ROO, Dr. P. THOMAS, *and* R. W. KROPHOLLER
LEYDEN, NETHERLANDS

DURING recent years lymphography (lymphangio-adenography) has been employed with increasing frequency in the evaluation of the extent of malignant processes. Although marked loss of weight, fatigue, and severe anemia may raise the suspicion of metastases, these lesions are often difficult to demonstrate conclusively. At present, contrast media containing oil are used to achieve roentgenographic visualization of the lymphatic system because, unlike water soluble solutions, these substances remain in the lymph nodes for a period of months, thus greatly increasing the roentgenologic possibilities. Normally, the contrast material is distributed equally over the entire lymph node; demonstration of lacunae in the opaque medium cast shadow indicates the absence of normal lymph node tissue. Lymphadenograms, *i.e.*, roentgenograms made after 24 and 48 hours, enable the best evaluation of the lymph nodes. Special attention must be given to the dimension and internal structure of the lymph nodes and to the appearance of the marginal sinus. A lymph node which is completely filled with abnormal tissue will not take up the contrast material and, therefore, will not be demonstrated on roentgenograms. In these cases the lymphangiograms, made during the injection of the contrast material, are of paramount importance, and abnormal pathways of flow of the opaque medium are indications of missing lymph nodes.

Certain characteristic aspects of the affected lymph nodes become obvious when a comparison of the anteroposterior, lateral, and oblique lymphadenograms is made. A definitely pathologic lymph node is generally not difficult to recognize among the normal lymph nodes. In our experience, however, lymphadenograms made in these three views are often insufficient for the evaluation of pathologic lymph nodes.

In lymphoreticular malignancy, the affected lymph nodes are almost always enlarged, and usually groups of these are involved. There may be doubt as to whether the lesions are due to Hodgkin's disease or lymphosarcoma, but usually there is no doubt about the fact that the lymph node or nodes are pathologic. In carcinomatous metastases the lymph nodes are not always enlarged and the metastases may be limited (macroscopically) to a single lymph node. It is, therefore, important in obtaining a correct roentgenologic diagnosis to be able to observe any small changes in the internal structure as well as any involvement of the marginal sinus of the lymph nodes. Interpretation becomes difficult when a number of lymph nodes lie superimposed over parts of the skeleton with inhomogeneous structure, when the patient is very obese, or when several lymph nodes are matted together. To gain more information concerning the location, shape, and structure of normal and pathologic lymph nodes and to establish a more reliable evaluation of metastases of carcinoma in lymph nodes, we have attempted tomography as a supplementary method of examination.

On tomograms the following characteristic findings according to the degree of infiltration of the lymph nodes by metastatic carcinoma are demonstrated:

(a) The lymph node may show no enlargement; the marginal sinus is inter-

* From the Department of Radiology (Director: Prof. Dr. J. R. von Ronnen), University of Leyden, Netherlands.

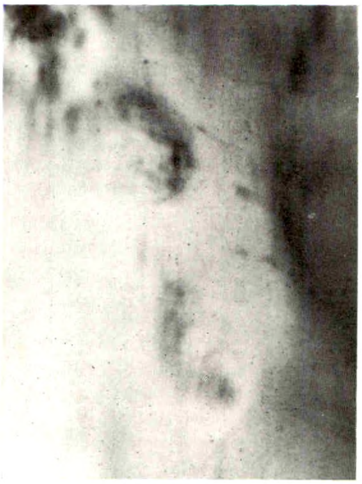

Fig. 1

Fig. 2

Fig. 3

FIG. 1. Tomogram showing the marginal lesions due to metastases. The boundary between the metastases and the normal lymph node tissue is indistinct and irregular.

FIG. 2. Tomogram showing 2 enlarged lymph nodes in which the destruction caused by the metastases has progressed so far that only a small remnant of the lymph node tissue is visible.

FIG. 3. Tomogram showing the greatly enlarged lymph node, whose internal structure has almost entirely disappeared. The marginal sinus is still clearly delineated but shows several interruptions.

rupted at one or more places; and the boundary between metastatic and normal lymph node tissue is blurred and irregular (Fig. 1).

(b) The lymph node is usually enlarged; the metastatic lesions have progressed so far that only a small amount of macroscopically normal lymph node tissue remains; and the marginal sinus has largely disappeared (Fig. 2).

(c) The lymph node is enlarged; the internal structure has almost entirely disappeared; and the original shape of the lymph node is indicated by the marginal sinus which can be clearly distinguished although a few interruptions are present (Fig. 3).

(d) The lymph node is completely replaced by carcinoma and is consequently no longer visible.

On the *lymphangiograms* the lymphatic drainage channels may be seen arched around the pathologic lymph node which has not taken up the contrast medium.

The *lymphadenograms* show an abrupt interruption of the glandular chain. When drainage is obstructed, the supply channels are visible on the lymphadenograms and the tomograms.

The *tomograms* are made with a rectilinear tube and film motion, a focus-film distance of 1.50 m. and an angle of 40 degrees. The distance between the various sections is 0.5 cm., or in some cases 0.25 cm. When possible, the patient is placed in a prone position. The usefulness of tomography in evaluation is illustrated by the cases cited below.

## REPORT OF CASES

CASE I. Mr. K.F. (3552/64), a 25 year old male, had surgery performed on the right lower leg for the first time in September, 1964. For a period of 6 months prior to that, he had had a pigmented nevus suggestive of melanoma; in the groin there was a lymph node which increased rapidly in size. The nevus was totally excised with extensive lymph node dissection. Histologic examination of the nevus and lymph nodes showed malignant melanoma with lymph node metastases. At a follow-up examination in December, 1964, a swelling was palpated above Poupart's ligament on the right side. The cytologic diagnosis from a sample obtained by puncture of the lymph node was malignant

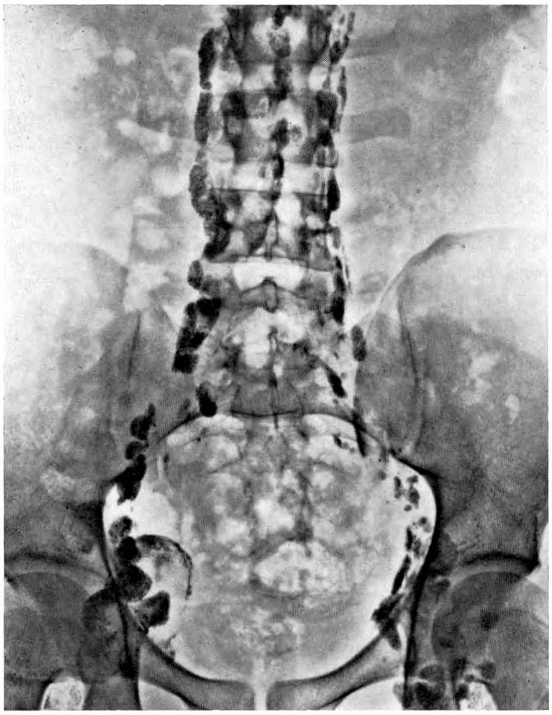

FIG. 4. Case I. Melanosarcoma. Lymphadenogram showing a large pathologic lymph node in the right iliac region.

metastasis from the melanoma. Clinical examination revealed no indications of metastases to the liver or lung.

A lymphographic examination was then carried out to determine the extent of the metastases. The lymphadenogram (Fig. 4) demonstrated a pathologic lymph node, the size of a hen's egg on the right, in the lower iliac region.

Tomography gave the following results: Figure 5*a* (Section 13½) showed a normal iliac lymph node (A) and a pathologic iliac lymph node (B). The latter lymph node was markedly enlarged, the marginal sinus was interrupted, and the internal structure was barely recognizable. The pathologic iliac lymph node (Fig. 5*b*, C) became distinctly visible on Section 15. An interrupted marginal sinus with almost no internal structure was visualized. More ventrally, 3 other lymph nodes were seen on Section 16 (Fig. 5*c*). These were an inguinal lymph node (D) and 2 iliac lymph nodes (E and F); all were roentgenologically normal. The lymph nodes along the common and external iliac vessels as well as the lumbar and aortic lymph nodes were also examined tomographically and were found to be normal. Tomograms give a better idea of the shape and structure of the lymph nodes in this region.

On the basis of the lymphographic findings, surgery was again performed. The lymph nodes in the right inguinal, iliac, lumbar, and aortic regions were removed. The pathologist's report confirmed the roentgenologic diagnosis.

CASE II. Mr. A.N. (16212/63), a 46 year old male, underwent an orchidectomy on the right side in April, 1964 for a seminoma of the testis. The patient reacted well to postoperative irradiation. In October, 1964 he complained of fatigue and pain in the back. The intravenous pyelogram showed a lateral displacement of the right kidney.

Because there were clinical reasons for suspecting retroperitoneal metastases, lymphography was performed. On the anteroposterior (Fig. 6), lateral (Fig. 7) and oblique lymphadenograms, the paralumbar and para-aortic lymph nodes on the left side were seen to be displaced to the left. These lymph nodes did not appear enlarged but were irregular in shape (A, B and C in Fig. 6 and 7).

Only on tomograms were the affected lymph nodes clearly demonstrated (Fig. 8, *a*, *b* and *c*).

On the basis of the lymphographic findings, the patient was again treated by radiation, this time with telecobalt, to which he reacted well. On follow-up examinations the pathologic lymph nodes were distinctly smaller and the displacement of the paralumbar and para-aortic lymph nodes was reduced.

CASE III. Mr. N.v.W. (7067/64), a 29 year old male, was admitted in April, 1964 with a large malignant lymphogranuloma in the left groin. The left testicle was stone-hard. The cytologic diagnosis based on a sample obtained by puncture of the lymph node showed metastasis of a seminoma of the testis.

A lymphographic examination was carried out to determine the extent of the malignant process. On the lymphadenogram (Fig. 9), in the left inguinal region, not only a normal lymph node (A) but also several lymph nodes raising the suspicion of metastases (B and C) were seen. Also noteworthy is that on both sides only a few lymph nodes were visible in the inguinal region. The iliac, paralumbar, and para-aortic lymph nodes are difficult to evaluate on the lymphadenogram.

Tomograms of the paralumbar, para-aortic,

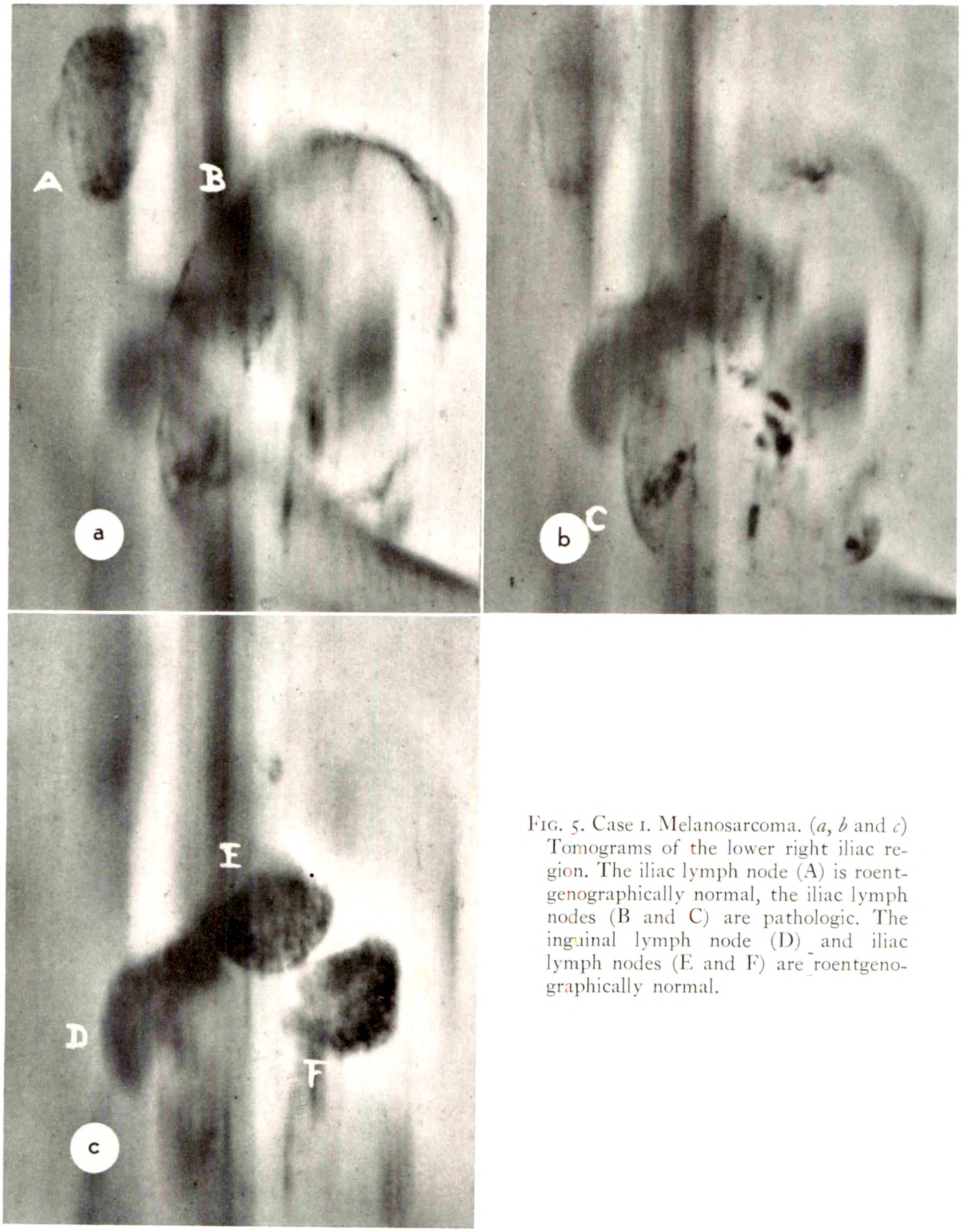


Fig. 5. Case 1. Melanosarcoma. (*a*, *b* and *c*) Tomograms of the lower right iliac region. The iliac lymph node (A) is roentgenographically normal, the iliac lymph nodes (B and C) are pathologic. The inguinal lymph node (D) and iliac lymph nodes (E and F) are roentgenographically normal.

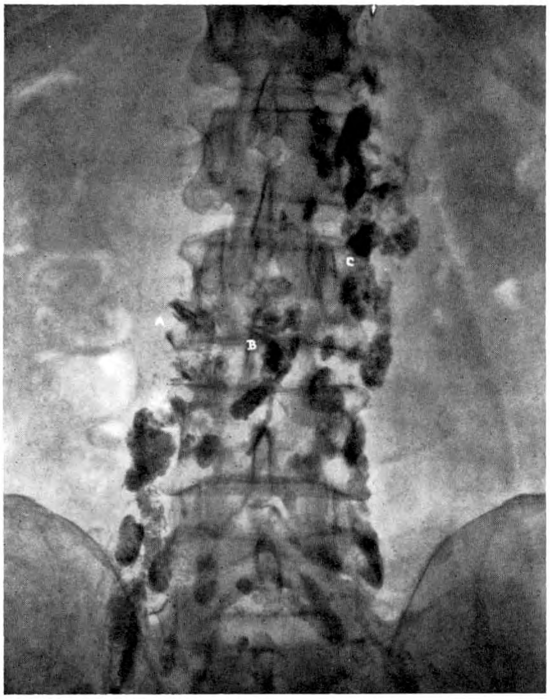

FIG. 6. Case II. Seminoma of testis. Anteroposterior lymphadenogram. The right paralumbar and para-aortic lymph nodes are displaced to the left. The lymph nodes (A, B and C) show no marked enlargement but the shape is irregular.

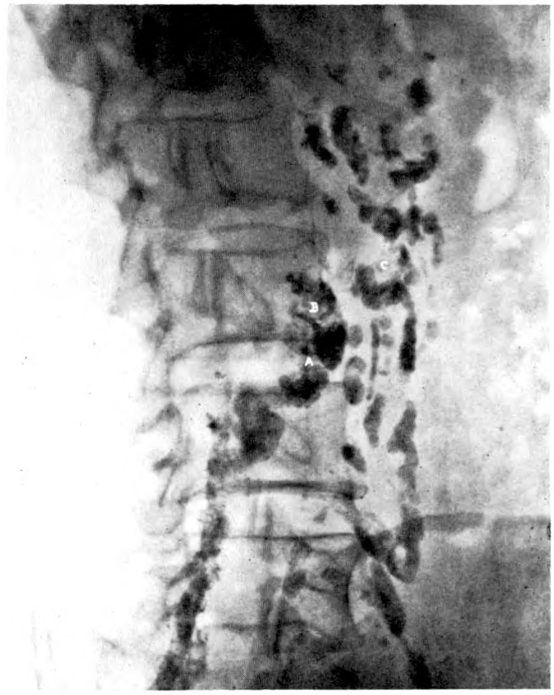

FIG. 7. Case II. Oblique lymphadenogram showing the same findings as Figure 6.

iliac, and right inguinal regions appeared normal. Tomograms of the inguinal lymph nodes on the left side (Fig. 10, *a* and *b*) showed a normal (A) and a pathologic (B) lymph node. The questionable lymph node (C) on the lymphadenogram, however, appeared roentgenologically normal.

On the basis of the lymphographic findings, a left hemicastration and extirpation of the lymph nodes in the inguinal and iliac regions on the left were performed. During the operation, it was found that no lymph nodes other than those which had been filled with contrast medium were present. The histologic examination confirmed the roentgenologic diagnosis. It is assumed that the abnormal course of the

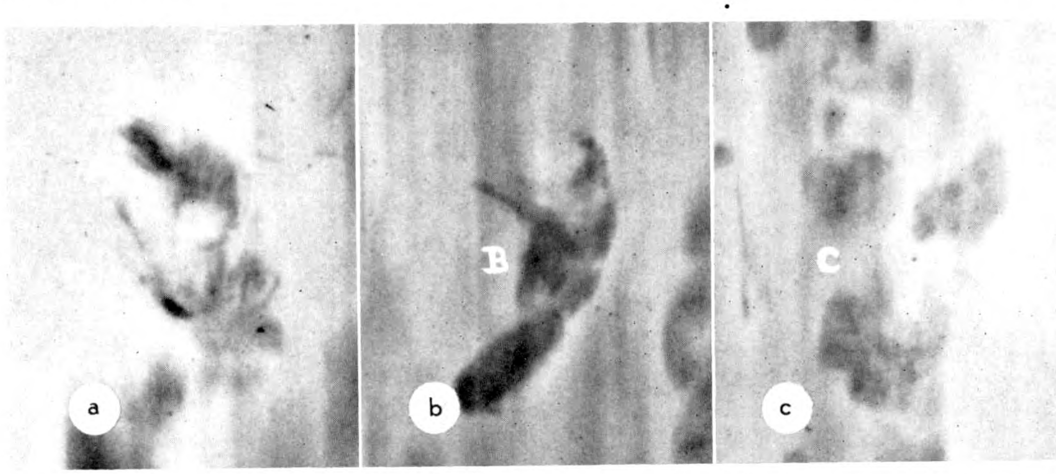


FIG. 8. Case II. Seminoma of testis. (*a*, *b*, and *c*) Tomograms showing clearly the changes in the lymph nodes (A, B and C).

Fig. 9. Case III. Seminoma of testis. Lymphadenogram showing in the left inguinal region a normal lymph node (A), while lymph nodes (B and C) raise suspicion of metastases.

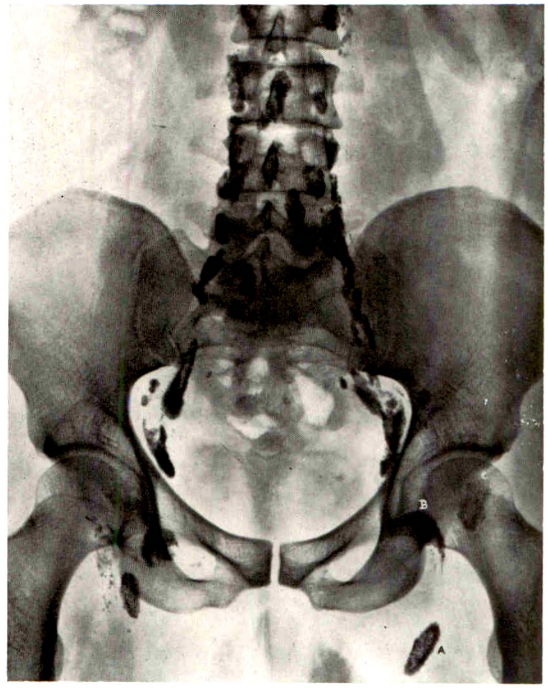


metastases was due to an operation at the age of 12 years for undescended testicles.

Case IV. Mrs. J.H.E. (5805/64), a 48 year old female, had for some time experienced a burning pain in the right leg. A firm swelling, measuring approximately 8 by 3 cm., was palpable in the right groin. Cytologic examination (based on a puncture) revealed fibrosarcoma. Before surgery, a lymphographic examination was carried out.

The lymphadenogram (Fig. 11) provided no further information about the palpable swelling in the right groin. The lymph nodes in the inguinal, iliac, paralumbar, and para-aortic regions could not all be properly evaluated be-

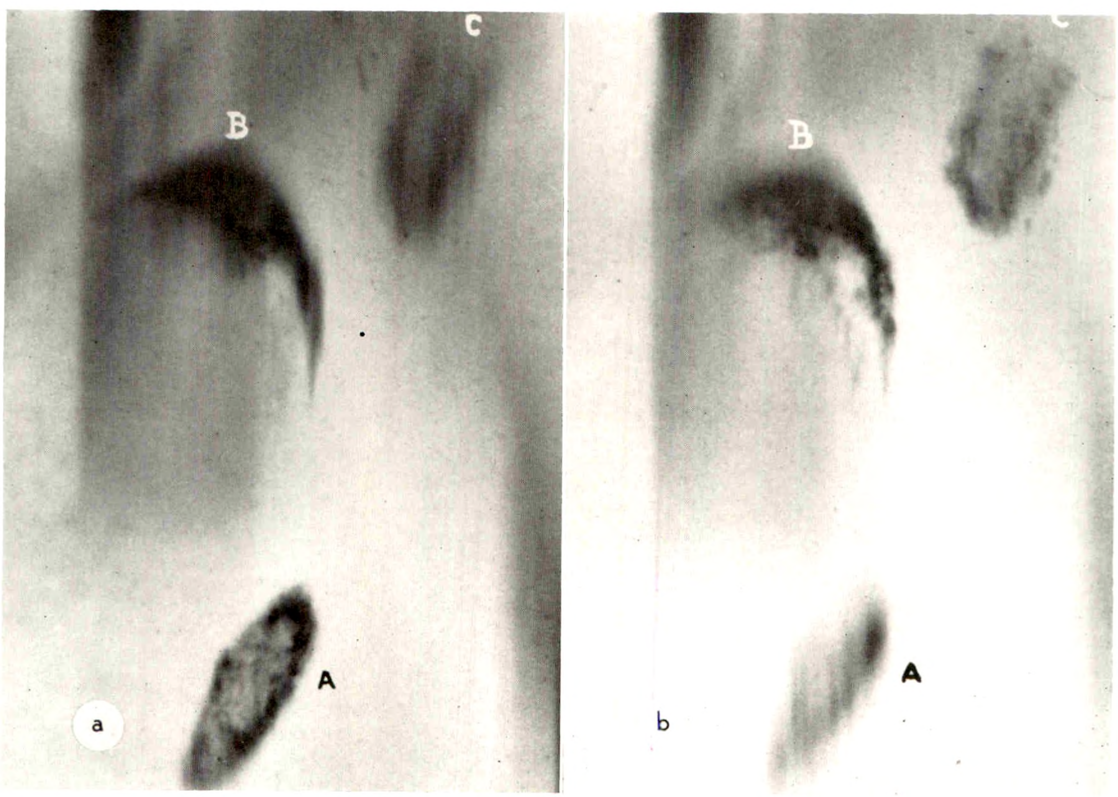


Fig. 10. Case III. Seminoma of testis. (*a* and *b*) Tomograms showing normal inguinal lymph nodes (A and C) and one (B) which is pathologic.

FIG. 11. Case IV. Fibrosarcoma. Lymphadenogram showing that the lymph nodes in the inguinal, iliac, paralumbar and para-aortic regions cannot be properly evaluated.

cause of overprojection of intestinal contents and skeletal elements on the anteroposterior, lateral, and oblique lymphadenograms.

Tomograms showed the paralumbar, para-aortic, and iliac lymph nodes to be normal. A tomogram of the right inguinal region showed a pathologic lymph node (A in Fig. 12), the others appeared normal.

At surgery, a tumor measuring 10 cm. in cross-section was removed from the right groin and the lymph nodes in the inguinal and iliac regions were extirpated. Histologic examination showed that the pathologic lymph node (A) was almost entirely replaced by metastases. The other lymph nodes appeared normal.

CASE V. Mrs. N.J.S. (8209/64), a 48 year old female, was admitted in April, 1964 for menopausal flux. Curettage provided evidence of an undifferentiated adenocarcinoma. Roentgenographic examination of the kidneys, thorax and thoracic and lumbar vertebrae revealed no metastases. A liver function test showed slight disturbance.

A lymphographic examination was done to determine whether metastases were present in the lymph nodes. At the level of the right arteria iliaca communis, the lymphadenogram showed an area which was bordered on both the upper and lower side by small, apparently normal lymph nodes (A, B, C, D and E in Figure 13).

On the tomographic sections (Fig. 14, *a*, *b* and *c*), some lymph nodes (A and C) were normal; one (B) appeared to be the remnant of an enlarged metastatic lymph node whose marginal sinus was only partially intact; and lymph nodes (D) and (E) were remnants of an enlarged pathologic lymph node which showed only a partially intact marginal sinus.

The patient was treated surgically with total extirpation of the uterus and its adnexa. Histologic examination showed that the lymph nodes with a pathologic appearance on the lymphograms were invaded by metastases of the adenocarcinoma of the corpus uteri.


FIG. 12. Case IV. Fibrosarcoma. Tomogram showing that the lymph node (A) is pathologic.


Fig. 13. Case v. Carcinoma of corpus uteri. Lymphadenogram showing at the level of the right arteria iliaca communis a large area, bordered above and below by small lymph nodes (A, B, C, D and E); it is not clear whether these are a number of small normal lymph nodes or partially eroded larger lymph nodes.

Case vi. Mrs. A.A.B. (1343/63), a 53 year old female, came for treatment of menopausal flux. Vaginal examination showed an eroded cervix with a slight thickening of the medial portion of the left parametrium. On speculum inspection a polypoid tumor of the cervix was noted. Histologic examination of a biopsy sample revealed squamous cell carcinoma. A diagnosis of squamous cell carcinoma of the cervix uteri Stage II was made.

Lymphography was carried out to determine the presence of metastases in the lymph nodes. The anteroposterior (Fig. 15*a*), lateral, and oblique (Fig. 15*b*) lymphadenograms showed an enlarged lymph node which appeared to contain metastases in the left lumbar region. However, tomograms (Fig. 16, *a*, *b*, *c* and *d*, representing Sections 13, 13½, 14 and 14½) demonstrated an oblong lymph node (A), a round lymph node (B), and a few small contrast spots (C). The appearance of the lymph nodes was normal. The deceptively pathologic picture on the lymphadenograms had been caused by overprojection of several lymph nodes.

Treatment consisted of intrauterine application of radium followed by percutaneous irradiation of the parametria.

Repeated lymphographic examinations after 18 months showed no changes.

## SUMMARY AND CONCLUSIONS

The evaluation of and differentiation between normal and metastatically invaded lymph nodes offer serious difficulties when the lesions and the changes in the lymph nodes are not pronounced.

The presently reported cases clearly show that tomography in addition to anteroposterior, lateral and oblique lymphadenography can supply important additional information concerning the location, shape, and structure of pathologic changes in lymph nodes. Furthermore, this method reveals metastases which are not distinctly visible on the follow-up examinations and permits the identification of suspected metastases by overprojection of small but healthy lymph nodes.

We are of the opinion that when applied as a supplementary examination, tomography is indispensable in arriving at the most reliable roentgenologic diagnosis.

Dr. T. de Roo
Afdeling Radiologie
Academisch Ziekenhuis
Leyden, Netherlands

## REFERENCES

1. Baum, S., Bron, K. M., Wexler, L., and Abrams, H. L. Lymphangiography, cavography and urography: comparative accuracy in diagnosis of pelvic and abdominal metastases. *Radiology*, 1963, *81*, 207–218.
2. Fischer, H. W. Editorial. Lymphography. *Radiology*, 1963, *80*, 1002–1004.
3. Herman, P. G., Benninghoff, D. L., Nelson, J. H., Jr., and Mellins, H. Z. Roentgen anatomy of ilio-pelvic-aortic lymphatic system. *Radiology*, 1963, *80*, 182–193.

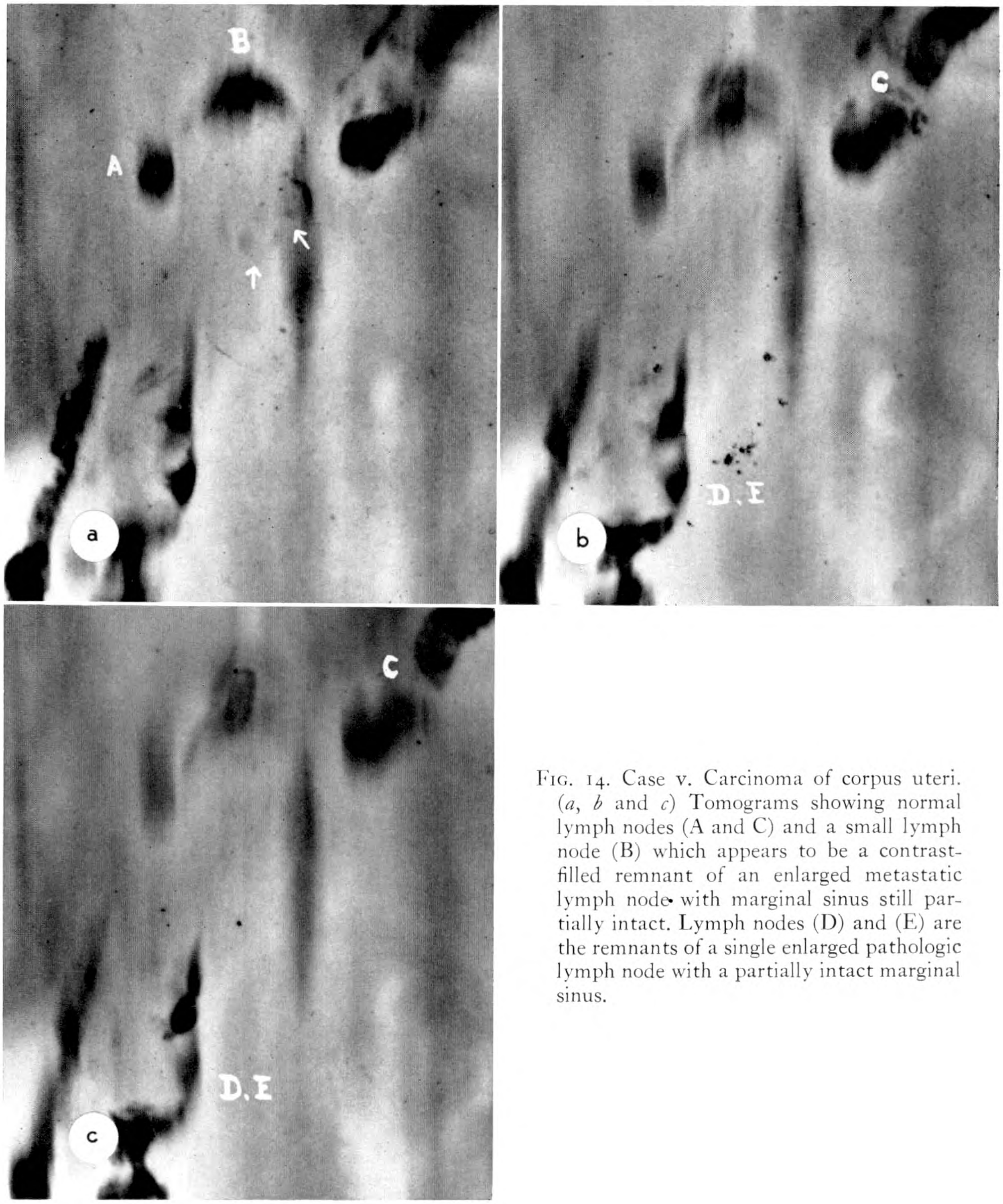


Fig. 14. Case v. Carcinoma of corpus uteri. (*a*, *b* and *c*) Tomograms showing normal lymph nodes (A and C) and a small lymph node (B) which appears to be a contrast-filled remnant of an enlarged metastatic lymph node with marginal sinus still partially intact. Lymph nodes (D) and (E) are the remnants of a single enlarged pathologic lymph node with a partially intact marginal sinus.

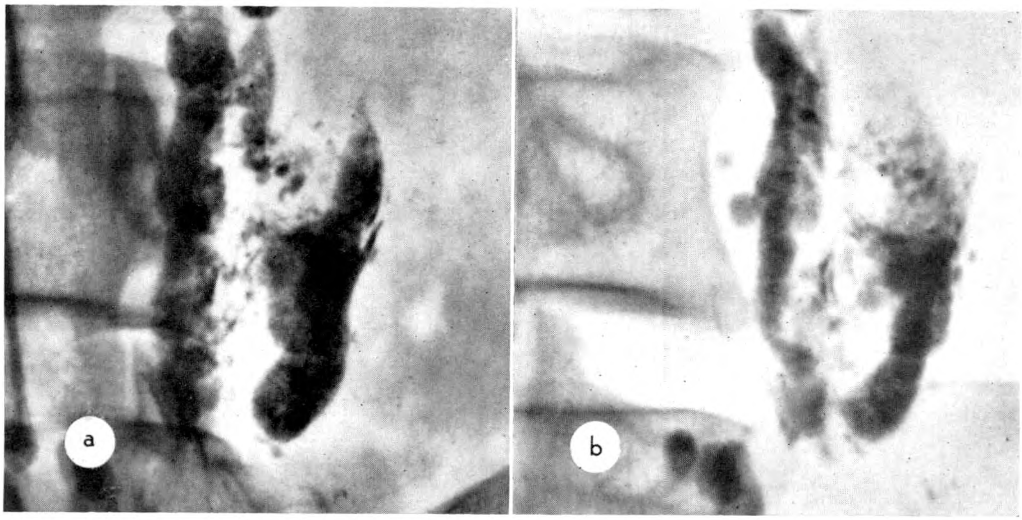


Fig. 15. Case vi. Carcinoma of cervix uteri. (*a* and *b*) Anteroposterior, and oblique lymphadenograms showing an enlarged lymph node apparently affected by metastases in the left lumbar region.

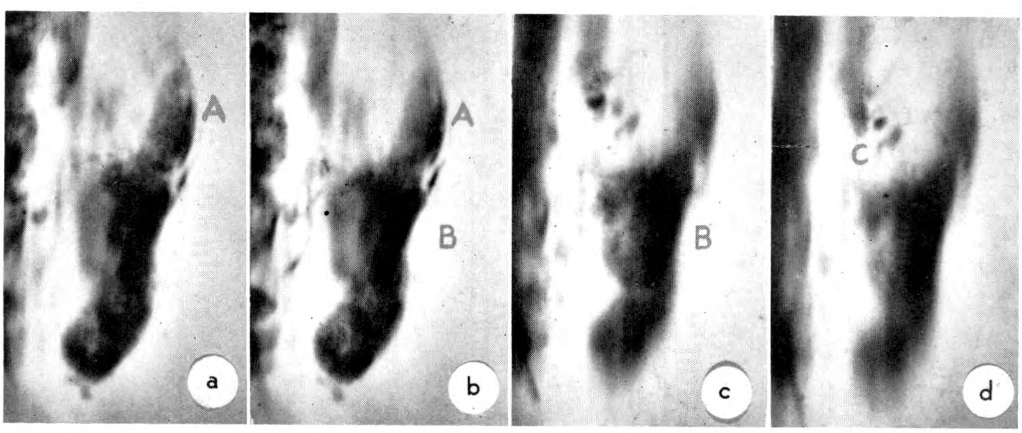


Fig. 16. Case vi. Carcinoma of cervix uteri. (*a*, *b*, *c* and *d*) Tomograms showing that the apparently pathologic lymph node seen in Figure 15, *a* and *b* is composed of one oblong lymph node (A), one round lymph node, (B), and several spots of contrast medium (C). The lymph nodes here have a roentgenologically normal appearance.

4. HRESHCHYSHYN, M. M., SHEEHAN, F. R., and HOLLAND, J. F. Visualization of retroperitoneal lymph nodes: lymphangiography as aid in measurement of tumor growth. *Cancer*, 1961, *14*, 205–209.
5. JACKSON, L., WALLACE, S., SCHAFFER, B., GOULD, J., KRAMER, S., and WEISS, A. J. Diagnostic value of lymphangiography. *Ann. Int. Med.*, 1961, *54*, 870–882.
6. ROO, DE, T. Lymphografie: een studie van de diagnostische en therapeutische mogelijkheden in de praktijk. Thesis. Leyden, 1964.
7. ROO, DE, T. Une nouvelle technique simple pour la lymphographie. *Ann. Radiol.*, 1965, *8*, 97–100.
8. ROO, DE, T. Valeur de la tomographie en lymphadenographie. *Ann. Radiol.*, 1965, *8*, 17–24.
9. SCHAFFER, B., KOEHLER, P. R., DANIEL, C. R., WOHL, G. T., RIVERA, E., MEYERS, W. A., and SKELLEY, J. F. Critical evaluation of lymphangiography. *Radiology*, 1963, *80*, 917–930.
10. SHEEHAN, R., HRESHCHYSHYN, M., LIN, R. K., and LESSMANN, F. P. Use of lymphography as diagnostic method. *Radiology*, 1961, *76*, 47–53.
11. VIAMONTE, M., JR., ALTMAN, D., PARKS, R., BLUM, E., BEVILACQUA, M., and RECHER, L. Radiographic-pathologic correlation in interpretation of lymphangioadenograms. *Radiology*, 1963, *80*, 903–916.
12. VIAMONTE, M., JR., and PARKS, R. E. Progress in Angiography. Charles C Thomas, Publisher, Springfield, Ill., 1964.
13. WALLACE, S., JACKSON, L., and GREENING, R. R. Clinical applications of lymphangiography. AM. J. ROENTGENOL., RAD. THERAPY & NUCLEAR MED., 1962, *88*, 97–109.
14. WALLACE, S., JACKSON, L., DODD, G. D., and GREENING, R. R. Lymphatic dynamics in certain abnormal states. AM. J. ROENTGENOL., RAD. THERAPY & NUCLEAR MED., 1964, *91*, 1187–1206.
15. ZEIDMAN, I., COPELAND, B. E., and WARREN, S. Experimental studies on spread of cancer in lymphatic system: absence of lymphatic supply in carcinoma. *Cancer*, 1955, *8*, 123–127.
16. ZHEUTLIN, N., and SHAMBROM, E. Contrast visualization of lymph nodes. *Radiology*, 1958, *71*, 702–708.

# LYMPHANGIOGRAPHY IN LYMPHOMA*

*By* RICHARD D. KITTREDGE, M.D., *and* NATHANIEL FINBY, M.D.
NEW YORK, NEW YORK

LYMPHOMA often presents as a local problem which commonly becomes more diffuse as the disease progresses. The initial localized lesion can be effectively treated, but the physician must be alert to the long progressive problem in diagnosis and management which often requires all the clinical diagnostic help available. Loss of weight, anorexia, anemia and fever will commonly occur and may be difficult to evaluate in a patient who has no evidence of recurrent disease in the original area of involvement. With the clear memory of past patients, the physician balances along the narrow line between widespread subclinical disease and overt local breakthrough, between low grade bearable symptomatology and overwhelming malaise; withholding therapy until the optimum time so that the most will be gained therapeutically. It is often stated that the most successful response will be seen in the first use of a therapeutic modality and effectiveness in lymphoma will decrease with retreatment. Even though it may be medically judicious to wait for objective evidence of disease in an area before treatment, this may not be possible in a patient whose symptoms are uncontrolled with usual medication. For these reasons, it is important to be aware of the objective evaluation of inaccessible areas made possible by lymphangiography.[3–11,13–18]

Retroperitoneal involvement of lymph nodes appears to be one of the major areas of occult involvement concomitant with more peripheral disease, for example, neck and axilla. Retroperitoneal disease may be the unrecognized cause of serious systemic symptomatology. Because of the multicentric nature of lymphoma with its chain-like lymph node distribution, it is common not to palpate a localized retroperitoneal mass. To document this involvement on roentgenograms offers important visual data for decisions in therapy.

In the majority of cases, the onset is insidious rather than abrupt and the earliest symptoms fall into the following three groups: (1) general or systemic; (2) local, referable to the blood-forming or lymphatic organs; and (3) local, referable to other organs. The general symptoms include malaise, lack of energy, fatigue, fever, night sweats, loss of appetite, loss of weight, weakness, pallor and shortness of breath. Most common in the group of local symptoms referable to the blood-forming or lymphatic organs is enlargement of the lymph nodes. Since such swellings are generally painless, patients will often take no action about them unless they become unsightly or mechanically troublesome. Unfortunately, the delay permits the development of generalized lymphadenopathy in the axillae, epitrochlear regions, groin, pelvis, and abdominal lymph nodes. Symptoms referable to other organ systems are uncommon and are more often seen in the later stages of the disease than the onset. All organ systems can be the site of lymphomatous involvement.

## PATHOLOGY

The distribution of disease in the "malignant lymphoma" groups varies from case to case. In some instances, the local growth is followed by enlargement of the regional lymph nodes and spleen and may simulate leukemia. This spectrum is further widened if the tumor cells enter the blood stream in sufficient numbers to present a "leukemic" blood picture.[1,2] Lymphosarcoma has been observed to terminate with a leukemic blood picture. Hodgkin's sarcoma and reticulum cell sarcoma have been observed with leukemia. The follicular forms of lymphoma can eventually lose the follicular

* From the Department of Radiology, St. Luke's Hospital, New York, New York.

TABLE I

| | Age and Sex | Presenting Problems | Pathology | Roentgen Findings |
|---|---|---|---|---|
| Case 1 | 40 M | Fever of unknown origin; abdominal disease to be ruled out | No positive pathology | Negative lymphangiogram |
| Case 2 | 64 F | Chronic lung disease; shortness of breath; cervical lymphadenopathy; recurrent fever; chills and weight loss led to lymphangiography | Lymphoma—lymphocytic cell type | Lymphangiogram positive |
| Case 3 | 35 M | Fever; right lower quadrant abdominal mass; enlarged posterior cervical lymph nodes; recurrent fever | Hodgkin's disease | Inferior vena cavagram revealed mass; ureters displaced on intravenous pyelogram; lymphangiogram positive |
| Case 4 | 59 F | Numbness from the waist down; diffculty in walking; bilateral Babinski signs | Lymphoma—reticulum cell type | Osteoblastic vertebra; left ureter deviated; vena cava displaced slightly; lymphangiogram positive |
| Case 5 | 34 M | Enlarged neck and axillary lymph nodes; dysphagia; night sweats; recurrent shortness of breath; splenic pain | Lymphoma—lymphoblastic cell type | Bone destruction; lymphangiogram positive |
| Case 6 | 75 M | Anemia; weakness; shortness of breath | No positive pathology | Lymphangiogram negative |
| Case 7 | 23 M | Pain; swelling; masses of right neck and both axillae; abdominal disease to be ruled out | Hodgkin's disease | Lymphangiogram negative; vena cavagram negative |
| Case 8 | 23 M | Abdominal and flank pain; enlarged inguinal lymph nodes; recurrent back pain; right lower abdominal pain; mass in inguinal areas. Developed thigh swelling 9 months after radiation treatment | Hodgkin's disease | Lymphangiogram showed dilated vessels in thigh; no positive lymph nodes |
| Case 9 | 23 M | Nodular swelling in left neck; recurrent fever and enlarged spleen | Hodgkin's disease | Lymphangiogram positive |
| Case 10 | 70 F | Vague abdominal pain; anorexia; mass in right lower abdomen; anemia; inguinal lymph nodes enlarged; recurrent disease showed leg swelling and pleural effusion | Lymphoma—lymphoblastic or reticulum cell type | Lymphangiogram negative |

Table I (*Continued*)

| | Age and Sex | Presenting Problems | Pathology | Roentgen Findings |
|---|---|---|---|---|
| Case 11 | 58 F | Enlarged cervical lymph nodes with dysphagia; recurrent disease; inguinal lymph nodes enlarged; right lower abdominal mass; edema of feet and legs | Lymphoma—reticulum cell type | Lymphangiogram abnormal |
| Case 12 | 61 M | Right axillary lymphadenopathy; diarrhea; anorexia; weakness | Lymphoma—reticulum cell type | Lymphangiogram negative |
| Case 13 | 65 F | Rectal mass | Lymphoma—reticulum cell type | Lymphangiogram negative |
| Case 14 | 9 F | Enlarged cervical lymph nodes; right superior mediastinal mass; recurrent fever and anemia | Hodgkin's disease | Lymphangiogram negative |
| Case 15 | 65 F | Inguinal lymph nodes enlarged | Lymphoma | Lymphangiogram positive |
| Case 16 | 40 F | Inguinal lymph nodes enlarged | Lymphoma | Lymphangiogram positive |

character. Other combinations and transitions have been reported, but there is a tendency to continue as the same general type of disease throughout the course.

All primary tumors of lymph nodes are malignant. They almost invariably arise either from lymphoid cells or from reticuloendothelial cells (histiocytes) or their derivatives. In this connection, it should be recalled that lymphocytes probably arise from reticulum cells, either directly or indirectly through the more primitive "lymphoblast" stage.

The tumor may arise from these cells at any stage in their development. For example, it may be composed mainly of small adult lymphocytes or of larger primitive lymphoid cells (lymphoblasts) or of any intermediate stage in the lymphoid series. It may consist largely of reticulum cells, with or without the formation of reticulin fibers, and, occasionally, with the development of bizarre giant multinuclear or polymorphonuclear forms similar to those seen in Hodgkin's disease.

When an individual lymph node is examined histologically without knowledge of changes elsewhere in the body, it may be impossible to correctly designate the subgroup to which each belongs. An example of this is seen in tumors composed principally of lymphocytes. Without further information, it cannot be determined whether or not the tumor cells have already entered the blood in large numbers and, therefore, whether the condition should be called "leukemia" or "lymphosarcoma."[1] Malignant neoplastic disease of the lymphoid cells apparently occurs in all species in which these cells are recognized. The disease is not known in species below the vertebrates.

## CLINICAL MATERIAL

Sixteen consecutive patients are listed in Table I. Five cases are reported in detail

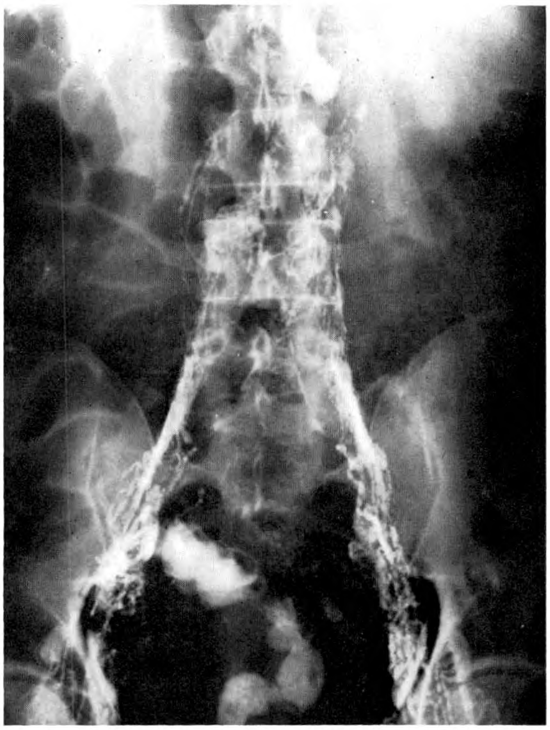

FIG. 1. Case 1. Recurrent fever, unexplained by extensive work-up, suggested the possibility of retroperitoneal disease. The lymphangiogram immediately following the procedure was normal.

(Case 1, 2, 3, 4 and 5). In all patients at some point in their course, it was deemed medically important to evaluate the retroperitoneal lymph nodes. Two patients, after an extensive but unrevealing work up, were suspected of retroperitoneal lymphoma. Lymphangiography showed no evidence of retroperitoneal disease (Case 1 and 6). Five patients, after varied courses of lymphomatous disease with at least one modality of treatment, demonstrated recurrent signs and symptoms suggestive of retroperitoneal disease. Lymphangiography was confirmatory in these cases (Case 2, 3, 5, 9 and 11). Six patients with positive biopsy of peripheral lymph nodes or a localized lymphoma had clinical suspicion of retroperitoneal lymphoma, but lymphangiography was normal (Case 7, 8, 10, 12, 13 and 14). Three patients with apparent local disease proved to have retroperitoneal lymphoma when studied during their initial admission (Case 4, 15 and 16). It is important to recognize that this information is usually not available short of laparotomy; therefore, lymphangiography takes a logical place in the work-up in this type of problem.

REPORT OF CASES

CASE 1. This 40 year old policeman was admitted to the hospital following laceration of his forehead and fracture of the frontal sinuses. He had two re-admissions since that time with postconcussion headaches. His most recent admission was prompted by convulsions.

Four days prior to this last admission, fever spiked to 102°F. with severe frontal headache. The evening prior to his current admission, his temperature rose to 104°F. Work-up was completely negative. Bilateral carotid arteriograms and lymphangiograms were normal (Fig. 1–4). Liver biopsy was normal. The fever seemed to resolve spontaneously.

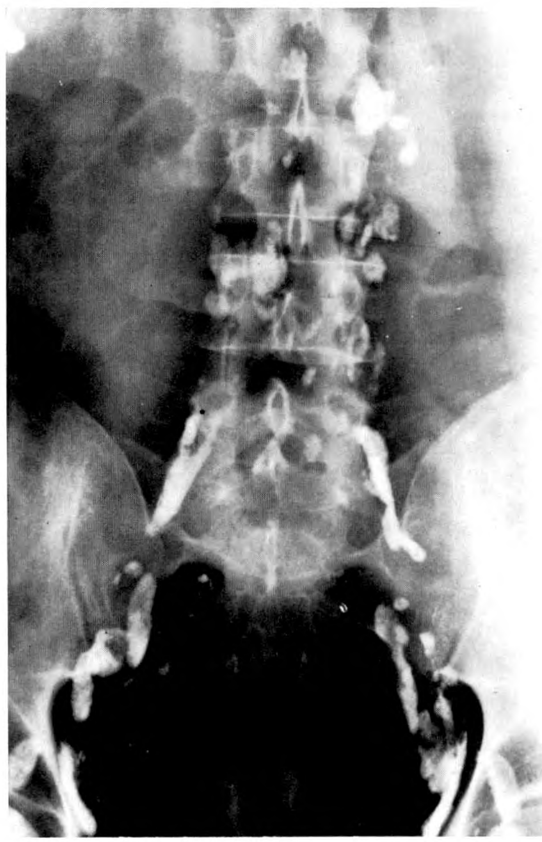

FIG. 2. Case 1. Twenty-four hour follow-up lymphangiogram demonstrated the normal lymph node shape and distribution.

Comment. In this patient severe febrile episodes recurred daily for 3 weeks. Detailed clinical investigation revealed no pertinent information. Surgical exploration to rule out lymphoma was considered but normal lymphangiograms ruled out this possibility.

CASE 2. This 64 year old white female entered with the chief complaint of shortness of breath of 2 weeks' duration. She had a long history of chronic lung disease with recurrent pulmonary infection and complicating infection in other sites (mastoiditis and brain abscess). On this admission cervical lymphadenopathy was noted. Biopsy revealed lymphoma, lymphocytic type. Nitrogen mustard was given with considerable regression of the lymphadenopathy. The patient was re-admitted in 3 months with complaints of increasing weakness and shortness of breath. The clinical picture was again dominated by pulmonary infection with increasing pulmonary effusion. The patient was again treated with nitrogen mustard.

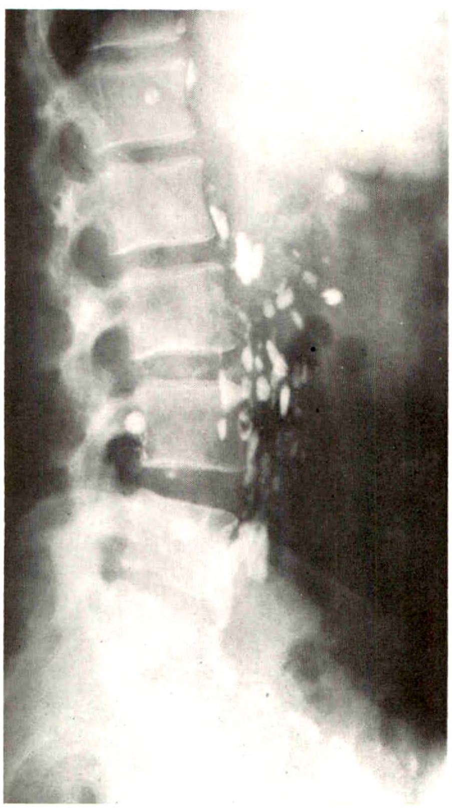

FIG. 3. Case 1. Twenty-four hour follow-up lateral lymphangiogram.

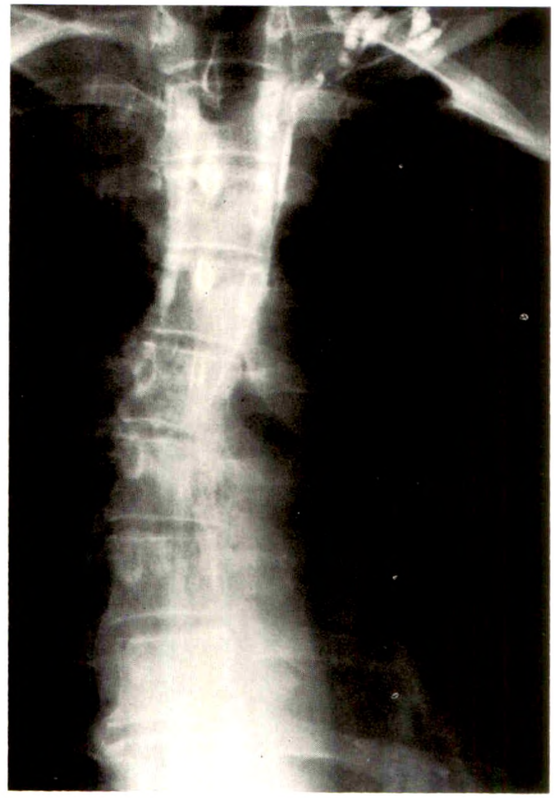

FIG. 4. Case 1. The thoracic duct was seen immediately following injection and appeared normal.

In 8 months, the patient was re-admitted with chills and weight loss.

Lymphangiograms showed typical changes of lymphoma throughout the iliac and para-aortic lymph nodes (Fig. 5–7). A course of radiation therapy was given. Roentgenograms showed a decrease in the size of the lymph nodes post therapy and condensation of contrast material (Fig. 8 and 9).

Comment. Systemic treatment twice with nitrogen mustard was very effective; however, eventually a more localized agent was needed. A complete visualization of the retroperitoneal lymph node chains was obtained to better localize the radiation.

CASE 3. A 35 year old man was admitted to the hospital with the chief complaint of spiking fever of several weeks' duration. Positive findings were a right lower quadrant mass on abdominal examination and posterior cervical lymphadenopathy. He had lost 45 pounds in 5 months and 10 pounds in the previous week. His appetite had decreased. He complained of

FIG. 6. Case 2. Twenty-four hour lymphangiogram after injection showed the vessels cleared and a grossly disturbed lymph node anatomy.

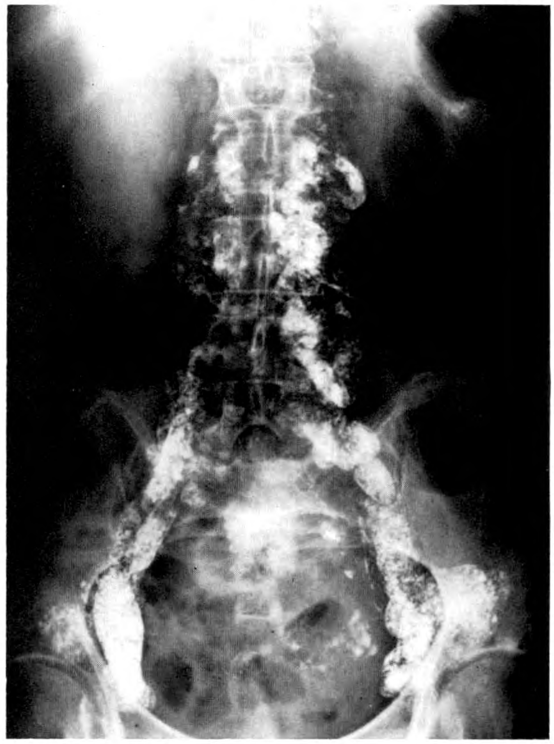

a steady ache in the lumbar spine for several months. A cervical lymph node was removed which was reported histopathologically as Hodgkin's disease. Radiation therapy to the neck lymph nodes and lower abdomen was given; however, the fever continued.

Inferior vena cavagrams and intravenous pyelograms revealed a residual abdominal mass overlying the lower lumbar spine with obstruction of the inferior vena cava and displacement of the ureters at this point.

Lymphangiography was performed and revealed abnormal inguinal and para-aortic lymph nodes characteristic of Hodgkin's disease (Fig. 10). The patient was retreated with

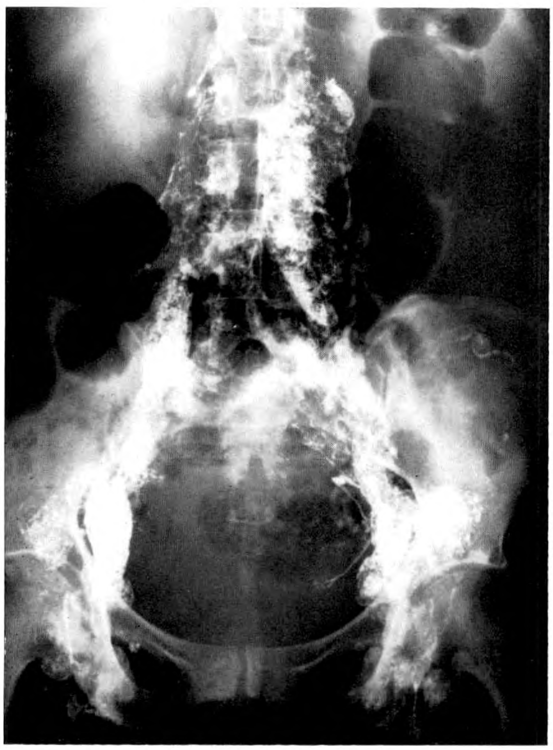

FIG. 5. Case 2. Anatomic appearance of lymph nodes immediately following injection is shown above. Recurrent fever, chills and weight loss led to lymphangiography. The iliac and para-aortic lymph nodes were diffusely enlarged with a foamy reticular replacement pattern characteristic of lymphoma.

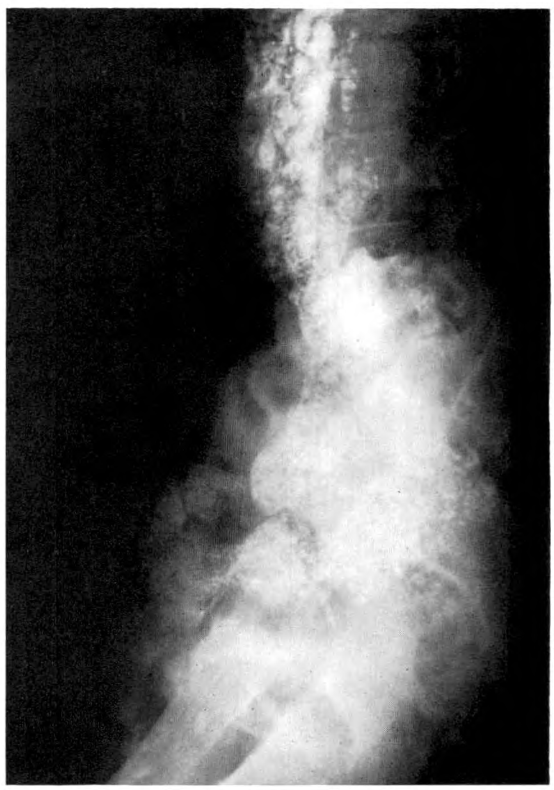

FIG. 7. Case 2. Lateral lymphangiogram showing lymph node involvement.

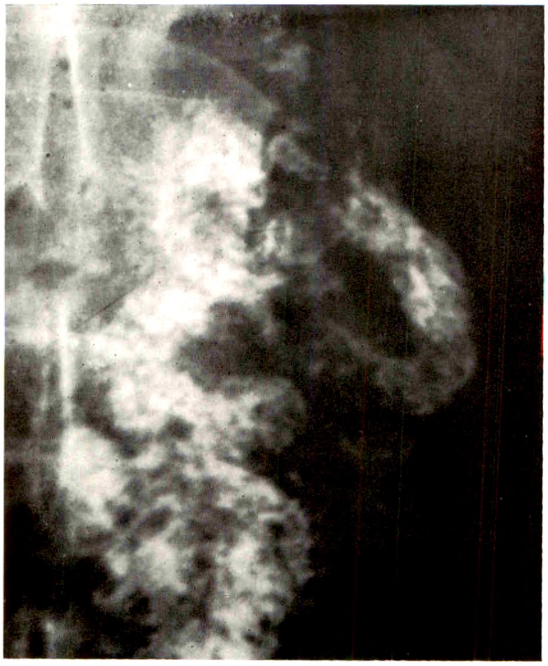

Fig. 8. Case 2. Closer view of the para-aortic lymph nodes before therapy.

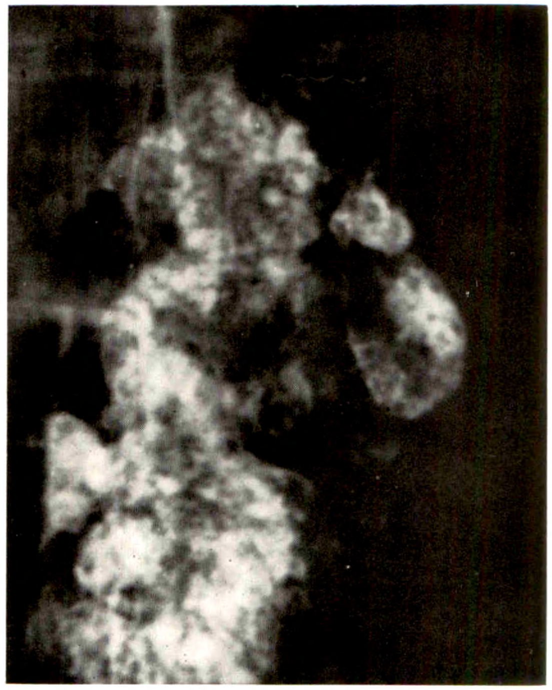

Fig. 9. Case 2. View of para-aortic lymph nodes after therapy. Note the condensation of the contrast medium as the lymph nodes shrink in size.

radiation and definite improvement was obtained (Fig. 11 and 12).

Comment. Following an initial course of irradiation of the lower abdomen, residual tumor was felt to be present. An inferior vena cavagram showed some degree of obstruction. Lymphangiography defined the need for additional inguinal and para-aortic irradiation.

Case 4. A 59 year old white female was admitted with chief complaints of hematuria, urinary frequency and urgency. One night prior to admission, she had gross painless hematuria. Physical examination revealed an obese woman in no acute distress. There was no evidence of intra-abdominal mass or costovertebral angle tenderness. She was admitted to the urologic service for evaluation and subsequently treated for cystitis. The patient was discharged and re-admitted 3 months later, complaining of numbness from the waist down and difficulty in

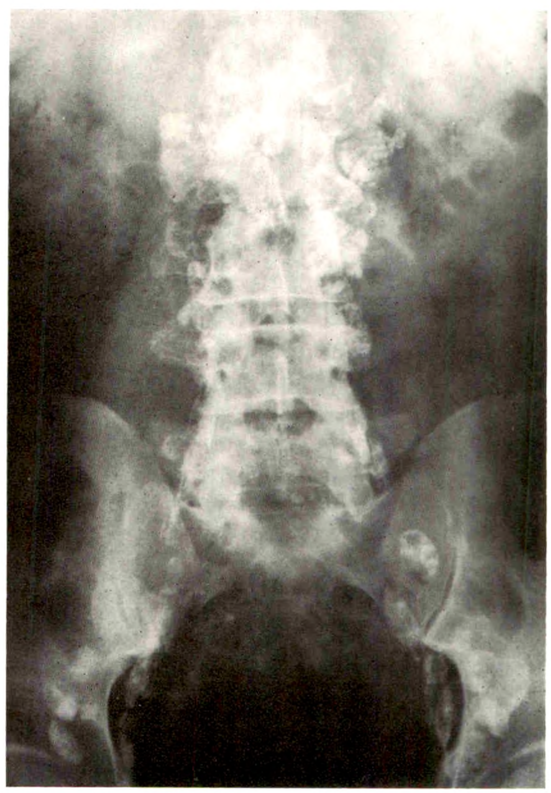

Fig. 10. Case 3. Enlarged partially replaced lymph nodes characteristic of lymphoma are well shown on this 24 hour postinjection study. Recurrent fever led to lymphangiography.

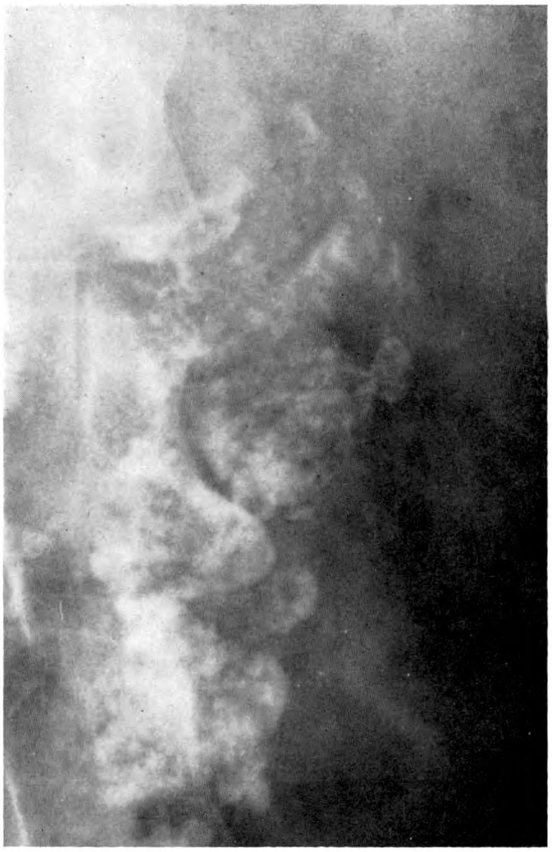

←

Fig. 11. Case 3. Closer view of involved lymph nodes before therapy.

Fig. 12. Case 3. View of involved lymph nodes after therapy. Decrease in size and condensation of contrast material are well seen.

walking. Examination revealed weakness of the lower extremities with moderate spasticity and bilateral Babinski signs with decreased pin prick perception at T5 and T6 distribution. A neurosurgical consultation was obtained and a laminectomy was performed at the area of T5 through T7. A large firm tumor constricting the cord was removed. The histopathologic report

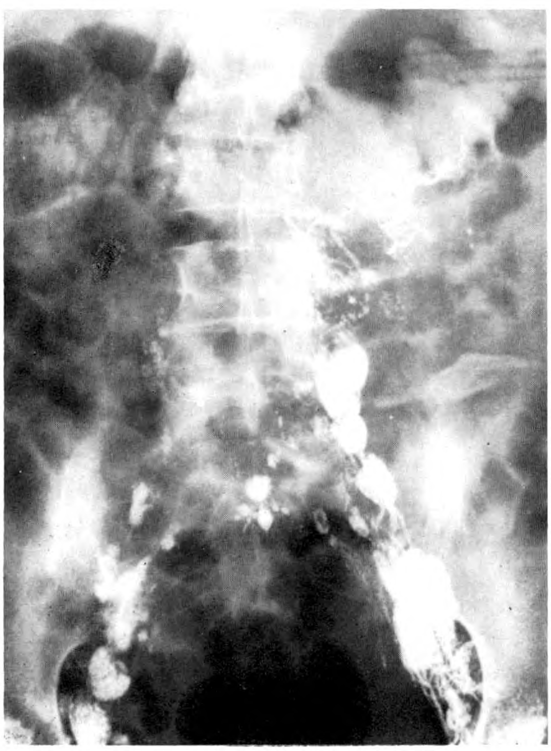

←

Fig. 13. Case 4. Lymphangiogram demonstrated abnormal channels and lymph node replacement at the level of L4 with vessels dissecting into the lateral retroperitoneal area. The second lumbar vertebra showed blastic change which proved to be reticulum cell lymphoma.

was lymphoma, reticulum cell type, involving the epidural space. Roentgenograms of the lumbar spine area revealed osteoblastic change of L2. Retroperitoneal disease was strongly suggested and lymphangiography was performed. Partial obstruction at the L3-L4 level was demonstrated with abnormal vessels dissecting into the lateral retroperitoneal area (Fig. 13). Delayed roentgenograms with intravenous pyelography showed a mass of abnormal lymph nodes displacing the ureter laterally (Fig. 14). An inferior vena cavagram showed no displacement (Fig. 15).

Comment. This patient certainly illustrated the variability of initial involvement. Lymphangiography demonstrated extensive retroperitoneal disease. Lymphatic collateral vessels dissected into the lateral retroperitoneal tissue to circumvent the main para-aortic involvement.

Case 5. This 34 year old white male entered with the chief complaint of swollen glands on the right side of the neck of 5 weeks' duration. The patient had experienced dysphagia and night sweats for the preceding 3 months. Excisional biopsy of a cervical lymph node revealed malignant lymphoma, lymphoblastic type. Radiation therapy to the neck lymph nodes produced a good response.

In 6 months the patient was re-admitted with shortness of breath, axillary pain, low chest pain and splenic pain. Roentgenograms showed a left pleural effusion and destruction of the ribs and pelvis (Fig. 20). Lymphangiograms demonstrated grossly involved lymph nodes in the para-aortic area (Fig. 16 and 17). Seven months later the lymph node involvement had increased markedly (Fig. 18 and 19).

Comment. Lymphangiography will allow for a variable period of visualization, often many months. Demonstration of lymph node shrinkage during therapy and recurrence with increase in size can be a great advantage.

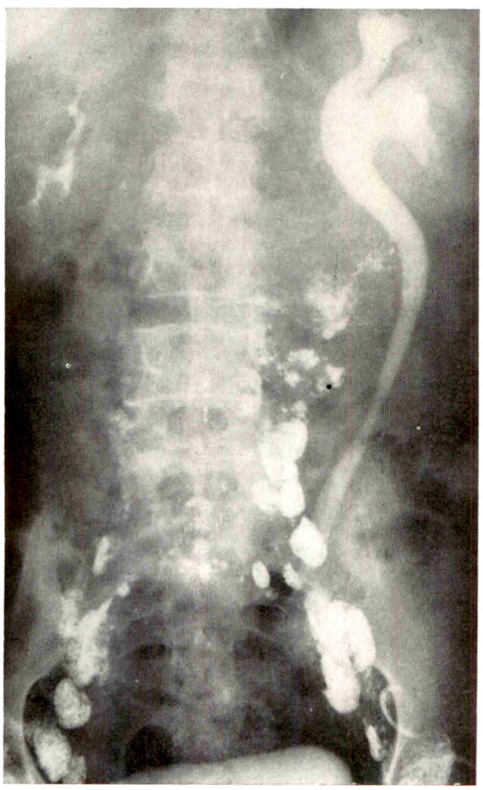

Fig. 14. Case 4. Twenty-four hour study post lymphangiography showed a mass of abnormal lymph nodes at the L3–L4 level, displacing the ureter laterally.

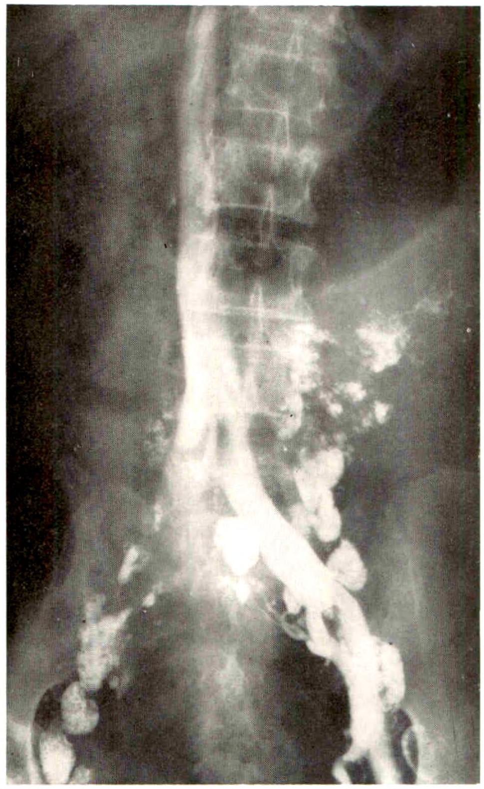

Fig. 15. Case 4. The inferior vena cava was not displaced by the mass of abnormal vessels and lymph nodes.

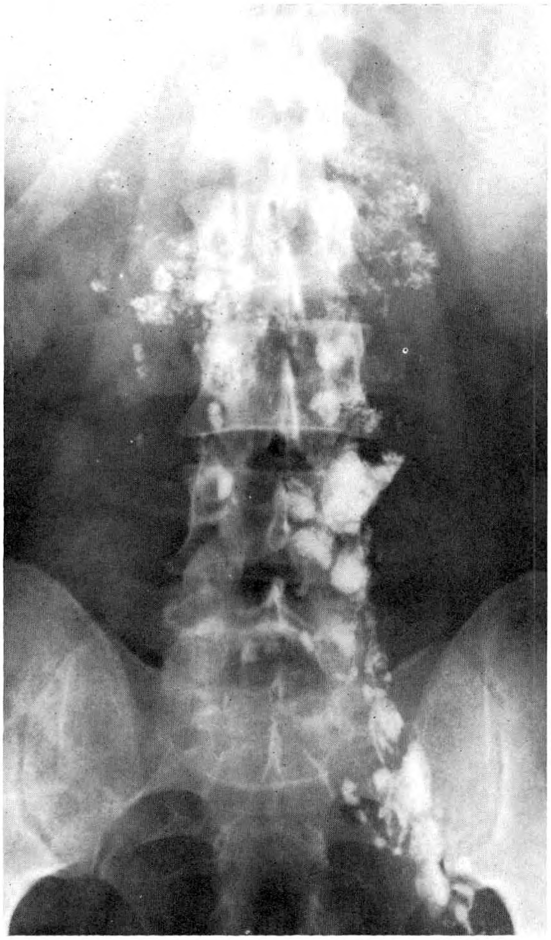

FIG. 16. Case 5. Shortness of breath, axillary pain and pleural pain prompted lymphangiography. Grossly involved lymph nodes were shown in the para-aortic area.

FIG. 17. Case 5. Closer view in lateral projection showed the enlarged partially replaced lymphomatous lymph nodes.

SUMMARY

Sixteen cases were studied by lymphangiography for lymphoma. Fourteen cases were known lymphoma patients in whom lymphangiography was utilized to evaluate the retroperitoneal space. Two patients without positive pathology were studied to rule out retroperitoneal lymphoma. Five cases are reported in detail to demonstrate the integral part that lymphangiography can play in the lymphoma patient. In the absence of overwhelming objective evidence of retroperitoneal disease, lymphangiography stands alone as the one single, easily tolerated, specific, highly reliable, direct method of evaluation.

Richard D. Kittredge, M.D.
Department of Radiology
St. Luke's Hospital
Amsterdam Avenue and 113th Street
New York, New York 10025

REFERENCES

1. ANDERSON, W. A. D. Pathology. Fourth edition. C. V. Mosby Company, St. Louis, 1961.
2. DAMESHEK, W., and GUNZ, F. Leukemia. Grune & Stratton, Inc., New York, 1964.
3. FISCHER, H. W., LAWRENCE, M. S., and THORNBURY, J. R. Lymphography of normal adult male: observations and their relations to diagnosis of metastatic neoplasm. *Radiology*, 1962, *78*, 399–406.

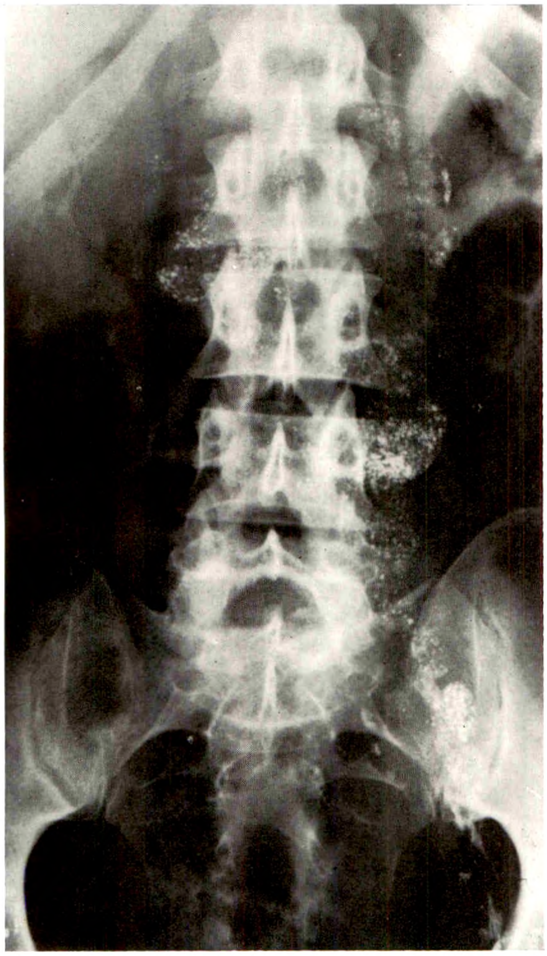

FIG. 18. Case 5. Seven months later the lymph node involvement had increased markedly.

FIG. 19. Case 5. Closer view in lateral projection showed progressing replacement and enlargement of lymph nodes.

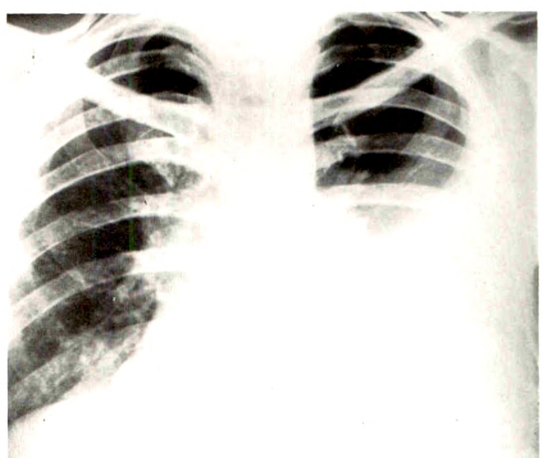

FIG. 20. Case 5. Bone destruction and pleural effusion developed at this time.

4. JACKSON, L., WALLACE, S., SCHAFFER, B., GOULD, J., KRAMER, S., and WEISS, A. J. Diagnostic value of lymphangiography. *Ann. Int. Med.*, 1961, *54*, 870–882.
5. JACOBSSON, S., and JOHANSSON, S. Normal roentgen anatomy of lymph vessels of upper and lower extremities. *Acta radiol.*, 1959, *51*, 321–328.
6. KENYON, N. M., SOTO, M., VIAMONTE, M., JR., PARKS, R. E., and FARRELL, J. J. Improved techniques and results of lymphography. *Surg., Gynec. & Obst.*, 1962, *114*, 677–682.
7. KINMONTH, J. B. Lymphangiography in clinical surgery and particularly in treatment of lymphoedema. *Ann. Roy. Coll. Surgeons England*, 1954, *15*, 300–315.
8. KINMONTH, J. B. Lymphangiography in man. *Clin. Sc.*, 1952, *11*, 13–20.
9. KITTREDGE, R. D., and FINBY, N. Lymphangiography in obstruction. AM. J. ROENTGENOL.,

Rad. Therapy & Nuclear Med., 1964, *91*, 444–447.

10. Kittredge, R. D., Burger, R., Finby, N., and Draper, J. W. Illustration of approach to diagnosis of pelvic disease. *J. Urol.*, 1963, *89*, 607–610.
11. Koehler, P. R., Wohl, G. T., and Schaffer, B. Lymphangiography—survey of its current status. Am. J. Roentgenol., Rad. Therapy & Nuclear Med., 1964, *91*, 1216–1221.
12. Rebuck, J. W. The Lymphocyte and Lymphocytic Tissue. Paul B. Hoeber, Inc., New York, 1960.
13. Schaffer, B., Koehler, P. R., Daniel, C. R., Wohl, G. T., Rivera, E., Meyers, W. A., and Skelley, J. F. Critical evaluation of lymphangiography. *Radiology*, 1963, *80*, 917–930.
14. Shanbrom, E., and Zheutlin, N. Radiographic studies of lymphatic system. *A.M.A. Arch. Int. Med.*, 1959, *104*, 589–593.
15. Sheehan, R., Hreschyshyn, M., Lin, R. K., and Lessmann, F. P. Use of lymphography as diagnostic method. *Radiology*, 1961, *76*, 47–53.
16. Viamonte, M., Jr., Altman, D., Parks, R., Blum, E., Bevilacqua, M., and Recher, L. Radiographic-pathologic correlation in interpretation of lymphangioadenograms. *Radiology*, 1963, *80*, 903–916.
17. Wallace, S., Jackson, L., Schaffer, B., Gould, J., Greening, R. R., Weiss, A., and Kramer, S. Lymphangiograms: their diagnostic and therapeutic potential. *Radiology*, 1961, *76*, 179–199.
18. Wallace, S., Jackson, L., and Greening, R. R. Clinical applications of lymphangiography. Am. J. Roentgenol., Rad. Therapy & Nuclear Med., 1962, *88*, 97–109.

# THE DORSAL PARASPINAL MASS IN HODGKIN'S DISEASE*

*By* RICHARD M. WITTEN, M.D., JUAN V. FAYOS, M.D., *and* ISADORE LAMPE, M.D.
ANN ARBOR, MICHIGAN

IN A review of 403 cases of Hodgkin's disease treated by radiation therapy at the University of Michigan Medical Center from the years 1940 through 1962, a paraspinal mass was diagnosed in 22 patients, an incidence of 5.5 per cent. Our report describes this manifestation of Hodgkin's disease.

## CLINICAL MATERIAL

The 22 patients were between 4 and 56 years of age. The majority was between 20 and 40 years of age. There were 17 males and 5 females. The histologic material has been reviewed in each case. A pathologic diagnosis of Hodgkin's granuloma was made in 19, paragranuloma in 1 and Hodgkin's disease unclassified in 2.

Pain in the dorsal region was described by 19 of 22 patients. Their pain was constant, aching and often severe. Shortness of breath was the only complaint in 1 patient. The remaining 2 patients were children, ages 6 and 8 years and no history of back pain was recorded.

In only 1 patient was the paraspinal mass present on initial evaluation. In 21 patients there was an interval of 5 to 150 months from the initial diagnosis until the development of the paraspinal mass. The average interval was 37 months.

At the time of appearance of the dorsal paraspinal mass, 6 patients had no other manifestation of their disease. Generalized lymphadenopathy with splenomegaly and/or hepatomegaly was present in 5 patients. Generalized lymphadenopathy without hepatosplenomegaly was present in 1 while a localized lymphadenopathy was concurrent with the appearance of a dorsal paraspinal mass in 6 cases. Systemic symptoms without lymphadenopathy or hepatosplenomegaly were present in the remaining 4 patients. All patients with paraspinal masses developed other manifestations of Hodgkin's disease during the course of the disease.

Survival after the appearance of the dorsal paraspinal mass ranged from 2 to 28 months and averaged 12 months in 18 patients who died of the disease. The remaining 4 patients were alive slightly more than 2, 4, 7, and 9 years after the paraspinal mass was recognized and each of these 4 patients has survived more than 5 years since the onset of the disease. Of 22 patients 11 survived at least 5 years with Hodgkin's disease. No clear association between survival and the appearance of the paraspinal mass or other coexisting manifestations of Hodgkin's disease was noted.

In 3 of 22 patients there were signs of spinal cord compression associated with the paravertebral mass. Laminectomy for decompression was done in 1 of these. The surgical specimen showed infiltration of bone meninges and paraspinal soft tissues by Hodgkin's disease.

The role of osseous involvement in the development of these masses is not clear. Contiguous osseous infiltration was recognized on roentgenograms in 6 of 22 patients. Of these, the mass was limited to the left side in 3, was bilateral in 2 and limited to the right side in 1.

## ROENTGENOGRAPHIC FINDINGS

The roentgen anatomy of the paraspinal soft tissues was discussed by Lachman[4] in 1942 and by Brailsford[1] and Garland[3] in 1943. The shadow cast by the paravertebral soft tissues contrasted against the lung

* From the Department of Radiology, Alice Crocker Lloyd Radiation Therapy Center, University of Michigan, Ann Arbor, Michigan.

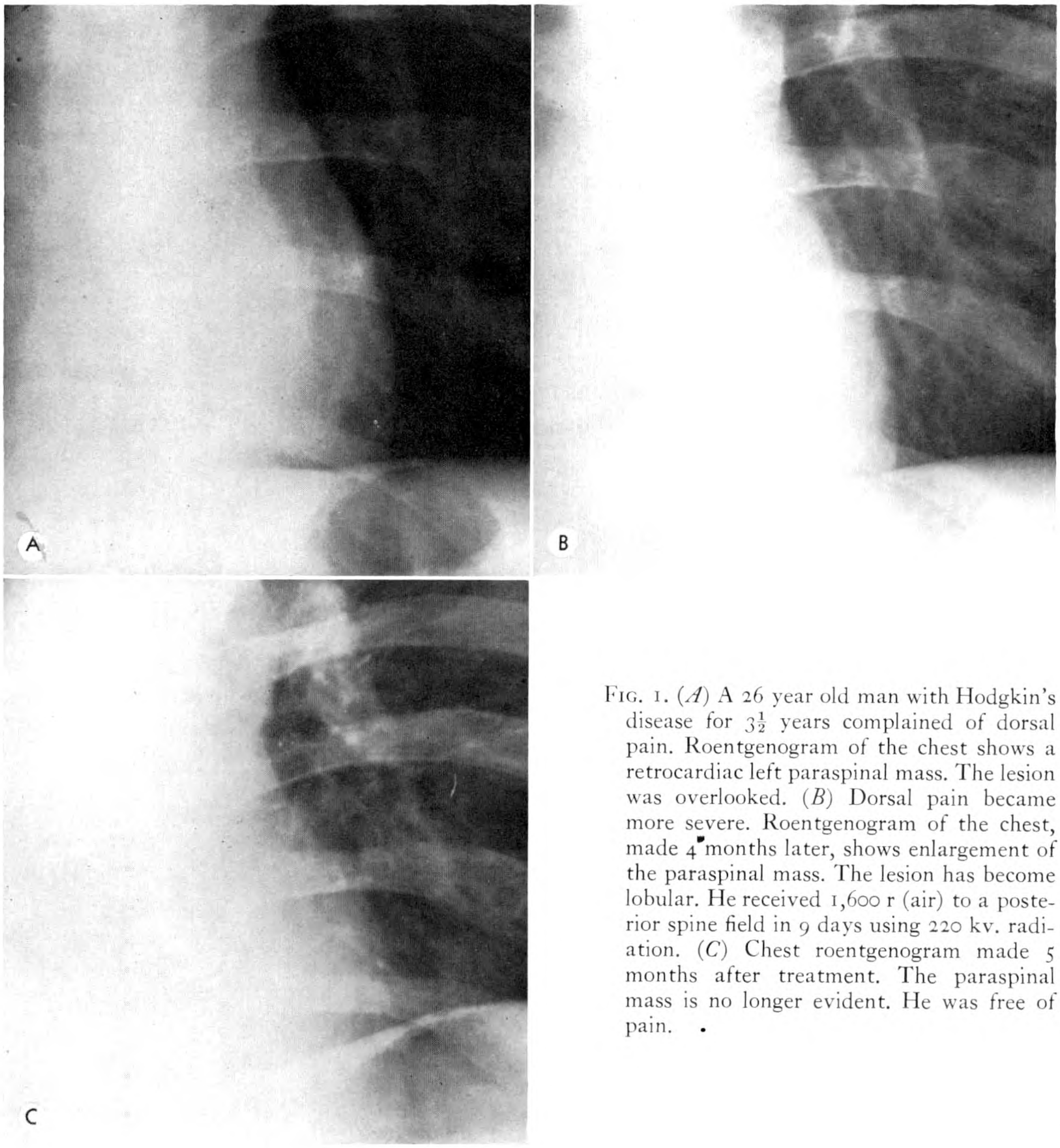


FIG. 1. (*A*) A 26 year old man with Hodgkin's disease for $3\frac{1}{2}$ years complained of dorsal pain. Roentgenogram of the chest shows a retrocardiac left paraspinal mass. The lesion was overlooked. (*B*) Dorsal pain became more severe. Roentgenogram of the chest, made 4 months later, shows enlargement of the paraspinal mass. The lesion has become lobular. He received 1,600 r (air) to a posterior spine field in 9 days using 220 kv. radiation. (*C*) Chest roentgenogram made 5 months after treatment. The paraspinal mass is no longer evident. He was free of pain.

has been called "the linear thoracic paraspinal shadow" and "the posteromesial pleural line." This normal anatomic finding is frequently encountered in roentgenograms of the dorsal spine in the anteroposterior projection and is usually better defined on the left than on the right. This line parallels the vertical axis of the spine and is not more than 3 mm. lateral to the lateral margins of the dorsal vertebral bodies.

Lateral displacement of this line has been noted in tuberculosis of the spine, hematoma secondary to fracture, and in neoplasms.[5] Recently, Millard[6] has called attention to such displacement in the early diagnosis of spinal osteomyelitis and has named this roentgen anatomic feature the "linear thoracic paraspinal shadow of Brailsford." These masses can be related to the linear paraspinal shadow by the principle of the silhouette sign of Felson.[2]

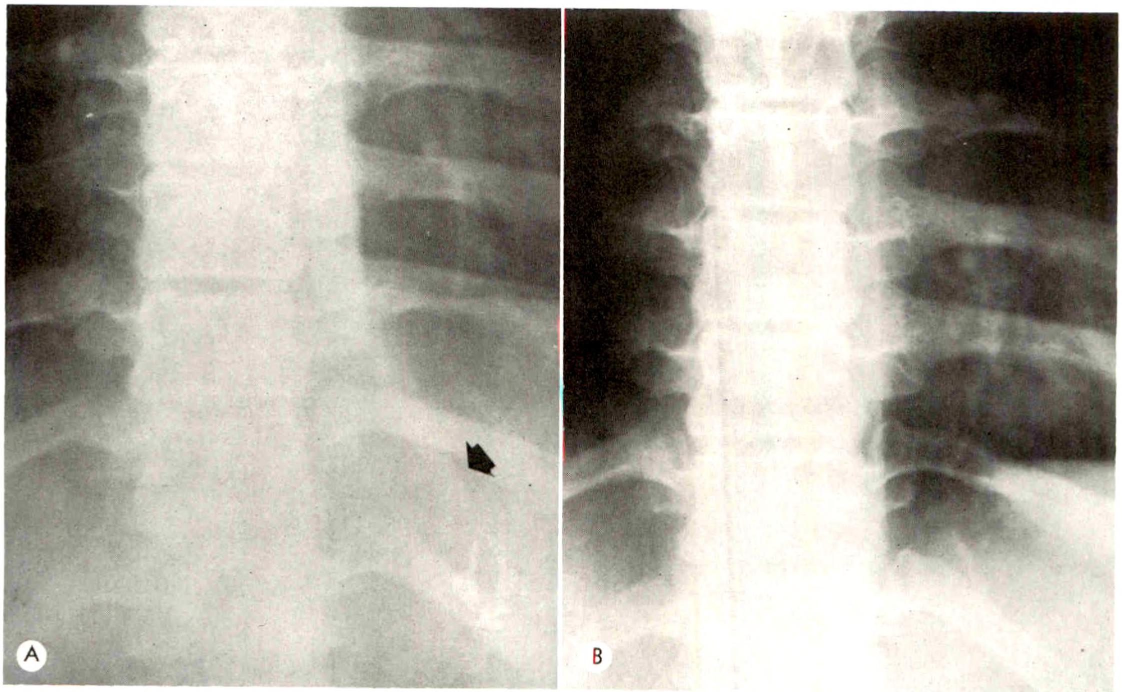


Fig. 2. (*A*) A 19 year old girl with Hodgkin's disease complained of dorsal pain. Roentgenogram of the dorsal spine shows a long, fusiform, paraspinal mass on the left. The greatest displacement of the paraspinal line is at D11–12. She received 3,000 r incident dose to a posterior spine field in 18 days using cesium 137 radiation. (*B*) Roentgenogram of the dorsal spine made more than 3 years after treatment. The mass has disappeared. She was free of pain.

We have observed displacement of this shadow in 22 patients with Hodgkin's disease. Twenty-three paraspinal masses will be considered since one child developed 2 paraspinal masses at separate sites with an interval of 10 months between episodes.

These masses tend to be fusiform and extend over more than one dorsal vertebral segment. The larger lesions may have a lobular contour (Fig. 1, *A*, *B* and *C*). There was a rather specific pattern of localization of the paraspinal masses in our patients.

Thirteen of 23 masses were limited to the left paravertebral soft tissues and greatest displacement appeared between the eighth and twelfth dorsal vertebrae (Fig. 2, *A* and *B*). In 6 instances they were bilateral and were also limited to the same lower dorsal region (Fig. 3, *A*, *B* and *C*). In 4 patients the paraspinal mass was limited to the right side and each of these was found at a higher, mid-dorsal level from the fifth to the eighth dorsal vertebrae (Fig. 4). The anatomic and physiologic basis for the predilection for these sites is unknown.

On routine posteroanterior chest roentgenograms, left sided paraspinal masses are seen as soft tissue densities in the paraspinal region through the heart shadow.

The right paraspinal portion of a bilateral mass presents as a displacement of the right linear paraspinal shadow and may be seen as an abnormal contour in addition to the normal right heart border and the lateral margin of the inferior vena cava.

Lesions limited to the right side may be more difficult to diagnosis on routine chest roentgenograms because of the possibility of confusing them with a hilar or mediastinal, especially subcarinal, lymphadenopathy. Careful observation in cases of paraspinal masses will show the gradual displacement of the paraspinal line at the upper and lower limits of the lesion, which is not observed in mediastinal or hilar lymphadenopathy.

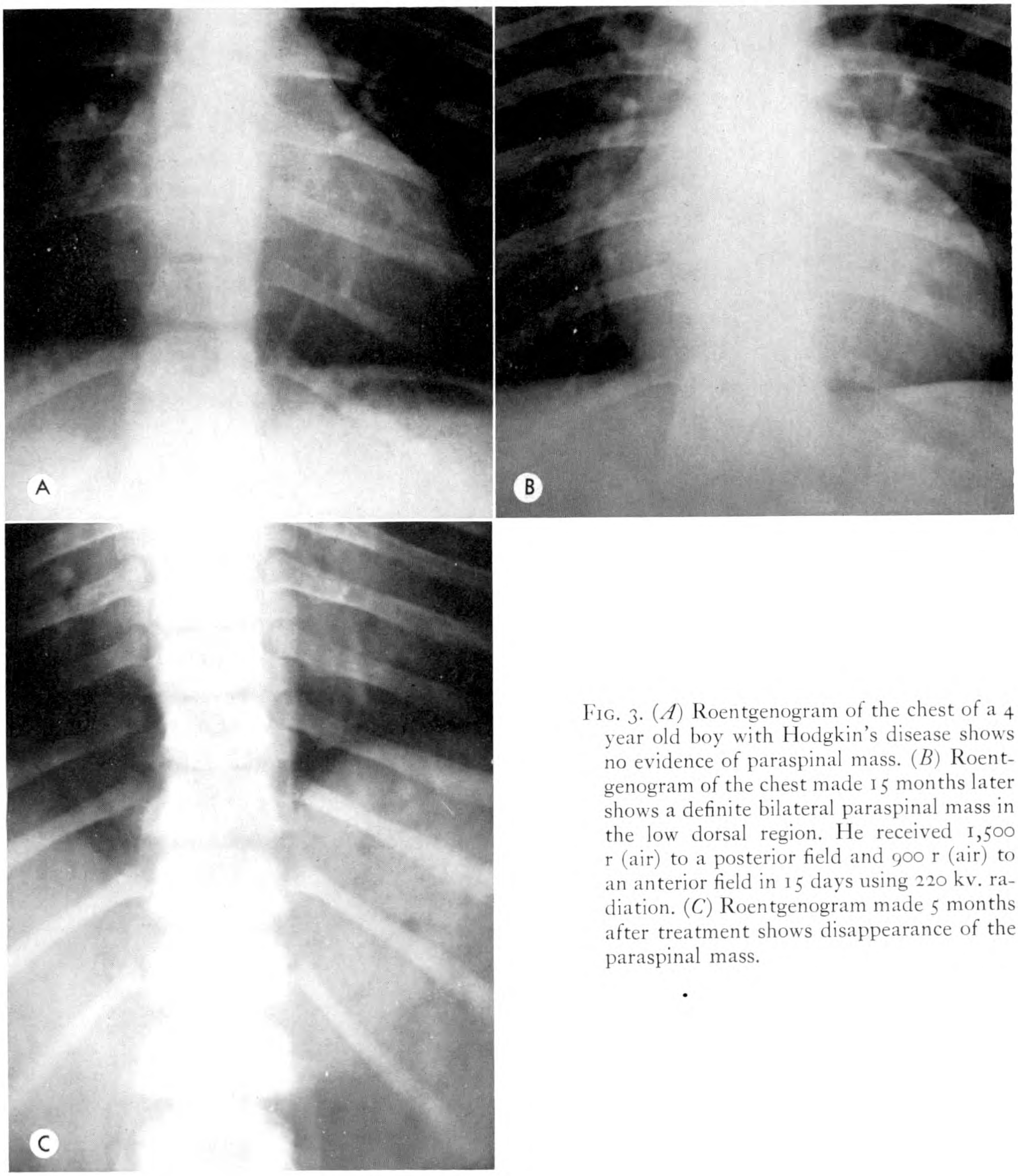


Fig. 3. (*A*) Roentgenogram of the chest of a 4 year old boy with Hodgkin's disease shows no evidence of paraspinal mass. (*B*) Roentgenogram of the chest made 15 months later shows a definite bilateral paraspinal mass in the low dorsal region. He received 1,500 r (air) to a posterior field and 900 r (air) to an anterior field in 15 days using 220 kv. radiation. (*C*) Roentgenogram made 5 months after treatment shows disappearance of the paraspinal mass.

In all the cases the routine posteroanterior roentgenogram of the chest has been diagnostic. Anteroposterior roentgenograms of the dorsal spine show this mass to better advantage. The lateral roentgenograms are normal unless there is osseous involvement.

In several of our cases where serial roentgenograms are available, it has been possible to follow the growth of these masses and their disappearance after treatment. In 15 of 23 paraspinal masses, roentgenograms after treatment are available and show disappearance of the paraspinal mass following treatment.

## TREATMENT

The treatment of Hodgkin's disease has

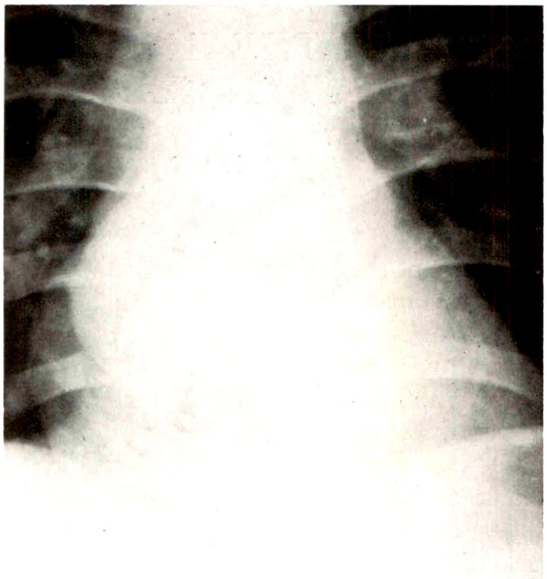

Fig. 4. A 14 year old white boy with Hodgkin's disease complained of dorsal pain. Roentgenogram of the chest shows a right paraspinal mass displacing the right paraspinal line. He received 1,000 r (air) to each of anterior and posterior mediastinal fields in 11 days using 220 kv. radiation. No follow-up roentgenograms are available.

varied considerably in this institution since 1940. All of the patients except 2 were irradiated. These 2 had systemic manifestations of Hodgkin's disease when the paraspinal mass appeared, and were treated with chemotherapy alone. One showed disappearance of the paraspinal mass on follow-up roentgenograms.

Most of the irradiated patients were treated using 200 kv. or 250 kv. radiation to a single dorsal port. Doses varied from 400 r (air) given in one day to 3,000 r (air) given in 24 days. A few cases were treated with opposing ports to doses that ranged from 1,200 r to 2,400 r in air to each port in 4 to 14 days.

Recently, $Cs^{137}$ radiation has been employed. The dose given at 1.5 mm. beneath the surface of the skin through a single dorsal port has been of the order of 3,000 r to 4,050 r in 11 to 24 days.

Complete regression of the paraspinal mass after irradiation was verified in all of the 14 lesions that had follow-up roentgenograms of the region involved. It is indeed remarkable to note the good response of this mass to radiation therapy, particularly in view of the diverse techniques employed. Some cases received a low radiation dose when compared to that currently employed.

## SUMMARY

1. In a review of 403 patients with Hodgkin's disease, 22 were found to have paraspinal mass.

2. In 19 out of 22 patients, the appearance of the paraspinal mass was associated with dorsal pain, often severe.

3. Twenty-three masses were found in 22 patients. Thirteen of the paravertebral masses were found in the left lower paradorsal region. Similar location was found in the 6 instances of bilateral masses. The 4 right paravertebral masses appeared at a higher level, generally from the fifth to the eighth dorsal vertebrae.

4. Complete disappearance of the paraspinal mass after radiation therapy was noted in all of the 14 lesions in which follow-up roentgenograms were available.

Richard M. Witten, M.D.
Radiation Therapy Center
Department of Radiology
University Hospital
Ann Arbor, Michigan

## REFERENCES

1. Brailsford, J. F. Radiographic postero-medial border of lung, or linear thoracic paraspinal shadow. *Radiology*, 1943, *41*, 34–37.
2. Felson, B. Fundamentals of Chest Roentgenology. W. B. Saunders Company, Philadelphia, 1960.
3. Garland, L. H. Postero-mesial pleural line. *Radiology*, 1943, *41*, 29–33.
4. Lachman, E. Comparison of posterior boundaries of lungs and pleura as demonstrated on cadaver and on roentgenogram of living. *Anat. Rec.*, 1942, *83*, 521–542.
5. Leigh, T. F., and Weens, H. S. The Mediastinum. Charles C Thomas, Publisher, Springfield, Ill., 1959.
6. Millard, D. G. Displacement of linear thoracic paraspinal shadow of Brailsford: early sign in osteomyelitis of thoracic spine. Am. J. Roentgenol., Rad. Therapy & Nuclear Med., 1963, *90*, 1231–1235.

# THE EFFECT OF IRRADIATION ON THE INTACT SUPRAVITALLY STAINED MAMMALIAN CELL*

*By* PAUL W. SCANLON, M.D., *Section of Therapeutic Radiology, Mayo Clinic and Mayo Foundation*
ROCHESTER, MINNESOTA

IN SPITE of the emphasis placed on the damage to desoxyribonucleic acid (DNA) or the replicating genetic system of mammalian cells following irradiation, recent investigators are questioning whether this is the only or even the chief means of cellular damage. Much recent work has lent support to the "enzyme-release" hypothesis in which damage to the integrity of the plasma membranes and intracellular permeability barriers is an important and perhaps primary result of radiation-induced cell death. Goldfeder,[4] in 1963, clearly distinguishing between reproductive death or that caused by radiation injury to the genetic material of the dividing cell and interphase death or radiation effects on nondividing cells leading to their destruction, presented two types of evidence supporting her conclusion that interphase or acute cell death is caused by radiation damage to the plasma membranes of the cell. With an enzyme-analysis method, she demonstrated a shift in catalase activity from the mitochondrial to the cell-sap fraction following irradiation of tumors *in situ*. This shift in catalase activity from one intracellular compartment to the other she explained by changes produced by radiation in the permeability or fragility of the mitochondrial membranous systems. Secondly, by means of electron microscopy studies, profound changes in the mitochondrial structures in irradiated cells together with ruptures of the limiting plasma membranes were shown. This rupture with a corresponding outflow of the intracellular organelles together with dilatation or segmental enlargement of various segments of the endoplasmic reticulum was explained by Goldfeder as an actual physical change produced in limiting plasma membranes by the impact of ionizing radiation. The chief criticism of this work at the time was the fact that such changes as were demonstrated and attributed to the effect of ionizing radiation could not, in fact, be differentiated from traumatic effects produced by the ordinary method of cell fixation and staining in preparation for electron microscopy.

Alexander,[1] more recently, expressed the opinion that while damage to DNA probably played an important role in the reproductive type of cell death following irradiation, this effect conceivably might not be the most important one leading to cell death. He, too, was of the opinion that damage to intracellular permeability barriers constituted an important primary effect of radiant energy. He found, for example, that with leukemia cells, release of ribonuclease activity in the nucleus can be observed within 5 minutes after 500 r has been given *in vitro* and that this constitutes perhaps the earliest biochemical lesion seen in dividing cells after exposure to roentgen rays. He further pointed out that extremely radioresistant micrococci have apparently the same DNA complement as more radiosensitive bacteria, so that damage to the DNA-replicating system is probably not the reason for the radiosensitivity of the microorganism. He said further that the plasma membranes are probably more logically indicated as a site of radiation damage, because it can be shown that neither cysteamine nor iodoacetamide diffuse into

* Presented at the Sixty-fifth Annual Meeting of the American Roentgen Ray Society, Minneapolis, Minnesota, September 29–October 2, 1964.

the interior of cells under conditions wherein they give rise to protection or marked sensitization, respectively.

Along these lines, it is the purpose of this paper to report on similar observable changes in the limiting plasma membranes produced by radiation in the intact living and metabolizing supravitally stained cell. The changes to be described are dynamic structural ones constantly changing with time, which can be fully appreciated only by close observation with a light microscope using magnifications of ×970 to ×1,450 over a period of several hours or even days. To obviate extraneous influences and to standardize conditions as much as possible, the bulk of this work has been carried out with mouse sarcoma 180 cells in their native ascitic fluid or human leukemia cells with only edathamil (EDTA) added to the blood sample. Occasionally, human carcinosarcoma or reticulum cell sarcoma cells in their native ascitic or pleural fluid have been used, and, as an example of normal nonmalignant cells, buccal or vaginal squamous cells in 5 per cent dextrose solution have been employed.

In wet drop preparations, after suitable supravital staining, mainly with Janus green B, the effects of radiant energy on intact living mammalian cells have been studied and classified in 2 main groups: (1) changes produced in limiting plasma membranes, the outer cellular membrane, membranes of the various cytoplasmic vesicles, and the limiting nuclear and nucleolar membranes; and (2) changes produced in the ability of the cell to metabolize the dark blue-green stain of Janus green B, originally taken up in the cytoplasmic vesicles, through a normal degradation process whereby the stain is changed to a bright-red coloration which diffusely and uniformly spreads throughout the entire cytoplasm of the cell, then to a lesser pink coloration, and finally to a completely colorless phase. The time factor in both these groups of changes is most important and it is essential to follow closely the dynamic changes produced in the wet drop preparations over the course of many hours.

It must be stressed from the outset that the structural changes observed in the various plasma membranes and the color changes observed in the metabolism of the supravital dye are not characteristic of irradiation alone. At any given moment, depending on the age and vitality of the cells studied, the pH of the medium employed, whether the cells are in a saline, buffered or glucose medium, and many other variables, there are always a few cells in various stages of cell death with changes similar to those described as radiation-induced. Other modalities of cellular death, including various cytotoxins, heavy metal poisons, chemotherapeutic agents, and normal cell death from anoxia and drying of the cell preparation, can produce changes in lesser or greater degree which mimic radiation-induced changes to a remarkable extent. It is only by constant comparison against unirradiated controls prepared in exactly the same manner that the observer can be assured that the changes seen are, in fact, due to the impact of ionizing radiation. No attempt has been made to quantitate numerically the changes observed, as they represent a broad spectrum of responses which the author has found impossible to express numerically. The changes observed are dose-dependent only in the very broadest sense. Marked morphologic alterations usually seen in great numbers at higher dose levels can be seen in a few cells at lower dose levels and, conversely, even maximal dose levels may leave some cells unscathed or with minor changes, usually thought characteristic of low dose levels.

Cells are usually studied in their native ascitic or pleural fluid to minimize extraneous influences. EDTA is added to prevent coagulation, and a wet drop preparation is prepared and stained with 0.5 to 1 per cent solution of Janus green B. Observations are serially made with an ordinary binocular microscope under oil immersion at a magni-

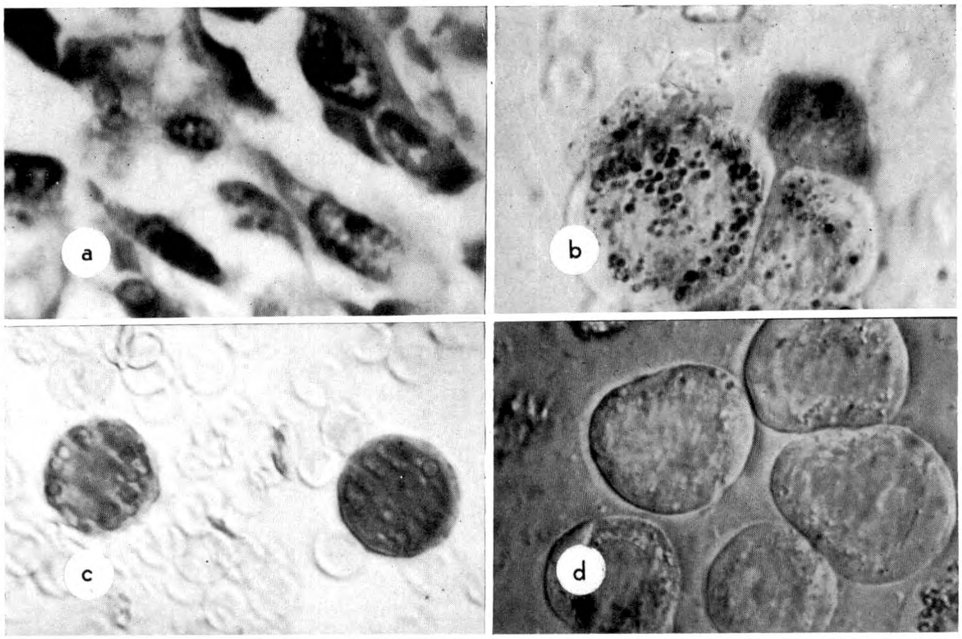


Fig. 1. (*a*) Hematoxylin and eosin preparation of mouse sarcoma 180. (*b*) Supravitally stained (Janus green B) sarcoma 180 showing early uptake of stain in cytoplasmic vesicles. (*c*) After conversion of phase shown in *b* to diffuse red coloration phase. (*d*) After conversion of phase shown in *c* to completely colorless phase.

fication of ×970. Photomicrographs were taken at magnifications of ×1,455, using Kodachrome II with exposure times of ½ to 1 second. It is obvious that in using such high degrees of magnification there is little or no depth of focus, and with the cells in fluid suspension, only a small central point of interest can be in focus, contrary to the usual medical photomicrograph which is sharp from edge to edge.

While many different types of supravital dyes or stains have been tried, the dye Janus green B has been found most satisfactory for the studies here made. This dye, which is diethylsafranine-azo-dimethylaniline, is thought to be a selective stain for mitochondria. It has long been known that the Janus green originally taken up primarily in cytoplasmic vesicles in a dark-blue or blue-green color is rapidly converted by the intact healthy metabolizing cell through a series of oxidative processes into a red coloration which spreads diffusely and uniformly throughout the cytoplasm and eventually is metabolized to a completely colorless state. The production of the pink color from the Janus green by mitochondria is now thought to be due to DPN (diphosphopyridine nucleotide)-specific dehydrogenases.[3] Interference by radiation in the ability of the normally metabolizing cell to oxidize this dye through to its colorless state will be shown later. Unfortunately, these color changes cannot be fully appreciated in the black-and-white illustrations which follow.

Figure 1*a* illustrates the paucity of cytoplasmic detail seen in the ordinary hematoxylin and eosin stain of the mouse sarcoma 180 cell and, by way of comparison, the much more informative cytoplasmic detail noted in the supravitally stained and intact sarcoma 180 cell as shown in Figure 1, *b*, *c* and *d*. Figure 1*b* illustrates the preliminary pickup of the dye in the cytoplasmic vesicles which are colored a rich dark blue-green against a light blue-green background of more general cytoplasmic staining. Figure 1*c* illustrates the diffusion of the blue-green dye out of the cytoplasmic vesicles and its conversion to a bright red cytoplasmic coloration, most of which is

unfortunately lost in black-and-white reproduction, and Figure 1*d* represents the final colorless state of the cell after complete degradation of the dye.

Dynamic changes in the integrity of various plasma membranes in the cell, progressive in time, can be categorized in 4 main types: (1) changes produced in the limiting outer cell membrane leading to bubbling, ballooning, and vesiculation of the outer membrane with or without loss of stainable cytoplasmic organelles; (2) changes in the cytoplasmic vacuoles leading to either enlargement of vacuoles with entrapment in the cytoplasm or (3) extrusion of these altered vesicles through the outer cell membrane into the surrounding medium; and (4) changes in the nuclear and nucleolar membranes leading to enlargement of the nucleus itself with vesiculation produced in the nuclear infrastructure and vesiculation produced within the nucleolus itself.

The actual structure of the limiting plasma membranes has a uniform pattern, and, in fact, seems to be universal in all living systems. Membrane systems generally show the same features: two protein membranes separated by a space thought to be a bimolecular double-layer phospholipid. The membrane is very thin, only 70 to 100 Å. thick, but it shows up clearly in electron micrographs of sections of fixed cells as a thin dense double line. Damage to this double-protein-layer membrane with a phospholipid interface and the dynamic changes which follow this damage are thought to constitute the chief mechanism of interphase cellular damage following irradiation. Once the integrity of one or both of the protein layers is breeched by radiant energy, either by actual physical breaking of the polypeptide leakage or as a result of interference in the function of natural polar pores occurring in this protein lining, the osmotic equilibrium of the organelle is disturbed, fluid is imbibed and the organelle swells, presumably because of the elasticity of the phospholipid interface.

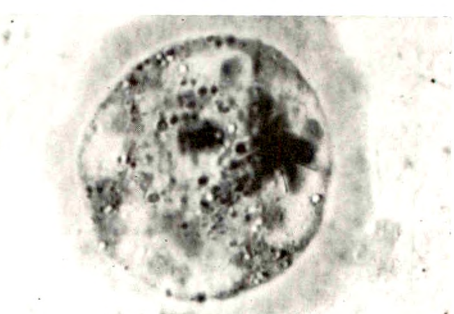

FIG. 2. Ballooning of outer cellular membrane, intervening space being filled with red-colored cytoplasmic material.

### CHANGES IN THE OUTER LIMITING CELL MEMBRANE

The earliest and most easily discernible structural changes following irradiation are those produced in the outer limiting cell membrane. Very early, and the time interval is somewhat dependent on the dose of irradiation given, there is an apparent ballooning of the outermost layer of the peripheral cell membrane. Whether this enlargement comprises the entirety of the outer cell membrane or merely separation at the phospholipoid interface is not certain. There should be only a single cell membrane, but after ballooning of this membrane the cytoplasmic periphery is noted to be intact (Fig. 2) and unchanged so that it is evident that there is some restraining force to the outflow of the cytoplasmic content at this stage. It may be that this inner restraining membrane is analogous to the protoplast membrane seen when the rigid outer cell membrane is stripped from bacteria or to the limiting membrane seen in PPLO (pleuropneumonia-like) or L forms of bacteria without rigid outer cell walls. As ballooning progresses, it seldom if ever remains symmetrical; instead, very shortly small bubbles appear on the outer membrane, which sometimes swells to enormous proportions before either separating or rupturing (Fig. 3).

When the outermost of the limiting cell membranes alone is disturbed, the content of the enlarged bubble appearing in the cell

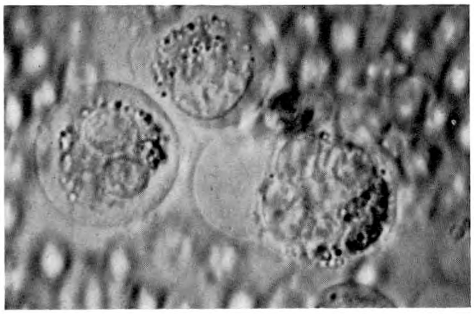

FIG. 3. Ballooning and bubbling of outer cellular membrane after irradiation. Content of bubble is colorless at this stage.

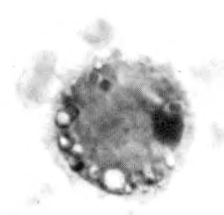

FIG. 5. Multiple smaller bubbles originating from outer cellular membrane, the content of which is diffusely red-stained cytoplasm.

surface contains a clear colorless fluid without any internal morphology. However, when the inner of the two limiting membranes is breeched, there is seen a rapid outpouring of blue (Fig. 4) or red (Fig. 5)-staining cytoplasmic microparticles into the outer balloon, depending on the phase of the dye conversion. These microparticles do not show clearly on photomicrographs as they are invariably in rapid brownian motion and are manifested in the photomicrographs only by a light dusty discoloration of the membrane bubbles. Occasionally, secretory cytoplasmic vesicles are extruded into the outer bubbles on the limiting cell membrane where they immediately start to swell, giving the appearance of bubbles within bubbles such as is seen in Figure 6, *a* and *b*. These bubbles, if watched long enough, are seen to eventually separate and float off into the surrounding medium as intact spheres which presumably eventually rupture and disperse their cytoplasmic content (Fig. 7). Occasionally, and presumably where the break in the outer limiting membrane is less marked, instead of actual bubble formation there is a wormlike or fingerlike projection seen to emerge from the outer limiting membrane, many times led by a small cytoplasmic vesicle (Fig. 8 and 9). Such a projection sometimes reaches a length many times the diameter of the cell before eventual separation of the leading secretory vesicle. In fact, this is a rather characteristic pattern assumed when any of the cytoplasmic vesi-

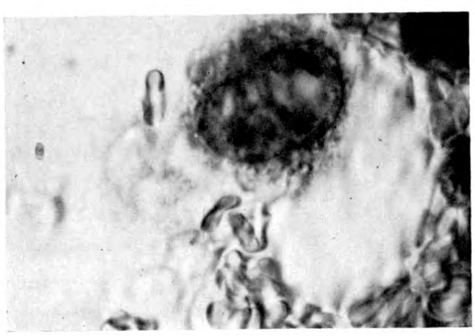

FIG. 4. Ballooning of outer cellular membrane. Content of bubble consists of blue-stained cytoplasmic microparticles in rapid brownian motion.

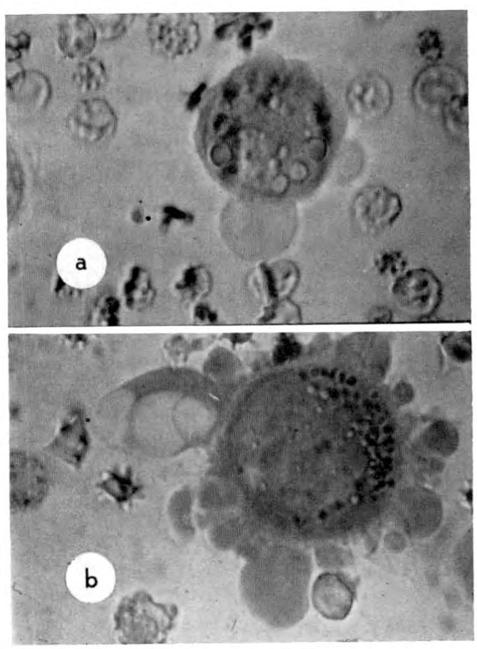


FIG. 6. (*a* and *b*) Examples of outer cellular membrane bubbles which contain rapidly expanding cytoplasmic vesicles.

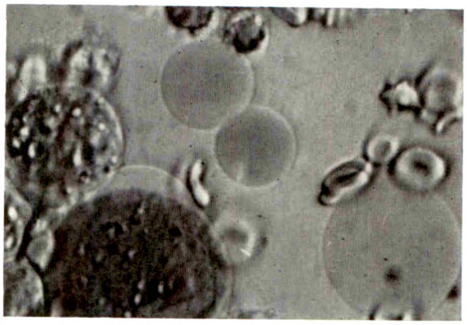

Fig. 7. Membrane bubbles containing red-colored cytoplasmic contents which have separated from cell.

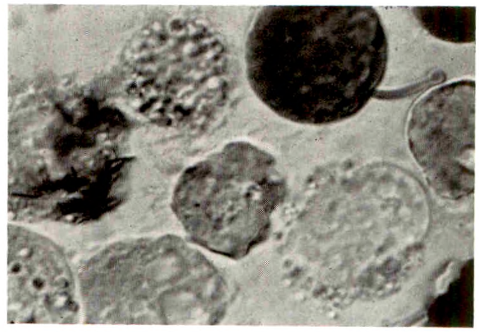

Fig. 8. Cytoplasmic vesicle extruded from cell membrane on a pedicle.

cles leave the cell. They invariably leave on a pedicle or stalk formation and once separated leave a collapsed frondlike pedicle extruding from the peripheral cell membrane. Cells with a frondlike periphery, and this is characteristic of many types of malignant cells, are those which have extruded a large component of their cytoplasmic vesicles. This observation of the egress of much of cytoplasmic content through breaks produced in the outer limiting membrane raises the question whether the decreased levels of DNA and RNA observed after irradiation might not be the result of actual physical loss of these substances into the surrounding medium rather than any suppression of their formation induced by irradiation.

## CHANGES PRODUCED IN SECRETORY CYTOPLASMIC VESICLES

Secretory cytoplasmic vesicles form a most prominent part in the morphology of the intact supravitally stained cell. Very comprehensively studied and described by Apffel and Baker,[2] these refractive cytoplasmic bodies, 0.3 and 0.8 $\mu$ in diameter, can be seen in normal cells but are found in much greater numbers in malignant cells. They are apparently lipidic in nature, contain phosphatids, and probably have a very thin protein coating. Their exact function is unknown but they are thought by some to be part of the Golgi secretory apparatus.[6] These cytoplasmic vesicles appear very similar to the secretory vesicles seen in amoebae which selectively concentrate the supravital dye in the first observable uptake of dye within the cell. Protein reactants such as weak acids or 10 per cent potassium cyanide are found to break the protein jackets of these vesicles, allowing immediate swelling. The swelling of these secretory cytoplasmic vesicles noted following irradiation (Fig. 10) is assumed to be due to actual physical breaks in their protein jackets produced by ionizing radiation with a rapid imbibing of fluid. It can be seen that the cytoplasmic vesicles can swell to enormous size before either rupture or liberation from the cell (Fig. 11). They may or may not contain supravital dye, depending on the stage of metabolism of the cell, although they are usually colorless. This swelling of the cytoplasmic vesicles is thought to be the basis for the cytoplasmic vacuolization characteristically noted in irradiated cells fixed and stained in the usual manner. Figure 12*a* demonstrates the

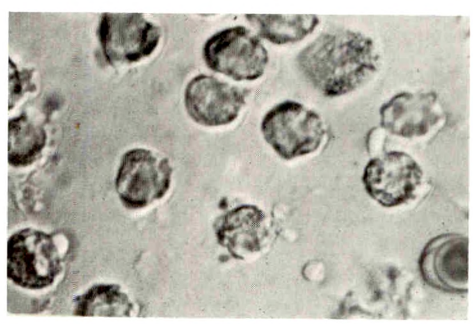

Fig. 9. Chronic myelogenous leukemia cells after 5,000 r in various stages of cellular membrane bubbling, distortion and cellular disintegration.

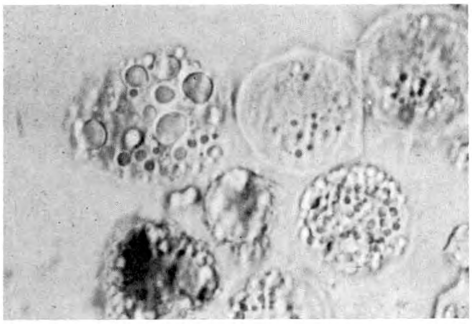

Fig. 10. Beginning enlargement of cytoplasmic vesicles of sarcoma 180 cell.

cytoplasmic vacuolization found in a supravitally stained squamous cell after a dose of 2,400 r in a patient with squamous cell epithelioma of the external auditory canal, and Figure 12*b* shows the vacuolization seen in a buccal squamous cell after a dose of approximately 3,000 r in a patient with carcinoma of the base of the tongue. This phenomenon is undoubtedly identical to the vacuolization noted in the cytoplasm of irradiated vaginal squamous cells and which is important in the evaluation of the "radiation response" described by Graham and co-workers (Fig. 13).

## DISCHARGE OF CYTOPLASMIC VESICLES FOLLOWING IRRADIATION

In addition to the enlargement and entrapment of cytoplasmic vesicles within the substance of the cytoplasmic confines, perhaps an even more common and characteristic change is noted in the early discharge of these cytoplasmic vesicles through the cell membrane into the surrounding me-

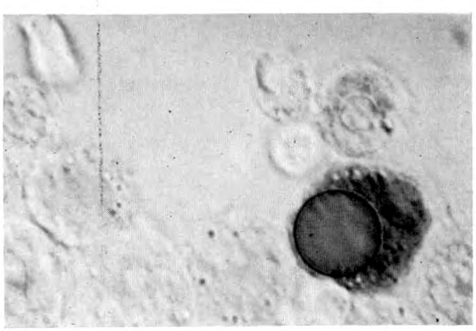

Fig. 11. Marked enlargement of a single cytoplasmic vesicle.

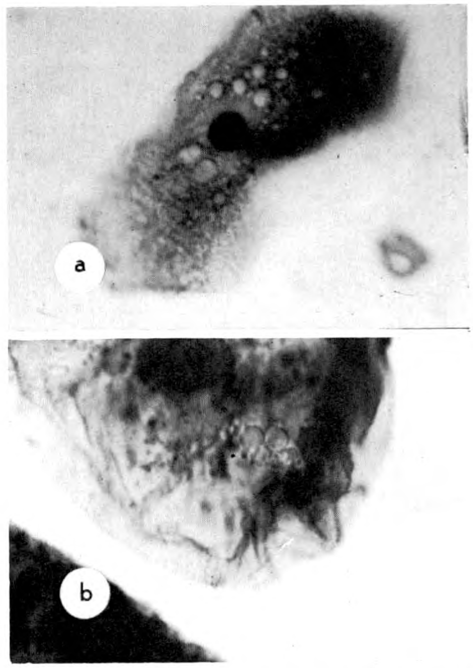


Fig. 12. (*a* and *b*) Squamous cells with radiation-induced cytoplasmic vacuolization.

dium as seen in Figure 14. As noted previously, these cytoplasmic vesicles on emerging from the cell either rupture in the surrounding fluid and disappear or persist for a time, intact in the surrounding fluid medium (Fig. 7).

## CHANGES IN RAPIDITY OF UPTAKE OF SUPRAVITAL DYES

The rapidity with which cytoplasmic

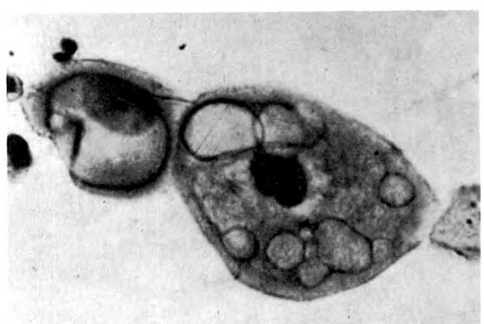

Fig. 13. Radiation response (×1,000) showing large vacuoles in cytoplasm. (From: Graham, J. B., Sotto, L. S. J., and Paloucek, F. P. Carcinoma of the Cervix. W. B. Saunders Company, Philadelphia, 1962, pp. 184–185. Courtesy of the publisher.)

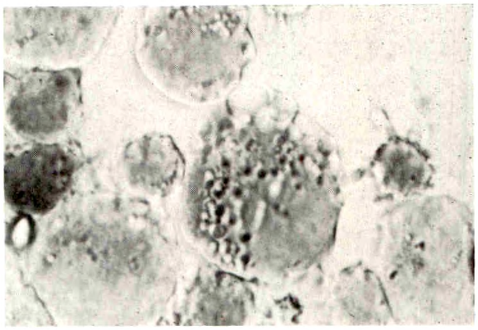

Fig. 14. Enlarging cytoplasmic vesicles in process of extrusion through cell membrane.

vesicles absorb supravital stains depends in large measure on the integrity of the involved plasma membranes and their state of vitality at the time of application of the dye. Devitalized cells, whether as the result of aging, trauma, anoxia or cellular toxins of various sorts, take up the dye with considerably greater avidity than do normal cells and this is first seen as a collection of the dye within the larger, more peripheral of the cytoplasmic vesicles. Immediately after irradiation in dosage of 2,500 to 5,000 r the cytoplasmic vesicles of sarcoma 180 cells can be seen to take up Janus green B with considerably more avidity than unirradiated controls. This effect is rather more apparent in slightly aged cells, 2 to 4 days old, where the conversion of the supravital dye through its color phases is slightly slowed down, taking up to several hours, in contrast to extremely fresh cells where the entire conversion takes place in ½ to 1 hour. This phenomenon is assumed to be due to actual physical breeching of the integrity of the plasma membranes of these vesicles with a resultant increased porosity and a passive rather than an active transport of the dye across the membranes involved. The changes produced by irradiation, however, are much more subtle than those produced by more noxious cellular toxins and poisons such as the chemotherapeutic agents and heavy metal poisons. Again, it must be emphasized that these changes are not quantitative except in a very broad sense. At any given moment in any given cell preparation, there are always devitalized aged cells which can mimic the changes described. It is only in the comparison of many irradiated specimens against normal controls that one can say with any assurance that irradiation does, in fact, increase the porosity of the plasma membranes leading to a more rapid uptake of the dye in the cytoplasmic vesicles.

### CHANGES IN THE ABILITY OF THE CELL TO METABOLIZE JANUS GREEN B

After the normal, intact, fresh, actively metabolizing cell initially takes up Janus green B in the larger of the cytoplasmic secretory vesicles, under ordinary circumstances within the space of a few hours, the dark-blue or blue-green coloration in the secretory vesicles diffuses out of the vesicles where it is actively metabolized presumably by the mitochondria so as to produce a homogeneous diffuse red and/or pink coloration of the entire cytoplasm. Eventually, this red coloration is degraded through a pink color to a completely colorless state in the normal cell. It was early noted, however, that cells around the periphery of the cover-slip preparation or those cells around entrapped air bubbles in the center part of the preparation, instead of going through this degradation from dark blue-green through red to colorless, maintain the dark blue-green coloration within the larger cytoplasmic vesicles for an indefinite period. In certain instances this maintenance of coloration within the larger of the cytoplasmic vesicles is continued until the death of the cell; in other instances there is much more retarded conversion through the pink to the colorless form. Access to oxygen is thought to supply sufficient hydroxy radicals to neutralize the effect of the acid hydrolysates which have to do with the metabolism of this supravital dye. Irradiation has a much less pronounced and more subtle effect along the same line, again perhaps by its production of hydroxy radicals and the neutralization of the acid hydrolysates responsible for the conversion of this dye or

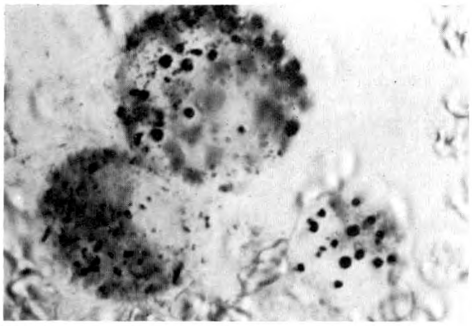

FIG. 15. Persistence of supravital dye within cytoplasmic vesicles.

possibly by simple enzyme deactivation. Hydrogen peroxide in the same concentration as is currently being used to increase the effect of clinical radiotherapy also maximally retards the color degradation of Janus green. Figure 15 demonstrates the persistence of the blue-green coloration of the dye in the cytoplasmic vesicles 20 hours after a dose of 2,500 r, many hours after the unirradiated cell would have converted the dye to a completely colorless phase. Figure 16 illustrates a partially arrested conversion of the dye 24 hours after a dose of 5,000 r. There is persistence of the dye within the cytoplasmic vesicles albeit with some degradation of the dye to produce a diffuse red coloration of the cytoplasmic background. It is thus apparent that many factors including irradiation, access to a supply of oxygen, chemotherapeutic agents, weak bases, heavy metal poisoning and even aging or anoxia of these cells will bring a complete or partial halt of the metabolism of Janus green B to its colorless phase. Whether this is due to enzyme deactivation by the various agents mentioned or the production of hydroxy radicals which neutralize the acid hydrolysates normally contained in the cytoplasmic lysosomes or whether it represents a general suppression in the active metabolism of the cell is not known and can be only postulated at this time.

In addition to the metabolic changes noted in the ability of the cell to metabolize this dye, there are actual structural changes which occur in the dye-containing vesicles which I have called vesicular stain and vesicular rupture. The processes are probably quite similar and the difference between the two probably has to do with the rapidity with which the dye is suddenly liberated into surrounding cytoplasm. With a sudden complete rupture of the secretory dye-containing vesicles, there is immediate liberation of the contents of the vesicle with crystallization of the dye in a starburst pattern (Fig. 17). This is distinguishable from the slower gradual leaking of the dye through the walls of the vesicles into the surrounding cytoplasm such as to produce a more homogeneous staining effect in the immediate vicinity of the ruptured vesicles (Fig. 18). The majority of cells which exhibit either vesicular rupture or vesicular stain effect usually have a combination of both (Fig. 19). The higher the dose of radiation or the more potent the chemotherapeutic agent or the more toxic the heavy metal employed, the more likely

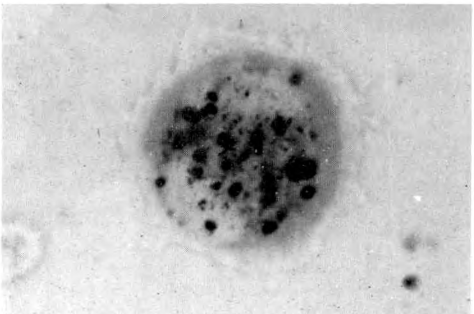

FIG. 16. Persistence of supravital dye within cytoplasmic vesicles but with some conversion to red coloration phase.

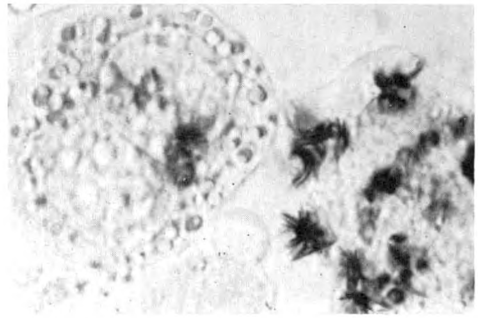

FIG. 17. Vesicular rupture with crystallization of dye in a star-burst pattern.

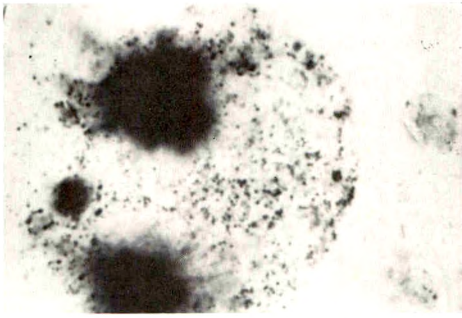

Fig. 18. Vesicular stain effect.

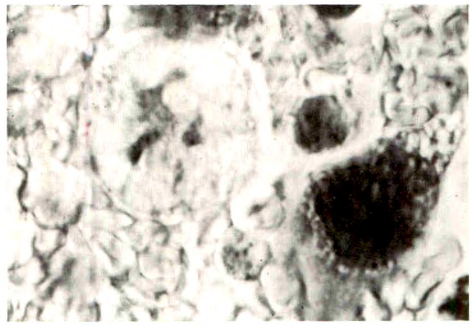

Fig. 20. Enlarged nucleus of an irradiated sarcoma 180 cell showing nuclear infrastructure with early penetration of supravital stain.

one is to see the star-burst formation indicating complete and sudden dissolution of the integrity of the dye-containing vesicle. Conversely, the less the dose of radiation and the more innocuous the chemotherapeutic agent or poison employed, the more likely one is to observe the vesicular stain effect. I think that unquestionably these changes can be explained only by physical loss of continuity of the vesicular wall, produced by the various agents mentioned.

## NUCLEAR AND NUCLEOLAR CHANGES

These changes have been left to the last because they constitute a combination of the structural changes mentioned above, namely, enlargement of the nucleus and nucleolus together with an early acceptance of stain by the injured nucleus. In the normal cell the nucleus is one of the last structures to accept supravital stain. In most instances, with healthy fresh cells, the cytoplasm may go through the entire cycle of conversion of the Janus green B without any stain whatever being accepted by the nucleus, depending on the concentration of the stain employed.

However, when the structural integrity of the nucleus is affected for any reason, and this is especially apparent in old, aged, or anoxic cells, the nucleus readily accepts stain, many times in a preferential fashion over and above acceptance by the cytoplasm. This nuclear stain, however, is not uniform throughout the entire nucleus. Instead, a definite nuclear morphology becomes apparent in the form of canaliculi and lacunae distributed throughout the nuclear sap. These canals and lacunae become filled with the dye as illustrated in Figures 20 and 21. This configuration is thought to be a much more accurate representation of nuclear morphology than is obtained in the ordinarily fixed and stained cell. It should be noted that in every instance the enlarged lacuna or nucleolus is attached to the nuclear wall by a fine reticular network.

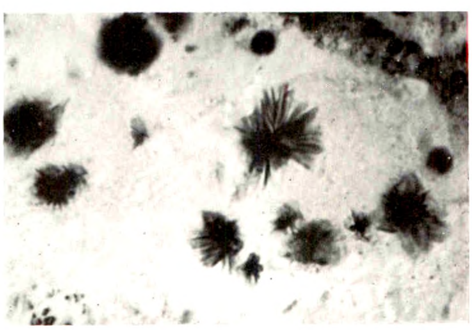

Fig. 19. Combination of vesicular stain and vesicular rupture.

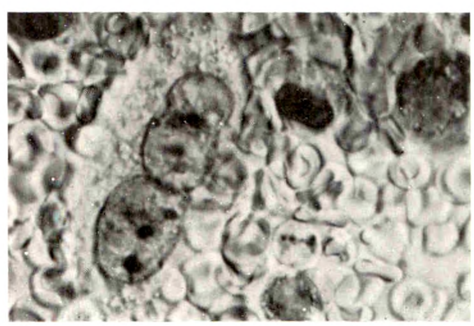

Fig. 21. Dividing nucleus of an irradiated sarcoma 180 cell with early acceptance of supravital stain.

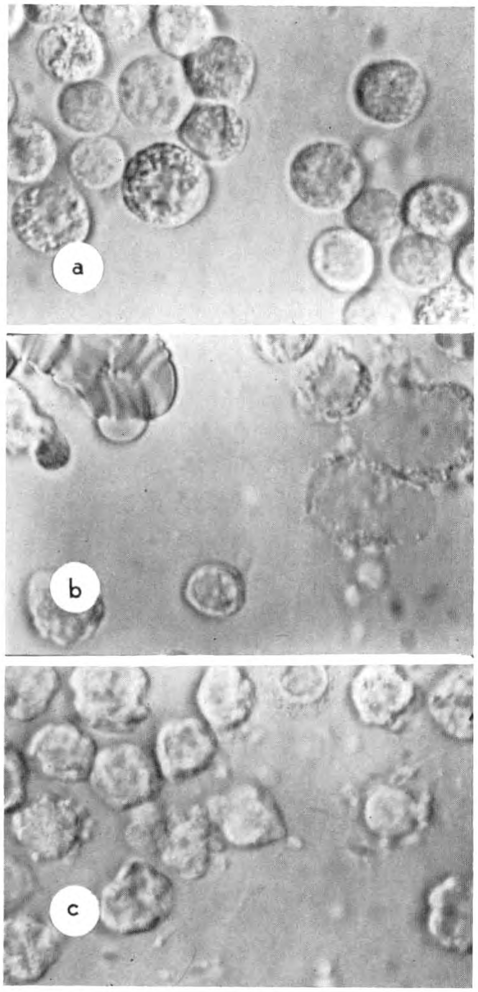


FIG. 22. Chronic myelogenous leukemia cells. (*a*) Unirradiated cells. (*b*) Irradiated cells (2,500 r) with nuclear enlargement. (*c*) Irradiated cells (2,500 r) with nuclear enlargement, membrane dissolution and fragmentation.

The coloration produced by dye acceptance in the injured nucleus incident to irradiation or other toxic agent is principally a function of time. Constant comparison to normal controls must be followed throughout the entire period of observation. In general, and again dependent on the dose of irradiation employed, the nucleus of an irradiated cell is seen to accept supravital dye staining much more quickly than does the normal cell. At the same time, there is usually a concomitant over-all nuclear enlargement, many times so pronounced that the enlarged nucleus gives the appearance of filling almost the entire cell (Fig. 22, *a*, *b* and *c*). This phenomenon is especially well seen in chronic leukemic cells, whereas the earlier takeup of the supravital dye by an injured nucleus is better demonstrated in the nucleus of the sarcoma 180 cell. In addition to the earlier acceptance of the dye and the over-all gross enlargement of the nucleus, there can, in many instances, be seen an active vesiculation produced in the lacunae within the nuclear substructure and also within the nucleolus (Fig. 23). It is assumed that this vesiculation has the same basis as the much larger vesicles produced in the cytoplasm, namely, a physical rupture of the protein jackets of the various subcellular organelles.

Finally, the most drastic of the cellular changes following irradiation and probably the one most often thought of as typical of the changes induced by radiation is that of complete cellular fragmentation and dissolution. Figure 22, *b* and *c* demonstrates the effect on chronic myelogenous leukemia cells immediately after the administration of 2,500 r. It can be noted that these cells which have gone through their dye-metabolism stage very rapidly have in many instances completely disrupted. This disruption, incidentally, is much more marked within clumps of cells. Those cells left on the periphery remain essentially intact and it is assumed that the cellular disruption incident to irradiation is, in large part, due to the concentrated effect of extravasated acid hydrolysates liberated in

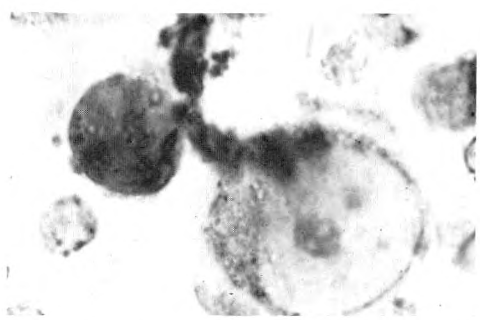

FIG. 23. Enlarged nucleus of an irradiated sarcoma 180 cell showing nucleolar vacuolization.

the process of cell dissolution in which there is a cumulative effect in the interior of cell clumps.

## SUMMARY

It is believed that the changes described herein are in the main changes produced by interruption in the integrity of limiting plasma membranes—both the outer limiting membranes and those of the cytoplasmic vesicles and nuclear structures produced as a result of physical damage incident to the application of radiant energy. These changes are all dynamic structural changes which can be seen only in the intact supravitally stained cell studied over a period of time under the light microscope. It is thought that in the process of ordinary fixation and staining the subtle plasma-membrane changes described herein are destroyed and are not readily apparent. It is obvious that much more work needs to be done with the supravital staining of malignant cells to define more clearly the process of radiation damage. Certain it is that the colorful metabolic changes produced by the conversion of certain supravital dyes could never be appreciated either from the study of fixed cells viewed under the light microscope or cells prepared for the electron microscope. It is entirely possible that many other supravital dyes with which the author has not had experience could be equally or more helpful in the study of the metabolic activity of mammalian cells and it is hoped that further work will elucidate these. In recent work the use of a combination of Janus green B and toluidine blue, the latter for nuclear detail, has proven more informative than the use of either alone. One of the greatest assets of such study is the ease with which cells can be obtained, stained and observed. Most of the morphologic studies carried out to date using conventional staining methods represent a single slice in time, which, pertinent though they may be, do not represent the continuing dynamic changes that are much more readily apparent in studies using intact supravitally stained cells. It is true that the supravital stains are cytotoxic and poisonous to a degree to the metabolism of normal cells, but they have the advantage usually of being very slow poisoners so that, by constant comparison against normal controls, this effect can be minimized. Further, such study allows for easy comparison between the lethal effects of irradiation and the somewhat similar effects produced by other causes of cell death. It is hoped that the changes described will lend some support to the plasma-membrane-disruption theory or enzyme-release hypothesis of interphase radiation damage.

Mayo Clinic
Rochester, Minnesota

## REFERENCES

1. Alexander, P. Intracellular permeability barriers as site of primary lesion for ionizing radiations. Presented at the Eighteenth Annual Symposium on Fundamental Cancer Research; Cellular Radiation Biology, Houston, Tex., March, 1964.
2. Apffel, C. A., and Baker, J. R. Lipid droplets in cytoplasm of malignant cells. *Cancer*, 1964, *17*, 176–184.
3. Bourne, G. H. Division of Labor in Cells. Academic Press, Inc., New York, 1962, p. 192.
4. Goldfeder, A. Radiosensitivity at subcellular level. *Laval méd.*, 1963, *34*, 12–43.
5. Graham, J. B., Sotta, L. S. J., and Paloucek, F. P. Carcinoma of the Cervix. W. B. Saunders Company, Philadelphia, 1962, pp. 184–185.
6. Mercer, E. H. Cells: Their Structure and Function. Doubleday & Company, Inc., Garden City, N. Y., 1962, p. 39.

# THE RESPONSE OF THE OLFACTORY EPITHELIUM OF THE ADULT AXOLOTL (*SIREDON MEXICANUM*) TO ROENTGEN IRRADIATION*

*By* V. V. BRUNST, D.Sc.
BUFFALO, NEW YORK

PREVIOUSLY reported work comparing the effects of roentgen irradiation on the tissues of young and adult axolotls[11] has been extended in the present investigation. This study was designed to compare the effects of local roentgen irradiation on the olfactory chambers, particularly on the olfactory epithelium, in adult axolotls and in young axolotls. Previous investigations[6,10] have shown considerable differences between adult and young animals in the responses of various types of tissue to radiation.

Olfactory epithelium is epithelium of a specialized type, derived from skin epithelium and closely associated with it. That being the case, some attention should be given here to the response of the skin epithelium of axolotls to roentgen irradiation.

The most typical change in the skin epithelium in young axolotls[5] is the development of what is known as giant-cell degenerating epithelium. This type of epithelium is characterized by the development of maximally large giant cells with giant nuclei, the formation of both large and small vacuoles in the cytoplasm of epithelial cells, an extremely uneven outer surface on the epithelium, the protrusion of individual giant cells from the outer surface, the formation of deep cracks and spaces between epithelial cells, and complete separation of some giant cells and cell complexes.

The response of the skin epithelium in adult axolotls is very different.[6] Giant-cell degenerating epithelium does not develop in adult axolotls. After very large doses of radiation, the epithelium may become atypical, containing cells with large nuclei, and no Leydig cells; but there are no actual giant cells. In some areas, the size of the nuclei may be normal. In other areas, however, the epithelium may be transformed into homogeneous tissue, without nuclei or cell borders.

The corneal epithelium is also derived from the skin epithelium, and is even more closely associated with it than is the olfactory epithelium. On comparing the effects of roentgen radiation on the cornea in adult axolotls with those in young axolotls,[9,11] it is obvious that some phenomena typical of the response of the young animals are not observed in the adults. For example, the irradiated cornea in the young axolotl is characterized by a highly uneven outer surface, and by the development of isolated projections consisting of separate epithelial cells, and the formation of abnormal outgrowths consisting of groups of several epithelial cells. The irradiated cornea in the adult axolotl, however, is characterized by a much less uneven outer surface, and the formation of isolated projections and outgrowths is never observed after irradiation of the adult cornea.

On the other hand, the formation of Leydig cells and pigment cells in the irradiated cornea is observed in both young and adult axolotls. Furthermore, melanophores and blood vessels develop in the substantia propria of the irradiated cornea in the adults, but not in the young animals. Under the circumstances, it is reasonable to expect the response of the olfactory epithelium to roentgen irradiation to be different in young and adult axolotls.

* From the Laboratory of Radiobiology, Roswell Park Memorial Institute (New York State Department of Health).
This investigation was supported by Grant CA-05579-04 from the United States Public Health Service.

## MATERIALS AND METHODS

In the present investigation, 75 adult axolotls (Siredon mexicanum), 4 to 5 years old, were used. The anterior portion of the head was irradiated with 1,000 r in 10 animals, 3,000 r in 20, 6,000 r in 10, 8,000 r in 10, and 10,000 r in 20; 5 animals served as untreated controls. Irradiation conditions were as follows: 250 kv., 30 ma., 0.25 mm. Al filter, beryllium window tube; half-value layer 1.0 mm. Al; 465 r/min. in air; target-to-object distance, 30 cm.

During irradiation, the animals were not anesthetized, but were kept under restraint by means of elastic bandages. The region of the gills was covered with a thin layer of moist cotton held in place with an elastic bandage. The animals were placed on a piece of cardboard covered with waxed paper and several layers of moistened filter paper. Body areas not to be irradiated were shielded with a lead covering made from a sheet of lead 4 mm. thick, with a round radiation localizer 6.5 cm. in diameter.[2] During irradiation, the animals were arranged in radial positions within a circle. Immediately after irradiation, the animals were put into water.

For histologic studies, animals were sacrificed, and tissues were fixed in Stieve's acetic mercuric chloride formalin.[18] Specimens were embedded in paraffin containing 5 per cent beeswax, and were sectioned at 8 $\mu$. The sections were stained with Ehrlich's hematoxylin and eosin, and photomicrographs were made under small ($\times$170) and large ($\times$570) magnifications.

## NORMAL OLFACTORY CHAMBERS IN THE ADULT AXOLOTL

The olfactory chambers are large organs that take up considerable space in the anterior portion of the head of the normal adult axolotl. The large interior cavities of the olfactory chambers are connected through the nostrils to the water of the exterior environment. Most of the interior surface of the olfactory chambers is covered with a specialized and sensitive type of epithelium, the olfactory epithelium. This type of epithelium has a characteristic structure, and includes many sensitive buds of various sizes (Fig. 2 and 3). The olfactory sensitive buds are modifications of the cutaneous sensitive buds distributed in some regions of the skin. They have a rich nerve supply.

The olfactory epithelium is stratified, columnar, and ciliated. In this kind of epithelium, it is typical for the most proximal (basal) layers to have round nuclei, the less proximal to have an intermediate type of nuclei, the several more distal layers to have nuclei that are comparatively large and elongated, and the most distal portion to be almost without nuclei. In this last "anucleate" portion, usually only a few isolated nuclei can be observed (Fig. 1–3). Ordinarily the distal portion of an olfactory bud is much narrower than the basal, and the cilia-covered distal surface facing the interior of the olfactory chamber is concave (Fig. 1–3).

Usually, each olfactory sensitive bud is separated from neighboring buds by septa. These septa consist of loose connective tissue with many blood vessels, especially capillaries, and pigment cells (Fig. 2 and 3). Very typical is the epithelium that covers the distal portion of the septa. This is interstitial epithelium, which is very different from the olfactory epithelium of the sensitive buds. The interstitial epithelium is also stratified, but it consists of large cells with large nuclei (Fig. 2, 3 and 5).

## EFFECTS OF IRRADIATION

For realistic evaluation of the effects of irradiation, it is necessary to take into consideration the major variations that occur in the response of the epithelium of the olfactory chambers. Such variations were observed in all cases, even after irradiation with the largest dose, 10,000 r. Various degrees of damage were observed not only in different animals irradiated with the same dose, but even in the same olfactory chamber. In a single irradiated olfactory chamber, it was possible to find normal epithelium, slightly damaged epithelium, and

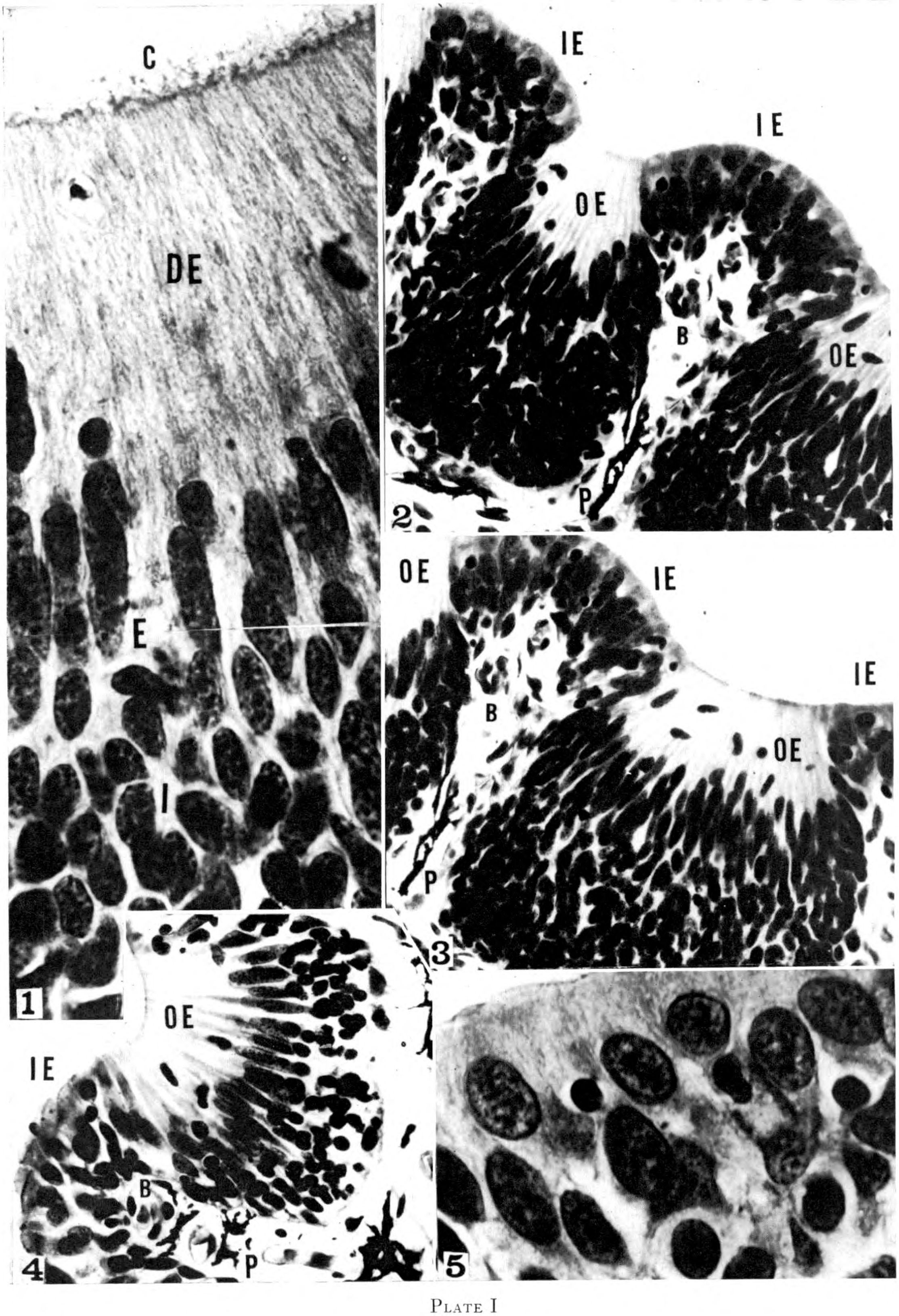


Plate I

very seriously damaged epithelium. This was highly typical, even after irradiation with maximum doses.

*1,000 r.* After irradiation with 1,000 r, definite changes in the irradiated olfactory chambers were not detectable. Grossly, the olfactory epithelium appeared normal (Fig. 4).

*3,000 r.* In many instances, the olfactory epithelium had a completely normal appearance after irradiation with 3,000 r. This was the case not only a short time after irradiation (Fig. 6), but also 76 days after (Fig. 8), and even 104 days after (Fig. 9). It is difficult, however, to explain the abnormal appearance of the interstitial epithelium 7 days after irradiation (Fig. 6). The cells have slightly enlarged nuclei (Fig. 7). It is possible that this development is a variation not connected with the radiation effect.

Slightly damaged olfactory epithelium was characterized by changes that occurred mostly in the distal portions (Fig. 10). Cell boundaries disappeared in many places, and the distal portion of the epithelium, which is usually almost without nuclei (Fig. 6, 8 and 9), was greatly reduced (Fig. 10).

Seriously damaged olfactory epithelium was characterized by complete disorganization of all layers and by complete absence of the distal "anucleate' portion. Typical interstitial epithelium was not visible (Fig. 11).

Various responses to irradiation with 3,000 r of the olfactory epithelium are illustrated in the case of an animal fixed 89 days after irradiation (Fig. 12–16). All of the photomicrographs involved are of sections of the same olfactory chamber. In some places the olfactory epithelium is normal, and in others it is only slightly damaged. There may be damage to the cytoplasm in the distal portions of the olfactory cells, with the appearance of many spaces and vacuoles (Fig. 12 and 14). In other places, the cell layers of the olfactory epithelium

←

Fig. 1–5. The normal olfactory epithelium of adult axolotl and the olfactory chamber of the adult axolotl after irradiation with 1,000 r.

Fig. 1. Part of the frontal section through the normal olfactory epithelium. C, cilia; DE, distal (anucleate) portions of olfactory cells; E, elongated nuclei of olfactory epithelium; I, intermediate type of nuclei of olfactory epithelium. Photomicrograph ×570.

Fig. 2 and 3. Various portions of the frontal section through the normal olfactory chamber of the adult axolotl. IE, interstitial epithelium; OE, olfactory epithelium; P, pigment cells; B, blood vessel. Photomicrographs ×170.

Fig. 4. Part of the frontal section through the olfactory chamber of adult axolotl 104 days after irradiation with 1,000 r. B, blood vessel; IE, interstitial epithelium; OE, olfactory epithelium; P, pigment cells. Photomicrograph ×170.

Fig. 5. Part of the section through the interstitial epithelium of olfactory chamber of normal adult axolotl. Photomicrograph ×570.

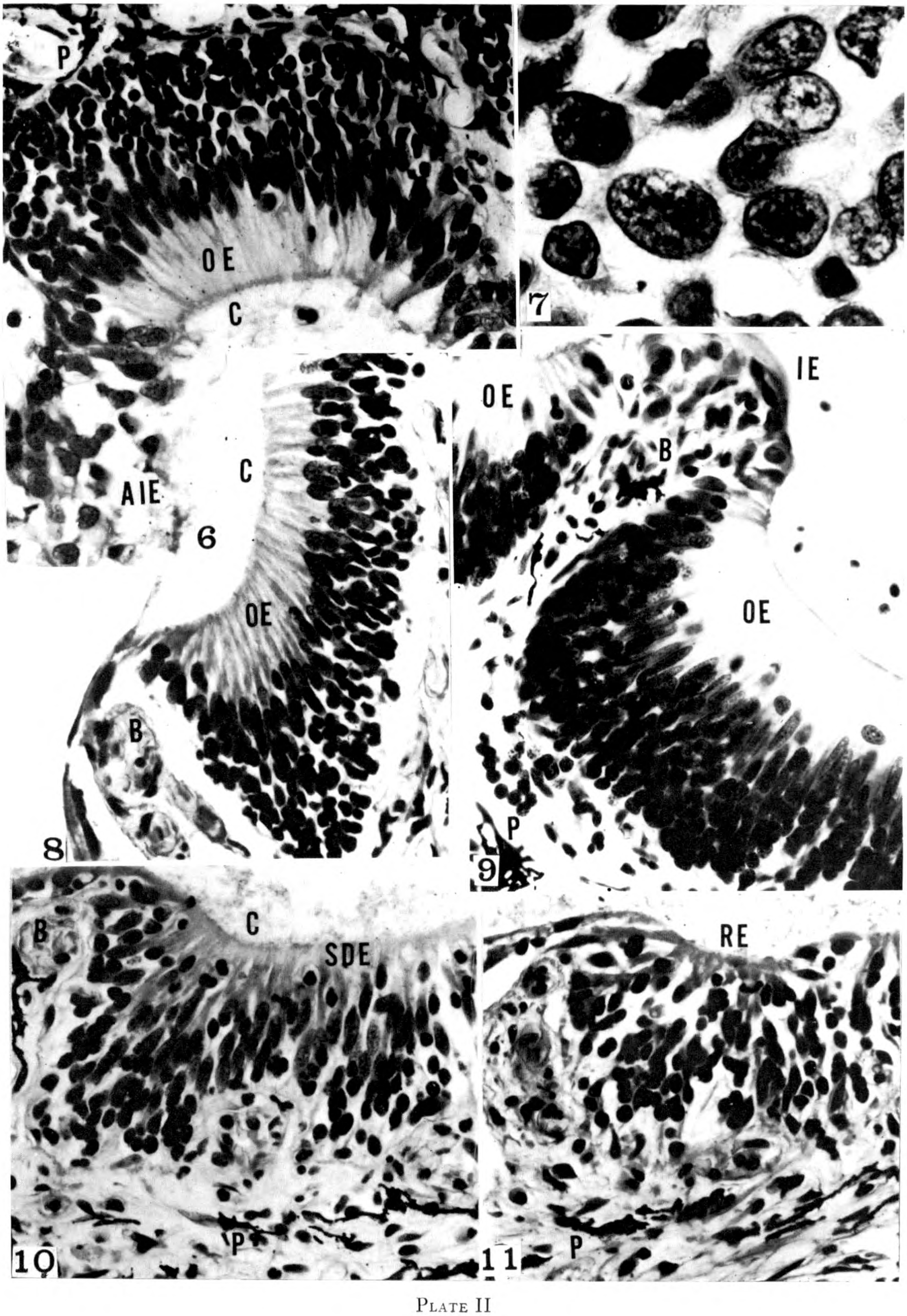


Plate II

are partially disorganized, and the number of cells is reduced (Fig. 14). In some places, more serious damage to the olfactory epithelium was observed. In some cases, most of the round cells disappeared (Fig. 15); in other cases, it was the large, elongated cells that almost all disappeared, the distal portion of the cytoplasm developing many spaces and an extremely atypical appearance (Fig. 13). Under large magnification (Fig. 16), it is possible to see the development of spaces and vacuoles, some pyknotic nuclei, and the formation of very small granules as a result of the destruction of nuclei.

*6,000 r.* In some places, the olfactory epithelium was normal after irradiation with 6,000 r (Fig. 17 and 26). Sometimes, when the olfactory epithelium was normal (Fig. 18) or only slightly damaged (Fig. 19), definite abnormalities developed in the interstitial epithelium. Nuclei became abnormally large (Fig. 18 and 19), and in some cases reached a truly giant size (Fig. 27). In some places, the interstitial epithelium became abnormally thick (Fig. 24). The area shown in Figure 24 still has the appearance of abnormally thick epithelium, but areas like that shown in Figure 28 exhibited a completely irregular expansion of mostly loose-connected atypical epithelial cells with abnormal nuclei, which might be very large or even of giant size.

Serious damage to the olfactory epithelium was characterized by reductions in the number of cells, disorganization in all layers, and disappearance of the distal "anucleate" portion (Fig. 22). In extreme cases, all typical structures disappeared, leaving behind only irregular clusters of otherwise isolated epithelial cells (Fig. 20 and 21).

Under large magnification, even slight damage to epithelial cells was clearly visible (Fig. 23, 25 and 29). Some of the nuclei became pyknotic. Such developments occurred 34 to 39 days after irradiation.

*8,000 r.* In some places, the olfactory epi-

FIG. 6–11. The olfactory chambers of adult axolotl after irradiation with 3,000 r.

FIG. 6 and 7. Various portions of the frontal section through the olfactory chamber of adult axolotl 7 days after irradiation with 3,000 r. AIE, abnormal interstitial epithelium; C, cilia; OE, olfactory epithelium; P, pigment cells. Photomicrographs: Fig. 6, ×170; Fig. 7, interstitial epithelium, ×570.

FIG. 8. Part of the section through the olfactory chamber of adult axolotl 76 days after irradiation with 3,000 r. B, blood vessel; C, cilia; OE, olfactory epithelium. Photomicrograph ×170.

FIG. 9. Part of the section through the olfactory chamber of adult axolotl 104 days after irradiation with 3,000 r. B, blood vessel; IE, interstitial epithelium; OE, olfactory epithelium; P, pigment cell. Photomicrograph ×170.

FIG. 10 and 11. Various portions of the frontal section through the olfactory chamber of adult axolotl 89 days after irradiation with 3,000 r. B, blood vessel; C, cilia; RE, remnants of olfactory epithelium; SDE, slightly damaged olfactory epithelium; P, pigment cells. Photomicrographs ×170.

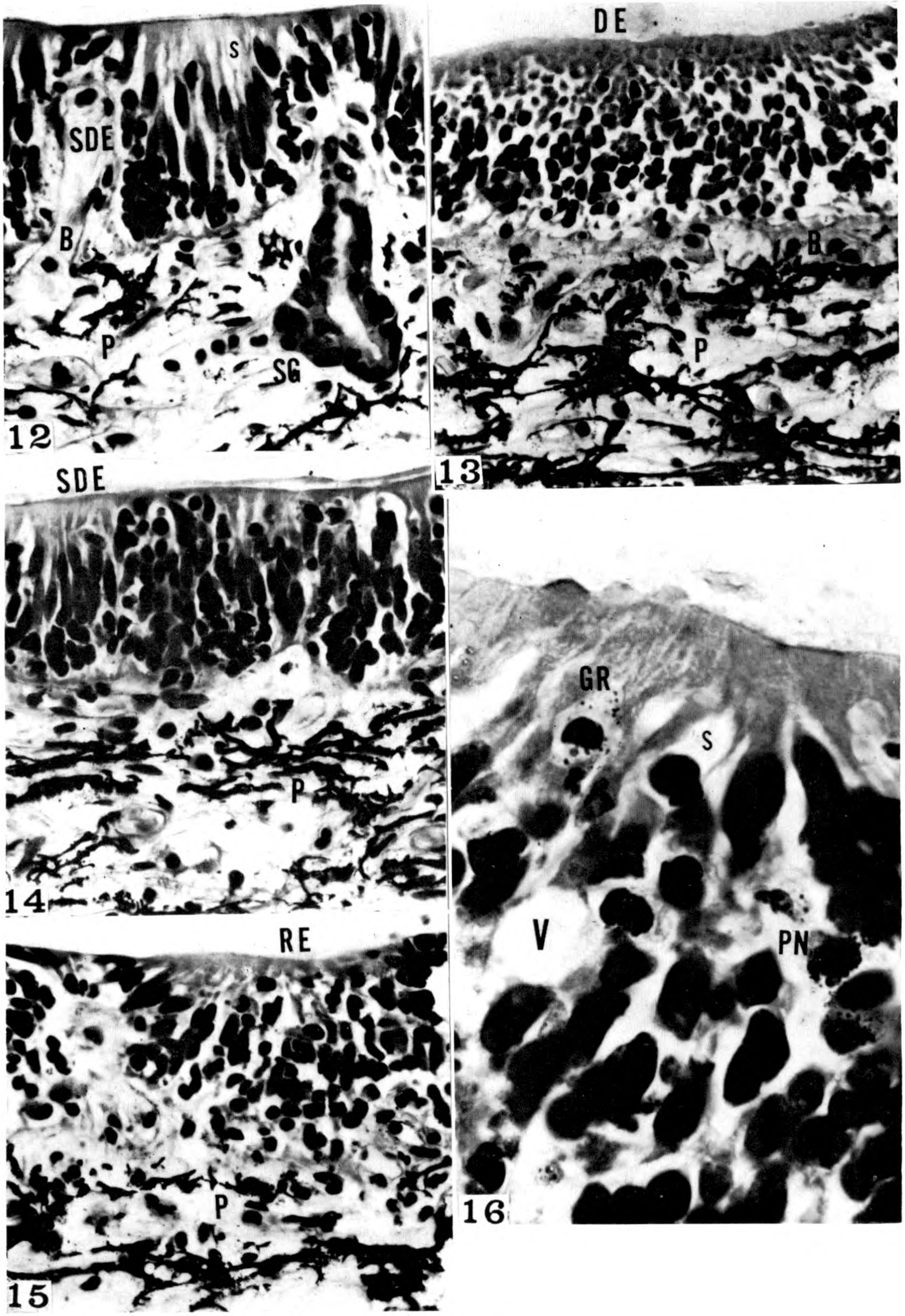


Plate III

thelium was normal after irradiation with 8,000 r (Fig. 34). In other places, it was only slightly damaged, with reductions in the number of cells, partial disorganization in the various layers, and reduction of the distal "anucleate" portion (Fig. 36).

Serious damage to the olfactory epithelium was characterized by the complete disappearance of the distal "anucleate" portion (Fig. 37–39). In some cases, the various layers of the epithelium underwent complete disorganization (Fig. 35). In other cases, the elongated cells disappeared almost entirely (Fig. 37). In many places, cells emigrated from the epithelium to the interior cavity of the olfactory chamber (Fig. 38 and 39).

Abnormal development of the interstitial epithelium, with enlargement of nuclei, was also observed after irradiation with 8,000 r (Fig. 30–32). Nevertheless, the interstitial epithelium never became as thick after 8,000 r as after 6,000 r and the nuclei never reached giant size (compare Fig. 33 with Fig. 27).

*10,000 r.* Even after irradiation with 10,000 r, it was possible to find completely normal olfactory epithelium in some places (Fig. 40 and 41). This was the case both 15 and 36 days after irradiation, the latent period being definitely over in the latter case. In the same olfactory chamber, however, it was also possible to find considerable damage to the epithelium (Fig. 42 and 44). This damage was of the same types as occurred after irradiation with smaller doses: reductions in the number of cells, disorganization of the various layers, and disappearance of the distal "anucleate" portion (Fig. 42 and 44). In some areas, the elongated cells disappeared completely (Fig. 45). Under large magnification, it is evident that some epithelial nuclei are definitely pyknotic (Fig. 43), and that some are considerably enlarged (Fig. 48).

Maximum damage was characterized by complete disorganization of the cells, major reductions in the numbers of cells, complete disappearance of the distal "anucleate" portion, and development of many irregular

←

Fig. 12–16. Various portions of the frontal section through the olfactory chamber of adult axolotl 61 days after irradiation with 3,000 r. B, blood vessel; DE, damaged olfactory epithelium; GR, granules; PN, pyknotic nucleus; S, spaces between the cells; SDE, slightly damaged olfactory epithelium; SG, subepithelial gland; RE, remnants of olfactory epithelium; P, pigment cells; V, vacuole. Photomicrographs: Fig. 12–15, ×170; Fig. 16, ×570.

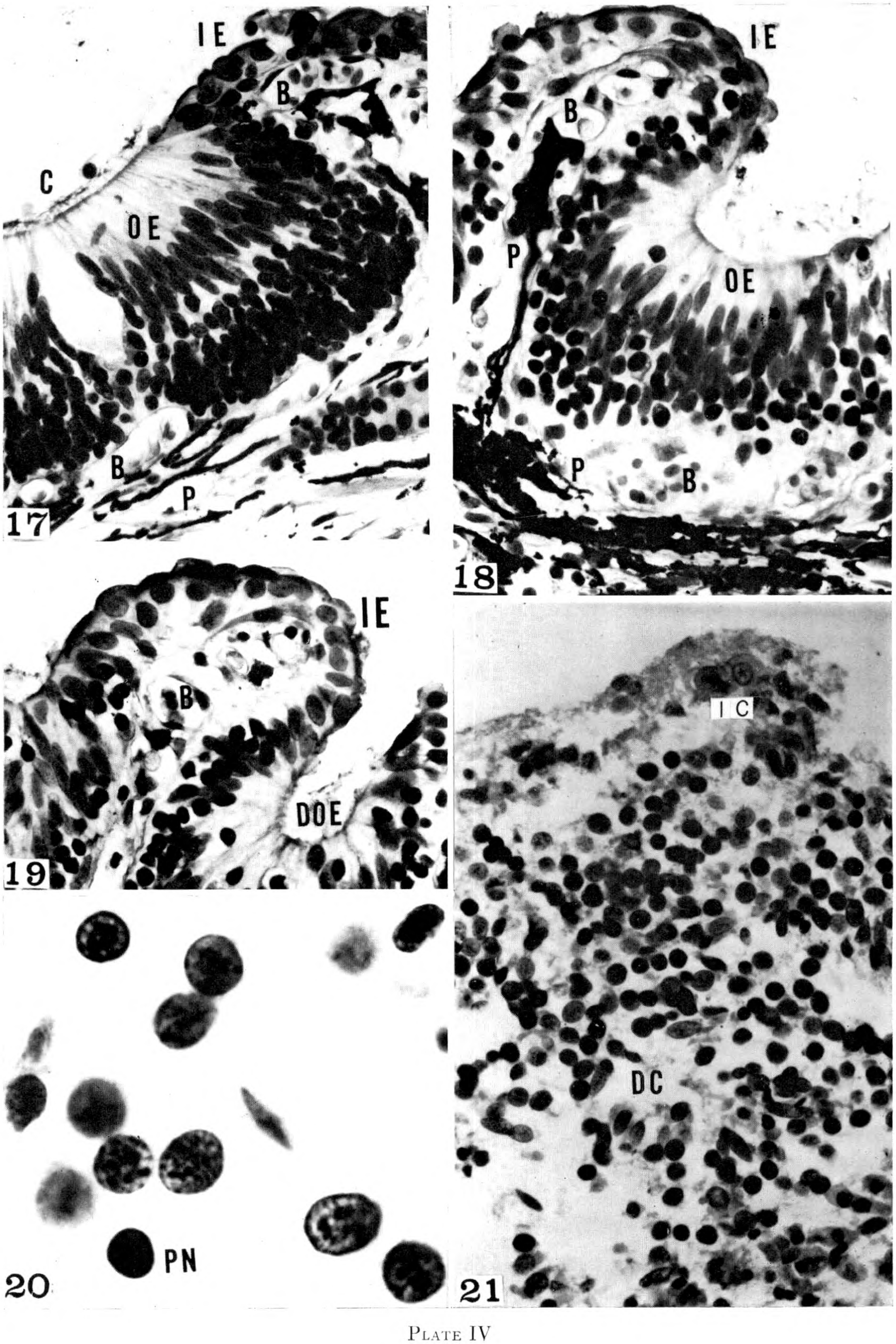


Plate IV

spaces among the cells. The appearance of the olfactory epithelium was radically changed; it looked much less like epithelium and more like loose connective tissue. This loss of the structure typical of epithelium is due to the destruction of a large number of cells, together with the resultant progressive loosening of the factors holding the cells together. Such a development could be observed even when the damage was comparatively slight (Fig. 46); the changes were especially obvious when the damage was appreciable (Fig. 42 and 47). Associated with the loosening process was a migration of the epithelial cells: partly from one layer of the epithelium to another, resulting in mixture of the various layers; and partly from the epithelium to the interior cavity of the olfactory chamber (Fig. 46).

The loosening process was typical of roentgen damage to not only olfactory but also interstitial epithelium. It could be observed in some parts of the interstitial epithelium even more clearly than in the olfactory epithelium (Fig. 46). The progressive reduction of connections and development of spaces and vacuoles between the cells was characteristic (Fig. 49–51). The nuclei of the interstitial cells became enlarged, but did not reach giant size.

## DISCUSSION

In axolotls, the olfactory epithelium is obviously far more resistant to roentgen radiation in adults than in young animals. In the latter, the olfactory epithelium is one of the most radiosensitive of all areas of the head, and truly normal olfactory epithelium was never found after irradiation.[7] In adult axolotls, however, normal olfactory epithelium was still present after irradiation with any dose, including the largest (10,000 r). In 27.7 per cent of the young animals irradiated, the olfactory epithelium completely disappeared, and was replaced by typical skin epithelium with many Leydig cells.[7] Complete disappear-

←

Fig. 17–21. The olfactory chambers of adult axolotls after irradiation with 6,000 r.

Fig. 17. Part of the section through the olfactory chamber of adult axolotl 13 days after irradiation with 6,000 r. B, blood vessel; C, cilia; IE, interstitial epithelium; OE, olfactory epithelium; P, pigment cells. Photomicrograph ×170.

Fig. 18 and 19. Various portions of the frontal section through the olfactory chamber of adult axolotl 32 days after irradiation with 6,000 r. B, blood vessel; DOE, damaged olfactory epithelium; IE, interstitial epithelium; OE, olfactory epithelium; P, pigment cells. Photomicrographs ×170.

Fig. 20 and 21. Various portions of the frontal section through the olfactory chamber of adult axolotl 44 days after irradiation with 6,000 r. DC, disarranged cells of olfactory epithelium; IC, isolated cells of interstitial epithelium; PN, pyknotic nucleus. Photomicrographs: Fig. 20, ×570; Fig. 21, ×170.

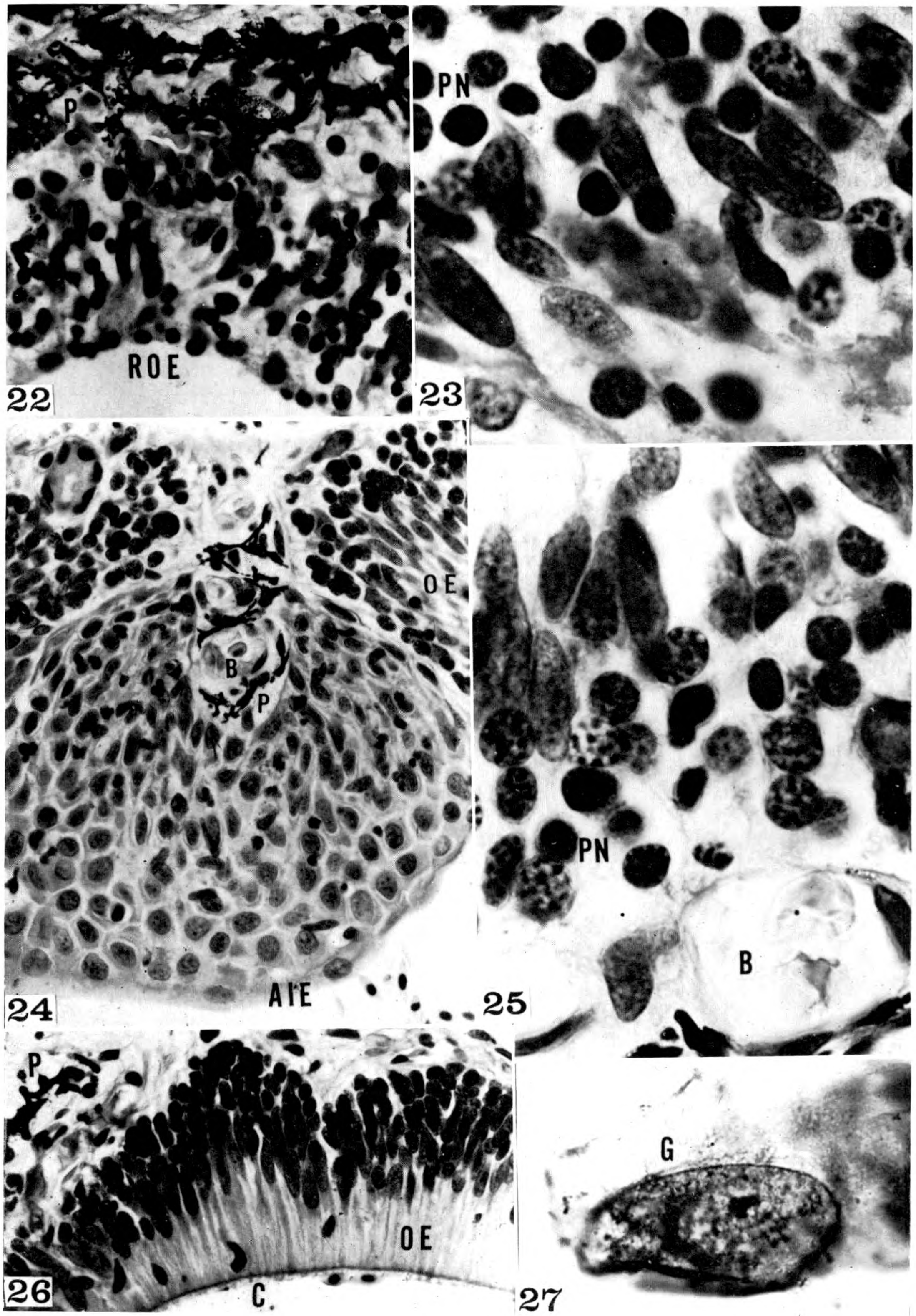


Plate V

ance of olfactory epithelium and its replacement with skin epithelium were never observed in irradiated adult animals.

In 54.3 per cent of the irradiated young axolotls, the olfactory epithelium did not disappear, but underwent major damage. In none of the irradiated adults, not even those exhibiting the greatest damage, were the olfactory chambers completely damaged; some areas were damaged only moderately, and others not at all. This was the case in spite of the fact that the adult animals were irradiated with much larger doses, the maximum for the young animals being 6,000 r and that for the adults being 10,000 r.

In young axolotls, the olfactory epithelium is more radiosensitive than the cornea;[9] but, in adult animals, the cornea is much more radiosensitive than the olfactory epithelium. In adult axolotls, irradiation of the cornea with even a minimum dose of 1,000 r gave definite results, comprising a thickening of the corneal epithelium and the development of Leydig cells and melanophores;[11] but irradiation of the olfactory epithelium with the same dose produced no observable effect, the tissue remaining completely normal. Irradiation of the cornea with 6,000 to 10,000 r was followed by severe damage: the substantia propria underwent thickening and stratification, and blood vessels penetrated into it; the epithelium became much thicker, and giant cells, melanophores, and Leydig cells developed; and sometimes the corneal epithelium disappeared and was replaced with skin epithelium. Irradiation of the olfactory epithelium with 6,000 to 10,000 r, however, was followed only by variable results, ranging from severe damage down to no visible effect whatever.

The axolotl cornea has almost the same sensitivity in adults as in young animals, but the response is somewhat different. The formation of Leydig cells and pigment cells in the corneal epithelium occurs in both young and adult axolotls; but the

←

Fig. 22–27. The olfactory chambers of adult axolotls after irradiation with 6,000 r.

Fig. 22–26. Various portions of the frontal section through the olfactory chamber of adult axolotl 39 days after irradiation with 6,000 r. AIE, abnormal interstitial epithelium; C, cilia; B, blood vessel; OE, olfactory epithelium; P, pigment cells; PN, pyknotic nucleus; ROE, remnants of olfactory epithelium. Photomicrographs: Fig. 22, 24 and 26, ×170; Fig. 23 and 25, ×570.

Fig. 27. Part of the section through the olfactory chamber of adult axolotl 36 days after irradiation with 6,000 r. G, giant nucleus in interstitial epithelium. Photomicrograph ×570.

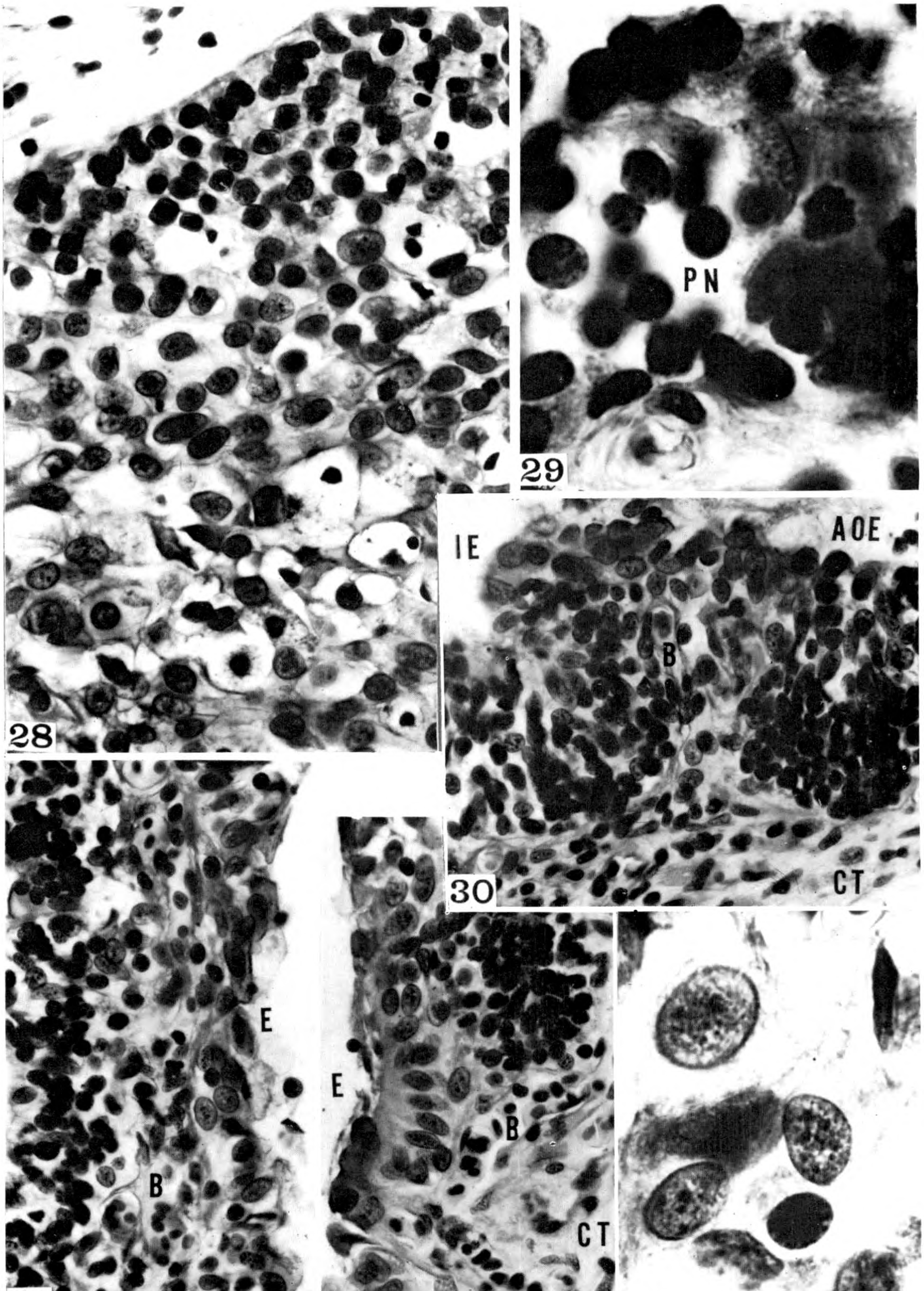


PLATE VI

development of an uneven outer surface and the formation of abnormal outgrowths occur only in the young animals, and the development of melanophores and blood vessels in the substantia propria occurs only in the adults.

The observed facts make it possible to draw certain general conclusions. In axolotls, the radiosensitivity of a specific type of tissue is a function of the age of the animal as well as of the type of tissue; but the radiosensitivities of different types of tissue vary with age in different ways. Thus, some types of tissues have much the same sensitivities in adults as in young animals, whereas other types are far less sensitive in adults.

In various animals, the radioresistance of the liver is remarkable. A dose greater than 12,000 r is needed in order to cause significant injury, and some liver cells remain uninjured even after exposure to as much as 60,000 r.[17] At the other extreme is the lens of the eye of the mouse, which has been found to be sensitive to doses as small as 15 r.

In young axolotls, radiation produces the most severe damage in lymph nodes, connective tissue, skin and gill epithelium, cloacal epithelium, kidney epithelium, and the spleen; the spinal cord, however, is the most resistant.[7] In adult axolotls, the most severe damage occurs in the lymphatic tissue in the peripheral portion of the liver, as well as in the spleen, in intestinal epithelium, and in gill epithelium.[6]

The comparative radiosensitivities of different tissues in axolotls and various mammals have been studied in several laboratories.[14,16,20,21] All of the investigators found that the most radiosensitive tissue is that of the lymph nodes, and nearly all found that the most resistant is that of the nervous system.

Recent investigations emphasize the extreme radiosensitivity of early embryos. According to Hammer-Jacobsen,[15] as little as 1 to 10 r administered to a fetus is sometimes able to cause such injuries as

←

Fig. 28–33. The olfactory chambers of adult axolotls after irradiation with 6,000 and 8,000 r.

Fig. 28 and 29. Various portions of the frontal section through the olfactory chamber of adult axolotl 34 days after irradiation with 6,000 r.

Fig. 28. Abnormal thickening of interstitial epithelium. Photomicrograph ×170.

Fig. 29. PN, pyknotic nucleus. Photomicrograph ×570.

Fig. 30–33. Various portions of the frontal section through the olfactory chamber of adult axolotl (albino) 37 days after irradiation with 8,000 r. AOE, abnormal olfactory epithelium; B, blood vessel; CT, loose connective tissue; E, abnormal interstitial epithelium; IE, interstitial epithelium. Photomicrographs: Fig. 30–32, ×170; Fig. 33, ×570.

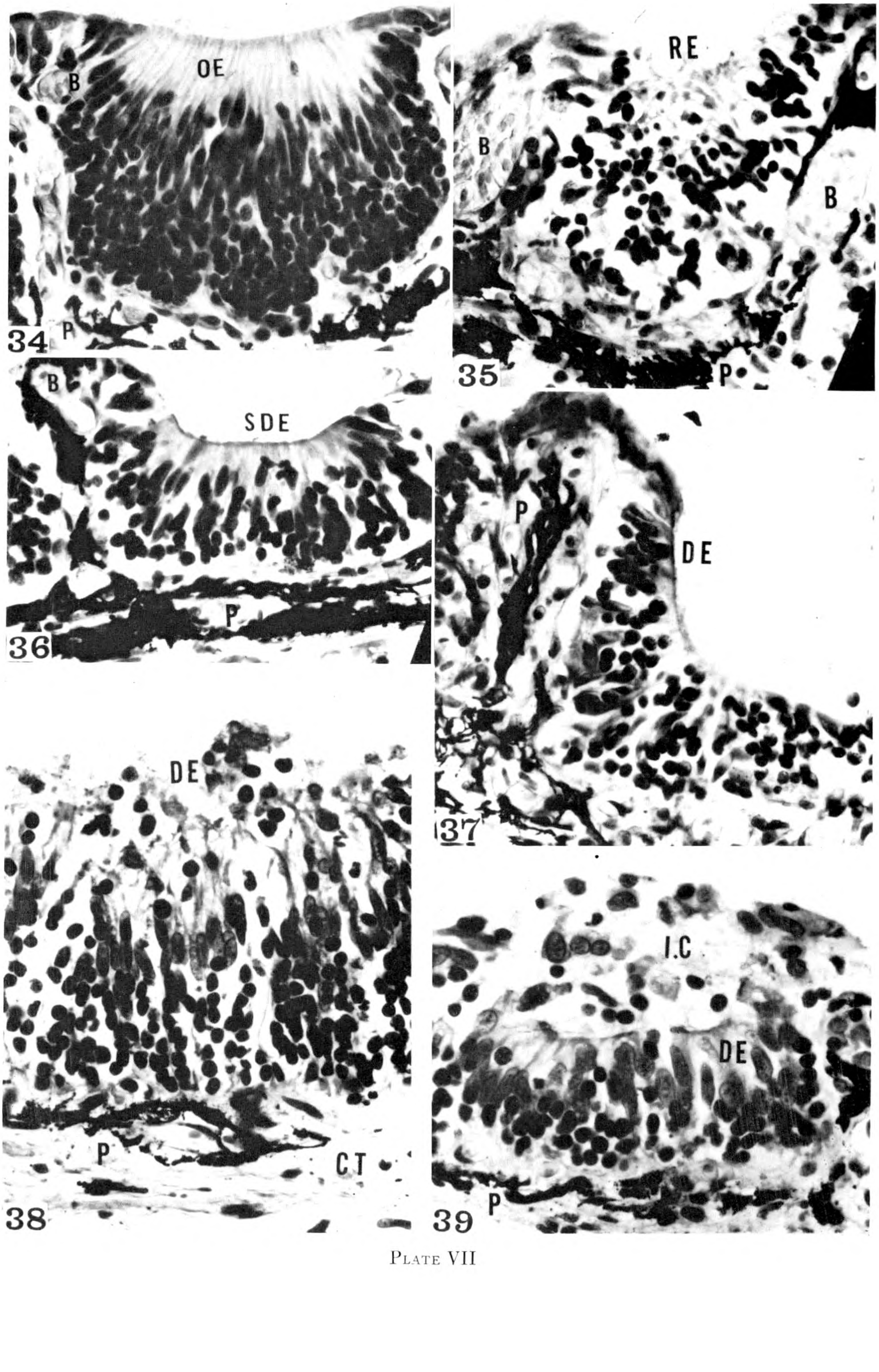


PLATE VII

malformation, slow development, or reduced resistance. "The embryo can be killed by irradiations which for any species are less than the lethal dose for the adult," says Rugh,[19] "and congenital effects may be produced by exposures of about 2 per cent of that of the $LD_{50/30}$ level."

In grasshopper neuroblasts, reports Carlson,[13] as little as 3 r will reduce mitosis to 25 per cent of normal, and 16 r reduces it almost to zero in less than an hour. "Cells vary enormously in their ability to survive ionizing radiations," comments Carlson,[13] "and this seems to have no relation to the mitotic effect of the radiation. It requires, for example, 72 r to depress mitosis in cells of the developing rat retina to approximately the same extent as 8 r depresses it in the grasshopper neuroblast. On the other hand, 72 r kills approximately 11 per cent of the developing rat retina cells as determined 6 hours after treatment, while 10,000 r produces virtually no deaths of grasshopper neuroblasts within at least 8 hours after treatment."

The abnormally extensive development of the interstitial epithelium following irradiation can be considered a result of roentgen stimulation. This phenomenon need not be discussed here, since it has been discussed at great length in previous publications.[1,3–5,8,9,12]

## SUMMARY

1. The anterior portion of the head was irradiated in 70 adult axolotls (*Siredon mexicanum*), 4 to 5 years old, 1,000 r being administered to 10 animals, 3,000 r to 20, 6,000 r to 20, 8,000 r to 10, and 10,000 r to 20; 5 animals served as untreated controls. Specimens fixed at various intervals following irradiation were studied histologically.

2. After irradiation with 1,000 r, the olfactory epithelium appears normal.

3. After irradiation with 3,000 r, the olfactory epithelium appears normal in many places. Elsewhere in the olfactory epithelium there may be slight damage, characterized by reduction of the distal "anucleate" portion, or serious damage, characterized

←

Fig. 34–39. The olfactory chambers of adult axolotls after irradiation with 8,000 r.

Fig. 34. Part of the section through the olfactory chamber of adult axolotl 32 days after irradiation with 8,000 r. B, blood vessel; OE, olfactory epithelium; P, pigment cell. Photomicrograph ×170.

Fig. 35–37. Various portions of the frontal section through the olfactory chamber of adult axolotl 30 days after irradiation with 8,000 r. B, blood vessel; DE, damaged olfactory epithelium; P, pigment cells; SDE, slightly damaged olfactory epithelium. Photomicrographs ×170.

Fig. 38–39. Various portions of the frontal section through the olfactory chamber of adult axolotl 35 days after irradiation with 8,000 r. CT, connective tissue; DE, damaged olfactory epithelium; IC, isolated cells emigrated from the epithelium. Photomicrographs ×170.

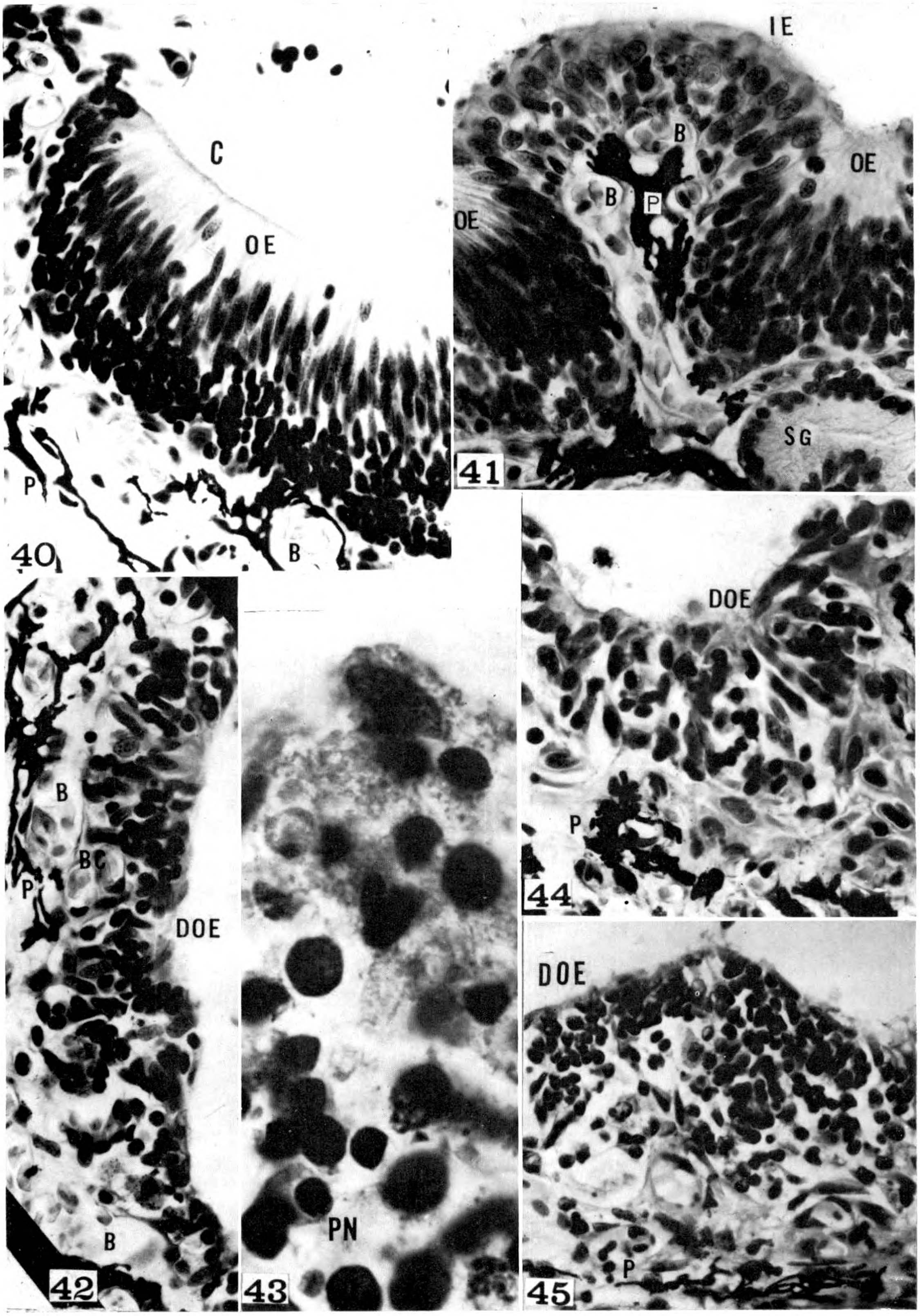


Plate VIII

by complete disorganization of all layers and disappearance of the "anucleate" portion.

4. After irradiation with 6,000 r, the olfactory epithelium appears normal in some places. Occasionally, the interstitial epithelium undergoes abnormal developments, becoming unusually thick, with very large or even giant nuclei. Serious damage to the olfactory epithelium is characterized by reductions in the number of cells, disorganization of all layers, and disappearance of the distal "anucleate" portion.

5. After irradiation with 8,000 or 10,000 r, the olfactory epithelium appears normal in some places. Elsewhere in the olfactory epithelium, there may be the same kinds of damage as occur after irradiation with smaller doses.

6. In axolotls, the olfactory epithelium is far more radioresistant in adults than in young animals. In the latter, the olfactory epithelium is one of the most radiosensitive areas of the head.

7. The olfactory epithelium is more radiosensitive than the cornea in young animals, but the reverse is true in adults.

8. The radiosensitivities of different tissues vary with age in different ways. Some tissues have much the same radiosensitivities in adults as in young animals, whereas others are far less sensitive.

Laboratory of Radiobiology
Roswell Park Memorial Institute
Buffalo, New York

REFERENCES

1. Brunst, V. V. Influence of local x-ray treatment on development of extremities of young axolotl (Siredon mexicanum). *J. Exper. Zool.*, 1950, *114*, 1–49.
2. Brunst, V. V. Technics of local low voltage roentgen ray irradiation of experimental animals. *Lab. Invest.*, 1952, *1*, 432–438.
3. Brunst, V. V. Problem of roentgen stimulation. Am. J. Roentgenol., Rad. Therapy & Nuclear Med., 1952, *68*, 281–289.
4. Brunst, V. V. Reaction of skin epithelium of tails of Rana catesbiana tadpoles to local x-irradiation. *Radiation Res.*, 1955, *2*, 556–567.
5. Brunst, V. V. Histopathology of roentgen death of young axolotl (Siredon mexicanum). Am. J.

Fig. 40–45. The olfactory chambers of adult axolotls after irradiation with 10,000 r.

Fig. 40, 42 and 44. Various portions of the frontal section through the olfactory chamber of adult axolotl 36 days after irradiation with 10,000 r. B, blood vessel; C, cilia; DOE, damaged olfactory epithelium; OE, olfactory epithelium; BC, blood capillary; P, pigment cells. Photomicrographs ×170.

Fig. 41. Part of the section through the olfactory chamber of adult axolotl 15 days after irradiation with 10,000 r. B, blood vessel; IE, interstitial epithelium; OE, olfactory epithelium; P, pigment cells; SG, subepithelial gland. Photomicrograph ×170.

Fig. 43. Part of the section through the olfactory chamber of adult axolotl 44 days after irradiation with 10,000 r. PN, pyknotic nuclei. Photomicrograph ×570.

Fig. 45. Part of the section through the olfactory chamber of adult axolotl 30 days after irradiation with 10,000 r. DOE, damaged olfactory epithelium; P, pigment cells. Photomicrograph ×170.

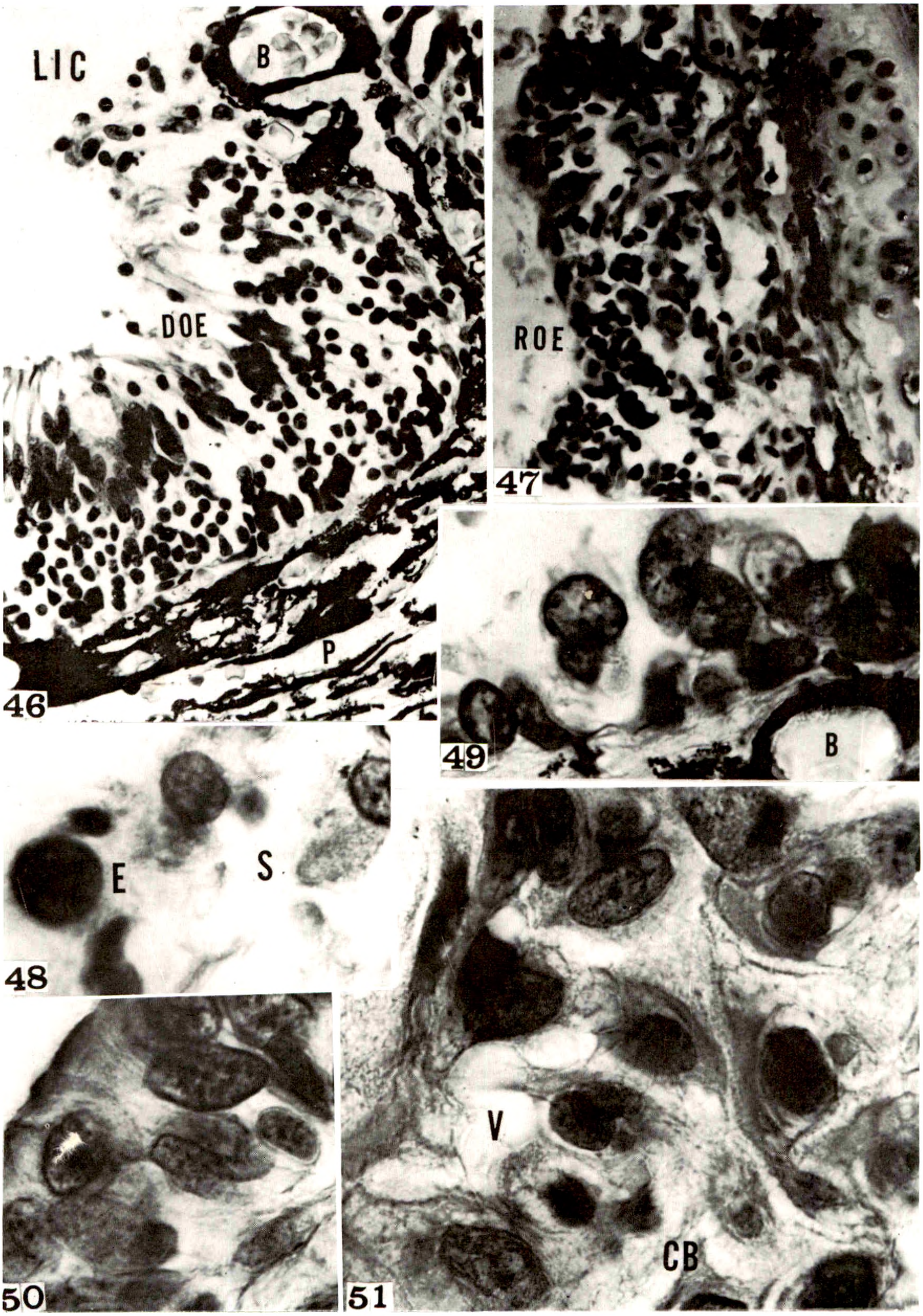


Plate IX

Roentgenol., Rad. Therapy & Nuclear Med., 1957, *78*, 518–545.

6. Brunst, V. V. Effect of different doses of roentgen rays on adult axolotl (Siredon mexicanum). Am. J. Roentgenol., Rad. Therapy & Nuclear Med., 1958, *80*, 126–142.
7. Brunst, V. V. Further investigation of effect of roentgen irradiation upon development of head of young axolotl. Am. J. Roentgenol., Rad. Therapy & Nuclear Med., 1959, *82*, 708–719.
8. Brunst, V. V. Roentgen regression and roentgen stimulation in axolotl (Siredon mexicanum). *Acta Unio internat. contra cancrum*, 1959, *15*, 568–576.
9. Brunst, V. V. Successive changes in cornea of young axolotl (Siredon mexicanum) after x-irradiation. *Radiation Res.*, 1963, *20*, 325–340.
10. Brunst, V. V. Successive changes in skin epithelium of young axolotl (Siredon mexicanum) after roentgen irradiation. Am. J. Roentgenol., Rad. Therapy & Nuclear Med., 1963, *89*, 624–647.
11. Brunst, V. V. Response of cornea of adult axolotl (Siredon mexicanum) to x-radiation. To be published.
12. Brunst, V. V., and Figge, F. H. J. Development of secondary tails in young axolotls after local x-ray irradiation. *J. Morphol.*, 1951, *89*, 111–113.
13. Carlson, J. G. Immediate cytological effects of ionizing radiations. *Bios*, 1958, *29*, 106–117.
14. Desjardins, A. U. Radiosensitiveness of cells and tissues, and some medical implications. *Arch. Surg.*, 1932, *25*, 926–942.
15. Hammer-Jacobsen, E. Therapeutic abortion on account of x-ray examination during pregnancy. *Danish M. Bull.*, 1959, *6*, 113–122.
16. Henshaw, P. S., and Snider, R. S. Correlation of tissue responses following exposure to penetrating radiations. *M.D.D.C.*, 1946, 569, (U. S. Atomic Energy Comm.)
17. Koletsky, S., and Gustafson, G. Liver damage in rats from radioactive colloidal gold. *Lab. Invest.*, 1952, *1*, 312–323.
18. Romeis, B. Mikroskopische Technik. Leibniz Verlag, München, 1948.
19. Rugh, R. Major radiobiological concepts and effects of ionizing radiation on embryo and fetus. In: Response of the Nervous System to Ionizing Radiation. Edited by T. J. Haley. Academic Press, Inc., New York, 1962.
20. Schlumberger, H. G., and Vasquez, J. J. Pathology of total body irradiation in monkey. *Am. J. Path.*, 1954, *30*, 1013–1047.
21. Warren, S. Histopathology of radiation lesions. *Physiol. Rev.*, 1944, *24*, 225–238.

---

Fig. 46–51. The olfactory chambers of adult axolotls after irradiation with 10,000 r.

Fig. 46. Part of the section through the olfactory chamber of adult axolotl 10 days after irradiation with 10,000 r. B, blood vessel; DOE, damaged olfactory epithelium; P, pigment cells. Photomicrograph × 170.

Fig. 47. Part of the section through the olfactory chamber of adult axolotl 30 days after irradiation with 10,000 r. ROE, remnants of olfactory epithelium. Photomicrograph ×170.

Fig. 48. Some of olfactory cells of adult axolotl 44 days after irradiation with 10,000 r. E, enlarged cell nucleus; S, spaces between the cells. Photomicrograph ×570.

Fig. 49–51. The interstitial epithelium 10, 15 and 36 days after irradiation with 10,000 r. CB, cell border; V, vacuoles in cytoplasm and between the cells. Photomicrographs ×570.

# INTERNAL $Sr^{90}$ BETA-RAY DOSIMETRY WITH FLUORODS*

*By* JACOB KASTNER, PH.D., DONALD R. ROBERTS, M.A., *and* WILLIAM PREPEJCHAL, B.E.E.†
ARGONNE, ILLINOIS

SCHULMAN-ETZEL[9,24] fluorod dosimeters have been employed for the measurement of $Sr^{90}$, $Y^{90}$, beta-ray dose *in vivo* and *in vitro*. The following is a description of the dosimetric problems associated with these fluorods.

## MEASUREMENT SYSTEM

Fluorods made from silver phosphate glass are now commercially available in the form of cylindrical rods 1 mm. in diameter and 6 mm. long. The Bausch and Lomb (B and L) Optical Company manufactures both high- and low-Z* (lithium phosphate) glass rods whose output was determined with their "microdosimeter reader."[6]

Very early in our work it was determined that the high-Z rods gave nonreproducible data and also faded quickly. The low-Z rods, however, are relatively permanent and some institutions routinely locate these fluorods in personnel film badge holders as additional monitors.[10] Measurements were also made with Toshiba[20] low-Z fluorods which were read using the B and L instrument. The chuck (rod-holder) of this instrument was modified to provide a firmer grip and thus more reproducible data even though the sensitivity was somewhat reduced in the process (see Appendix).

The rods must be carefully cleaned before reading. For example, we use a succession of rinses in acetone, distilled water, and alcohol, or, alternatively, an ultrasonic bath in soap solution followed by rinsing in water and alcohol. After the rod is placed in the chuck, it must be dusted by a puff of dry air.

Prior to reading the fluorod, the open chuck background was determined for each range. This value was subtracted from the mean of replicate fluorod readings to determine the photoluminescent output. In this work the pre-dose luminescence for each rod was subtracted from the final reading, but in most cases of biological interest the use of a pre-dose value, which is the mean for a batch, seems sufficiently precise.

A 2 hour wait after exposure was sufficient to provide essential stability. The "Reader" was on for about an hour before measurements were made and its stability was checked periodically by means of the photoluminescence from manganese-doped glass standards.[8]

* Bausch and Lomb Microdosimeter, Catalog No. 33-66-00.

## $Co^{60}$ GAMMA-RAY CALIBRATION

Fluorods, in cylindrical lucite holders with 4 mm. thick walls, were exposed to various doses in the high intensity $Co^{60}$ gamma facility of the Division of Biological and Medical Research. Figure 1 shows the relationship of instrument fluorescent units to the $Co^{60}$ gamma ray absorbed dose in rads. Over the region of interest, the mean ratio of fluorescent units (F.U.) to $Co^{60}$ dose in rads is: F.U./$\gamma$ rad$=0.67$. It should be noted, of course, that the specific ratio obtained is peculiar to the system used, and, furthermore, that the fluorescence is not really proportional to the dose over more than three decades.

## BETA-RAY CALIBRATION

Since there is a variation in beta flux through the internal volume of the dosimeter, the latter cannot be considered a point detector. For this reason the response of the dosimeter system per unit of dose received

* Work performed under the auspices of the U. S. Atomic Energy Commission.
† Radiological Physics Division, Argonne National Laboratory, Argonne, Illinois.

must be determined with the particular beta emitter being studied.

To provide isotropic $4\pi$ sources of $Sr^{90}-Y^{90}$, we first employed aqueous solutions of $SrCl_2$ with approximately 1 and 10 $\mu c$ per ml. The fluorods, in plastic tubing, were suspended so that the thickness of the surrounding solution exceeded the maximum range ($\sim$1 cm.) of the $Y^{90}$ beta rays. The results with these solutions were somewhat erratic and recourse was made to the use of gelatin molds containing a known concentration of $Sr^{90}$. These provided very reproducible and useful sources for delivering beta-ray doses in an isotropic manner and were made in the following way. The open gelatin surfaces were covered by a $\frac{1}{4}$-mil Mylar film and the complete molds were sprayed with a light acrylic coat. The molds were kept in glass sealers with some water on the bottom to provide 100 per cent humidity. Exposures and storage were carried out in a refrigerator at $+7°$ C. The gels have been stable and have provided reproducible data for more than a year and show no signs of deterioration. The use of thin plastic sleeves* to protect and hold the fluorods proved to be convenient and efficient and yet lowered the net fluorescence by less than 10 per cent. It is recommended that such sleeving be used in all tissue implants.

To verify the isotropic character of the gelatin system, the fluorescence of fluorods sandwiched between two beta-ray gelatin molds was compared with the fluorescent output when one of the molds was blank, *i.e.*, contained no activity. This was done for times varying from a couple of hours to as much as a week. In all cases the ratio of fluorescent output for $4\pi$ irradiation was almost exactly twice the $2\pi$ case. Furthermore, as can be seen in Figure 1, proportionality held over the complete range of measurements. The $Sr^{90}-Y^{90}$ dose rate was computed using the well-known relation[13]

$$R_\beta = 51.2\ \overline{E}_\beta\ C \text{ rad/day},$$

* Intramedic Polyethylene tubing, No. PE160, Clay-Adams, Inc., New York.

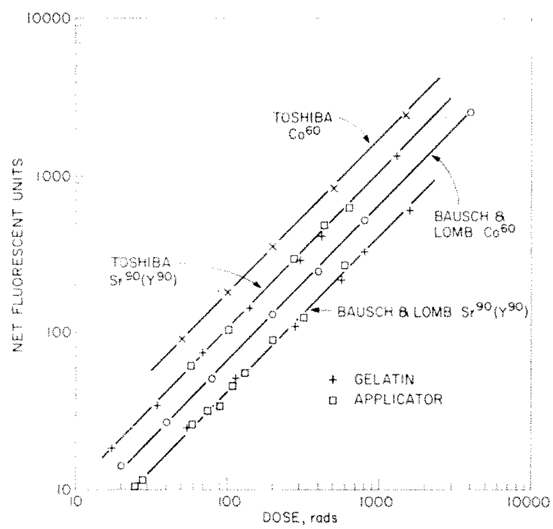


Fig. 1. Fluorod dosimeter fluorescence versus absorbed dose.

where $C$ is the concentration in $\mu c$/gm., $\overline{E}_\beta$ is the average beta-ray energy, 1.1 mev.

A measurement of $Sr^{90}$ concentration in the gelatin was made upon completion of the fluorod calibration to check the concentration of activity.

There is available in our laboratory a $Sr^{90}-Y^{90}$ beta-ray applicator which has been calibrated for dosage in a lucite phantom by Chhabra using a Failla extrapolation ion chamber.[7] We decided to use the $Y^{90}$ source to check the beta-ray response of the fluorods and, in particular, to simulate the nonuniform source distribution which obtains in therapeutic practice. A lucite holder was constructed to position the rods under the applicator with provision for various lucite absorbers. In this way, dose rates as well as exposure times could be varied over wide limits. As Figure 1 shows, the fluorescent response to the absorbed dose in rads was identical with that observed for the uniform irradiation supplied by the gelatin source. Furthermore, the response was proportional to the dose and independent of the dose rate over a range of at least two decades.

A summary of the responses of the fluorods to various sources is given in Table 1.

Although the Toshiba fluorods are 2.7 times as sensitive as the B and L dosime-

TABLE I

FLUORESCENT UNITS PER RAD

| | Bausch and Lomb | Toshiba | Tosh/ B and L |
|---|---|---|---|
| Cobalt 60 | 0.67 | 1.78 | 2.7 |
| Strontium 90 ($Y^{90}$) | 0.42 | 1.10 | 2.7 |
| $Sr^{90}/Co^{60}$ | 0.62 | 0.62 | |

ters, the beta-ray to gamma-ray response ratio is essentially the same in both despite their different glass composition. The density variation for the two glasses was less than 10 per cent.

The beta-gamma ratio of fluorescent response is in good agreement with the results of other workers[14,21] provided one corrects their data for the small extra dose contributed by the $Sr^{90}$ in their source.

The two glasses also behaved similarly

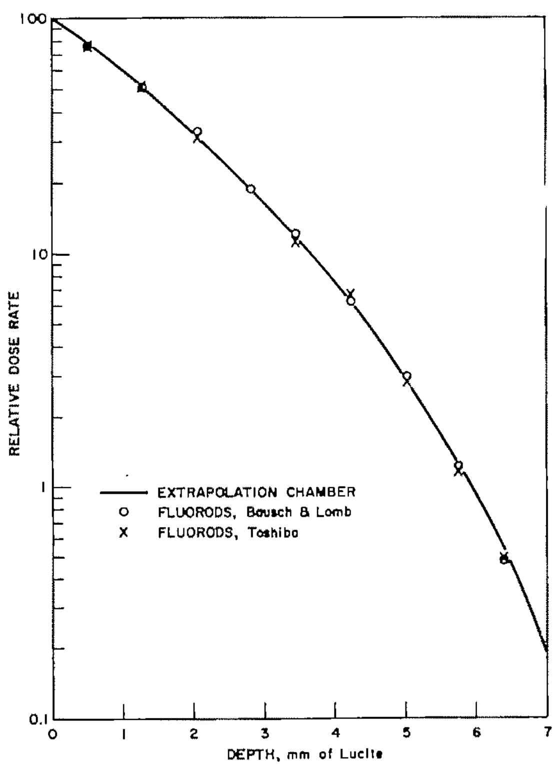


FIG. 2. Comparison of depth-dose measurements in lucite; fluorods versus extrapolation chamber.

with regard to relative fluorescent output versus depth in lucite. Figure 2 shows the excellent fit with Chhabra's extrapolation chamber data. Thus, even though the fluorods are *not* point detectors, they may give surprisingly useful information about beta-ray dose distributions. Incidentally, using the gelatin mold as a source of beta rays, one obtains the same depth dose curve in lucite as for the applicator. This observation, together with the identity of response for the two sources, implies similarity in their beta-ray spectra.

*Reader Geometry*. The possible effect of the geometry of excitation of luminescent centers by the B and L reader was checked by using another reading system which has been described by Barr *et al.*[1,2] We were fortunate to be able to borrow this apparatus from the Division of Biophysics of the Sloan-Kettering Institute. No significant difference was observed in the beta-gamma ratio of fluorescent response.

*Temperature Dependence*. Although we have not carried out extensive tests, the fluorods seem to be relatively insensitive to temperature in the range of 0 to 25°C. Barr,[2] and Miyanaga and Yamamoto[20] reported temperature coefficients of +0.4%/°C. and +0.2%/°C. for B and L and Toshiba fluorods, respectively. The maximum variation therefore can be no more than 10 per cent.

## CONCLUSION

The use of Schulman and Etzel fluorods for *in vivo* and *in vitro* dosimetry for $Sr^{90}$ beta rays and, for that matter, other beta rays is quite feasible, provided careful precalibration is carried out on a sample of the specific batch of dosimeters to be used. A reproducible technique for calibration employing gelatin phantoms is described. The convenience, in practice, of using such gelatin techniques for calibrating beta-ray applicators should not be overlooked. Comparison with the work of other laboratories can always be made if a $Co^{60}$ gamma-ray calibration is included.

The response is linear to dose over a large

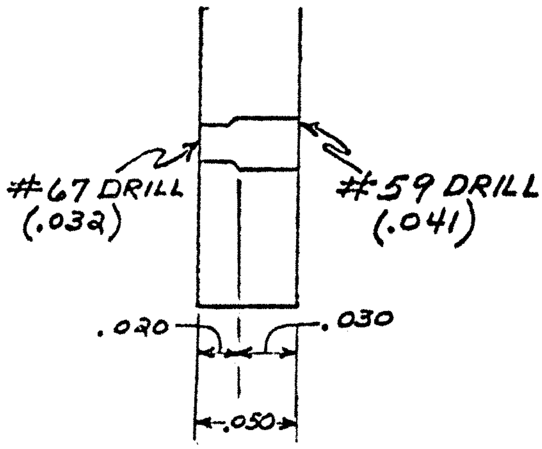


Fig. 3. Reader chuck modification.

range and is also independent of dose rate. If one uses low-Z fluorods, the fluorescence does not fade over many months and thus the dosage can be reread at any time. Of the two commercially available materials, the Toshiba fluorods are superior with regard to sensitivity and low pre-dose reading; however, both the Toshiba and the B and L products offer good reproducibility if the B and L reader is slightly modified to provide better alignment of the fluorods.

Jacob Kastner, Ph.D.
Radiological Physics Division
Argonne National Laboratory
9700 South Cass Avenue
Argonne, Illinois

It is a pleasure to acknowledge the encouragement and advice of Mr. L. D. Marinelli, Director of the Radiological Physics Division of this Laboratory. Stimulation of this work and fruitful discussion were also provided by Dr. L. Voyvodic of the High Energy Physics Division and Dr. A. M. Brues of the Division of Biological and Medical Research. We also appreciate the ingenuity of Mr. Edward Fudala in modifying the reader chuck, and the help of Mr. Billie G. Oltman in making some special scintillator measurements.

## APPENDIX

### MODIFICATION OF BAUSCH AND LOMB FLUOROD MICRODOSIMETER READER #33

Modification of the B and L reader chuck involves only the .055 inch stainless steel plate on the light source side of the chuck. The original plate is removed and used to locate all holes on a new plate (ours is .050 inch aluminum). All holes are drilled and counterbored to duplicate the original with the exception of the window which admits ultraviolet light to the rods. This hole is first drilled through with a #67 drill; then, from the photocell side, and to a full diameter depth of .030 inch, the hole is enlarged with a #59 drill (see Fig. 3). The fluorods will now sit in this hole to a depth of .030 inch. This is sufficient to maintain reproducible alignment. The small spring in the chuck still provides a firm grip for the rod.

Handling of the rods can also be made more efficient by clipping 5/16 inch-long sections of #PE 160 intermedic polyethylene tubing in a #88 Mueller Electric Co. battery clip, so that $\frac{1}{8}$ inch of tubing protrudes. The rods are slipped into the tubing from the chuck or from the rod holder and are firmly held by the tubing. The clips merely serve as handles and are not opened and closed.

## REFERENCES

1. Barr, N. F., Stark, M., and Laughlin, J. S. Comparison of two fluorometers designed to measure radiation-induced fluorescence of silver-activated glass rods. *Radiology*, 1961, *76*, 113–115.
2. Barr, N. F., Stark, M. B., Hands, J., and Laughlin, J. S. Dosimetry with small silver-activated glass rods. *Health Physics*, 1961, *7*, 48–53.
3. Becker, K. Phosphate glass for routine personnel monitoring. AEC-TR-5781, 1963.
4. Bernard, C. H., Thornton, W. T., and Auxier, J. A. Silver metaphosphate glass for x-ray measurements in coexistent neutron and γ-radiation fields. *Health Physics*, 1961, *4*, 236–243.
5. Blair, G. E. Applications of radiation effects in glasses in low- and high-level dosimetry. *J. Am. Ceramic Soc.*, 1960, *43*, 426–429.
6. Blair, G. E., Brumley, C. H., Meltzer, R. J., and Rood, J. L. Commercial microdosimeter uses glass fluorescence. *Nucleonics*, 1959, *17*, No. 9, 128–129.
7. Chhabra, A. S. $Sr^{90}-Y^{90}$ beta-ray (and bremsstrahlung) depth-dose measurements in lucite. *Radiology*, 1962, *79*, 1001–1007.
8. Degelman, J., Callahan, A. B., and Fulton, G. P. Improved fluorometer for miniature

glass rod radiation detectors. *Radiation Res.*, 1957, *6*, 548–553.
9. Etzel, H. W., and Schulman, J. H. Silver-activated alkali halides. *J. Chem. Phys.*, 1954, *22*, 1549–1554.
10. Gupton, E. D., Davis, D. M., and Hart, J. C. Criticality accident application of Oak Ridge National Laboratory badge dosimeter. *Health Physics*, 1961, *5*, 57–62.
11. Hamilton, J. F., Hamm, F. A., and Brady, L. E. Motion of electrons and holes in photographic emulsion grains. *J. Appl. Physics.*, 1956, *27*, 874–885.
12. Hayes, R. L., Nold, M. M., Comar, C. L., and Kakehi, H. Internal radiation dose measurements in live experimental animals. *Health Physics*, 1960, *4*, 79–85.
13. Hine, G. J., and Brownell, G. L., Editors. Radiation Dosimetry. Academic Press, Inc., New York, 1956, p. 824.
14. Hine, G. J., Hodara, M., and Friedman, M. Accuracy of fluorod dose measurements. *Radiology*, 1962, *78*, 44–48.
15. Hodara, M., Friedman, M., and Hine, G. J. Radiation dosimetry with fluorods. *Radiology*, 1959, *73*, 693–705.
16. Kondo, S. Neutron response of silver-activated phosphate glass. *Health Physics*, 1960, *4*, 21–31.
17. Lee, P. K., Ballinger, E. R., and Schweitzer, W. H. Heat treatment which extends usable range of $AgPO_3$ glass dosimeters. Los Alamos Report-LA-2575, September 13, 1961.
18. Malsky, S. J., Amato, C. G., and Reid, C. Miniature versatile dosimeter. IRE Trans. Med. Electronics ME-7, 1960, 193–196.
19. Malsky, S. J., Amato, C. G., Reid, C. B., Spreckels, C., and Maddalone, L. *In vivo* dosimetry with miniature glass rods. I. Physical aspects and recent developments. Am. J. Roentgenol., Rad. Therapy & Nuclear Med., 1961, *85*, 568–571.
20. Miyanaga, I., and Yamamoto, H. Studies on silver-activated metaphosphate glass on personnel monitoring dosimeter. *Health Physics*, 1963, *9*, 965.
21. Nold, M. M., Tapper, D. N., and Comar, C. L. $Cs^{137}$ dose measurements in tissue. II. *Health Physics*, 1962, *8*, 217–229.
22. Riegert, A. L., Johns, H. E., and Spinks, J. W. T. Ag-phosphate glass needles for measuring gamma dose. *Nucleonics*, 1956, *14*, 134–137.
23. Roswit, B. *In vivo* dosimetry with gold-sheathed miniature glass rods. II. Clinical applications in radiation therapy. Am. J. Roentgenol., Rad. Therapy & Nuclear Med., 1961, *85*, 572–582.
24. Schulman, J. H., and Etzel, H. W. Small-volume dosimeter for x-rays and gamma-rays. *Science*, 1953, *118*, 184–186.
25. Schulman, J. H., Ginther, F. J., Klick, C. C., Alger, R. S., and Levy, R. A. Dosimetry of x-rays and gamma-rays by radiophotoluminescence. *J. Appl. Physics.*, 1951, *22*, 1479–1487.
26. Schulman, J. H., Shurcliff, W., Ginther, R., and Attix, F. Radiophotoluminescence dosimetry system of the U. S. Navy. *Nucleonics*, 1953, *11*, 52–56.
27. Tapper, D. N., Nold, M. M., and Comar, C. L. $Cs^{137}$ dose measurements in tissue. I. *Health Physics*, 1962, *8*, 207–216.
28. Yokota, R., Nakajima, S., and Sakai, E. High sensitivity silver-activated phosphate glass for simultaneous measurement of thermal neutrons, $\gamma$ and/or $\beta$-rays. *Health Physics*, 1961, *5*, 219–224.

# USE OF PINHOLE CAMERA FOR TESTING UNIFORMITY OF BETA-RAY APPLICATORS

S. J. SUPE*
BOMBAY, INDIA

THE principle of the pinhole camera has been applied in a wide variety of problems. In the field of radiation physics, it has been extensively used in the determination of the focal spot size.[2,3,4,7,8,11] In fact, the technique is as old as the roentgen technique itself. It has been used: (a) in locating unknown sources of radiation arising from contamination;[16] (b) in determining the area from which secondary emission occurs in dental roentgenography;[10] and (c) in aligning roentgen tubes in their housing.[1] The method has also been applied in testing the uniformity of emission from the different parts of the target area in a roentgen tube.[2,6,7,14]

Kuntke[5] and Vuorinen[15] have discussed the inaccuracies which occur with the use of the pinhole method for roentgen rays due to penumbra, the tunnel effect and the size and shape of the pinhole. In the case of beta rays, additional errors arise due to: (1) bremsstrahlung; (2) significant electron scattering in air; and (3) the absorption by the thin foil covering the source in order to seal the source "in." There is, however, one favorable feature of this method in the case of beta rays. This is the fact that the "tunnel effect" correction for a given source can be made to depend simply on the tunnel diameter by fixing the tunnel length to be equal to the maximum range of beta rays in the material of the pinhole plate. This feature has not been widely investigated and the few studies reported so far[9] are confined to the determination of the size and shape of areas contaminated with beta emitting radioisotopes. The purpose of the author is to describe the construction and use of a pinhole camera for testing the uniformity of the beta emission from a plane beta source.

## CONSTRUCTION OF THE PINHOLE CAMERA

In a pinhole camera, the pinhole length must be kept to a minimum in order to minimize the tunnel effect. Hence, the use of high density material (usually also high Z) is necessary. This, however, leads to considerable bremsstrahlung emission. The bremsstrahlung contribution can be minimized, provided that (1) the thickness of the pinhole plate is much greater than the maximum range of the beta particles in the material of the plate (care being taken to ensure that the length of the pinhole is not more than the beta range in order to minimize the tunnel effect), and (2) a low Z material is appropriately interposed between the source and the pinhole plate.

Certain preliminary investigations have been carried out with a pinhole camera and a $Sr^{90}$ eye applicator. The experimental set-up is shown in Figure 1. The only modification in this set-up adopted for study of the bremsstrahlung contribution was that, instead of the pinhole plate, lead sheets of thicknesses varying from 1 mm. to 4 mm., but without pinholes, were used. This enabled us to estimate the extent of fogging of the film due to bremsstrahlung. The study was repeated with a 1 cm. thick perspex sheet interposed between the beta source and a 4 mm. thick lead plate. These results are shown in Figure 2. It can be seen from this graph that if a 1 mm. thick lead plate is used for the pinhole, the optical density of the fog due to bremsstrahlung on the Agfa Printon K film is as high as 0.6. However, using a combination of 1 cm. perspex and 4 mm. lead, the fog did not exceed an optical density of 0.01. This combination was therefore employed in constructing the pinhole plate shown in Figure 1.

* Directorate of Radiation Protection, Atomic Energy Establishment Trombay, Bombay, India.

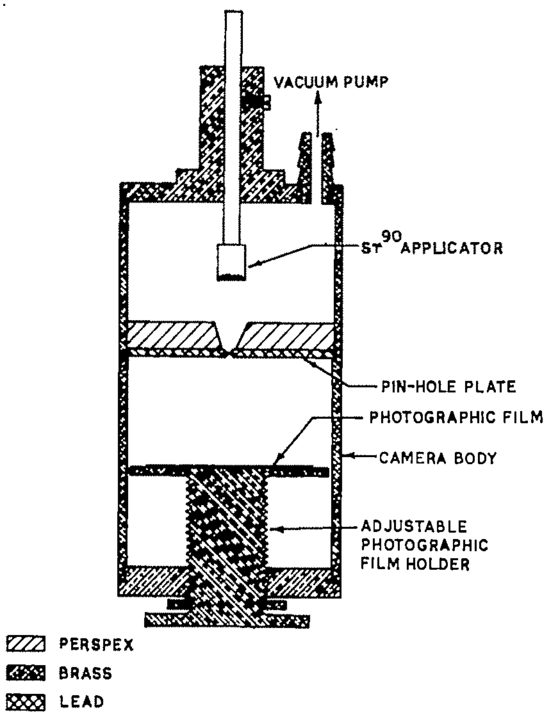


FIG. 1. Pinhole camera arrangement.

The principle involved in the use of the pinhole camera for studies of the uniformity of radiation emission from area sources is simple. If two point sources, A and B (Fig. 3*a*), on the surface of a large source have the same flux, points A′ and B′ on the film will have equal optical densities. The successful use of the pinhole camera principle demands that the radiation emitted from any point on the source should not be scattered in its path before reaching the film. The effect on the film of any scattered radiation from the source side of the pinhole plate is mostly eliminated by the plate itself. However, the scattering taking place on the film side results in the introduction of considerable additional fog on the film. Furthermore, owing to preferential forward scattering, this fogging is not uniform over all the film. It is maximal in the center—the point of intersection of the axis of the pinhole with the plane of the film, and decreases with increasing radius.

Since, for the same path length, the scattering of beta particles is significantly greater than that of photons, the error induced by scattering, which is usually unimportant in the case of roentgen and gamma rays, cannot be ignored in the case of beta radiation. The error can, however, be reduced considerably by lessening the distance between the pinhole plate and the film. Even this approach has its limitations when one deals with small area sources as the pinhole-to-film distance has to be kept long enough in order to obtain a magnified image of the source on the film for accurate densitometry. In the present investigation, these problems were overcome by producing a partial vacuum in the camera, thereby achieving considerable reduction in the scattering radiation. Fogging of the film due to scatter, which was as high as 0.2 at atmospheric pressure, was reduced to 0.01 when the pressure in the camera was kept below about 1 mm. mercury.

The drilling of the pinhole itself must be

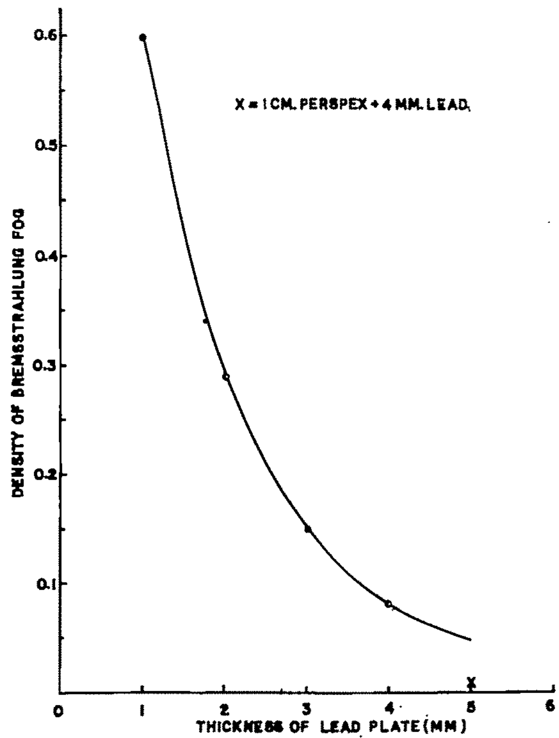


FIG. 2. Bremsstrahlung fog density of the film when different thicknesses of lead sheets were used for pinhole plate.

done very carefully; for, normally, vignetting occurs at the pinhole circumference and the scattered radiation from such a surface introduces nonuniformity in the optical density of the film. This defect was minimized by carefully smoothening the pinhole under a microscope.

## CORRECTIONS TO BE APPLIED IN THE USE OF THE CAMERA

When a large area source is used in conjunction with a pinhole camera, it subtends an appreciable angle at the pinhole. In such a case the density of the film decreases from the center to the edge of the image produced. Three factors are responsible for this: (1) the reduction in beta flux due to the inverse square law; (2) the nonuniform attenuation of radiation by the thin film providing a protective cover for the source; and (3) the tunnel effect. The corrections to be applied in order to take these factors into account are detailed below.

1. The correction factor for the reduction in the flux reaching the edges due to the inverse square law is

$$\frac{1}{1+\left(\frac{r}{x}\right)^2},$$

where $r$ is the radius at the source and $x$ the source to pinhole distance.

2. All plane beta sources are usually covered with a thin foil of some suitable protective material. The beta particles emitted from the center of the source and reaching the pinhole pass normally through the thickness of the protecting material, while those reaching the pinhole from the edges pass obliquely through it (Fig. 3*a*). If $t$ is the thickness and $\mu$ the linear absorption coefficient of the material of the film, the corresponding reduction in the intensity of the beam at the edges is given by the factor

$$e^{-\mu t(\sqrt{1+(r/x)^2}-1)}.$$

The effect of the obliquity will be considerable if $\mu t$ is large. However, since the correct value of $\mu$ is difficult to obtain, this factor has to be evaluated using the central axis depth dose data reported elsewhere.[12] Such evaluations were made in the present case for: (1) a $Sr^{90}$ eye applicator which was covered by 0.010 inch of Al and 0.002 inch of stainless steel (100 mg./cm.$^2$); and (2) two $P^{32}$ plaques covered by 50 mg./cm.$^2$ perspex and 100 mg./cm.$^2$ perspex, respectively. The results of these evaluations are shown in Table I. It can be seen that, although for low values of $r/x$ this correction is negligible, it increases as $r/x$ increases and becomes significant for values of $r/x$ higher than 0.15.

3. The surface area of a source contributing radiation dose to the central point (C′ in Fig. 3*b*) is circular, while the area contributing to any off center point is bound between two arcs of nearly equal radii. It can be readily seen that the ratio of the area at D′ to that at C′ is $2(\theta-\sin\theta\cos\theta)/\pi$. $\theta$ is in radians and is given by

$$\cos^{-1}\frac{l}{d_p}\cdot\frac{r}{x},$$

where $l$ and $d_p$ are the length and diameter of the pinhole respectively. When

$$\frac{l}{d_p}\cdot\frac{r}{x}\ll 1,$$

this reduces to

$$1-\frac{4}{\pi}\cdot\frac{l}{d_p}\cdot\frac{r}{x}.$$

In the case of roentgen rays, the value of $l$ is uncertain as the photons are not totally absorbed in the pinhole plate unless very large thicknesses are used. Therefore, both length and diameter of the pinhole must be chosen arbitrarily[5] and a compilation of data for "tunnel effect" correction is rather difficult. In the case of beta rays, however, the optimum tunnel length is given by the maximum range ($R_0$) of the beta particles in the material of the pinhole plate, and the tunnel effect correction depends only upon the diameter selected. Thus, by putting $l=R_0$, the value of $\theta$ is

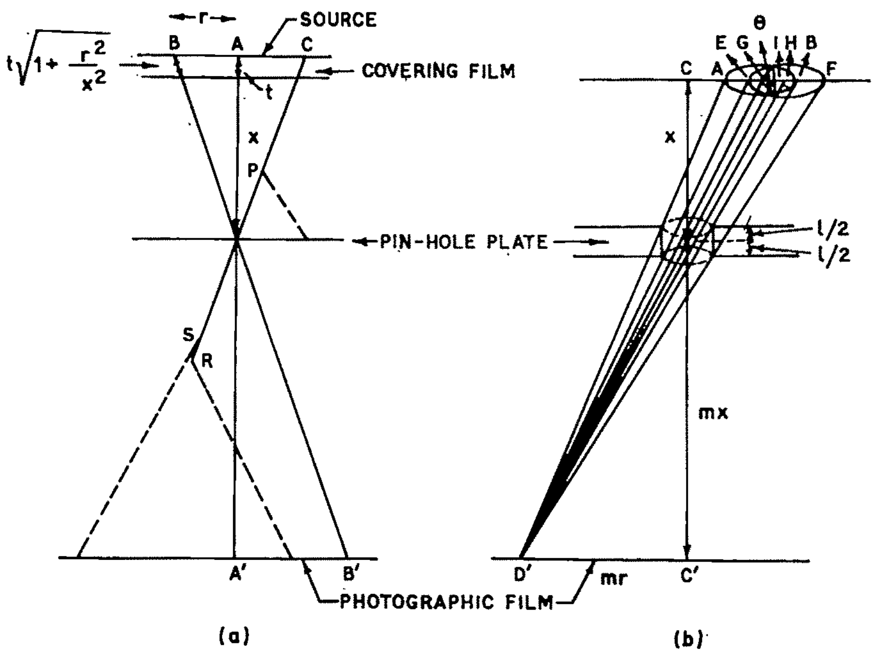


FIG. 3. (*a*) The scattering taking place on the source side of the pinhole is attenuated by the pinhole plate while that taking place on the film side results in fog. It can also be seen that the beta rays starting from the edge of the source are attenuated more in the covering foil. (*b*) The tunnel effect due to the oblique path of the beta rays. The area of the source contributing dose at C′ is circular while that contributing the dose at D′ is the area between two arcs.

$$\cos^{-1}\frac{R_0}{d_p}\cdot\frac{r}{x}.$$

The tunnel effect factor has been calculated using $Sr^{90}$ ($E$ max. = 2.23 mev.) for $d_p$ = 0.2, 0.4, 0.6, 0.8, 1.0 and 1.5 mm.; and using $P^{32}$ ($E$ max. = 1.71 mev.) and $Ca^{45}$ ($E$ max. = 0.216 mev.) for $d_p$ = 0.8 mm. The results are presented in Figure 4. The curves show that this factor varies with the energy of beta rays and the diameter of the pinhole.

TABLE I

VALUES OF THE CORRECTION FACTORS FOR THE NONUNIFORM ABSORPTION IN THE COVERING FOIL

| $r/x$ | Correction Factor for | | |
|---|---|---|---|
| | $P^{32}$ $t$ = 50 mg./cm.$^2$ | $P^{32}$ $t$ = 100 mg./cm.$^2$ | $Sr^{90}$ $t$ = 100 mg./cm.$^2$ |
| 0.00 | 1 | 1 | 1 |
| 0.05 | 0.9994 | 0.9988 | 0.9991 |
| 0.10 | 0.9977 | 0.9953 | 0.9963 |
| 0.15 | 0.9948 | 0.9897 | 0.9919 |
| 0.20 | 0.9908 | 0.9817 | 0.9856 |
| 0.25 | 0.9858 | 0.9723 | 0.9778 |

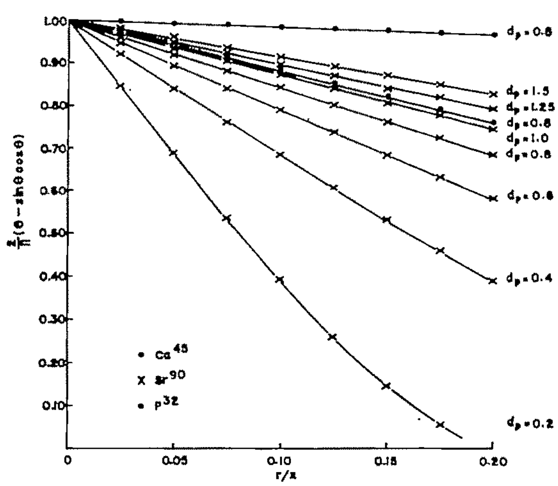


FIG. 4. The tunnel effect for various beta-ray energies and various pinhole diameters (see text).

The expression for the total reduction in intensity due to factors 1, 2 and 3 is given by

$$\frac{1}{1+\left(\frac{r}{x}\right)^2} \cdot e^{-\mu t(\sqrt{1+(r/x)^2}-1)} \cdot \frac{2}{\pi} (\theta - \sin\theta\cos\theta).$$

As $r/x$ increases, the contribution towards reduction in the intensity of beta radiation by each of these three factors also increases. Thus, the value of $r/x$ should be kept at a minimum, *i.e.*, $x$ should be large. This is not always possible. In any case, the air absorption (even when there is partial vacuum), as well as the exposure time increases with $x$. Further, the greater the value of $x$, the larger the area of the source which contributes radiation dose to any point on the film. This results in a fuzzy photographic image which is not a faithful reproduction of the point to point variation of surface activity of the source. Thus, the experimental parameters chosen will necessitate the application of these correction factors. The actual magnitude of such a correction factor was calculated for a $Sr^{90}$ source for $d_p$ =0.8mm. and $t$=100 mg./cm.$^2$. These are plotted in Figure 5, as curve A. Curve A thus represents the variation of density on a film exposed to a uniform plane $Sr^{90}$ source, when a pinhole

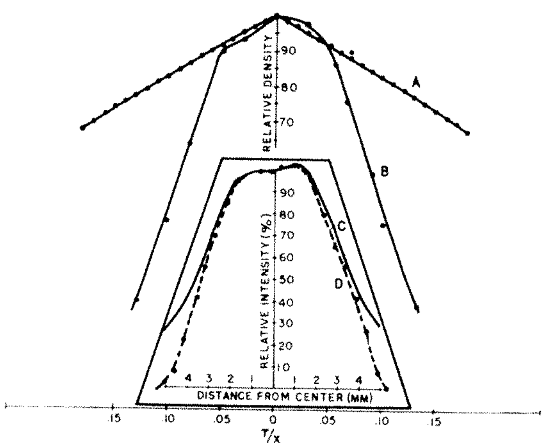


Fig. 5. Density variation on the films exposed using a pinhole camera. The inset figure shows the beta flux variations as obtained by using pinhole camera and extrapolation chamber (see text).

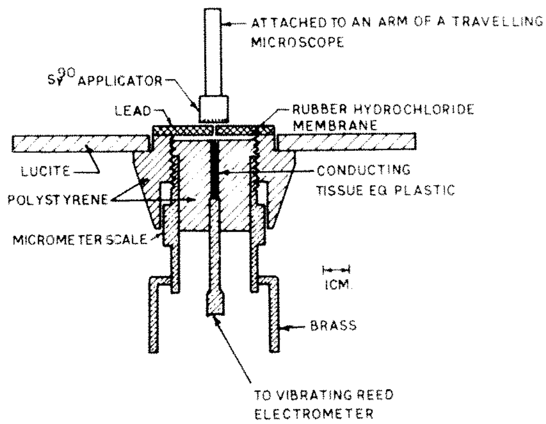


Fig. 6. Arrangement for scanning the surface of the beta applicator through a small collimator with an extrapolation chamber.

camera is used. In the same figure, curve B represents the variation of density on a film exposed to an actual $Sr^{90}$ eye applicator under identical conditions of source to film geometry. The ratio of the densities of corresponding points of the curves gives the extent of the deviation from uniformity of the beta flux distribution for the $Sr^{90}$ eye applicator. These ratios are plotted as percentages in the inset figure as a continuous curve C.

As a further check on the flux data obtained above, the measurements were also carried out by scanning the active surface of the source, using a 0.02 inch diameter collimator made in a sufficiently thick lead plate and kept concentric with the central electrode of an extrapolation chamber (Fig. 6). The source was put on an arm of a traveling microscope and the area was scanned systematically. The curve for the flux distribution so obtained is shown by curve D in Figure 5. It can be seen that curves C and D in Figure 5 are in fairly good agreement. They indicate that the beta flux from the central region of diameter $\simeq$3 mm. of the $Sr^{90}$ beta source is uniform within $\pm$3 per cent, and that the flux falls off rapidly beyond this diameter.

The exact diameter of the source (which is circular) was determined by using the following method:[13] Several autoradiographs of the source were made after plac-

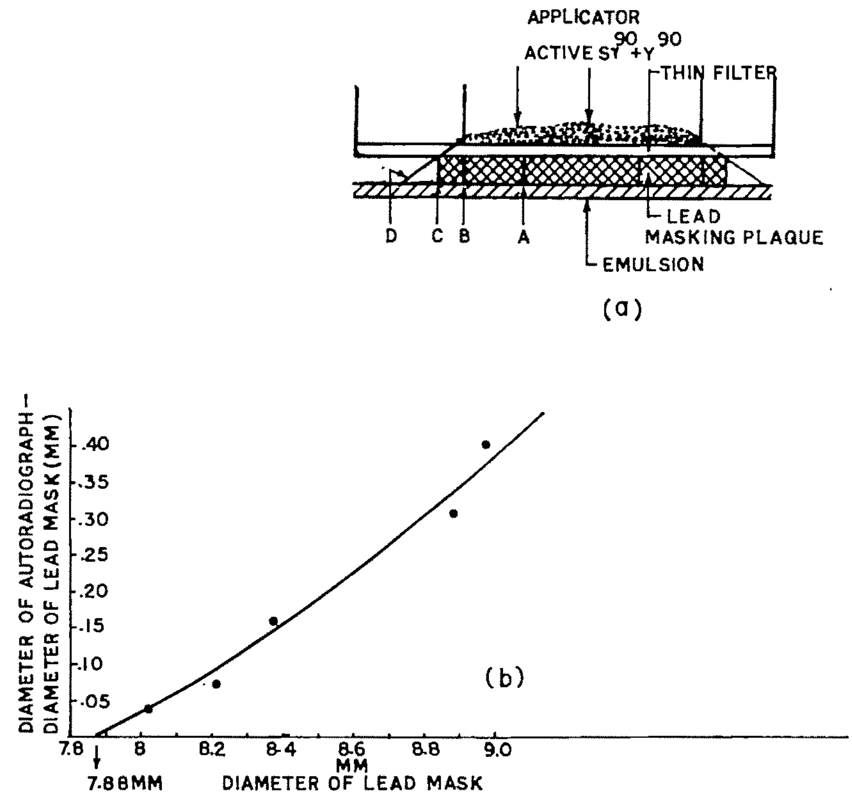


Fig. 7. (*a* and *b*) Diagrams showing the principle of the use of masking plaques to determine the size of the active area of the applicator.

ing it in contact with a number of circular masking plaques of 1 mm. thick lead of varying diameters. As long as the size of the masking plaque was smaller than the diameter of the source, the diameter of the shadow of the plaque was equal to the diameter of the plaque itself (Fig. 7*a*). When, however, the plaques were larger than the $Sr^{90}$ source, the difference between the diameters of the plaque and its shadow became greater. By plotting the difference between the diameters of the plaques and their shadows against the diameters of the plaques (Fig. 7*b*) and by extrapolating the curve to zero difference, the diameter of the source was determined. In the present case it was found to be 7.9 mm. It can thus be seen that with the $Sr^{90}$ beta source used, the flux of beta rays was not uniform over the entire area of the source.

## SUMMARY AND CONCLUSION

Thin sealed beta sources, such as $Sr^{90}$ eye applicators, are commonly used for treatment of surface lesions in clinical work. A knowledge of the surface dose rate, the size of the active area and the distribution of the beta flux on the surface is essential in planning treatment. The surface dose rate and the size of the active area are available from the suppliers. The measurement of the distribution of the beta flux is usually carried out by using an extrapolation chamber with sensitive current measuring instruments. Inasmuch as such equipment is rarely available in most laboratories and hospitals where these beta applicators are used, a pinhole camera suitable for studying the variation of beta flux at the surface of these applicators was designed. It was found that the defects normally associated with this technique, such as fogging of the film due to bremsstrahlung production and scattering of beta rays, could be reduced to negligible levels by choosing an appropriate material of opti-

mum thickness for the pinhole plate and by conducting the exposures under partial vacuum. The corrections to be applied for defects arising from such factors as the tunnel effect and absorption in the thin foil covering the source are outlined. The flux variation so obtained for a $Sr^{90}$ eye applicator was found to be in fairly good agreement with that observed by scanning the surface through a very small size collimator coupled to an extrapolation chamber.

It is concluded that important information concerning the uniformity of distribution in thin sealed beta sources such as eye applicators can be easily obtained by the use of a simple pinhole camera technique.

Directorate of Radiation Protection
Atomic Energy Establishment Trombay
Bombay 74 (AS), India

The author gratefully acknowledges the assistance of Mr. S. M. Rao in exposing the various films and making measurements with the extrapolation chamber and of Mr. Sethumadhavachar in fabricating the camera. Grateful thanks are due to Dr. K. S. Korgaonkar for guidance and to Mr. A. S. Rao for advice and encouragement. The author also wishes to thank Mr. G. Subrahmanian and Mr. U. Madhvanath for many helpful suggestions.

REFERENCES

1. Cohen, B. S. Multiple pinhole camera for accurate centering of roentgen-ray tube in its housing. Am. J. Roentgenol., Rad. Therapy & Nuclear Med., 1956, *75*, 149–152.
2. Frantzell, A. Effect of focal size, shape and "structure" on roentgenographic representation of small-calibre metal objects. *Acta radiol.*, 1951, *35*, 265–276.
3. Greening, J. R. Testing x-ray equipment by examining emitted x-rays. *Radiography*, 1959, *25*, 199–210.
4. Kemp, F. H., and Nichols, A. F. Focal spot sizes. *Brit. J. Radiol.*, 1958, *31*, 486–488.
5. Kuntke, A. H. G. On determination of roentgen tube focal spot sizes by pin-hole camera roentgenography. *Acta radiol.*, 1957, *47*, 55–64.
6. Mallet, L., and Maurin, R. Study of quality and origin of parasitic radiation from target of x-ray tube. *Radiology*, 1947, *48*, 628–632.
7. Mattsson, O. Practical photographic problems in radiography with special reference to high voltage technique. *Acta radiol.*, 1955, Suppl. 120.
8. Polansky, D., and O'Connor, D. T. X-ray focal spot measurement. *Nondestructive Testing*, 1954, *12*, 37.
9. Preuss, L. E., and Jenkins, G. Pinhole camera maps beta-active deposits. *Nucleonics*, 1958, *16*, No. 10, 98–99.
10. Richards, A. G. Radiation protection via pinhole camera. *Oral Surg.*, 1960, *13*, 953–963.
11. Robertson, C. W., and Watson, G. Precise measurements of focal areas in diagnostic x-ray tubes and their applications in tube development. *Brit. J. Radiol.*, 1958, *31*, 489–491.
12. Supe, S. J., and Cunningham, J. R. Physical study of strontium 90 $\beta$-ray applicator. Am. J. Roentgenol., Rad. Therapy & Nuclear Med., 1963, *89*, 570–574.
13. Supe, S. J., and Cunningham, J. R. Internal report of Physics Department, Ontario Cancer Institute, Toronto, Ontario.
14. Thoraeus, R. Amount of off-focus radiation in beams from various types of roentgen tubes. *Acta radiol.*, 1937, *18*, 753–760.
15. Vuorinen, P. Reliability of pinhole methods in evaluation of radiation from emission area in roentgen tubes. *Acta radiol.*, 1960, *54*, 41–44.
16. Wiltshire, L. L. Pinhole camera locates sources of gamma radiation. *Nucleonics*, 1962, *20*, No. 3, 76.

# SHIELDING DOOR WITH FLUSH THRESHOLD FOR A MEGAVOLTAGE THERAPY ROOM*

*By* C. J. KARZMARK *and* P. A. HUISMAN
PALO ALTO, CALIFORNIA

ACCESS to high-energy therapy rooms must be either via a maze or a heavy shielding door. A maze restricts personnel exposure by requiring that any primary photon be at least twice scattered. This arrangement provides access free of mechanical maintenance problems but requires greater space as well as increased walking for personnel. Often the maze entry is radiation interlocked with a lightweight door, a simple barrier, or a light beam-photo cell system. Ruddy[2] has described several types of radiation shielding doors: hinged, lift, hanging, and rolling; while Wadley[3] gives details for a hinged design.

For therapy installations, a motorized heavy shielded door is often dictated by limitations of space or because of its quicker, easier access for bed patients as compared with a maze. We have encountered two difficulties in our previous experience with heavy therapy room doors: providing fast, reliable door operation, and finding a threshold design which affords good shielding without impeding traffic or requiring maintenance.

Both of these door problems have been solved for the therapy room layout shown in Figure 1. The first problem is solved by a substantial mechanical design which includes a heavy-duty door operator.* The door hangs from trolleys mounted on an overhead track. The time for this 10,000 pound door to open fully is 10 seconds. A half-open position, affording rapid and adequate access for ambulatory patients and therapy personnel, may be activated from two locations, one at the console and the other near the door itself. The door may be fully opened by activating the push-button switch a second time.

A flush, floor-level threshold (Fig. 2, *A* and *B*) is provided by a solid steel section placed beneath the door and flush with the floor covering. This steel member, which is buried in the concrete floor, is 8 inches wide and 8 inches deep and attenuates scatter and leakage radiation passing under the door through the floor. The door is 5 inches thick, and it is adjusted for a 0.060 inch clearance above the threshold. The door bottom and threshold have machined surfaces so that smaller as well as larger gaps are possible. This narrow adjustable gap passes only a small amount of scatter radiation. The gap-target geometry requires leakage radiation emerging from the gap to be at least singly scattered after leaving the target. On the door exterior surface, the contribution from primary scatter appears small compared with leakage radiation for all accelerator orientations. Maximum transmission through the door occurs with the accelerator beaming upward. The x-ray target is about 6 inches above the floor level for this accelerator orientation.

Measurements indicate that the maximum exposure rate, which occurs near floor level just outside the door, does not exceed 10 mr/hr. for 100 rad/min. at 1 meter in the phantom position. For reasonable occupancy and use factors, the cumulative contribution to personnel exposure is well below accepted values. A recent weekly total, measured with personnel monitoring film, was under 30 mr at all points on the door exterior surface except for a narrow strip adjoining floor level. Here the corresponding weekly exposure increased to about 50 mr in the gap. Such an increase appears qualitatively consistent with the

* Richards-Wilcox Company, Aurora, Illinois, No. 1265.

* From the Department of Radiology, Stanford University School of Medicine, Palo Alto, California.
This work was in part aided by Grant C-5838 from the National Cancer Institute, National Institutes of Health, USPHS.

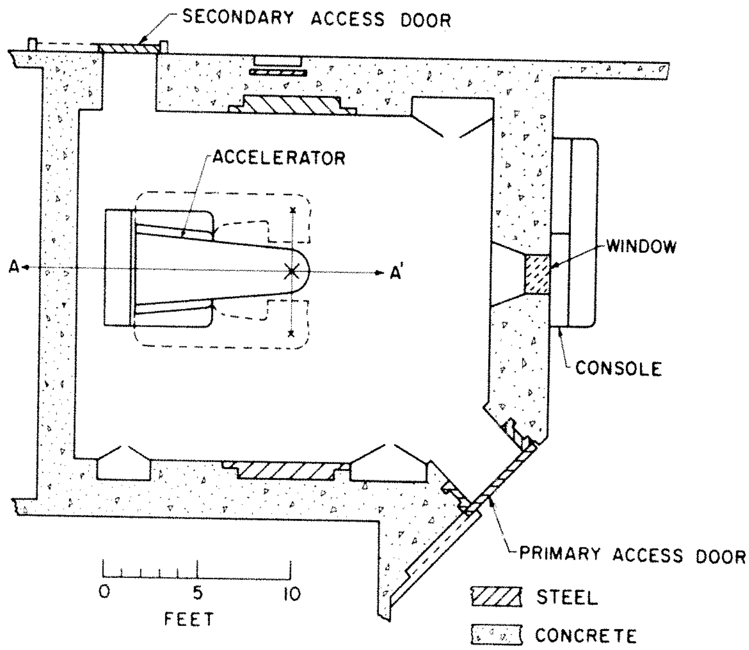


Fig. 1. Plan View, 6 mev. linear accelerator megavoltage therapy room. An isocentric accelerator system which is incorporated in this facility, has been recently described by Haimson and Karzmark.[1] The 45° orientation of the primary access door is convenient for ambulatory and bed patients, as well as therapy personnel. The accelerator is isocentrically mounted and rotates about the horizontal axis A-A', the axis being 46 inches above the floor. The x-ray target rotates on a circle of one meter radius, whose center is located at the isocenter X, a point along accelerator axis A-A'. The x-ray beam axis is always perpendicular to and directed through axis A-A'. The projection on the plan view of all target locations lies along the line x-X-x. The dotted accelerator outlines correspond to the two horizontal beam accelerator orientations. The primary-beam wall shielding includes steel sections (diagonal stripes) inserted flush with the side walls. A secondary access door is for emergency use only.

(*Please turn the page for Fig. 2*)

presence of a gap and the decreased attenuation of the bottom edge of the door where a 0.5 inch steel plate substitutes for the lead core.

SUMMARY

A design objective for megavoltage therapy room doors is to limit leakage radiation at floor level without encumbering access or creating door-threshold maintenance problems. This goal is met in a new design in which the threshold is a wide deep, steel section placed flush with the floor surface. A precise narrow gap is maintained between the threshold and the undersurface of the shielding door such that the radiation leakage under the door is below accepted values.

C. J. Karzmark
Department of Radiology
Stanford University School of Medicine
300 Pasteur Drive
Palo Alto, California

We are indebted to Fire Protection Products Company of San Francisco for aid in design of the door and for a high standard of construction. We thank Dr. R. Loevinger for useful discussion and comments.

REFERENCES

1. Haimson, J., and Karzmark, C. J. New design 6 MeV linear accelerator system for supervoltage therapy. *Brit. J. Radiol.*, 1963, *36*, 650–659.
2. Ruddy, J. M. How to select gamma shielding doors. *Nucleonics*, 1962, *20*, No. 6, 94–95.
3. Wadley, W. G. Simple radiation shielding doors. *Nucleonics*, 1954, *12*, No. 5, 54.

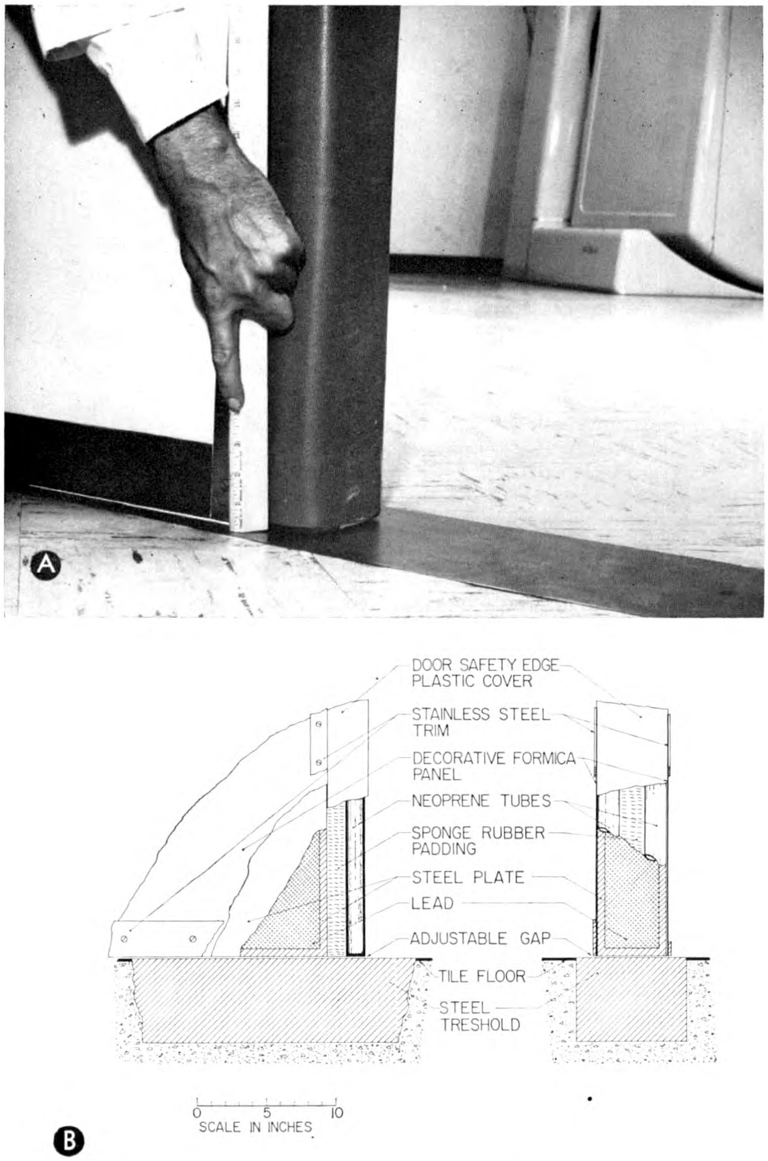


FIG. 2. (*A*) Photograph of primary access shielding door near floor level. In this view, the 0.060 inch gap near the floor is emphasized by a folded white paper placed just below the door. The flush steel threshold is seen at floor level. The threshold is welded at each corner of the door opening to vertical steel members which provide additional radiation shielding at these vulnerable locations (see Fig. 1). The threshold and vertical shield members are integrally tied to the concrete shielding. Door hangers run on a hardened steel "I" beam track, the position of which is adjustable. This beam is supported on both ends by structural steel angles tied to the concrete and in addition by intermediate concrete anchored suspensions. (*B*) Primary access door detail near floor level. The door itself is 4 inches of sheet lead tightly contained in a rectangular box made of 0.5 inch steel plate. Decorative plastic panels* cover the door surface and also the removable panels behind which the door retracts in its open position. Stainless steel trim is used at the door edges. A horizontal stainless steel strip is attached to the outer door surface near the floor to provide a contact surface for a positioning roller. The door safety edge consists of two adjacent, vertical 1.5 inch neoprene tubes, a "T" shaped section of sponge rubber, and a plastic cover overall. The sealed tubes are filled with air at atmospheric pressure; when the door is closing, physical contact with the safety edge activates a pressure-sensitive switch, opening the door. The door-operator clutch and brake are adjusted so that door over-travel is less than an inch.

* These phenol formaldehyde laminations are available in a wide variety of colors and patterns under different trade names; *e.g.*, Formica, Formica Insulation Company, Cincinnati, Ohio.

VOL. 94, NO. 4

# THE AMERICAN JOURNAL OF ROENTGENOLOGY RADIUM THERAPY AND NUCLEAR MEDICINE

*Editor:* TRAIAN LEUCUTIA, M.D.
*Assistant to the Editor:* KENNETH L. KRABBENHOFT, M.D.
*Associate Editors:* HARRY HAUSER, M.D., RUSSELL H. MORGAN, M.D., EDWARD B. D. NEUHAUSER, M.D., WENDELL G. SCOTT, M.D.
*Consulting Editorial Board:* See front cover.
*Published by:* CHARLES C THOMAS, Publisher, 301–327 East Lawrence Avenue, Springfield, Illinois.

*Issued monthly. Annual subscription: United States, Mexico, Cuba, Central and South America, and Canada $15.00; other countries, $17.00. Current single numbers, $1.50. Advertising rates submitted on application. Editorial office, 110 Professional Building, Detroit 1, Michigan. Office of publication, 301–327 East Lawrence Avenue, Springfield, Illinois. Information of interest to authors and readers will be found on page ii.*

AMERICAN ROENTGEN RAY SOCIETY

*President:* H. O. Peterson, Minneapolis, Minn.; *President-Elect:* J. P. Medelman, White Bear Lake, Minn.; *1st Vice-President:* C. B. Peirce, Montreal, Que., Canada; *2nd Vice-President:* H. C. Sehested, Fort Worth, Tex.; *Secretary:* C. A. Good, Mayo Clinic, Rochester, Minn.; *Treasurer:* S. W. Brown, 1467 Harper Street, Augusta, Ga.

*Executive Council:* H. O. Peterson, J. P. Medelman, C. B. Peirce, C. A. Good, S. W. Brown, C. B. Holman, R. R. Greening, J. F. Roach, H. G. Reineke, J. C. Cook, R. M. Caulk, E. E. Barth, T. Leucutia, E. F. Van Epps, S. F. Ochsner, J. S. Dunbar, H. M. Stauffer, T. F. Leigh, Chairman, Emory University Clinic, Atlanta, Ga. 30322

*Program Committee:* C. A. Good, J. F. Roach, T. Leucutia, R. R. Greening, H. O. Peterson, J. P. Medelman, Chairman, White Bear Lake, Minn.

*Publication Committee:* J. A. Campbell, M. M. Figley, R. N. Cooley, J. F. Holt, J. F. Roach, Chairman, Albany, N. Y.

*Finance and Budget Committee:* J. S. Dunbar, H. M. Stauffer, R. E. Parks, T. M. Fullenlove, C. B. Holman, Chairman, Rochester, Minn.

*Committee on Scientific Exhibits:* R. G. Lester, J. O. Reed, R. R. Greening, Chairman, Philadelphia, Pa.

*Advisory Committee on Education and Research:* A. Raventos, A. R. Margulis, E. C. Lasser, F. J. Bonte, H. G. Reineke, Chairman, Cincinnati, Ohio.

*Representatives on the American Board of Radiology:* C. A. Good, Rochester, Minn.; C. A. Stevenson, Spokane, Wash.; J. F. Roach, Albany, N. Y.

*Director of Instruction Courses:* H. O. Peterson, Minneapolis, Minn.; *Assoc. Director:* D. G. Mosser, Minneapolis, Minn.

*Manager of the Annual Meeting:* J. C. Cook, 110 Professional Building, Detroit, Mich. 48201

*Editor:* T. Leucutia, 110 Professional Building, Detroit, Mich. 48201

*Representative on the Board of Chancellors of the American College of Radiology:* Seymour F. Ochsner.

*Sixty-sixth Annual Meeting:* Washington Hilton Hotel, Washington, D. C., Sept. 28-Oct. 1, 1965.

AMERICAN RADIUM SOCIETY

*President:* Justin J. Stein, Los Angeles, Calif.; *President-Elect:* Milton Friedman, New York, N. Y.; *1st Vice-President:* Manuel Garcia, New Orleans, La.; *2nd Vice-President:* Richard J. Jesse, Houston, Tex.; *Secretary:* John L. Pool, New York, N. Y.; *Treasurer:* Juan A. del Regato, Penrose Cancer Hospital, 2215 North Cascade Ave., Colorado Springs, Colorado 80907.

*Executive Committee:* Gilbert H. Fletcher, Chairman, Houston, Tex.; Charles G. Stetson; Joseph H. Farrow; Justin J. Stein; John L. Pool; Milton Friedman; Manuel Garcia; Richard H. Jesse; Juan A. del Regato.

*Scientific Program Committee:* Justin J. Stein, Chairman; Glenn E. Sheline; Robert C. Hickey; Lewis W. Guiss; Harvey P. Groesbeck, Jr.; Roald N. Grant; Milton Friedman; Joseph H. Farrow, Ex officio.

*Committee on Arrangements:* R. Lee Foster, Chairman, The Medical Center, 1313 North 2nd Street, Phoenix, Ariz. 85004; Clifford L. Ash; James M. Ovens; Jerome M. Vaeth.

*Publication Committee:* Harry Hauser, Chairman, Cleveland, Ohio; Wendell C. Hall, Hartford, Conn.; Martin Van Herik, Rochester, Minn.

*Public Relations Committee:* James M. Ovens, Chairman, Phoenix, Ariz.; John Day Peake; R. C. Burr.

*Janeway Lecture Committee:* William S. MacComb, Chairman, Houston, Tex.; Clifford L. Ash; A. N. Arneson.

*Representatives on the American Board of Radiology:* Donald S. Childs, Jr., Rochester, Minn.; Justin J. Stein, Los Angeles, Calif.; Bernard P. Widman, Philadelphia, Pa.

*Representative on the National Council on Radiation Protection and Measurements:* Herbert M. Parker, Richland, Wash., Liaison Member.

*Representative on the Board of Chancellors of the American College of Radiology:* Charles G. Stetson.

*Forty-eighth Annual Meeting—Golden Anniversary of the American Radium Society:* Camelback Inn, Phoenix, Ariz., April 13–16, 1966.

# EDITORIAL

## INSTRUCTION COURSES OF THE SIXTY-SIXTH ANNUAL MEETING OF THE AMERICAN ROENTGEN RAY SOCIETY

PRESIDENT-ELECT J. Paul Medelman asked that the Section on Instruction continue the excellent work of the past by arranging a series of Instruction Courses also for the Sixty-sixth Annual Meeting of the American Roentgen Ray Society, which will be held at the Washington Hilton Hotel, Washington, D. C., September 28–October 1, 1965.

As is known, these courses were initiated by President-Elect Edward L. Jenkinson, who at the Fortieth Annual Meeting in Chicago in 1939, with the approval of the Executive Council, created a Section on Instruction of that year's annual meeting. Since then, every President-Elect considered it most important to ensure continuation of these courses as an essential feature of the over-all program of the annual meeting. During these years, the rapid advances made in all branches of clinical radiology, the commensurate progress achieved in the domain of radiation physics, radiobiology and some other allied sciences and, in particular, the broadening scope of nuclear medicine, gradually but steadily contributed to further enhance the importance of these courses. As a result of such phenomenal growth, dissemination of the new accomplishments has become an inescapable task, and this task is admirably fulfilled by the Section on Instruction.

The Society is in the enviable position of having had 3 eminent Directors of the Section on Instruction who shaped the pattern of our quest for knowledge during the past quarter century: Dr. B. R. Kirklin, 1939–1948; Dr. H. M. Weber, 1948–1957; and Dr. Harold O. Peterson, 1957–1963. During his tenure of office as President-Elect of the Society in 1964, Dr. Peterson was substituted by Dr. Donn G. Mosser, his able Associate.

This year the Director of the Section on Instruction is again Dr. Harold O. Peterson, and the Associate Director, Dr. Donn G. Mosser. They have assembled an outstanding Faculty of Instructors, comprising many new members, who will present new topics in conforming with Dr. Peterson's "intent of keeping abreast with the demands of modern radiology."

The Section will present this year: 16 single period courses on Diagnostic Roentgenology; 7 single period courses on Therapeutic Radiology, Nuclear Medicine, Physics and Radiobiology; 10 two period courses and 2 three period courses in Diagnostic Roentgenology, and 1 four period sequential course on Therapeutic Radiology. This latter course will be given, on special invitation of the Society, by the distinguished Radiotherapist, M. Lederman, M.B., D.M.R.E., F.F.R., Deputy Director of the Radiotherapy Department of the Royal Marsden Hospital, London, England.

A detailed description of the courses and of the instructions on registration appears elsewhere in this issue of the Journal.

# AMERICAN ROENTGEN RAY SOCIETY

## Section on Instruction

Harold O. Peterson, M.D., *Director*
Donn G. Mosser, M.D., *Associate Director*

*Titles and Abstracts of Courses Offered*
*Sixty-Sixth Annual Meeting*
September 28 to October 1, 1965

The Instruction Courses for the Sixty-sixth Annual Meeting of the American Roentgen Ray Society will be held on Tuesday, Wednesday and Thursday afternoons, September 28, 29 and 30, at 3:00 P.M., and Friday afternoon, October 1, at 1:30 P.M. Each course period will be of 90 minutes' duration and no other official activity will be scheduled for this time.

A special registration desk for these courses will be set up near the general registration area. Complete information concerning the courses as well as tickets for those courses still available can be obtained Monday, September 27, from 8:30 A.M. to 4:30 P.M. and daily, Tuesday through Friday, September 28–October 1, 8:30 A.M. to 4:30 P.M.

Fifteen daily courses will be given on each of the first three days, eight courses on Friday. Please note that several of the courses will be given in two and three sessions. A brief abstract for each course will be found on the following pages as well as a complete list of the faculty and the registration form. There will be one 4-day continuous therapy course by a British Radiotherapist.

Admission to all courses will be by ticket. To avoid the confusion usually present on the first day of the meeting, tickets will be mailed to all those whose registration forms (Pink Sheets) reach the office of the Director before September 17, 1965. The envelope containing the tickets will be labelled in a conspicuous manner. Please be on the lookout for your tickets and remember to bring them to the meeting. Tickets will be issued in the order that the requests are received but the first mailing will be shortly *after September 7, 1965*.

### How to Register and Obtain Tickets

After reviewing the abstracts of the available courses on the following pages, fill out the pink order sheet. Please make three choices for each day and include the course number and name of Instructor for each choice. A $2.00 registration fee is required from *nonmembers* for each course attended. Since it is possible to attend only one course a day for four days, the maximum fee is $8.00. Members of the American Roentgen Ray Society and graduate students or residents in Radiology are not required to pay for these courses but must fill out the pink order sheet indicating their choices.

Please mail these order sheets to Dr. Harold O. Peterson, 1995 West County Road "B," St. Paul, Minnesota 55113.

### THE FACULTY

### 1965

Malcolm A. Bagshaw, M.D., Associate Professor of Radiology, Director of Radiotherapy, Stanford University School of Medicine, Palo Alto, California

Stanley Baum, M.D., Assistant Professor of Radiology, School of Medicine University of Pennsylvania, Philadelphia, Pennsylvania

Lewis S. Carey, M.D., Department of Radiology, Saint Joseph's Hospital, Saint Paul, Minnesota

Giovanni Di Chiro, M.D., Head, Section on Neuroradiology, National Institute of Neurological Diseases and Blindness, Department of Health, Education and Welfare, Bethesda, Maryland

Gerald D. Dodd, M.D., Clinical Professor of Radiology, Jefferson Medical College Hospital, Philadelphia, Pennsylvania

J. Scott Dunbar, M.D., Associate Professor of Radiology, McGill University; Director of Department of Radiology, Montreal Children's Hospital, Montreal, Quebec, Canada

Robert L. Egan, M.D., Emory University Clinic, Atlanta, Georgia

Lewis E. Etter, M.D., Professor of Radiology, Falk Clinic, School of Medicine, University of Pittsburgh; Consultant, Western Psychiatric Institute and Clinic, Pittsburgh, Pennsylvania

Benjamin Felson, M.D., Professor and Director, Department of Radiology, University of Cincinnati College of Medicine, Cincinnati, Ohio

Arthur K. Finkelstein, M.D., Professor of Radiology, School of Medicine, University of Pennsylvania, Philadelphia, Pennsylvania

William E. Gannon, M.D., Associate Professor of Radiology, College of Medicine, State University of New York, Brooklyn, New York

Roy R. Greening, M.D., Professor of Radiology, Jefferson Medical College Hospital, Philadelphia, Pennsylvania

George Jacobson, M.D., Professor of Radiology, Chairman, Department of Radiology, School of Medicine, University of Southern California, Los Angeles, California

Harold G. Jacobson, M.D., Head of the Division of Diagnostic Radiology, Montefiore Hospital; Professor of Clinical Radiology, New York University College of Medicine; Senior Consultant in Radiology to the Veterans Hospital in the Bronx, New York, New York

M. Lederman, M.B., D.M.R.E., F.F.R., Deputy Director, Radiotherapy Department, Royal Marsden Hospital, London; Consulting and Radiotherapist to the Royal National Throat, Nose & Ear Hospital, The Metropolitan Ear, Nose & Throat Hospital, Moorfields Eye Hospital, The Royal Eye Hospital, and Chelsea Hospital for Women, London, England

Richard G. Lester, M.D., Professor and Chairman, Department of Radiology, Duke University Medical Center, Durham, North Carolina

Alexander S. Macmillan, Jr., M.D., Instructor in Radiology, Harvard Medical School; Radiologist, Massachusetts Eye and Ear Infirmary; Radiologist to the Harvard Medical and Surgical Services, Boston City Hospital, Boston, Massachusetts

John T. Mallams, M.D., Director, Charles A. Sammons Department of Radiation Therapy and Nuclear Medicine, Baylor University Medical Center, Dallas, Texas

Richard H. Marshak, M.D., Attending Radiologist, The Mount Sinai Hospital, New York, New York

William Martel, M.D., Associate Professor, Department of Radiology, The University of Michigan Medical Center, Ann Arbor, Michigan

Harry Z. Mellins, M.D., Department of Radiology, State University of New York, Downstate Medical Center, Brooklyn, New York

Harvey Meyers, M.D., Associate Professor of Radiology, School of Medicine, University of Southern California, Los Angeles, California

Russell H. Morgan, M.D., Radiologist-in-Chief, The Johns Hopkins Hospital, Baltimore, Maryland

Sidney W. Nelson, M.D., Professor and Chairman, Department of Radiology, The Ohio State University Medical School, Columbus, Ohio

Charles M. Nice, Jr., M.D., Professor and Chairman, Department of Radiology, Tulane University School of Medicine; Director of Diagnostic Radiology, Charity Hospital, New Olreans, Louisiana

M. Vera Peters, M.D., Assistant Professor in Therapeutic Radiology, University of Toronto; Assistant Professor, Department of Medical Biophysics, University of Toronto; Senior Radiotherapist, Princess Margaret Hospital, Toronto, Ontario, Canada

Gordon Potts, M.D., Assistant Professor of Radiology, College of Physicians and Surgeons, Columbia University, New York, New York

Maurice D. Sachs, M.D., Chief, Radiology Service, Veterans Administration Hospital, Associate Professor of Radiology, Western Reserve University School of Medicine; Director, Radiology Forest City Hospital, Cleveland, Ohio

Frederic N. Silverman, M.D., Director, Division of Roentgenology, The Children's Hospital, Cincinnati, Ohio

Norman Simon, M.D., Associate Radiotherapist, The Mount Sinai Hospital, New York, New York

Warren K. Sinclair; Senior Biophysicist, Division of Biological and Medical Research, Argonne National Laboratory, Argonne, Illinois

Edward B. Singleton, M.D., Clinical Associate Professor of Radiology, Baylor University College of Medicine; Director of Radiology, St. Luke's and Texas Children's Hospital, Houston, Texas

Harry L. Stein, M.D., Assistant Professor Radiology, Cornell University Medical College, New York, New York

George N. Stein, M.D., Professor of Clinical Radiology, School of Medicine, University of Pennsylvania, Philadelphia, Pennsylvania

Melvin Tefft, M.D., Consultant in Radiology to the Massachusetts General Hospital; Radiotherapist, Children's Hospital and Medical Center, and Children's Cancer Research Foundation; Assistant in

Radiology, Harvard Medical School, Boston, Massachusetts

Sidney Wallace, M.D., Instructor in Radiology, Jefferson Medical College Hospital, Philadelphia, Pennsylvania

Don C. Weir, M.D., Clinical Professor and Acting Director of Radiology, St. Louis University School of Medicine, St. Louis, Missouri

Marvin M.D. Williams, Ph.D., Professor of Biophysics, Mayo Graduate School, University of Minnesota, Rochester, Minnesota

Robert E. Wise, M.D., Chairman, Department of Diagnostic Radiology, Lahey Clinic Foundation; Chairman, Department of Radiology, New England Baptist Hospital, Boston, Massachusetts

Martin H. Wittenborg, M.D., Radiologist, Children's Hospital Medical Center; Associate Clinical Professor of Radiology, Harvard Medical School, Boston, Massachusetts

Ernest H. Wood, M.D., Professor of Radiology in the College of Physicians and Surgeons, Columbia University; Director of Radiology, Neurological Institute, Columbia-Presbyterian Medical Center, New York, New York

## DESCRIPTION OF COURSES

### COURSE 101 and COURSE 201

**Tuesday and Wednesday**

**WILLIAM MARTEL, M.D.**
**Ann Arbor, Michigan**

**Arthropathies: Differential Diagnosis**

This course will be given in two parts:

**Course 101. Part I**

**Course 201. Part II**

Skeletal manifestations of various arthritic diseases will be discussed, largely from the viewpoint of the differential diagnosis. Features are often present which permit a definite radiologic diagnosis.

The following conditions, among others, will be discussed: rheumatoid arthritis; ankylosing spondylitis; psoriatic arthritis; Reiter's syndrome; scleroderma; lupus erythematosus; villonodular synovitis; degenerative joint disease; neuropathic joint disease; gout; chondrocalcinosis; and infectious arthritis.

### COURSE 102

**Tuesday**

**CHARLES M. NICE, JR., M.D.**
**New Orleans, Louisiana**

**Roentgen Examination of the Small Bowel: Factors Affecting Motility, Pattern and Diagnosis**

A series of over 200 normal individuals was studied to indicate how preparation of the patient, type of barium suspension and position of the patient affected the motility and pattern of the small bowel examination. Three very important factors influencing the examination were found to be the amount of fecal material in the cecum, the volume of the opaque medium, and the position of the patient while the procedure was in progress.

The use of saline, suspending agents, and micronized forms of barium also will be discussed. Several cases to demonstrate the value of the small bowel examination when properly performed will be presented.

### COURSE 103

**Tuesday**

**RUSSELL H. MORGAN, M.D.**
**Baltimore, Maryland**

**Screen Intensification and Cineradiography**

This course will deal with the physics and technical problems associated with screen intensification and cineradiography. The discussion will consider those aspects of x-ray image formation and perception which are important in the fields of screen intensified fluoroscopy and motion picture recording. Particular attention will be given to the practical problems associated with the use of various intensifier and cineradiographic systems in clinical radiology.

### COURSE 104

**Tuesday**

**GEORGE JACOBSON, M.D.**
**Los Angeles, California**
**HARVEY MEYERS, M.D.**
**Los Angeles, California**

**The Acute Abdomen: Intestinal Obstruction and Other Selected Conditions**

*Intestinal Obstruction:* A logical approach to the roentgenographic diagnosis of small and large bowel obstruction will be presented relating the roentgen features to altered physiology. The recognition of vascular impairment will be stressed.

*Perforated Peptic Ulcer:* The use of a water-soluble contrast medium to examine the upper gastrointestinal tract of patients suspected of having per-

forated peptic ulcer and the rationale for the procedure will be discussed.

*Non-penetrating Injuries of the Abdomen:* The discussion will pertain to the roentgen manifestations in blunt trauma to the gastrointestinal tract, liver and spleen.

---

### COURSE 105

**Tuesday**

**ERNEST H. WOOD, M.D.**
**New York, New York**

**The Radiology of Subarachnoid Hemorrhage**

Subarachnoid bleeding from potentially treatable lesions is being recognized with increasing frequency as a cause of acute cerebrovascular accidents. The diagnosis of such lesions is one of the most important indications for cerebral angiography. The radiologist must know when various angiographic procedures should be performed and exactly how they should be carried out. It is important to have a thorough understanding of the pathogenesis of subarachnoid hemorrhage for radiologic differential diagnosis. The radiologist must appreciate the limitations as well as the value of angiography in demonstrating the various types of lesions causing bleeding.

Impending complications of subarachnoid hemorrhage frequently elude clinical recognition, but their existence must be known to institute proper treatment at the optimum time. Incipient infarction, the formation of a hematoma, or the development of a cerebral herniation can often be diagnosed only by radiologic means, and there are many angiographic findings that denote such naturally developing threats to life. Clinical, radiologic and pathologic correlative studies have made it possible to assess for prognosis the importance of arterial spasm, hematoma formation, impaired blood flow to vital centers, collateral circulation, anatomic variations, degenerative vascular disease, and numerous other angiographic changes. The radiologist plays a significant role in judging the precarious balance in cerebral circulation after intracerebral or subarachnoid hemorrhage; his analysis of the angiogram may be the decisive factor in the choice of treatment.

---

### COURSE 106

**Tuesday**

**EDWARD B. SINGLETON, M.D.**
**Houston, Texas**

**Pediatric Chest Abnormalities**

1. Technique
2. The normal chest and variations of normal
3. Abnormalities of the thoracic cage
4. Newborn pulmonary complications: a. variations of perinatal distress—hyalin membrane disease, aspiration syndrome and pulmonary hemorrhage; b. pneumonias including aspiration secondary to pharyngeal incoordination and esophageal atresia
5. Congenital anomalies: congenital lobar emphysema, congenital cystic malformation, diaphragmatic abnormalities, pulmonary agenesis and hypoplasia
6. Pulmonary abnormalities acquired in later infancy and childhood: a. types of pneumonia and their complications; b. acquired tracheo-esophageal fistula; c. foreign bodies; d. fibrocystic disease; e. bronchiolitis
7. Rare pulmonary conditions: pulmonary alveolar microlithiasis, neoplastic diseases, pulmonary fibrosis, hemosiderosis, cytomegalic inclusion disease

---

### COURSE 107
### and
### COURSE 207

**Tuesday and Wednesday**

**M. H. WITTENBORG, M.D.**
**Boston, Massachusetts**

**Osseous Manifestations of Systemic Disease in Infancy and Childhood**

This course will be given in two parts:
**Course 107. Part I**
**Course 207. Part II**

The roentgen diagnostic aspects of bone changes in systemic disease will be reviewed. Emphasis will be on the changes that are unique to growing bones. This will include examples of nutritional, hematologic, metabolic, and endocrine disorders that are reflected in the skeleton by characteristic roentgenographic appearances.

---

### COURSE 108
### and
### COURSE 208

**Tuesday and Wednesday**

**FREDERICK N. SILVERMAN, M.D.**
**Cincinnati, Ohio**

**Course 108. What's New in Pediatric Radiology?**

Selected recent reports of subjects in the field of Pediatric Radiology will be evaluated critically. Presentation will be on a body system basis including skeletal, neuromuscular, genitourinary, gastrointestinal and respiratory systems. The selection of subjects will be arbitrary but a question period should allow for consideration of any important omissions.

**Course 208. Gastrointestinal System**

Techniques of examination and review of impor-

tant pathologic findings in infants and children will be reviewed. Emphasis will be on the recognizable and remediable abnormalities.

---

**COURSE 109**
**COURSE 209**
**and**
**COURSE 309**

**Tuesday, Wednesday and Thursday**

**ALEXANDER S. MACMILLAN, JR., M.D.**
**Boston, Massachusetts**

**Sinuses, Mastoids and Laryngopharynx**

**Course 109. Sinuses and Orbits**
**Course 209. Mastoids and Temporal Bone**
**Course 309. Laryngopharynx**

Following a discussion of positioning, normal and some acceptable variations of the normal plus various pathologic states will be presented. As much information as possible will be given in as short a time as possible. Following the presentation, there will be opportunity for questions.

---

**COURSE 110**

**Tuesday**

**STANLEY BAUM, M.D.**
**Philadelphia, Pennsylvania**
**GEORGE N. STEIN, M.D.**
**Philadelphia, Pennsylvania**
**ARTHUR K. FINKELSTEIN, M.D.**
**Philadelphia, Pennsylvania**

**Selective Mesenteric Angiography in the Diagnosis of Gastrointestinal Abnormalities**

Selective mesenteric angiography in the diagnosis of gastrointestinal abnormalities is a relatively new procedure in this country, but it is rapidly receiving widespread acceptance. Its proper and safe employment depends upon a skillful team. This course is not arranged for experts in this field, but is being presented for radiologists who are interested in the subject and who may be contemplating the establishment of such a facility in their own hospital practice.

There will be a demonstration of the present areas of usefulness, and the advantages and limitations of abdominal angiography in gastrointestinal diagnosis, as compared with conventional radiologic studies of these areas.

Following a brief review of the historical background and a similarly brief explanation of the technical procedure and equipment required, the major anatomic features will be quickly shown. Most of the presentation will be devoted to discussion of the use of selective arteriography in certain abnormalities of the liver, spleen, pancreas, gastrointestinal tumors, vascular anomalies and occlusive vascular disease. These topics will be illustrated by brief case histories and the conventional film studies by one of the panelists, followed by the other panelist who will explain the reason for deciding to perform angiographic studies in the specific case and a demonstration of the results of those studies.

At the conclusion of the presentation, questions will be invited, and answers will be attempted.

---

**COURSE 111**

**Tuesday**

**HARRY L. STEIN, M.D.**
**New York, New York**

**The Application of Angiocardiographic and Arteriographic Procedures in Emergency Situations**

In the past decade, angiographic techniques have assumed a prominent place in the routine daily practice of diagnostic roentgenology. These procedures are being requested and applied more frequently on an emergency basis than ever before.

The various angiocardiographic and arteriographic methods employed in these situations will be covered. The types of emergencies encountered, citing representative cases, will be shown and discussed.

The broad areas thus covered will include: (A) The Heart and Great Vessels; (B) Visceral and Peripheral Arteriography; and (C) Cerebrovascular Emergencies. Such entities as pulmonary embolus, dissecting aortic aneurysm, renal embolus, visceral and peripheral trauma are included.

---

**COURSE 112**
**and**
**COURSE 212**

**Tuesday and Wednesday**

**SIDNEY W. NELSON, M.D.**
**Columbus, Ohio**

**Bronchography**

Course 112. The radiologist who can properly perform and interpret bronchograms is in a position where he can make outstanding contributions to the diagnosis and understanding of many chest diseases. The proper therapy for any disease which affects the bronchial tree is often dependent upon the accurate determination of the nature and extent of the bronchial involvement. Inasmuch as the interpretation of bronchograms requires considerable knowledge of the normal anatomy of the tracheobronchial tree and some of the common anatomic variations, the pertinent anatomy will be discussed and illustrated. A good knowledge of bronchial anatomy will enable the radiologist to systematically identify each of the major segmental bronchi, because of his knowledge of the expected distribution of each of these bronchi. The identification of each of the major segmental bronchi is extremely important in interpretation.

Once the basic bronchographic anatomy has been considered, the details of the bronchographic technique will be described. This will include the method of performing topical anesthesia, introduction of intranasal catheter, method of injecting contrast medium in order to assure systematic filling of the desired segmental bronchi, proper positioning of patient for filling of each segment, and the spot filming techniques employed to thoroughly record the filling of the desired segmental bronchi. This portion of the discussion will also include a description of some of the characteristic features of various contrast materials. The advantages of fluoroscopically controlled spot filming in comparison with conventional large film techniques will be emphasized. Good bronchographic technique can be mastered with little effort and can be quickly performed by the radiologist and his technical staff, thus precluding the necessity for resorting to the "team" approach which is often so time-consuming and frustrating in large busy hospitals.

Course 212. During the second session the majority of the different types of bronchopulmonary pathology will be discussed including the following: 1. Chronic bronchitis: a. spasm; b. excessive secretions; c. dilated mucosal glands; d. destruction of mucosa. 2. Emphysema. 3. Segmental bronchiectasis. 4. Cystic lesions. 5. Bronchogenic carcinoma. 6. Pulmonary "coin" lesions. 7. Bronchial adenoma. 8. Erosion of bronchi by adjacent calcified lymph nodes. 9. Inflammatory strictures. 10. Bronchial relocation following atelectasis of surgical removal.

The value of bronchography in the differential diagnosis of many bronchopulmonary diseases will be emphasized throughout the course, as for instance, atelectasis due to bronchogenic carcinoma or other intrabronchial lesions. Segmental bronchiectasis with associated chronic pneumonic changes may mimic neoplasms on plain chest roentgenograms, but can be clearly identified by bronchographic methods. Chronic granulomas and other infections can frequently be identified by virtue of the bronchiectatic changes produced in adjacent bronchi, thus helping to differentiate these diseases from neoplastic processes. Certain pulmonary diseases have very specific bronchographic appearances; *e.g.*, bronchial adenomata, polycystic lung, etc.

It is hoped that this presentation will encourage radiologists to perform this extremely useful roentgenographic procedure more frequently in the future. In so doing, they will be able to make more significant contributions to the diagnosis and treatment of the patients referred to them for study by their colleagues who are not radiologists.

---

## COURSE 121

**Tuesday**

**M. LEDERMAN, M.B., D.M.R.E., F.F.R.**
**London, England**

### Anatomy in Relation to Cancer with Special Reference to Head and Neck Tumors

The upper air and food passages are defined and the possible reasons for development of cancers in certain parts of the buccal cavity and pharynx deduced from a study of the alimentary grooves. These extend from the floor of the mouth to the esophageal opening past the tongue and larynx. The grooves are in 3 segments: (I) buccal, (II) oropharyngeal, and (III) laryngopharyngeal, and each of them is a frequent site for cancer.

The natural history of the cancers encountered will be discussed with special reference to their therapeutic implications.

---

## COURSE 122

**Tuesday**

**MELVIN TEFFT, M.D.**
**Boston, Massachusetts**

### The Radiotherapeutic Management of Malignant Disease in the Pediatric Age Group

The radiotherapeutic management of children with malignant disease will be discussed.

The disease entities to be included will be: Wilms' tumor, neuroblastoma, soft tissue sarcoma, lymphoma, acute leukemia, primary bone neoplasia, central nervous system tumors, and other miscellaneous entities.

The discussion will comprise mode of clinical presentation, diagnostic investigations, and therapeutic management.

Prognosis in terms of survival will be discussed in regard to age at diagnosis, site of the primary lesion, and mode of therapy.

Special emphasis will be placed on radiotherapeutic techniques peculiar to the pediatric age group.

---

## COURSE 123

**Tuesday**

**M. VERA PETERS, M.D.**
**Toronto, Ontario, Canada**

### The Place of Radiotherapy in the Management of Lymphomas

The differences in the clinical manifestations and in the clinical course will be discussed with reference to Hodgkin's disease, lymphosarcoma, reticulum cell sarcoma and giant follicular lymphoma. A knowledge of these variations is helpful in the management of the individual patient since it allows one to anticipate the expected course and prescribe accordingly.

The curative approach will be stressed for the groups of patients offering a good prognosis and the plan of management will be presented for each stage of the disease in each morphologic group.

---

## COURSE 202

**Wednesday**

**DON C. WEIR, M.D.**
**St. Louis, Missouri**

### Roentgen Diagnosis of Injury of the Cervical Spine

The ever increasing burden of traffic on the streets and highways is resulting in an increase in the frequency of cervical spine injuries. These injuries represent acute medical emergencies and are also important in the realm of medico-legal litigation.

The atlanto-axial segment of the cervical spine is unlike the remainder of the spine both anatomically and functionally. Variations in normal alignment, dislocations, "rotation deformities," and fractures will be discussed. Reversal, or loss of the normal lordotic curve will be evaluated along with a discussion of the so-called "whip-lash," the "darling" of the plaintiff's attorney and the "bane" of the defendant's attorney.

The relative value of cervical diskograms and myelograms in injury will be presented. Luschka's joints will be discussed and their clinical significance evaluated.

Technical aspects of cervical spine examinations will be outlined and evaluation of conventional views, flexion and extension, oblique studies, laminagraphy and special pillar views will be considered.

---

## COURSE 203

**Wednesday**

**LEWIS S. CAREY, M.D.**
**Saint Paul, Minnesota**

### Congenital Heart Disease

This course consists of an analysis of the normal and abnormal cardiovascular silhouette. The significance of alterations in cardiovascular contour in various congenital cardiac malformations will be explained in correlative fashion by angiocardiographic studies.

---

## COURSE 204
## COURSE 304
## and
## COURSE 404

**Wednesday, Thursday and Friday**

**RICHARD H. MARSHAK, M.D.**
**New York, New York**

The following entities will be discussed:

**Course 204. Stomach and Duodenum**

1. Gastric Ulcer
2. Gastritis including Menetrière's disease (exudative enteropathy)
3. Differential diagnosis of circular defects of the stomach including submucosal tumors, aberrant pancreatic tissue, polyps, metastatic lesions, and lymphosarcoma
4. Abnormalities in the duodenal bulb not due to duodenal ulcer
5. Duodenitis??

**Course 304. Small Bowel**

1. Technique
2. The malabsorption syndrome
3. Regional enteritis
4. Infarction
5. Tumors
6. Intramural hemorrhage

**Course 404. Colon**

1. Inflammatory lesions of the colon
2. Tumors of the colon not including carcinoma

---

## COURSE 205
## and
## COURSE 305

**Wednesday and Thursday**

**ROBERT E. WISE, M.D.**
**Boston, Massachusetts**

### Cholangiography

The course will be divided into two periods.

Course 205. The first will be devoted to a discussion of oral and intravenous techniques of examination of the gallbladder and biliary ducts. Included will be current concepts and techniques of oral cholecystography. The indications, technique, interpretation, and pitfalls of intravenous cholangiography will be described in detail.

Course 305. The second period will be devoted to a discussion of direct cholangiography including percutaneous, operative and postoperative "T-tube" techniques.

---

### COURSE 206

**Wednesday**

**GIOVANNI DI CHIRO, M.D.**
**Bethesda, Maryland**

**Cisterns and Sulcuses in the Normal Pneumoencephalogram**

The normal pneumoencephalographic anatomy of cisterns and sulcuses will be reviewed in detail. Particular emphasis will be placed on the "critical" areas of the endocranial subarachnoidal pathways, *i.e.* on those segments which more often are displaced or distorted in cases of intracranial space-occupying lesions. The pitfalls in the interpretation of the cisternal images and the normal variations, at the borderline with the pathologic, will be discussed at length.

---

### COURSE 210 and COURSE 310

**Wednesday and Thursday**

**J. S. DUNBAR, M.D.**
**Montreal, Quebec, Canada**

**Pediatric Urology**

Course 210. *Technique.* The technique of urography will be discussed, with particular emphasis on infants and young children. The methods of roentgenography, the use and dosage of contrast medium, and the indications and contraindications for examination will be outlined. Particular emphasis will be placed on the diagnosis of chronic urinary infection and on lower tract disease. The value of excretory urography will be stressed, and the methods of using both radiography and cine-fluorography to derive maximum information by this method will be outlined.

Course 310. *Urinary Tract Abnormalities.* Some of the normal variants which may be confused with urinary tract disease will be discussed first. Abnormalities will then be demonstrated, including upper tract and lower tract obstruction, inflammatory disease, renal trauma and new growth. Particular emphasis will again be placed on diagnosis of abnormalities in early life, since these are the problems which are least familiar to the general radiologist.

---

### COURSE 211 and COURSE 311

**Wednesday and Thursday**

**BENJAMIN FELSON, M.D.**
**Cincinnati, Ohio**

**Course 211. The Hili and Pulmonary Vessels**

The hili and pulmonary vasculature often provide important clues in chest roentgen interpretation. However, variations within the normal range are so broad that it often is difficult to distinguish between the normal and the abnormal. Working from a background of the normal, the course will deal with minimal changes in the roentgenogram which indicate important disease. The discussion will include the following areas: (1) hili, (2) pulmonary arteries, (3) pulmonary veins, (4) lymphatics, (5) bronchial circulation, and (6) azygos system.

**Course 311. Alveolar and Interstitial Lesions in the Lung.**

The problem of differential diagnosis of the vast array of disseminated pulmonary lesions is an almost insurmountable one unless specific patterns can be identified on the roentgenogram. It is often possible to recognize the diffuse alveolar pattern and, once identified, the list of its causes is relatively short. The recognition of diffuse interstitial disease is considerably more difficult, but even here it is sometimes possible to reliably distinguish this pattern and thereby reduce the etiologic possibilities to a reasonable number. In this course the roentgen features of the alveolar and interstitial patterns will be described and the various causes of each will be illustrated.

---

### COURSE 221

**Wednesday**

**M. LEDERMAN, M.B., D.M.R.E., F.F.R.**
**London, England**

**Tumors of the Nasal Fossae and Paranasal Sinuses**

The natural history and the wide histologic variety of these tumors can be best understood by a study of the anatomy and development of this region. Tumors may arise from: (1) the nasal fossae; (2) the maxillary antra; (3) the ethmoidal air cells; (4) the sphenoidal sinus; and (5) the frontal sinus.

The various clinical and radiologic methods of studying and classifying these tumors will be discussed. Any treatment policy adopted must take into account:

(1) The limitations of radiotherapy when bone is invaded by cancer
(2) The limitations of surgery in the presence of ethmoidal invasion
(3) The need to conserve the normal eye

Treatment by radiotherapy alone does not give satisfactory results, nor are the results of surgery gratifying since most patients present with advanced lesions. The policy recommended is radiotherapy and surgery in combination, the irradiation with few exceptions preceding surgery.

The preparation and care of the patient and the radiation techniques employed at different energies will be discussed. Special emphasis will be placed on the need for orbital irradiation and the problems and techniques of ocular protection.

The complications of radiotherapy and the results of radiation treatment used alone or in combination with surgery will be given—based on a series of 600 cases seen and treated by the lecturer.

## COURSE 222

**Wednesday**

**MALCOLM A. BAGSHAW, M.D.**
**Palo Alto, California**

### Combined Radiation and Intra-Arterial Antimetabolite Therapy

This course will include a discussion of the theoretic considerations in the selection of certain antimetabolite compounds which might be used in combination with radiation therapy for advanced carcinoma of the head and neck or pelvis. The technical aspects of intra-arterial infusion will be discussed in detail, the results and complications in the treatment of over 50 patients by this method will be described. The agents to be considered will include methotrexate, 6-mercaptopurine and 5-bromodeoxyuridine.

## COURSE 223

**Wednesday**

**MARVIN M. D. WILLIAMS, Ph.D.**
**Rochester, Minnesota**

### Preparing for an Examination in Radiological Physics

The answers given to various types of questions in radiological physics, although not entirely incorrect, are often unsatisfactory. Frequently, the answer given is an equation, a numerical constant, or a memorized statement. The examinee frequently cannot tell (1) what conditions must be satisfied in order that the use of the equation is justified, (2) what the numerical constant represents, or (3) what the memorized statement means. This problem and some of these questions will be discussed with the aim not only of indicating a correct answer but also of showing that an acceptable answer is likely to follow naturally when the subject matter is understood. The discussion will include suggestions from other examiners in radiological physics.

## COURSE 301

**Thursday**

**HARRY Z. MELLINS, M.D.**
**Brooklyn, New York**

### Voiding Cystourethrography

The present status of the procedure in both children and adults will be discussed. Methods, criteria for diagnosis and limitations of the procedure will be covered. The presentation will be based upon a critical review of over 4,000 cases studied during the past 5 years.

## COURSE 302 and COURSE 402

**Thursday and Friday**

**HAROLD G. JACOBSON, M.D.**
**New York, New York**

### Roentgen Aspects of Some Miscellaneous Skeletal Abnormalities

The skeletal manifestations of the following entities will be discussed in two sessions: (1) Paget's disease; (2) fibrous dysplasia; (3) aseptic necrosis and allied disorders; (4) the reticuloses; (5) Gaucher's disease; (6) lymphoma; (7) leukemia; (8) agnogenic myeloid metaplasia; (9) neuropathic bone disease; (10) pigmented villonodular synovitis; (11) sarcoid; (12) tuberculosis; and (13) syphilis.

The roentgen features of these entities will be described, and although the commonplace findings will be demonstrated, a fair amount of emphasis will be placed on the unusual manifestations of these disorders. In all instances pathologic findings will be briefly described, and the concept of relating these findings to the roentgen patterns and appearances will be stressed.

## COURSE 303 and COURSE 403

**Thursday and Friday**

**ROBERT L. EGAN, M.D.**
**Indianapolis, Indiana**

### Over Nine Years' Experience with Mammography

**Course 303. Introduction and Technique of Mammography**

**Course 403. Diagnosis of Breast Lesions by Mammography**

Over 9 years' experience has been gained with soft tissue roentgenography of the breast in a Tumor Institute with an active breast service. These studies have proved a highly accurate and valuable adjunct to the clinical and pathologic evaluation of breast lesions.

A simple and readily adaptable roentgenographic technique will be presented. Cases illustrative of typical benign and malignant disease will be shown and the diagnostic features of each described and tabulated. Differential diagnosis, sources of error, limitations of the procedure and the clinical and pathologic implications of the method will be discussed.

The results of a statistical analysis of the first 1,000 consecutive examinations (all with a follow-up

from 1 to 9 years) will be reviewed. The error in 245 cases of malignant disease was 0.82 per cent.

---

### COURSE 306
### and
### COURSE 406

**Thursday and Friday**

**LEWIS E. ETTER, M.D.**
**Pittsburgh, Pennsylvania**

**Normal and Pathologic Roentgen Anatomy of the Skull, Paranasal Sinuses and Mastoids**

Course 306. Description of standard techniques and positions with illustrated slides for roentgen examination of the skull and paranasal sinuses. Comparison of advantages of one projection over another with respect to visibility of particular structures. General considerations with reference to the cerebral and facial components of the cranium with analysis of individual bone components that produce the various lines and shadows seen in plain roentgenograms of the skull. Examples of pathologic alterations of these normal structures will be shown. The analysis will cover studies of the sphenoid, frontal, temporal, ethmoid, parietal and occipital bones in various projections.

Course 406. Detailed roentgen anatomic analysis of the paranasal sinuses, middle ear and mastoid processes with description of precision roentgenographic techniques employed. Study of the roentgen features of the middle cranial fossa and their relations to the sphenoid and other paranasal sinuses. Consideration of the orbits and optic foramina with special attention to the frontal, ethmoid and sphenoid bone components in various projections as well as the features contributed by the zygomatic and maxillary bones.

---

### COURSE 307

**Thursday**

**GERALD D. DODD, M.D.**
**Philadelphia, Pennsylvania**
**ROY R. GREENING, M.D.**
**Philadelphia, Pennsylvania**
**SIDNEY WALLACE, M.D.**
**Philadelphia, Pennsylvania**

**Lymphangiography**

This discussion will include a brief review of the historical and experimental background of lymphangiography and detail the technique, indications and complications of the intralymphatic injection of various contrast media. The roentgen appearance of normal lymphatic channels and lymph nodes will be stressed with comment on normal variants which frequently lead to erroneous interpretation. Various abnormal states will be illustrated and current and future avenues of investigation considered. Time will be reserved for discussion from the floor.

---

### COURSE 308

**Thursday**

**RICHARD G. LESTER, M.D.**
**Durham, North Carolina**

**Selective Angiocardiography**

In this course consideration will be given to the diagnostic applications of several methods of selective angiocardiography, including right sided cardioangiography, left sided cardioangiography and selective thoracic aortography.

Following an analysis of the indications of these various types of selective angiocardiography, there will be a discussion of methodology with emphasis on X-ray apparatus, including cine-radiographic techniques, photo-radiographic devices, rapid film units, etc. The problem of providing optimal anatomic detail with data concerning dynamic changes in normal and pathologic structures will be outlined.

The major portion of the session will be devoted to the step by step analysis of the details of the diagnostic interpretation of these examinations in a wide variety of congenital cardiovascular diseases. Emphasis will be placed on the correlation of angiocardiographic findings with the findings at surgery and necropsy. The importance of detailed analysis of fine changes will be stressed. The necessity of precise definition of the various lesions and the significance of anatomic variations from the point of view of surgical correction will be brought out. More common congenital cardiovascular lesions will be discussed with emphasis on important variations within single diagnostic categories. Less common and rare lesions will be demonstrated from the point of view of recognition and their importance in terms of operability and correction. A brief discussion of the role of selective angiocardiography in acquired heart disease will also be presented.

Registrants in the course are invited to bring problem cases for discussion and analysis following the formal program.

---

### COURSE 312

**Thursday**

**GORDON POTTS, M.D.**
**New York, New York**

**The Normal Carotid Angiogram**

In this course the following aspects of carotid angiography will be discussed:

1. Technique of puncturing the carotid artery
2. Selective internal and external carotid angiography
3. Some aspects of simultaneous biplane filming techniques

4. The anatomy of the vessels filled during carotid angiography

The more important anatomic variations will be described with particular reference to those which may simulate the changes caused by mass lesions. The angiographic anatomy will be related to the gross anatomy of the brain.

---

### COURSE 321

**Thursday**

**M. LEDERMAN, M.B., D.M.R.E., F.F.R.**
**London, England**

#### Oropharynx

Anatomy and physiology of the different parts of the pharynx with special reference to the differing histologic tumor types encountered, and importance of Waldeyer's Ring in relation to tumor pathology.

Demographic factors in pharyngeal cancer and the significance of the Plummer-Vinson syndrome.

Clinical features of the different forms of cancer arising in:

(1) nasopharynx;
(2) the oropharynx and its subdivisions; *i.e.* soft palate, fauces, tonsil, base of tongue and postero-lateral pharyngeal walls.

General principles of treatment with special reference to the place of radiotherapy.

The techniques of radiotherapy for the different tumor sites using orthovoltage or megavoltage roentgen-rays, and telecurietherapy will be described.

The complications and results of radiotherapy will be given—based on a series of 1,200 cases seen and treated by the lecturer.

---

### COURSE 322

**Thursday**

**WARREN K. SINCLAIR**
**Argonne, Illinois**

#### Mammalian Cell Radiobiology and Radiotherapy

Techniques of establishing radiation survival curves in single mammalian cells both *in vitro* and *in vivo* have resulted in a better understanding of the kinetics of cell destruction *in vivo.* Radiobiologic responses which have been examined in detail by *in vitro* culture methods include the oxygen effect, recovery from sublethal damage, variation of response with age in the cell cycle, chromosome changes and variations in the properties of surviving cells. Representative results obtained in one cell line both with synchronized and asynchronous populations will be outlined as an illustration. Some of the problems of translating cell culture results to *in vivo* situations will be pointed out and the possible significance of results of culture studies for dose fractionation schedules in radiotherapy discussed. (Work supported by the U. S. Atomic Energy Commission.)

---

### COURSE 323

**Thursday**

**NORMAN SIMON, M.D.**
**New York, New York**

#### Iridium 192 as a Substitute for Radium

Iridium 192 has become a useful and practical substitute for radium in removable implants of tumors. It is more flexible and accurate than radium, and the exposure to personnel is less than with radium. Afterloading is feasible, and surgical techniques in implantation of tumors with iridium 192 are varied. Dosimetry is still a problem, and direct measurement of radiation in implants should be helpful. Iridium 192 should replace radium for removable implants, and its advantages may even extend the indications for implant of tumors.

---

### COURSE 401

**Friday**

**WILLIAM E. GANNON, M.D.**
**Brooklyn, New York**

#### The Localization of Intracranial Masses by Cerebral Angiography

This course will consist of a method of analyzing a cerebral angiogram to localize a space-occupying lesion. It will be assumed that there is no tumor stain present. The various types of displacement of the anterior cerebral artery, the frontopolar sign and the falx sign will be demonstrated. The significance of elevation of the middle cerebral group will be discussed. The value of the capillary and venous phases in the localization of mass lesions will be illustrated. Examples of the near and distant effects of a mass lesion will also be included.

---

### COURSE 405

**Friday**

**MAURICE D. SACHS, M.D.**
**Cleveland, Ohio**

#### A Practical Approach to Roentgenology of the Biliary Tract

The physiologic anatomy of the biliary tract as well as the abnormal findings will be considered in an effort to help improve diagnostic acumen.

Proper dosage will be discussed including a plea for discontinuance of so-called "double dose" methods.

A routine technique for oral, intravenous, operative and postoperative cholangiography will be presented.

The value of a fat meal, a delayed fat meal and the role of laminagraphy will be shown.

Examples of abnormal findings of the biliary tract, particularly dysfunction and fibrosis of the sphincter of Oddi, adenomyosis, pancreatitis, and carcinoma will be presented.

## COURSE 421

**Friday**

**M. LEDERMAN, M.B., D.M.R.E., F.F.R.**
**London, England**

### Larynx and Laryngopharynx

Problems of tumor classification with special reference to the TNM system.

Natural history of tumors affecting the larynx and laryngopharynx and its influence on radiation techniques.

Treatment policy and selection of cases for radiotherapy. Relationship between surgery and radiotherapy.

Radiation techniques available for treating tumors of the larynx and laryngopharynx at various energies.

Postradiation complications and their avoidance.

Results to be expected from radiation treatment based on a series of over 2,000 cases seen and treated by the lecturer.

## COURSE 422

**Friday**

**JOHN T. MALLAMS, M.D.**
**Dallas, Texas**

### Pre-Surgical Adjuvant Radiation Therapy

The experimental information on the adjuvant effects of radiation therapy will be reviewed. The clinical results and pathologic data of our own and other programs will be evaluated. New programs in progress at Baylor University Medical Center and their rationale will be presented in detail.

The discussion will consider lesions of the head and neck, lung, esophagus, ovary, urinary bladder, bone, colon, rectum, and the intra-abdominal sarcomata.

## CONDENSED SCHEDULE OF COURSES

**TUESDAY** 3:00 to 4:30 P.M. September 28, 1965

| Diagnostic Roentgenology | | Therapeutic Radiology, Nuclear Medicine, Physics and Radiobiology | |
|---|---|---|---|
| 101—Martel | Arthropathies: Differential Diagnosis, Part I | 121—Lederman | Anatomy in Relation to Cancer with Special Reference to Head and Neck Tumors |
| 102—Nice | Roentgen Examination of the Small Bowel: Factors Affecting Motility, Pattern and Diagnosis | 122—Tefft | The Radiotherapeutic Management of Malignant Disease in the Pediatric Age Group |
| 103—Morgan | Screen Intensification and Cineradiography | 123—Peters | The Place of Radiotherapy in the Management of Lymphomas |
| 104—Jacobson, Meyers | The Acute Abdomen: Intestinal Obstruction and Other Selected Conditions | | |
| 105—Wood | The Radiology of Subarachnoid Hemorrhage | | |
| 106—Singleton | Pediatric Chest Abnormalities | | |
| 107—Wittenborg | Osseous Manifestations of Systemic Disease in Infancy and Childhood, Part I | | |
| 108—Silverman | What's New in Pediatric Radiology? | | |
| 109—Macmillan | Sinuses and Orbits | | |
| 110—Baum, Stein, Finkelstein | Selective Mesenteric Angiography in the Diagnosis of Gastrointestinal Abnormalities | | |
| 111—Stein, H. | The Application of Angiocardiographic and Arteriographic Procedures in Emergency Situations | | |
| 112—Nelson | Bronchography, Part I | | |

## CONDENSED SCHEDULE OF COURSES

**WEDNESDAY** — **3:00 to 4:30 P.M.** — **September 29, 1965**

### Diagnostic Roentgenology

| | |
|---|---|
| **201—Martel** | Arthropathies: Differential Diagnosis, Part II |
| **202—Weir** | Roentgen Diagnosis of Injury of the Cervical Spine |
| **203—Carey** | Congenital Heart Disease |
| **204—Marshak** | Stomach and Duodenum |
| **205—Wise** | Cholangiography |
| **206—Di Chiro** | Cisterns and Sulcuses in the Normal Pneumoencephalogram |
| **207—Wittenborg** | Osseous Manifestations of Systemic Disease in Infancy and Childhood, Part II |
| **208—Silverman** | Gastrointestinal System |
| **209—Macmillan** | Mastoids and Temporal Bone |
| **210—Dunbar** | Pediatric Urology, Technique |
| **211—Felson** | The Hili and Pulmonary Vessels |
| **212—Nelson** | Bronchography, Part II |

### Therapeutic Radiology, Nuclear Medicine, Physics and Radiobiology

| | |
|---|---|
| **221—Lederman** | Tumors of the Nasal Fossae and Paranasal Sinuses |
| **222—Bagshaw** | Combined Radiation and Intra-Arterial Antimetabolite Therapy |
| **223—Williams** | Preparing for an Examination in Radiological Physics |

## CONDENSED SCHEDULE OF COURSES

**THURSDAY** — **3:00 to 4:30 P.M.** — **September 30, 1965**

| **Diagnostic Roentgenology** | | **Therapeutic Radiology, Nuclear Medicine, Physics and Radiobiology** | |
|---|---|---|---|
| **301—Mellins** | Voiding Cystourethrography | **321—Lederman** | Oropharynx |
| **302—Jacobson, H.** | Roentgen Aspects of some Miscellaneous Skeletal Abnormalities | **322—Sinclair** | Mammalian Cell Radiobiology and Radiotherapy |
| **303—Egan** | Introduction and Technique of Mammography | **323—Simon** | Iridium 192 as a Substitute for Radium |
| **304—Marshak** | Small Bowel | | |
| **304—Wise** | Cholangiography | | |
| **306—Etter** | Normal and Pathologic Roentgen Anatomy of the Skull, Paranasal Sinuses and Mastoids, Part I | | |
| **307—Dodd Greening Wallace** | Lymphangiography | | |
| **308—Lester** | Selective Angiocardiography | | |
| **309—Macmillan** | Laryngopharynx | | |
| **310—Dunbar** | Pediatric Urology, Urinary Tract Abnormalities | | |
| **311—Felson** | Alveolar and Interstitial Lesions in the Lung | | |
| **312—Potts** | The Normal Carotid Angiogram | | |

**CONDENSED SCHEDULE OF COURSES**

**FRIDAY** **1:30 to 3:00 P.M.** **October 1, 1965**

| Diagnostic Roentgenology | | Therapeutic Radiology, Nuclear Medicine, Physics and Radiobiology | |
|---|---|---|---|
| **401—Gannon** | The Localization of Intracranial Masses by Cerebral Angiography | **421—Lederman** | Larynx and Laryngopharynx |
| **402—Jacobson, H.** | Roentgen Aspects of Some Miscellaneous Skeletal Abnormalities | **422—Mallams** | Pre-Surgical Adjuvant Radiation Therapy |
| **403—Egan** | Diagnosis of Breast Lesions by Mammography | | |
| **404—Marshak** | Colon | | |
| **405—Sachs** | A Practical Approach to Roentgenology of the Biliary Tract | | |
| **406—Etter** | Normal and Pathologic Roentgen Anatomy of the Skull, Paranasal Sinuses and Mastoids, Part II | | |

# BOOK REVIEWS

*Books sent for review are acknowledged under: Books Received. This must be regarded as a sufficient return for the courtesy of the sender. Selections will be made for review in the interest of our readers as space permits.*

X-Ray Examination of the Stomach. A Description of the Roentgenologic Anatomy, Physiology, and Pathology of the Esophagus, Stomach, and Duodenum. Revised edition. By Frederic E. Templeton, M.D., Clinical Professor of Radiology, The University of Washington, Seattle, Wash. Pp. 598, with many illustrations. Price, $15.00. University of Chicago Press, Chicago, Ill., 1964.

This volume is listed as a revised edition, written 20 years after the first appearance of the book. Although the title remains the same and mentions only the stomach, the subtitle tells more accurately that this book is: "a description of the roentgenologic anatomy, physiology, and pathology of the esophagus, stomach and duodenum." It is slightly larger than the original. The figures have increased from 297 to 322. There are 82 more pages, but each contains slightly fewer printed words.

There is an interesting introduction by Paul Hodges, the former mentor of the author. The introduction has been expanded and there are up-to-date data about radiographic equipment, especially fluoroscopes. A brief chapter on protection and additional information concerning examination procedures have been added. New radiographic figures illustrate the lower esophagus, hiatal herniation and the duodenal bulb. An expanded section on varieties of examination and useful hints on practical technique show the touch of an experienced and thoughtful clinical radiologist. The reviewer believes this book is the best available account of how to perform a fluoroscopic examination, stressing as it does the procedural steps in fluoroscopy and spot-filming.

In the chapters considering various disease entities, anatomic, physiologic and pathologic features are closely correlated to radiographic appearance. The chapters on inflammations, ulcers, and neoplasms are excellent. As do most explanations of the complexities of the lower esophagus, the account in this book leaves some confusion in the reader's mind. It is interesting that the author claims priority for illustrating the lower esophageal ring (in the first edition, 1944), and says that the ring is a structural portion of the phrenic ampulla of the esophagus.

From the literature of the last 20 years, the author selects only 40 new references to add to almost 400 from the prior 30 years. If this seems a little ungenerous to workers of the past two decades, one may note in the prologue a quotation from Ecclesiastes: "Nothing under the sun is new. . . . For it hath already gone before in the ages that were before us." In a sense, therefore, this is the testament of an older radiologist, although it is still the basis on which most of us have to work. Image amplification, cineradiography and video-taping will have to be evaluated by a new generation.

In summary, this is a conscientious report by a very able radiologist. It will be extremely helpful to the resident who is trying to develop a personal competence in examination. It will also appeal to most experienced radiologists as an excellent practical review of a phase of radiology that occupies a considerable share of their personal attention.

Seymour Fiske Ochsner, M.D.

Anatomico-Roentgenographic Studies of the Spine. By Lee A. Hadley, M.D., Senior Attending Roentgenologist, Syracuse Memorial Hospital, Syracuse, N.Y.; Lecturer in Radiology, Upstate Medical Center, New York State University, Syracuse, N.Y.; Former Clinical Associate Professor of Public Health, Syracuse University College of Medicine, Syracuse, N.Y. Cloth. Pp. 545, with many illustrations. Price, $26.00. Charles C Thomas, Publisher, 301–327 East Lawrence Avenue, Springfield, Ill., 1964.

This book merits attention because it focuses on the correlation between the radiologic appearance and the morphologic and histologic findings in a variety of conditions. It is enriched by the frequent and effective use of long term follow-up studies of individual patients clearly showing the late sequelae of particular lesions. The illustrations are quite plentiful and of excellent quality. Often different examples of the same type of abnormality are included and, in places where the text is concise

and the illustrations numerous, the book takes on the appearance of an atlas. The legends are comprehensive and many include capsules of clinical information which enhance the reader's interest.

The book is not intended as a "complete text book" of spinal diseases. As a result, the subject matter is dealt with unevenly and the chapter organization is rather unconventional. Some chapters are organized on an etiologic basis, others on anatomic or regional considerations and some include rather diverse and miscellaneous conditions. Chapters which are particularly well done are those on normal and abnormal development, the cervical region, the intervertebral articulations and the effects of degenerative changes. Subjects which are dealt with less extensively include endocrine and metabolic diseases, infections and tumors. A bibliography, organized according to subject, appears at the end of each chapter. However, there are relatively few specific references in the text. It would have been preferable to indicate more often the source of the observations.

The book reflects the author's long experience. It is recommended to radiologists, orthopedic surgeons, neurologists and allied specialists interested in spinal diseases.

William Martel, M.D.

## BOOKS RECEIVED

International Conference on Avian Tumor Viruses. National Cancer Institute Monograph 17, December, 1964. Sponsored by National Cancer Institute, National Institutes of Health, Bethesda, Md., and Duke University School of Medicine, Durham, N. C. Edited by Joseph W. Beard. Cloth. Pp. 803, with many illustrations. Price, $6.25. Superintendent of Documents, U. S. Government Printing Office, Washington, D. C., 1965.

Practical Gamma Spectrometry. By A. J. Duivenstijn and L. A. J. Venverloo. Cloth. Pp. 146, with 67 illustrations. Price, $7.50. Charles C Thomas, Publisher, 301–327 East Lawrence Avenue, Springfield, Ill., 1965.

Dosemeters for X-Ray Diagnosis. By K.Reinsma. Cloth. Pp. 110, with 36 figures. Price, $4.50. Charles C Thomas, Publisher, 301–327 East Lawrence Avenue, Springfield, Ill., 1965.

Medical X-Ray Technique: Principles and Applications. Second edition. By G. J. van der Plaats, M.D. Cloth. Pp. 496, with 260 illustrations. Price, $14.50. Charles C Thomas, Publisher, 301–327 East Lawrence Avenue, Springfield, Ill., 1965.

Radioisotopes and Their Industrial Applications. By H. Piraux. Cloth. Pp. 266, with many illustrations. Price, $14.50. Charles C Thomas, Publisher, 301–327 East Lawrence Avenue, Springfield, Ill., 1965.

Myelography. By Vincenzo Valentino, Docent of Neuroradiology, University of Naples, Naples, Italy. Cloth. Pp. 273, with 221 illustrations. Price, $19.50. Charles C Thomas, Publisher, 301–327 East Lawrence Avenue, Springfield, Ill., 1965.

Ultrasonic Engineering. By Julian R. Frederick, Associate Professor of Mechanical Engineering, University of Michigan. Cloth. Pp. 379, with many illustrations. Price, $15.00. John Wiley & Sons, Inc., Publishers, 605 Third Avenue, New York, N. Y., 1965.

A Diagnostic Approach to Chest Diseases: Differential Diagnoses Based on Roentgenographic Patterns. By Glen A. Lillington, B.Sc., M.D., M.S. (Med), F.R.C.P. (C), Section of Medicine, Palo Alto Medical Clinic; Research Associate, Palo Alto Medical Research Foundation; Clinical Assistant Professor of Medicine, Stanford University School of Medicine; and Robert W. Jamplis, B.A., M.D., M.S. (Surg), F.A.C.S., Section of Thoracic Surgery, Palo Alto Medical Clinic; Research Associate, Palo Alto Medical Research Foundation; Clinical Assistant Professor of Surgery, Stanford University School of Medicine. Cloth. Pp. 508, with many illustrations. Price, $14.50. The Williams & Wilkins Company, Baltimore, Md., 1965.

Planning for Medical Progress Through Education. A Report Submitted to the Executive Council of the Association of American Medical Colleges. By Lowell T. Coggeshall, M.D. Paper. Pp. 107, with some charts. Price, $2.00. Association of American Medical Colleges, 2530 Ridge Avenue, Evanston, Ill., 1965.

Medical Uses of Radium and Radium Substitutes. Conference Summary and Conclusions, University of Chicago, September 3 & 4, 1964. Paper. Pp. 40. U. S. Department of Health, Education, and Welfare, Public Health Service, Washington, D. C., 20201, 1965.

Pulmonary Diffusing Capacity for Carbon Monoxide in Relation to Cardiac Output in Man. By Jan Bjure, Department of Clinical Physiology, Sahlgrenska Sjukhuset, University of Göteborg, and Department of Clinical Physiology, University of Umeå, Sweden. Paper. Pp. 113. The Scandinavian Journal of Clinical & Laboratory Investigation, Volume 17, Supplementum 81, 1965.

Visual Principles of Elementary Human Anatomy. By Charles E. Tobin, Ph.D., Professor of Anatomy; and Peter Ng, B.F.A., M.S., Medical Illustrator, The University of Rochester School of

Medicine and Dentistry, Rochester, N.Y. Paper. Pp. 102, with many illustrations. Price, $2.50. F. A. Davis Company, Publishers, 1914–16 Cherry Street, Philadelphia, Pa., 1965.

IMPLICATIONS TO MAN OF IRRADIATION BY INTERNALLY DEPOSITED STRONTIUM-89, STRONTIUM-90, and CESIUM-137. A report of an Advisory Committee from the Division of Medical Sciences, National Academy of Sciences, National Research Council, Washington, D.C., December 1964. Paper. Pp. 34. Federal Radiation Council, Washington, D. C., 1965.

BACKGROUND MATERIAL FOR THE DEVELOPMENT OF RADIATION PROTECTION STANDARDS: PROTECTIVE ACTION GUIDES FOR STRONTIUM-89, STRONTIUM-90, and CESIUM-137. Staff Report of the Federal Radiation Council, May, 1965. Report No. 7. Paper. Pp. 44. Price, $0.30. Superintendent of Documents, U. S. Government Printing Office, Washington, D. C., 20402, 1965.

RÖNTGEN-UND KERNPHYSIK: FÜR MEDIZINER UND BIOPHYSIKER. By Prof. Dr. Dr. h. c. Richard Glocker, and Doz. Dr. Eckard Macherauch. Cloth. Pp. 520, with 375 illustrations. Price, Ganzleinen DM 69,-. Georg Thieme Verlag, Postfach 732, Herdweg 63, 7000 Stuttgart 1, Germany, 1965.

NEUE ERGEBNISSE DER BIOPHYSIKALISCHEN FORSCHUNG. From the Max Planck-Institut für Biophysik Frankfurt am Main, aus Anlass seines fünfundzwanzigjährigen Bestehens. Paper. Pp. 168, with 64 illustrations. Price, DM 26,-. Georg Thieme Verlag, Postfach 732, Herdweg 63, 7000 Stuttgart 1, Germany, 1965.

AN EVALUATION OF A METHOD FOR DETERMINATION OF FREE CORTICOSTEROIDS IN MINUTE QUANTITIES OF MOUSE PLASMA. By J. H. Solem, and T. Brinck-Johnsen. Paper. Pp. 14 with some illustrations. The Scandinavian Journal of Clinical & Laboratory Investigation. Volume 17, Supplementum 80. Oslo, 1965.

ABRIDGED SCIENTIFIC PUBLICATIONS. Volume 40, 1963. From the Kodak Laboratories. Paper. Pp. 257, with many illustrations. Published by Department of Information Services, Research Laboratories, Eastman Kodak Company, Rochester, N.Y., 1965.

EINE UNTERSUCHUNG DER FERSENBELASTUNG BEIM GEHEN: EINE METHODE FÜR DIE MESSUNG DER FERSENBELASTUNG IM SCHUH. By Hilding Wetzenstein. Paper. Pp. 94, with many illustrations. Acta Orthopaedica Scandinavica. Supplementum No. 75. Stockholm, 1964.

THE GEORGE BANTA COMPANY STORY, 1902–1962. By C. A. Peerenboom. Paper. Pp. 255, with many illustrations. George Banta Company, Inc., Menasha, Wis., 1965.

## THE BRITISH INSTITUTE OF RADIOLOGY

LONDON—13th–17th September, 1965.

Radiologists, Radiotherapists, Physicists and Radiobiologists visiting England on their way to the Rome International Congress of Radiology are invited to write to The Secretary of The British Institute of Radiology, 32 Welbeck Street, London, W. 1., where assistance may be obtained in planning hospital visits and where it is hoped to hold scientific and social meetings.

# ABSTRACTS OF RADIOLOGICAL LITERATURE

## INDEX TO ABSTRACTS

## ROENTGEN DIAGNOSIS

### Head

Gros, Ch. M., and Wachenheim, A. Critique radiologique de l'impression basilaire. (A radiologic critique of basilar impression.) *J. de radiol., d'électrol. et de méd. nucléaire*, Dec., 1964, *45*, 781–788. (From: Service Central de Radiologie and Clinique Neurologique de Strasbourg, France.)

Basilar impression usually is congenital and due to lack of expansion of the posterior fossa, so that the region of the foramen magnum is invaginated. It is *not* due to ascension of the first two cervical vertebrae, although the radiologist may be put off the track and fail to evaluate the hypoplasia because he is accustomed to making the diagnosis from certain bench-marks, usually those found in lateral views. The authors find these insufficient and rely also on 3 lines, all drawn on posteroanterior tomograms made in the nose-forehead position with the cuts at the level of the odontoid. These are: (1) the bidigastric line, drawn between the digastric grooves (mastoid notches); (2) the bimastoid line, drawn through the tips of the mastoids; here the tip of the odontoid should be tangent to this or not more than 7 mm. above it; and (3) the condylo-atloid angle. Lines through the joint surfaces here will normally meet in the midline at 124° to 134°.

The basilar line is one in the lateral view which also is of particular use. The odontoid is just tangential to this line, which is a downward prolongation of the clivus. It is used not so much to show a basilar impression as it is to differentiate occipital luxations.

It is not enough for the radiologist to make the diagnosis, but he should describe the distinct osseous aberration which has produced the deformity. These are:

1. DYSHARMONIC BASILAR IMPRESSIONS.
   a. *Basi-occipital dysplasia.*
      —*simple shortening of the clivus*, which normally is 3.2 cm. $\pm$.3. A shortening gives an anterior basilar impression.
      —*shortening, straightening and hypoplasia of the clivus* which give an anterior impression, plus a posterolateral one associated with condylar and lateral occipital deformities.
   b. *Occipital condylo-lateral or posterolateral impressions.*
      —*condylar form.* Hypoplasia or aplasia of the condyles. The condylo-atloid angle is in excess of 135°.
      —*posterolateral form.* This is best demonstrated by evaluating the bidigastric line.
   c. *Partly or completely unilateral* due to condylolateral dysplasia.
2. HARMONIC BASILAR IMPRESSIONS. The aplasia is proportionate.
   a. *Associated impressions.* These are slight and often accompany other deformities of the cervico-occipital joint.
   b. *Acquired impressions.* These may appear in Paget's, Lobstein's, Recklinghausen's and Bechterew's diseases. Generally they are of the posterolateral type.

There are lesions in which the odontoid passes above Chamberlain's line which are not basilar impressions, specifically an anterior luxation of the occiput, odonto-atloid diastasis and malformations of the atlas. These are differentiated from basilar impressions by evaluating the base of the occiput, the bidigastric line and the condylo-atloid angle.—*Frank A. Riebel, M.D.*

Gass, J. Donald M. Orbital and ocular involvement in fibrous dysplasia. *South. M. J.*, March, 1965, *58*, 324–329. (From: University of Miami School of Medicine, and the Bascom Palmer Eye Institute, Miami, Fla.)

This report concerns itself with case histories of 3 patients having progressive unilateral occular complaints secondary to fibrous dysplasia limited to the orbit. In each instance, the disease was eradicated by surgical excision.

Fibrous dysplasia of the skull, as elsewhere, usually has a characteristic roentgenographic appearance. However, when the orbital plate of the frontal bone is involved fibrous dysplasia may resemble a meningioma. In this respect, it is well to remember that fibrous dysplasia usually occurs in children and adolescents, while meningioma is typically seen in adults.—*John H. Harris, Jr., M.D.*

Terrahe, K. Missbildungen des Inner- und Mittelohres als Folge der Thalidomidembryopathie—Ergebnisse von Röntgenschichtuntersuchungen des Ohres. (Malformations of the inner and middle ear due to thalidomidembryopathy—results of roentgentomographic examinations of the ear.) *Fortschr. a. d. Geb. d. Röntgenstrahlen u. d. Nuklearmedizin*, Jan., 1965, *102*, 14–29. (Address: Kardinal-von-Galen-Ring 10, 4400 Münster/Westfalen, Germany.)

Tomography of the middle and inner ear has made great progress in recent years since the introduction of pluridimensional blurring with the polytome. Its aid in the investigation of congenital defects is invaluable. Thalidomidembryopathy of the ear occurs frequently, being only second to dysplasias of the extremities. Less often encountered are atresias of the gastrointestinal tract, congenital heart lesions and facial hemangiomas.

Tomographic studies are most important in deciding operability and specific surgical planning. Thirty-seven out of 180 patients have been selected so far, because bilateral involvement resulting in deafness makes a plastic operation at an early date desirable. Technically, tomograms in the anteroposterior and Stenvers projection yield sufficient information.

The inner ear was involved 55 times, unilaterally in 19 and bilaterally in 17 patients. Dysplasia and aplasia of the lateral semicircular canal occurred most frequently (25 times). The superior semicircular canal and the cochlea were less often involved. When the posterior semicircular canal was also absent, the entire inner ear was aplastic. This happened 12 times with 2 patients exhibiting bilateral involvement and narrow internal auditory canal, elevation of the bulbus of the jugular vein and a flattened carotid canal. In 3 instances, the entire labyrinth was aplastic.

The middle ear displayed a variety of malformations of the tympanic cavity and of the ossicles. The facial-nerve canal was often narrowed due to mechanical compression. A frequently encountered facial paralysis, however, was unrelated but rather due to dysplasia of the central nucleus of the facial nerve. On the other hand, a narrow or obliterated internal auditory canal suggested aplasia or hypoplasia of the acoustic nerve.—*Ernest Kraft, M.D.*

FRANK, R. M., HERDLY, J., and PHILIPPE, E. Acquired dental defects and salivary gland lesions after irradiation for carcinoma. *J. Am. Dent. A.*, April, 1965, *70*, 868–883. (Address: Dr. Frank, Institut Dentaire, Faculté de Médecine, Strasbourg, France.)

The authors followed 61 patients, who had received radiation therapy for carcinomas of the oral cavity, ora- and nasopharynx, hypopharynx and larynx, in an attempt to substantiate the premise that acquired dental defects after irradiation bear a direct relationship to alterations of the salivary glands and the secretion of saliva. A careful review of the literature seemed to point strongly to this cause and effect relationship. The patients who made up the present study consisted of 59 who had been treated with cobalt 60 teletherapy and 2 who had radium implants combined with external roentgenray irradiation. Particular care was taken to note whether or not the teeth were outside or inside the treatment field, and also the dose to the parotid and submandibular glands, which with cobalt 60 therapy usually ran in the neighborhood of 5,000 to 6,000 r on each side. Symptoms such as a loss of taste, dryness to the mouth and a sensation of bitterness were also recorded. The salivary flow was determined, and its quality noted. A histologic study of the salivary glands, secured from radical neck dissections, was carried out.

The authors found that in all patients who had dental defects acquired after radiation therapy, the salivary glands had been included in the field of irradiation. In 6 patients with no subsequent dental defects, the salivary glands had been completely outside of the radiation field; or only one side had been irradiated. In the patients with acquired dental defects, it was found that the dental lesions were identical regardless of whether the teeth were outside or inside the radiation field. Histologically, the dental lesions were similar to dental caries, differing only in their location. The acquired defects were located usually on the buccal, palatal, or lingual surfaces, and the incisal or occlusal edges, areas usually spared by dental caries. These are areas similiar to those seen in children with congenitally absent salivary glands or in Sjogren syndromes—areas that in normal individuals are protected by salivary flow.

It was found that in patients who received considerable radiation to their salivary glands, there was a drastic reduction in salivary flow, which on occasion lasted as long as 5 years after therapy, but which usually increased again after 2 to 6 months. After irradiation of the salivary glands, the saliva that was produced consisted of a thick, viscid, cloudy, discolored solution. There was a definite increase in the nitrogen content and a marked lowering of the pH. This was most dramatic 2 to 3 months after irradiation, and tended to rise again 2 to 6 years later. This altered saliva covered the teeth and provided an excellent substrate for bacterial attacks. The salivary glands themselves showed pronounced glandular atrophy, fibrosis, and adiposis. In contrast to this, patients who were given radiation directly to the jaws and teeth, but not to the salivary glands, failed to develop dental lesions even 3 years after therapy, and had a normal production and appearance of their saliva. The lubricating, moistening, diluting, cleansing, neutralizing, and antibacterial actions of the saliva were in evidence.

The authors would like to see a reappraisal of the commonly held belief that teeth must be extracted prior to radiotherapy as a preventive measure. They also suggest that the radiotherapist should carefully consider the possibility of avoiding salivary gland irradiation whenever technically possible.—*Kenneth M. Nowicki, M.D.*

BRABAND, H. Probleme der Röntgendiagnostik des Ameloblastoms in Westafrika. (Problems of the roentgen diagnosis of ameloblastoma in West Africa.) *Fortschr. a. d. Geb. d. Röntgenstrahlen u. d. Nuklearmedizin*, March, 1965, *102*, 310–319. (From: Department of Radiology of University College Hospital, Ibadan, Nigeria.)

Ameloblastoma of the mandible originates from the dental epithelium. Several variations exist

roentgenologically and histologically. In West Africa, the disease is predominantly encountered in the native Bantu population. It develops especially in the third decade of life, and there is a male preponderance of 3:1.

The author observed the tumor in 50 patients. The histories suggested a gradual swelling of the mandible, especially the left, over a period of 2 to 3 years. Occasionally, the tumor could be traced back 5 years without causing any considerable inconvenience or pain. The area between the third lower molar and the angle of the mandible was the usual starting point, from where it extended to the horizontal and the ascending rami. The tumor consisted of larger and smaller cysts containing clear to turbid fluid. Secondary infection and ulceration were rarely observed.

Histologically, the following types can be distinguished: (1) fibro-ameloblastoma, (2) melano-ameloblastoma, (3) hemangio-ameloblastoma, and (4) adeno-ameloblastoma.

Roentgenologically, the unilocular or monocystic form causes difficulties of differential diagnosis. It may simulate a dental cyst when it extends to the root of a tooth. A very large cyst, however, suggests ameloblastoma. The development of osseous septa and trabeculae within the tumor is quite characteristic. Multiple cystic cavities are most typical although they can masquerade as multiple dental cysts, giant-cell tumors, aneurysmal bone cysts, osteofibroma and fibrous dysplasia.

In 5 per cent of all tumors of the jaw, atypical roentgen appearances prevented a definite diagnosis due to a far advanced stage and degenerative changes.—*Ernest Kraft, M.D.*

Hastings-James, R. Tumors of the eighth cranial nerve in roentgen diagnosis. *J. Canad. A. Radiologists*, March, 1965, *16*, 19–24. (From: The Victoria General Hospital, Halifax, Nova Scotia, Canada.)

This paper discusses the roentgeonologic findings in 18 cases of 8th nerve tumor. There were 12 male and 6 female patients. The time of onset was for the most part in later middle age.

The clinical findings are listed according to frequency of occurrence. It is noted that increased intracranial pressure is a rather frequent finding. The sella turcica was considered to be normal in 5 patients. The 13 abnormal appearing sellae showed varying degrees of thinning and demineralization of the dorsum sellae and posterior clinoids, the changes being considered marked in 7 and slight in 6. Prominent emissary channels were seen in 10 cases.

The roentgenologic appearances produced by the tumor involving the 8th nerve in its course through the temporal bone have been described in previous reports. Bone changes are seen in about 85 per cent of cases by the time the patients present for examination. The alterations produced may be considered as both quantitative and qualitative, the former consisting of a widening of the internal auditory canal, and the latter a change in the appearance of the bone locally.

The author made careful measurements of the width of the internal auditory canal at corresponding points on the two sides, and believes that this comparison is important. While the 17 normal canals measured an average of 5.5 mm., the 19 abnormal ones averaged 9.5 mm. in width. The finding of a normally wide meatus in the presence of an acoustic neuroma is rarely due to the small size of the tumor but rather to its central location, with absence of extension into the more peripheral canal. Changes of a qualitative nature are frequently the chief finding. These were seen in 10 cases and consisted of local decalcification or erosion of the bone.

Pneumoencephalography was found to be the most useful of the special procedures.—*Douglas S. Kellogg, M.D.*

Courville, Cyril B. Contrecoup injuries of the brain in infancy: remarks on the mechanism of fatal traumatic lesions of early life. *A.M.A. Arch. Surg.*, Jan., 1965, *90*, 157–165. (Address: 1200 N. State Street, Los Angeles, Calif. 90033.)

The author analyzed the clinical and postmortem data in 48 cases of craniocerebral injury in childhood, to assess the age and incidence at which the typical lesions first appear.

Before the age of 3 years, contrecoup injury was noted in 10 per cent of his cases. The incidence increased to 71 per cent in the 4 year age group. This represents a significant difference from the adult population in which 85 per cent of craniocerebral trauma is accompanied by contrecoup lesions.

The greatest incidence of contrecoup injuries was noted with blows to the lateral side of the head in which contra-lateral temporal lobe contusions are to be expected. Impact on the postero-lateral region of the skull may produce contra-lateral fronto-temporal contusions. Contra-lateral subfrontal and anterior temporal lobe contusions may be expected when the impact is in the occipital region. Basal contusions may occur when the impact is on the vertex.

The author postulates the low occurrence of contrecoup injuries in children below the age of 4 years to be due to the greater plasticity of the infant's cranium; less convolutional markings within the skull's inner table; and the softer textures of the infant's brain.

A conclusive diagnosis of contrecoup injury in children (contusion or intracerebral hemorrhage) cannot be made without actual visual confirmation at surgery or postmortem examination.—*James F. Martin, M.D.*

Adapon, Benjamin D., Chase, Norman E., Kricheff, Irvin I., and Battista, Arthur F. Cerebral ultrasonic tomography. *Radiology*, Jan., 1965, *84*, 115–121. (From: Departments of Radiology [Neuroradiology], Neurology and Neurosurgery, New York University Medical Center, New York, N. Y.)

The purpose of the authors is to illustrate some of the techniques employed and results obtained in ultrasonic echo scans of patients with intracranial masses. The scanning instrument employed in this study was the Hoffrel Model 100 Medical Ultra-Sonoscope, equipped with the Hoffrel Model 500 Precision Rectangular Co-ordinate Scanner and scanner-control unit.

With the patient in the decubitus position on the stretcher, the transducer probe is applied along a line drawn on the occipito-temporal-frontal region 6 cm. above the canthomeatal line. The tracing is marked at the level of the external auditory meatus. The motorized transducer holder regulates the speed of the probe along the surface of the skull. The direction in which the transducer is aimed may be adjusted up to 30° from the vertical. This aids in obtaining a proper beam entrance and good acoustical contact along irregular contours. The transducer is moved along this path from posterior to anterior. Paired tracings are usually obtained on both sides of the skull for comparison, and the tracings are photographed with the Polaroid Land camera.

The scanning methods are employed and are classified as Type "A" and Type "B." Type "A" scanning is used to locate the midline and to determine whether or not it has shifted. There is also a differential absorption transmission and reflection of ultra-sound waves between many pathologic lesions and normal brain tissues. The "B" scan identifies and projects these differences and has the potential of actually delineating intracranial masses.

One hundred neurologic patients were subjected to "A" and "B" scans. All had either neuroradiologic diagnostic procedures, and/or surgical exploration or autopsy. The midline echo was considered normal if it was within 1.5 mm. of the midline. Forty-two patients had roentgenographically proved midline shifts. Thirty-eight of these were predicted correctly on the "A" scan, giving an accuracy of 90.4 per cent. There were 3 false negatives.

In 49 cases no midline shift could be determined by echo or conventional neuroradiologic diagnostic procedures. There was one false positive midline echo shift of 1.7 mm. Two of the echo tracings were technically unsatisfactory for analysis. This gave an accuracy of 94.2 per cent in patients with no midline shifts.

In 43 patients with "B" scans intracranial masses were histologically verified. There were 10 subdural hematomas, 1 epidural hematoma, 8 deep intracerebral clots, 3 meningiomas, 11 gliomas, 5 metastatic tumors, 2 craniopharyngiomas, and 1 pituitary adenoma. Six masses (14 per cent) were accurately demonstrated, and fifteen (34.9 per cent) were not well defined but displayed abnormal echo patterns suggestive of masses. Twenty-two cases were entirely normal on the "B" scan. One of two posterior fossa tumors was accurately diagnosed. Hydrocephalus in children was readily demonstraed by the "B" scan in 4 instances.

The authors conclude that the accuracy of the method is still low; however, it is simple, easily reproducible, and quite inexpensive. It may find great importance as a screening test for more elaborate neuroradiologic examination in cases with clinical suspicion of mass lesions.—*Howard R. Stewart, M.D.*

Gillot, Cl., Aaron, Cl., Chassaing, P., and Delmas, A. Les veines cérébrales et les sinus craniens: aspects normaux obtenus par la méthode de phlébographie occlusive. (Cerebral veins and cranial sinuses: normal aspects demonstrated by the occlusive phlebographic method.) *Presse méd.*, Jan., 1965, *73*, 229–234. (From: Laboratoire d'Anatomie de la Faculté de Médecine de Paris, Paris, France.)

Noting that in the venous phase of routine cerebral angiography not all the veins of the skull, particularly those at the base, are fully opacified, the authors developed this technique for opacifying all the cerebral veins. A catheter is introduced through the saphenous vein at a point approximately 2.0 cm. lateral and below the spine of the os pubis. The catheter has a balloon at its end which, without the aid of roentgenoscopic control, is passed through the right heart into the jugular vein in the neck. As the tip reaches the jugular foramen at the base of the skull, the rubber balloon is inflated by the addition of 10 ml. of water, thus occluding the internal jugular vein. This is followed by the injection of an iodized contrast medium, and 5 films are exposed successively, after the injection of 15, 30, 50, 70 and 100 ml. of the contrast medium. This results in opacification of the entire venous system including the superficial cerebral veins.

For the purpose of this study the cerebral venous system is divided in three parts, best seen in the lateral projection. The contrast medium flows against the current and opacifies, in the following order: (1) the veins at the base; (2) the deep cerebral veins; and (3) the superficial veins or the veins of the convexity of the brain.

The procedure was first performed on 20 dogs and subsequently on 100 cadavers, before it was used in the human subject.

Other methods for opacification of the cerebral

veins have been tried, but have proved unsatisfactory. These include injection through the ophthalmic vein, which leads to the cavernous sinus, and a direct injection into the internal jugular vein. At this point the authors consider their work to be essentially a basic study of anatomy.

The practical or clinical applications of this method, particularly in cerebral trauma, will be the subject of a subsequent publication.

Reproductions of 17 roentgenograms and diagrams accompany this interesting work.—*William H. Shehadi, M.D.*

Kricheff, Irvin I., Chase, Norman E., and Ransohoff, Joseph R. The angiographic investigation of ruptured intracranial aneurysms. *Radiology*, Dec., 1964, *83*, 1016–1025. (From: Departments of Radiology [Neuroradiology] and Neurosurgery, New York University Medical Center, New York, N. Y.)

Angiography is the only means by which vascular lesions causing spontaneous subarachnoid hemorrhage may be identified during life. Non-hypertensive spontaneous subarachnoid hemorrhage is usually associated with rupture of a congenital aneurysm although a few patients bleed from arteriovenous malformations and tumors. The authors confine the present communication to the angiographic investigation of intracranial aneurysms.

The initial investigation of these patients should be undertaken as soon as practical after admission to the hospital. Since aneurysms are multiple in 15 per cent of patients having one such lesion, angiography should include at least bilateral carotid studies and preferably visualization of all the intracranial vessels. Occasionally, only one side is studied initially when a space-occupying mass such as an intracerebral clot is demonstrated along with the aneurysm. Such cases require immediate surgical intervention. However, a midline intracerebral clot may result from an aneurysm on either side and in such cases a bilateral study is indicated.

Direct carotid puncture is the technique preferred by the authors since right brachial or subclavian injections allow overlapping vascular shadows in the frontal plane due to vertebral artery filling. A needle, with a non-cutting bevel such as a Cournand, is carefully positioned and after a test injection, serial biplane filming is performed with pressure injection.

The standard positions are a true lateral and a frontal projection with 12° caudal angulation of the tube. Following the initial study, several special examinations are performed as indicated to best demonstrate the presence of single or multiple aneurysms. These include cross-compression techniques and special projections such as an oblique, frontal projection with cranial angulation and occasionally, the submentovertex view when the aneurysm is of posterior communicating origin.

Postoperative angiograms are urged in all patients and are especially indicated in those patients who do poorly after surgery. The reason for the poor result may be demonstrated as increased spasm, inadvertent occlusion of a major vessel, hydrocephalus, or the presence of a hematoma which may be surgically correctable.

The careful roentgenographic interpretation of a complete angiographic investigation is most important in evaluating these patients for surgery. Aneurysms must be differentiated from vascular loops and tortuosity and a single important differential point is that such configurations are usually denser than an aneurysm of the same diameter. Junctional dilatations, which usually occur at the level of the posterior communicating artery, are generally triangular in shape, under 3 mm. in diameter, and have their base on the carotid artery with the branch vessel arising from their dome. Vascular spasm may be local or diffuse and can be difficult to evaluate. Diffuse spasm may extend widely and should be diagnosed whenever the cerebral arteries, especially the more proximal vessels at the base of the brain, are narrower than experience would indicate.

Space-occupying lesions are not uncommonly associated with subarachnoid hemorrhage and frequently are due to intracerebral, intraventricular and subdural clots. The intracerebral clots appear as an avascular space occupying lesion adjacent to the site of bleeding and should be promptly removed. The presence of multiple aneurysms is not a contraindication to surgery if the currently bleeding aneurysm can be identified with any sense of security. Hydrocephalus is a common complication of subarachnoid hemorrhage, due to a basilar arachnoid reaction, and has been identified as developing within a 2 week period.

The authors admonish that the complications of angiography are largely the result of technical errors and are preventable. Particular care must be directed against damage from the needle, the embolization of particulate matter as well as air and prolonged cross compression or too vigorous post-angiography compression. In essence, angiography in subarachnoid hemorrhage should be performed by the most experienced operator available in each particular institution.—*Edward B. Best, M.D.*

## Neck and Chest

Harper, R. A. Kemp, and Guyer, P. B. The radiological features of thymic tumors: a review of sixty-five cases. *Clin. Radiol.*, April, 1965, *16*, 97–105. (From: St. Bartholomew's Hospital, London, England.)

In a group of 65 patients with thymic tumors seen since 1948, 51 had myasthenia gravis and 14

did not. Radiologic investigation consisted of initial fluoroscopy, followed by anteroposterior and lateral chest roentgenograms, and a coned lateral roentgenogram of the anterior mediastinum (with the shoulders back), somewhat underexposed as compared to the usual lateral chest roentgenogram. Tomography in the lateral, posteroanterior and, occasionally, the oblique projections was used if additional definition was necessary. Calcification was found in 17 patients. This was usually small in amount, measuring not more than 1×2 cm., but a few massive tumors showed very extensive calcification. The occurrence of diffuse or amorphous calcification is the only radiologic feature in nonmyasthenic patients which is at all suggestive of the thymic origin of a mediastinal tumor.

Roentgenologic evidence of metastases involving the pleura was found in 4 patients. These deposits presented as discrete peripheral nodules. The size of the tumors was often greatly altered by radiotherapy. In 44 cases studied microscopically, these tumors included 19 lymphoepitheliomas, 6 thymomas, 2 malignant and 2 benign thymomas, 1 thymic carcinoma, 1 thymic cyst, 1 epithelioid tumor, 1 fibrous nodule, 1 reticulosarcoma, 1 secondary metastasis, 1 failure of involution and 8 cases were inconclusive.

In this series only one small tumor was not detected, and there were no instances of a false positive diagnosis.—*Samuel G. Henderson, M.D.*

Lang, Erich K. Arteriographic diagnosis of the thoracic outlet syndromes. *Radiology*, Feb., 1965, *84*, 296–303. (From: Department of Radiology, Methodist Hospital, Indianapolis, Ind.)

Retrograde catheter aortography offers a new diagnostic means of locating the exact site of compression or obstruction responsible for the thoracic outlet syndromes. Accurate reproduction of the offending positions can be carried out and the artery studied under these conditions by injection of contrast medium and recording on serial roentgenograms. This eliminates the element of chance in surgical correction.

The author presents an analysis of 136 patients with thoracic outlet syndromes diagnosed by arteriography. Obstructing defects were demonstrated in the following conditions: scalenus anticus syndrome, pectoralis minor syndrome, thoracic outlet syndrome, cervical rib syndrome, combined lesions, vertebral steal and pseudosteal syndromes.

A small Seldinger catheter is advanced under fluoroscopic control into the subclavian artery. Introduction of the catheter into the femoral artery is favored since this offers the advantage of catheterization of both subclavian arteries without the presence of an irritating and splinting intraluminal foreign body at the point of interest. About 12 cc. of 50 per cent iodinated contrast medium is hand injected with the arm in neutral position. Smaller amounts will suffice for injections in positions which result in dampening of the pulse. The examinations are performed in various positions: the neutral, the Adson and the modified Adson as well as a position showing maximal clinical symptoms and dampening of the pulse. The decreased flow rate can also be studied by isotropic flow studies.

Arteriographically, four distinct types of scalenus anticus syndromes are readily recognized. Demonstration of the type of compression will usually permit identification of cause: (1) an oblique compression defect due to scalenus medius tendon; (2) torsion of the subclavian artery between the scalenus anticus and medius tendon; (3) concentric ridge-like compression of the entire subclavian artery over its entire passage through the scalenus tunnel; and (4) a sharp, linear cut-off at the point of entry into the scalenus tunnel. Post-stenotic dilatation is most often seen with concentric compression.

The cervical rib syndrome is readily recognized on plain chest roentgenograms. Arteriograms usually show huge post-stenotic dilatation of the subclavian artery in neutral position.

The pectoralis minor syndrome mimics the scalenus anticus syndrome. On arteriograms the two are readily differentiated. A marked depression and deflection of the junction segment of the subclavian and axillary artery are caused by the pectoralis minor tendon.

Various intrinsic arterial disease entities may closely mimic these conditions. Arteriosclerotic plaque formation and obliterative disease of the subclavian artery, fibromuscular dysplasia with intimal and subendothelial hyperplasia, as well as fibrous replacement of the subclavian artery belong in this group. These conditions are readily differentiated on arteriograms. Depending upon the site of the obstructing lesion, various "steal" syndromes may result.—*A. W. Sommer, M.D.*

Steckel, Richard J., and Grillo, Hermes C. Catheterization of the trachea and bronchi by modified Seldinger technic: a new approach to bronchography. *Radiology*, Dec., 1964, *83*, 1035–1038. (From: Department of Radiology and Surgical Services of Harvard Medical School, Massachusetts General Hospital, Boston, Mass.)

In 15 patients, a modified Seldinger technique has been employed to introduce a radiopaque teflon catheter through the cricothyroid membrane and then to maneuver it into various primary and secondary bronchi under fluoroscopic control. Selective bronchograms of superior quality have been obtained with no complications encountered.

The pharynx is lightly anesthetized, and the patient is then placed in the supine position with the

head well extended. The skin overlying the cricothyroid membrane is infiltrated in the midline with 2 per cent xylocaine, and with the same syringe a small amount of xylocaine is injected through the membrane to anesthetize the trachea locally. A Seldinger 160 needle is then introduced into the trachea with the tip pointed toward the carina. The wire guide is inserted and the catheter (inside diameter 1.35 mm.) threaded over it. After the wire guide is removed, the patient's head can be returned to a neutral position and the catheter manipulated under fluoroscopic control into, or adjacent to, the desired bronchial orifice. During placement of the catheter, anesthesia is obtained by repeated injections of xylocaine through the catheter. Television monitoring with image amplification is desirable but not a necessity.

Most patients who had had previous conventional bronchography agreed that this method was incomparably more comfortable. Local anesthesia and introduction of the catheter required an average of 5 minutes. A minimum of local anesthesia is required. In patients with diminished respiratory reserve, excellent filling of selected bronchi can be obtained with a minimum amount of contrast medium.—*Howard R. Stewart, M.D.*

Koch, Bernd. Familial fibrocystic pulmonary dysplasia: observations in one family. *Canad. M. A. J.*, April 10, 1965, *92*, 801–808. (From: Department of Medicine and Division of Research, Ottawa Civic Hospital, Ottawa, Ontario, Canada.)

Familial fibrocystic pulmonary dysplasia (FFPD) is a similar but distinct syndrome from idiopathic acute diffuse interstitial fibrosis of the lungs and from idiopathic bronchiolar emphysema. This study concerns 56 members of one family in which 8 members exhibited features of FFPD. Diagnostic criteria included progressive dyspnea and cyanosis, digital clubbing, pulmonary hypertension, negative sweat tests, polycythemia, arterial hypoxia and hypocapnia, roentgenograms showing diffuse bilateral pulmonary fibrosis, and diffuse fibrocystic pulmonary dysplasia at postmortem examination.

Clinical and pathologic evidence indicates that the disease is genetically determined. In one instance, there was a father-to-son transmission, and probably another son and daughter were also affected, which rules out a sex-linked genetic defect and establishes the autosomal dominant inheritance of FFPD. Although the pathogenesis remains obscure, an enzyme defect is probably the underlying agent. It is thought that pulmonary morphologic changes are a secondary nonspecific reaction, and that bronchogenic carcinoma is a tertiary nonspecific complication.—*Lois Cowan Collins, M.D.*

Hafter, E. The so-called "lower esophageal ring." *German Med. Monthly*, Feb., 1965, *10*, 65–71. (Address: Tödistr. 36, Zürich, Switzerland.)

In 1944, in his book entitled "X-Ray Examination of the Stomach," Templeton described a ring-like constriction in the epiphrenic ampulla. Jutras (1949), Evans (1952), Ingelfinger and Kramer (1953), and Schatzki and Gray (1953) reported a number of patients with similar findings. The latter authors used the descriptive term, "lower esophageal ring."

This ring was demonstrable only on maximum inspiration after swallowing, at which time the lumen of the adjacent esophagus was distended to a width greater than the diameter of the ring. It disappeared when the adjacent esophagus collapsed. The band measured 2 to 4 mm. in width and was located 4 to 5.5 cm. above the level of the diaphragm. Its diameter ranged from 6 to 15 mm. in Ingelfinger's cases and from 3 to 18 mm. in Schatzki's group. There was no obstruction to flow of fluid contrast medium, but a swallowed capsule was temporarily delayed at this level. In 1956, Schatzki and Gray reviewed their cases and found little interval change in most patients.

Wolf (1956), in a paper on hiatus hernia, demonstrated a transverse "sulcus" in several cases at the proximal end of the hernia. He subsequently suggested that this sulcus and Schatzki's ring were probably identical. If this were correct, the "lower esophageal ring" would in fact correspond to the esophagogastric junction displaced above the diaphragm by the presence of a small hiatus hernia.

MacMahon has described the findings at necropsy in a case of "lower esophageal ring." There was a small sliding hiatus hernia and a thin mucosal shelf at the esophagogastric junction. The upper surface of this membranous shelf was covered by esophageal mucosa and the lower surface by gastric mucosa. There was increased connective tissue in the tunica propria of the ring which suggested to Barrett that the ring represents an inflammatory scar. However, the total absence of inflammatory reaction in cases studied histologically makes this hypothesis unlikely.

The author feels that it is possible to accurately localize the esophagogastric junction by demonstrating the "lower esophageal ring." Thus, one can differentiate with certainty a small hiatus hernia from an epiphrenic ampulla. His technique includes roentgenograms obtained in full expiration (open hiatus) and in full inspiration (closed hiatus) with barium in the esophagus. Of the patients with a small hiatus hernia, more than half show three transverse rings.

The lower ring is caused by closure of the hiatus during inspiration. It cannot be demonstrated when the hiatus is abnormally enlarged and incompetent. The upper ring lies 3–6 cm. proximal to the lower

ring. This is the site of transition between the tubular esophagus and the vestibule.

The middle ring is only demonstrated when the adjacent lumen is fully distended with contrast medium. In 42 patients, the diameter of this middle ring was less than 25 mm. In 9 patients with intermittent dysphagia, the diameter of the ring was less than 14 mm.

The author believes that the middle ring fits the description of the "lower esophageal ring" of Schatzki and Ingelfinger and agrees with them that this represents a reliable roentgenologic landmark for the esophagogastric junction. Mucosal folds proximal to the ring were always fine and narrow like folds of the tubular esophagus. Distal to the ring, the mucosal folds are wide similar to gastric mucosa.

This ring is seen predominantly in men over age 50. The youngest case in this series is a female aged 20. In all cases, there appeared to be a small hiatus hernia in association with the ring. Dysphagia was present in every case when the ring diameter was less than 14 mm. It was frequent in the 14 to 20 mm. range, and was not recorded with a ring diameter greater than 25 mm.—*E. Gedgaudas, M.D.*

## ABDOMEN

WEINBERG, PETER E., and LEVIN, BERTRAM. Hyperplasia of Brunner's glands. *Radiology*, Feb., 1965, *84*, 259–262. (From: Michael Reese Hospital and Medical Center, Chicago, Ill.)

A brief historic review and classification along with 2 cases of surgically proven hyperplasia of Brunner's glands are presented.

Brunner first described hyperplasia of the duodenal glands in 1876. They are located in the mucosa and submucosa, being most numerous in the first portion and decreasing in number and size distally, disappearing beyond the ligament of Treitz. They are normally 3–5 mm. in diameter and their physiologic function is to protect the duodenal mucosa from the acid gastric chyme.

Hyperplasia was classified into three types by Feyrter in 1934. The first is a diffuse nodularity consisting of coarse mucosal folds and irregularly circumscribed nodules of duodenal glands which are distributed throughout the greater portion of the duodenum. The second type is a circumscribed nodular hyperplasia in which isolated nodules, often accompanied by atrophy of the intervening glands, are found in the suprapapillary segment of the duodenum. The third type is the single nodule of adenomatous hyperplasia. This solitary type may be either sessile or pedunculated and may be as large as several centimeters in diameter.

Erb and Johnson introduced hyperplasia of Brunner's glands as a clinical entity in 1948, and it is noted that the clinical picture is extremely variable. However, the roentgenologic appearance of hyperplasia is considered reliable and characteristic.

The roentgenologic differential diagnosis includes: duodenal polyposis, localized hyperplasia of lymphoid follicles, and duodenitis. Reported reviews of the literature have not uncovered a single case of carcinoma of Brunner gland origin.

Case data, along with photographs and roentgenographic reproductions, are included.—*John Bond, M.D.*

HOUSTON, C. STUART, and WITTENBORG, M. H. Roentgen evaluation of anomalies of rotation and fixation of the bowel in children. *Radiology*, Jan., 1965, *84*, 1–18. (Address: Dr. Houston, University Hospital, Saskatoon, Saskatchewan, Canada.)

The roentgenologic aspects of anomalies of rotation and fixation of the bowel in children are presented. Basis for this report is a review of 147 cases seen over a 10 year period at Children's Hospital Medical Center of Boston.

Diagnosis of anomalies of rotation and fixation of the bowel requires an understanding of the embryology of normal and abnormal intestinal rotation. Interruptions or aberrations of the orderly process of rotations may occur at any stage of development. A rigid classification of these anomalies is neither practical nor useful but the defects can be grouped as follows:

1. Extroversion of the cloaca, with no rotation of the bowel. The ileum and colon each open separately onto the extroverted area in the mid line, below the umbilical cord.
2. Omphalocele, resulting from failure of the midgut to return from the umbilical cord.
3. Congenital left diaphragmatic hernia, always accompanied by an anomaly of rotation.
4. Congenital right diaphragmatic hernia, associated with neurenteric and vertebral anomalies in 2 cases in this series.
5. "90 degree rotation," also termed "nonrotation" or "situs inversus partialis commune mesenterium," with continuation of the eighth fetal week relationship within the abdomen. The colon lies in the left abdomen and the small bowel in the right, on either side of the superior mesenteric artery, with a common unattached mesentery.
6. Nonfixation. The viscera are normally placed, with the exception of the ascending colon and cecum, which are freely movable.
7. Reverse rotations, a rare anomaly, with rotation in the opposite or clockwise direction. The jejunum and duodenum lie anterior to the superior mesenteric artery.
8. Reverse nonrotation, with the colon on the right side and the small bowel on the left.

In this series of 147 patients, 22 had no symptoms related to the malrotation. Only when complications are superimposed upon the anomalies of rotation and fixation do symptoms appear. They arise from: (a) mechanical obstruction; (b) vascular obstruction; (c) a celiac-like syndrome.

Abdominal survey roentgenograms will rarely be of value unless there are complications. Duodenal obstruction secondary to "malrotation" often cannot be differentiated from duodenal obstruction due to atresia, stenosis or annular pancreas. In "malrotation," a large gastric bubble with a smaller duodenal one just proximal to the obstruction is frequently seen. Low small bowel obstruction due to volvulus may be recognized by the gas trapped within distended small bowel loops, with fluid levels in the upright position. Rapid progression from one intestinal gas pattern to another may occur. Vascular complications rapidly result in ileus and free peritoneal fluid, with symptoms of gastrointestinal bleeding and shock.

In approximately two-thirds of the patients in this series, barium enema examinations or a gastrointestinal series, or both, were performed prior to surgery. Contrast studies will: (a) localize and characterize the obstruction; (b) detect the abnormal position of the bowel; (c) reveal abnormal fixation in the majority of the cases in which it exists. The practical problem is not whether barium studies are to be undertaken, but to decide whether one examination or both should be performed. Barium is preferred to water-soluble agents by the authors.

Obstruction may be acute or chronic, partial or complete, compensated or intermittent. Complete or nearly complete obstructions are usually in the duodenum and associated with volvulus, bands or both. A dilated proximal duodenum and pylorus, with sudden dumping of barium into the duodenum when the patient is turned from supine to prone position may be observed. Abnormal fixation of the bowel is demonstrated when the duodenojejunal junction is abnormally placed and/or when the ileocecal valve lacks normal fixation in the right lower quadrant. A jejunum confined to the right side of the abdomen indicates anomalous rotation.

The cecum may be abnormally fixed posteriorly or abnormally mobile anteriorly. There may be a primitive fan-shaped mesentery or a longitudinal mesentery suspending the cecum and ascending colon.

The roentgenologic findings often proved the crucial factor in correct and accurate diagnosis. Unusual position of bowel loops should alert the radiologist to the possibility of an error in rotation. Identification of the fixation points of the mesentery permits evaluation of abnormal fixation.—*A. W. Sommer, M.D.*

Rudhe, Ulf, and Keats, Theodore E. Granulomatous colitis in children. *Radiology*, Jan., 1965, *84*, 24–32. (From: Department of Diagnostic Radiology, Children's Clinic, Karolinska Sjukhuset, Stockholm, Sweden.)

The purpose of this report is to emphasize the occurrence of granulomatous colitis in children, to describe some of its roentgenologic aspects in this age group, and to present an apparently undescribed roentgen alteration. This series comprises 15 patients, 11 males and 4 females, ranging in age from 10 to 16 years, with diagnosis proven in 10 cases by surgical and histologic specimens.

The disease tends to be segmental, with simultaneous involvement of the colon and ileum, and is likely to be confused with idiopathic ulcerative colitis. Anal and perirectal fistulae and abscesses are frequently the presenting signs and internal fistulae are a frequent complication.

Roentgenologically, the disease is characterized by segmental involvement with sharply demarcated skip areas, by longitudinal ulcerations which later present as penetrating spicules with interposed cobblestone mucosa, and by segmental exaggerated haustration. The exaggerated haustration is described as differing from the corrugation associated with idiopathic ulcerative colitis and is presented as a motor defect and early sign of granulomatous colitis. It is important to emphasize that this type of motor disorder of the bowel may be present long before any mucosal change is detectable at roentgen examination of the bowel.

The cases presented are illustrated by 16 roentgenographic reproductions and 2 schematic diagrams.—*John L. Bond, M.D.*

Ching, Nathaniel P. H., and Ballinger, Walter F., II. Perforation of the colon: secondary to the meconium plug syndrome. *A.M.A. Arch. Surg.*, Jan., 1965, *90*, 65–67. (Address: Dr. Ballinger, The Johns Hopkins Hospital, Baltimore, Md. 21218.)

The authors discuss perforation of the colon in the newborn, and present a case caused by the meconium plug syndrome. Within 27 hours after an uncomplicated delivery, vomiting and abdominal distention was noted in a 2.6 kg. Negro male. A barium enema study revealed a meconium plug in the rectum. Following a digital examination, a "tadpole-like" stool was passed and the infant appeared improved. At 48 hours of age, the patient's abdomen was again distended and abdominal roentgenograms revealed free air in the peritoneal cavity. Exploratory laparotomy disclosed a perforation in the cecum and a temporary cecostomy was performed.

The infant did well postoperatively with passage of a meconium stool after lubricating his rectum.

The cecostomy was repaired on his 20th day of

life and he was discharged 32 days after birth at a weight of 3.0 kg.

The mortality in this condition is stressed and a plea is made for early diagnosis and surgical correction.—*James F. Martin, M.D.*

Brown, B. St. J. Defecography or anorectal studies in children including cinefluorographic observations. *J. Canad. A. Radiologists*, March, 1965, *16*, 66–76. (From: The Montreal Children's Hospital, Montreal, Quebec, Canada.)

Defecography is a technique of roentgenologic examination which has been used at The Montreal Children's Hospital to study the mechanism and effectiveness of defecation. It can be applied as a modification of the standard barium enema procedure in most infants and children. The patients are examined with no preparation whatever. This method of study provides more complete and, at times, new information in the following groups of conditions: (1) megacolon, due to chronic constipation or to aganglionosis; (2) evaluation of surgical procedures; (3) fecal incontinence and other disorders of function of the anorectal region; (4) imperforate anus and malformation of the pelvic floor and perineum; (5) miscellaneous conditions including fistulae and sinuses in the anorectal region.

Fourteen case reports are presented. In addition, this examination was carried out in 50 children of various ages (7 weeks to 13½ years) with normal bowel habits. Most of these were done for the investigation of abdominal pain or bleeding per rectum unassociated with anorectal disease. Detailed description of the technique is given, and numerous reproductions of roentgenograms are included.—*Douglas S. Kellogg, M.D.*

Neaman, Montague Philip. Comparative evaluation of adjuvants to barium enema examinations: use of oxyphenisatin and tannic acid. *J. Canad. A. Radiologists*, March, 1965, *16*, 17–18. (Address: 105 Northgate Building, Edmonton, Alberta, Canada.)

Many radiologists have used tannic acid for a number of years to improve mucosal definition in the colon. Recently there have appeared case reports linking fatal liver damage with barium enemas containing tannic acid. Since little work had been done in the use of adjuvants other than tannic acid, it was felt worthwhile to conduct a further study of the value of a recent colonic evacuant, oxyphenisatin (Lavema-Winthrop).

The roentgenograms of 303 barium enema examinations were reviewed by the author without knowledge as to the presence or absence of added Lavema, tannic acid, or whether no additive was used.

The patients were divided into three groups as follows: Group 1—102 patients received an estimated 0.30 per cent solution of tannic acid-barium sulphate (Merck); Group 2—100 patients had Lavema added in graduated doses according to patient size; Group 3—101 patients had no additive in the barium suspension.

All patients were prepared with castor oil the day prior to the examination. The postevacuation roentgenograms were interpreted as belonging to 1 of 4 categories, according to the degree of evacuation and the excellence of mucosal definition. There were fewer good examinations with Lavema than with tannic acid, probably because of excessive evacuation. With barium sulphate only, there were fewer excellent examinations and a higher percentage of poor examinations.

A plea is made for further critical evaluation of drug adjuvants in barium enema examinations.—*Douglas S. Kellogg, M.D.*

## Gynecology and Obstetrics

Warfield, Charles I., and Sherer, Max G. (Silver Spring, Md.) Stein-Leventhal syndrome. *South. M. J.*, March, 1965, *58*, 333–336.

This report concerns 56 patients who met the authors' criteria of the Stein-Leventhal syndrome.

The authors routinely use gas gynecography according to the method of Schultz and Rosen. Ninety-four gynecograms were obtained, employing nitrous oxide, without untoward effects.

In addition to ovarian enlargement, a spherical (rather than a cylindrical) ovarian configuration has been found to be highly suggestive of polycystic ovarian disease. The demonstration of this spherical configuration is particularly valuable when ovarian enlargement is not obvious.—*John H. Harris, Jr., M.D.*

Bank, H., Beer, R., Lunenfeld, B., Rabau, E., and Rumney, G. Recurrence of adrenal carcinoma during pregnancy with delivery of a normal child. *J. Clin. Endocrinol. & Metabol.*, March, 1965, *25*, 359–364. (From: Department of Endocrinology, Tel-Hashomer Government Hospital, Israel.)

A case of adrenocortical carcinoma in a 24 year old woman, who has to date survived 8 years, is reported.

The findings discussed include the local recurrence of the tumor during a third pregnancy, the demonstration of a partial placental barrier to cortisol, the birth of a normal child with well-functioning adrenals in the presence of high levels of maternal cortisol, and the management of pregnancy in the presence of functioning adrenocortical carcinoma.—*John H. Harris, Jr., M.D.*

## Genitourinary System

Antoine, B., Anagnostopoulos, T., Watchi, J. M., and Parienty, R. L'ectasie canaliculaire précalicielle: étude basée sur 21 cas de maladie de Cacchi et Ricci, dite "reins en éponge." (Precalyceal canalicular ectasia: study based on 21 cases of Cacchi and Ricci disease, so-called "sponge kidneys.") *J. de radiol., d'électrol. et de méd. nucléaire*, Nov., 1964, *45*, 663–680. (From: Clinique des Maladies métaboliques de la Faculté de Médecine de Paris, et du Centre de Recherches sur l'Insuffisance rénale de l'Association Claude-Bernard, Paris, France.)

This condition was first described in 1948 by Cacchi and Ricci, a urologist-radiologist team who recognized its distinctive identity. The authors stress that although the credit for the original description of this disease should go to Cacchi and Ricci, the term "sponge kidney" is erroneous and misleading.

The condition is characterized by the following: (1) It is discovered as an incidental finding during a routine examination of the urinary tract, often during intravenous urography for urinary infection or lithiasis; (2) the roentgenologic appearance is striking, the findings being diffuse and bilateral. They consist of small tubular dilatations presenting an appearance of "a bouquet of flowers" at the apex of the calyces extending to the pyramids, but exclusive of the cortex; (3) the renal function is surprisingly well preserved, occasionally there being slightly decreased concentration of urine and the clinically noted polyuria; (4) the roentgenologic appearance remains unchanged with the passage of time, as evidenced by serial follow-up examinations on several patients; (5) the histologic study of a surgically removed kidney demonstrates total absence of an inflammatory process, the presence of cystic tubular dilatations involving the renal tubules in the precalyceal portion of the collecting system, which coincides with and explains the roentgenologic appearance.

The disease is quite rare as evidenced by the paucity of reports in the literature. It is relatively benign and is distributed practically equally between the two sexes. In some instances a familial tendency has been observed.

In the series studied by the authors the patients varied in age between 3 weeks and 71 years.

Precalyceal tubular ectasia, noncomplicated, is practically asymptomatic, and only when complications set in does the condition become symptomatic. Urinary infection and calculus formation may be associated with the condition.

Of the 21 patients examined by the authors, 11 presented symptoms of urinary infection, 5 were benign and afebrile, while 6 presented acute symptoms of pyelonephritis and pyuria. Eight patients presented symptoms of pain in the loins and 6 had renal colic (in 4 the calculi were passed). Microscopic hematuria was observed in 7 cases. None of the patients presented symptoms to suggest hypertension, hepatomegaly, portal hypertension or splenomegaly.

Exclusive of occasional episodes of hematuria, the absence of blood in the urine is the rule, with microscopic hematuria demonstrated in 20 per cent. Blood chemistry and routine urine studies show no remarkable findings. Renal function is well maintained.

Calcareous deposits with the formation of small calculi in the dilated tubules are noted. There is minimal blunting of the calyces. An early precalyceal tubular nephrogram is obtained during intravenous urography, which distinguishes this condition from tubular reflux due to other causes.

The cyst-like or tubular dilatations are about 1–2 mm. in diameter. When opacified, they present a converging or radiating pattern towards the papilla. This may be a fine cystic network, a striated pattern, or an indistinct and a more or less nebulous arrangement. The best demonstration is obtained on roentgenograms obtained 1 minute after the injection, revealing an early and characteristic nephrogram.

Nephrocalcinosis within the dilated precalyceal tubules was found in 43 per cent of the cases observed by the authors. This is characteristically pyramidal in location and excludes calcinosis due to other causes such as tuberculosis, papillary necrosis and hyperparathyroidism.

Seventeen figures, including reproductions of roentgenograms, anatomic and microscopic sections, and 1 table accompany this interesting article.—*William H. Shehadi, M.D.*

## RADIATION THERAPY

Minton, John Peter, Ketcham, Alfred S., Dearman, James R., and McKnight, William B. The effect of neodymium laser radiation on two experimental malignant tumor systems. *Surg., Gynec. & Obst.*, Mar., 1965, *120*, 481–487. (From: Surgery Branch, National Cancer Institute, National Institutes of Health, Bethesda, and the Applied Physics Branch, Redstone Arsenal, Huntsville, Ala.)

The laser is a source of high intensity photon energy described as coherent monochromatic light. The neodymium laser produces energy at a wave length of 10,600 Å units which is in the infrared portion of the electromagnetic spectrum. Since laser energy can be optically focused, the possible application of laser radiation as an oncolytic agent has been investigated.

The authors conducted this study to determine the capabilities of laser radiation regarding permanent tumor destruction and the dependency of such destruction on tumor size.

Two separate tumor systems were employed, one a melanoma and the other a sarcoma, in 2 different strains of mice. An important factor in tumor destruction is the transfer of the neodymium laser energy into the tumor cells and the production of an intense amount of heat in the target area. The most constant observation following a laser pulse was the immediate appearance of a thermal burn at the site of laser impact. The size and degree of the burn was proportional to the amount of energy delivered. Recent studies have indicated that during the laser impact the temperature rise can be as great as 1,000°C.

The results of these laser tumor experiments indicated clearly that greater amounts of laser energy were necessary to destroy larger tumors. In certain cases both the sarcoma and melanoma were permanently destroyed. However, the melanoma was more easily destroyed supporting the theory that more heavily pigmented tumors are capable of greater energy absorption of laser radiation per unit volume than non-pigmented tumors.

From this study, no apparent survival benefit was afforded mice with incompletely destroyed tumors.—*Francis Shea, M.D.*

## RADIOISOTOPES

Morrison, Robert T., Afifi, Adel K., Van Allen, Maurice W., and Evans, Titus C. Scintiencephalography for the detection and localization of non-neoplastic intracranial lesions. *J. Nuclear Med.*, Jan., 1965, *6*, 7–15. (From: Radiation Research Laboratory and Department of Neurology, State University of Iowa, Iowa City, Iowa.)

Five hundred patients with a variety of intracranial diseases were scanned using RIHSA, $I^{131}$ colloidal human albumin, or $Hg^{203}$ chloromerodrin. All these agents appear to be of equal value in detecting intracranial lesions. Any advantage of one over the other concerns the time interval between the dose and the scan and the radiation to the patient.

Eighty-five per cent (64 of 75) of confirmed neoplasms were demonstrated by scanning. Fifty-two per cent (29 of 56) with a clinical diagnosis of cerebral infarction showed abnormal scans. The scan of an infarct, in most cases, appeared no different than that of a neoplasm, but infarcts tended to show more irregular borders, while neoplasms exhibited a more regular and rounded appearance. The incidence of abnormal scans decreased as the time interval between the onset of the infarction and the scan increased. Usually by 8–10 weeks after the abnormal scan (if done early in the course of the infarct), rescanning showed no abnormality, unless in reality a neoplasm was present. Seven of 8 arteriovenous malformations were demonstrated and 7 of 8 subdural hematomas.

Five abnormal scans of non-neoplastic lesions are illustrated.—*William K. Littman, M.D.*

Overton, Marvin C., III, Otte, William K., Beentjes, Lucas B., and Haynie, Thomas P. A comparison of $^{197}$mercury and $^{203}$mercury chlormerodrin in clinical brain scanning. *J. Nuclear Med.*, Jan., 1965, *6*, 28–37. (From: Departments of Neurosurgery, Radiology and Internal Medicine and the Nuclear Medicine Service, The University of Texas Medical Center, Galveston, Texas.)

The radiation dose advantage of $Hg^{197}$ over $Hg^{203}$ primarily concerns the dose to the kidneys. $Hg^{197}$ causes about one-eight that of the longer lived $Hg^{203}$.

$Hg^{203}$ was given intravenously in a dose of 10 μc/kg., but not exceeding 700 μc. One cc. mercuhydrin was injected intramuscularly prior to the $Hg^{203}$. $Hg^{197}$ was given in a dose of 700 μc for adults and 500 μc for children.

The over-all rate of correctly diagnosing neoplastic lesions as positive revealed little difference between $Hg^{203}$ (82 per cent) and $Hg^{197}$ (88 per cent). For unknown reasons in non-neoplastic diseases $Hg^{197}$ (75 per cent positive) appeared superior to $Hg^{203}$ (50 per cent positive).

Thus $Hg^{197}$ gives results comparable to those obtained with $Hg^{203}$ chlormerodrin, but $Hg^{197}$ has the advantage of a lower radiation dose to the patient.—*William K. Littman, M.D.*

Caniggia, A., Gennari, C., and Cesari, L. Intestinal absorption of $^{45}$Ca in stone-forming patients. *Brit. M. J.*, Feb. 13, 1965, *1*, 427–429. (From: Institute of Medical Semeiology, University of Siena, Siena, Italy.)

The authors studied 6 patients who had multiple renal calculi; 1 had nephrocalcinosis, and 1 had hyperparathyroidism.

All were found to absorb calcium more than normally. This has been previously demonstrated in hyperparathyroidism.

The authors postulate that the principal metabolic abnormality in some patients with calcium nephrolithiasis could be an increased intestinal absorption of calcium.—*George L. Sackett, Jr., M.D.*

Mena, Ismael, and Thomsen, Pablo. Detection of heart shunts by means of $^{125}$I. *J. Nuclear Med.*, Jan., 1965, *6*, 16–27. (From: Department of Medicine, Divisions of Nu-

clear Medicine and Cardiology, Catholic University Hospital, Santiago, Chile.)

Both normal subjects and individuals with pathologic defects were studied. The pathologic defects included 20 atrial septal and 9 ventricular septal defects.

A detailed description is given of the procedure of external counting over the heart chambers, of the equipment used, and of the dosage of $I^{125}$.

All but 1 of the patients with atrial septal defect showed an abnormality of early recirculation of the right heart. There was less accuracy in detecting those with ventricular septal defect.

The conclusion from the study is that it seems possible to perform selective right heart radiocardiography by means of external precordial detection of $I^{125}$ and that the method is simple, safe, and reproducible.—*William K. Littman, M.D.*

Fava, G., and Roncoroni, L. Possibilità ed applicazioni pratiche dello "scanner" Nukab con memoria magnetica. (Possibilities and practical applications of the "scanner" Nukab with magnetic memory.) *Radiol. med.*, Dec., 1964, *50*, 1264–1276. (Address: Dott. Giannino Fava, Piazzale Gorini, 22, Milan, Italy.)

The authors report on and discuss the advantages of the new Nukab scintiscanning system.

This scintillation scanner has the same characteristics as most of the commercially available scanners and, furthermore, records on magnetic tape and on graph paper all the data obtained which can be processed later and/or reproduced on Polaroid film.

The machine will scan the whole body and permit also body profile scanning.

A few cases are reported which illustrate the advantages of this scintigraphic system.—*A. F. Govoni, M.D.*

# SUBJECT INDEX TO VOLUME 94

(ab) = abstract (E) = editorial

# AUTHOR INDEX TO VOLUME 94

* = Original Article

# Answer to a problem

When minimum exposure is all-impo
tant, KODAK ROYAL BLUE Medical X-r
Film can record the maximum amou
of radiographic information.

Add its day-after-day uniformity, a
you have the answer to the problem
obtaining clear, accurate radiograp
on which to base your diagnoses.

**EASTMAN KODAK COMPANY,**
**Radiography**
**Markets Division,**
**Rochester, N. Y.**

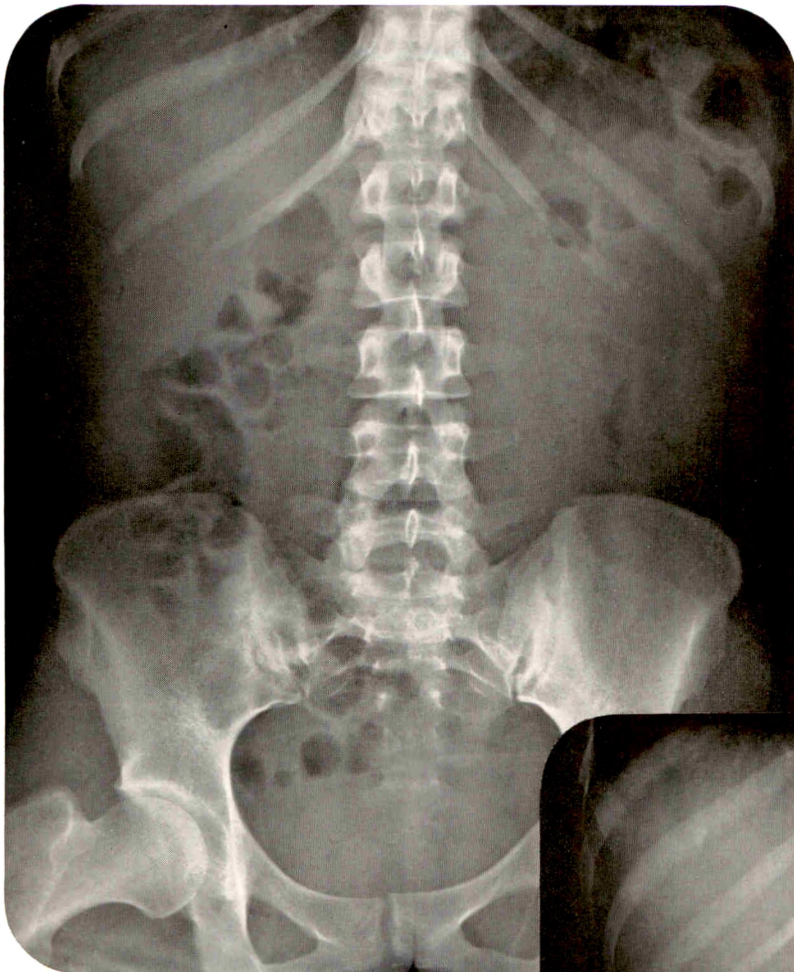

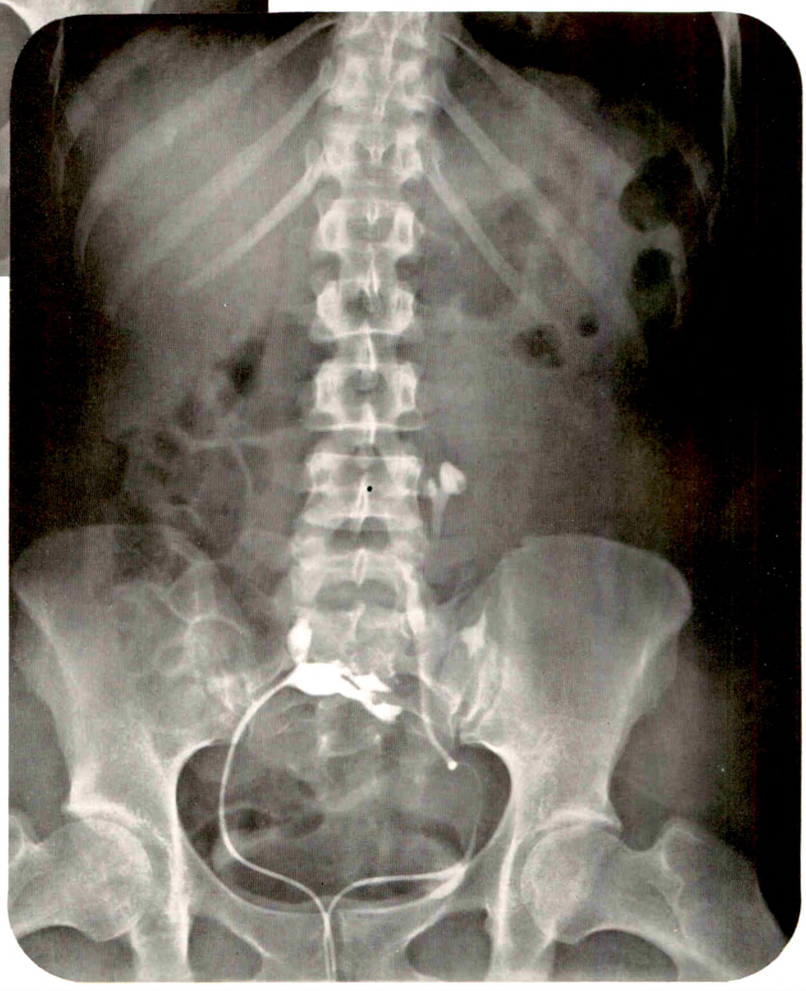

Reproduced from radiographs made on

KODAK **ROYAL BLUE** Medical X-ray Film

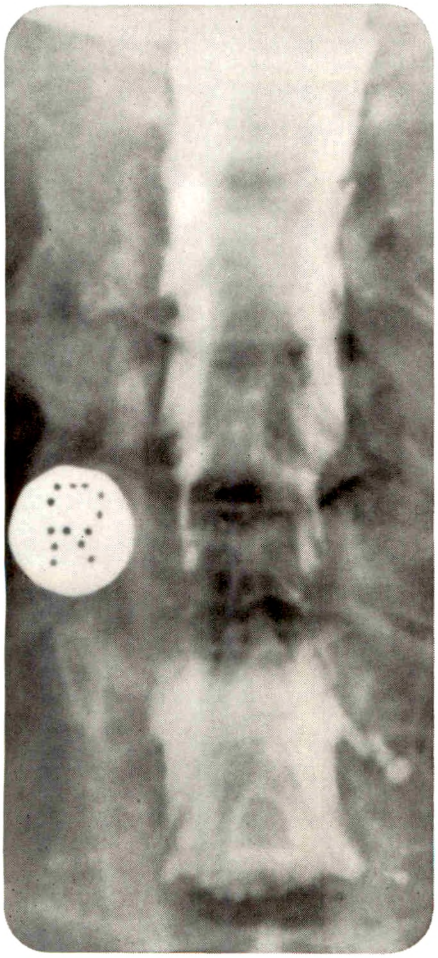

Progressive bilateral numbness, weakness, and muscle atrophy that had been present for one year in a 57-year-old man was attributed to cervical spondylosis. A myelogram using 12 cc of PANTOPAQUE [Iophendylate Injection] demonstrated the large defect at the level of the fifth cervical vertebra. The patient recovered rapidly following laminectomy and posterior decompression of the fifth cervical spinal nerve roots.

"PANTOPAQUE" *is the registered trademark under which all leading x-ray dealers supply the compound ethyl iodophenylundecylate, which is synthesized in the laboratories of Eastman Kodak Company and prepared as the myelographic contrast medium Iophendylate Injection, U.S.P., by Lafayette Pharmacal Inc. The trademark serves to indicate to the radiologist continuity of experience in the manufacture of this medium.*

# BARNES-HIND BAROTRAST®

□ Barotrast suspends easily—and **stays** in suspension. Coverage is complete... coating is thin, elastic, tenacious... flow is steady, consistent, and columnar. Barotrast is ideal for routinely precise examinations. □ BAROTRAST® (Specially compounded and micronized form of barium sulfate) □

**BARNES-HIND BARIUM PRODUCTS**
DIVISION OF BARNES-HIND PHARMACEUTICALS, INC.
Sunnyvale, California

## the original high-density barium product for unsurpassed delineation

Barotrast used in an air contrast study of the mid transverse colon.

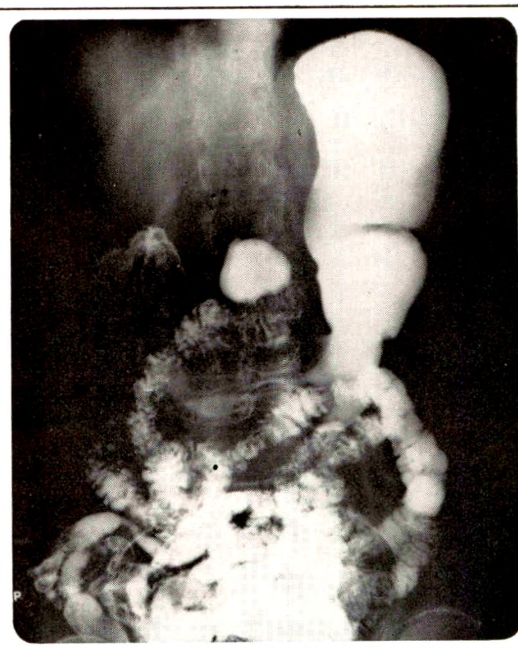

Barotrast used in an upper GI study of the stomach.

25 POUNDS

LIST NO. 821

Barotrast®

BARNES-HIND BARIUM PRODUCTS
Division of Barnes-Hind Pharmaceuticals, Inc.
Sunnyvale, California Made in U.S.A.

©1964 BPA 101


*the clinical situation demands conclusive, differential diagnosis consider these contrast media*

**Hytrast**® (iopydone, iopydol)
**Ethiodol**® (ethiodized oil)
**Lipiodol**® **28%** (iodized oil)
**Lipiodol**® **40%** (iodized oil)
**Ascendant Lipiodol**® (floating iodized oil)
**Visciodol**® (Lipiodol-sulfanilamide)

*...and procedural aids*

**Colo-Bar**® (ready-to-eat cholagogue)
**Polysorb**® **Hydrate** (for radiation dry skin)

CONTRAST MEDIA — DEVELOPMENTS OF GUERBET LABORATORIES

FOUGERA **E. FOUGERA & COMPANY, INC.** HICKSVILLE, L. I., NEW YORK

# INDEX TO ADVERTISERS



•

**We try to present an accurate index. Occasionally this may not be possible because of a last-minute change or an omission.**

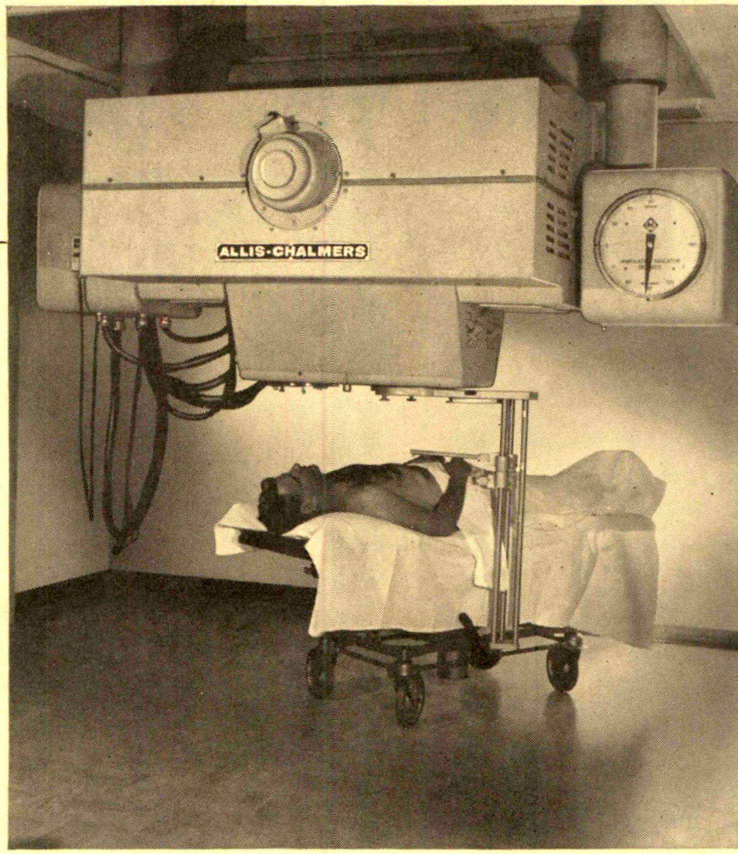


**If you're ready to consider super-voltage X-ray equipment...**

**The most**
# reliable
**unit you can buy is the Allis-Chalmers 25 Mev Betatron**

*Here's why.* In three words: simplicity of design. Because it has fewer gadgets, there's less to go wrong. Another reason? The Allis-Chalmers warranty. Every part, every casting, every piece of wiring is as good as 21 years of Betatron experience can make it. So good Allis-Chalmers backs all mechanicals with a full-year warranty. Even the X-ray tube is warranted against premature failure. Or we make it right, at our expense. If you're considering a super-voltage X-ray unit, evaluate it on the basis of reliability. Consider how you may have to use it every day in therapy. Therapy that shouldn't wait. Evaluate reliability in terms of costly maintenance. Then evaluate the Allis-Chalmers 25 Mev Betatron, with the greatest *proven* reliability PLUS performance that gives you 30-50% more tumor dose, 45-50% less entrance dose. Think reliability. Write for descriptive 25 Mev Betatron brochure. Allis-Chalmers, Electrical Apparatus and Systems Division, Milwaukee, Wisconsin 53201.

A-2010

ALLIS-CHALMERS

# four generations of technological advance in Cobalt[60] teletherapy apparatus


30 OCT 1965

Into the C8M80 — latest in the long line of Picker Cobalt[60] Therapy Units — has gone the fully-matured expertise of the most experienced engineering group in the teletherapy field. The performance data accumulated in hundreds of installations (over half the Cobalt[60] installations in the Free World are Picker-equipped) has been uniquely theirs to build upon.

Add to this the voices of the many distinguished therapists who were good enough to give of their counsel in its development, and you arrive at an apparatus in which is concentrated a depth of capabilities* equal to the performance of the most sophisticated current techniques.

*Recounted in detail in Picker Publication #5-133. Get a copy from your local Picker office or write
PICKER X-RAY CORPORATION
White Plains, New York.

**the PICKER**

**C8M80**

**COBALT[60]**

**TELETHERAPY APPARATUS**

Picker x-ray